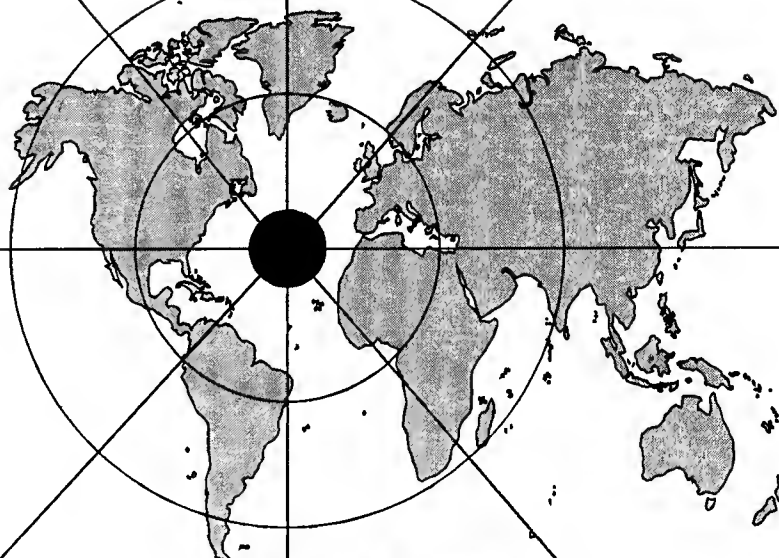
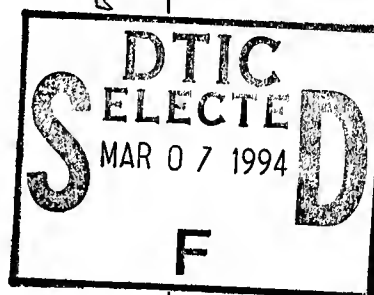


Proceedings of the Forty-Third IWCS



19950302 140



INTERNATIONAL WIRE AND CABLE SYMPOSIUM

NOVEMBER 14 THRU 17, 1994

This document has been approved
for public release and sale; its
distribution is unlimited.

Sponsored by
International Wire and Cable Symposium,
Inc. (IWCS)
Eatontown, New Jersey

With Participation by
US Army Communications-Electronics Command
(CECOM)
Fort Monmouth, New Jersey

PROCEEDINGS OF 43RD INTERNATIONAL WIRE AND CABLE SYMPOSIUM

Sponsored by
International Wire and Cable Symposium, Inc. (IWCS)
Eatontown, New Jersey

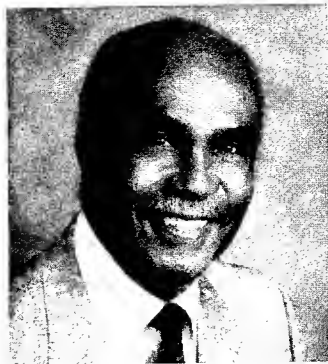
With Participation by
US Army Communications-Electronics Command (CECOM)
Fort Monmouth, New Jersey

ATLANTA HILTON & TOWERS HOTEL
ATLANTA, GEORGIA
NOVEMBER 14, 15, 16 and 17, 1994

APPROVED FOR PUBLIC RELEASE: DISTRIBUTION UNLIMITED

Accession For	
NTIS CRA&I	<input checked="" type="checkbox"/>
DTIC TAB	<input type="checkbox"/>
Unannounced	<input type="checkbox"/>
Justification	
By	
Distribution /	
Availability Codes	
Dist	Avail and/or Special
A-1	

1994-11-17 10:00:00



MESSAGE FROM THE PRESIDENT/DIRECTOR

A warm welcome is extended to all attendees of the 43rd International Wire and Cable Symposium (IWCS). It is hard to believe that another symposium is upon us. The expectation of seeing many familiar and also new faces at each symposium is always exciting. This year's program of over 125 presentations should include topics of special interest for nearly everyone, especially the opening tutorial session on Tuesday entitled "Choices of Local Distribution Network." The technical program includes four full days of activities, beginning on Monday with ten educational short courses, that covers a variety of subjects, followed by three days of technical presentations. The suppliers forum on Monday and Tuesday plus the hospitality suites located throughout the hotel, will provide additional sources for technical information and discussions.

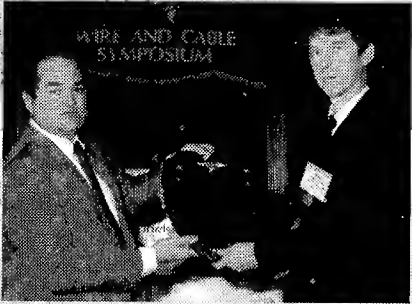
To add some diversion from all the technical discussions and for your enjoyment you must attend the special activities scheduled during the symposium, beginning with Monday Night Football sponsored by the AlphaGary Corp.; the usually popular hospitality hour on Tuesday and the award's luncheon on Wednesday. During the awards's luncheon, the winners and first recipients of the Elmer F. "Ace" Godwin scholarships will be announced.

This has been a great year for the IWCS Committee. The committee held one of its quarterly planning meetings in Japan. During our stay in Japan, we had the opportunity to visit several Japanese companies. It was a most enjoyable and educational experience. A trip that will always be remembered. The committee also held one of its planning meetings in Sturbridge, Mass. During our stay in Sturbridge, the committee took the opportunity to invite representatives of companies that are located in the area to an informal evening affair. Similar informal meetings will be scheduled in other locations, for the purpose of discussing ways to improve the value and interest of the symposium to the wire/cable industry.

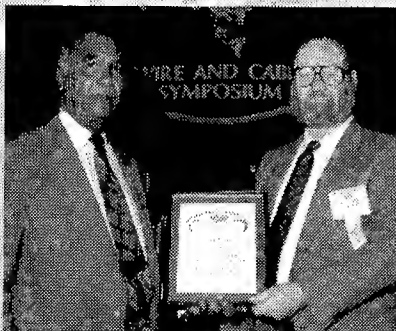
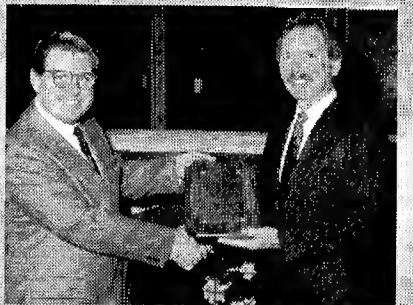
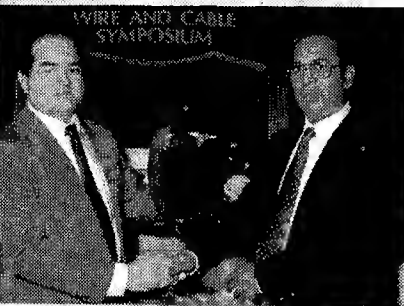
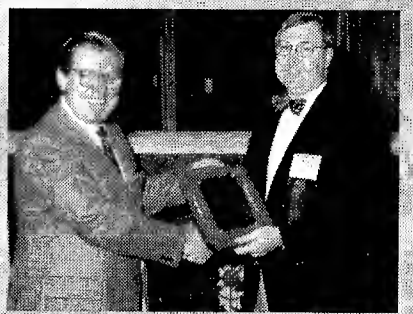
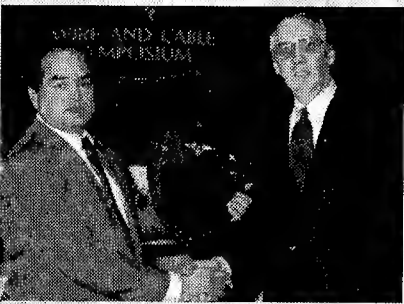
Four members on the committee are retiring this year. Rene Freeman, Xavier Mann, Dieter Nordmann and Homero Vela, each during their tenure and by their dedication, contributed significantly to the continued success of the symposium. I extend to each, the committee's sincere thanks and appreciation for their cooperation and support.

Again I ask each and every attendee of the symposium, the wire/cable industry and government activities to continue their support of the IWCS. Please plan to attend the 1995 symposium scheduled for the week of November the 12th at the new Marriott Hotel located in downtown Philadelphia. This will represent the IWCS's return to the northeast, where it began some forty-three years ago.

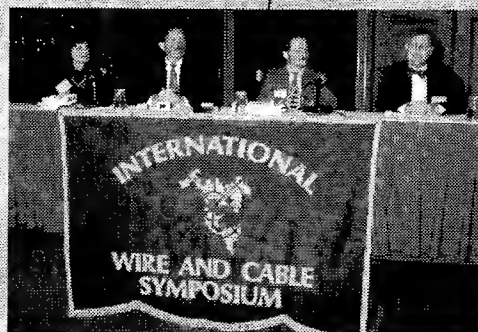
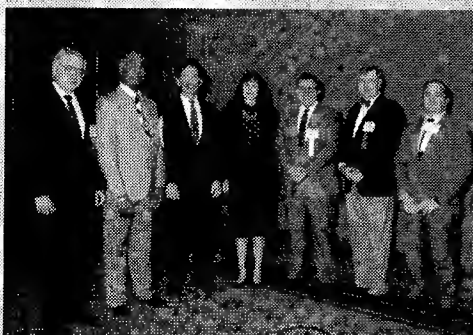
Elmer F. Godwin
Elmer F. Godwin
President/Director

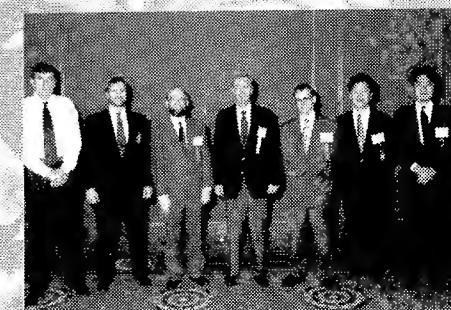
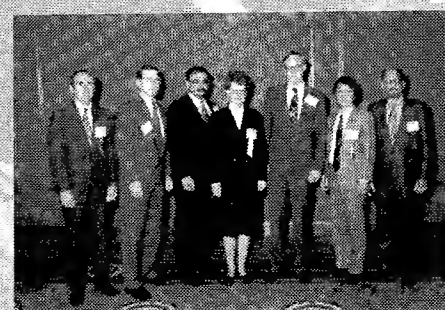
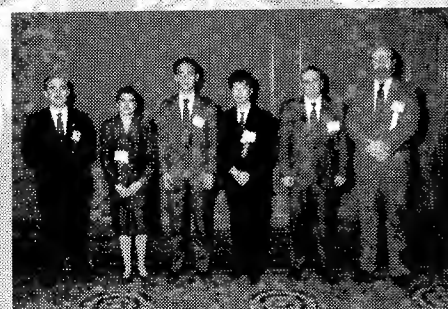
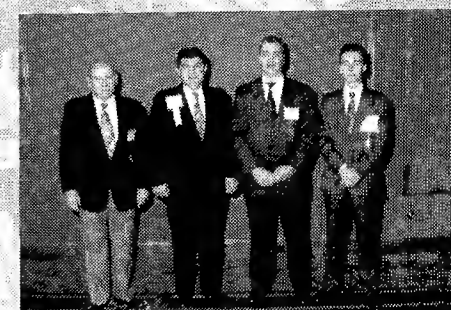
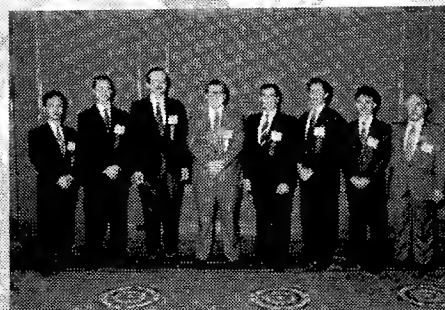
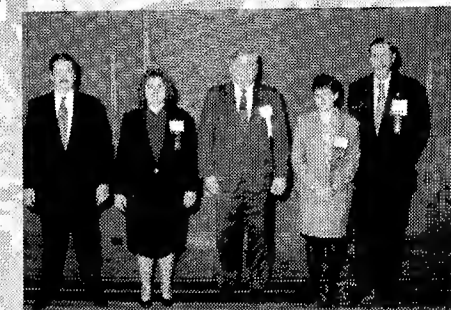
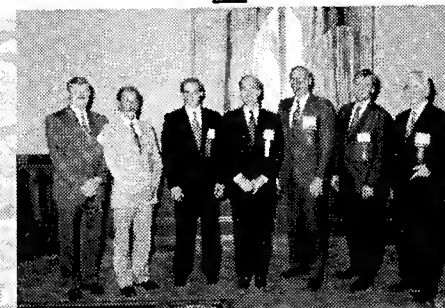
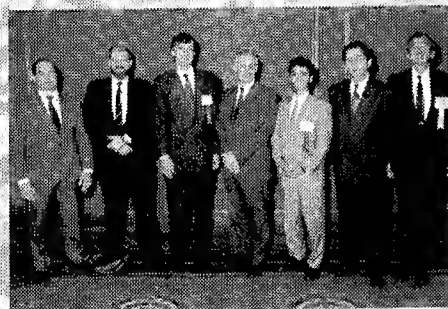
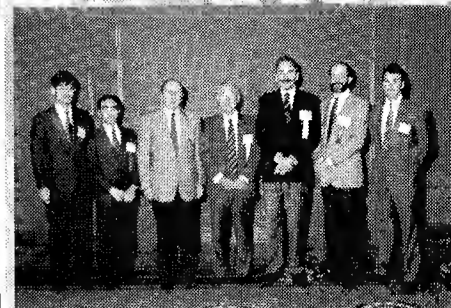
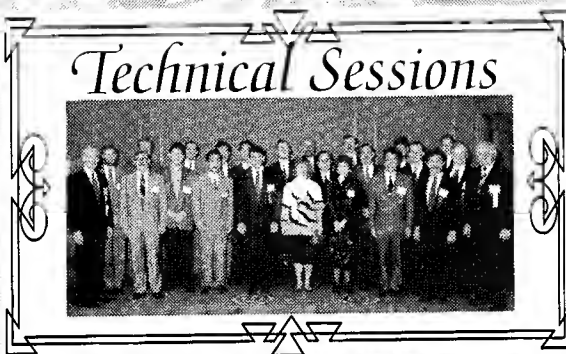
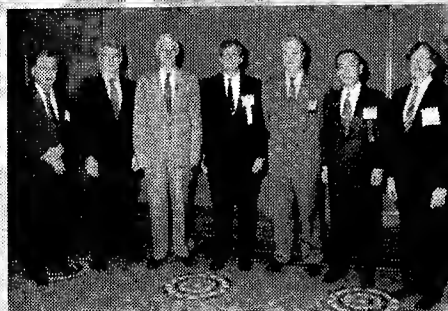
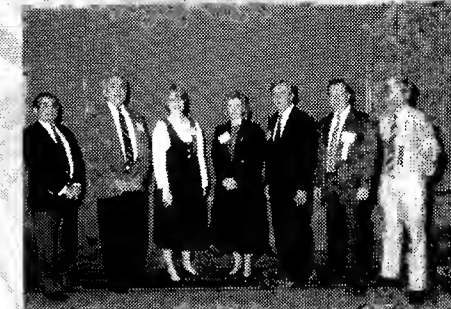
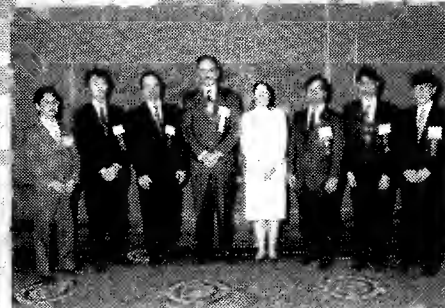
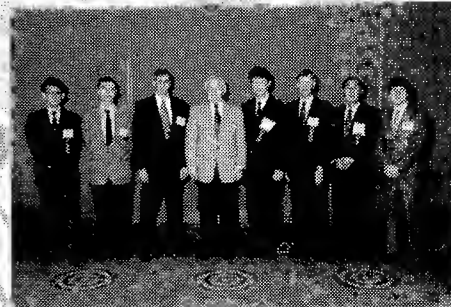
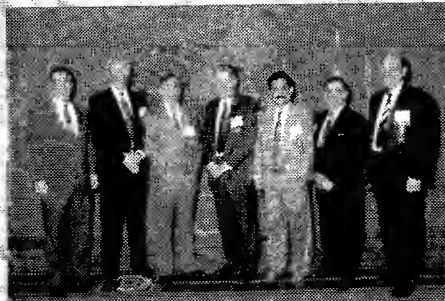
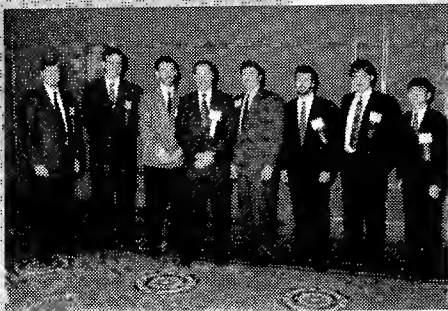


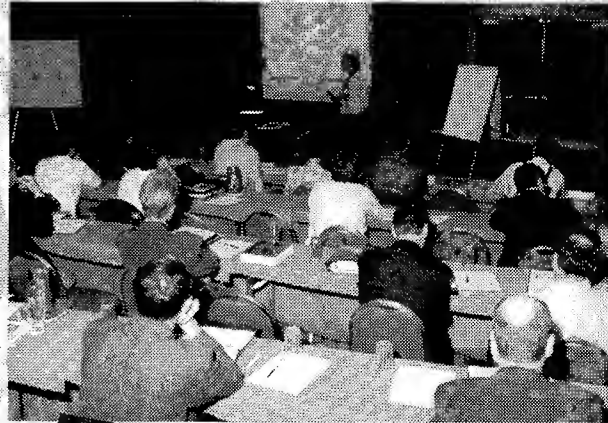
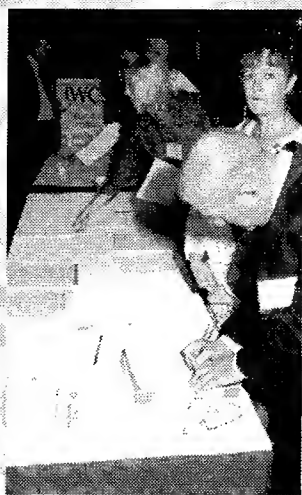
Adam's Mark Award Winners *mark*



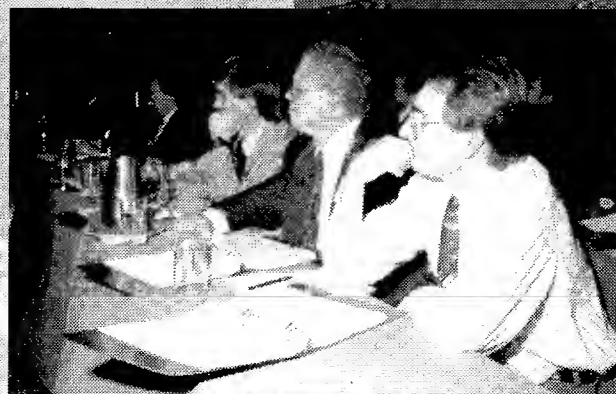
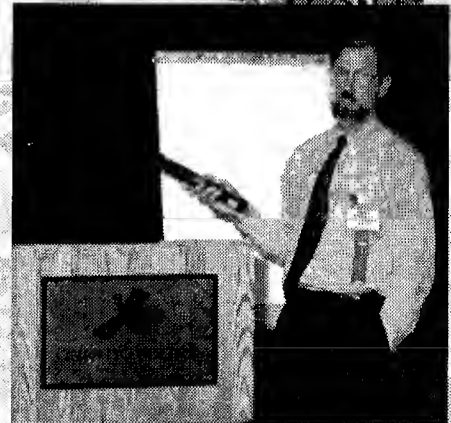
Tutorial Speakers

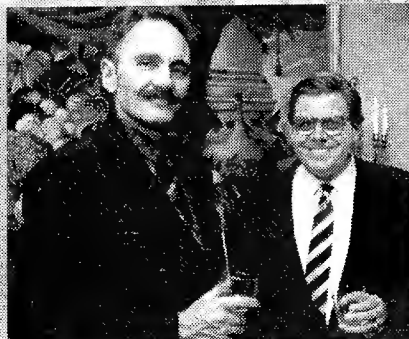
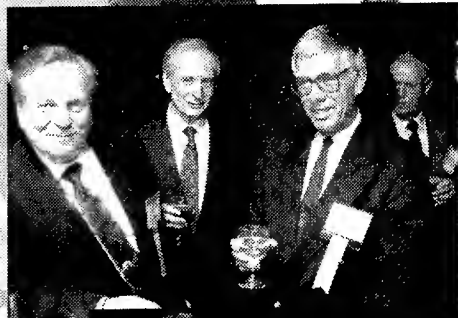
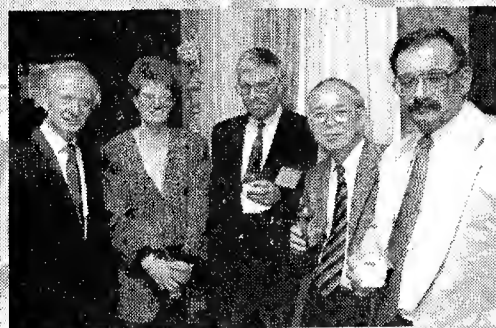


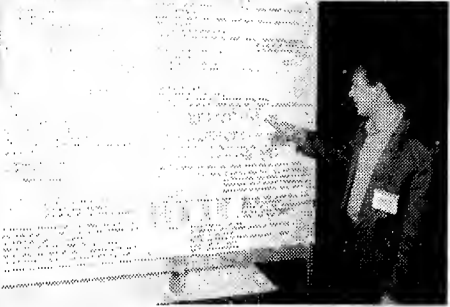
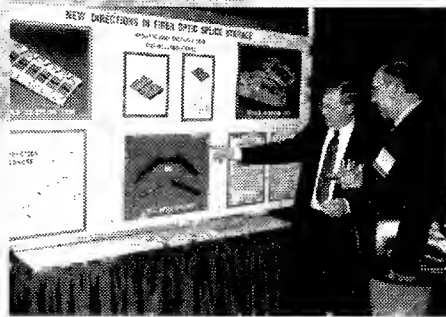
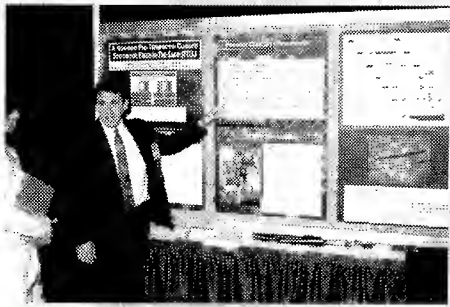




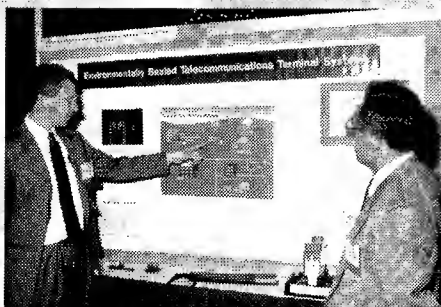
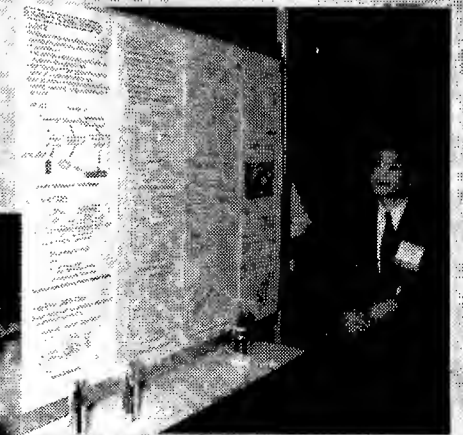
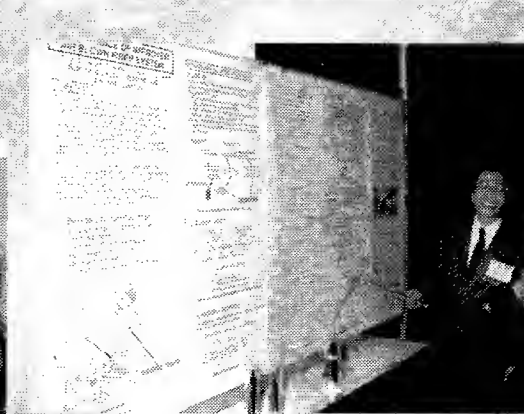
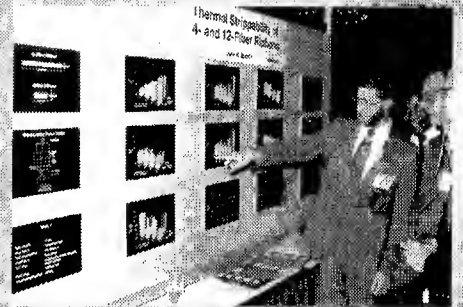
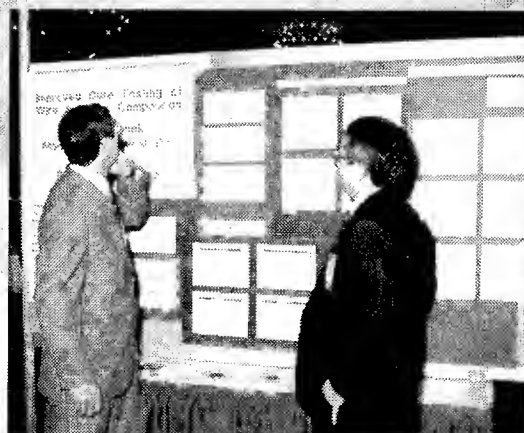
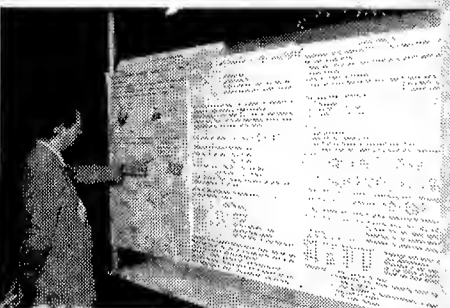
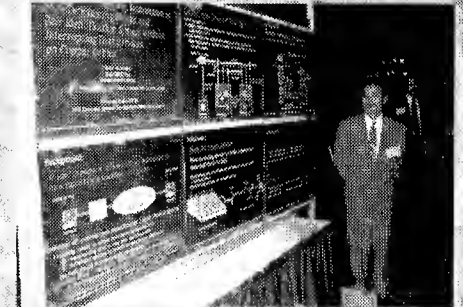
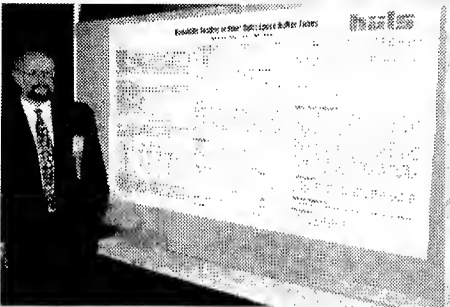
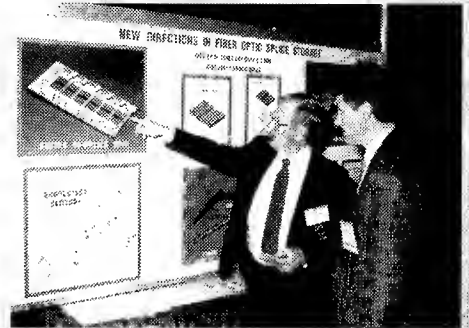
*Educational
Short
Courses*

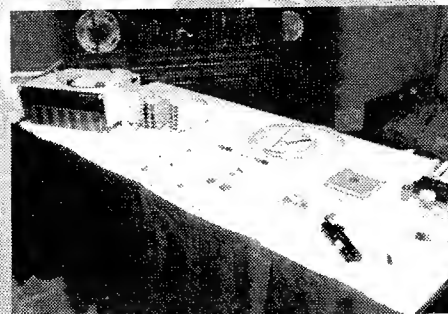
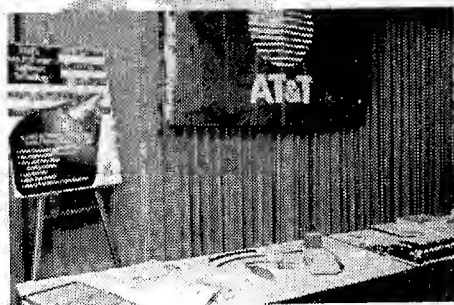
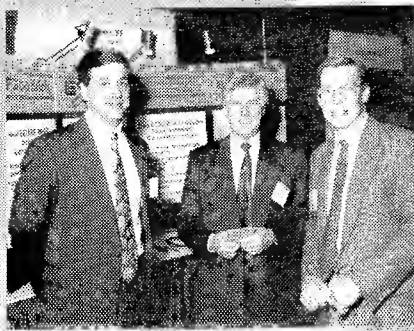






IWCS 1994 *Displays*





GOLD SUSTAINING CONTRIBUTORS

AFA Industries

20 Jewell Street
Garfield, NJ 07026

Akzo Fibers Inc.

801-F Blacklawn Road
Conyers, GA 30207

Alcatel Cable

30, rue des Chasses
92111 Clichy Cedex
France

Alcatel Telecommunications Cable

2512 Penny Road
Claremont, NC 28610

AlphaGary Corporation

Pioneer Industrial Park
Leominster, MA 01453

Amoco Chemical

200 E. Randolph, MC 4101
Chicago, IL 60601-7125

AT&T Bell Laboratories

2000 NE Expressway
Norcross, GA 30071

Belding Thread Group

6100 Fairview Rd, Suite 350
Charlotte, NC 28210

Borealis Compounds, Inc.

176 Thomas Road
Port Murray, NJ 07865

Camden Wire Company, Inc.

12 Masonic Ave.
Camden, NY 13316

Chase & Sons

19 Highland Avenue
Randolph, MA 02368

Commscope, Inc.

3642 US 70 East
Claremont, NC 28610-0879

Corning Inc.

35 West Market St.
MP-RO-2
Corning, NY 14831

DCM Industries, Inc.

2930 Faber Street
Union City, CA 94587

DSM Desotech Inc.

1122 Saint Charles Street
Elgin, IL 60120

DuPont Company

Chestnut Run Plaza
Bldg. 711, Room 231
Wilmington, DE 19880-0711

E.I. DuPont Company

5401 Jefferson Davis Highway
Richmond, VA 23234

The Furukawa Electric Co., Ltd.

6 Yawata-Kaigandori
Ichihara Chiba 290
Japan

Fusion UV Curing Systems

7600 Standish Place
Rockville, MD 20855-2798

GE Plastics

One Plastics Avenue
Pittsfield, MA 01201

General Cable Co.

160 Fieldcrest Avenue
Edison, NJ 08837

The Geon Company

6100 Oak Tree Blvd.
Cleveland, OH 44131

Kabelmetal Electro GmbH

Kabelkamp 20
D30179 Hannover, Germany

KT Industries Inc.

3925 Ardmore Ave.
Fort Wayne, IN 46802

MM Cables

71 Whiteside Road
Clayton 3168
Australia

Neptco, Inc.

30 Hamlet Street
Pawtucket, RI 02861-0323

Nippon Telegraph and Telephone Corp.

1-7-1, Hanabatake
Tsukuba, Ibaraki, 305
Japan

Nokia-Maillefer

1856 Corporate Dr., Suite 135
Norcross, GA 30093

Olex Cables, A Division of Pacific Dunlop Ltd.

207 Sunshine Road
Tottenham VIC 3012
Melbourne, Australia

Optical Fibres

Second Avenue
Deeside Industrial Park
Deeside, Clwyd CH5 2NX
Great Britain

Owens-Corning Fiberglas Corp.

Fiberglas Tower
Toledo, OH 43659

43RD INTERNATIONAL WIRE AND CABLE SYMPOSIUM (IWCS) SYMPOSIUM COMMITTEE

IWCS STAFF

ELMER F. GODWIN
(President/Director)
GEF Associates
3A Buttonwood Drive
Shrewsbury, NJ 07702
Ofc: (908) 389-0990
Fax: (908) 389-0991
Home: (908) 741-8864

IRVING KOLODNY
(Director's Assistant)
80-56 230th Street
Bellerose Manor, NY 11427
Tel & Fax: (718) 464-9197

PATRICIA HUDAK
(Administrative Assistant)
IWCS, Inc.
174 Main Street
Eatontown, NJ 07724
Tel: (908) 389-0990
Fax: (908) 389-0991

1994 OFFICERS

XAVIER MANN
(Chairman)
AT&T Fitel
P.O. Box 486
Carrollton, GA 30117
Tel: (404) 830-6616
Fax: (404) 836-8820

BRIAN D. GARRETT
(Vice-Chairman)
CommScope, Inc.
P.O. Box 879
Claremont, NC 28610
Tel: (704) 459-5003
Fax: (704) 459-5097

RENE G. FREEMAN
(Secretary)
Union Carbide Corp.
505 North 51st Avenue
Phoenix, AZ 85043
Tel: (602) 233-5904
Fax: (602) 233-5905

RICHARD ROSSI
(Treasurer)
General Cable Co.
160 Fieldcrest Avenue
Edison, NJ 08837
Tel: (908) 417-3132
Fax: (908) 225-3185

1994 COMMITTEE MEMBERS

Nils Artlove
Telia AB
Network Services
S-123 86 Farsta, Sweden
Tel: +46-8-7133746
Fax: +46-8-7132926

Dr. Stephen Hornung
120/B67
British Telecom Laboratories
Martlesham Heath
Ipswich IP5 7RE
United Kingdom
Tel: +44-473-644685
Fax: +44-473-644142

Dr. Koichi Inada
Fujikura Ltd.
Opto-Electronics Laboratory
1440 Mutsuzaki, Sakura-shi
Chiba-ken, 285 Japan
Tel: +81-43-484-3940
Fax: +81-43-484-3988

Dr. Felix P. Kapron
Bellcore
445 South Street
MRE- 2K140
Morristown, NJ 07960
Tel: (201) 829-5225
Fax: (201) 829-5965

Dr. Joyce P. Kilmer
Optotec, N.A.A.
Suite 300
151 First Ave.
New York, NY 10003
Tel: (212) 475-0093
Fax: (212) 475-0625

Inge B. Kovacs
Borealis Compounds, Inc.
176 Thomas Road
Port Murray, NJ 07865
Tel: (908) 850-6219
Fax: (908) 850-6268

Dieter S. Nordmann
Kabelmetal Electro GmbH
P.O. Box 260; Kabelkamp 20
D30179 Hannover, Germany
Tel: +49-511-676-2020
Fax: +49-511-676-2664

Michel Rousseau
Alcatel Cable
30, rue des Chasses
BP 309
92111 Clichy Cedex, France
Tel: +33-1-4756-6900
Fax: +33-1-4756-6739

Homero Vela
AT&T ELECON
Telesistemas C.A.
Calle Milano No. 70
Urb. Paraiso del Tuy
Santa Lucia, Estado Miranda
Venezuela
Tel: +58-39-31-1089
Fax: +58-2-575-4129

Roland H.W. Watkins
1158 Sedgefield Court
Oldsmar, FL 34677
Tel: (813) 787-6527
Fax: (813) 787-8780

ADVISORY

Dr. Peter R. Bark
Siecor Corporation
P.O. Box 489
489 Siecor Park
Hickory, NC 28603
Tel: (704) 323-6205
Fax: (704) 323-6264

Leo Chattler
DCM Industries, Inc.
2930 Faber Street
Union City, CA 94587
Tel: (510) 429-9500
Fax: (510) 429-1250

Michael A. DeLucia
Naval Surface Warfare Center
Carderock Div., Annapolis Detach.
Energy R&D Office, Code 859
Annapolis, MD 21402-5067
Tel: (410) 293-3825
Fax: (410) 293-2875

Dave Fallowfield
AGT Limited
Floor 21-G
10020 100 St.
Edmonton, Alberta
Canada T5J 0N5
Tel: (403) 493-5575
Fax: (403) 493-4829

Manuel R. Santana
AT&T Bell Laboratories
2000 NE Expressway; Rm 1D32
Norcross, GA 30071
Tel: (404) 798-2754
Fax: (404) 798-4654

CONSULTANTS

Dr. Reiner J. Gerdes
Gerdes Consulting
& TransTel Group Inc.
812 Oakdale Rd., N.E.
Atlanta, GA 30307-1210
Tel: (404) 368-8343
Fax: (404) 368-8382

Dr. Raymond E. Jaeger
SpecTran Corporation
50 Hall Road
Sturbridge, MA 01566
Tel: (508) 347-2261
Fax: (508) 347-2747

Hans A. Mayer
Olex Cables (Division of Pacific
Dunlop Ltd.)
207 Sunshine Road
Tottenham, VIC 3012
Melbourne, Australia
Tel: +61-3-316-2240
Fax: +61-3-314-1436

GOLD SUSTAINING CONTRIBUTORS

Penreco

Div. of Pennzoil Products Co.
4401 Park Ave.
Dickinson, TX 77539

Photon Kinetics, Inc.

9405 S.W. Gemini Drive
Beaverton, OR 97008-7160

PPG Industries, Inc.

One PPG Place, 33rd Floor West
Pittsburgh, PA 15272

Quantum Chemical Co.

11500 Northlake Drive
Cincinnati, OH 45249

Siecor Corp.

1928 Main Avenue SE
Hickory, NC 28603

SpecTran Corporation

50 Hall Road
Sturbridge, MA 01566

The Stewart Group Ltd.

259 Steelcase Road West
Markham, Ontario L3R 2P6
Canada

Sumitomo Electric U.S.A., Inc.

21221 S. Western Ave., Suite 200
Torrance, CA 90501

Teknor Apex Company

505 Central Avenue
Pawtucket, RI 02861

Telia AB

Network Services Division
S-123 86 Farsta
Sweden

UBE Industries (America), Inc.

666 Fifth Avenue, 14th Floor
New York, NY 10103-0074

Union Carbide Corp.

39 Old Ridgebury Road
Danbury, CT 06817

WaterGuard Cable Products, Inc.

14135 I-10 East
Houston, TX 77015

Witco Corp.

520 Madison Ave.
New York, NY 10022

SILVER SUSTAINING CONTRIBUTORS

ACOME

Paris & Mortain, France

Ericsson Cables AB Telecom Cables Division

Hudiksvall, Sweden

Hitachi Cable Ltd.

Hitachi-shi, Japan

Kabel Rheydt Aktiengesellschaft

Mönchengladbach, Germany

Kroschu-Kabelwerke

Kromberg & Schubert GmbH u. Co.

Wuppertal, Germany

Mitsubishi Cable Industries, Ltd.

Chiyoda-ku, Tokyo, Japan

Mohawk/CDT

Leominster, MA 01453

T&T Marketing, Inc.

Allamuchy, NJ 07820

TABLE OF CONTENTS

TUESDAY MORNING—9:00 AM—12:00 PM (NOON) Grand Ballroom East (Ballrooms A&B), Second Floor

Announcements/Greetings

Elmer F. Godwin, President/Director, IWCS, Inc., Eatontown, NJ

Xavier Mann, AT&T Fitel, Carrollton, GA, Chairman, IWCS

Joseph J. Pucilowski, Jr., Director, Space and Terrestrial Communications, U.S. Army CECOM, Fort Monmouth, NJ

SESSION 1: CHOICES IN THE LOCAL DISTRIBUTION NETWORK

Chairperson: Dr. Joyce P. Kilmer, Optotec, N.A.A., New York, NY

Panelists (Invited Presentations)

Evolution of the Optical Access Network in Japan—*Y. Wakui, K. Ishihara*, NTT Access Network Systems Laboratories, Ibaraki, Japan 3

Choices in the Local Distribution Network—*E. Flor*, Deutsche Bundespost Telekom, Darmstadt, Germany 5

Choices in the Local Distribution Network—*K. Oakley*, British Telecom, London, United Kingdom ... 8

Today, Tomorrow and the Twenty-First Century (The Three Phases of Cable TV)—*A. B. Best*, Cox Cable Communications, Inc., Atlanta, GA 9

G. R. Boyer, Bellcore, Morristown, NJ 11

TUESDAY AFTERNOON—1:00 PM—5:00 PM TRACK 1—FIBER OPTIC CABLES Grand Ballroom, Second Floor Ballroom A

SESSION 2: FIBER OPTIC CABLE DESIGN I

Chairperson: Dr. Peter R. Bark, Siecor Corporation, Hickory, NC

Design Concepts for a 4000-Fiber Cable with Thinly Coated Fiber—*R. S. Wagman, P. R. Bark, H. G. Cooke, C. K. Eoll, R. O. Livingston, G. A. Lochkovic, W. W. McAlpine, F. M. Sears, S. S. Sodhi*, Siecor Corp., Hickory, NC 12

Design and Development of High-Density Optical Fiber Slotted-Core Cable—*R. Matsuoka, M. Saito, M. Hara, A. Otake*, The Furukawa Electric Co., Ltd., Chiba, Japan 22

Ultra High-Density Optical Fiber Cable with Thin Coated Multi-Fiber Ribbons for Subscriber Networks—*N. Okada, K. Watanabe, K. Kobayashi, M. Miyamoto*, Fujikura, Ltd., Chiba, Japan 28

Ultra-High-Count Optical Fiber Cable using Single-Helical-Groove Unit—*W. Katsurashima, Y. Kitayama, S. Tanaka*, Sumitomo Electric Industries, Ltd., Yokohama, Japan 36

A New Compact Ribbon Cable—*M. Yamanaka, N. Okada, M. Miyamoto, T. Maruoka*, Fujikura Ltd., Chiba, Japan 43

Design of Loose Tube Fiber Optic Cable with Adjusted Contraction and Strain Windows—*J. Horska*, CommScope, Inc., Catawba, NC 50

TUESDAY AFTERNOON—1:00 PM—5:00 PM Grand Ballroom, Second Floor Ballroom B

SESSION 3: FIBER COATINGS

Chairperson: Mr. Michel Rousseau, Alcatel Cable, Clichy Cedex, France

Substrate Effects on Cure of UV Curable Fiber Optic Materials—*D. M. Szum*, DSM Desotech Inc., Elgin, IL 59

Influence of Glass-Coating Adhesion on the Optical and Mechanical Performances of Fibres in Water—*F. Cocchini, D. Cuomo, G. Ferri, A. Pudia*, FOS-Fibre Ottiche Sud, Battipaglia, Italy 66

Effect of Curing Temperature on Curing Rate and Mechanical Properties of Polyurethane Acrylate Coatings for Optical Fiber—*H. Takase, Y. Hashiguchi, Y. Takasugi, N. Saito, T. Ukachi*, Japan Synthetic Rubber Co., Ltd., Kawasaki, Japan 72

The Effect of Cure Dose on the Aging Behavior of UV Cured Optical Fiber Coatings—*C. P. Chawla*, DSM Desotech Inc., Elgin, IL 78

Enhanced UV Cure Material Properties in the Development of a Next Generation Optical Fiber Coating—*E. H. Urruti, J. R. Toler, G. Kar, C.-K. Chien, J. W. Botelho*, Corning Inc., Corning, NY 89

A New Coating System for Fibers with Enhanced Resistance to Environmental Conditions—*A. Ginocchio, A. Portinari, E. Consonni*, Pirelli Cavi SpA, Milano, Italy; *G. Roba*, FOS - Fibre Ottiche Sud, Battipaglia, Italy; and *F. Nanni*, Società Italiana per l'Esercizio delle Telecomunicazioni, Roma, Italy 96

TUESDAY AFTERNOON—1:00 PM—5:00 PM Grand Ballroom, Second Floor Ballroom C

SESSION 4: MATERIALS PROCESSES & MANUFACTURING

Chairperson: Ms. Inge B. Kovacs, Borealis Compounds, Incorporated, Port Murray, NJ

The Application of Synthetic Silica Tubing for Large Preform Manufacture Using MCVD—*P. F. Glodis, C. F. Gridley, W. M. Flegal, A. A. Klein, D. P. Jablonowski, D. Kalish*, AT&T Network Cable Systems, Norcross, GA; *A. Sorby, H. Damsgaard, G. Knudsen*, Lycom, Brondby, Denmark; *H. Schaper, N. Treber, H. Fabian*, Heraeus Quarzglas, Hanau, Germany; and *P. C. Schultz*, Heraeus Amersil, Duluth, GA 105

Sonic Tension Control at High Draw Speed—*M. Luukkala, H. Rääkkönen*, University of Helsinki; *J. Kurki, L. Stormbom*, Nokia Cables, Vantaa, Finland; and *J. Kohtala*, Nokia-Maillefer, Norcross, GA 116

Damage Development in Small-Diameter, Pultruded, GRP Rod Used in Optical Fibre Cables—*S. N. Kukureka, R. Leetham*, The University of Birmingham, Birmingham, UK 121

Effect of Novel Cleaning Solvents on Optical Fiber Coatings—*J. R. Petisce, K. W. Jackson, N. W. Sollenberger, C. R. Taylor*, AT&T Bell Laboratories, Norcross, GA; *A. J. Muller*, AT&T Bell Laboratories, Murray Hill, NJ 126

Flame Retardant Optical Cables for Central Office, Underground or Other Specific Applications—*G. Hög*, Kabel Rheydt, Mönchengladbach, Germany; *J. O. Karlsson*, Alcatel IKO Kabel, Grimsas, Sweden; *N. Mariette*, O. Tatat, Alcatel Cable, Bezons Cedex, France; *G. Paternostro*, Alcatel Cavi, Latina, Italy; *J. Rauchs*, Opticable, Frameries, Belgium; and *J. Schulte*, Alcatel Kabelmetal Electro, Stadthagen, Germany 134

OEMI Parallel Channel Cable: Flame Test Performance of Nonhalogen and Halogen Containing Constructions—*G. A. Schmidt*, Union Carbide Corp., Somerset, NJ; and *L. G. Polhemus*, IBM, Poughkeepsie, NY 142

TUESDAY AFTERNOON—1:00 PM–5:00 PM
TRACK 2—COPPER CABLES
 Grand Ballroom, Second Floor
 Ballroom D

SESSION 5: SUPERCONDUCTIVITY UPDATE

Chairperson: Mr. Leo Chatler, DCM Industries, Incorporated, Union City, CA

Moderator: Dr. Paul Chu, University of Houston, Houston, TX

MIT Program to Demonstrate Superconductive Components in Microwave Systems—*R. W. Ralston*, MIT Lincoln Laboratory, Lexington, MA 150

Advances in High Temperature Superconducting Materials and Components—*A. Lauder*, *C. Wilker*, *Z. Y. Shen*, *P. S. W. Pang*, *W. L. Holstein*, *D. J. Kountz*, *D. W. Face*, DuPont, Wilmington, DE 155

The ARPA High Temperature Superconductivity Program—*S. A. Wolf*, ARPA/DSO, Arlington, VA 163

High Performance Superconducting Filters for Wireless Systems—*O. E. Smith*, Illinois Superconductor Corp., Evanston, IL 167

High Temperature Superconducting Materials Research: Problems and Potentials—*L. Gao*, *Y. Y. Xue*, *R. L. Meng*, *C. W. Chu*, University of Houston, Houston, TX 174

Navy Program in Superconductivity—*D. U. Gubser*, Naval Research Laboratory, Washington, DC 179

TUESDAY EVENING
Hospitality Hour—6:00 PM–8:00 PM
 Admission by badges issued to all registrants

WEDNESDAY MORNING—8:00 AM–11:45 AM
TRACK 1—FIBER OPTIC CABLES
 Grand Ballroom, Second Floor
 Ballroom A

SESSION 6: FIBER OPTIC CABLE DESIGN II

Chairperson: Mr. Manuel R. Santana, AT&T Bell Laboratories, Norcross, GA

Miniature Optical Fiber Cables for Jumper Applications—*D. Mathis*, *M. Viriyayuthakorn*, *J. Holman*, *L. Graham*, *R. Reagan*, AT&T Bell Laboratories, Norcross, GA 183

New Low Count Optical Fiber Cables—*S. Saito*, *N. Okada*, *K. Watanabe*, *M. Miyamoto*, Fujikura, Ltd., Chiba, Japan 189

Manufacturing and Field Experimentation of Microsheath Cable for Low Cost Subscriber Loop—*P. Jamet*, *A. Jarlot*, SILEC, Montereau, France 196

Ultra High Density Cables Using a New Concept of Bunched Multicore Monomode Fibers: A Key for the Future FTTH Networks—*G. Le Noane*, *D. Boscher*, *P. Grosso*, *J. C. Bizeul*, *C. Botton*, France Telecom CNET, Lannion, France 203

Strain Analysis of U-Groove Type Cable with Multi Fiber Ribbons—*N. Okada*, *K. Watanabe*, *M. Miyamoto*, Fujikura, Ltd., Chiba, Japan 211

Low Fiber Count Cables for Emerging Broadband Networks—*M. D. Kinard*, *T. D. Mathis*, *A. J. Panuska*, *P. D. Patel*, AT&T Bell Laboratories, Norcross, GA 219

Development of Dielectric Fiber Optic Drop Cable—*S. T. Ferguson*, *W. J. McCallum*, *Siecor Corp.*, Hickory, NC 227

WEDNESDAY MORNING—8:00 AM–11:45 AM
 Grand Salon, Second Floor
 Salon C

SESSION 7: SUBMARINE CABLES I

Chairperson: Mr. Dieter S. Nordmann, Kabelmetal Electro GmbH, Hannover, Germany

Development of Small Size Optical Fiber Submarine Cable—*M. Nunokawa*, KDD Submarine Cable Systems, Inc., Tokyo, Japan; and *M. Kiuchi*, *T. Akasaka*, *S. Suzuki*, *H. Yoshioka*, Ocean Cable Co., Ltd., Yokohama, Japan 234

Direct Mechanical Fiber Strain Measurement and the Cabled Fiber Strain of an Undersea Cable—*C. S. Ma*, AT&T Submarine Systems Inc., Holmdel, NJ; *L. L. Blyler*, *G. E. Johnson*, AT&T Bell Laboratories, Murray Hill, NJ; and *R. T. Traut*, *C. E. Murphy*, *M. W. Jones*, *F. C. Gibson*, *W. M. Keith*, Simplex Technologies, Inc., Newington, NH 241

New Low Weight/Small Diameter Optical Fibre Submarine Cable for Unrepeated System—*G. Berthelsen*, *I. Vintermyr*, Alcatel Kable Norge AS, Oslo, Norway 249

Design and Development of High Fibre Count Repeaterless Submarine Cable—*W. F. Wright*, *C. E. Murphy*, *W. D. Beland*, *M. J. Cyr*, *G. N. Fontaine*, *R. T. Traut*, Simplex Technologies, Inc., Portsmouth, NH; *C. S. Ma*, *T. Lee*, *D. Stroumbakis*, *R. Giangrossi*, *R. Stathum*, *R. Rue*, AT&T Submarine Systems Inc., Holmdel, NJ; and *L. Blyler*, AT&T Bell Laboratories, Murray Hill, NJ 256

Design and Development of High Fibre Count Cables for Unrepeated Systems—*G. McGurk*, *J. R. Ford*, *L. J. Parker*, *G. C. Miller*, STC Submarine Systems Ltd., Southampton, United Kingdom 265

Hydrogen Generation and Diffusion at Submarine Cable Joints: An Experimental Investigation—*B. R. Ridd*, *C. J. Brown*, STC, Portsmouth, United Kingdom; and *G. McGurk*, STC Submarine Systems Ltd., Southampton, United Kingdom 273

WEDNESDAY MORNING—8:00 AM–11:45 AM
 Grand Salon, Second Floor
 Salon D

SESSION 8: OVERVIEW OF INTERNATIONAL DEFENSE INITIATIVES IN FIBER OPTICS AND PHOTONICS

Chairperson: Mr. Michael A. DeLucia, Naval Surface Warfare Center, Annapolis, MD

Moderator: Dr. Howard Wichansky, U.S. Army CECOM, Fort Monmouth, NJ

Overview of Wideband Analog Components and Systems—*M. J. Wale, C. Edge*, GEC-Marconi Materials Technology (GMMT), Northants, United Kingdom.....

281

Fundamental Design of Integrated Photonic Systems for Phased Array Antenna Control—*J. G. Wright, L. A. Coryell*, U.S. Army Communications-Electronics Command, Fort Monmouth, NJ; *W. H. Chang, R. A. Lux*, U.S. Army Research Laboratory, Fort Monmouth, NJ; and *T. J. Tayag*, U.S. Army Research Laboratory, Adelphi, MD.....

291

Optical Fiber Network Characterization: Work in Progress at NATO Panel IV, Research Study Group 12—*J. Isbert, J.-M. Maisonneuve*, Centre d'Etudes et de Recherches de Toulouse, Toulouse, France ..

298

Development of Standardized Test Procedures for Radiation Effects in Optical Fibers by the NATO Nuclear Effects Task Group—*E. J. Friebele*, Naval Research Laboratory, Washington, DC

310

A Four-Fiber Tactical Fiber-Optic Connector—*H. Muth*, AT&T Network Cable Systems, Norcross, GA; and *V. E. Kalomiris*, CECOM, Fort Monmouth, NJ ...

315

WEDNESDAY MORNING—8:00 AM—11:45 AM

TRACK 2—COPPER CABLES

Grand Salon, Second Floor

Salon E

SESSION 9: HIGH PERFORMANCE CABLES

Chairperson: Mr. Roland H. W. Watkins, Gillett Lehman & Associates, Town & Country, MO

Optimization of High Performance Unshielded Twisted Pair Media—*P. Z. Vanderlaan*, Belden Inc., Richmond, IN

320

Performance Evaluation of Multiple Pair Category 5 Backbone Cable for High Speed Data Services—*J.-H. Walling, M. Bélanger, B. Lord*, Northern Telecom, Quebec, Canada.....

328

Analysis and Improvement of Crosstalk (NEXT & FEXT) For Multi-Unit, Backbone UTP Cable Applied up to FDDI/ATM Data Speed—*S. Hinoshita, S. Ishii, K. Ishii*, Hitachi Cable, Ltd., Hitachi, Japan

341

100 Megabit per second LAN Utilizing Four and 25 Pair Unshielded Twisted Pair Media—*R. A. Wessels, Jr.*, CommScope, Inc., Claremont, NC.....

351

Enhanced Multi-Pair Cable Designs: Power Sum Validations—*W. F. Reichert*, Champlain Cable Corp., Colchester, VT

355

Data Cables and System Components for the Use up to 100 (300) MHz—*P. E. Gregor, T. Tholen*, Kabel Rheydt AG, Mönchengladbach, Germany; and *H. Knop*, BETEFA GmbH, Berlin, Germany

363

WEDNESDAY AFTERNOON—11:45 AM—2:15 PM

Awards Luncheon

Grand Ballroom West

Admission by badges issued to all registrants

WEDNESDAY AFTERNOON—2:15 PM—5:00 PM

TRACK 1—FIBER OPTIC CABLES

Grand Ballroom, Second Floor

Ballroom A

SESSION 10: AERIAL CABLES

Chairperson: Mr. Rene G. Freeman, Union Carbide Corporation, Phoenix, AZ

Aerial Fiber Optic Cable for Railway Applications Metallic or Dielectric Solutions—*J. P. Bonicel, O. Tatat, G. Couvrie*, Alcatel Cable, Bezons Cedex, France; *L. Rapebach*, SNCF, France; *P. Zamzow*, Kabel Rheydt, Mönchengladbach, Germany; *J. Rauchs*, Opticable, Belgium; and *C. Vergez*, Alcatel Contracting, France

368

High Count Optical Fiber Compositing Ground Wire (OPGW)—*J. Sumita, Y. Kashihara*, The Kansai Electric Power Co., Inc., Osaka, Japan; and *J. Ohta, I. Sakabe, T. Saito*, Sumitomo Electric Industries, Ltd., Yokohama, Japan

376

Optical Ground Wire and All Dielectric Self-Supporting Cable - A Technical Comparison—*H. G. Haag, G. Hög, U. Jansen, P. E. Zamzow*, Kabel Rheydt AG, Mönchengladbach, Germany; and *J. Schulte*, Kabelmetal Electro GmbH, Hannover, Germany

380

WEDNESDAY AFTERNOON—2:15 PM—5:00 PM

Grand Salon, Second Floor

Salon C

SESSION 11: SUBMARINE CABLES II

Chairperson: Mr. Dave Fallowfield, AGT Limited, Alberta, Canada

The Development of a New Submarine Cable Design for Repeaterless Application—*K. Sjölin, L. Lidén, N. E. Grip*, Ericsson Cables AB, Hudiksvall, Sweden; and *S. Lindohf, J. Björkman*, Telia AB, Farsta, Sweden.....

388

Next Generation of Cable Designs for Optically Amplified Systems—*J. Power, C. Rochester, P. Worthington*, STC Submarine Systems Ltd., Southampton, United Kingdom.....

395

Characteristics of Optical Fiber Submarine Cables for Long-Haul Submarine Optical Amplifier Systems—*Y. Yoshida, N. Norimatsu, H. Abe, H. Yamamoto*, Kokusai Denshin Denwa Co. Ltd., Tokyo, Japan

402

The Development of a New Land and Beach Joint with Potential Universal Applications—*J. Bishop*, STC Submarine Systems Ltd., Southampton, United Kingdom.....

408

WEDNESDAY AFTERNOON—2:15 PM—5:00 PM

Grand Salon, Second Floor

Salon D

SESSION 12: FIBER RIBBONS

Chairperson: Mr. Nils Artlove, Telia AB, Farsta, Sweden

Experimental Investigation of the Microbending Behavior of Fiber Optical Ribbons—*C. Unger, W. Stöcklein, S. Unterberger, W. Pfandl*, Siemens AG, Neustadt, Germany.....

413

A Study of 16-Fiber Ribbon for Ultra High Density Optical Fiber Cable—*T. Kakuta, K. Oishi, W. Katsurashima, H. Hongo, Y. Matsuda*, Sumitomo Electric Industries, Ltd., Yokohama, Japan

423

A Comprehensive Approach to Ribbon Design with a Focus on Materials—*J. R. Keese, G. A. Lochkovic*, Siecor Corporation, Hickory, NC; and *D. Smith, J. R. Toler*, Corning Inc., Corning, NY

430

TRACK 2—COPPER CABLES

Grand Salon, Second Floor

Salon E

SESSION 13: POWER AND INDUSTRIAL CABLES

Chairperson: Mr. Hans A. Mayer, Olex Cables, A Division of Pacific Dunlop Limited, Melbourne, Australia

Fundamental Characteristics of the 500 kV XLPE Cable—*M. Fukawa, M. Asakawa*, Tokyo Electric Power Company, Tokyo, Japan; and *T. Fujui, S. Fukunaga, H. Inoue, S. Osawa, K. Fudamoto, T. Hasegawa*, Sumitomo Electric Industries, Ltd., Osaka, Japan..... 440

Evaluation of Service Aged EPR Cables—*C. Katz*, Cable Technology Laboratories, Inc., New Brunswick, NJ; and *M. Walker*, Houston Lighting & Power Company, Houston, TX 450

Moisture Crosslinkable Polyethylene with Improved Processing and Crosslinking Performance—*B. Å. Sultan*, Borealis Polyeten AB, Stenungsund, Sweden 460

WEDNESDAY AFTERNOON—4:00 PM–6:30 PM

Grand Salons (Salons A&B), Second Floor

SESSION 14: POSTER PAPERS

Chairpersons: Dr. Reiner J. Gerdes, Gerdes Consulting; TransTel Group Incorporated, Atlanta, GA and Mr. Dieter S. Nordmann, Kabelmetal Electro GmbH, Hannover, Germany

A New Automatic System for Installing Aerial Round Cable—*H. Nakanishi, K. Yamamoto*, Nippon Telegraph and Telephone Corp., Ibaraki, Japan 468

Apparatus for Determining Condition of Cables Inside Plant—*T. Hamade, Y. Shimo*, Nippon Telegraph and Telephone Corp., Ishikawa, Japan; *M. Sakata*, NTT Fanet Systems Co., Tokyo, Japan; and *K. Sega*, Sony Tektronix Company, Tokyo, Japan 473

Release of Lead from Lead-Sheathed Telecom Cables in Soil—*S. Forsberg*, Swedish University of Agricultural Sciences, Uppsala, Sweden; and *J. Björkman*, Telia AB, Farsta, Sweden 478

The Influence of Reflective Components in Lightwave AM-VSB CATV Systems Performance—*T. J. Sheu, K.-Y. Chen, C.-Y. Wang, H.-T. Chen, F.-Y. Tsai, W.-S. Chien*, Telecommunication Laboratories, Taiwan, Republic of China 483

The Effect of Sulfate-Reducing Bacteria on the Metallic Corrosion in Fiber Optic Cable—*J.-H. Wang, Y.-T. Horng, H.-P. Hsh, K.-Y. Chen*, Telecommunication Laboratories, Taiwan, Republic of China 488

Optical Fiber Monitoring Systems for Passive Optical Networks—*C.-C. Lee, K.-Y. Chen, F.-Y. Tsai, K.-H. Lai, T.-J. Liaw, B.-H. Wann*, Telecommunication Laboratory, Taiwan, Republic of China ... 494

Study, Manufacture and Test on a S-Z Stranded Loose Tube Optical Fibre Ribbon Cable with No Pretwisting and No Filling Compound—*L. Baguer, P. Blasco, J. Cobo, C. Día, F. Escribano*, Cables de Comunicaciones, S.A., Zaragoza, Spain 499

Evaluation of the Environmental Resistance of 900µm-jacket Optical Fibers Using Stripping Profiles as a Monitoring Method—*H.-F. Lin, C.-H. Hsieh, S.-I. Wang, Y.-C. Lin, K.-Y. Chen*, Telecommunication Laboratories, Taiwan, Republic of China 504

A New, Sealed, High Capacity Universal Fiber Optics Closure—*J. S. Mullaney, T. H. Wermke, W. N. Beauchamp*, Raychem Corporation, Fuquay-Varina, NC 509

Effect of Superabsorbent Materials on the Performance of Optical Fiber Ribbons—*Y.-C. Lin, T.-C. Chang, J.-M. Hsiao, W.-J. Chen, K.-Y. Chen*, Telecommunication Laboratories, Taiwan, Republic of China 513

The Stability of Optical Fiber Color Codes: Effects of Material Choices and Service Environments—*B. J. Keon*, Telstra, Melbourne, Australia; and *R. A. Frantz*, Bellcore, Morristown, NJ 522

Fiber Curl: A New Measurement Method and a Statistical Prediction of the Influence of Fiber Ribbon Splice Losses—*M. Bottanelli*, SIRT S.p.A., Milanino, Italy 528

A Cost-Effective Technique for the Glanding of Optical Fibre Bundles into Submerged Repeaters—*S. J. McManus, I. G. Watson, G. Waterworth*, STC Submarine Systems Ltd., London, England 533

Properties of Loose Tube Optical Cables Contributing to Low-Temperature Optical Loss—*M. J. Zammit, P. B. Grimado, G. D. Kiss*, Bellcore, Morristown, NJ; and *O. S. Gebizlioglu*, Bellcore, Red Bank, NJ 538

Long Term Environmental and Process Tests of On-Line Colored Fiber Optic Ribbons—*B. Arvidsson, M. Eriksson*, Ericsson Cables, Hudiksvall, Sweden; *J. Kohtala*, Nokia-Maillefer, Norcross, GA; and *J. Tanskanen*, Nokia-Maillefer, Vantaa, Finland 545

Push in Modulus Test for the Primary Coating of Dual-Coated Fiber—*K. Oishi, N. Akasaka, T. Hattori, T. Kakuta, Y. Matsuda*, Sumitomo Electric Industries, Ltd., Yokohama, Japan 552

Reducing Toxic Air Emissions by Replacing Methyl Ethyl Ketone Inks and Solvents with Aqueous Inks for Marking PVC Insulated Conductors—*B. M. Brokke, J. E. Bosak*, AT&T Network Cable Systems, Phoenix, AZ; and *T. Davidow*, Toncee Inc., Smyrna, GA 559

Mechanical Properties of Aged Fiber Coatings by Dynamic Mechanical Analysis of Optical Fibers—*O. S. Gebizlioglu, I. M. Plitz*, Bellcore, Red Bank, NJ; and *R. A. Frantz*, Bellcore, Morristown, NJ 564

THURSDAY MORNING—8:30 AM–12:00 PM (NOON)

TRACK 1—FIBER OPTIC CABLES

Grand Ballroom, Second Floor

Ballroom A

SESSION 15: FIBER OPTIC INSTALLATION & APPLICATIONS

Chairperson: Mr. Homero Vela, AT&T ELECON Tele-sistemas C.A., Estado Miranda, Venezuela

Economical Fiber Migration in the Local Loop: New Technologies and Concepts Cut into the Cable Plant—*W. Liese, W. Wenski, H. Schönfeld*, Kabelmetal Electro GmbH, Hannover, Germany 571

Optical Power Measuring System for High Count Fiber Ribbons— <i>T. Takashima, Y. Unami, T. Yamada, Fujikura Ltd., Chiba-ken, Japan; and K. C. Au, Fujikura Asia Ltd., Chiba-ken, Japan</i>	582
Restoration of the Mechanical Strength of Aged Optical Fiber— <i>G. Ljungqvist, M. Johansson, L. Stensland, Ericsson Cables AB, Sundbyberg, Sweden</i>	589
Measurement of Distributed Strain in Frozen Cables and Its Potential for Use in Predicting Cable Failure— <i>T. Kurashima, K. Hogari, S. Matsuhashi, T. Horiguchi, Y. Koyamada, Y. Wakui, Nippon Telegraph and Telephone Corporation, Ibaraki-ken, Japan; and H. Hirano, Nippon Telegraph and Telephone Corporation, Tokyo, Japan</i>	593
Effect of Parameter Differences on the Fiber Splice Loss and Easy Bidirectional OTDR Measurement in the Field Installation— <i>Z. Wanchun, Dalian Vastone Communication Cable Corp., Dalian, Republic of China; and R. Yang, F. Schank, Siecor GmbH & Company KG, Neustadt/Coburg, Germany</i>	603
Remote Optical-Fiber Testing System For Unrepeated Long-Span Optical-Fiber Trunk Lines— <i>S. Goto, N. Atobe, Nippon Telegraph and Telephone Corporation, Chiba, Japan; I. Sankawa, Nippon Telegraph and Telephone Corporation, Tokyo, Japan; and T. Horiguchi, Nippon Telegraph and Telephone Corporation, Ibaraki-Ken, Japan</i>	608

THURSDAY MORNING—8:30 AM—12:00 PM (NOON)
Grand Ballroom, Second Floor
Ballroom B

SESSION 16: FIBER OPTIC SPLICING & CONNECTORS

Chairperson: Dr. Stephen Hornung, British Telecom Laboratories, Ipswich, United Kingdom

80-Fiber Connector— <i>H. Yanagase, T. Shigematsu, J. Yamakawa, K. Kanai, The Furukawa Electric Company, Ltd., Chiba, Japan</i>	614
Precision-Length Oblique Cleaving of Ribbon Fibers for High-Performance Mechanical Splices— <i>R. J. Ferina, Jr., Radiall, Inc., Stratford, CT; and H. B. Yin, Radiall S.A., Voreppe, France</i>	620
High Fiber Count Push-On Pull-Off Connector— <i>Y. Kikuchi, H. Furukawa, Y. Nomura, H. Yokosuka, Fujikura Ltd., Chiba, Japan</i>	627
Integral Multi-Fiber Management for Economic Mass-Fusion Splicing— <i>M. Loch, Siemens AG, Munich, Germany; and G. Boscher, RXS Schrumpftechnik-Garnituren GmbH, Hagen, Germany</i>	633
Improved Splice Loss of Optical Fiber Ribbon at Altitudes— <i>M. Hamada, T. Yanagi, Y. Okamoto, T. Watanabe, K. Osaka, T. Taguchi, Sumitomo Electric Industries, Ltd., Yokohama, Japan</i>	638

THURSDAY MORNING—8:30 AM—12:00 PM (NOON)
Grand Ballroom, Second Floor
Ballroom C

SESSION 17: OPTICAL FIBER PROPERTIES

Chairperson: Mr. Xavier Mann, AT&T Fitel, Carrollton, GA

Structures and Characteristics of Carbon Films on Optical Fibers— <i>M. Nakamura, A. Urano, H. Aikawa, H. Ishikawa, T. Danzuka, Sumitomo Electric Industries, Ltd., Yokohama, Japan</i>	644
---	-----

In-Line Methods of Assuring the Characteristics of Hermetically Carbon-Coated Optical Fibers— <i>T. Shimomichi, K. Oohashi, S. Araki, T. Maruoka, Fujikura, Ltd., Chiba, Japan</i>	651
Improved PMD Stability in Optical Fibers and Cables— <i>A. F. Judy, AT&T Bell Laboratories, Norcross, GA</i>	658
Bending Induced Polarization Mode Dispersion with Random Mode Coupling— <i>T. Sekito, Y. Suetsugu, Y. Yamazaki, Y. Saito, Sumitomo Electric Industries, Ltd., Yokohama, Japan</i>	665
Thermal Characteristics of the Propagation Delay for Bare and Cabled Single Mode OVD Fibers— <i>W. S. Jia, T. H. Chen, Chengdu Cable Plant of P&T Ministry, Sichuan, People's Republic of China; and R. Yang, E. Baumann, A. Landers, Siecor GmbH & Company KG, Neustadt/Coburg, Germany</i>	672
Photo-Elastic Correction Factor for Fiber Strain Measurements in a Cable Under Tensile Load— <i>K. Abe, i/FO Technologies, Ontario, Canada; K. Yoshida, Phillips-Fitel Incorporated, Ontario, Canada; O. Daneshvar, ATT-Fitel Inc., Carrollton, GA; and J. J. Carr, Corning Inc., Corning, NY</i>	678

THURSDAY MORNING—8:30 AM—12:00 PM (NOON)
TRACK 2—COPPER CABLES
Grand Ballroom, Second Floor
Ballroom D

SESSION 18: COAXIAL CABLES

Chairperson: Mr. Brian D. Garrett, CommScope, Incorporated, Claremont, NC

Long-Term Operating Experience of Large Diameter Flexible Coaxial Cable in High-Power Broadcasting Stations— <i>M. Franz, Kabelmetal Electro GmbH, Hannover, Germany; G. Schweiger, German Bundespost TELEKOM, Darmstadt, Germany; and D. R. Stein, Cable Consultants Corp., Larchmont, NY</i>	684
Shielding Effectiveness of Coaxial Drop Cable and Simulated Aging by Flexure— <i>J. Elko, T. McAlister, K. Gantt, CommScope, Inc., Catawba, NC</i>	694
Electrical Properties of Thermoplastic Polyimide Insulated Coaxial Cable for Use at High Temperature and Under Radioactive Condition— <i>S. Sudo, S. Ono, M. Ushiki, T. Murase, Y. Sato, T. Shiono, Showa Electric Wire & Cable Company, Ltd., Kanagawa-ken, Japan; and H. Mitsui, Toshiba Corporation, Kanagawa-ken, Japan</i>	700
Optimized VARIO Leaky Feeders for 900 and 1800 MHz Frequency Bands with Optical Fibers Integrated in the Inner Conductor for Use in Mobile Radio Communication Systems in Tunnels and Buildings— <i>G. Brambilla, Sirti S.p.A., Milano, Italy; H. G. Haag, A. Weiss, Kabel Rheydt AG, Mönchengladbach, Germany; and K. Schulze-Buxloh, Kabelmetal Electro GmbH, Hannover, Germany</i>	710
Design of VHF-UHF Super-Wideband Leaky Coaxial Cable (LCX)— <i>I. Sakabe, K. Aihara, S. Hisano, Y. Sakata, S. Suzuki, Sumitomo Electric Industries, Ltd., Yokohama, Japan</i>	715
The Close-Coupling Radio (CCR) System— <i>T. Ando, T. Watari, Hitachi Cable Ltd., Hitachi, Japan</i>	721

THURSDAY AFTERNOON—1:00 PM–5:00 PM
TRACK 1—FIBER OPTIC CABLES
Grand Ballroom, Second Floor
Ballroom A

SESSION 19: FIBER RELIABILITY

Chairperson: Dr. Felix P. Kapron, Bellcore, Morristown, NJ

Optical Fiber Strength, Fatigue and Handleability After Aging in a Cable—*A. Dwivedi, G. S. Glaesemann, Corning Inc., Corning, NY; and C. K. Eoll, Siecor Corporation, Hickory, NC*..... 728

Stress Assisted Corrosion Mechanism of Pristine and Corroded Silica Glass Fibers—*D. Inniss, Q. Zhong, C. R. Kurkjian, AT&T Bell Laboratories, Murray Hill, NJ*..... 736

The Effects of Optical Fiber Coating and Ink Materials on the Corrosion of the Glass Surface—*R. A. Frantz, E. M. Vogel, H. H. Yuce, Bellcore, Morristown, NJ; B. J. Keon, Telstra, Melbourne, Australia; and T. N. Bowmer, Bellcore, Red Bank, NJ*..... 742

Optical Fiber Inert Strength and B-Value—*W. Griffioen, B. Friderich, PTT Research, Leidschendam, The Netherlands; and T. Svensson, Telia Research AB, Haninge, Sweden*..... 750

Distributed Strain Technique, Verified by Applying Slant Two-Point Bending of Optical Fibres—*T. Svensson, Telia Research AB, Haninge, Sweden*..... 759

The Tube Test. A Small-Size Sturdy Specimen for Static Fatigue of Long Optical Fibres under Uniaxial Stress—*T. Svensson, P.-O. Karlsson, Telia Research AB, Haninge, Sweden*..... 763

THURSDAY AFTERNOON—1:00 PM–5:00 PM
Grand Ballroom, Second Floor
Ballroom B

SESSION 20: FIBER OPTIC CONNECTORS

Chairperson: Dr. Koichi Inada, Fujikura Limited, Chiba-ken, Japan

Development of 16-Fiber Push-On Type Optical Connector—*I. Matsuura, T. Ueda, M. Honjo, T. Yamanishi, Sumitomo Electric Industries, Ltd., Yokohama, Japan*..... 768

Field Test Results for Pre-Connectorized Cable with 16-Fiber Ribbons—*H. Iwata, M. Matsumoto, Y. Ishino, S. Tomita, S. Nagasawa, T. Tanifuji, Nippon Telegraph and Telephone Corporation, Ibaraki, Japan*..... 774

Automated Connectorizing Line for Optical Cables—*M. Tsuda, R. Yuguchi, T. Isobe, K. Ito, Y. Takeuchi, T. Uchida, K. Suzuki, T. Matsuoka, K. Higuchi, I. Kinoshita, The Furukawa Electric Company, Ltd., Chiba, Japan*..... 781

Reliability of Epoxy Adhesives in Ceramic-Ferrule Optical Connectors—*L. A. Reith, R. A. Frantz, P. B. Grimado, D. A. Dolinoy, Bellcore, Morristown, NJ; and I. M. Plitz, O. S. Gebizlioglu, Bellcore, Red Bank, NJ*..... 790

Reliability of Optical Fiber Cables for New Connector Systems—*J. R. Holman, A. C. Jenkins, N. T. Subh, R. Travieso, AT&T Bell Laboratories, Norcross, GA*..... 795

A "Universal" Buildout System for Fiber-Optic Connections—*W. W. King, B. G. LeFevre, D. L. Stephenson, C. Gonzalez, S. C. Perry, AT&T Bell Laboratories, Norcross, GA*..... 802

THURSDAY AFTERNOON—1:00 PM–5:00 PM
TRACK 2—COPPER CABLES
Grand Ballroom, Second Floor
Ballroom D

SESSION 21: BROADBAND NETWORK APPLICATIONS

Chairperson: Mr. Richard Rossi, General Cable Company, Edison, NJ

Moderator: Mr. O. Wes Summers, BellSouth Telecommunications Incorporated, Atlanta, GA - President, Building Industry Consulting Service International (BICSI), Tampa, FL

High Frequency Characteristics of Outside Plant Multipair Telephone Cables—*J. Schulte, C. Chojetzki, G. D. Maltz, G. Verdenhalven, Kabelmetal Electro GmbH, Hannover, Germany*..... 809

Symmetrical Copper Trunk Cables for Use Up to 20 MHz Optionally to be Combined with Optical Fibres—*P. E. Gregor, Kabel Rheydt AG, Oberhausen, Germany; G. Hög, Kabel Rheydt AG, Mönchengladbach, Germany; P. E. Zamzow, Kabel Rheydt AG, Bochum, Germany; and G. Thönnessen, Kabel Rheydt AG, Mannheim, Germany*..... 819

Powering Study of Broadband Coaxial Cable Distribution Plants—*H. D. Pixley, CommScope, Inc., Catawba, NC*..... 827

Process Control of Multipair Cable for Crosstalk Performance—*D. Kang, Z. Fengqi, Chengdu Cable Plant, Chengdu, China*..... 837

TV and the Twisted Pair—*D. J. Meskell, Jr., DJM Techniques, Eatonton, GA*..... 843

OPENING SPEAKERS



XAVIER MANN
Chairman, IWCS
Senior Product Manager
AT&T Fitel
Carrollton, Georgia

Xavier Mann is the 1994 Chairman of the International Wire and Cable Symposium (IWCS). During his four years as a member on the IWCS Board of Trustees he has also served as secretary and vice chairman.

Mr. Mann holds a Bachelor of Science and Master of Science in Ceramic Engineering, both from the Georgia Institute of Technology. He has worked in both technical and commercial areas of the fiber optic cable industry for over a decade with Siccior Corporation and AT&T Fitel. He has been with Fitel since 1987 where he is currently the head of Fitel's product management department.

Mr. Mann's office is located at AT&T Fitel's manufacturing facility in Carrollton, Georgia.



JOSEPH J. PUCILOWSKI, JR.
Director, Space and Terrestrial Communications
R&D Center
U.S. Army Communications-Electronics Command
Fort Monmouth, New Jersey

Mr. Joseph J. Pucilowski, Jr. was appointed as Director for Space and Terrestrial Communications, U.S. Army Communications-Electronics Command (CECOM), Research, Development and Engineering Center (RDEC) on 27 December 1992. He has command responsibility for formulating, coordinating, managing and implementing internal and external research, development, engineering and support programs to provide the Army with seamless communications across the tactical battlefield, while also providing full technical support to U.S. Army Program Executive Officers and Project Managers in communications.

He was awarded a Bachelor of Arts in Physics, with a minor in mathematics from Rutgers University, and a Master of Science in electrical engineering from Fairleigh Dickinson University. He was appointed by the Secretary of the Army to the Senior Executive Service in November 1986.

Mr. Pucilowski was appointed Acting Deputy Chief of Staff for Concurrent Engineering at the U.S. Army Materiel Command Headquarters from February 1991 to September 1991. In that capacity he had command responsibility for Concurrent Engineering planning and implementation as well as test and evaluation, production base planning and product assurance for AMC.

Mr. Pucilowski began his government career in 1963 as a physicist for the U.S. Atomic Energy Commission. He transferred to Fort Monmouth in 1967 and has held various technical and managerial assignments at Fort Monmouth to include: Director of the Center for Command, Control and Communications (C3) Systems, CECOM RDEC; Director of Product Assurance and Test; Associate Director for Research & Technology, CECOM RDEC; Associate Technical Director for Automation, CECOM RDEC; Associate Director for Information Processing Technology, Center for COMM/ADP; and Deputy Director and Acting Director of the Center for Tactical Computer Systems.

He has served on various NATO panels. Mr. Pucilowski served as President of the Armed Forces Communications-Electronics Association (AFCEA) Fort Monmouth Chapter and as the Chairman of the 14th and 17th Annual AFCEA Symposia. He also serves as an Honorary Advisor Member of the Board of AUSA, Fort Monmouth Chapter. He has been a member of the NJ Dept of Higher Education's Panel on Faculty Development in Telecommunications and Army Member of the Joint Directors of Laboratories Technology Panel on C3.

He has published or presented over thirty-five technical papers. He was recipient of the Presidential Meritorious Rank Award in 1994.

A native of New Jersey, Mr. Pucilowski currently resides in Howell with his wife Maryann. They have six children... Adam, Joseph, Linda Ann, Mary, Kristin and Francine.

CHOICES IN THE LOCAL DISTRIBUTION NETWORK

CHAIRMAN



DR. JOYCE P. KILMER
Optotec, N.A.A.
New York, New York

Dr. Joyce P. Kilmer received the Ph.D. degree in electrical engineering from the University of Florida and joined Bellcore as a Member Technical Staff of the Optical Cables District in the Fiber Optic Technology Division in 1984. In 1988, he was temporarily reassigned to Fiber Optic Systems District to study the effects of reflections on fiber optic system performance. In 1989, he was promoted to District Manager of the Optical Connector, Splicing and

Closures District. In 1990, he became Director of the Optical Cables & Distribution Terminals/Closures Group. In this capacity he was responsible for writing generic requirements, performing product and post-mortem analyses, and developing long term reliability testing of optical fiber, optical fiber cable, and distribution terminals for Fiber-in-the-Loop (FITL). Currently, Dr. Kilmer is the North American Agent for Optotec.

PANELISTS

Yutaka Wakui, Vice President, Executive Manager of NTT Telecommunication Field Systems R&D Center, Ibaraki, Japan

Eckart Flor, Head of Division Synchronous Network and Fibre Optics in the Subscriber Line Area
Deutsche Bundespost Telekom, Darmstadt, Germany

Keith Oakley, Manager, Transport Network Strategy, BT Laboratories, London, United Kingdom

Alex B. Best, Senior Vice President of Engineering, Cox Cable Communications, Atlanta, Georgia

Gerald R. (Gerry) Boyer, Director Access Network System Engineering, Bellcore, Morristown, NJ

Evolution of the Optical Access Network in Japan

Yutaka Wakui and Koshi Ishihara

NTT Access Network Systems Laboratories

The service network is currently being improved to provide advanced services flexibly through the introduction of digital network and fiber-optic transmission technologies. NTT plans to complete the introduction of digital switches and fiber-optic systems into the nationwide trunk network by 1998. In 1985, NTT built a trunk network extending throughout Japan which employs single-mode optical fiber cable. At present, there are about 100,000km of cable in this network. In order to provide multimedia communication services, such as audio, video and data transmission between computers, it is necessary to introduce an optical fiber network into the access network, which consists of mainly a huge amount of metallic cable, that can provide various services, ranging from narrowband to broadband.

The advisory committee of the Ministry of Posts and Telecommunications announced this year that they plan to construct a nationwide optical fiber network by the year 2010. NTT plans to realize fiber-to-the-home (FTTH) nationwide by the year 2015 and, in the business areas of major cities in particular, we will promote the extension of optical fiber cables into or near customers' buildings and plan to complete the optical fiber network in these areas by the year 2000.

At present, we use optical fiber to provide high-speed and broadband services such as primary rate ISDN, video transmission and high-speed data transmission with a one-to-one fiber-use system, which directly links each user to a central office, and narrowband services, such as plain old telephone services, by using multiplexed transmission systems called optical access systems or central terminal/remote terminal (CT/RT) systems. In order to realize FTTH,

NTT is developing new powerful fiber-optic access systems to provide attractive multimedia communication services economically.

We have selected the single star configuration for optical fiber distribution in outside plant so that an optical fiber directly links each user to an NTT central office. There are two main reasons for this: to realize sufficient transparency in terms of connecting with the above mentioned optical access systems; and to allow easy maintenance. For the business areas of large cities where there are many sources of demand for optical fiber and an insistence on communication reliability, we have adopted a cable ring distribution configuration which provides greater flexibility with regard to demand fluctuations and greater reliability by fiber route duplication.

In order to realize this network concept, we have developed a number of optical fiber network technologies. These include high-density optical fiber cable technology which realizes high-fiber count cable and long-span cable installation, high-fiber count and high-fiber density connector technology which can reduce fiber joining and rejoining work, and fiber access technology which allows fibers to be accessed at the midspan of a cable. We have developed technology for providing optical fibers for home use. Furthermore, to reduce the total cost, including running costs, we have developed advanced operation systems, such as remote and automatic optical fiber testing technology.

In this lecture, I will describe the current status of optical fiber network deployment and the trends in optical fiber technology at NTT.

Biography

Yutaka Wakui was born in Tokyo in 1943. He received a B.S. degree in electronics and communication engineering from Waseda University in 1966. Since joining NTT in 1966, he has been engaged in outside plant planning and telephone office management. He was made manager of the Facility Division in the Hokkaido Telecommunications Bureau in 1981, executive manager of facility planning in Engineering Strategy Planning Headquarters in 1986, and deputy general manager of the Tokai Regional Communications Section in 1989. He is currently vice president, executive manager of the NTT Access Network Systems Laboratories.



Koshi Ishihara was born in Yamanashi Prefecture, Japan, on January 31, 1943. He received the B.S. degree in mechanics from Tokai University in 1967, the M.S. degree in mechanics from Yamanashi University, Yamanashi, Japan, in 1969, and the Ph.D. degree in communication engineering from Osaka University, Osaka, Japan, in 1981. In 1969, he joined the Ibaraki Electrical Communication Laboratory, Nippon Telegraph and Telephone Public Corporation, Ibaraki, Japan, and worked on design of coaxial and optical Subscriber Cable Systems Laboratory of NTT Access Network Systems Laboratories, and is responsible for optical subscriber cable technology. Dr. Ishihara is a member of the Institute of Electronics, Information and Communication Engineers of Japan.



CHOICES IN THE LOCAL DISTRIBUTION NETWORK

ECKART FLOR

DEUTSCHE BUNDESPOST TELEKOM, DARMSTADT, GERMANY

The pressure on all established network carriers to employ optical fibres in the local loop network is growing steadily. In times of deregulation and migration of the traditional telephone services to mobile communications, every operator must examine carefully how he can capitalize on the usage of expensive "fixed networks," especially in the subscriber line area. For the big carriers the implementation of broadband accesses to a maximum possible number of customers may well become a question of survival.

Now the reunification of Germany has offered Telekom the unique chance of taking a decisive step on the way to the network of the future. In 1994 the OPAL (short for Optical Access Line) project led to a breakthrough of fibre-optics. Already today it is obvious that this technology has economical advantages over copper when the entire local access area is optimized under switching and transmission engineering aspects.

But also in the western part of Germany with its well-developed copper infrastructure the perspectives, no doubt, are favorable.

The basic infrastructure installed at the upper network level in the course of transition to fibre-optic technology can be adapted relatively fast and at comparatively moderate cost to the requirements of new broadband services. Wideband usage of these resources will be doomed to failure, however, because of the insufficient opportunities offered by the access network. A conversion of this network level, which has been optimized for telephony and the transmission medium "copper," is achievable only in the very long run. This is attributable, on the one hand, to the high costs involved, and, on the other, to the fact that a nation-wide introduction of optical-fibre systems calls for a multitude of construction projects, this causing the time-to-market to become much too long for a rapidly

developing broadband service, even if no strict limits were to be imposed on capital investment.

The German reunification, however, confronted Telekom with a unique situation. The necessity to build up a completely new telecommunications network in the eastern part of Germany started the discussions about the use of optical fibres in the subscriber line network anew. The fact that the expenditure for the civil engineering work required must be raised anyway has led to completely new perspectives for optical fibres.

In response to the situation prevailing in the new federal states, the Board of Directors set the following objectives:

Optical Fibre lines for:

200,000 households in 1993,
500,000 households in 1994 and another
500,000 households in 1995.

Since the fibre-based network extensions had to be accomplished not only in financial but also in temporal competition with copper, recourse was made to pilot systems in 1993 (OPAL 1 to 7), because a standardized technology was not available before 1994. Selection of coverage areas was based on copper projects, where attempts at achieving maximum economy were made by choosing a high building density and large residential complexes. As no established market existed for such projects, contracts were awarded on a turn-key basis, prices being quoted for the number of connectible residential units.

The first line units provided under this programme were taken into service in Gera (Raynet) and Quedlinburg (ke) on 13 October 1993.

Under the OPAL 94 programme two essential changes have been made:

- Contract award was based on a worldwide invitation to tender in line with a detailed specification.
- The local projects involved were selected under planning aspects, making due allowance for an overall economic concept for switching and transmission engineering.

The active fibre-optic technology was financed largely by savings in the transmission sector. While the restricted range of the transmission medium "copper" requires a number of switching facilities, the application of optical fibres offers the opportunity of bridging great distances passively and concentrating the necessary switching functions in a few points. The remote peripheral equipment envisaged as a substitute for small exchanges is relatively expensive. Their original traffic concentration function with the aim of saving transmission capacity for their interconnection to parent exchanges is rather questionable in the optical fibre era characterized by the low channel-kilometre costs of high bit rate systems.

The invitation to tender achieved excellent results on the world market. The prices quoted fell by far below those quoted for OPAL 93. Together with the funds saved by an all-encompassing optimization, the total cost volume of Fibre-To-The-Building (FTTB) was proved to be equal to that of copper. This is also noteworthy insofar as the OPAL 94 programme comprises a high percentage of single-family homes in rural districts, a situation which so far has been considered as really "anti-fibre-optic." It became apparent, however, that just in this area the large-scale reorganization of the entire network allowed substantial savings to be reached in the transmission sector, which compensated for the extra expenditure spent for active fibre-optic transmission systems.

Whereas the OPAL 93 and 94 projects capitalized on the "start-from-the-scratch" situation in the new federal states, the OPAL 95 programme is intended to provide the transition to the western part of the Federal

Republic of Germany. Here the environment is fundamentally different. Even though there are a number of new building areas in the old federal states, too, the copper-based infrastructure is normally well developed, so that the network conversion costs, inclusive of all civil engineering expenses, fully arise from optical-fibre technology deployment.

The transition to a fibre-optic network in the old federal states therefore is a problem of the migration concept chosen and will have to take place stepwise.

The requirements set on this implementation strategy are:

- Fast transition to countrywide coverage,
- Definition of a new service platform above telephony,
- No pre-investments in future services, that is, each step taken has to pay.

Like for OPAL 94, recommendable financial resources are the comparatively high expenses necessary for a further network digitization in the switching sector.

The replacement of these remote peripheral switching facilities by transmission technology creates a service-neutral platform which permits services operating up to 2 Mbit/s to be introduced into the network quickly and at no extra cost.

If there is the necessity of upgrading the feeder cables, this should be done on an optical-fibre basis. The civil engineering work needed for that purpose is relatively cheap, because these cables are largely laid in tubes. Due to the high costs involved, fibre application in the junction network will not be feasible in the first stage, however.

The remaining pairs of the distribution cable network with their comparatively short lengths can then be equipped as required with active transmission facilities for broadband signals (2 Mbit/s, 6 Mbit/s), the use of active transmission systems for narrowband services avoiding the otherwise necessary investments in junction cable network expansions.



Dipl.-Ing. Eckart Flor
Head of Division Synchronous Network &
Fibre Optics in the Subscriber Line Area

Deutsche Bundespost Telekom
Forschungs- und Technologiezentrum
P.O. Box 10 00 03
D-64276 Darmstadt, Germany
Telephone: +49-6151-83-64-56
Fax: +49-6151-83-64-59

Eckart H. Flor received the Dipl.-Ing. degree in Telecommunication Engineering from the University of Aachen in 1968. He joined the DBP Telekom and started his work at the research and development centre FTZ in Darmstadt. After 3 years experience with the design of analog equipment he became head of the department of reliability and quality control.

In 1981 he went back to the design group, where he started the activities in the field of SDH. Following the decision of a general transition to SDH in 1989 he became the coordinator of all SDH activities.

After the reunification of Germany all FITL-activities were concentrated in his division. He is responsible for the Telekom's OPAL program installing 230,000 lines in 1993, followed by 500,000 lines in 1994 and continuing in 1995.

CHOICES IN THE LOCAL DISTRIBUTION NETWORK

KEITH OAKLEY

BRITISH TELECOM, LONDON, UNITED KINGDOM

INTRODUCTION

Conventional telco copper networks are coming under increasing pressure from new technologies. The concept of one circuit per copper pair leads to a high operational costs and the risk of significant stranded investment whilst copper's restricted range and bandwidth capability limits the ability to support the future information superhighway. In the UK there is fierce competition from various forms of cellular radio and telephony provided on the margins of CATV networks. British Telecom like many other operators is examining its options for the future.

OBJECTIVES

The ideal network must meet the following major objectives:

- Providing flexibility and breadth in service provision.
- Minimised the whole network costs.
- Ensure future proofing of the installed broadband infrastructure against unpredictable service evolution.
- Cope efficiently with the ongoing needs of narrowband customers. Serve both business and residential customers via a common integrated network infrastructure.

PASSIVE OPTICAL NETWORKS

BT is increasingly using fibre systems to address the above requirements.

Conventional PDH fibre systems for 2mbit/s and above delivery to business customers have been used for some time but BT is now beginning to deploy both point to point SDH and point to multi-point passive optical network (PON) systems to customers. Systems have been developed in FTTB (Fibre to the Building) and FTTC (Fibre to the Curb) form. The latter variant, aimed at achieving viable costs for residential customers, extends fibre to a small active node at the curb with conventional copper technology being used for the final customer drops typically 100 metres.

Whilst these early PON systems have focused on the delivery of existing narrowband services, systems are now emerging aimed at the delivery of broadband multi media services to both business and residential customers.

PONS are most closely associated with the use of digital baseband modulation - the fundamental preferred format for most optical fibre systems to date. The basic idea of PONS stemmed from the realisation that digital fibre baseband systems typically have substantial power budget margins over local loop distances which can be exploited with advantage via the use of optical splitters.

PONS offer little cost advantage over conventional coaxial cable systems for the delivery of analogue cable TV channels. However, future networks will focus on the digital delivery of Interactive Multimedia Services such as Video on Demand, home banking, home shopping etc. where the benefits of digital baseband system design, coupled with a PON architectural approach will become increasingly significant.

CONCLUSION

A key issue for the design of any future network is the balance of emphasis to place on delivery of today's services as opposed to tomorrow's. For telcos with no embedded coaxial networks a digital baseband approach to network design coupled with the use of PON techniques offers both cost savings and maximum network efficiency for today's services and significant advantages for the delivery of future digital interactive multimedia services.



Keith Oakley
Manager for Core and Access
Transport Network Strategy
British Telecom
PP 310 Williams National House
11/13 Holborn Viaduct
London EC1A 2AT, England

Much of Keith Oakley's long career with British Telecom has been spent introducing new technology into the access network. Most recently he has been heavily involved in Passive Optical Network (PON) technology. In his current roles as Manager for Core and Access Transport Networks Strategy he has responsibility over the future strategy for most of BT's physical network, a network under intense competitive pressure.

TODAY, TOMORROW AND THE TWENTY-FIRST CENTURY (The Three Phases of Cable TV)

Alex B. Best
Cox Cable Communications, Inc.
Atlanta, GA

Phase I - The Broadcast Delivery of Analog Services

Since the beginning of the late '40's/early '50's, cable operators have offered consumers an increasing array of programming choices that are viewed in a non-contentious manner. By non-contentious, I mean that all customers have simultaneous access to all services. Stating it another way, the services are transmitted through the network in a "broadcast" mode. Until a few years ago, the network structure consisted of a series cascade of coaxial cable segments whose loss was overcome by a broadband amplifier, repeated until the entire service area was covered. The topology of this network was configured in what was referred to as a "tree-and-branch" architecture. The channel capacity of such a system was determined by two factors. One is the bandwidth of an analog television signal, which for the U.S. is 6 Mhz per channel (NTSC standard). The second is the bandwidth capability of the broadband amplifier. Due to improvements in the distortion capabilities of transistor technology, this bandwidth has continued to increase over the years, starting at 216 Mhz in the early days and increasing to 750 Mhz today. With 750 Mhz technology, a cable operator is capable of offering up to 110 analog channels of cable programming services.

In 1988, cable operators began deploying fiber optic technology from the headend (origination point) to locations throughout the existing coaxial cable based system. This new technology offered cable operators a way to substantially improve the picture quality and reliability to customers at the extremities of the plant. This problem was caused by the long cascade of amplifiers required to reach these customers.

A typical system today (recently upgraded) is capable of offering 110 analog channels of television, through a fiber/coax network that is configured in star/bus fiber-to-the serving area topology.

Phase II - The Broadcast Delivery of Digital Services

Additional new technology was recently introduced which allowed an analog television signal to be converted to the computer language of ones and zeros, and compressed by removing redundant information in a very sophisticated computer using a software algorithm agreed to by a standards organization called the Motion Picture Expert Group (MPEG). By deploying this technology in a cable headend the number of channels offered

by a cable operator could be increased by a factor of 4 to 10, depending upon the compression ratio selected in the MPEG compression process. Obviously, picture quality is somewhat compromised at the higher compression ratios.

Unfortunately, very few cable systems are large enough to support the cost associated with compressing a large number of program services since each compression costs approximately \$75,000. To overcome this cost in each headend, several entities have set up facilities to compress services at a single location and deliver them over satellite in a compressed format. A cable operator can receive these services in a compressed format and pass them through the headend to be offered to subscribers on a subscription basis.

Using this concept, a cable operator can substantially increase the number of channels offered over their existing cable plant, without the need for a bandwidth upgrade.

It should be pointed out however, that these digitally compressed services are still being offered to the customer in a broadcast mode, i.e., there is no contention for these services.

Obviously, for a customer to receive programs offered in a compressed format, they must be offered a "decompression" set-top decoder. These boxes will be available in quantity in the fourth quarter of 1995.

Phase III - On-Demand Delivery of Video, Voice, and Data

Several trials are presently underway in the cable industry which will allow the customer to access programming in an on-demand scenario. Movies-on-demand is an obvious example of such a service. Several pieces of new technology are required to offer services in this manner. One is a file server with adequate memory to store the huge amount of data required for video. This server must also have the output bandwidth to serve thousands of customers simultaneously. The second is a switch which directs the bits for a given movie onto the appropriate fiber feeding the neighborhood of the customer requesting the movie. Third, the system network configuration and channel capacity must be adequate to handle the traffic problem associated with offering personalized programming to a customer in an on-demand scenario.

Variables which must be considered in the traffic modeling process include the number of movies offered, the compressed bit rate, the RF modulation scheme, the number of customers per node, and the buying habits for the types of movies offered.

Similar traffic models must be dealt with when other on-demand services are offered, such as telephony services and data services including Prodigy, America On-Line, and the InterNet.

In the end, it is very likely that a cable operator will continue to offer services, both analog and digital, transmitted in a broadcast mode. Additionally, a certain percent of the capacity of the fiber/coax network will be dedicated to services offered in an on-demand scenario. It is these video, voice, and data services that are offered in an on-demand scenario that defines the much publicized concept referred to as the Information Highway to the Home.



ALEX B. BEST
Senior Vice President, Engineering
Cox Cable Communications
1400 Lake Hearn Drive
Atlanta, Georgia 30319

Alex B. Best, Senior Vice President of Engineering, joined Cox Cable Communications in April 1986 as Vice President of Engineering. He was promoted to his present position in January 1989.

Mr. Best joined Cox following twenty years with Scientific Atlanta, where he was involved in nearly every aspect of that Company's CATV product development and business application. His last position prior to his appointment at Cox was that of Principal Engineer.

Mr. Best Received a B.S. and M.S. degrees in Electrical Engineering from Georgia Institute of Technology, and completed the Program for Management Development (PMD) at Harvard Business School.

Mr. Best has been a member of the National Cable Television Association's Engineering Committee since 1978 and Chairman of that Committee's Ad Hoc Subcommittee to investigate the implications of Broadcast Stereo Compatibility (BTSC) on cable communications. He has also been a member of the Society for Cable Television Engineers since 1975. Mr. Best is a member of the Board of Directors of Cable Labs, Inc., a research and development group funded by the cable television industry, and serves as Chairman of their Technical Advisory Committee and its Steering Subcommittee. He was the 1977 recipient of the National Cable Television Association's Vanguard Award for Science and Technology; and received the Southern Cable Television Association's Polly Dunn Award in 1992 for his dedication to the cable industry.



GERALD R. (GERRY) BOYER
Director Access Network System Engineering
Bellcore
Morristown, New Jersey

Gerald Boyer received his B.S. and M.S. degrees in Theoretical and Applied Mechanics from, respectively, the University of Illinois and Columbia University. He began his career in the communications industry in 1968 with Bell Laboratories and accepted a management position with Bellcore at its inception in 1984.

Gerry has worked in a variety of areas involving applied research, product development, and systems engineering. He managed development of Bellcore's generic

requirements for Fiber In The Loop ("TR-909"). He led the systems engineering effort that assessed potential end-to-end video delivery technologies for Bellcore's Video Dial Tone Prospectus. Most recently, Gerry defined the broadband access technology behind Bellcore's "RBOC of the Future" - a low cost, operationally efficient access network that integrates telephony, mobility, broadcast video and interactive multimedia services. This work triggered interest in aggressive hybrid fiber/coax upgrades in some major telephone companies.

LUNCHEON SPEAKER



DURWOOD FINCHER
"MR. DOUBLETALK"
Atlanta, Georgia

Sometimes you wonder if the speaker you hire is going to make any sense. Not with Durwood Fincher -- he never makes sense.

He's been called "Mr. Doubletalk" by Candid Camera's Allen Funt. Corporate executives have called him "the great imposter" and "the perfect icebreaker." Who knows what you'll call him, but you'll agree that Durwood Fincher is like no other speaker in America today.

He's usually introduced as Dr. Robert Payne, a highly-touted government "expert" straight from Washington. His speech, custom-tailored to your theme or requirements is a delicious diatribe filled with bureaucratic rhetoric and platitudes and delivered with that all-too-familiar boring speaker's monotone.

"Oh, no!" the audience thinks to itself as the sentences grow longer and the words become more obscure. Soon everyone is squirming and frowning as "words" begin to appear that really aren't words at all.

Suddenly, someone realizes what's happening and snickers. Then two of three others catch on and begin to chuckle. Finally a wave of realization passes over the audience and frowns turn into laughter as everyone becomes aware that he or she has been "had."

Recognizing that he has been "discovered," Durwood concludes on a positive note that leaves your people relieved, relaxed and ready to get the most out of the remainder of your meeting.

Design Concepts for a 4000-Fiber Cable with Thinly Coated Fiber

R. S. Wagman, P. R. Bark, H. G. Cooke, C. K. Eoll, R. O. Livingston, G. A. Lochkovic,
W. W. McAlpine, F. M. Sears and S. S. Sodhi

Siecor Corporation
489 Siecor Park, Hickory, North Carolina 28603

Abstract

A U-groove ribbon cable using 200 μm outer diameter, single-mode optical fibers was designed, manufactured and tested. The cable design can accommodate up to 4000 fibers. Standard cable design concepts had to be reassessed, and development efforts were focused on three critical issues: (1) the ribbon matrix material, (2) U-groove design and (3) the stranding process. A low modulus, low friction ribbon matrix material was used to isolate the fibers from microbending forces and allow easy ribbon slippage for minimal fiber strain. The U-groove material and shape were chosen to minimize the cable diameter. Performance of this cable with its ultra-high fiber density is shown to be comparable to that of conventional outside plant cable. This confirms that U-groove ribbon cables incorporating thinly coated optical fiber is a viable technology.

1.0 Introduction

Nippon Telephone and Telegraph (NTT) is preparing to implement B-ISDN subscriber networks in Japan and is developing the associated technologies necessary for such an undertaking. Ultra-high-fiber-count optical fiber cables [1] represent one such technology which NTT is developing for both high-speed broadband and narrowband applications in the subscriber network. Initially, the goal of this development program was a 4,000-fiber U-groove (U-channel) cable with an outside diameter of 35 mm. This equates to a fiber density of 4 fibers/ mm^2 . In conventional cable technologies, 1 fiber/ mm^2 is considered to be high density. Other innovations needed for ultra-high fiber density include a thinly coated optical fiber, 16-fiber ribbons and 160 fibers per U-groove.

Originally, thinly coated optical fibers that were 180 μm in outside diameter were suggested for this development [2]. During the development program,

however, reliability concerns and microbending attenuation increases due to reduced protection for the glass prompted a change to fiber that was 200 μm in outside diameter [3]. At the same time, a new outer primary (secondary) fiber coating with a high Young's modulus was chosen because fibers with such a coating were found to have less microbending sensitivity than fibers with a conventional outer primary coating material [4].

This paper reports on the design, manufacture and testing of a U-groove cable capable of incorporating up to 4000 fibers. A cross-section of the cable with the maximum complement of fibers is shown in Fig. 1. In this design, U-grooves are stranded in two layers around an overcoated steel central element. Each U-groove contains a stack of ten 16-fiber ribbons, and each layer of U-grooves is wrapped with water-blocking tape.

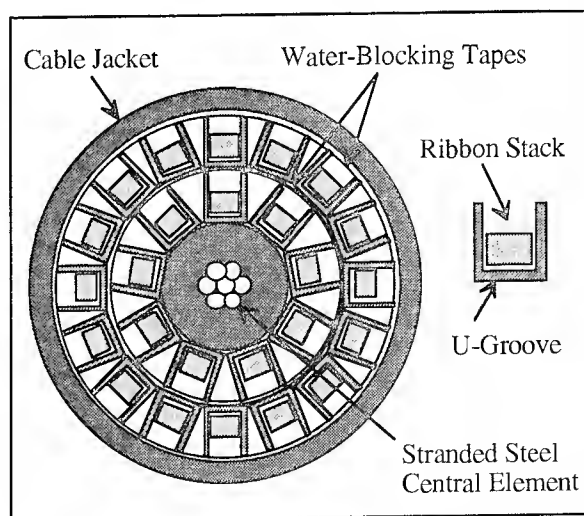


Fig. 1. Example of a 4000-Fiber U-Groove Cable

A key challenge in this development program has been attenuation performance. When a cable is bent or taken to low temperatures, for example,

attenuation increases due to microbending of the fibers can occur if the ribbons are exposed to significant lateral forces. Such forces can be reduced or avoided if there is sufficient room in the cable for the ribbons to move freely, whether it be radial movement, longitudinal slippage or twisting. Of course, such forces are less important for ribbon designs which are less sensitive to microbending under lateral load. The challenge of good attenuation performance was met by focusing on three critical issues: (1) the ribbon matrix material, (2) U-groove design and (3) the stranding process.

2.0 Ribbon Matrix Material

Besides holding the fibers together in a ribbon, the ribbon matrix material helps to isolate the optical fibers from lateral forces that can lead to microbending. It has been shown [5] that matrix materials with a low Young's modulus provide better isolation than do high modulus materials. On the other hand, low modulus materials typically have relatively high coefficients of friction. Such materials would be undesirable as matrix materials. Low ribbon-to-ribbon friction is needed to allow slippage of the ribbons relative to each other when a cable is bent. Otherwise, cable bends could cause high fiber strains and large lateral loads on the ribbons. The former would be a fiber reliability issue, while the latter could cause unacceptable attenuation increases.

Two tests were developed [5] to characterize experimental ribbons, and, in particular, to assess matrix materials. The first test measured fiber attenuation in ribbons in a simulated cable environment. The second measured ribbon-to-ribbon coefficients of friction.

The following method was used to measure attenuation. Using 400 g of tension, 500 m of ribbon are wound in several layers onto a drum with a 225 mm diameter. One hour later, the attenuation of each of the fibers in the middle 200 m of the ribbon is measured using an OTDR. In this test, the (relatively long) measured portion is sandwiched between other layers of ribbon; this simulates the ribbon-to-ribbon contact within a cable.

In the ribbon-to-ribbon friction test, one length of a ribbon is fixed to a mandrel while another length of the same ribbon is pulled along the upper surface of the fixed ribbon. A static coefficient of friction is estimated using the peak force generated.

Many different types of ribbon matrix materials were evaluated; however, one matrix material was developed that had both a low modulus and a low ribbon-to-ribbon coefficient of friction. This is the material that was used to make the ribbons for the cable described in this paper. The ribbon-to-ribbon coefficient is indicated by the diamond in Fig. 2.

Incidentally, it is important to use ribbon-to-ribbon coefficients of friction rather than film-to-film coefficients in assessing the suitability of matrix materials. Measurements of the coefficients of friction using films prepared from the matrix materials can yield results that are very different from the results of ribbon-to-ribbon tests. This effect is illustrated in Fig. 2. The differences are due to dissimilar surface finishes and the composite nature of ribbons.

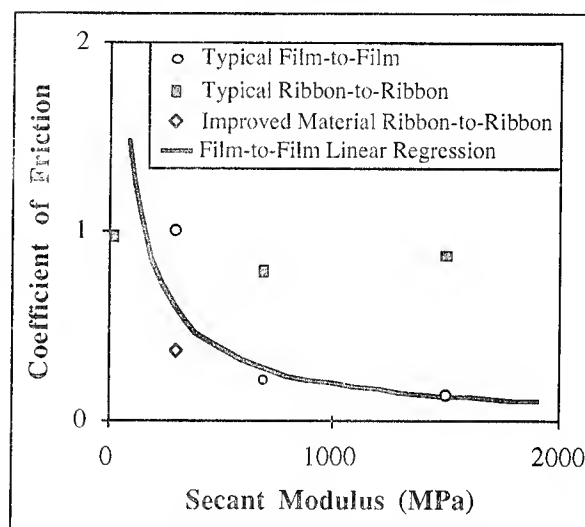


Fig. 2. UV Ribbon Matrix Material Coefficient of Friction Versus Secant Modulus

3.0 U-Groove Optimization

An important goal was to develop a cable with as small a diameter as possible. To minimize the outside diameter of the cable, U-grooves should have the thinnest walls structurally possible, with a shape which promotes cable compactness; but crush resistance cannot be sacrificed. U-groove optimization offers the greatest opportunity to minimize the outside diameter since so many of the other cable variables are fixed – for example, the number of fibers per ribbon (16), the number of ribbons per stack (10) and the number of U-grooves (25). Testing for the structural integrity of U-grooves, either

individually or in cables, was performed using parallel plate crush (lateral load) tests.

The function of the U-groove in the cable is to provide a dimensionally and structurally stable space for the ribbons to move and rotate. In particular, rotation of the ribbon stack during cable bending must be considered. Fig. 3 shows how the ribbon stack rotates to relieve bending strains. Using experimental results, inside U-groove dimensions were found which provide the proper amount of free space for stack rotation during bending, as well as for radial stack movement during cable expansion and contraction.

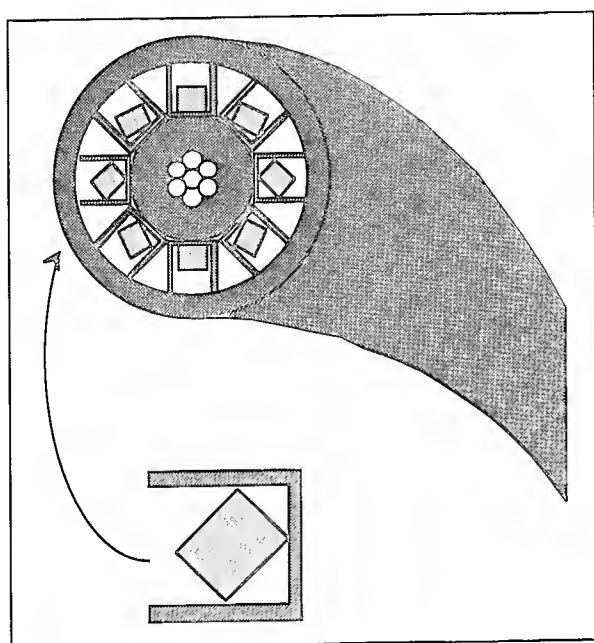


Fig. 3. Rotation of the Ribbon Stack During Bending

Theoretical and experimental studies were done on the relationships among U-groove material, wall thickness and height with respect to crush performance when individual U-grooves were tested. In the crush testing, the failure force was defined as the force at the onset of inelastic compression. At this force, the U-groove was being permanently deformed. Test results correlated well with Euler's slender column theory [6].

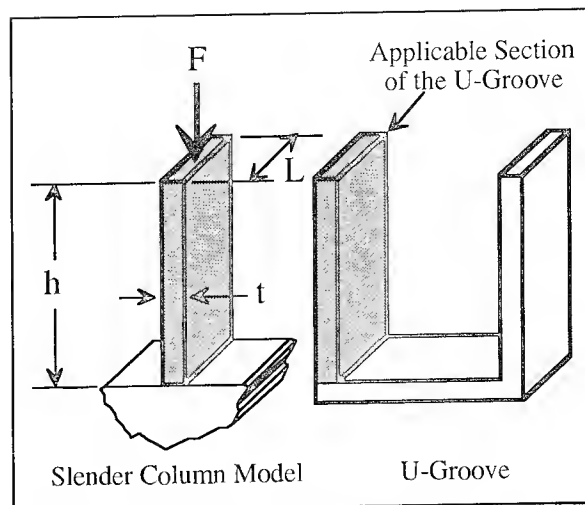


Fig. 4. Application of Euler's Column Theory to U-Grooves

Application of the theory to the U-groove structure is shown in Fig. 4. Euler's equation for a section of U-groove wall which is fixed at the bottom of the wall and free at the top is given by

$$\frac{F_{\text{critical}}}{L} = \frac{\pi^2 E t^3}{48 h^2} \quad (1)$$

where F_{critical} is the force required for failure, L is the length of U-groove under test, E is Young's modulus for the material, and t and h are the thickness and height of the wall, respectively.

The average of 30 measured values of the left-hand side of Eq.(1) was found to fall within 10% of the average of the corresponding values predicted by the right-hand side. In addition, the square of the correlation coefficient for the measured and predicted values was 0.83. Therefore, Eq.(1) was used to help select the optimum combination of material modulus, wall thickness and height. The material chosen has a modulus greater than 2400 MPa.

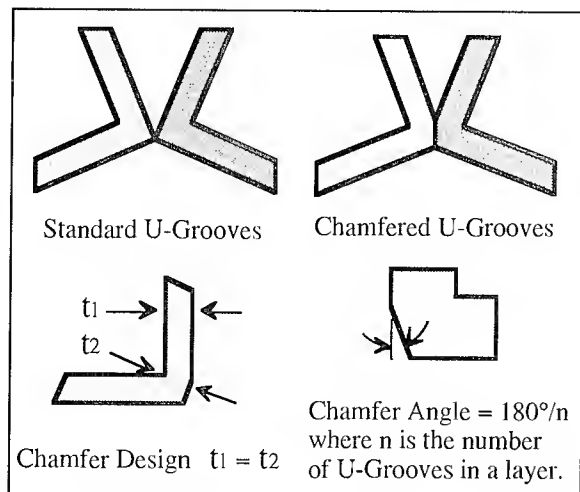


Fig. 5. Chamfering of U-Groove

The shape of the outside of the U-groove was optimized by chamfering the corners. In the simplest form of the U-groove, sharp bottom corners contact each other in the cable as shown in Fig. 5. By chamfering these corners, the cable diameter is reduced. The chamfer is designed as follows: the chamfer angle is one-half the angle at which the U-grooves contact each other, while the minimum thickness in the corner is set equal to the wall thickness of the sides. By doing so, crush resistance is not compromised, and the stability of the cable package is increased due to the larger contact areas between the U-grooves.

Table 1. 4000-Fiber Cable Diameters for Two Materials With and Without Chamfered Corners

Cable OD (mm)	Material 1 700 MPa Modulus	Material 2 2400 MPa Modulus
Without Chamfer	46.6	43.7
With Chamfer	45.4	42.5

Table 1 shows the diameter of a 4000-fiber cable with and without the chamfered corners. Overall, the cable diameter is reduced by about 4 mm through U-groove material and shape optimization.

4.0 Cable Stranding Process

To achieve acceptable attenuation performance and have low fiber strain during bending, the cable stranding process must be very exacting. The task is further complicated by the need to strand up to 160 ribbons in one layer during one operation. A schematic of the stranding line is shown in Fig. 6. This stranding method and layout was chosen for simplicity of organization and the ease of ribbon tension control. In addition, this method allows the ribbons to be stranded at desired helix angle of each ribbon. In the stranding line development, particular attention was paid to the tension, rotation and line speed controls.

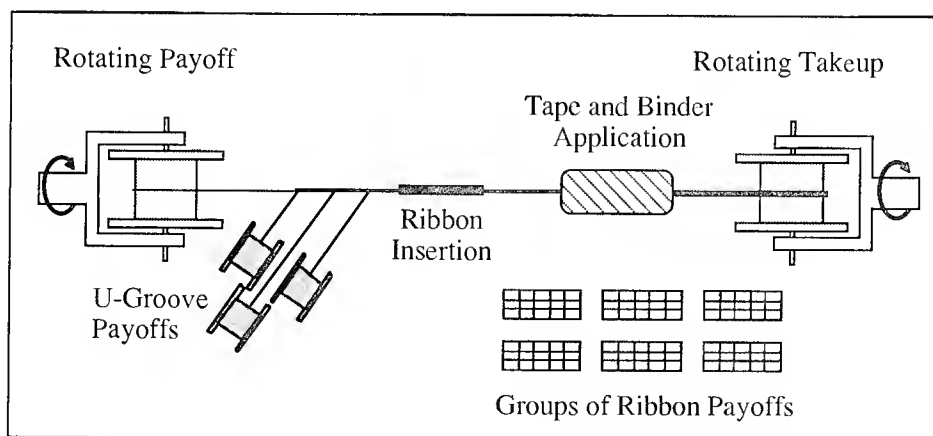


Fig. 6. Schematic of the Stranding Line for the 4000-Fiber Cable

To evaluate the stranding process, the helical length of the ribbons is measured. In the 4000-fiber cable design, each ribbon in a stack has a different length because each ribbon is a different distance from the center of the cable. In addition, the tensions used in stranding affect the relative length of the ribbons in the cable. Helical length is a good measure of stranding control.

A technique was developed to measure the helical length of ribbons in 10 m of cable with a precision of better than 0.01%. The accuracy of this technique allowed optimization of the stranding process. In initial stranding trials, certain stranding parameters were causing inappropriate values of excess ribbon length (the difference between the helical length of a ribbon and the corresponding cable length). This is seen in Fig. 7, where Cables 1 and 2 are identical except for being made with different stranding parameters. Some adjacent ribbons even have about the same excess ribbon lengths. There should be a nearly uniform difference between the excess lengths of adjacent ribbons in each stack. Changes in the stranding parameters and the ribbon insertion method corrected these problems. Fig. 8 shows the results for a cable made using those modified stranding conditions. The three sets of results in this figure correspond to samples from three different locations along the length of the cable. The three overlapping lines show the consistency of the stranding and the precision of the helical length measurements.

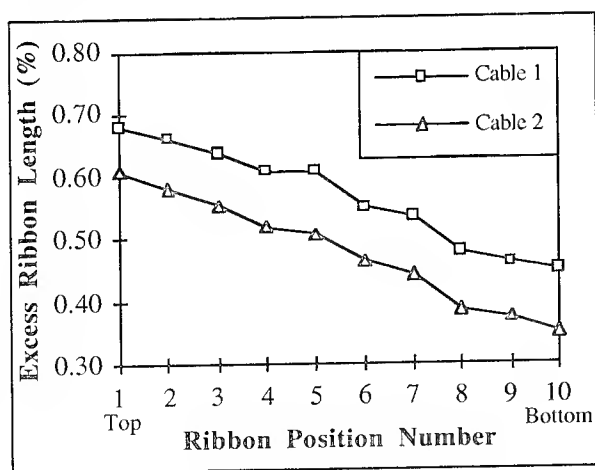


Fig. 7. Cable Excess Ribbon Length

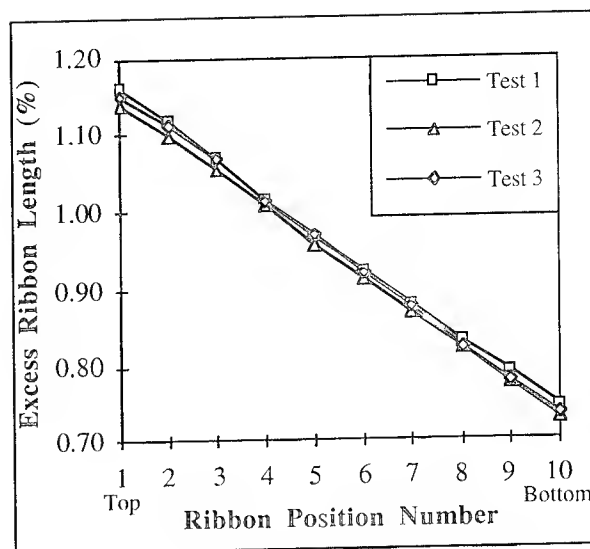


Fig. 8. Cable Excess Ribbon Length with Strander Improvements

5.0 Cable Results

A cable was manufactured with the new ribbon matrix material, two layers of optimized U-grooves and an improved stranding process as described in the previous sections. Though the cable design is capable of accommodating 4,000 fibers, this experimental cable contained 320 fibers. One U-groove in the inner layer and another in the outer layer were each filled with a stack of ten ribbons. For this cable, 200 μ m uncolored fibers were used to make ribbons 3.25 mm wide and 0.25 mm thick. Printing was used to identify each ribbon and its polarity. The inner layer of nine U-grooves was stranded around a polyethylene-overcoated, 6.0 mm stranded steel central member, and a water-blocking tape was wrapped over the U-grooves. The outer layer of sixteen U-grooves was then applied with a lay opposite to that in the first layer, and water-blocking tape was again applied. Finally, a polyethylene jacket with a 2.5 mm nominal wall thickness was extruded over the core. The overall cable diameter was 42.5 mm.

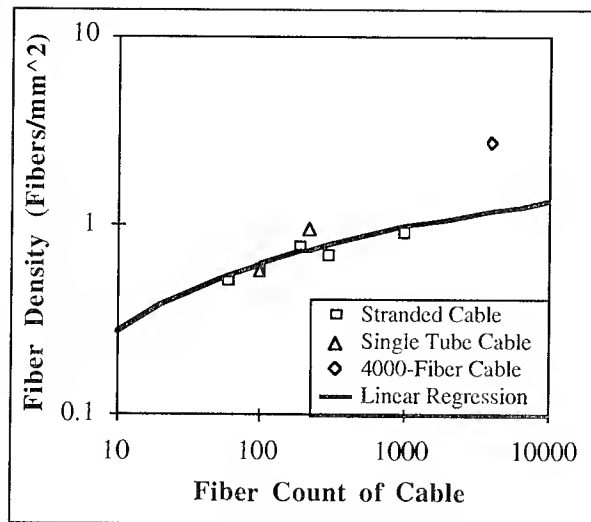


Fig. 9. Fiber Density Versus Fiber Count

In Fig. 9, fiber density (fibers/mm² of cable cross-sectional area) for conventional cables and the current 4000-fiber cable design are plotted versus fiber count. If the experimental cable contained the complete complement of 4000 fibers, it would have a fiber density of 2.82 which is well above the regression line for conventional cables.

5.1 Attenuation Performance

The experimental cable has been extensively tested to determine attenuation performance. The results show that this cable with thinly coated fibers performs as well as or better than cables made with conventional cable technology and standard optical fibers.

5.1.1 Method of Analysis

Analysis of the results for cable with ribbon stacks requires special treatment. During early cable development, the most significant increases in attenuation were often found for fibers on the outside edges of a ribbon stack, especially in the four corners of the ribbon stack. Fibers in the four corners have the potential to see higher stresses than other fibers in the ribbon stack.

One way to describe cable performance is to use the mean attenuation for all the fibers in the cable. However, the mean attenuation can be deceiving if there are a large number of fibers measured in the ribbon stack. The effect of high corner-fiber attenuation can be masked by more numerous low attenuation values for fibers elsewhere in the ribbon stack. Thus, the performance of the corner fibers is sometimes considered separately from that of the remaining fibers in the results presented below.

Table 2. Cable Attenuation

Test Item		Result	
As Manufactured (dB/km)	non-corner fibers	0.22 / 0.01	Mean / Std Dev @1550 nm
	corner fibers	0.22 / 0.02	
Temperature Cycling at -30°C (dB/km)	non-corner fibers	0.22 / 0.02	
	corner fibers	0.22 / 0.01	
Temperature Cycling at 60°C (dB/km)	non-corner fibers	0.22 / 0.02	
	corner fibers	0.23 / 0.02	
Bending (dB)	200 mm Radius	<0.02	Maximum Loss @1550 nm
Crushing (dB)	2000 N	<0.02	
Squeezing (dB)	0.20% Elongation 600 mm Radius	<0.03	
Tensile Loading (dB)	0.25%	<0.02	

In this analysis, attenuation at 1550 nm is the primary focus; however, 1310 nm was also examined to differentiate between microbending and macrobending effects.

5.1.2 Attenuation Results

Attenuation performance of the experimental cable was monitored during cable manufacturing, mechanical handling (bending, crushing, squeezing, and tensile loading) and temperature cycling. The corner fiber effect found in some of the earlier developmental cables was not present in this cable. A summary of the results is shown in Table 2.

As manufactured, the mean attenuation at 1550 nm of all the fibers was 0.22 dB/km with a standard deviation of 0.02 dB/km. The maximum attenuation of any fiber in the cable was 0.26 dB/km. The maximum corner fiber attenuation was 0.24 dB/km.

In the following attenuation tests, representative samples of the fibers were chosen for measurement.

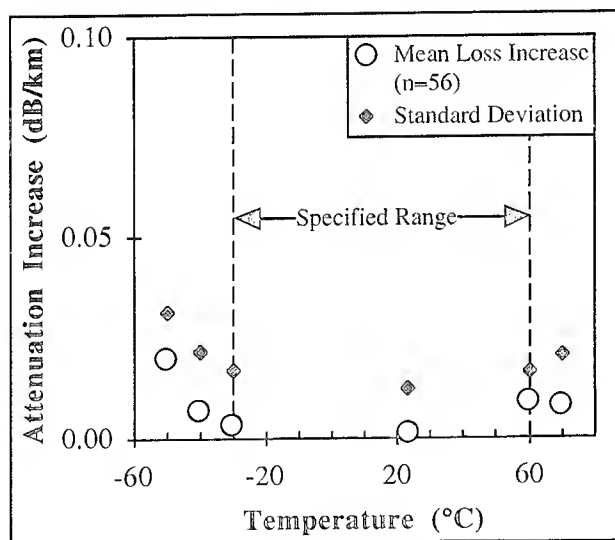


Fig. 10. Attenuation Increase versus Temperature

Temperature Cycling: The cable was subjected to a series of temperature cycles in the range from -30°C to +60°C. In this specified range, the cable exhibited minimal attenuation change. Additionally, to investigate the temperature limits of the cable, it was cycled through a temperature range of -50°C to +70°C. At +70°C, there was no increase in attenuation. The cable did experience

some attenuation change at -50°C. One fiber along the outer edge of the stack exhibited a change of 0.16 dB/km. The other fibers showed little or no attenuation change. Fig. 10 graphs the results.

Bending: The cable was repeatedly bent 90° around a series of mandrels with radii from 200 to 600 mm. No attenuation increase was detected during bending.

Crushing: A lateral force up to 2000 N/100 mm was applied to the cable. The resultant measurements showed no significant attenuation increase. Furthermore, cable deformation did not occur until a lateral force of 3000 N/100 mm was reached.

Squeezing: The cable was pulled 90° over a 600 mm mandrel with a tension of 800 kg. During repeated cycling, there was no attenuation increase.

Tensile Loading: The cable was subjected to a tensile force which elongated the cable up to 0.25% of the original cable length. No increase in attenuation was detected during the tensile test.

6.0 Conclusion

A cable with the potential for incorporating 4000 fibers was successfully designed, manufactured and tested. The cable utilizes 200 µm diameter optical fibers, 16-fiber ribbons and 160-fiber ribbon stacks in two layers of U-grooves to obtain an ultra-high fiber density of 2.82 fibers per square millimeter of cable cross-section. During temperature cycling, only at -50°C did one fiber show a significant increase in attenuation.

Three main areas of study contributed to the optimized cable design:

- Ribbon matrix materials were investigated using a ribbon-to-ribbon friction test and a simulated cable attenuation test as the main criteria for choosing among the materials. A material was found that provided both low friction and low modulus. The low modulus reduced the microbending sensitivity of the ribbons.
- The U-groove design was optimized by the choice of material and shape. A relatively high modulus material was selected and the thickness of the

U-groove walls were minimized. A chamfer was developed for the bottom corners of the U-grooves to increase the packing density and add stability to the cable construction.

- Stranding processes were developed to lay the ribbons into the core in a highly controlled manner. A high precision method of measuring ribbon length relative to cable length was developed to help in the optimization of the stranding process.

The performance of the experimental cable is comparable to that of current outside plant cables. This demonstrates that U-groove cables incorporating thinly coated fiber is a viable technology.

Acknowledgements

The authors thank the many people who contributed to this development program. Special thanks go to Scott McDowell, Larry Herman, Jeff Dellinger, Jeff Clampitt and John Keesee.

References

- [1] S. Tomita, M. Matsumoto, T. Yabuta and T. Uenoya, "Preliminary Research into Ultra High Density and High Count Optical Fiber Cables," *40th International Wire and Cable Symposium Proceedings*, pp. 8-15, 1991.
- [2] F. Sears, H. Cooke, C. Eoll, W. Jackman, G. Lochkovic, W. McAlpine, S. Sodhi and R. Wagman, "Effect of U-groove Torsional Rigidity on Performance of High-Fiber-Count Cable," *Optical Fiber Communication Conference Technical Digest*, pp. 178-180, 1994.
- [3] G. S. Glaesemann, "Process Handleability of Thin-Coated Optical Fibers," *Optical Fiber Communication Conference Technical Digest*, pp. 243-244, 1994.
- [4] W. Katsurashima, Y. Kitayama, K. Oishi, T. Kakuta and N. Akasaka, "Microbending Loss of Thin Coating Single Mode Fiber for Ultra-High-Count Cable," *41st International Wire and Cable Symposium Proceedings*, pp. 13-19, 1992.
- [5] J. Keesee, G. Lochkovic, J. R. Toler and D. Smith, "A Comprehensive Approach to Ribbon Design with a Focus on Materials," *43rd International Wire and Cable Symposium Proceedings*, this issue, 1994.
- [6] Joseph E. Shigley and Charles R. Miske, *Mechanical Engineering Design*, 5th Edition, McGraw-Hill Inc., pp. 120-128, 1989.



Richard S. Wagman was born in Dallastown, PA in 1956. He received his B.S. degree in the Engineering Science honors program at Pennsylvania State University in 1978, and his B.S. in Electrical Engineering from Johns Hopkins University in 1984. He

worked for seven years as a Product Engineer at Continental Wire & Cable before joining Siecor Corporation in 1985. At Siecor, he has worked with cable, materials and test design. He is currently employed as a Staff Engineer in the Research, Development and Engineering Department. He has been granted four patents and has co-authored two previous IWCS papers.



Peter R. Bark was born and educated in Germany. In 1963, he received his bachelor of science degree (Diplom-Ingenieur) from the Technical University at Munich. In 1968, he received his doctorate in engineering from the same university. From 1968 to 1971, he was

involved in research in molecular beam physics in Munich and in Peymenade, France.

In 1971, he joined Siemens AG in Munich and became involved in the development of telecommunications cable and related hardware. Since 1973, he has been working exclusively in optical fiber technology. In 1978, he joined Siecor Optical Cables, Inc. in the United States as VP of Engineering. In 1980, he became VP and General Manager for Optical Cable Manufacturing and Development. His key task was to build a new factory for fiber optic cables in Hickory, NC, and transfer technology from Siemens in Germany. In 1985, he became VP and Director of Research, Development & Engineering at Siecor Corporation. Dr. Bark is currently the Senior Vice President & Director of Research, Development & Engineering at Siecor

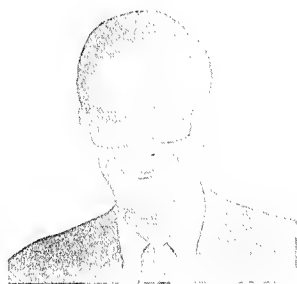
Corporation.

He has authored and coauthored numerous papers and made a number of key contributions in optical communications.



Harriet G. Cooke was born in Carmel, CA in 1966. She received her B.M.E. from Georgia Institute of Technology in 1991. At Georgia Tech. she was involved in NASA sponsored research and design of mechanical arms for lunar applications. Since 1991, she has been

employed at Siecor Corporation, where she has worked with profile extrusion and stranding. She is currently employed as a Process Development Engineer in the Research, Development and Engineering Department.



Christopher K. Eoll was born in Thunder Bay, Ont., Canada in 1940. He received a B.Sc. in physics and an M.Sc. in theoretical physics from Queen's University in Kingston, Ont., Canada in 1962 and 1964, respectively. In 1967, he was granted a Ph.D. in mathematical

physics by the University of Toronto in Toronto, Ont., Canada. Subsequently, he spent two years as a Postdoctoral Fellow at the University of Sussex in Brighton, England, and the International Centre for Theoretical Physics in Trieste, Italy.

From 1969 to 1977, he was employed by Canada Wire & Cable Ltd., where his final position was Product Development Manager for the Communications Products Div. He joined Superior Cable Corp. in 1977 as Technical Director. At present, Dr. Eoll holds the position of Scientist in the Research, Development and Engineering Department of Siecor Corporation. He has recently been focusing on aspects of optical cable design, materials properties and light transmission.



count cables and database management. He is currently employed as a Research Data Analyst in the Research, Development and Engineering Department.

Ronnie O. Livingston was born in Loris, SC in 1968. He received his B.S. in Physics and Applied Mathematics from Presbyterian College in 1990. Since 1992, he has been employed at Siecor Corporation, where he has worked with statistical analysis of high-fiber-



development since graduation in 1985, and has been with Siecor Corporation since 1991. His responsibilities include the development of UV-curable and related products for both the domestic and the Japanese markets. He currently is the Supervisor for UV Development in the Research, Development and Engineering Department. He has been awarded two patents and has two publications.

Gregory A. Lochkovic was born in Evansville, IN in 1962. He received a B.S.M.E. in 1985 from Purdue University and an M.S. in Manufacturing Systems from Clarkson University in 1993. He has worked in various areas of fiber optic cable product and process



as the Process Development Supervisor, Track III in the Research, Development and Engineering Department.

Warren W. McAlpine was born in Bennettsville, SC in 1960. He received his B.S.M.E. from Clemson University in 1983. Since 1984, he has been employed at Siecor Corporation, where he has worked with process and equipment development. He is currently employed



Frederick M. Sears was born in Houston, TX in 1952. He received S.B. and S.M. degrees from M.I.T. in 1975, in the five year honors program, and a Ph.D. degree from the University of California at Berkeley in 1980, all in mechanical engineering.

In 1980, he joined AT&T Bell Laboratories in Murray Hill, NJ, as a Member of Technical Staff, where he pursued research and development on optical fiber characterization techniques including fiber interferometry, single-polarization fibers, polarization-maintaining fibers and measurements, and optical time-domain reflectometry. In 1984, he transferred to the Atlanta Bell Laboratories location, pursuing optical fiber research and development on modal noise in single-mode lightguide systems, cutoff wavelength, characterization of polarization-maintaining fibers, interconnection of polarization-maintaining fibers, Fabry-Perot fiber interferometry and fiber-optic cable design.

Since 1990, he has been at Siecor Corporation in Hickory, NC, where he manages the Ultra-High-Fiber-Count Cable development. This project involves developing optical fiber cables with up to 4000 fibers for fiber-to-the-home in the Japanese market. He is Project Manager in the Research, Development & Engineering Department.

Dr. Sears is a member of the Optical Society of America, Pi Tau Sigma, and the Optical Fiber Communications subcommittee on Fibers, Cables, and Fiber Components.



Shami S. Sodhi was born in Amritsar, India in 1964. He received his M.S. in Electrical Engineering from Virginia Polytechnic Institute and State University in 1989. Since 1989 he has been with Siecor Corporation in Hickory and is presently Supervisor of

the Product Evaluation Lab in the Research, Development and Engineering Department. He is a member of IEEE.

Design and Development of High-Density Optical Fiber Slotted-Core Cable

Ryuichi MATSUOKA, Minoru SAITO, Masami HARA, Akihiro OTAKE

The Furukawa Electric Co., Ltd.
6, Yawata-Kaigandori, Ichihara, Chiba, 290, Japan

Abstract

We developed high count and high density optical fiber cable with slotted-core structure. To realize higher density than the conventional cables, we have tried to reduce the diameter of slotted rod as possible and used 16-fiber ribbon composed of downsized coated optical fibers. We investigated optimum structure of downsized coated optical fiber, 16-fiber ribbon and slotted rod, in order to achieve satisfactory transmission and mechanical characteristics.

1. Introduction

High count and high density optical fiber cable must be developed to construct optical subscriber networks in future, which expand optical fiber cables and various services to all users. Therefore, various cable structures have been proposed and investigated to realize higher density cable.⁽¹⁾

Slotted-core structure cable has been widely used at present and is one of the most suitable for high density optical fiber cable. We have tried to achieve higher density of slotted-core cable.

In order to realize higher density than that of conventional slotted-core ribbon cable, we have downsized each components in the cable: coated optical fiber, optical fiber ribbon, and slotted rod.

Coated optical fiber had been downsized to 180 μ m in diameter by reducing coating thickness. Thickness of 16-fiber ribbon composed of downsized coated optical fibers had been reduced to 0.20–0.25mm. Diameter of slotted rod had been downsized by minimizing width between slots.

However, downsizing these components causes the deterioration of mechanical strength or optical transmission characteristics of them. So we investigated the effect of structure of coated optical fiber, optical fiber ribbon and slotted rod on the characteristics, for instance, loss increase of optical fiber by the lateral pressure. And we found the optimum structure which realize high density and satisfy the characteristics.

In this paper, we present the design and performance of a developed 800-fiber single slotted-core cable, which realized approximately three times as high-density as conventional slotted-core ribbon cable.

2. Downsized Coated Optical Fiber

Downsizing coated optical fiber has been severally studied in order to realize high density optical fiber cable.⁽²⁾⁽³⁾ We manufactured and investigated coated single mode optical fiber 180 μ m in diameter as shown in Figure 1: Hard coating mainly prevents glass fiber cracking and breaking by external force, while soft coating performs as a cushion and reduces microbending caused by lateral pressure.

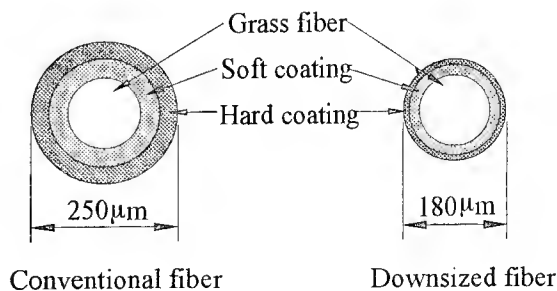


Figure 1 Downsized Optical Fiber

Major problems of downsized coated optical fibers are the deterioration of their mechanical strength and their lateral pressure characteristics. Hard coating should be thick and hard for the mechanical strength, but on the other hand, soft coating should be kept sufficiently to improve the lateral pressure characteristics. Therefore, their two layer coating structure should be optimized.

We mainly investigated optimum two layer coating structure to improve the lateral pressure characteristics, which should seriously affect the characteristics of optical fiber cable. In order to improve the lateral pressure characteristics, we have studied the effects of coating structure by multi-layer winding drum microbending testing.⁽³⁾ The attenuation increase of these experiments were analyzed by multi-regression analysis with the parameters expressing buffer effect and stiffness of the coating structure, and we have introduced a regression formula of microbending loss. For example, Figure 2 shows a relation between R_p/R_s (a ratio of soft coating diameter to hard coating diameter) and attenuation increase calculated by this formula, when outer diameter is 180 μm .

In result, we have found optimum coating structure and manufactured the downsized coated optical fibers having superior lateral pressure characteristics.

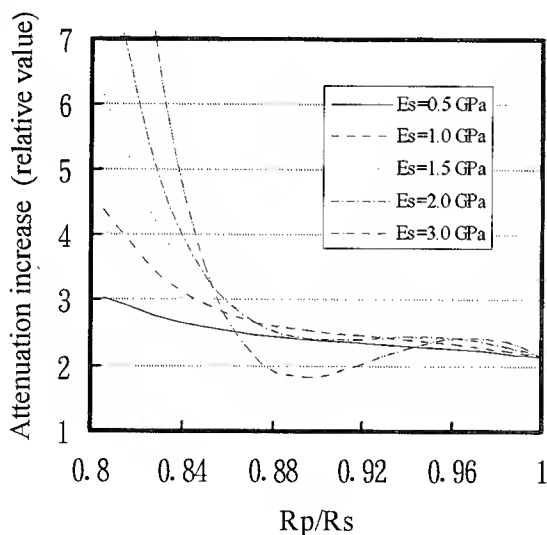


Figure 2 Relation between R_p/R_s and attenuation increase calculated by a regression formula of microbending loss
(E_s : Young's modulus of hard coating)

3. 16-fiber Ribbon

Higher count fiber ribbon should be effective for increasing fiber density, and furthermore, their coating thickness should be minimized. We developed 16-fiber ribbon composed of downsized coated optical fibers mentioned above. Figure 3 shows the structure of conventional 8-fiber ribbon and developed 16-fiber ribbon.

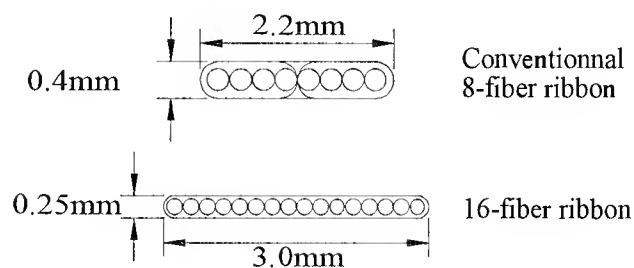


Figure 3 Optical Fiber Ribbon

The reduction of thickness of ribbon, however, causes protection of the fiber to be worse, against external force during manufacturing and installing the optical cable. Hard ribbon coating should be advantageous for the protection of optical fiber, but the lateral pressure characteristics must be also taken into consideration. So, we have analyzed lateral pressure characteristics of the ribbon, and found optimum structure.⁽⁴⁾

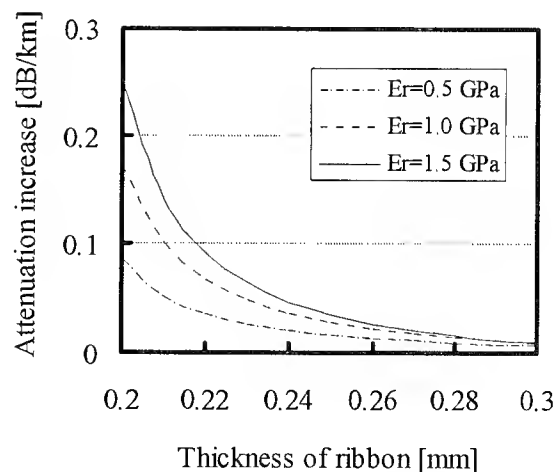


Figure 4 Relation between thickness of ribbon and calculated attenuation increase
(E_r : Young's modulus of ribbon coating)

We estimated lateral pressure characteristics of 16-fiber ribbons by multi-layer winding drum microbending testing; 16-fiber ribbons were wound around a plastic bobbin at tension of 2N and 6N. We obtained the optimum regression formula of bobbin winding attenuation increase using parameter related with stiffness of fiber ribbon and buffer effect of ribbon coating, by the same way as downsized coated optical fibers. Figure 4 shows the relation between ribbon thickness and attenuation increase calculated by this formula. From this figure, we found that ribbon thickness should be more than 0.23mm at least to satisfy the lateral pressure characteristics.

4. Slotted Rod

We had tried to reduce a diameter of slotted rod for high density cable. Slotted rod, which we discuss in this paper, has five helical slots which contain ten stacked 16-fiber ribbons.

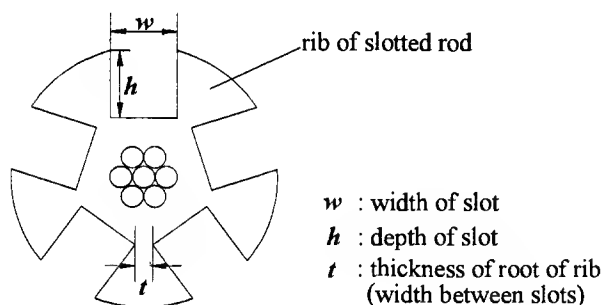


Figure 5 Structure of slotted rod

As shown in Figure 5, the diameter of slotted rod is dependent on width w and depth h of slots and thickness of root of rib t , or, say in other word, width between slots. Width and depth of slots should be determined by the dimension of stacked ribbon fibers so that the thickness t should be minimized for downsizing the cable (Figure 6).

However, the endurance of the slotted rod against external force would be worse as the thickness t becomes smaller. We have studied the effects of the thickness t and the elasticity of material, on the endurance of the slotted rod.

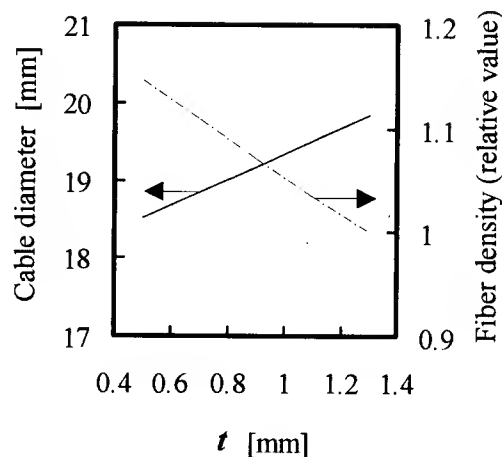


Figure 6 Diameter and fiber density of cable dependent on thickness of root of rib

We evaluated the endurance of slotted rod as follows. Firstly, we evaluated endurance of the rib of slotted rods by measuring forces to break down the rib on equal conditions. Figure 7 shows the endurance of rib correlated with t . The endurance was nearly proportional to t in case elasticity of material was equal. Figure 8 shows the endurance roughly proportional to modulus of elasticity of material.

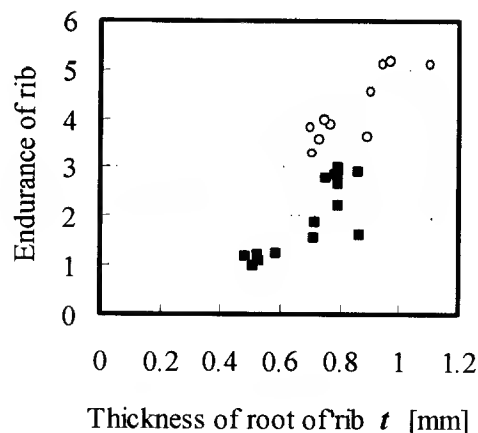


Figure 7 Endurance of rib correlated with the thickness of root of rib. (a ratio of modulus of elasticity : $\bigcirc / \blacksquare = 1.3$)

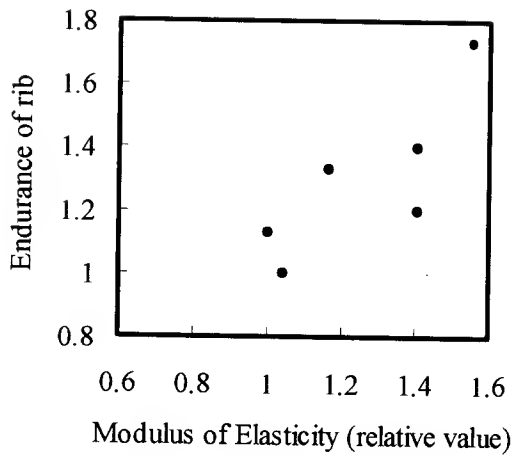


Figure 8 Endurance of rib correlated with elasticity of material

Secondly, we examined the ability of slotted rods to withstand crushing. The slotted rod was crushed between two flat steel base plates, and the plates applied the crushing force uniformly upon a 100mm length. We measured the reduction of slotted rod diameter toward the crushing force applied.

Table 1 shows the structure of slotted rods which we examined the crushing test. Figure 9 and Figure 10 show the reduction of slotted rod diameter dependent on the crushing force applied. At relatively low crushing forces, reductions were directly proportional to crushing force, and didn't depend on t . Their proportions seem to be determined by elasticity of material. But over a certain crushing force, slotted rod began to crush rapidly, that was caused by breakdown of rib of slotted rod. Their breakdowns depend on t and elasticity of material as mentioned above, and as shown in Figure 9 and Figure 10. These breakdowns of ribs were not recovered as it was before, and they affect seriously the characteristics of optical fiber ribbon stacked in slots.

As a result, slotted rod for high density optical fiber cable should be designed taking into consideration that structure of slotted rod effects on the endurance.

Table 1 Structure of Sample

Sample	t [mm]	Modulus of Elasticity (relative value)
A	0.7	1
B	0.9	1
C	1.1	1
D	0.7	1.3
E	0.9	1.3

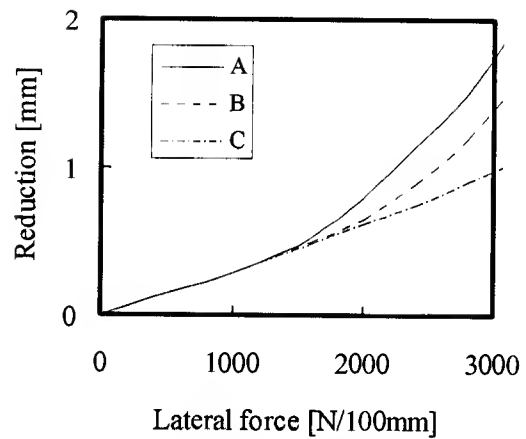


Figure 9 Crushing test of Slotted rod (Sample A, B, C)

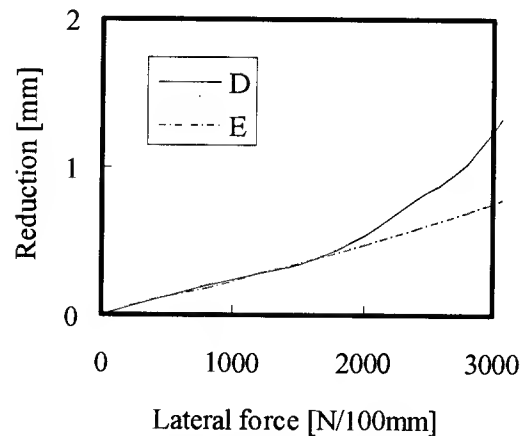


Figure 10 Crushing test of Slotted rod (Sample D, E)

5. Cable structure

Figure 11 shows the structure of our trial cable compared with the conventional 1000-fiber slotted-core cable. Our trial cable is the single slotted rod structure which has five helical slots containing ten stacked 16-fiber ribbon; it can contain 800 fibers. Each components in the cable: coated optical fiber, optical fiber ribbon, and slotted rod, have been downsized and their structure have been optimized according to the condition as mentioned above. In result, our trial cable was approximately three and a half times as high-density as conventional 1000-fiber slotted-core cable.

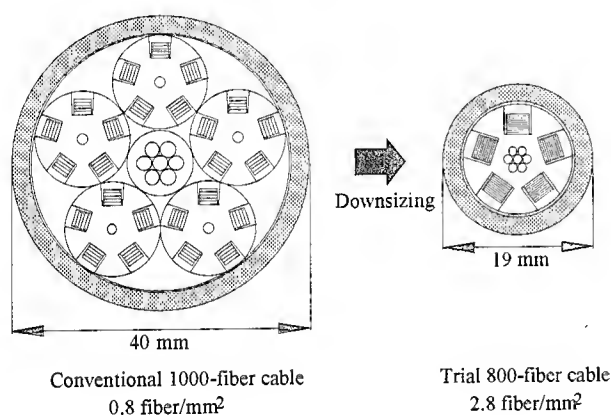


Figure 11 Structure of trial cable compared with the conventional slotted-core cable

6. Characteristics of Cable

Figure 12 shows the change of optical attenuation during cable manufacturing process. Attenuation was almost stable at both 1.3 μ m and 1.55 μ m wavelength in downsized optical fiber, 16-fiber ribbon and Slotted-Core cable.

The mechanical performances and temperature characteristics of this cable were tested and we found no problems as shown in Table 2.

7. Conclusion

In order to realize high density slotted-core optical fiber cable, it is necessary to downsize each components in the cable. We optimized the structure of the components, that is, downsized coated optical fiber, 16-

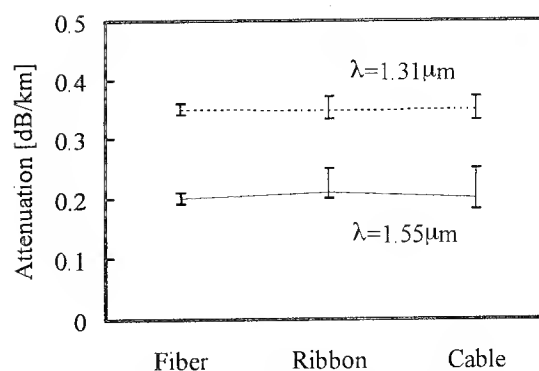


Figure 12 Change of attenuation during cable manufacturing process

Table 2 Mechanical performances of trial cable

Test items	Conditions	Loss increase
Temperature Characteristics	from -20 to +60°C (off the reel)	< 0.1dB/km
Bending	bending at 300mm radius	< 0.1dB
Crushing	crushing force 2000N/100mm	no loss increase
Squeezing	0.2% elongation 600mm radius	< 0.1dB

fiber ribbon and slotted rod, to prevent the deterioration of their lateral pressure characteristics, which should seriously affect the optical transmission characteristics of cable.

In result, we realized slotted-core optical fiber cable which was approximately three and a half times as high-density as conventional cable.

References

1. S. Tomita *et al.*, "Ultra High-Density Optical Fiber Cable with Thin Coated Fibers and Multi-Fiber Connectors", 42nd IWCS, 1993.
2. W. Katsurashima *et al.*, "Microbending Loss of Coating Single Mode Fiber for Ultra-High-Count Cable", 41st IWCS, 1992.
3. M. Hara *et al.*, "Design of downsized coated optical fibers to minimize microbending loss", 41st IWCS, 1992.
4. M. Saito *et al.*, "16-fiber ribbon for ultra-high-density and high-count optical fiber cable", 42nd IWCS, 1993.



Ryuichi MATSUOKA

The Furukawa Electric
Co., Ltd.

6, Yawata-Kaigandori,
Ichihara, Chiba, 290, Japan

Mr. Matsuoka received his M.E. degree in electronics from Osaka University in 1991. He joined The Furukawa Electric Co., Ltd. and has been engaged in research and development of optical fiber cable. He is now a research engineer of optical fiber transmission research department, opto-technology laboratory.



Masami HARA

The Furukawa Electric
Co., Ltd.

6, Yawata-Kaigandori,
Ichihara, Chiba, 290, Japan

Mr. Hara received his M.E. degree in Physics from Osaka University in 1987. He joined The Furukawa Electric Co., Ltd. and has been engaged in research and development of optical fiber cable. He is now a research engineer of optical fiber transmission research department, opto-technology laboratory.



Minoru SAITO

The Furukawa Electric
Co., Ltd.

6, Yawata-Kaigandori,
Ichihara, Chiba, 290, Japan

Mr. Saito received his M.E. degree in chemistry from Kyushu University in 1992. He joined The Furukawa Electric Co., Ltd. and has been engaged in research and development of optical fiber cable. He is now a research engineer of optical fiber transmission research department, opto-technology laboratory.



Akihiro OTAKE

The Furukawa Electric
Co., Ltd.

6, Yawata-Kaigandori,
Ichihara, Chiba, 290, Japan

Mr. Otake graduated from Tohoku University in 1974. He joined The Furukawa Electric Co., Ltd. and has been engaged in research and development of optical fiber cables and those accessories. He is now the chief of optical fiber transmission research department, opto-technology laboratory.

Ultra High-Density Optical Fiber Cable with Thin Coated Multi-Fiber Ribbons for Subscriber Networks

Naoki Okada, Kohichiro Watanabe, Kazunaga Kobayashi, Matsuhiro Miyamoto

Fujikura, Ltd. Telecommunication Cable Section Opt-electronics Laboratory

1440 Mutuzaki, Sakura, Chiba, 285, Japan

Abstract

Ultra high-count and high-density optical fiber cables for the future subscriber optical networks have been studied. In order to realize new cables above-mentioned, we have tried following three methods; reducing fiber diameter, increasing fiber-ribbon count, optimization of cable structure. In this study, the thin coated 16-fiber ribbons are adopted, from the view point of not only increasing fiber packing density, but also reducing fiber splicing time to construct the networks and compatibility with the conventional ribbon structures such as 4 or 8-fiber ribbons. We have investigated three types of new cable structures of different concepts; U-groove cable, H-groove cable, and large U-groove cable. Moreover 4000-fiber structure cable have been manufactured actually. It was confirmed that the new high-count and high-density cables with sufficient characteristics can be obtained successfully.

1. Introduction

Aiming at implementing a Fiber-to-Home (FTTH) system [1], studies have been made of a ultra-high-density, high-fiber-count optical cable containing about 4,000 fibers [2,3]. In order to build very extensive fiber-optic subscriber networks economically, it is important to reduce cable diameter and weight, and it is strongly

desired to increase the fiber-packing density of cable. For this, investigations have lately been carried on to reduce fiber or fiber-ribbon diameter by decreasing fiber coating thickness and to increase the fiber count with consideration for ease of splicing [4,5]. Though intended primarily for protection of silica fiber, the coating on the fiber has an important function of reducing transmission loss (microbending loss) that is caused when lateral pressure is applied to fibers during cabling. Therefore, reducing fiber or fiber-ribbon diameter by decreasing fiber coating thickness is very effective for packing fibers at higher densities, but is expected to constitute a factor that makes cabling difficult. Structural design of cable is also considered important. In this paper, we will report the results obtained by investigating various cable structures of different design concepts chiefly by using thin coated 16-fiber ribbons on which we have made investigations so far.

2. Structural Design of Cable

In order to pack fibers in fiber-optic cables at higher densities, the three following methods are effective:

a) Reducing fiber diameter

This method is very effective for higher-density packing of fibers. In this study, the fiber diameter was reduced by

decreasing the thickness of the primary and secondary layers of fiber coating with the silica fiber outside diameter of 125 μ m unchanged for matching with existing fibers. When designing a coating structure, it would be necessary to take into account the microbending loss that will be caused by application of lateral pressure.

b) Increasing fiber-ribbon count

Increasing fiber-ribbon count is expected not only to contribute to higher-density packing of fibers, but also to facilitate ease of splicing. Particularly for high-fiber-count cables, this method is considered beneficial to shortening of splicing time. In this study, a 16-fiber ribbon structure was adopted.

c) Optimization of cable structure

The results of investigating various cable structures of different design concepts by using the thin coated 16-fiber ribbons on which we have made investigations so far will be described later.

3. Fiber-Ribbon Structure

A thin coated 16-fiber ribbon was obtained in the following ways. That is, 16 fibers coated to 180 μ m in outside diameter are arranged in parallel and entirely coated with a UV resin. The section of the thin coated fiber ribbon is shown in Fig.1.

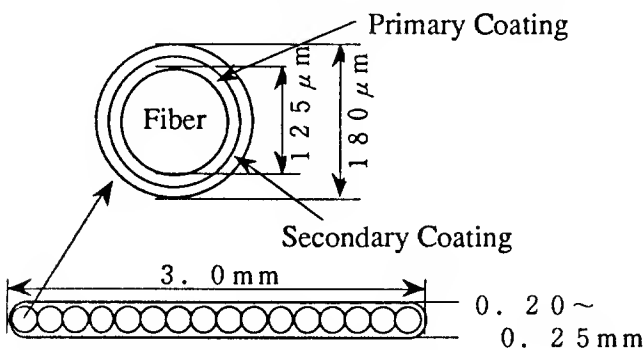


Fig.1 Thin Coated 16 Fiber Ribbons

The evaluation results from a tension winding test shown in Fig.2 have been used so far as a guide to the structural design of fiber coating that is high in resistance to lateral pressure.

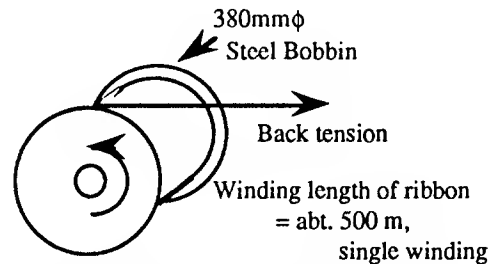


Fig.2 Tension winding test method

As a result, it has been found possible to estimate resistance to lateral pressure from the coefficient that determines coating structure (given in Equation (1) "coating structure coefficient") [6].

$$C_{\text{mech}} = \frac{k_s^2}{D_0^{0.375} H_0^{0.625}} \quad [\text{Eq.1}]$$

where $\left\{ \begin{array}{l} k_s : \text{spring constant} \\ D_0 : \text{resistance to deformation of coating} \\ H_0 : \text{flexural rigidity of coating secondary layer} \end{array} \right.$

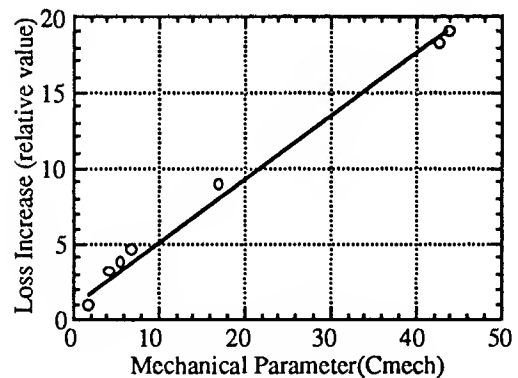


Fig.3 Tension winding characteristic of small-diameter fiber ribbon

The relation between this coefficient and the microbending loss at tension winding is shown in Fig.3. From this graph, it can be seen that the resistance to lateral

pressure varies greatly with the type of coating structure. Moreover, the coating structure for a thin coated fiber ribbon, whose resistance to lateral pressure is equal to or higher than that of existing fiber ribbons, has been established.

4. Cable Structure

Fig.4 shows conventional 1000-fiber cable. This cable is composed of 8-fiber ribbons and multi slotted rods. This cable structure is not suitable for high-count and high-density cable. If we try 4000-fiber cable with 8-fiber ribbons and multi slotted rods, the cable diameter will be about 70mm ϕ [2].

We have investigated three types of cable structures of different concepts to optimize the cable structure with thin coated 16-fiber ribbons. Trial cables were made using the afore-mentioned thin coated 16-fiber ribbons having a high resistance to lateral pressure, and their characteristics were examined. The fibers used here were of single-mode type: MFD = $9.5 \pm 0.5 \mu\text{m}$; $\lambda_c = 1.24$ to $1.28 \mu\text{m}$.

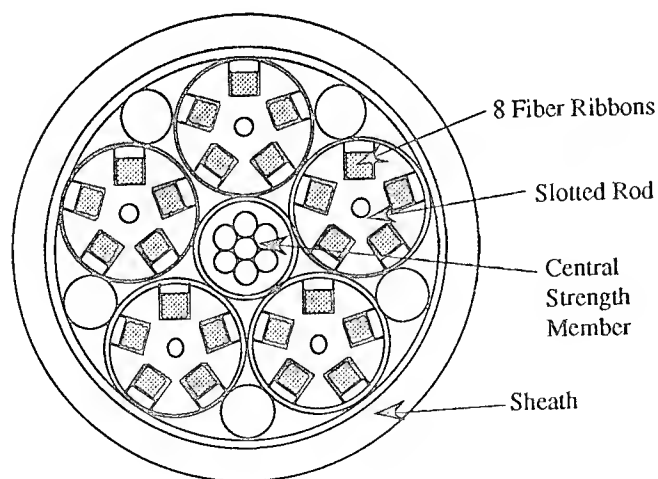


Fig.4 Cross Sectional View of
Conventional 1000-Fiber Cable

4-1. U-groove type cable

As shown in Fig.5, U-grooves are arranged around central tension members and 10 each thin coated 16-fiber ribbons packed in the grooves. This structure is designed to reduce the space which is not participated to accommodate the fibers. A ultra-high-fiber-count cable is obtained by multi-stranding of the U-groove ribbons. This proves that higher-density packing of fibers is possible. We also have tried to manufacture 4000-fiber structure cable as shown in Fig.5-b.

4-2. H-groove type cable

The cable structure is shown in Fig.6. As seen from the figure, 5 each thin coated 16-fiber ribbons are packed as units in H-grooves each consisting of two spiral grooves. The structure is the units-stranded type in which the H-groove type units are stranded around central tension members. Use of H-grooves enables minimization of the central area as compared with conventional slotted rods as shown in Fig.4, making it possible to obtain units that are excellent in fiber-packing density. The 4000-fiber structure trial cable has been manufactured as shown in Fig.6-b.

4-3. Large U-groove type cable

The cable structure is shown in Fig.7. As seen from the figure, 15 each thin coated 16-fiber ribbons are twisted and packed in large U-grooves loosely. The loose structure is used to minimize the stress applied to the thin coated 16-fiber ribbons. We designed this cable which has very thin coated fiber ribbons and 15 each fiber ribbons in a large U-groove to increase the fiber density making up for the loose structure. The trial cable was investigated for two types: air core type and jelly-filled type.

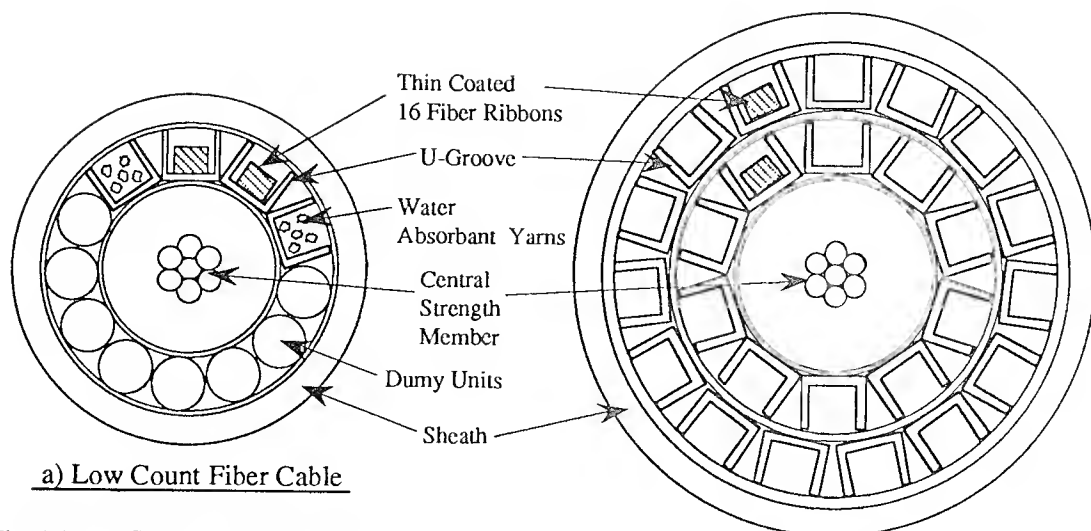


Fig.5 Cross Sectional View of Prototype U-Groove Cable

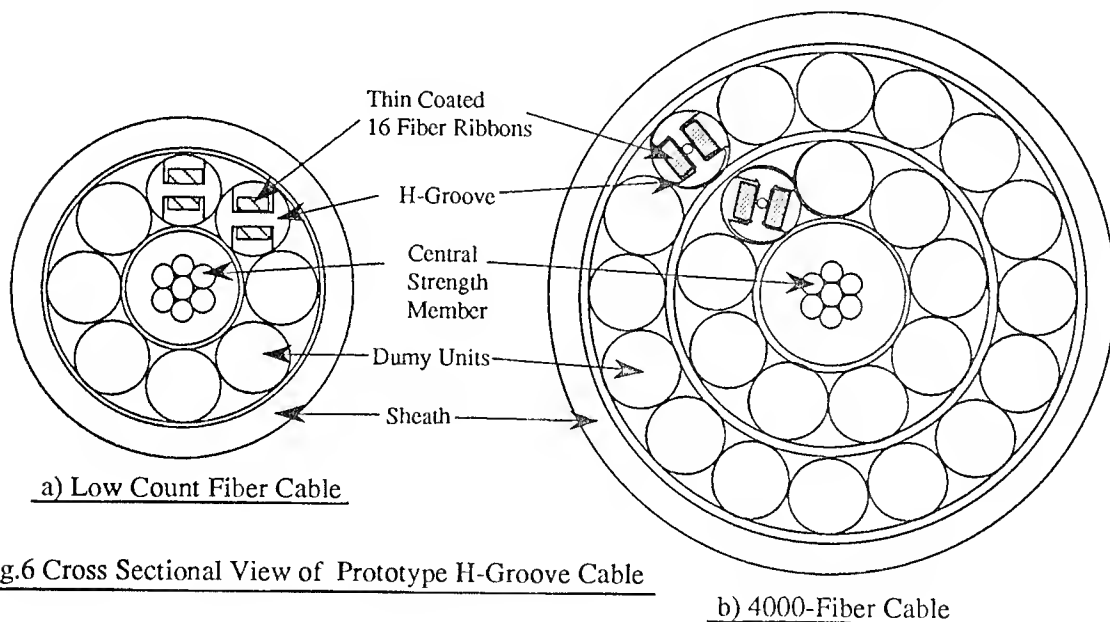


Fig.6 Cross Sectional View of Prototype H-Groove Cable

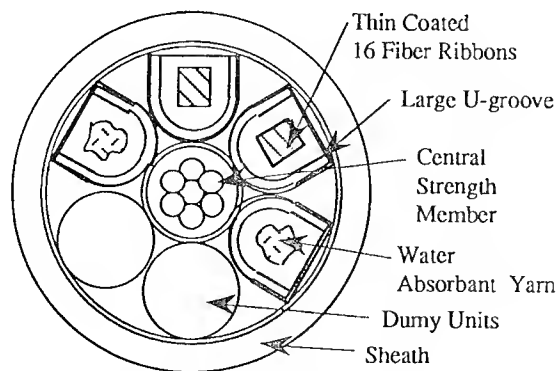


Fig.7 Cross Sectional View of Prototype Large U-Groove Cable

5. Cable Characteristics

The characteristics of the above-mentioned three types of trial cables were evaluated. The results are as follows:

5-1. In-process change in transmission loss

The trial cables were investigated for changes in transmission loss between the stages of the manufacturing process. The results are given in Fig.8. The cables showed no change in transmission loss, so they were all confirmed to be able to be satisfactorily manufactured.

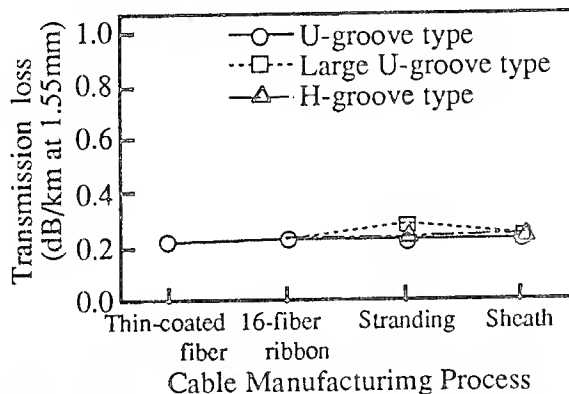


Fig. 8 In-process change in transmission loss

5-2. Tensile characteristic

Tensile tests were made by applying tension up to 1,000 kgf (equivalent to 0.2% cable elongation). Changes in transmission loss and fiber strain caused by application of tensile force were measured. The changes in transmission loss were very small for all of the three types of cables. The changes in fiber strain are shown in Fig.9. As for fiber strain, only the large U-type structure shows a considerably small elongation of the fibers as compared with that of the cable. Therefore, the fibers are considered to be packed loosely, with excess length, in the cable.

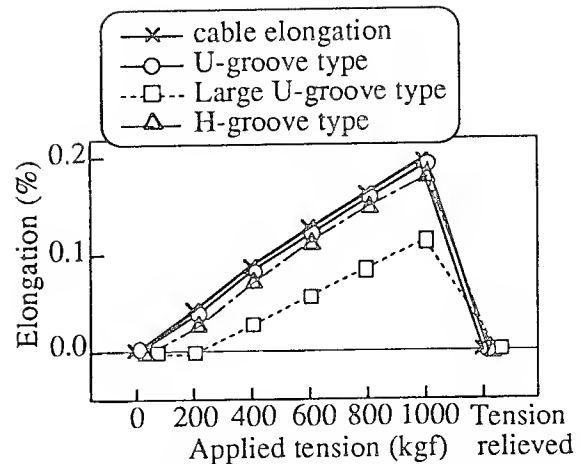


Fig. 9 Tensile characteristic (fiber strain)

5-3. Temperature characteristic

Changes in transmission loss within the temperature limits of -30 to +60°C were investigated with the cable wound on a reel. The results are given in Fig.10. Virtually no changes in transmission loss were observed at temperatures of -30 to +60 °C

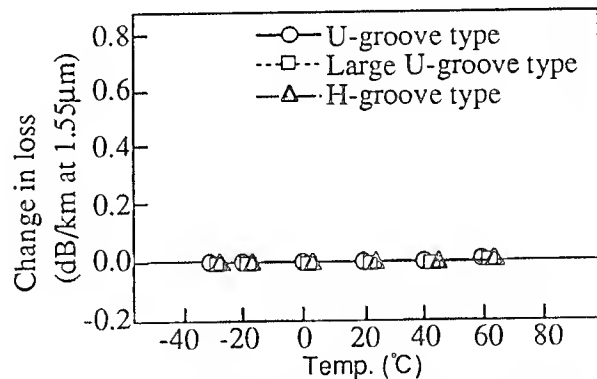


Fig. 10 Transmission loss Vs. temperature

5-4. Other mechanical tests

The cables were evaluated for bending, resistance to lateral pressure, and squeezing characteristics. The test conditions and results are given in Table 1. All of the cables exhibited good results.

Table 1 Mechanical test results

Test items	Test conditions	Results
Bending	400 mm ϕ $\pm 90^\circ$ bending	No change in loss
Lateral pressure	300 kgf/100 mm	No change in loss
Tensile	1000 kgf	No change in loss
Squeezing	800 kgf/600 mmR-roller	No change in loss

5-5. Water blocking characteristic

The small size trial cables are made capable of water blocking with a water swellable tape or jelly compound. The U-groove type and the H-groove type cable have the water absorbent tape to get water blocking characteristics. As for the large U-groove type cable, the air core type and the jelly-filled type whose large U-grooves were filled with jelly compound were investigated. The water blocking test as shown in Fig.11 was performed, assuming water infiltration from the cable end. The results are given in Table 2. It can be seen from the table that the cables show excellent water blocking performance without the large U-groove type cable not jelly filled.

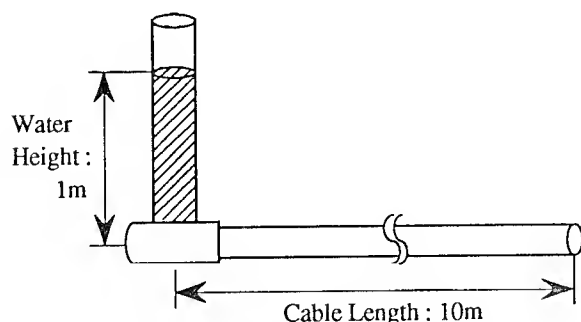


Fig.11 Water Blocking Test Set Up

Table 2 Water blocking test results

Cables		Test results
U-groove type		No leak
H-groove type		No leak
Large U-groove type	Jelly	No leak
	Non-jelly	N.G.

* Water leak at the cable end was examined 24 hours after water injection.

6. Comparison of each cable structure

As mentioned above, it was verified that the newly designed high-count and high-density cable shows good cable characteristics. Here, the four types of cable structures containing conventional multi slotted rods type cable were laboratory designed for applications for packing more than 4,000 fibers per cable. The results shows Table 3.

Multi slotted rods type structure is not so good for ultra-high-count cable such as 4000-fiber cable, because the cable diameter will be too large to install the cable into conventional ducts.

U-groove type structure is one of the best cable structures to pack ultra-high-count fibers. This fiber density highest in these cables designed. However, stranding process will be complex because of large number of stranding elements such as grooves, ribbons forming each layer.

As for H-groove structure, fiber packing density may be decreased a little compared with U-groove type structure. However, the cable is advantageous in that individual units are easy to handle at the time of branching. Moreover, the manufacturing process is similar to conventional slotted rods type cable, therefore this H-groove type cable can be manufactured easily using ordinary stranding equipment.

Large U-groove type structure is useful to protect the thin coated multi fiber

Table 3 Comparison of each cable structure

Cables		Fiber count	Cable dia.	Fiber density	Waterproof
Conventional Multi slotted rods type		4000-fiber	70mm ϕ	1.1 fibers/mm ²	Good
U-groove type		4000-fiber	42mm ϕ	2.9 fibers/mm ²	Good
H-groove type		4000-fiber	47mm ϕ	2.3 fibers/mm ²	Good
Large U-groove type	Jelly	4800-fiber	45mm ϕ	3.0 fibers/mm ²	Good
	Non-jelly	4800-fiber	45mm ϕ	3.0 fibers/mm ²	N.G.

* Multi slotted type has ordinarily 8-fiber ribbons

* New cable structures have thin coated 16-fiber ribbons

ribbons. But, the jelly compound will be must filled in the cable to obtain good water blocking characteristics. The water blocking by wrapping water swellable tape seems difficult in this large U-groove structure.

7. Conclusion

We investigated cabling of 16-fiber ribbons using thin coated 180 μ m fibers. Trial cables were made using three types of structures: the U-groove type structure, which is considered as one of the cable structures most suitable for higher-density packing of fibers; the large U-groove type structure designed to minimize the stress applied to fiber ribbons; and the H-groove type structure of the unit-stranded type with the per-unit fiber density increased by making improvement to the existing multi-slot type cable. The characteristics of the trial cables were evaluated. As a result, it was verified that all of them possess satisfactory initial characteristics. By investigating a cable containing about 4,000 fibers, we have found it possible to expect to attain a drastic increase in fiber-packing density as compared with the existing multi-slot type 1,000-fiber cable.

References

- [1] T. Uenoya, "The Optical Fiber Loop 21 Plan", OEC, 1990
- [2] T. Tomita et al., "Preliminary Research into Ultra High Density and High Count Optical Fiber Cables", 40th IWCS, 1991
- [3] T. Tomita et al., "Ultra High-Density Optical Fiber Cable with Thin Coated Fibers and Multi-Fiber Connectors", 42th IWCS, 1993
- [4] K. Kobayashi et al., "Study of Microbending Loss in Thin Coated Fibers and Fiber Ribbons", 42th IWCS, 1993
- [5] M. Miyamoto et al., "Low Microbend Loss Coating Design for High Density Optical Cable", OEC'94, Technical Digest, July 1994
- [6] J. Baldauf et al., "Relationship of Mechanical Characteristics of Dual Coated Single Mode Optical Fibers and Microbending Loss", IEICE TRANS. COMMUN., VOL.E76-B, NO.4 APRIL 1993

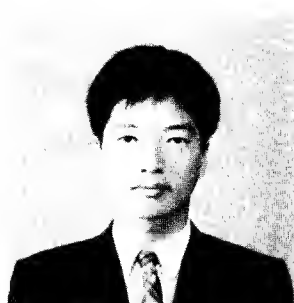


Naoki Okada

Opto-Electronics
Laboratory
Fujikura Ltd.

1440, Mutsuzaki,
Sakura-shi, Chiba,
285, Japan

Naoki Okada was born in 1964. He joined Fujikura Ltd. after his graduation from Chiba University with a B.E. degree in 1986 and has been engaged in research and development of optical fiber cables. He is now an engineer in the Telecommunication Cable Section and a member of the IEICE of Japan.



Kazunaga Kobayashi

Opto-Electronics
Laboratory
Fujikura Ltd.

1440, Mutsuzaki,
Sakura-shi, Chiba,
285, Japan

Kazunaga Kobayashi was born in 1961. He joined Fujikura Ltd. after his graduation from Gunma University with a M.E. degree in 1985 and has been engaged in research and development of optical fibers. He is now an engineer in the Telecommunication Cable Material Section and a member of the IEICE of Japan.



Kohichiro Watanabe

Opto-Electronics
Laboratory
Fujikura Ltd.

1440, Mutsuzaki,
Sakura-shi, Chiba,
285, Japan

Kohichiro Watanabe was born in 1959. He received a B.E. degree in electrical engineering from Tohoku University in 1982. Since joining Fujikura, Ltd. in 1988, he has worked on the development of optical fiber cables. He is currently employed in the Telecommunications Cable Section of the Opto-electronics laboratory.



Matsuhiro Miyamoto

Opto-Electronics
Laboratory
Fujikura Ltd.

1440, Mutsuzaki,
Sakura-shi, Chiba,
285, Japan

Matsuhiro Miyamoto was born in 1953. He graduated from Nagoya Institute of Technology with a B.E. degree of electrical engineering. He joined Fujikura Ltd. after his graduation from Tokyo Institute of Technology with a M.S. degree in 1978 and has been engaged in research and development of optical fiber and optical fiber cables. He is now a manager of the optical fiber cable section.

Ultra-High-Count Optical Fiber Cable using Single-Helical-Groove Unit

W. Katsurashima, Y. Kitayama, S. Tanaka

Sumitomo Electric Industries, Ltd.

Abstract

We have developed ultra-high-count optical fiber cable that can accommodate up to 4000 fibers. Downsized coated fibers were adopted to minimize cable size. New unit structure incorporates stacked 16-fiber ribbons in a slot formed on a plastic rod without jelly filling compound. Manufactured test samples indicated good transmission and mechanical properties. We also investigated SZ stranding (ROL) of the units around the central member and it showed excellent performances as well.

1. Introduction

Cables have their life span and they must be replaced continually. Now copper pair lines are widely spread around all over Japan. If these cables are replaced by optical fiber cables, it leads to FTTH by single star network that is the most flexible construction to any further integrated services in future. This subscriber network consists of cables incorporating up to 3600 copper pairs (Fig.1), so several thousands of optical fibers must be included in a cable for replacement. We are now manufacturing up to 1000-fiber count cables for commercial use, however have no menus on such high-fiber-count cables. Novel development is requested.

Studies on optical cables that accommodate 4000 fibers are prevailed from 1991(1)(2). Mr. Tomita in NTT suggested in his paper that reducing coating diameter of optical fiber is effective to minimize cable size. However downsized coated fiber inevitably induces the deterioration on microbending durability against lateral forces(3). So we concluded that preferably few stresses ought to be applied on downsized coated fibers and have studied new cable structure

accommodating stacked fiber ribbon units loosely without jelly filling compound.

Our single-helical groove unit accommodates up to ten fiber ribbons, so the assembling machine requires only ten ribbon supplying systems. By simply assembling these units around central member we can get optical fiber cable of fiber count by multiples of numbers of fibers in a unit. This cable can take two layer structure of units and 4000-fiber count cable is realized by assembling 9 units in inner layer and 16 units in outer layer using 160-fiber units. Cable diameter was 48 mm when we used 200 μ m fiber in diameter and would be 46 mm when 180 μ m fiber.

We also studied SZ stranding (ROL) of the units and experimental cable indicated good transmission loss.

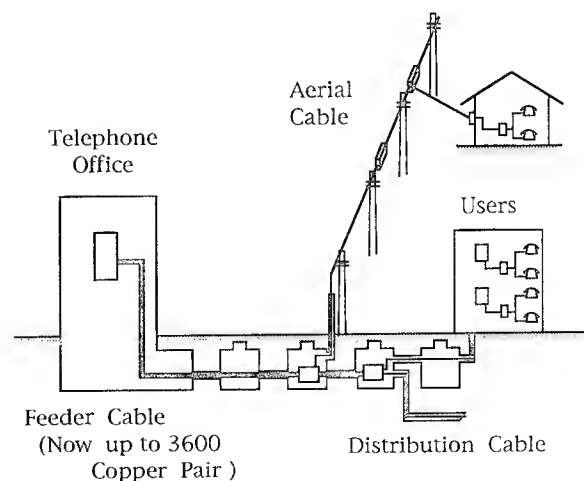


Fig. 1 Subscriber Network

2. Design concept

2.1 Downsized Coated Fiber

Downsizing coated fiber is effective for minimize the cable diameter and we must remain glass fiber diameter of $125\text{ }\mu\text{m}$ for the compatibility with other optical fiber components. So downsizing fiber diameter should be realized by reducing coating thickness. Fig.2 is the example of downsized coated fiber.

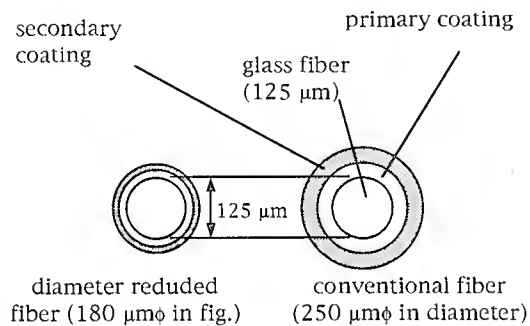


Fig. 2 Downsized coated fiber (left) and conventional 250 μm fiber (right)

Fiber coating is not only for protecting glass fiber from the abrasion but also has important function of restraining microbending loss increase(3)(5). Reducing coating thickness directly causes the deterioration of fiber against microbending. Fig.4 is the test result for long span winding test(Fig.3). Fibers with various coated diameter were wound around the reel with sand-paper and loss deviation were measured. Loss increases are adjusted by PML(presumed microbending loss) method(2) and compared with the data of conventional coated 250 μm fiber. Calculated PML is 3.1 times greater in 200 μm fiber to that of 250 μm fiber, 3.7 times in 180 μm fiber, 5.2 times in 170 μm fiber and 8.7 times in 160 μm fiber. Microbending loss is ranked according to the coating diameter of fiber and it shows the close relationship between coating thickness and the durability against microbending loss.

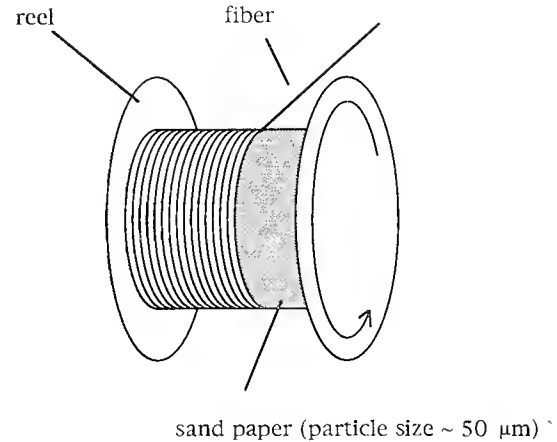


Fig. 3 long span wingind test

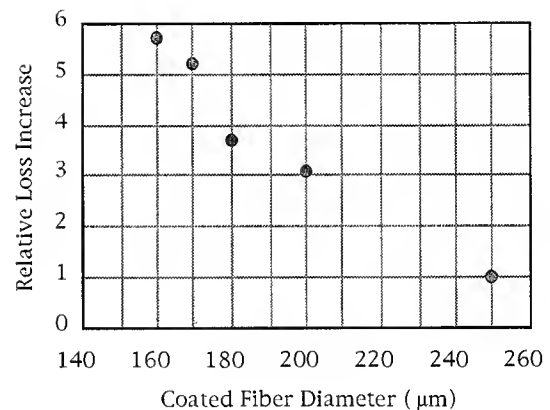


Fig. 4 Loss increase caused by long span winding test

2.2 Cable

We have developed and are manufacturing Tape-Slot type (ribbon units in slots on rod) optical cable for our commercial products (Fig.5). In this structure optical ribbon units must be accommodated tightly in slots so that the arrangements of each ribbon may not be disturbed by the undesirable movement of each ribbon and the cable performance is kept proper in any conditions. However this tight structure inevitably induces lateral forces against ribbon unit and the downsized coated fiber could suffer the microbending loss increase caused by these stresses. So we decided preferably few stress ought to be applied on downsized coated fibers.

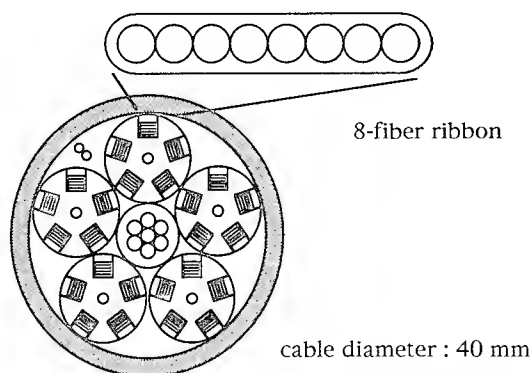


Fig. 5 Tape-Slot type optical cable
(1000-fiber cable in fig.)

3. Helical Single Groove Unit Cable

3.1 Cable Structure

We adopted 16-fiber ribbon considering the fiber density in a cable and the workability on connecting. Fiber diameters in our cables are 180 μm (4) and 200 μm .

Fig. 6 indicates the cross sectional view of single groove unit cable. Ten 16-fiber ribbons are twisted and inserted into a helical groove on a plastic rod accordingly and wrapping is formed. We wrapped the water swellable tape on a stranded core and didn't used jelly filling compound. The fiber strain in the cable can be reduced, if the stranded 16-fiber ribbons are loosely accommodated in the groove with an adequate clearance so that its center position can coincide with that of the groove unit. Fibers may touch the wall of the groove, but not be strongly suppressed. By this configuration the stress free cable can be realized with this structure and is suitable for downsized coated fibers.

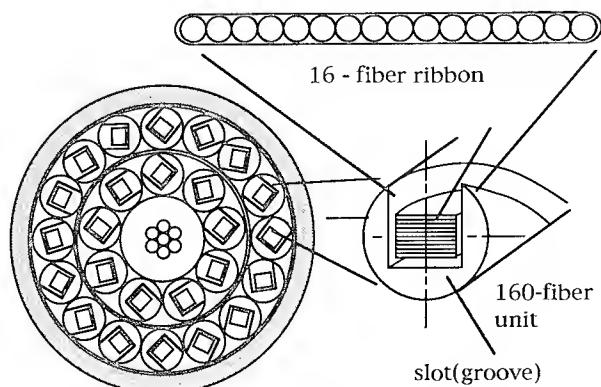


Fig. 6 single-helical-groove unit cable

3.2 Spacer

Diameter of the spacer D is expressed by

$$D = d \sqrt{(d^2 + w^2 - c^2) / (d^2 - c^2)} + c \quad \dots (1)$$

where d is the depth of slot, w is the width and c is the thickness of the edge (Fig. 7). Stress free condition is realized by the relationship

$$(D - 2c)^2 > (nt)^2 + w^2 \quad \dots (2)$$

where n is the number of the stacked ribbons and t is the thickness of ribbon unit.

Thickness c must be thick enough to endure crushing during cable installation. At most 8000 N is applied to a cable and the roller in corner

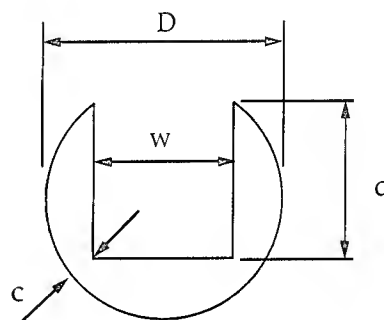


Fig. 7 Spacer

has its radius of 600 mm. So the unit should work under the pressure of 13.3 N/mm. We used the plates of 100 mm in length for the crushing test, so the unit should overcome the pressure more than 1330 N. Fig. 8 shows the test result. Spacer is not center symmetry and deformation differs by the direction you put force. We put the weight on the plates between which we hold the unit (see Table 2: crushing test). Our unit indicated good crush performances and we cannot find any residual deformation after release of the stress.

Spacer diameter is determined by equation(1). In that case, spacer size must satisfy the relation (2) and the crushing performance.

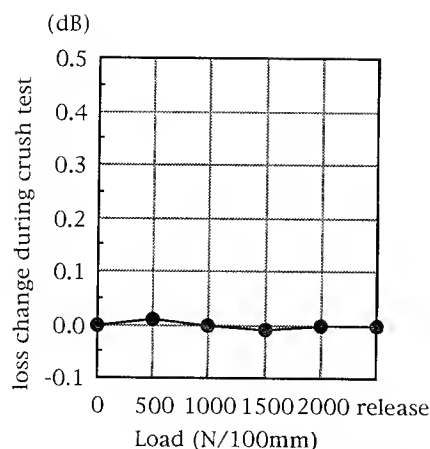


Fig. 8 crush test on single groove unit

3.3 Experimental Cable

Cross sections of our test cables are shown in Fig. 9. Fig. 9(a) constructs 1600-fiber cable structure with 180 μm fiber, and Fig. 9(b) is the 4000-fiber construction with 200 μm fiber. True unit is located in each layer by one and other unit is dummy. Cable diameter is 32 mm and 48 mm. If we construct 4000-fiber cable by same size unit for 180 μm fiber, cable diameter would be 46 mm. Manufactured cable was 500 m in length. Transmission loss is indicated in Table 1. Loss distribution in a unit is indicated in Fig. 10. Extreme outer position fiber and inner position fiber indicate the same distribution patterns due to the stress free conception of this single helical groove unit.

We performed several mechanical and thermal tests on our experimental cable. These are indicated in Table 2. In the squeezing test we set the roller on a trail and let the trail go on rails. There were few loss changes during these tests at 1.31 and 1.55 μm .

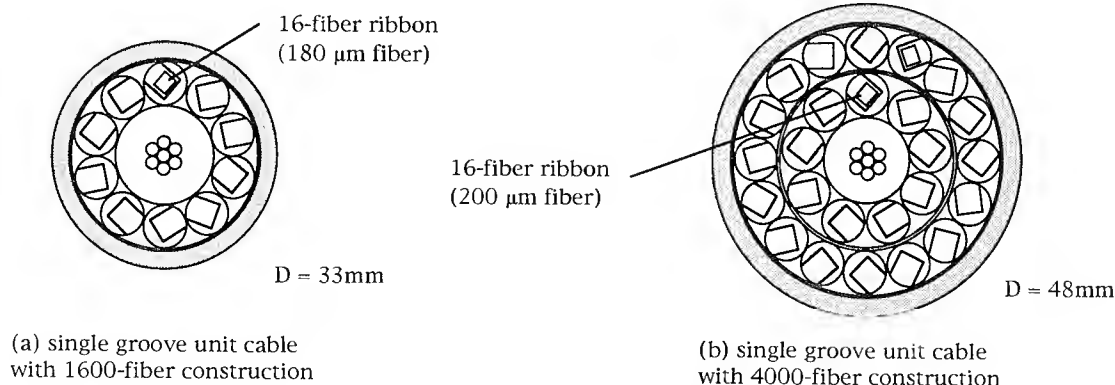


Fig. 9 Our experimental cable

3.4 Investigation of SZ stranding of the units

SZ stranding (ROL) is preferable for downsizing the assembling machines and has merits in mid-span sheath entry.

Fig. 11 indicates the model of the SZ stranding. When cable is bent, fiber is stretched in outside portion of the bending and is suppressed in inner portion. To compensate these imbalance the amount of these two kind of stress must be same. The track of SZ stranding is expressed as follows

$$x = a \cos \left(\frac{\phi}{2} \sin k \right) \quad \dots (3)$$

$$y = a \sin \left(\frac{\phi}{2} \sin k \right) \quad \dots (4)$$

$$z = \frac{\phi}{2\pi} k + c_1 \quad \dots (5)$$

where a is the spiral radius and ϕ is the ROL angle. When cable is bent by the radius R , the fiber elongation Δl_{sz} through half pitch of SZ stranding $P_{sz}/2$ is given by

$$\Delta l_z = \frac{P_{sz}}{2\pi R} a \int_{-\pi/2}^{\pi/2} \cos \left(\frac{\phi}{2} \sin k \right) dk = P_{sz} a J_0 \left(\frac{\phi}{2} \right) \quad \dots (6)$$

J_0 is the Bessel function. Smallest ϕ that gives equation (6) zero is 275.5 deg. However we must consider the situation the stranded angle deviate from this best angle in actual cable. In that case fiber strain is approximately given by

$$\epsilon = \frac{\frac{1}{R} a J_0 \left(\frac{\phi}{2} \right)}{1 + \left(\frac{\pi a \phi}{2 P_{sz}} \right)^2} \quad \dots (7)$$

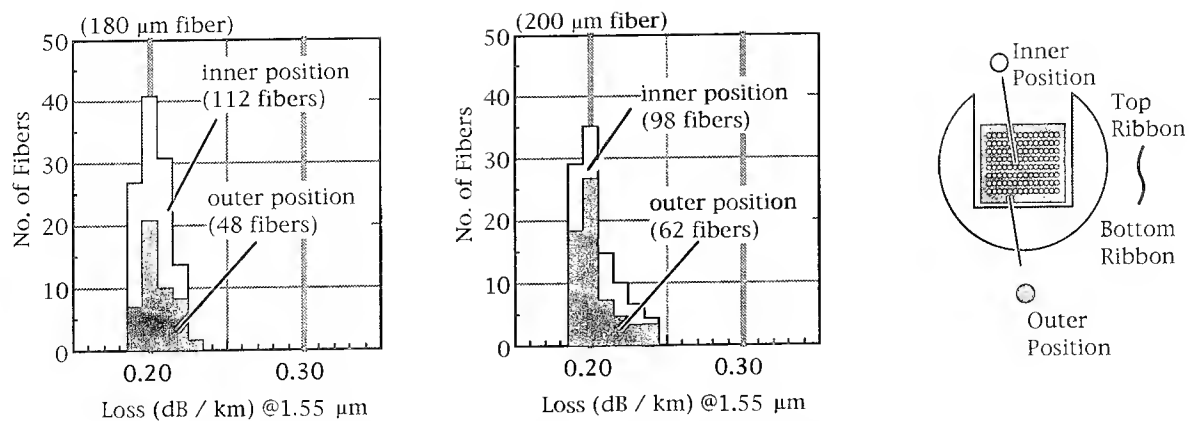
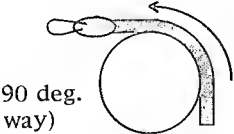
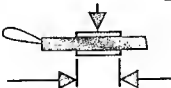
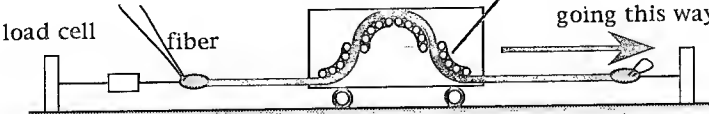


Fig. 10 loss distribution of our test cable (left: 180 μm fiber, right: 200 μm fiber)

Table 1 Transmission loss (@ 1.55 μm) of our test cable

fiber diameter	cable structure	cable diameter	average loss(@1.55)	maximum loss(@1.55)
180 μm	1600-fiber type	33 mm	0.203 dB/km	0.23 dB/km
200 μm	4000-fiber type	48 mm	0.204 dB/km	0.24 dB/km

Table 2 mechanical and thermal test

Bending	(R = 200 mm)	optical loss change during test < 0.02 dB (@ 1.31 & 1.55 μm)	
Crashing	(3000N / 100mm)		
Tension	(10000N)		
Squeezing	(8000N, R 600)		
Temperature	-30 °C to 60 °C		
[Bending]	 <p>R ~ 200mm 90 deg. (right & left both way)</p>	[Crushing]	 <p>weight (up to 3000 N) 100 mm</p>
[Tension]	load : up to 10000 N	[Temperature]	- 30 °C to 60 °C condition : on reel (1600mm φ)
[Squeezing]	 <p>load : up to 8000 N roller (R = 600 mm) going this way</p>		

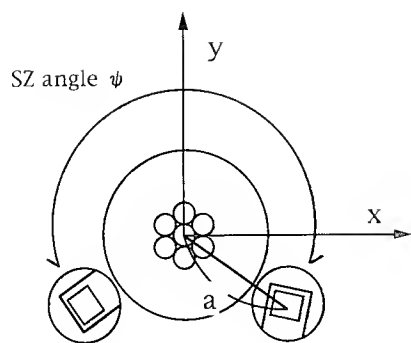


Fig. 11 calculation model of SZ stranding

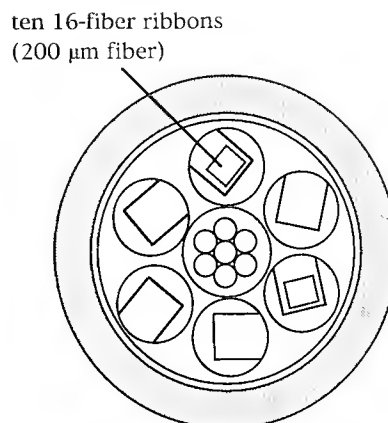


Fig. 12 our experimental cable (SZ stranding)

Provided that bending radius is 500 mm and the deviation from the best angle is 10 degree, fiber strain reaches 0.07 %. In this case fibers may suffer the compressive strains or the fiber bending caused by excess length. We have designed the depth of the groove deep enough to absorb the excess length more than 0.2 %, so only the compressive stress must be considered. In our experimental cable two kinds of units were prepared. One of which has the fiber excess length of 0.1 % considering the deviation of ROL angle from the best angle. Another has no excess length. Cross section of the test cable is indicated in Fig. 12. That is 960-fiber count construction, however 4 unit is empty dummies. Coated fiber diameter was 200 μm . Transmission properties of this cable is in Table 3. Average losses are almost the same in both two units, however, the one without excess length indicated the loss increase in edge fiber. On contrary another unit

showed good transmission loss properties. And we performed the mechanical test indicated in Table 2 and no loss change was observed during the tests.

4. Conclusion

We have investigated new optical cable using single helical groove as one of the candidates for ultra-high count optical fiber cable that can accommodate up to 4000 fibers. In spite of the deterioration of microbending characteristics due to downsized coated fiber, our cable indicated good performance. And we confirmed the possibility of assembling our units in SZ direction.

5. Reference

- (1) S.Tomita et al, IWCS '93 pp.5-15
- (2) S.Tomita et al, IWCS '91
- (3) W.Katsurashima et al, IWCS '92
- (4) Y.Kitayama et al, OFC 94, pp.178
- (5) K.Oishi et al, IWCS '93, pp.687-693

Table 3 Transmission loss of our test cable (SZ stranding)

fiber diameter	200 μm	
cable structure	960-fiber type	
cable diameter	30 mm	
EXL (design)	0 %	0.1 %
average loss	0.202 dB/km	0.203 dB/km
maximum loss	0.28 dB/km	0.24 dB/km



Wataru Katsurashima

Sumitomo Electric
Industries, Ltd.

1, Taya-cho, Sakae-ku
Yokohama, Japan

Wataru Katsurashima graduated from Tokyo University in 1987. He joined Sumitomo Electric Industries, Ltd. in 1987 and has been engaged in optical fiber and cables. Mr. Katsurashima is a member of Institute of Electronics, Information and Communication Engineers of Japan.



Shigeru Tanaka

Sumitomo Electric
Industries, Ltd.

1, Taya-cho, Sakae-ku
Yokohama, Japan

Shigeru Tanaka received the B.S. and M.S. degree from Tokyo University in 1974 and 1976. He received Ph.D degree in 1989. He joined Sumitomo Electric Industries Ltd. in 1976 and has been engaged in the design and characterization of optical fibers and cables. He is a Chief Research Associate of Communication R&D department. Dr. Tanaka is a member of Institute of Electronics, Information and Communication Engineers of Japan.



Yoshinobu Kitayama

Sumitomo Electric
Industries, Ltd.

1, Taya-cho, Sakae-ku
Yokohama, Japan

Yoshinobu Kitayama received his M.S. degree in Electrical Engineering from Kyoto Univ. in 1982. He then joined Sumitomo Electric Industries and has been engaged in research and development of optical fiber and cables. Mr. Kitayama is a senior engineer of Communication R&D department in Yokohama Research Laboratories, and a member of the Institute of Electronics, Information and Communication Engineers of Japan.

A New Compact Ribbon Cable

Masayoshi Yamanaka, Naoki Okada, Matsuhiro Miyamoto, and Toshikuni Maruoka

Fujikura Ltd.

Telecommunication Cable Section Opt-Electronics Laboratory

1440 Mutuzaki, Sakura, Chiba, 285, Japan

Abstract

In this paper we will discuss the design, construction, and testing of a new lower-count ribbon cable with an open channel that includes several fiber ribbons. Both straight and twisted ribbon structures were investigated for fiber accommodation in a channel. It seems to be difficult to realize a compact size for the straight ribbon cable structure. By twisting the stacked fiber ribbons in an open channel, problems caused by difference in ribbon length can be reduced. Five 8-fiber ribbons were used in trial cables designed for 40-fiber cable. The trial cable revealed excellent performance in mechanical and environmental tests.

1. Introduction

In the subscriber loop, lower-count cables featuring easy mid-span entry will be required for access to user homes. An optical fiber ribbon is suitable for increasing fiber-packing density, for reducing fiber-joining time, and for being joined with higher-fiber count cables. A tube unit containing several optical fiber ribbons has been studied for its higher fiber count and for tube ribbon cables. In terms of mid-span access, an open channel structure is more easily branched than a tube structure as a buffer shell for ribbons. It seems to be difficult to remove a ribbon from a tube without damaging the

ribbons. A single-channel structure can provide easy access to ribbons and storage space for several ribbons.

We studied two types of channel ribbon cables. In Section 2, the straight and twisted ribbon structures are examined theoretically.

In Section 3, a compact ribbon cable is experimentally examined.

2. Cable Design

In designing a new subscriber cable, we considered the following four criteria: (1) rapid cable-joining capacity, (2) mid-span access capacity, (3) simple and compact design, and (4) low fiber count up to 40. To realize first requirement, it is a common practice to use fiber ribbons. In order to achieve easy mid-span access and realize a simple, compact cable, the cable structure is such that ribbons are stored in a straight open channel. Five 8-fiber ribbons are stacked in a straight open channel.

2-1. Straight ribbon structure

One of the simplest structures is that of straight stacked ribbons in a straight channel as shown in Fig. 1. The excess length is one of the most important considerations when designing cable. The excess length of the stacked fiber ribbons inserted in the open channel is determined by the curvature of blocking region, as shown

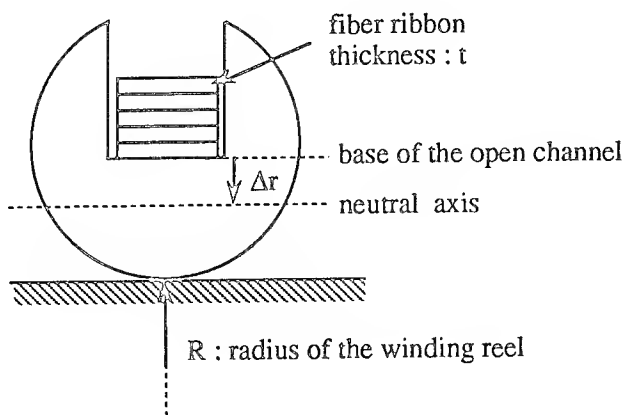


Fig.1 The structure of most simple cable and the parameters for calculating the excess fiber length

R: radius of the winding reel

Δr: distance between the neutral axis and the base of an open channel

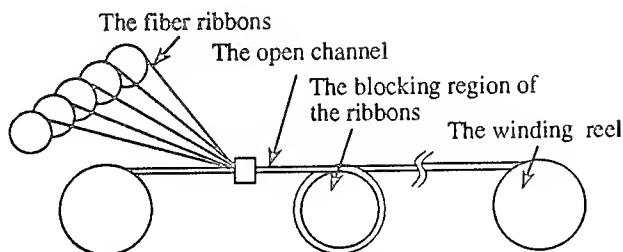


Fig.2 The scheme of the cable manufacturing process

in Fig. 2. The difference in distance between each ribbon stacked to the neutral axis of the rod section obviously gives rise to varying lengths of the fiber ribbons in an open channel. When cable parameters such as Δr, t, and R are established as shown in Fig. 1, the excess fiber length α is derived as the equation (1) and (2). In this calculation, the open side of the channel is directed outward in bending. The values, n and t are the number of fiber ribbons from the base and the thickness of the fiber ribbon. The result

$$\alpha(\%) = \frac{L_f L_c}{L_c} \times 100 \quad (1)$$

$$= \frac{\Delta r - \frac{t}{2}(2n-1)}{R} \times 100 \quad (2)$$

L_f: Length of ribbons

L_c: Length of a channel

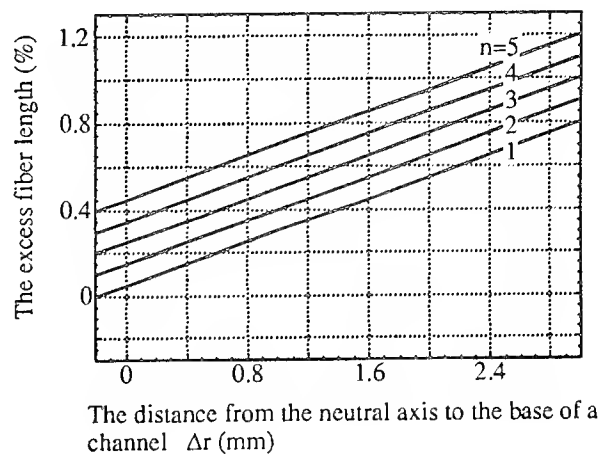
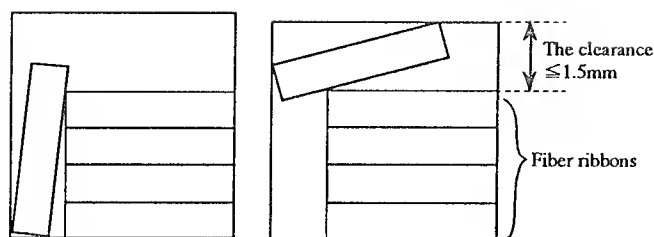


Fig.3 The dependence of the excess fiber length on Δr

is shown in Fig. 3. The excess length α of each fiber ribbon also strongly depends on Δr, which is the neutral axis position in the channel. The larger n becomes, the larger the excess length becomes.

For this type of cable, disordering of the stacked fiber ribbons must be avoided. The fiber ribbons may be subjected to unpredictable mechanical conditions caused by such disorder. The disordering of stacked fiber ribbons often causes an increase in attenuation. Therefore, the clearance in an open channel should be limited so that disorder does not occur. For cables with five fiber ribbons, the clearance must be less than 1.5 mm to eliminate disordering, as illustrated in Fig. 4. In this calculation, the horizontal clearance



Example of
disordered fiber ribbon

Fig.4 The scheme of the disordered fiber ribbon

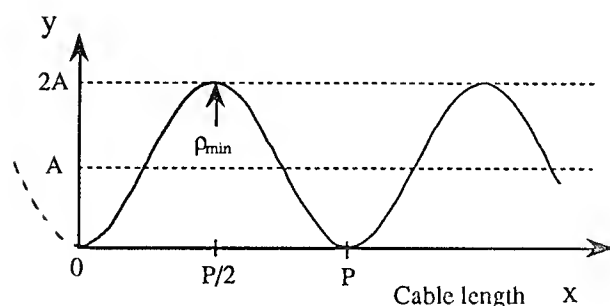


Fig.5 Sinusoidal fiber in a channel

in the channel is assumed to be 0.4 mm.

When the fibers have a positive excess length in the channel, the fiber will meander¹⁾. The clearance in the channel should be designed to avoid small bending radius of the fiber which occurs loss increase. Assuming that the fibers meander sinusoidally in the channel, as shown in Fig. 5, a fiber coordinate can be determined from equation (3). In such a case, the minimum radius of curvature ρ_{min} is expressed in terms of the amplitude of sinuous fiber A and fiber excess length α , as shown in equation (4)^{2), 3)}. The amplitude of the sinuous fiber is proportional to the excess fiber length when minimum curvature ρ_{min} is given. As shown in Fig. 3, the ribbons in an open channel each have different excess lengths. The loss-free depth of the channel is calculated from the sum of the amplitude of each sinuous ribbon. The result

$$y = A \sin\left(\frac{2\pi}{P} z\right) \quad (3)$$

$$\rho_{min} = \frac{A}{4\alpha} \quad (4)$$

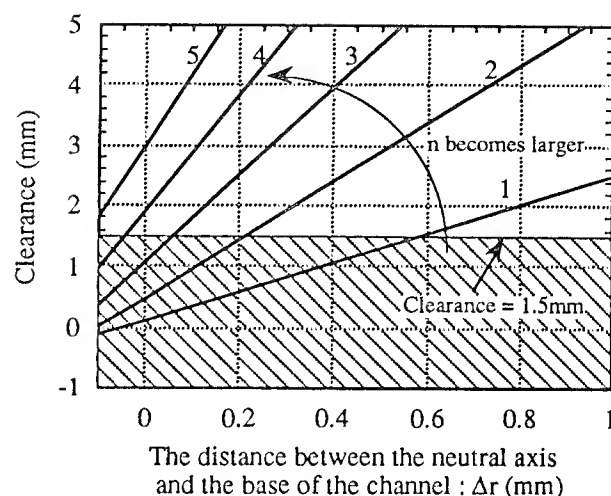


Fig. 6 Clearance required for stable attenuation

of this calculation is shown in Fig. 6, where ρ_{min} is sufficiently large that the bending loss is negligible. In the same figure, the hatched area indicates allowable clearance conditions that avoid disordering and bending loss resulting from excess ribbon length. According to Fig. 6, the number of fiber ribbons that can be inserted into an open channel is no more than three. As a result, it appears that such a cable structure cannot accommodate more than 24 fibers.

2-2. Twisted ribbon structure

In order to improve the problems of the straight ribbon structure mention above, we also designed the twisted ribbon struc-

ture. The stacked fiber ribbons are twisted and inserted into an open channel loosely so as to reduce the variation in length of the fiber ribbons. Such a cable structure is suitable for easy control of the excess fiber length because the stacked and twisted fiber ribbons are regarded as one unit.

The most important cable parameters are 1) excess fiber length, 2) open-channel clearance, and 3) the twisting pitch of the stacked fiber ribbons. These parameters are determined as follows.

1) Excess fiber length

Considering the stacked and twisted fiber ribbons as one unit, the dependence of the excess unit length on the neutral axis position was calculated according to equation (1). The results of this are shown in Fig. 7. We decided to use a positive value as the excess length because the negative values indicate that the fiber ribbons are always stretched.

2) Open-channel clearance

The excess length of a unit as described above increases at low temperatures because of differences in the linear expansion coefficients of glass fibers and plastic rods with steel members. The open-channel clearance is determined in consideration of the increase in the excess ribbon length of a unit at low temperatures.

3) Twisting pitch of the stacked fiber ribbons

The twisting pitch of the stacked fiber ribbons are determined according to our study of the ribbon loose tube cable^(4),5).

3. Experiments

3-1. Cable fabrication

According to the theoretical study in Section 2, we fabricated a twisted-ribbon-

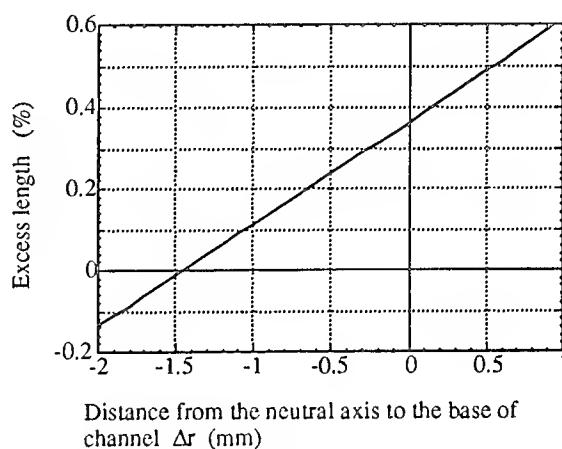
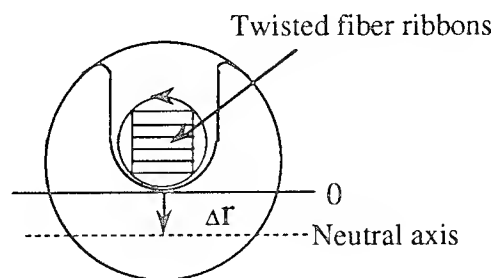


Fig.7 Dependence of the excess length on Δr

type trial ribbon cable as shown in Fig. 8. The 8-fiber ribbons are stacked, twisted, and then inserted into an open channel. The two strength members are inserted into the rod in parallel. The rod material is chosen in consideration of its mechanical strength at lower temperatures, its thermal stability during the sheathing process, and aging. The open channel is filled with jelly compounds. The rod is wrapped and sheathed with polyethylene. Sheathing and the insertion of several fiber ribbons into an open channel can be performed in one process. The twisting pitch and excess ribbon length were optimized experimentally. The finished cable is very compact, with an outer diameter less than 12 mm.

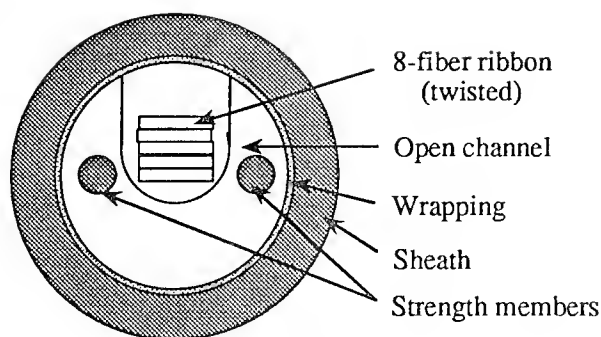


Fig.8 Cross section of an open-channel ribbon cable

3-2. Performance of the trial cable

Trial cables were examined and subjected to various tests, including the mechanical and environmental tests.

(1) Increase in optical attenuation during the manufacturing process

The changes in optical attenuation during the cable manufacturing process of the trial cable is given in Fig. 9. During the fabrication process, no change in loss was observed.

(2) Temperature-cycling test

To predict the long-term reliability of the optical attenuation of the cable, we subjected a trial cable to a heat-cycle test. The temperature-cycle pattern for this test and the obtained results are given in Fig. 10. During the test, the change in attenuation was less than 0.1dB/km at both measured wavelengths.

(3) Installation test

As mentioned above, the trial cable featured stable transmission characteristics when wound on a reel. To simulate installation, the attenuation loss in the

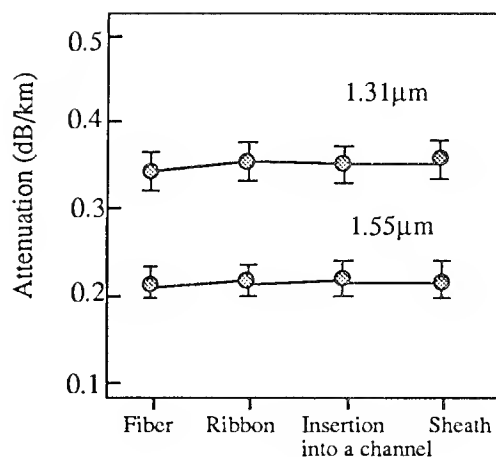


Fig.9 Attenuation changes during the cable manufacturing process

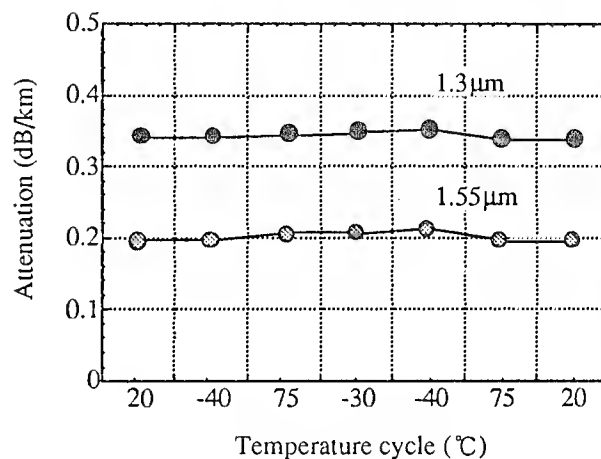


Fig.10 Results of the heat-cycling test for the trial cable

straightened cable was measured. In the test, no change in loss was observed.

(4) Mechanical tests

The mechanical tests involve the tensile strength of the cable, cable twist, bending, impact, and compressive strength. During these tests, the change in transmission loss was below 0.01 dB. The conditions and results of the mechanical tests are summarized in Table 1.

In the tensile load test, the load on the cable was increased gradually to 1500 N. During the test, the increase in attenuation was below 0.01 dB, and there was no evidence of cracking or slitting on the cable after the test.

In the compression test, the cable subjected to a load of 440N/cm revealed no changes in residual attenuation. After releasing the load from the cable, no residual attenuation was found in the cable.

Table. 1 Mechanical test results

Items	Condition	Cable Performance
Tensile	Tensile load :50m/1500N	During test ≤ 0.01 dB
Twist	10 cycles of $\pm 180^\circ$	During test ≤ 0.01 dB After test no cracking or splitting
Compression	Compressive load :440 N/cm Compressive Plate :100 mm	During test ≤ 0.01 dB
Bending	Mandrel :200mm ϕ	During test ≤ 0.01 dB
Impact	2.5 mm ϕ /2.0 kg Impact cycle:10 1 m drop	During test ≤ 0.05 dB

*) all tests measured at 1.55 μ m

5. Conclusion

A new type of ribbon cable in which ribbons are stored into an open channel has been designed, manufactured, and tested. At first, we designed two types of open channel cables which are straight and twisted ribbon structure. As a result of examination, the straight ribbon structure with 8-fiber ribbons is not suitable for more than 24 fiber cables, so we adopted the twisted ribbon structure. The stacked ribbon fibers are twisted in an open chan-

nel in order to eliminate the differences in the excess lengths of ribbons and minimize the strain on the ribbon fibers when the cable is bent.

The features of this cable are; 1) use of the 8-fiber ribbons to join each cables rapidly when constructing networks, 2) use of an open channel to pack the 8-fiber ribbons considering easy mid-span entry, 3) simple and compact structure to achieve the economical network construction. The trial cable with five 8-fiber ribbons showed stable characteristics in mechanical and environmental tests. This new compact ribbon cable seems just suitable for the future subscriber loops such as "fiber to the home".

References

- (1) P.D. Patel and A.J. Panuska, "Light-weight fiber optic cable", 39th International Wire and Cable Symposium Proceeding, 1990, pp.158-164.
- (2) D. Bosher, B. Missout, and P. Cheron, "Low-loss optical fiber cable design and manufacture", 30th International Wire and Cable Symposium Proceeding, 1981, pp.139-146.
- (3) S. Hatano, Y. Katsuyama, T. Kokubun, and K. Hogari, "Design and Characteristics of Multi-Hundred-Core Optical-Fiber Cable For Use in Subscriber Feeder Lines", J of Light Technology, vol. LT-4, No.8, pp.1189-1193.
- (4) Y. Kurosawa, H. Sawano, M. Miyamoto, and N. Sato, "Development of ribbon loose tube cable for optical subscriber loop", 41st International Wire and Cable Symposium Proceeding, 1992, pp.151-157.
- (5) M. Yamanaka, N. Okada, H. Sawano, and M. Miyamoto, "A study on reverse lay stranding loose tube cable containing ribbon fibers", 42nd International Wire and Cable Symposium Proceeding, 1993, pp.521-526.



Masayoshi Yamanaka

Opto-Electronics
Laboratory
Fujikura LTD.
1440 Mutsuzaki,
Sakura, Chiba,
285, Japan

Mr. Yamanaka was born in 1966. He joined Fujikura Ltd. after graduating from Tohoku University in 1992 with an M.E. degree, and has since been engaged in the research and development of optical-fiber cables. He is now an engineer in the optical-fiber cable section.

Matsuhiro Miyamoto

Opto-Electronics
Laboratory
Fujikura LTD.
1440 Mutsuzaki,
Sakura, Chiba,
285, Japan

Mr. Miyamoto was born in 1953. He joined Fujikura Ltd. after graduating from Tokyo Institute of Technology in 1978 with an M.S. degree, and has since been engaged in the design and research of optical fibers and cables. He is now a section chief of the Telecommunication Cable Section and is a member of IEICE of Japan.



Naoki Okada

Opto-Electronics
Laboratory
Fujikura LTD.
1440 Mutsuzaki,
Sakura, Chiba,
285, Japan

Mr. Okada was born in 1964. He joined Fujikura Ltd. after graduating from Chiba University in 1986 with a B.E. degree, and has since been engaged in the research and development of optical-fiber cables. He is now an engineer in the optical-fiber cable section and is a member of IEICE of Japan.



Toshikuni Maruoka

Opto-Electronics
Laboratory
Fujikura LTD.
1440 Mutsuzaki,
Sakura, Chiba,
285, Japan

Mr. Maruoka was born in 1943. He joined Fujikura Ltd. after graduating from Tokyo University in 1967 with a B.E. degree, and has since been engaged in the design, research, and development of transmission cables. He is now the manager of the Transmission Line Department and is a member of IEICE of Japan.

DESIGN OF LOOSE TUBE FIBER OPTIC CABLE WITH ADJUSTED CONTRACTION AND STRAIN WINDOWS

Jana Horska

CommScope, Inc.
General Instrument Corporation
Catawba, North Carolina 28609, U.S.A.

ABSTRACT

This paper describes methods for balancing the contraction and strain windows in stranded loose tube fiber optic cables by an accurate positioning of fibers inside the buffer tubes. Enhanced low temperature performance and more economical cable design can be achieved by implementing these techniques.

The mathematical model used in the traditional cable design is reviewed and generalized equations for the adjusted contraction and strain windows are presented. The new design approach was tested and verified in the development of a dual layer loose tube fiber optic cable. The experience gained in this process, typical production challenges and benefits are discussed.

Finally, a potential to use these methods to increase fiber packing density and decrease cable dimensions is analyzed.

INTRODUCTION

Traditional stranded loose tube fiber optic cable uses as a basis certain standard components. These include a central anti-buckling member, a plurality of buffer tubes, strength elements, and a protective jacket surrounding the buffer tubes. The cable components typically expand and contract to a greater extent than do optical fibers as the temperature increases and decreases, respectively.

The maximum strain withstood by a fiber optic cable without imparting strain to the optical fibers is typically termed the strain window of the cable. Likewise, the maximum contraction withstood by a cable without excessively bending the optical fibers and significantly attenuating the signal transmission is termed the contraction window.

Generally, a traditional loose tube cable design provides a large strain window, while the contraction window

often is not sufficient. Therefore, excessive attenuation of the transmitted optical signal may occur at low temperatures. In order to avoid this problem, methods of adjusting the contraction and strain windows of the cable at the predetermined range of temperatures and loads can be employed.³ These methods are based on the positioning of the optical fibers within the buffer tubes so as to have an average position offset in a direction extending radially inward from the buffer tube axis toward the central support member at a reference temperature.

LOOSE TUBE FIBER OPTIC CABLE DESIGN

Cable Structure

A fiber optic cable consists of a core, strength elements, and an outer protective jacket. The core of a loose tube fiber optic cable includes a series of buffer tubes stranded around a central support member in one or more concentric layers. Optical fibers are placed in buffer tubes in a loose buffered relationship. The buffer tubes are arranged in either a reverse oscillating helical lay pattern or in a helical lay pattern. The protective jacket is extruded over the core.

Cable Components

The central support member may be formed of a dielectric material, such as glass or aramid reinforced plastic, or one or more metal wires. The buffer tubes and the protective jacket are usually plastic. More specifically, the protective jacket may be polyethylene and the buffer tubes may be polybutylene terephthalate, polyethylene, or polypropylene. The buffer tubes are filled with filling compound, typically a thixotropic synthetic oil based gel. A variety of yarns, rovings, wires, or rods may be used over the outer layer of buffer tubes to enhance tensile strength of the cable. The fiber optic cable may also include an armor layer to provide additional protection for the cable.

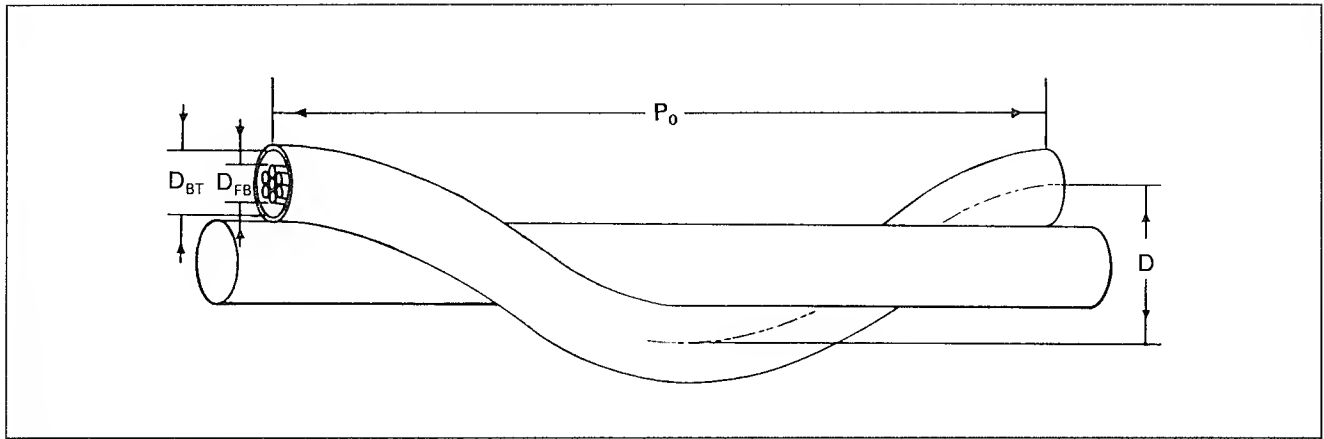


Figure 1. Helically Stranded Buffer Tube

Effective Coefficient of Thermal Expansion of Cable

With the exception of the optical fibers, the cable components are bound together such that they expand and contract in substantially equal amounts. Therefore, an effective coefficient of thermal expansion of the cable, $\alpha_{EFF}(T)$, may be defined as:

$$\alpha_{EFF}(T) = \frac{\sum_{i=1}^n A_i(T) E_i(T) \alpha_i(T)}{\sum_{i=1}^n A_i(T) E_i(T)}, \quad (1)$$

where T is temperature, $A_i(T)$ is the respective cross-sectional area of each cable material, designated i , $E_i(T)$ is the respective secant modulus of each material, and $\alpha_i(T)$ is the respective coefficient of thermal expansion of each material.¹

Typically, the effective coefficient of thermal expansion of the cable, $\alpha_{EFF}(T)$, is significantly higher than the coefficient of thermal expansion, $\alpha_F(T)$, of the optical fibers. Thus, the cable components expand and contract more than the optical fibers as the temperature increases and decreases, respectively.

Because of the different contraction rates of the optical fibers and cable components, excessive bending of the fibers and signal attenuation increase may occur at low temperatures. Similarly, at relatively high temperatures and loads, excessively elongated fibers may show an attenuation increase or a complete mechanical failure. Therefore, sufficient contraction and strain windows for predetermined temperature and load ranges are required. Typically, the contraction and strain windows of a fiber optic cable are determined at a reference temperature, such as room temperature, and with no tensile load applied to cable.

Traditional Design

Contraction Window. The contraction window for an ideal helix and a traditional design (reference Appendix, Part I, II, and IV-A) may be determined as:

$$\epsilon_C = 1 - \sqrt{1 - \frac{\pi^2}{P_0^2} (D_{BT} - D_{FB}) (2D + D_{BT} - D_{FB})}, \quad (2)$$

where P_0 is a pitch length (lay length) of the helically wound buffer tubes at the reference temperature (see Fig. 1), D_{BT} is the inner diameter of the buffer tube, D_{FB} is the diameter of the fiber bundle, and D is the center-to-center spacing between the buffer tube axes.

Strain Window. The strain window for an ideal helix and a traditional design (reference Appendix, Part I, II and IV-A) may be determined as:

$$\epsilon_S = \sqrt{1 + \frac{\pi^2}{P_0^2} (D_{BT} - D_{FB}) (2D - D_{BT} + D_{FB})} - 1. \quad (3)$$

New Design Approach

Two methods can be used in the cable manufacturing process to adjust the contraction and strain windows of the stranded loose tube cable:

Method 1:

This method requires applying tension to each of the buffer tubes while stranding the buffer tubes around the central support member. This tension causes an elongation of the buffer tubes and a movement of the fibers toward the central support member in a stranded core.

Method 2:

In this method, a negative excess fiber length (EFL) is created in buffer tubes during the buffering process. Thus, fibers are under tension inside the buffer tube. After positioning the buffer tubes around the central support member, fibers assume the average position offset radially inward from the buffer tube axis toward the central support member to relieve the tension.

Desired contraction and strain windows for a certain cable design can be achieved by either of these processing methods or their combination. Alternatively, the first method may be used to compensate for excessively high EFL in a buffer tube after buffering.

Offset of Optical Fibers. By adjusting the contraction and strain windows, the optical fibers inside the buffer tube assume the average position offset in a direction extending radially inward from the buffer tube axis toward the central support member (reference Appendix, Part IV-B). This offset may be calculated as:

$$d = \frac{1}{2} \left[D - \frac{1}{\pi} \sqrt{(\pi^2 D^2 + P_0^2) (\epsilon + 1)^2 - P_0^2} \right] \quad (4)$$

Parameter ϵ is defined as:

$$\epsilon = \frac{L_{FB}}{L_{BT}} - 1 \quad (5)$$

where L_{FB} is the length of the fibers in a reference length of the cable at a reference temperature, and L_{BT} is the length of buffer tubes in the same reference length of the cable at the same reference temperature.

In relation to two methods of balancing the contraction and strain windows, ϵ may be expressed as:

$$\epsilon = \frac{\epsilon_{EFL} - \epsilon_{BT}}{\epsilon_{BT} + 1} \quad (6)$$

where ϵ_{EFL} is the excess fiber length (EFL) in the buffer tube after buffering and ϵ_{BT} is the elongation of the buffer tube after the stranding process.

For fiber optic cables fabricated with tension applied to the buffer tubes during stranding of the core, ϵ_{BT} may be calculated as:

$$\epsilon_{BT} = \frac{4F}{\pi E (D_2^2 - D_1^2)} \quad (7)$$

where E is the secant modulus of the buffer tube material, F is the tension applied on the buffer tube

during the stranding process, D_1 is the inner diameter of the buffer tube, and D_2 is the outer diameter of the buffer tube.

Contraction Window. The contraction window for an ideal helix and a fiber position offset (reference Appendix, Part IV-B) may be determined as:

$$\epsilon_{Cd} = 1 - \sqrt{1 - \frac{\pi^2 (D_{BT} - D_{FB}) (2D + D_{BT} - D_{FB})}{P_0^2} - \frac{\pi^2 4d(D-d)}{P_0^2}} \quad (8)$$

Strain Window. The strain window for an ideal helix and a fiber position offset (reference Appendix, Part IV-B) may be determined as:

$$\epsilon_{Sd} = \sqrt{1 + \frac{\pi^2 (D_{BT} - D_{FB}) (2D - D_{BT} + D_{FB})}{P_0^2} - \frac{\pi^2 4d(D-d)}{P_0^2}} - 1 \quad (9)$$

If a more accurate model of the contraction and strain windows for S-Z stranded cables is desired, a reverse oscillating helix (reference Appendix - Part III) should be used in the calculations.

Advantages of New Design Approach

Development of Standard Loose Tube Fiber Optic Cable.

The principles of adjusting the contraction and strain windows may be implemented in the design of a standard loose tube cable to shorten the development process. In addition, this cable is less sensitive to variations of buffer tube lay length.

Loose Tube Fiber Optic Cable with Enhanced Performance at Low Temperatures.

Typically, fiber optic cables are designed for an operational temperature range of -40°C (-40°F) to $+70^\circ\text{C}$ ($+158^\circ\text{F}$). A proper adjustment of the contraction window may allow for an excellent optical performance even at temperatures below -40°C (-40°F). However, this improvement is limited by the properties of a filling compound.² The viscosity of a typical filling compound (a thixotropic synthetic oil based gel) increases rapidly at temperatures below -40°C (-40°F) (see Fig. 2).

Increase in Fiber Packing Density.

The balancing of contraction and strain windows can be employed to increase the number of fibers placed in the buffer tube, such that a traditional cable design may be used for higher fiber counts. Respectively the dimensions of the cable developed for a certain number of fibers can be decreased. Potential cost reductions are obvious.

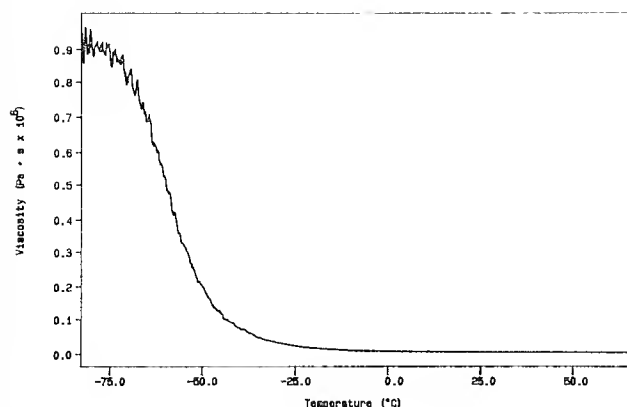


Figure 2. Viscosity of Filling Compound vs Temperature

PRODUCTION ISSUES

Method 1:

Typical stranding equipment is designed to place little to no tension on the buffer tubes during payoff. Tensioning of buffer tubes for the desired elongation, however, requires payoffs capable of tension in the 10 - 40 N (2.3 - 9.0 lb) range. Buffer tube tension during reverse oscillating lay stranding varies periodically as a function of the imparted twist geometry. The payoffs must have some degree of accumulation and enough responsiveness so as to minimize buffer tube tension fluctuations. The desired buffer tube tension must therefore be a time weighted average over the periodic tension fluctuations as measured at the closing and binding point of the tubes.

Increased buffer tube tensions can worsen a condition known as "core rocking" - a back and forth imparted rotation of the core at the stranding point. This motion tends to increase the buffer tube lay length and decrease the number of captured cycles between switchpoints. On the other hand, cable designs with adjusted contraction and strain windows are generally less sensitive to these degradations of the stranding geometry.

Method 2:

Most loose buffering lines have the capability to produce buffer tubes with an EFL range of -0.1% to +0.5%. In order to achieve the desired negative EFL, variations in fiber payoff tensions, plastic cooling rates, tube routing during processing, and buffer tube tensions can be employed.^{4, 5}

With negative EFL, increases in optical attenuation may be experienced after buffering. Excessive microbending may occur as the fibers act against one another after being pulled to the inner radius of the tube while being

coiled at put-up. If increases occur they will be temporary in nature and will revert to nominal values after helically stranding of the buffer tubes.

EXPERIMENTAL DATA

The methods of balancing the contraction and strain windows were tested and verified in the design of a dual layer loose tube fiber optic cable. The development of this cable is usually a difficult process because of the relatively high effective coefficient of thermal expansion of the cable, α_{EFF} . By implementing the first method to adjust the contraction window, excellent performance at -40°C (-40°F) was achieved.

Two samples of a dual layer loose tube cable were manufactured and tested per Bellcore TR-NWT-000020, Issue 5.⁷ Sample 1 - an armored version of the cable - was processed with an adjusted tension on all buffer tubes during stranding. In Sample 2 - an all dielectric version - each layer contained the buffer tubes stranded with standard as well as higher payoff tensions. The results of the Temperature Cycling and Aging Tests for these samples are shown in Table 1a).

In addition, Sample 3 - an all dielectric dual layer loose tube cable - was specially designed and manufactured to have an optical performance at low temperatures "on the edge". A combination of the buffer tubes processed with standard and higher tensions was placed at each layer. The optical performance of this sample at temperatures -40°C (-40°F), -45°C (-49°F), -50°C (-58°F), and -55°C (-67°F) was monitored. The test results are summarized in Table 1b).

CONCLUSION

This paper presented methods for adjusting the contraction and strain windows in loose tube fiber optic cables. These techniques were tested and verified in the development of a dual layer stranded cable. Excellent optical performance of this cable at low temperatures was achieved.

By implementing these design principles to increase fiber packing density and decrease cable dimensions, significant cost reductions may be accomplished. In addition, cables with balanced contraction and strain windows allow for a higher degree of variation at certain stages of processing. More specifically, an excessively high EFL in a buffer tube after buffering may be compensated at the stranding process. Also, this cable design is less sensitive to lay length irregularities caused by limitations of stranding machinery.

		Attenuation Change at -40°C (-40°F) [dB/km]					
		Temperature Cycling Test			Aging Test		
		Min	Max	Avg	Min	Max	Avg
Sample 1	1st Layer - Adjusted Payoff Tension	-0.01	0.02	0.00	-0.01	0.03	0.01
	2nd Layer - Adjusted Payoff Tension	-0.01	0.03	0.00	-0.01	0.02	0.00
Sample 2	1st Layer - Adjusted Payoff Tension	-0.02	0.00	-0.01	-0.02	0.00	-0.01
	1st Layer - Standard Payoff Tension	0.00	0.00	0.00	0.00	0.00	0.00
	2nd Layer - Adjusted Payoff Tension	-0.01	0.00	-0.01	-0.02	0.00	-0.01
	2nd Layer - Standard Payoff Tension	-0.01	0.02	0.00	0.18	1.23	0.78

	Attenuation Change [dB/km]											
	Test Temperature -40°C (-40°F)			Test Temperature -45°C (-49°F)			Test Temperature -50°C (-58°F)			Test Temperature -55°C (-67°F)		
Sample 3	Min	Max	Avg	Min	Max	Avg	Min	Max	Avg	Min	Max	Avg
1st Layer - Adjusted	-0.01	0.00	-0.01	-0.01	0.00	-0.01	-0.01	0.02	0.01	0.01	0.04	0.03
1st Layer - Standard	-0.02	0.01	0.00	-0.03	0.03	0.00	-0.02	0.02	0.00	0.01	0.02	0.02
2nd Layer - Adjusted	-0.01	0.03	0.01	-0.01	0.01	0.00	-0.02	0.05	0.01	0.00	0.03	0.02
2nd Layer - Standard	-0.01	0.06	0.03	0.00	0.04	0.02	0.05	0.15	0.10	0.03	0.25	0.17

Table 1a), b). Experimental Data

ACKNOWLEDGEMENTS

The author wishes to gratefully acknowledge the assistance and cooperation of her colleagues from R&D and Fiber Optics Manufacturing Division of CommScope, Inc. Thanks to Mr. Doug Blew, Fiber Optics Operations Manager, for his excellent advice and comments in processing issues, and to Mr. Bruce Carlson, Mr. Chris Story, and Mr. John Chamberlain for their help on this project. The author would like to extend her sincere appreciation to Mr. David Esker, Materials Engineer, for his exceptional work on thermo-analytical and tensile measurements. In addition, special thanks to Mr. Brent Hager, Product Development Technician, for test data he provided.

REFERENCES

1. S. M. Cooper, K. L. Coupe, B. D. Zimmermann, "The Effect of Temperature Dependent Materials Properties on Fiber Optic Cable Design", *Proceedings of the 35th International Wire and Cable Symposium*, pp 148 -158, 1986.
2. M. C. Light, J. A. Moses, M. A. Sigmon, C. A. Story, "Design and Performance of Telecommunication Cables Optimized for Low Fiber Counts", *Proceedings of the 37th International Wire and Cable Symposium*, pp 63-70, 1988.
3. J. Horska, "Fiber Optic Cable Having Extended Contraction Window and Associated Method and Apparatus for Fabricating the Cable", *U.S. Patent Application*, Serial Number 08/258,532, June 1994.
4. D. J. Blew, "Apparatus for Controlling Excess Fiber Length in a Loose Tube Optical Fiber Buffer Tube", *U.S. Patent*, Patent Number 4,921,413, May 1990.
5. D. J. Blew, "Method for Controlling Excess Fiber Length in a Loose Tube Optical Fiber Buffer Tube", *U.S. Patent*, Patent Number 4,983,333, January 1991.
6. T. Salat, et al, "Mala Encyklopedia Matematiky", *Obzor - Bratislava*, 1981.
7. Bellcore, "Generic Requirements for Optical Fiber and Optical Fiber Cable", *Technical Reference TR-NWT-000020, Issue 5*, December 1992.

APPENDIX

Part I: Theory of Curve in Three Dimensions

Definition (1)

Let C be the curve consisting of all ordered triples $[f(t), g(t), h(t)]$, where the functions f , g , and h are continuous on an interval I . The equations

$$x = f(t), y = g(t), z = h(t),$$

where t is in I , are called parametric equations for C , and t is called a parameter.

Definition (2)

Let $\mathbf{r}(t)$ be a vector-valued function expressible in the form

$$\mathbf{r}(t) = f(t)\mathbf{i} + g(t)\mathbf{j} + h(t)\mathbf{k},$$

where

$$x = f(t), y = g(t), z = h(t)$$

are parametric equations for a curve C , and t is a parameter. The vector-valued function $\mathbf{r}(t)$ is called a parametric expression of C .

Theorem (1)

If a parametric expression $\mathbf{r}(t)$ of a curve C , where t is in I , is a function of r -class (\exists r derivatives that are continuous), and $r \geq 1$, and $\mathbf{r}'(t) \neq 0$, then a curve C is called a regular curve.⁶

Theorem (2)

If $\mathbf{r}(t)$, $t \in \langle \alpha, \beta \rangle$, is a parametric expression of a regular curve C , then the length, L , of C is given by

$$L = \int_{\alpha}^{\beta} |\mathbf{r}'(t)| dt,$$

$$L = \int_{\alpha}^{\beta} \sqrt{f'(t)^2 + g'(t)^2 + h'(t)^2} dt.$$

Part II: Circular Helix

Parametric Expression

A parametric expression of a circular helix is

$$\mathbf{r}(t) = [a \cos t, a \sin t, bt],$$

where $a > 0$, $b \neq 0$, $t \in \langle \alpha, \beta \rangle$. The first derivative of $\mathbf{r}(t)$ is

$$\mathbf{r}'(t) = [-a \sin t, a \cos t, b].$$

A circular helix is a regular curve, because $\mathbf{r}'(t) \neq 0$.

Length of Circular Helix

According to Theorem (2) in Part I, the length of a circular helix between points A and B (see Fig. 3) is

$$L(A, B) = \left| \int_0^{2\pi} \sqrt{a^2 \sin^2 t + a^2 \cos^2 t + b^2} dt \right|,$$

$$L(A, B) = 2\pi \sqrt{a^2 + b^2}.$$

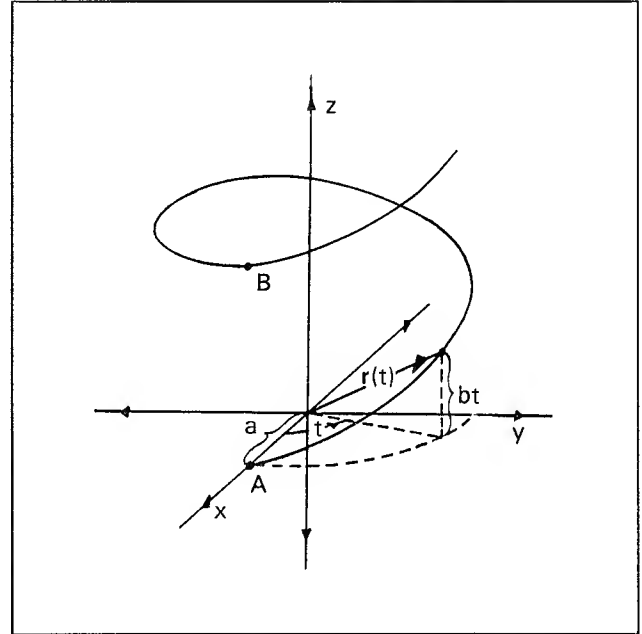


Figure 3. Circular Helix

Let D_H be a diameter of a circular helix and P a pitch length (lay length) of a circular helix. Then $a = D_H/2$, $b = P/(2\pi)$, and a length of a helix is

$$L = \sqrt{\pi^2 D_H^2 + P^2}.$$

Part III: Reverse Oscillating Helix

In a typical loose tube fiber optic cable, buffer tubes are arranged in a reverse oscillating helical lay pattern. A pitch length of helices varies in this cable configuration. Generally, the pitch length of the cycles around switchpoints is higher than it is in the rest of the cable. An irregularity of the reverse oscillating helical lay pattern is caused by limitations of the stranding machinery.

In order to provide a more accurate mathematical model

of this situation, a varying pitch length is considered in equation for the length of the helix.

Parametric Expression

A parametric expression $r(t)$ of a curve C for a reverse oscillating helix is

$$r(t) = [f(t), g(t), h(t)],$$

where $f(t) = a \cos t$ and $g(t) = a \sin t$. Typically, a function $h(t)$ in a form of a polynomial of the third order represents a pitch length irregularity with a sufficient accuracy. Then

$$r(t) = [a \cos t, a \sin t, bt^3 + ct^2 + dt + e],$$

$$r'(t) = [-a \sin t, a \cos t, 3bt^2 + 2ct + d].$$

Let $r(t)$ be a parametric expression of a curve C . Then length, $L(A_0, A_n)$, of C between points A_0 and A_n is:

$$L(A_0, A_n) = \left| \int_0^{2n\pi} \sqrt{a^2 \sin^2 t + a^2 \cos^2 t + (3bt^2 + 2ct + d)^2} dt \right|,$$

$$L(A_0, A_n) = \left| \int_0^{2n\pi} \sqrt{a^2 + (3bt^2 + 2ct + d)^2} dt \right|, \quad (10)$$

where $n \in \mathbb{N}$, $a = D_H/2$, and coefficients b , c , d , and e may be determined from test data by an interpolating method. Integral (10) may be solved numerically.

Part IV: Circular Helix Model of Contraction and Strain Windows

A) Traditional Design

Contraction Window. Let's assume that centers of a fiber bundle, C_{FBO} , and a buffer tube, C_{BTO} , are identical (see Fig. 4) at a reference temperature, typically room temperature. As the temperature decreases, a fiber bundle shifts in a direction extending radially outward from the buffer tube axis and away from the central support member to compensate for different rates of thermal contraction between optical fibers and other cable components. The cable contraction inducing a movement of a fiber bundle to position C_{FBC} is termed the contraction window, ϵ_C , of the fiber optic cable.

Let L_{FBO} be a length of the optical fibers in the reference length of cable, L_0 , at the reference temperature, T_0 . Typically, the reference length, L_0 , is equal to pitch length, P_0 , of the helically stranded buffer tubes. As the cable contracts as temperature decreases, also the pitch length decreases. Let L_{FBC} be a length of unbuckled optical fibers in the position C_{FBC} in the reference cable length, $L_C = P_C$, at the temperature T_c , where $T_c < T_0$. Then $L_{FBO} = L_{FBC}$ and contraction window may be

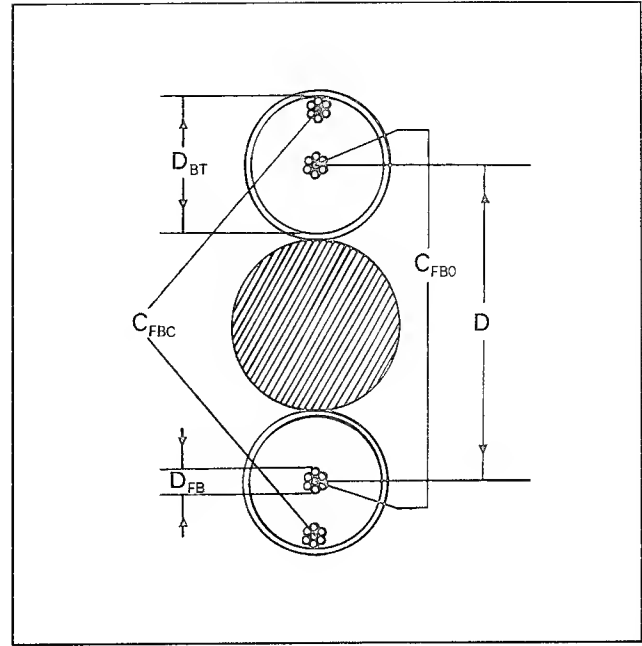


Figure 4.

determined as follows:

$$L_{FBO}^2 = \pi^2 D^2 + P_0^2$$

$$L_{FBC}^2 = \pi^2 (D + D_{BT} - D_{FB})^2 + P_C^2$$

$$P_C = P_0(1 - \epsilon_C) \Rightarrow \epsilon_C \in <0; 1>$$

where D is the center-to-center spacing between the buffer tube axes, D_{BT} is the inner diameter of the buffer tube, and D_{FB} is the diameter of the fiber bundle.

$$\pi^2 D^2 + P_0^2 = \pi^2 (D + D_{BT} - D_{FB})^2 + P_C^2$$

$$\epsilon_C = 1 \pm \sqrt{1 - \frac{\pi^2}{P_0^2} (D_{BT} - D_{FB}) (2D + D_{BT} - D_{FB})},$$

$$a) \text{ If } \epsilon_C = 1 + \sqrt{1 - \frac{\pi^2}{P_0^2} (D_{BT} - D_{FB}) (2D + D_{BT} - D_{FB})},$$

then $\epsilon_C \in <1; 2> \wedge \epsilon_C \in <0; 1>$.

It means that

$$\epsilon_C \neq 1 + \sqrt{1 - \frac{\pi^2}{P_0^2} (D_{BT} - D_{FB}) (2D + D_{BT} - D_{FB})}.$$

$$b) \text{ If } \epsilon_C = 1 - \sqrt{1 - \frac{\pi^2}{P_0^2} (D_{BT} - D_{FB}) (2D + D_{BT} - D_{FB})},$$

then $\epsilon_C \in <0; 1>$.

It means that

$$\epsilon_C = 1 - \sqrt{1 - \frac{\pi^2}{P_0^2} (D_{BT} - D_{FB}) (2D + D_{BT} - D_{FB})}.$$

Contraction window ϵ_C is

$$\epsilon_C = 1 - \sqrt{1 - \frac{\pi^2}{P_0^2} (D_{BT} - D_{FB}) (2D + D_{BT} - D_{FB})}.$$

Strain Window. Let's assume that centers of a fiber bundle, C_{FB0} , and a buffer tube, C_{BT0} , are identical at a reference temperature, typically room temperature (see Fig. 5). As the temperature increases or as a tensile load is applied to the cable, a fiber bundle shifts in a direction extending radially inward from the buffer tube axis and toward the central support member. The cable strain inducing a movement of a fiber bundle to position C_{FBS} is termed the strain window, ϵ_S , of the fiber optic cable.

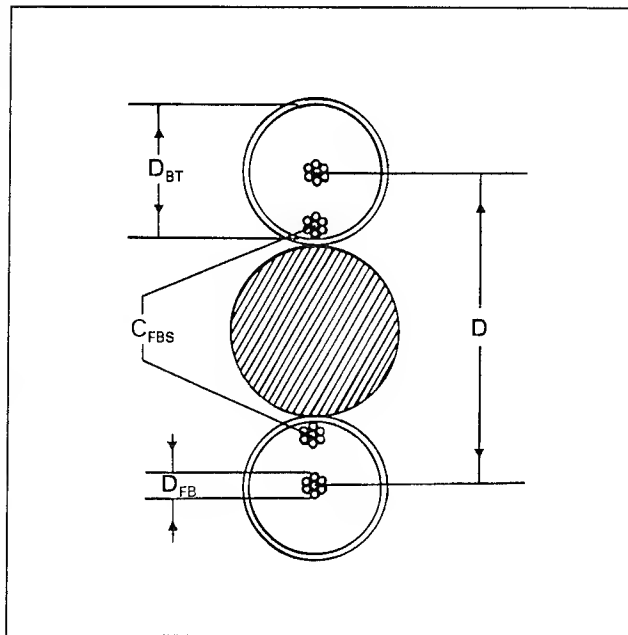


Figure 5.

The same logic as used in the section above is applied to determine the strain window as:

$$\epsilon_S = \sqrt{1 + \frac{\pi^2}{P_0^2} (D_{BT} - D_{FB}) (2D - D_{BT} + D_{FB})} - 1.$$

B) New Design Approach

Offset of Optical Fibers. By adjusting the contraction and strain windows, the optical fibers inside the buffer tube assume an average position offset (see Fig. 6).

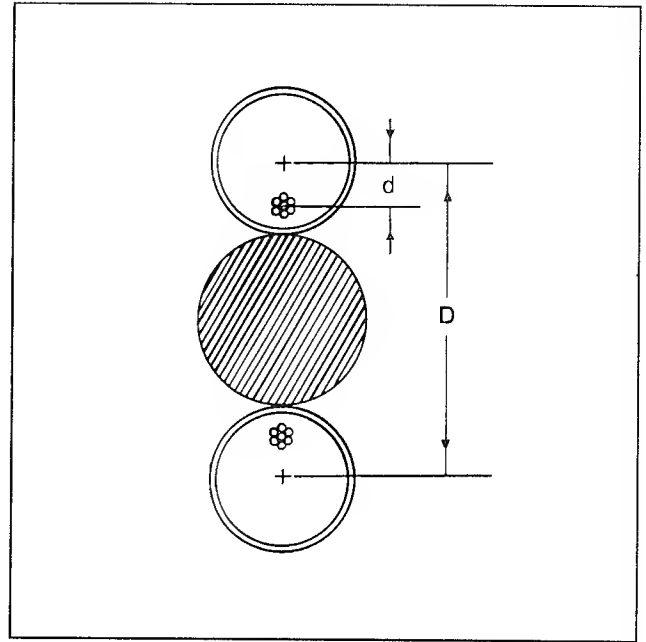


Figure 6.

The logic from previous sections is used to quantify this offset as:

$$d = \frac{1}{2} \left[D - \frac{1}{\pi} \sqrt{(\pi^2 D^2 + P_0^2) (\epsilon + 1)^2 - P_0^2} \right],$$

where ϵ relates the length of buffer tube, L_{BT} , and length of fiber bundle, L_{FB} , in the reference length of the cable:

$$\epsilon = \frac{L_{FB}}{L_{BT}} - 1.$$

If L_{BT0} is the length of the buffer tube after buffering, then the elongation of buffer tube after stranding process, ϵ_{BT} , and the excess fiber length in buffer tube after buffering, ϵ_{EFL} , are defined as:

$$\epsilon_{BT} = \frac{L_{BT}}{L_{BT0}} - 1,$$

$$\epsilon_{EFL} = \frac{L_{FB}}{L_{BT0}} - 1.$$

Parameter ϵ may be expressed in the form:

$$\epsilon = \frac{\epsilon_{EFL} - \epsilon_{BT}}{\epsilon_{BT} + 1}.$$

For the fiber optic cable fabricated with tension applied to the buffer tubes during stranding of the core, ϵ_{BT} may be calculated as follows:

$$\epsilon_{BT} = \frac{4F}{\pi E (D_2^2 - D_1^2)},$$

where E is the secant modulus of the buffer tube material, F is the tension applied on the buffer tube during stranding process, and D_1 (D_2) is the inner (outer) diameter of the buffer tube.

Contraction Window. The contraction window, ϵ_{Cd} , in cable with the fiber offset, d , may be determined similarly as the contraction window in traditional cable:

$$\epsilon_{Cd} = 1 - \sqrt{1 - \frac{\pi^2}{P_0^2}(D_{BT} - D_{FB})(2D + D_{BT} - D_{FB}) - \frac{\pi^2}{P_0^2}4d(D-d)}.$$

Strain Window. Likewise, the strain window, ϵ_{Sd} , in a new design approach is:

$$\epsilon_{Sd} = \sqrt{1 + \frac{\pi^2}{P_0^2}(D_{BT} - D_{FB})(2D - D_{BT} + D_{FB}) - \frac{\pi^2}{P_0^2}4d(D-d)} - 1.$$



Jana Horska

CommScope, Inc.
General Instrument Corp.
6519 CommScope Rd.
Catawba, NC 28609
U.S.A.

Jana Horska is Product Development Engineer at CommScope, Inc. She received her M.S. Degree in Optics and Optoelectronics from Comenius University, Bratislava, Slovakia, in June 1991. She joined CommScope, Inc. in June 1993.

SUBSTRATE EFFECTS ON CURE OF UV CURABLE FIBER OPTIC MATERIALS

David M. Szum

DSM Desotech Inc.
Elgin, Illinois

ABSTRACT

The ultimate physical properties of a coating may be underdeveloped when the coating is cured on a substrate that may act as a heat sink. Such is the case when the substrate has a significantly greater mass than the coating. Data are presented which compare the properties of coating cured on optical fiber with those of the same coating cured on glass plates, release paper, and thin polyester sheets. Two independent test methods were used to verify this effect. Glass transition temperatures were taken from modulus versus temperature sweeps (isochronal thermal sweeps) as generated on a solids analyzer rheometer. The degree of cure was measured using a Fourier Transform Infrared technique. In this technique, the percent of reacted acrylate unsaturation (% RAU) was calculated by ratioing the acrylate absorbance of the cured coating at 810 cm^{-1} to the corresponding absorbance of the liquid. Tensile properties (from an Instron) were also generated to provide a practical link to a common Quality Control test provided by coating manufacturers. The data indicates that caution needs to be exercised when modeling coating behavior on fiber using coating physical property data generated on glass plates. This effect is only seen in coatings with glass transition temperatures above ambient cure conditions (outer primary coatings and some matrix materials). Alternative substrates are proposed which allow the coatings to cure to a larger degree and more closely resemble properties of coatings as cured on fiber.

INTRODUCTION

Many optical fiber and optical fiber ribbon manufacturers are attempting to generate mathematical models based on cured coating physical properties. These models are developed with the assumption that bulk coating properties either do not significantly change or change in a linear manner when the coating substrate mass is altered. As a result, the developed models may be misleading or fail altogether when trying to accurately predict fiber properties. By carefully choosing the substrate for the polymer flat film testing, one can more accurately model coating behavior on optical fiber and optical fiber ribbon.

The crosslinking of UV curable materials is similar to the crosslinking of other thermosetting materials and generally involves the transformation of low molecular weight liquids to high molecular weight amorphous solids by means of chemical reactions. An understanding of the curing process is of particular

importance in the fiber optic telecommunications industry, especially considering the emphasis on modeling optical fiber and optical fiber ribbon behavior based on polymer physical properties. A useful framework for understanding the changes which occur during cure of a thermosetting system is the isothermal time-temperature-transformation (TTT) cure diagram. This type of phase diagram was developed for thermosetting materials in an attempt to understand cure phenomena¹. A TTT diagram, schematically shown in Figure 1, is a plot of the times required to reach gelation and vitrification, as a function of cure temperature. This paper shows that UV curable coatings can be understood by treatment in a similar manner.

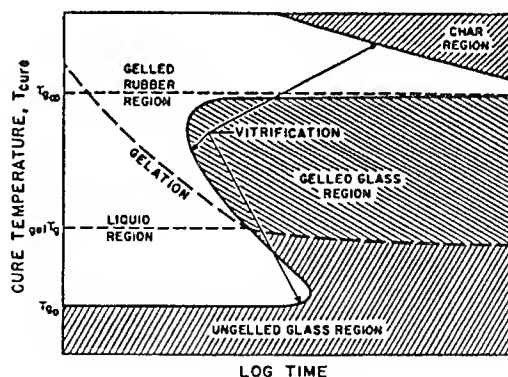


Figure 1 Time-temperature-transformation (TTT) cure diagram (schematic)

A brief summary of how the TTT cure diagram relates to UV curable polymers is required. In short, in order to achieve a maximum degree of crosslinking, the cure temperature must exceed the ultimate maximum glass transition temperature of the polymer ($T_{g_{\infty}}$). Since this temperature during cure is a critical factor in physical property development, then it follows that any condition during cure which would reduce or dissipate the heat generated (so that the temperature during cure could not attain $T_{g_{\infty}}$) would also retard the degree of

cure of the polymer. The result is a lower degree of cure and, therefore, a lower glass transition temperature (as well as a lower room temperature modulus). One goal of this work is to understand any conditions during cure which would affect the cured polymer properties in the ways described. Furthermore, since the TTT cure diagram is unique for each UV curable polymer (dependent on polymer morphology and degree of exotherm), the extent of cure inhibition will also be unique for each UV curable polymer. In fact, *at any given cure temperature below $T_{g\infty}$ two polymers can have very similar physical properties, whereas, if allowed to fully cure at temperatures above $T_{g\infty}$, they can have drastically different physical properties.* It is important, therefore, to mimic the temperature during cure of the application (in this case, a UV curable coating applied on optical fiber) as closely as possible to be able to accurately model fiber performance based on polymer coating physical properties. If this is not done, then contradicting data may occur and erroneous conclusions may be made. The main goal of this work, therefore, is to not only find what factors influence the temperature during cure, but to see if those factors can be controlled to mimic the temperature during cure on optical glass fiber.

Experimental

Coating Preparation:

The formulations used were typical high modulus fiber optic outer primary coatings or matrix materials. They were manufactured using reactants and diluents obtained from the suppliers without further purification. After blending, the solution was filtered through a 1.2 micron (absolute) Cuno filter. Three different coatings were used in this study. Coating A is a typical outer primary coating and Coatings B and C are typical matrix materials.

Film Preparation:

The coatings were drawn down on one of three different substrates 1) A 22.68 cm x 27.72 cm glass plates (mass = 360 grams), 2) A 75 micron (nominal) piece of release paper which was secured to a glass plate (mass = 6 grams), or 3) A 125 micron thick 22.68 cm x 27.72 cm Mylar® film (mass = 10 grams). All drawdowns were made using a Pacific Scientific Automatic Drawdown Apparatus and Gardner bird bar film applicators of the appropriate film thickness. Actual measured film thicknesses are reported with the data. The coating was cured to 100% of its achievable ultimate modulus (dependent on the substrate and substrate mass) using a Fusion Systems Model K523/2

Fusion Unit with a single "D" bulb. An 8.0 cfm nitrogen atmosphere was employed. Curing was accomplished using a dose of 1.0 J/cm² as measured by an International Light, Inc. IL 390 Light Bug, which measures light in the 257-390 nm wavelength range.

The same outer primary coating was also applied to 125 micron OD optical fiber glass resulting in a total OD of 246 microns. The draw rate was 50 m/min and the curing lamp was a 120 W/cm Fusion D bulb. The estimated UV dose was 0.6 J/cm². No inner primary coating was applied and a technique was found to remove the coating intact (as a tube). Subsequent testing, such as DMA, was run with several "tubes" in tandem with geometry calculated appropriately. As much as was possible, the "tube" samples were treated identically to the films.

Dynamic Mechanical Analysis:

Rheological data was obtained from a Rheometrics Solids Analyzer (Model RSA II). Temperature sweeps were employed, starting and finishing at appropriate temperatures. The frequency was set at 1.0 radian/second and temperature sweep values of the elastic modulus (E'), loss modulus (E''), and tan delta were recorded at two degree intervals. Before starting a temperature sweep experiment, the sample was preheated to 80°C for a minimum of five minutes in the dry nitrogen atmosphere (less than 1% RH) of the rheometer's environmental chamber. This was done not only to remove ambient water that may be present and act as a plasticizer, but also to erase any prior heat history effects present from physical aging². The temperature sweep sample was cooled from 80°C to -60°C and then a temperature sweep was run from -60°C to 90°C.

Fourier Transform Infrared Spectroscopy (FTIR):

FTIR spectra were obtained using a Nicolet model 60SX. Samples of the uncured liquids, the cured polymers, and coated optical fibers were examined using an attenuated total reflectance (ATR) accessory equipped with a KRS-5 crystal. The angle of incidence was set at 45°. Data was collected using 100 co-added scans at 4 cm⁻¹ resolution with a DTGS detector. ATR is a surface technique so data was obtained on both surfaces of coatings cured on glass, Mylar, and release paper. Only the outer surface was examined on coated optical fiber.

For each spectrum, the acrylate absorbance at 810 cm⁻¹ was normalized to a reference peak. Comparison of the acrylate absorbance of the cured sample to that of the uncured liquid coating yielded the percent of

reacted acrylate unsaturation (% RAU). Further details of this test are available upon request.

Tensile Properties:

Tensile properties were measured using an Instron Model 4201. The gauge length was 50 mm and the strain rate was 25 mm/minute. The secant modulus at 2.5% strain was the selected measure of modulus. It is defined as the stress at 2.5% strain divided by that strain value (.025 in absolute terms). The details of this method are available upon request.

RESULTS AND DISCUSSION

To better understand the significance of the TTT cure diagram, some descriptive definitions and some background information are required. The *glass transition temperature* (T_g) and its variations ($T_{g_{\infty}}$, T_{g0} , etc.) represents the point at which a polymer (regardless of its degree of cure) becomes a vitrified glass. This point has been defined many ways. For the purposes of this work, however, it will be defined by three points on a dynamic mechanical analysis (DMA) scan as follows: 1) The temperature for which the elastic modulus is 1000 MPa; 2) The temperature for which the elastic modulus is 100 MPa; 3) The temperature at which the tan delta curve attains its maximum value. As long as the reference points are consistently used, the observations will be valid. *Gelation* is defined as that (fixed) point in the progress of the reaction at which rubbery elastic properties appear. It is the result of the formation of a crosslinked network. Curing reactions which do not produce crosslinks also do not produce gelation³. *Vitrification* is defined as the (fixed) point where the reaction mixture attains a glassy state. The point can be reached with or without prior gelation. Vitrification cannot occur in a curing reaction if the glass transition temperature of the fully cured material is below the temperature of curing.⁴ Below $_{gel}T_g$, the temperature at which the time to gel is the same as the time to vitrify, the resin can remain ungelled, even though it can become hardened during storage. The resin remains flowable and fusible as long as it is in its ungelled state. Below T_{g0} , the glass transition temperature of the unreacted UV curable resin, essentially no reaction occurs because the reactive species are immobilized in the glassy state.

The resin will not vitrify on isothermal cure if the cure temperature is above $T_{g_{\infty}}$, the glass transition temperature of the fully cured resin. The cure can then proceed to near completion *since it will not be quenched prematurely as it would be below $T_{g_{\infty}}$* . At cure temperatures sufficiently below $T_{g_{\infty}}$, the reaction will not go to completion. As the viscosity increases (a result of

the increasing molecular weight), the reaction becomes diffusion controlled and the living free radical chains ends are no longer mobile enough to find and react with other living free radical chain ends. Thus the cessation of reaction is not necessarily an indication that the reaction is complete, i.e., the reaction may have been quenched due to vitrification. The extent of conversion attained when the reaction is quenched increases as the temperature during UV cure is raised, as evidenced by a corresponding increase in the glass transition temperature.⁵ This being the case, then, it becomes necessary to understand the factors which influence the temperature of the UV curable resin during the curing process. Some of the considerations for understanding these factors are as follows:

1) The true temperature during cure is likely to be *different than* the ambient temperature, due to exothermic heat of reaction raising the coating temperature above ambient.^{6,7} In addition, the UV curing process usually involves the emission of heat, in the form of infrared radiation, from the bulbs of the UV processor.

2) The extent of this extra boost in temperature will be strongly affected by heat loss to the surroundings. Therefore:

a) Lower surface-to-volume geometries will favor heat retention and higher peak temperatures during cure.

b) The mass per unit area of the substrate and its thermal diffusivity will influence the amount of heat that it can draw away from the reacting coating.

From these considerations, we conclude that thick coatings will retain more heat than thin ones and that low mass/unit surface area substrates will allow the coating to retain more heat.

The first step in this study was to examine any differences in the coating bulk properties for a coating applied on fiber versus the same coating cured on glass at different thicknesses as well as coating cured on release paper. Release paper was used since its mass was about the same as the coating and would provide a thermal barrier between the glass and coating. Different thicknesses on glass were used to examine any potential "insulation" effect of the polymer from the glass "heat sink". Polymers are very poor heat conductors compared to glass.⁸ Coating A was examined and the results are shown in Table I. All samples were compared by DMA and, also, extent of conversion (% RAU) was measured by FTIR. These two techniques were chosen to examine cure suppression because they are significantly different in

Sample ID	Substrate	Sample Thickness (microns)	T at $E_{1000\text{MPa}}$ (°C)	T at $E_{100\text{MPa}}$ (°C)	T at Tan Delta Max (°C)	Equilibrium Modulus (MPa)	Tensile Modulus ^e (MPa)	%RAU on Top of Film	%RAU on Bottom of Film
A	Glass	49	30	49	50	18.8	650 (52.6)	93	94
B	Glass	60	31	50	51	20.5	700 (64.5)	95	92
C	Glass	72	32	51	53	20.4	730 (82.8)	96	92
D	Glass	188	39	66	67	30.5	900 (184.4)	100	95
E	Glass	315	41	71	70	34.3	1070 (289.6)	99	97
F	Glass	639	36	69	67	31.0	960 (632.5)	100	95
G	Release Paper	102 ¹	43	73	72	33.9	1050 (106.7)	100	99
H	Release Paper	719 ¹	36	69	69	29.8	900 (713.7)	100	95
I	Glass	56 ²	31	50	52	19.3	830 (79.8)	94	96
J	Glass	647 ²	36	68	67	30.4	960 (642.62)	100	94
K	Release Paper	102 ³	43	75	72	----	980 (114.3)	100	99
L	Release Paper	655 ³	38	70	69	30.8	870 (670.6)	100	95
M	Optical Fiber	62.5 ⁴	42	74	72	32.3	----	98	----

Table I
Effect of Thickness and Substrate on Cured Coating Properties of Coating A

- ¹ Cured on white release paper to get the insulating effect of the coated paper.
- ² Cured at 2.0 J/cm² on glass to find the contribution of 100% reflection from the white release paper towards cure.
- ³ Cured at 2.0 J/cm² on release paper to study the effect of increased cure and/or heat on properties.
- ⁴ Outer primary (only) coated fiber obtained from a draw tower. The coating was mechanically stripped from the fiber as described in the experimental section. The resulting films were taped together (so that several tubes were run in parallel) and DMA scans were run.
- ⁵ Numbers in parentheses are film thicknesses (in microns) measured for the modulus result (alone). These are from the same film samples as cured above, however, different gauge lengths were required for the tensile modulus test.

data collection (the DMA is purely a physical measurement and FTIR is a spectroscopic measurement) and thus operates as an independent verification of the cure suppression effect. Tensile modulus results were also generated for all samples, except for the coating stripped from the fiber, to provide a reference point.

The results from Table I may be summarized as follows:

1) As coating thickness increases (samples A-F), the T_g and the modulus of the material actually increases, reaches a maximum, and then starts to decrease. It is only at the T_g maximum that the coating properties resemble the properties of the coating cured on fiber (sample M).

2) The 102 micron sample (sample G) cured on release paper has the highest T_g and most closely resembles the coating applied on fiber (sample M). The 719 micron sample (sample H) cured on release paper

shows a reversal of the trend for modulus, T_g , and % RAU on the bottom. It is believed that, at this thickness, the sample is starting to show incomplete cure due to absorption of light (the Beer's Law effect), however, it still indicates a larger degree of cure (by DMA and FTIR) than the 72 micron (sample C) as cured on glass.

3) The experiment with the 56 micron sample and the 647 micron sample cured on glass at 2.0 J/cm² (samples I and J, respectively) was performed to show that this effect is not due to "reflection" of the light from the white release paper. If 1.0 J/cm² light was 100% reflected (an unlikely event) then the sample would receive a total of 2.0 J/cm². As can be seen, the T_g of the sample is similar to the samples cured at 1.0 J/cm².

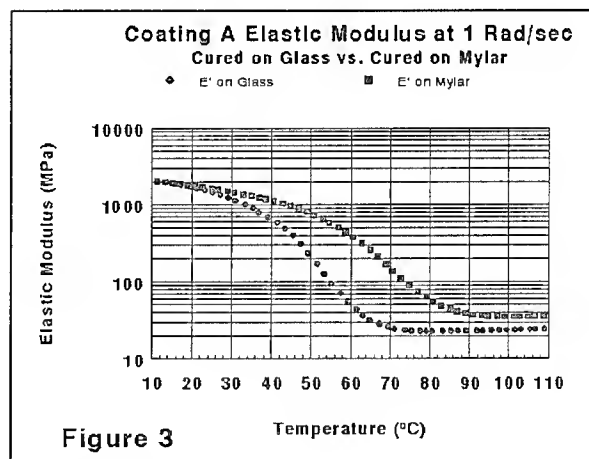
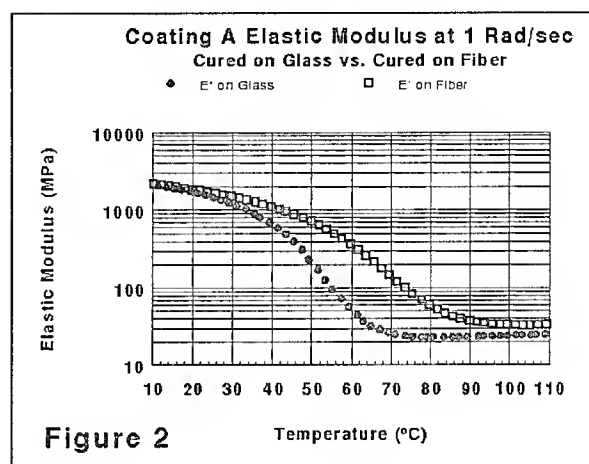
4) Samples K and L were cured on release paper at 2.0 J/cm² to see if any further cure could be obtained. There is no evidence of further cure.

A few sources of heat generation have already been mentioned (exotherm and IR from UV lamps). If these could be kept constant for any given UV curable polymer, then only the variables between coating application (on fiber) and data generation (on glass plates) need to be examined. The most obvious variable is the nature of the substrate itself. Currently, optical fiber coating manufacturers provide data as cured on glass plates. While the silica surface is not as high a quality as that of optical fiber silica, it has been assumed that the two substrates should be similar enough that coating bulk properties, such as T_g , from the two substrates are comparable. This assumption was verified experimentally. The only remaining difference, then, is the actual differences in the coating/glass mass ratios. In the case of a typical 250 micron silica optical fiber, the coating/glass mass ratio is close to 1:1. In the case of coating cured on a glass plate, the coating/glass mass ratio is on the order of 1:100 (assuming 4 grams of coating on a 400 gram glass plate). Since silica glass, in general, is relatively transparent to UV and IR radiation, it does not generate any significant heat upon exposure to these wavelengths of light. As a consequence, to maintain thermal equilibrium the silica substrate will act as a "heat sink" and absorbs as much heat from the coating as it possibly can. This removal of heat from the coating, therefore, lowers the temperature during cure thus resulting in suppression of the coating's "true" T_g .

In general, the effectiveness of a "heat sink" is proportional to its mass and to the surface area of exposure, both relative to the mass of the "heated" object (in this case, the UV curable coating). The mass ratios have already been discussed. The surface/volume ratio for a 250 micron coated fiber (assuming standard 125 micron optical fiber glass) is approximately 11000/m and the surface/volume ratio for an average 15.12 cm x 22.68 cm x 75 micron drawdown is approximately 13000/m. These values are within the same order of magnitude and thus, for this experiment, were not considered significantly different.

The data in Table I indicates that the glass plate was acting as a heat sink and that this effect is the largest contributor to the T_g suppression. The next step was to find a substrate which would allow full T_g development (by thermally insulating the coating from the glass plate) and still be of practical everyday use. Release paper is not an ideal candidate for the latter purpose since it provides a somewhat textured surface on the cured film and does not provide much substrate support. Among some of the other substrates tested was 125 micron polyester (Mylar). This substrate was stiff enough to provide good support when secured to a glass plate, yet provided a good thermal insulation barrier. The data in Figures 2,3, and 4 are DMA

comparisons of the same material cured on glass versus fiber (Figure 2), glass versus Mylar (Figure 3), and finally Mylar versus Fiber (Figure 4). As can be readily seen, the sample cured on Mylar and optical fiber are almost identical, while the sample cured on glass is significantly different.



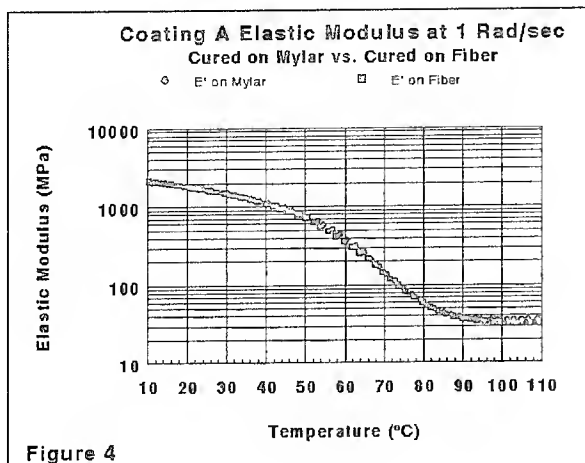


Figure 4

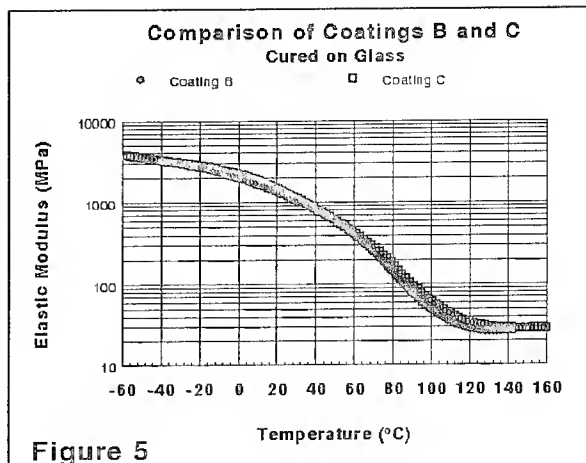


Figure 5

The presence of this effect in itself should not pose a problem to fiber manufacturers. Most of the important coating data gathered is generated on optical fiber. Recently, however, more manufacturers are interested in developing models and databases to predict fiber performance from data supplied by coating manufacturers. For these purposes, the heat effect described herein poses a real problem. This effect is not only significant, it is also non-linear. An explanation of this can best be seen in Figures 5 and 6. Figure 5 is a comparison of the DMA's of Coatings B and C cured on glass. They appear to be very similar. However, when compared on Mylar (Figure 6), there is a very large difference. Therefore, the assumption that since these materials appear the same on glass, they should be similar on Mylar or fiber, would be a faulty assumption. In fact, since the discovery of this phenomena, a few actual reverses in predictions based on coating properties as cured on glass have been observed which were subsequently explained by comparing the materials as cured on Mylar. This effect will be completely dependent on the unique vitrification and gelation temperatures for the different oligomers and monomers used in any given UV curable formulation. This fact has far reaching implications. We have studied only a couple of physical properties in this work, however, it is reasonable to conclude that assumptions regarding (high T_g) coating physical properties as cured on glass will be unreliable predictors of coating performance on optical glass fiber.

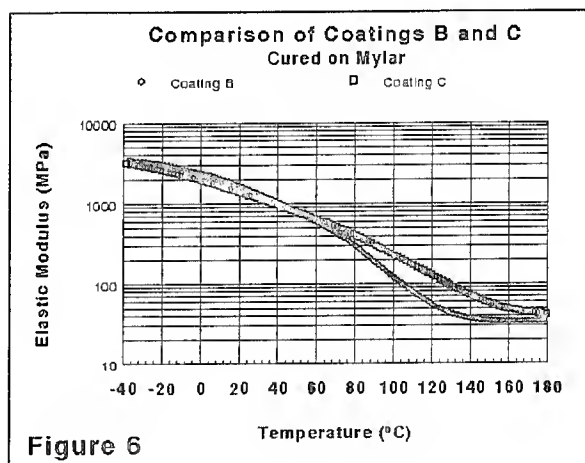


Figure 6

It can be inferred from the theory described above that only materials which have a T_g above ambient temperature will be susceptible to this "vitrification effect".

It is well known that the UV cure reaction is an exothermic reaction and, as such, generates a good deal of heat during the curing process. The irradiating lamps also generate IR radiation which also is transformed into heat. This means that the temperature during cure will always be above ambient temperature and, hence, low T_g inner primary coatings, by definition, will always cure above their T_g . Outer primary optical fiber coatings and higher T_g matrix materials, however, will be subject to this "vitrification effect".

CONCLUSIONS

The following are a summary of the conclusions that can be made from this study:

- 1) Due to substrate mass differences, the properties of high T_g UV curable coatings cured on glass plates are substantially different from those of identical coatings cured on optical fiber.
- 2) When high T_g coatings are cured on thin mylar, release paper, or any other low mass substrate (even if secured to glass), then the physical properties will closely match those of identical coatings cured on optical fiber.
- 3) Physical properties of UV curable coatings cured on glass plates are not useful or reliable for predicting the corresponding optical fiber properties.

¹ J.K. Gillham, "Torsional Braid Analysis (TBA) of Polymers," *Developments in Polymer Characterisation-3*, J.V. Dawkins, Ed., Applied Science, London, 1982, Chap. 5.

² "Polymer Relaxation Effects on Physical Properties of UV Curable Materials", D. M. Szum, **Radtech '94 North America UV/EB Conference and Exhibition Proceedings**, May 1-5 1994, pages 220-228

³ P.J. Flory, *Principles of Polymer Chemistry*, Cornell University Press, Ithaca, N.Y., 1953

⁴ J.B. Enns and J.K. Gillham, *J. Appl. Polym. Sci.*, **28**, 2567 (1983)

⁵ J.B. Enns and J.K. Gillham, *J. Appl. Polym. Sci.*, **28**, 2831 (1983)

⁶ J.E. Moore, in: *U.V. Curing: Science and Technology*, Vol. 1 (S.P. Pappas, ed.), Technology Marketing Corp., Norwalk, Conn. (1978).

⁷ C.E. Hoyle, in: *Radiation Curing: Science and Technology*, (S.P. Pappas, ed.), Plenum Press, New York, N.Y. (1992)

⁸ E.V. Thompson, in: *Encyclopedia of Polymer Science and Engineering*, 2nd Edition, Vol. 16 (Mark, Bikales, Overberger, and Menges, ed.), John Wiley & Sons, New York (1989), pp. 711-747

Acknowledgements

The author would like to acknowledge the following for their invaluable assistance:

John Zimmerman (for a crucial observation)
Dr. Robert Johnson
Timothy Bishop
Steven Schmid
Roger Salvesen
Dr. James Julian
DSM Desotech



Biography

David M. Szum received a BS in Biochemistry at Illinois Benedictine College, Lisle Illinois. He also holds a M.S. in Chemistry from the University of Illinois at Chicago. He is currently a senior research chemist for DSM Desotech, Inc. He has been engaged in research and development of coatings for optical fibers since January 1989. He is also a member of EIA/TIA working committees 6.6.7, fiber coatings, 6.6.8, fiber reliability, and 6.7.10, color coding of fiber optic cables.

INFLUENCE OF GLASS-COATING ADHESION ON THE OPTICAL AND MECHANICAL PERFORMANCES OF FIBRES IN WATER

F.Cocchini, D.Cuomo, G.Ferri, A.Pudia

FOS - Fibre Ottiche Sud
Strada Provinciale 135 - Km 4.5
84091 Battipaglia (SA) ITALY

ABSTRACT

UV-curable acrylic resins, currently the most used coating materials for optical fibres, are intrinsically permeable to water and are known to undergo the swelling phenomenon. As a consequence, unbalanced stresses may arise after immersion in water, and possibly delamination and microbending losses may develop. Moreover, permeation through the coating in presence of delamination allows the water molecules to break the glass SiO linkages, thus degrading the mechanical strength of the fibres.

In this paper a possible correlation between water soak fibre performances and some characteristics of coating materials is suggested.

1. INTRODUCTION

Immersion of fibres in water has been shown to cause an increase of the attenuation coefficient and a decrease of the tensile strength.

The presence of unbalanced stresses, arising after immersion in water, is a possible cause for delamination, depending on the intermolecular forces at the glass-coating interface; asymmetric stresses (due to swelling), in turn, cause an increase of transmission losses (attenuation) due to the μ -bending phenomenon.

The strength degradation of the glass is most probably due to the water molecules which, freely moving at the glass surface after delamination, easily break the glass SiO linkages (particularly in presence of OH^- or H^+ excess) [1,2].

Experiments have been carried out to investigate these two items: three types of double-layer coating (denoted X, Y and Z) have been considered. The coated fibres have been immersed in water at controlled temperatures. The added losses, the tensile strength and the occurrence of delamination have been monitored with time, and mutually correlated.

It has been possible to associate the occurrence of delamination to low values of the "threshold strength" at the glass-coating interface for the X pairs: this quantity is defined as the limit of the adhesion energy for very low rates of

deformation, and is better measured above the glass transition temperature, in order to minimise energy dissipation [3]. The different behaviour of the Y and Z coatings, which turn out to have similar threshold strengths, is probably connected with dimensional changes correlated to the weight changes and extractables.

2. EXPERIMENTALS

2.1 Equipment

In order to evaluate the glass transition temperatures (T_g) of the cured coatings, a Thermo-Mechanical Analyzer (TMA) was used: the set-up of the equipment, configured according to the tensional scheme, included a temperature variation from -40 to 60 °C, a 0.03 N static load and a (superimposed) 0.01 N step-dynamic load at frequency 1/12 Hz: when the material under test passes the T_g , its behaviour changes from glassy to rubbery, and an abrupt change in the response is clearly visible.

Measurements of adhesion between glass and cured films of coating were carried out using a precision dynamometer; coating samples were fully cured, over a glass plate, in the form of thin parallelepipeds, 0.1 mm thick and 16-20 mm wide. Peeling load was measured, at rates varying from 0.05 mm/min to 10 mm/min, and at temperature ranging from 20 to 60 °C. The adhesion energy per unit area G_a is defined as [1]

$$G_a = (1 - \cos\theta) F/W \quad (1)$$

where (fig.1) F is the peeling force, W is the width of the strip, θ is the peeling angle (in our experiments 45°, 90° or 135°), and a negligible stretching of the non-adherent part of the strip has been assumed.

Finally, the extractable content of the different materials was measured [4,5]: this was done by weighing cured samples of coatings before and after immersion in hot (60 °C) water; the results are given according to

$$\% \text{ Extractables} = 100 \cdot (W_0 - W_d)/W_0 \quad (2)$$

where W_0 is the initial weight of the (dried) sample and W_d is the final weight of the soaked and dried sample. This parameter is thought to be connected with the swelling, for water immersion, of the acrylic resins: the lower the extractables, the lower the swelling.

2.2 Conditioning

Water soak test was conducted according to the temperatures commonly adopted in Italy, i.e. 20 and 60 °C; fibres characteristics were monitored, measuring attenuation coefficients and tensile strength; care was given to the onset of delamination, checked with the aid of an optical microscope.

Tensile strength of conditioned fibres was measured at a rate of 50 mm/min on samples 0.5 m long; measurements (averaged on 10 samples) were taken every month, up to 9 months.

Attenuation coefficients were measured with an OTDR at 1550 nm: data were collected every hour at the beginning of the test, and then every week.

The onset of delamination was checked after 1, 3, 5, 15, 30 days: samples can be very short, but care must be taken to keep the extremities of the samples out of the water, in order to prevent water penetration by capillarity; the "degree" of delamination can be different with respect to the number and the size of observed separation points.

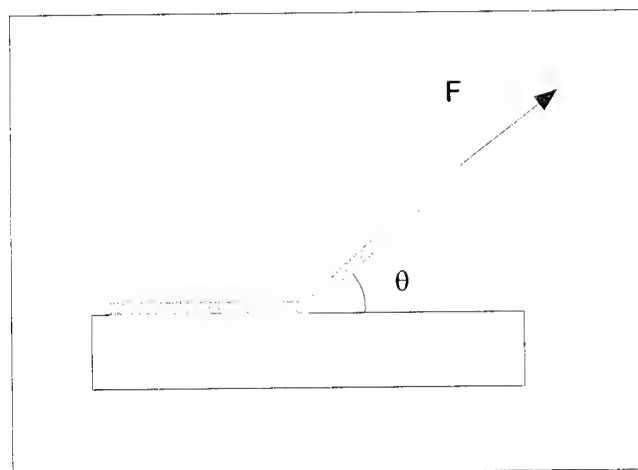


Figure 1 - Peel test.

3. RESULTS

3.1 Material Properties

Figs. 2, 3 show the results of TMA tests carried out on the material for the first layer of, respectively, the Y and the Z couple (in this respect, X is equivalent to Y): the T_g for X and Y first layer materials is greater than 25 °C, while the T_g for the first layer material of Z is clearly lower than 0° C.

Figs. 4 and 5 show the adhesion energy vs the speed of the dynamometer for two different temperatures. The results were dependent on the peeling angle according to eqn.(1). As already mentioned, an important parameter is the threshold strength, i.e. the limit of the adhesion energy for very low

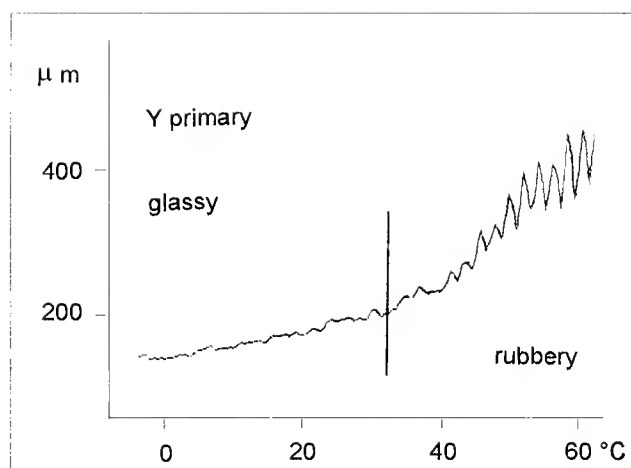


Figure 2 - Strain vs temperature for a Y primary sample under a 0.01 N step-dynamic load.

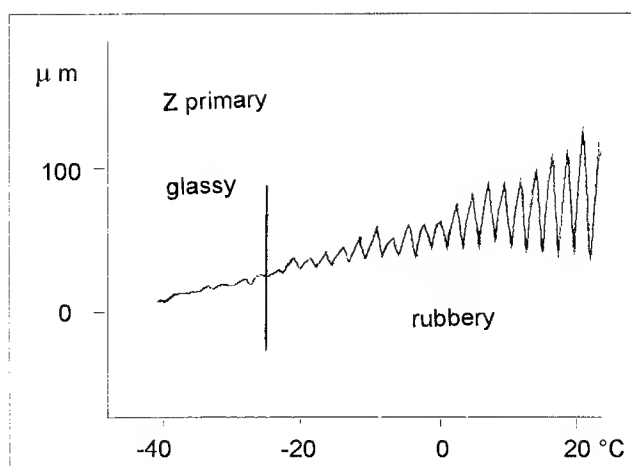


Figure 3 - Strain vs temperature for a Z primary sample under a 0.01 N step-dynamic load.

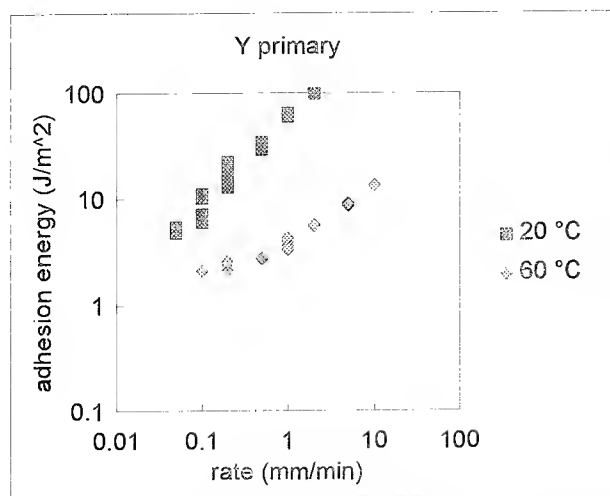


Figure 4 - Adhesion energy vs peeling rate at two temperatures for the Y primary.

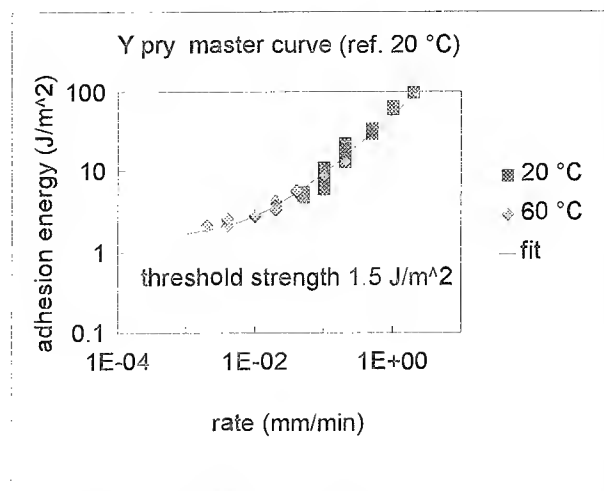


Figure 6 - Master curve of the adhesion energy vs peeling rate at the reference temperature of 20 °C for the Y primary.

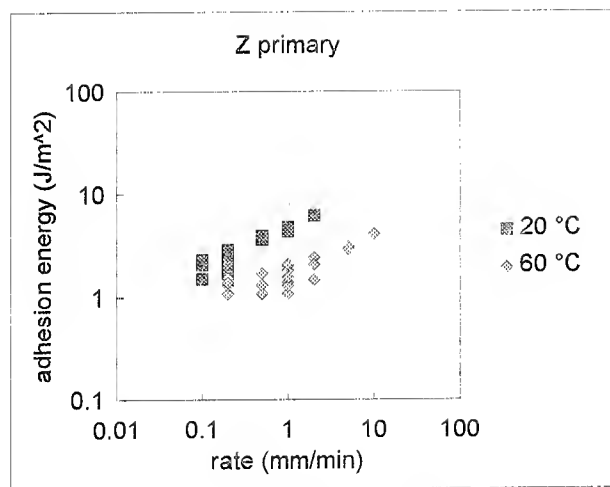


Figure 5 - Adhesion energy vs peeling rate at two temperatures for the Z primary.

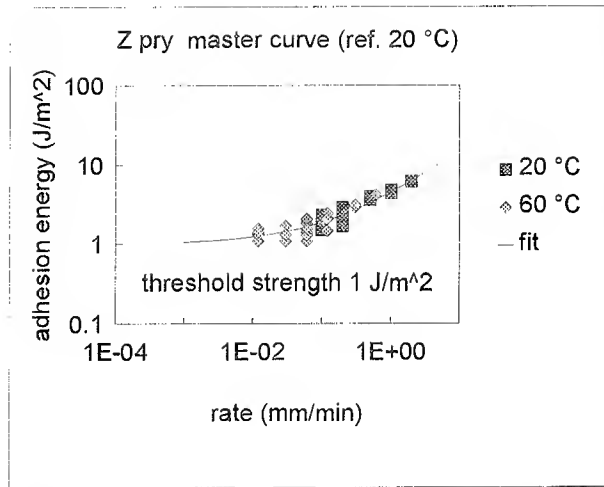


Figure 7 - Master curve of the adhesion energy vs peeling rate at the reference temperature of 20 °C for the Z primary.

rates. To obtain that parameter a rigid shift of the 60 °C data is applied, according to the time-temperature superposition principle, thus obtaining the master curves shown in Figs. 6 and 7 at the reference temperature of 20 °C for the materials of the first layer of Y and Z coatings; an equivalent curve for the X coating is not available, since a dramatic decrease of the peeling force is observed at low rate and/or high temperature, thus giving very noisy data. In Table I, we report the large adhesion energy (G_a) of the X coating at room temperature and high rate, which dramatically decreases (below the instrument sensitivity) at high temperature and/or low rate (threshold strength in Table I).

Values of extractables for the different materials are also given in Table I, where some other data are presented which are discussed in the next clause.

3.2 Fibres behaviour

Fig. 8 shows in detail the tensile strength degradation for the three different coatings over a period of 9 months ageing in hot (60 °C) water.

Transient losses (attenuation coefficients increase) are given (on a log scale) in fig. 9, where X was tested at 20 °C,

pair	Primary layer				Secondary layer	Fiber	
	Tg (°C)	Ga @ 20 °C 1 mm/min (J/m ²)	Threshold Strength (J/m ²)	Extractables @ 60 °C (%)	Extractables @ 60 °C (%)	Delamination & Added Loss	Mechanical Strength
X	high > 25	high 60	small < 0.5	medium 3.5	medium 3.3	short times/low temp. (hours @ 20 °C)	decreases
Y	high > 25	high 60	medium 1.5	high 5.5	medium 3.3	medium times/high temp. (days @ 60 °C)	decreases
Z	low < 0	medium 5	medium 1	low 2	low 1.2	not observed (> 1 month @ 60 °C)	stable

Table I - Summary of the results.

while Y and Z were tested at 60 °C; after the complete delamination, the stresses relax, and consequently the attenuation decreases (complete delamination occurs immediately on coating X at 60 °C, so that testing it at this temperature is meaningless).

Delamination was observed with an optical microscope: in fig. 10 is shown an example of partial delamination.

These observations are summarized in Table I; the following remarks apply:

- both coatings X and Y delaminate (and show large transient losses), respectively in short times (hours) at room temperature and in medium times (days) at 60 °C; mechanical degradation occurs for both types of coatings, over the typical long times (months at 60 °C) required for glass corrosion in water;
- coating Z does not delaminate over long times in water at 60 °C and maintains stable optical and mechanical performances.

These two remarks confirm that (as already stated in the introduction) transient losses are the macroscopic manifestation of delamination, which is responsible, in presence of water, of glass corrosion (strength degradation).

4. DISCUSSION

Delamination has been correlated to the swelling and, rather than to the adhesion force at room temperature and high rate, to the threshold strength between glass and primary coating, defined as the limit of the adhesion energy for very low rates of deformation, measured above the glass transition temperature: in fact, the delamination due to water sorption and swelling is physically a low rate phenomenon. In this respect the Z coating, which apparently have poor adhesion at room temperature, well behaves in the soak tests.

The strong adhesion energy of both the X and Y coatings at room temperature is due to the contribution of the energy dissipated in the internal motion of molecular segments

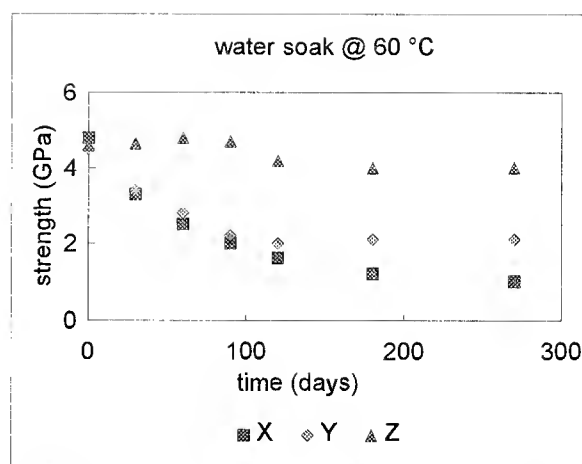


Figure 8 - Fibre mechanical strength vs time in water soak test at 60 °C for the three pairs of coating.

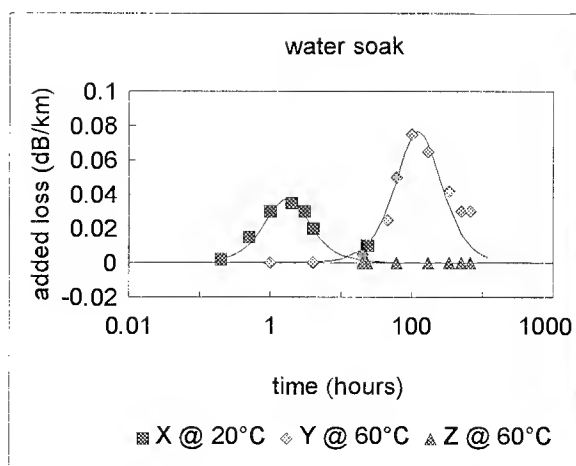


Figure 9 - Added losses at 1550 nm vs time in water soak test for the three pairs of coating at 20 or 60 °C.



Figure 10 - Example of partial delamination at the glass-coating interface.

ACKNOWLEDGMENTS

We wish to gratefully acknowledge our friends A.Mazzotti, G.Sabbato, C.Viscido and A.Pannullo for their unvaluable support in all the experimental activities.

REFERENCES

- [1] H.H Yuce, IWCS 92 Proc. (1992)605
- [2] W.Griffioen, IWCS 92 Proc. (1992)622
- [3] A.Ahagon and A.N.Gent, J.Polym.Sci. Polym.Phys.Ed. 13(1975)1285
- [4] C.P.Chawla, T.E.Bishop, D.M.Szum and K.P.Murray, Opt.Eng. 30(1991)763
- [5] A.Abel and J.Van Eekelen, EFOC 93 Proc. (1993)298

during the peeling. This contribution is large at high rates since those materials are below their T_g 's at room temperature.

Delamination and added losses are contemporary phenomena, with characteristic times depending on the threshold strength and the level of swelling (i.e. level of stress at the glass-coating interface). Mechanical degradation is a slower phenomenon fully activated, in our case, after the delamination occurrence.

The attitude of a coating to suffer delamination is connected to the threshold strength (coating X in Table I): however, other parameters can play an important role, such as the extractable content and the subsequent dimensional changes for water soak; the Y coating, for instance, has a "good" threshold strength, but its poor behaviour in water is due to the large dimensional changes (high extractables) which are responsible for intense stresses.

5. CONCLUSIONS

The occurrence of delamination at the glass-coating interfaces of optical fibres after immersion of samples in water has been shown to induce:

- i) a large increase of the transmission losses, and
- ii) zero stress ageing, that is a decrease of the mechanical strength other than stress corrosion.

Delamination has been correlated to the swelling and to the threshold strength between glass and primary coating. The threshold strength can thus be considered a critical parameter.



Franco Cocchini, after graduating in Physics at the University of Pisa in 1983, received a PhD in Solid State Physics from the Scuola Normale Superiore of Pisa. He has worked with EniChem R&D on the rheological and mechanical properties of polymeric materials. He joined FOS in 1990 where he is currently involved in the development of coating materials for optical fibres.



Giuseppe Ferri received the degree in Electronic Engineering from University of Naples "Federico II" in 1988. In the same year he joined FOS as a researcher in the technology area. Since 1990 he is involved in the optical and mechanical characterization of standard fibres, and in the development of new products. He is a member of COST (Cohoperation in Science and Technology) 246 WG1, an European study group on fibre mechanical reliability, and of ITU-T (former CCITT). He is co-author of more than 10 papers on optical fibres.



Daniele Cuomo received the Physics degree from the University of Naples in 1982. He worked at the same University in the Electronic Engineering Department for five years, initially studying gravitational waves and their interaction with electromagnetic (E.M.) fields, then working in the area of E.M. wave propagation. He has been a fellow at the Italian National Research Council (CNR) for one year, working on plasma physics. In 1988, he joined FOS, in the Research and Development Group, starting several research project dealing with both light propagation inside the fibre and coating materials optimization. He is member of several International Standardization Committees (e.g. IEC SC86A, ITU-T SG15, and others). He is an OSA member since 1992.



Antonello Pudia received the degree in Chemistry from the University of Naples "Federico II" in 1990. He worked for the Italian National Research Council (CNR) on the development and characterization of polymer blends. He joined FOS in 1993 where he is working on the chemical and physical characterization of acrylic resins for optical fibre coating.

EFFECT OF CURING TEMPERATURE ON CURING RATE AND MECHANICAL PROPERTIES OF POLYURETHANE ACRYLATE COATINGS FOR OPTICAL FIBER

H. Takase, Y. Hashiguchi, Y. Takasugi, N. Saito, and T. Ukachi

Tokyo Research Laboratory Japan Synthetic Rubber Co., Ltd.
3-5-1 Higashiurigaoka Asao-Ku, Kawasaki 215, Japan

Abstract

Effects of curing temperature on curing rate and physical properties of a particular urethane acrylate coating were studied by using real-time infra-red spectroscopy and dynamic mechanical thermal analysis techniques. It was found that the phase-separation took place when the coating was cured at the temperatures above 50 °C. Owing to the phase-separation, Young's modulus of the cured coating varied from 32 kg/mm² to 54 kg/mm² as a function of the curing temperature. The maximum reaction rate of acrylic double bonds was obtained when the coating was cured at around 50°C. This temperature closely related to the glass transition temperature of the hard-segment of cured coating. Not only the reaction rate of acrylic double bonds but also the physical properties of the cured coating were found to be affected by the curing temperature through the change in the microstructure of the cured coating.

Introduction

Ultraviolet (UV) curable urethane acrylates have been favorably used as protective coatings for optical fibers because of their demonstrated well-balanced physical properties and good chemical and weathering resistance. In addition to these properties, the fast cure rate of UV curable coatings allows us to realize better productivity in manufacturing the optical fibers. In optical fiber manufacturing, a tandem dual coating system has been employed for double layer coatings. As we reported in the previous paper, the surface temperatures of glass core and/or a primary coating layer after being cured were strongly depending on the drawing rate and the cooling distance.⁽¹⁾ Consequently, the tensile properties of a particular secondary coating were found to be greatly affected by the surface temperature of the primary coating.

Curing of urethane acrylates induced by UV radiation takes place through the free radical polymerization process. Thus, the curing kinetics of urethane acrylates are considered to be affected by the curing temperature because of not only the

change in a reaction rate of radicals but also the change in a microstructure, such as soft- and hard- segments phase-separation, of urethane acrylates during curing. Overton *et al.* reported that equilibrium modulus of UV curable coating decreased with an increase of the curing temperature and suggested that this was caused by an increase of the rate of termination reaction of acrylic double bonds.⁽²⁾ The polymerization induced by UV radiation is initiated and completed within order of milliseconds, it is thus very difficult to evaluate the polymerization mechanism of UV curable coatings.

We prepared a model coating of which Young's modulus showed relatively strong dependence on the curing temperature to clarify the origin of this temperature dependence. Using this model coating, we evaluated the physical properties of the coating cured at various temperatures and analyzed the temperature dependence of a consumption rate of acrylic double bonds during UV curing by using a real-time infra-red (RT-IR) spectroscopy technique.^{(3), (4)} We discuss here how the curing temperature affects the reaction rate of acrylic double bonds and the physical properties of resultant coating.

Experimental

1) Sample Preparation

According to the results presented in the previous work, it was suggested that urethane acrylates which had a tendency of forming soft- and hard-segments phase-separation might show the relatively strong dependence of the curing temperature on the physical properties of cured coating.^{(1), (5)} We prepared the model coating, A-1, of which physical properties of cured film have relatively strong dependence on the curing temperature, by formulating following components: (a) 55 wt% of polytetramethylene glycol based di-functional urethane oligomer endcapped with hydroxyethylacrylate, Mw ~ 2500, (b) 17 wt% of mono-functional aliphatic acrylate monomer, Mw ~ 500, (c) 25 wt% of di-functional aliphatic acrylate monomer, Mw ~ 800, and (d) 3 wt% of acetophenone type

photoinitiator.

The coating was casted on to a groove, $50 \times 10 \times 0.1$ mm, which was equipped on a 5 mm-thick glass plate. In order to eliminate the effects of oxygen inhibition and evaporation of the coating components at elevated temperature, the surface of the coating was laminated with a polyethyleneterephthalate (PET) film of 50 μm thickness. After being stood at desired temperature for at least 10 minutes to reach an equilibrium, the glass plate with the coating was passed under a metal-halide lamp (275 mW/cm^2). The UV dose was controlled at 500 mJ/cm^2 . The cured coating was removed from the glass plate and employed for the following measurements after being conditioned for 24 hours at 23 $^{\circ}\text{C}$, 50 % RH.

2) Evaluation of Physical Properties of Cured Coating

Young's modulus of the cured coating was measured at 23 $^{\circ}\text{C}$ by using a standard method.⁽¹⁾ The modulus was defined by the 2.5 %-secant modulus. The extent of cure of coatings was evaluated by measuring the methylethylketone (MEK) unextractable content (gel fraction). The cured coating was extracted by refluxing in MEK for 12 hours and the remaining coating was dried to obtain the percent unextractables. Swelling ratio was also measured for the coatings in tetrahydrofuran (THF) to estimate the extent of the crosslink density of the cured coating. The cured coating, $15 \times 8 \times 0.1$ mm, was soaked in THF for 24 hours at 23 $^{\circ}\text{C}$. The swelling ratio of the cured coating was determined by the ratio of the size of the swollen coating and that of the original one.

Dynamic mechanical response of the cured coating was measured by using a viscoelastometer in the temperature range of -100 $^{\circ}\text{C}$ to 200 $^{\circ}\text{C}$ with a heating rate of 2 $^{\circ}\text{C}/\text{min}$ and with a frequency of 1 Hz. Temperature dependence of storage modulus (E') and loss tangent ($\tan \delta$) for the cured coating were measured.

3) RT-IR Analysis of Reaction Mechanism

An RT-IR spectroscopy was employed to analyze the reaction mechanism of the coating during UV irradiation. The coating, A-1, with a thickness of 20 μm was put between two plates of potassium bromide (KBr) crystals to eliminate the effects of oxygen inhibition and evaporation of the coating components. We introduced the KBr disc with the coating into the RT-IR spectroscopy apparatus to irradiate it at desired UV dose and simultaneously to detect the change in absorbance of IR band at 812 cm^{-1} which is an identical wave number of the absorption of acrylic double bonds. The UV light generated by a high-pressure mercury lamp was guided to the sample through an infra-red cut filter to give an intensity of

50 mW/cm^2 . The KBr disc was enclosed within an aluminum block equipped with resistive heaters which could maintain the temperature from 25 $^{\circ}\text{C}$ to 120 $^{\circ}\text{C}$ with an accuracy of ± 1 $^{\circ}\text{C}$. The IR absorption of coating was monitored at every 2 milliseconds and the data obtained were sent to a digital oscilloscope and a personal computer for data processing.

The IR absorption at 812 cm^{-1} directly relates to the degree of reaction conversion through the equation,

$$\text{Reaction Conversion (\%)} = 100 \times (A_0^{812} - A_t^{812}) / A_0^{812} \quad \dots\dots (1)$$

where A_0^{812} and A_t^{812} represent absorption intensities before and after UV exposure for time t , respectively. While the polymerization rate at time t is defined by the equation,

$$R_p = [M_0] \times (A_t^{812} - A_{t+\Delta t}^{812}) / A_0^{812} \cdot \Delta t \quad \dots\dots (2)$$

where $[M_0]$ is the initial concentration of acrylic double bonds in the coating.

Results and Discussion

The curing temperature dependence of the Young's modulus of the coating, A-1 is shown in Figure 1. Young's modulus of the coating varied as a function of the curing temperature. When the coating was cured at the temperatures below 50 $^{\circ}\text{C}$, Young's modulus increased with an increase of the curing temperature. On the contrary, Young's modulus became to decrease when the coating was cured at the temperatures above 50 $^{\circ}\text{C}$.

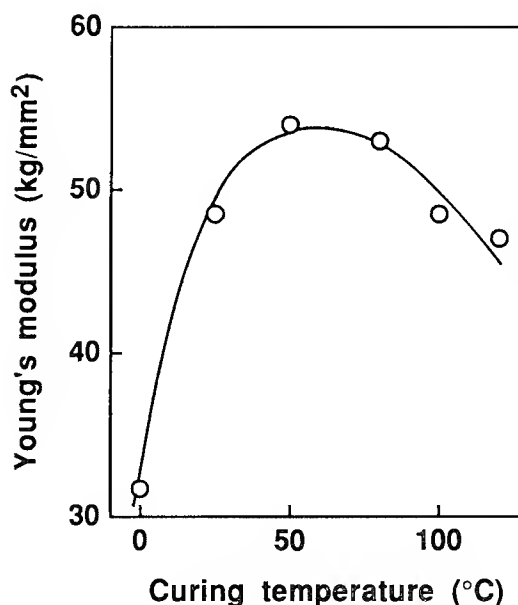


Figure 1. Curing temperature dependence of the Young's modulus of the coating, A-1.

The gel fractions and the swelling ratios of the cured coating are plotted as a function of the curing temperature in Figure 2. The swelling ratio is inversely proportional to the crosslink density and the crosslink density is proportional to the Young's modulus of the cured coating, generally. The lower swelling ratios seen on coatings cured at higher temperatures, thus, indicate the higher crosslink densities comparing to those cured at lower temperatures. Similarly, the gel fractions increased with an increase of the curing temperature and this also indicates that the higher curing temperature tends to give higher extent of cure. These behaviors obtained from the swelling ratio and the gel fraction are consistent with the data of Young's modulus of the coatings cured at the temperatures below 50 °C. However, in spite of relatively low swelling ratio and high gel fraction which correspond to the high crosslink density, lower Young's modulus was obtained on the coating cured at the temperatures above 50 °C.

Figure 3 shows the dynamic mechanical response, storage modulus and loss tangent, of the coatings cured at different temperatures. Although three independent peaks are found in the loss tangent curve of the coating cured at 120 °C, only a single peak was found in the loss tangent curve cured at 0 °C. The first and the second peaks become to appear as the curing temperature increases. This indicates that the soft- and hard-segments phase-separation is induced as the curing

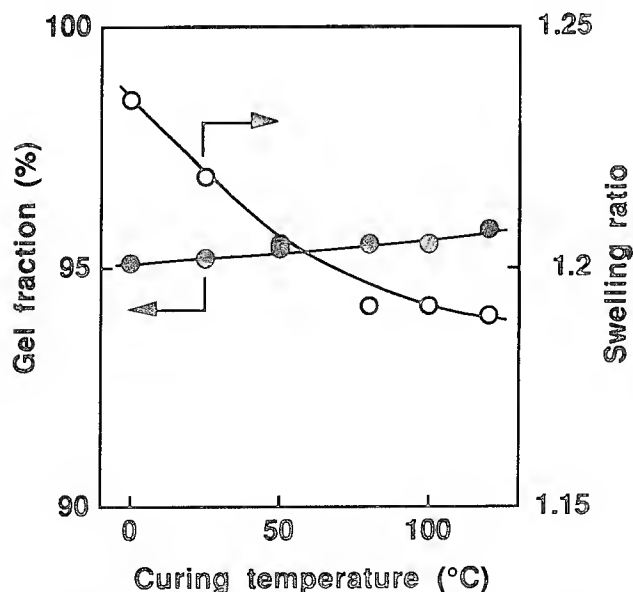


Figure 2. Curing temperature dependence of the swelling ratio (open circle) and the gel fraction (closed circle) of the coating, A-1.

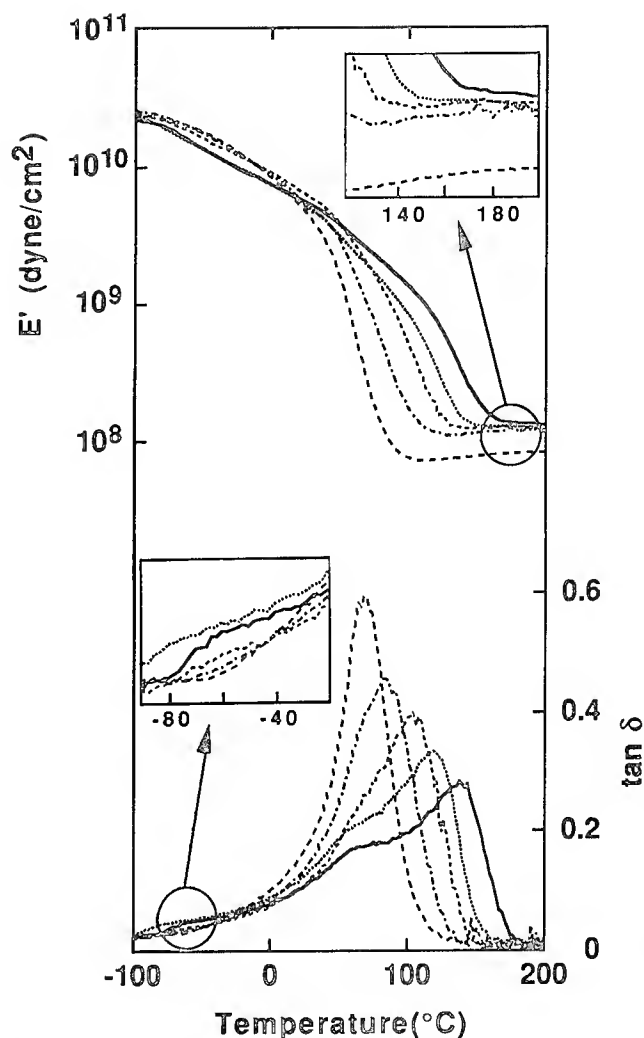


Figure 3. Dynamic mechanical response, storage modulus (E') and loss tangent (δ), of the coating cured at various temperatures.

----- cured at 0°C ----- cured at 25°C
 ----- cured at 50°C ----- cured at 80°C
 ————— cured at 120°C

temperature increases. Since the first peak around -60°C is assigned to the glass transition temperature (T_g) of polytetramethylene glycol which is employed as the soft-segment component of the urethane acrylate oligomer, the second one around 60°C represents the T_g of the hard-segment component and is originated from hydrogen bonds between urethane linkages, and the third one around 150°C is the T_g of the chemically crosslinked network. As shown in Figure 3, the peak maximum of the third peak also shifts to the higher temperature as the curing temperature increases. On the other hand, the storage modulus at the temperature range above 150°C increases with an increase of curing temperature. The storage modulus at high temperature corresponds to the equilibrium modulus and represents the extent of crosslink density of the cured coating. From the equilibrium modulus seen in Figure 3, the crosslink density increases with an increase of the curing temperature. This is also consistent with the results obtained from the swelling ratio and the gel fraction. For the coatings cured at higher temperature, however relatively low Young's modulus was obtained in spite of the higher crosslink density. This inconsistency between the Young's modulus and the crosslink density will be explained by the effect of the phase-separation in the cured coatings. The soft-segment domain of which T_g appeared around -60°C was created when the coating cured at higher temperature. The temperature at which the Young's modulus was measured was 23°C and is higher than this T_g of the soft domain, thus the domain becomes rubbery at this temperature. The lower Young's modulus obtained in the coatings cured at higher temperatures is due to the contribution

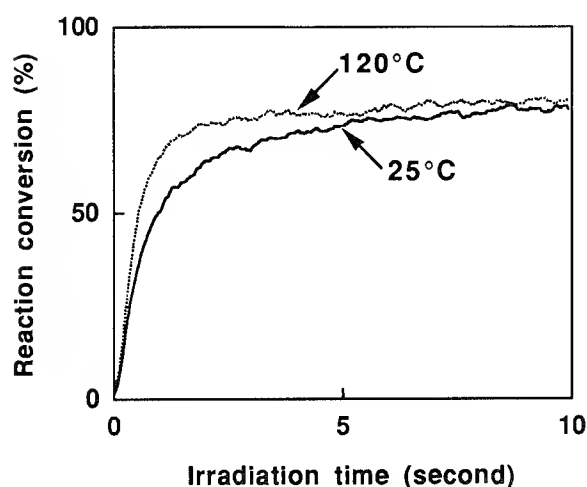


Figure 4. Reaction conversion curves of the coating, A-1, obtained at 25°C and 120°C .

from this rubbery soft-segment. The change in the microstructure of the cured coating is considered to affect not only the physical properties of the cured coating but also the reaction mechanism of the coating. We, thus carried out the following RT-IR analysis during UV curing.

The reaction conversion was measured on the coating, A-1, by changing the temperature, ranging from 25°C to 120°C , with the UV dose of 500 mJ/cm^2 ($50\text{ mW/cm}^2 \times 10\text{ sec}$). Figure 4 represents typical conversion curves of the coating cured at 25°C and 120°C . The reaction of coating irradiated by the UV light at higher temperature proceeds more rapidly than that irradiated at lower temperature. Assuming that the steady-state approximation is valid, the reaction rate of a radical with a monomer is independent of a particular radical, and the chain transfer reaction is negligible, the reaction rate of UV induced free radical polymerization can be written by the equation:

$$d[M]/dt \propto k_p (k_t)^{-0.5} \times [M] \quad \dots\dots\dots (3)$$

where $[M]$ is the concentration of the acrylic double bonds in the coating, and, k_p and k_t are the rate constants of radicals for propagation and termination reactions, respectively.

Assuming an Arrhenius-type relation, logarithm of reaction rates obtained at the reaction conversion less than 60 % was plotted against the reciprocal temperature in Figure 5. The slope of the Arrhenius-type plot gives an apparent activation energy for the reaction of acrylic double bonds. From the equation (3), the apparent activation energy, E_{ap} corresponds to $(E_p - E_t/2)$ where E_p and E_t are the activation energies for the propagation and the termination reactions of the chain radicals, respectively.

As can be seen in Figure 5, regardless of the reaction conversion, the slopes of the Arrhenius-type plot become positive at the curing temperature below 50°C , and become negative at above 50°C . The reaction rate shows the maximum at the temperature around 50°C . This characteristic curing temperature corresponds to the temperature where the second peak in loss tangent curve appeared. From the measurements of loss tangent of the cured coatings, the peak around -60°C , which is assigned to the T_g of the phase-separated soft-segment domain, appeared much clearly at the curing temperature above 50°C . This temperature is also very close to the characteristic temperature obtained in the experiments on the reaction kinetics.

The negative apparent activation energy is given when a half value of the activation energy for the termination reaction, E_t , is larger than that for the propagation reaction, E_p .⁽⁶⁾ When the coating is cured at high temperature, both of

termination and propagation rates are accelerated, however, the termination rate can be easily affected by the mobility of chain radicals and the extent of network formation. Thus the half value of the activation energy for the termination reaction, $E_t/2$, turned to be larger than the activation energy for the propagation reaction, E_p , and this makes the apparent activation energy, E_{ap} , negative at this higher temperature range. On the other hand, the positive activation energy indicates that the reaction of propagating radical with monomer is accelerated more easily than the coupling reaction of radicals on growing polymer terminals. The coating cured at lower temperature, the reaction medium is much homogeneous than that cured at higher temperature. Assuming that the temperature dependence of the diffusion rate of chain radicals was larger than that of low molecular weight monomers, the overall activation energy might turn to be positive at low temperature.

The reaction rate of acrylic double bonds could be strongly affected by the change in the microstructure, soft- and hard-segments phase-separation, of the cured coating which is created by the change of the curing temperature.

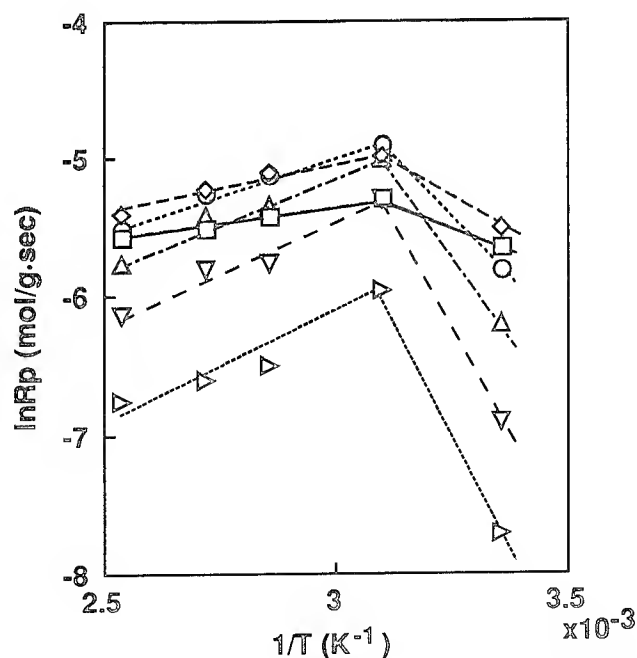


Figure 5. Arrhenius-type plot of the reaction rate of the coating, A-1, as a function of reciprocal temperature.

—□— 10% conversion -◇- 20% conversion
 ---○--- 30% conversion -△- 40% conversion
 -▽- 50% conversion ---▷--- 60% conversion

Conclusions

We reported here that the temperature during UV curing was an important factor to determine the physical properties of the resultant coating. For the particular model coating, Young's modulus varied from 32 kg/mm² to 54 kg/mm² as a function of the curing temperature ranging from 0 °C to 120 °C. From the results obtained by a dynamic mechanical thermal analysis of the cured coating, it was found that the phase-separation was induced when the coating was cured at higher temperature and consequently the physical properties of resultant coating varied as a function of the curing temperature. The reaction rate of the acrylic double bonds in the coating was also studied by using the real-time infra-red spectroscopy technique during UV curing at various temperatures. The maximum reaction rate was obtained at the temperature around 50 °C. This temperature range corresponds to the temperature where the phase-separation takes place in the cured coating. The occurrence of the phase-separation in the cured coating was found to affect not only the physical properties but also the reaction rate of acrylic double bonds in the coatings.

References

- 1) T.Ukachi, A.Aoyama, Y.Naito, and K. Igarashi, Proc. 41st IWCS, 261 (1992).
- 2) B.J.Overton, C.R.Taylor, and A.J.Muller, Polymer Engineering and Science 29, 1165 (1989).
- 3) N.Saito, Y.Hashiguchi, Y.Takasugi, and T.Ukachi, Proc. RadTech Asia 93, 221 (1993).
- 4) C.Decker and K.Moussa, Macromol. Chem. 189, 2381 (1988).
- 5) Z.Komiya, Y.Takasugi, T.Ukachi, and G.Pasternack, Proc. 42nd IWCS, 531 (1993).
- 6) G.R.Tryson and A.R.Shultz, J. Polym. Sci. Polym. Phys. Ed. 17, 2059 (1979).

H. Takase received his ME degree in Applied Chemistry from Tohoku University, Sendai, Japan, in 1992 and joined Tokyo Research Laboratory of Japan Synthetic Rubber Co., Ltd. He has been currently working on the development of UV curable materials for optical fiber coatings.





Y. Hashiguchi received his MS in Synthetic Organic Chemistry from Kyusyu University, Japan, and joined Japan Synthetic Rubber Co., Ltd. in 1984. He has been engaged in research and development of radiation curable materials for optical fiber coatings.



Y. Takasugi received his ME degree in Nuclear Engineering from Hokkaido University, Japan, in 1991. He started work at Tokyo Research Laboratory of Japan Synthetic Rubber Co., Ltd. on the development of radiation curable materials for optical fiber coatings.



N. Saito received his ME degree in Applied Chemistry from Keio University, Japan, in 1990. He started work at Tokyo Research Laboratory of Japan Synthetic Rubber Co., Ltd. on the development of radiation curable materials.



Takashi Ukachi received his BE degree in Biophysics and Bioengineering from Osaka University and Ph. D. degree in Material Science from Kyusyu University. He started his professional carrier at Tokyo Research Laboratory of JSR in 1976 and has been engaged in research on development of radiation curable materials.

THE EFFECT OF CURE DOSE ON THE AGING BEHAVIOR OF UV CURED OPTICAL FIBER COATINGS

Chander P. Chawla

DSM Desotech Inc.
Elgin, Illinois

ABSTRACT

Possibilities exist for UV cured optical fiber coatings to be either under or over exposed to UV irradiation when applied on fiber drawing towers. This could have an effect on the aging behavior of these coatings. Four UV curable optical fiber coatings were cured to varying levels and then aged under hydrolytic, thermo-oxidative, and fluorescent light conditions for various periods of times. Changes in coating color, weight, and dynamic mechanical properties, glass transition temperature and equilibrium modulus, were measured. Under-cured coatings showed larger changes in weight, T_g , and E_p upon exposure to various accelerated aging conditions. Increasing exposure past the nominal dose required for cure increased the color change on aging.

INTRODUCTION

Ultra-violet (UV) light curable optical fiber coatings have been used for the protection of optical fiber for nearly two decades. These coatings have the advantage of curing to a solid state at a very fast rate thereby allowing high fiber draw speeds. In addition to fast cure speed, the UV curable coatings have a number of other desirable properties e.g. low glass transition temperature (T_g) and low modulus for inner primary coatings and high T_g and high modulus for outer primary coating. These coatings should maintain their properties for the expected fiber life time, normally 25 years, in order to provide reliable performance. The modulus of a UV curable coating increases upon exposure to light as the cross-link density increases. After a certain exposure dose (depending upon the coating composition) the modulus reaches a plateau, indicating that almost all of the available reactive groups (e.g. (meth)acrylate) have reacted and the system has reached a limiting cross-link density (Figure 1). In particular, the outer primary coatings may still have some reactive groups available, but these may not be able to react due to mobility restrictions in a tightly cross-linked system.

Depending upon the fiber draw speed and the tower's UV lamp configuration, it may be possible that the inner and or the outer primary coatings are not cured to an optimum level. These coatings may be

under or over exposed to UV light, both of which are undesirable. Under-curing may lead to lower than desired modulus, incompletely developed adhesion of the inner coating to glass, or higher extractables etc. The coating may be lower in cross-link density and will tend to be more unstable and prone to attack by the environment e.g. gel filling compounds or various chemical environments. Over exposure of coating to UV irradiation may lead more directly to degradation of the coating.

Few investigations have been conducted on determining the effect of exposure dose on the aging behavior of UV cured optical fiber coatings. Recently, some work was done to understand the effect of varying UV exposure of optical fiber coatings on fiber properties. Yuce¹ et al reported that the mechanical properties of optical fibers depended on the extent of cure. Frantz² et al studied the aging of optical fibers with different degrees of cure. There have also been a number of aging studies conducted on degradation of optical fiber coatings under thermo-oxidative³, hydrolytic⁴, and UV⁵ light conditions. In this work, we have investigated the effect of varying cure dose on the changes in the dynamic mechanical properties, weight, and color of some UV curable optical fiber coatings upon aging under fluorescent light, humid heat (95°C/95%RH) and dry heat (125°C).

EXPERIMENTAL

Coatings:

We examined four urethane acrylate oligomer based coatings (three inner primaries and one outer primary) for this study. Coatings 1, 2, and 3 are inner primaries and coating 4 is an outer primary coating used.

Curing: A 75 micrometer Bird Film Applicator was used to draw coatings down on clean 23 cm X 30 cm glass plates with the aid of a Pacific Scientific Automatic Drawdown Apparatus. These coatings cure at very different doses, hence the doses representing

low to high values varied for each coatings. The low values were also limited by the instrument. The cure doses used for each coating have been summarized in Table I. Coatings 1, 2, 3, and 4 cure to 95% of their ultimate modulus at 1.0, 0.25, 0.50, and 1.7 J/cm₂ respectively.

Cured film aging:

The cured films were aged for 10, 20 and 30 days at 95°C/95%RH in a Blue M Temperature/Humidity Chamber Model FR 251C 240V. Cured films were also aged for the same time intervals under ambient temperature and humidity in a chamber equipped with 2 fluorescent lamps positioned 6 inches away from the sample. Finally, coatings were aged at 125°C (thermo-oxidative aging) in a convection oven for 7, 14, and 28 days.

Dynamic mechanical analysis:

A Rheometrics Solids Analyzer RSA II was used to perform the dynamic mechanical analysis measurements on the aged and unaged samples. The sample dimensions were 12 mm X 23 mm. The frequency employed was set at 1.0 radian/second. Prior to initiating a temperature sweep, the sample underwent an 80°C preheat for a minimum of five minutes in the dry N₂ atmosphere of the Rheometer's environment, to remove any water that could be present which might act as a plasticizer.

Color changes:

Color measurement data was obtained from a Macbeth Series 1500 Color Measurement System (Model 2020). The colorimeter was calibrated and set to the following parameters:

Illuminant: D for primary and secondary illuminant
Color difference: FMC-2
Mode: 2, COL
Area of Measurement: Large Area View
Specular Component: Excluded (SCE)
UV Filter: Included
Background: White Calibration Standard

Weight Changes:

Weight changes were measured after conditioning the thermo-oxidative and fluorescent light aged samples (3 cm X 3 cm) for fifteen minutes in a desiccator. The samples aged at 95°C/95%RH were dried at 60°C for one hour and conditioned in a desiccator for 15 minutes.

RESULTS AND DISCUSSION

The variation in cured film parameters, $\tan \delta$ peak (T_g) and equilibrium modulus (E_0), as a function of time are summarized in Table I. These doses were selected based on the previously determined cure behavior of these coatings. In general, as the exposure dose increases, the T_g and E_0 increase as a result of increased cross-link density.

Color Changes:

It is desirable to minimize color development in optical fiber coatings due to potential problems in fiber identification. At times, color changes can also be accompanied by deterioration of physical properties leading to fiber handling problems. The color (ΔE values)^{6,7} changes of these coatings cured at different doses and then aged under light, humidity, and heat aging have been summarized in Tables II, III and IV. Part of this data has been plotted in Figure 2.

Fluorescent light aging provided the smallest changes in film color of the three aging conditions. As the dose increased for coating 1, changes in color (Δ color) showed small decreases. For coatings 2 and 3, the Δ color was larger as the dose was increased. Δ color increased with aging time for all doses for coating 4. For coating 2, there appeared to be a decrease in Δ color in going from 20 to 30 days of aging.

Under hydrolytic (95°C/95%RH) thermo-oxidative aging conditions, all four coatings showed increases in Δ color as a function of increasing dose. Also, Δ color increased as a function of increasing aging time for all four coatings. Thermo-oxidative aging produced the largest color changes.

Weight Changes:

Most of UV curable coating materials contain some potentially volatile material which is not cross-linked to the rest of the matrix, e.g. residual photoinitiator, additives etc. In addition, depending on the degree of cure, there may be some additional non-cross-linked material. Upon aging, some or all of these materials could be lost from the cured film. It is desirable to have very low film weight losses in order to maintain coating integrity. Results of weight changes under various aging conditions for different doses have been summarized in Tables V, VI, and VIII. Part of this data has been plotted in Figure 3.

In general, as the cure dose increased, the weight losses (Δ weight) under all aging conditions decreased. The weight losses for all coatings, under all aging conditions increased as a function of aging time. The

weight losses were the lowest for fluorescent light aging. Hydrolytic and thermo-oxidative aging conditions produced similar weight loss behavior. similar.

Dynamic Mechanical Properties:

It is important that UV curable optical fiber coatings maintain their T_g 's and E_0 's. Shifts in these properties on aging can cause problems with fiber attenuation and handling. Results of changes in T_g and E_0 have been summarized in Tables VIII through XIII. Part of this data has been plotted in Figure 4.

Fluorescent Light Aging:

T_g values showed small increases upon aging for coatings 1, 2, and 3, which could result from weight loss upon aging. In an unaged film, non-cross-linked material acts as plasticizer and depresses the T_g of the coating. Coating 4 showed similar behavior, except for the fact that aging changes in T_g were much larger compared to coatings 1, 2, and 3. Also, as the dose increased, the changes became smaller.

The E_0 values for coatings 1 and 2 decreased upon aging. There was little effect of cure dose on the amount of decrease in E_0 . Coatings 3 and 4 showed increases in E_0 upon aging. ΔE_0 were not significantly affected by increase in dose for coating 3. For Coating 4, ΔT_g decreased with increasing dose.

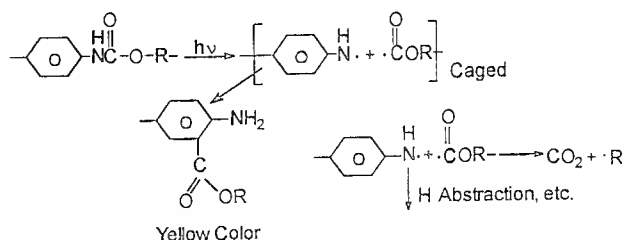
Hydrolytic and Thermo-oxidative Aging: T_g values generally increased for all coatings as a function of aging time due to loss of non-cross-linked material for both hydrolytic and thermo-oxidative aging conditions. Coating 4 showed the largest increases in T_g . Changes in T_g for coatings 1 and 2 were almost independent of cure dose. For coating 4, as the cure dose increased, the changes in T_g became smaller.

Under hydrolytic aging conditions, E_0 values decreased for coatings 1, 2, and 4, indicating a possible chain-scission type of mechanism which leads to reduced cross-link density and reduced E_0 (E_0 is directly proportional to the cross-link density)⁸. As the aging time increased, the ΔE_0 increased. For coating 4, increased cure dose resulted in relatively larger ΔE_0 indicating that chain scission mechanism is predominant for the higher cross-linked density state. For thermo-oxidative aging, the ΔE_0 values decreased as a function of aging time for coatings 1 and 2. Coating 3 showed the lowest amount of changes followed by coatings 1 and 2. These changes were not greatly affected by the cure dose. The ΔE_0 values for coating 4 increased as a function of aging time and decreased as a function of cure dose.

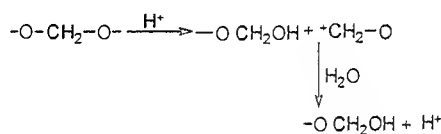
Discussion:

Exposure of cured coating films to various aging conditions, these can lead to formation of a number of different degradation products⁹ e.g.

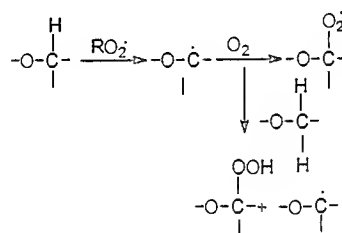
Q-UV or Fluorescent Light Aging:



Hydrolysis:



Thermo-oxidative Aging:



These are some of the possible reactions of the cured film constituents. Light absorption leads to excitation of the functional group, followed by formation of free radicals, which can undergo a variety of reactions. Some of the degradation products could be colored (e.g. the Photo-Fries yellow product shown above from a polyurethane degradation) leading to film discoloration. As the exposure continues, the colored species may absorb light and fragment to give products which may not be colored. This might explain the decrease in Δ color for fluorescent light aging of coating 2 after 20 days. Oxygen can play a part in the reactions shown above by forming peroxide radicals or hydroperoxides from radical species. Various linkages in polyurethane oligomer based coatings are subjected to degradation. Ether or ester linkages contained in polyols used in the polyurethane oligomer can undergo degradation on exposure to light. The various degradation mechanisms taking place and their extent

will depend on coating compositions and the degree of cure of the coating.

Color Changes:

Larger cure doses resulted in increased Δ color for all aging conditions. Δ Color, in general, increased for all doses as a function of time for all aging conditions. Color changes were the highest for thermo-oxidative and hydrolytic conditions. There were coating to coating differences which could be rationalized based on coating compositions. Coating 4 is the slowest curing of all and showed the largest effect of exposure dose. Coating 1 was the only coating to show a slight decrease in Δ color upon increasing dose for fluorescent light aging. This could be due to the degradation of color forming species on further exposure to light.

Weight Changes: In general, lower exposure doses, resulted in larger weight losses. Increased dose leads to a more cross-linked structure and hence should result in lower weight losses upon aging. Weight losses on aging were most likely due to loss of non-cross-linked or volatile material. Weight losses upon aging also correlated with increases in T_g . Loss of material on aging reduces the plasticization effect of these materials resulting in increased T_g 's. The extent of Δ weight varied depending upon the cure behavior and the chemical composition of the coating. At the highest doses, coatings 2 and 4 showed the lowest weight losses under all aging conditions. Coating 4 is a highly cross-linked coating and should have very little non-cross-linked material when cured at a high dose. Coating 2 is a relatively lightly cross-linked inner primary coating which contains very little volatile material.

T_g and E_0 Changes: The T_g increased for all coatings under all aging conditions for all doses. In general, the ΔT_g values were smaller for increasing doses. The largest increases were again seen for coating 4. The increase in T_g is explained by the weight loss as a result of aging.

The effect on E_0 was more complicated. Thermo-oxidative and hydrolytic aging both can lead to degradation of coatings through chain scission or cross-linking mechanisms. Chain scission leads to reduced E_0 and in addition could also depress the T_g . Cross-linking on the other hand, would lead to an increased E_0 and may also increase T_g . Coatings 1 and 2 showed a decrease of ΔE_0 (and cross-link density) under all of the aging conditions indicating that chain scission is the main reaction. The decreases in ΔE_0 were generally smaller, the larger the dose. Coating 4 showed a decrease in ΔE_0 on humidity aging and an increase on fluorescent light and heat aging. Coating

3 showed increases in E_0 for aging under humidity and fluorescent light aging and decreases for heat aging conditions. The increase in ΔE_0 for coatings 3 and 4 at lower doses (aged under fluorescent light) could be explained by the fact that these might be insufficiently cured to begin with and exposure to light increased the cure level.

CONCLUSIONS

The effect of exposure dose on the aging behavior of UV curable optical fiber coatings varied depending upon the coating cure behavior and chemical composition. In general, lower degree of cure can produce pronounced changes in color, weight, and glass transition temperature (T_g) and equilibrium moduli (E_0) of a coating. Under-curing produced smaller changes in E_0 for coating 4 upon hydrolytic aging. Over-exposure, on the other hand, leads to larger color changes in the cured films on aging.

REFERENCES

- ¹ H. H. Yuce, I.M.Plitz, R.A.Frantz, and M.Ardejco, "The Effect of Coating Cure on the Mechanical Characteristics of Optical Fibers", Proc. of IWCS, pp.716-721 (1990).
- ² R. A. Frantz, I. M. Plitz, H. H. Yuce, and O. S. Gebizlioglu, "The Effect of Aging on Optical Fibers With Incompletely Cured Coatings", Proc. of IWCS, pp. 279-284 (1992).
- ³ D. Simoff, M. Chan, J. Chapin, and B. Overton, "Thermo-oxidative Aging of A Primary Lightguide Coating in Films and Dual Cured Fibers", Proc. of ANTEC, pp 586-589 (1988).
- ⁴ D. Szum, C. Chawla, T. Bishop, K. Murray, J. Zimmerman, "Water Sensitivity and Its Relationship to Stability in Optical Fiber Coatings", Proc. of IWCS, pp. 708-714 (1990).
- ⁵ T. Hosoya and Y. Matsuda, "UV Resistance Properties of UV-Cured Resin Coated Optical Fibers", Proc. of IWCS, pp. 149-154 (1991).
- ⁶ D. Szum and R. Salvesen, "A New Method for Measuring the Contribution of UV Cured Coatings towards Color Changes Upon Aging of UV Cured Inks", Proc. of Sixth Intntnl. Conf. on Plasts. in Telecomm. London, U.K., (1992).
- ⁷ T. Bishop, C. Chawla, D. Szum, and E. Poklacki, "Aspects of Thermo-oxidative and Hydrolytic Degradation in Optical Fiber Cable Matrix Material", Proc. of IWCS, pp. 442-446 (1992).
- ⁸ L. E. Nielsen, "Mechanical Properties of Polymers and Composites", Vol. 1, Marcel Dekker Inc., NY, 176 (1974).
- ⁹ J. J. Kroshwitz et al ed., Encyclopedia of Polym. Sc. & Eng., Vol. 4, pp. 630-696, John Wiley & Sons, NY (1986).

ACKNOWLEDGEMENT

The author would like to acknowledge the help of Marc Skaddan in preparing all the samples and carrying out most of the testing. The author would also like to acknowledge the help of Steven R. Schmid and Dr. Robert Johnson for their helpful comments during the preparation of this manuscript. Finally, the author would like to thank DSM Desotech for giving him the opportunity to present this paper.



BIOGRAPHY

Chander P. Chawla received his Ph.D. in polymer science from the University of Southern Mississippi in May 1990. He obtained a Master's degree in polymer science and technology from the Indian Institute of Technology, New Delhi, in 1984, and a Master's degree in chemistry from the University of Delhi, New Delhi, in 1982. He has been working in the area of fiber optic coatings since October 1989. He is currently a research associate in the optical fiber coatings group of DSM Desotech Inc.

Table I
Effect of Increasing Cure Dose on Glass
Transition Temperature (peak $\tan \delta$) and
Equilibrium Modulus of the Coatings

	CURE DOSE, J/cm ²	TAN δ PEAK, °C	E ₀ , MPa
COATING 1	0.7	23	2.1
	1.5	25	2.1
	3.0	23	2.1
COATING 2	0.2	-20	1.7
	0.3	-20	1.8
	0.7	-18	1.9
	1.5	-19	2.0
COATING 3	0.2	-12	1.4
	0.4	-9	1.9
	1.0	-8	2.1
	2.0	-6	2.1
COATING 4	0.2	35	19.2
	0.7	51	31.5
	2.0	51	32.0
	4.0	55	37.5

Table II
Effect of Cure Dose on Δ Color After Fluorescent Light Aging

	COATING 1			COATING 2				COATING 3				COATING 4			
CURE DOSE, J/cm ² -	0.7	1.5	3.0	0.2	0.3	0.7	1.5	0.2	0.4	1.0	2.0	0.2	0.7	2.0	4.0
AGING TIME, DAYS I															
10	+2.5	+1.6	+0.8	+3.4	+4.9	+6.5	+5.7	+4.6	+5.9	+5.2	+6.5	+6.1	+8.0	+7.6	+6.7
20	+3.3	+2.8	+1.5	+5.4	+7.5	+7.7	+6.0	+7.4	+5.2	+5.7	+5.9	+7.5	+8.4	+7.8	+8.0
30	+2.9	+2.7	+1.4	+1.9	+3.1	+2.3	+1.7	+4.4	+7.0	+4.0	+4.2	+9.0	+9.4	+7.8	+8.3

Table III
Effect of Cure Dose on Δ Color Under 95%/95%RH Aging Conditions

	COATING 1			COATING 2				COATING 3				COATING 4			
CURE DOSE, J/cm ² -	0.7	1.5	3.0	0.2	0.3	0.7	1.5	0.2	0.4	1.0	2.0	0.2	0.7	2.0	4.0
AGING TIME, DAYS I															
10	+8.1	+9.7	+13.7	+3.6	+4.2	+6.6	+6.4	+2.2	+3.5	+3.0	+4.7	+5.5	+8.8	+9.8	+11.4
20	+12.6	+13.7	+15.2	+4.2	+5.3	+9.1	+8.8	+3.4	+4.2	+4.9	+7.6	+9.8	+17.0	+18.2	+19.6
30	+24.4	+21.0	+20.9	+8.5	+10.2	+7.4	+5.7	+6.8	+8.6	+7.8	+11.0	+18.9	+27.0	+29.0	+32.6

Table IV
Effect of Cure Dose on Δ Color Under 125°C Aging Conditions

	COATING 1			COATING 2				COATING 3				COATING 4			
CURE DOSE, J/cm ² -	0.7	1.5	3.0	0.2	0.3	0.7	1.5	0.2	0.4	1.0	2.0	0.2	0.7	2.0	4.0
AGING TIME, DAYS I															
7	+36.6	+36.4	+42.9	+15.7	+16.6	+18.3	+15.5	+10.0	+9.9	+14.0	+17.7	+20.4	+21.5	+21.2	+26.0
14	+58.7	+66.2	+77.6	+22.5	+25.0	+24.0	+25.6	+12.6	+12.1	+14.3	+19.5	+45.4	+44.0	+54.3	+40.4
28	+80.1	+87.6	+88.7	+52.4	+53.2	+57.8	+50.4	+26.2	+24.4	+39.3	+33.0	+60.1	+73.9	+60.4	+73.4

Table V
Effect of Cure Dose on Δ Weight Under Fluorescent Light Aging Conditions

	COATING 1			COATING 2				COATING 3				COATING 4			
CURE DOSE , J/cm ² -	0.7	1.5	3.0	0.2	0.3	0.7	1.5	0.2	0.4	1.0	2.0	0.2	0.7	2.0	4.0
AGING TIME, DAYS :															
10	3.3	2.4	2.8	0.7	1.1	0.5	0.9	4.5	3.8	3.0	3.0	1.0	0.4	0.2	0.5
20	4.1	2.8	3.1	0.6	1.1	0.6	0.9	4.7	4.0	3.5	3.3	0.9	0.5	0.2	0.5
30	4.6	3.1	3.6	0.3	1.1	0.6	0.9	5.0	4.1	3.5	3.4	1.0	0.6	0.2	0.2

Table VI
Effect of Cure Dose on Δ Weight Under 95°C/95%RH Aging Conditions

	COATING 1			COATING 2				COATING 3				COATING 4			
CURE DOSE , J/cm ² -	0.7	1.5	3.0	0.2	0.3	0.7	1.5	0.2	0.4	1.0	2.0	0.2	0.7	2.0	4.0
AGING TIME, DAYS :															
10	6.7	5.3	6.1	2.4	2.2	1.7	2.4	8.4	5.6	4.5	4.2	6.5	3.7	2.4	2.9
20	7.8	6.6	7.1	3.2	2.6	2.0	2.8	9.1	5.9	4.8	4.5	7.0	4.4	4.0	3.8
30	9.1	7.6	7.7	3.6	3.1	2.5	3.1	9.6	6.1	4.9	4.7	7.4	4.3	3.3	3.6

Table VII
Effect of Cure Dose on Δ Weight Under 125°C Aging Conditions

	COATING 1			COATING 2				COATING 3				COATING 4			
CURE DOSE , J/cm ² -	0.7	1.5	3.0	0.2	0.3	0.7	1.5	0.2	0.4	1.0	2.0	0.2	0.7	2.0	4.0
AGING TIME, DAYS :															
7	5.2	4.2	4.7	2.3	1.6	0.7	1.2	7.8	4.6	3.4	3.5	6.0	3.3	2.6	2.8
14	6.1	4.9	5.4	2.6	1.9	1.1	1.8	8.7	4.9	4.0	3.8	6.1	3.5	2.7	3.0
28	7.0	5.7	6.1	4.1	3.0	2.2	2.6	10.0	5.1	3.9	4.0	6.5	3.9	3.2	3.4

Table VIII
Effect of Cure Dose on ΔT_g (peak $\tan \delta$) Under Fluorescent Light Aging Conditions

	COATING 1			COATING 2				COATING 3				COATING 4			
CURE DOSE , J/cm ² -	0.7	1.5	3.0	0.2	0.3	0.7	1.5	0.2	0.4	1.0	2.0	0.2	0.7	2.0	4.0
AGING TIME, DAYS I															
10	+5	+3	+4	+4	+4	+6	+5	+4	+3	+2	+1	+15	+8	+10	+9
20	+4	+2	+4	+4	+4	+3	+5	+5	+4	+3	+2	+14	+10	+12	
30	+5	+3	+5	+5	+3	+4	+3	+4	+3	+2	+1	+18	+11	+12	+13

Table IX
Effect of Cure Dose on ΔT_g Under 95°C/95%RH Aging Conditions

	COATING 1			COATING 2				COATING 3				COATING 4			
CURE DOSE , J/cm ² -	0.7	1.5	3.0	0.2	0.3	0.7	1.5	0.2	0.4	1.0	2.0	0.2	0.7	2.0	4.0
AGING TIME, DAYS I															
10	+8	+6	+8	+4	+4	+2	+4	+4	+3	+2	+1	+7	+4	+6	+5
20	+9	+6	+9	+6	+6	+4	+4	+3	+3	+3	0	+10	+4	+4	+4
30	+12	+9	+10			+5	+7	+3	+1	+2	-1	+8	+4	+5	+4

Table X
Effect of Cure Dose on ΔT_g (peak $\tan \delta$) Under 125°C Aging Conditions

	COATING 1			COATING 2				COATING 3				COATING 4			
CURE DOSE , J/cm ² -	0.7	1.5	3.0	0.2	0.3	0.7	1.5	0.2	0.4	1.0	2.0	0.2	0.7	2.0	4.0
AGING TIME, DAYS I															
7	+6	+3	+6	+2	+1	+2	+2	+2	+2	+1	0	+17	+11	+12	+6
14	+7	+6	+9	+1	+3	+1	+4	+4	+3	+2	+2	+18	+14	+11	+13
28	+10	+8	+9	+3	+3	+3	+5	+4	+3	+2	+1	+32	+27		+24

Table XI
Effect of Cure Dose on ΔE_g Under Fluorescent Light Aging Conditions

	COATING 1			COATING 2				COATING 3				COATING 4			
CURE DOSE, J/cm^2	0.7	1.5	3.0	0.2	0.3	0.7	1.5	0.2	0.4	1.0	2.0	0.2	0.7	2.0	4.0
AGING TIME, DAYS															
10	-1.0	-0.9	-0.8	-0.1	-0.5	-0.2	-0.2	+0.2	+0.3	+0.3	+0.2	+7.1	+5.2	+6.2	+4.9
20	-1.2	-1.0	-1.2	-0.3	-0.3	-0.2	-0.3	+0.2	+0.3	+0.3	+0.4	+9.9	+5.1	+7.8	
30	-1.4	-1.3	-1.4	-0.4	-0.3	-0.4	-0.3	+0.5	+0.4	+0.4	+0.3	+8.3	+5.6	+5.2	+4.5

Table XII
Effect of Cure Dose on ΔE_g Under 95°C/95%RH Aging Conditions

	COATING 1			COATING 2				COATING 3				COATING 4			
CURE DOSE, J/cm^2	0.7	1.5	3.0	0.2	0.3	0.7	1.5	0.2	0.4	1.0	2.0	0.2	0.7	2.0	4.0
AGING TIME, DAYS															
10	-0.4	-0.2	0	0	0	-0.1	-0.1	+0.2	+0.3	+0.3	+0.3	-1.6	-3.4	-1.0	-3.4
20	-0.5	-0.4	-0.2	-0.4	-0.4	-0.5	-0.6	0	+0.3	+0.3	0.4	-0.1	-3.2	-1.8	-4.2
30		-0.5	-0.4			-0.7	-1.0	+0.1	+0.1	+0.3	+0.3	-0.7	-3.9	-3.5	-7.6

Table XIII
Effect of Cure Dose on ΔE_g Under 125°C Aging Conditions

	COATING 1			COATING 2				COATING 3				COATING 4			
CURE DOSE, J/cm^2	0.7	1.5	3.0	0.2	0.3	0.7	1.5	0.2	0.4	1.0	2.0	0.2	0.7	2.0	4.0
AGING TIME, DAYS															
7	-0.2	-0.3	-0.1	+0.2	-0.1	-0.1	0	0	+0.3	+0.2	+0.2	+5.5	+1.9	+4.5	+0.1
14	-0.3	-0.4	-0.4	-0.3	-0.6	-0.6	-0.4	-0.2	-0.1	-0.1	-0.2	+5.2	+4	+3.2	+3.3
28	-0.4	-0.2	-0.2	-0.7	-0.7	-0.8	-0.8	0	-0.1	-0.2	-0.2	+12.9	+11		+8.4

Figure I Dose Versus Modulus For A Typical Optical Fiber Coating

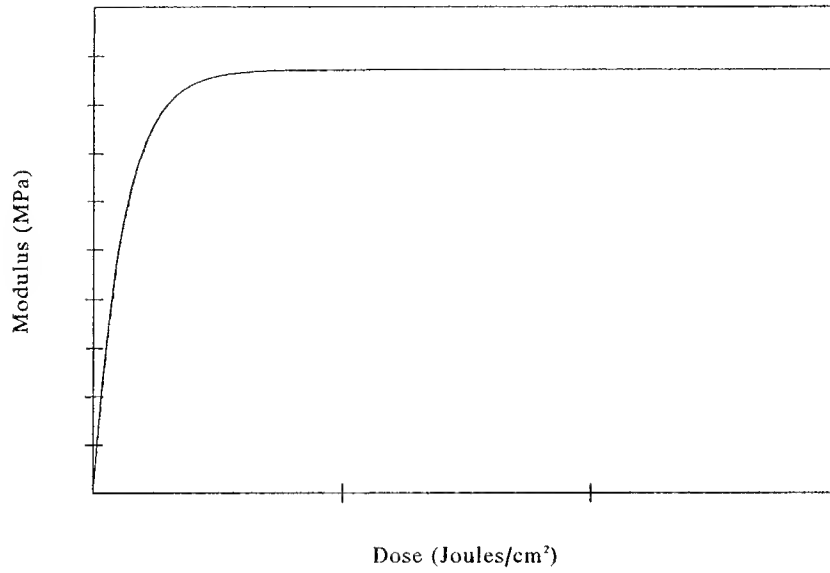


Figure II Effect Of Cure Dose On Color Change At 125°C For Coatings 1 and 3

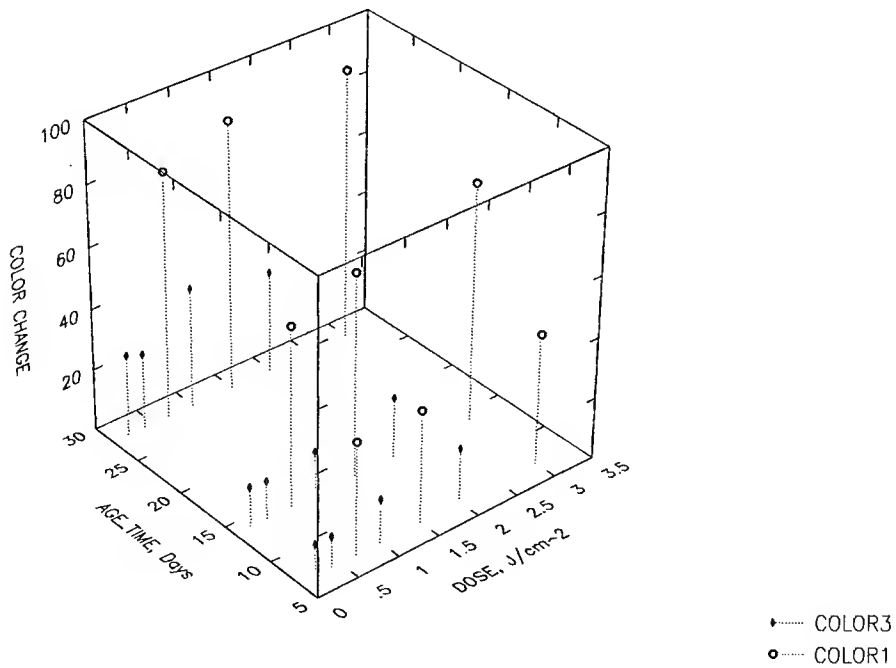


Figure III Effect of Dose And Aging Time On Weight changes at 125°C

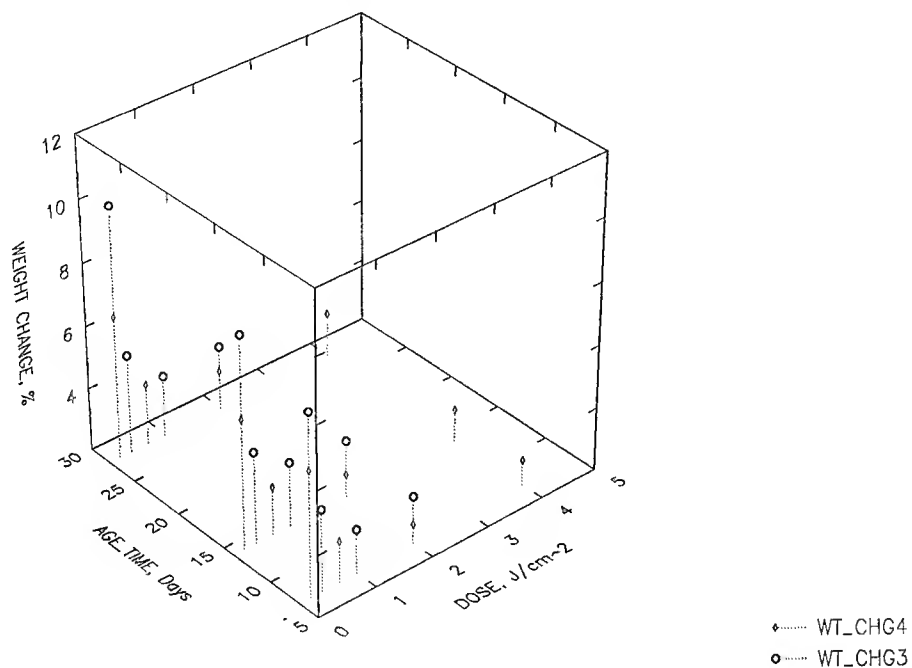
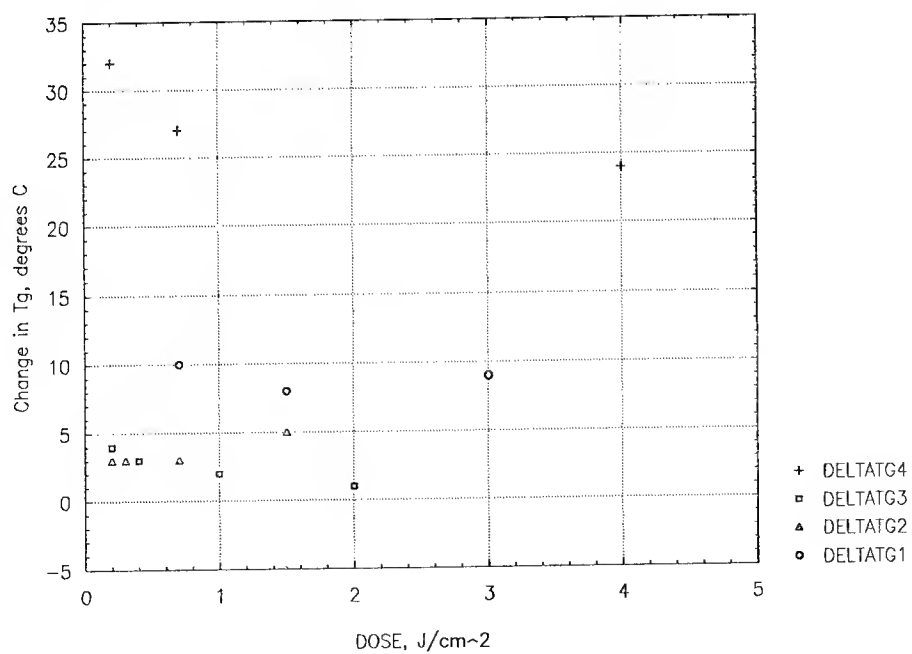


Figure IV Effect Of Dose On Tg After Aging At 125°C For Four Weeks



ENHANCED UV CURE MATERIAL PROPERTIES IN THE DEVELOPMENT OF A NEXT GENERATION OPTICAL FIBER COATING

Eric H. Urruti, J. Richard Toler, Git Kar, Ching-Kee Chien, John W. Botelho

Corning Incorporated, Corning, NY, 14831, USA

ABSTRACT

A new optical fiber coating system has been designed and developed for enhanced environmental stability. A robust fiber coating system is a prerequisite as fiber is deployed in the rigorous environments found in the local loop. The new coating has been successfully designed for universal application in loose tube, ribbon, and tight buffer cable designs. It is compatible with existing fibers, field practices, and tools. Testing has shown this new system to have improved performance while retaining the critical features of current coating systems.

INTRODUCTION

When optical fibers were first used for telephony applications, fiber strength retention and chemical removal were the primary performance concerns for the coating materials. As technology improved, advancements in coating materials were required, such as mechanical removal, enhanced low temperature performance, and environmental stability. As fiber networks become more pervasive, the requirements placed on the fiber itself are becoming more stringent. A key feature required for fiber-in-the-loop applications to proceed is to reduce installed costs. To reduce these costs, fiber manufacturers have improved fiber geometric precision to allow mass connectorization of ribbon and/or ribbonized fibers. To accomplish this procedure quickly and effectively, coating and ribbon matrix material removal in a clean and efficient manner is required. To maximize efficiencies, it is advantageous if the requirements can be met with a single coating system for both ribbon and loose tube cables. Since severe environmental exposures can be anticipated for fiber-in-the-loop applications, the following capabilities of the coating system are essential:

- Reduce installation cost via ribbon or ribbonizing
- Improve ability to handle fiber and strip coating
- Enhance resistance to environmental exposure
- Single coating system for loose tube and ribbons to increase flexibility

The approach undertaken to deliver a coating system which can address these requirements was to enhance bend resistance, to gain added control of the coating removal process by material selection, and to improve the chemical stability of the coating system.

It is possible to influence the microbend performance of the fiber through proper material selection of the inner and outer primary coatings. Improved microbend resistance allows for ease in ribbon manufacture, while still providing a robust coating system for loose tube cables. Coating strip characteristics are controlled through proper adhesion of the inner primary coating to the glass, coating geometry selection, and the material selection of the outer primary coating. Chemical stability is addressed at a molecular level by the proper choice of oligomers and monomers which are resistant to aging and to environmental attack.

The result of this work is a superior, versatile coating system which can be used for both loose tube, ribbon, and tight buffer applications. The bend performance exhibited by the preferred coating system allows for low attenuation ribbons, as well as enhanced cabling consistency. The focus on coating removal resulted in a system which is consistent with all present day craft practices, allowing for the clean removal of the coating materials in single, ribbonized, or ribbon fibers. The improved chemical stability resulted in a system that exhibits enhanced environmental stability for coating removal, and optical and color performance. These attributes, combined with excellent manufacturing control and tight geometric tolerances, result in the most consistent strip performance across a broad range of environmental extremes which may be encountered in the local loop.

RESISTANCE TO MICROBENDING

In the development of environmentally resistant fibers, with a coating system that is ribbon compatible, resistance to optical loss is critical. Optical loss due to microbending can occur from thermal shrinkage and point stresses, during and after the cabling process. The ability of fibers with the preferred coating to resist microbending as experienced in a cable can be simulated with the "Basketweave" test.^{1,2} This test has been demonstrated as an excellent surrogate for the

relative cable performance at low temperatures. Use of a longer test fiber and the ability to characterize microbending performance at low temperatures are two clear advantages of this technique over previously used microbending tests on fibers. A 2.5 km long fiber is wound at 70 g tension onto a 140 mm diameter x 80 mm wide glass spool with a 2 mm take-up pitch and 0.5 mm per pass taper. The spool containing the test fiber is placed in a temperature chamber. The change in attenuation over the range of -40°C to 85°C is measured and the maximum excursion is noted. The measurement variability is very small at 0.01 dB/km for measurements at 1300 nm and 0.02 dB/km for 1550 nm. Table 1 shows the superior performance of fibers with the preferred coating compared to fibers with the Commercial 1 coating.

Table 1: Maximum Attenuation Loss in the Basketweave Test from -40°C to 85°C

Coating	Mean Attenuation Change at 1300 nm (dB/km)	Mean Attenuation Change at 1550 nm (dB/km)
Preferred Coating	0.03	0.06
Commercial 1	0.08	0.21

Given the small variability seen for this test, fibers with the preferred coating are clearly superior to fibers with the Commercial 1 coating for microbending.

THERMAL STABILITY

Thermal stability studies can be used to assess the environmental stability of coatings. Prolonged exposure to elevated temperatures, as well as hot, humid environments, aggressively challenge the physical properties of coatings. The thermal stability of the outer primary coating in the preferred coating system was studied using dynamic mechanical analysis (DMA). This technique has been used in the past to evaluate the effects of various chemicals and solvents on optical fiber coatings.³ Films of the coating were exposed to three accelerated aging conditions and then measured with the DMA for changes in their modulus and in their glass transition temperatures (peak tan delta). The changes in modulus were assessed by comparing the temperatures where the E' curve crosses the 1000 MPa and the 100 MPa levels and by comparing their equilibrium moduli. The equilibrium moduli of coatings are a function of their crosslink density. Reference 3 established the error of measurement for these tests at $\pm 4^\circ\text{C}$. The results are shown in Table 2.

Table 2: Physical Property Changes of the Preferred Outer Primary Coating on Thermal Aging

	7 Days 125°C	30 Days 95°C, dry heat	30 Days 95°C, 95% RH
E' = 1000 MPa (°C Change)	+5	+5	+2
E' = 100 MPa (°C Change)	+3	+2	0
Peak Tan Delta (°C Change)	+2	+2	-1
Equilibrium Modulus (MPa)	-1	-1	-5

The results in Table 2 show very little to no change in the modulus when coating films of the preferred system outer primary coating are exposed to such conditions. The efforts to design-in thermally stable molecules has resulted in a coating system that is stable at elevated temperatures in both dry and humid environments.

Furthermore, the preferred coating shows virtually no color change when exposed to a variety of accelerated aging environments. Color changes in fiber coatings, particularly yellowing, hinder or prevent the easy discrimination of fiber colors in the field.⁴ The chemical stability of the preferred coating system, as demonstrated above, suggests superior environmental stability.

STRIPPABILITY

Single fiber strippability

Fiber coatings are generally removed by mechanical stripping for splicing and termination operations. The coating removal normally is carried out using a stripping tool. Craft people in the field want the stripping to be easy, consistent, and to leave a clean fiber. Bellcore's TR-20 document⁵ "Generic Requirements for Optical Fiber and Fiber Optic Cable" requires the peak force to be in the range of 0.3 to 2 pounds. Lower force generally means easier stripping. The standard deviation of the peak strip force is a general indicator of fiber manufacturing and strip performance. The preference is to have no coating residue left on the glass fiber after stripping. However, it is accepted practice to use a single wipe with a solvent-moistened cloth to remove the residue.

Figure 1 and Table 3 show the peak strip force and its standard deviation for fibers with the preferred and with other commercial coatings. In all cases, the mean and standard deviation values are based on ten tests. The preferred coating shows a low strip force and a small standard deviation. By comparison, Commercial coatings 2, 3, and 4 have a much larger standard deviation. This shows that the preferred coating is easier and more consistent to strip than Commercial coatings 2 and 3.

Figure 1. Strip Force Performance of Fiber as Received

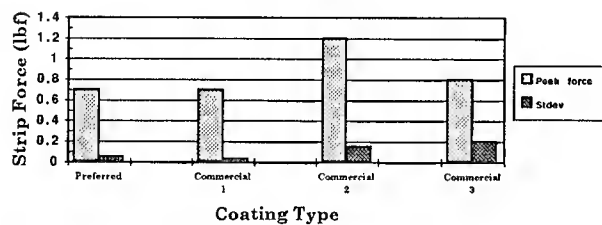


Table 3: Strip Performance of Various Fiber Optic Coating Systems

	Preferred	Com. 1	Com. 2	Com. 3	Com. 4
Ave. Peak Strip Force (lbf)	0.7	0.7	1.2	0.8	0.9
Standard Deviation (n = 10)	0.05	0.03	0.15	0.19	0.08

The Bellcore TR-20 document also specifies that the strip force at 0 and 45°C should be between 0.3 and 2.0 lbf. Peak strip forces at these two extreme temperatures are shown in Figure 2 and Table 4 for fibers with the preferred coating and with other commercial coatings. While all of the results shown meet the requirements of TR-20, fibers with the preferred coating have the lowest strip force and are the easiest to strip at these temperature extremes.

Figure 2. Strip Force as a Function of Temperature

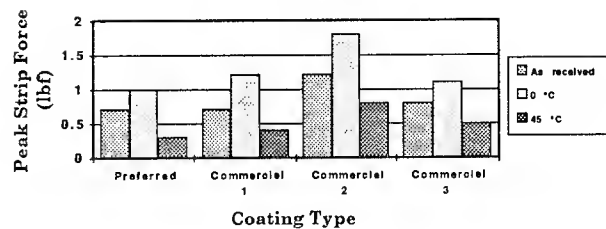


Table 4: Strip Performance as a Function of Temperature

Ave. Peak Strip Force (lbf)	Preferred	Com. 1	Com. 2	Com. 3	Com. 4
As Received	0.7	0.7	1.2	0.8	0.9
0°C	1.0	1.2	1.8	1.1	1.1
45°C	0.3	0.4	0.8	0.5	.63

The strippability of these fibers after exposure to a variety of environments was also evaluated to ensure that they will strip acceptably for the duration of the cable's expected life. The strip force test was performed under various simulated aging environments to test the fiber coating for its water sensitivity, hydrolytic stability, and compatibility with gel compounds. The results, shown in Figure 3 and Table 5, show that the preferred coating does not change after aging under various environments. A fiber coating may be exposed to environments that can be very different chemically, for example water and mineral oil. Mineral oil is chemically similar to many of the cable fill compounds used commercially, and has been used as a test surrogate for fill compounds as a worse case condition.^{6,7} The preferred coating performs well under both conditions. The test results indicate that other fiber coatings may perform well in one environment, but not so in others.

Figure 3. Strip Performance under Accelerated Aging Conditions

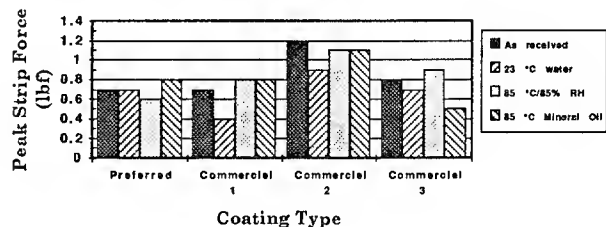


Table 5: Strip Performance in a Variety of Accelerated Aging Conditions

Ave. Peak Strip Force (lbf)	Preferred	Com. 1	Com. 2	Com. 3
As received	0.7	0.7	1.2	0.8
23°C water-14 days	0.7	0.4	0.9	0.7
85°C/85% RH-30 days	0.6	0.8	1.1	0.9
85°C Mineral oil-30 days	0.8	0.8	1.1	0.5

RESISTANCE TO SOLVENTS

Since solvents are used in the field to remove cable fill compounds from fibers, a fiber coating must not be adversely affected by exposure to such solvents. To test this, fibers with the preferred coating were exposed 12 times over a 6 hour period to the solvent by dipping the fiber into the solvent for 5 seconds, then letting the fiber air dry until the next exposure. The fiber was then tested for its peak strip force. Fiber coatings adversely affected by exposure to solvents cause the fiber to become either significantly harder or easier to strip. The results obtained from the preferred coating system are shown in Table 6.

Table 6: Strip Performance After Exposure to Various Solvents

Exposure	Mean Peak Strip Force (Lbf)
Control - no exposure	0.7
Wasp Spray	0.7
Acetone	0.7
Isopropyl Alcohol	0.6
Aqueous Ammonia	0.6

These results show no effect of strip force from exposure to acetone and a very minimal effect from exposure to alcohol and ammonia. The chemical stability provided by this coating system results in consistent strip force performance even after temperature extremes, temperature/humidity cycling, and solvents exposure.

A very aggressive test which challenges the coating in many respects is temperature cycling in mineral oil. This test shows the attenuation loss after one cycle from -40°C to +85°C, followed by 7 days at 85°C, then cycling the fiber again from -40°C to +85°C. This test, the results of which are shown in Table 7, clearly demonstrates the thermal and solvent resistance of the preferred coating system and its effect on the optical performance of the fiber. An attenuation change of only 0.02 dB/km at 1550 nm demonstrates the robustness of this product in very aggressive environments.

Table 7: Temperature Cycling in Mineral Oil

	Attenuation Increase (dB/km @ 1550 nm) *	
	Preferred Coating	Commercial 1
Mean	0.02	0.22
Maximum	0.04	0.29

* Cycle condition: -40°C to +85°C, 7 days at +85°C, followed by -40°C to +85°C cycle.

PERFORMANCE IN RIBBONS

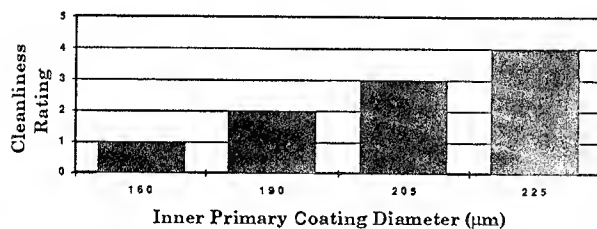
The deployment of fiber rich network architectures dictated the development of mass fusion splicing of optical fiber ribbons to reduce installation costs and time. Mass stripping of the matrix materials and fiber coatings from optical fiber ribbons is an integral part of mass splicing.

Mass stripping imposes some stringent requirements upon the fiber coating properties. The most fundamental of all fiber coating requirements is that the coating protect the glass from its environment, and also be easily removed, leaving the fiber free from any residual debris. In single fiber applications, the optical fiber is cleaned relatively easily via a single wipe with a solvent-moistened cloth. In contrast, ribbon structures are more compact and relatively difficult to clean efficiently and effectively after stripping. Ribbon fibers that are not adequately cleaned can contribute to splices having higher than acceptable optical losses. Thus, post strip-cleanliness of the ribbon fibers is of critical importance.

Several key coating properties have been identified as significantly influencing the post-strip cleanliness of mass-stripped optical fiber ribbons. Figure 4 shows the effect of the diameter of the fiber's inner primary coating on strip cleanliness while the outer primary was held at a nominal 245 microns. The rating scale used in Figure 4 ranges from 1, a very clean strip with no visible coating or matrix particles left adhering to the glass fiber, to 5, a very incomplete strip in which large areas of matrix material are left along with the fiber coatings

underneath (unacceptable). As the thickness of the fiber inner primary increases, the shear applied to the inner primary causes the low modulus, low tensile strength coating to tear. This leads to some of the inner primary being left behind on the stripped glass fiber, i.e., a less clean strip. A thinner inner primary layer would give a cleaner ribbon strip; however, an inner primary that is too thin would provide less protection against microbending of the fiber caused by loads applied to the side of the fiber. Thus, it is necessary to optimize coating geometry based on physical properties of the coatings relative to fiber performance.

Figure 4. Ribbon Strip Cleanliness vs. Inner Primary Diameter



Another factor which influences the strip cleanliness is the level of adhesion of the fiber's inner primary coating to the glass fiber. When ribbons are stripped, the desired result is for the inner primary to cleanly shear from the glass surface. However, if the adhesion is too low, the fiber becomes susceptible to handling damage in the fiber and ribbon manufacturing operations, or in the field handling of the ribbon. Figure 5 shows the ribbon strip cleanliness for both 4-fiber and 12-fiber ribbons when the inner primary adhesion to glass is varied. Adhesion was measured on coating films on glass plates using the 180 degree peel test. As expected, the differences seen for 4-fiber ribbons are much less than are seen for 12-fiber ribbons. Adhesion levels of 225 g/in of film width cause excessive debris to be left on the stripped fibers. Decreasing levels of adhesion results in cleaner ribbon strips until approximately 25 g/in of film width is reached.

As part of a continuous effort to improve fiber coating systems beyond their current level of performance, the preferred system utilizes an inner primary coating material that enables extreme low temperature performance in a ribbon. As shown in Table 8, the typical added loss at -60°C is 0.05 dB/km or less for both 4-fiber and 12-fiber ribbons containing fibers with the preferred coating, along with DSM-Desotech's LTS UV-curable inks and DSM-Desotech's 950-706 UV-curable Cabellite™ matrix material.

Figure 5. Ribbon Strip Cleanliness vs. Inner Primary Adhesion

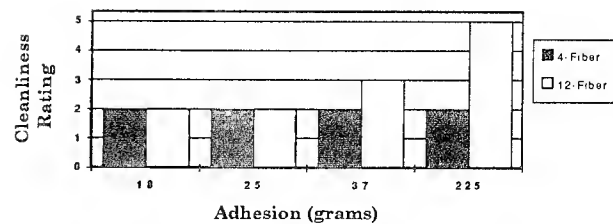


Table 8: Attenuation Loss at 1550 nm at -60°C for the Preferred Coating System in 12 and 4 Fiber Ribbons

Ribbon Fiber Number	12-Fiber Ribbon Loss at -60°C (ΔdB/km)	4-Fiber Ribbon Loss at -60°C (ΔdB/km)
1	0.00	0.02
2	0.00	0.03
3	0.00	0.02
4	0.00	0.01
5	0.00	
6	0.00	
7	0.00	
8	0.00	
9	0.00	
10	0.00	
11	0.00	
12	0.00	

The 12-fiber ribbon exhibits no added loss for any of its fibers down to -60°C. The 4-fiber ribbon shows more loss, primarily because it contains a much thicker layer of matrix material which can bend the fibers during thermal contraction. In this case, the 12-fiber ribbon thickness dimension was 270 μm while the 4-fiber thickness dimension was 400 μm.

RELIABILITY

No examination of fiber coating systems would be complete without addressing the issue of reliability. Two measures that are commonly referred to are: EIA/TIA 455-76, dynamic fatigue; and draft EIA/TIA 455-97, static fatigue.

Bellcore's TR-20 document requires dynamic fatigue values of greater than or equal to 20. The mean value obtained for silica fiber with the preferred coating is 20.4.

Analysis of the preferred coating system resulted in a static fatigue value of 27.3 after 7 days of testing in an in situ environment of 85°C/85% RH. However, a cautionary note should be taken that this test procedure has not been accepted by EIA/TIA, and much disagreement on the meaningfulness of the results exists. Until the disagreements can be fully resolved, it

is advisable that all results obtained with this test be viewed as preliminary, and that traditional silica values of 20 for fatigue be used in all reliability calculations.

SUMMARY

As fibers are deployed more widely, the requirements on fiber coatings are becoming more stringent. Results presented herein demonstrate that the preferred coating system has enhanced bend performance, enhanced thermal and chemical stability, and consistent strip performance over a wide range of temperatures and solvents. The result is a versatile coating system which is appropriate for loose tube, ribbon, and tight buffer applications, and which is consistent with all present craft practices.

ACKNOWLEDGEMENTS

The authors gratefully acknowledge our colleagues at DSM Desotech Inc., Steve Schmid, Gregg Kuetemeyer, David Szum, and Chander Chawla. Without their help and insight this work would not have been possible. We are also grateful for testing support from the Center of Fiber Optic Testing, and the ongoing support and encouragement from Margot Botelho and Dale Niebur.

REFERENCES

1. "Microbend Loss of Colored Optical Fibers Measured Over Extended Temperature Range", by Z. Pasturczyk and C. Saravanos, *42nd International Wire and Cable Symposium Proceedings* (1993), p. 527.
2. Under development as FOTP-112 by EIATIA Working Group 6.6.7.
3. "Effect of Chemical Environments on UV Curable Optical Fiber Coatings", by C. P. Chawla and D. M. Szum, *40th International Wire and Cable Symposium Proceedings* (1991), p. 141.
4. "The Effects of Aging on the Discernibility of the Color Identification of Optical Fibers", by R. A. Frantz and I. M. Plitz, *42nd International Wire and Cable Symposium Proceedings*, (1993), p. 850.
5. "Generic Requirements for Optical Fiber and Fiber Optic Cables", TR-NWT-000020, Bell Communications Research, Morristown, NJ, Issue 5, 1992.
6. "Self-stripping of Optical Fiber Coatings in Hydrocarbon Liquids and Cable Filling Compounds", by O. S. Gebizlioglu and I. M. Plitz, *Optical Engineering*, **30**, No. 6, page 749 (1991).
7. "Fiber Coating Interactions with Buffer Tube Gels", by R. A. Frantz and I. M. Plitz, *Optical Engineering*, **30**, No. 6, page 767 (1991)



Eric H. Urruti
Corning Incorporated
Corning, NY 14831

Eric Urruti received his B. S. degree in Chemistry from Indiana University in 1981, and his Ph. D. in Polymers and Coatings from North Dakota State University in 1986. He joined Corning, Incorporated in 1986 in Corporate R&D in Corning, New York, working on fiber optic coatings. In 1989, Eric joined the development group in Corning's Wilmington, North Carolina, fiber production facility working on hermetic coatings. In 1993, Eric returned to Corning, New York, to work as a Project manager for new coating development, and is presently supervisor of Corning's coating development group in Corporate R&D.



J. Richard Toler
Corning Incorporated
Corning, NY 14831

Dick Toler received his B. S. in Chemistry from Virginia Commonwealth University and his Ph.D. degree in Organic Chemistry from the University of Virginia. He worked with Owens-Corning Fiberglas until 1986 when he joined Corning Incorporated. At Corning, he has worked on the development of fiber coatings for optical fibers.



Git Kar
Corning Incorporated
Corning, NY 14831

Dr. Gitimoy Kar joined Corning in 1973 after receiving his Ph. D. degree in materials science and engineering from the University of California at Berkeley. He first became involved in optical fiber RD&E in 1977 and has held various technical and managerial positions in engineering, manufacturing and product development. His area of expertise includes preform processing, fiber draw and coating. Currently, Dr. Kar is responsible for new product development for future optical fiber networks.



John W. Botelho
Corning Incorporated
Corning, NY 14831

Mr. Botelho joined Corning Incorporated in 1981 with a B. S. degree in Mechanical Engineering from Southeastern Massachusetts University. He has held a variety of engineering positions in both the Electronic Components Business as well as the Optical Fiber Business. He is currently engaged in Optical Coating Development with focus on emerging ribbon applications.



Ching-Kee Chien
Corning Incorporated
Corning, NY 14831

Ching-Kee was born in China. He received his B. S. degree in Chemistry in Taiwan and his Ph.D. degree in Polymer Chemistry from the State University of New York. After working at the Carnegie Mellon Institute and City College of New York, he joined Corning Incorporated in 1985 where he has worked on coating development for optical fibers.

A NEW COATING SYSTEM FOR FIBERS WITH ENHANCED RESISTANCE TO ENVIRONMENTAL CONDITIONS

A.Ginocchio, A.Portinari, E.Consonni (1) G.Roba (2) F.Nanni (3)

(1) Pirelli Cavi Spa - Divisione Italia (2) FOS-Fibre Ottiche Sud
(3) SIP-Societa' Italiana per l'Esercizio delle Telecomunicazioni

ABSTRACT

The challenge for successful penetration of optical fibers into the subscriber loop is dependent on the development of new cables that must be small, light, flexible, and cost effective. In such a prospect, intrinsically reliable fibers are needed which can ensure, by means of their "coating system", significantly steady transmission performance also in harsh environments. A new optical fiber dual coating system specifically designed to meet the above mentioned need is presented. The laboratory tests carried out on this new fiber and on different fibers available on the market are described. The results obtained demonstrate that fibers made with this new double layer coating are suitable for ribbon cables and appear to be a promising solution for most cable structures.

INTRODUCTION

During the last ten years, optical cables have found their main application in long distance networks. Consequently manufacturing technology has been developed to produce high quality optical cables, generally characterized by robust protection structures for the optical fibers.

Nowadays the new field of application of optical fibers is the subscriber loop. However, a successful introduction of optical fibers in this context requires light, flexible, small, cost effective but nevertheless intrinsically reliable cables.

In developing these new cables the use of optical fibers that can ensure, by means of their "coating system", stable and reliable transmission characteristics both in the case of compact cable structures (i.e. ribbon cables), where there is tight contact among the fibers, and in a "harsh environment" (high humidity and/or water immersion) is critical.

This paper describes a series of tests carried out on a new coating named Z1 developed for meeting the requirements mentioned above. The results, compared with other commercial fibers, confirm the reliability of this fiber for ribbon cables; moreover the Z1 fiber appears to be a promising solution also for other cable structures.

FIBER DESIGN

The new coated fiber has been designed to optimize its use in those structures where the tight contact between the fibers and/or the multilayer geometry may cause a degradation of

the optical performance of the cabled fibers. A typical example is the ribbon fiber cable.

Most current ribbons consist of 4 fiber units encapsulated in a common coating where each fiber consists of 4 elements: glass, double layer coating and ink layer (see figure 1).

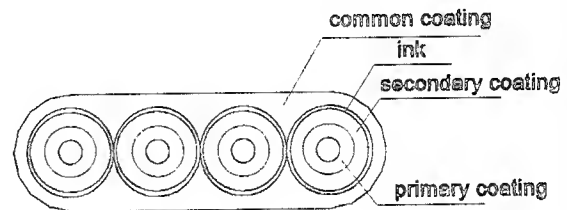


Fig.1 - Four fibers ribbon cross section

The numerous interfacial contacts and the asymmetrical geometry have an influence on the overall ribbon performance and make the ribbon more sensitive than the single fiber to those phenomena that can cause dimensional changes in the coating layer.

In fact the optical transmission loss is influenced by the mechanical stresses transferred to the fiber. These mechanical stresses can be caused both by forces applied to the external ribbon surface and by internal forces distributed along the interfacial layer contacts.

Moreover, the presence of delaminations between the glass-coating and coating-ink-common coating interfaces when the fiber or ribbon is subjected to a wet environment can emphasize the negative influence of these external or internal stresses on the optical performance.

It should be noted that the dimensional changes of the coating layers and the presence of delaminations are tightly correlated, since the former can definitely promote the latter. For this reason it's important to consider not only the ribbon design but at a prior stage also the fiber design. This must be optimized in order to achieve high dimensional stability in harsh environments and low side pressure dependence.

The new double layer coated fiber has been developed to optimize the optical and mechanical performance in particularly severe conditions caused by side pressure, temperature cycling and/or "wet" environments.

In addition, the basic performance criteria (i.e.: strippability and individual fiber break out, color coding for identification, mass fusion splice reliability, etc.) requested for ribbon and ribbon cable have also been satisfied. As far as the mass fusion splice is concerned, the optimization has also been devoted to the reduction of the fiber axis deflection after the coating stripping ("fiber curl").

Side pressure/ thermal cycling behavior

The side pressure dependence is related to the dimensional and physical characteristics of the coating layers. As far as the side pressure is concerned, when the overall diameter and the dimensions of the ribbon have been established, an optimal thickness of the first coating layer must be chosen for reducing the mechanical stresses transferred to the fiber structure. Furthermore the first and second coating layers must satisfy the conflicting requirements of mechanical protection and damping of the glass fiber. As the thickness of the second layer increases, there is a reduction in the stress applied to the underlying first layer but the consequent thinning of the first layer can give rise to a minor damping effect on the residual stress [2].

The calculation of the residual stress acting on the fiber structure when a concentrated force is applied along a generatrix of the overall coating can be performed with a finite element method. Since the elastic modulus of the coating layers depends on the temperature, the evaluation must be carried out at temperatures related to the thermal working conditions of the fiber (generally between -30°C and +60°C). The results carried out considering the physical characteristics of raw materials used have shown an optimum first layer thickness of about 30 microns.

On the other hand, the thermal contraction analysis indicates that the fiber behavior improves as the thickness of the first layer decreases. However the loss increase due to the side pressure remains the more relevant effect for design consideration.

Aging in a high humidity environment / water soak

Acrylic resins, which are at present the most commonly used coating materials for optical fibers worldwide, are permeable to water and consequently susceptible to swelling.

Unbalanced stresses may arise after immersion in water and, in some cases, delamination may develop depending on the intermolecular forces at the glass-coating and coating-ink interfaces. Asymmetric stresses in the optical fibers cause added microbending transmission losses. Water molecules, freely moving at the glass surface after delamination, easily break the glass SiO linkage (particularly in presence of OH- or H+ excess), causing a decrease of the mechanical strength of the fibers.

The occurrence of delamination at the glass-coating and ink-coating interfaces of optical fibers after immersion of samples in water, especially in case of ribbon structure, has been shown to induce:

- an increase of the transmission losses;
- zero stress aging, that is a decrease of the mechanical strength.

In this context, by decreasing the presence of extractable particles in the coating materials and increasing the threshold strengths, the coating materials must be selected in order to optimize the ribbon and/or fiber structure stability during immersion in water [3].

EXPERIMENTAL

The tests have been initially oriented towards the evaluation of the fiber behavior in ribbon structures. However, after the encouraging results obtained, they have been extended in order to test the fiber performances also in loose cable structures.

The scope of the tests carried out was to determine the sensitivity of ribbons and fibers to side pressure, thermal cycling and water.

For each test some results obtained on different fibers or ribbons available on the market will be reported for comparison.

Mechanical tests.

Fiber breaking strengths before and after accelerated aging in water have been determined in order to test the coating as protection element. In fact, the fiber axial strength is strongly influenced by the dimension and by the shape of the microflaws distributed on its surface. The microflaw dimensional growth is highly influenced by the environmental conditions and is strongly accelerated in presence of water.

In this context, the fiber strength and the effectiveness of the coating as protection element are highly correlated. The results, performed on different natural fibers are reported on figure 2.

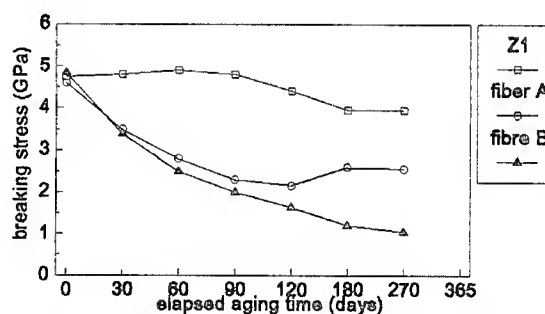


Fig.2 - Breaking stress of fibers aged in water at 60°C

The Z1 fiber shows a lower reduction in strength due to the absence of delaminations at the glass-coating interface.

Thermal cycling.

This test is mainly devoted to evaluate the microbending losses caused by thermal contraction of the coating. The test must be performed on natural fibers, colored fibers and ribbons, being more critical for ribbons. Several ribbons produced with Z1 fibers underwent thermal cycling, with temperatures ranging from -40 °C to + 60 °C. Figures 3 and

4 show some groups of attenuation measurements performed at -40°C and $+60^{\circ}\text{C}$.

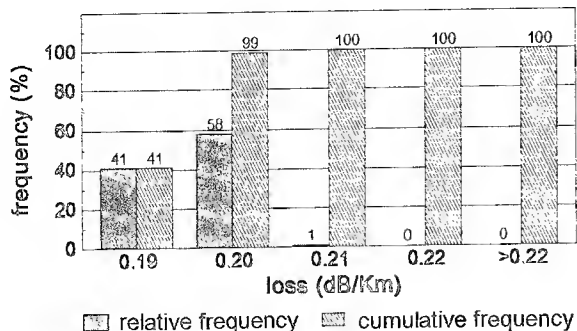


Fig.3 - Thermal cycling on Z1 ribbon (60°C , 1550 nm)

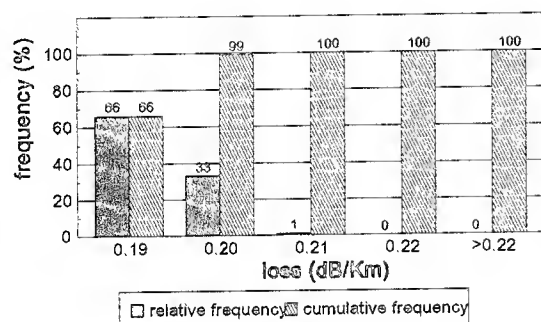


Fig.4 - Thermal cycling on Z1 ribbon (-40°C , 1550 nm)

It can be seen that the optical attenuation is highly stable in all temperature ranges.

Side-pressure test.

This test is to evaluate the behavior of fibers and ribbons when subjected to microbending caused by "side pressure". In fact, as far as the ribbon cable design is concerned, ribbons are expected to be in contact with the plastic slotted core, and therefore, to be subjected to a side pressure depending on the applied tension and on the slotted core geometrical shape [2].

The side pressure is obtained by means of radial expansion of a cylindrical bobbin on which the sample of ribbon or fiber is wound in a single layer. The bobbin surface is covered with a thin sheet having a pliability and roughness power spectrum similar to those of the cable slotted core. The ribbon or fiber samples are 100 meters long to obtain the necessary sensitivity.

The measurements are taken at different temperatures covering the cable's thermal working range to take into account the variation of the mechanical characteristics of the different materials vs. temperature.

In figure 5, Z1 fiber ribbon performances are compared with those of a standard fiber ribbon at different temperatures.

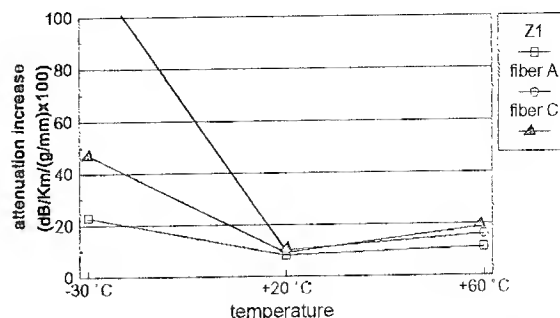


Fig.5 - Expandable bobbin: attenuation increase vs temperature for fiber ribbons

It can be seen that the attenuation increase vs the lateral pressure is less pronounced for Z1 ribbon in comparison with the other ribbons especially at low temperatures.

Aging in filling compound at high humidity/temperature

Optical measurements are carried out on fibers and ribbons aged in filling compound at high temperature and high humidity (temperature between 70°C and 90°C , relative humidity of 95 %). The 70°C test condition has been considered because at this temperature a lot of data are available for comparison among different fibers. The 4 months aging time and the 90°C test conditions correspond to a period of about 30 years at the temperature of 20°C , established using the Arrhenius law.

Figure 6 shows the attenuation measured at -30°C for ribbon samples, while figures 7 and 8 show the loss increases at -30°C for fibre samples. The measurements are carried out at different aging elapsed times.

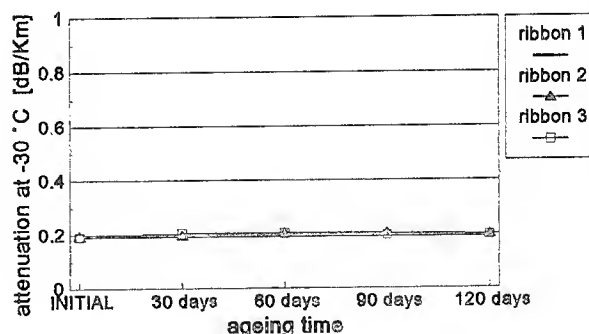


Fig. 6 - Aging on Z1 fiber ribbons: attenuation at -30°C and 1550 nm after immersion in filling compound at 90°C and 95% RH.

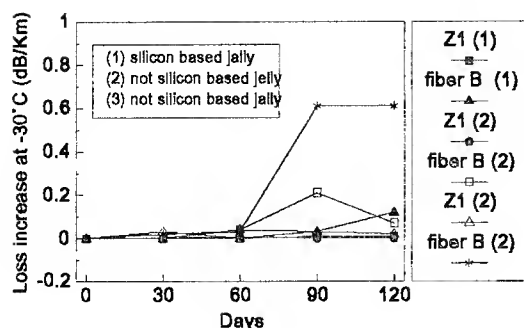


Fig. 7 - Aging on natural fibers: attenuation at -30°C and 1550 nm after immersion in filling compound at 70°C and 95% RH.

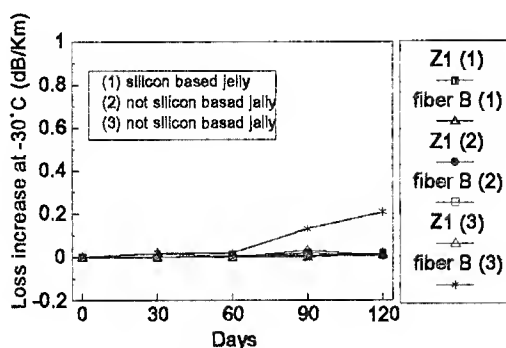


Fig. 8 - Aging on colored fibers: attenuation at -30°C and 1550 nm after immersion in filling compound at 70°C and 95% RH.

The results obtained show that the Z1 fiber behavior is characterized by a very low dependence on the filling compound or ink used.

Aging in water.

This test is necessary to directly evaluate the fiber or ribbon water "sensitivity". The importance of this behavior is related to the high demands of cables to be used in subscriber loops where harsh environments have to be tolerated and more economical cable overall protections are required.

Two temperature conditions have been considered for the tests namely 20°C and 60°C .

The 60°C condition has been chosen in order to evaluate the fibre/ribbon performance in an extremely harsh environment. It should be noted that, on the basis of the experience gained so far, the 60°C test on ribbons, due to its severity on the multilayer structure, can be used as a relative indicator of behavior tendencies but cannot be considered as a simple accelerated test in place of the 20°C test.

In fact, all chemical and mechanical coating characteristics related to the fiber water soak sensitivity are highly dependent on the temperature. In particular the mechanical performance of the coating, the osmotic pressure and the presence of hydrolytic phenomena can play a different role

at 60°C in comparison with lower temperatures. For instance the growth of bubbles between glass and coating surfaces can be emphasized by a low coating Young modulus and by a greater osmotic pressure. While some hydrolytic traces can be seen after aging of acrylate materials at $100 - 120^{\circ}\text{C}$ in water, this is not the case for lower temperatures. However some hidden hydrolytic phenomena are more likely to influence the overall fiber performance at 60°C test conditions than at 20°C test conditions. As a conclusion testing at 60°C is very far from being a simple acceleration of lower temperature testing, but must be considered as a peculiar environment, involving substantial differences in aging mechanism.

To check water sensitivity for fiber or ribbon it is essential to monitor the attenuation variations during the whole test. For the first 7 days a continuous monitoring of attenuation (every 15 minutes) is recommended. In fact the ribbon/fibre behavior during the first week can be representative of a longer period of time for cabled ribbons and fibers. As an example, water soak test (fig. 9/12) shows a poor performance of fiber A in spite of the regular behavior in the long term.

The sample length is around 1000 meter for better OTDR measurements. Tests on natural fiber, colored fiber and ribbon have been performed with different combinations of fiber types, inks and common coatings.

Figures 9, 10 and 11 describe water soak tests at room temperature carried out on natural and colored fibers, while figures 12, 13 and 14 show the same tests at 60°C .

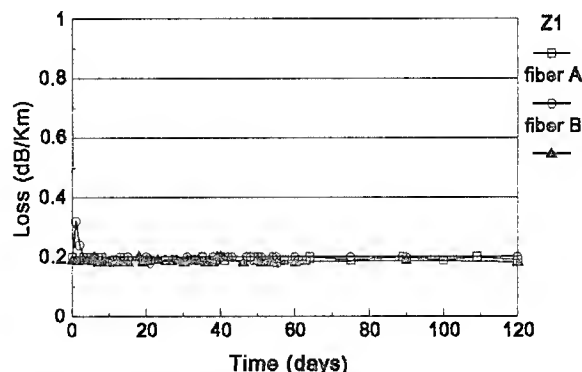


Fig. 9 - Water soak test on natural fibers at 20°C

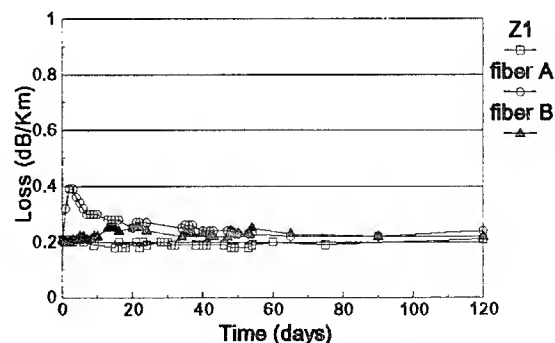


Fig. 10 - Water soak test on colored fibers at 20°C (transparent ink)

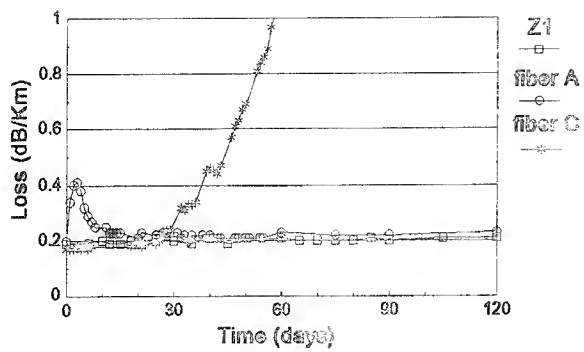


Fig. 11 - Water soak test on colored fibers at 20°C (opaque ink)

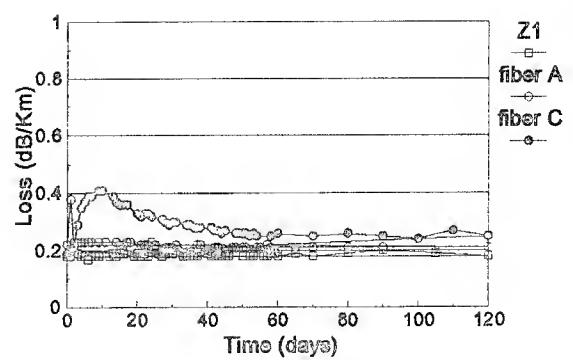


Fig. 14 - Water soak test on colored fibers at 60°C (opaque ink)

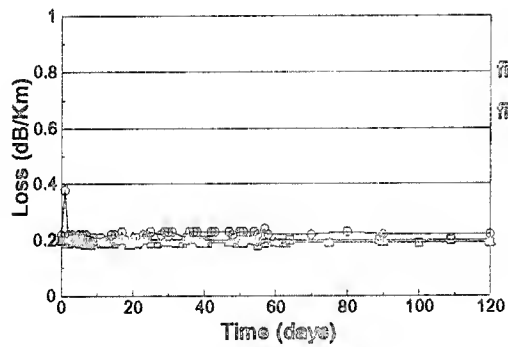


Fig. 12 - Water soak test on natural fibers at 60°C

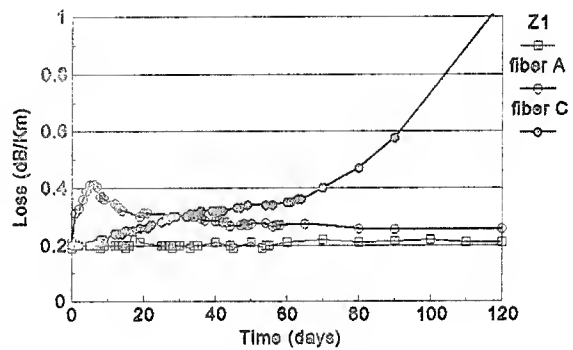


Fig. 15 - Water soak test on ribbons at 20°C

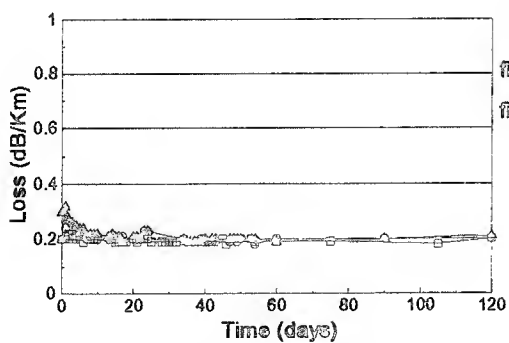


Fig. 13 - Water soak test on colored fibers at 60°C (transparent ink)

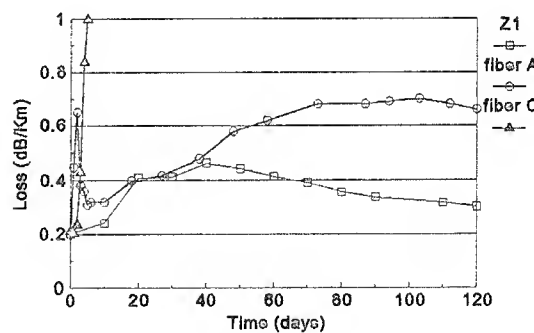


Fig. 16 - Water soak test on ribbons at 60°C

Figures 15 and 16 show water soak tests carried out on fiber ribbons.

The behavior of Z1 fiber seems to be very independent of the kind of ink used, and the results obtained on ribbon structures demonstrate that the Z1 fiber shows reduced optical loss increase due to water soak phenomena compared to other tested fibers.

A complementary water soak test is the measurement of pull-out forces on fiber samples aged in water at 60 °C for 30 days. The measurements are performed on 10 mm of fiber embedded in resin with a gauge length of 100 mm and a crosshead speed of 10 mm/min (see figure 17).

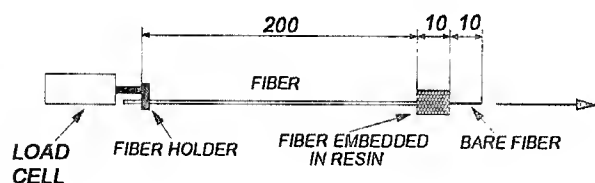


Fig.17 - Test apparatus for the pull-out force measurement

This test allows to verify the adhesion between glass and coating before and after aging in water. These measurements compared to the optical performances tested on the same fibers in the same environments can give interesting information on the effect of glass-coating delaminations on the optical fiber performance. Figures 18, 19, 20 show the results obtained on different fibers compared to Z1 fiber.

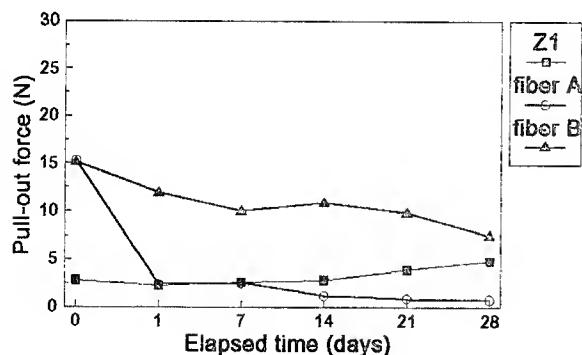


Fig.18 - Pull-out test on natural fibers aged in water at 60 °C

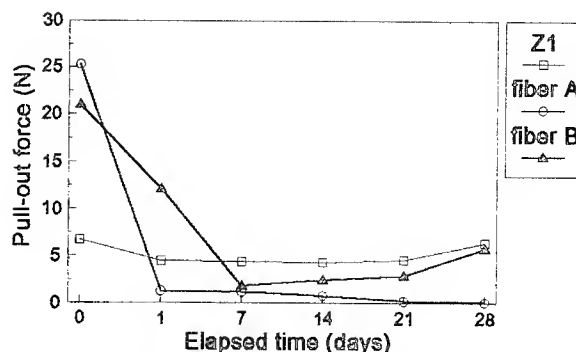


Fig.19 - Pull-out test on colored fibers (transparent ink 1) aged in water at 60 °C

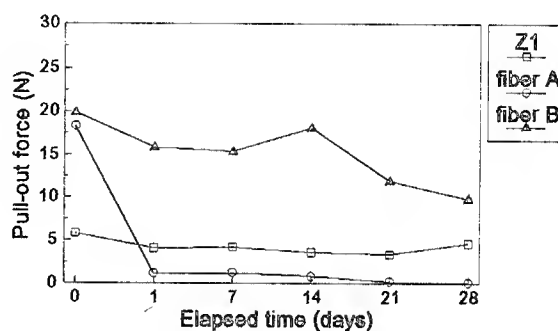


Fig.20 - Pull-out test on colored fibers (transparent ink 2) aged in water at 60 °C

It can be easily seen that the change in pull-out force is highly correlated to the optical performance of the fibers. More in detail, three different behaviors can be observed:

- absence of delaminations: no loss increases
- quick grow of delaminations and complete separation between glass and coating after 1 day in water; there is loss increase only during the first aging day
- presence of delaminations distributed in irregular way or low growth of delamination; there is a constant change of loss at low rate.

The final test is performed on cable structures immersed in water for long aging time at an average temperature of 20 °C. Two different cable structures are considered: ribbon cables and loose tube cables. The cabled fiber behaviors (described in figures from 21 to 26) correspond to the performances evaluated during the laboratory tests on loose coil samples.

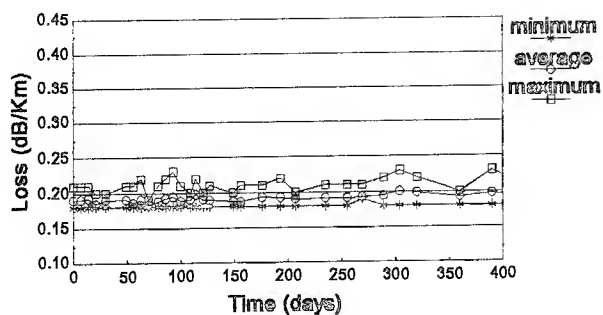


Fig. 21 - 100 optical fiber ribbon cable: aging in water (Z1 fiber)

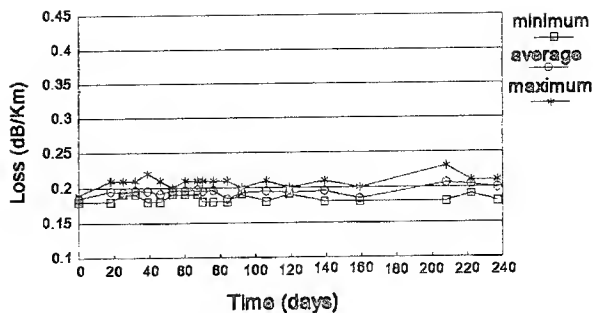


Fig. 24 - Optical loose tube cable: aging in water (Z1 fiber)

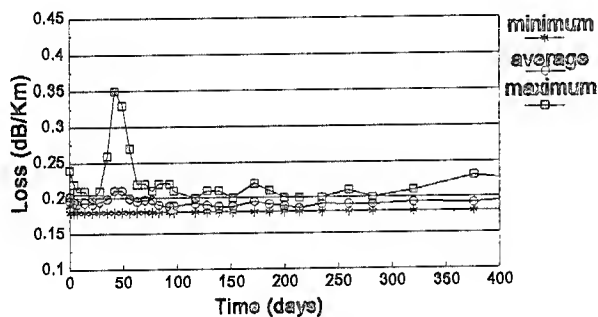


Fig. 22 - 100 optical fiber ribbon cable: aging in water (fiber A)

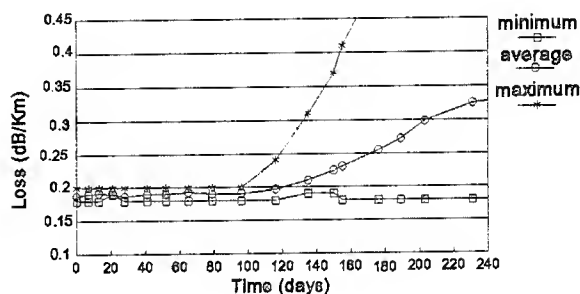


Fig. 25 - Optical loose tube cable: aging in water (fiber A)

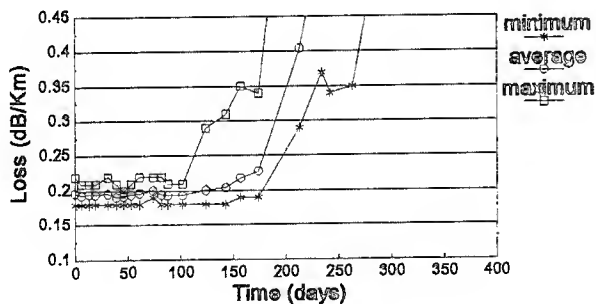


Fig. 23 - 100 optical fiber ribbon cable: aging in water (fiber C)

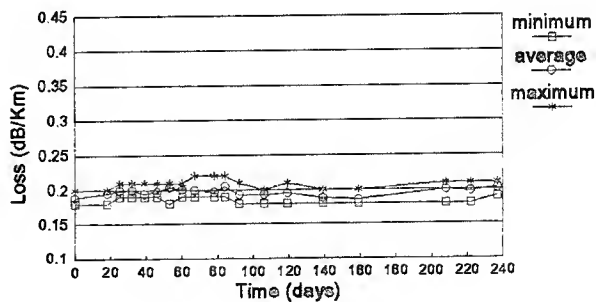


Fig. 26 - Optical loose tube cable: aging in water (fiber B)

Fiber "curl"

The "fiber curl" phenomenon is related to a fiber memory of the drawing process and can have a relevant impact on the optical splice performance, especially in case of fiber ribbons (mass fusion splice). In fact, as far as the cleaving operations are concerned, a fiber axis deflection after the coating stripping has a negative influence on the end face cleaving and, consequently, on the final result in terms of optical splice performance.

A lot of tests have been performed on Z1 and commercial fibers in order to evaluate the fiber "curl". The measurement procedure involves: - removing the coating for a length of 30 mm with an hot mechanical stripper; - placing the optical fiber in a microscope equipment; - measuring the distance Y_d and Y_s as indicated in figure 27.

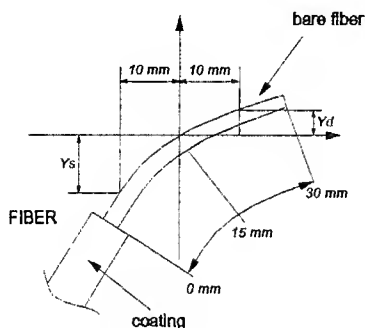


Fig. 27 - Fiber curvature degree: measurement method

The degree of curvature is computed as the absolute value of the difference between Y_d and Y_s . The results carried out are summarized in figure 28.

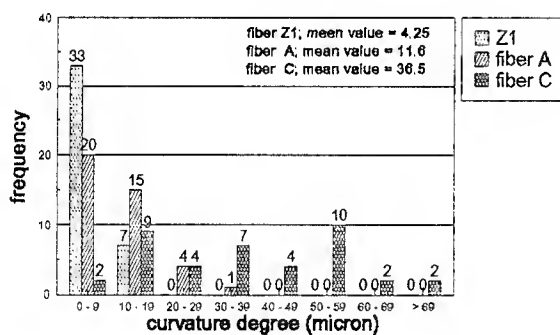


Fig. 28 - Curvature degree measurements

FIELD TRIALS

More than 30 thousand kilometers of Z1 fiber has been employed for ribbon cable production mainly with one hundred fiber count. About ten thousand kilometers of fiber has already been installed. During the field trials, evaluation

of fiber performances in terms of handling, jointing and installation have been carried-out. The results obtained are completely satisfactory.

CONCLUSIONS

Aging tests in water and in filling compound carried out on fibers available on the market have shown that the behavior of the fibers aged in such environments is strongly influenced by the coating system (double layer coating and ink layer).

A new double layer coating able to assure stable fiber performance after long aging time in water and in filling compound and optimized for use in ribbon structures has been developed and tested. This new fiber has been thoroughly characterized and implemented in ribbon cable design; furthermore, on the basis of laboratory tests, it has been demonstrated to be suitable for other cabling structures.

REFERENCES

1. F.Montalti, F.Nanni, F.Caviglia, D.Suino, "Evolving new technologies for the Italian Optical Cable Plants" 1993, IWCS p.36-41
2. F.Donazzi, R.Gaspari, A.Portinari, "Problems related to the Design and Manufacture of Optical Fibre Ribbons" 1991, EFOC p.116-121
3. A.Abel, J.van Eekelen, "Dynamic water sensitivity of U.V. acrylate inks and matrix coating, and its relationship to the water soak performance of optical fiber ribbons." 1993, EFOC & N p.298-302
4. G.Carones, A.Pannullo and A.Zuccala, "A novel optical Fibre for Ribbon Application" 1993 EFOC&N p.222-228



A. Ginocchio

Pirelli Cavi - Divisione
Italia
Milano, Italy

A. Ginocchio was born in Milan in 1947. He graduated in Electrical Engineering from Politecnico di Milano in 1972 and joined Pirelli in 1974, where he was engaged in the research and development on submarine cables. Since 1987 he has been responsible for the technological development of optical fiber cables in Pirelli Cavi - Divisione Italia.

E. Consonni

Pirelli Cavi - Divisione
Italia
Milano, Italy

E. Consonni was born in Seregno (Mi) in 1964. He graduated in Aeronautical Engineering from Politecnico di Milano in 1991 and joined Pirelli in 1991, where he has been engaged in research and development of telecommunication Cables, dealing mostly with environmental tests on optical fibres/cables and manufacturing technology.

F. Nanni

SIP-Societa' Italiana per
l'Esercizio delle
Telecomunicazioni

Fabrizio Nanni was born in Rome, Italy, in 1960. He received his doctorate in Physics from the University of Rome. During his studies from 1986 he has collaborated with a laboratory of research on optical communications: Fondazione "U. Bordon" in Rome working on photoconductivity ultrafast phenomena, semi-conductor laser and ultrafast photodiodes characterization. In 1988 he joined SIP (Italian Telecommunication Operating Company) Headquarters where he has been engaged in the study and development of optical and copper cables and in optical cable specification and characterization both in laboratory and field. Moreover his present responsibilities include CCITT Com.XV, ETSI-TM1, CECC-WG28 and COST 246 activities.

A. Portinari

Pirelli Cavi - Divisione
Italia
Milano, Italy



A. Portinari was born in Sesto San Giovanni (Milan) in 1933. Degree in Electrical Engineering from University of Padova. He joined Pirelli in 1961. He was engaged in Research & Development and manufacturing technology of Telecommunication cables. Since 1989 he was Pirelli's officer responsible for the product development for SIP.

G. Roba

FOS-Fibre Ottiche Sud
Battipaglia, Italy



G. Roba was born in Cogoleto (Genova) in 1951. He received his Doctorate in Physics in 1976 from the University of Genova where he spent a short postgraduate period working in the field of superconducting detectors. In 1977 he joined CSELT where he was involved in R&D activity on optical fibre technology. In 1985 he joined 3M ITALIA RICERCHE with the responsibility of advanced electro-optic technologies development in cooperation with main Japanese O.E.M.s. In 1989, on secondment from PIRELLI CAVI - ITALY, he joined PIRELLI CABLES - UK where he has been Manager of the Optical System Group R&D activity included the development of Erbium-Doped fibers for the Optical Amplifier. Since Oct. 1994 he is R&D Manager of FOS - Fibre Ottiche Sud in Battipaglia. Dr. Roba holds 20 international patents and is author/co-author of some 35 publications. He is member of OSA.

THE APPLICATION OF SYNTHETIC SILICA TUBING FOR LARGE PREFORM MANUFACTURE USING MCVD

P.F. Glodis, C.F. Gridley, W.M. Flegal, A.A. Klein, D.P. Jablonowski,
D. Kalish

AT&T Network Cable Systems, Norcross, Ga.

A. Sorby, H. Damsgaard, G. Knudsen
Lycom, Brondby, Denmark

H. Schaper, N. Treber, H. Fabian
Heraeus Quarzglas, Hanau, Germany

P.C. Schultz

Heraeus Amersil, Duluth, Ga.

ABSTRACT - The MCVD process is used widely as a manufacturing process for optical fiber. The application of high purity synthetic silica tubing to MCVD in a large production environment has allowed improved productivity by increasing preform size. This has been accomplished while maintaining or improving quality in all fiber parameters. In addition, the development and application of both undoped and fluorine doped synthetic silica has resulted in the straightforward manufacture of large MCVD preforms with depressed clad, matched clad, and dispersion shifted profile designs. This new direction for MCVD opens a wide array of options for improved productivity with high quality.

1.0. INTRODUCTION

The Modified Chemical Vapor Deposition (MCVD) process has been used extensively as a method of manufacturing high quality optical waveguide preforms since 1974¹. At present, the percentage of fiber manufactured worldwide using MCVD is estimated to be 37%. Major fiber designs required by the customer are matched clad or depressed clad single mode (for operation at 1310 nm), dispersion shifted single mode (for operation at or near 1550 nm), and 62.5 μ m multimode. The same basic MCVD process has proven to be very adaptable in manufacturing all these designs in a production environment.

The basic concept of MCVD has been documented in numerous review papers^{2,3}. The process is sometimes characterized as an inside deposition process in that the reaction of

halides and oxygen to form oxide particles and their subsequent deposition occurs inside a quartz tube. The tube and its deposit is then heated and collapsed to a solid rod. To make a larger preform a second tube is normally collapsed over the rod. Standard fiber drawing and coating operations are used to transform the preform into multi-kilometer lengths of optical fiber.

The availability of high quality tubing in the late 1970's and throughout the 1980's was crucial to the successful application of MCVD. Fortunately, glass processes using high quality natural quartz existed for producing lamp tubing. Adapting these processes to needs of MCVD, glass companies responded to supply natural fused quartz tubes made with such raw materials (so called "natural quartz tubing"). These tubes had the necessary properties for successful fiber manufacture using MCVD at reasonably low costs.

While the simplicity and flexibility of MCVD allows for rapid application of different fiber designs, its use of natural quartz tubing for single mode designs has resulted in some limitations. Because of the relatively high attenuation of the natural quartz tube it becomes necessary to place some amount of MCVD deposit between the single mode core and the tube. Also, since the deposition is inside a tube, there are limitations as to the amount of glass than can be deposited; 75-125 mm^2 is typical. These two factors combine to limit the preform size and the resultant productivity of a MCVD lathe station. With natural quartz tubing, maximum preform sizes for single mode designs are 50-70 km.

The development of low loss fused silica tubing made by flame hydrolysis of SiCl_4 (so called "synthetic silica tubing") has altered this limitation. Preform sizes and productivity have been dramatically increased by the application of synthetic silica tubing to the MCVD process. Similar improvements have been demonstrated for the PCVD fiber fabrication process^{4,5}.

2.0. SYNTHETIC SILICA TUBING AND MCVD

2.1 MCVD and single mode fiber manufacturing productivity

To further describe the relationship between MCVD deposit and preform size, Figure 2.1 shows the fraction of the total glass in a typical single mode fiber contributed by the MCVD process as a function of preform size. The preform size is expressed as the fiber kilometers obtained by drawing a 100 cm preform length. We assume a typical MCVD practice in which about 80 mm^2 of glass is deposited inside the starting tube and an overclad process is used whereby a second tube (overclad tube) is collapsed over the rod obtained from the MCVD step. In the finished preform the diameter of the core and MCVD cladding is 10 mm. In Figure 2.1, preform size is assumed to be increased by increasing the core size, holding the total amount of MCVD deposition to 80 mm^2 and increasing the size of the overclad tube to match the larger core diameter.

For example, in a 30 km preform MCVD would contribute 21% of the glass in the fiber. For a 150 km preform, the MCVD fraction drops to less than 5%. This substitution of starting and overclad material for MCVD deposit results in increased productivity since the total MCVD cycle time essentially does not change while the preform size increases by a factor of five. In effect, the MCVD deposition rate is much less important since the fraction of glass from MCVD is lowered. The economics of the process are greatly influenced by the cost of the tubing material

which in turn depend upon deposition rates in the tube manufacturing process.

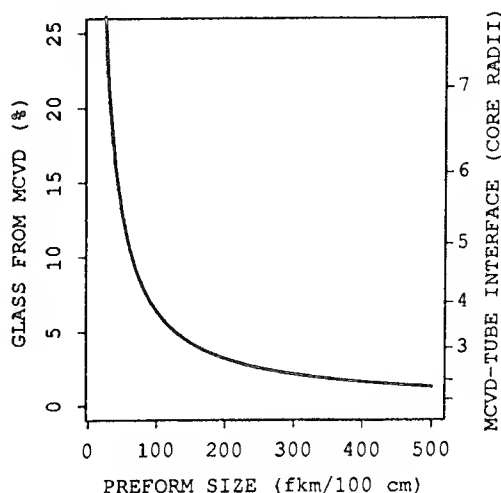


Fig. 2.1 - Increases in preform size with a constant 80 mm^2 MCVD deposit

Figure 2.1 also shows the location of the interface between the MCVD glass and the inside surface of the starting tube in the collapsed preform. This is expressed in units of core radii. For a 30 km preform, the MCVD tube interface to core ratio is 7. For a 150 km preform, the ratio drops to 3.1. Since the starting tube is much closer to the core in the large preform, the optical quality of the starting tube has a much greater effect on the fiber loss. Therefore, the availability of tubing with optical loss comparable to MCVD derived material is necessary for the successful implementation of the scaleup in MCVD preform size outlined above.

2.2 Fiber profiles and large MCVD preforms

MCVD is a versatile process in terms of the refractive index profiles that can be realized. The profile is built up radially, step by step, with each glass layer deposited and sintered individually. This minimizes the diffusion of dopants across layers. Fluorine doping is easily accommodated (typically C_2F_6 or SiF_4 is used) and allows fiber profiles with regions of depressed

index. Usually, switching between different single mode designs such as matched clad, depressed clad or dispersion shifted fiber has required only software changes to the MCVD preform recipe.

It is desirable to preserve this manufacturing versatility with synthetic silica tubes and larger preforms. The difficulty is that typical depressed clad single mode profiles require lowering the cladding index out to radial distances of 5 to 7 core radii. In a 30 km preform, this is achieved by simply depositing all of the depressed cladding in the MCVD part of the process. For a 150 km preform, the MCVD-tube boundary is located at a clad to core ratio of 3.1 (with a 10 mm MCVD deposit thickness) so a new approach became necessary.

The solution was found in the development and use of fluorine doped (downdoped) starting tubes in the MCVD process. This was essential for the manufacture of large depressed clad MCVD preforms. The range of index depression possible in the tube manufacturing process matches that used in MCVD. For a typical depressed cladding single mode preform, tubes with an average index depression of -12×10^{-4} are used. The downdoped section of the preform profile then consists of the MCVD cladding material out to 3 core radii at the starting tube boundary (for a 150 km preform) followed by the downdoped starting tube out to 5.5 core radii at the boundary with the undoped synthetic silica overclad tube.

Figure 2.2 illustrates this approach. The refractive index profiles for matched clad, depressed clad, and dispersion shifted single mode fibers are shown along with a cross section for a 49 mm (dia.) preform, indicating the contribution of the various process components or steps. The shaded areas show the MCVD material (4% of the fiber cross section), the starting tube (9%) and the overclad tube (87%). The major process change between the manufacture of large matched clad or dispersion shifted fiber and the

manufacture of depressed single mode preforms is the use of a fluorine doped starting tube for depressed clad.

In Section 3.0, we describe the production methods and quality of the synthetic silica tubing.

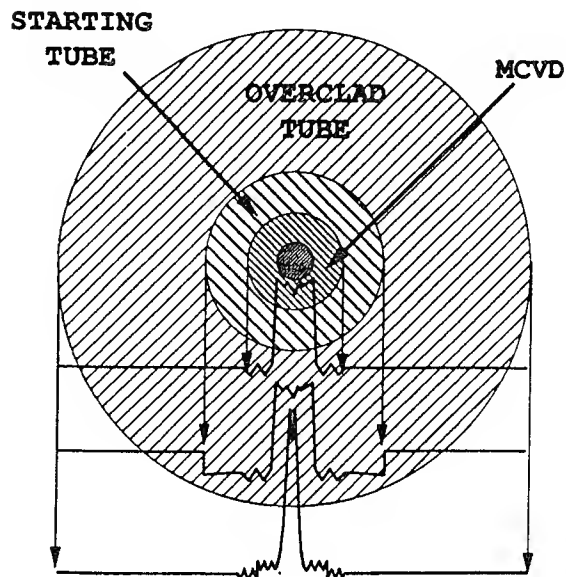


Fig. 2.2 - A preform cross-section with fiber profiles for depressed clad, matched clad, and dispersion shifted fiber designs.

3.0 SYNTHETIC SILICA TUBING

3.1 Production Method

Synthetic silica tube materials are produced in a flame hydrolysis reaction starting with silicon tetrachloride in an oxyhydrogen torch. The primary SiO_2 particles are collected to form a porous body which in subsequent process steps is conventionally dehydrated using chlorine in inert gas mixtures (for undoped tubes) or gas phase doped with fluorohydrocarbons (for downdoped tubes). Vacuum sintering then follows.

The product which is thus obtained is a hollow cylinder with a weight in excess of one hundred kilograms. The material qualification is carried out by means of IR for OH and UV spectrometry for transition metals.

The geometry of these hollow cylinders is perfected through a series of inside and outside precision grinding steps. By this, deviations from circularity and concentricity of the inside and outside surface can be reduced to levels of no more than 0.1%.

From these high precision hollow cylinders the waveguide tubes are pulled. This process is similar to that used for cylinders made from natural quartz wherein tubes are free drawn (e.g., without forming dies) in an electrically heated furnace.

The technology for manufacturing synthetic silica tube materials has been developed and improved greatly over the past few years. In early 1993, a large volume production plant located in Bitterfeld, Germany (formally GDR) started its operation.

3.2 Materials Properties

Refractive index

As described in Section 2.0, both doped and undoped synthetic silica materials are used in MCVD. Undoped synthetic silica tubing is used as jacket material with a refractive index close to that of natural quartz tubing. The index is increased by about 1×10^{-4} due to the chlorine incorporated.

Substrate tubes are located closer to the core region of the optical fiber and therefore need to be adjusted with their refractive index to the MCVD cladding layers. For matched clad fibers undoped synthetic silica (code name F300) provides the refractive index level needed. In the case of depressed clad design the index of the substrate tube is reduced by fluorine doping (code name F320) to refractive index values of about 12×10^{-4} below that of undoped silica.

For special applications where even further depression of the cladding region is desired synthetic silica tubing with refractive indices 45×10^{-4} below that of undoped silica is available (code name F325). Fig. 3.1 summarizes the optical indices discussed above. Natural silica

(code name Heralux) was taken as reference with the refractive index of the synthetic material given as the difference measured by a P104 profile analyzer (York, UK).

Purity

Synthetic silica tubing is well known for its high purity and the corresponding low attenuation levels and high tensile strength. In standard production and quality control most methods for analyzing

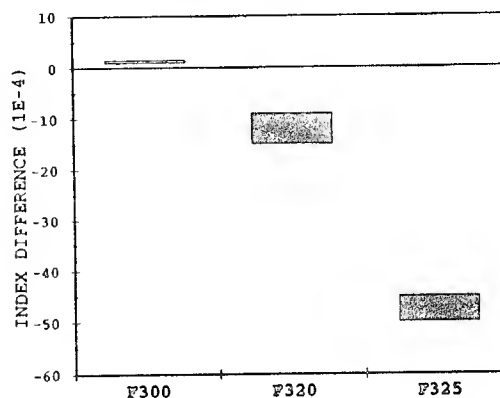


Fig. 3.1 - Refractive indices of the synthetic material.

impurity levels in the ppb range are quite complicated and cause unacceptable time delay. To avoid such problems UV attenuation measurements may be introduced. For evaluation of metallic impurities the absorption coefficient at 200 nm is a very reliable parameter. It is measured in units of 1/cm and is referred to as K_{200} -value.

All synthetic silica tubing is specified to have K_{200} -values of less than 0.1 cm^{-1} . The mean production values are about one order of magnitude below the specification limit indicating a typical overall metallic impurity level to be about 50 ppb. A histogram of measured K_{200} -values is shown in Fig. 3.2.

OH-content

For low fiber attenuation, OH levels of <1 ppm are desirable for preform sizes of 100 km or greater. Through proper dehydration using chlorine or

fluorohydrocarbons, we are able to keep the tubing below this limit. In Fig. 3.3 a histogram of production OH values is plotted, showing median values between 0.10 and 0.15 ppm. In comparison, natural quartz tubing for waveguide applications contains 150-200 ppm of OH. OH values were measured by the intensity of fundamental OH absorption at 2.7 μm .

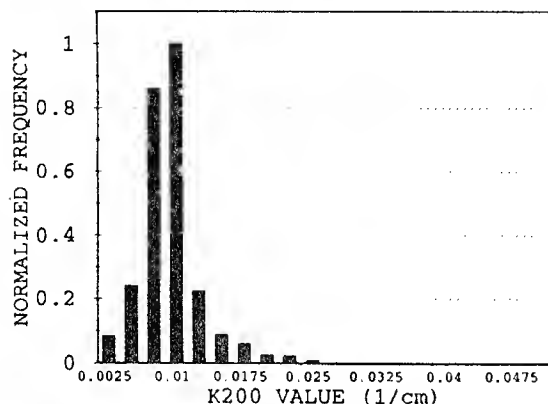


Fig. 3.2 - Purity of synthetic material as represented by K200 values from standard production.

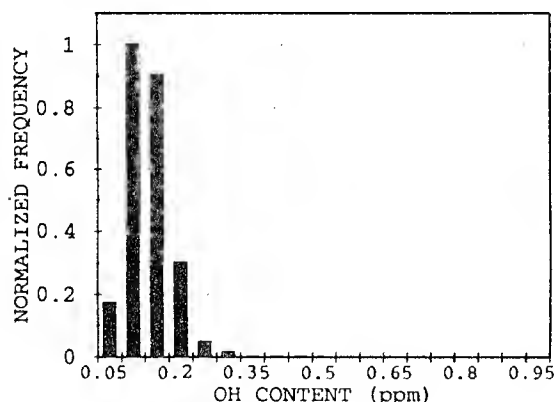


Fig. 3.3 - OH levels in synthetic tubing as measured from standard production.

Viscosity

In optical fiber preforms synthetic silica materials from different production methods with different doping levels are combined forming the desired refractive index profile and geometry. To obtain sufficient tensile strength and to avoid changes in optical performance due to internal stresses the viscosities of

the different materials need to be adjusted.

For synthetic silica tubing and natural quartz tubing the viscosity data were determined as a function of temperature (Fig. 3.4). In the temperature range between 1000°K and 2000°K the torsion method⁶ was used. Data for temperatures between 1700°K and 2300°K were determined by the fiber drawing method⁷. Natural quartz tubing shows the highest viscosity due to the absence of chlorine and the presence of trace metallic impurities. F300 is softer because of the chlorine incorporated in the glass. Lowest viscosity was recorded for F320 due to the presence of fluorine.

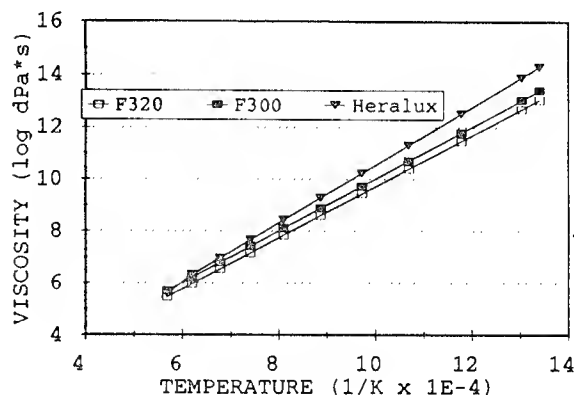


Fig. 3.4 - Viscosity vs. temperature for natural and synthetic material.

In Fig. 3.5 the differences in viscosity were calculated for the three types of silica discussed above. F300 was taken as the reference sample given by the zero line. The temperature dependencies of the synthetic silicas match quite well resulting in very low stress levels in the final optical fiber. Natural quartz tubing combined with synthetic silica tubing may cause undesirable stress profiles due to the different temperature dependence of viscosities.

3.3 Tube Geometry

Fiber performance is affected not only by material properties but also by its dimensional characteristics. Parameters like eccentricity and clad

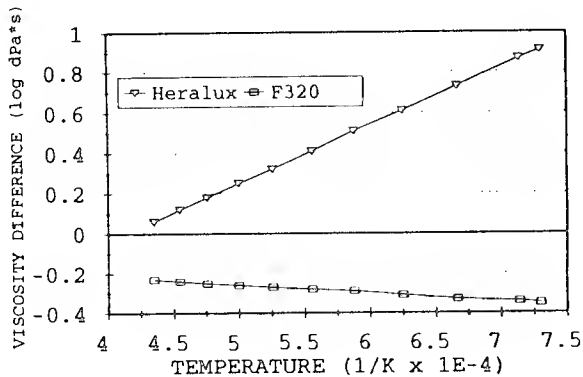


Fig. 3.5 - Viscosity differences of natural and doped synthetic materials as referenced to undoped synthetic.

noncircularity are determined not only by preform manufacturing but also by the geometry of the starting and overclad tubes. Dimensional deviations of the tubes are transformed via the preform into the fiber. To improve these fiber parameters, cylinder geometry and tube pulling technique have become the central topics of development programs over the last decade. Significant progress has been made which in turn has contributed to the outstanding performance of today's optical fibers.

Whereas in fiber drawing dimensional control is limited to the fiber diameter, in tube pulling two parameters, diameter and wall thickness, need to be controlled. Complex automatic control systems were introduced in the mid 1980's resulting in significant improvements. With the increasing power of computer systems new software with special algorithms for on-line process control have been developed exclusively for tube pulling and implemented into production in 1993. Table I shows the impact of these process improvements on tube geometry control.

Tube dimensions are governed by the capability of the manufacturer to ensure parameter control during the pulling process. Because of the

YEAR	STANDARD DEV. (typ.)		
	OUTER DIA. (mm)	WALL THICKNESS (mm)	CROSS SECTIONAL AREA (mm)
1983	0.60	0.18	12.8
1991	0.28	0.11	6.9
1992	0.13	0.07	1.2

Table I - Improvements of substrate tube geometry. Typical standard deviation values of production are given for different periods of process control development.

multitude of diameter and wall thickness combinations tube dimensions are preferably described by the cross sectional area (CSA) given in units of mm^2 . Table II shows the development of CSA values for synthetic silica tubing in the past and near future. Future tube sizes are already pulled on a small R&D and pilot production volume basis and can be scaled to full production quantities when required.

YEAR	CSA Value (mm^2)
1991	700
1992	940
1993	1650
1994	2120
1995	3140

Table II - Development of CSA values for synthetic silica tubing in the past and near future.

4.0 IMPLEMENTATION AND RESULTS

The potential of the synthetic silica tubing has been realized under production conditions for the major fiber designs of depressed clad single mode, matched clad single mode, and dispersion shifted single mode. Concurrent with the development of synthetic silica tubing, the MCVD process was adapted to allow for its application. The result has been large preform sizes, high productivity, and excellent fiber quality.

As discussed in Section 2.0, the application of synthetic silica tubing to MCVD is conceptually very

straightforward. Approximately the same amount of deposit is required inside the tube, and an overclad step is necessary to realize larger preform diameters. One key difference in the deposit, however, is that the core is 1.5-2.5 times larger. Thus a greater percentage of the deposit is core material and a lesser percentage is deposited cladding. A key difference in the overclad operation is that the overclad tube is larger, with a wall thickness of 11-15 mm vs 3-4 mm for a natural quartz process.

Although the equipment and process modifications for these differences are critical, they are not necessarily overwhelming. The same basic MCVD and overclad equipment that was used for a natural quartz tubing process is now manufacturing synthetic preforms that are 3-6 times larger. Considerations must be made with regard to the tubing viscosity which, as described earlier, is lower for synthetic silica tubing.

Synthetic MCVD preforms are now a part of routine production at AT&T for the primary single mode designs of depressed clad, matched clad, and dispersion shifted. Large preform sizes of 200-400 km are in development. The increased preform size is realized without significant changes to the MCVD cycle time, thus providing a 2-3 X improvement in productivity.

This productivity is realized with a fiber quality that is equivalent or better than the natural quartz MCVD process. For the depressed clad design, median losses at 1310 nm are 0.331 db/km, with median 1385 nm losses (representative of the OH peak) less than 0.45 db/km. The median 1550 nm losses are 0.195 db/km. Geometry is also very good, with median eccentricities of 0.25 μ m and median clad noncircularities of 0.35 %. All parameters show very tight distributions that result in high yields.

The following figures fully describe the production performance of the synthetic process for the single mode designs of depressed clad, matched clad, and dispersion shifted. The

data bases for all except matched clad are taken as 500 preform samples from standard production. The matched clad data base was much smaller, and therefore all production from a specified period is represented.

4.1 Depressed Clad

Histograms that detail the loss performance described above for depressed clad single mode fiber are shown in Fig. 4.1. Control of the OH in the starting tubes, described earlier in Section 3.0, is a key factor in the tight distribution of loss at the system operating wavelength of 1310 nm. Median 1385 nm and 1550 nm attenuation values of 0.426 and 0.195 db/km are also noted in Table III.

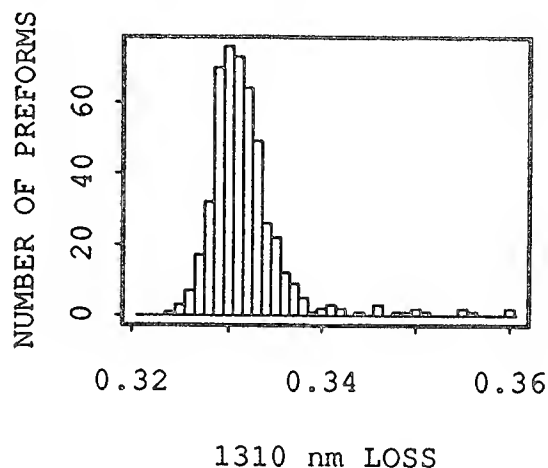


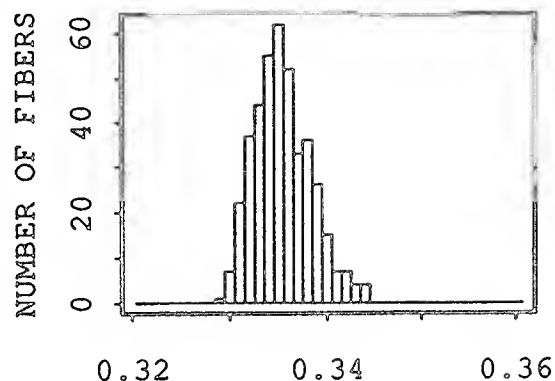
Fig. 4.1 - A distribution of 1310 nm loss for a depressed fiber design.

Key geometric factors of eccentricity and clad noncircularity are important in obtaining good fusion splicing, particularly for mass splicing applications. The distributions obtained with the synthetic tubes in a production environment allow a high yield to the specifications of 0.8 μ m for eccentricity and 1% for clad noncircularity. Table III lists the median values for these parameters.

4.2 Matched Clad

The flexibility of MCVD allows the manufacture of synthetic matched clad fiber in a fashion similar to that

used for the depressed clad fiber. Loss histograms in Fig. 4.2 illustrate the same excellent attenuation distributions at 1310 nm. The same argument for geometry control is true for matched clad, and production data for this fiber design is also well within the same specification limits. See Table II for median values of 1550 nm attenuation, eccentricity, and clad noncircularity.



1310 nm LOSS

Fig. 4.2 - A distribution of 1310 nm loss for a matched clad design.

4.3 Dispersion Shifted

The applications for dispersion shifted fiber are at the 1550 nm wavelength, and the histogram in Fig. 4.3 shows a median loss of 0.201 db/km. Eccentricity and clad non-circularity have the same excellent distribution as was described for depressed and matched clad. Median values for the production sample are noted in Table II.

4.4 Strength

The high purity of synthetic materials also results in striking improvements in the break frequency of fiber. All fiber is prooftested to 100 Kpsi before being shipped or placed in cable. With natural quartz there are always residual inclusions that find their way into the tubing, in spite of the stringent methods used to find the best material.

On the other hand, by the nature of its manufacturing process the

synthetic material has effectively no inclusions that can cause proof test breaks. A comparison of production break rates in the second half of 1993 attributed to only the natural

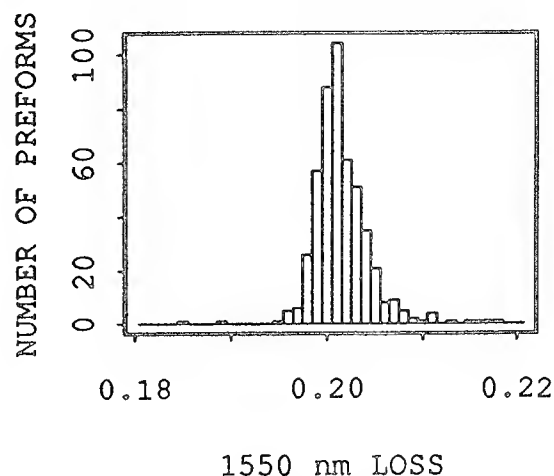


Fig. 4.3 - A distribution of 1550 nm loss for a dispersion shifted design.

MEDIAN PRODUCTION VALUES			
	DEPRESSED CLAD	MATCHED CLAD	DISPERSION SHIFTED
1385 nm LOSS (db/km)	0.426	0.430	0.464
1550 nm LOSS (db/km)	0.195	0.193	0.201
ECCENTRICITY (um)	0.21	0.30	0.22
CLAD NON-CIRCULARITY (%)	0.35	0.30	0.29

Table III - Median production values for key fiber quality parameters.

and synthetic material defects is shown in Fig. 4.4. Whereas the natural material exhibited 10-20 breaks/1000 km, the synthetic material is much less than 1 break/1000 km. This also allows much higher proof test levels of 200 Kpsi or above to be applied for ocean fiber or other high strength applications.

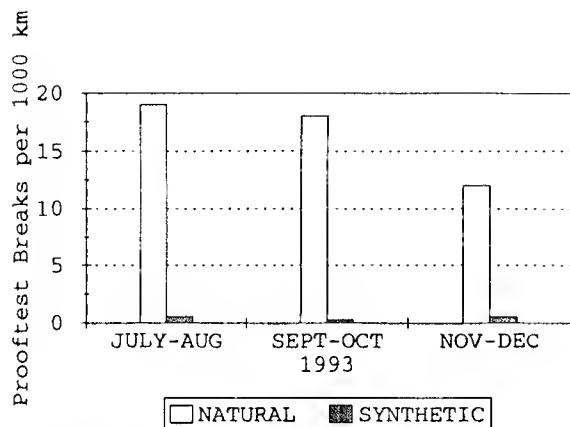


Fig. 4.4 - A comparison of fiber break rates for natural and synthetic materials.

5.0 OUTLOOK

As described, preforms using synthetic silica tubing have been fabricated in a production environment for depressed clad, matched clad, and dispersion shifted fiber designs.

There is potential for larger preform sizes. As synthetic silica tubing quality improves and techniques to add more deposit in the MCVD process are refined, it is anticipated that preforms on the order of 200-400 km presently in development will be transferred to production. Referring to Fig. 2.1, it is only a matter of reducing the core/clad ratio and using more tubing material. Of course, the tubing quality and purity becomes a larger factor.

In summary, the development and application of production methods for undoped and doped synthetic silica tubing and the corresponding development and application of these tubes to the MCVD process has opened a new array of options for fiber manufacture using MCVD. All the conventional single mode fiber designs can be fabricated at higher productivity. In the future with further refinements in tube manufacture and MCVD processing, even more advantages are expected to be gained.

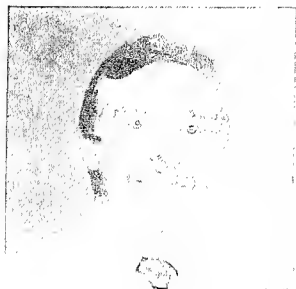
REFERENCES

1. J.B. MacChesney, P.B. O'Connor, and H.M. Presley, "A new technique for the preparation of low-loss and graded-index optical fibers," *Proc. IEEE*, vol. 62, p. 1280 (1974).
2. S.R. Nagel, J.B. MacChesney, K.L. Walker, "Modified Chemical Vapor Deposition", *Optical Fiber Communications, Vol 1*, (New York: Academic Press, 1985), p. 1.
3. S.R. Nagel, J.B. MacChesney, K.L. Walker, "An Overview of the Modified Chemical Vapor Deposition Process and Performance", *IEEE J. Quan. Elec.*, vol. QE18, p. 459 (1982).
4. P. Geittner, H.J. Hagemann, H. Lydtin, and J. Warnier, "Hybrid technology for large SM fiber preforms", *J. Lightwave Tech.*, vol 6, p. 1451 (1988).
5. A.H. van Bergen, and A.H.E. Breuls, "Large, all synthetic PCVD preform manufacturing", *EFOC92 Proc.*, p. 220 (1992).
6. W. Weiss, "A rapid torsion method for measuring the viscosity of silica glasses up to 2200 °C", *J. Am. Ceram. Soc.*, vol 67, p. 213 (1984).
7. U.C. Paek, C.M. Schroeder, C.R. Kurkjian, "Determination of the viscosity of high silica glasses during fiber drawing", *Glass Technol.*, vol 29, p. 263 (1988).



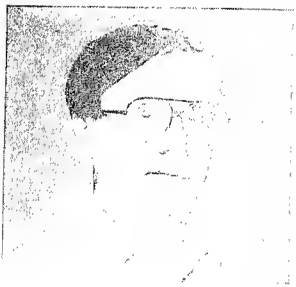
Paul Glodis received the B.Sc. degree in physics from Polytechnic Institute, Worcester, MA. in 1966 and the Ph.D. degree in physics from Yale University, New Haven, CT. in 1972. From 1972 to 1980 he worked in the Medium Energy Particle

Physics Group in the Physics Department of the University of California, Los Angeles. In 1980 he joined AT&T Bell Laboratories, Norcross, GA., as a Member of the Technical Staff and since then has worked in the areas of single-mode fiber design and manufacture. Dr. Glodis is a member of the American Physical Society.



Charles Gridley is a Product Development Engineer with the AT&T Network Cable System's Lightguide Engineering Staff. He holds a Bachelor of Chemical Engineering degree from the Georgia Institute of Technology. Since joining AT&T in 1986,

Mr. Gridley has worked on various preform fabrication projects utilizing synthetic tubing.



William Flegal is currently Optical Fiber Product Manager for AT&T Network Cable Systems. He joined AT&T in 1970 as a Senior Development Engineer and has had responsibilities for development in both plastic insulating and optical preform

processing. He received the Doctor of Philosophy degree from the Georgia Institute of Technology and is a Professional Engineer. He is a previous contributor to IWCS.



Alan Klein received his B. S. Degree in Mechanical Engineering from Rensselaer Polytechnic Institute in 1972 and his M. S. Degree in Mechanical Engineering from Georgia Institute of Technology in 1989. His 14 years of

experience in the fiber and preform process development has led to development of various multimode and single mode fiber designs, most notably the

development of dispersion shifted fiber for optical amplifiers. He is currently a Member of Technical Staff with AT&T in Atlanta, Georgia.



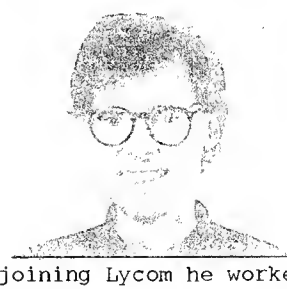
Donald Jablonowski is a Technical Manager with AT&T Network Cable Systems. He received the PhD degree in Electrical Engineering from Carnegie-Mellon University in 1973. That same year, he joined AT&T's Western Electric

Engineering Research Center in Princeton, N.J. In 1978, he moved to the Atlanta Works where he has had responsibility for the development and implementation of fiber manufacturing processes.



David Kalish is Optical Fiber Development and Engineering Director, AT&T Network Cable Systems. He joined AT&T Bell Laboratories in 1971 and, in various assignments, has been involved with fiber design, physical characterization of

fibers, development of fiber facturing processes and fiber systems engineering. He has S.B., S.M. and Sc.D degrees from M.I.T.



Atle Sorby was born in Norway in 1959. He is a graduate of the Technical University of Norway in Physics and Electronics (1983). He joined Lycom in Denmark in 1988. His current responsibilities include MC-SM fiber designs. Prior to

joining Lycom he worked for Alcatel Cable Norway as a research engineer on fiber characterization and cable designs.



Hans Damsgaard was born in Denmark in 1956. He is a graduate of the University of Aarhus in Physics (1981). In 1984 he received a Ph.D. degree from the Technical University of Denmark and NKT. From 1981 to 1987 he worked on optical fiber development at NKT in Denmark. In 1987 he joined Lycom and is now Manager of Development and Engineering.



Heinz Fabian is Manager of Product Development of waveguide tubes at Heraeus Quarzglas. He joined the company in 1988 after receiving his diploma degree in physics from the University of Munster. From 1988 to 1993 he led R&D projects concerning material research and development for new silica materials. In 1993 he assumed his present responsibility for product development.



Gudmund Knudsen was born in Denmark in 1957. He is a graduate of the Technical University of Denmark in Electrical Engineering (1980) and Solid State Physics (Ph.D., 1983). In 1983 he began working in the optical fibers Development and

Engineering department of NKT. In 1987 he moved to Lycom where he is now Vice-President, Engineering and Manufacturing.



Peter Schultz, is President of Heraeus Amersil, Inc.. Following graduation from Rutgers University (BS 1964, PhD 1967), Dr. Schultz was part of the original Corning research team which fabricated the world's

first practical glass optical fiber for communications in 1970. He has written over 20 research papers, holds 25 patents, and is expert in fused silica glasses. Until 1984 Dr. Schultz managed glass materials research at Corning Glass Works. Prior to joining Heraeus Amersil in 1987, Dr. Schultz attended MIT Sloan Business School and was Vice President of Engineering for Spectran Corporation and Galileo Optics, Inc., both located in Massachusetts.



Hartwig Schaper received the Ph.D. in Inorganic Chemistry from the University of Erlangen (Germany). From 1985 to 1990 he was Head of Development for Philips Optical Fibre in Eindhoven, The Netherlands. In 1990 he joined Heraeus

Quarzglas to work in the area of synthetic tubing. He presently is Vice President of their Fiber Optic Product Division.



Norbert Treber graduated from the Fachhochschule in Frankfurt, Germany with an engineer degree (Dipl. Ing) in 1969.

Since January 1974 he has been with Heraeus Quarzglas, initially as Head of Fiber Optic Products

Development and later in various sales and marketing positions. In 1987 he was appointed to his present position as Vice President and General Manager of the Fiber Optic Product Division.

Sonic Tension Control At High Draw Speed

Mauri Luukkala, University of Helsinki
Heikki Räikkönen, University of Helsinki
Jouko Kurki and Lena Stormbom, Nokia Cables
Jukka Kohtala, Nokia-Maillefer

Abstract

A new instrument to measure the drawtension of bare optical fiber is described. The instrument is using acousticstring waves. From the measured string wave velocity the tension can be calculated from basic physics rules.

Background

While optical fiber is being drawn from the heated preform in the drawing tower the physical properties of the fiber are mainly determined by the draw tension. The draw tension, on the other hand, is quite difficult to measure on-line without contact as the fiber is usually hot, fragile and quite sensitive to mechanical contact. The tension can be measured by a set of mechanical pulley-type wheels which touch the fibers but which can easily break the fiber at production speeds. However, these mechanical contact wheels are currently used as a standard device to measure the initial tension when the draw process is being set-up in the beginning of the draw process when the speed is low. The tension at higher production speeds is then theoretically estimated. The tension can also be estimated from mechanical loaded pulleys after the polymer coating unit, but even here the estimation of the real tension of the bare, uncoated fiber is inaccurate as the shear forces of the coating polymer and unknown and can vary due to changes in viscosity of the coating material. Thus, there is a need to measure the draw tension of bare optical fiber on-line, without mechanical contact, continuously.

If the draw tension is known on-line, the fiber drawing process becomes much better under control, the set-up time is shortened, the fiber quality becomes more uniform and possible

troubleshooting becomes easier. The importance of these things grow further as the draw speeds are increasing more and more. Furthermore, if the draw tension is known continuously, the tension value can be used to control the furnace and draw speed as a part of a feedback loop. However, even an 'off-line' tension readout would be most valuable.

We have built a novel instrument that is measuring the draw tension on-line using string wave packets that travel along the fiber. By measuring the velocity of the string wave packets the tension can be calculated provided the linear density of the fiber is known. The new instrument has been so successful that it has been commercialized.

There has been reports of other tension measurement units that are using standing wave resonances of the fiber between the heated preform and the polymer coating unit (1). However, we feel that standing-wave dependent instruments may be excessively sensitive to various parameters in industrial surroundings. Our instrument is using traveling string wave packets avoiding any reflections making the unit insensitive and robust against industrial environment.

Instrument

The measurement principle is using string wave packets that are launched along the fiber. From basic physics we know that the velocity of the string waves is $v = \sqrt{T/m}$, where m is the linear density of the fiber and T the tension. For thin fibers this simple equation holds very well. In our case we launch string wave packets along the fiber with a loudspeaker box that has a slit in front in order to create a periodic displacement along the fiber. The displacement propagates as a string wave burst in the two opposite directions

along the fiber. (See Fig. 1)

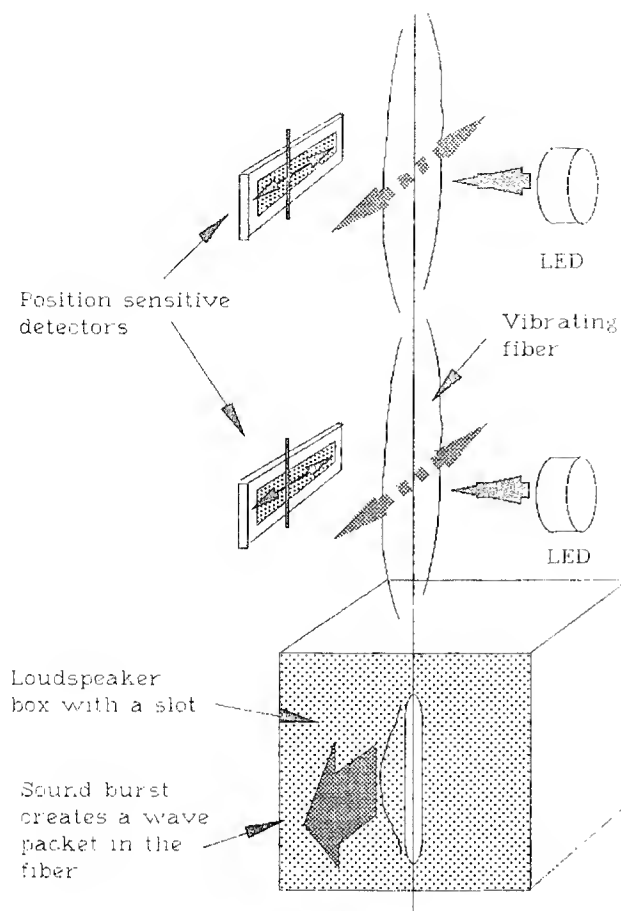


Fig 1. The measurement principle

The propagation time or velocity of the wave is then measured by two optical measurement stations or sensors at known separation along the fiber and then the measured time-of-flight of the wave burst is fed into a PC which then calculates the speed of the string wave, the tension and also displays the tension value both numerically and graphically on the PC screen. The drawing speed of the fiber is causing an error in the string wave velocity, however. This speed is causing a shift in the velocity of the string wave but it can be compensated in the computer by adding (or subtracting) the speed of the fiber to the measured string wave speed. This compensation can be done either manually or automatically. As we are using propagating string wave bursts, the total fiber length, tower height or other stranding wave sensitive features do not affect our

measurement principle. Moreover, speed compensation is difficult to implement in a standing wave system.

The optical time-of-flight measurement is done at right angles against the linear fiber displacement. To improve accuracy we launch linearly polarized string waves by using a suitably orientated acoustic excitation from the loudspeaker which emits a 300 Hertz burst.

In laboratory, stand-still conditions the accuracy of the instrument has been better than 1 percent with the resolution the same or better provided the linear density of the fiber is known accurately enough. These calibration measurements have been carried out by suspending a known weight from the laboratory holder. Note that when the loudspeaker makes a displacement on the fiber, the restoring force is not elastic but rather the tension. Thus, in principle, the fiber material does not affect the measurement. This implies that the fiber displacement is much smaller than the wavelength of the string wave. In our case this requirement is satisfied as the used displacement is of the order of the fiber diameter and wavelength of the order of 50 cm. In practice we have observed differences in displacements between fibers of different make indicating the role of the bending stiffness of the fiber. The practical, on-line measurement range has turned out to be from about 20 grams up to about 130 grams (0.2-1.3 Newtons). At low tension the fiber tends to sway or swing too much in front of the measurement aperture for the measurement to be reliable; at high values of the tension the fiber displacement is too small to give a good reading. As mentioned above, the speed shift created by the fiber itself can be compensated simply by inputting the draw speed value into the computer by the keyboard. In this way measurements up to 600 m/min has been carried out. The practical, operational accuracy has turned out to be about 3-4 percent of the maximum tension value (about 10 grams of tension). Somewhat unexpectedly the tension appears to become rather noisy at high draw tension.

The measured values can be stored in the computer for later reference or retrieval. In such a way the 'history' of each fiber lot can be stored for later study. The PC also has a digital, 8-bit parallel output for possible control or feedback

purposes. However, in practice it has turned out that the real-time graphical tension display is most valuable for the operator of the draw tower.

Measurement Results

The instrument is being operated by several commercial drawing towers with good results. For the moment it is being used as an off-line graphic display mode device. No feedback control installations have yet been built. This will be a subject for further studies.

The mechanical mounting or installation is straightforward, only the optical alignment needs some care as the fiber has to run within 1 mm of the optical window.

The vertical height of the device is about 75 cm and the optical measurement span is only 50 cm. This short optical measurement span means that temperature gradients along the fiber have minimal effects.

Extensive industrial testing (2) has shown that the measurement principle has no measurable effect upon the fiber quality like attenuation, core diameter, concentricity, etc. There was some scatter in the concentricity values from 0.25 micrometers to 0.38 micrometers but this is well within the allowed tolerance of 0.8.

As mentioned, the instrument is routinely used in production (2,3) at speeds up to 600 m/min and draw tensions of up to 140 grams. The use of the instrument shortens the set-up time after preform change and guarantees uniform and repeatable draw conditions, etc.

The tension data can be stored in the PC and it can be transformed into Excel or QuattroPro format for later use. In addition the computer has a useful running average mode which allows the tension to be smoothed with a selectable number of counts.

Another useful property of the instrument is that according to the measurement principle no calibration is needed after the first initial calibration. The measurement principle is based upon time difference measurement which may be regarded as inherently accurate or absolute. The only input parameter needed is the linear density of the fiber (and draw speed) which is known anyway.

Figure 2 displays a tension measurement run done at Nokia Cables/Fiber Optics draw facility at speed of 600 m/min.

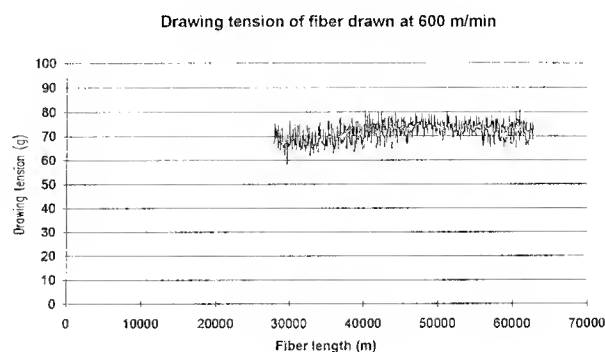


Fig 2. Tension variation recorded at 1 s intervals at 600 m/min draw speed, (Nokia Cables/Fiber Optics). The tension measurement did not affect the attenuations which were 0.328/0.196 dB/km at 1.31/1.55 μ m wavelengths.

Further Considerations

Even though the measurement principle can be regarded as inherently accurate, several external factors have to be taken into account as follows:

- Vibration. The loudspeaker excites the fiber into transverse vibration which at first sight might affect the fiber properties in an undesired way. As mentioned earlier, even though the vibration amplitude is about 1 - 2 fiber diameters, no effect has been detected in attenuation by OTDR measurements at both 1310 and 1550 nm (2). Some towers seem to have a natural mode of vibration which may harm the fiber and also the measurement accuracy. Also low tension sway or wobble may make the operation of the instrument impossible.

- Diameter or density variations. If the diameter of the fiber varies then also the linear density of the fiber varies creating a corresponding error in the readout. However, the diameter or density of the fiber is kept constant with a high degree of accuracy.

- Torsional effects. The torsion of the fiber may cause additional tension increase. Torsion is usually 'invisible' but it becomes visible by our instrument.
- Tension noise. It has turned out that tension is rather noisy (3), particularly at high tension values. This may be an indication that the furnace control may be somewhat slow.
- Misalignment of the measuring head. The optical measurement arm or head has to be aligned vertical and parallel to the fiber so that the fiber stays within the optical measurement window. After preform change and subsequent set-up the instrument may need re-alignment.
- Speed compensation. As has been described before, our instrument has speed compensation facility in the PC. As the velocity of the string wave is in the range of 150 m/s, a draw speed of 2 - 3 m/s represents an error of only about 1 - 2%. The speed compensation becomes important only when the draw speeds reach values of 500 - 600

m/min as the error caused by the draw speed is in the range of 10%. However, high speed drawing is no particular difficulty for our instrument due to the speed compensation property. Also fiber acceleration has minimal effect as the measurement period is 1 second.

- Temperature gradients. Electro-optical tension measurement systems are very sensitive to temperature gradients. On the other hand, our instrument is practically insensitive to temperature effects.

References

1. US pat No 5,079,433 C.G.Askins, M.A.Putnam and E.J.Friebele, J. Lightwave Techn., vol 9, No8 p.945-947 (1991)
2. Ericsson Cables, Hudiksvall, Sweden, private communication
3. Nokia Cables/Fiber Optics, Vantaa, Finland

Authors



Prof. Mauri Luukkala,
Dept. of Physics,
University of Helsinki,
POB 9, FIN-00014
Univ. of Helsinki,
Finland.

Mauri Luukkala works as a professor at the Physics Department, University of Helsinki. He specializes in various sensors and industrial instrumentation using ultrasound and optics. He also works for Soundek Oy, a company that makes ultrasonic instrumentation.



Heikki Räikkönen
Dept. of Physics,
University of Helsinki,
POB 9, FIN-00014
Univ. of Helsinki,
Finland.

Heikki Räikkönen works as a research assistant at the Physics Department, University of Helsinki. He also works as a technology assistant in Soundek Oy.



Jouko Kurki
POB 77,
Nokia Cables/Fiber Optics,
FIN-01511 Vantaa,
Finland

Jouko Kurki has received the Dipl.Eng. and Dr. of Techn. degrees in Electrical Engineering from Helsinki University of Technology in 1977 and 1983, respectively. His work has included development of optical fiber manufacturing processes, machinery and

fiber measurements in the Technical Research Centre of Finland, Nokia-Maillefer Ltd. and Nokia Cables Fiber Optics since 1977. He is currently responsible for fiber R&D at Nokia Cables Fiber Optics.



Lena Stormbom
Nokia Cables/Fiber Optics,
POB 77,
FIN-01511 Vantaa,
Finland

Lena Stormbom received the Dipl.Eng. degree in Physics in 1986 from the Helsinki University of Technology. Before joining the product development group for Fiber Optics at Nokia Cables in 1987 focusing on the fiber drawing area, she worked at Nokia Cable Machinery at the Fiber Optic Center.



Jukka Kohtala
Nokia-Maillefer
1856 Corporate Drive
Norcross, GA
USA

Jukka Kohtala received the Msc degree in Physics from Turku University, Finland in 1983. After working two years with Nokia Cables as a research engineer he joined Nokia Maillefer in 1990. He is currently responsible for Nokia-Maillefer fiber optics operations in America.

DAMAGE DEVELOPMENT IN SMALL-DIAMETER, PULTRUDED, GRP ROD USED IN OPTICAL FIBRE CABLES

S N Kukureka and R Leetham

The University of Birmingham, School of Metallurgy and Materials,
Edgbaston, Birmingham B15 2TT, UK

Abstract

This paper is a study of the mechanical reliability of GRP strength members used for optical fibre cables. In particular it considers damage development in pultruded GRP rod subject to severe bending stresses. The extreme anisotropy, high volume fraction of fibres and small diameter of the rod make conventional test techniques difficult. The acoustic resonance method is a non-destructive technique allowing measurements of Young's modulus deterioration and changes in internal friction. Its application to small-diameter rod is considered and some results presented. Internal friction, characterised by Q^{-1} , appears to be more sensitive to the onset of damage than Young's modulus changes alone. This damage appears to be fibre debonding leading to final failure by longitudinal splitting over the whole length of the rod. Further work is under way to quantify strength member reliability in terms of these failure modes.

Background

Optical fibres need to be protected if they are to be installed, used and maintained effectively in telecommunications. The fibres themselves are given primary coatings to protect them from abrasion and damage. They are subsequently buffered with further layers to protect from the mechanical and chemical environment and to prevent microbending which results in unacceptable attenuation. The protected fibres are then incorporated into cables to allow installation and use. A typical optical-fibre cable construction is shown in Fig 1.

The functions of the cable can be summarised under four main headings [1]: fibre protection; stability of fibre transmission characteristics; cable strength; identification and jointing. The third function - cable strength - usually requires the addition of a cable strength member as well as a thick outer sheath. Optical cables must have similar mechanical properties to electrical transmission cables to allow installation by similar techniques. These mechanical properties include resistance to tension, torsion, compression, bending, squeezing and vibration [1]. The cable strength member is essential in providing such properties.

Furthermore, there are many circumstances in which strength members are required not to conduct electricity and so must be made of dielectric materials such as polymer composite materials. This is often because of the proximity of large electric fields as, for instance, in communications cables installed along the power transmission network, or in many military applications. Composite strength members have found many applications in cables and their light weight and ease of manufacture makes them a viable alternative to steel in many cases. Composite strength members can also provide neutral buoyancy which is often a requirement of submarine cables in naval use.

If the whole optical fibre cable is to have a substantial guaranteed lifetime then the composite strength member must have the appropriate reliability. This paper is a contribution to the study of reliability in cable strength members made from glass reinforced plastics (GRP). It will focus on alternative methods of monitoring damage development in strength members under severe mechanical conditions and hence contribute to the understanding of cable reliability.

GRP Strength Members

GRP strength members are based on glass-reinforced thermoset matrices. The matrix material is usually an epoxy or a vinyl ester resin. The fibres are continuous and unidirectional and are impregnated with resin by the pultrusion method. This is illustrated schematically in Fig 2. A continuous strand roving is drawn through a resin bath and the impregnated strand is then drawn through a heated die where curing and shaping take place simultaneously. Although fibre reinforcements which are possible with pultrusion include glass, aramid and carbon, in practice 90 % of pultruded products are made with unsaturated polyesters reinforced with glass [2]. Pultrusion is currently one of the only major manufacturing processes for composites which is continuous. High stresses are generated by compaction at the die entrance, by viscous forces during gelation and from friction of the cured profile. These limit line speeds during manufacture to be much less than those of conventional thermoplastics extrusion. Nevertheless line speeds of up to 0.05 m/s can be achieved and small diameter rod for strength members can be made continuously in lengths of up to several kilometres.

Large volume fractions of 60 or 70 % glass are necessary to provide the high stiffnesses and strengths required. Fibre reinforcement which is continuous and unidirectional with such high volume fractions is relatively unusual for GRP. More often GRP is used in laminate or filament-wound form. Other pultruded products are typically used in larger sections or with less critical applied stresses. In this application not only are high stresses and possibly aggressive chemical environments applied during installation, but also whilst in service the strength member may be subjected to a continuous tensile stress.

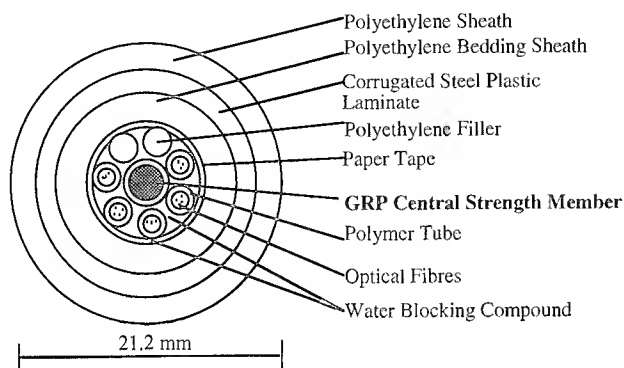


Figure 1 Typical optical fibre cable cross-section. (Courtesy of BNR Europe Ltd.)

Damage development and assessment in GRP strength members

Cable lifetimes are often specified as 25 years or more [3] and so a knowledge of the reliability of the strength member is vital for cable design. A sufficient body of information does not yet exist on the long-term mechanical reliability of GRP strength members. In order to provide data on cable reliability we need to study the response of the GRP strength members to damage. This can take many forms. Examples include fibre failure, resin cracking, interfacial debonding and delamination [4 - 9]. Many of these mechanisms co-exist and the high degree of anisotropy exhibited by unidirectional composites makes stress analysis difficult. Damage development is likely to be cumulative and widespread [10]. Its effects are difficult to predict and considerable loads can often be sustained by damaged composites before the effects become catastrophic.

Sectioning and microscopic examination is perhaps the most reliable way of determining the extent of damage. However, a destructive method is clearly not feasible as a method of examining damage over large areas of the composite or of determining damage in a specimen which is required to undergo further loading. Some form of non-destructive testing is required if we are to assess damage development in a realistic manner.

As discussed above, the strength members are of a geometry which is unusual for composite materials. Small diameter cylindrical rod is rather difficult to access by conventional non-destructive test techniques [11]. Surface microscopy, ultrasonic scanning or X-ray inspection are all more easily performed on rectangular or flat specimens - the traditional laminate geometry. Similarly, the alternative static methods involving strain gauges are equally unsuitable.

What is needed is a method of assessing damage in rods typically 3 mm in diameter without further damaging the specimens. One such method is the resonance method which can be used for the measurement of Young's modulus and internal friction. The remainder of this paper is an examination of the application of this method to composite strength members and an evaluation of its usefulness as a test method.

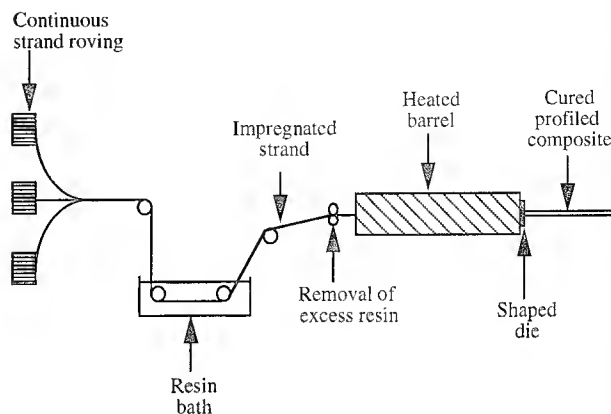


Figure 2 A schematic diagram of the pultrusion process.

The resonance method

The dynamic techniques for studying damage in composites are all based on the propagation of elastic stress waves in solids. These methods may be divided into (i) free vibration methods (ii) forced vibration resonance methods and (iii) attenuation of elastic waves [12]. The first two methods - free vibration and resonance - are based on standing waves caused by the interference of continuous waves reflected from the specimen boundaries. The third method is based on measurements of the attenuation in a pulsed wave.

The free vibration method is usually performed with large amplitude oscillations in torsion or flexure. Although the method is relatively straightforward experimentally it is slow since many oscillations are necessary for accurate measurement. Wave propagation methods suffer from the requirement for complex instrumentation and the difficulties of generating and measuring pulsed waves of a known character [12].

In this work the resonance technique, using forced vibrations was employed. This enabled a variety of parameters to be determined as measures of damage development. The method has the advantage that the apparatus is readily available and that tests can be performed in a relatively short time period. Also the tests do not cause further damage to the specimen and so damage development can be monitored during a mechanical testing regime.

Experimental method

In order to introduce damage into the material, four-point bend tests were carried out [13]. Four steel rollers equally spaced and at right angles to the rod provide loading in bend. The two central ones move downwards (under the force of a cross-head from a mechanical testing machine) as the two outer ones remain fixed. This has the advantage over three-point bend that the position of maximum curvature in the middle of the rod is not under the direct contact of a roller. This is important since these uniaxial composites are extremely anisotropic and lateral crushing must be prevented. For this reason, tensile testing is very difficult to perform [14] since any gripping of the specimen sufficient to transfer axial load is usually greater than the crushing strength. Bend tests also have the advantage that they are more realistic simulation of service conditions. Strength members are unlikely to see short-term tensile loads which are large enough to cause failure whereas high bending stresses can easily be introduced by storage on drums and during installation. The short (100 mm) bend samples are also convenient for direct use in the dynamic vibration apparatus. Since the geometry is similar it is possible to remove samples during a sequence of mechanical tests, monitor them in the vibration apparatus then return them to the mechanical testing machine. In this way the development of damage can be studied.

The resonance apparatus is shown schematically in Fig 3. The specimen (a cylindrical rod) is 100 mm in length. It is freely supported in a horizontal position by two fine cotton threads. An audio oscillator and amplifier provide mechanical vibration which is transmitted through the thread to the specimen. The second thread is used to transmit the signal to the detecting transducer as well as for supporting the specimen. Typical frequencies were around 1.3 kHz.

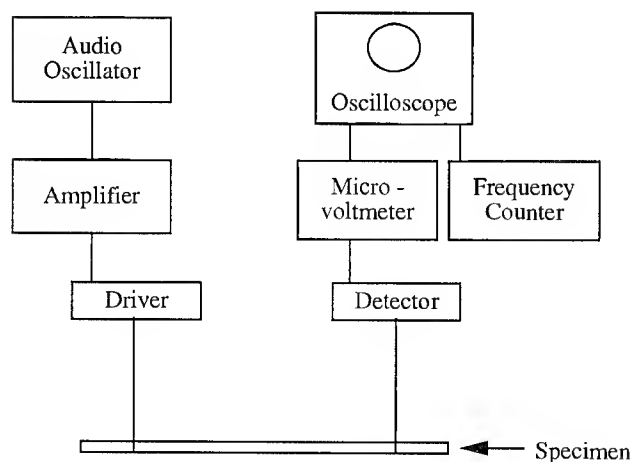


Figure 3 Schematic diagram of the resonance technique equipment.

The specimen is excited over a range of frequencies until the resonant frequency is found. This allows the elastic modulus to be found [15] according to:

$$E = (1.261886 \rho L^4 f^2 T_1) / D^2$$

where E = Young's Modulus

ρ = specimen density

L = length of rod

D = diameter of rod

f = resonant frequency in first fundamental mode

T_1 = correction factor for Poisson's ratio and finite thickness effects.

Previous work [14] has shown the initial behaviour of the material to be linearly elastic before the onset of damage and so the use of Young's Modulus is justified.

The elastic modulus depends only on the resonant frequency - the amplitude of the resonance peak rather than its shape. An alternative technique (analogous to the use of the Q factor in electrical engineering) is to consider the sharpness of the resonance peak and so determine the internal friction. If ΔN is the applied frequency necessary to change the amplitude from half its maximum value N at one side of the resonant frequency to half its maximum value on the other side then $\Delta N / N$ is a measure of the internal friction [12]. For a solid damped specimen the usual assumptions are that the restoring force is proportional to the displacement (Hooke's law) and that the dissipation is proportional to the velocity [12]. It can be shown that Q^{-1} as a measure of internal friction is given by

$$Q^{-1} = 3^{-1/2} (f_u - f_L) / f_r$$

where f_u and f_L are the driven frequencies above and below the resonant frequency f_r [16].

This does not presuppose anything about the mechanisms leading to internal friction and damping. These are likely to include fibre debonding and fibre fracture as well as matrix cracking. In order to characterise damage phenomenologically by these dynamic techniques we introduce a damage variable D defined by $D = 1 - (E / E_0)$ where E_0 is the elastic modulus of the material in the undamaged state and E is the modulus in the damaged state [11]. This parameter varies from zero for an undamaged specimen to a theoretical maximum of one when there is no residual modulus in the specimen. It is possible to define a critical value of the damage variable D_c at which catastrophic failure occurs. For instance Jessen and Plumtree [7] considered failure in their composite specimens to occur when the damage variable D reached 0.2

Results and discussion

A number of tests were performed in bend and the damage development monitored by the resonance technique. Two different regimes of sequential loading were employed. In the first, bend tests were performed by incrementing load and monitoring resonance at regular intervals. In the second, the cross-head displacement was incremented. The results are shown in Figs 4 and 5.

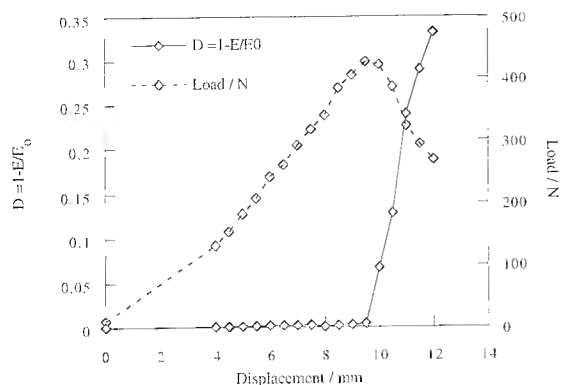


Figure 4 Change in Damage Variable with increasing crosshead displacement in four-point bend.

Fig 4 shows the results of increasing load. In an attempt to compare different measures of damage, the data are plotted as % change in Young's modulus (E) and as % change in internal friction given by Q^{-1} . It can be seen that very little change occurs until a catastrophic increase at a load of about 450 N. However, it is clear that the internal friction measurements are more sensitive in that they indicate damage at a far earlier stage than the change in Young's modulus alone.

The final failures are characterised by debonding and longitudinal splitting along the whole length of the sample [10]. Clearly the interfacial strength of the fibre resin combination is less than the strength of the fibres, and fibre bundles remain largely intact even at failure. This means that the material is still able to support load even at high percentages of the failure load but the internal friction measurements indicate clearly the onset of damage before it becomes catastrophic. This behaviour is in contrast to stress corrosion failure [17] characterised by fibre breakage and lateral cracking in a localised area.

In Fig 5 the alternative measurements based on a step increase in displacement are shown. Here the damage variable D remains virtually zero until rapid failure occurs whereas the load, as expected, peaks at this transition. The damage variable rises rapidly to 0.35 over a 2 mm increase in cross-head displacement.

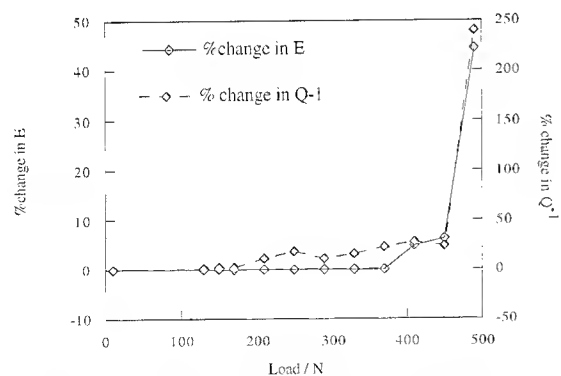


Figure 5 Comparison between percentage change in Internal Friction and Young's Modulus with increasing load.

These results clearly indicate that although final failure does take place in a very short period of time it is not instantaneous. If cable reliability is important then it is necessary to predict failure in strength members. Further work is proceeding to develop models of residual strength and strength member reliability more quantitatively but this work does indicate that resonance techniques provide a method of monitoring damage development in GRP strength members.

Conclusions

1 Resonance measurements provide an accessible method of non-destructive testing in small-diameter pultruded GRP rod.

2 Both Young's modulus changes and internal friction are able to detect the onset of damage.

3 Internal friction appears to be more sensitive in monitoring the initiation of damage and pre-catastrophic deterioration in properties.

4 Final failure in bend tests in the absence of an aggressive environment is more usually by fibre-matrix delamination along the whole length of the sample than by fibre breakage.

Acknowledgement

We would like to thank BNR (Europe) Ltd and Northern Telecom for the supply of samples and for their interest in this work.

References

- [1] J M Senior, *Optical Fiber Communications* (Prentice Hall, London, 2nd ed, 1992)
- [2] A W Birley, B Haworth, J Batchelor, *Physics of Plastics* (Hanser, Munich, 1992)
- [3] P R Bark, D O Lawrence, *Optical Fiber Transmission* ed E Bausch, (Sams, New York, 1986)
- [4] H T Hahn, *Composite Materials: Testing and Design* (5th Conf) ASTM STP 674 ed S W Tsai (1979)
- [5] D Dew-Hughes, J L Way, *Composites*, **4**, 167, (1973)
- [6] P T Curtis, *Journal of Strain Analysis*, **24**, 235, (1989)
- [7] S M Jessen, A Plumtree, *Composites*, **20**, 559, (1989)
- [8] B Harris, *Composites*, **8**, 214, (1977)
- [9] K Reifsnider, *Int Journal of Fracture*, **16**, 563, (1980)
- [10] R Leatham, S N Kukureka, *Advancing with Composites 94*, Vol 2, p277 (Woodhead, Milan, 1994)
- [11] R Leatham, S N Kukureka, *Proc 9th Int Conference on Composite Materials (ICCM-9)*, Vol III, p745 (Woodhead, Madrid, 1993)
- [12] H Kolsky, *Stress Waves in Solids* (Dover, New York, 1963)

- [13] R F Gibson, *Principles of Composite Material Mechanics*, p381 (McGraw-Hill, New York, 1994)
- [14] S N Kukureka, R Leetham, I F Scanlan, D L Walters, *Plastics in Telecommunications VI*, (PRI, London, 1992).
- [15] S Spinner, W E Tefft, *Proc ASTM*, **61**, 1221, (1961)
- [16] C B Ponton, *PhD dissertation*, University of London, (1987)
- [17] R Leetham, S N Kukureka, *Journal de Physique IV*, **3**, 1665, (1993)



Dr S N Kukureka
 The University of Birmingham
 School of Metallurgy and Materials
 Edgbaston
 Birmingham B15 2TT
 UK

Stephen Kukureka gained a BSc from Bristol University followed by a PhD from Cambridge University. After research with IMI plc and at the universities of Leeds and North London he is now a lecturer in Metallurgy and Materials at the University of Birmingham. His current research interests lie in the mechanical properties of polymers and composites. Dr Kukureka is a Chartered Engineer and a Member of the Institute of Materials and of the Institution of Mechanical Engineers.

Rachel Leetham graduated with a BEng in Materials Science and Technology from the University of Birmingham and is an Associate of the Institute of Materials. She is currently a research student undertaking a PhD in the reliability of composite strength members for cables.

Effect of Novel Cleaning Solvents on Optical Fiber Coatings

J.R. Petisce, K.W. Jackson, N.W. Sollenberger, and C.R. Taylor

AT&T Bell Laboratories
Norcross, Georgia 30071

A.J. Muller

AT&T Bell Laboratories
Murray Hill, New Jersey 07974

Abstract

Splicing of optical fibers or optical fiber ribbons contained within a cabled assembly requires the removal of cable filling compounds after retrieval from the cabled assembly so that subsequent mechanical stripping of polymeric coatings can be achieved. Safe handling and environmental concerns associated with conventional organic solvents commonly used to remove filling compounds have prompted the introduction of cleaners containing novel organic compounds into commerce. Compositional analysis of these novel cleaners was obtained through gas chromatography/mass spectroscopy. Sheet swelling data for three primary/secondary optical fiber coating systems after immersion in three commercially available cleaners were obtained. The immersion effects of these cleaners on optical fibers having these coating systems were evaluated by measuring the following coating properties insitu: 1) strip force, 2) coating pullout, 3) primary coating modulus, and 4) delamination resistance.

Introduction

Most optical fiber utilized in telecommunication networks are contained within a cabled assembly. One telephone cable architecture consists of bundles of coated optical fiber distinguished from one another by different color coded yarns.^[1] Several fiber bundles are contained within a central core tube and surrounded by a sheathing system. Another telephone cable architecture consists of a stack of fiber optic ribbons within a central core tube also surrounded by a sheathing system.^[2] Central core tubes of both cable architectures usually contain a jellylike filling compound which inhibits water ingress.^[3]

In splicing applications, filling compound removal from the surface of coated optical fibers or fiber ribbons after retrieval from a cable has commonly been achieved through the use of chlorinated hydrocarbons such as 1,1,1 trichloroethane or methylene chloride. Production and import of 1,1,1 trichloroethane has been banned by the Environmental Protection Agency beginning January 1, 1996 because of its ozone depletion potential.^[4] Safe handling concerns associated with methylene chloride have been reported.^[5] These facts have lead to the commercial introduction of cleaners containing organic compounds which do not have the environmental or safe handling concerns associated with 1,1,1 trichloroethane or methylene chloride. The ability of some organic compounds to adversely interact with optical fiber coatings^[6] prompted our study of the effects of these new cleaners on optical fiber coatings.

Compositional Analysis

Experimental

Gas chromatography-mass spectroscopy was used to identify and quantify the volatile components of three cleaners. Samples of each cleaner were diluted with HPLC grade methylene chloride to a nominal final concentration of 1 mg/ml. All samples were analyzed using a Hewlett-Packard 5890 capillary gas chromatograph interfaced to a 5970B mass selective detector and equipped with a 0.2 mm x 0.33 micron film thickness crosslinked 5% phenyl/95% methyl silicone column (Hewlett-Packard Ultra II). Helium at 0.8 ml/min was used as the carrier gas and the injection volume was 1.0 microliter. The injection port was maintained at 250°C and the detector interface was 280°C. The column temperature was

held at 75°C for 5 minutes, increased to 300°C at 8°C/min., and held at 300°C for 17 minutes. All chromatograms were acquired in the scan mode. The mass spectrometer conditions were as follows: electron impact 70 eV, 1800 eV multiplier voltage, and scans of 45 to 700 amu were acquired at a rate of 0.6 seconds/scan. Compound identifications were made through comparison of their mass spectra with authentic known compounds.

The amount of limonene (the predominant terpene) present in each formulation was determined using external calibration. A series of dilutions of limonene (Aldrich, 97% purity) was prepared in methylene chloride and analyzed under standard conditions. Peak areas were used to construct the calibration curves from which the unknown concentrations were derived.

Results

In all formulations, limonene was identified as the predominant terpene. Trace amounts of related terpenes, most likely impurities in the limonene, were also detected.

Table I
Cleaner Analysis

Cleaner	Limonene	Petroleum Solvents	Alcohols
A	100 wt%	0 wt%	0 wt%
B	34 wt%	0 wt%	66 wt%
C	4 wt%	96 wt%	0 wt%

As shown in Table I, cleaner A has the highest limonene concentration, cleaner C has the lowest limonene concentration, and cleaner B has a limonene concentration intermediate between that of cleaners A and C. Cleaner B contains approximately 66 weight per cent of an alcohol mixture comprised of ethanol, isopropanol, and methanol. Cleaner C contains a mixture of petroleum solvents comprised of linear and branched alkanes having 10 to 20 carbons.

Sheet Swelling

Experimental

Sheets of three primary optical fiber coatings, P1, P2, P3, and three secondary optical fiber coatings, S1, S2, S3, were cured on Pyrex glass using a conveyor unit

equipped with a Fusion Systems D lamp. The conveyor speed was adjusted to provide a UV dose of 0.7 Joules per square centimeter. The lamp height was adjusted to provide a UV intensity of 1.5 watts per square centimeter. UV dose and intensity measurements were made using an International Light IL 390 radiometer equipped with a "Lightbug" sensor. The sheet thicknesses ranged from 0.14 to 0.19 mm.

Test specimens measuring 4.3 mm x 62.5 mm were cut from cured sheets. Two test specimens of each coating were placed in separate Pyrex petri dishes filled with cleaner A, B, or C. After immersion for a specified test period, the specimens were measured while immersed in the cleaner. The volume swell was calculated by measuring changes in test specimen length and assuming isotropic swelling. The temperature and humidity during immersion were maintained at 22°C and 50% RH. Results are reported as an average of the volume swell of the two test specimens.

Results

As shown in Figure 1, primary coatings P1, P2, and P3 swell very differently upon immersion in cleaner A. After only a 5 minute immersion, P2 swells to over 200% its original volume. P1 and P3 both ultimately swell to approximately the same 60% level after 6 hours of immersion, but P1 swells more than P3 at immersion times less than 6 hours.

The effect of primary coating immersion in cleaner B is somewhat different than the effects of immersion in cleaner A (Figure 2). At cleaner B immersion times up to 60 minutes, coating P2 swells more than coatings P3 and P1. After 6 hours or 24 hours of cleaner B immersion, coating P3 swells to the greatest extent. Coatings P1 and P3 swell the same after 1 minute cleaner B immersion, but at all longer immersion times coating P1 swells less than either coating P2 or P3.

Cleaner C swells coatings P1 and P3 to a much lower extent than both cleaners A and B (Figure 3). However, swell data for coating P2 were unavailable after cleaner C immersion for 1, 5, 10, 60, and 360 minutes because the P2 test specimens twisted upon immersion.

In general, secondary coatings S1, S2, and S3 are much less affected by immersion into cleaners A, B,

or C than the primary coatings P1, P2, or P3. For example, no swelling of coatings S1 and S3 could be detected after cleaner A immersion for up to 10 minutes (Figure 4). After 24 hour cleaner A immersion, coating S3 was swollen by only about 5% and coatings S1 and S2 were affected to a smaller extent.

Similarly, all secondary coatings remained relatively unaffected even after 24 hours of cleaner C immersion (Figure 6).

Cleaner B has the greatest effect on the secondary coatings (Figure 5). Coating S2 swells to over 30% of its original volume after 1 hour immersion. Coatings S1 and S3 swell to over 20% of their original volumes after 6 hours immersion. Only coating S3 swells significantly after 10 minutes immersion, yet coatings S1 and S2 are relatively unaffected.

Discussion

From the sheet swelling data, predictions of immersion effects on coated fibers can be made. Immersion of fiber having primary coating P2 into cleaner A would be predicted to have the greatest effect of all primary coatings and cleaners evaluated. Conversely, immersion of fiber having either primary coatings P1, P2, or P3 into cleaner C would be predicted to have the least effect. Immersion of fibers having any of the evaluated primary coatings into cleaner B is predicted to have an intermediate effect.

Immersion of fiber having any of the tested secondary coatings into cleaners A or C is predicted to be unaffected. In contrast, prolonged immersion of fibers having any of the evaluated secondary coatings into cleaner B might be affected.

Effects on Coated Fibers

Experimental

Coils of coated fibers drawn with coating systems P1/S1, P2/S2, and P3/S3 were placed in Pyrex petri dishes and covered with a liquid cleaner for a specified test time. Immersion test times of 1.0 and 5.0 minutes were chosen as representative time periods that the coated fibers could contact the cleaners under actual field use conditions. Fiber ends were placed in the liquid cleaner during immersion

testing. The temperature and humidity during fiber immersion were maintained at 22°C and 50% RH. Fiber ends were examined for delaminations by optical microscopy immediately after removal from the liquid cleaner. The ability to mechanically remove the coating system was determined before and after immersion by measuring the coating strip force.^[7] The primary coating crosslink density was measured before and after immersion using an insitu modulus measurement.^[8] The force required to pull the fiber from the coating system was measured before and after immersion by measuring the pullout force.^[9] Approximately 0.5 meter of fiber was discarded from both fiber ends which were immersed in liquid cleaner before either pullout force, strip force, or insitu modulus measurement.

Results

Delaminations

The coated fibers were examined by optical microscopy immediately after cleaner immersion for the presence of delaminations between the primary optical fiber coating layer and the optical fiber glass surface. No delaminations were detected after either 1.0 or 5.0 minute immersion in cleaners A, B, or C for all coated fibers evaluated.

Coating Strip Force

Coating strip force measurements after cleaner immersion were normalized to the strip force measurement before cleaner immersion for each coating system. Results presented in Figure 7 show that the coating systems P1/S1 and P3/S3 display comparable changes in strip force after immersion in cleaners A, B, and C. Specifically, a small strip force reduction occurs after immersion in cleaner A or C and a larger strip force reduction occurs after immersion in cleaner B. In contrast, coating system P2/S2 displays greater strip force reductions after immersion in any cleaner than the other coating systems, but cleaner B more greatly affects the strip force than it does for the other coating systems.

Primary Coating Insitu Modulus

Insitu modulus measurements after cleaner immersion were normalized to the insitu modulus measurement before cleaner immersion for each coating system (Figure 8). The insitu moduli of fibers having coating

system P1/S1 were increased after immersion in cleaner A, B, or C. After one minute immersion all three cleaners three cleaners had a comparable effect on the P1/S1 insitu modulus; however, after five minute cleaner B immersion the insitu modulus change was somewhat less than for immersion in either cleaner A or B.

The insitu moduli of fibers having coating system P2/S2 were also increased after immersion in cleaner A, B, or C. The insitu modulus changes are comparable for immersion in all cleaners with the exception of the modulus change after one minute cleaner C immersion which caused a slight insitu modulus decrease.

The insitu modulus increase for fibers having coating system P3/S3 is greater after immersion in either cleaner A or C than after cleaner B immersion. A one minute immersion in cleaner B apparently causes a slight reduction in P3/S3 insitu modulus.

Coating Pullout Force

The coating pullout force for fibers having coating system P1/S1 is slightly reduced after a one or five minute cleaner A immersion and slightly increased after cleaner B or C immersion for the same time periods (Figure 9).

One minute cleaner A immersion slightly reduces the pullout force for fibers having coating system P2/S2, but a five minute immersion reduces the pullout force to a greater extent. One minute cleaner B immersion slightly increases the P2/S2 coated fiber pullout force, whereas a five minute cleaner B immersion causes a large pullout force reduction. Comparable pullout force increase occurs after either a one or five minute cleaner C immersion of P2/S2 coated fibers.

Slight changes in P3/S3 pullout force occurs after either a one or five minute immersion in cleaners A or C. A one minute cleaner B immersion causes a significant increase in P3/S3 pullout force, whereas a five minute cleaner B immersion results in a pullout force reduction.

Conclusions

The inability of cleaner A, B, or C immersion 1) to induce delamination formation or 2) increase coating strip force for all coated fibers evaluated provides

reasonable confidence that these cleaners can be safely used without adversely affecting coating performance or handling characteristics of fibers having these coating systems. Although decreases in strip force and pullout force of P2/S2 coated fibers after cleaner B immersion indicate that the primary coating/glass optical fiber interface has been altered, sufficient primary coating glass adhesion persists as evidenced by the absence of coating delaminations after short immersion times. Since cleaner A is comprised of 100% limonene, short contact times with this novel cleaning solvent can be tolerated without adverse effects on optical fiber having the urethane acrylate coating systems evaluated.

Close examination of the sheet swelling data reveals its limited utility as a predictor of cleaner compatibility with coated optical fiber. Predictions of cleaner compatibility can be obtained by comparison of coating sheet swelling data shown in Figures 1 through 6. The greatest primary coating sheet swelling occurs when P2 is immersed in cleaner A. After a five minute cleaner A immersion, P2 swells approximately 200%. By assigning an arbitrary value of 10 as a relative standard to this 200% swelling, the swelling of all other primary coatings after a five minute immersion can be numerically ranked. Since the swelling of all secondary coatings after a five minute immersion in either cleaner A, B, or C is very small, it is assumed that all secondary coatings contribute little to the use of sheet swelling data as a predictor of on-fiber cleaner compatibility. A possible reason for the absence of any correlation between sheet swelling data and on-fiber coating data is that the secondary coatings may serve as a barrier to the evaluated cleaners. It is possible that the secondary coatings may serve as a barrier to the evaluated cleaners. The predictions of cleaner compatibility with optical fibers having specific coating systems based on five minute immersion sheet swelling data are presented in Table II.

Table II
Compatibility Predictions

Coating System	Cleaner A	Cleaner B	Cleaner C
P1/S1	2	2	1
P2/S2	10	3	N/A
P3/S3	1	2	1

N/A = data not available.

A value of 10 connotes a large predicted effect of a specific cleaner on a coating system, whereas a value of 1 connotes little predicted effect.

Since all fibers having either of the three coating systems evaluated did not delaminate after up to five minute immersion in cleaner A, B, or C, the coating sheet swell data is not a good predictor of the ability of a cleaner to induce delaminations on coated fiber. No correlation exists between the predictions listed in Table II and the strip force data presented in Figure 7. Finally, no correlations exist between the predictions listed in Table II and the insitu moduli or pullout data presented in Figures 8 and 9, respectively.

Acknowledgements

The authors thank Daniel Harper, Brian Dritschler, and Claire Plaganis for coating sheet swell data and in-situ coating measurements. The authors also thank Melissa Kuck for analytical data. The assistance of Patricia Zang of the AT&T Bell Laboratories-Norcross, Georgia technical library and Mark Gaeth of the AT&T Atlanta Works Environmental Health and Safety Department in obtaining references for this paper is appreciated.

References

1. Patel, P.D. and Gartside, C.H., III, "Compact Lightguide Cable Design", 34th IWCS, 1985, 21-27.
2. Gagen, P.F. and Santana, M.R., "Design and Performance of a Crossply Lightguide Cable Sheath", 28th IWCS 1979, 391-395.
3. a) Bury, J.R. and Joiner, D.A., "Versatile High Performance Filling Compounds for Telecoms Cable Applications", 34th IWCS, 1985, 38-43 . b) Hattori, T., et. al., "Optimal Design of Jelly Compound for Optical Cable", 37th IWCS 1988, 12-15 . c) Hsiao, J.M., et. al., "Effects of Waterproofing Compounds on the Long Term Reliability of Polymeric Coated Optical Fibers", 41st IWCS, 1992, 435-441.
4. Nudo, L., "Heirs to the Throne", Pollution Engineering, 1993, 54-58.
5. Wedin, R.E., "How New Solvents Washed Away Bad Press", Today's Chemist At Work, 1993, 10-14.
6. a) Chandan , H.C., et. al., "Fiber Protective Coating Design for Evolving Telecommunication Applications", 41st IWCS, 1992, 239-48. b) Gebizlioglu, O. and Plitz, I.M., "Self Stripping of Optical Fiber Coatings in Hydrocarbon Liquids and Cable Filling Compounds", Optical Engineering, 1991, 749-62.
7. Electronics Industry Association (EIA) Fiber Optic Test Procedure (FOTP) 178.
8. J.W. Shea, et. al., "Characterization of Critical Properties of Optical Fiber Coatings", Material Research Society, 1991, 85-90.
9. EIA FOTP 106.

Biography



James R. Petisce is a Member of Technical Staff in the Materials Engineering Department at AT&T Bell Laboratories in Norcross, Georgia. After receiving a BA/MA in Chemistry from Boston University in 1980, he received a Ph.D. in Organic Chemistry (Photochemistry) from Northwestern University (Evanston, IL.) in 1984. Since joining Bell Laboratories in 1984, he has worked in the design and development of optical fiber coatings, bonded ribbon matrix materials, UV curable adhesives, index matching compounds, optical fiber color codings, and polyimide optical fiber coating. His present responsibilities include design and development of materials for optical fiber and cable.



Kenneth W. Jackson is a Distinguished Member of Technical Staff in the Lightguide Technology Department at AT&T Bell Laboratories, Norcross, GA. He joined the Western Electric Company in 1970 having received a B.S.M.E. from Auburn University. He joined AT&T Bell Laboratories in 1981 having received a M.S.M.E. and Ph.D. from the Georgia Institute of Technology. Since 1981, he has worked in the areas of Lightguide Fiber Fabrication, Lightguide Connectors, Materials Design, and Lightguide Cable and Development.



Neil W. Sollenberger is a Member of Technical Staff in the Outside Plant Fiber Group at AT&T Bell Laboratories in Norcross, Georgia. He is responsible for various aspects in the design and development of outside plant fiber optic cables. Prior to his current assignment, his responsibilities have included the design and development of both copper and fiber optic closures and terminals, as well as cabinets for loop electronics. Neil Sollenberger joined AT&T Bell Laboratories in 1978. He has a B.S. degree in Agricultural Engineering from the University of Georgia, and has a M.S. degree in Mechanical Engineering from the Georgia Institute of Technology.



Carl R. Taylor is currently Technical Manager of the Materials Technology and Quality Group at AT&T's main Fiber Optic Manufacturing site in Atlanta. The group has responsibility for the design and engineering of materials used in fiber optic cable and apparatus products as well as responsibility for the quality of all incoming materials and components. He has previously been Supervisor of the Plastics Engineering and Characterization Group in Atlanta and Supervisor of the Polymer Materials Research Engineering Group at AT&T Bell Laboratories in Murray Hill, NJ. Prior to joining AT&T Bell Laboratories in 1977, he earned a B.S. in Chemistry from the College of Wooster in Ohio and a Ph.D. in Physical Chemistry from the University of Wisconsin in Madison. His graduate work focused on the physical and viscoelastic properties of polymers.



Amy J. Muller graduated from Dartmouth College in 1978 where she majored in chemistry. In 1984, she received a Ph.D. degree in Analytical Chemistry from the University of Minnesota. Amy joined AT&T Bell Laboratories in 1984 as a Member of Technical Staff in the Materials Science Division. Her current position as Supervisor of Process Analytical Control Technology involves the development of process control technology and instrumentation for research and manufacturing applications.

Figure 1
Cleaner A

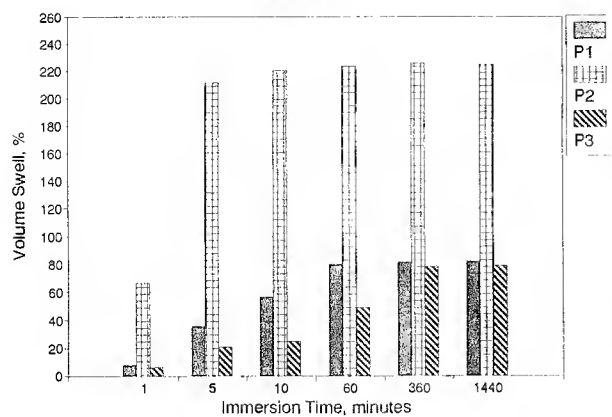


Figure 4
Cleaner A

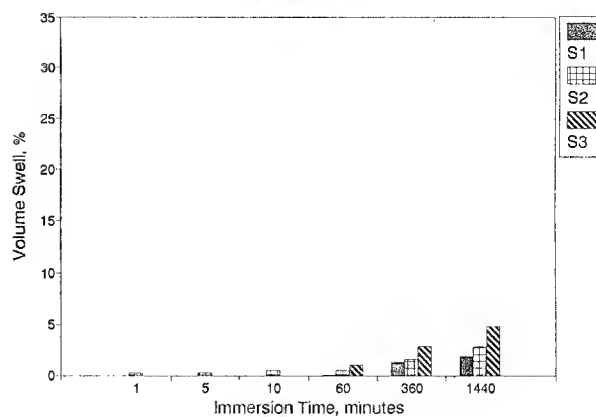


Figure 2
Cleaner B

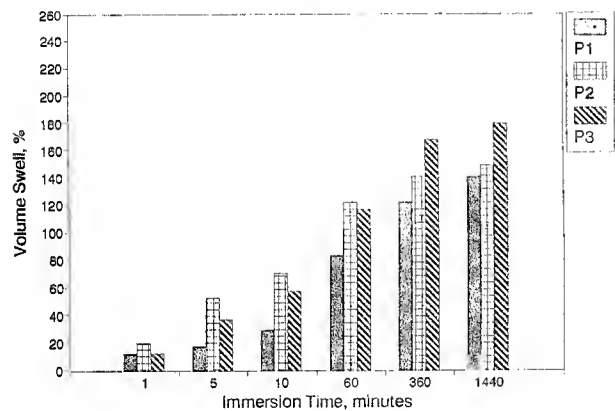


Figure 5
Cleaner B

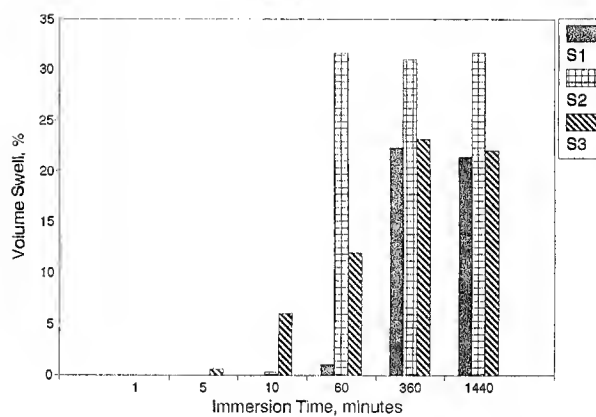


Figure 3
Cleaner C

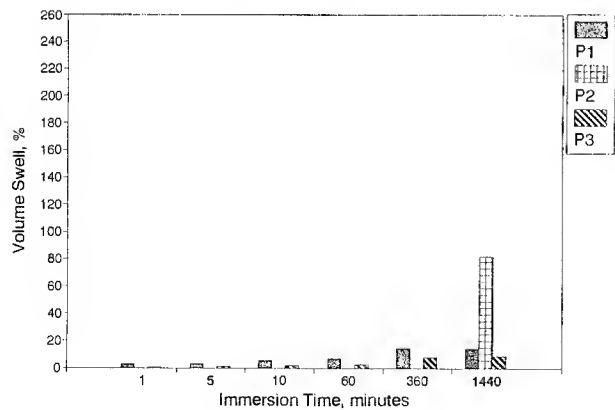


Figure 6
Cleaner C

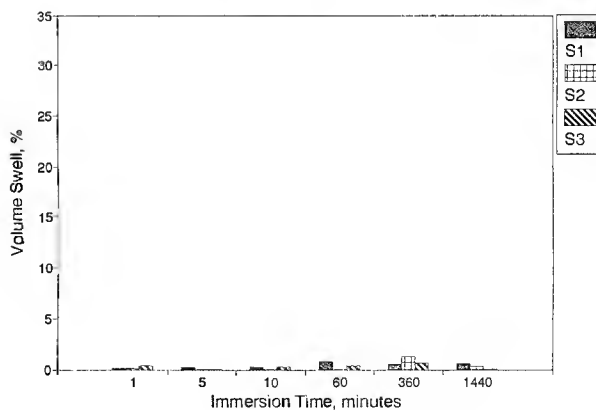


Figure 7
Effect of 5 Minute Immersion

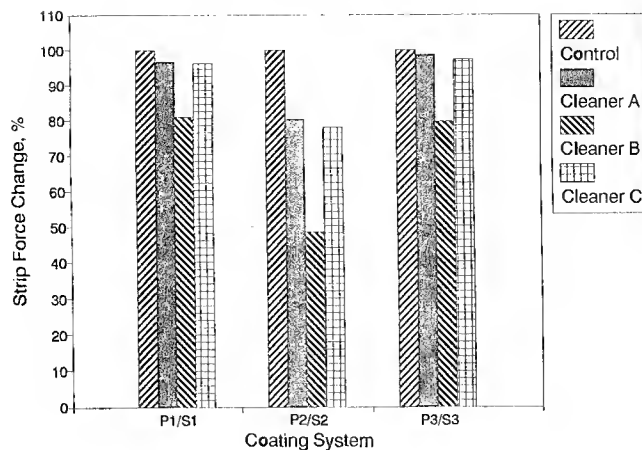


Figure 8
Effect of Immersion on Insitu Modulus

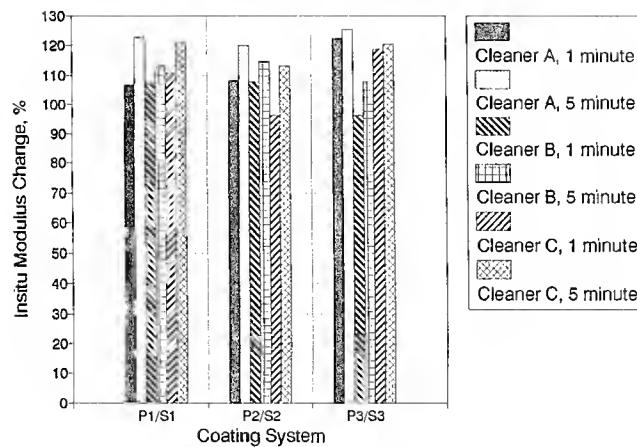
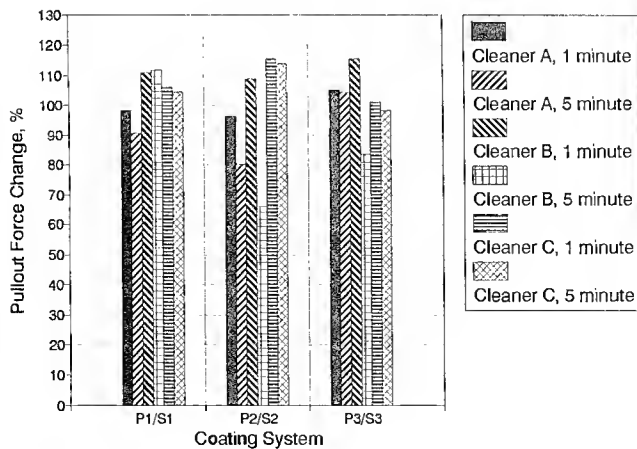


Figure 9
Effect of Immersion on Pullout Force



FLAME RETARDANT OPTICAL CABLES FOR CENTRAL OFFICE, UNDERGROUND OR OTHER SPECIFIC APPLICATIONS

G. HÖG ¹, JO.KARLSSON ², N. MARIETTE ³, G. PATERNOSTRO ⁴, J. RAUCHS ⁵, J. SCHULTE ⁶, O. TATAT ³

¹ KABEL RHEYDT, GERMANY - ² ALCATEL IKO KABEL, SWEDEN - ³ ALCATEL CABLE - OFCCC, FRANCE -
⁴ ALCATEL CAVI, ITALY - ⁵ OPTICABLE, BELGIUM - ⁶ ALCATEL KABELMETAL, GERMANY

Abstract

Optical cables used in a Central Office shall be flame retardant. Their constructions are generally depending on the country where they are used. Most of them are all dielectric, but loose tube, slotted core or tight designs are possible.

This paper establishes a state of the art of the cables developed in our group around the world. The different designs are presented and discussed. Performances are compared, including fire performances.

1 - Introduction

The main requirement for an optical cable for underground application is a low fire propagation. In addition to that, other requirements such as low smoke emission, low toxicity are added. To comply, halogen free flame retardant materials are used for jacketing.

Functional requirements can be requested : rodent resistance, oil resistance, chemical resistance, watertightness,...

Several loose tube cables have been developed in our group and are presented in the second part of this paper.

Due to its international position, our Group has a broad overview about the needs of customers and their relevant standards in term of flame retardant optical cables. From one country to another, or from one continent to another, these specifications are differing. At the moment, a typical example is Europe compared to United States. In Europe, in addition to rather stringent fire retardancy requirements, the specifier places the accent on the people safety and tries to avoid corrosivity risks during fire. In United States, a very high fire retardancy level is required, corrosivity or toxicity being of less importance. This debate about non halogen versus halogen materials has already been pointed out (1).

In the field of fire resistant cables, work has been performed with power cables years ago. For such kinds of cables, different developments have been made, particularly for shipboard cables, cables for subway, and for nuclear power plants where people safety problems, as well as equipment reliability is a major concern. Consequently, a large Research and Development study concerning materials and cable constructions has been realised. Now we are benefiting from these developments and more work is going on in close collaboration with the Alcatel Material Cable Competence Center and with Alcatel Alsthom Recherche.

2 - Test methods and requirements

We have summarized in table 1 the different test methods used to check the adequation of an optical fiber flame resistant cable to its environment. the cables have been divided into :

- cables for tunnels,
- cables for buildings (plenum, riser, electronic equipment rooms, terminations).

We have tried to include in this table the test methods used either in Europe or in the USA.

The most suited jacketing material families are given for each cable environment in table 1.

		tunnel	plenum	riser	electronic equipment room	other terminations
fire tests	IEC 332/1					X
	NFC 32070 C2					
	NFC 32070 C1	X			X	
	IEEE 383 UL 1581 IEC 332/3	X	X (Europe)	X	X	X
	UL 1566			X		
	UL 910		X (USA)			
smoke		X	X	X (Europe)	X (optionally)	
corrosivity					X	
toxicity		X	X		X (optionally)	
recommended jacketing material		low smoke PVC or preferably HFFR	HFFR (Europe) or low smoke fluorinated (USA)	PVC preferably low smoke	low corrosive halogen, preferably HFFR	PVC
concerned cable type (typical)		12 to 36 OF, loose construction, metallic armor	1 to 12 OF, loose or tight, all dielectric	12 to 36 OF (and more), loose or ribbons, all dielectric or metallic	1 to 36 OF, all dielectric, tight or small loose tubes	1 or 2 OF, all dielectric

table 1 : jacketing material families

Concerning the cable constructions, this table gives only the main guidelines. Should the cable be all dielectric, should it be loose or tight, with or without metallic armor,...

Then, different constructions may fulfill the requirements and the final cable design will be influenced either by the customer specification, if it is descriptive, or by their preferences.

3 - Cables for central telephone exchanges

The optical cables used in Central Telephone Exchanges can be classified by category number 4 in the previous table (electronic equipment rooms or buildings), and then must fulfill a series of requirements. They must be designed for indoor installation, and connectorizable in order to work with the transmission equipment. For that matter, the basic unit is a flexible, reinforced, single fiber cable and the multifiber cables shall be easily splittable into such basic units.

These cables shall be flame retardant and must not release corrosive components when exposed to a fire in order to reduce potential damage to the electronic components of the equipment. Low smoke emission can be an additional requirement depending on customer specification or national regulations.

Test procedures to verify the flame retardancy of the cables are generally international for example the well known :

- IEC 332/1 : »Test on a single, vertical insulated wire or cable»,
- IEC 332/3 : »Test on bunched wires or cables»,

but national standards can also be applicable depending on the customer (for example NFC 32070 category C1 in France).

These tests have been developed years ago for electrical wire and cable testing. Due to the lack of specific test procedures for optical cables and in order to use standardised test equipment, they are now used to evaluate flame resistance of fiber optic cables.

Regarding corrosivity, all the customers agree that corrosive element emissions during a fire must be avoided in such an environment, but two different ways to achieve this have been chosen :

- some customers have chosen to specify Zero Halogen materials and their corrosivity is controlled using the international IEC 754-2 standard;
- other customers have chosen to specify a maximum acceptable level of corrosivity measured according to a specific test method, for example France Telecom CNET test method.

According to this second philosophy, the materials shall be low corrosive, but not only limited to Zero Halogen. The advantage of these materials compared to Zero Halogen is mainly better flexibility which is very often required for the single fiber cable.

The single fiber cable, which is also the basic unit of the multifiber constructions, is generally a tight construction, but depending on the customer's specification or preference, it can also be a small loose design. Both have been developed in order to satisfy most of the demands.

The first family is based on a fiber, tight jacketed to 0.9 mm diameter and the second one on a 0.6/1.1 mm dry loose tube. The single fiber cable is finished with aramid yarns as strength elements and jacketed to 2.5 to 3.0 mm diameter either with a Zero Halogen or a low corrosive material. For example polyurethane can be used in order to get high flexibility or abrasion resistance (2). On the other side, such materials have a high coefficient of friction which could be a drawback when cables are installed one over the others in cable paths.

In order to build multifiber cables, these units are stranded around a bare or jacketed dielectric strength member and protected by flame barrier (special tapes) and a flame retardant jacket, generally Zero Halogen as the flexibility is not an issue, less important for multifiber cable than for single fiber. These two cable families are presented in fig.1.

Table 2 presents examples of requirements requested by customers for single fiber cables based on tight and loose OF that we have produced. The tight cable has been proposed either with polyurethane, low corrosive PVC or HFFR jacketing material.

Table 3 presents the characteristics of two multi fiber cables. One is based on 10, tight, single fiber cables stranded around a jacketed, dielectric strength member, protected with mica/wooven glass tapes and jacketed with a HFFR material ; the other is very similar, but based on stranded 0.6/1.1 mm loose tubes.

In order to achieve higher fiber count and lower cable diameter, 0.9 mm diameter tight jacketed fibers can be

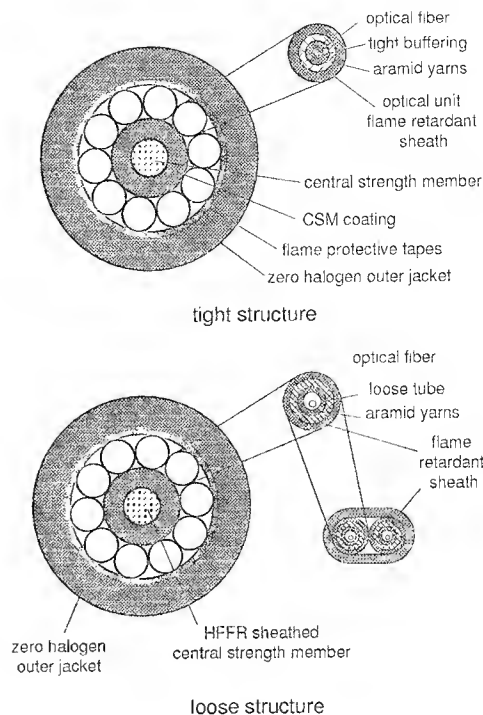


fig 1: tight and loose fiber cable families

directly stranded around a central dielectric strength member (6 or 12 OF cables in table 4) or stranded in sub-units which are stranded around a central, dielectric strength member (36 OF cable in table 4).

	Tight cables		loose cable
	French market	Italian market	Belgian market
jacketing material	polyurethane, low corrosive PVC or Zero Halogen jacket	Zero Halogen jacket	Zero Halogen jacket
diameter	2.7 mm	2.55 mm	3.0 mm
Thermal cycling	≤ 0.1 dB/km at 1310 and 1550 nm (-5/+60°C)	≤ 0.2 dB/km at 1550 nm (-25/+70°C)	≤ 1.0 dB/km at 1550 nm (-5/+50°C)
tensile	30 daN : no attenuation increase	14 daN : ≤ 0.05 dB/km at 1550 nm	50 daN : ≤ 0.1 dB/km at 1550 nm
crush resistance	25 daN/cm : < 0.1 dB at 1550 nm, reversible	10 daN/cm : ≤ 0.05 dB at 1550 nm	40 daN/cm : ≤ 0.05 dB at 1550 nm
bending radius	10 turns, $r = 30$ mm ≤ 0.1 dB at 1550 nm ≤ 0.1 dB at 1310 nm	6 turns, $r = 20$ mm 10 cycles ≤ 0.1 dB at 1550 nm	-
torsion	10 turns/m: ≤ 0.1 dB at 1310 and 1550 nm	80 turns/m: ≤ 0.1 dB at 1550 nm	-
friction coefficient	0.94 : PU jacket (non compliant) 0.16 : PVC jacket 0.13 : HFFR jacket	-	-
cyclic bending	$r = 30$ mm, 500 cycles : < 0.1 dB at 1550 nm	$r = 5$ mm, 5000 cycles : < 0.1 dB at 1550 nm	$r = 15$ mm, 1000 cycles : ≤ 0.05 dB at 1550 nm
kink test	no kink or attenuation increase on 60 mm diameter	-	-
flame retardancy	comply with IEC 332/1 except cable break during the test comply with needle burner test NFC 20922	comply with IEC 332/1 comply with IEC 332/3 cat.C	comply with IEC 332/1 comply with IEC 332/3 cat.C

table 2 : single fiber cable characteristics

	loose tube 0.6/1.1 mm	tight 0.9 mm fibres
diameter	15.7	17
thermal cycling	-5/+50 °C : ≤0.10 dB/km at 1310 and 1550 nm	-5/+45 °C : ≤0.1 dB/km -30/+70 °C : ≤1.0 dB/km reversible (1310 nm and 1550 nm)
tensile	160 daN : ≤0.2 dB/km at 1550 nm	70 daN : ≤1.0 dB/km at 1310 and 1550 nm
crush	80 daN/cm : ≤0.1 dB at 1550 nm	25 daN/cm : ≤0.1 dB at 1550 nm
bending radius	r=140 mm : no attenuation increase at 1310 and 1550 nm	r=150 mm : no attenuation increase at 1310 and 1550 nm
flame retardancy	comply with IEC 332/3 cat C	comply with IEC 332/1 comply with NFC 32070 cat.C1

table 3 : tight and loose 10 fibers cable

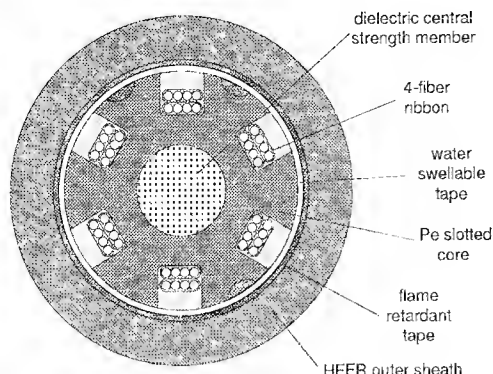
These constructions are smaller, splittable and directly connectorizable, but are generally limited to connections that must not be connected and disconnected very often. They are more dedicated to commercial and industrial buildings than to telephone exchanges and consequently must use flame retardant materials with low smoke and low toxic emissions in order to insure people safety. Performances of these cables are

summarized in table 4; they are jacketed with LSZH (Low Smoke Zero Halogen) compounds to meet the flame retardancy, smoke emission and toxicity requirements.

Finally, we have also produced, on customer request, an halogen free flame retardant ribbon cable. Its description and characteristics are given in table 5.

	6 fibers cable	12 fibers cable	36 fibers cable
diameter	6.9	8.6	12
thermal cycling	-40/+70 °C : ≤0.1 dB/km at 1550 nm	-40/+70 °C : ≤0.1 dB/km at 1550 nm	-30/+60 °C : ≤0.4 dB/km at 1310 and 1550nm
tensile	70 daN : ≤0.5 dB/km at 1550 nm	up to 250 daNdaN : ≤0.5 dB/km at 1550 nm	150 daN : ≤0.1 dB/km at 1550
crush	20 daN/cm : ≤0.2 dB at 1550, reversible	26 daN/cm : ≤ 0.1 dB at 1550, reversible	30 daN/cm : ≤0.15 dB at 1550
bending radius	r=80mm : ≤0.1 dB at 1550	r=120mm : ≤0.1 dB at 1550nm	r=180mm : no attenuation increase
repeated bending	-	-	r=37.5mm, 1000 cycles : ≤0.05 dB at 1310 and 1550
impact resistance	-	-	100 impacts, 2N.m ≤0.05 dB at 1310 and 1550
flame retardancy	comply with IEC 332/1 comply with NFC 32070 cat.C1	comply with IEC 332/1 comply with NFC 32070 cat.C1	comply with IEC 332/3 cat C

table 4 : tight multifiber cables characteristics



diameter : 14 mm
weight : 160 kg/km
fibre count : 48
temperature operating range : -30/+60°C
max pulling strength (no loss increase) : 200 daN
longitudinal watertightness : yes
fire propagation test : comply with IEC 332/3 cat C

table 5 : ribbon HFFR cable

In order to be able to propose cables for telephone central exchange and commercial or industrial buildings for an international market, different cable constructions have been developed. The cable designs are optimized to the customer in terms of basic unit construction to satisfy his preference or specification for connectorisation and in terms of jacketing material choice in order to comply with its specifications or with national regulations.

4 - Cables for tunnels

Even more specific and stringent is the tunnel application for optical cables.

These cables are installed in the cable path along the tunnels, but also for subway application through the stations.

In addition to conventional requirements applicable to optical cables such as operating temperature range or maximum pulling strength, they may have to be resistant to :

- rodents,
- fungus growth,
- chemicals, because of their hostile environment,
- insect,
- radiations.

Last but not least, they must not propagate the fire and must not generate smoke or toxic components when exposed to fire.

A typical example is the French specification (3) issued by R.A.T.P. (Réseau Autonome des Transports Parisiens) which lists the requirements of optical cables for the Paris subway. This specification considers the whole problem of optical cables installed in public areas. The main cable parameters to be taken under consideration for this application are summarized in table 6:

Parameter	requirement
Diameter	≤ 13 mm
Thermal cycling -15/+50°C	≤ 0.1 dB/km
Tensile 200 daN	≤ 1.0 dB/km at 1310 nm ≤ 2.0 dB/km at 1550 nm
Crush 10 daN/cm	≤ 0.2 dB
Bending radius 40d	≤ 0.2 dB
Kink on D = 15d	no kink
Watertightness	option : 1 meter height, 168h
Flame resistance	C2 according NFC32070 C1 according NFC32070, less than 300 mm damaged
Smoke emission (NBS)	Dm ≤ 350 VOF4 ≤ 100
Toxicity	toxicity index ≤ 5 at 800°C
Corrosivity	pH ≥ 4

table 6 : RATP main requirements

For such cables, the jacketing materials are fundamental in order to reach the objectives of the customer. For R.A.T.P., the jacketing materials are described in the specification K20 which is prescribing halogen free flame retardant crosslinked materials. The main characteristics of such materials are listed in table 7:

Characteristics	Requirement
mechanical characteristics	$R_r \geq 7$ MPa $A_r \geq 100\%$ $E_{50} \geq 7$ MPa
mechanical characteristics after aging 10d at 100°C	$ \Delta R_r \leq 25\%$ $ \Delta A_r \leq 25\%$ $ \Delta E_{50} \leq 30\%$ shrinkage $\leq 5\%$
Oil immersion 4 hours 70°C	$R_r \geq 7$ MPa $A_r \geq 100\%$ $ \Delta E_{50} \leq 30\%$ volume variation $\leq 20\%$
Acids and bases immersion 28 days at 23°C	$R_r \geq 7$ MPa $A_r \geq 100\%$ $ \Delta E_{50} \leq 30\%$
Pressure at high temperature	$\leq 50\%$ at 80°C
Low temperature bending	-15°C
Tear strength	≥ 20 N/mm

table 7 : RATP main requirements for HFFR material

In order to select the best HFFR raw materials suitable for cables for subway, we carried out a comparative study on eight cables based on :

- a conventional, dielectric core made of stranded loose tubes,
- a corrugated steel tape for the rodent and crush resistance.

Then, fire resistance had been evaluated with several Halogen Free Flame Retardant (HFFR) jacketing compounds made in our Group or commercially available.

The flame retardancy was evaluated according to the international IEC 332/3 standard using the category B test method configuration (3.5 litres per meter). This configuration has been found suitable for comparison and selection of the cable constructions and HFFR jacketing compounds.

Eight different cables using eight different HFFR compounds were screened using that test. They are referenced A to H in table 8.

The HFFR materials have been selected based on their Limit Oxygen Index (LOI), and mechanical properties. They are either thermoplastic or crosslinkable.

Table 8 gives the results of the IEC 332/3 catB screening

Cable ref.	Material ref.	L.O.I. (%)	IEC 332/3 test result (damaged height in cm)	
			front side	rear side
A	1	45	104	63
B	2	38	78	55
C	3 Xlinked	36	burn	burn
D	4	36	burn	burn
E	5	33	burn	burn
F	6	35	burn	burn
G	7	34	76	104
H	8	37	78	87

Table 8 : IEC 332/3 test results

Nota : The IEC 332/3 requirement is «less than 250 cm damaged at the end of the test».

For conclusions :

- only cables A, B, G, H complied,
- for similar constructions, as previously mentioned (4), LOI can not be considered as a very accurate way to predict the cable fire resistance. For example, cable G passed the test, its jacketing material having a rather low L.O.I.
- cross-linking does not necessarily mean good fire resistance.

Obviously, cables for subway (or for tunnels) are then developed on special customer request and most of their performances are strongly depending on the jacketing material used. Halogen Free Flame Retardant materials are used.

Three different cables developed for such applications are presented here after :

- two cables were designed for subway,
- the third one to be installed in the CERN (Centre Européen de Recherche Nucléaire) particle accelerator.

Table 9 summarizes the cable characteristics and figure 2 gives the cables cross section.

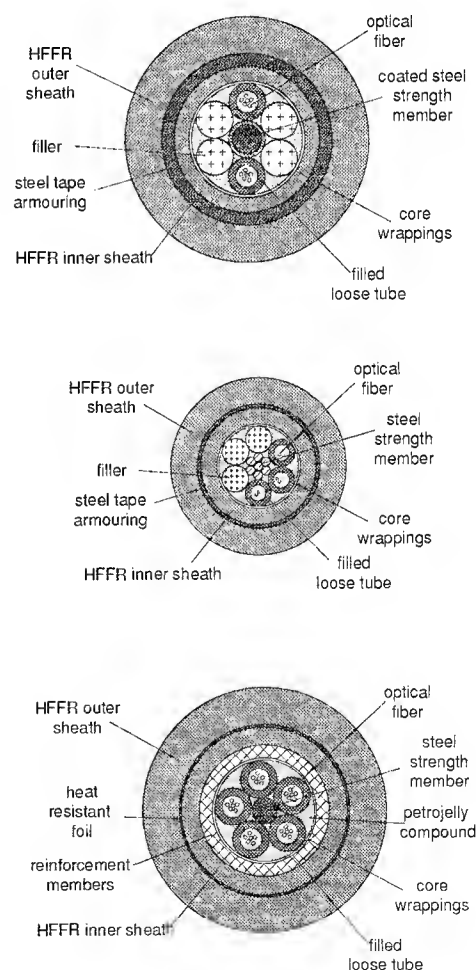


fig. 2 : cables for tunnel

property	unit	cable 1	cable 2	cable 3
diameter	mm	18	12.7	19
weight	kg/km	350	220	
operating range	°C	-30/+70	-20/+60	-25/+60
max tensile load	daN	270	280	440
crush resistance	daN/cm	50	-	-
min bending radius	mm	200	220	400
flame retardancy		NFC 32070 C2 NFC 32070 C1 IEC 331	IEC 332/1 IEC 332/3 IEC 331	IEC 332/1 IEC 332/3
toxicity				ATS 1000.001
smoke emission			IEC 1034	ASTM E 662
resistant to :		rodents fungus	rodents insects	rodents radiation
corrosivity		IEC 754/1- 754/2	IEC 754/1 754/2	DIN 57472 part 813
water - tightness		yes	no	yes

table 9 : cables for tunnel

In addition to the IEC 332/3 flame propagation test, fire resisting characteristics were requested for cables 1 and 2. It means that these cables must continue to work during fire. The test used to simulate this situation was IEC 331 which is up to now dedicated to power cables. For power cable, the insulation resistance between conductors is controlled during the test. For optical fiber cable, we decided to control the fiber attenuation during the test. IEC 331 test equipment is described in figure 3.

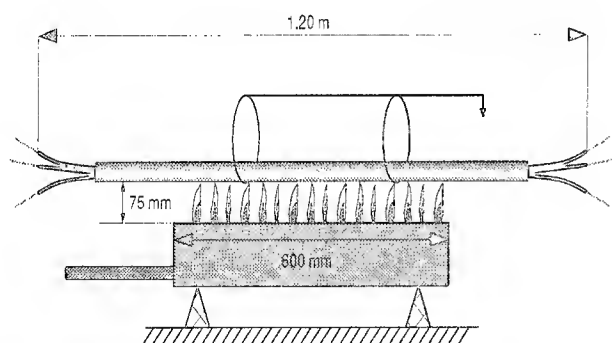


fig. 3 : IEC 331 test equipment

Hereafter are in table 10 typical results obtained with cable 1 (5 different samples taken from 4 different cables).

No fiber broke during the test and the average attenuation increase was maximum 0.2 dB per fiber.

sample ref.	attenuation variation in dB			
	after 1 hour burning		after 1 hour burning and 15 min cooling down	
	1 fiber	15 looped fibers	1 fiber	15 looped fibers
1	0.21	2.14	0.20	2.53
2	0.03	0.40	0.05	0.89
3	0.08	1.22	0.08	1.32
4	0.05	0.73	0.05	0.90
5	0.06	0.95	0.06	1.26

table 10 : IEC 331 test results

After a careful selection of the HFFR jacketing materials, different cables have been developed according to special customer demands. They fulfill most of the standardized tests for halogen free flame retardant cables and are suited for tunnel environments. Their protection is made of 2 HFFR jackets and steel tape in between and their diameter depends on their fiber count. These cables do not propagate the fire, do not generate smoke, and, for some of them, are resistant to fire according to IEC 331 test method.

5 - Conclusion

Flame retardant optical fiber cables cannot be considered just as an extension of conventional fiber optic cables with a different jacket material. Their construction is highly directed by their environment, in addition to their necessity to be flame resistant. Parameters such as number of fibers, connectorization, rodent or oil resistance, toxicity or corrosivity,... shall be taken under consideration.

HFFR material selection cannot be done only according to raw material supplier information. Parameters such as Limit Oxygen Index are not sufficient for that matter. This selection must include standardized fire tests performed on cables.

This paper presented three different flame retardant cable applications and the related cables developed in order to answer to the customer demands :

- cables for telephone central exchange,
- cables for buildings,
- cables for tunnels.

For each of these applications, in order to be an international supplier, not only one but several constructions are proposed by our group to satisfy most of the customers specifications or preferences.

REFERENCES

- (1) : Guerry L. Grune «Wire and cable materials selection criteria for the 90's...», IWCS 1990
- (2) : S. Camara «Evaluation of optical fiber terminating cables with flame retardant polyurethane jacketing» ; IWCS 1988
- (3) : RATP Specification K209
- (4) : L. Colla «AXE exchange cable fire performance testing»; IWCS 1988

AUTHORS

Georg HÖG - KABEL RHEYDT AG
Mönchengladbach, GERMANY

Georg Hög (43) is head of the Development Group for Optical Fiber Cables. He obtained his Dip.-Ing.-Degree from the University of Aachen and joined AEG Kabel in 1977. After being engaged in the development of symmetrical telecommunications cables he became responsible for this group in 1980. He is in his present position since 1985.



Jan-Olof KARLSSON - ALCATEL IKO KABEL
S-510 94 Grimsås, SWEDEN

Jan-Olof KARLSSON holds a Master of science degree in Electronic Engineering from the University of Chalmers in Gothenburg, Sweden, where he graduated in 1970. He joined Alcatel IKO Kabel in 1976 as a development engineer for telecom cables and he is now responsible for technical activities in the Telecom Cables Division.



Nicolas MARIETTE - ALCATEL CABLE
35 rue Jean Jaurès 95871 Bezons, FRANCE

Nicolas MARIETTE was born in 1968 and received his chemical engineering degree (DUT) from the Institut Universitaire de Technologie, Béthune, France. He worked for five years on new materials and plastics before he joined Alcatel Cable in 1993 where he is particularly in charge of flame retardant cables testing.



G. PATERNOSTRO - ALCATEL CAVI
18 Via Crocifisso - 04100 Latina, ITALY

Giovanni PATERNOSTRO was born in 1946 and received his Dott. Ing. degrees in electronics engineering from Roma university. He is manager of Telecom Cables design and development of Alcatel Cavi.

He is author of technical papers and patents on cable process and measures.

Jean RAUCHS - OPTICABLE SA
Frameries, BELGIUM

Jean RAUCHS was born in 1965. He obtained his Dip. Ing. Degree in mechanics from the Faculté Polytechnique de Mons, Belgium, in 1989. He joined Opticable in August 1989 in the R&D department. He became in 1991 responsible for the Engineering department.



J. SCHULTE - ALCATEL KABELMETAL
Gubener Str. 1 - 3060 Stadthagen, GERMANY

J. SCHULTE received his physics degree in quantum optics in 1981 and his Ph.D. in engineering in 1986 from the Technical University Hannover. After a research fellowship at IBM, Yorktown Heights, he joined Kabelmetal in 1987, where he is currently in charge of cable engineering.



Olivier TATAT - ALCATEL CABLE
35 rue Jean Jaurès 95871 Bezons, FRANCE

Olivier TATAT was born in 1959. He received his engineering degree from the Institut des Sciences de l'Ingénieur de Montpellier (ISIM) in 1982. He joined Les Câbles de Lyon in 1985 where he was in charge of material and mechanical problems for telecommunications cables. He is now working as project engineer in the Optical Fiber Cable Competence Center of Alcatel Cable.



OEMI PARALLEL CHANNEL CABLE: FLAME TEST PERFORMANCE OF NONHALOGEN AND HALOGEN CONTAINING CONSTRUCTIONS

G. A. Schmidt
Union Carbide Corporation
Somerset, NJ

L. G. Polhemus
IBM
Poughkeepsie, NY

ABSTRACT

This paper discusses the performance of three IBM 20/C Bus and Tag cables during the UL 1685 Vertical Tray Cable burn test and during the UL 1666 Riser Cable burn test. The three cables have identical electrical performance, but they are constructed from different thermoplastic and shielding materials. The flame propagation, smoke obscuration and heat release are discussed. Information is provided on the corrosive effects of materials similar to those used for the three cables.

A. INTRODUCTION

I. Application and Electrical Properties

Three IBM 20/C Bus and Tag cable types are discussed in this paper. The cables are used mainly as "in and out" cables for mainframe computers and to interconnect computers. Different thermoplastic and shielding materials were applied to construct these cables. All three cables comply with the specified electrical performance:

Capacitance	44.3 pf/m max.
Impedance	95 + or - 3 Ω
Attenuation, 400 Mc	10.2 db/30.5 m max.
Velocity of Propagation	81.5% to 84.5%

B. 20/C BUS AND TAG CABLES: MATERIALS AND CONSTRUCTION

The outside diameter of all cables is within 20.3 mm + - 0.8 mm, (0.80" + - 0.03"). The significant differences among the three cables are as follows:

IBM CL2 Blue, Standard Cable (Halogen)

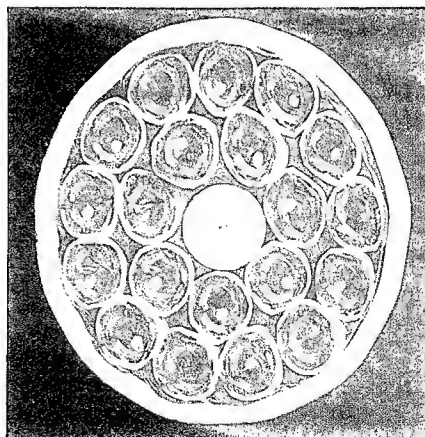
Coaxes: LDPE filament, FRPE tube,
80°C PVC jacket
Cable: PVC filler, 20 coaxes, aluminum/
polyester wrap, 80°C PVC jacket

IBM CL2, Halogen Free

Coaxes: LDPE filament, LDPE tube,
nonhalogen jacket
Cable: Nonhalogen filler, 20 coaxes,
aluminum/polyester wrap,
nonhalogen jacket.

IBM CL2P, Flexible Plenum (Halogen)

Coaxes: Foam FEP, PVDF Jacket
Cable: Proprietary construction with
20 coaxes and chlorinated polymer
jacket.



IBM CL2, Halogen Free, Cross Section
Actual Average OD: 20.3 mm (0.80")

C. UL 1685: VERTICAL TRAY FIRE PROPAGATION AND SMOKE RELEASE TEST FOR ELECTRICAL AND OPTICAL FIBER CABLES

I. TEST PROCEDURE

The three cables were tested in the enclosure described in Figure 1. The test procedure per UL 1685 was selected, because it specifies an exhaust during the test. It can be seen in Table 1 that the procedure per IEEE-383 is very similar to the UL 1685 test.

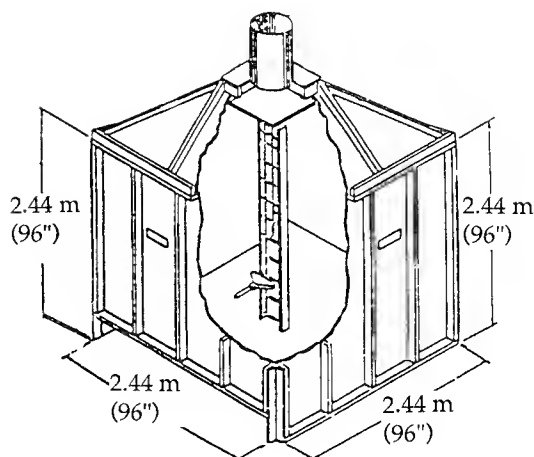


Figure 1: UL 1685/IEEE-383 Test Enclosure

Table 1: Comparison of Tray Cable
Burn Tests

	<u>UL 1685</u>	<u>IEEE-383</u>
Sample:	2.44 m (96")	2.44 m (96")
Horizontal burner:	0.46 m (18") from floor	0.61 m (24") from floor
Exhaust velocity:	393 meters per minute	none specified
Fails:	If it burns to the top of the 2.44 m (96") sample and/or if it fails smoke requirements	If it burns to the top of the 2.44 m (96") sample

II. TEST RESULTS

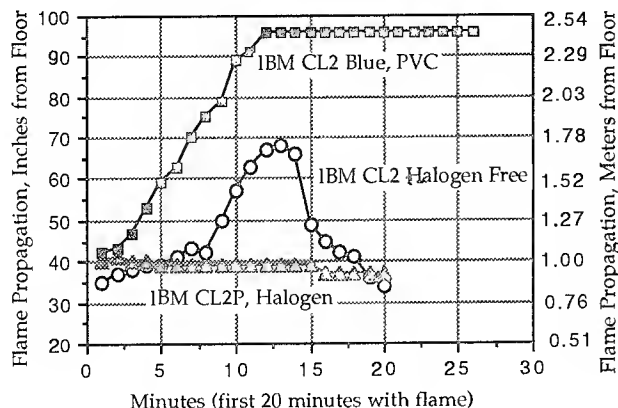
1. Flame Propagation

Figure 2 below shows the flame propagation of the three cables after the 70000 Btu/hour flame has been ignited. The flame is applied for 20 minutes. It can be seen that the flames move upward quickly on the standard cable and they reach the top of it after 14 minutes. Cables that are required to meet the flame requirement of the UL 1685 vertical tray cable test pass when the flames do not reach the top of the 2.44 m (96") cable sample.

The nonhalogen cable starts burning after 8 minutes, the flames move up to 1.72 m (67.72") after 13 minutes and they decline thereafter.

The plenum rated halogen cable has minimal flame propagation. Basically it burns only in the burner's flame. The maximum flame height is 1.02 m (40"). Towards the end of the test, the flame height is 0.94 m (37").

Figure 2: Flame Propagation

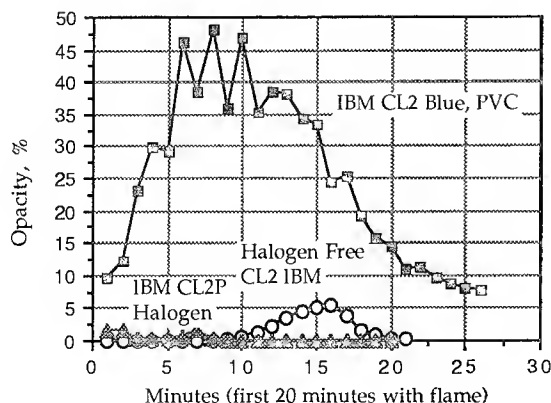


2. Smoke Obscuration

The visible smoke that develops during the vertical tray cable test is detected by a light source that is located in the exhaust duct. Figure 3 is a recording of the visible smoke produced by each of the three cable samples. The standard cable developed much black smoke early during the test. The first peak of 46% opacity was reached after 6 minutes. The standard cable continued to smoke after the 20 minute flame application. The test was discontinued after 26 minutes.

The halogen cable had slight development of visible smoke at the start of the test. The nonhalogen cable reached 5.5% opacity after 16 minutes. The test was discontinued after 26 minutes.

Figure 3: Smoke Obscuration versus Time



3. Actual Weight Loss

It was of interest to note the actual weight loss of the three cables that occurred during the UL 1685 burn test. The data are shown in Table 2.

Table 2: Net Cable Weight Loss During the UL 1685 Tray Cable Burn Test

	CL2 PVC	CL2 Halogen Free	CL2P Halogen
Number of cable lengths on the ladder	5	5	5
Initial cable weight			
kg	6.1	6.2	6.9
Pounds	13.4	13.6	15.3
Weight of materials consumed			
kg	1.9	0.5	0.3
Pounds	4.2	1.2	0.7

It can be seen, that the CL2 PVC cable has the highest weight loss. The CL2 PVC cable was dissected and it was determined that the total amount of filled and unfilled organic materials that are represented by the 5 lengths of the CL2 PVC cable on the ladder during the UL 1685 test is 2.77 kg (6.11 pounds). The PVC compound and the FRPE tubes may contain about 30% of inorganic material; 70% of 2.77 kg (6.11lbs) is 1.94 kg (4.3 pounds). The actual loss of 1.9 kg (4.2 pounds) is an indication that all organic materials have burned off.

In the case of the Zero Halogen cable, some of the weight loss is water of hydration from the flame retardant additive.

4. Weights of Cable Components

Figures 4 and 5 provide information about the weights of components of the CL2 PVC and the CL2 nonhalogen cables. Information regarding the CL2P plenum rated cable was excluded, since it is a proprietary construction.

CL2 Halogen Free 20/C Coax. Cable:
Weights of Cable Components

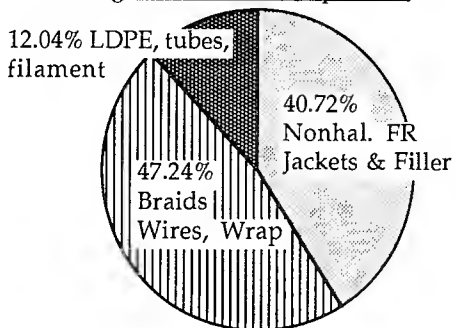


Figure 4

CL2 PVC Blue 20/C Coax. Cable:
Weights of Cable Components

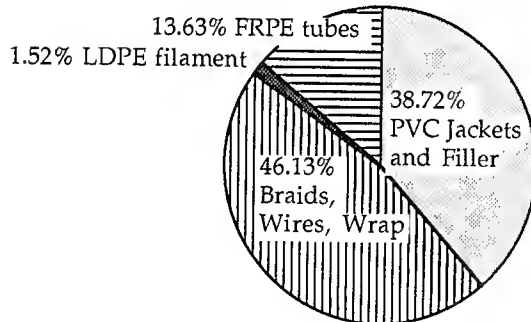


Figure 5

D. UL 1666: TEST FOR FLAME PROPAGATION HEIGHT OF ELECTRICAL AND OPTICAL-FIBER CABLES INSTALLED VERTICALLY IN SHAFTS

I. TEST PROCEDURE

The UL 1666, the vertical riser cable burn test, was performed as a second fire test on the three IBM cables. The test chamber is shown on page 6 in the UL 1666 Standard, dated January 22, 1991, and it is reproduced as Figure 6 below.

- * A slot measuring 305 mm by 610 mm (1 ft by 2 ft) is located in the first floor, and an identical slot is located directly above in the second floor.
- * Each set of IBM cables that was tested per UL 1666 consisted of fifteen 5.33 m (17.5 ft) lengths. The cable lengths were lashed together in a single layer and installed through both slots against the long sides of the slots that are closest to the ignition flame.
- * Commercial grade propane was used as fuel having a heating value of approximately 2500 Btu per cubic foot (83.1 MJ/m³) or 22.2 kilocalories per cubic meter.
- * The maximum flame height with reference to the first floor level was observed at intervals of 60 seconds.
- * The thermocouple temperature at the 3.66 m (12 ft) level and the air velocity probe were recorded every 10 seconds.
- * The test flame was applied to the cable lengths for 30 minutes. After the test flame was extinguished and all flaming of the cable specimens ceased, the maximum height of continuous cable damage was measured and recorded.
- * A coating of soot on the cable specimens was ignored if, when wiped off, the original surface of the cables was unblemished.

- * Damage was considered to have occurred anywhere that a cable specimen showed evidence of its combustible material having been softened (recorded as "melt"), having been partially consumed (recorded as "char"), or having been completely consumed (recorded as "ash").

II. REQUIREMENTS PER UL 1666

1. The flame propagation height shall be less than 3.66 m (12 ft).
2. The temperature of any thermocouple at the 3.66 m (12 ft) height is not to exceed 454.4°C (850.0°F).

UL 1666 Fire Test Chamber

Drawings of the fire test chamber are shown in Figure 6 and 7. The drawings were reproduced from the Standard UL 1666, dated January 22, 1991, page 6.

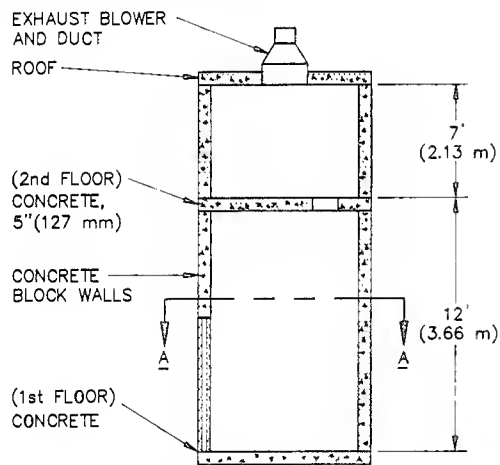


Figure 6: View of the Chamber

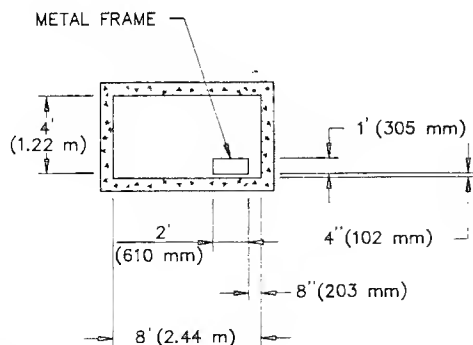
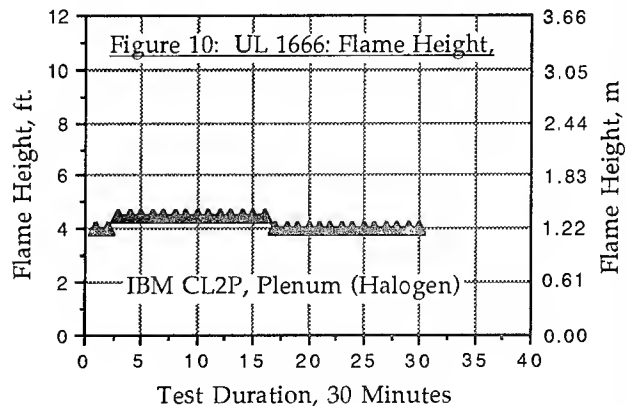
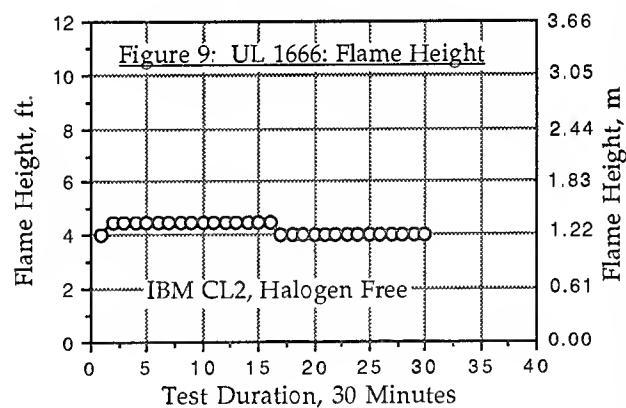
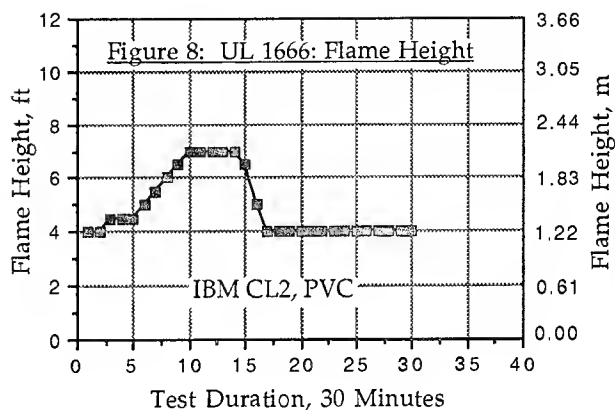


Figure 7: View of floor section with the metal frame where the cables will be located. An identical slot is located directly above in the second floor.

III. TEST RESULTS

1. Flame Propagation

The flame propagation of the three cables during the UL 1666 riser cable burn test is graphically displayed in Figures 8, 9, and 10. It can be seen that all three cables passed the test, the flame propagation height is less than 3.66 m (12 ft.) and the temperature in the shaft during the three tests did not exceed 454.4°C (850°F), see Table 3.



It was not expected that the CL2 PVC cable would pass the riser cable burn test, because the UL 1666 test is considered to be more severe than the UL 1685 test.

Figure 11 is a reproduction of Figure 760-53 from the 1993 National Electric Code, it shows the Cable Substitution Hierarchy.

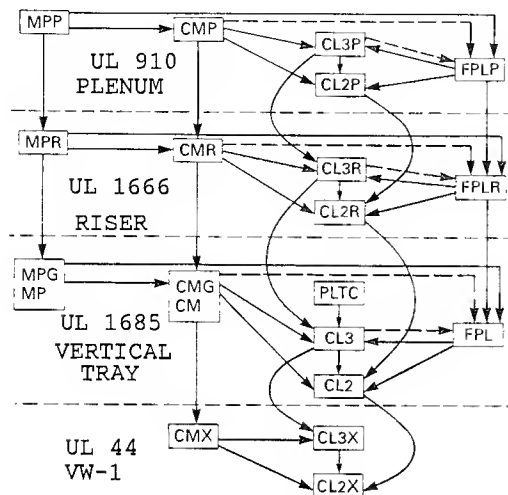


Figure 11: From 1993 NEC: Cable Substitution Hierarchy

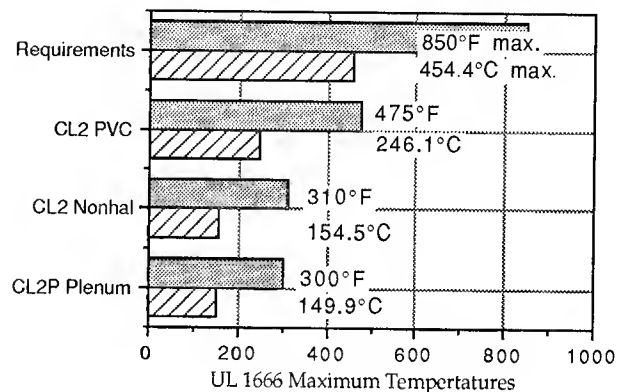
The identifications of the applicable burn tests were added to Figure 11.

It is possible that the presence of the ladder during the UL 1685 may be the reason that a cable can pass the UL 1666 test, but fail the UL 1685 test. During UL 1685 tests of coaxial cables such as types RG-223 and RG-58, it was observed that pure polyethylene that is surrounding the center conductor and covered with the braided outer conductor melts during the test and covers the rung where the fire is moving up slowly. The liquid polymer will start burning and support the fire. In order for such a cable to pass, the fire must self extinguish before it reaches the next rung of the ladder. The fire of the IBM CL2 cable was too strong to observe the above described scenario, but the presence of the ladder may have been the reason for its failure during the UL 1685 test. For the UL 1666 test, the cables are lashed together, melting material can run down and burn near the bottom of the cable assembly.

2. Maximum Temperatures in the Riser Shaft

The maximum temperature that is permitted during the test in the shaft and the temperatures that were reached during the test of the three cables are recorded in Figure 12. None of the cables tested approached the permitted temperature limit.

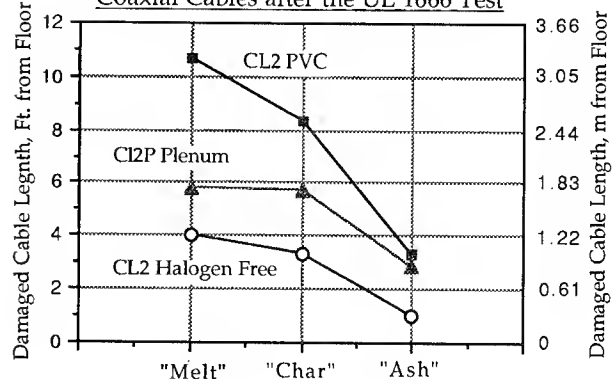
Figure 12: UL 1666, Maximum Temperatures



3. Cable Damage

After the completion of the UL 1666 riser cable burn tests, the cable assemblies were lowered from the shaft and the damaged sections were measured and recorded. The results are shown in Figure 13. It is possible that some of the reacted intumescent flame retardant in the jacket of the CL2P cable was identified as damage, because the reported flame height of the CL2P plenum cable and the CL2 nonhalogen cable was 1.37 m (4.50 ft.), see Table 3.

Figure 13: Condition of IBM 20/C Coaxial Cables after the UL 1666 Test



4. Summary of Test Results

Data that were collected during the UL 1666 riser cable burn tests are recorded in Table 3.

Table 3: UL 1666 Riser Cable Test Results

General Information:

Length of Cable Sections Tested	m (ft.)	5.33 (17.5)
Number of Cable Lengths Tested		15
Average Outside Diameter of Cables	mm (Inches)	20.3 (0.80)

	CL2 PVC	CL2 Halogen Free	CL2P Plenum
Time to Ignition, Minutes:Seconds	00:35	00:35	00:35
Flame Height, maximum, m (ft.)	2.13 (7)	1.37 (4.50)	1.37 (4.50)
Time to Maximum Flame Height Minutes:Seconds	10:00	2:00	3:00
Maximum Temperature, °C (°F)	246.1 (475)	154.5 (310)	149.9 (300)
Afterburn Minutes:Seconds	0:11	4:45	0:05
Condition of Cable Lengths after the UL 1666 Riser Test:			
Evidence of softening, "Melt" m (ft.)	3.25 (10.67)	1.22 (4.00)	1.77 (5.83)
Partially consumed "Char" m (ft.)	2.54 (8.33)	1.01 (3.30)	1.75 (5.75)
Completely consumed "Ash" m (ft.)	1.01 (3.33)	0.30 (1.00)	0.86 (2.83)

D. CORROSION

The corrosive effects of the combustion gases of the three cables was not measured. The data shown in Table 4 (3) were obtained on materials similar to those used for the three cables. The data are presented as an indication of the corrosive effects that can be expected from the combustion gases of the three cables. The test method used is an indirect determination of the corrosive effect of combustion gases from insulating and jacketing materials of a

cable by measurement of the conductivity of the aqueous solution used to absorb the combustion gases.

Table 4: Corrosivity of Combustion Gases:
VDE 0472, Part 813

Significant Test Conditions:

Combustion at 800°C for 30 minutes

Material

Conductivity
of Aqueous
Solution, $\mu\text{S}/\text{cm}$

Halogen Free Compound	16
Polyvinylidene Fluoride Compound	4540
Commercial PVC Compound	7208

E. CONCLUSIONS

All three cables have identical electrical performance. The nonhalogen cable and the halogen (plenum rated cable), are superior with respect to flame propagation, smoke obscuration and heat release. In assessing the corrosive effects of the combustion gases, the nonhalogen cable shows by far the best results of the three cables.

Acknowledgements

The authors wish to acknowledge the contributions of Richard Wagner of Montrose Products Company for producing and providing the cable samples used in the fire tests, and technical assistance, and Al Soto and Grant Apgar of UCC who performed the UL 1685 fire tests.

Reference:

- (1) UL 1685: Vertical Tray Fire Propagation and Smoke Release Test for Electrical and Optical Fiber Cables.
- (2) UL 1666: Test for Flame Propagation Height of Electrical and Optical Fiber Cables Installed Vertically in Shafts.
- (3) Corrosivity Test Methods for Polymeric Materials Part 5, a Comparison of four Test Methods, S. L. Kessel et al., presented during the 18th International Conference on Fire Safety, January 1993, Clarion Hotel San Francisco International Airport, Millbrae, California.

Biographical Sketches of the Authors



Gertraud A. (Trudy) Schmidt is a Senior Research Scientist with the Polyolefins Specialties R&D Wire and Cable Materials Group of Union Carbide Corporation. Trudy has been associated with Union Carbide since 1985, developing and commercializing nonhalogen flame retardant cable compounds. She was formerly affiliated with General Cable Corporation in the position of Assistant Director of Research and Development, later as Director of Material Science.

Trudy was born in Coburg, Germany. She is a graduate of the Ohm-Polytechnikum in Nürnberg, Germany with a MS degree in Chemical Engineering. She is a Senior Member of IEEE, a member of the National Fire Protection Association, the American Chemical Society and the Society of Plastic Engineers.

(Union Carbide Corporation, Weston Canal Center, 1 Riverview Drive, Somerset, NJ 08875; Phone: 908-271-7909; FAX: 908-271-7679)



Leonard G. (Len) Polhemus is an Advisory Engineer with IBM in the Enterprise Systems Division. He has been working since 1982 in the Cable/Connector Technology Group. He has been with IBM since 1964.

A resident of Poughkeepsie NY, he has an AAS degree in Electronic Technology, he is a member of the NFPA Panel 12, CBEMA and he has served on U.L. Ad Hoc committees.

During the past few years, he has been very active with wire designs and materials to meet the worlds changing performance and environmental requirements. Len has also been active with IBM's effort to provide Environmentally Conscious Products.

(IBM Corporation, 522 South Road,
Poughkeepsie, NY 12601-5400
Phone: 914-435-1363; FAX: 914-432-9807)

MIT PROGRAM TO DEMONSTRATE SUPERCONDUCTIVE COMPONENTS IN MICROWAVE SYSTEMS*

Richard W. Ralston

MIT Lincoln Laboratory, Lexington, Massachusetts 02173

ABSTRACT

The Massachusetts Institute of Technology (MIT) is the host institution and a founding member of the Consortium for Superconducting Electronics (CSE). This Consortium joins AT&T, IBM, Conductus, CTI-Cryogenics and MIT in developing superconductive technology for practical electronic applications. The CSE progress toward demonstrating well-engineered microwave components and qualifying them as system-worthy prototypes for communication and signal-processing purposes is described.

INTRODUCTION

The CSE was formed in October 1989 by IBM, AT&T, MIT, and Lincoln Laboratory (which is run for the Federal government by MIT) with the goal of developing technology leading to practical applications for superconducting electronics.¹ The Advanced Research Projects Agency (ARPA) and the industrial members have shared the development costs. Since the CSE is concerned with electronic (as opposed to large-current) applications, it deals with superconductors in thin-film form.

Early in the life of the CSE the primary focus was on the development of substrate materials and film-deposition techniques for specific applications. Three application areas were targeted: microwave networks, magnetic sensors, and digital circuits. The vision is that all three areas will ultimately be implemented in the high-transition-temperature superconducting (HTS) materials. Although strong progress has been made in all three circuit areas, the multilayer film technology for sophisticated digital circuits is still primarily the domain of low-transition-temperature superconductors (LTS), and that LTS technology has been recently transferred out of the CSE for use at Lincoln Laboratory in support of Department of Defense (DoD) applications. The microwave and magnetic applications remain as twin thrusts of the CSE for dual-use HTS applications. Two smaller companies, Conductus and CTI-Cryogenics have joined the microwave effort, and it is this larger of the two CSE application thrusts which is described here.

*This work was conducted under the auspices of the Consortium for Superconducting Electronics with support by the Advanced Research Projects Agency and industry.

THIN FILM MATERIALS FOR MICROWAVE CIRCUITS

The HTS microwave thrust is exploiting two properties of superconductors which make them attractive for microwave circuits: (1) low surface resistance which results both in very low propagation loss in transmission structures and in very high quality factors (Q) in resonant structures, and (2) frequency-independent magnetic penetration depth which results in dispersionless transmission structures.²

Figure 1 shows the surface resistance R_s of Cu, Nb, and $\text{YBa}_2\text{Cu}_3\text{O}_{7-x}$ (YBCO) films as a function of frequency in the 0.1 - 100 GHz frequency range.³ The Cu and YBCO data are for 77 K temperature, while the Nb data is for 7.7 K. This temperature was chosen for Nb so that it would be at the same "reduced" temperature (*i.e.*, normalized to its transition temperature) as YBCO at 77 K. It is clear that both superconductors offer a nearly two-order-of-magnitude improvement over the performance of even cold copper at X-band (10 GHz) and lower frequencies. It is in this frequency region where the CSE is targeting near-term applications.

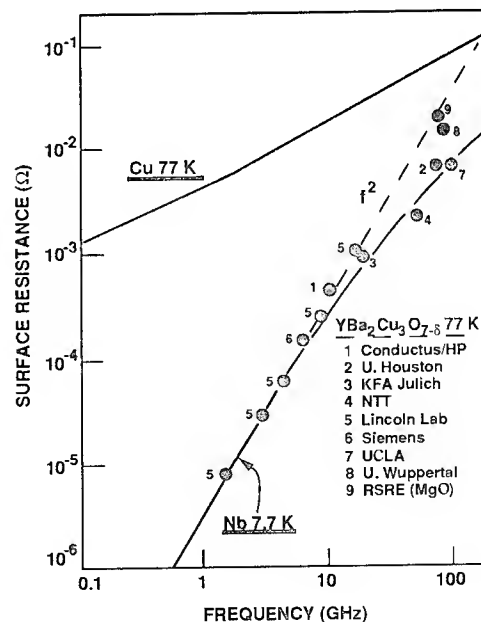


Figure 1. Surface resistance as a function of frequency for cooled Cu and superconducting Nb and YBCO.

This low surface resistance of the superconductors permits a great size reduction for microwave circuits. Planar superconducting transmission lines have been fabricated in the forms familiar to microwave engineers — stripline, microstrip, and coplanar — by the relatively straight forward substitution of superconducting films for copper or gold. Figure 2 shows the standard structures.

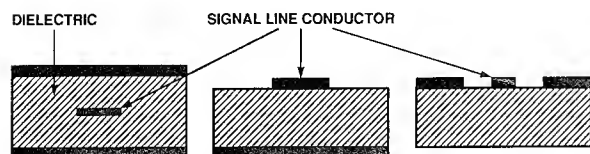


Figure 2. Cross sectional view of typical transmission line structures: (left) stripline, (middle) microstrip, (right) coplanar.

These transmission lines are used to form filters, and specific implementations are described later. In order to manipulate, or "process", signals these filters must retain the signal energy for many cycles (typically 100 to 10,000) of the microwave carrier frequency. Hence high conductor quality factor is required. For the simple limit of a parallel-plate structure, that is microstrip with very wide conductors, the Q is $3.95 \times 10^{-3} f h / R_s$ where f is in GHz, R_s is in ohms and h is in micrometers. As will be illustrated later, high Q drives the technology in terms of (1) large-area, low-dielectric-loss substrates, and (2) smooth, thick deposited films which support sufficient signal current. Filter performance also requires (3) accurate line-patterning methods, and (4) precise electrical design models. The CSE has made substantial contributions in all areas.

Lanthanum Aluminate (LaAlO_3) is provided on a commercial basis in boule and wafer form in up to 4-inch-dia. sizes by AT&T. This material is the best currently available microwave substrate, and is routinely used by the CSE and others in the field for growth of HTS films. The CSE has concentrated on YBCO as the most reproducible microwave film. Its primary attribute is that it is conveniently grown by a number of in-situ techniques, while the competing materials require complex post-growth, ex-situ anneals to achieve the desired superconducting properties.

Coating both sides of a substrate with YBCO is necessary to implement the microstrip and stripline transmission structures. These two structures are preferred over the coplanar configuration because they provide both higher Q and more convenient filter layouts. Lincoln Laboratory has pioneered the use of a gas-conduction heater to facilitate film deposition on both sides of substrates. Versions of the heater are in operation at Lincoln Laboratory, Conductus, and IBM for film production by both sputtering and laser ablation. A drawing of the heater for 2-inch-dia.

substrates is shown in Figure 3. The heater obviates the need for "gluing" substrates to heater blocks. It achieves uniformity of $\pm 1^\circ\text{C}$ near the growth temperature of 740°C , withstands the hot oxygen ambient, and facilitates flipping the substrate for high-yield coating on both wafer surfaces.

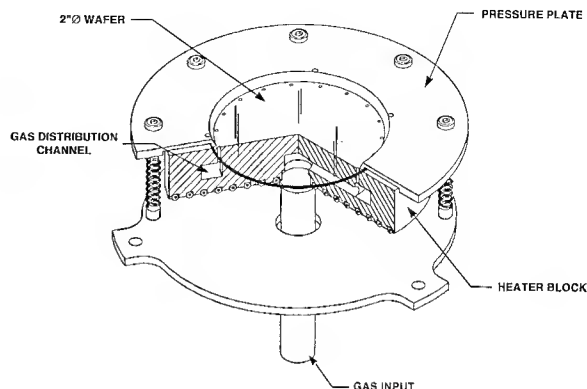


Figure 3. Heater which incorporates pocket of hot gas behind substrate to provide uniform heat by conduction and avoid film contamination.

A variety of YBCO deposition techniques are being refined within the CSE. The primary sources for microwave films today are planar- and cylindrical-magnetron sputter systems in which a relatively high background pressure (280 mTorr) including oxygen is used. The deposition tool used at Lincoln Laboratory was developed specifically to support microwave component development. The substrate, premounted on the top segment of the gas-pocket heater, is extended through a load lock to speed pump down. Once heated, the deposition proceeds at a 300-nm/hr rate for up to three hours. Following a cool down in 1 Torr oxygen, the substrate is removed to the load-lock chamber (and flipped for second-side coating if desired). The magnetron source, with a 4-inch-inside-dia. YBCO cylindrical target, has a magnetic field designed both to produce high deposition rates and to keep substrate ion bombardment low. The reduced surface bombardment provides smooth, dense films to a thickness of 0.7- μm or more. Making these thicker films permits higher microwave currents to flow through filter structures, thus enabling high Q s to be sustained at high throughput powers. The use of the films in two types of microwave filters is described below.

CHIRP FILTER FOR CUEING RECEIVER

This first application example is a nonresonant tapped-delay-line chirp filter. The device is the basis for a cueing receiver. The DoD needs cueing receivers to detect the presence of multiple emitters in a wide band of interest and to pass this information to other receivers with narrower bandwidth and greater selectivity. The cued receivers that

follow are concerned with the information content of the signals, while the cueing receiver must very rapidly determine the frequency and, to a limited extent, the amplitude of the signals.

Figure 4 shows how a YBCO tapped delay line can be used for spectrum analysis.² The taps, in the form of backward-wave couplers, are tuned and arranged so that the highest frequency undergoes the shortest delay, and the lower frequencies receive delay that is linearly proportional to their difference from the highest frequency. Thus a broadband input impulse applied to the filter will produce a down-chirp response, *i.e.*, with the output frequency decreasing linearly with time.

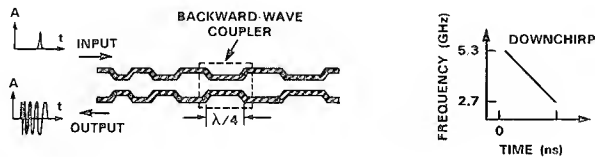


Figure 4. Superconductive chirp filter structure using superconductive striplines and backward-wave couplers.

Spectrum analysis using the chirp transform is illustrated in Figure 5. The chirp filter visible in the photograph is patterned as a spiral on the 2-inch-dia. wafer. Suppose that the input is a number of narrowband tones. The dashed line in the figure will allow us to follow a single tone through the chirp-transform system. The input signal is mixed with a chirp waveform, produced by sweeping the frequency of an oscillator linearly in time. Here an upchirp is used and the sum frequency from the mixer is selected. This results in an upchirp for each tone present at the input. The following chirp filter (compressor) has an impulse response with the frequency-time slope equal to the negative of that from the swept oscillator, so each upchirp is compressed into a pulse at the output. Pulses containing the energy of the higher input frequencies emerge from the output earlier, since they experience less delay in the compressor. It is easy to see that the time of arrival of pulses at the output is linearly related to the frequency of the input signal. The amplitude of the output pulse is linearly related to the input signal amplitude as long as the mixer is operating in its linear range.

The pulse-processing electronics is based on high-speed silicon technology and uses a 2-GHz clock to time the arrival of pulses from the chirp filter. First the pulses are stripped of the carrier by an envelope detector and then are sent to a threshold detector. The arrival of a pulse from the threshold detector latches the clock time elapsed from the start of the chirp generator, *i.e.*, proportional to the frequency of the input signal that produced the pulse. This frequency report provides the cueing message.

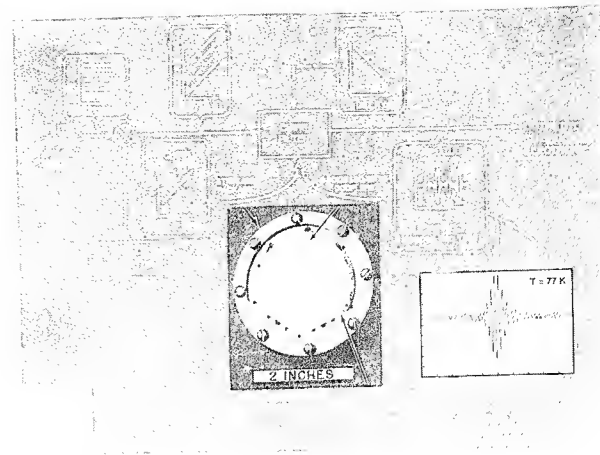


Figure 5. Block diagram of the cueing receiver

Figure 6 shows the room-temperature electronics, power supply, and the cryogenic YBCO chirp filter that implemented the design.⁴ The chirp filter in this prototype receiver has 3-GHz bandwidth (from 9 to 12 GHz) and provides 12 ns of delay, which is equivalent to a 120-MHz resolution, or 24 frequency bins across the analysis band. *The system provides a new look across the spectrum every 50 nsec, and promises substantial advantage in the real-time intercept and sorting of signals from dense emitter environments of concern to our DoD.* A satellite version of this receiver is scheduled to go into orbit soon on an Argos platform as part of the Navy High Temperature Superconductive Space Experiment. Chirp filter delay time and coupler count are being increased for future receivers to provide up to 40 ns of delay and 40-MHz resolution.

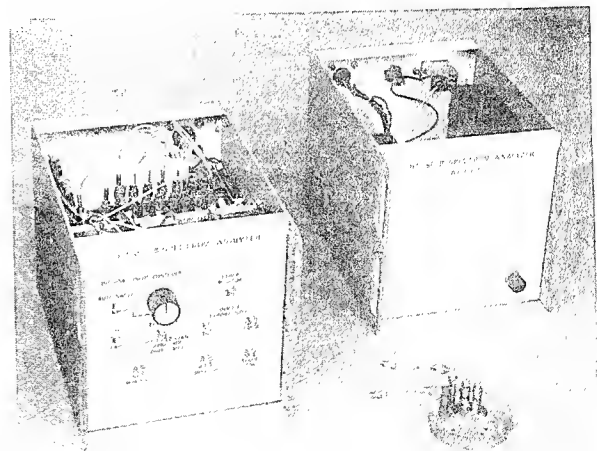


Figure 6. Preprototype cueing receiver comprising (left) output processing electronics, (right) power supplies, and (below) chirp filter.

BANDPASS FILTER FOR CELLULAR BASE STATION

The second application example is a resonant bandpass filter, and is the primary thrust of the CSE for civilian use. The cellular telephone market is growing dramatically, with new bands being auctioned for use. The spectral regions allocated for cellular use are rather narrow, and are certain to have a high density of users. Thus proper filtering of transmit and receive signals into the allocated bands, and precise channelization of the multiple simultaneous signals within each band, are essential to providing adequate customer service. The CSE is driving HTS filters into both transmit and receive segments of the base station as the means to maximize frequency use. By far the more difficult challenge is to support transmit, for the filter must pass 10 W or more.

Bandpass filters are typically realized by appropriately coupling a set of resonant sections. Resonators may be in the form of three-dimensional cavities, bulk rods, or planar circuits like microstrip. The latter are especially attractive because of their compactness and low cost. However, the Q of normal-metal microstrip lines is too low to support the low insertion loss and sharp filter skirts needed for channelizing communications bands. This is especially true for filters with narrow fractional bandwidth because the insertion losses (in dB) of filters scale as $1/(wQ)$ where w is the fractional bandwidth and Q is the unloaded Q of the resonators. As an example, a five-pole, 1% bandwidth filter with element Q s of 20,000 would have a dissipation-induced insertion loss of only 0.2 at midband and three times this amount at the passband edges. As explained previously cooled normal metals are unable to achieve even Q s of 1000 in compact planar form. Hence a filter in a normal metal would have a loss of 6 to 9 dB at the band edges and would be unacceptable, for it would deny communication at those edge frequencies. Thus, communications engineers are currently forced to use bulky, expensive and handcrafted bulk-cavity filters or dielectric-resonator filters.

The development issues for planar HTS filters include: (1) sufficiently accurate design models and (2) high-power-handling films. In the early days of HTS filter development, commercial computer-aided-design (CAD) packages provided accuracy sufficient to produce filters of a few percent bandwidth. These CAD routines, however, are not adequate for highly accurate, narrowband components. A full-wave synthesis routine developed at MIT under the auspices of the CSE provides very accurate loss and kinetic inductance calculations.⁵ Figure 7 illustrates the effects of different conductors on a 4-pole, 1%-bandwidth filter design. Note the substantial pulling of frequency caused by the higher kinetic inductance of YBCO. The film thickness, as well as the resonator linewidth and substrate thickness must be carefully controlled to support filter designs of 1% bandwidth and narrower, and these aggressive requirements must be met for cellular applications.

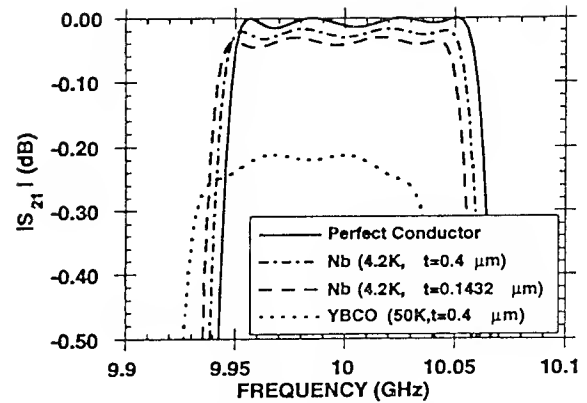


Figure 7. Design calculations for an aggressive 4-pole, 1%-bandpass filter showing the importance of proper models for the superconductor.

Substantial progress is also being made in handling practical transmit powers. The emerging communication systems near 2-GHz will probably require ≥ 10 W confined to no more than 15-MHz (0.6%) bandwidth. The layout of a 5-pole interdigital microstrip filter for such a band is shown in Figure 8. The design was done at Conductus, and employs resonators with 10- Ω internal characteristic impedance.⁶ Each resonator must have a minimum unloaded Q of 20,000 at full transmit power if the insertion loss and bandshape are to remain acceptable. The surface resistance in YBCO increases as increased rf current flows through grain boundaries, hence the Q drops for increased power. Low impedance resonators, because they approach the parallel-plate limit and reduce edge currents, can sustain higher powers. At 50 K and approximately 2 GHz, good CSE YBCO films on LaAlO_3 can routinely support adequate Q at several Watts of applied power.

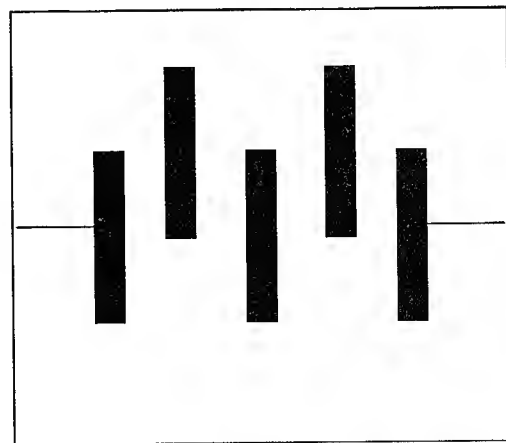


Figure 8. Layout of a 5-pole microstrip interdigital filter designed for 0.6% bandwidth at 2 GHz. The resonators have 10- Ω characteristic impedance.

Filters with various coupling structures and resonator configurations are being tested for power handling. A recent result is shown in Figure 9. The filter bandpass begins to distort at an input power of 38 dBm and significant distortion has set in at 41 dBm. With this high throughput power of 10 W, careful package and cryocooler design is essential to preventing thermal runaway. *The CSE projects that optimized filters of this type will provide excellent base-station performance at several tens of Watts or transmitter power.*

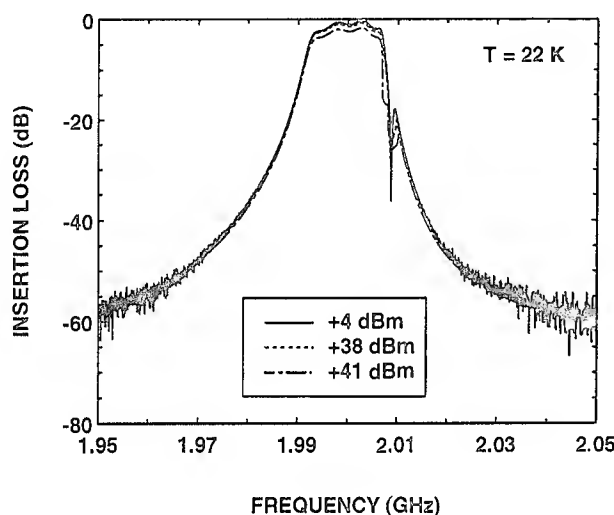


Figure 9. Bandpass filter characteristic demonstrating potential for cellular-telephone transmit applications.

SUMMARY

The CSE has combined the technological strengths of scientists and engineers from the university, government, and commercial sectors to advance HTS thin film components toward practical DoD and civilian system applications. Prototype demonstrations are occurring at a brisk pace as evidenced by the cueing receiver and cellular base station examples.

ACKNOWLEDGEMENT

It is not possible to list the many contributors to whom the author is indebted for their creative and diligent teamwork. The CSE participants have successfully penetrated both institutional and technological barriers to converge on practical HTS technology. Thank you all.

REFERENCES

- [1] R.W. Ralston, M.A. Kastner, W.J. Gallagher, B. Batlogg, *IEEE Spectrum* 29, 50 (1992).
- [2] R.S. Withers, in *The New Superconducting Electronics*, H. Weinstock and R.W. Ralston, eds. (Kluwer Academic Publishers, Boston, 1993), p. 277.
- [3] H. Piel, H. Chaloupka, and G. Müller, in *Advances in Superconductivity IV*, H. Hayakawa and N. Koshizuka, eds. (Springer Verlag, 1992), p. 925.
- [4] W.G. Lyons, M.M. Seaver, D.R. Arsenault, R.R. Boisvert, and T.C.L.G. Sollner, *Micro. and Opt. Techn. Lett.* 6, 728 (1993).
- [5] L. Lee, and W.G. Lyons, *Proceedings 1994 IEEE International Microwave Symposium*, (IEEE, New York, 1994), p. XIV.
- [6] G-C. Liang, C.F. Shin, D. Zhang, R.S. Withers, M.E. Johansson, W. Rudy, B.F. Cole, M. Krivoruchko, and D.E. Oates, *Proceedings 1994 IEEE International Microwave Symposium*, (IEEE, New York, 1994), p. 183.



Richard W. Ralston
MIT Lincoln Laboratory
Lexington, MA 02173

BIOGRAPHY

Richard W. Ralston received the B.S. and M.S. degrees in electrical engineering from Lehigh University in 1965 and 1966 and the Ph.D degree in applied physics from Yale University in 1971. From 1965 to 1966 he was at Bell Telephone Laboratories, where he participated in the development of microwave devices. He joined MIT Lincoln Laboratory in 1971, and first researched tunable-wavelength diode lasers and then investigated programmable acoustoelectric filters. He has been working in the Analog Device Technology Group since 1974. Appointed in 1984 as leader of that group, he oversees the development of charge-coupled devices and superconductive circuits. Both device categories are targeted at real-time signal-processing applications. Dr. Ralston has also served as principal director of the Consortium for Superconductive Electronic, since its formation in 1989.

ADVANCES IN HIGH TEMPERATURE SUPERCONDUCTING MATERIALS AND COMPONENTS

Alan Lauder, Charles Wilker, Zhi Yuan Shen, Philip S. W. Pang,
William L. Holstein, Dennis J. Kountz, and Dean W. Face

DuPont
Wilmington, Delaware

ABSTRACT

The key to product performance is the understanding and precise control of materials. Large area high temperature superconductor (HTS) thin films in several materials $\text{YBa}_2\text{Cu}_3\text{O}_7$, $\text{Ti}_2\text{Ba}_2\text{CaCu}_2\text{O}_8$, and $(\text{Ti,Pb})\text{Sr}_2\text{Ca}_2\text{Cu}_3\text{O}_9$ are available now and ready for use in rf and microwave components. Important materials properties, critical temperature and surface resistance, their uniformity and reproducibility are discussed. The ability to handle high current in long meander lines at dc is reviewed and more importantly for microwave and high speed digital applications, the excellent high power handling performance of HTS materials are shown. The demonstration of HTS materials in low insertion loss filters and low phase noise oscillators operational up to 107 K is also summarized.

INTRODUCTION

Materials requirements for high temperature superconductors (HTS) needed to fabricate HTS microwave and high speed digital devices and systems are applications specific. In order to avoid sub-optimal system performance, HTS components manufacturers will need to acquire a "tool chest" that includes several HTS compositions, multiple substrate options, new passivation materials and high resolution fabrication processing. Key HTS materials performance factors are critical temperature (T_c), surface resistance (R_s), critical current (J_c), power handling, and performance parameter stability to small thermal changes around the HTS device operating temperature. In addition, HTS wafers must be available in large area, coated on both top and bottom surfaces, with excellent uniformity across the wafer in both performance factors and HTS film thickness, environmentally stable or with an appropriate

passivation layer, containing zero defects and low cost. The processes to manufacture these superconducting wafers must therefore be safe, zero polluting, highly reproducible, with high throughput and yield. HTS thin film wafer production has been demonstrated at low throughput rates and modest yields which has enabled the fabrication of many prototype high performance HTS passive microwave devices.

In this paper we describe several superconducting thin film compositions developed on large area substrates which show excellent T_c , R_s , and J_c performance properties uniformity and run to run reproducibility. As power handling is critical for several applications, we describe three methods to measure a HTS-sapphire resonator for the evaluation of unpatterned thin films, a third order intercept (TOI) measurement and a stripline resonator operated at multiple power levels. Performance of $\text{Ti}_2\text{Ba}_2\text{CaCu}_2\text{O}_8$ material is shown for all techniques and $\text{YBa}_2\text{Cu}_3\text{O}_7$ and $\text{Ti}_2\text{Ba}_2\text{CaCu}_2\text{O}_8$ materials are compared at 5.55 GHz in the HTS-sapphire resonator. Finally, examples of high performance HTS filters and oscillators are also shown.

MATERIAL PERFORMANCE

Critical Temperature, T_c . The critical temperature, T_c , is an intrinsic property of the superconducting material and reflects the chemical composition, stoichiometry and crystallographic phase. It is also potentially impacted by any interaction with the substrate, defect in the thin film, or loss of epitaxy. T_c is important from a device and system operational perspective, (i) the higher the T_c is above the operating temperature, the greater the

operating safety margin, (ii) performance factors, such as R_s , degrade rapidly as T_c is approached and sensitivity in performance to small variations in temperature, $\Delta R_s/\Delta T$, can translate into device degradation such as frequency drift in a resonator and (iii) if the device is contained in a cryocooler, then the operating temperature has a direct impact on the cryocooler power requirements and hence size, weight and reliability.

We have fabricated thin films of several HTS compositions with T_c values ranging from 90 to 123 K as shown in Table 1. The preferred substrate which produces the best epitaxy in thallium containing superconductors, is lanthanum aluminate, LaAlO_3 . $\text{YBa}_2\text{Cu}_3\text{O}_7$ is compatible with LaAlO_3 , magnesium oxide, and yttrium stabilized zirconia (YSZ). In some cases a buffer layer of cerium oxide, CeO_2 , is used to improve the superconductor epitaxy. For sapphire, such a buffer layer is essential to engender superconductor chemical compatibility with the substrate. The thin film compositions featured primarily in this paper are $\text{YBa}_2\text{Cu}_3\text{O}_7$, $\text{Ti}_2\text{Ba}_2\text{CaCu}_2\text{O}_8$, and $(\text{Ti,Pb})\text{Sr}_2\text{Ca}_2\text{Cu}_3\text{O}_9$ as performance characteristics of these materials have been largely optimized through extensive process development, and all are produced as 2-inch (5.1 cm) and 3-inch (7.6 cm) diameter wafers.

Table 1. High temperature superconducting thin film compositions and respective T_c values.

Superconductor	T_c (K)
$\text{YBa}_2\text{Cu}_3\text{O}_7$	92
$\text{TiBa}_2\text{CaCu}_2\text{O}_7$	90
$\text{TiBa}_2(\text{Ca,Y})\text{Cu}_2\text{O}_7$	98
$\text{Ti}_2\text{Ba}_2\text{CaCu}_2\text{O}_8$	106
$\text{TiBa}_2\text{Ca}_2\text{Cu}_3\text{O}_9$	110
$\text{Ti}_2\text{Ba}_2\text{Ca}_2\text{Cu}_3\text{O}_{10}$	120
$(\text{Ti,Pb})\text{Sr}_2\text{CaCu}_2\text{O}_7$	91
$(\text{Ti,Pb})\text{Sr}_2(\text{Ca,Y})\text{Cu}_2\text{O}_7$	108
$(\text{Ti,Pb})\text{Sr}_2\text{Ca}_2\text{Cu}_3\text{O}_9$	123

Surface Resistance, R_s . Low R_s is a critical performance parameter for HTS thin films and translates directly to low insertion loss and high Q-values in passive microwave circuits such as resonators, filters, multiplexers, power splitters/combiners, delay lines, antennas and

antenna feed networks as well as HTS/semiconductor hybrid circuits such as amplifiers, oscillators and mixers.^{1,2} At microwave frequencies, HTS thin films have 10 to 1000 times lower R_s than copper. The R_s of HTS films can be measured by a variety of methods.² Measurements reported in this paper were made by the parallel plate resonator technique³ and more extensively by the HTS-sapphire resonator technique.⁴ The lowest reported R_s performance obtained with a pair of $\text{Ti}_2\text{Ba}_2\text{CaCu}_2\text{O}_8$ thin films demonstrates the close correlation between these two techniques and is shown in Figure 1.

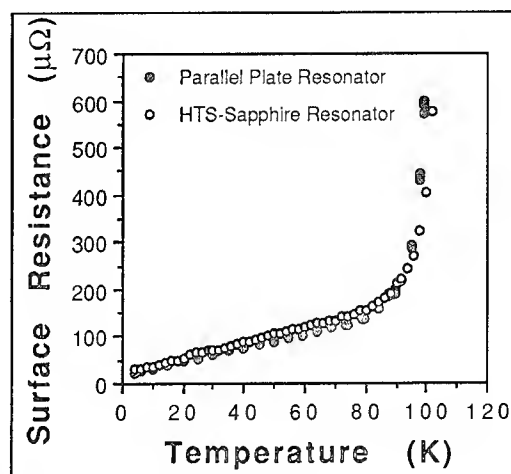


Figure 1. R_s scaled to 10 GHz as f^2 versus temperature for a pair of $\text{Ti}_2\text{Ba}_2\text{CaCu}_2\text{O}_8$ thin films on LaAlO_3 as measured by the parallel plate resonator technique at 12 GHz and the HTS-sapphire resonator technique at 27.45 GHz.

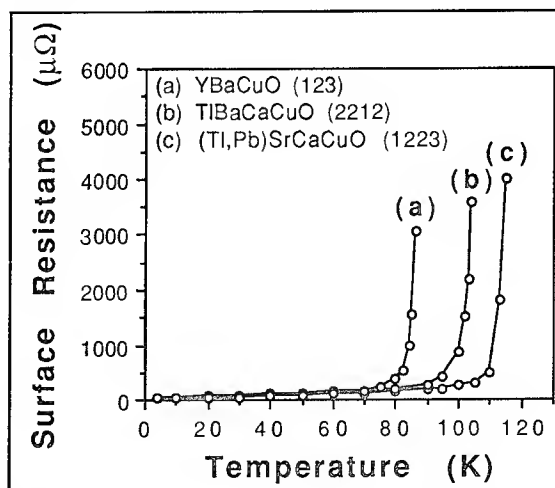


Figure 2. Comparison of HTS thin film materials on LaAlO_3 substrates measured by the HTS-sapphire resonator technique at 27.45 GHz and scaled to 10 GHz by f^2 .

At 77K and 10 GHz R_s is $130 \pm 20 \mu\Omega$ and $150 \pm 10 \mu\Omega$ for the two respective techniques. At 90K, R_s values are $200 \pm 40 \mu\Omega$ and $212 \pm 20 \mu\Omega$, respectively. A comparison of $\text{YBa}_2\text{Cu}_3\text{O}_7$, $\text{Ti}_2\text{Ba}_2\text{CaCu}_2\text{O}_8$ and $(\text{Ti,Pb})\text{Sr}_2\text{Ca}_2\text{Cu}_3\text{O}_9$ on LaAlO_3 substrates shows the impact of T_c on R_s temperature sensitivity, $\Delta R_s/\Delta T$, Figure 2. Below 70 K temperature sensitivity for all three materials is comparable. At 77 K, $\Delta R_s/\Delta T$ is increasing for $\text{YBa}_2\text{Cu}_3\text{O}_7$ while the thallium superconductors display a flat response to changes in temperatures. HTS materials R_s properties can also be compared versus oxygen free high conductivity copper (OFHC), Table 2.

Table 2. Comparison of R_s for three HTS materials versus copper at the same temperature as measured by the HTS-sapphire resonator technique at 27.45 GHz and scaled to 10 GHz by f^2 .

Composition	Improvement in R_s vs. OFHC Copper					
	70K	80K	90K	100K	110K	115K
$\text{YBa}_2\text{Cu}_3\text{O}_7$	52x	26x	-	-	-	-
$\text{Ti}_2\text{Ba}_2\text{CaCu}_2\text{O}_8$	50x	61x	61x	30x	-	-
$(\text{Ti,Pb})\text{Sr}_2\text{Ca}_2\text{Cu}_3\text{O}_9$	60x	65x	62x	49x	26x	9x

R_s and T_c Uniformity Within A Wafer. The uniformity of the R_s properties across a 3 inch

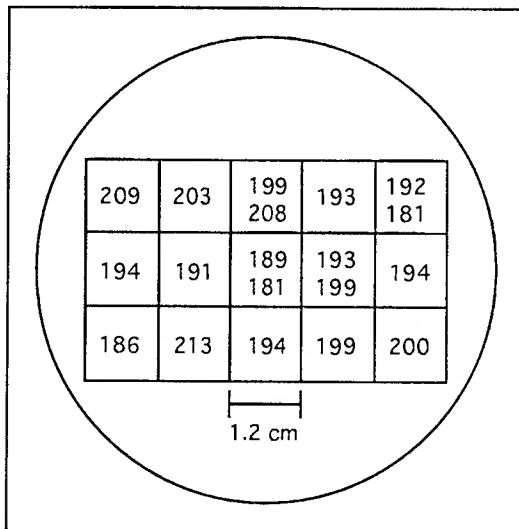


Figure 3. R_s values in $\mu\Omega$ at 10 GHz and 80 K for a 3 inch (7.6 cm) diameter LaAlO_3 wafer coated with $\text{Ti}_2\text{Ba}_2\text{CaCu}_2\text{O}_8$ thin film and diced into fifteen 1.2 cm squares for evaluation by the 27.45 GHz HTS-sapphire resonator technique.

(7.6 cm) diameter LaAlO_3 wafer coated with a $\text{Ti}_2\text{Ba}_2\text{CaCu}_2\text{O}_8$ thin film was determined by dicing the wafer into 15 squares and measuring the R_s of each in the 27.45 GHz HTS-sapphire resonator. R_s , scaled to 10 GHz by f^2 , at 80 K is shown in Figure 3 and ranges from $181 \mu\Omega$ to $213 \mu\Omega$ with an average value of $196 \mu\Omega$. HTS film thickness ranges from $0.55 \mu\text{m}$ at the edge of the 3 inch wafer to $0.70 \mu\text{m}$ in the center. Within the ± 1 K measurement accuracy of the inductive T_c technique, all fifteen films are identical with a T_c of 103 ± 1 K.⁵

R_s and T_c Reproducibility - Wafer to Wafer. The process to fabricate $\text{Ti}_2\text{Ba}_2\text{CaCu}_2\text{O}_8$ thin films on LaAlO_3 substrates comprises two steps. First Ba, Ca, and Cu oxides are deposited as a precursor film by rf sputtering and followed by a separate thallination anneal step. In order to evaluate wafer to wafer reproducibility a series of forty successive depositions of precursor were made.⁵ Three of these depositions were on silicon wafers for the determination of compositional uniformity throughout the run. The remaining 37 substrates were thallinated and annealed. These substrates comprised 29 LaAlO_3 2 inch (5.1 cm) diameter wafers for component development purposes and 8 LaAlO_3 1.2 cm squares interspersed throughout the run for T_c and R_s quality control evaluation. The positions of the test wafers in the run, the T_c and R_s values measured at 27.45 GHz in the HTS-sapphire resonator and scaled to 10 GHz f^2 are shown in Table 3. Within the limits of the inductive T_c measurement technique, all 8 test samples are equivalent with $T_c = 104 \pm 1$ K. R_s at 10 GHz and 80 K average $168 \mu\Omega$ and ranges from a low of $147 \mu\Omega$ to a high of $214 \mu\Omega$.

Table 3. R_s and T_c reproducibility over a run of 40 wafers encompassing 8 test samples.

Run Number	T_c (K)	R_s ($\mu\Omega$)
		at 10 GHz and 80 K
2	105	147
6	105	148
10	104	147
14	105	175
18	105	147
26	105	214
33	103	175
39	105	189

Critical Current, J_c . The current density at which a superconductor shows a non-zero dc resistivity is known as the critical current density, J_c . A standard four-point measurement of a patterned HTS meander is used to measure the volume resistivity, ρ , versus J , shown in Figure 4.

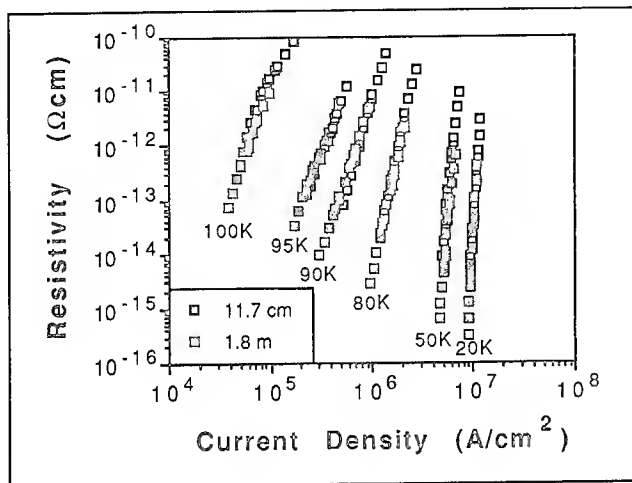


Figure 4. Resistivity versus current density, J , for a 12 μm wide by 1,800 mm long section and a 117 mm long subsection of a $\text{Tl}_2\text{Ba}_2\text{CaCu}_2\text{O}_8$ meander on a LaAlO_3 substrate. This data was collected by a standard dc four-point measurement.

$\rho = (R A)/L = (V/L)/(I/A) = E/J$ where L is the length of the meander, A is cross sectional the area and E is the tangential electric field. All of these data show that the HTS ρ values are at least four orders of magnitude lower than copper at the same temperature. It is also important to note that the J_c of a HTS depends not only upon its intrinsic properties but also upon extrinsic properties, e.g. film defects. Since the data for the 1.8 meter long meander are coincident with those of the 11.7 cm meander the HTS film used to fabricate these meanders is high quality with low defect density.

Using the criterion that the transverse electric field, $E = 1 \mu\text{V}/\text{cm}$, the plot of J_c versus temperature can be generated, Figure 5.^{6,7} At 20 K, J_c is $1 \times 10^7 \text{ A}/\text{cm}^2$ and at 77 K, J_c is $2 \times 10^6 \text{ A}/\text{cm}^2$. Retesting of the meander after aging for three months under ambient laboratory conditions showed essentially identical performance indicating the

environmental stability of the $\text{Tl}_2\text{Ba}_2\text{CaCu}_2\text{O}_8$ system.

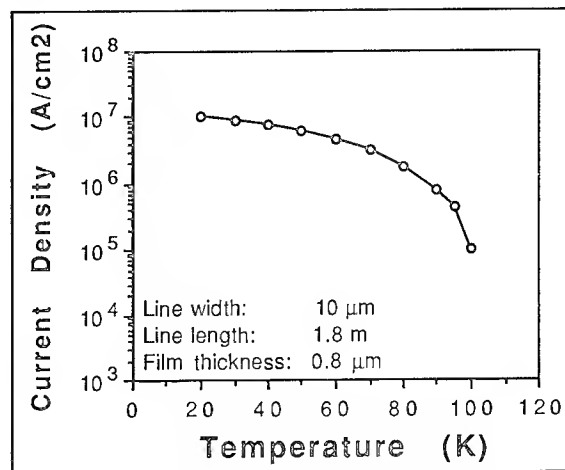


Figure 5. Critical current, J_c , for $\text{Tl}_2\text{Ba}_2\text{CaCu}_2\text{O}_8$ on LaAlO_3 patterned as a meander line 1.8 m long and 10 μm wide.

POWER HANDLING

The critical current, J_c , is a dc phenomenon that is inadequate as a measure of power handling in rf and high speed digital applications. The simplest way to measure the rf power handling of a HTS circuit is to fabricate the circuit and increase the input power while measuring one of its key properties. Power handling capability within any given circuit is, however, a reflection of (i) the HTS material quality, (ii) deterioration created by the fabrication processing and (iii) the design of the circuit.

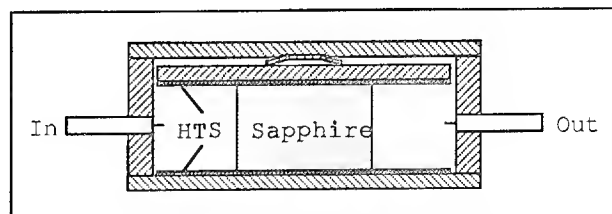


Figure 6. HTS-sapphire resonator formed as a HTS-sapphire-HTS sandwich held in an oxygen-free copper package using a beryllium copper spring.

Ideally, for HTS thin film development, comparison and quality assurance, we need a power handling method that evaluates the unpatterned HTS wafer and hence the uncompromised materials contribution. We have

therefore developed a HTS-sapphire resonator technique for this purpose.⁴ The 5.55 GHz resonator shown in Figure 6 utilizes a sapphire rod 1.00 x 0.47 inches (2.54 x 1.20 cm) sandwiched between a pair of HTS films of 2 inch (5.1 cm) diameter. Operating frequency is a function of the sapphire rod dimensions. The material property R_s , and the resonator property, Q-value, can be measured as a function of local rf magnetic field, rf current density, or circulating power stored in the cavity. Excellent power handling is observed for both $\text{YBa}_2\text{Cu}_3\text{O}_7$ on LaAlO_3 , Figure 7, and $\text{Tl}_2\text{Ba}_2\text{CaCu}_2\text{O}_8$ on LaAlO_3 , Figure 8.

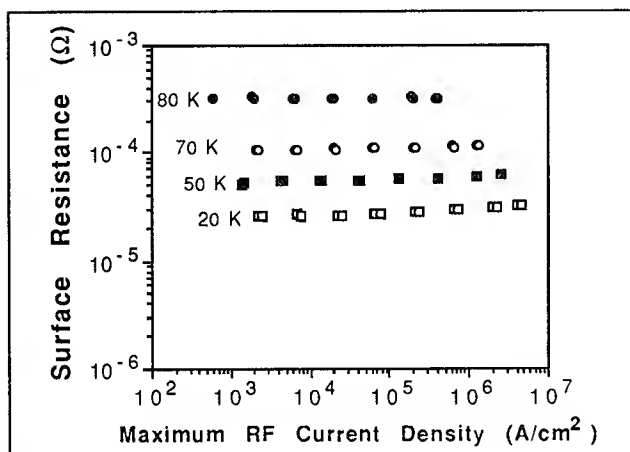


Figure 7. Surface resistance versus maximum rf current density for a pair of 2 inch (5.1 cm) diameter $\text{YBa}_2\text{Cu}_3\text{O}_7$ thin films measured at 5.55 GHz using a HTS-sapphire resonator technique.

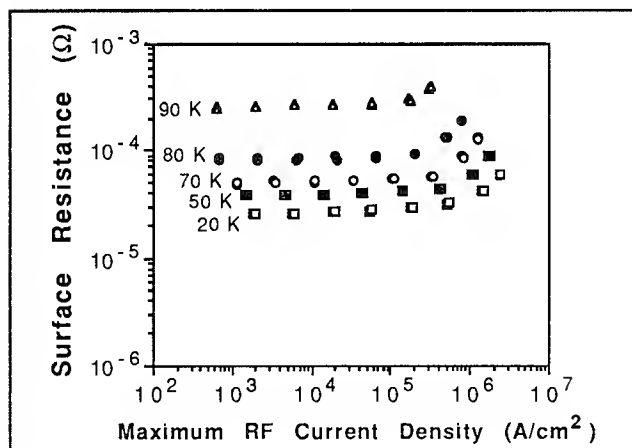


Figure 8. Surface resistance versus maximum rf current density for a pair of 2 inch (5.1 cm) diameter $\text{Tl}_2\text{Ba}_2\text{CaCu}_2\text{O}_8$ thin films measured at 5.55 GHz using a HTS-sapphire resonator technique.

At 80 K and 5.55 GHz the surface resistance of $\text{YBa}_2\text{Cu}_3\text{O}_7$ thin films is ca. $300 \mu\Omega$ up to a maximum rf current density of $3 \times 10^5 \text{ A/cm}^2$. At 70 K, R_s is ca. $100 \mu\Omega$ up to $1 \times 10^6 \text{ A/cm}^2$ before the superconductor turns "normal". At any given temperature, the R_s of the thallium thin film is typically lower, i.e. superior, to that of $\text{YBa}_2\text{Cu}_3\text{O}_7$ although this advantage is reversed at low temperatures and high current densities. The surface resistance for $\text{Tl}_2\text{Ba}_2\text{CaCu}_2\text{O}_8$ films at 80 K and 5.55 GHz is ca. $100 \mu\Omega$ up to $2 \times 10^5 \text{ A/cm}^2$ maximum rf current density, and remains $<100 \mu\Omega$ at 70 K to $1 \times 10^6 \text{ A/cm}^2$.

The surface impedance, Z_s , of a HTS thin film is not only a function of the temperature and frequency but also of the local current density or the local magnetic field. It is this dependence upon the local current density that yields a nonlinearity that can generate harmonics or mix different frequency components causing intermodulation distortion. Microwave circuits made from inferior HTS materials typically show nonlinear effects at relatively low power level. Such materials deficiencies can be erroneously interpreted resulting in the belief that harmonic generation and intermodulation distortion are a serious limitation for HTS microwave applications which require a clean spectrum. We have developed and extensively characterized a third order intercept procedure that measures harmonic generation utilizing a simply

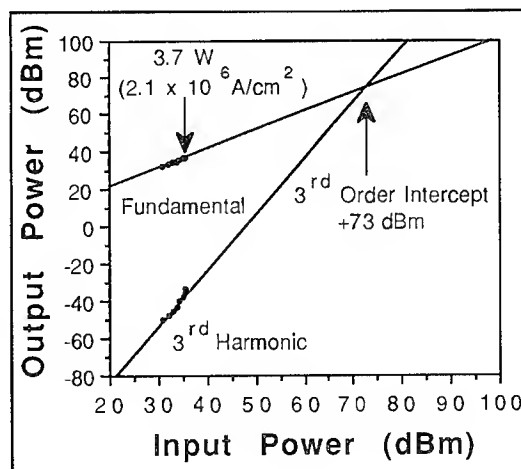


Figure 9. Output power versus input power for a $30 \mu\text{m}$ wide by 5 mm long 50Ω $\text{Tl}_2\text{Ba}_2\text{CaCu}_2\text{O}_8$ coplanar transmission line at 1.0 GHz and 80 K. This data was collected using a single tone as an input.

patterned HTS coplanar transmission line. A plot of the input power versus the output power for a 5 mm long by 30 μm wide 50 Ω HTS coplanar transmission line is shown in Figure 9. For a fundamental input frequency of 1 GHz, at 80 K, the third order intercept is +73 dBm. At a input power level of 3.7 W (which corresponds to a current density of $2.1 \times 10^6 \text{ A/cm}^2$), the third harmonic is more than 75 dB down from the fundamental. This excellent material performance provides new opportunities for microwave engineers to design innovative HTS microwave circuits that realize unprecedented high performance not only for low power applications but also for moderate and high power applications.

The rf power handling of a circuit can be measured directly. As an example, the power handling of a half-wave length microstrip line resonator is shown in Figure 10.⁸

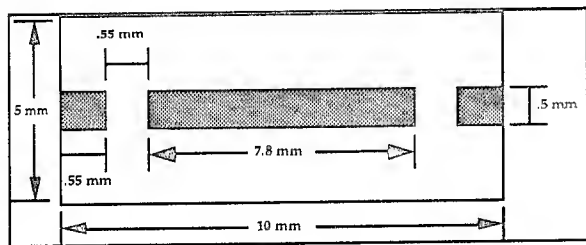


Figure 10. $\text{Ti}_2\text{Ba}_2\text{CaCu}_2\text{O}_8$ microstrip line resonator.

The loaded Q-values, Q_L , are plotted versus the input power measured at several temperatures in Figure 11.

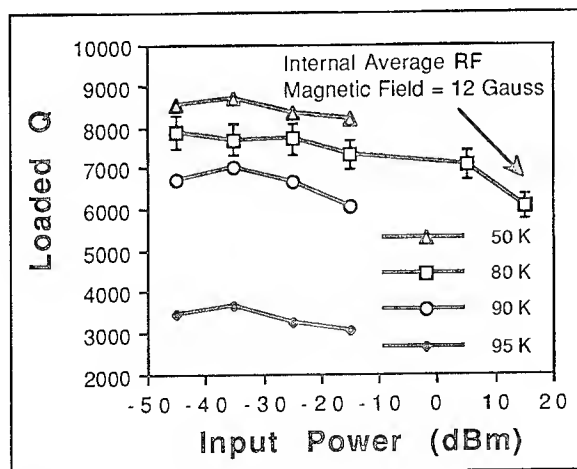


Figure 11. Loaded Q-value versus input power for a $\text{Ti}_2\text{Ba}_2\text{CaCu}_2\text{O}_8$ microstripline resonator.

At 80 K and +15 dBm the loaded Q-value drops 25% from its low power value. This resonator can handle 32 mW of input power, of which only about ten percent is actually dissipated within the resonator, the rest of the power is either reflected or transmitted. For a Q_L of 6,000, this corresponds to approximately 20 W of circulating power. This means that if the two coupling gaps of the resonator were eliminated to form a 500 μm wide HTS microstrip transmission line, then the line would be capable of carrying up to 20 W of continuous (cw) power with only a 25% degradation of its insertion loss. Other resonant type HTS components such as filters show a similar power handling behavior.

HTS MICROWAVE DEVICES

We have fabricated a large number of HTS passive microwave circuits such as resonators, filters, multiplexers, power splitter/combiners, delay lines, antennas and antenna feed networks as well as several HTS/semiconductor hybrid circuits such as amplifiers, oscillators, mixers and receiver front ends, which have shown exceptionally good performance.^{1,2} The unique benefits of HTS materials are exemplified here by two examples, filters and oscillators.

Filters, filter banks and multiplexers are important components of wireless communications equipment which requires narrow bandwidth, low in-band insertion loss, high out of band rejection and steep skirts. A C-band, 3-pole microstrip line filter made from $\text{Ti}_2\text{Ba}_2\text{CaCu}_2\text{O}_8$ on LaAlO_3 , is shown in Figure 12 and its performance is shown in Figure 13.

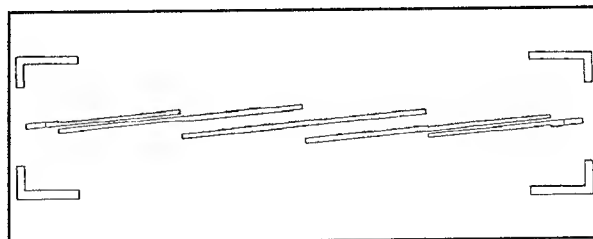


Figure 12. C-band, 3-pole microstrip line filter made from $\text{Ti}_2\text{Ba}_2\text{CaCu}_2\text{O}_8$ on LaAlO_3 .

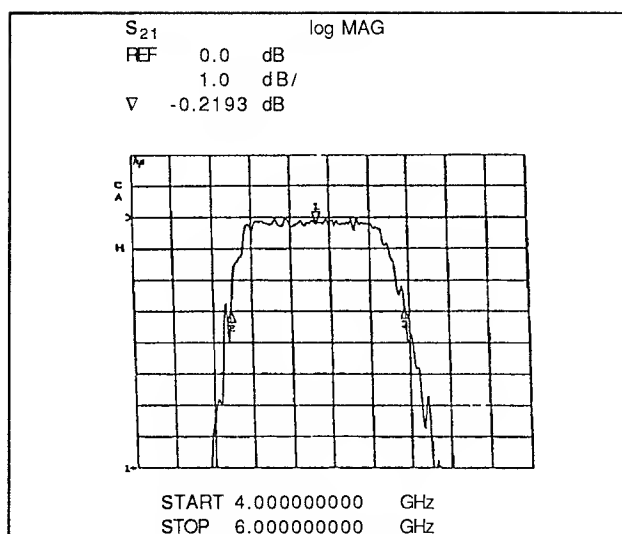


Figure 13. A 3-pole $\text{Ti}_2\text{Ba}_2\text{CaCu}_2\text{O}_8$ microstrip line filter showing in-band insertion loss of 0.2 dB.

The total in-band insertion loss for the HTS filter is 0.2 dB, which is mainly due to the reflection loss from the input and output connectors. Such miniature microstrip line filters are ideal for replacing the bulky waveguide filters in receivers. Where high power handling capability is required for transmitters, compact HTS-sapphire cavity filters can be used.

HTS resonators are also ideally suited to be used in oscillators as the extremely high Q-values achievable translate into low phase noise and small size. The block diagram of such an oscillator is shown in Figure 14 and a schematic, utilizing a HTS microstrip resonator as the feedback element, is shown in Figure 15.

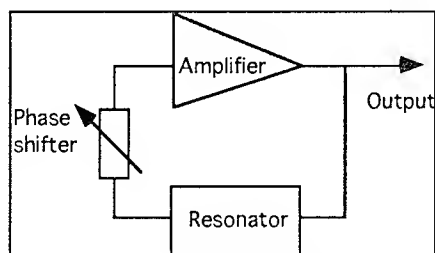


Figure 14. Block diagram for a HTS low phase noise oscillator.

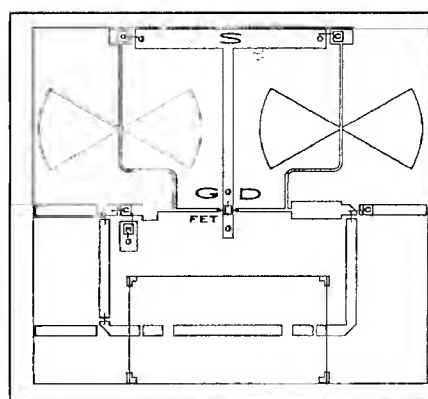


Figure 15. Schematic of a HTS low phase noise oscillator, utilizing a microstrip line HTS resonator.

The total noise of the oscillator shown in Figure 15 is -106 dBc/Hz at 10 kHz off-set from the 5 GHz carrier frequency. In order to achieve even lower phase noise, the microstrip resonator was replaced with a high Q-value HTS-sapphire resonator. A Fujitsu FHR10X HEMT which exhibits 3 dB more gain and 0.4 dB less noise at cryogenic temperature compared to room temperature was selected as the active device in the amplifier.¹² This amplifier was incorporated with the HTS-sapphire resonator as the frequency stabilizer operated at 5.55 GHz and 80 K. This oscillator provides 10 mW output power with an efficiency of 30%. Figure 16 shows the measured phase noise versus off-set frequency from the carrier. At 10 kHz off-set, the measured phase noise was -125 dBc/Hz, which was actually limited by the measurement instrumentation.

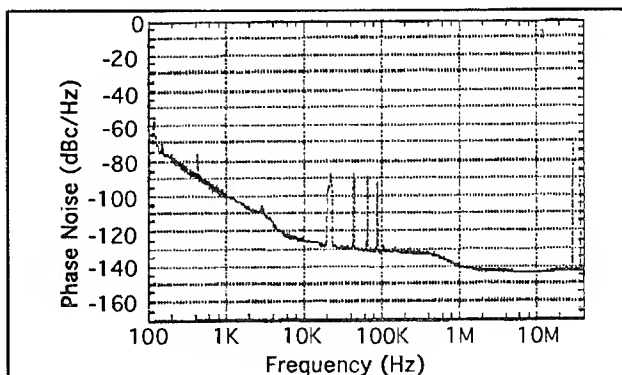


Figure 16. Phase noise versus frequency for a C-band HTS oscillator. At 10 kHz off-set the phase noise is -125 dBc/Hz which is a measurement limit within the test setup.

Through appropriate selection of HTS materials, the operating temperature can be changed substantially or the operating safety margin of the component enhanced. Utilizing the same block diagram shown in Figure 14, we fabricated a low phase noise Ka-band HTS oscillator. A MITEQ 25002800-24-S-4 custom made amplifier with 25 dB gain and 2.4 dB noise figure was used in the circuit. Frequency stabilization was effected with a 27.45 GHz HTS-sapphire resonator using (TiPb)Sr₂Ca₂Cu₃O₉ on LaAlO₃ superconductor and a sapphire rod 5 x 2 mm. Operating as high as 107.5 K, the measured total noise is -94.5 dBc/Hz at 10 kHz off-set, which is again limited by the test setup, Figure 17.

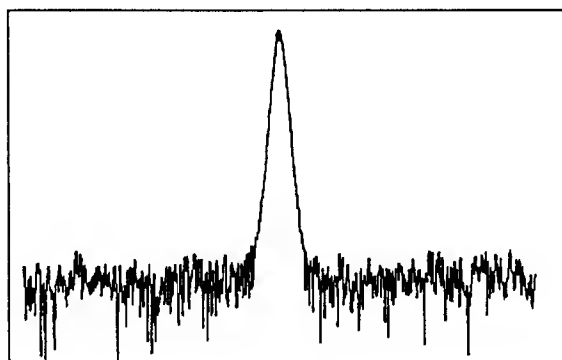


Figure 17. Total noise spectrum for a HTS-sapphire oscillator operating at 107.5 K and 27.45 GHz. The horizontal scale is centered at 27.453 GHz with a span of 100 kHz. The vertical scale is -100 to 0 dB. The total noise, including phase noise, is less than -94 dBc/Hz at 10 kHz offset and is limited by the spectrum analyzer.

The entire oscillator can be packaged into a one cubic inch case and powered by a small battery. The small size and the low power requirement make it very attractive for portable equipment.

SUMMARY

Considerable progress has been made at DuPont towards the goal of achieving practical circuits for rf, microwave and digital applications. Demonstration devices reviewed in this paper include a compact filter with in-band insertion loss < 0.2 dB, and a compact oscillator operating at 107.5 K and 27.5 GHz with total noise less than -94.5 dBc/Hz at 10 kHz off-set. Noise values were limited by the measurement equipment. High temperature superconductor thin films are fabricated as large area high performance wafers on a variety

of substrates. Extremely low surface resistance and high power handling capability of these superconductors is demonstrated thereby establishing the materials underpinning for superconducting systems development.

ACKNOWLEDGMENTS

The authors wish to acknowledge the invaluable assistance in film and device fabrication and testing of Charles Carter, III, Michael S. Brenner, Louis A. Parisi, Robert J. Small, Frank M. Pellicone, Mark S. Warrington, Joseph P. Nestlerode and Steven P. McKenna.

REFERENCES

- [1] J. Brown, "Superconducting Circuits Make Practical Strides," *Microwave & RF*, July 1993, pp. 123-126.
- [2] Z-Y. Shen, "High Temperature Superconducting Microwave Circuits," *Artech House*, Boston, 1994.
- [3] R.C. Taber, *Rev. Sci. Instrumen.*, vol. 61, pp. 2200, 1990.
- [4] C. Wilker, Z-Y. Shen, V.X. Nguyen and M.S. Brenner, "A Sapphire Resonator for Microwave Characterization of Superconducting Thin Films," *IEEE Trans. Appl. Supercon.*, vol. 3, pp. 1457-1460, 1993.
- [5] W.L. Holstein, L.A. Parisi, Z-Y. Shen, C. Wilker and M.S. Brenner, "Surface Resistance of Large Area Ti₂Ba₂CaCu₂O₈ Thin Films at Microwave and Millimeter Wave Frequencies Measured by Three Non-Cavity Techniques," *J. Supercon.*, vol. 6, pp. 191-200, 1993.
- [6] W.L. Holstein, C. Wilker, D.B. Laubacher, D.W. Face, P.S.W. Pang, M.S. Warrington, C.F. Carter and L.A. Parisi, "Critical Current Density and Resistivity Measurements for Long Patterned Lines in Ti₂Ba₂CaCu₂O₈ Thin Films," *J. Appl. Phys.*, vol. 74, pp. 1426-1430, 1993.
- [7] A. Lauder, C. Wilker, D.J. Kountz, W.L. Holstein and D.W. Face, "High Performance Superconducting Thin Films on Large Area Substrates," *IEEE Trans. Appl. Supercon.*, vol. 3, pp. 1683-1686, 1993.
- [8] C. Wilker, Z-Y. Shen, P.S.W. Pang, D.W. Face, W.L. Holstein, A.L. Matthews and D.B. Laubacher, "5 GHz High-Temperature-Superconductor Resonators with High Q and Low Power Dependence up to 90 K," *IEEE Trans. MTT*, vol. 39, pp. 1462-1467, 1991.
- [9] Z-Y. Shen, C. Wilker, P.S.W. Pang, W.L. Holstein, D.W. Face, and D.J. Kountz, "High T_c Superconductor-Sapphire Resonator with Extremely High Q-Values up to 90 K," *IEEE Trans. MTT*, vol. 40, pp. 2424-2432, 1992.
- [10] Z-Y. Shen, C. Wilker, P.S.W. Pang, D.B. Laubacher, W.L. Holstein, D.W. Face, D.J. Kountz, A.L. Matthews, J.M. Meriwether and C.F. Carter, "High T_c Superconducting Device Development at DuPont," *1992 IEEE Antenna & Propagation Society International Symposium Digest*, vol. 2, pp. 970-973, 1992.

- [11] Z-Y. Shen, C. Wilker, P.S.W. Pang, C.F. Carter, V.X. Nguyen and D.B. Laubacher, "High Temperature Superconductor/III-V Hybrid Microwave Circuits," *Microwave and Optical Technology Letters*, vol. 6, pp. 728-732, 1993.
- [12] C. Wilker, P.S.W. Pang, C.F. Carter and Z-Y. Shen, "S-Parameter, I-V Curve and Noise Figure Measurements of III-V Devices at Cryogenic Temperatures," *1992 Automatic RF Techniques Conference Digest*, pp. 71-79, 1992.

AUTHORS



Alan Lauder
DuPont
Wilmington, Delaware

Alan Lauder is General Manager, Superconductivity in DuPont's Central Research and Development. For the past seven years he has had global responsibility for DuPont's new business development program in superconductivity. At DuPont he has more than 20 years of management experience in bringing research technology from

the laboratory to the commercial marketplace and plant manufacturing site. He is the current Chairman of CSAC, the U.S. trade association representing the superconductivity industry. Dr. Lauder has a B.Sc. (Hons.) and a Ph.D. in Chemistry from the University of Durham in England and a MBA from the University of Delaware.



Charles Wilker
DuPont
Wilmington, Delaware

Charles Wilker is a Senior Research Physicist in DuPont's Superconductivity organization where he has for 7 years been responsible for the characterization of HTS thin films and components. He has a B.A. in Physics from Swarthmore and an M.S. and Ph.D. in Chemistry from Cornell.



Zhi-Yuan Shen
DuPont
Wilmington, Delaware

Zhi-Yuan Shen is an Engineering Fellow in DuPont's Superconductivity organization. He is responsible for the design and development of passive HTS components and active HTS/III-V hybrids. Dr. Shen has a B.S. and Ph.D. (Electrical Engineering) from the Zhejiang University where he was the Director of the University Microwave and Millimeter-Wave Laboratory.



Philip S. W. Pang
DuPont
Wilmington, Delaware

Philip Pang is a Senior Research Engineer in DuPont's Superconductivity organization and is responsible for the layout and fabrication of HTS components. He has a B.Sc. from Polytechnic of North London and an M.Sc. and Ph.D. in Electronics from University of Kent.



William L. Holstein
DuPont
Wilmington, Delaware

William Holstein is a Research Associate in DuPont's Superconductivity organization. He has developed processes for the fabrication of thallium thin films and contributed to the fundamental understanding of the mechanisms of film growth. Dr. Holstein has a B.S.E. in Chemical Engineering from Princeton and an M.S. and Ph.D. (Chemical Engineering) from Stanford University.



Dennis J. Kountz
DuPont
Wilmington, Delaware

Dennis Kountz is a Senior Research Chemist in DuPont's Superconductivity organization and is responsible for thallium/lead thin film development of applications of superconductor technology to non-destructive tests applications. He has a B.A. in Physics and Chemistry from Wittenberg University and an M.S. and Ph.D. in Physical Chemistry from Ohio State University.



Dean W. Face
DuPont
Wilmington, Delaware

Dean Face is a Senior Research Physicist in DuPont's Superconductivity organization. He is currently working on the development of in situ thallium processing buffer layers, SQUIDs, tunnel junctions and high Tc thin films and devices. Dr. Face has a B.S. from Caltech and an M.S. and Ph.D. in Applied Physics from Yale University.

THE ARPA HIGH TEMPERATURE SUPERCONDUCTIVITY PROGRAM

Stuart A. Wolf

Advanced Research Projects Agency, Arlington VA 22203
Permanent Address: Naval Research Laboratory, Washington DC 20375-5000

ABSTRACT

This paper will present an overview of the ARPA project on high temperature superconductivity. This multidisciplinary effort has, since 1987, spent well over \$200,000,000 on promoting the science and technology of these materials. The program has recently been focused on several very promising applications of this emerging technology. Support of many aspects of R and D has been provided to universities, national laboratories and an emerging industrial base. The current program is focused on 1) the development of RF and microwave passive components and subsystems for applications to radar, electronic warfare, wireless communications and medical instrumentation 2) developing digital applications of cryogenic technology both utilizing superconductors as well as semiconductors 3) contributing to the development of a conductor for power applications and 4) developing a variety of low-cost reliable cryocoolers that will be the enabler for many of the aforementioned applications.

INTRODUCTION

The Advanced Research Projects Agency (ARPA) effort on High Temperature Superconductivity (HTSC) is, we believe, the largest single program in the U. S. that has been devoted to the development of the science and technology of these exciting and revolutionary materials. Since 1987, ARPA has supported efforts at universities, national laboratories and industry in efforts that to date have significantly exceeded \$200M.

The program has had three phases. The first phase which extended from the inception of the program in 1987 until approximately 1991 saw the maturation of the synthesis process for the powder precursors as well as the development of various processing techniques for providing bulk monolithic samples as well as the first useful thin films. The limits of the performance of these materials was being explored and projections as to the quality of various components were being made. This phase of the program supported more than 50 projects at a wide variety of contractors.

The second phase started in approximately 1990 and is in its final stages. In this phase various components and simple subsystems were developed. In the RF and microwave area they included simple components such as filters, delay lines, down converters, resonators antennas and antenna coupling networks. In fact many of these were packaged into a satellite payload and were prepared for a launch on the Navy high temperature superconductivity space experiment HTSSE I. It was also clear that these components in a system or subsystem could have a significant impact on many Air Force and Army applications as well. This phase also saw the start of an large effort to develop multi-chip-modules (MCM's) utilizing traces of the cuprate superconductors for wiring. The advantage of these modules would be the ability to connect a very large dense array of semiconductor chips with just two wiring layers compared to the tens of layers that would be required with copper traces. The final demonstration of a superconducting MCM is slated for early 1995.

In the area of bulk materials, monolithic flux trapped magnets were produced that had potential as clamps for adaptive tooling in the aircraft industry as well as magnets for simple motors. Also in this phase we started a joint program with the Navy to develop conductors based on bismuth-strontium-calcium-copper oxide (BSCCO) powder in silver tube (PIT) for use in a prototype motor for shipboard applications.

The Consortium for superconducting Electronic was also started in the second phase and it has been exploring various ways in which companies AT&T, IBM, Conductus and CTI in collaboration with MIT, Cornell and Lincoln Lab can provide a significant technology base for commercial applications. After three years of developing the technology base they are entering the second phase of funding in coincidence with the last phase of the ARPA program and will be pursuing two system applications, cellular base stations for wireless communications and medical instrumentation utilizing Superconducting QUantum Interference Device (SQUID) magnetometers and gradiometers. These very sensitive instruments can non-invasively monitor the heart and other circulatory organs similar to the electrocardiograph.

The last phase of the program started in approximately 1993 and will continue until it transitions to a cryogenics program in 1996. One

of the most important aspects of this phase is the resources that will be applied to develop a number of reliable, low-cost cryocoolers that will be both electrically and physically sized for specific applications of cryogenic systems. The availability of appropriate cryocoolers will be an important enabler for this technology to make it to the marketplace. Overall, the goal of this phase is the development of a series of system demonstrations as well as some military insertions. The results of this last phase will be a justification for the 9 years of support that ARPA provided to the academic, scientific and engineering community to bring this revolutionary technology to the commercial and military marketplace. Some of the major projects that are being pursued in this third and last phase of the high temperature superconductivity program will be described in the next part of this overview.

SYSTEM DEMONSTRATIONS AND INSERTIONS

In this section we will describe some of the major efforts currently underway that we feel will lead to significant military and commercial products for the fledgling superconductor industry.

Filterbanks for Dual Use Applications

One problem with many of our existing aircraft is the degree of interoperability of many of the electronic systems that must work together to provide a highly survivable platform. For example a high power frequency agile radar emanating from one antenna might be picked up by a radar-warning receiver (RWR) antenna located nearby on the same aircraft. It is necessary that the radar signal be filtered out from the input of the RWR so that it is not saturated. Such a complex switched notch filterbank is being developed by Superconductor Technologies Inc. (STI) under ARPA and Air Force sponsorship. A demonstration filterbank consisting of 32 contiguous channels each separately switchable in well under a millisecond has recently been demonstrated. This program will integrate a flightworthy version of these filters into a complete cryogenic package (including cryocooler) that can be directly inserted onto an existing airborne platform so as to demonstrate the efficacy of this approach. The goal will be for the Air Force to commit to buy a superconducting upgrade to its existing electronics. Band pass filterbanks also can be utilized in many other military receivers as preselectors for the signals of interest. For some of these other systems (see radar application below) additional superconducting components are also crucial to enhanced performance.

Similar problems with interference are being experienced by cellular phone providers. Since every large geographic area has two providers A and B with interleaving frequency allocations, it is very important that signals from the A provider don't leak into the B band. Non-superconducting filters do this job, but in the process lose part of each usefull band and hence lose the ability to serve as many customers as

they might with better filters. The superconducting filters can provide significantly better characteristics and hence salvage more of the frequency spectrum that is allotted to each carrier. This can be a very large market for the superconductivity companies if they can meet the cost and performance specifications of the wireless industry.

Stable Oscillators for Radar Applications

The need for better ship defense is well documented especially in a littoral environment with large clutter associated with nearby land masses. Superconductivity offers the ability to fabricate extremely stable resonant cavities that can ultimately reduce the phase noise of the radar by more than an order of magnitude. These resonant cavities with superconducting walls can have quality factors (Q's) of many million, much more than can be achieved with conventional materials. Westinghouse, in collaboration with NRL will be developing and testing an advanced radar incorporating a superconducting stabilized local oscillator that will form the foundation for a significantly improved radar capability.

Cryoelectronics

It has been known for some time that conventional CMOS circuits will function several times faster and with lower voltage requirements at cryogenic temperatures. In fact the original goal of the superconducting MCM effort was to capitalize on this improvement as well as the simpler MCM possible with superconducting traces to provide a strong impetus to go cryogenic for some mainstream electronics. Over the last several year it has become clear that the impediment to a rapid transition to cryoelectronics has been the perception of unreliable, expensive cryocoolers and the lack of cryogenic capability in the mainstream companies. We have decided to take a more conservative approach and get to the goal of liquid nitrogen temperature (77K) in stages. In order to eventually take full advantage of the benefits of a superconducting MCM the I/O's of the semiconductor chips must be increased. This can be accomplished using area array connections rather than edge array interconnects which are currently in general use. Furthermore, much needs to be done to optimize the processing of the chips for low temperature operation. Finally some experience needs to be obtained in cooling the circuits reliably. Cray Research and Motorola are tackling the first few tasks related directly to the chips and the semiconductor processing and STI is addressing the cryocooling issue by developing a simple cooled workstation module that will not contain any superconductivity. Finally the integration of the cooled semiconductor chips with a superconducting MCM will be undertaken when low enough temperatures are reliably reached.

High Performance Network Switch

As we begin to fully utilize the Information Infrastructure and the requirements for high speed transmission and dissemination of voice, images and data expand, there will be the need for a new generation of high performance network

switches. Superconducting Josephson Junction (JJ) devices offer an important benefit for such a new generation of switches. These JJ devices have a fundamental switching time of a small fraction of a picosecond and dissipate nanowatts of power. Thus as the requirements for high throughput network switches handling 100's of channels of data at 10 gigabits persecond per channel rates the size, power and complexity of a conventional technology switch become overwhelming whereas the superconducting JJ implementation of such a switch would be quite small and would dissipate watts as compared to hundreds of kilowatts for a semiconductor switch. Unfortunately a mature JJ technology for the high transition temperature cuprate superconductors has not yet been developed. Thus there is a large risk associated with a program that has the goal of demonstrating a superconducting switch base on a JJ technology that is very immature. Like the cryoelectronics program outlined just above, we will tackle this problem in two stages. We will develop a cryogenic switch with improved performance based on cooled semiconductor technology (Tektronix) and in several years when the HTSC JJ technology matures (being developed by Westinghouse and Conductus), it will be inserted into the highest performance requirement part of the network switch and will ultimately provide the capabilities mentioned above.

Stuart A. Wolf
ARPA/DSO
3701 N. Fairfax Dr
Arlington VA 22203



Dr. Wolf is currently a Program Manager at ARPA but is permanently assigned to the Naval Research Laboratory as the Head of the Materials Physics Branch. Dr. Wolf has been actively involved in superconductivity research for the bulk of his professional career.

Low Cost Manufacturing

For HTSC to be a commercial success will require more than just a few demonstration projects. It will require a low cost supply of superconducting films on large area substrates (>4 inches in diameter) that are compatible with the further processing into the RF and Microwave components and subsystems described above. We will be supporting efforts to provide the vendors of superconducting films with the necessary tools to become cost effective manufacturers so that they can truly compete in the marketplace and reap the benefits of this high performance technology.

SUMMARY

In summary, the HTSC program at ARPA has been pursuing the science and technology of these very important materials since they were discovered and we believe that the field is now poised to make some significant system demonstrations and insertions that will justify the time, money and effort that has been put into this field over the last nine years.

ACKNOWLEDGEMENT

It is a great pleasure to thank Dr. Frank Patten of ARPA who I have been working with for the past several years and is responsible for most of the efforts that have been described in this overview. Without Frank's support and encouragement this manuscript would not have been possible.

High Performance Superconducting Filters for Wireless Systems

Ora E. Smith, President and CEO

Illinois Superconductor Corporation

Abstract

Superconducting RF bandpass filters can increase the capacity and quality of wireless telecommunications systems by enhancing and improving adjacent channel rejection; improving base station receiver sensitivity for weak signals by increasing the signal to noise ratio; improving call quality; and reducing filter insertion losses.

Introduction

The rapid expansion of the wireless telecommunication industry is producing increasing congestion in the UHF and low-microwave RF spectrum. There is a limited amount of RF spectrum available, and each wireless telecommunications service wants to increase its allocation of the limited RF spectrum resource when possible, while maximizing the communications capacity of its allocated spectrum space. New RF spectrum allocations are not an ideal solution to the need for increased communications capacity. The additional spectrum allocation for a specific telecommunications service requires the displacement of existing users of that spectrum space, and the new channels will soon fill to capacity if the service is expanding rapidly. Therefore, the wireless telecommunications industry continues to support new technological solutions that will maximize the communications capacity of the RF spectrum space available to each telecommunications service.

The rapidly expanding cellular telephone communications service provides a good example of the need for improvements in utilization of RF spectrum. The 30% annual growth rate in cellular users that has occurred over the past several years led the Federal Communications Commission (FCC) to allocate additional RF spectrum for cellular telephone use. That spectrum, which has already been saturated in many metropolitan areas, was made available by discontinuing use of some frequencies previously allocated for UHF television services.

The FCC recently auctioned about 790 KHz of spectrum in the frequency range near 2 GHz for use by private licensees. This spectrum auction, which brought in over \$600 million, gives a good indication as to how the marketplace values RF spectrum. For example, the cost for an auctioned nationwide license for spectrum equivalent to a full duplex FM channel (60 KHz) was about \$47 million.

The new spectrum allocation, like all other allocations, is really a re-allocation, requiring existing users to be discontinued. The best analogy is perhaps real estate development in desirable areas. There is only so much land to go around, and buildings are constantly being torn down and existing residences and businesses being evicted to make way for higher value uses.

Since the extent of the RF spectrum is finite, the growth in demand for wireless services creates an enormous drive for new technologies which will help make more efficient use of this limited resource.

Illinois Superconductor Corporation (ISC) has analyzed the problems arising from the present congestion and signal load on the cellular communication channels and has designed a superconducting RF filter that will reduce the communications degradation arising from the existing spectrum loading and also make it possible to maximize cell density and channel loading in the future. The superconducting RF filter that ISC is preparing for on-site testing in an operating cellular communications facility is a package with two independent 26 pole dual bandpass RF signal filters for the cellular base station receiver front-end.

The superconducting RF filter will work with the existing Advanced Mobile Phone System (AMPS) analog communications systems, and it will also substantially improve the performance of systems using the Time Division Multiple Access (TDMA) digital modulation protocol.

A variant of the ISC superconducting RF filter will work with systems using the Code Division Multiple Access (CDMA) protocol. The CDMA protocol is expected to become of great importance in the future of digital communications in cellular applications because of its ability to increase system capacity by a factor of four to six times that obtainable with the TDMA digital modulation and by a factor of nearly twenty over the conventional AMPS analog cellular communications modulation technique.

Therefore, ISC's superconducting RF filter design for the receiver front end in cellular base stations has current and future applicability that will enhance cellular communications by a significant factor and increase the system capacity of existing and future cellular systems. Because ISC has developed its filter technology using thick-film ceramic high temperature superconductor technology, the costs of incorporating a superconducting filter into a cellular communications site are much less than for a filter using thin-film technology. In fact, ISC's cellular base station receiver front end filter is expected to be cost competitive with conventional filter technology that provides substantially less performance.

Before the introduction of High Temperature Superconductors, superconducting technology required very low operating temperatures of about 5° Kelvin. High Temperature Superconductors operate at liquid nitrogen temperature, 77° Kelvin and above. The higher operating temperature of HTSC superconducting RF components makes the use of closed-cycle refrigerators feasible, which permits superconducting components to be used in applications where low maintenance requirements and high reliability are necessary.

Benefits of Superconducting RF Filters

The increasing load on the cellular communication channels from voice and data traffic is degrading the quality of connections and decreasing the reliability of connections. Crosstalk and garbled transmissions become annoying intrusions on voice communications and the bit rate of digital data transmissions drops. Adjacent channel interference overloads the base station receiver front ends which increases the signal to noise ratio required to maintain contact and causes calls to terminate unexpectedly.

Part of the current problem arises because the FCC originally structured the cellular telephone system in the United States so

there are two competing operators in every service areas using adjacent frequency bands. The signaling channels are located at the interface of the two bands, and originally did not pose much of a problem in terms of voice quality degradation. However, due to the explosive growth of cellular communications, the FCC allocated additional cellular spectrum and the carriers no longer had contiguous spectrum to operate in. The new allocation allowed voice channels from competing carriers to be adjacent and this increases the probability of adjacent channel interference at the base station receiver.

As the number of cells and mobile users continue to increase, it is necessary to split cells and reassign frequencies. This makes it difficult for carriers to make sure that competing carriers do not have frequency plans that will cause adjacent channel interference to their systems. Cellular systems use power control techniques in which the base station instructs the mobile unit to lower or increase its power level to maintain communications while avoiding interference and base station receiver overload. However, when a mobile unit belonging to operator "A," for example, is far from the "A" base station, it will be instructed to raise its power level to the maximum in order to maintain contact with the "A" base station. If this "A" mobile happens to be near a "B" operator's cell site, the "B" cell base station may receive an unexpectedly strong signal on a frequency adjacent to the channels it is trying to use to hear its "B" mobile units. This strong signal results in adjacent channel interference and consequent degradation of quality and capacity of the "B" operator's system.

The channel quality degradation problem for AMPS analog communications is most severe at the base station receivers because most mobile radio telephones are very low power units compared to the cellular base station transmitters. So, the maximum performance enhancement for the system will occur if the adjacent channel interference is minimized at the base station receiver. At present, cellular base station receivers are using low to medium Q bandpass filters based on normal conductors such as silver-plated copper that are sometimes combined with ceramic dielectric loaded cavities.

The superconducting RF passband filter offers substantial improvements over conventional filters because the superconducting bandpass filter has a much lower insertion loss than conventional filters with the same number of poles. It absorbs less signal energy than the conventional filter and

this results in a higher signal to noise ratio. Lower insertion loss results from the very high Q of the superconducting resonators compared to the lower Q resonators of its conventional counterpart. The Q of a filter is a function of the inverse ratio of the signal energy consumed by the filter to the signal energy entering the filter element and it is typically measured in terms of insertion loss in a complete filter. The higher Q of the superconducting filter resonators allows the construction of complex resonator arrays with more resonators than conventional filters. The complex resonator arrays produce extremely steep skirts on the bandpass signal strength curve which approaches the theoretical value for the filter without increasing the insertion loss. The steep skirts on the filter's bandpass minimize adjacent channel interference, while they also provide a narrower passband for the communications channel. The narrower passband reduces receiver front-end overload from adjacent channel interference and reduces spurious intermodulation signal mixing in the base station receiver front-end caused by high power transmitters in other cellular systems and communication services.

In cells in which voice quality and call capacity are now reduced because of high adjacent channel interference from the alternate cellular service and spurious intermodulation signal mixing products from other RF spectrum users, the superconducting RF filter will increase the cell's usable spectrum and enhance the operator's flexibility in frequency assignments by a substantial amount, if all channels are in use, and by an even greater percentage if the improved off-channel signal rejection permits the use of one or more channels that are currently locked out.

Superconducting RF Filters for CDMA

While the above considerations are primarily directed at the existing analog Advanced Mobile Phone Service (AMPS) protocol and the time-slicing single channel TDMA digital protocol, the superconducting bandpass filter may also offer even more improvements in capacity in systems using the spread-spectrum CDMA digital protocol. The CDMA protocol is likely to become a common protocol for digital communications in the future.

Capacity is the most meaningful way to quantify the performance of a cellular system and it is often used as the comparison index for different cellular communication protocols. A CDMA system takes advantage of voice activity and spatial isolation, and it makes full use of the total allocated spectrum for the communications service.

With CDMA, the cellular provider's assigned channels are used equally by all signals at all times. Theoretical considerations predict that a CDMA cellular system will show a net improvement on the order four to six times the capacity of an equivalent TDMA system and that it will have a capacity more than twenty times that of the present analog AMPS system.

CDMA's performance advantages are significant, but they can be degraded by interference from RF spectrum users on adjacent spectrum allocations and by inter-system interference from the alternate cellular service provider using the alternate channels within the assigned spectrum block. CDMA performance degradation results when there is intermodulation between neighboring channel signals in the RF front end of the receiver.

Predictions of CDMA system performance assume that the cellular base station receiver front end RF filter suppresses adjacent channel interference from other commercial users, mobile units, and other cells; and that the RF amplifier would have a wide enough dynamic range to make the interference from adjacent channel intermodulation insignificant. Or, the predictions assume that the CDMA spectrum space is shielded by a guard band. However, these analyses do not sufficiently consider the problem of a foreign mobile unit operating within the cell. The mobility of a mobile unit accessing the operating base station receiver unit within the cell in fringe or border areas can result in a signal with low enough strength that the inter-system interference power becomes significant and even dominating compared to the mobile unit's signal. This causes a significant intermodulation effect that can degrade or even interrupt communications despite the large dynamic range of the cellular base station receiver's RF amplifier.

The situation in which the interfering signal dominates the desired signal is basically caused by relative distances between the cellular mobile user and the base stations of the two systems, and also by the power control employed by both systems. At very low signal levels, the interference effects from the neighboring base station must be attenuated. The superconducting RF filter will be capable of suppressing the interfering frequencies from the neighboring base station and this will lead to superior CDMA system performance in terms of decreased signal outage probability.

ISC has developed a mathematical model that incorporates the effects of a superconducting RF front end filter on intermodulation interference and predicts the increase in system capacity that will result from using the filter. The model uses conservative as-

assumptions about system loading and user mobility. The key factor is the mobility of the cellular user, and the mobility becomes of increasing importance as the cell size decreases. The model shows that with the CDMA digital modulation technique, the base station receiver front-end is highly sensitive to the sharpness of the passband of the RF filter when user mobility is taken into account. A filter approaching theoretical performance can improve base station receiver performance under these conditions, and the filter can reduce, or eliminate, the requirement for guard band for the CDMA spectrum.

The Superconducting RF Filter

ISC's Spectrum Master™ filter is currently configured as two filters in one package with two signal inputs and two signal outputs. Each filter is a 26 pole filter with two passbands having 10 poles and 16 poles respectively. The filter has performance specifications approaching the theoretical values for an ideal filter. It installs between the cellular base station antenna and the receiver multicoupler. It significantly reduces intermodulation, crosstalk, noise, and the false foreign carrier detection caused by out-of-band transmitters. The present configuration of the dual filter package permits two separate receive paths for diversity sufficient to meet the needs for a typical cell site. Other configurations are under design.

The Q of each 26 pole filter in the dual filter package is in excess of 40,000 for designs suitable for installation in cellular base station sites. As would be expected, given the high Q resonators used in this design, the insertion loss and selectivity of the filter are greatly superior to what is achievable with current technology. The insertion loss is typically better than 1.5 dB for each 26 pole filter. The ripple is less than 0.75 dB and the return loss is greater than 20 dB. The high Q provides filter skirts with very sharp roll-off at the edges of the passband. In notch configuration, each 26 pole filter has an attenuation of up to 50 dB for in-band foreign signal suppression. Maximum attenuation for out-of-band signals reaches a maximum of 90 dB to 100 dB for designs suitable for cellular installations.

The power dependence of the 26 pole filter has been tested up to an input power of 40 dBm. These tests indicate that the thick film materials based 26 pole filter has a relatively stable insertion loss up to 30 dBm (between -40 and 30 dBm, the insertion loss increases from 1.5 to 2.5 dB). Above this signal level, the insertion loss increases sharply, but with an incubation time indicative of surface heating of the

superconductor. It is expected that more efficient cooling schemes would improve the ability of these materials to accommodate higher power levels, although the current signal power levels sustainable by the superconducting filter components is sufficient for receiver front-end filtering applications with a healthy margin to spare.

Of course, use of HTSC components in an RF filter requires cooling the filter to liquid nitrogen temperatures. The use of bulk liquid nitrogen is probably impractical in a cellular telecommunications site. Recent advances in cryogenic refrigerator technology have made it possible to package the 52 pole dual filter unit with a closed-cycle refrigerator, that maintains cryogenic operating temperatures for the filter.

With the present filter configuration, cryogenic cooling does not unduly increase the overall system cost. Further, the maintenance required for the closed-cycle cryogenic refrigerator is minimal since it does not require an external supply of cryogen, and its proprietary refrigerant does not require periodic replenishment. Maintenance of the filter with its cryogenic cooling system may be scheduled to conform to the routine maintenance procedures of the cellular base station receiver. This makes the filter practical and desirable for commercial applications.

Thick Film HTSC Materials For RF Filters

ISC currently has an aggressive program aimed at the development of additional high performance RF components based on high temperature superconductors. The YBCO thick-film HTSC technology is ideal for the design and manufacture of RF components. With proper attention to substrates, and with proper adhesion techniques, the YBCO thick-film materials may be painted on and heat-processed using techniques comparable to those for industrial enamels. ISC's YBCO HTSC materials development program is, at present, heavily focused on the cellular base station receiver front-end filter, but the technology being developed to address this application is generic. Similar materials formulation and processing techniques can be used for a wide variety of components suitable for RF applications over a wide range of frequencies.

ISC combines the development of device-specific materials, device design, packaging, and cryogenics in a unique systems approach for producing RF components. Fabricating RF components from textured HTSC thick films permits economical commercial manufacture of cavities and waveguide resonant structures having Q 's of $10^4 - 10^6$. This performance level is substantially higher than those obtainable with other HTSC RF component fabrication techniques.

Before ISC developed its thick film fabrication techniques for RF components, the majority of HTSC device work in the cellular telecommunications frequency range was based on thin film technology which works well in its range of application. However, HTSC thin film technology is limited to the fabrication of planar structures which, even with very low surface resistance (R_s) HTSC films, have relatively low Q 's. Planar structures are two-dimensional and they are not suitable for the commercial manufacture of generalized RF component shapes. It is necessary to produce RF components with complex three-dimensional geometries to obtain high Q 's and produce components that can easily replace existing components in wireless telecommunication equipment. The thick film or bulk technique for producing HTSC RF components was originally avoided by most developers because the early work on bulk HTSC materials showed them to have very high R_s values that were thought to be unacceptable for practical applications.

However, improved processing techniques have resulted in thick film materials with low R_s values that are ideal for the fabrication of RF components. The use of ISC's textured thick film technology permits filter designs to be based on resonant cavities or waveguides that are intrinsically high Q structures because of their low insertion loss. While the surface resistances of the present thick film formulations are still somewhat greater than what has been measured on state-of-the-art epitaxial thin films, the combination of reduced surface resistance and high Q resonant structures can result in filters whose performance substantially exceeds what can be achieved with either conventional RF devices or thin film HTSC RF devices.

The thick film fabrication technique developed and patented at ISC is aimed at the production of a highly textured $\text{YBa}_2\text{Cu}_3\text{O}_{7-x}$ (YBCO) microstructure on an inexpensive substrate material. Recognizing that the commercialization of textured YBCO thick film structures in lower frequency RF applications requires the fabrication of large area thick film coatings on inexpensive substrates, ISC has focused its internal development effort on developing a thick film process capable of meeting these needs. Consequently, ISC has developed a unique variation of the directional solidification process for YBCO, commonly referred to as "melt-texturing" that enables the formation of textured thick films on arbitrary substrates at substantially reduced temperatures. Instead of relying on the crystallization of YBCO out of a peritectic liquid, similar microstructures can be obtained by crystallizing YBCO out of a number of non-equilibrium liquids.

This process, called "reactive texturing", has the advantage of being much more rapid than the peritectic recrystallization (due to the much larger thermodynamic driving force involved) and it occurs at a substantially lower temperature (typically in the 850° to 890°C range). In addition, as both the temperature and the time-at-temperature are substantially reduced in the reactive texturing process compared with the conventional process, a much wider variety of substrate materials can be used, including base metals such as stainless steel that have been buffered with a "suitable" noble metal.

ISC's thick film process involves the deposition of a slurry of YBCO powder and an organic vehicle on the substrate using any of a number of standard coating techniques, including spraying, dip-coating, and brushing. Using one of these techniques, it is possible to quickly and economically coat a wide variety of geometries and sizes of parts. The development of the textured microstructure occurs during firing which is accomplished in conventional ceramic processing furnaces. The texturing process is reliable and repeatable. The rate of material production by this process is sufficient for commercial exploitation at a cost consistent with the bulk production of RF devices.

Typical Superconducting RF Filter Performance

The 26 pole filter produced by ISC is consistent with the theoretical projections, allowing for the design specifications of the filter and the expected deviations of the YBCO material as formed in the reactive texturing process from theoretical values.

The performance figures for ISC's 26 pole filter design represent a very substantial increase in filter performance over conventional filter technology and reflect a unique approach to filter design which combines the low surface resistance of HTSC materials with resonant cavities with intrinsically high Q values.

Potential Market

The present concentration of ISC's development effort is focused on the existing cellular communications service, but work is also proceeding on products for future enhancements to the existing cellular communications industry, such as the Personal Communications System (PCS). The cellular telephone market continues to exhibit extraordinary growth. By current estimates, the cellular telephone business is evaluated at about \$11 billion dollars annually¹ in the United States alone.

There are currently more than 13,000 cellular base station sites in the United States and more than 25,000 cellular sites worldwide. Each cellular base station site represents an average equipment investment of about \$1 million. This implies a worldwide investment in cellular base station equipment of about \$25 billion. The value of the existing investment is impressive, but even more impressive is its rate of expansion which is currently over 30% annually.

ISC's superconducting RF filter for cellular base station receiver front ends will be an attractive product for retrofit applications into existing cellular sites because it substantially increases the system capacity in high load environments. New cellular sites in high load environments will wish to take advantage of the increased performance resulting from improved reception also. The annual market for new cellular site installations is now about \$5 to \$6 billion worldwide, which provides a substantial opportunity for the insertion of the ISC's new superconducting RF filter technology.

ISC also estimates that there is a substantial market for retrofit of its superconducting RF filter into cellular base station receiver front ends. Many urban cellular sites are loaded beyond their capacity and they also have channel allocations that are locked out and unusable because of alternate channel interference and because of interference from other RF spectrum users. A product that will maximize channel selectivity and sensitivity while minimizing out-of-channel interference will be a very attractive solution to cellular telephone congestion in urban areas. ISC's solution is even more attractive now that the required cryogenic cooling of the superconducting filter is now accomplished by a low-maintenance closed-cycle cryogenic refrigerator.

Future Development

ISC is presently designing other HTSC ceramic RF components for cellular system base station receivers to further enhance their sensitivity, selectivity, and immunity to off-channel signals. To achieve the design goals, ISC is co-developing with AT&T a new generation of cellular base station receivers which will be complex systems using a large number of both superconducting and cryo-cooled components. The new receivers will be configured for both analog and digital communication modes.

Conclusions

The development of the reactive texturing method for the deposition and processing YBCO HTSC materials on economical substrates such as stainless steel has made possible the fabrication of RF components suitable for commercial use in wireless telecommunication receiver applications. The first practical component developed with this technique, a dual 26 pole cellular base station receiver front-end filter, has met the design goals required for superior performance in an operating base station site. The performance specifications of the filter as measured show that superconducting RF components for receivers are not only possible, but also offer substantial and attractive performance gains over conventional technology products.

The introduction of closed-cycle cryogenic refrigeration units at an attractive unit price, combined with the inherently low manufacturing costs of HTSC RF filter components will make it possible to offer a superconducting receiver front-end filter to cellular base station operators that will enhance the quality of communications in their cells and increase the cell capacity while reducing the number of dropped calls.

The success of the HTSC RF cellular base station receiver front-end filter means that other HTSC superconducting RF components are feasible for a wide range of applications and frequency ranges for the wireless telecommunication services that need the enhanced receiver sensitivity, resistance to front-end overload, and out-of-band signal rejection that superconducting RF receiver components can provide.

¹ Herschel Schostick and Associates Limited, 10 Post Office Road, Silver Springs, Md, 20910-1103



Ora E. Smith
Illinois Superconductor
Corporation
1840 Oak Avenue
Evanston, IL 60202

Ora Smith is President and Chief Executive Officer of Illinois Superconductor Corporation, headquartered in Evanston, Illinois.

Ora holds B.S. and M.S. degrees in mechanical engineering from MIT and a J.D. from Harvard Law School. He was previously Vice President and Chief Marketing Officer at Conductus, Inc., in Sunnyvale, California, and has held a variety of executive positions at Rockwell International. He also has served as the Industrial Research Institute Fellow in the White House Office of Science and Technology Policy, as well as on the boards and advisory bodies of several other organizations.

High Temperature Superconducting Material Research: Problems and Potentials

L. Gao, Y. Y. Xue, R. L. Meng and C. W. Chu

Texas Center for Superconductivity, University of Houston, Houston, TX 77204-5932

ABSTRACT

Great strides have been made in the effort to commercialize the great potential of high temperature superconductors. We shall summarize the current status of high temperature superconducting material research concentrating on physical limitations such as transition temperature, critical current density irreversibility line, etc., on the application of existing high temperature superconductors.

Ever since the discovery¹ of superconductivity in the element Hg back in 1911 by the Dutch low temperature physicist Kamerlingh Onnes working on the liquefaction of helium, the unique property of zero resistance for dc current flow below certain critical temperature called transition temperature (T_c) in a superconductor has fascinated both the scientific community as well as the engineering community. For the scientists, the challenges are to find better superconductors with ever increasing T_c , to understand, and to improve existing superconductors. At the same time, to find ways to harvest the potentials for application of existing superconductors remains to be the goal of the engineers working in the field of superconductivity. This fascination with superconductors was rekindled by the discovery² of the $\text{La}_{2-x}\text{Ba}_x\text{CuO}_4$ compound in 1986 which has a T_c of ~ 30 K. The interest of the scientific community and the engineering community as well as the general public at large reached the apex in 1987 with the discovery³ of $\text{YBa}_2\text{Cu}_3\text{O}_7$, the so-called "123" material with a T_c of ~ 90 K. For the first time, superconductivity can be sustained by using liquid nitrogen (boiling point 77 K) instead of liquid helium (boiling point 4.2 K). The era of High Temperature Superconductivity (HTS) thus began.

More than seven years have passed since the dawn of HTS. Thanks to the hard works of scientists that belong to diverse disciplines including physics, chemistry, material sciences, chemical, electrical and mechanical engineering all over the world, great advances have been achieved in the study of these HTS materials. For example, the transition temperature has been pushed up to 164 K in the Hg-1223 compound. While HTS wires with length exceeds 1 km have been manufactured by American Superconductors as well as by Sumitomo in Japan with their critical current density approaching 10^4 A/cm². Since it is impossible to do justice to

the intense activities in all fields of HTS material research in a short paper, we shall instead concentrate on several aspects of these materials.

For a superconductor to be in its superconducting state, several conditions have to be satisfied. These conditions differ for different materials. First, the temperature of a superconductor has to be below certain temperature. Second, the magnetic field surrounding a superconductor cannot exceed certain value. Third, the current carried by a superconductor cannot surpass certain limit. Associated with these three requirements are the well-known critical temperature T_c , critical field H_c and critical current density J_c . For HTS materials, it is found that the so-called irreversibility field H_i sets an upper limit for any application of HTS in the presence of a magnetic field, and hence a more meaningful parameter for practical purposes. Therefore, we shall concentrate on T_c , J_c and H_i only.

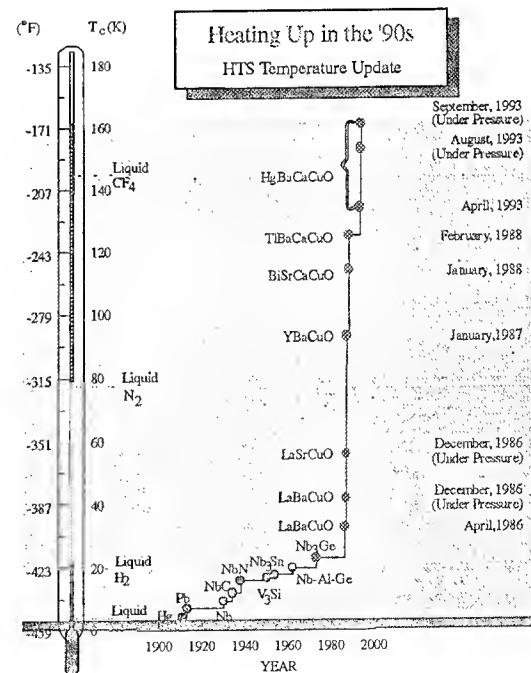


Fig. 1: T_c of various superconductors and their year of discoveries.

Critical Temperature T_c

The most well-known character of a superconductor is definitely its critical transition temperature. Over the last seven years, more than 90 compounds have been discovered with T_c above 23 K, the pre-HTS record set back in 1973, while about 30 of these have $T_c > 77$ K. These compounds can be divided into three families: cuprates, bismuthates, and fullerenes. The cuprates account for the majority of the known HTS' and include all materials with T_c 's above 77 K. The increase of T_c with time is sketched in Fig. 1.

Table 1: Several typical high temperature superconductors with T_c above 77 K.

Formula	Name	T_c (K)	Application Form
$\text{YBa}_2\text{Cu}_3\text{O}_7$	Y-123 (YBCO)	92	film, bulk, wire
$\text{Bi}_2\text{Sr}_2\text{CaCu}_2\text{O}_8$	Bi-2212 (BSCCO)	80	tape, wire
$\text{Bi}_2\text{Sr}_2\text{Ca}_2\text{Cu}_3\text{O}_{10}$	Bi-2223	110	tape, wire
$\text{TlBa}_2\text{Ca}_2\text{Cu}_3\text{O}_{10}$	Tl-1223 (TBCCO)	120	tape, wire
$\text{Tl}_2\text{Ba}_2\text{Ca}_2\text{Cu}_3\text{O}_{10}$	Tl-2223	125	tape, wire
$\text{HgBa}_2\text{CuO}_4$	Hg-1201	97	?
$\text{HgBa}_2\text{CaCu}_2\text{O}_6$	Hg-1212	120	?
$\text{HgBa}_2\text{Ca}_2\text{Cu}_3\text{O}_8$	Hg-1223 (HBCCO)	133 *164	?

* under pressure

In Table 1, the chemical formulae, abbreviated names, T_c 's and material forms of application currently pursued for several HTS materials are listed. In addition to the Y-, Bi- and Tl- compounds, the newly discovered Hg-compounds are also listed. For Y-, Bi- and Tl- compounds, intensive research for their applications has been going on for quite some time since their discoveries. The recently discovered Hg-compounds just start to attract attention for their potential for applications. Hence the question marks in Table 1.

Of all existing HTS compounds, the highest T_c of 134 K at ambient pressure belongs to $\text{HgBa}_2\text{Ca}_2\text{Cu}_3\text{O}_y$ (Hg-1223), the $n = 3$ member of the family of Hg-compounds $\text{HgBa}_2\text{Ca}_n\text{Cu}_{n+1}\text{O}_{2n+2+\delta}$ (Hg-12[n-1]n) with $n = 1, 2, 3, 4, \dots$ being the number of CuO_2 layers.

Shortly after the discovery of the mixed phase Hg-compound by Schilling *et al.*⁴ in 1993, we succeeded in developing an easy and dependable synthesis method⁵ to produce nearly single phase 1, 2, and 3 layer compounds. By subjecting these materials to high pressures generated by two opposing tungsten-carbide anvils, we found that superconductivity can be readily pushed toward higher

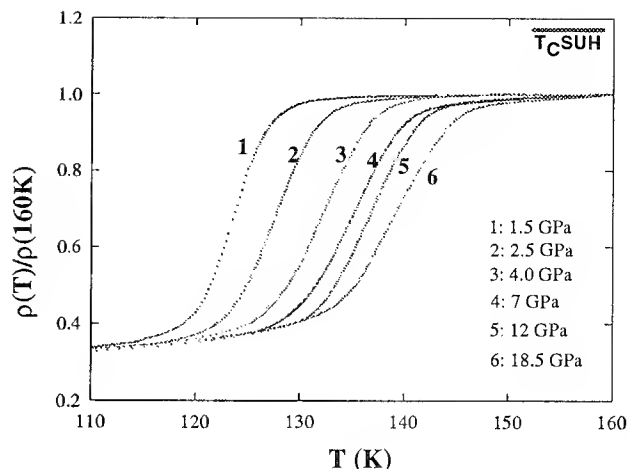


Fig. 2: Resistivity of $\text{HgBa}_2\text{CaCu}_2\text{O}_{6+\delta}$ normalized to 160 K under various quasi-hydrostatic pressures. The non-zero resistance tail is due to cracks produced during sample thinning process. (From Ref. 6)

temperatures by pressure as shown in Fig. 2, where the temperature dependence of the resistance of a Hg-1212 sample is plotted for several pressures. One can clearly see the upward shift of the superconducting transition with increasing pressure. With this encouraging result, we extended the pressure up to 45 GPa with the collaboration of Mao and Eggert of the Geophysical Laboratory in Washington using the diamond anvil cell technique, the final result⁷ is a record high 164 K at 30 GPa for the onset of superconducting transition temperature in

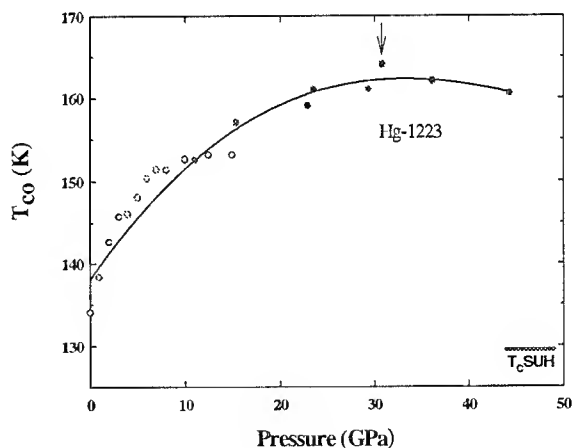


Fig. 3: The onset transition temperature T_{co} of Hg-1223 under quasi-hydrostatic pressure. Arrow points to the 164 K T_{co} at ~ 30 GPa.

the 3-layer $\text{HgBa}_2\text{Ca}_2\text{Cu}_3\text{O}_{8+\delta}$ shown in Fig. 3. This demonstrates that T_c can exceed 160 K in cuprates. The challenge now is to find chemical/physical means to stabilize such high T_c so as to make this material suitable for practical applications. Since the application of pressure reduces the

interatomic distances inside the material, one can think of a simple way to "mimic" the pressure in the Hg-compound by replacing the Ba atom with a slightly smaller Sr atom. Following this line of thinking, by using high pressure synthesis technique, we succeeded in making both Sr-doped $\text{Hg}(\text{Sr}_x\text{Ba}_{2-x})\text{Ca}_2\text{Cu}_3\text{O}_{8+\delta}$ and 100% Sr-based $(\text{Hg}, \text{M})\text{Sr}_2\text{Ca}_2\text{Cu}_3\text{O}_{8+\delta}$ with $\text{M} = \text{Pb}$ or Mo . Here M is needed for the stabilization of the crystal structure. Unfortunately, the introduction of Sr into the Hg-compound results in a steady reduction of T_c instead.

In spite of all the pitfalls and frustrations, it continues to be the main goal for scientists working in the field of superconductivity to look for new superconductors of ever increasing T_c s. This is because the increase of T_c , hence the operational temperature of a high temperature superconductor will result in huge benefits from both physical as well as economical fronts. For example, by switching from liquid helium cooling to liquid nitrogen cooling, one has a saving of 95% in energy and 60-fold increase in cooling efficiency, plus the reduction in cost of cryogenic liquids (\$5/liter for liquid helium vs. \$25/liter for liquid nitrogen). Another important benefit of a higher operational temperature is the enhancement of the so-called thermal stability. The reduced specific heat of

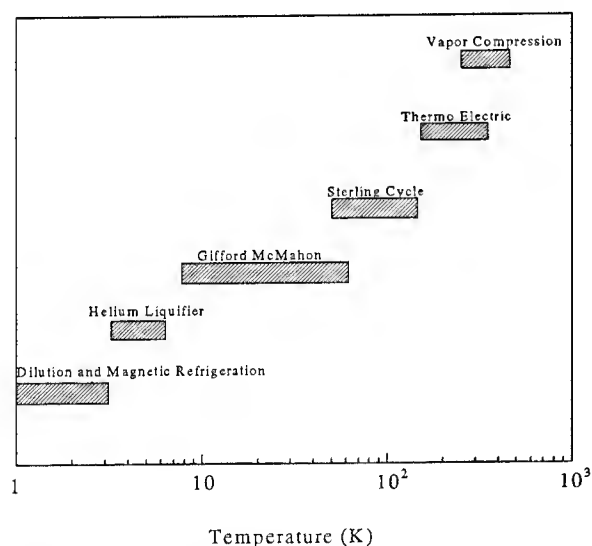


Fig. 4: Operational temperature ranges for commercial refrigerators. (From Ref. 8)

superconductors at low temperatures makes them quite susceptible to small thermal disturbances resulting in catastrophic flux avalanches. Increase the operating temperature will result in the increase of the specific heat, thus alleviate the thermal instability problem. Furthermore, as temperature increases, there are more means available for refrigeration (Fig. 4). We may even be able to use commercial refrigerators to cool the high temperature superconductors and eliminate cryogenic fluids all together.

Critical Current Density J_c

The current carrying capability of a superconductor is the second critical factor governing its applications. The upper limit of this capability is the critical current density J_c , usually described in A/cm^2 . There are number of factors affecting J_c for a given superconductor. The most dominant factors are granularity and magnetic flux pinning strength for the HTS materials. The granularity of the ceramic nature of HTS materials results in the so-called weak-link grain-boundary gap. Associated with the flux pinning strength is another gap called flux pinning gap.

Over the past years, the granularity gap has been partially overcome for some of the HTS compounds. *e.g.*, the J_c at 77 K for bulk YBCO material has increased from $10 \text{ A}/\text{cm}^2$ right after the discovery of YBCO to the current value of $8 \times 10^4 \text{ A}/\text{cm}^2$ and $2 \times 10^5 \text{ A}/\text{cm}^2$ in melt-textured Y-123 samples at zero and 30 tesla magnetic field, respectively. Applications for such bulk materials are being sought in magnetic bearings, motors, fly wheels, etc. Unfortunately, successful melt-textured BSCCO, TBCCO and HBCCO compounds have yet to be achieved.

The flux pinning gap has also been overcome in thin films. State of the art high quality YBCO thin films have J_c values well into $10^6 \text{ A}/\text{cm}^2$ at 77 K, which is not too far below the theoretical limit of the depairing limit estimated to be $\sim 10^7 \text{ A}/\text{cm}^2$ at the same temperature. Irradiation by fast neutrons and heavy ions have also been proven to be quite successful in increasing the flux pinning force in HTS materials.

For power applications, long superconducting wires are required. Since HTS materials are mechanically brittle and electrically anisotropic, the fabrication of HTS wires, tapes or ribbons with large J_c and great length is truly a formidable task.

Table 2: ASC Multifilament composite BSCCO conductor performance (77K, self field). (Courtesy of Dr. William Carter of ASC).

Length(m)	$J_c (\text{A}/\text{cm}^2)$ ($10^{-11}\Omega\text{-cm}$)	$J_e (\text{A}/\text{cm}^2)$ ($10^{-11}\Omega\text{-cm}$)
0.03	22,100*	6,200*
60	17,800	5,000
280	10,900	2,500
1,160	8,800	2,120

* $1 \mu\text{V}/\text{cm}$ criterion.

Note: J_c is the critical current density when only the superconducting core area is considered. J_e is the effective critical current density when the overall area (superconducting core plus Ag cladding material) is considered.

Over the last few of years, giant strides have been made in the fabrication of long superconducting tapes. BSCCO compounds play a significant role in these development thanks to the high

anisotropy in these compounds which make grain-alignment possible. The Powder In Tube (PIT) method has yielded short ribbons with $J_c \sim 10^5$ A/cm² at 4.2 K even at fields higher than 20 T. BSCCO wires of lengths of more than 1,000 m have been manufactured by Sumitomo in Japan and American Superconductors Corporation. In Table 2, J_c for ASC multifilamentary composite BSCCO conductors at 77 K in self field at different lengths are compared.

The TBCCO with its superior behavior under magnetic field is starting to attract attention and promising preliminary results have been reported for TI-1223 ribbons.

Irreversibility Field H_i

The third most crucial factor in the application of HTS material is their performance under magnetic field. All HTS materials have a so-called irreversibility line which separates a reversible region of finite diamagnetism above it and

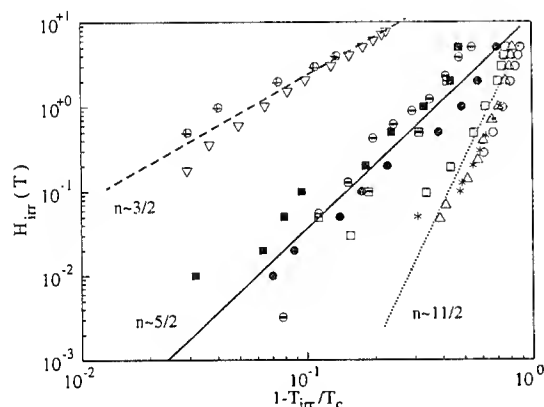


Fig. 5: H_i (T) for some HTS compounds. Δ Bi-2212, * TI-2223, \blacksquare TI-2212, \bigcirc Bi-2223, \oplus Y-123 melt-textured, ∇ Y-123 single crystal, \bullet and \blacksquare Hg-1212, \boxplus Hg-1223, \ominus Hg-1201. (From Ref. 9)

irreversible magnetic behavior below. Transport current can only be supported below this line. Therefore, the irreversibility line is utterly important in defining the temperature and magnetic field limitations for a given HTS compound. Figure 5. depicts the irreversibility lines for some HTS compounds.

In this respect, the BSCCO wire has a major problem: its J_c drops dramatically even under modestly low magnetic field. Increasing temperature to 77 K also has a detrimental effect. For TI-1223, the problem is much less serious while Y-123 is the least affected by magnetic field. This is due to the fact that these compounds have a increasing irreversibility field in the order of Bi-2223, TI-1223, and Y-1233 as can be seen in Fig. 5. Notice that HBCCO has its irreversibility line just

between BSCCO and YBCO. Therefore, HBCCO should outperform BSCCO under magnetic field.

One can correlate the irreversibility line with the strength of inter-layer coupling between neighboring conducting Cu-O layers. This strength can be represented by the inter-layer distance between Cu-O planes in these compounds. In Fig. 6, the irreversibility fields for several HTS compounds is plotted against the separation of the Cu-O planes.

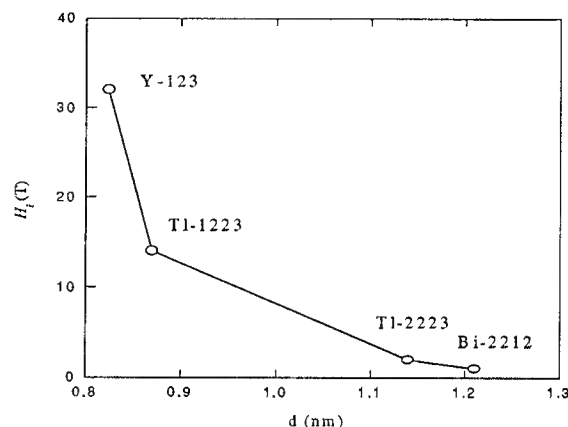


Fig. 6: Correlation between the irreversibility field and distance d for neighboring Cu-O planes for several HTS compounds. (From Ref. 10)

From Fig. 6, it is clear that BSCCO compounds have the longest Cu-O plane distance hence the weakest inter-plane coupling strength which cause the J_c drop. However, it is exactly due to this weak coupling that allow easy grain alignment during the rolling process in the PIT technique which is responsible for the success of BSCCO wires. On the other hand, wire making using YBCO, the HTS having the strongest inter plane coupling, remains to be far from satisfactory.

From the above discussion, it is clear that in order to apply HTS to their potential, one has to maintain a careful balance among the many competing factors such as pinning strength, easiness of processing, chemical stability, etc. In Table 3, several typical HTS compounds are "graded" by comparing the these factors. Roughly the smaller the number, the better the property. It should be emphasized that such a

Table 3: Comparison of the properties of some HTS compounds

Compound	process- sibility	Pinning strength	Flexibility	Chemical stability
Y-123	4	1	4	4
BSCCO	1	5	1	1
TI-2223	2	4	2	3
TI-1223	3	3	3	3
HBCCO	4*	3*	3*	4*

* not enough data

comparison is only meaningful when combined with other criteria. For example, even though YBCO is difficult to process, and is not flexible, still it is by far the best material for 77 K thin film applications.

To summarize, unprecedentedly rapid progress has been made since the beginning of the HTS era. New HTS compounds are still being discovered continuously. Studies of the physical, chemical properties have resulted in better processing techniques that produces long HTS wires, high quality thin films reproducibly. New HTS device prototypes have been built and tested. However, other than a few commercially available HTS items, major commercial HTS products have yet to be identified. This is expected in view of the complexity of HTS materials. More in-depth studies are called before the full potential of the HTS materials can be realized.

Acknowledgment:

The authors would like to thank their colleges for their hard work and dedication. This work is supported in part by NSF, USAFOSR, ARPAR, the State of Texas through the Texas Center for Superconductivity at the University of Houston, and T. L. L. Temple Foundation.

References

1. H. K. Onnes, Communications from the Physical Laboratory of the University of Leiden, No. 124c (1911).
2. J. G. Bednorz and K. A. Muller, Z. Phys. B 63, 189 (1986).
3. M. K. Wu, J. R. Ashburn, C. J. Torng, P. H. Hor, R. L. Meng, L. Gao, Z. J. Huang, Y. Q. Wang and C. W. Chu, Phys. Rev. Lett. 58, 908 (1987).
4. A. Schilling *et al.*, Nature 363, 56 (1993).
5. R. L. Meng *et al.*, Physica C 216 21 (1993).
6. L. Gao *et al.* Philosophical Magazine Lett. 68, 345(1993).
7. L. Gao *et al.* Phys. Rev. Rapid Comm. in press.
8. R. A. Ackermann, presented at SMES Utility Interest Group Meeting, Buffalo, NY (1992).
9. Z. J. Huang *et al.*, Phys. Rev. B 49, 4218 (1994).
10. T. Nabatame *et al.*, Physica C 193 (1992).

NAVY PROGRAM IN SUPERCONDUCTIVITY

D.U. Gubser

Naval Research Laboratory
Washington, DC 20375-5343

ABSTRACT

The Navy program in superconductivity is a multi-faceted program with strong efforts in fundamental theory and properties, in materials and processing, and in prototype demonstrations. Work includes development of several application areas including satellite communications, missile guidance, magnetic anomaly detection, digital electronics, and wires and magnets for ship propulsion and other power devices. The focus of the program is on systems demonstrations of superconductivity and includes integration of high temperature superconductors, low temperature superconductors, and cooled semiconductors. This talk will provide a review of the various focused efforts in the Navy's Superconductivity Program.

INTRODUCTION

The Navy has had an active program in superconductivity since shortly after World War II. The present level of effort and focus of the Navy's program began in 1987 shortly after the discovery of high temperature superconductivity (HTS). At that time, the Navy formed the Naval Consortium for Superconductivity (NCS) with the specific charter of providing oversight to the Navy's science and technology programs in superconductivity (Figure 1).

The Navy program encompasses both HTS and low temperature superconductors (LTS) in its programs. The LTS components of the program is focused more on systems demonstrations since the technology is more mature. The HTS components of the program are focused on science and technology issues and prototype device demonstrations, consistent with a less mature technology. Figure 2 contrasts the differences between LTS and HTS in a very succinct form. The four main differences are: 1) LTS materials generally have simpler crystal structures and are easier to fabricate; 2) LTS materials have large isotropic coherence lengths whereas HTS materials have small anisotropic coherence lengths (the spatial distance over which superconducting properties vary); 3) LTS materials are generally more malleable than the extremely brittle HTS materials; and 4) LTS materials form integral components of present day commercial

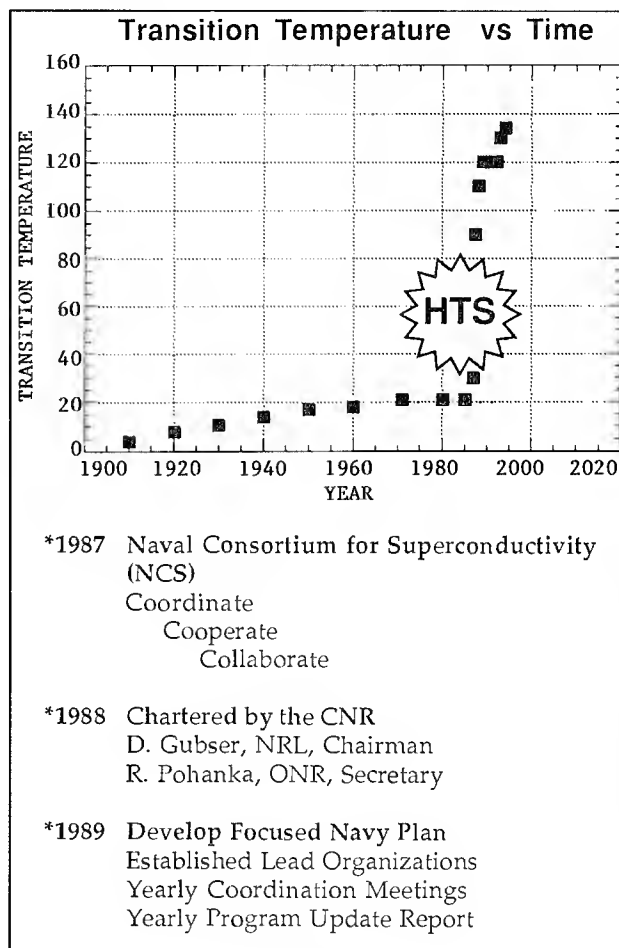


Figure 1.

systems whereas HTS materials are only ready for prototype device demonstrations. HTS materials, on the other hand, offer significantly higher operating temperatures than LTS materials which in turn leads to less overall refrigeration requirements, greater refrigeration efficiency, and greater system reliability.

The progress in the field of HTS materials has been truly remarkable in the past seven years. The maximum transition temperature, T_c , has risen to approximately 140 K at the time of writing this article. First principle calculations of the electron band structure

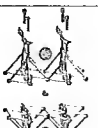



Low Temperature Superconductors vs High Temperature Superconductors			
1.	Simple Structures	Complex Structures	
2.	Large, Isotropic Coherence Length	Small anisotropic Coherence length	
3.	Malleable	Brittle	
4.	MRI Applications	4.2K Demonstrations	

Figure 2.

have been performed and verified with sophisticated experiments. Outstanding science issues remain with respect to the fundamental origin of superconductivity in HTS materials and with the nature of magnetic flux motion in them. There remains a clear need for improved quality and characterization of the materials in order to distinguish between the various theoretical models.

Similarly with technological developments, progress has been rapid. Small modest size magnets of HTS materials are now available for prototype demonstrations. Thin films of high quality HTS materials have made HTS passive electronic devices a reality. Film multi-layer structures are coupling complex integrated HTS and semiconductor electronic circuitry. Focus is now shifting to the total system package including the need for reliable and affordable refrigeration systems.

NAVY PROGRAM

The Navy has a well-rounded superconductivity program with efforts in the fundamental science issues, technology development, and prototype demonstrations. The program encompasses both HTS and LTS programs. The remainder of this article will briefly discuss several of these programs.

Fundamental Properties

Navy scientists and contractors have been pursuing electronic band structure calculations to determine the nature of the electronic states. Such calculations are essential to understanding the origin of superconductivity in the HTS materials. Similarly model calculations are ongoing which extend the Eliashberg

formulation of superconductivity to take into account the unique features of HTS materials; namely, the extreme anisotropy and the short coherence lengths. These calculations, coupled with the band structure calculations, have led to a number of successes in explaining the unusual features of the HTS materials.

The search for new materials remains a small but important feature of the Navy's Superconductivity Program. Recent progress in fabricating mercury cuprate materials with T_c exceeding 130K has been a result of this program. Other programs in the Navy are focused on understanding the nature of magnetic flux flow in HTS materials and the nature superconductivity at the interface between HTS and other materials. Both of these fundamental issues have important bearing on the technology of HTS. The ultimate performance of HTS devices cannot be predicted without improved understanding of these fundamental issues.

High Temperature Superconductivity Space Experiment (HTSSE)

The Naval Research Laboratory (NRL) has a major initiative to demonstrate HTS electronic devices for space applications. This initiative has been funded by Navy, ARPA, and SDI (now BMDO) and supports development at over 20 different industry, university, and government laboratories. The initial experiment, HTSSE I, was completed in 1993 and space-qualified 14 different passive electronic components. These devices were integrated with a refrigeration unit, assembled in a launch payload, and tested operational at the launch site. Unfortunately, the launch failed to achieve orbit, and the space test was voided.

HTSSE II

Deliverables	Vendor
Channelized Filterbanks	COM DEV Naval Research Lab Space Systems/Loral Westinghouse S&T Center
Delay Line	Westinghouse S&T Center
Analog Signal Processor	Conductus MIT Lincoln Lab
Bandpass Receiver	NASA (JPL and Lewis Research Center)
Analog-to-Digital Converter GHz Digital Multiplexer	Conductus TRW

Figure 3.

A second HTSSE is now being completed. HTSSE II contains HTS components linked into operational sub-systems to test the performance of the subsystems in space. Subsystems include HTS components, cooled semiconductor components, and digital as well as passive devices. HTSSE II is scheduled for launch in late 1995. Figure 3 is a listing of the sub-systems and manufacturers included in HTSSE II.

HTS Motor Demonstration

The Naval Surface Warfare Center-Annapolis (NSWC), the Navy-supported National Center for Excellence in Metalworking Technology (NCEMT), and NRL have another major demonstration program focusing of HTS wires and magnets. This program, jointly supported by the Navy and ARPA, is to demonstrate HTS conductor and magnet technology by insertion of an HTS magnet into an existing superconducting 400 HP motor. This program supports 3 industrial efforts, 3 university efforts, and 3 government laboratories, all working to produce conductors and magnets suitable for the superconducting motor test bed.

The first of the motor magnets has been delivered to the NSWC laboratory where the motor tests will be conducted. The initial magnets are of sufficient quality to enable initial tests to begin this year, with follow-on tests in 1995 and 1996. The goal of this program is to accelerate and monitor the progress in HTS conductors and magnets, and to demonstrate to the Navy the utility of these materials for power applications.

SQUID Magnetometry

The Naval Surface Warfare Center-Coastal Systems Center (CSS) has an active program in SQUID magnetometry for Magnetic Anomaly Detection. This program has produced a field deployable SQUID system based on bulk LTS technology. Current efforts are focused on thin film LTS technology and improved cryogenics, both of which are designed to improve the performance and logistics of operation.

A new initiative is focused on extending SQUID magnetometry systems to HTS materials including cooled electronic packages for signal to noise reductions. Final design of this system should be completed in 1996, and field testing of the HTS system should begin in 1998. A final demonstration, including coupling with acoustic sensors, is scheduled for 1999.

Antennae

The Naval Air Warfare Center-China Lake has a program focused on HTS antennae development. Antennae in the frequency range below 1 GHz are used for missile guidance and active tracking. These antennae can be made with greater directionality and effi-

ciency if HTS antennae arrays can be developed. Both tunability and cooling issues are being addressed in this program. Several prototypes are currently being assessed.

A major materials issue is being encountered in the HTS antennae; namely, power limitations. Although thin film antennae are of sufficient quality to make good receiver elements, higher power applications for sending signals remain an unsolved problem, although progress is being made.

Radar

To improve the ability of advanced radar to detect weak signals from clutter noise, HTS stabilized oscillators and HTS filters are being developed. Improved signal to noise of more than a factor of 2 is envisioned from the first demonstration radar models. Further improvements are expected as HTS digital devices become available for digital signal processing.

Mine Sweeping

NSWC (Annapolis and CSS) have a program to develop a LTS magnet system for magnetic mine sweeping. This program began in 1993 and will culminate in 1997 with a field demonstration unit which will include a niobium-tin superconducting magnet operating at a temperature near 10K, conductively cooled by a cryocooler, and possessing HTS downleads to reduce the heat flow from room temperature to the 10K magnet system. Part of this program is to develop the LTS conductor technology to make it lighter weight and less susceptible to shock and vibration which will occur in the proposed application.

Superconducting Magnetic Energy Storage (SMES)

NSWC-Annapolis has been active in the development of a SMES system for large scale energy storage and pulsed power applications. A new initiative involving the Navy, ARPA, and DOE for the development of SMES for utility applications has been initiated this year. This program will focus on the development of LTS conductors, system design, and prototype demonstration of a 0.5 megajoule energy storage unit. A successful demonstration should lead to a new appreciation of SMES as a useful component in our nation's energy planning for the future.

SUMMARY

This article provides a brief summary of the Navy's interests and programs in superconductivity. The next few years will be crucial to the technology as the planned demonstrations are essential to continue the interest of the Navy and the nation toward the development of this new technology.



D. U. Gubser
Naval Research Laboratory
Washington, DC

Dr. Donald U. Gubser is Superintendent of the Materials Science and Technology Division at the Naval Research Laboratory (NRL). He was graduated from the University of Illinois with degrees in Physics (BS, 1963; MS, 1964; and Ph.D., 1969) and has been employed at NRL since that time. Dr. Gubser's scientific training and personal research have been in superconductivity, magnetism, electron transport, and cryogenic properties of materials. He is also a professorial lecturer at the George Washington University, teaching both graduate and undergraduate courses in Materials Science. Dr. Gubser is a Fellow in the American Physical Society (APS). He has received the Naval Meritorious Service Award for his scientific leadership and research accomplishments, and the Senior Executive Service Meritorious Service Award for excellence in science management. He has received many other NRL awards for his research and leadership.

MINIATURE OPTICAL FIBER CABLES FOR JUMPER APPLICATIONS

Don Mathis, Montri Viriyayuthakorn, Jim Holman,
Lionell Graham, Randy Reagan

AT&T Bell Laboratories
Norcross, Georgia

ABSTRACT

As more and more optical fiber systems come on line, the Central Office will become more congested. This is due to the large number of racks, troughs, and cables required. Customers are requiring miniaturization of products for Central Offices in order to reduce congestion and cost. Smaller cables allow greater packing densities in the cable troughs. Decreasing the size and space requirements reduces the man-hours for both the initial installation and future rearrangements. A cable smaller than the standard 2.4 mm or 3 mm cable, currently available on the market, is needed. This paper covers the design, manufacture and testing of two miniature fiber optic jumper cables. These two designs use cables with diameters of 1.6 mm as a basic unit. Although the size of the cables has been greatly reduced, they are designed to meet the Bellcore Qualification requirements. Unusually high strengths will be shown for Bellcore mechanical tests, specifically the compression and tension tests. These miniature cables have been designed with an "enhanced" nylon buffered fiber which meets the strippability requirements down to both the coating and glass.

I. Miniature Jumpers Needed For New Fiber Distribution Frames

Increasingly, Local Exchange Carriers are adding fiber to their systems. These optical fiber systems include Fiber-to-the-Home, Fiber-to-the-Curb, Hybrid Fiber-Coax, Digital Loop Carrier, and Interoffice carrier. The result is that the Fiber Distribution Frame (FDF) is becoming more congested with fiber jumpers. One solution to this congestion is to design cables that are robust and can handle the installation and fiber maintenance but are also miniature in size compared to present jumper designs. Another driver for small cables is the fact that many connector companies are developing high performance compact connectors. These connector designs will require smaller cables for application.

New Fiber Distribution Frames are being designed that will hold 96, 144, and 216 jumpers on the same shelf size that presently holds only 72. Plans call for the entire 7 foot high distribution frame to hold between 648 and 2160 jumpers. These developments initiated the design of new miniature jumper cables.

II. Minicord Designs

Minicord

The Minicord consists of both a single fiber design and a duplex design. The single fiber design uses the standard size 900 μ m (0.035") buffer covered with an aramid yarn. A PVC jacket covers the package producing a total outside diameter of 1.60 mm (0.063"). A duplex design consists of two 900 μ m (.035") buffered fibers covered with aramid strength members and then covered with a PVC jacket in a figure "8" design. The dimensions are 1.60 mm (0.063") and 4.2 mm (0.165"). These designs are shown below in Figure 1.

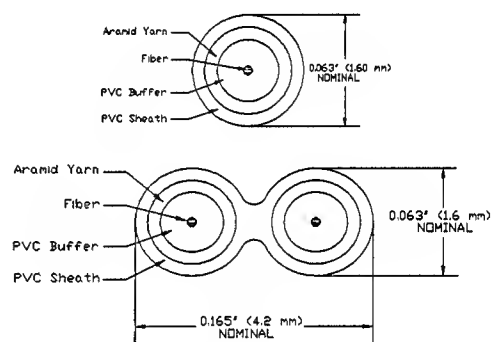


Figure 1 : Minicord Cable Designs

III. Buffer

Material

In the FC and SC connectors the ceramic ferrule moves with respect to the body of the connector. Jenkins et al (Ref. 1) showed that when the buffered fiber is connected to the ferrule, the buffered fiber must move within the cable jacket or there will be a sharp bend of the buffered fiber at the jacket. This sharp bend of the buffered fiber can produce mechanical fatigue and ultimately cause the fiber to break. The buffer material in the Minicord used for this application is an "enhanced" nylon. The nylon buffer is designed to be stiff enough and smooth enough such that it will slide within the cable. This prevents the sharp bend in the buffered fiber (and consequently mechanical fatigue) when used with the FC and SC connectors.

Material-Jacket Test

For initial development and quality control, a test was developed to test the ability of the nylon buffer to slide within the jacket. An 18 inch sample is used with 1 inch of buffer extending from one end. A force gauge is used to push the buffered fiber back into the jacket. The force, P , should be as shown below :

$$0.2 \text{ lbs} < P < 0.7 \text{ lbs}$$

The lower limit is to assure that there is sufficient frictional force to prevent the buffer from sliding too freely. The upper limit provides a force that is less than that needed to cause the buffered fiber to buckle.

The critical force of buckling, P_{cr} , is given by Euler's equation for a beam fixed at both ends. This equation can be applied to the buffered fiber when one end is fixed in the ceramic ferrule and the other end is fixed inside of the cable jacket. Therefore,

$$P_{cr} = \frac{4\pi^2 EI}{l^2}$$

where : l is the length of the buffered fiber between the ferrule and entry into the jacket.
 E is the effective modulus of elasticity of the buffered fiber
 I is the area moment of inertia

The force required to push the buffered fiber into the jacket is,

$$P = \mu \sigma_{rr} A$$

where : μ is the coefficient of friction between the buffer and the aramid yarn inside of the jacket.
 σ_{rr} is the hoop stress exerted by the jacket on the buffered fiber.
 A is the surface area of the buffer within the jacket.

Equating these two equations and solving for σ_{rr} gives,

$$\sigma'_{rr} = \frac{4\pi^2 EI}{l^2 \mu A}$$

σ'_{rr} is the critical hoop stress at which the buffer can just be pushed into the jacket. Increasing the modulus, E , allows the buffered fiber to be pushed back into the jacket at a higher hoop stress. Decreasing the coefficient, μ , also helps the buffered fiber to slide more easily. The new enhanced buffer material has a very slick surface for this purpose. Proprietary process techniques are required to provide an enhanced nylon material with these features.

Strippability

It was found during the course of this work that increasing the nylon modulus made the cable compatible with the SC and FC connectors but it also increased the buffer hoop stress making it more difficult to strip. When a high modulus nylon material is applied directly to a coated optical fiber, it becomes difficult to remove due to higher hoop stress and adhesion. Major effort has been directed toward developing methods that provide an easy-to-strip nylon buffered fiber. Earlier work (Ref. 2) used a pre-treatment prior to applying the nylon buffer. This method improved the strippability down to the coating but could not meet the Bellcore requirement of 3 pounds maximum strip force to either the coating or glass.

It was recognized during the optimization of the buffer processing that an "enhanced" nylon buffer could be manufactured. The strippability of this material surpasses Hytrel and other nylon buffers while comparing favorably with AT&T's proprietary PVC. Stripping down to the coating and glass can be achieved by using a variety of commercial stripping tools. The strippability results for this "enhanced" nylon buffer is well within the Bellcore requirements of 3 pound strip force and is very consistent, as shown in figure 2.

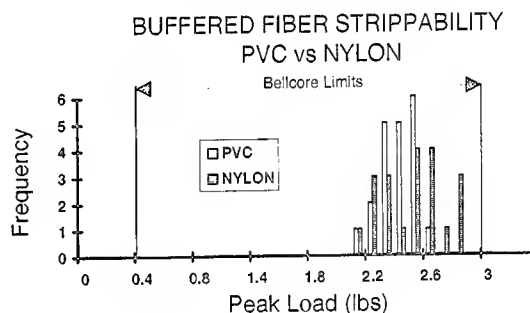


Figure 2 : Buffer Fiber Strippability

IV. Duplex Compact Transition

Existing duplex jumper cables in the marketplace usually consist of two buffered fibers helically wound with aramid yarn with a jacket placed around the yarn. The cable is connectorized by stripping the outer jacket and feeding the aramid yarn and the buffered fiber through a PVC or nylon tube. Otherwise, the connectorized end would have no strength member. A short piece of material is placed at the junction of the two tubes to hold them on the cable. The two tubes and the plastic material at the junction are called a "bifurcation kit".

The Minicord duplex cables were designed such that the aramid strength members are placed around individual buffered fibers. No "bifurcation kit" is needed when the duplex is separated into two single-fiber cables for connectorization. This results in :

- less cost for parts,
- lower connectorization labor costs,
- a strength member continuity from connector to connector
- no large hump at the junction of the "Y".

Avoiding a large hump at the point of bifurcation reduces jumper build-up in the FDF trough which allows more cables to be placed into the trough. Another valuable feature is that the length of each leg of the "Y" can be lengthened in the field in order to connect widely spaced connectors. Jumpers using a "bifurcation kit" cannot.

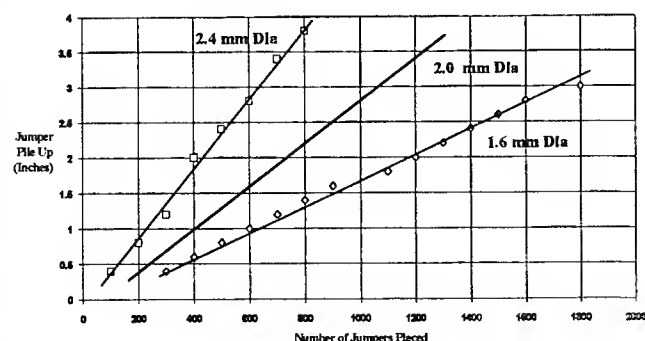
V. Improved Packing and Handling

It has been shown (Ref. 3) by human factors analysis and craft testing that the new Minicords provide a significant advantage in installation, tracing, and removal operations. A simple way to compare the various cordage products presently available in the marketplace is via cross-sectional area.

Diameter	1.6 mm	2.0 mm	2.4 mm
Cross-Sectional Area	2.0 mm ²	3.1 mm ²	4.5 mm ²

The cross-sectional area of 1.6 mm cordage takes up 55% less space than the 2.4 mm cordage and 35% less space than the 2.0 mm cordage.

Bellcore recommends that the jumper pile-up depth be limited to a maximum of 2 inches so that jumpers are not subjected to excessive stress during handling. The chart below shows the advantage of the 1.6 mm Minicord over larger cordage. For a 2 inch pile-up of jumpers, the trough will hold 1200 Minicords as compared with 750 of the 2.0 mm jumpers and only 400 of the 2.4 mm jumpers. Thus the 1.6 mm cordage provides a packing density that is 60% greater than the 2.0 mm cordage and 200% greater than the 2.4 mm cordage.



The capacity of a particular FDF trough should be determined empirically. This is due to the theoretical packing density being reduced by jumpers crossing over each other in the trough. The table below demonstrates the difference between theoretical and empirical packing densities.

Calculated Density at 2 inch Pile up (Jumpers per sq. inch)			
Cordage	Theoretical Based on Dimensions	Empirical Based on pileup data	Avg. Packing Factor ^a
2.4 mm dia	112	35-to-45	0.36
2.0 mm dia	205	65-to-85	0.40
1.6 mm dia	252	100-to-125	0.45

^aAvg. Packing Factor = Empirical / Theoretical

VI. Cable Requirements

There are certain Bellcore Qualification tests (Ref. 4) that are especially difficult to pass as the diameter of a jumper decreases. These are Tensile load, Compression, Twist, and Cyclic Flex. For this reason much attention was paid to these tests in the design of a miniature cable. The results are shown for these more demanding tests in the table below.

Specifications	Bellcore Requirement	Minicord Results
Tensile Load	50 lbs	135 lbs
Compression	20 lbs/inch	508 lbs/inch
Twist	180°, 0.3m (11.8 inches)	360°, 0.075 m (2.97 inches)
Cyclic Flex - 300 cycles, 180°	32 mm rod (1.26 inches)	12.7 mm rod (0.5 inches)

The full range of Bellcore qualification tests and results are shown below for the 1.6 mm duplex Minicord with the enhanced nylon buffer.

**Fiber Optic Cable Qualification Laboratory
Summary of Mechanical Test Results
1.6 mm Duplex Minicord with Nylon Buffer**

IEC Fiber EIA/Optic Test Procedure Requirement	Bellcore TR-NWT-000409	Laboratory Test Level	Cable Performance (1310/1550 nm)
EIA FOTP-25 Impact Test (\cong IEC 794-1-E4 Impact Test)	.5 kg Mass 20 Impacts @ 30 Cycles/min. Avg. Δ Loss \leq 0.20 dB	.5 kg Mass 25 impacts @ 30 Cycles/min.	Δ Loss = -.008/- .003 dB Δ Loss = .000/.010 dB No Visual Damage Observed @ 10 X mag.
EIA FOTP-33 Tensile Load & Bend Test (IEC 794-1E1 Tensile Strength Test)	220 N Tensile Load, 10 min. duration, 550 mm Universal Sheave Dia. Avg. Δ Loss \leq 0.20 dB	600 N Tensile Load 1 hour duration, 400 mm Universal Sheave Dia.	Δ Loss = -.001/- .004 dB Δ Loss = -.003/- .002 dB No Visual Damage Observed @ 10 X mag.
EIA FOTP-37A High Temperature Bend Test (IEC-794-1-E11 Proc. 1 Cable Bend Test)	4 hours @ + 50°C, 20 Wraps on Mandrel Dia. = 51 mm Avg. Δ Loss \leq 0.20 dB	4 hours @ + 50°C, 20 Wraps on Mandrel Dia. = 51 mm	Δ Loss = .030/.035 dB Δ Loss = -.003/.005 dB No Visual Damage Observed @ 10 X mag.
EIA FOTP-37A Low Temperature Bend Test (IEC-794-1-E11 Proc. 1 Cable Bend Test)	4 hours @ 0°C, 20 Wraps on Mandrel Dia. = 51 mm Avg. Δ Loss \leq 0.20 dB	4 hours @ 0°C, 20 Wraps on Mandrel Dia. = 51 mm	Δ Loss = -.016/- .013 dB Δ Loss = .010/.021 dB No Visual Damage Observed @ 10 X mag.
EIA FOTP-41 Compressive Loading Resistance Test (IEC 794-E3 Crush Test)	356 N Compressive Load, 100 mm Compressive Plates, 10 minute Duration Avg. Δ Loss \leq 0.20 dB	8,900 N Compressive Load, 100 mm Compressive Plates, 1 hour Duration	Δ Loss = .013/.089 dB Δ Loss = .014/.185 dB No Residual Δ Loss No Visual Damage Observed @ 10 X mag.
EIA FOTP-85 Twist Test (IEC 794-E7 Torsion Test)	10 Cycles Of: 180° CW Twist, 180° CCW Twist, L= .3 Meters Avg. Δ Loss \leq 0.20 dB	10 Cycles Of: 360° CW Twist, 360° CCW Twist, L= .075 Meter	Δ Loss = -.008/- .004 dB Δ Loss = .002/.005 dB No Visual Damage Observed @ 10 X mag.
EIA FOTP-104 Cyclic Flexing Test (IEC 794-E6 Repeated Bending Test)	300 180° Flexes, Sheave Dia. \leq 20 X Cable Dia., or 32 mm Avg. Δ Loss \leq 0.20 dB	300 180° Flexes, Sheave Dia. 12.7 mm	Δ Loss = -.006/- .011 dB Δ Loss = -.003/.001 dB No Visual Damage Observed @ 10 X mag.

VII. Summary

The ever-increasing use of fiber optics by the Local Exchange Carriers is increasing jumper congestion in the Fiber Distribution Frames (FDF). Miniature jumper designs using a 1.6 mm OD cable as a basic unit have been developed to help relieve this congestion. These jumpers will tolerate the installation, handling, and removal operation during normal FDF use. An enhanced nylon buffer has been developed that has a low coefficient of friction and high modulus. This buffer will slide within the jacket and is compatible with the SC, FC, and all other optic fiber connectors available in the industry. This enhanced nylon buffer compares with PVC in strippability and is well within the requirements as given by Bellcore. These cable designs are available in both single fiber and duplex configurations.

VIII. References

1. Jenkins, A., Holman, J.R., Subh, N.T., Travieso, R. Reliability of Optical Fiber Interconnect Cables For New Connector Technology, International Wire and Cable Symposium Proceedings, Atlanta, 1994
2. Mathis, Don, Holman, Jim. Design of Buried Service Lightguide (BSL) Cables, International Wire and Cable Symposium Proceedings, Reno, 1990
3. Reagan, R. A. Comparison of 2.4 mm, 2.0 mm and New 1.6 mm Cordage Products, AT&T Internal memorandum, August 8, 1994
4. Bellcore. 'Technical Reference, TR-NTW-000409, Generic Requirements for Intrabuilding Optical Fiber, Issue 2, 1990



Don Mathis is a Member of Technical Staff in the Fiber Optic Cable and Materials Development and Engineering Department, at AT&T Bell Laboratories in Norcross, Georgia. He is responsible for the design of Fiber Optic Premises Cable products.

Dr. Mathis joined AT&T Bell Laboratories in 1972. He has B.S. and M.S. degrees in Mechanical Engineering from Oklahoma State University, and a Ph.D. degree in Mechanical Engineering from the University of Houston.

He has been granted 10 patents in the area of optic fiber connectors and cables.



Montri Viriyayuthakorn is a Member of Technical Staff in the Fiber Optic Cable and Materials Development and Engineering Department, at AT&T Bell Laboratories in Norcross, Georgia. He is responsible for product design and manufacturing process development for Fiber Optic Building and Specialty Cables.

Dr. Viriyayuthakorn joined AT&T Bell Laboratories in 1979. He has a B.S. degree in Civil Engineering and an M.S. degree in Mechanical Engineering from Worcester Polytechnic Institute, and a Ph.D. degree in Chemical Engineering from Brown University.

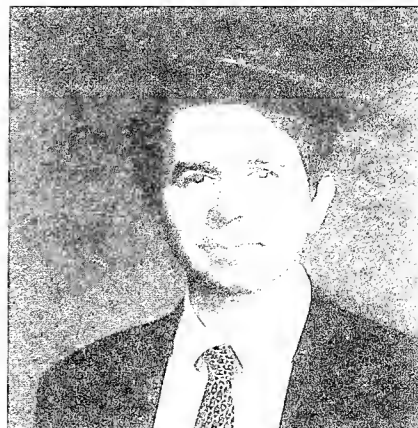
He has been granted 10 patents.



Jim Holman is a Senior Development Engineer in the Fiber Optic Cable and Materials Development and Engineering Department, at AT&T in Norcross, Georgia. He is responsible for the development of manufacturing processes for Fiber Optic Premises Cable products.

Mr. Holman began his career with AT&T Bell Laboratories in 1966 and later transferred to Network Cable Systems. He has a B.S. degree in Electrical Engineering from the Georgia Institute of Technology.

He has been granted three patents with one pending.



Randy Reagan is a technical manager of the Fiber Interconnection Equipment and Enclosure Department at AT&T Bell Laboratories in Whippany, N.J. His group's responsibilities include development of new fiber optic apparatus products for cable interconnection in the Central Office, Outside Plant, and Private Network applications.

Mr. Reagan holds a B.S. degree in Mechanical Engineering from NJIT, a M.S. degree from the University of Michigan, and an MBA from New York University.



Lionell Graham is a Technical Manager in the Fiber Optic Cable and Materials Development and Engineering Department. His group's responsibilities include design, development, process engineering, and testing for the manufacturing of Fiber Optic Building and Specialty Cables.

Dr. Graham joined AT&T's Engineering Research Center in 1978 and in 1991 transferred to Network Cable Systems. He has a B.S. degree in Chemistry from Tougaloo College and a Ph.D. degree in Inorganic Chemistry from the University of California at Berkeley.

NEW LOW COUNT OPTICAL FIBER CABLES

Susumu Saito, Naoki Okada, Kohichiro Watanabe, Matsuhiro Miyamoto

Telecommunication Cable Section, Opt-electronics Laboratory, Fujikura, Ltd.
1440 Mutuzaki, Sakura, Chiba, 285, Japan

Abstract

Recently, digital network systems using optical fiber transmission to serve subscribers in large cities are rapidly expanding. However, digital transmission systems are demanded not only in large cities but also in rural areas. The subscribers in rural areas are scattered so a distribution cable with a few fibers is expected to be used frequently there. A new lowest count cable consisting of only two 4-fiber ribbons has been developed. The cable structure was designed to be light weight and small in diameter for easy casual, quick and economical installation.

1. Introduction

The optical fiber transmission is spreading to subscriber networks, and Fiber-To-The Office (FTTO) is being constructed mainly for business users in urban areas. And optical fiber loops are constructed using higher count cables including 1000-fiber cables in metropolitan areas [1]. On the other hand, the demand for digital service in rural areas is growing as well as in urban areas although the density of users of this service is considerably low. To attain distribution to these users in a

short time, a thin, lightweight low-count cable is required [2-4]. In Japan, conventional distribution routes to subscribers are of duct and aerial. A slotted-rod type optical cables consisting of 4-fiber ribbons, with a typical count of more than 100 is widely used not only for duct routes but also for aerial routes. Therefore, two types (duct and aerial) of low count optical fiber cables each consisting of 4-fiber ribbons have been developed. The cable structures have been designed to accommodate 4 to 8 fibers in a small diameter.

2. New low count duct cable

2.1 Cable Structure

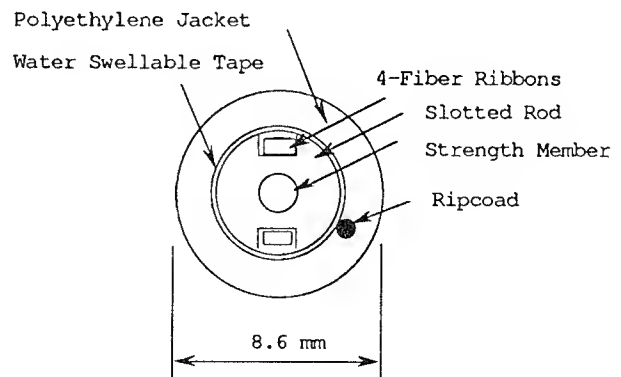


Fig. 1 Cross section of new low count cable for duct use

The design criteria for the new low count duct cable are 1) accommodation of one or two 4-fiber ribbons, 2) water blocking, 3) flame-retardant, 4) thin and lightweight for instant installation, and 5) sufficient mechanical strength. To meet these requirements, new small diameter slotted-rod cable was designed. The slotted-rod has two helical slots each capable of accommodating a 4-fiber ribbon can be accommodated in each slot. The diameter of the cable is reduced to be about 9 mm. A cross-sectional view of the new low count cable is shown in Fig. 1. The slotted-rod structure was chosen because of many advantages: high lateral pressure resistance, easy grip of central strength member for pulling, and dry type water blocking by water swellable tape. Moreover, the cable was made flame retardant by adopting a non-halogen polyethylene sheath. The new duct cable is compatible with conventional higher count slotted-rod ribbon cables in terms of splicing and installation.

2.2 Cable Fabrication

The new small slotted-rod cable was fabricated in the same manner as conventional slotted-rod cables. Ribbons were stacked into a slotted-rod. The core rod was wrapped with water blocking tape and sheathed. The dimensional characteristics of fabricated cable is shown in Table 1. The weight of the new

Table 1 Dimentional characteristics of new low count duct cable

	8 fiber duct cable
fiber	4, or 8
O.D	9 mm
Weight	60 kg/km

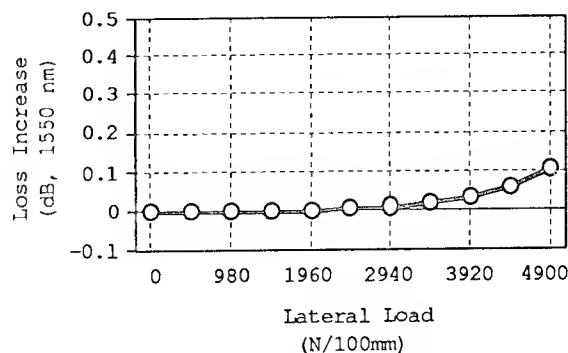


Fig. 2 Loss Characteristics of Lateral Pressure Test

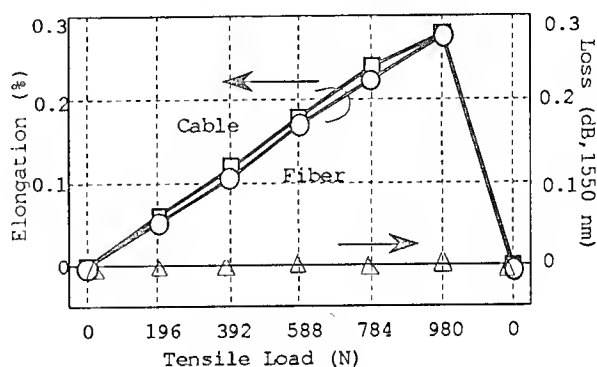


Fig. 3 Fiber and cable elongation under tensile test

duct cable is limited to 60 kg per km for ease of installation. The transmission loss performance of fabricated trial cable was as stable as that of conventional slotted-rod cables.

2.3 Cable Performance

The new low count fiber cable was subjected to environmental and mechanical tests. The results are as follows.

(1) Lateral Pressure Test (Crush):

Fig. 2 shows the lateral pressure characteristics of a trial cable. There was no loss increase at lateral loads up to 2940 N/10cm.

(2) Tensile Test:

Fig. 3 shows the fiber and cable elongations as a function of tensile

Table 2. The test condition and results of environmental and mechanical test of new lowcount cable.

Test	Condition	Results
Heat Cycle	-30,+70 deg.C	Loss change <0.1 dB/km at 1550 nm
Tensile	Maximum Load 245 N	loss change <0.1dB/km
Crush	Maximum Load 1960 N/100mm	loss change <0.1dB/km
Impact	1kg, 1m height 25mm flat head	residual loss <0.1dB/km
Twisting	1m length, $\pm 180^\circ$	loss change <0.1dB/km
Squeezing	Radi. 250mm Angle 90°	loss change <0.1dB/km

load. The elongation of the cable agreed with that of the fiber. The loss increase was not observed on the tension of 980 N.

(3) Water Blocking Test:

A 1 m static head was applied to one end of the trial cables. The water penetration length was less than 1 m even after 10 days. The water blocking performance of the cable was excellent owing to the relatively small slot size.

(4) Flame Retardant Test

We fabricated flame retardant type of duct cable by adopting non-halogen polyethylene sheath. The test was executed in accordance with "JIS C 3521", "Flame Test Method for Flame Retardant Sheath of Telecommunication Cables". This standard is based on "IEEE Standard 383". Flame could not continue to extend

over 1 m in height. The results were satisfactory.

Other environmental and mechanical test results are summarized and shown in Table 2.

3. New low count aerial Cable

3.1 Cable design

The new low count aerial cable was designed based on the conventional optical drop wire. A cross-sectional view of the new ribbon type aerial cable is shown in Fig. 5. The drop wire is composed of two single fibers with polyamid jacket and two parallel steel tension members embedded in polyvinyl chloride [PVC] sheath. The new cable has, in place of single fibers, 4-fiber ribbons with plastic jacket arranged between the parallel tension members.

The new cable is stranded around a supporting tension member (messenger wire). This simple cable design, which does not use any conventional protection slotted rod and water blocking tape is suitable for fabrication of a low cost, small diameter cable. The self-supporting structure is effective for quick and easy installation. The installation length of the drop wire is typically within 100 m. The new low count ribbon cable is required to be distributed more than several hundred meters in length. The supporting member is made as small as possible with consideration to cable handling and wind resistance. The increase in equivalent weight by wind is relatively small because the projected area of the cable is small.

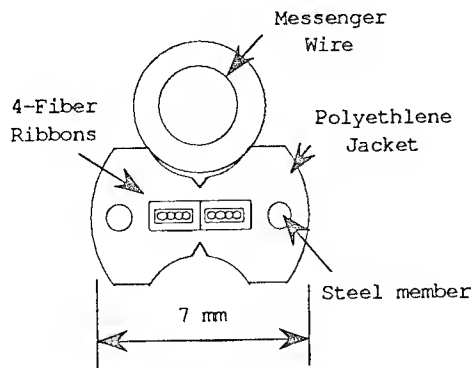


Fig. 4 Cross section of new low count aerial cable

The shape of cable cross-section is not circular but flat. And sheath surface is notched for ease of sheath removal.

3.2 Cable Manufacturing

We constructed trial cables in accordance with the above-mentioned design as follows:

(1) Jacketed fiber ribbon

Single mode fibers were arrayed and formed into 4-fiber ribbons in a standard process. Then, ribbons were jacketed with polyamid resin to improve robustness in the same manner as the single fibers of the drop wire. The jacketed ribbon is 0.6 mm in thickness and 1.3 mm in width.

(2) Sheathing

The two parallel steel members and ribbons are covered with polyethylene [PE] sheath. Polyethylene is adopted instead of PVC because of excellent mechanical and environmental reliability. The lateral pressure characteristics of unstranded cable with PVC and PE sheaths are shown in Fig. 5. In this comparison, our typical grade of PE and PVC for sheathing were used.

(3) Self-support stranding

The new cable is stranded around the supporting member without twisting and with a appropriate stranding pitch. The stranding pitch are determined in accordance with reel diameter. Fig. 6. shows the fiber strain of the cable wound on a reel as a function of reel diameter and stranding pitch. The fiber strain is determined by the change in fiber length by bending. A small reel for cable storing and carrying is desirable for economical installation.

3.3 Cable Performance

The transmission loss histogram and the loss change in the trial cable making process were shown in Fig. 7. and 8. No loss change were observed in the process. The transmission loss of cable was stable in repeated cable making processes.

The newly developed aerial cable was subjected to various environmental and mechanical tests. The results of other basic tests such as temperature cycle, tensile, crush, impact, twisting, squeezing and bending showed the sufficient performance of the new low

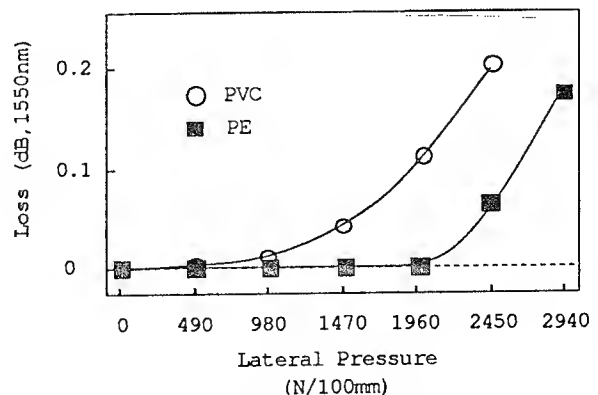


Fig. 5 Lateral compression test of aerial cables with PE and PVC sheath.

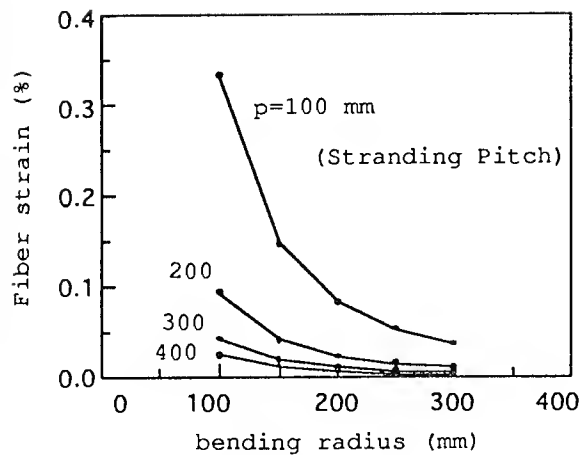


Fig. 6 Calculated fiber strain of bent aerial cable as a function of bending radius and stranding pitch.

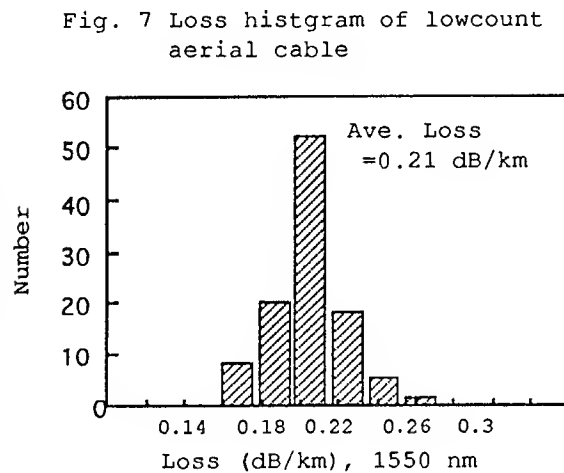
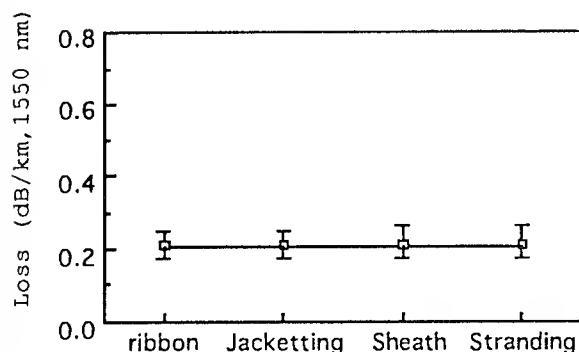


Fig. 8 Loss change of low count aerial cable in fabrication process



count aerial cable. Additionally we investigated the following characteristics and confirmed total performance by field test.

(1) Water Immersion Test

Fig. 9 shows the loss change of the newly developed aerial cable in water immersion test. The temperature of water was kept at 70 degree C. No loss change was observed during three months. The cable exhibited stable loss performance when immersed in water.

(2) Fiber strain in a reel

The fiber strain of the cable wound on a reel was measured by the Brillouin gain analysis in the same manner as the low count duct cable. Fig. 10 shows the Brillouin gain spectra in both straight and bent states. It is noted that the fiber strain caused by winding on the reel was small because the gain broadening were small. The change in fiber strain was roughly estimated at 0.002%. The two parallel members within the sheath would govern the cable bending direction. Fibers are positioned on the neutral axis of the flat cable. The cable is stranded around the supporting member without twisting. This is because the fiber strain of the cable wound on the reel is small. No loss change by winding were observed for a reel diameter of 250 mm. Use of a small and lightweight storage reel is essential for easy and economical installation.

(3) Installation Test

A new low count aerial cable was installed in the field to investigate the total performance including long term reliability. This test cable was strung on poles as shown in Fig. 11. The supporting member was easy to grab and

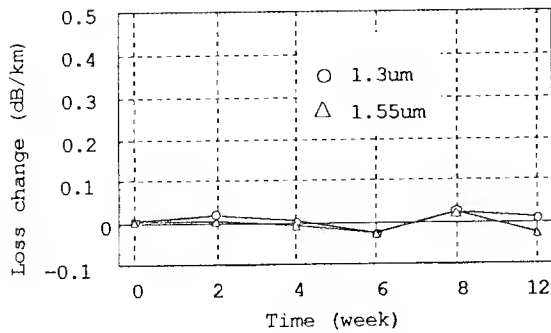


Fig. 9 Water Immersion Test

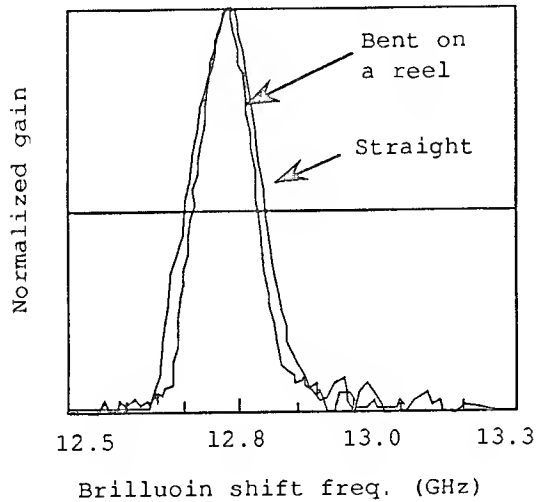


Fig. 10 Brilluoin gain spectra of aerial cable in straight and bent in reel.

fix on the poles by hand tools. The maximum pole interval was 50 m. Total route length was about 250 m. The stringing tension was only several tens of kg due to the lightweight of the cable which gives from 300 to 500 mm of dip for each span. The loss change was not observed just after installation. The optical attenuation and dips has been monitored since the end of cable installation. The loss change after installation is shown in Fig.12. No loss change was observed during four months. The monitored dip showed no change.

4. Conclusion

We have developed new duct and aerial cables each consisting of two 4-fiber ribbons for distribution in rural area. In the new cable design, the slotted-rod is minimized in size for two ribbons only. The aerial cable has a simple structure different from that of slotted-rod type. The new cables are light weight and small in diameter, so they are suitable for economical distribution. The cables can also be wound on a small reel with low fiber strain. Environmental, mechanical tests verified the excellent performance of the cables.

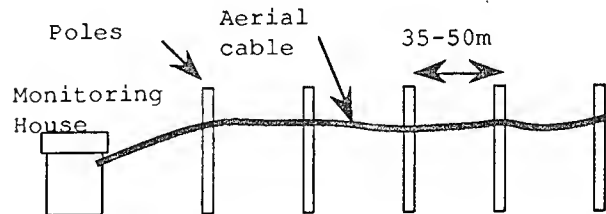


Fig.11 Field test of the new aerial cable.

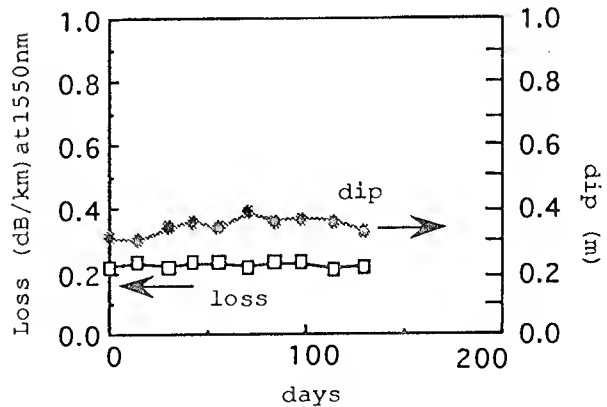


Fig. 12 Loss and dip change of installed cable

References

- [1] H. Ishihara, "Plan for Optical Access Network", NTT R&D, Vol.43, No.2, 1994
- [2] E. Kondo, M. Uesugi, N. Ohno, and T. Sano, "Characteristics of Low Count Optical Fiber Cable with Small Diameter" The Institute of Electronics, Information and Communication Engineers, B-874, 1993.
- [3] E. Kondo, H. Matsumoto, and K. Sato, "A Study on The Structure of Optical Fiber Cable" The Institute of Electronics, Information and Communication Engineers, B-630, 1992.
- [4] T. Nakayama, H. Okabayashi, E. Kondo, and S. Matsushashi, "To Make The Economical Deployment of Subscriber Networks" 42nd IWCS, pp.339-345, 1993.
- [5] T. Horiguchi et.al, Journal of IEICE of Japan, J73-B-I, No.2, pp.144, 1990



Naoki Okada was born in 1964. He joined Fujikura Ltd. after his graduation from Chiba University with a B.E. Degree

in 1986 and has been engaged in research and development of optical fiber cables. He is now an engineer in the Telecommunication Cable Section and a member of the IEICE of Japan.



Kohichiro Watanabe was born in 1959. He received a B.E. degree in electrical engineering from Tohoku University in 1982. Since

joining Fujikura, Ltd. in 1988, he has worked on the development of optical fiber cables. He is currently employed in the Telecommunications Cable Section of the Opto-electronics laboratory.

Acknowledgment



Susumu Saito was born in 1964. He received a B.S. degree in physics from Sophia University in 1987.

Since joining Fujikura, Ltd. in 1987, he has worked on the development of optical fiber cables. He is currently employed in the Telecommunications Cable Section of the Opto-electronics laboratory.



Matsuhiko Miyamoto was born in 1953. He graduated from Nagoya Institute of Technology with a B.E.

degree of electrical engineering. He joined Fujikura Ltd. after his graduation from Tokyo Institute of Technology with a M.S. degree in 1978 and has been engaged in research and development of optical fiber and optical fiber cables. He is now a manager of the optical fiber cable section.

MANUFACTURING AND FIELD EXPERIMENTATION OF MICROSHEATH CABLE FOR LOW COST SUBSCRIBER LOOP.

P. JAMET - A. JARLOT

SILEC - MONTEREAU - FRANCE

1. ABSTRACT

This paper gives detailed informations about the microsheath cable concept, in terms of structure, packing density, weight and main mechanical and optical characteristics.

It also describes the technical solutions which have been found in order to have a pre-industrial production of microsheath cables.

Then, the results obtained by such a cable in a field experimentation of FTTB/FTTH network are described.

The papers published at the 40th IWCS⁴ and at the EFOC in june 1992⁵ presented the microsheath cable concept to be the best solution for low cost subscriber loop.

At the moment microsheath cable is coming from concept to pre-industrial reality with field experimentations.

3. CONCEPT AND STRUCTURE OF MICROSHEATH CABLES

3.1. CONCEPT.

The classic long distance optical cables require fiber overlength mainly to obtain no strain on the fibers during laying (high tensile strength, crush resistance, ...) and thermal cycling (wide range of temperatures). So these cables are not totally optimized in terms of compacity and cost.

It has been demonstrated that a limited strain (fiber elongation $\leq 0.3\%$), mainly during cable laying, is acceptable without damage for transmission performance and lifetime. So it is possible to manufacture cables with adapted sheathing, without fiber overlength, meeting the following characteristics :

- longitudinal performance : low thermal dilatation coefficient, high tensile modulus,
- radial performance : crush and bend resistance.

Therefore packing density increases and weight decreases substantially.

Generally cables and cable elements cross section are circular : in the past, many other solutions have been investigated but, finally, circular structures are always the best solution to design and manufacture cables easily. So it is better for all cable elements, such as fiber modules, to be circular.

2. INTRODUCTION

FTTL development depends on the emergency of low cost technical solutions. It has been demonstrated that the passive infrastructure (civil works, cables, laying, splicing and closures) has a major impact on the global costs.

So, the use of cables specifically adapted is needed. In a wide range of fiber counts^{1,2,3}, cables have to present the main following characteristics :

- small external diameter (high packing density),
- low weight,
- modularity,
- suitable performance.

All these adapted characteristics should results in :

- low cost cable (small diameter, easy manufacturing with a limited number of operations),
- low cost laying (small diameter and small weight),
- low cost splicing (modularity, single and multi fiber splicing, ...).

All these considerations lead to the microsheath cable concept i.e. :

- circular modules without fiber overlength inside each module,
- circular assembly of modules,
- circular sheathing with minimum empty space between the assembly and the sheath(s).

3.2. STRUCTURE OF THE MICROSHEATH CABLES.

3.2.1. Microsheath modules

They are constituted of a circular assembly of coloured fibers (for instance 4, 6 or 12 fibers) covered with a tight thin sheath. Between fibers and the sheath a watertightness compound may be applied. The microsheath has to be easily removable without any tool.

3.2.2. Module assembly

Modules are SZ stranded in order to make units of 4, 6 or 12 modules for instance. Each unit is identified by a coloured binder.

3.2.3. Sheathing

SZ stranded units are covered by one or several sheath(s) tightly applied on the assembly.

The structure is described in figures 1.

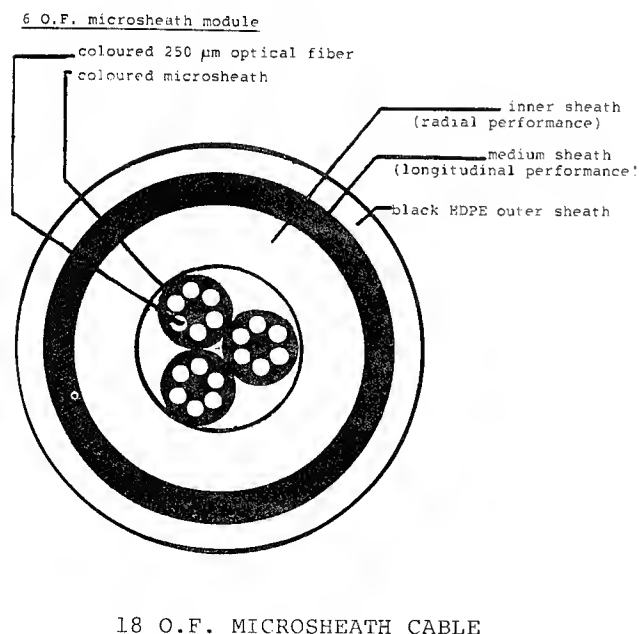


Fig. 1a

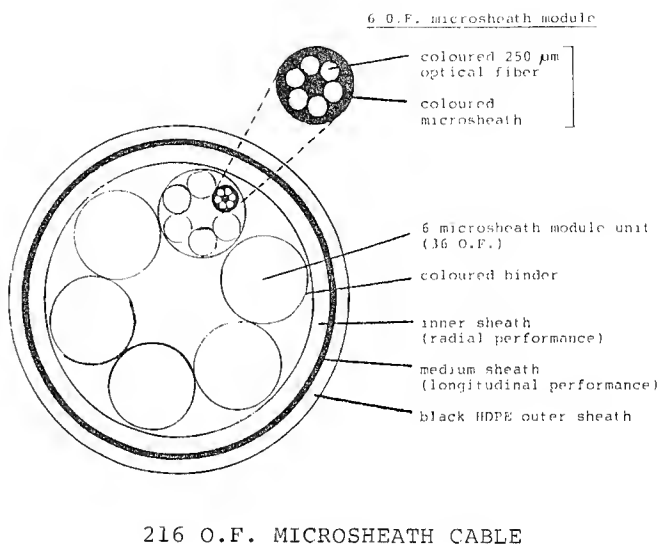


Fig. 1b

Remarks :

1/ In the same way it is possible to manufacture higher fiber count cables by :

- increasing the microsheath module number,
- increasing the optical fiber number inside the microsheath module.

2/ An alternative solution consists in cabling several medium fiber count super- units, for instance 7 x 216 O.F. (see figure 2).

As for telecom copper cables, fiber identification is easily obtained by the combination of :

- coloured binder (unit identification),
- coloured microsheath (module identification)
- coloured coating (fiber identification).

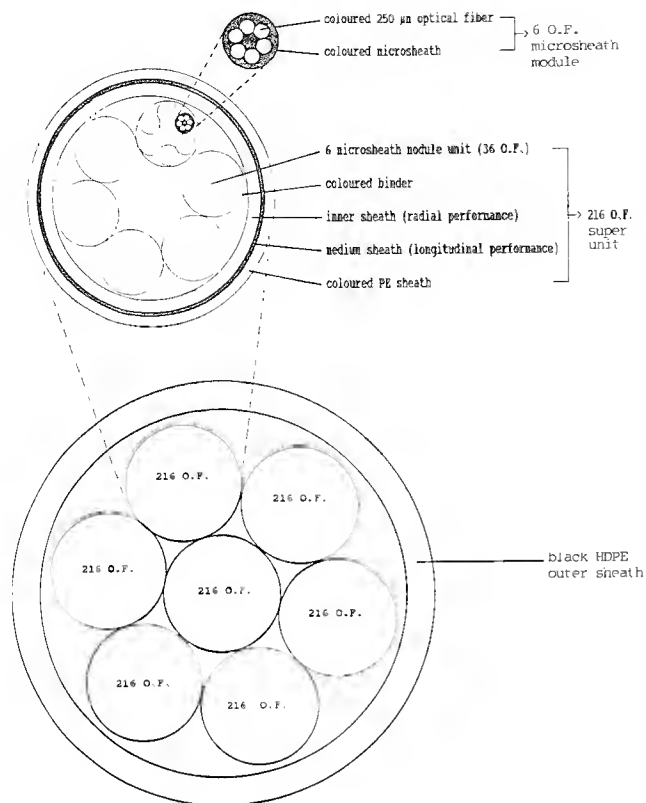


Fig. 2

3.3. MATERIAL ASPECTS

3.3.1. Microsheath modules

Microsheath materials have to comply with the following requirements :

- high speed manufacture,
- low modulus (section X Young modulus) to obtain no residual strain on the fibers in a large range of temperatures, good flexibility and removability,
- long term stability.

SILEC has developed such a thermoplastic compound.

3.3.2. Sheathing

First sheath : radial characteristics (crushing and bending) are easily obtained with classical hard thermoplastics.

Second sheath : longitudinal characteristics (high tensile modulus and low thermal expansion coefficient) are obtained when using composite thermoplastics, or liquid crystalline resins or solid strength members (FRP or steel).

It is possible to combine the two types of characteristics, using only one inner special sheath.

External sheath : polyethylene, PVC or flam retardant halogen free sheath, depending of the application.

3.4. MAIN CHARACTERISTICS

3.4.1. Microsheath modules

For instance, with 250 µm coated fibers the outer diameter of the module is 0.95 mm for 6 fibers and 1.30 mm for 12 fibers.

It is demonstrated that the manufacture of microsheath modules induces no change in the attenuation values at 1300 and 1550 nm with single mode fibers (see fig. 3).

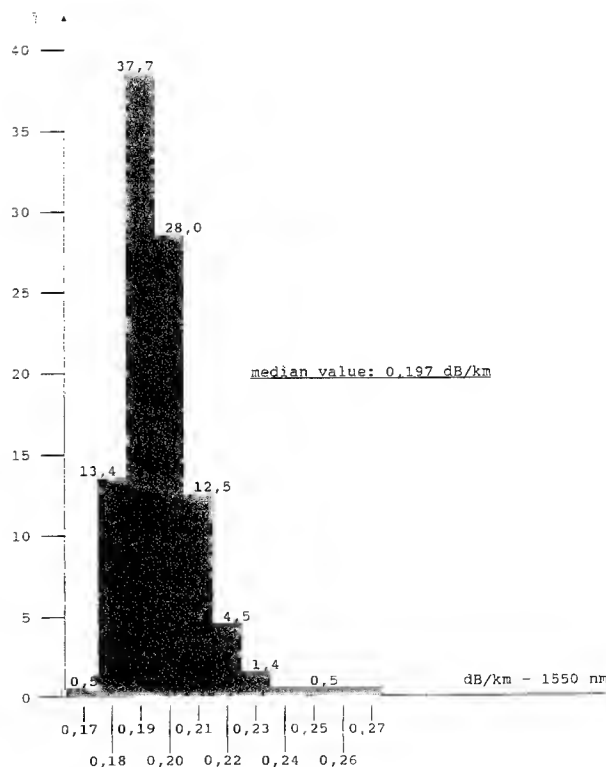


Fig. 3

During thermal cycling (see fig. 4) between -30 and +60°C the maximum reversible attenuation change at 1550 nm is lower than 0.10 dB/km (generally ≈ 0 dB/km).

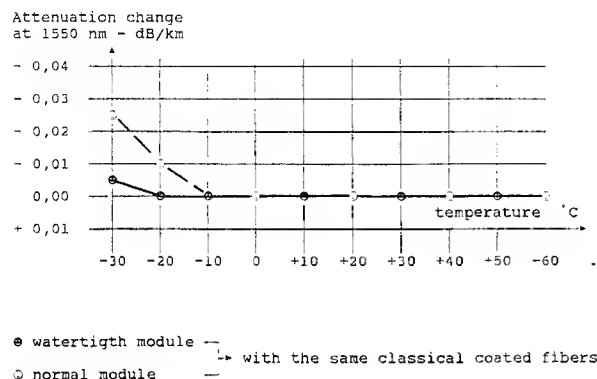


Fig. 4

Modules dipped in water at 20°C during 3 months present no significant attenuation change at 1300 and 1550 nm (see fig. 5) with classical and specially coated (for ribbon production) single mode fibers. After 10 days in water the coating strippability decreases and is the same after 3 months. With microsheath modules this reversible decrease (after drying) is limited (20 % lower) if compared to single optical fibers dipped in water.

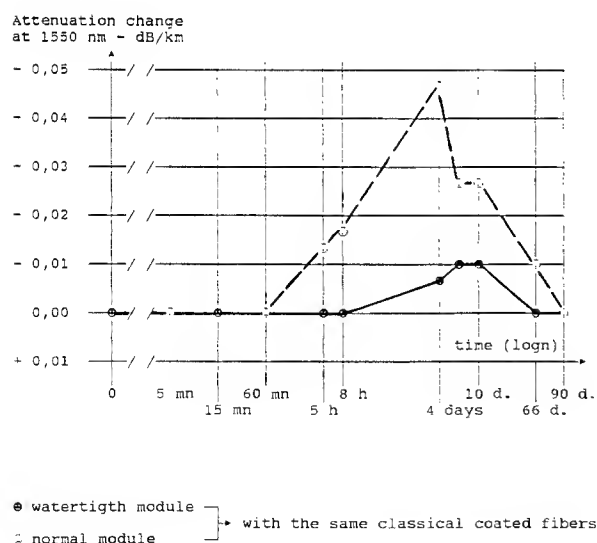


Fig. 5

In the same way a damp heat test (following "Draft I-ETS for single mode optical ribbon cable - amended version of Madrid TD 90 / TD 16 A for WGI - 1993 October 1st) gives good results :

- no attenuation change at 1550 nm,
- stability of the coating strippability.

3.4.2. Microsheath cables

The following cables are designed with 250 μ m coated optical fibers.

Actually each module contents 6 fibers according to FRANCE TELECOM requirements (other modularities are available).

The external sheath of indoor cables is made of an halogen free flame retardant compound.

The outer sheath of outdoor cables is made of black HDPE.

Main characteristics of 100 % extruded thermoplastic sheathed cables (except direct burial cable with a corrugated steel armour and aerial cable with steel messenger) are summarized in the following tables. They comply with FRANCE TELECOM requirements for local networks.

DIMENSIONAL CHARACTERISTICS				
Application	Fiber count	External diameter mm	Packing* density O.F./mm ²	Weight kg/km
INDOOR	6	5.6	0.24	33
	18	7.0	0.47	77
	36	8.1	0.70	88
LAYING IN DUCTS	6	4.5	0.38	15
	18	6.3	0.58	32
	36	7.8	0.75	50
	72	10.0	0.92	80
	144	12.0	1.25	130
	216	14.3	1.34	185
	612	22.0	1.61	380
	1 512	31.0	2.00	780
DIRECT BURIAL	36	12.0	0.32	120
AERIAL	18	$\leq 7 \times 15$	-	-

* Packing density is multiplied by 2.5 to 4.0 if microsheath modules are made of 12 smaller optical fibers (180 μ m diameter over coating).

If we compare microsheath cables packing density to ribbon cables packing density⁶ (see figure 6) it is easy to demonstrate that the ribbon concept needs special 180 μm coated optical fibers to obtain the same compacity that microsheath cables with 250 μm coated optical fibers : the microsheath concept gives systematically the best packing density.

PACKING DENSITY: O.F. / sq mm

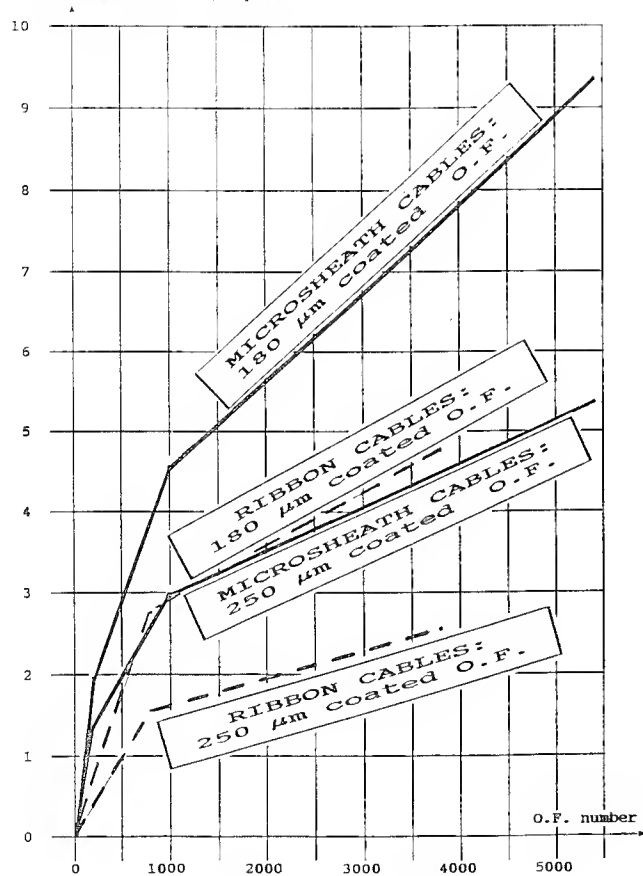


Fig. 6

MECHANICAL CHARACTERISTICS WITHOUT ATTENUATION CHANGE				
Application	Fiber count	Crush resistance daN/cm	Mini.bend radius mm	Tensile strength daN
INDOOR	6	20	30	35
	18	25	40	80
	36	25	50	90
LAYING IN DUCTS	6	25	50	25
	18	25	65	35
	36	30	80	50
	72	30	120	80
	144	30	150	150
	216	30	170	200
	612	30	250	380
	1 512	30	300	800
DIRECT BURIAL	36	40	150	100
AERIAL	18	30	100	240

THERMAL CHARACTERISTICS			
Application	Fiber count	Temperatures with $\delta\alpha$ 1550 nm ≤ 0.10 dB/km*	Temperatures with $\delta\alpha$ 1550 nm reversible
INDOOR	6 to 36	-10 to +40°C	-30 to +60°C
LAYING IN DUCT	6 to 1512	-20 to +60°C	-30 to +60°C
DIRECT BURIAL	36	-20 to +60°C	-30 to +60°C
AERIAL	18	-30 to +60°C	-40 to +70°C

* typical value ≈ 0.02 dB/km

It is possible to improve performance with other thermoplastic materials or when cables are not 100 % extruded : for instance better cold temperature and tensile strength characteristics.

4. PROCESS CONSIDERATIONS

Most of new cable designs require specific investissements in machinery or extensive modifications of the existing manufacturing process. On the contrary, the manufacture of microsheath cables requires only conventional telecom cable operations.

4.1. MANUFACTURE MODULE PROCESS

For instance a loose tube high speed production line is quite convenient for microsheath modules manufacturing. The following equipments are required :

- fiber unwinding with low and regulated tensile strength,
- SZ twisting,
- watertightness compound injection,
- extruder with screw and tools designed for low material flow,
- capstan or caterpillar modified in such a manner that the module is not crushed
- winding with low tensile strength.

4.2. STRANDING OF THE MODULES

For instance a SZ loose tube stranding line with low tensile modules unwinding and low tensile binding is convenient.

4.3. SHEATHING

A classical sheathing line with 2 - 3 serial or attached extruders adapted to each thermoplastic material is recommended.

4.4. REMARKS

It is quite possible to associate stranding and sheathing. So manufacture of microsheath cables is limited to 2 operations :

- microsheath module extrusion,
- stranding/sheathing.

High speeds may be obtained with these processes, after optimization, taking under consideration productivity and quality purposes.

5. INSTALLATION OF CABLES

4,8 kms of microsheath 36 O.F. duct cables (see point 3.4.2), with 6 usefull single mode optical fibers have been supplied for a FITL experimentation by FRANCE TELECOM in Arcachon.

5.1. GENERAL CONDITIONS OF THE EXPERIMENTATION

Some of the objects of the experimentation consist in the field evaluation of different technics, such as :

- laying in duct a microsheath cable without any specific equipment,
- using opto-couplers (2 -> 8),
- splicing fibers from microsheath modules,
- measuring the final optical budget.

The cable lengths repartition is the following :

- middle length : 215 m
- maximum length : 570 m
- minimum length : 45 m

5.2. INSTALLATION OF THE CABLES

Most of the individual cable lengths being of some tens of meters have been directly and manually pushed inside ducts without any preparation.

The longest individual lengths (570 m, 470 m ...) have been layed with the same technic, the intermediary chambers being used as a relay to push the cable.

Systematically, no specific equipment has been used except, for each drum of 2.4 km of cable, a standard take up lightly braked.

For all lengths layed, the maximum tensile strength was very small (some daN), even when ducts contained cables yet installed and when 3 microsheath cables were pushed simultaneously in the same duct.

The materials used to make the cable, its light rigidity, small diameter and low weight explain these very good results.

No special tool except a cutter is needed to open the cable. The microsheath protecting the 6 fibers is manually removed (with nails). Fiber identification is easy. The microsheath modules are very flexible (they accept without damage, in all directions, the same minimum bending radius than the individual optical fibers) and are easy to arrange in small contents (for instance cassettes).

Classical individual optical fiber splices have been quickly made with good results without any problem [in laboratory, multi splices of 6 fibers (after a flat positioning) with a classical optical ribbon splicing machine give also good results]. The microsheath concept is compatible with low cost splicing operations.

The control tests of the installation show :

- no variation of the cables attenuation at 1300 and 1550 nm with regard to values given by the fiber manufacturer,
- that total optical budget is very low : the biggest attenuations are due to opto couplers. So optical attenuators are necessary.

6. CONCLUSION

Microsheath cables are now a pre-industrial reality in a wide range of fiber counts and applications. With their adapted characteristics, easiness of laying and splicing they are the best solution for low cost distribution networks.

ACKNOWLEDGEMENTS

The authors would like to associate to this paper teams of FRANCE TELECOM / CNET and SAT Company involved in the development of the microsheath cables and their applications within this project supported by FRANCE TELECOM.

REFERENCES

- 1/ M.H. REEVE - "Optical fibre network architectures for the local loop" - EFOC/LAN 1989, p. 168.
- 2/ J. ABIVEN - "La transmission de services à bas débit sur bus passif" - L'Echo des Recherches - n° 138 - 4ème trimestre 1989 - p. 13.
- 3/ U.H.P. OESTREICH - "Design considerations for short haul cables" - 35th IWCS, 1986, p. 24.
- 4/ P. TROMBERT, P. JAMET, P. CHERON / G. LE NOANE, D. BOSCHER - "The microsheath cable : a novel design of ultralightweight single mode optical cable for low cost subscriber loop" - 40th IWCS, 1991, p. 24.
- 5/ P. TROMBERT, P. JAMET, P. CHERON / G. LE NOANE, D. BOSCHER - "The microsheath cable : a novel design of ultralightweight single mode optical cable for low cost subscriber loop" - EFOC/LAN 1992, part 1, p. 45.

6/ S. TOMITA, M. MATSUMOTO, N. NAGASAWA, T. TANIFUJI - "Ultra high density fiber cable with thin coated fibers and multi fiber connectors" - NTT - JAPAN - 42th IWCS, 1993, p. 5.



Patrick JAMET

Société Industrielle
de Liaisons Electriques
S I L E C
B P n° 6
77871 MONTEREAU CEDEX
F R A N C E

Patrick JAMET, born in 1950, received his Ph.D of Physical Chemistry from the DIJON University in 1976 and is presently the R. & D. manager for copper and optical telecom cables.



Alain JARLOT

Société Industrielle
de Liaisons Electriques
S I L E C
B P n° 6
77871 MONTEREAU CEDEX
F R A N C E

Alain JARLOT, born in 1945, is graduated from the POITIERS Ecole Nationale Supérieure d'Ingénieurs. He joined SILEC in 1969 and is presently the copper and optical telecom cable product manager.

ULTRA HIGH DENSITY CABLES USING A NEW CONCEPT OF BUNCHED MULTICORE MONOMODE FIBERS : A KEY FOR THE FUTURE FTTH NETWORKS

G Le Noane , D Boscher , P Grosso , J C Bizeul , C Botton

France Telecom CNET LAB/FCI/FCM 22300 LANNION FRANCE

ABSTRACT

In comparison with FTTC/FTTB systems in economical terms , the full-star option remains more evolutionary and requires relative simple technologies to be cost competitive . To achieve this goal we propose a new concept of bunched multicore monomode fiber (BMMF) leading to a very precise matrix of monomode guides inscribed in a 125 μ m diameter and leading to a drastic increasing of density and a drastic decreasing of "cabled monomode guide cost". This paper describes the design of this new BMMF, the technological principle, the first experimental results with four, seven and nine cores monomode fibers. To ensure the credibility of the BMMF concept, we also investigate other main characteristics and components such as strength of the fiber, test of several cable structures, splices and fan out termination.

1 INTRODUCTION

Many topologies have been proposed in order to realise FTTH networks, but to day there is no clear indication of which configuration will be the best candidate and in any case much studies and development are needed before definitive choices can be made. The final choice will depend on economic factors and on other parameters like flexibility, ability to upgrade new services, reliability . However the economic factors are quite different according to a certain configuration and, in particular, the initial first cost including the cost installation of the primary and the secondary distribution sections , the economical weight of optical components like fibers, cables, splices, connectors, opto-electronical technologies can be clearly identified according to each main option for the local network leading to specific and ambitious technological programs.

Today among the three general options, full-star network, distributed-star network and passive

splitter network, and as a result of economical analysis, it is generally well-accepted that the full-star network, in which every subscriber has a dedicated fiber all the way back to the exchange, is not cost effective. Consequently, recent developments tend towards sharing customer access using much less fiber per subscriber and sharing the cost of optical transmitters and receivers among many subscribers. In such FTTC/FTTB systems it appears that recent progress on monomode fibers in term of cost and quality, new technologies of high count and high density cables like ribbon technique or micro sheath techniques give a correct answer to built efficient networks. However it remains a need for the development of specific components and some drawbacks can be clearly identified.

For the full-star option, the optical technologies are relatively simple but they need drastic evolution to be cost competitive. In particular, and in order to reduce the initial costs and the cost per subscriber, very high density and low cost cables and associated techniques are required. Several way are under investigation like ultra high density and high count preconnectorized optical fibre cables (1,2,3). In this technique a decreasing of the coated fiber diameter can be used to increase the fiber count in a ribbon (4,5) leading to a 4000 fiber cable 35 mm in diameter by replacing the five 12 fiber stack with a ten 16 fiber ribbon. In parallel and as a part of a large technological program on all the active and passive components at CNET, we have studied new technologies for low-cost and high precision fibers (6) and for ultra-light weight and high density cables (7). Nevertheless if these technologies appear well adapted and cost effective for some FTTC/ FTTB or FTTH sharing options, it seems that the FTTH full star option (which does not exclude however sharing aspects for optical transmitters) requires a new step in the high density and in the modularity of cables in order to realise very high count fiber networks while decreasing drastically the initial and the engineering costs.

Several years ago, a technical program, was managed in Japan on multicore multimode fibers leading to some interesting results (8,9,10). In the meantime, spectacular progress on monomode fibers in term of performances and cost have authorised their use in the local network. So in order to increase drastically the cable density and the cost of the "cabled monomode guide" (a new concept which replace the "cabled monomode fiber") we have studied a new concept of multicore-monomode fiber (BMMF). In particular, and as an example the structure and the manufacturing of a four cores bunched fiber is described in this paper. Then some fundamental characteristics such as optical loss and crosstalk are given with some experimental results.

II BUNCHED MULTICORE-MONOMODE FIBER (BMMF) DESIGN

2.1 design

To produce all synthetic glass monomode fibers with very precise geometrical characteristics, we have proposed recently (6) a direct deposition inside very thick and precisely bored silica lingots using a new manufacturing deposition and collapsing process, the FCVD(Furnace Chemical Vapour Deposition). This process achieves very precise geometrical characteristics thanks to the precise geometrical characteristics of the thick tubes before deposition and to the very stable and efficient collapsing. On the other hand, the use of a synthetic silica tube, typically 1ppm OH content gives the opportunity to reduce the core-cladding ratio b/a to about 3 leading to CVD glass volume fraction of about 4% for a classical monomode fiber of 125 μm outside diameter. One of the basic ideas for our multicore monomode design is to consider that these well-known and very precise geometrical characteristics and this low b/a ratio are quite interesting to bunch preform after a precise grinding to obtain the desired matrix. The other consideration is that there is no need in a bunched multicore monomode fiber for a silica cladding of 125 μm on each elementary preform in term of bending and micro-bending behaviour, in particular for a use in the 1,3 μm window, and taking into account some optimisation of the core parameters ($\phi_c, \Delta n$). So, associating these main considerations, the FIG1 indicates the principle of our four cores BMMF.

As an example of this design, a four cores fiber is inscribed in a 125 μm diameter circle, leading to a

density multiplied by four, and to a cost of "cabled monomode guide", which therefore replaces the classical "cabled monomode fiber", divided by a factor comprise between 3 and 4. The accuracy of the elementary preforms and consequently the accuracy of the bunched perform gives a very precise spatial reference for the four cores of the matrix which will be the basic criteria for the connecting devices.

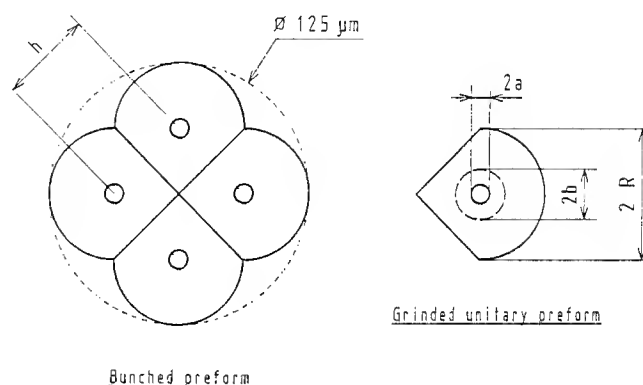


Fig1 : Design of four core BMMF

	External	Optical cladding	Core	h
	Diameter	Diameter	Diameter	Diameter
PREFORM	16 mm	6,15 mm	2 mm	11,3 mm
FIBER	62,5 μ	24 μ	8 μ	44,2 μ

Parameter of a 4 cores BMMF : $\Delta n = 5,1 \cdot 10^{-3}$

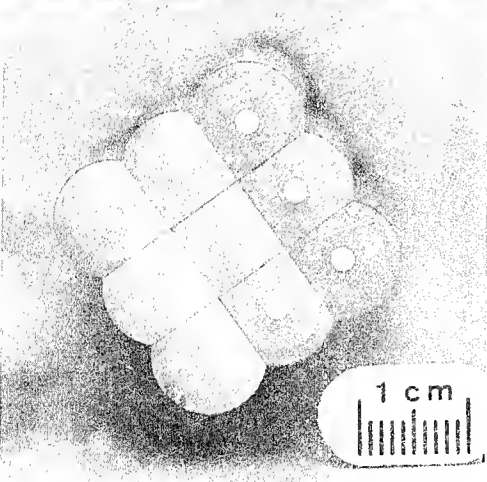
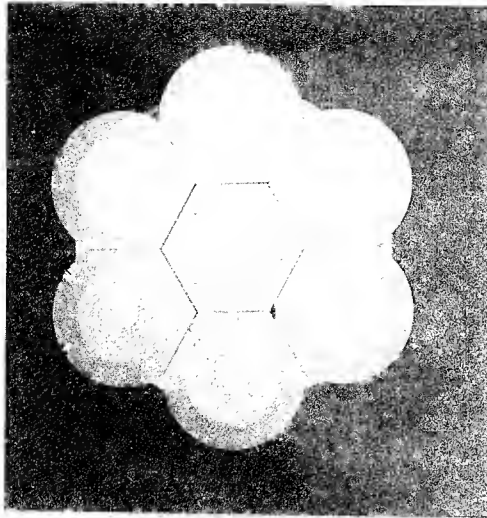


Fig2 : Assembled Preforms with 9 , 7 , and 4 cores

2.2 Manufacturing

The manufacturing process is divided into the following phases ;

- To realize the elementary performs with the opto-geometrical characteristics adapted to the desired bunched perform. This means that the perform process needs a good control and reproducibility to obtain the good nominal outside diameter with the good opto-geometrical characteristics of the core.

- To grind the elementary perform to obtain the shape in order to bunch them for the desired matrix.

- To bunch the elementary performs and fused the extremity of the bunched preform to a special beginning silica rod. With this concept we provided three types of preform which are presented on photography 2.

The preforms are then drawn in a classical HF furnace to obtain the 125μm fiber which is protected with a monolayer UV Epoxyacrylate coating.

III Theoretical aspects

The coupling of two parallel fibers was theoretically studied several years ago with coupled mode theories (11,12,13). These theories were applied to monomode optical couplers where the distance between the two cores was very short, giving a very high coupling coefficient. When the cores are non identically, the power coupling of one core to another is given by :

$$[1] \quad P_2 = P_0 F^2 \sin^2 \left(\frac{CL}{F} \right)$$

$$\text{with } F = \frac{1}{\sqrt{1 + \left\{ \frac{\beta}{2C} \left(\frac{\partial R_c}{R_c} - \frac{\partial \beta}{\beta} \right) \right\}^2}}$$

Where R_c is the radius of curvature of the fiber itself.

C is the coupling coefficient :

$$[2] \quad C = \frac{\sqrt{2\Delta} u^2 K_0(w h/a)}{a V^3 K_1^2(w)} \approx \sqrt{\frac{\pi \Delta}{w h a}} \frac{u^2 \exp(-w h/a)}{V^3 K_1^2(w)}$$

with a : core radius,

h : center-to-center distance,

Δ : profile height parameter $\left(\Delta = \frac{n_{co}^2 - n_{cl}^2}{2n_{co}^2} \approx \frac{\Delta n}{n_{co}}, \Delta n = n_{co} - n_{cl} \right)$,

n_{co}, n_{cl} : core and cladding index,

V : waveguide frequency $(V = k a n_{co} \sqrt{2\Delta}, k = 2\pi/\lambda)$,

u, w : respectively core and cladding parameters $(V^2 = u^2 + w^2)$

When the cores are strictly identical, we observe that the coupled power is strongly dependent on h value and wavelength (fig3). Fortunately, with a very small propagation constant variation $\Delta\beta$, we observe that the maximum coupled power go down drastically.

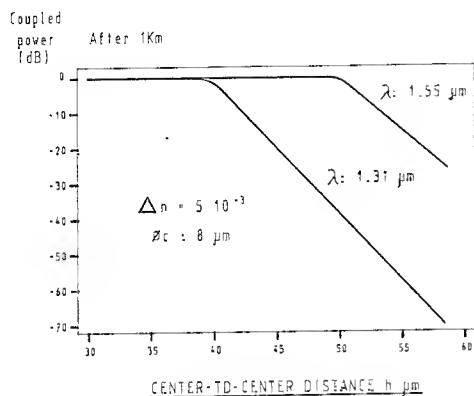


Fig 3 : Coupled power versus intercore distance with identical cores.

The figure 4 shows that $\Delta=10^{-7}$ index variation or 0.0001 micron core radius variation guarantees a maximum coupled power of 50db with $\Delta n = 7 \cdot 10^{-3}$.

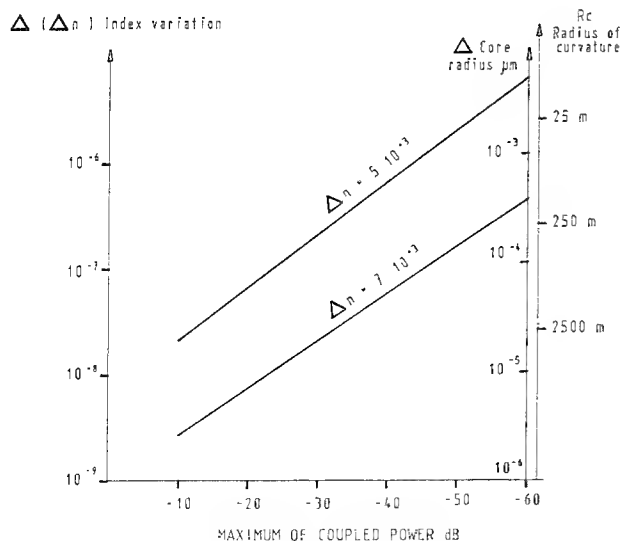


Fig 4 : Maximum coupled power for non identical cores.

We observe with relation 1 that, when the propagation constant variation $\Delta\beta$ increases, the coupling length L_c decreases in the same time and Fig 5 gives the coupling length versus the maximum coupled power for the four cores BMMF ($h=44.2\mu$).

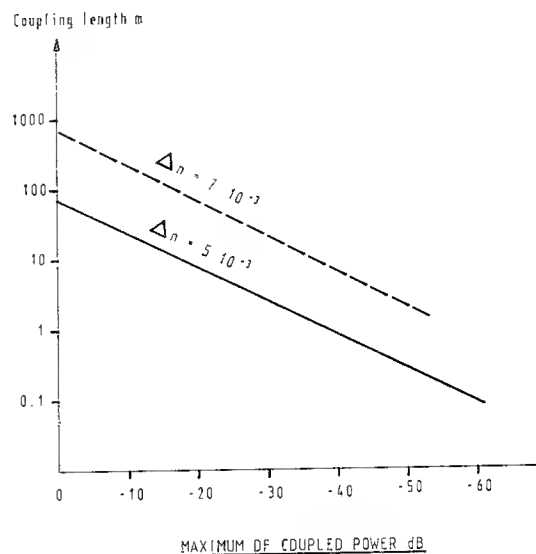


Fig 5 : Coupling length versus the maximum coupled power.

Previous result leads to a great practical interest for the design and the optimisation of our bunched multicore monomode fiber (BMMF). It is clear that taking into account these theoretical considerations, the design of very high density BMMF is the result of a good compromise between several opto-geometrical parameters of the monomode guides, preform process efficiency and specifications (attenuation, cabling ability, splicing ability...). In particular we have to consider that this new BMMF concept is completely adapted to a future full-star FTTH network where a monomode guide is completely or partially dedicated to a subscriber. It seems obvious that such approach opens the door for a redesign of the monomode guide to optimise the BMMF. In particular in a classical monomode fiber, the index difference and consequently the core diameter were optimised to obtain at a given λ_c the minimum attenuation in the second and third window compatible with a good cabling ability. In the BMMF concept, attenuation and dispersion are not

determinant parameters and consequently a redesign can be done in term of process efficiency, optimisation of density, micro-bend resistance and so on. More over we can consider that in a full-star concept the use of adjacent guides can be dedicated to two different ways (one for the central office to the subscriber and the other for the subscriber to the central) leading to an effective distance $\sqrt{2} h$ between two guides in terms of main crosstalk.

IV FIRST RESULTS OF FOUR CORES BMMF

4.1 Transmission

About hundred kilometers of four cores have been manufactured with several modified parameters such as welding or soldering perform, drawing temperature or mismatched refractive index.

In order to test the microbending behaviour in cable, we applied a hard single layer coating with 240 μ diameter without optimization particularly for the eccentricity of the coating and the photography 6 shows you the four cores BMMF and its coating.

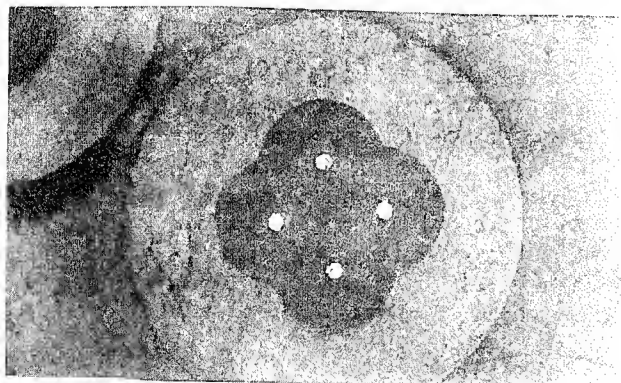


Fig 6 : Photography of the 4 cores BMMF with its coating.

Theoretical approach showing the wavelength, h and Δn dependence have been perfectly checked and the transmission measurements : are given in the table 7.

Index Variation				
	5 10 ⁻³		7 10 ⁻³	
	Attenuation	Crosstalk	Attenuation	Crosstalk
1,3 μ	0,35 db/km	40 db	0,33 db/km	>55 db
1,55 μ	0,54 db/km	18 db	0,28 db/km	38 db

Table 7 Optical Characteristics of 4 cores BMMF

The crosstalk could be a main factor for the transmission qualities and a first experiment has been carried out with a bad BMMF (20db diaphotie) at 1.55 μ .

The transmission bit error with a 140 mb/s bit rate on 2 km length at 1.55 μ was not measurable (BER< 10⁻¹²).

4.2 Mechanical behaviour

The four cores BMMF structure is not circular and the mechanical stress behaviour will be different from classical fibers. The first investigations which are made, show that drawing preparation and temperature influence the break level, but the first weibull diagram can be considered as satisfactory.

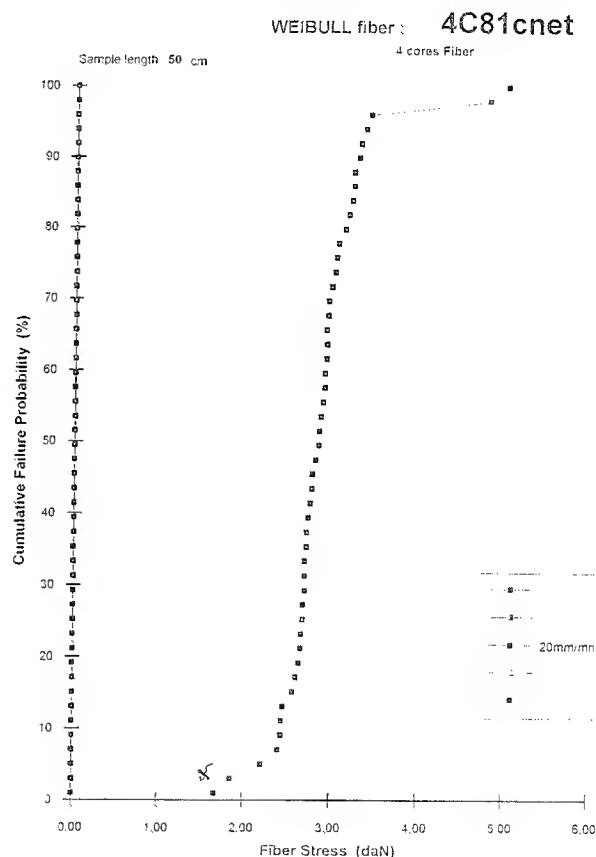


Fig 8 : Weibull diagram of the BMMF

The mean value which is close to 3 da N, must be in fact, applied to the minimum diameter of the

fiber ($\sqrt{2} R$) and this strength extended to the 125 μ fiber is in comparison with classical fibers.

4.3 BMMF Cabling

After drawing and characterization of the BMMF, several cable structures have been tested, for evaluation to provide a previous demonstrator including all network passive components.

The incidence of this new concept on the cable performance is very easy to demonstrate and it appears in particular that the concept of microsheath (7) or ribbon cable which appears very modular and leads to ultra light weight and high density cables is well adapted to receive the concept of BMMF. The table shows the evolution providing in a few years by the microsheath design and secondly by the microsheath design associated with the BMMF. The break is very impressive and leads to two important consequences :

- The new ultra high density of BMMF cables authorises a very flexible installation reducing the first cost of a full-star network and optimising the civil engineering cost. As an example it seems possible to realise cables of 200 to 800 optical cores capacities in a few millimetres diameters (6 to 10 mm) and weight of 35 to 60 kg/km . These data can be compared to a classical copper cable of 800 copper pairs (0.6 mm unit diameter lead to a 73.2 mm cable diameter weighting 9000 kg/km).

	Copper Pair (0.6 mm ϕ) Cable	Classical Optical Cable	Microsheath Cable	BMMF & microsheath cable (potentiality)
Diameter (mm)	70	48	25	10
Weight (Kg/km)	9000	1000	280	60

Diameter and weight of some 800 guides cables.

- The "cabled monomode guide cost "compared to the "monomode fiber cost" is directly divided by the BMMF capacity.

The test of four types of cables are in progress (fig 9)

- A semi tight structure from FOPTICA for cable terminations
- The microsheath structure from SILEC applied to 144 and 576 cores
- The ribbon structures from ACOME applied to 576 cores

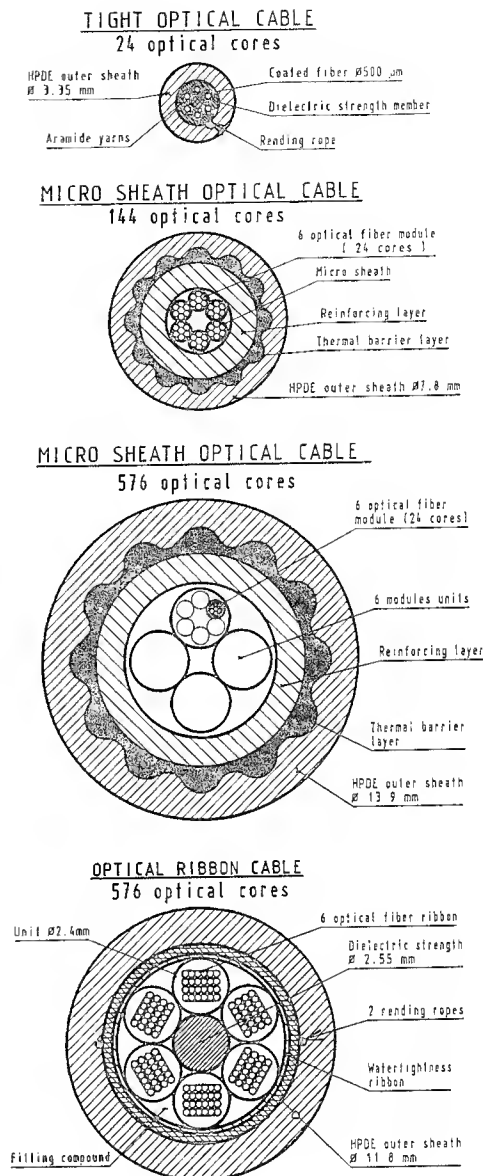


Fig 9 : Four tested cable structure with BMMF.

4.4 Connection Devices

The preform, fiber and cable feasibility is now ensured, but it is essential to propose connecting solutions which could be easily brought into operation.

The preform and fiber design giving precise perpendicular references, it is relatively easy to imagine connecting concepts.

4.4.1 Splices

The 90° assembling structure of the BMMF let us with the first investigations to connect very easily two multicore fibers in a fixed V groove or in an elastomeric U groove and the mean insertion loss is 0.4 dB with 1dB maximum value. Other kind of splice technique such as the fuse are now undertaken.

4.4.2 Fan out

For the full star network its essential to have access to OLT or subscriber with a single classical fiber and we therefore need fan out components to go to one BMMF toward four single fibers.

Several technical solutions have been evaluated and realized all types firstly need to obtain single fibers with a 44 microns diameter and after that, it is necessary to assemble the fibers in a circular or plane contact before to connect to the BMMF.

All the tested solutions which will later describe are advantages and disadvantages but they give insertion losses less than 1dB.

V CONCLUSION

In conclusion we have designed a new concept of bunched multicore monomode fiber (BMMF) based on the fabrication of very precise elementary performs precisely grounded and bunched to obtain a very precise matrix of multicore monomode guides easy to splice. Our first experiment have demonstrate the feasibility of 4 cores BMMF inscribed in a 125 µm diameter circle with an acceptable attenuation and a very low crosstalk at 1,3 µm authorising the transmission of high bit-rate systems. Associated with high density cable structure like the microsheat structure, we think that this new concept can constitute an important key for the

design of future economical FTTH interactive broadband networks where the fully or partly dedicated "cabled fiber" is replaced by a fully or partly dedicated "cabled monomode guide" with a drastic increasing of density and a drastic decreasing of elementary cost per subscriber, initial cost of installation and civil engineering cost. A large technical program is now conducted to optimise these BMMF, to design the cable and associated splicing and splitting technologies in order to get very cheap and well adapted materials for the subscriber FTTH network.

- REFERENCES -

- (1) T UENOYA "The Optical Fiber Loop 21 plan", OEC, 1990.
- (2) S TOMITA and Al "Preliminary research into ultra high density and high-count optical fibre cables" - Proc. IWCS 1991- pp 8-15.
- (3) T HAIBARA and al "High-Speed, low-loss connection techniques for high-count pre-connectorized cables" - Proc IWCS 1991- pp 296-302.
- (4) M HARA and Al. "Design of downsized coated optical fibers to minimize microbending loss" - Proc. IWCS 1992- pp 20-24.
- (5) W KATSURASHIMA and A1. "Microbending of thin coating single mode fiber for ultra-high-count cable" - Proc. IWCS 1992 - pp 13-19.
- (6) G LE NOANE - I HARDY- P GROSSO - Preform manufacturing by FCVD Proc IWCS93
- (7) G LE NOANE - P TROMBERT - D BOSCHER and al "The microsheat cable : a novel design of ultralight weight single mode optical cable for low cost subscriber loop" - Proc IWCS 1991- pp 24-29.
- (8) S INAO and al. "High density multicore-fiber cable" - Proc. 28th Wire and Cable Symp. - pp 370-384- Nov.78.
- (9) N KASHIMA and al. "High density multicore-fiber cable"- Proc. 28th Wire and Cable Symp. - pp 370-384 - Nov.78.
- (10) S SUMIDA and al. "Fundamental studies on flat bunched optical fibers" - Journal of lightwave techno - VOL LT 3 - n 1 - Feb. 1985.
- (11) R VAN CLOOSTER and D. PHARISEAU "The coupling of two parallel dielectric fibers Physica 47 (1970).
- (12) M.J.F. DIGONNET and H.J. SHAW "Analysis of a tunable single mode optical fiber coupler IEEE - Vol. QE 18 n 4 (19)
- (13) G SCHONER and G. "Coupling properties of a double-core single mode optical fiber - Siemens Forschung Entwickl Ber Bd.10 (1981) n 3.



Georges LE NOANE

FRANCE TELECOM
CNET/ LAB/ FCI
BP 40 22300 LANNION
FRANCE

Georges LE NOANE born in 1945 received his engineering degree from the Ecole Nationale des Arts et Metiers and joined CNET in 1974. He began working on optical fiber connector technique, then switched to cables. From 1979 to 1993 he was responsible of optical fibers and cables department. He is now head of division "fibers cables and interconnections".

Daniel BOSCHER

FRANCE TELECOM
CNET / LAB/ FCI / FCM
BP 40 22300 LANNION
FRANCE

Daniel BOSCHER born in 1951 received his engineering degree from the Ecole Nationale Supérieure des Arts et Métiers and Joined CNET in 1973.

Working on circular waveguide until 1979, he then joined the optical fibers and cables department. Since 1993 he is manager of the "Fibers, Cables and Measurements" Department.

P. GROSSO

FRANCE TELECOM
CNET/ LAB/ FCI/FCM
BP 40 22300 LANNION
FRANCE

Philippe GROSSO received his optic engineer diploma from CNAM in 1978. He joined CNET in 1983, where he is in charge of Preform and drawing studies in the fibers, Cables and Measurements Department.



JEAN CLAUDE BIZEUL

FRANCE TELECOM
CNET/ LAB/ FCI/ FCM
22300 LANNION
FRANCE

Jean Claude BIZEUL was born in 1948. In 1973 he joined the CNET in Lannion. He was engaged in research on fabrication and characterisation of optical fibers. Since 1988 he is involved in optical fiber and cable measurement group with special interests on transmission and geometrical single mode fiber features. He represents France Telecom in VIT/TS specially on optical Transmission Study Group.

CLAUDE BOTTON

FRANCE TELECOM
CNET/LAB/FCI/FCM
BP 40 22300 LANNION
FRANCE

Claude BOTTON was born in 1970 and received his optics/ electronics engineer diploma from ENIB in 1993. He is now pursuing the PH D degree at CNET Lannion, where he is engaged in research and development of BMMF.

Strain Analysis of U-groove Type Cable with Multi Fiber Ribbons

Naoki Okada, Kohichiro Watanabe, Matsuhiko Miyamoto

Fujikura, Ltd. Telecommunication Cable Section Opt-electronics Laboratory
1440 Mutuzaki, Sakura, Chiba, 285, Japan

Abstract

Ultra high-count, high-density optical fiber cable has been investigated toward the full optical fiber local loop. Multi fiber ribbons are suitable for realizing of high-density and high-count fiber cables. However, the low loss, compact, high-count cable may be difficult to design in general. Because, as the fiber count in a ribbon and the diameter of the cable are higher and larger, the strain of the ribbon in the cable will be large. We should design the cable structure carefully considering these effects.

In this paper, the U-groove type optical fiber cable with thin coated multi fiber ribbons are investigated. At first, the strain analysis are shown. And then, the characteristics of the experimental cable are shown comparing with analytical results. The transmission characteristics and the fiber strain measurement by the Brillouin spectroscopy method are investigated. As results, the characteristics of the cable are effected by ribbon width and drum diameter.

1. Introduction

Ultra high-count, high-density optical fiber cable for the full optical fiber local loop is currently under development[1,2,3]. To realize these cables, the following three methods are effective; the

reduction of fiber coating diameter, the multi-fiber ribbon structure, and the design of cable structure. Especially, multi-fiber ribbons are suitable for high-density and high-count fiber cables, considering efficient construction of the networks by reducing the connecting time. However, achieving these cables with good characteristics may be difficult. This is due to the fact that as the fiber count in a ribbon becomes greater and the diameter of the cable larger, the strain of the ribbon in the cable will become large. Therefore, we should design the cable structure carefully considering these effects.

2. Cable Structure

2-1. Multi-fiber Ribbon Structure

The multi fiber ribbon structures are shown in Fig.1. These are obtained by arranging the thin coated fibers in a line and covering with UV curable resin. We manufactured 8,12,16 180 μ m thin coated fiber ribbons as shown in Fig.1.

2-2. U-groove Type Cable Structure

The U-groove type optical fiber cable is shown in Fig.2. The U-shape grooves are stranded around a central strength member, and the 10 fiber ribbons are stacked in a U-groove. This cable structure is suitable for high-density and high-count cables. We investigated the behavior of the optical

fiber ribbons in the cable theoretically and experimentally.

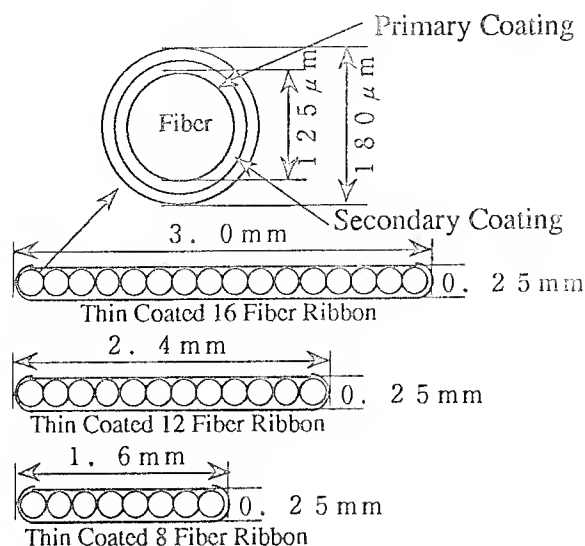


Fig.1 Thin Coated Fiber Ribbons

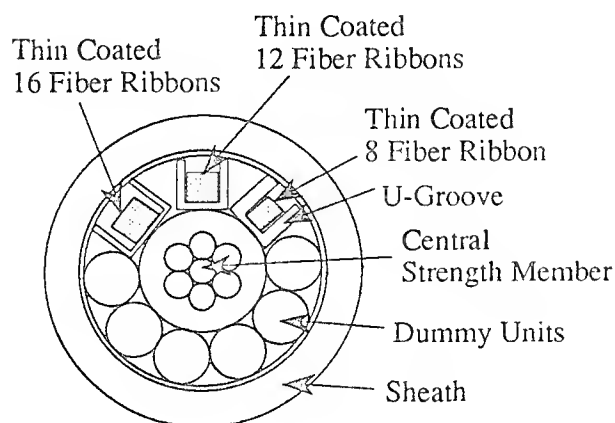


Fig.2 U-Groove Type Optical Fiber Cable

3. Theoretical Analysis

3-1. Theoretical Analysis Method

To obtain the good cable characteristics, we should design the cable structure considering the curvature radius and the strain of the fiber in the cable. Fig.3 shows the calculation model to research these factors. In this figure, P_c shows center position of the ribbon, P_{e1} and P_{e2}

show both edges of the ribbon, w is the ribbon width, a is the pitch radius of P_c , θ , ϕ_1 and ϕ_2 are the stranding rotation angles of P_c , P_{e1} , and P_{e2} , p is the stranding pitch. A fiber ribbon is stranding around the central strength member in the U-groove as shown in Fig.4.

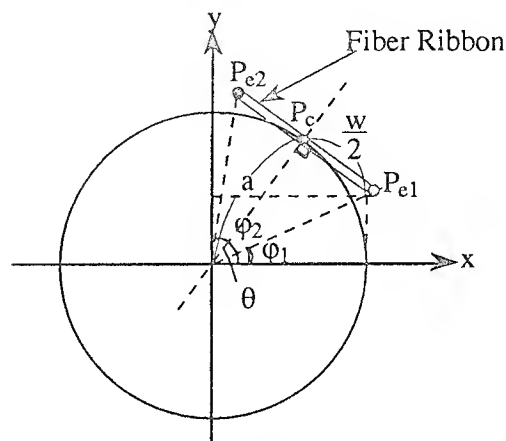


Fig.3 Calculation Model of Stranding Fiber Ribbon

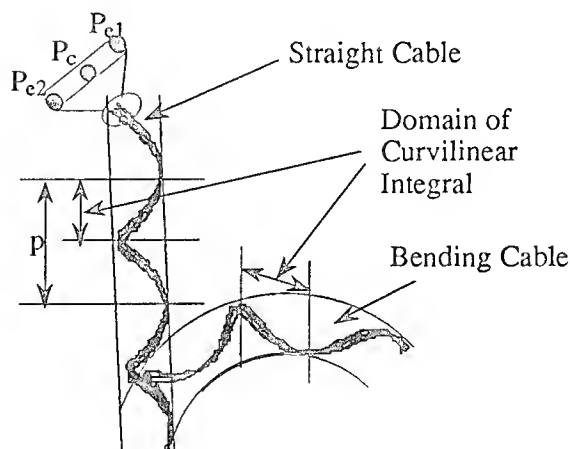


Fig.4 Stranding Fiber Ribbon in Straight and Bending Cable

The curvature radius and the strain of the fiber will be most critical at the both edges of ribbon in the bending cable. Therefore, the behavior of the ribbon edges in the bending cable was mainly investigated.

In the bending cable, such as drum winding cable, the stranding form of the

ribbon edges can be expressed by Eq.1. In this analysis, the ribbon width w is introduced into the stranding form equations as Eq.1. Therefore, we can evaluate the ribbon width effects on fiber curvature and strain. From Eq.1, the curvature radius of the ribbon edges ρ can be calculated by Eq.2.

On the other hand, the strain of the ribbon edges are calculated as following. We defined the strain in bending cable as the difference between the length of P_c in straight cable (which equals original ribbon length) and that of Pe_1 , Pe_2 in bending cable as shown in Fig.4. The length l is calculated by the following Eq.3 as curvilinear integral in a half stranding pitch using Eq.1. Moreover, the P_c length is LP_c , the Pe length in bending cable is LBP_e , the fiber strain ϵ is defined by Eq.4.

$$\begin{cases} x = r \cos \alpha - k_2 \cos \xi \cos \alpha \\ \quad + \sqrt{a^2 + \left(\frac{w}{2}\right)^2} \sin(\alpha - \phi) \sin \alpha \\ y = r \sin \alpha - k_2 \cos \xi \sin \alpha \\ \quad - \sqrt{a^2 + \left(\frac{w}{2}\right)^2} \sin(\alpha - \phi) \cos \alpha \\ z = k_2 \sin \xi \end{cases}$$

$$\begin{cases} \phi = \theta \pm \arctan \left(\frac{w}{2a} \right) \\ \xi = \frac{\theta p}{2\pi r} \\ k_1 = r - a \cos(\alpha - \theta) \\ k_2 = r - \sqrt{a^2 + \left(\frac{w}{2}\right)^2} \cos(\alpha - \phi) \end{cases}$$

---[Eq.1]

$$\frac{1}{\rho} = \sqrt{\left(\frac{d^2x}{dl^2}\right)^2 + \left(\frac{d^2y}{dl^2}\right)^2 + \left(\frac{d^2z}{dl^2}\right)^2}$$

---[Eq.2]

$$l = \int \sqrt{\left(\frac{dx}{d\theta}\right)^2 + \left(\frac{dy}{d\theta}\right)^2 + \left(\frac{dz}{d\theta}\right)^2} d\theta$$

---[Eq.3]

$$\epsilon = \frac{LBP_e - LP_c}{LP_c}$$

---[Eq.4]

3-2. Results of Theoretical Analysis

3-2-1. Ribbon Width Dependence of Fiber Curvature Radius and Fiber Strain

As analytical results, ribbon width dependence of fiber curvature radius and fiber strain are shown in Fig.5. The fiber curvature is not dependent on ribbon width. However, the fiber strain is strongly dependent on ribbon width. We should design the structure of the multi-fiber ribbon carefully, because of above effects.

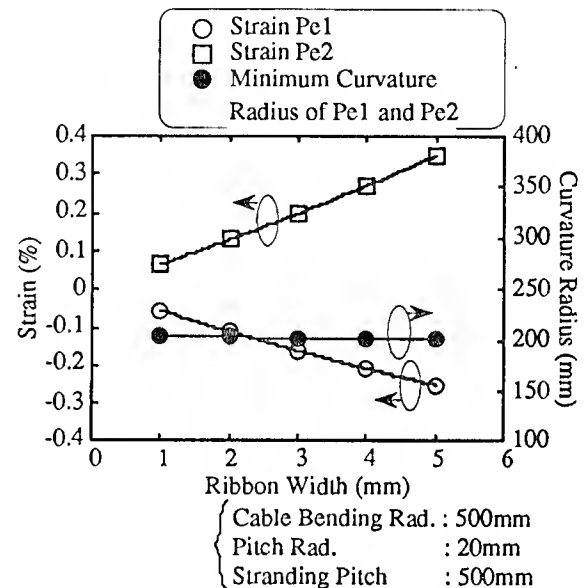


Fig.5 Ribbon Width Dependence of Fiber Curvature Radius and Fiber Strain

3-2-2. Cable Bending Radius Dependence of Fiber Curvature Radius and Fiber Strain

As analytical results, cable bending radius dependence of fiber curvature radius and fiber strain are shown in Fig.6. The fiber curvature is dependent on cable bending radius. The fiber strain is dependent on cable bending radius, too. It is expected that the good cable characteristics can be obtained at large cable bending radius, so the radius of the drum should be selected sufficiently large.

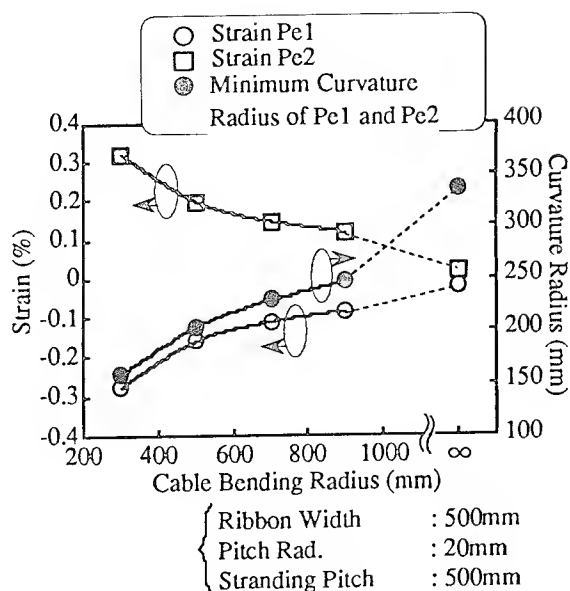


Fig.6 Cable Bending Radius Dependence of Fiber Curvature Radius and Fiber Strain

3-2-3. Stranding Pitch Dependence of Fiber Curvature Radius and Fiber Strain

As analytical results, stranding pitch dependence of fiber curvature radius and fiber strain are shown in Fig.7. The stranding pitch dependence of the fiber strain is not observed apparently. On the other hand, as the stranding pitch is shorter, the fiber curvature radius is smaller.

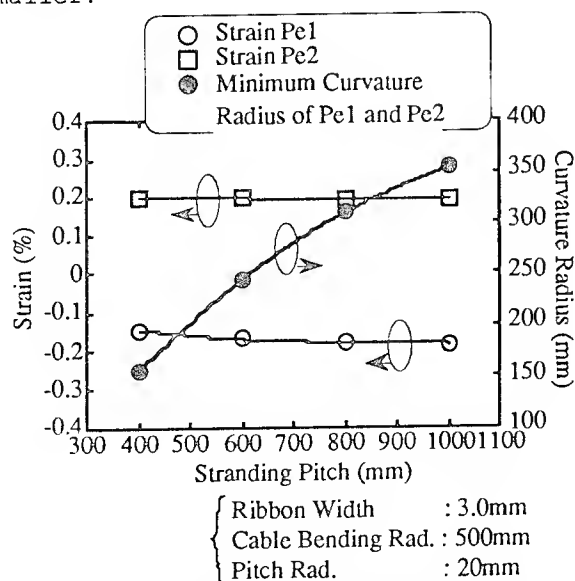


Fig.7 Stranding Pitch Dependence of Fiber Curvature Radius and Fiber Strain

3-2-4. Pitch Radius Dependence of Fiber Curvature Radius and Fiber Strain

As analytical results, pitch radius dependence of fiber curvature radius and fiber strain are shown in Fig.8. The pitch radius dependence of the fiber strain is not observed. The curvature radius is affected by the pitch radius.

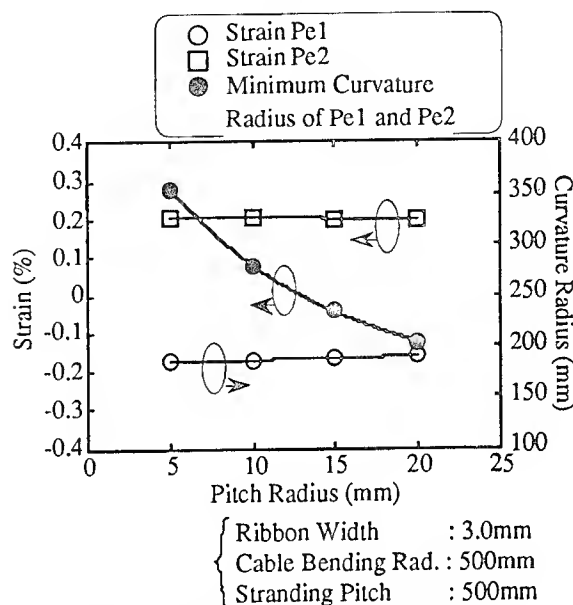


Fig.8 Pitch Radius Dependence of Fiber Curvature Radius and Fiber Strain

As results, the fiber curvature radius is affected by cable bending radius, stranding pitch, and pitch radius. Moreover, the fiber strain is affected by ribbon width and cable bending radius.

4. Experimental Results

The experimental cables with thin coated multi fiber ribbons were manufactured as shown in Fig.1 and Fig.2 to confirm the theoretical analysis. We reported that the microbending characteristics are influenced by coating structures; for example, thickness and Young's modulus of coating materials[4,5]. Conversely, we can get the several optical fibers which

have different microbending characteristics. Therefore, in order to investigate the cable characteristics clearly, we used the special thin coated multi fiber ribbon which are sensitive to lateral pressure. The parameters of our observation are a , p , w , r which determine the cable structure. Here, the used fibers are single mode fibers.

4-1. Transmission Characteristics

At first, we investigated the transmission loss of the experimental cable wound on the 1000mm ϕ drum. The results are shown in Fig.9. The ribbon width dependence was observed. The wider ribbon shows larger transmission loss.

Next, we investigated the drum radius dependence of the transmission loss. Fig.10 shows that the transmission loss is larger, as the drum radius is smaller. Here, the infinity means the straight installed cable.

These results shows the good agreement with the calculation results of theoretical fiber strain.

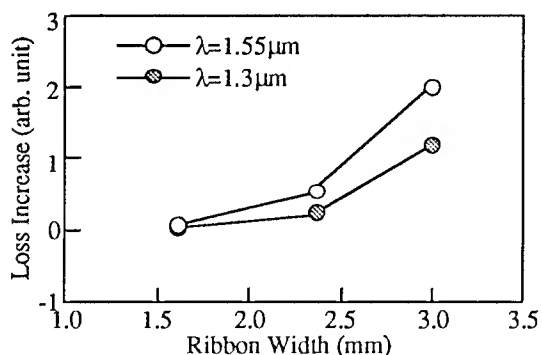


Fig.9 Ribbon Width Dependence of Maximum Transmission Loss in Experimental Cable

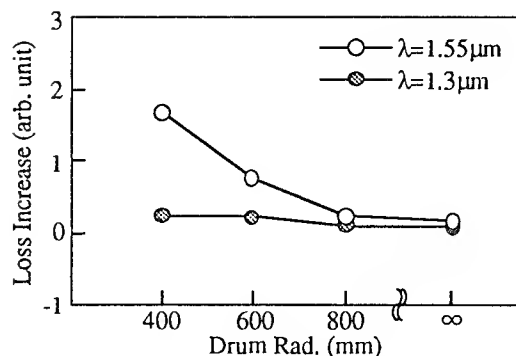


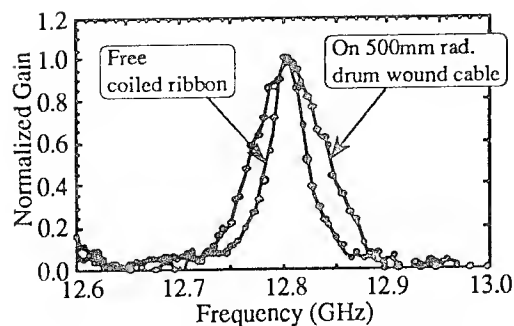
Fig.10 Drum Radius Dependence of Maximum Transmission Loss in Experimental Cable

4-2. Fiber Strain

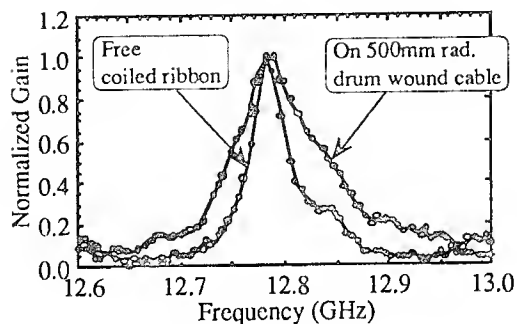
In recent years, the fiber strain analysis by the Brillouin spectroscopy method is reported[6]. This technique is based on the stress/strain dependence of the Brillouin frequency shift in optical fibers. The distributed fiber strain in the cable can be evaluated, therefore this method is very useful. The edge fiber of ribbon are measured. We can investigate the fiber strain by comparison of the spectra of free coiled fiber and that of stranded fiber in cable. The spectra will move to high frequency side at fiber elongation strain.

Fig.11 shows the ribbon width dependence of the Brillouin spectra. The spectra is extended, as the larger the ribbon width are. Therefore, the fiber strain is larger, as the ribbon width is wider.

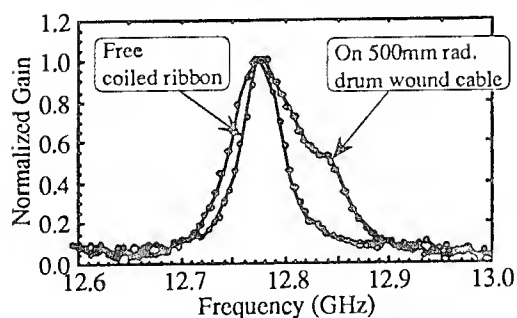
Fig.12 shows the drum radius dependence of the Brillouin spectra. As a result, it seems that the drum radius is larger, as the fiber strain is smaller. These results correspond to the transmission loss characteristics and theoretical fiber strain analysis.



a) 180μm × 8-fiber Ribbon

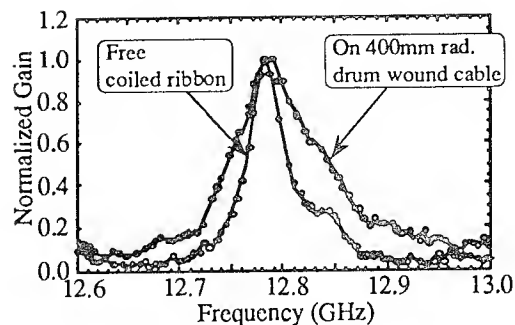


b) 180μm × 12-fiber Ribbon

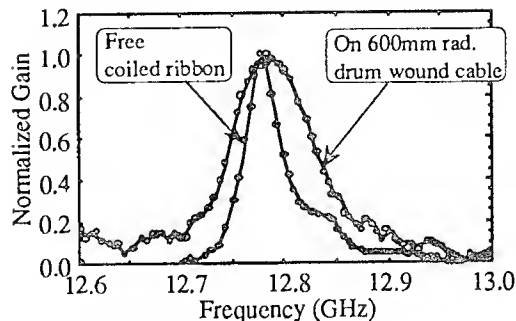


c) 180μm × 16-fiber Ribbon

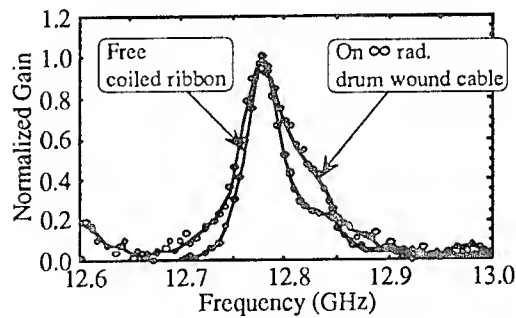
Fig.11 Ribbon Width Dependence of Brillouin Spectra



a) Drum Radius = 400mmφ



b) Drum Radius = 600mmφ



c) Straight Cable

Fig.12 Drum Radius Dependence of Brillouin Spectra

5. Comparison of Theoretical Analysis and Experimental Results on Fiber Strain

We have attempted to roughly estimate the relationship between theoretical analysis and experimental results on fiber strain. The both side (elongation side and compression side) of half band width ω_1 , ω_2 are obtained from Brillouin spectra. These values are compared with the theoretical fiber strain. The ribbon width dependence is shown as Fig.14, and winding drum radius

dependence is shown as Fig.15. Almost similar trends are observed in both theoretical and experimental results.

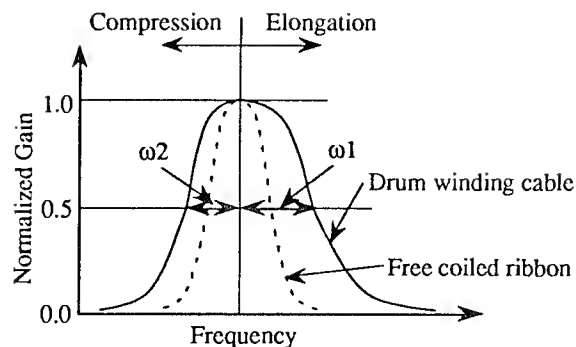


Fig.13 Brillouin spectra analysis

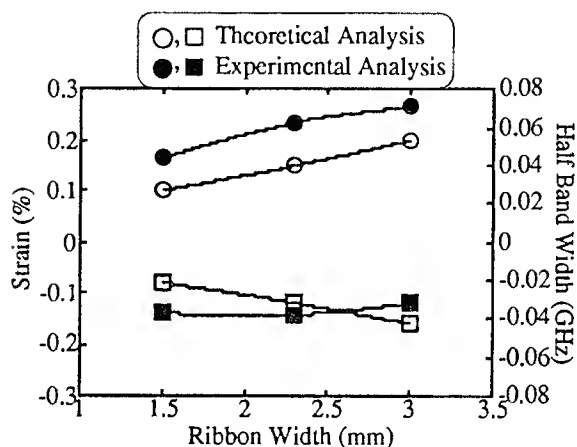


Fig.14 Relationship between theoretical and experimental fiber strain analysis dependent on ribbon width

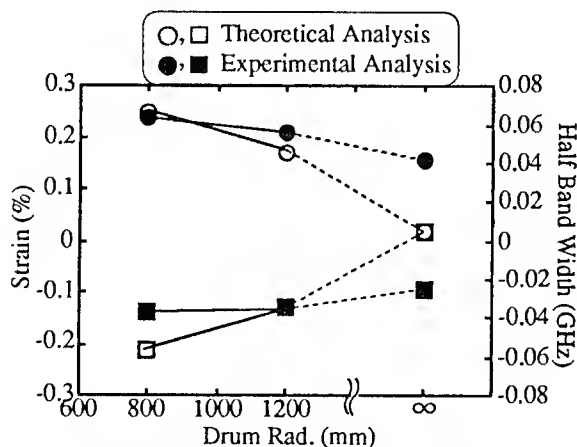


Fig.15 Relationship between theoretical and experimental fiber strain analysis dependent on winding drum radius

6. Conclusion

High-density optical fiber cables with multi fiber ribbons were studied. The theoretical and experimental analysis was performed on the multi fiber ribbon U-groove type cable. Especially, the curvature radius and the strain of the fiber ribbon edges were investigated. As a result, it was verified that the theoretical fiber strain and the attenuation loss of the experimental cable are affected by ribbon width and drum radius. Moreover, the experimental fiber strain analysis by the Brillouin spectroscopy method was tried. This results support to the theoretical fiber strain and the attenuation loss of the experimental cable.

References

- [1] T. Uenoya, "The Optical Fiber Loop 21 Plan", OEC, 1990
- [2] T. Tomita et al., "Preliminary Research into Ultra High Density and High Count Optical Fiber Cables", 40th IWCS, 1991
- [3] T. Tomita et al., "Ultra High-Density Optical Fiber Cable with Thin Coated Fibers and Multi-Fiber Connectors", 42th IWCS, 1993
- [4] J. Baldauf et al., "Relationship of Mechanical Characteristics of Dual Coated Single Mode Optical Fibers and Microbending Loss", IEICE TRANS. COMMUN., VOL.E76-B, NO.4 APRIL 1993
- [5] K. Kobayashi et al., "Study of Microbending Loss in Thin Coated Fibers and Fiber Ribbons", 42th IWCS, 1993
- [6] T. Horiguchi et al., "Brillouin Characterization of Fiber Strain in Bent Slot-Type Optical-Fiber Cables", Journal of lightwave technology, Vol.10, No.9, September 1992



Naoki Okada

Opto-Electronics
Laboratory
Fujikura Ltd.

1440, Mutsuzaki,
Sakura-shi, Chiba,
285, Japan

Naoki Okada was born in 1964. He joined Fujikura Ltd. after his graduation from Chiba University with a B.E. Degree in 1986 and has been engaged in research and development of optical fiber cables. He is now an engineer in the Telecommunication Cable Section and a member of the IEICE of Japan.



Matsuhiro Miyamoto

Opto-Electronics
Laboratory
Fujikura Ltd.

1440, Mutsuzaki,
Sakura-shi, Chiba,
285, Japan

Matsuhiro Miyamoto was born in 1953. He graduated from Nagoya Institute of Technology with a B.E. degree of electrical engineering. He joined Fujikura Ltd. after his graduation from Tokyo Institute of Technology with a M.S. degree in 1978 and has been engaged in research and development of optical fiber and optical fiber cables. He is now a manager of the optical fiber cable section.



Kohichiro Watanabe

Opto-Electronics
Laboratory
Fujikura Ltd.

1440, Mutsuzaki,
Sakura-shi, Chiba,
285, Japan

Kohichiro Watanabe was born in 1959. He received a B.E. degree in electrical engineering from Tohoku University in 1982. Since joining Fujikura, Ltd. in 1988, he has worked on the development of optical fiber cables. He is currently employed in the Telecommunications Cable Section of the Opto-electronics laboratory.

LOW FIBER COUNT CABLES FOR EMERGING BROADBAND NETWORKS

M. D. Kinard, T. D. Mathis, A. J. Panuska, P. D. Patel

AT&T Bell Laboratories
Norcross, Georgia 30071

Abstract

This paper describes the design and development of a family of low fiber count cables specifically engineered for emerging broadband networks. The design builds on the proven central tube design with stranded dielectric and linear metallic strength members successfully deployed in the fiber optic plant since 1985. The significant feature of this design is the use of a common core tube to offer a variety of fiber core options such as fiber bundles, buffered fibers, and ribboned fibers. The design is optimized for packing density and excess fiber length and offers load ratings that are appropriate for the emerging new markets. Particular attention is paid to the design and choice of materials to enhance the ease of handling and installation. A composite cable design is presented for those applications where both optical and copper media are envisioned. These designs are completely compatible with the existing line of connecting apparatus and fiber organization systems for an end-to-end fiber solution. Optical and mechanical qualification test results are presented for these cable designs.

as shown in Figure 1, seem to dominate the present networks but it has been predicted that this may change in the next 2 or 3 years. This has been the subject of much debate for both local exchange carriers (LEC) and cable TV (CATV) operators. Many of the changes are being driven by both the regulatory agencies and by the ever changing technology. As the local exchange carriers and the cable TV operators deploy optical fiber closer to the subscribers, a complete family of products will be needed to support this growing demand.

A family of Buried Service Lightguide (BSL) cables was developed in 1989³ which held from 1 to 4 buffered fibers in a water blocked nylon core tube. This design was provided in both armored and dielectric versions. However, present requirements demand greater flexibility of both fiber arrangements in the core and copper media within the cable configuration. For that reason a new family of cables has been developed to meet these new markets.

The fiber cable requirements for these local access networks are much different than the long-haul systems.

The cable requirements consist of:

1. flexible fiber core configurations
2. relatively short cable lengths
3. convenient fiber drop capability
4. ease of interconnections
5. increased handling capability
6. low and high fiber counts
7. and, most importantly, low installed cost

I. Introduction

In the present day business literature, there is a large amount of discussion concerning deployment of optical fiber for broadband networks. This is not a new subject since "Fiber-to-the-Home" has been discussed at least since 1988.¹ These networks will deliver voice, data, cable TV, and interactive broadband services. Fiber/coaxial systems², such

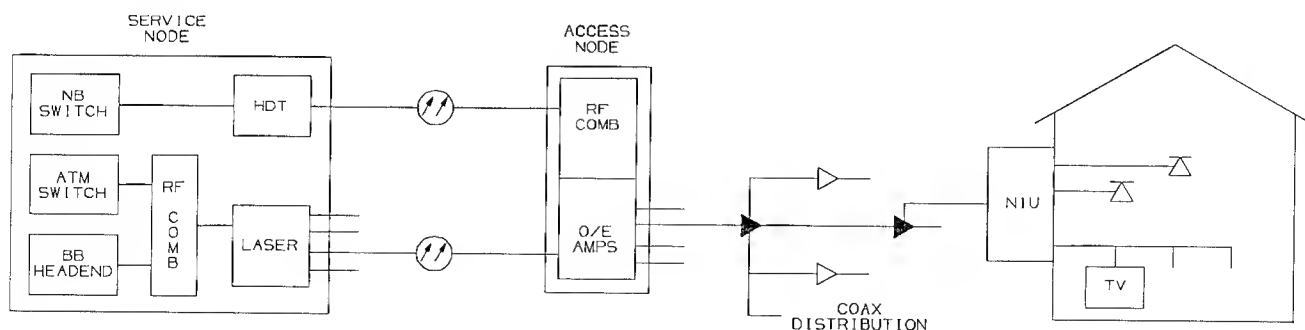


Figure 1. Integrated Fiber/Coax Architecture

A family of armored, dielectric, and composite drop cables has been developed to meet the technology demands unique to these new markets. This family of optical fiber cables was developed using extensive cable design experience, field tested cabling technology, and proven cabling materials. The family of cable products uses an optimized common core tube design to enhance manufacturing efficiency and also offer a variety of fiber core configuration and sheath options. This paper will discuss the fiber core design, the mechanics of the fibers within the core, the sheath design, and finally the Bellcore qualification tests and results.

II. Fiber Optic Cable Design Considerations

There has been intense interest in delivering broadband services over fiber based networks. The pressing issue, however, is not so much with fiber technology, but economics. Some of the telcos and CATV companies are moving to invest in multimedia services based on financial returns since they agree that integrated fiber/coax architectures offer a good promise based on price, performance, reliability, and easily upgradable platform. The telco and CATV architectures do require different considerations from those for trunking and feeder applications.

The demand for high fiber count cables, up to 240 fibers, is readily met by traditional loose tube, fiber bundle, and ribbon core designs. Cable designs with fiber counts as high as 288 fibers are also available, which may be necessary for feeding the broadband distribution systems. In addition, existing lower fiber count cables (i.e. up to 96 fibers) can offer the drop flexibility needed in the distribution network.

The traditionally available very low fiber count cables (i.e. up to 18 fibers) have not been optimized for size, flexibility, and lower installed cost. To meet the challenges of flexible cable solutions unique to the emerging broadband markets, a family of armored, dielectric and composite drop cables has been developed for aerial, buried and underground applications. Based on our customer inputs, it is quite clear that they prefer flexibility in fiber core arrangements. Therefore, a key feature considered in the development of this family of cable products is that it offers a variety of fiber core options within a common core tube design along with easy handling during installations, thus enabling flexible cabling solution for the broadband networks.

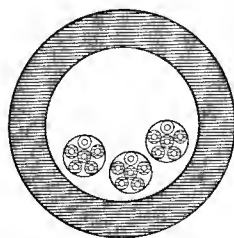


Fig. 2 Fiber Bundle Core

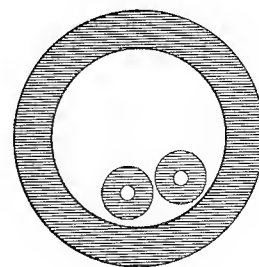


Fig. 3 Buffered Fiber Core

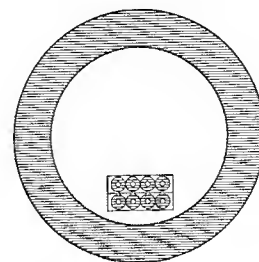


Fig. 4 Small Count Ribbon Core

III. Fiber Core Configurations

To satisfy the need for a wider choice of fiber core options and for flexibility in frequent drop/add capability, the fiber core design must incorporate a variety of fiber units and fiber types. Fibers must be readily accessible in unit sizes appropriate to the specific situation such as: fiber bundles, larger-diameter buffered fiber bundles and small fiber count ribbon units.

The flexibility is provided by an optimized filled central core tube structure that houses the following fiber core options:

1. Up to Eighteen 250 μ m Coated Fibers
2. Up to Two 900 μ m (PVC-buffered) Fibers
3. Up to Two 4/6-Fiber Ribbons

Figures 2 through 4 show cross-sections of the common core tube that accommodate all of the above fiber core options. The core tube is made from a polymer material that is traditionally used for outside plant cable applications, so that fibers are easily accessed, yet the structure is robust enough to provide mechanical protection for the fibers. The 4 mm outside diameter core tube is optimized to give maximum packing density with desired excess fiber length while maintaining excellent optical and mechanical performance.

The fibers in all core options, including ribbons and buffered fibers, may be placed in the tube with or without

intended stranding, but with a controlled amount of excess length to limit fiber strain during installation. The core tube is filled with water-blocking compound to prevent water migration along the core tube.

The various core options provide excellent interconnection capability with existing conventional feeder and distribution cable designs, whether they have a fiber bundle, ribbon or loose tube configuration. This common core tube design is used as a building block for the family of fiber drop cables described below.

Fiber Core Mechanics

"Could a range of fiber core arrangements be used in a common core-tube/sheath configuration?" was an initial question. The answer proved to be, "Yes", however one must pay careful attention to the mechanics of the core.

The most important consideration is to understand the mechanical and optical behavior of varied fiber types/arrangements in the form of fiber bundles⁴, buffered fibers, and fiber ribbons in a compact common core tube. It is desired that the cable design provide the *lowest attenuation* while maintaining *highest reliability* for various fiber types. One of the key parameters affecting the above characteristics is *strain* in the fiber. Higher strains induced during cabling and/or installations can cause higher attenuation and reduce mechanical reliability. Fiber strains are most commonly induced by tensile and bending loads during manufacturing and installation. Some of the key parameters affecting these strains are:

1. Packing density
2. Excess fiber length
3. Fiber unit stranding/twisting
4. Cable bending
5. Tensile load rating

In all cases, desired performance can be achieved with proper attention to these core mechanics parameters. While we will keep the actual attribute values proprietary, we will discuss design philosophy and overall physical effects in general. We will now examine the above parameters in more detail.

Packing Density: The two most common definitions used in the cable industry for packing density are based on core tube inside diameter and cable outside diameter. Packing density based on core tube inside diameter is defined as: *a ratio of total fiber unit area to core area in percent*, where as, based on cable outside diameter it is defined as: *fibers per cable area in mm²*. For the highest packing density a critical dimension (d_c) exists for different fiber arrangements. For fiber bundles or buffered fibers, this dimension is the minimum diameter (d_c) circumscribing all fibers (N_f) with diameter (d_f). For ribbons, this dimension is the diagonal of the ribbon stack.

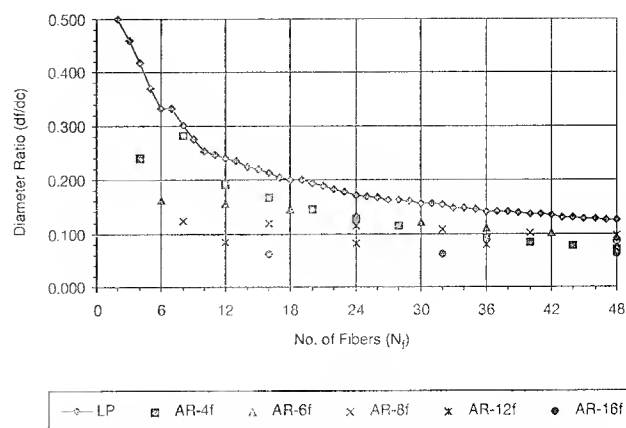


Figure 5 Critical Dimensions for Fiber Cores

Figure 5 shows the relationship between the ratio of d_f/d_c and total number of fibers, N_f (up to 48 fibers) for both fiber bundle and ribbon cores. It shows that the fiber bundles give the highest ratio (lowest critical dimension, d_c) as compared to the ribbon core for a given fiber count. Furthermore, the smaller count ribbons give higher ratio than the larger count ribbons. Therefore fiber arrangement into fiber bundles gives optimum packing density and it decreases for low count ribbons, and high count ribbons, respectively. The high packing density results in a compact and craft-friendly cable design that is cost effective. However, higher packing density can induce higher strains and attenuation. Furthermore, both the packing density and excess fiber length are related and will be discussed later.

Excess fiber length: It is generally desired that the length of fiber be longer than the cable and this excess fiber length (EFL) is expressed as a percent. In general, higher excess length is desired since it can help reduce tensile strain in fiber and/or reduce tensile stiffness requirement of the cable. However, it may induce undesirable bending strains in the fiber depending on the available free space in the core tube (packing density). Based on helix and sinusoidal model analysis presented by Patel and Panuska⁵, it is shown that the sinusoidal model is conservative and predicts lower minimum bend radius than the helix model. Assuming the sinusoidal model, the excess fiber length, e_{es} , is expressed in the following convenient form:

$$e_{es} = 100 \left[(1 + k^2)^{1/2} \{1 - p\} - 1 \right]$$

$$\text{where } p = \frac{1}{4}q^2 + \frac{3}{64}q^4 + \frac{1}{256}q^6 + \dots$$

$$q^2 = \frac{k^2}{1 + k^2}$$

$$k^2 = \frac{1 - (d_c / D)}{(D_s / D)}$$

and

d_c / D = ratio of critical dimension to tube diameter
 D_s / D = ratio of twice the minimum sinusoid radius to tube diameter

Above expression relates excess fiber length with two ratios involving critical dimension and bend diameter. Figure 6 shows three curves for the excess fiber length as a function of the ratio of fiber bend diameter to the core tube diameter (D_s / D) for three values of the critical dimension to the core tube diameter (d_c / D) ratio. For a given EFL, the curves predict smaller fiber bend diameter ratio for higher critical dimension ratio than lower one. These design curves can be used to optimize the core tube design by maximizing the fiber bend radius.

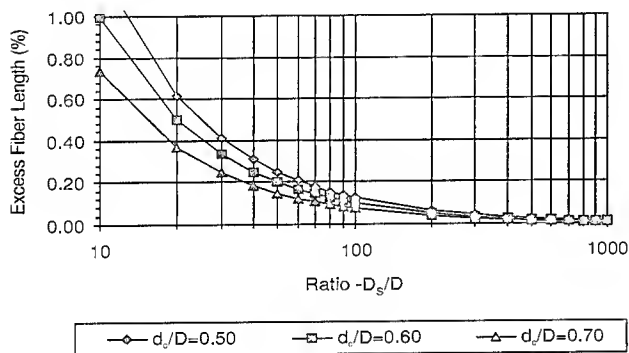


Figure 6 Effect of Critical Dimension on Excess Fiber Length

Fiber unit stranding/ twisting: Depending on cable design, the fiber units are either layed straight, stranded, or twisted during manufacturing. This process can impart further bending strain on the fiber.

For helical stranding with pitch diameter (D_p) and pitch (P_h), the radius of helix (R_h) is given by

$$R_h = \frac{D_p}{2} \left[\left\{ \frac{P_h}{\pi D_p} \right\}^2 + 1 \right]$$

The strain, ϵ_b , induced by bending a fiber to a diameter, D_b , about its own axis is given by

$$\epsilon_b = \frac{d_f / D}{D_b / D} = \frac{(d_f / d_c)(d_c / D)}{D_b / D}$$

Like excess fiber length, the above expression also relates the bending strain to critical dimension and bend diameter ratios. Figure 7 shows three curves for the fiber bending strain as a function of ratio of fiber bend diameter to core tube diameter (D_b / D) for three values of fiber diameter to core tube diameter ratio (d_f / D). The preceding design

curves along with past experience are helpful in the design of an optimum core tube.

The bending strains due to helical stranding can be high and are generally left on the fiber for the service life of the cable. Typical loose tube cable design can have up to 0.1% bending strain in the fiber. This could affect both attenuation and reliability.

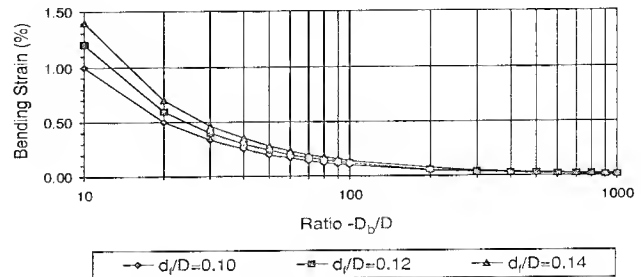


Figure 7 Bending Strain due to Fiber Bend

Cable bending: Cable must be flexible enough to bend at a specified radius without affecting attenuation or long term reliability during manufacture and installation. Cable bending can induce two types of strains in fiber; first, due to bending of fiber about its own axis as discussed above, and second, due to bending of fiber about cable neutral axis. The first strain is controlled by limiting minimum bend radius. However, the second strain is design dependent. Situations where the fibers in the core tube are located further away from the neutral axis, a common design technique requires one to average the strain by stranding or twisting the fiber cores. This is particularly important in high fiber count (large critical dimension) designs. In the low fiber count design with small critical dimension, it is less critical and can be used to advantage.

Tensile load rating: The fibers must be able to survive the total strain caused by rated tensile loading. For example, Bellcore's objective is that the fibers should not exhibit a strain greater than 66% of the fiber proof strain. This 66% design safety factor is based on static fatigue analysis⁶ and it gives 0.33% and 0.61% allowable fiber strains at 0.35 GPa and 0.69 GPa proof stress.

Core Structure Issues

The following three core types are considered in this cable family:

1. buffered fibers
2. fiber ribbons
3. fiber bundles

This listing is ordered in decreasing critical dimension ratio or increasing number of fibers in a given space. Each core type has a different "window" for both packing density and excess fiber length. The above analysis is used

to optimize a common core tube design and then verify the design by experiments for a variety of fiber types.

Buffered fibers are uncommon in the outside plant world. However, more and more customers are interested in them for fiber drop cables. Tight buffers may also be used in drop cables for compatibility with the building cables in commercial application. They are considered to be more robust than either coated fibers or fiber ribbons. They have the lowest fiber-number density, due to their overall size (typically 900 μm). Since they have the highest critical dimension, the above analysis is used to size the core tube for two buffered fibers.

Ribboned fibers are less common in low count cables but offer a high degree of organization. Two four-fiber and two six-fiber ribbons are found compatible with fiber unit breakouts needed in a typical broadband application and therefore are considered for the common core tube design.

Fiber bundles are most common in this low fiber count range and offer the most freedom of fiber movement. They have the highest fiber-number density, and have the most forgiving "windows". An optimum packing density and fiber excess length is established which gives a maximum of 18 fibers in the common core tube design.

IV. Sheath Design Options

Many of these broadband applications require the fiber cables to withstand a wide range of installation and environmental conditions. For the areas where rodent protection is a must, a robust armored cable design is needed, whereas a dielectric cable is preferred for lightning avoidance and/or for eliminating bonding and grounding. Moreover, in special situations where both fiber optic and metallic media is required, a composite cable is needed. In all cases, the tensile stiffness and fiber excess lengths are designed such that the cable provides the expected high performance in the field.

Armored Cable Design

The armored cable design is based on proven LXE sheath technology⁷ that has been used successfully in the outside plant network; however, it has been optimized for the low fiber counts. Because of its miniature size, several metal forming and water blocking challenges had to be overcome during the design process.

Figure 8 shows a cross-section of this design where two linear metallic wire strength members and electrolytically chrome coated steel (ECCS) armor provide the desired mechanical protection and tensile load rating of 1800 N. A medium density polyethylene jacket yields excellent bending flexibility, field handling and ease of fiber access. The overall diameter of the finished cable is 9.1 mm, and the weight of the cable is 92 kg/km.

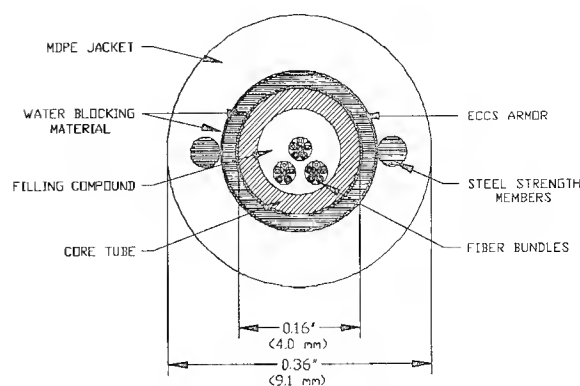


Figure 8. Armored Cable

Dielectric Cable Design

The Dielectric cable design is based on the proven dielectric crossply sheath technology that has been successfully deployed in the outside plant since 1985. This cable has been specifically designed for one or two buffered fibers needed in drop applications.

Figure 9 shows a cross-section of this design where a layer of dielectric strength members are applied over the common core tube to provide the desired mechanical protection and tensile load rating of 1350 N. For ease of sheath entry, two ripcords are provided and a water blocking material is used to prevent water migration through the cable sheath. A medium density polyethylene jacket completes the cable with an overall diameter of 7.6 mm and a weight of 45 kg/km.

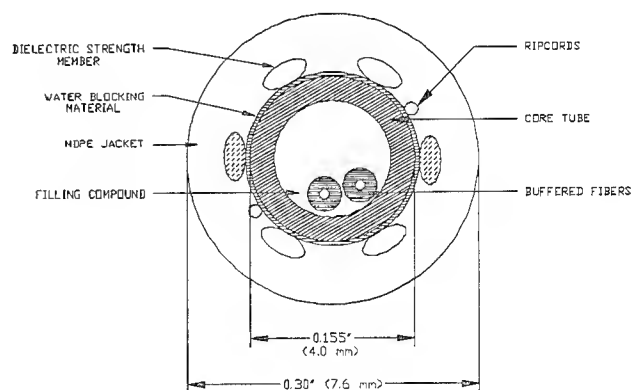


Figure 9. Dielectric Cable

Composite Cable Design

Presently considered broadband architectures rely on some combination of fiber optic, twisted-pair copper and coax media, which implies the need for a cable structure that contains both fiber and copper or fiber and coax

media. Such a structure offers compatibility with existing plant and labor cost savings through improved installation efficiency.

Figure 10 shows a cross-section of a composite cable which includes a dielectric cable with two buffered fibers and a two pair buried service wire. This cable offers the needed flexibility of installing multiple media in a single operation, and the ability to terminate multiple media in one or more closures, depending on the application. The design uses a traditional figure-8 concept with two individual cables combined in one common polyethylene over-jacket. The over-jacket is constructed such that it is easily separated from the individual cables for termination. The overall dimensions for this cable are 9.4 mm x 17.0 mm and the weight is 134 kg/km.

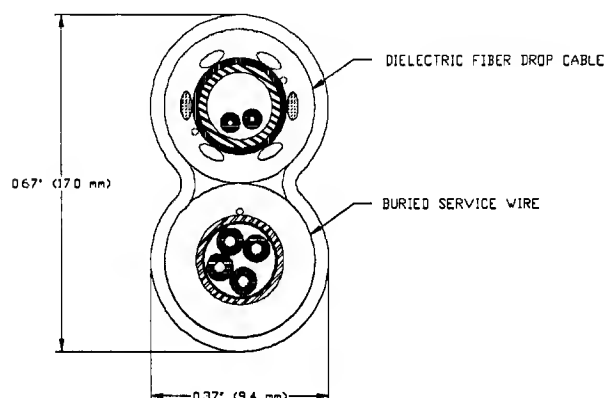


Figure 10. Composite Cable

V. Qualification Tests

Industry standard qualification testing verified that these designs fully met Bellcore TR-TSY-000843, *Generic Requirements for Optical/Metallic Buried Service Cable*, Issue 1, January 1989 and in addition met most of the intended requirements of TR-NWT-000020, *Generic Requirements for Optical Fiber and Optical Fiber Cables*, Issue 5, December 1992. Moreover, a series of field tests are being conducted at our Chester, N.J. facility and customer feedbacks are being gathered.

Figure 11 shows production data for armored cable for over 6FMM of fibers with a mean loss of 0.19 / 0.33 dB/km and a sigma of 0.006 dB at 1310 nm / 1550 nm,

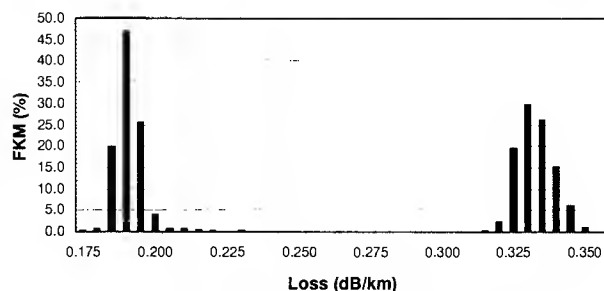


Figure 11. Optical Loss Data For Armored Cable

respectively. Figures 12 and 13 illustrate mechanical test results for Armored and Dielectric cables, respectively. In addition, the armored design also passes the Category II lightning requirement of 80 kA. Furthermore, it passes the gopher test damage index requirement rating of 3.0 as conducted by the Denver Wildlife Research Center. At the request of a customer this cable was also tested at a low temperature of -60°C and performed very well.

Test Procedure	Cable Performance
Impact Test	Passes All Requirements With Max Δ Loss @ 1310/1550 nm Mech. : 0.014/0.051 dB Env. : 0.048/0.071 dB/km
Tensile Load & Bend	
High/Low Temp. Bend	
Compressive Load	
Twist	
Cyclic Flexing	
External Freezing	
Temp Cycling & Aging	

Figure 12. Mechanical Testing - Armored Cable (Fiber Bundle & Ribbon Core)

Test Procedure	Cable Performance
Impact Test	Passes All Requirements With Max Δ Loss @ 1310/1550 nm Mech. : 0.004/0.019 dB Env. : 0.018/0.022 dB/km
Tensile Load & Bend	
High/Low Temp. Bend	
Compressive Load	
Twist	
Cyclic Flexing	
External Freezing	
Temp Cycling & Aging	

Figure 13. Mechanical Testing - Dielectric Cable (Buffered Fiber Core)

VI. Interconnection Apparatus

A variety of closures² are available to aid in splicing fibers in feeder cables, and splicing and dropping fibers in distribution cables. Because of flexible fiber core arrangements in these lower fiber counts and smaller size cables, the closures also need to be compatible, smaller and less expensive. For example, some customers would like to be able to take two six-fiber ribbons and splice them to a single twelve-fiber ribbon. AT&T closures are specifically designed to accommodate these and other needs and work with the above described armored, dielectric, and composite cables to offer an economical solution.

The compact nature of both the armored and dielectric cables make them highly attractive for tight interconnection situations in cabinets and closures in the fiber broadband architectures. In addition, both fiber optic cable de-

signs are available in pre-terminated assemblies which offer a fast installation solution for dropping small groups of fibers to Access Nodes or Optical Network Units (ONU).

VII. Conclusions

This paper describes a family of cable products specifically developed to support the emerging fiber based broadband implementations. Existing fiber bundle and ribbon core technologies are extended to optimize the cable designs for today's needs. Design curves are also presented based on sinusoidal model for excess fiber length and applied to optimize the cable designs presented herein. These designs have been tested in the laboratory, qualified, and are presently being deployed by our customers.

¹J. B. Haber, D. Kalish, and J.J. Refi, "Single-mode Media and Apparatus for Fiber-to-the-Home", International Wire and Cable Symposium Proceedings, Reno, 1988.

²L. T. Carlton, G. S. Cobb, M. D. Kinard, T. F. McIntosh, P. D. Patel, "Cabling and Preterm Solutions for Broadband Networks", NFOEC'94, Vol. 2, pp 387-399.

³D. Mathis, J. Holman, "Design of Buried Service Lightguide (BSL) Cables", 39th International Wire and Cable Symposium Proceedings, Reno, 1990.

⁴P. D. Patel and C. H. Gartside, III, "Compact Lightguide Design," 34th International Wire and Cable Symposium Proceedings, 1985, pp. 21-27.

⁵P. D. Patel and A. J. Panuska, "Lightweight Fiber Optic Cable," 39th International Wire and Cable Symposium Proceedings, 1990, pp. 158-165.

⁶Stewart E. Miller and Ivan P. Kaminov, "Optical Fiber Communications II," Academic Press, Inc., 1988, pp 227.

⁷P. D. Patel, M. R. Reynolds, M. D. Kinard, A. J. Panuska, "LXE- A Fiber-optic Cable Sheath Family with Enhanced Fiber Access," 37th International Wire and Cable Symposium Proceedings, 1988, pp. 72-78.



Michael D. Kinard is a Senior Development Engineer with AT&T Bell Laboratories, Norcross, GA. He holds a BSME from Old Dominion University and an MSME from Georgia Tech. He has worked in cable design and development for fifteen years. He holds several patents in the cable design and processing areas.



Don Mathis is a Member of the Technical Staff in the Lightguide Technology Department at AT&T Bell Laboratories in Norcross, GA. He is responsible for design of optical fiber service cables and premise cables.

Dr. Mathis joined AT&T Bell Laboratories in 1972. He has B.S. and M.S. degrees from Oklahoma State University, and a PhD degree in Mechanical Engineering from the University of Houston.

He has been granted ten patents with three more pending.



Andrew J. Panuska is a Member of Technical Staff with AT&T Network Cable Systems in Norcross, Georgia. He received B.S. Degrees in Mechanical Engineering and Civil Engineering from the John Hopkins University. He joined AT&T in 1963 on the Ocean Cable Project and in 1969 was assigned to copper cable sheathing and jacketing. Since 1979, he has worked in the Fiber Optic Cable Development Department responsible for the development of fiber optic cable products and processes.



P. D. Patel is a Distinguished Member of Technical Staff at AT&T Bell Laboratories, Norcross, GA. He joined Bell Laboratories in 1969 after receiving degrees in Mechanical Engineering, including a B.E. from Maharaja Sayajirao University, India, and an Engr. Sc. D. degree from Columbia University.

Since 1979, he has worked in the Transmission Media Laboratory at Norcross and is currently working in the Specialty and Premise Cables & Measurements Group.

Dr. Patel's assignments include development of fiber optic cables for outside plant, loop, campus and CATV applications. He holds 19 U.S. Patents and has published 15 technical papers, mostly in the field of fiber optics.

DEVELOPMENT OF DIELECTRIC FIBER OPTIC DROP CABLE

Stephen T. Ferguson and William J. McCallum

Siecor Corporation
Research, Development, and Engineering
Hickory, North Carolina 28603 U.S.A.

Abstract

A new cable has been developed and tested to meet the requirements for low fiber count dielectric drop, intelligent highways, security video, cellular and other emerging cable applications. These applications expose the cable to harsh environmental and mechanical extremes. The cable must be water blocked and flame retardant. Low flexural modulus and compact construction is important for ease of installation and cable routing. The cable must also be rugged to withstand installation pulling forces and long-term loading.

This paper addresses the design considerations and performance of this new low fiber count cable to meet the demands of these cable applications.

Introduction

As fiber is installed in the loop network and other specialized cable environments, the need for lower fiber count cable is apparent. In recent years, telephone and cable operating companies have begun deploying fiber into the subscriber loop to provide broadband services. With existing multiplex technology, the architecture exists for low fiber count drop cables to Optical Network Units (ONUs) or fiber nodes placed in neighborhoods for signal distribution. Local and state governments are exploring the utilization of low fiber count cables in construction of intelligent vehicle highway systems with the ability to control traffic flow at ramps and stoplights, assist mass transit systems, and support toll collection. At locations involving extreme distances between monitoring stations, low fiber count optical cables are used to provide signals from security cameras and sensors which would otherwise be inaccessible for conventional copper cables without signal regeneration. An emerging technology is the use of optical fiber cables for transporting radio frequency (RF) signals between cellular base stations and remote microcell centers for high speed transportation of wireless signals.

The operating environment in these cable applications is very demanding. The cable experiences temperature extremes, installation tensile and crush loads, as well as harsh outdoor hazards such as UV radiation, humidity, ice, and heat aging found in ONU and pedestal applications. The cable is typically routed into this hardware with small bend diameters; therefore, cable flexibility and small diameter is critical. Flame resistance is also desired since the cable could be routed in close proximity to structures or near existing electronics. Because the installation of these cables may vary according to the type of electronics and termination hardware, the optical fibers in these cables must be flexible. The fibers must allow for field connectorization and handling, but should also facilitate easier fusion splicing and stress-reduced routing in splice hardware.

Given these design considerations, a low fiber count flame retardant dielectric cable has been developed and tested.

Cable Design

Several key performance characteristics were identified for this cable design: rugged optical fiber buffer design, attenuation performance over a -40° to +70 °C temperature range, cable and buffered fiber flexibility, water penetration resistance and flame resistance. Current industry specifications for outdoor fiber optic cable and buried service wire were used for compliance versus specifications. The diagram for the cable cross section is shown in Figure 1.

Buffered Fiber

Rugged fiber design is critical for the demanding installation conditions found in the application environments for this product. This cable was designed with 900 μm tight buffered fiber to improve handling characteristics and reduce opportunity for fiber damage during installation. Each fiber is positively identified through surface coloring. Since 900 μm fibers are employed throughout the entire cable length, fiber furcation or special fiber protection

is not required upon cable termination. The field craftsperson can simply route the 900 μm fibers in the installation hardware and/or directly terminate the optical fibers with connectors.

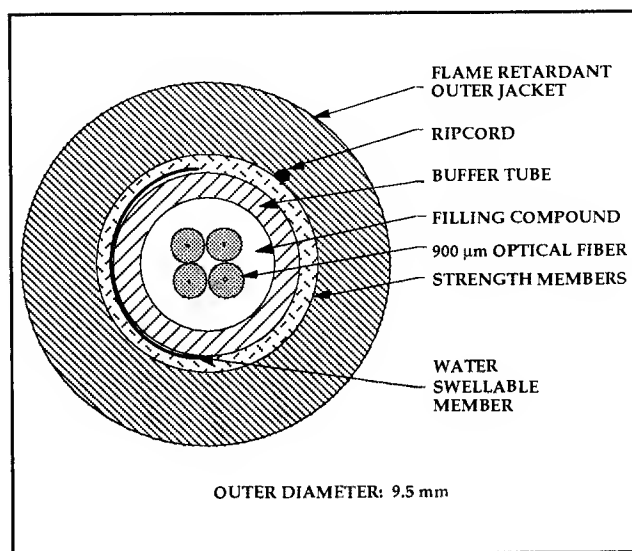


Figure 1: Dielectric Drop Cable Cross Section Diagram

Some tight buffered fibers hold a set or "memory" from buffer tube excess fiber length or from remaining in small loops formed during splice tray installation. Buffer material selection included process steps and material rejection criteria based on minimizing fiber "memory." Additionally, the buffer material was tested for compatibility with filling compound at high temperature (85 °C) for extended periods (> 24 weeks) with negligible change in material strength and elongation.

Another buffer design objective was to identify a material that would contribute virtually no attenuation increase to the overall fiber performance during temperature cycling and mechanical testing. Attenuation changes in excess of 0.20 dB/km at 1550 nm were common for previously available tight buffered fibers when subjected to the -40 °C to +70 °C temperature range. The tight buffer material chosen for this cable exhibits a coefficient of thermal expansion and secant modulus similar to the optical fiber coating, contributing to low levels of strain induced in the fiber during temperature cycling, thereby reducing its effect on fiber attenuation.

A unique feature was added to aid with fiber termination. A synthetic resin slip layer was placed on the outer surface of the 250 μm fibers to aid with

removal of the outer tight buffer. This layer provides for a light bond between the tight buffer material and the optical fiber. The field craftsperson can easily strip 100 mm or more of the tight buffer material in a single pass using conventional buffer strippers to expose the 250 μm fiber. A second pass with a conventional coating stripping tool removes the fiber coating, exposing the optical waveguide for termination and/or cleaving. If desired, the 900 μm tight buffer material can be stripped directly to the 125 μm optical fiber with conventional buffer strippers in a single pass.

Buffer Tube

A central tube cable design incorporates up to four (4) optical fibers. The buffer tube is comprised of thermoplastic material and is filled with water blocking filling compound. The material selection for the buffer tube plays an important role in cable flexibility. The tube must be flexible during handling, yet offer additional fiber protection during crush and other mechanical loading.

Strength Elements

Aramid and impregnated fiberglass yarns are helically wound over the buffer tube for increased cable tensile strength and enhanced anti-buckling during temperature cycling. The Young's modulus of the anti-buckling fiberglass rovings and the yarn's lay length over the tube were found to contribute to the overall flexibility of the cable. Longer yarn lays and high yarn modulus tend to increase cable stiffness. An optimized combination of yarn lay and modulus was required to meet the installation tensile strengths up to 1350 N while not adversely affecting the overall cable flexibility.

Water Penetration Protection

Water swellable material is dispersed with the yarns to effectively meet water penetration requirements. Adhesives and water blocking greases are eliminated between the buffer tube and outer jacket. Cable end preparation is simplified during installation since solvents are not required to remove flooding compounds from the yarns and buffer tube prior to cable termination.

Jacket Material

The jacket material was compounded to provide a flexible, flame retardant, UV light stabilized outer jacket that offers rugged cable protection and increased handleability. Care was taken to select a material with the desired flexibility and handling characteristics. Flame retardants were added to increase the resistance

TEST	RESULT *	TEST METHOD
Temperature Cycling (-40° to +70 °C, 4 cycles)	< 0.05 dB/km increase	EIA/TIA-455-3A
Cable Aging (85°C, 168 hrs)	< 0.05 dB/km increase	EIA/TIA-455-3A
High Temperature Bend (+60 °C, 4 turns)	< 0.05 dB increase	EIA/TIA-455-37A
Low Temperature Bend (-20 °C, 4 turns)	< 0.05 dB increase	EIA/TIA-455-37A
Impact (20 cycles)	< 0.05 dB increase	EIA/TIA-455-25A
Compression (220 N/cm)	< 0.05 dB increase	ANSI/EIA-455-41
Tensile Strength (1350 N)	< 0.05 dB increase	ANSI/EIA-455-33A
Cable Twist (2 turns)	< 0.05 dB increase	EIA/TIA-455-85A
Cyclic Flex (100 cycles)	< 0.05 dB increase	EIA/TIA-455-104A
Flame Resistance	Pass	UL-1581, VW-1
Water Penetration (1 m: 24 hrs-Unaged, 1 hr-Aged)	No Water Leakage	EIA/TIA-455-82A
Lightning Test (w/Braided Steel Messenger)	> 150 kA	EIA/TIA-455-181
Resistance to Fungus Growth	Grade 0 - 0% growth	ASTM G-21
Filling Compound Flow (80 °C)	No Compound Flow	EIA/TIA-455-81

* Note: Attenuation measurements performed at 1550 nm.

Table 1: Dielectric Drop Cable Performance

of this material to ignition and hinder the propagation of flame. The material was enhanced with carbon black and other stabilizers to meet the requirements of an outdoor environment. Additionally, this material was designed for resistance to wasp spray and fungus growth.

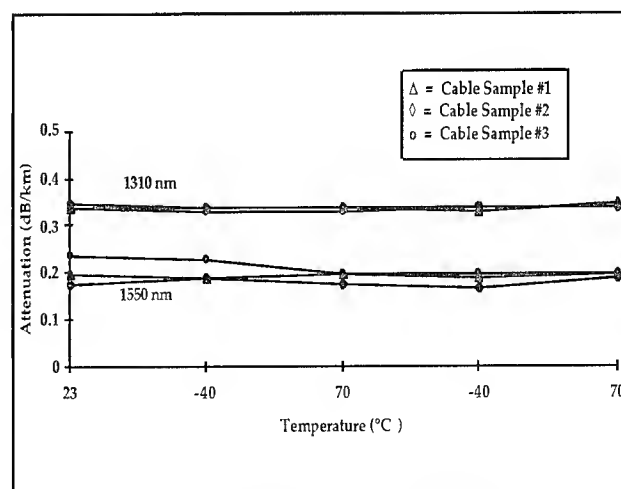
Cable Performance

Developmental cables were produced and evaluated for optical, mechanical, and environmental performance. Typical cable performance and test methods are summarized in Table 1.

Temperature Cycling/Heat Aging

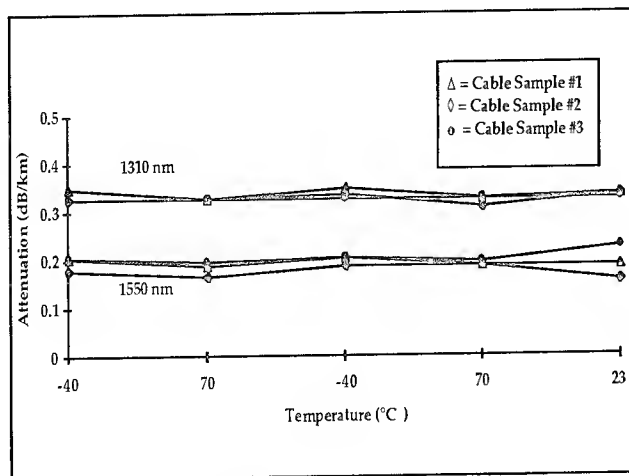
This cable was designed to exhibit superior low and high temperature performance both in temperature cycling and heat aging. Several factors contributed to cable performance. First, the outer jacket material was developed to have a low coefficient of thermal expansion (CTE), thereby reducing the amount of expansion and contraction with temperature change. Second, the 900 μ m buffer was designed to closely match the CTE of the acrylate coating on the optical fiber. Third, the excess fiber length in the buffer tube was optimized to isolate the optical fibers from the induced mechanical forces during tube contraction.

Figure 2 illustrates the actual attenuation performance of various cable samples during temperature cycling. Figure 3 illustrates the actual attenuation performance of these same cable samples after heat aging (168 hrs, 85 °C) for an additional two temperature cycles. The temperature cycling/heat aging cycle time profile is shown in Figure 4.



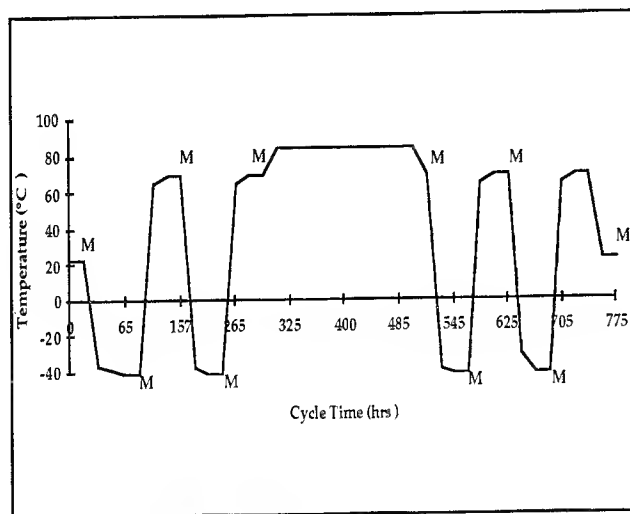
Note: Actual attenuation measurements.

Figure 2: Temperature Cycling Results - Unaged Cables



Note: Actual attenuation measurements.

Figure 3: Temperature Cycling Results - Aged Cables



Note: M = Attenuation Measurement Points

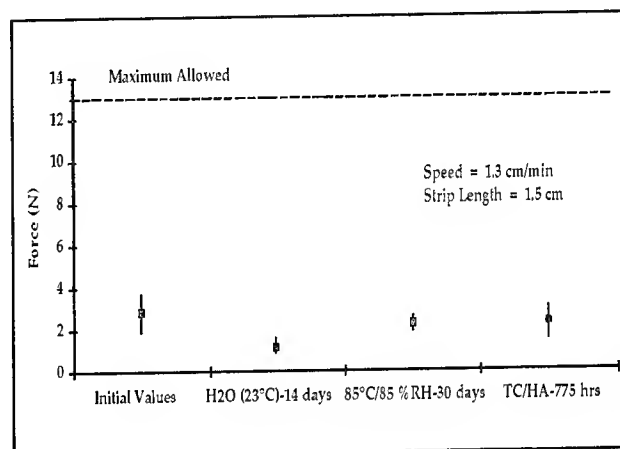
Figure 4: Cable Temperature Cycling/Heat Aging Cycle Time Profile

Fiber Strip Force

Optical fibers were buffered to 900 μm for improved field connectorization and handling, so a process was developed to allow this protective buffer to be removed down to the 250 μm acrylate coating. This fiber can also be stripped directly to the 125 μm optical fiber. This one or two pass stripping option allows for expanded choices of termination and/or splicing during cable installation. Due to the varied installation environments, characterizing the coating strip force was especially important in assuring the

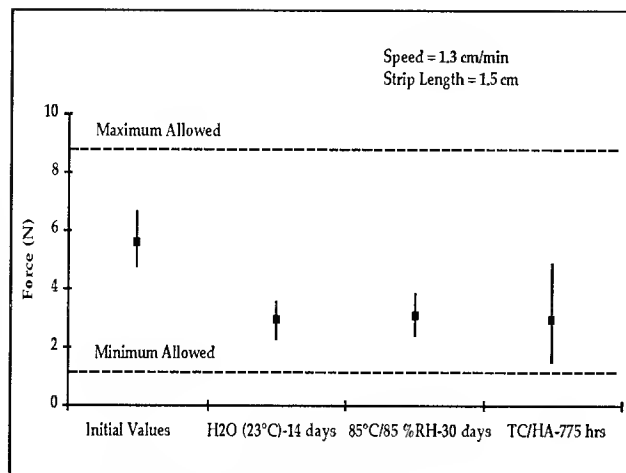
overall stability of the fiber buffer and coating to moisture and extreme conditions.

In order to evaluate the strip force of the buffered fibers under a variety of conditions, individual fibers were placed in three test environments: initial room temperature, 85 °C/85 % RH for 30 days, and 23 °C tap water for 14 days. The testing indicated that the strip force to remove the 900 μm buffer material down to the 250 μm fiber coating and to remove the 250 μm fiber coating down to the 125 μm optical fiber slightly decreases in both test conditions; however, minimum strip force integrity was maintained. See Figures 5 and 6 for the results of this testing.



Note: 1) Bar indicates range of data, solid block indicates nominal value.
2) TC/HA = Temperature cycled/heat aged cable sample

Figure 5: Strip Force Required for Buffer Removal (900 μm -250 μm)



Note: 1) Bar indicates range of data, solid block indicates nominal value.
2) TC/HA = Temperature cycled/heat aged cable sample.

Figure 6: Strip Force Required to Remove Fiber Coating (250 µm-125 µm)

Flame Resistance

This cable is a flame retardant design for applications where flame resistance is a requirement. The cable design also utilizes materials which provide water penetration resistance and UV stability. Therefore, the overall cable construction allows for installation in both flame retardant and conventional outdoor telecommunications applications. Additionally, emerging cable technologies may require cables which bridge the gap between outdoor and flame retardant cable designs.

The UL VW-1 flame test was used to determine finished cable construction compliance. This test utilizes three acceptance criteria:

- The flame must self-extinguish within 60 seconds after each of five - 15 second applications of the test flame.
- The cable specimen shall not ignite combustible materials located below the vertically mounted sample.
- The cable specimen shall not damage more than 25 percent of the indicator flag located 254 mm above the flame application.

The finished cables met these requirements. Additionally, cable was submitted for independent testing and found to meet the flame spread requirements of UL-1581, the Vertical-Tray Flame Test (OFN).

Cable Flexibility

Cable flexibility was a key design consideration since this cable will be deployed in environments with limited space and where enhanced cable flexibility is required. Cable handling characteristics were optimized for this application.

For comparison purposes, a very flexible single tube cable with a similar diameter to the developmental drop cable was evaluated for handleability by bending it into a 50 mm diameter loop. Although the cable bent very easily, it was vulnerable to kinking as the loop diameter approached 50 mm. A second single tube cable of comparable size that was very stiff and difficult to bend was selected for evaluation. This stiff cable did not exhibit enough flexibility for deployment in small bend diameters. The new drop cable was designed to be stiff enough not to kink when bent into small loop diameters but not so rigid that it was difficult to handle during installation.

A test was developed to determine an estimate of the cable flexural modulus (see Figure 7) by modifying Test Method I of ASTM D 790-92, "Standard Test Methods for Flexural Properties of Unreinforced and Reinforced Plastics and Electrical Insulating Materials." In order to test a completed cable, the procedure was modified as follows:

- Cable support span: 8x cable OD
- Crosshead speed: 10 mm/min

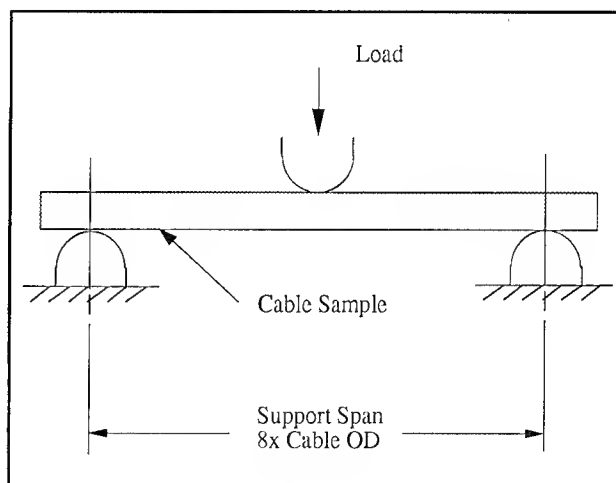


Figure 7: Flexural Modulus Test Configuration

By using this test method, cable flexibility was measured and the results were used to characterize a cable with the desired handling characteristics. As seen in Table 2, the cable with high flexibility had a lower flexural modulus when compared with the more rigid cable. The developmental drop cable flexibility was optimized and the flexural modulus was determined to be 85 MPa. Figure 8 shows the typical load versus cable strain curve for each cable tested.

CABLE TYPE	CHARACTERISTICS		
	FLEXIBILITY	CABLE KINK (2" diameter loop)	FLEXURAL MODULUS* (MPa)
1	High	Yes	40
2	Low	No	435
Developmental Drop Cable	Optimized	No	85

*Note: Measurements at ambient temperature

Table 2: Physical Characteristics for Cables Used in Modulus Test

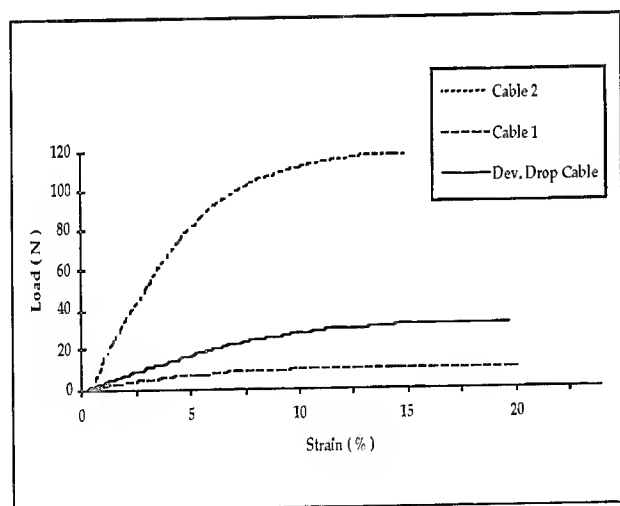


Figure 8: Graph of Load versus Cable Strain for Tested Cables

Conclusions

An enhanced dielectric fiber optic drop cable has been developed that meets the demanding requirements found in the distribution environment and other emerging communication applications. The cable is designed to meet four primary objectives:

- Performance in rugged installation environments
- Optimized cable flexibility
- Flame resistance
- Fiber strippability

The cable design incorporates 900µm tight buffered fibers that are capable of excellent attenuation performance over a wide temperature range. Performance and durability of this buffer design was optimized to meet demanding installation conditions.

Acknowledgments

The success of this cable development project is the result of significant contributions of many people. The authors would like to thank all who participated in the design, development, construction and testing. Special thanks to Dr. Ilona Schmidt and Greg Mills for their support during all phases of this project.

References

1. ASTM D 790-92, "Standard Test Methods for Flexural Properties of Unreinforced and Reinforced Plastics and Electrical Insulating Materials."
2. Bernard W., Grant S.C., "Fiber Optic Drop Cables in the Subscriber Loop," *Proceedings of the 39th IWCS*, 1989, pp. 402 - 407.
3. Leistad, J. E., "Fibre-Optic Cables for the Subscriber Network," *Revue E-108 éme année-n°3-92* (Janvier 93), pp. 37-44.
4. Carson, P., "Cellular Calls On Fiber," *Fiberoptic Product News*, May 1994, Volume 9, Number 5, pp. 17-19.
5. Barrett, M., "FITL-An Outside Plant Economic Model," *Lightwave*, May 1993, Volume 10, Number 6, pp. 36-42.
6. ANSI/UL 1581-1985, "Reference Standard for Electrical Wires, Cables, and Flexible Cords," First Edition.
7. S-87-640-1992, "Fiber Optic Outside Plant Communications Cable," Insulated Cable Engineers Association, Inc.
8. TR-NWT-000020, "Generic Requirements for Optical Fiber and Optical Fiber Cable," Issue 5, December 1992.
9. TR-TSY-000843, "Generic Requirements for Optical and Optical/Metallic Buried Service Cable," Issue 1, January 1989.



Stephen T. Ferguson
Siecor Corporation
PO Box 489
Hickory, NC 28603

Stephen T. Ferguson received a B.S. degree in Mechanical Engineering from Virginia Polytechnic Institute and State University in 1989. Since joining Siecor Corporation in 1989, he has coordinated and supervised installation and maintenance of fiber optic cable systems at customer locations; and planned and directed technical support to internal departments and customers. Currently, he is with the Research, Development and Engineering Department as a Product Development Engineer responsible for design, development and implementation of telecommunications cable products. Mr. Ferguson is a member of the American Society of Mechanical Engineers and Insulated Cable Engineers Association.



William J. McCallum
Siecor Corporation
PO Box 489
Hickory, NC 28603

William J. McCallum received a B.S. degree in Engineering from the University of North Carolina at Charlotte in 1982. Since joining Siecor Corporation in 1982, he has been actively involved with design and development activities for copper and fiber optic telecommunications cables and elevator control cables. He is currently Supervisor, Process Development for Telco and Customer Premises Products with Research, Development, and Engineering. Mr. McCallum is a Professional Engineer and is a member of the National Society of Professional Engineers.

Development of Small Size Optical Fiber Submarine Cable

Makoto Nunokawa*, Masahiko Kiuchi**, Toshikazu Akasaka**, Shigeru Suzuki**, Hiroyuki Yoshioka**

* KDD Submarine Cable Systems, Inc.
KDD Building, 3-2, Nishi-Shinjuku 2-chome
Shinjuku-ku, Tokyo 163-03, Japan

** Ocean Cable Co., Ltd.
3-12-1, Shin-Yamashita
Naka-ku, Yokohama 231, Japan

Abstract

The new cable design to meet the market's needs for medium - haul repeatered system, which is more suitable for the total cost performance of the system than the conventional cable design for long - haul repeatered system, has been required .

Therefore, we designed and developed a small and lightweight optical submarine cable, SS cable, to meet the requirement . This cable provides high reliability for more than 25 years, whereas its dimension and weight are minimized about 2 / 3 of conventional cable, i.e in case of non - armored cable type, the outer diameter is approx. 17mm and the weight in water is approx. 350kg / km .

This cable has been provided to several medium - haul repeatered systems including the systems between Southeast Asia, that total is more than 3,000km .

Introduction

We have already developed optical fiber submarine cables for use in international and long - haul repeatered systems, and have provided them in practical use . These cables have a excellent characteristics such as deployment and recovery up to 8,000 m water depth .

On the other hand, the market recently shows such a tendency that the optical submarine cable systems have been extensively constructed between neighboring countries. (We will express as " Medium - haul repeatered system " herein after.)

The feature of these systems are summarized as follows :

1. Maximum system length is limited to approx. 2,000km .
2. Deployed water depth is comparatively shallow and it is mostly within 1,500m .
3. Due to the deployed water depth, the armored cables are mainly applied to the system .

We considered there should be the optimum designing of the cables applied to the above systems in place of the cables for the long - haul repeatered system and it could be reduce the system total cost.

We reviewed our OS Cable design (for long - haul repeatered system) and designed Small Size Optical Submarine Cable for the medium - haul repeatered system by minimizing the diameter and the weight.

The following merits are expected by applying the new designed cables to the medium - haul repeatered system. :

1. Cable cost reduction
2. Transportation and installation cost reduction due to increase of loaded cable length.

This report describes the design and the evaluation test results of the optical fiber submarine cable (called as SS cable) for medium - haul repeatered system.

Cable Design

We set the designing concept shown in Table.1 on the basis of the following consideration and started the development.

Table. 1 Designing Concept of New cable

	Concept
1	Number of fiber : ≤ 6 fibers
2	Water depth : $\leq 5,000\text{m}$
3	System length : $\leq 2,000\text{km}$
4	Design lifetime : ≥ 25 years
5	To minimize the cable diameter and weight
6	Joining techniques (Joint Box and Coupling) of OS cable substantially be applied.
7	Manufacturing facilities for OS cable be applied to the production.

We decided to minimize the diameter and the weight of the following OS cable because it has been applied to various projects for long - haul repeatered system, and its fine characteristics as to the performance and the productivity have been proved.

Moreover, if the development can be accomplished by modifying the OS cable design, we can minimize the new investment in the cable manufacturing facilities and the joining technique of OS cable can be applied substantially. The application of the common joining technique has a beneficial effect on reducing the cable maintenance cost.

Further, it is estimated that most of cables are deployed within 1,500m water depth, but taking into consideration to be deployed in the deep sea as the non - armored cable, the design target should be set as 5,000m water depth .

Even in the medium - haul repeated systems, the transmission characteristics and the reliability required for the optical fiber submarine cables are the same as these of long - haul repeated systems. Hence, we decided to design each components of cable including the optical fiber unit, considering the reliability and optical, mechanical characteristics, and its productivity.

Here, a thorough consideration is required for the composite conductor (copper tube, 3 - divided steel segments and tension member) designing as the power supply path for submersible repeaters. To minimize the size of the composite conductor is attributed to the increase electric resistance, hence its design should be optimized considering the haul length.

On the basis of above discussion, the optimum cable dimension for medium - haul repeatered system, was determined .

The structure and characteristics of SS cable are shown in comparison with OS cable as Fig. 1 and Table . 2 respectively .

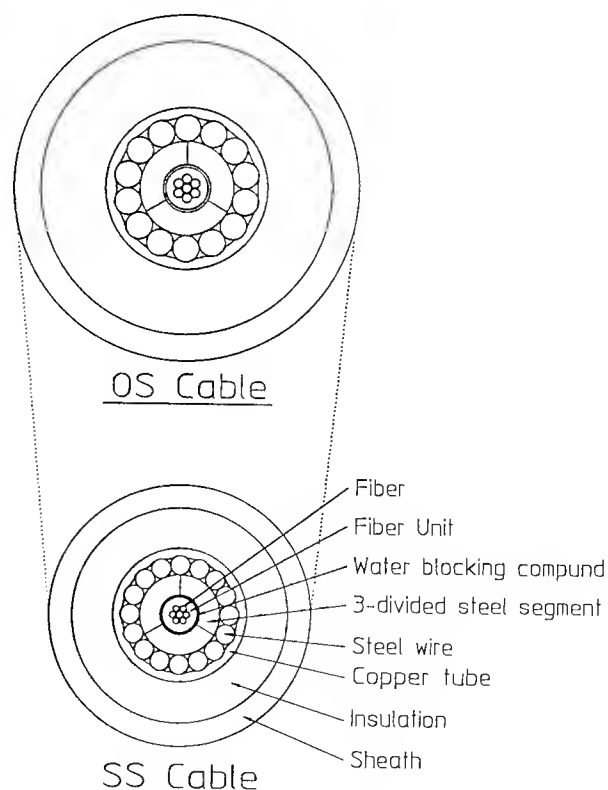


Fig. 1 Structure of SS cable

Table. 2 Characteristics of SS cable and OS cable

Item	SS Cable	OS Cable
Cable diameter	Approx. 17mm \varnothing	Approx 22.5mm \varnothing
Cable weight in air	5.62kN / km	8.88kN / km
Cable weight in water	3.40kN / km	4.98kN / km
Stowage factor	0.324m ³ / km	0.568m ³ / km
MBL (※)	60kN	98kN
DC resistance (3°C)	1.0 Ω / km	0.7 Ω / km
Cable modulus	17km	20km
Hydrodynamics constant	43.5deg - knots	43.6deg - knots

(※) Minimum Cable Breaking Load

The structure is as follows :

1. Fiber unit
The fiber unit are stranded around a steel wire and embedded in UV - cured resin .
2. Three - divided steel segments
The three - divided steel segments are assembled longitudinally over the fiber unit to form pressure resistance tube .
3. Steel wire
Around the steel segments, high tensile steel wires are stranded .
4. Water blocking compound
The water blocking compound is continuously filled in to the space between the fiber unit, steel segments and each steel wire.
5. Copper tube
The copper tube is applied tightly around steel wires .
6. Insulation
The low density polyethylene is applied around the composite conductor to insulate from sea water .
7. Sheath
The sheath is applied over the insulation to protect from abrasion on a sea bottom .

The dimension and weight of SS cable are minimized about 2 / 3 of OS cable .

The armored cable is applied to the shallow water area to protect from fishing activity or ship's anchor etc . We have designed and developed several kinds of armored cables corresponding to each sea area (the water depth and the sea bed condition) . For example , the structure and characteristics of the single armored cables and the double armored cables are shown in Fig . 2 and Table . 3 respectively .

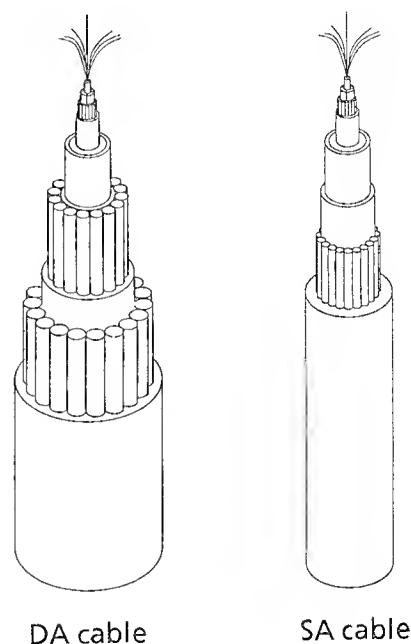


Fig. 2 Structure of Type SA and DA cable

Table. 3 Characteristics of Type SA and DA cable

	Type SA Cable	Type DA Cable
Cable diameter	Approx. 33mm \varnothing	Approx 55mm \varnothing
Cable weight in air	22.7kN / km	88.1kN / km
Cable weight in water	15.6kN / km	68.8kN / km
MBL (※)	156kN	424kN
Stowage factor	1.22m ³ / km	3.39m ³ / km

(※) Minimum Cable Breaking Load

Evaluation Test

Various tests were carried out on the developed SS cables to evaluate the performance as for the handling, the installation and the long term stability on the sea bed. Typical testing items and test results are shown in Table 4.

Furthermore, for the purpose of final confirmation, the sea trial was performed. Non - armored cable was installed into 5300m water depth and recovered. The continuous measurement for optical characteristics was conducted during the sea trial, and the performance after recovering was examined.

Throughout the sea trial, no optical loss increase was observed and no degradation of cable characteristics was confirmed.

As the result of these evaluation, we confirmed the SS cable has the excellent performance to construct the medium - haul repeatered system.

Table . 4 Evaluation Test Results of SS cable

Test Item	Purpose	Test Condition	Test Result						
Temperature test	To simulate that the cable withstands operating and storage temperature	Optical loss change is measured continuously in the temperature range form -20°C to 60°C.	• Optical loss change is within ± 0.002dB/km. (refer to Fig. 3)						
Water pressure	To simulate that the cable withstands maximum deployment water pressure	Water pressure 100kg/cm ² , 550kg/cm ² and 800kg/cm ² is applied to cable, optical loss change is measured continuously.	• Optical loss change is within ± 0.001dB/km.						
Lateral load	To simulate that the cable withstands the stowage in the cable tank or holding at the cable ship machinery	When 20kN lateral load is applied to cable mounted between flat plates with 20cm in length, cable loss change is measured continuously and cable mechanical characteristics test is conducted after the test.	• Cable loss is not changed. • Cable mechanical characteristics is not degradation.						
Reverse bend	To simulate that the cable withstands the bend at the handling	When 30 reverse bending on 0.9m radius is applied to cable, cable loss change is measured continuously and cable mechanical characteristic test is conducted after the test.	• Cable loss is not changed. • Cable mechanical characteristics is not degradation.						
Load - torque -elongation	To evaluate the cable characteristics	When the tension is applied to the cable with both end fix, the cable elongation , torque and optical loss is measured continuously.	• Optical loss is not changed. • Cable torque is within 0.15kg - m / 10kN.						
Load - rotation - elongation	To evaluate the cable withstands the laying and recovery tension	When the tension is applied to the cable with one end fix, the cable elongation and optical loss is measured continuously.	• Optical loss is not changed. • Cable elongation characteristics is Fig.4.						
Sheave Test	To simulate that cable withstands the cable joint condition	The sham sheave is moved a axle - direction to cable that is applied tension . (refer to Fig.5) In the above condition, optical loss is measured continuously and the cable mechanical characteristics test is conducted after the test.	• Optical loss is not changed. • The cable mechanical characteristic is not degradation. (refer to Fig.5)						
Water ingress	To simulate the water blocking characteristics of cable	When the 100kg/cm ² and 550kg/cm ² water pressure is applied to the one cable end for, the water ingress length of the cable is measured.	• Water ingress length is within the following specification . <table><tr><td>Water pressure</td><td>Specification</td></tr><tr><td>100kg/cm²</td><td>250m / 2weeks</td></tr><tr><td>550kg/cm²</td><td>1,000m / 2weeks</td></tr></table>	Water pressure	Specification	100kg/cm ²	250m / 2weeks	550kg/cm ²	1,000m / 2weeks
Water pressure	Specification								
100kg/cm ²	250m / 2weeks								
550kg/cm ²	1,000m / 2weeks								

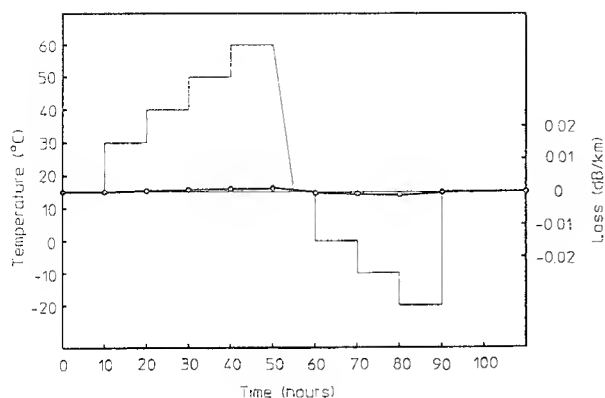


Fig. 3 Temperature Test

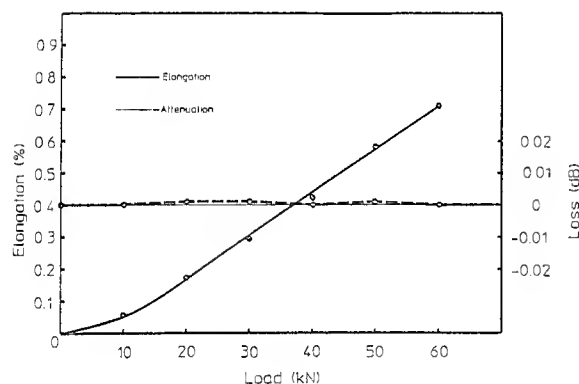


Fig. 4 Tensile Test

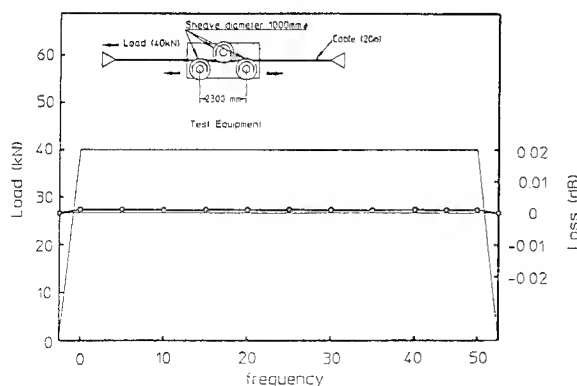


Fig. 5 Sheave Test

Joining

As described in above, we decided to apply OS cable joining technique to SS cable joining, because the common joining technique is very beneficial in the point of the system maintenance cost.

The developed Coupling and Joint Box for SS cable are almost in common with these for OS cable, so that the same joining techniques (Method, Equipments and Parts) can be utilized. Because of the cable dimension difference, the anchoring parts and some attachments for joining equipments are only different from those for OS cable.

Fig. 6 shows an example of the joint box for SS cable, which is employed for mutual joint between the single armored cable and double armored cable. And the tensile test result of this joint box is shown in Fig. 7.

The alternate load due to the pitching of cable ship and the load (140kN) close to the breaking load of single armored cable were applied to this joint box.

As the results, no degradation of the performance of the joint box is observed.

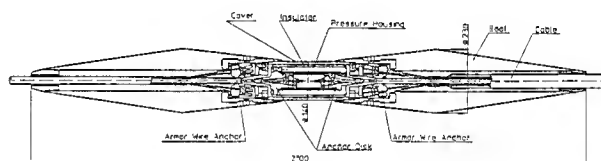


Fig. 6 Joint Box for SS cable

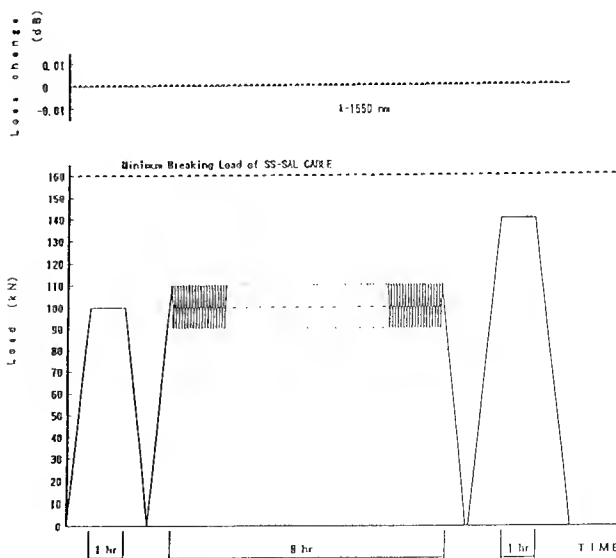


Fig. 7 Tensile Test with Joint Box

Conclusion

We anew developed small and lightweight optical submarine cable, SS cable, for use in a medium - haul repeatered system.

In case of non - armored type of SS cable, the size and weight were minimized into about 2 / 3 of OS cable's, whereas it provides high reliability for more than 25 years.

SS cable has been already provided to several medium - haul repeatered systems including the systems between Southeast Asia, that total length is more than 3,000km.

Now we are developing of a fiber unit which contain 24 fibers and further optimization of this cable for use in non - repeatered system.

Acknowledgement

The authors wish to acknowledge KDD for their advice and discussion, and also wish to acknowledge all parties concerned in the development for their assistance and co-operation .

Reference

- (1) Y. Yamazaki, et al., " The OS-280M optical Fiber Submarine Cable " Suboptics '86 123-128 (1986)
- (2) M. Nunokawa, et al., "A study of Small - diameter Optical Submarine Cable " IEICE of Japan, '88 B588 (1988)
- (3) H. Yamamoto, et al., " Design and Test Result of OS-560M Optical Submarine Cable, Repeater Housing and Coupling " IWCS '91 620-627 (1991)



Makoto Nunokawa
KDD Submarine Cable
Systems, Inc.
KDD Building, 3-2,
Nishi-Shinjuku 2-Chome
Shinjuku-ku, Tokyo
163-03, Japan

Makoto Nunokawa was born in 1945. He received B.E. degree in 1968 and M.E. degree in 1970 from Waseda University, Tokyo, Japan. He joined the Research and Development Laboratories, Kokusai Denshin Denwa Company, Ltd. (KDD) in 1970 where he was engaged in the research and development of coaxial and optical fiber submarine cable systems. He is presently Senior Managing Director of KDD Submarine Cable systems, Inc. He is a member of IEICE of Japan.



Shigeru Suzuki
Ocean Cable Co., Ltd.
3-12-1, Shin-Yamashita
Naka-ku, Yokohama
Japan

Shigeru Suzuki was born in 1956. He graduated from Tokyo Metropolitan university with B.E degree in 1979. He joined Ocean Cable Co., Ltd. and he has been engaged in research and development of optical fiber submarine cable. He is now an assistant manager of Submarine cable division and a member of IEICE of Japan.



Masahiko Kiuchi
Ocean Cable Co., Ltd.
3-12-1, Shin-Yamashita
Naka-ku, Yokohama
Japan

Masahiko Kiuchi was born in 1967. He graduated from Tokai University with B.E degree in 1990. He joined Ocean Cable Co., Ltd. and he has been engaged in development of optical fiber submarine cable. He is now an engineer of submarine cable division.



Hiroyuki Yoshioka
Ocean Cable Co., Ltd.
3-12-1, Shin-Yamashita
Naka-ku, Yokohama
Japan

Hiroyuki Yoshioka was born in 1954. He graduated from Kyoto Institute of Technology with B.E degree in 1979. He joined Ocean Cable Co., Ltd. and he has been engaged in research and development of optical fiber submarine cable. He is now an assistant manager of submarine cable division and a member of IEICE and JSME of Japan.



Toshikazu Akasaka
Ocean Cable Co., Ltd.
3-12-1, Shin-Yamashita
Naka-ku, Yokohama
Japan

Toshikazu Akasaka was born in 1964. He graduated from Kanagawa University with B.E degree in 1988. He joined Ocean Cable Co., Ltd. and he has been engaged in development of optical fiber submarine cable. He is now an engineer of submarine cable division.

DIRECT MECHANICAL FIBER STRAIN MEASUREMENT AND THE CABLED FIBER STRAIN OF AN UNDERSEA CABLE

C. S. Ma, L. L. Blyler, G. E. Johnson
AT&T Submarine Systems, Inc., Holmdel, New Jersey
AT&T Bell Laboratories, Murray Hill, New Jersey

R. T. Traut, C. E. Murphy, M. W. Jones, F. C. Gibson, W. M. Keith
Simplex Technologies Inc., Newington, New Hampshire

ABSTRACT

A reliable mechanical method has been developed to measure the strain of an optical fiber in an undersea cable. The strain is measured in both a tightly-coupled Submarine Lightguide (SL) cable Unit Fiber Structure (UFS) optical core and in a completed SL cable. Cabled fiber strain values are used in optical fiber static fatigue calculations to assure the long term reliability of optical fibers. This strain is designed to be slightly compressive and therefore provides an additional margin of safety for long term fiber reliability. The direct mechanical strain measurement method presented in this paper verifies that fiber strains are at the designed strain values in SL cables and that these strains are consistent from cable to cable. The basic principle of the method is to directly measure and compare the free lengths of each fiber, the central kingwire, and the cable structure of an SL cable sample, and calculate the cabled fiber strain in the UFS and completed cable.

The measurement set includes a test bed, two X-Y positioners, two microscopes, and two dial indicators. Measurement accuracy is better than 0.01% strain for a 36 inch (914.4 mm) long sample and 0.04% strain for a 5 inch (127 mm) long sample of an SL UFS or cable.

The cabled strain of a fiber in an SL UFS is related to the UFS processing parameters and tooling used in the UFS manufacture. Consistent fiber strain is achieved when tooling and fiber coating surfaces are smooth and uniform. Strain in the completed cable results from the superimposed combination of UFS fiber strain and the strain induced during the steel wire stranding and copper power conductor manufacturing operation. A determined amount of strain variation results from the effects of variation of the coupling between the UFS and the cable structure.

I. INTRODUCTION

Fiber strain in a tightly-coupled unit fiber structure (UFS) has been measured previously using optical methods. The time lag of an optical pulse associated with the length change was accurately measured using a York S18 optical measurement set. Measurements were taken after sequential manufacturing processes and fiber strains were calculated at each stage. The optical measurement procedure is tedious and requires

extreme attention to procedures and environmental conditions. Fiber preparation, temperature, air flow, and vibration may impart variation. Also, this optical method is limited by fiber length. The optical method can be applied to short UFS samples. However, chemicals such as methylene chloride are needed to dissolve the elastomer matrix to expose the fibers. For this procedure, ambient environmental conditions must be well under control. Therefore, a direct mechanical measurement has been introduced to improve and simplify the fiber strain determinations. The method was developed to accurately measure 5 inch (127 mm) and 36 inch (914.4 mm) samples.

To directly measure fiber strain the lengths of the completed cable and components (kingwire and fibers) are required. A diagram of an SL Light Weight cable is shown in Figure 1. The cable sample is first cut to the desired length with a diamond blade saw and the UFS is removed. The fibers and kingwire are then removed from the UFS by softening the elastomer with warm air. At various stages of this operation the samples are placed on a precision length test bed and measured in a free (untensioned) condition. The length information is used to calculate the fiber strain associated with the relative length changes at each stage in the sample dissection.

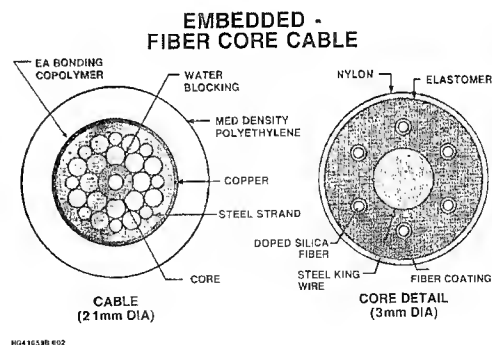


Figure 1. SL Light Weight Cable

Although a six fiber cable was used as a basis for establishing the statistical reliability of the measurement, other fiber count cables (four through

twenty-four) have been measured, yielding important data and an improved understanding of the manufacturing processes. The following sections discuss the instrumentation, measurement accuracy, and the fiber strain in an SL cable.

II. CABLE DESCRIPTION

A diagram of an SL Cable is shown in Figure 1. Submarine Lightguide (SL) cable^{[1] [2]} was developed to provide the medium for transoceanic transmission of digital optical signals. In order to provide high reliability, SL cable was designed to ensure close control of cabled fiber strain. This was accomplished by enclosing a central Unit Fiber Structure (UFS) within a high strength steel strand package designed to provide high yield strength and low strain. The compact strength package, as well as the low steel strand lay angles, provides a cable structure which imparts very low residual strain to the UFS, even after tensioning to the maximum permissible tensions. The reliability of the fibers within SL cable, even after recovery from the deepest ocean water, is ensured by this low residual strain characteristic and by close control of the fiber strain during cable manufacture.

Deep water SL cable is manufactured in three primary processes. The first is the UFS process. In this process three simultaneous extrusions occur. The first layer, extruded over the central copperclad steel kingwire, provides the medium to support the coated optical fibers. Through special tooling the fibers are immediately positioned and slightly embedded in the first layer elastomer. The second layer elastomer is then immediately extruded, to encapsulate the ring of fibers, and then a third extrusion encloses the UFS within a thin layer of nylon. The amount of cabled fiber strain at UFS is closely controlled. This is accomplished through control of kingwire tension, fiber tensions, temperatures, dimensions, tooling surfaces and fiber coating surfaces.

The second SL cable process is the Power Conductor (PC) process. Here, the nominal 0.117 inch (2.97 mm) diameter UFS is fed into the central cavity of the steel strand package. The UFS is maintained at a prescribed level of backtension. At the closing point, 24 steel strand wires are helically formed around the UFS while the waterblocking filling compound is simultaneously applied. Next, a longitudinal copper tube is formed, continuously TIG welded, and swaged down into the outer steel strand wires to the design diameter. The swaging of the copper into the steel strand interstices increases copper/steel friction and ensures positive shear coupling. The amount of change in the fiber strain is controlled by the UFS backtension, strand wire tension, closing and swaging tensions, and the degree of coupling.

The final deep water SL cable process is the extrusion of a medium density polyethylene jacket. The clean Power Conductor is first coated with a thin layer of adhesive polymer to ensure positive shear coupling between the copper and the polyethylene. Next, the polyethylene jacket is extruded to a nominal 0.827 inch (21.0 mm) diameter. The polyethylene jacket functions as both an electrical insulation for powering of repeaters or optical amplifiers, and as a protective jacket for the Power Conductor. Because the UFS is well-coupled to the Power Conductor, there is no change in the cable fiber strain as a result of the polyethylene jacketing process.

A smaller and lower cost version of SL cable has been developed^[3] for repeaterless system applications. This design is known as SL-100 and a diagram is shown in Figure 2. SL-100 is produced in three processes similar to SL cable and the descriptions above apply also to SL-100. The UFS diameter for SL-100 is the same as with SL. For fiber counts up to 12, the above UFS description applies. For fiber counts from 13 to 24, the UFS is produced by a UV-cured matrix process^[4] but the key process control parameters, as described above, also apply.

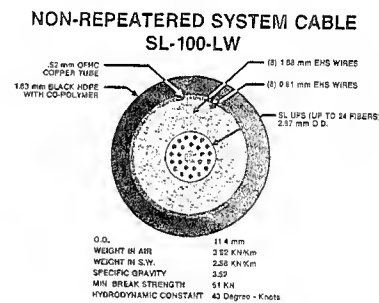


Figure 2. SL-100 Light Weight Cable

SL-100 has a smaller Power Conductor diameter and is formed with 16 high strength steel wires. Although smaller in size, the SL-100 PC process is like the SL PC process described above.

The SL-100 deep water cable is jacketed with high density polyethylene to a final diameter of 0.450 inches (11.43 mm). As with SL, a thin layer of adhesive polymer is extruded over the Power Conductor immediately before the polyethylene jacket to ensure positive shear coupling.

III. INSTRUMENTATION

The complete measurement set includes: one test bed, two X-Y positioners, two holders, two compact microscopes, and two dial indicators.

1. Test Bed

The test bed is a 1.5 inch thick solid aluminum block. The size was selected in order to minimize any physical changes due to temperature variation during sample measurement. Additionally, the test bed is enclosed in a controlled room where air temperature variation is less than $\pm 3^{\circ}\text{C}$.

The test bed is shown in Figure 3. It has 4 parallel sample slots which are capable of lodging 36 inch (914.4 mm) long samples of fiber, kingwire, and cable. The two inner slots are designated for cable and kingwire samples respectively. The two outer slots are reserved for fiber samples and can also be used for parallel checking of the test bed. The test bed can accommodate a variety of cable designs by using "L" shaped filling blocks.

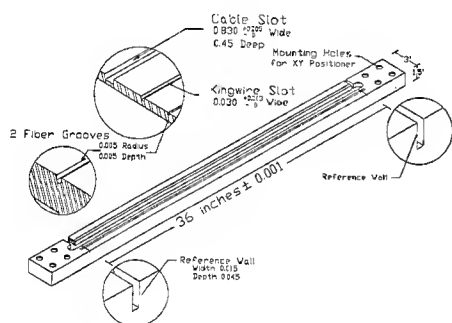


Figure 3. Test Bed

The comparison between lengths of cable, kingwire, and fiber samples is facilitated with precisely machined reference slots located at each end of the test bed. The reference slots are perpendicular to the sample slots and the length between their interior sides is 36 ± 0.001 inches (914.4 ± 0.025 mm).

Shorter cable samples can also be accommodated by machining additional reference slots at the desired sample length. For our application, the additional slot is 5 ± 0.001 inches (127 ± 0.025 mm) away from the primary reference slot.

The maximum absolute strain error due to the test bed itself is 0.003% for a 36 inch (914.4 mm) sample and 0.02% for a 5 inch (127 mm) sample.

2. X-Y Positioner and Microscope

The fiber and kingwire lengths are measured using compact microscopes (Edmund Scientific Co. Model # A38837). They are mounted on X-Y positioner platforms located at each end of the test bed (see Figure 4). One end of the sample is aligned with the interior side of the primary reference slot and its position is verified using the microscope reticle. At the opposite end the second microscope is used to measure the position of the sample with respect to the interior side of the reference slot. Using the micrometer on the X-Y positioner the sample length is determined.

The resolution of the X-Y positioner micrometer is 0.00004 inch (0.001 mm) which is associated with a 0.0001% strain resolution on a 36 inch (914.4 mm) sample. For a 5 inch (127 mm) sample the associated strain resolution is 0.0007%.

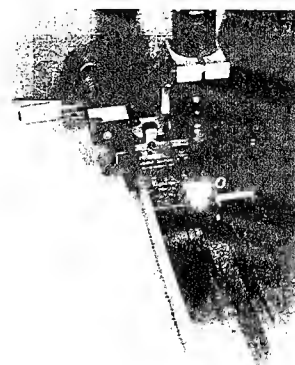


Figure 4. X-Y Positioner with Compact Microscope

3. Indicator

For cable length measurements, the microscopes are not sufficient due to their short depth of field. Therefore, Mitutoyo 513-104 dial test indicators are used to replace the scopes (see Figure 5).

The dial indicator contact ball and the associated zero setting in the dial are used as the reference to measure two parameters. First, by placing the ball on the reference slot wall and then on the kingwire at each end of the sample and reading the X-Y positioner, values the tensioned kingwire length in a cable can be measured. Using the same procedure the overall cable sample length can be measured by placing the dial indicator contact balls on each end of the steel strand wires.

The 0.0001 inch (0.0025 mm) resolution of the dial test indicator is associated with a negligible strain error reading of 0.0003% out of a 36 inch (914.4 mm)

sample, and 0.002% error for a 5 inch (127 mm) sample.



Figure 5. X-Y Positioner with Dial Indicator

IV. SAMPLE PREPARATION

A sample of UFS or cable is prepared by cutting it to the desired length. For our application this consists of sample lengths of approximately 36 inches (914.4 mm) or 5 inches (127 mm). A Buehler 11-1180 Isomet® precision, low speed saw is used to perpendicularly cut the samples. The saw has a water cooled, diamond blade which makes a clean and smooth cross section cut without deforming the sample.

If the sample is in the form of a UFS, the fibers and kingwire are separated using a heat stripping technique. If the sample is in cable form, it is first measured and then the UFS is removed from the cable. The fibers and kingwire are subsequently separated from the UFS using the heat stripping technique.

V. MEASUREMENT

The basic principle of this direct strain measurement is to compare the lengths among fiber, kingwire and cable, to calculate the relative length changes, and to convert them to fiber strain.

1. Fiber in UFS

The natural fiber length (neither tension nor compression) in an SL UFS is calculated based on the lay length and the kingwire length of a UFS sample. Since the same lay length is used for all six fibers in a cable, and because of the different visibility of the fibers within the polymeric matrix, only one lay length of the six fibers is measured (usually the dark color fiber). The equation to calculate the fiber strain in a UFS under no-load condition is as below:

$$\epsilon_{ufs} = \frac{(L_{kw} - L_f \cos(\alpha))}{L_f \cos(\alpha)} \quad (1)$$

$$\alpha = \arctan\left(\pi \frac{OD_{ufs1} + OD_f}{lay}\right)$$

where ϵ_{ufs} is the fiber strain in a UFS without any load, L_{kw} is the length of the kingwire out of UFS, lay is the fiber lay length, OD_{ufs1} is the first polymer layer OD, OD_f is the fiber OD, L_f is the measured fiber length out of UFS matrix and α is the lay angle.

2. Fiber in Cable

For the fiber strain in a cable, the dial test indicators and X-Y positioners are used on the clean cut end cross sections of a cable to measure the positions of the strand wires and kingwire ends relative to the test bed fixture reference wall slots. The position of a cable end is determined from the average of two steel strand positions which are next to the UFS but opposite to each other. The cable length is calculated by comparing the end positions to the test bed fixture reference wall slots. The end position of a kingwire is measured directly by dial indicator and the micrometer of the X-Y positioner. The UFS (or kingwire) strain in a cable is calculated by using the following equation:

$$\epsilon_{kw} = \frac{(L_{st} - L_{kw})}{L_{kw}} \quad (2)$$

where ϵ_{kw} is the kingwire strain in a complete cable, L_{st} is the average steel strand length (or cable length), and L_{kw} is the measured length of the kingwire out of the UFS of the cable sample.

The fiber strain in a finished cable sample ϵ_{cable} is the sum of the kingwire strain in a cable sample and the fiber strain in the UFS from the same cable sample:

$$\epsilon_{cable} = \epsilon_{kw} + \epsilon_{ufs} \quad (3)$$

VI. ACCURACY ANALYSIS

1. Instrumentation Precision

As to the instrumentation precision itself, the measurements for UFS and cable samples are different: one is the combination of compact microscopes and X-Y positioners for the measurement of the fibers and kingwire in a UFS, the other is the combination of indicators and X-Y positioners for the measurement of a cable. The combined instrumentation accuracy of the measurements of a fiber and kingwire is less than 0.003% strain for a 36 inch long sample and less than 0.02% for a 5 inch long sample. The accuracy of the measurement of a cable is less than 0.0005% strain for a 36 inch sample and 0.004% for a 5 inch sample in terms of the combined instrumentation. Therefore, the total accuracy of fiber strain measured from a cable under the worst condition is less than 0.004% for a 36 inch sample and 0.024% for a 5 inch sample.

2. UFS Manufacture

a. Fiber Lay

The error, with the assumption of the same lay of each fiber in a cable sample, is less than 0.003% strain under the most unlikely case of fibers touching. Also, the measurement error of the lay length itself is small, i.e. a 2 mm error of lay length measurement can induce a strain error less than 0.0001%.

b. First Layer Elastomer Diameter

The strain measurement error due to the variation of the first layer elastomer diameter is small. The maximum error from the diameter variation to the nominal diameter is less than 0.001% strain according to the specification of the first layer elastomer diameter.

3. Overall Error of Direct Strain Measurement

From Parts 1 and 2 above, the overall error of a 36 inch cable sample, by using this direct strain measurement technique, is less than 0.009% without consideration of the possible 0.003% offset of the machining accuracy of the test bed fixture reference wall slots. The overall error for a 5 inch cable sample is less than 0.031% without the possible 0.02% offset from the reference walls.

VII. COMPARISON OF DIRECT STRAIN AND OPTICAL STRAIN MEASUREMENT

The direct strain measurement was compared to an established optical strain measurement to verify similar results between the two methods. Three adjacent samples of UFS were used for the comparison.

The optical method consisted of using a York S18 test set to measure the length change when a 31.5 inch (800 mm) section of fiber was removed from a 66.9 inch (1700 mm) sample of UFS. This method resulted in measurements of -0.088% and -0.092% (minus sign indicates compression) for the two samples tested. The reports from the York S18 test set are displayed in Figure 6. A direct strain measurement, using methods described in this paper, was performed on the third UFS sample. The measurements yielded a fiber strain of -0.090% which accurately demonstrated the capability of the direct mechanical fiber strain measurement method.

The direct measurement method has advantages over the optical measurement method. First, chemicals, and their associated hazards, used to free the fibers from the elastomer are eliminated by implementing the direct method. Also, the need to control ambient environmental conditions, which is critical to the optical measurement method, is minimized with the

direct strain measurement technique. Finally, samples as short as five inches can be measured with the direct method which provides useful information regarding strain uniformity in SL cables.

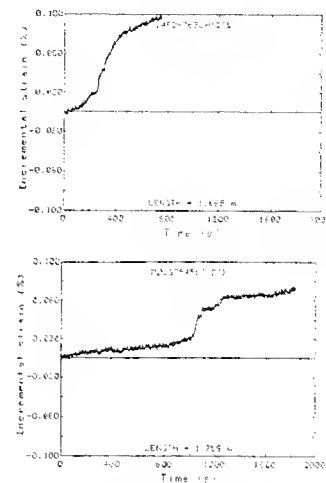


Figure 6. Strain Measurement
From YORK S18 Optical Measurement Set

VIII. FIBER STRAIN IN SL CABLE

1. Post UFS Manufacturing Stage

After UFS manufacture, the fibers are locked in the UFS at a strain level determined by processing conditions and material properties. Using the direct strain measurement method, a large number of 6-fiber UFS (comprising a total of 95 fibers) was subjected to measurement to determine the fiber strain capability of the UFS process. The average fiber strain determined for 36-inch UFS samples in this study was -0.08% with a standard deviation of 0.023%. This result is shown as the large boxplot of Figure 7, labeled "prior to change."

From UFS processing conditions, the calculated fiber strain level in a UFS should be approximately -0.13%. This value is based on the applied fiber back tension, the kingwire line tension, and the thermal expansion and contraction of the components of the UFS during the extrusion process. It assumes that no changes in fiber tension occur in the process caused by fiber friction against the tooling along its path. The lower measured value of average fiber compressive strain, -0.08%, and its large variation indicated that the above assumption was invalid.

In order to improve the control of fiber strain in the UFS, a development was undertaken to reduce fiber friction during UFS processing. Both the fiber path tooling and the fiber surface condition were improved to reduce both friction and abrasive wear or damage.

After implementation of these improvements, fiber strain was measured in four representative 6-fiber UFS. The results are shown as the individual UFS boxplots of Figure 6. After the improvements the average fiber compressive strain became -0.12% and the standard deviation decreased to 0.015%. Because the measured fiber strain after the change of tooling and control of the fiber surface condition is very close to the calculated strain, the friction between the fiber and tooling is now considered to be under adequate control.

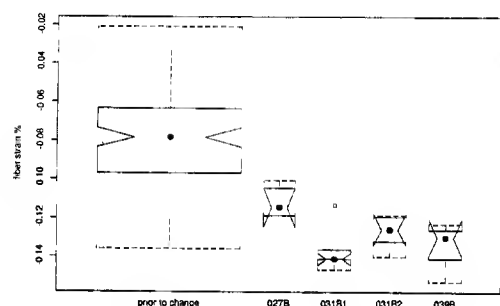


Figure 7. Fiber Strain in the 6-Fiber UFSs
Before and after Tooling Change and
Fiber Surface Control

In a further study of fiber strain process capability, the direct strain measurement was applied to a series of UFS containing 4, 6 or 12 fibers. All UFS were manufactured under the same conditions of individual fiber back tension, kingwire line tension and nominal processing temperatures. The tooling and fiber surface condition improvements were implemented in this study. The results are shown in Table I. It is remarkable that the average fiber strains are independent of fiber count in the UFS and that the standard deviations are nearly identical. This result indicates that differences in total fiber back tension arising from different fiber counts do not significantly impact fiber strain in the UFS.

TABLE I: POST UFS FIBER STRAIN

Fiber Count	Avg. Fiber Strain	Std. Dev.
4	-0.12%	0.015%
6	-0.12%	0.015%
12	-0.12%	0.019%

2. PC Process

The power conductor (PC) process strands steel wires around the UFS and forms the copper power conductor into the steel strand. During this process, waterblock material fills interstitial spaces between copper, wires and UFS. Through the use of different UFS, wire and line tensions and the application of waterblock compound, the UFS is coupled to the steel strand package at the desired strain level. The UFS back tension is adjusted to the specified value to ensure that the UFS to PC coupling is within the most desirable range. The measured UFS to PC strain is 0.054% average tension with a standard deviation of 0.033%. The variation of this stretch occasionally can reach lows close to zero and highs up to 0.09%. From the consistency of the UFS, wire, and line tensions, it is evident that the coupling between the steel strand package and the UFS through the waterblock compound varied within a known acceptable range.

For an SL-100 cable, a small version of the SL cable and a non-repeated cable (see Figure 2), the UFS strain in the PC is controlled about the same as an SL cable. The average strain of UFS measured in an SL-100 cable is about 0.05%.

3. Cabled Fiber Strain

The final fiber strain in an SL cable after the jacket insulation is extruded on the PC is the combination of the UFS and PC processes. Therefore, the average cabled fiber strain of a six-fiber SL cable is about -0.066%. For cables of different fiber count, there is no significant difference of the average fiber strain at both the post UFS stage and in completed cable.

IX. CONCLUSIONS

This direct-mechanical strain measurement set and technique has proven to be capable of reliably and accurately measuring the cabled fiber strain. The measured strain results help us to understand the manufacturing processes and to improve them. The cabled fiber strain meets the requirement of SL cable reliability. This slightly compressive fiber strain maintains the cabled fiber strain in a compression mode or very close to zero tension mode regardless of the coupling variation from the PC process.

X. ACKNOWLEDGEMENT

We would like to thank K. S. Kim, A. I. Quigley, and D. B. Rue from AT&T Submarine Systems, Inc. for their assistance in this program.

REFERENCES

1. C. D. Anderson, R. F. Gleason, P. T. Hutchison, P. K. Runge, "An Undersea Communication System Using Fiberguide Cables," IEEE Undersea Lightwave Communications, 1986, pp. 39-47.
2. A. Adl, T. M. Chien, T. C. Chu, "Design and Testing of the SL Cable," IEEE Undersea Lightwave Communications, 1986, pp. 233-249.
3. T. C. Chu, R. J. Rue, N. Koltunovich, G. N. Fontaine, "A High-Performance, Low-cost Submarine Lightguide Cable for Non-Repeatered System Applications," Proceedings of International Conference on Electronic Components and Materials, ICECM '92, Hangzhou, China 1992.
4. W. F. Wright, C. E. Murphy, W. D. Beland, M. J. Cyr, G. N. Fontaine, R. T. Traut, C. S. Ma, L. L. Blyler, T. C. Lee, D. Stroumbakis, R. V. Giangrossi, R. Stathum, R. J. Rue, "Design and Development of High Fiber Count Repeaterless Submarine Cable," IWCS '94, 1994.



L. L. Blyler, Jr.
AT&T Bell Laboratories
Murray Hill, New Jersey

L. L. Blyler, Jr. attended Princeton University where he received his Ph.D. in Aerospace and Mechanical Sciences in 1966. He joined AT&T Bell Laboratories in 1965 where he is currently Technical Manager of the Plastics Applied Research, Properties and Processing Group. His research interests include physical properties and characterization of polymers, polymer melt rheology and processing, and polymer applications in lightwave technology and undersea cable systems.




C. S. Ma
AT&T Submarine Systems, Inc.
Holmdel, New Jersey

C. S. Ma was born in 1949 in Taiwan, Republic of China. He received his Ph.D. in Engineering Mechanics from Iowa State University in 1984. After graduation, he joined AT&T Bell Laboratories, Holmdel, New Jersey, and worked in the Undersea Lightwave Cable Characterization Group on hydrogen, fiber loss, and cable heat transfer areas. Later, he worked in the Undersea Lightwave Cable Development Group till present on cable processing, cabling loss, fiber strain, and new cable development.




G. E. Johnson
AT&T Bell Laboratories
Murray Hill, New Jersey

G. E. Johnson joined AT&T Bell Laboratories in 1960. He received a B.S. in Electrical Engineering (1966) and an M.S. in Physics (1970) at Newark College of Engineering (now NJIT) while working. He has worked on the insulating properties of materials with particular use in ocean cable systems for most of his career. He is currently a Member of Technical Staff in the Plastics Applied Research, Properties and Processing Group. His current work includes diffusion in polymers, dielectric behavior of materials and development work on materials for SL cable systems.




R. T. Traut
Simplex Technologies Inc.
Newington, New Hampshire

R. T. Traut is Manager of Development Engineering with Simplex Technologies Inc. He joined Simplex as a Senior Development Engineer in 1978. His experience includes 27 years in product design and R&D engineering in the power and communications cable industries. He has written numerous technical papers and holds 3 patents. He is a member of IEEE. His education includes a B.S.E.E.T. degree from Roger Williams College (1976) and an M.B.A. from New Hampshire College (1983).




C. E. Murphy
Simplex Technologies Inc.
Newington, New Hampshire

C. E. Murphy is a Development Engineer with Simplex Technologies Inc. He joined Simplex in 1985 and is currently involved in the characterization/enhancement of optical and mechanical cable properties. He is a member of IEEE and holds an A.S.E.T. degree from New Hampshire Technical College (1985).




M. W. Jones
Simplex Technologies Inc.
Newington, New Hampshire

M. W. Jones manages the Quality Control Laboratories at Simplex Technologies Inc. He joined Simplex in 1986 after completing a Bachelor's in Microbiology from the University of New Hampshire. He has held a few positions at Simplex including Materials Specialist and Development Engineer. His major contributions to fiber optic ocean cable have been in the chemical and polymer sciences.



F. C. Gibson
Simplex Technologies Inc.
Newington, New Hampshire

F. C. Gibson is a Development Engineering Technician with Simplex Technologies Inc. He joined Simplex in 1993 and is involved with cable testing in the Development Laboratory. Previously he has had over 20 years experience with optical tooling.



W. M. Keith
Simplex Technologies Inc.
Newington, New Hampshire

W. M. Keith is a member of the Development Engineering Laboratory at Simplex Technologies Inc. He joined Simplex as a Development Technician in 1978 and has been involved with optical measurements, cable terminations, fiber splicing, and testing of undersea cables. He served 4 years in the U.S. Navy as an Avionics Specialist and received an A.A. degree from El Camino Junior College, Torrance, California in 1971.

NEW LOW WEIGHT/SMALL DIAMETER OPTICAL FIBRE SUBMARINE CABLE FOR UNREPEATERED SYSTEM

G. Berthelsen, I. Vintermyr

Alcatel Kabel Norge AS
Østre Aker vei 33, N-0509 Oslo, Norway

ABSTRACT

This paper describes a new cable design developed specifically for coastal submarine networks. The design has emphasised high fibre count, moderate deployment depths, low weight, small diameter and simple manufacture and installation.

Extensive testing of the new design has shown that the cable will maintain its mechanical and optical integrity during sea operations and furthermore throughout the design life period.

1. THE MARKET

As the possible distance between terminals has increased dramatically, it has become economical to use repeaterless fibre optic submarine systems for:

- "short haul" international links
- coastal city-to-city systems (festoons).

Repeaterless systems are therefore replacing former practice with repeatered coax- or fibre optic submarine systems, and terrestrial deployment respectively.

Cables for the first application are normally governed by the same specifications and requirements as repeatered systems, and often the same cable designs are used. These systems may require from 4 to 12 fibres and deployment to large depths (because they are laid beyond the continental shelf).

The second application is part of a domestic backbone network, and is designed with the same capacity as terrestrial high level transmission routes, requiring 16 to 48 fibres. Cable lengths can be short, or very long, depending on the distance between population centres. As the cable is normally laid on the continental shelf along the coast, the deployment depth is moderate (i.e. less than 3000 m).

Norway and Italy were the first countries in the world to use fibre optic submarine cables instead of a massive network of terrestrial systems. During the last two years, however, the interest for this way of quickly building a high capacity network has exploded. Systems are already installed in Thailand, and projects in the Americas and Asia, totalling more than 5000 km of cable, are presently being tendered.

2. DESIGN REQUIREMENTS

The scope of the design process was to develop a cable with performances matched to the new service requirements recently seen for the unrepeatered cable market.

The following features were emphasised during the design process:

- Reliable and robust design
- Low weight and small diameter in order to reduce transportation and deployment costs
- Perform reliably in water depths down to 3000 m, in shallow water and on land
- Maximum fibre count of 48
- Use of 1% proof stress fibres
- Maintain mechanical and optical properties during handling and installation throughout the design lifeperiod.
- Proper jointing properties, allow no-mould jointing
- Design lifeperiod of minimum 25 years

3. DESIGN AND MANUFACTURING

The cable design is based on a loose tube concept, in which the optical fibres are protected by a 3.7 mm OD longitudinally welded stainless steel tube situated in the cable centre.

The steel tube is made from a stainless steel strip which is formed into a tube through a precision forming mill. Optical fibres and thixotropic filling compound are introduced into the tube, which is then welded longitudinally with a CO₂ laser beam. The welded tube is then reduced in size through a set of diamond dies and checked for defects. The weld has a 100% penetration, virtually indistinguishable to the naked eye and with a smooth inner surface at the welding area.

The optical fibres are inserted into the formed tube with low tension and with a nominal excess length of 0.3 %. The 3.7 OD steel tube can accommodate a maximum of 48 fibres. All interstices inside the tube are filled with jelly. All types of fibres with a proof stress level of minimum 1 % can be used.

If required for electrical purposes (electroding and fault location), a copper conductor, in the form of a copper tape, can be applied over the steel tube. A polyethylene sheath is then extruded over the steel tube/copper conductor to complete the cable core.

The cable core is shown in Figure 1.

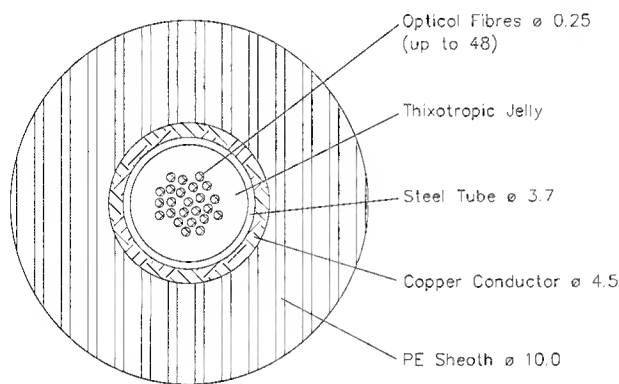


Figure 1 Cable core

The cable core is armoured with one or two layers of high grade steel wires. A full range of armouring designs have been qualified to comply with worldwide requirements. Customers require different tensile strengths depending on deployment method, burial or surface lay, deployment depth, potential damage probability and tradition. The cable "family" encompasses the following armour strengths in terms of NTTS (maximum short term tension that can be applied to the cable designs):

Light wire armour (LWA)	30 kN
Single armour (SA)	70 kN
Double armour 1 (DA 1)	120 kN
Double armour 2 (DA 2)	250 kN
Heavy armour (HA)	400 kN

Outer protection can either be a polyethylene sheath or the traditional PP-yarns embedded in a bitumenous compound.

All 5 designs are shown in Figure 2.

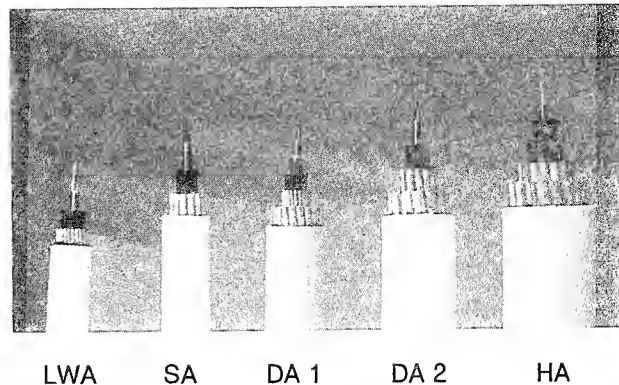


Figure 2. New Cable family

Armouring Design Description

The basic characteristics of the cable range are listed below.

LWA (Light Wire Armoured Cable)

The cable core is protected with a single layer of 1.6 mm high grade steel wires.

The LWA design is intended for use in lakes, at deep sea water (down to 3000 m), at sea floors with no significant hazards, or buried in most types of sea waters.

The design is also well suited as land cable from the beach joint to the terminal station.

SA (Single Armoured Cable)

The cable core is protected with one layer of 3.2 mm high grade steel wires.

The SA design is intended for use where there are medium hazards. The armouring will provide adequate impact and tensile strength which will protect the cable core from severe impacts and abrasion in a wide range of sea waters.

DA 1 (Double Armoured 1 Cable)

The armouring consists of 2 layers (1.6 and 3.2 mm wires) of high strength steel wires over the cable core. The wires are of the same dimensions as for the LWA and SA designs. Thus, transitions between the different cable designs are simplified. Even with outer PE sheath, smooth transitions can be made between SA and DA1..

The DA 1 design is intended for use in areas where moderate protection is required, typically system shore ends.

DA 2 (Double Armoured 2 Cable)

The SA design is overarmoured with a layer of 5.0 mm high strength wires.

The DA 2 design is intended for use in areas where high protection is required, typically at the system shore ends and in routes with shallow waters and abrasive sea floors.

HA (Heavy Armoured Cable)

An extra PP-yarn bedding is applied over the cable core, followed by two layers (4.2 and 5.0 mm wires) of high strength steel wires.

The HA design is intended for use in areas where maximum protection is required, typically at shore ends and in shallow waters with abrasive sea floors.

The respective main characteristics for all 5 armour versions are:

	Outer diam (mm)	Weight in air/sea (kg/m)		Specific gravity (g/cm ³)	Min bend diam at NTTS (m)
LWA	17	0.5	0.3	2.2	0.75
SA	21	1.1	0.7	3.2	1.5
DA 1	25	1.7	1.2	3.5	1.5
DA 2	31	3.1	2.3	4.1	2.5
HA	38	4.8	3.7	4.2	2.5

Compared with most cables used for unrepeated cable systems, this new design represents a reduction both in diameter and weight of about 25 %, and an increase in specific gravity of about 10 % for cables with comparable mechanical strengths.

4 JOINTING TECHNIQUES

A cable joint has been designed for the new cable, and this is currently undergoing qualification testing. The joint shall provide optical, electrical and mechanical continuity between contiguous cable sections required during manufacturing and repair/installation operations. The joint has cylindrical outer shape with rubber bend restrictors, and can accommodate 48 fibre splices in the internal splice trays. Anchoring of the cable armour is provided by locking cones preloaded by a hydraulic press tool. Pressure integrity is preserved using metal seals, while additional elastomeric seals preserve electrical insulation. Thus no time-consuming moulding, or X-ray examination is necessary.

Electrical continuity of both the armouring and inner conductor allows fault location by electroding, and facilitates shunt fault location by pulse-echo metering. The choice of joint housing materials eliminates potential sea-water corrosion of both cable armour and joint.

The joint is able to be handled as an integral part of the cable through standard cable-vessel equipment such as cable guides, caterpillars, capstan engines and bow wheels.

In addition to the cable joint, a tubular joint with almost the same characteristics as the steel tube itself, has been developed for splicing the steel tube/fibres during the manufacturing process. Consequently, the number of cable jointing boxes in a link will be very limited, and extra precautions due to cable joint boxes will be strongly reduced during cable handling, deployment or burial.

5. CABLE QUALIFICATION PROGRAMME AND TEST RESULTS

An extensive test programme, designed to explore the extremes of anticipated in-service conditions, has been performed. These tests have included both land based tests and sea trials.

The following tests comprised the qualification test

- Crush
- Impact
- Temperature Cycling
- Ageing
- Water Ingress
- Hydrostatic Pressure Resistance
- Tensile Strength
- Tensile and Bend
- Alternate Bending
- Tension/Torque
- Coiling
- Electrical
- Hydrodynamic Test
- Sea Trial

Test results from the above tests on all 5 designs are summarized below

Crush and Impact Resistance

The crush and impact resistance of all 5 cable designs has been evaluated in accordance with IEC 794-1-E3 and IEC 794-1-E4, respectively. In the crush test, cable samples were placed between two metal plates of 100 mm length. In the impact test, a hammer was dropped vertically onto an intermediate steel piece with diameter of 50 mm, which was placed on top of the cable sample being tested.

Test results, showing maximum load/impact without giving any loss effects, are shown in Figure 3.

From the experimental results, we may conclude that all designs show high crush and impact resistance.

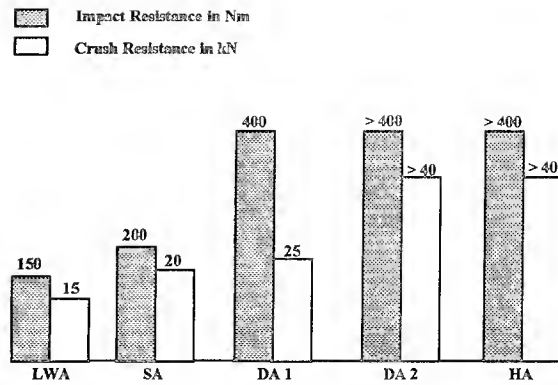


Figure 3. Crush and Impact Resistance

Tensile and Bending Performance

Cable and fibre strain characteristics versus cable tension up to the respective NTTS loads are similar for all 5 armour designs. Typical mechanical and optical properties, visualized by the tensile strength test for the DA 1 cable design, are shown in Figure 4.

Cable strain at the NTTS load is typically 0.4 - 0.5% for all 5 designs, and the corresponding fibre strain is 0.3% lower due to the fibre excess length in the tube. The loose tube design ensures that the fibres are well protected from external stresses such as compression and crushing during high strain operation such as cable recovery. No attenuation increase are seen on the fibres at the NTTS. Due to the fibre excess length, only limited strain is exerted on fibres at the NTTS load, and no strain or loss increase is exerted on fibres after installation.

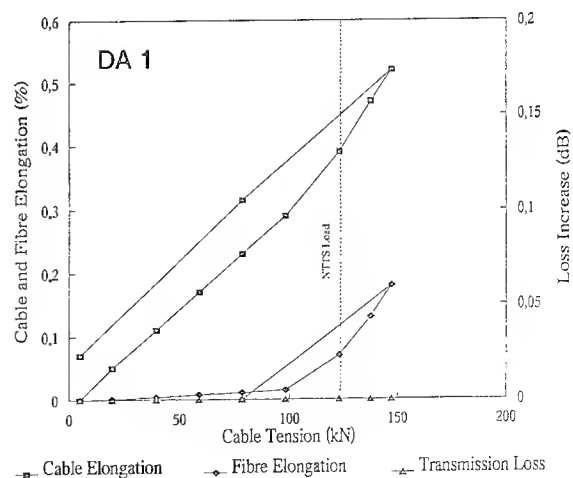


Figure 4. Tensile Strength Performance

Tensile bend tests have shown that all designs can be handled at their respective NTTS loads, at their minimum bending diameters, without degradation of either optical or mechanical properties.

No signs of degradation has been seen after bending the cable designs, at low load, in alternate direction 100 times around a form with a 1.5 m diameter (ref IEC 794-1-E6).

Tensile/torque tests have shown the following figures for the torque moment:

	LWA	SA	DA1	DA2	HA
Torque (Nm/kN)	0.5	0.8	1.1	1.4	2.2

We may conclude that the fibres are well protected inside the steel tube when straining the cables to their respective NTTS loads. Furthermore, excellent bending performances, both at high and low loads, should enable maximum flexibility in transportation, laying methods and installation equipment.

Temperature Characteristics.

Temperature cycling tests have been conducted in accordance with IEC 794-1-F1. All cable designs have shown similar effects with respect to temperature cycling, i.e the cable core is not affected by the type of armouring.

A typical time record for optical loss at 1550 nm versus temperature is shown in Figure 5.

As can be seen from this record, the cable design has a wide operational temperature range showing no change in optical loss. At low temperature, attenuation starts to increase at -30°C. At higher temperatures, no effects have been measured.

No permanent change in loss has been measured after the temperature cycling test.

Ageing tests have been carried out at 80°C for a period of 30 days without seeing any loss effects between 1100 and 1600 nm.

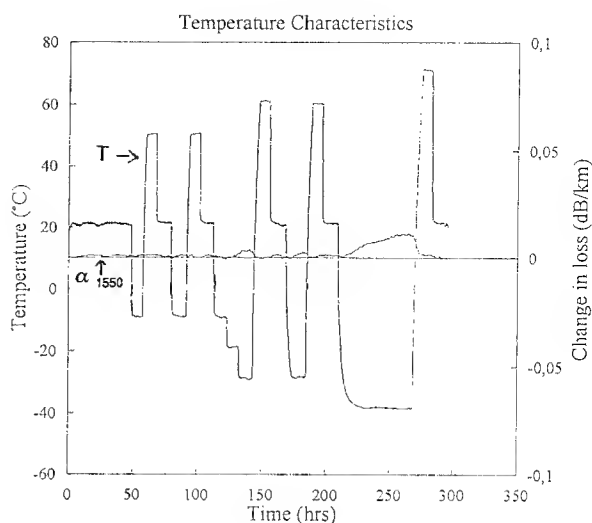


Figure 5. Temperature Cycling Performance

Water ingress

A 200 m cable core length with one end open to water, and the other sealed, was exposed to a hydrostatic pressure of 200 bar inside a pressure vessel for 3 days..

The penetrated cable length was less than 50 m after 3 days.

Hydrostatic Pressure Resistance

The critical pressure for the steel tube can be calculated from the following formula /Ref 1/:

$$P_{CR} = \frac{\sigma_{YP} * h}{R}$$

where σ_{YP} = Yield point for steel tube material
 h = Wall thickness of steel tube
 R = Steel tube radius (OD/2 - h/2)

Inserting OD = 3.7 mm, h = 0.2 mm and σ_{YP} = 700 MPa into the above formula yields a collapse pressure of 800 bar for the 3.7 OD steel tube being used in the cable designs.

Thus, it is not surprising that all cable designs have passed a 250 bar test.

Electrical Test

All designs showed no sign of degradation or breakdown after application of a DC voltage of 15 kV for 5 minutes.

Hydrodynamic Test

The tests were performed in a 160 m long towing tank. Cable test lengths with outer PE sheath were attached to a two-component force transducer giving the towing force components in the X- and Z-direction. The two-component force transducer was fixed to a towing carriage trailer, capable of obtaining a maximum speed of 20 knots.

Test results, showing the sinking speed (hydrodynamic constant, H), in both m/s and degree*knots, and the drag coefficient, C_{dn} are shown below.

	LW	SA	DA1	DA2	HA
H(m/s)	0.56 ^{*)}	0.69	0.87	1.08	1.23
H(degree*knots)	60	77	97	120	137
C_{dn}	1.1	1.26	1.19	1.27	1.21

^{*)} Test results for LWA are based on calculations only.

The experimental figures for the hydrodynamic constant conform very well to theoretical calculations for smooth cable designs, shown in /Ref. 2/.

The experimental figures for the drag coefficient conform very well to calculations, shown in Ref 3, for cylinders. These calculations show that the drag coefficient will be very close to 1.2 within a relatively wide range of Re numbers (Re 8000 - Re 200 000).

The Re - number is given by /Ref 3/:

$$Re = \frac{U \cdot D}{\nu}$$

where

- U = Speed of fluid close to cylinder (cable)
- D = Cylinder (cable) diameter
- ν = Kinematic viscosity ($1.2 \cdot 10^{-6} \text{ m}^2/\text{s}$)

For the cable towing tests, U will be equal to towing speed(V) times $\sin \alpha$. It can be shown that Re will be well inside the above Re-range, where the drag coefficient is 1.2, for towing speeds in the range 1 -10 knots for all designs, except from the LWA design, which from /Ref. 3/ will be expected to have a slightly less drag coefficient.

Cable geometry (layback after the towing vessel), based on the experimental towing tests at a speed of 3 knots, is shown for all 5 cable designs in Figure 6.

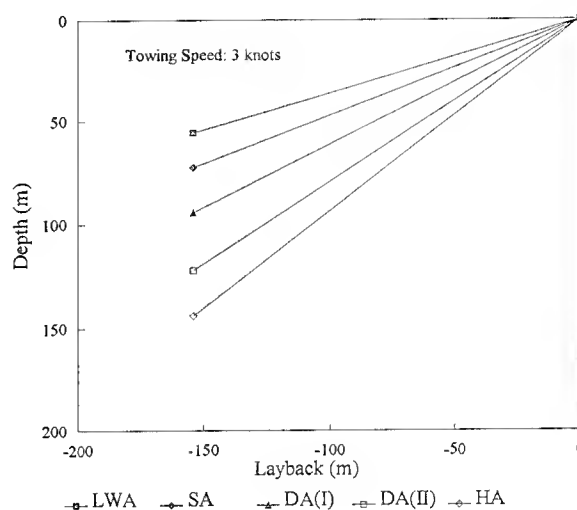


Figure 6 Towed cable geometries for all 5 cable designs at a towing speed of 3 knots.

From the towing tests, we may conclude that all designs have relatively high hydrodynamic constants. Thus good performance, such as better following the contour of an irregular sea bed, during laying and recovery operations should be expected.

Furthermore, the high cable density improves the self burial properties. This makes the cables more stable in the sea bed currents, thereby reducing abrasion damage.

Sea Trial

The excellent cable performance seen for all armouring designs in the comprehensive land-based test program, has been validated in a sea trial down to 500 m in a rugged bottom terrain.

6. CONCLUSION

A new low weight/high fibre count cable for use in unrepeated submarine links has been described. Extensive testing has been performed which demonstrates that the new cable design will maintain its mechanical and optical integrity during sea operations and throughout the designlife period.

ACKNOWLEDGEMENTS

The authors wish to thank Christian Reinaudo and Jean Francois Libert, Alcatel Submarcom, France, for valuable support and discussions.

REFERENCES

- /1/ S. Timoshenko
"Strength of Materials", part II, 3rd edition,
pp 186-193
- /2/ E. E. Zajac
"Dynamic and Kinematics of the Laying and Recovery
of Submarine Cables". Bell System Technical Journal,
September 1957, p 1180.
- /3/ H. Schlichting
"Boundary Layer Theory"
McGraw-Hill series in mechanical engineering, 1979,
p17

Biography

Mr. G. Berthelsen
Alcatel Kabel Norge AS
Østre Aker vei 33
P.O. Box 130, Økern
N-0509 Oslo
Norway

Gunnar Berthelsen graduated from Heriot-Watt University, Edinburgh, UK in 1971 and joined Standard Telefon og Kabelfabrik (now Alcatel Kabel Norge) the same year. He started work with fibre optics in 1977 and is currently Technical Manager at Alcatel Kabel Norge.



Dr. I. Vintermyr
Alcatel Kabel Norge AS
Østre Aker vei 33
P.O. Box 130, Økern
N-0509 Oslo
Norway

Inge Vintermyr graduated from the Norwegian Institute of Technology in 1989 with a Ph.D in Materials Science. He joined Alcatel Kabel Norge AS in 1989, and is currently working as a development engineer at the Optical Cable R&D Department.

DESIGN AND DEVELOPMENT OF HIGH FIBER COUNT REPEATERLESS SUBMARINE CABLE

¹W.F. Wright, C.E. Murphy, W.D. Beland, M.J. Cyr, G.N. Fontaine, R.T. Traut.

²C.S. Ma, T. Lee, D. Stroumbakis, R. Giangrossi, R. Statham, R. Rue, ³L. Blyler

¹Simplex Technologies Inc., Portsmouth, NH; ²AT&T Submarine Systems Inc., Holmdel, NJ; ³AT&T Bell Labs, Murray Hill, NJ

ABSTRACT

Traditional submarine fiber optic cable systems have typically utilized a small number of fibers along with high speed regenerators or optical amplifiers. The lightwave circuits were operated at high data rates to provide the maximum possible transmission capacity. Increased interest in repeaterless systems has led to the development of a cable that is utilized as an extension of the local terrestrial telephone network, thereby requiring a higher number of fibers. This new type of high fiber count submarine cable contains proven design elements of the deep water submarine cable and provides a cost effective solution for the requirements of a non-repeatered cable system. This paper discusses cable design and testing criteria. The testing provides confirmation that this cable meets the handling and operational requirements of a high reliability, repeaterless submarine cable.

INTRODUCTION

Non-repeatered Submarine Optical Fiber Cable must meet the demands of a different market place, in comparison to the traditional trans-oceanic deep water cable. Submarine cables used for coastal links and inter-island links are installed primarily in shallow water. Also, since these cables do not require repeaters, it is possible to reduce the volume of material used for cable powering such as copper and polyethylene, thereby reducing manufacturing costs.

This new high fiber count structure was designed for compatibility with the AT&T/Simplex SL100 Repeaterless Submarine Cable. The Unit Fiber Structure (UFS) uses a UV-curable acrylate matrix to encapsulate the fibers along with a central kingwire. This type of tight buffer structure has proven performance in thousands of kilometers of submarine cable

manufactured for systems installed world wide.

Fiber splicing procedures for a high fiber count cable are potentially very time consuming. This concern has led to the development of mass fusion splicing techniques. Factory and ship-board splicing personnel utilize the same efficient procedures that enable splicing and cable termination activities to be completed in approximately the same time as traditional (low fiber count) long haul cables.

The un-armored cable has a maximum deployment depth of 6000 meters. Steel tape protection and several types of armor designs have been developed as well.

This work was the result of a cooperative effort between Simplex Technologies Inc., and AT&T Submarine Systems Inc. The AT&T "Product Realization Process" (PRP), was used as a program management tool to define the program goals and implement the activities that resulted in the introduction of this new product to manufacturing.

I. CABLE DESIGN CONCEPTS

The new High Fiber Count UFS was designed to be used in conjunction with the existing SL100 Repeaterless Submarine Cable. The SL100 cable was designed specifically to meet the requirements of repeaterless cable systems with a maximum deployment depth of 6000 meters, and a 25 year service life.

The SL100 repeaterless cable consists of a central UFS surrounded by 16 steel strand wires, waterblock material, a metallic sheath and a high density polyethylene jacket. The metallic sheath provides a hermetic seal and protects the fiber core from hydrostatic pressure.¹ Various protective armor designs are available

to suit any installation environment. Figure 1 shows a diagram of the unarmored SL100 Repeaterless Cable.

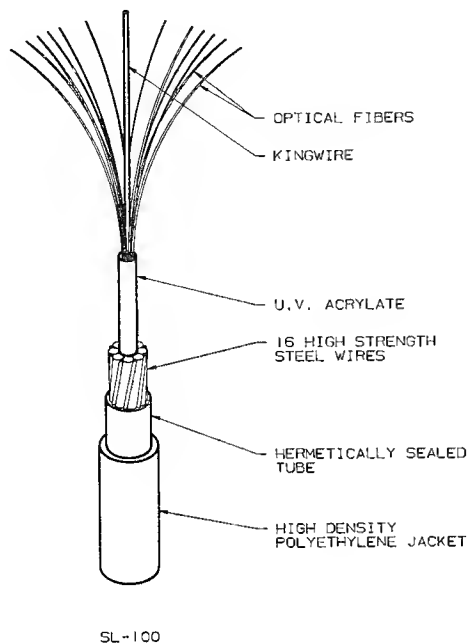


Figure 1.

The basic design of the central fiber structure for this 24 fiber repeaterless cable was based on the existing UFS with a proven performance of nearly seventy thousand kilometers of installed cable throughout the world. This new UFS contains a central kingwire and an UV-Curable matrix to tightly couple the fibers. The fibers are placed around the kingwire in two concentric rings. Fiber counts greater than 24 are also available.

The following design criteria were among those considered for this high fiber count repeaterless cable.

- Reliability
- Environmental performance
- Fiber count flexibility
- Manufacturing simplicity
- Maximum manufacturable length
- Cabled fiber loss performance
- Simplicity of fiber breakout
- Simplicity of fiber splicing and cable joining
- Cost

Although loosely coupled optical fiber submarine cable designs have been introduced to the "repeaterless" market, this new design combines the proven reliability and performance of the tight coupled central fiber structure with the easy fiber access typically associated

with loosely coupled designs. The tight coupled structure allows for a controlled amount of residual compressive strain to be installed on each fiber, which provides low fiber stress and high reliability.

II. HIGH FIBER COUNT UFS DEVELOPMENT

It was advantageous for the new high fiber count UFS to be compatible with the existing SL100 cable manufacturing and jointing technology. This compatibility eliminated the need for new manufacturing hardware and engineering studies, and consequently provides better control over cable production and system assembly costs. Several different fiber structure designs, both loose and tight coupled types, were considered for this new high fiber count UFS. The final decision to pursue the traditional tight coupled fiber structure with a central kingwire was based in part on the high degree of reliability offered by this structure, and because the application of UV curable material (i.e., in the form of fiber coatings) was considered to be a well understood technology.

A block diagram of the High Fiber Count UV-UFS manufacturing line is shown in Figure 2.

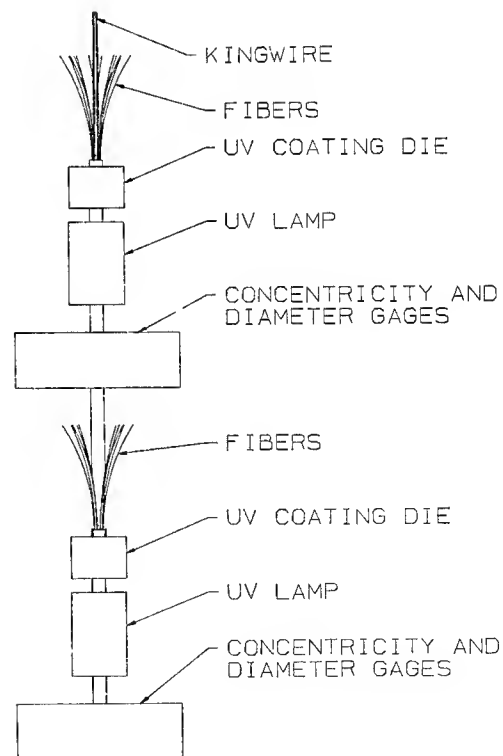


Figure 2.

The process system consists of two coating dies in tandem, in a vertical configuration. The kingwire and fibers enter the top of the die and exit with the uncured matrix material surrounding the fibers. Each die is immediately followed by UV curing lamps, along with diameter and concentricity monitoring instrumentation.

UV-curable acrylate material is delivered to the coating dies through pressurized lines. The feed lines, valves and pumps are specially selected for their compatibility with the acrylate material.

The diameter of the UFS is controlled primarily through the pressure of the UV-curable acrylate material entering the die, along with the selection of the proper die diameter. The dies and delivery system are engineered to avoid air incorporation in order for the UFS to be free of voids and diameter irregularities.

Fibers are delivered to the respective dies from tension controlled payout systems. Static discharge devices are used to keep dust from accumulating on the fibers and sheaves. Diameter and concentricity monitoring gauges installed in the processing line insure that the product is made to specification.

During the high fiber count UFS Development Program, process variables and product performance characteristics were optimized through the use of designed experiments. This work has resulted in producing a robust product with reliable performance features.

III. UV MATRIX MATERIAL PERFORMANCE AND TESTING

The UV-curable matrix material is engineered to incorporate a number of performance advantages in the high fiber count UFS. Some of the key performance features are:

1. Tight coupling of the fibers to the kingwire.
2. Buffering the fibers from radially-directed stresses which could induce microbending losses.
3. Mechanical ruggedness.
4. Low friction surface for ease of handling.
5. Release properties which allow the fibers to be mechanically removed from the UFS without adherence of residual clumps of matrix or color coat loss.

6. Excellent long term oxidative and hydrolytic stability.
7. No promotion of hydrogen generation by the finished UFS.

The tensile mechanical properties of the UV-cured matrix material, compared with those of a typical thermoplastic elastomer used as a UFS buffer material in submarine lightwave cable, are displayed in Table 1. The tensile strengths of the two materials are comparable, however the ultimate elongation of the UV cured matrix is considerably lower than that of the thermoplastic elastomer. This property allows the UV-cured matrix to be failed in a controlled manner during the mechanical fiber stripping process. Mechanical fiber stripping is highly desirable over chemical stripping because it eliminates potential safety and fire hazards in the cable factory and onboard ship. On the other hand, the ultimate elongation is sufficiently high that the material withstands deformations encountered during normal handling operations without suffering damage.

TENSILE PROPERTIES OF UFS
BUFFER MATERIALS

<u>MATERIAL</u>	<u>TENSILE STRENGTH (MPa)</u>	<u>ULTIMATE ELONGATION (%)</u>
Thermoplastic Elastomer 14		>200
UV-Cured Matrix	12	55

Table 1.

The relaxation modulus characteristics of the thermoplastic elastomer and UV-cured matrix materials are shown in Figure 3. Relaxation curves obtained from dynamic mechanical analysis are compared at 0° and 25°C, which covers the temperature range of operation of undersea cable systems. The relaxation modulus of the UV-cured matrix material is more time dependent than that of the thermoplastic elastomer. At short times (<1 hr.) it is stiffer than the thermoplastic elastomer, so that it is more resistant to handling deformation, which is of short duration. At longer times, the modulus of the UV-cured matrix relaxes to lower values than that of the thermoplastic elastomer. Therefore the UV-cured matrix is more efficient in its ability to relax stresses which might be transmitted to the fibers by cabling, cable handling, or environmental changes.

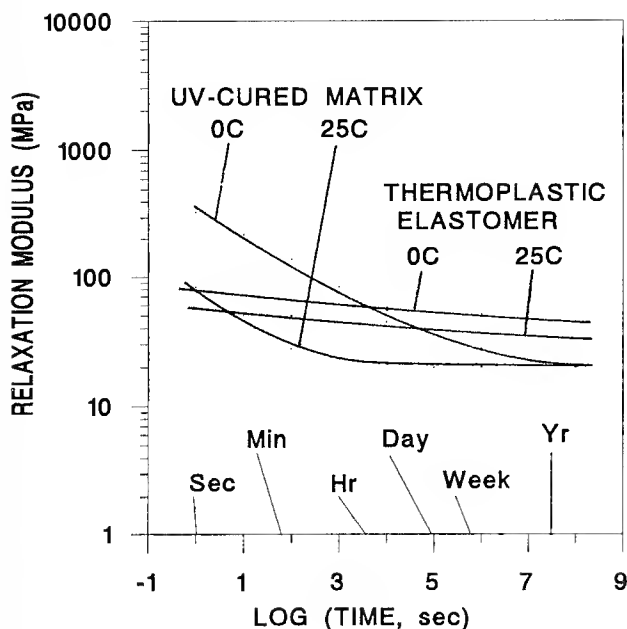


Figure 3.

IV. FIBER SPLICING AND CABLE JOINTING

In mass fusion splicing of the SL 100 HFC cable, loose fibers are formed into a ribbon structure with the use of adhesives and commercial ribbon forming tools. The ribbonized fibers are stripped, cleaved, spliced, proof tested and reinforced up to 12 fibers at a time. The claddings of the fibers are aligned in high precision V-grooves. Low loss splicing of single mode fiber has become more reliable since core to cladding eccentricity has been reduced with improvements in fiber fabrication technology.

Typical mass fusion splice loss results for three fiber types, single mode (SM), Z fiber (Z), and dispersion-shifted fiber (DSF), are shown in Figure 4. SM and Z fibers had comparable loss to single fiber splice results (active core alignment) although a slightly higher variation in the process capability was seen. DSF was found to be more difficult to splice because of its smaller mode-field radius and complex index of refraction profile.

When transverse offset is controlled, good splice loss results are attainable. However, the higher the fiber count (above 6) the more difficult it becomes to maintain consistently low fiber offsets. Therefore, confirmation of the fiber axis offsets prior to fusion is critical to the success of a mass fusion

splice, especially for DSF splicing. Figure 5 shows a graph of measured DSF splice loss as a function of pre-splice fiber offset. SM and Z fibers are much more tolerable to pre-splice offsets. A comparison of DSF mass fusion splice loss to identical and non-identical (different MFD's and core-cladding eccentricities) single fiber splicing is shown in Figure 6.

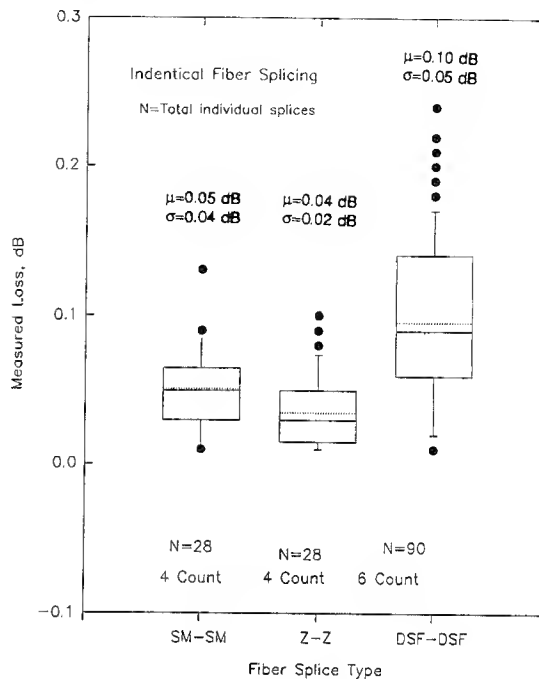


Figure 4.

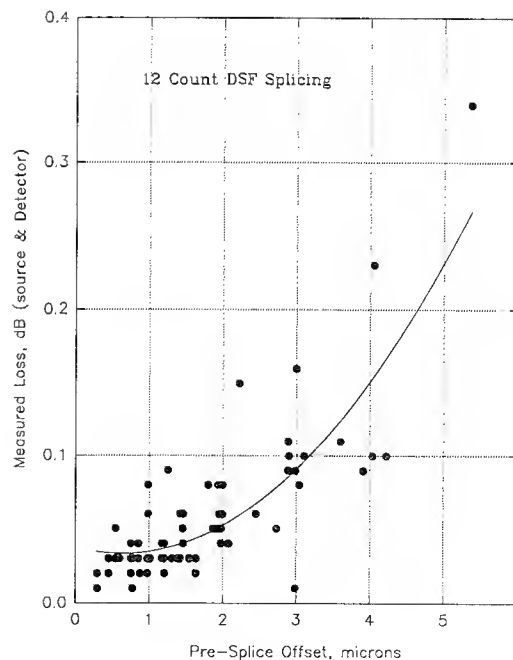


Figure 5.

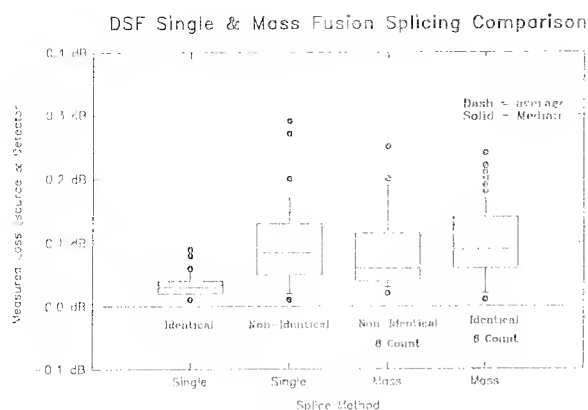


Figure 6.

The finished splice is stored in a small metallic U-channel which is then encapsulated in a UV-curable polymer. A specially designed applicator fixture (patent pending) is used to place the fibers into the U-channel and apply the UV-curable polymer.

The optical performance of the protected splices were tested for 2 months at 85°C at 85% relative humidity, followed by temperature cycling between -20°C to +50°C for 1 month with no change in mechanical integrity and no change in optical loss at 1550 nm to within the stability of the test system of ± 0.02 dB. The use of a rigid U-channel alleviated the requirement to proof test to the 200 ksi level, since the fiber splice is reinforced and held permanently straight.

Mass fusion splicing of fibers up to 12 at a time for a 24 count cable can decrease the splicing time by a factor of 7. Time savings are gained not only from the stripping step to fusion, but also during proof testing, coating restoration, and coiling.

Individual sections of high fiber count cable are connected together by an electrical-mechanical-optical connection called a splice-box. The strength of the steel strand package is transferred to a mechanical device, called a socket, which is connected to another cable by a similar socket.

The color coated fibers are mechanically removed (stripped) from the UV matrix. The outer matrix layer can be separated (peeled) from the inner layer in three to four sections. The fibers from the outer matrix layer are then individually removed. The same procedure is applied to the inner layer fibers. After all fibers are stripped from the UV-UFS they are individually proof tested.

Upon completion of mass fusion fiber splicing, the fibers are coiled inside a fiber tray for protection. After the fibers are coiled, a cover is placed over the opening in the fiber tray and secured.

A steel cylinder is placed over one of the sockets and the fiber tray. A threaded locking ring is placed over the other socket and screwed into the open end of the cylinder, securing the steel cylinder in place. The steel cylinder provides tensional support of the splice box and seals the fiber tray from the molten polyethylene during the molding process.

Finally, a polyethylene sleeve is slid over the steel cylinder, the splice-box assembly is placed in a mold cavity, and it is overmolded. When the overmolded splice-box is completed, a beryllium-copper cylinder is slid over the overmolded splice-box and two strain-relief bushings are screwed into both ends of the beryllium-copper cylinder.

V. ENVIRONMENTAL TESTING PERFORMANCE

A prototype cable was manufactured and subjected to various tensile and temperature tests. Since this cable market is expected to use a variety of fiber types, this cable contained a combination of 24 Dispersion Shifted and Non-Dispersion Shifted fibers. All fibers were color coated with a commercial UV-curable material. The test cable was unarmored.

A seven kilometer section of High Fiber Count (HFC) SL100 Cable, placed on a reel, was subjected to an Extended Range Temperature Test. The temperature was cycled from +50°C to -20°C, with additional stabilization points at +3° and +20°C. The limits of -20°C and +50°C are storage temperature requirements, and +3°C is the typical operating temperature. The cable's temperature stability was verified by monitoring the kingwire resistance.

Fibers of the same type were looped together and spliced to a high stability optical source/detector instrument to monitor the optical power during the test. The Temperature versus Optical Power graph (Figure 7) shows that fiber test loops of 35 and 42 kilometers exhibited negligible temperature induced change (<0.004 dB/Km) in optical power during the 25 day test. All fibers followed a typical loss curve, and all fibers returned to their original attenuation values. (A small amount of

test set drift was responsible for the apparent offset at the end of the test).

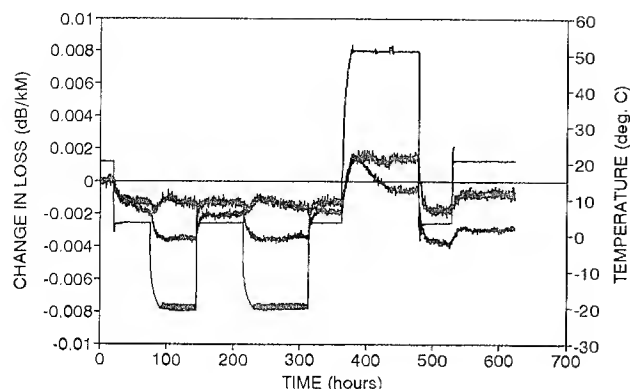


Figure 7.

In another test, a 100 meter cable sample was terminated and placed in a tensile test bed. The test cable was tensioned from 1000 pounds to 7500 pounds. At each tension increment, the tension was stabilized, and one end of the cable was rotated to match the torque level seen at the 1000 pound preload level. Tension was held at 7500 pounds for one hour, then systematically reduced back to 1000 pounds. The graph of fiber loss versus cable tension, shown in Figure 8, indicates that the attenuation was very stable over the entire range of cable tensions in this Tension-Rotation-Elongation Test.

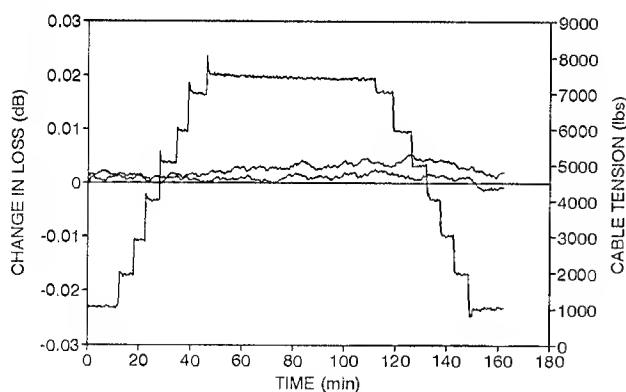


Figure 8.

Among the other tests that we performed were: Tension-Torque-Elongation, Reverse Bend, and Temperature with Flexure. This 24 fiber repeaterless cable passed all mechanical and optical testing criteria.

VI. CONCLUSION

The High Fiber Count SL100 Repeaterless Submarine Cable described in this paper, has passed all standard qualification tests. This new fiber encapsulation structure provides excellent optical fiber attenuation performance, and is fully compatible with existing cable processing and termination hardware. Performance characteristics of this product include:

1. Proven high reliability tight coupled UFS.
2. Flexible fiber count.
3. Mechanically strippable fiber structure.
4. Excellent handling and environmental performance.

The cable and termination hardware have been qualified to meet the demands of repeaterless submarine installations such as coastal festoons and inter-island links.

VII. ACKNOWLEDGEMENTS

The authors wish to thank the many people at Simplex and AT&T whose efforts were critical to the timely success of this program, especially Debra Simoff, Mark Paczkowski, Bud Parsons, Frank Gibson, Russ Day, Dave Dumont, and Wayne Keith.

REFERENCES

1. Chu, T.C., Rue, R. J., Koltunovich, N., and Fontaine, G.N., "High Performance Low Cost Submarine Cable for Non-repeatered System Applications", AT&T Technical Memorandum, Oct. 14, 1992.



William F. Wright,
Simplex Technologies Inc
Newington, NH

William Wright is a Senior Engineer in the Development Engineering Group at Simplex Technologies Inc. He received his B.S. in Physics from Saint Mary's University in 1979. His primary responsibilities include development and testing of undersea fiber optic cables, and the evaluation of optical fiber performance.



Michael J. Cyr
Simplex Technologies Inc
Newington, NH

Michael J. Cyr is a Senior Development Engineer with Simplex Technologies Inc. He joined Simplex in 1986 as a Process Engineer where he worked on the splicing and coupling of both co-axial and fiber-optic cables. In September of 1993, he joined the Development engineering group at Simplex and is currently working on the development and coupling of high-fiber count cables. Mike received his B.S.Che from the University of Maine in 1986.



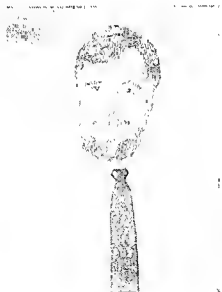
Craig E. Murphy
Simplex Technologies Inc
Newington, NH

Craig E. Murphy is a Development Engineer with Simplex Technologies Inc. He joined Simplex in 1985 and is currently involved in the characterization/enhancement of optical and mechanical cable properties. He is a member of IEEE and holds an A.S.E.T. degree from New Hampshire Technical College (1985).



Greg N. Fontaine
Simplex Technologies Inc
Newington, NH

Greg Fontaine is the Manager of Product Design and Applications Engineering at Simplex Technologies Inc. He joined Simplex in 1978 and has a B.S.M.E. degree from the U.S. Naval Academy and an M.B.A. degree from New Hampshire College.



Wayne Beland
Simplex Technologies Inc
Newington, NH

Wayne Beland has worked in R&D and Quality organizations for 12 years. He joined Simplex Technologies in 1986, and has been supervisor of the Development Engineering Lab and is currently the R&D Facilities Coordinator.



Richard T. Traut
Simplex Technologies Inc
Newington, NH

Richard T. Traut is Manager of Development Engineering with Simplex Technologies Inc. He joined Simplex as a Senior Development Engineer in 1978. His experience includes 27 years in product design and R&D engineering in the power and communications cable industries. He has written numerous technical papers and holds 3 patents. He is a member of IEEE. His education includes a B.S.E.E.T. degree from Roger Williams College (1976) and an M.B.A. from New Hampshire College (1983).



C. S. Ma
AT&T Bell Laboratories
Holmdel, NJ

C.S. Ma was born in 1949 in Taiwan, Republic of China. He received his PhD in Engineering Mechanics from Iowa State University in 1984. After graduation, he joined the AT&T Bell Laboratories, and worked in the Undersea Lightwave Cable Characterization Group on hydrogen, fiber loss, and cable heat transfer areas. Later, he worked in the Undersea Lightwave Cable Development Group till present on cable processing, cabling loss, fiber strain, and new cable development.



D. Stroubakis
AT&T Bell Laboratories
Holmdel, NJ

Dimitrios Stroubakis, born in 1964, is a Member of Technical Staff at AT&T Submarine Systems in the Undersea Cable Development Laboratory. He holds a BS in Mechanical Engineering from Polytechnic Institute of New York and an MS in Mechanical Engineering from Columbia University. After graduation, Dimitri joined AT&T Bell Laboratories in 1987, where his responsibilities have been in the design and test of specialty undersea lightwave cables for military applications, inspection technologies, and cable mechanics. His current efforts involve supporting platform splicing technologies for optical amplifiers, cable jointing, and for shipboard applications, including mass fusion splicing and high loss fusion splice attenuators



T. C. Lee
AT&T Bell Laboratories
Holmdel, NJ

T.C. Lee was born in 1957 in Hong Kong. He received his Bachelor degree from The City College, New York, in 1981. He joined AT&T Bell Laboratories and worked on Undersea Lightwave Cable termination and joints since 1981.



R. V. Giangrossi
AT&T Bell Laboratories
Holmdel, NJ

R. V. Giangrossi joined AT&T Bell Laboratories in February 1970 after working 10 years with Bendix Semiconductor Division. At Bendix he was employed as a senior technician in the reliability and environmental testing of semi-conductor components. He has been with the Undersea Cable Group at AT&T since 1970, spending the first 7 years with the Coaxial Cable Repeater Testing and Characterization Group. In 1977, he was assigned to a new group called Fiber Optics. His duties involved testing and characterizing optical fiber and splicing. Since 1977, he has been involved with electric arc, laser and gas flame fusion fiber splicing. He is currently involved with electric arc mass fusion splicing technology.



R. Stathum
AT&T Bell Laboratories
Holmdel, NJ

R. Stathum was born in 1964 in Long Branch, New Jersey. He joined AT&T Bell Laboratories in 1984 and worked in the Undersea Lightwave Fiber Splicing, Characterization and Measurements Group on optical fiber splicing techniques, qualification measurements, failure mode analysis and procedural development. Currently he works in the Undersea Lightwave Cable Jointing Group.



Ralph Rue
AT&T Bell Laboratories
Holmdel, NJ

Ralph Rue received his AAE-MET degree from Vermont Technical College, and his BS-MET degree from Trenton State College. He joined the Undersea Systems Cable Development & Implementation Department at AT&T Bell Laboratories in 1984. His work has been focused on the development testing and analysis of fiber optic undersea cable designs and related hardware.



Lee L. Blyler, Jr.
AT&T Bell Laboratories
Murray Hill, NJ

Lee L. Blyler, Jr. attended Princeton University where he received his Ph.D. in Aerospace and Mechanical Sciences in 1966. He joined AT&T Bell Laboratories in 1965 where he is currently Technical Manager of the Plastics Applied Research, Properties and Processing Group. His research interests include physical properties and characterization of polymers, polymer melt rheology and processing, and polymer applications in lightwave technology and undersea cable systems.

DESIGN AND DEVELOPMENT OF HIGH FIBRE COUNT CABLES FOR UNREPEATERED SYSTEMS

G. McGurk, J.R. Ford, L.J. Parker, G.C. Miller

STC Submarine Systems Limited, Southampton, UK
(A company of Alcatel Submarine Systems)

ABSTRACT

The use of low loss multi-fibre ribbons (4, 6 or 8 fibres) has allowed the development of compact fibre packages with a high fibre density. By careful selection of materials and process design these packages have been inserted into established submarine cable structures with zero incremental losses. This modular approach to cable development has allowed the quick and cost-effective introduction of unrepeatered cables and joints accommodating up to a maximum of 48 fibres.

A rigorous design verification programme has been successfully completed including extensive land based tests and sea trials. This programme has demonstrated the suitability of cables containing various fibre counts (12 - 48) to the maximum design depth of 4000 metres over a wide range of installation and environmental conditions. The excellent optical characteristics of the fibre package over the entire range of test conditions demonstrates the suitability of the cable design for future long-haul submarine applications.

1.0 INTRODUCTION

STC has a long established reputation for excellence in the design and supply of long-haul regenerated submarine systems. The cornerstone of this success is the optical stability of the fibre package which provides zero incremental cable losses at all stages of manufacture and installation. This design is based on straight lay individual fibres around a central steel kingwire encapsulated in a thermoplastic elastomer.

The increase in demand for low cost unrepeatered cable systems necessitated the development of new products without the 8000m depth performance and power feed capabilities characteristic of long-haul systems. As part of a two phase programme STC developed an unrepeatered cable carcass based around the established fibre package[1] which has been installed in a number of applications.

Whilst this design proved extremely successful[2] the package construction is not suited to satisfy the growing market of unrepeatered cable systems with high fibre counts. This paper describes the next phase of the product development cycle concerned with the design of unrepeatered cables and joints containing up to 48 low loss fibres. Details of the manufacturing performance and extensive product test regime are described.

2.0 DESIGN PRINCIPLES

2.1 Cable carcass

The qualified cable design established in the first phase of the development programme[3,4] is shown in Figure 1 and contains many principles successfully employed in repeatered cables. The central package is located within a closed steel c-section which offers resistance to hydrostatic pressure. A layer of high tensile steel wires acts as the main strength member with a welded copper tube providing both hermeticity and torsional stability. The polyethylene sheathing layers and corrugated steel tape provide excellent abrasion resistance. Over 20,000 fibre km of this cable has been successfully deployed and the design provides a fully qualified submarine cable capable of deployment in water depths down to 4000 metres.

2.2 Fibre package construction

The basic function of any fibre package is to enable safe fibre handling during cable manufacturing processes and to maintain the ribbons in a fixed orientation for identification purposes. In order to satisfy the modular design approach for this particular product any option was limited in size to fit the constraints of the internal dimensions of the cable carcass.

A range of alternative designs were considered including slotted core, fibre bundles, tight buffering and loose tube. Each alternative also had the further option of employing individual fibres or multi-fibre ribbons.

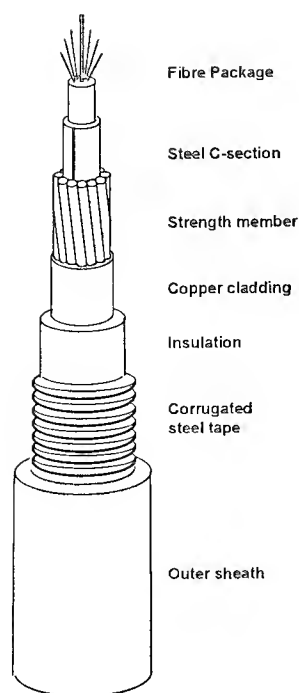


FIGURE 1
STEEL TAPE PROTECTED S3 CABLE

A number of key parameters were assessed for each design option with particular emphasis placed upon manufacturing related issues. The raw material costs associated with cables containing up to 48 fibres and the tight optical requirements of many unrepeatable systems make process reliability of critical importance to reduce costs. Furthermore, a cable designed for simple jointing processes can also help reduce total system assembly and installation costs.

The cable design selected was based on fibre ribbon technology arranged in a tight buffered configuration. This achieves extremely high fibre packing densities thus allowing a maximum of 48 fibres within the dimensional constraints of the cable c-section. The diameter of the fibre package is identical to that qualified in the Phase I cable design thus maintaining a fully modular approach to the development and qualification programme.

Alternative stack geometries (Figure 2) allow high flexibility in achieving intermediate fibre counts by the use of 4, 6 or 8 fibre ribbons. Each ribbon type employs an identical sequence of individually coloured fibres to provide maximum flexibility in manufacture. Individual fibre identification is achieved by the lateral inversion of the top ribbon in the stack as shown in Figure 2. This ribbon is then allocated ribbon 1 and fibres identified as Red 1, Green 3 etc. according to their position in the stack.

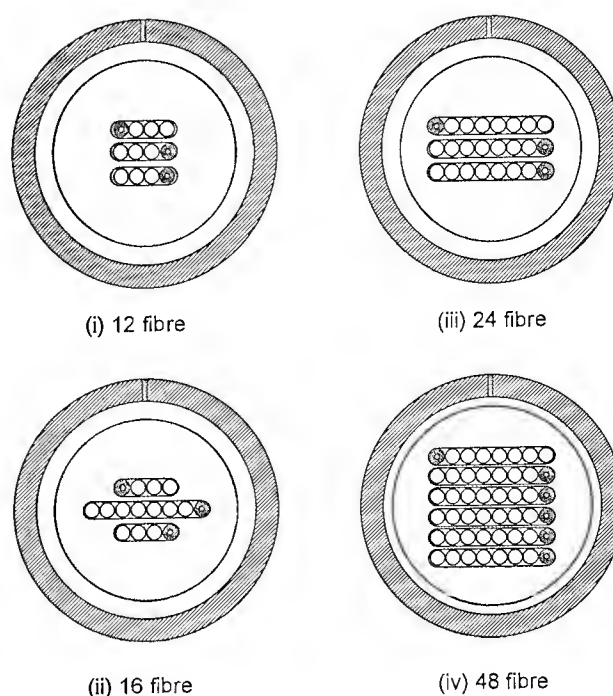


FIGURE 2
ALTERNATIVE RIBBON STACK GEOMETRIES

2.3 Package material selection

The package encapsulant material is required to bond the fibre ribbons within a stable matrix to minimise optical losses and also protect the fibres from the influence of external stresses during cable manufacture and installation. The selection of this material also had a major impact on the cable manufacturing processes and subsequent jointing operations. Table 1 gives the main selection criteria identified for the package material and the principal material properties. Final material selection used Taguchi analysis as a major experimental tool in order to reduce the development cycle time and minimise development costs[5].

In order to provide effective waterblocking between the package and steel c-section a cold-filling thixotropic gel was also incorporated. This material was selected primarily for its simple processing characteristics although the blending of water-swellable and hydrogen-scavenging agents into these compounds provide added flexibility when required. Compatibility testing was used extensively to guarantee no adverse interaction between the waterblocking compounds and other package materials.

The use of these materials resulted in extremely low axial water penetration (< 100 m) after 14 days under hydrostatic pressures equivalent to 4 km water depth.

	Cable requirements	Material requirements
Mechanical Requirements	Ribbon stack buffering Effective waterblock Temperature stability	Elasticity Adhesive properties High T _g
Chemical Requirements	Long term stability Low hydrogen generation Environmental	Compatibility Thermal stability Hydrolytic stability Health & Safety
Cable Manufacture	Proprietary equipment High process speeds Environmental	Low temp/viscosity Rapid cure/solidification Health & Safety
Joint assembly	Simple ribbon peel out	Tensile > tear > adhesive strength

TABLE 1
PACKAGE MATERIAL SELECTION CRITERIA

2.4 Joint design and splice management.

In order to accommodate multiple attempts at fusion splicing, joint design for optical fibre cables typically requires the preparation of excess fibre and subsequent storage of spare fibre within the joint housing. Cable systems containing high fibre counts present a number of potential problems in storing additional fibre, especially for joints based upon rigid splice technology.

The use of a ribbon fibre package does present a number of joint design options based on mass fusion splicing and ribbon storage. This approach offers potential saving in assembly time and reduced space required for splice storage. However, the torsional characteristics of fibre ribbons make some traditional single fibre storage designs unsuitable for ribbon handling. In addition the splice losses associated with current mass fusion splice technology, without the benefit of active core alignment, can introduce a significant loss penalty in systems with very tight optical power budgets.

As an alternative, a fibre and splice management system has been developed which accommodates up to 48 individual fibres within an existing joint housing (Figure 3). This use of a fully mechanically qualified joint housing maintains the modular approach to the product development and qualification programme.

The STC unrepeated cable joint design was initially developed to accommodate 12 individual fibres and rigid splices. The tensile and compressive load on the joint is supported by the steel housing forming the outer casing of the joint. This leaves the maximum possible free volume within the joint housing to store both fibre and fibre splices. A modular approach was adopted which stores up to 24 fibres in flat storage trays located on either side of the joint centre line. In this way many common components can be used for all fibre counts between 12 and 48 fibres.

Recent advances in single fibre splicing technology have produced highly reliable splicing machines which produce consistent low loss splices. The selection of package materials which allow simple ribbon peel out saves considerable jointing time and eliminates the need for specialised equipment. This simple fibre preparation stage more than compensates for the increased assembly time required to complete individual fibre splices and as a result assembly times of 8 hours have been demonstrated for 24 fibre joints and less than 12 hours are required to complete a 48 fibre joint.

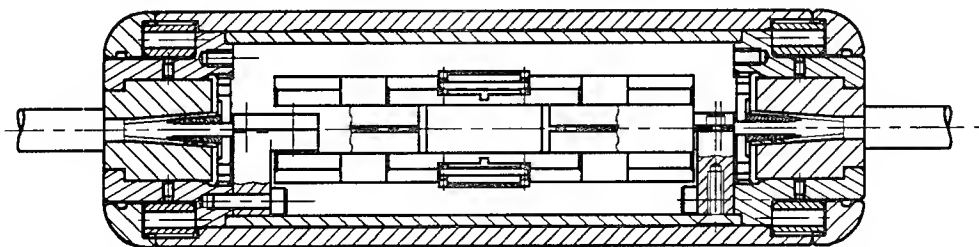


FIGURE 3
S3 HIGH FIBRE COUNT CABLE JOINT

3.0 CABLE MANUFACTURING

During the development of the ribbon package cables containing multiple fibre counts were manufactured using both step index and dispersion shifted fibres in 8, 6 and 4 fibre ribbons. Losses comparable with the established 12 fibre package were achieved in all cable types and process reliability proved excellent with no incidents of fibre/ribbon damage during the package and c-section insertion process stages.

The ribbon encapsulation process was developed with particular emphasis placed on manufacturability. As a result of the careful selection of package materials simple technology was available at all stages in the process development. Consequently a complete manufacturing process was designed, manufactured, installed and fully operational in less than 16 weeks from completion of pilot scale manufacturing trials. Figure 4 shows a schematic diagram of the process equipment.

Whilst only relatively short lengths of cable were manufactured during the development and product qualification stage significant quantities of cable have been manufactured for a 1300 km, 24 fibre domestic festoon system. This system includes a number of coastal links up to a maximum single span length of 224 km.

Figure 5 shows the bi-directional average loss distribution (dB/km) in finished armoured cable. Data is presented for all fibres in a 3 x 8 dispersion shifted ribbon geometry measured at 1550 nm. This loss distribution is similar to that of incoming fibre and indicates zero fibre loss increment post cabling (mean 0.200 dB/km). The losses compare favourably with individual fibre package in established long-haul systems.

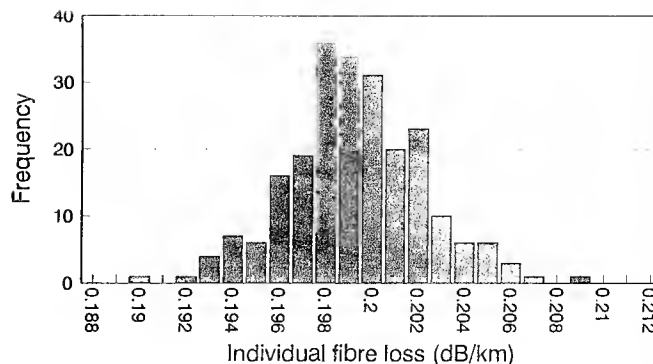


FIGURE 5
INDIVIDUAL FIBRE LOSS IN ARMoured CABLE

4.0 QUALIFICATION TESTS

4.1 Land based tests

Once the initial design selection stage had been completed a series of land based tests were carried out designed to characterise the cable performance under extreme operational conditions. These tests covered mechanical and optical characteristics of the cable and joints under three main operating regimes i.e. handling and storage, installation and recovery and sea bed conditions.

As the cable carcass had been fully evaluated using the original 12 fibre package[4] a test programme was devised which specifically investigated the interface between the cable and the performance of the ribbon package. Table 2 summarises the test programme and results which was performed on both armoured and STP cable and joints.

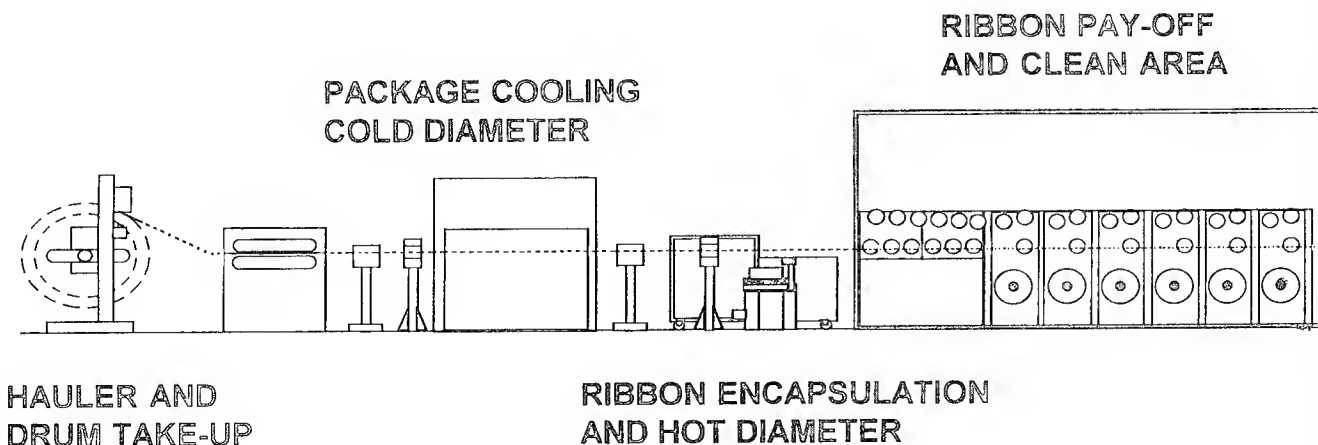


FIGURE 4
SCHEMATIC LAYOUT OF RIBBON PACKAGE PROCESS

	OPERATIONAL REQUIREMENT	QUALIFICATION TEST	RESULT
Handling and Storage	Crush in cable tank	Static crush	PASSED
	Dropped objects	Dynamic Impact	PASSED
	Temperature stability	Temperature Cycling (-20 to + 60 C)	PASSED
	General handling	Reverse Bend tests	PASSED
	Joint transfers	Bump & Vibration	PASSED
Installation and Recovery	Tensile strength	NTTS & NOTS	PASSED
	Twist on handling	Torsion at NOTS	PASSED
	Cable repair in adverse weather	Fatigue Cycling	PASSED
	Bending under tension on recovery	NTTS around 2 m sheave	PASSED
Sea bed conditions	Stability at deep sea pressures	Hydrostatic pressure resistance.	PASSED
	Low hydrogen outgassing	Cable ageing 25 years	PASSED
	Water penetration after break	Waterblocking test	PASSED

TABLE 2
SUMMARY OF CABLE QUALIFICATION TESTS

Of particular interest during the test programme was the performance of the rectangular ribbon stack under normal cable loading by crush and impact. Both qualification and characterisation tests were carried out on STP and armoured cables in order to gain direct comparison with other established cable designs. For qualification tests the conditions are pre-determined to simulate a given operational limit (i.e. crush at the bottom of a cable tank) and each sample undergoes hydrostatic pressure tests to simulate deep sea conditions on completion of the test. For characterisation purposes samples were also tested until the point at which a fibre break was recorded by optical monitoring. Cables containing 24 and 48 fibres all satisfied these specified requirements. During characterisation tests the loading required to cause fibre breaks was comparable with standard 12 fibre cables.

In the case of dynamic impact testing a cylindrical weight is dropped on the cable from a known height to achieve the desired level of impact energy. In the static crush test compressive loads are applied between two parallel plates for a given period. In both cases optical power is monitored throughout the test and on completion destructive examination takes place to determine the degree of ovality in the c-section and orientation of the ribbon stack.

In order to assess the thermal stability of the ribbon package and encapsulant materials, temperature cycling tests, and hydrogen outgassing to simulate long-term ageing, were also carried out. The hydrogen ageing test is performed on a long length of cable (1 km) configured to allow optical monitoring through multiple fibre paths. The sample is then held in an elevated temperature environment for a period to simulate operating conditions over 25 years. The precise test conditions and duration are derived using an Arrhenius time - temperature relationship but typically the test lasts up to 16 weeks. Regular cut-back attenuation measurements at 1550 nm and 1240 nm were performed and, based upon the most pessimistic statistical interpretation of the data, the increase in attenuation due to cable ageing is comparable to established cable designs.

4.2 Sea trials

As part of a general philosophy for the release of new products sea trials are used to further complement the extensive range of land-based tests. Whilst it is not always possible to experience the full range of installation conditions during the course of a sea trial it provides an opportunity to cover many aspects of the land-based test programme under real service conditions. By careful selection of the trial route and system design it is possible to generate invaluable data over relatively long lengths of cable and also provide an early opportunity to experience full scale manufacturing and system assembly procedures prior to the award of a major submarine contract.

Deep Water Sea Trial	Shallow Water Sea Trial
25 km STP cable	4 km SA cable
12, 24 & 48 DS & nDS Fibre	24 DS Fibres
5 cable joints	3 cable joints
5 x 72 km Optical loops	2 x 12 km Optical loops
System loss 0.21 dB/km	System loss 0.21 dB/km
Max. depth 3750 metres	Max. depth 610 metres
Sea state 7	Sea state 6
Installation: 16 w/p LCE	Installation: 8 w/p LCE
Recovery: 3 metre drum	Recovery: 3 metre drum

TABLE 3
SEA TRIAL SUMMARY

Two sea trials were specified to cover a range of operational conditions and cable types. In the first case a deep water trial was identified in order to test the STP cable and joints to the maximum design depth of 4000 metres. A further sea trial was also completed in armoured cable to a nominal depth of 600 metres. Table 3 gives the basic conditions and parameters for each trial.

4.2.1 Deep water sea trial

A total of 25 km of STC's (STP) unrepeated cable with different fibre packages was manufactured and assembled for the trial. The cables consisted of approximately 10 km of 12 fibre cable (12 individual fibres in tight buffered package), 9 km of 24 fibre (3 x 8 dispersion shifted fibre ribbons) and 1 km of 48 fibre cable (6 x 8 mixed fibre ribbons). A further 5 km of STP was employed as the anchor rope without optical monitoring. The system included 4 x 24 fibre cable joints and a block end seal and provided 5 optical paths to allow monitoring during all stages of loading, deployment, holding and recovery. A trial ground was identified in the Bay of Biscay which provided water depths up to the maximum design limit of 4000 metres.

The trial involved deployment, followed by holding for 36 hours to simulate a deep water repair operation (3 cable joints) and recovery. In order to fully evaluate the new ribbon package the holding period took place with the 24 fibre cable over the ship's bow.

Optical monitoring was achieved by the use of a high stability laser and detector with continuous output to a chart recorder. Simultaneously the length was recorded via a separate optical loop. Figure 6 shows the optical transmission loss and cable tension against time over the period of the trial. 3 further optical loops were configured and monitored using an OTDR. The optical performance of the system remained extremely stable throughout the trial and no permanent change was recorded on any fibre following recovery of the system.

Deployment of the system was achieved using a 16 wheel pair Linear Cable Engine in severe weather conditions (wind force 7/8; sea state 7). The maximum pay-out speed was limited by the conditions to 3 knots and a peak tension was recorded of 21.5 kN. Recovery took place at a maximum speed of 1.75 knots with a peak recovery tension of 27.5 kN. During the trial the electrical integrity of the cable insulation was evaluated by taking resistance readings and detailed dissection of all cables and joints identified no damage.

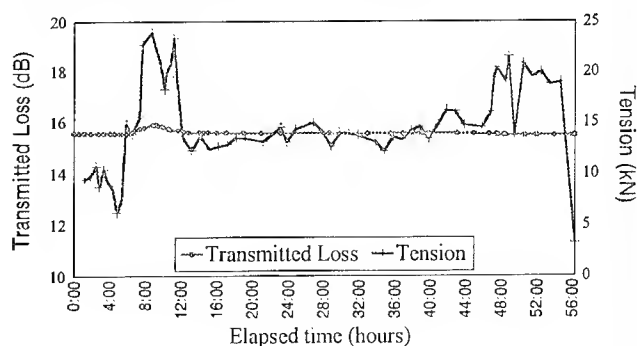


FIGURE 6
OPTICAL LOSS AND CABLE TENSION DURING
DEEP WATER SEA TRIAL

4.2.2 Shallow water sea trial.

The shallow water sea trial used a single armour cable surface laid to a nominal depth of 600 metres. The cable contained 24 dispersion shifted fibres in the form of a 3 x 8 fibre ribbon stack. The splice configuration allowed continuous monitoring over an 11 km optical path using a high stability source and detector. A separate optical path allowed simultaneous monitoring by OTDR.

The cable for this mini-system was loaded into a container in the UK and joints assembled using STC's modular containerised installation unit[5]. The complete assembled system was then transported by road to Denmark where the system was transferred onto a waiting cables ship. On completion of the trial the system was off-loaded into a container and returned to the cable factory for analysis and dissection.

The trial took place in the North sea off Norway in strong weather conditions (Wind force 6/7, Sea state 6). The system was deployed, held for 4 hours and then recovered. During the trial the optical signal showed no measurable change and the cable handled well during all operations.

5.0 CONCLUSIONS

A cable for unrepeaters systems has been developed and fully qualified to operate in water depths down to 4000 metres. This cable, based on a central ribbon fibre package, can contain up to 48 low loss fibres and has been successfully deployed and recovered from close to its maximum design limit. A 24 fibre armoured version of the same cable has also been deployed and recovered from 600 metres.

The fibre package has been designed using both encapsulated and edge-bonded ribbon types stacked and tightly buffered in a thermoplastic polymer. Results from land-based tests have demonstrated that this package compares favourably with more traditional package designs when subject to mechanical handling.

This cable has been selected for a coastal festoon system supplying 24 dispersion shifted fibres using 8 fibre ribbons. Manufacturing data has shown that cabling processes produce zero incremental loss on the ribbon fibre package. Transmission losses in finished cable compare extremely well with those achievable in single fibre package cables and this package design would be suitable for use in long-haul systems.

Full qualification tests and sea trials have been completed on a 24 fibre joint based upon the same modular design approach. Improvements in the cable design to assist in jointing operations have allowed joint assembly times of 8 hours without the need for mass fusion splicing.

Minor modifications to existing jointing technology have demonstrated the accommodation of up to 48 individual fibres in a submarine cable joint housing with joint assembly times of less than 12 hours.

6.0 Acknowledgements

The authors would like to thank the Directors of STC Submarine Systems Limited for their kind permission to publish this material. Additional thanks go to Mr. R. Clarke, Mr D. Kenney (BNR Europe Ltd.) and Mr. P.A. Norman (STC Submarine Systems) for their valuable contribution toward pilot scale manufacturing trials and prototype product testing.

7.0 References

- [1]. C.J. Rochester et. al. "Cable designs for unrepeaters single span systems." 39th International Wire and Cable Symposium, Reno, Nevada, November 1990.
- [2]. A.J. MacLeod "Unrepeaters systems." Suboptic 93, Versailles, France 29th March-1st April 1993.
- [3]. S.C. Beech, I.R. Doble, J.R. Ford, C.J. Rochester "New unrepeaters cable design testing methodology and results." 41st International Wire and Cable Symposium, Reno, Nevada, November 1992.
- [4]. J.R.Ford, C.J. Rochester "Performance verification of a new unrepeaters cable design." Suboptic 93. Versailles, March 29th - April 1st 1993
- [5]. I.M. Boardman "High fibre density cable systems for the unrepeaters market." Suboptic 93, Versailles, March 29th - April 1st 1993.
- [6]. S.C. Beech, R. Maxted "Development of a Jointing/Repair facility for high reliability submarine cables." 42nd International Wire and Cable Symposium, St. Louis, Missouri, November 1993.



G. McGurk BSc(Eng)
STC Submarine Systems Ltd
West Bay Road
Western Docks
Southampton
SO15 1DS
UK

Ged McGurk is currently Contract Support Manager in the Technical Department at STC Submarine Systems, Southampton. After joining STC in 1989 as a Materials Scientist he has worked on the development of a variety of cable products within the New Product Development Group.



J.R. Ford BSc. PhD
STC Submarine Systems Ltd
West Bay Road
Western Docks
Southampton
SO15 1DS
UK

Dr. John Ford joined STC Submarine Systems in 1988 after completing his PhD. in Polymer Science. He has been responsible for materials selection and qualification testing for unrepeated cable designs. He is currently Product Development Manager for Unrepeated Systems.



L.J. Parker BEng
STC Submarine Systems Ltd
West Bay Road
Western Docks
Southampton
SO15 1DS
UK

Luci Parker joined STC Submarine Systems in 1992 after completing her BEng. in Mechanical Engineering at the University of Southampton. She is currently employed as a Development Engineer working on the design of new unrepeated cables with particular reference to fibre and ribbon related issues.



G.C. Miller BSc.
STC Submarine Systems Ltd
West Bay Road
Western Docks
Southampton
SO15 1DS
UK

Gary Miller joined STC Submarine Systems as a Product Development Engineer and is now Section Head, Process Engineering, responsible for the introduction of new products into volume manufacture. He graduated from Southampton University in 1987 with a BSc in Mechanical Engineering.

Hydrogen Generation and Diffusion at Submarine Cable Joints: An Experimental Investigation

B.R.Ridd*, C.J.Brown* and G. McGurk

STC Submarine Systems Ltd, West Bay Road, Western Docks, Southampton, SO15 1DS

*STC/ University of Portsmouth Teaching Company Scheme, Department of Chemical and Physical Sciences, White Swan Road, Portsmouth, PO1 2DT

ABSTRACT

Cable ageing margins are applied to cable systems to account for attenuation increases over the operating life due to the ingress of hydrogen into the cable structure. In order to review the current ageing margins for submarine systems it is necessary to develop a comprehensive understanding of hydrogen permeation into optical fibre cable systems. Experimental methods are described which allow the amount of hydrogen inside joint housings to be monitored. Various techniques are discussed to determine and accelerate the extent of hydrogen diffusion into the joint. The effects of different operating environments are also considered to allow extrapolation to a wide range of service conditions. The possible sources of hydrogen are discussed including the extent of electrochemical corrosion due to local and galvanic effects.

1.0 INTRODUCTION

The effect of hydrogen on the attenuation of optical fibre systems is well understood [1-2]. Extensive measures, such as material selection to avoid hydrogen outgassing and the use of hermetic seals, have been employed by submarine cable designers in an attempt to eliminate its presence in the cable structure. Nonetheless, hydrogen is generated most notably by electrochemical corrosion of metallic cable components and possibly through bacterial action and can enter the system via discontinuities in the hermetic seal. Submarine cable joints and repeater terminations represent such a discontinuity in this seal and allow localised access to hydrogen leading to optical attenuation of the system.

Ageing effects and the prediction of end of system life (EOL) margins have always been a concern to system designers. Provision for increased attenuation through the life of the system is made in the system optical power budget. This allowance, at 1550nm, is typically of the order of 0.005 dB/km over 25 years. For an unrepeated system of 300 km this may therefore account for approximately 1.5 dB at the EOL. Modern fibre optic systems demand a greater understanding of the possible cable ageing mechanisms in order to provide the most cost-effective system design whilst maintaining operating margins to the 25 year EOL. It is important therefore to fully quantify all possible sources of hydrogen within the system to

determine the long-term effects on optical performance in a wide range of environmental conditions. A greater understanding of any mechanism that contributes to the loss, including hydrogen ingress at joints, may allow a more accurate prediction of EOL losses.

2.0 EFFECTS OF HYDROGEN ON SYSTEM PERFORMANCE

Optical fibres exposed to an atmosphere of hydrogen show an increase in optical attenuation across a broad spectrum that includes the operating wavelengths of current submarine cable systems [3]. Therefore quantifying the amount of hydrogen present inside a cable is of importance to the cable manufacturer and system operator.

Once hydrogen enters the fibre it may remain in the molecular state or may dissociate and chemically bond to the glass. In single mode fibres used for submarine systems, a combination of low dopant concentrations and low temperatures as encountered in the submarine environment, mean that hydrogen tends to remain in the molecular state and bonding to the glass is almost negligible. In this molecular state hydrogen produces an easily identifiable series of sharp absorption peaks in the 1100 - 1600 nm region, including one particularly strong, narrow peak at 1240 nm (Figure 1).

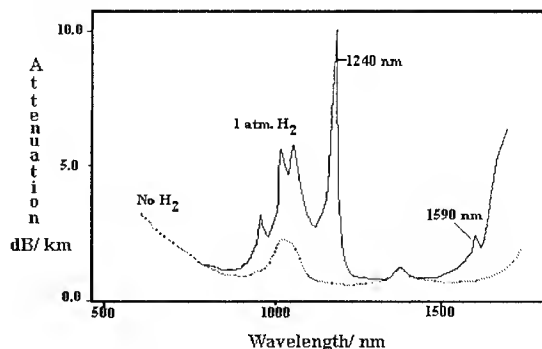


Figure 1. Spectral Attenuation due to Hydrogen

Empirically, the loss due to hydrogen at 1240 nm is fifteen times that as seen at the operating wavelength of 1550 nm.

The level of signal attenuation is directly proportional to the partial pressure of hydrogen inside the cable. To produce an increase in attenuation for single mode fibres, only several tenths of an atmosphere partial pressure of hydrogen are required. It is therefore important that all potential sources are fully understood to provide guarantees of performance over design life.

3.0 SOURCES OF HYDROGEN

There are two main sources of hydrogen at cable joints that have the potential to cause cable ageing for the fibre optic telecommunication system:

3.1 Electrochemical corrosion

Corrosion may be described as the degradation of a metal due to a chemical reaction with its environment [4-5]. In the submarine environment the process is electrochemical in nature, where the metal acts as an electrode and the sea water as an electrolyte. The process of corrosion can be easily understood by the consideration of a simple corrosion cell as shown in Figure 2.

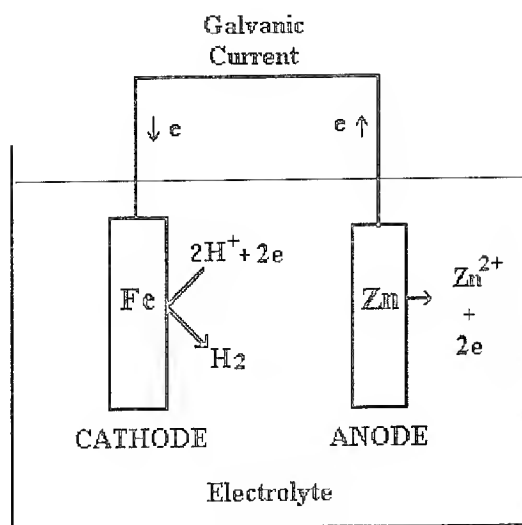


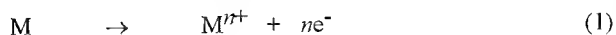
Figure 2. Schematic of a simple corrosion cell

This cell represents a specific example of a galvanic cell in which two dissimilar metals are in electrical contact with one another and immersed in an electrolyte. The process involves the oxidation of the zinc electrode which acts as an anode and the protection of the iron electrode which acts as a cathode. The zinc becomes the anode as it has a more negative electrode potential than iron in a specified electrolyte, sea water in this case (see Table 1). This results in an electrochemical reaction in which the transfer of electrons take place.

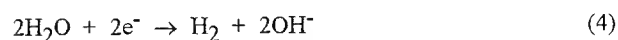
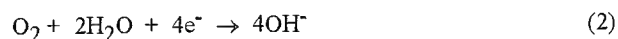
↑ Noble or cathodic	Platinum
	Gold
	Graphite
	Titanium
	Silver
	Stainless steel
	Nickel (passive)
	Bronzes (Cu-Sn)
	Copper
	Brasses
	Nickel (active)
	Tin
	Lead
	Cast iron
↓ Active or anodic	Steel or iron
	Aluminum
	Zinc
	Magnesium

Table 1. Galvanic series of some metals in sea water

The anodic process results in the corrosion of a metal. The anodic reaction usually involves the loss of electrons to form a metal cation. Other reactions can occur but metal dissolution is of greatest importance here:



The cathodic reaction parallels the anodic reaction. The electrons generated by the above reaction pass through the electronic contact to the cathode. Here they restore the electrical balance of the system by reaction with a cathodic reactant in the electrolyte. The most important cathode processes in sea water are predominantly the reduction of dissolved oxygen (Eqn2), the reduction of hydrogen ions (Eqn 3) and the reduction of water (Eqn4):



A combination of cathodic reactions can occur providing that the net total oxidation rate equals the net total reduction rate. A number of factors including solution composition, pH, aeration, flow conditions and the catalytic properties of the metal surface determine which reactions predominate.

In summary, the overall cell reaction involves oxidation at the anode and reduction at the cathode with the possible formation of hydrogen. An example of a corrosion cell in a submarine system is the galvanic corrosion between the armour wires of the cable and the various alloys used for joint housings. Galvanised zinc wires are commonly used in the armouring of

submarine cables. As zinc is anodic to many commonly used alloys, then electrical contact between the two may result in a corrosion cell with the possibility of hydrogen generation in the vicinity of cable joints.

The formation of these simple cells is not confined to situations involving two dissimilar metals but also occurs between different areas on the surface of one metal due to variations in the microstructure. Therefore corrosion of the joint components may occur without the influence of two metal corrosion i.e., it may occur on an apparently heterogeneous metal surface.

Other effects which may become significant in the submarine environment are stray current corrosion [4] and magnetohydrodynamics (MHD) [4,6]. These effects may influence small corrosion currents in the cable which supplement the above mechanisms of corrosion.

3.2 Bacterial Action

Polluted inshore waters containing industrial and organic waste are likely to contain bacteria which may enhance hydrogen generation. Research [7] has demonstrated that anaerobic processes play a major role in the degradation of organic matter in coastal marine sediments. Sulphate reduction of organics by sulphate reducing bacteria (SRB) to hydrogen sulphide accounts for approximately 50% of all organic matter that is degraded within these sediments. There has been considerable research into the problems of bacterial corrosion but progress is slow due to the problems of in-situ investigations and in assessing the extent of the microbial content in a complex series of reactions. Thus the microbial contribution to hydrogen levels in submarine systems could be better understood. However, SRB tend to enhance corrosion in oxygen free environments by acting as a cathodic depolariser i.e., they utilise atomic hydrogen in the process of sulphate reduction thus making the cathodic reaction easier.

Any undisturbed surface in the marine environment will be quickly coated with a layer of organic matter. Soon after, this layer of organic matter will be colonised by micro-organisms able to utilise it as a source of energy and hence a primary fouling layer will be formed. As this film grows, oxygen consumption by this film will become greater than the supply of oxygen and anaerobic conditions will develop in the film. Films of less than 100 μm are sufficient to allow the development of anaerobic conditions beneath them. In anaerobic sediments, stimulation of microbial activity due to the presence of metal surfaces may be sufficient to cause localised sulphate depletion, stunting the action of SRB and thus allowing the concentration of hydrogen to rise.

4.0 SUBMARINE CABLE JOINT DESIGN

The basic joint design for submarine cables is similar in principal for all cable types. The fundamental function of the cable joint is to maintain the mechanical integrity of the cable allowing the splicing of fibres in order to join different sections of cable. The joint ensures that the cable stresses are not imparted to the fibres. The joint is a point at which excess fibre is taken out of the hermetically sealed package to allow splicing. Thus the joint is a break in the hermetic seal which is difficult to avoid.

Armour and joint housing materials are usually metallic in nature and are likely to corrode to a certain degree in the lifetime of the system resulting in the generation of hydrogen. A proportion of this hydrogen enters the cable system causing an attenuation increase which has to be allowed for in ageing budgets.

Ageing margins are currently based upon worst case theoretical models using published diffusion co-efficients and partial pressures of hydrogen as expected in service. Whilst these have provided conservative estimates for current systems, more accurate predictions will provide opportunities for design optimisation. Experimental investigation will allow correlation of the models to evaluate the design of future products and provide a greater understanding of the ageing mechanism.

5.0 EXPERIMENTAL INVESTIGATION/ DESIGN

STC has embarked upon a programme of work in an attempt to quantify hydrogen ingress at cable joints. A means of analysing hydrogen generation and diffusion into a joint in different environments has been devised by making simple modifications to existing joint housings. A schematic diagram of the experimental set-up is shown in Figure 3.

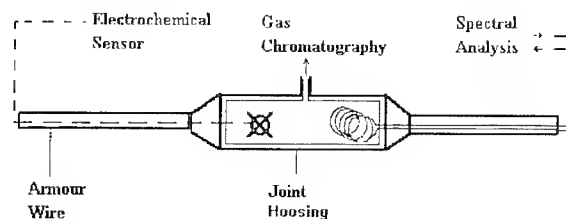
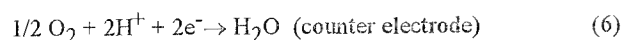
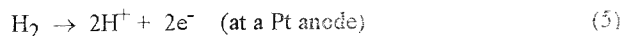


Figure 3. Schematic of Experimental Joint Design

The design allows hydrogen to be monitored within the housing by both direct and indirect means as described below. This allows for an effective cross calibration which greatly improves accuracy and confidence in the results.

5.1 Electrochemical Sensors

Slight joint modifications have been made to allow the insertion of commercially available electrochemical gas sensors directly within the joint housing. For long-term experiments both the power and output signals are routed through the cable by removal of the central fibre package. Careful sealing of the cable elements within the joint housing prevents axial diffusion from the joint. The sensors give a d.c. voltage output on the basis of a simple redox reaction:



The current flowing from the cathode is directly proportional to the concentration of hydrogen. The sensors are sensitive to temperature during assembly (i.e., moulding operations) and relative humidity. However, they provide real time gas monitoring down to levels of 0.1% and when used in conjunction with gas chromatography provide useful experimental data which is gained without affecting the joint sample.

5.2 Gas Chromatography

Gas chromatography (GC) is a well established, reliable and accurate technique for the quantitative measurement of hydrogen and many other gases. It has a lower limit of detection for hydrogen of approximately 0.01%. Gas sampling from within the joint housing provides the most accurate means of assessing the hydrogen concentration at any one time. Extraction of the gas must be completed carefully to avoid contamination. The volume of gas removed must be minimised to avoid disturbing any state of equilibrium in the diffusion process. The use of capillary tubes inserted in the cable structure allow gas extraction from the centre of the joint as shown in Figure 3.

5.3 Spectral Loss Analysis

The use of optical fibre stored in the joint housing provides the means of detecting hydrogen by spectral loss analysis. Up to 1km of fibre can be wrapped in the joint housing which may be measured periodically for hydrogen related loss effects. This indicates clearly the presence of hydrogen within a system. Hydrogen gives a fingerprint like trace with the greatest loss observed in the 1240 nm region with a further peak at 1590 nm (Figure 1). Comparative OTDR measurements at 1240 nm can also confirm the presence of hydrogen.

5.4 Experimental Facility for Corrosion Study

An experimental test facility has been designed to study the corrosion of immersed cable and joints. The facility consists of two flow tanks which can recirculate a corrosive electrolyte. The tanks allow the simulation of various submarine

environments. Variation and close control of the temperature, pH, salinity, conductivity and flow rate of the electrolyte is possible. The tanks will enable the study of samples in various sediments simulating the ocean floor. The facility can hold and allow the study of a number of sample joints as described in the next section.

A larger tank which can accommodate long cable lengths incorporating a number of test joints is also available to allow hydrogen analysis. Facilities also exist to allow immersion tests in real seawater environments over long time scales.

6.0 TESTS AND RESULTS

A number of experiments have been undertaken to quantify hydrogen permeation at cable joints arising from electrochemical corrosion. These consist of long and short-term laboratory and field based investigations.

6.1 Hydrogen Generation

Potential Monitoring- Monitoring the potential of all components in contact with sea water in the region of the joint gives an indication of the likelihood of hydrogen generation due to general corrosion upon each. Where the components are in electrical contact with one another, as for the armour wires and the joint housing, measurement of the combined potential allows calculations that determine whether hydrogen generation is thermodynamically possible. A simplified equation derived from the Nernst equation [7] which relates the pH of sea water to the likelihood of hydrogen generation is as follows:

$$E(\text{V}) = -0.059 \text{ pH} \quad \text{at } 298 \text{ K} \quad (7)$$

This enables the potential below which hydrogen generation is thermodynamically possible to be calculated. From this calculation, assuming the pH of normal sea water to be 8.2, it can be shown that hydrogen generation may occur on a metallic surface below a potential of approximately -480 mv versus a standard hydrogen reference electrode (or -720mV versus a standard calomel reference electrode (SCE)).

The potential of various alloys in flowing 3.5% sodium chloride at 20 C is shown in Table 2. Also shown is the combined potential of these alloys when coupled with a zinc electrode having a larger surface area (5:1).

Alloy	Potential/mv (vs SCE)	Combined Potential/ mv (vs SCE)
Low Alloy Steel	-610	-1025
Sherardised Steel	-850	-1025
Stainless Steel (Austenitic)	-100	-1025
Beryllium-Copper	-250	-1025
Galvanised Armour (Zinc)	-1030	-

Table 2. Potential of some alloys in 3.5 % NaCl.

The large zinc electrode represents armour wire and the alloys the joint housing. It can be seen that when a large surface area of zinc is coupled to alloys with a more positive electrode potential, the potential of the alloy is significantly lowered into a region where, theoretically, hydrogen evolution can occur.

Galvanic Current Measurement - Any electrical couple between two dissimilar metals can lead to galvanic corrosion (section 3.1). These dissimilar metals, e.g., armour wires and joint housing materials, may be electrically coupled through a Zero Resistance Ammeter (ZRA). An experiment which terminated the armour wires short of the joint housing as shown in Figure 4 was undertaken.

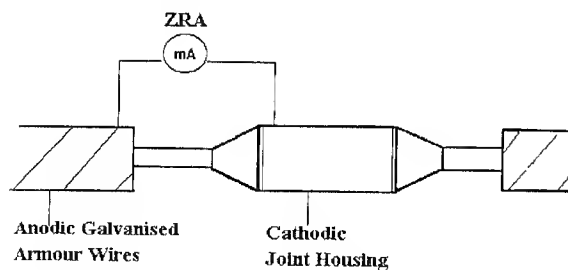


Figure 4. Galvanic current measurement

The ZRA provides an electrical coupling which, as the name suggests, provides effectively a zero resistance path to the galvanic current whilst giving an output reading of the current. The measured current may then be used to calculate the amount of hydrogen that can theoretically be produced if one assumes that all the current is consumed in the generation of hydrogen and that there is no competing cathodic reaction i.e., a worse case scenario. The mass of hydrogen produced may be

calculated using the following equation which is derived from Faraday's laws of electrolysis [8];

At constant current

$$w = M I t / n F \quad (8)$$

where w = mass produced (grams)
 M = molar mass of hydrogen
 I = current (A)
 t = time (s)
 F = Faraday constant (96485 C)
 n = number of electrons

A galvanic current of between 2 - 3 mA has been measured between 1.5 m lengths of galvanised armour wire on either side of a sherardised (zinc/iron alloy coating) joint housing immersed in flowing 3.5% sodium chloride solution at 20 C. This current was generated as a result of the potential difference between the electrode potentials of the armour and the joint components.

When in service, consideration must be given to the likelihood that greater lengths of cable may produce larger galvanic currents. The galvanic current may also be supplemented by such effects as stray current corrosion or magnetohydrodynamics.

Sherardised components have an electrode potential which is relatively close to zinc. Thus the potential difference which generates the galvanic current is relatively low in this instance. However, if the joint components were made from an alloy with a more positive electrode potential, such as copper, the potential difference would be much larger. This may also result in the generation of larger galvanic currents.

Tafel Analysis - This is a well-established electrochemical technique which allows the cathodic behaviour of metals in various environments to be understood in the laboratory. It identifies the likelihood of hydrogen generation from a kinetics viewpoint and displays the competing reactions. This allows an estimation to be made as to the proportion of galvanic current utilised by the hydrogen evolution reaction compared to the other cathodic reactions. The details of this technique [9] are beyond the scope of this paper but its usefulness in this area must be recognised.

6.2 Hydrogen Diffusion Into Joints

6.2.1 Impressed Current Studies

A method to rapidly determine whether generated hydrogen can enter the joint has been devised. The method can be

carried out in a number of days. The joint components are forced to become the cathode of a corrosion cell by the application of a large current (the cell is balanced by the use of an inert platinised titanium anode). The application of this extremely high current forces the cathodic reaction to occur at a much accelerated rate. The technique may be used to assess the relative performance of alternative joint designs.

A test joint constructed from sherardised steel components modified with a calibrated electrochemical sensor and a GC sample port was immersed in a flow tank for a period of 38 days prior to the application of an impressed current. At the end of this period the output from the sensor was below its lower limit of detection. An impressed current of 3.0 A was applied to the sea case. Under these extreme conditions large quantities of hydrogen were observed to be evolving from the surface of the joint components. The hydrogen concentration inside the joint as detected by the sensor increased steadily after the application of the current (Figure 5).

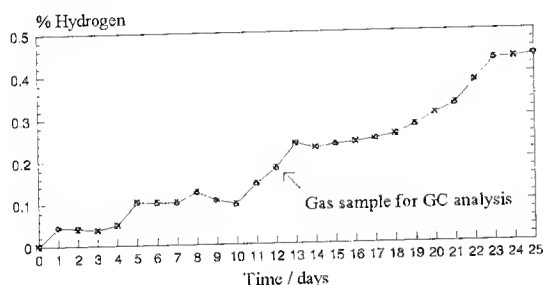


Figure 5. Increase in hydrogen concentration inside joint after impressing 3.0 A current

A gas sample from the joint was taken on day 12 and analysed using gas chromatography. Hydrogen was positively identified (Figure 6) at a concentration which compared well with an indicated sensor reading of 0.22 %.

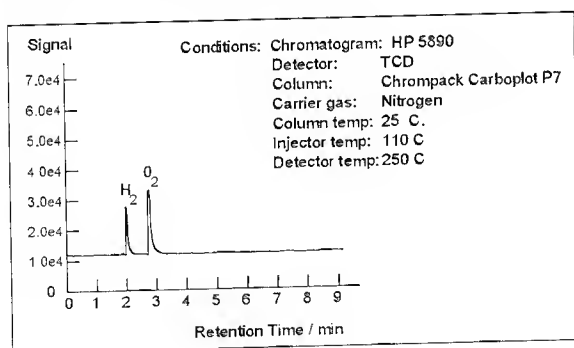


Figure 6. Gas Chromatogram showing presence of Hydrogen

The ratio of impressed current which is consumed specifically in the formation of hydrogen is to be calculated in the

laboratory using simple electrodes in a specially designed, enclosed cell similar to the simple corrosion cell in Figure 1. An impressed current will be applied to an electrode made of the joint material whilst an inert anode completes the circuit. The cell will allow the accurate measurement of generated hydrogen by analysis of gas in a head space above the electrolyte. This will allow calculations to be made with regard to the ratio of hydrogen generated to the amount which enters the joint.

Further tests will involve variation of joint materials, length of armour wire and armour type in a matrix of various conditions such as flow rate, temperature and pH to show the effect on the potential and galvanic current. This will allow extrapolation to a wide range of service conditions.

6.2.2 Corrosion Studies

Natural Corrosion - By the nature of the chemical processes involved, tests observing the natural corrosion of joint components must be long-term to produce meaningful results. Experiments include submerging joints in various environments such as flowing, still and polluted sea water, some of which are ongoing.

As many aspects of corrosion are specifically related to environmental factors, only generalised conclusions can be made concerning the experimental results obtained from any one test site. However, the results will show whether significant amounts of hydrogen enter the joint over extended periods of time. The most adverse environment with regard to hydrogen generation will also be identified.

An unarmoured joint containing a hydrogen sensor was manufactured as a control sample. After storage in the atmosphere at ambient temperature for 2 days it was immersed in a flow tank at 20°C for 4 days to confirm stability after the manufacturing process. The output of the sensor remained at zero during this time. This unarmoured joint was then refurbished as an armoured joint using the appropriate piece parts together with armour wires laid up around the cable. This sample, together with other samples in alternative cable types were re-immersed in the flow tank for long-term evaluation. No significant quantities of hydrogen have been detected to date and such tests are ongoing.

Accelerated Corrosion - An increase in temperature of 10°C may generally be approximated to a two fold increase in the rate of a chemical reaction. Therefore corrosion may be accelerated by increasing the electrolyte temperature. A joint is to be immersed in flowing, 3.5% sodium chloride solution at a temperature of 50°C to accelerate corrosion. Hydrogen will be monitored throughout.

7.0 DISCUSSION

Preliminary investigations including potential and galvanic current measurement have shown that the generation of hydrogen is thermodynamically plausible at armoured cable joints. The results indicate that the joint components become the cathode of a corrosion cell and that hydrogen generation may occur upon them. This may be most severe with joint components manufactured from materials where a significant potential difference exists between them and the galvanised armour wires. However long-term investigation is paramount to gain conclusive evidence.

The impressed current experiments have verified that when hydrogen is generated on outer joint components it can gain entry, by diffusion, to the joint splice cavity. This indicates that any hydrogen generated by natural corrosion can also enter the system at the joint. Whilst the lengths of fibre within the joint housing are usually low (2-4 m) and therefore do not contribute to a major loss increase, axial penetration along the cable may result in attenuation effects over a longer length of fibre. Axial penetration of the gas within the joint is dependant on the efficiency of the cable structure to block gas permeation. This aspect is the subject of a separate programme of research. In any case the concentration of gas within the joint housing under all conditions remains an important parameter.

It is evident that an enhanced understanding of cable ageing mechanisms due to corrosion is of prime importance to the cable designer. Hydrogen ingress at joints needs further investigation to fully quantify loss margins allotted to this phenomenon. Accurate predictions will allow the cable designer to properly assess the margins required for each cable system according to the number of joints. Tighter margins could be applied allowing wider repeater spacing for repeatered systems and increased spans for unrepeatered systems leading to significant cost reduction.

8.0 CONCLUSIONS

An experimental technique has been developed to monitor hydrogen concentration within submerged fibre optic joints. This method has confirmed that when hydrogen is generated externally on metallic joint components it can diffuse into the joint cavity.

Present levels of hydrogen generation by natural corrosion do not appear to present a risk to the ageing margins of existing submarine systems and current power budgets are adequate. Whilst ageing models may provide adequate safeguard to system performance, hydrogen ingress at cable joints needs to

be quantified to allow more accurate predictions of EOL losses and to evaluate new designs. This may allow increased system reliability and more cost-effective solutions for future submarine cable systems.

Long-term evaluation is required to identify exact levels of hydrogen ingress generated by natural corrosion at joints. A test programme is underway to fulfil this requirement to enable accurate predictions of required ageing margins in a wide range of service environments.

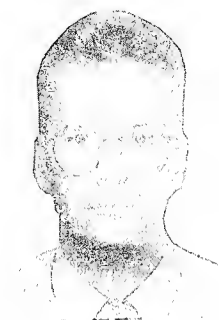
9.0 ACKNOWLEDGEMENTS

The authors would like to thank Ian Whyte of City Technology Limited, Portsmouth, U.K. who supplied the electrochemical sensors and the expertise of Martin Hill of the University of Portsmouth in the field of Gas Chromatography. Thanks are also given to Professor Frank Walsh and Dr. Des Barker of the University of Portsmouth for their assistance in the writing of this paper.

10.0 REFERENCES

1. **Hydrogen Related Degradation In Optical fibres: Implications And Practical Solutions**, J.D. Rush, K.J. Beales, D.M. Cooper, W.J. Duncan and N.H. Rabone, Br. Telecom Technol. J., 2, No. 4, 84, Sept 1984.
2. **Hydrogen Sources For Signal Attenuation In Optical Fibres**, G. Schick, K.A. Tellefsen, A.J. Johnson, C.J. Wiczorek, Proc 39th Int. Wire Cable Symp., 244, Nov. 1990.
3. **Lightwave Technology**, J. Stone, LT-5 (5), 712, 1987
4. **Corrosion In Submarine Systems And Test Methods For Evaluation Of Long Term Performance**, C.J. Brown, G. McGurk, F.C. Walsh, B.D. Barker, Proc 42nd Int. Wire Cable Symp., 463, 1993.
5. **Marine Corrosion**, F.L. LaQue, J. Wiley & Sons, Inc, New York, 1985.
6. **Corrosion Enhancement Of An Undersea Repeater Due To The Hall Effect**, E.A. Franke, IEE J. of Oceanic Eng., 4, 89, July 1979.
7. **Industrial Electrochemistry**, D. Pletcher, F.C. Walsh, Chapman & Hall, London 1990.
8. **Trans. Inst. Metal Finish.**, F.C Walsh, B.D. Barker, G. Ottewill, 71(3), 113, 1993.

9. Instrumental Methods In Electrochemistry, R. Greef, L.M. Peter, D. Pletcher and J. Robinson, Ellis Horwood, Chichester, 1985.



Bryan Ridd
STC Submarine Systems Ltd
West Bay Road
Western Docks
Southampton
SO15 1DS
UK.

Bryan Ridd is a Teaching Company Associate in the New Product Development Group at STC working on a joint project with the University of Portsmouth in the field of corrosion. He received a BSc (Hons) Degree in Applied Chemistry in July 1993 from the University of Portsmouth and joined STC in October of the same year.



Craig Brown
STC Submarine Systems Ltd
West Bay Road
Western Docks
Southampton
SO15 1DS
UK.

Craig Brown is also a Teaching Company Associate in the New Product Development Group at STC. Since joining the company in July 1993 he has been involved with the corrosion testing and design of cable components.

He received a BSc (Hons) in Applied Chemistry from the University of Portsmouth in 1989. He then went to the University of Southampton to study Electrochemistry completing his PhD in 1992.



Ged McGurk
STC Submarine Systems Ltd
West Bay Road
Western Docks
Southampton
SO15 1DS
UK.

Ged McGurk is currently Contract Support Manager in the Technical Department at STC Submarine Systems, Southampton. After joining STC in 1989 as a Materials Scientist he has worked on the development of a variety of cable products until recently as Product Development Manager for Unrepeated systems.

OVERVIEW OF WIDEBAND ANALOG COMPONENTS AND SYSTEMS

M J Wale and C Edge

GEC-Marconi Materials Technology (GMMT),
Caswell, Towcester, Northants, NN12 8EQ, UK

Abstract

Rapid progress is now being achieved in wideband analog optoelectronic and fiber optic technology. We review here a number of recent developments which exemplify the current state of the art both in component technology and in system applications, including radar and communications. Phased array antennas are discussed in particular detail since the advantages of using optics in these systems are particularly compelling.

Introduction

It has been known for some years that fiber optic transmission of high frequency analog signals offers considerable potential for improved system design. Fiber optics offers the following advantages in comparison with conventional microwave transmission media:

- Low incremental link loss (less than 1 dB/km)
- Link loss independent of microwave frequency, even up to mm-waves
- Constant group delay (very low dispersion)
- Freedom from electromagnetic interference
- Low temperature coefficients, especially of phase shift
- Very light, flexible transmission media
- Allow wavelength division multiplexing for multi-channel operation.

Optical transmission of analog signals is much more challenging than digital transmission, because of the wide dynamic range of the signals involved. In fact, it is only in the last five years that fiber optic links which are generally compatible with radar or microwave communications signals

have been demonstrated, whereas fiber optics has been the principal technology for digital telecommunications transmission systems for a decade or more. Progress is extremely rapid at the present time and analog fiber optic systems are now being qualified for very demanding military system applications, both in the UK and elsewhere. Many new applications for this technology are emerging, including delay lines with very wide time bandwidth product for radar signal processing and wide bandwidth antenna beamforming in phased array antennas, as well as more straightforward signal transmission and distribution functions.

In this paper, we shall first look at the component technology required to build RF optical links and signal processing subsystems, then examine the performance of the links themselves and finally explore the application of optical signal processing techniques to beamforming in phased array antennas for communications and radar.

Component Technology

The simplest optical link comprises a modulated optical source and an optical receiver, linked by optical fiber. A single mode fiber is usually preferred in wideband analog systems, since the varying partition of energy between the various propagating modes in a multimode fiber can be a significant source of noise. Propagation loss in the fiber itself is extremely small and may be neglected for most purposes: it is less than 0.5 dB/km at 1.3 μm , or around 0.1 dB per microsecond delay. Dispersion is also a relatively minor effect, particularly around 1.3 μm where the dispersion of typical optical fibres crosses zero; speciality fibres with the dispersion minimum at other wavelengths (e.g. 1.55 μm) are also available. Transmission system

performance is accordingly more often determined by the transmitter and receiver than by the fibre itself. In the following sections we give a brief review of the component performance which is currently available. More detailed coverage is given in [1].

Although it is possible to modulate the output power of a semiconductor laser directly through its injection current, for wide bandwidth high dynamic systems an externally modulated configuration using an auxiliary integrated optical modulator is usually preferred. This is because the noise and distortion characteristics of a directly modulated laser deteriorate significantly as the resonant frequency of the laser is approached. Nevertheless, directly modulated laser sources are widely employed in CATV applications at frequencies up to 1 GHz [2]. Auxiliary pre-distortion or feed-forward compensation electronics may be employed to improve the distortion performance. Directly modulated lasers are available commercially up to J-band, whilst laboratory results include multimode Fabry-Perot devices with bandwidths exceeding 25 GHz [3] and single frequency distributed feedback lasers with 22.5 GHz bandwidth [4].

Optical Sources

One of the major reasons for the recent performance improvements of optical RF links has been the availability of high power low noise optical sources. To date the best performance has been achieved using diode pumped solid state lasers (e.g. Nd:YAG or Nd:YLF at 1.3 μm), which are capable of generating single mode outputs at powers in excess of 100 mW with a relative intensity noise of less than -170 dB/Hz. These solid state sources are relatively large, have a low electrical to optical power conversion efficiency and require temperature control. Although it is possible to design for high performance over a wide environmental range [5], this typically requires a high power consumption for thermal control. Very high optical link performance is achievable using such high power, low noise devices, e.g. a dynamic range of 165 dB/Hz has been reported [25].

For applications where mass, space, power or environmental conditions are critical a semiconductor laser source is preferable. Packaged 1.3 μm sources coupling around 10

mW into the output fiber have recently become available from several manufacturers, principally for the CATV market. We have recently demonstrated 100 mW ex facet output power in a ridge-waveguide multi-quantum well DFB device operating at a single frequency in the 1.55 μm band [6]. The RIN of this device is better than -152 dB/Hz. Further improvements in output power, noise and packaging suitable for harsh environments are expected to occur rapidly.

External Modulators

The extension of analogue optical RF links into the microwave region has relied on the development of suitable external optical modulators. The more linear design are based on waveguide Mach-Zehnder interferometers and are available in either LiNbO₃ or GaAs substrate materials; a GaAs based device is illustrated in figure 1. Typical devices have bandwidths up to 20 GHz, require 5-10 volts for full switching and have a fibre to fibre loss of 6-9 dB. Commercial LiNbO₃ devices presently offer slightly lower fiber-coupled loss, whereas the GaAs units achieve a flatter frequency response, wider bandwidth and a much lower temperature dependence. The GaAs devices also have the advantage that close velocity matching between the microwave and optical signals can readily be achieved, while preserving a 50 Ω characteristic impedance. GaAs devices with bandwidths in excess of 50 GHz are now available [7,8]. Representative data are given in figure 2.

GaAs travelling wave modulator devices are attractive devices for incorporation into hybrid laser-modulator transmitters, where the coupling optics can be designed for accurate spot-size matching between the laser, modulator and output optical fiber. The use of laser-welded construction provides compatibility with demanding environmental specifications.

For links requiring a high spurious-free dynamic range, it may be necessary to use a modulators with lower third-order distortion than is available with the raised cosine response of the Mach-Zehnder modulator designs. Pre-distortion techniques have been shown to be suitable for low frequencies (<1GHz), but for improvements at higher

bandwidth optical techniques based on modifications to the waveguide design are required. A 20 GHz bandwidth GaAs travelling wave device has recently been demonstrated which provides an improvement of at least 6 dB in third order intermodulation distortion over the standard unit at a relatively high modulation depth of 10% [9].

Photodiodes

Microwave bandwidth photodiodes usually employ a p-i-n structure [10], although Schottky devices are also found. The primary design issue in high speed photodetectors is to achieve a satisfactory balance between quantum efficiency and bandwidth; in a vertical-entry structure there is usually a trade-off between the two performance parameters, since a deep absorption region within the device (for high efficiency) leads to longer transit time. The frequency response of a 20 GHz design developed in our own laboratory is shown in figure 3 [11]. By adopting a transverse, optical waveguide-based design, carrier transport is perpendicular to the direction of light propagation, thereby allowing much wider bandwidths to be obtained with high quantum efficiency [12]. Using these techniques detectors with bandwidth greater than 100 GHz are feasible [13].

Photoreceivers

For the highest performance the design of the photodiode and following amplifier should be considered as a single entity, i.e. a photoreceiver. The key performance parameters for a microwave bandwidth receiver are usually frequency response flatness and noise performance. In general, design techniques for wide bandwidth do not lead to the lowest noise, so a trade-off is necessary. Nevertheless, equivalent noise currents as low as $15 \text{ pA}/\sqrt{\text{Hz}}$ have been achieved with a frequency response flat within 2 dB in the 2-18 GHz range [14], using a travelling-wave amplifier design implemented as a monolithic microwave integrated circuit (MMIC) in high electron mobility transistor (HEMT) technology.

Impedance matching techniques can be applied to achieve lower noise and higher transimpedance in optical receivers for narrowband microwave systems. Using a matched p-i-n photodiode with a discrete HEMT amplifier, 450Ω transimpedance was achieved in the 12 GHz satellite

communications band with less than $6 \text{ pA}/\sqrt{\text{Hz}}$ equivalent input noise, representing an 19 dB improvement in transimpedance and 8 dB improvement in noise compared with the low noise broadband receiver mentioned earlier [15].

Optical Amplifiers

In direct point to point links the use of the above transmit and receive components can achieve very impressive results, comparable to short microwave links in performance but capable of much longer spans. If the link is long enough to have significant loss (i.e. several km) or there is additional loss owing to signal distribution to several destinations, the use of optical amplifiers is an alternative to producing yet higher power optical sources. Both semiconductor optical amplifiers and erbium-doped fiber amplifiers (EDFA) are applicable. The latter is particularly attractive for high dynamic range analog links because its gain dynamics are such that high linearity is preserved for signal modulation at frequencies above a few MHz even when operated in saturation. This type of amplifier does, however, limit the system to operating around the EDFA window $1550 \pm 20 \text{ nm}$. Gains up to 30 dB with noise figures as low as 4 dB are available. Extensive characterization of erbium-doped fibre amplifiers for microwave signal transmission is now in progress in several companies [16]. Semiconductor optical amplifiers (SOA) are much more flexible in operating wavelength, are very compact and have relatively low power requirements. In general the gain and noise figure of a SOA is not quite as good as the EDFA, partly because of the coupling loss between the amplifier and input fiber: 10 dB gain and 6 dB noise figure are typical values. Since the excited state lifetime in the SOA is very short, carrier density modulation can limit the achievable intermodulation performance in this type of device and considerable care must accordingly be taken in system designs employing this type of amplifier [17].

Analog Optical Links

The basic building block at system level is a point-to-point link, whose principal performance parameters are its RF

insertion loss, signal-to-noise ratio, spurious-free dynamic range, 1-dB compression point, third-order intermodulation intercept and noise figure. The usual definition of these parameters is shown in figure 4: the optical link is thus characterized by the same parameters as other microwave components and it is straightforward to compare the link parameters with the system requirements. The derivation of link performance from the component parameters has been extensively discussed in the literature [18]. The insertion loss of the link and its noise performance are determined by the optical power received at the photodetector, the relative intensity noise of the laser, the thermal noise of the amplifier which follows the photodiode and, when included, the spontaneous optical noise produced in the optical amplifiers. The spurious-free dynamic range is determined by the linearity of the modulation process, the optical amplifiers and of the photoreceiver.

It is worth mentioning that the third order intercept of an optical link often lies about 10 dB above 1 dB compression, just as in a microwave GaAs FET amplifier (though for very different reasons). The linearity of optical link is therefore comparable with other microwave components forming a practical system. Nevertheless the fact that optical links usually have a significant RF insertion loss (0-30 dB: see below) means that additional amplification has to be introduced. A particular characteristic of optical links is that an appreciable additive noise is intrinsic in the transmission process, owing to the quantization of the light wave into photons and the resulting shot noise in the photodetection process. Noise figures for basic unamplified optical links are in consequence often relatively high (10-40 dB), which determines that substantial preamplifier gain is required so that the overall system noise figure is not adversely affected.

Reported performance of microwave optical links has advanced at an extremely rapid rate in the last few years. Looking back to around 1988, link loss figures (measured from the optical modulator or laser drive connector to the photodiode output) were typically in the 45-70 dB range and noise figures were rarely less than 50 dB. Likewise the corresponding link dynamic range (often around 120 dB Hz) represented a substantial degradation of overall system

performance. The position today has been transformed quite dramatically. Bandpass optical links have now been designed which offer substantial optical gain [19], fundamental dynamic range has been extended to >160 dB Hz (>90 dB in 10 MHz bandwidth) and spurious-free dynamic range up to 117 dB Hz^{2/3} has been reported [20]. Noise figures down to 6 dB have been achieved without preamplification.

Several factors have been important in bringing about the dramatic improvement in link performance mentioned above. These include reductions in optical loss through the system (e.g. improvements in optical coupling efficiency in laser diode modules and integrated optical modulators), increased optical power output and lower relative intensity noise in laser sources (e.g. the use of high performance DFB lasers or solid state lasers) and improved design of optoelectronic interfaces with accurate impedance matching. A review of analog link design including a particularly detailed discussion of the implications of impedance matching is given in ref. [21]. Table 1 summarises some of the notable reported optical link results.

Measurements have confirmed that optical fiber links are capable of preserving low RF carrier phase noise. Newberg et al [28] achieved -138 dBc/Hz in phase and amplitude noise at 10 kHz from carrier in a short externally-modulated optical link, degrading by 8 dB over a link length of 2.25 km. Lee et al confirm this trend [29], with overall performance at L-band ranging from -130 dBc/Hz at 1 kHz from carrier to -150 dBc/Hz at 1 MHz. Logan and Lutes [30] measured the phase noise of an externally modulated 8.4 GHz link to be -115 dBc/Hz at 1 Hz from carrier. These results are better than most signal sources used in practice.

In the radar field, signals are often analysed in the range-Doppler plane and the ambiguity diagram provides a convenient way of characterising overall system performance, particularly with regard to phase noise. A recent characterisation of an externally modulated fibre optic link used for radar testing is described in [31], with results shown in figure 5.

Optics in Phased Array Antennas

The signal distribution and control system of a large phased array antenna is very complex and typically accounts for a large fraction of the total size, mass and complexity of the equipment, so the application of optical techniques to minimise these parameters is extremely attractive. Fiber optics may be used in a number of different ways and at a number of different levels within a phased array antenna system.

The most straightforward application is in distributing control signals and other digital data between transmit/receive modules and the central processor(s). Suitable technology for this application has been available for some time and indeed some phased array radar systems with optical data distribution have already been built: an important example in the UK is the MESAR ship-borne radar [32]. It is safe to assume that most designers contemplating a new phased array design would now look closely at optical distribution for digital data.

We believe there is an evolutionary path for optics in phased arrays from digital control networks, via local oscillator and transmit waveform distribution [33] to full signal beamforming. By performing the beamforming processing (time delay or phase shift) in the optical domain, further performance advantages in terms of multi-band and multifunction operation can be achieved. High accuracy and wide bandwidth are feasible, whilst simultaneously allowing the receive/transmit (R/T) module design to be simplified. Serious difficulties may often be encountered in accommodating the complex R/T modules needed in conventional microwave practice at the antenna face. This is particularly the case at mm-wave frequencies, since the spacing must be less than $\lambda/2$ in order to avoid spurious antenna "grating" modes. For a system operating at 60 GHz this separation can be at most 2.5 mm. Accordingly there is substantial motivation for keeping the circuitry at this point as simple as possible and using an optical system to define the phase and amplitude remotely from the antenna face itself.

Coherent Optical Beamforming

Coherent optical beamforming is based on the optical heterodyne principle, whereby two low noise optical signals with different frequencies ν_0 and ν_1 (optical carrier and local oscillator) are combined in a high speed photodetector to produce an RF signal at the difference frequency $f = \nu_1 - \nu_0$, the phase of this signal being determined by the phase difference between the two optical signals [34]. Figure 6 illustrates the basic implementation of a coherent optical beamformer. The optical source module generates the two optical signals (local oscillator and carrier) separated by the required RF frequency. The carrier signal can be modulated with the transmission signal waveform prior to splitting into the individual antenna channels. Static phase shifts for the antenna beamforming are applied to the carrier signal of each channel and amplitude tapering for antenna sidelobe control can also be provided using an optical voltage controlled attenuator. Distribution and optical control functions can both be achieved in a single integrated optical device, which can be small, fast and have extremely low power consumption; furthermore a single integrated optical chip will accommodate the phase and amplitude control for many channels. This approach can lead to significant reductions in power and weight compared with conventional microwave solutions.

The treatment of phase noise is critical in all heterodyne phase-shift beamforming systems. Since optical oscillators (lasers) have high phase noise in microwave terms (i.e. they have a wide spectral linewidth), it is necessary to employ a phase locked loop to reduce the relative phase noise between signal laser and frequency reference or to derive all of the signals from a common source using a single sideband modulator. We have employed both techniques in our work [35, 36]. A detailed proof of concept system based on coherent optical beamforming has been demonstrated for a communication applications where phase noise values between -90dBc Hz^{-1} and -100dBc Hz^{-1} were achieved. The basic transmit and receive links are illustrated in figure 7. A full description of the system is given in references [15] and [37].

It should be noted that the coherent optical beamforming technique has the same beam squint characteristics as other phase-steered antennas [38], i.e. effective antenna gain is reduced with wide bandwidth signals when a narrow spot beam is steered over a wide angle, since the beam direction is frequency-dependent. In order to avoid this effect, true time delay (TTD) techniques must be used. Optical techniques are also very important in the implementation of this type of antenna, particularly to achieve lower mass and size with wide bandwidth and high stability. Several notable system demonstrators are currently being built and tested [39]. Where the system criteria permit, coherent phase-shift systems provide an elegant solution to the beamforming problem with a much lower parts count, size, mass and power than a TTD network.

GMMT is currently evaluating coherent optical techniques for mm-wave communications antennas under contract to US Army CECOM, Ft. Monmouth, NJ.

Conclusions

Optoelectronic technology has now progressed to the point where its performance is compatible with a wide range of microwave systems. A number of major system developments which are underway worldwide are accordingly now incorporating optical links in order to realise the many advantages listed at the beginning of this paper. Furthermore, with the advent of new optical techniques such as coherent optical beamforming, entirely new system concepts will emerge. The application of such techniques to millimeter-wave antenna systems is particularly exciting in view of the high loss of conventional transmission media at these frequencies and the extremely limited space which is available for electronics behind each element of a millimeter-wave phased array. We believe optical technology is now beginning to show its potential for radically improving the design of a wide range of microwave systems including radar, communications and navigation, in airborne, marine, land-mobile and fixed installations.

References

- [1] Wale, M.J., "Wideband components for optical systems", MM '92, Brighton, September 1992, pp. 317-324; Wale, M.J., "Current developments in RF and microwave fibre optics", 19th European Conf. Optical Communication, Montreux, Switzerland, 12-16 September 1993.
- [2] Darcie, T.E., "Photonics in cable television systems", Optics & Photonics News, September 1992, pp. 16-23.
- [3] Morton, P.A., Logan, R.A., Tanbuk-Ek, T., Sciortino, P.F., Sergeant, A.M., Montgomery, R.K. and Lee, B.T., "25 GHz bandwidth 1.55 μm GaInAsP p-doped multiple quantum well lasers", Electron. Lett., **28**, pp. 2156-2157 (1992).
- [4] Morton, P.A., Logan, R.A., Tanbuk-Ek, T., Sciortino, P.F., Sergeant, A.M. and Wecht, K.W., "Superfast 1.55 μm DFB lasers", Electron. Lett., **29**, pp. 1429-1430 (1993).
- [5] Glomb, W.L., "Fiber optic links for antenna remoting", SPIE, **1703B**, pp. 523-527 (1992).
- [6] Reid, T.J., Williams, P., Hurley, J., Carr, N., Robbins, D.J. and Buus, J., "Strained-layer quantum-well laser with simultaneous high power and narrow linewidth", Technical Digest, OFC/IOOC 1993, paper WB2.
- [7] Walker, R.G., "High speed III-V semiconductor intensity modulators", IEEE J. Quantum Electronics, **27**(3), March 1991, pp. 654-667.
- [8] Walker, R.G., "High speed semiconductor guided-wave optical modulators", IEE Colloquium on Microwave Optoelectronics, London, 27 January 1994, IEE digest no. 1994/022.
- [9] Hall, D.D., Wale, M.J., Edge, C. and Parsons, N.J., "Advances in Microwave Optoelectronics", GEC J. Research, **10**(2), pp. 80-84 (1993).
- [10] Bowers, J.E., Burrus, C.A. and McCoy, R.J., "InGaAs photodetectors with modulation response to millimetre wavelengths", Electron. Lett., **21**, pp. 812-814 (1985).
- [11] Moseley, A.J., Carter, A.C., Kearley, M.Q., Park, C.A. and Humpreys, D.A., "High speed

- InGaAs/InP photodiodes for applications to 40 GHz", SPIE, **995**, pp. 61-67 (1988).
- [12] Kato, K., Hata, S., Kawano, K., Yoshida, J. and Kozen, A., "A high efficiency 50 GHz InGaAs multimode photodetector", IEEE J. Quantum Electron., **28**(12), pp. 2728-2735 (1992).
 - [13] Bowers, J., Giboney, K., Wey, Y-G. and Rodwell, M., "New concepts in 100 GHz bandwidth high-efficiency photodetectors", LEOS Summer Topical Meeting on Optical Microwave Interactions, Santa Barbara, Calif., 19-21 July 1993.
 - [14] Hankey, J., Howard, M.A., Long, A.P., Borley, S.J. and Holmes, S.J., "Low noise optical receiver operating at 2-20 GHz", Conference on Optical Fiber Communication, 1994 Technical Digest Series, **4**, Optical Society of America, paper WM3, pp. 155-156.
 - [15] Birkmayer, W.S. and Wale, M.J., "Proof-of-concept model of a coherent optical beam-forming network", IEE Proc., **139**, pt. J., pp. 301-304 (1992).
 - [16] Monardien, D., Moronville, C., Deborgies, F., "Microwave signal distribution using an optical amplifier", MTT-S, 1993, paper X4, pp. 731-734.
 - [17] Coles, A.N., Constable, J.A., White, I.H. and Cunningham, D.G., "Distortion of analogue intensity modulated signals in semiconductor optical amplifiers", Electron. Lett., **28**, pp. 1012-1013 (1992).
 - [18] Simons, R., "Optical control of microwave devices", Artech House, 1990, ch. 5.
 - [19] Betts, G.E., Johnson, L.M. and Cox, C.H., "Optimization of externally modulated analog optical links", SPIE, **1562**, *Devices for Optical Processing*, pp. 281-302 (1991).
 - [20] Ackerman, E., Kasemset, D. and Wanuga, S., "An external modulation L-band link with 117 dB spurious signal free dynamic range", Microwave J., Sept. 1991, pp. 158-163.
 - [21] Cox, C.H., "Gain and noise figure in analogue fibre optic links", IEE Proc., pt. J., **139**(4), pp. 238-242 (1992).
 - [22] Ackerman, E., Kasemset, D., Wanuga, S., Boudreau, R., Schlafer, J. and Lauer, R., "A low-loss Ku-band directly modulated fiber-optic link", IEEE Photonics Technol. Lett., **3**(2), pp. 185-187 (1991).
 - [23] Betts, G.E., Johnson, L.M., Cox, C.H. III and Lowney, S.D., "High sensitivity optical analog link using external modulator", CLEO 89.
 - [24] Betts, G.E., Cox, C.H. III and Ray, K.G., "20 GHz optical analog link using an external modulator", IEEE Photonics Technol. Lett., **2**, pp. 923-925 (1990).
 - [25] Cox, C.H. III, Betts, G.E. and Yee, A.C., "Incrementally lossless, broad bandwidth analog fiber optic link", IEEE/LEOS Summer Topical Meeting on Broadband Analog Optoelectronics, Devices and Systems, Monterey, CA, July 1990.
 - [26] Maignan, M., Brindel, P. and Karas, A., "Liaisons point-à-point hyperfréquence par voie optique", IEEE/MTT French Chapter meeting, Seillac, Nov. 1992.
 - [27] Wanuga, S., Ackerman, E.I., Kasemset, D., Hogue, D.W. and Chinn, S.R., "A low loss L-band microwave fiber optic link for control of a T/R module", SPIE, **1374**, *Integrated Optics and Optoelectronics II*, San Jose, CA, 17-19 Sept 1990, pp. 97-106.
 - [28] Newberg, I.L., Gee, C.M., Thurmond, G.D. and Yen, H.W., "Radar measurement applications of fiber optic links", 42nd Frequency Control Symposium, pp. 453-455 (1988).
 - [29] Lee, J.J., Yen, H.W., Loo, R.Y., Walston, A.A. and Newberg, I.L., "System applications of photonics to phased arrays", SPIE, **1703B**, pp. 490-501 (1992).
 - [30] Logan, R.T. and Lutes, G.F., "High stability microwave fiber optic systems: demonstrations and applications", 46th IEEE Frequency Control Symposium, pp. 310-316 (1992).
 - [31] Aitken, A.J.S., Shephard, D. and Hall, D.D., "Calibration of wideband radar systems using fibre optic delay lines", IEE Colloquium Digest 1994/002, London, January 1994.

Authors

- [32] Salter, D.M., "Multi-functional phased array radars", PESL New Technology, No. 4, Plessey Electronic Systems Ltd, Spring 1987.
- [33] Williams, M.O. et al, "Optical signal distribution for a satellite phased array", IEE Colloq. Digest 1990/008, paper no. 16.
- [34] Stewart, W.J., "Optical phased array control", Military Microwaves '84, pp. 287-291.
- [35] Wale, M.J. and Holliday, M.G., "Microwave signal generation using optical phase locked loops", Workshop on Microwave Optoelectronics, European Microwave Conference, Stuttgart, 13 September 1991.
- [36] Wale, M.J., Walker, R.G. and Edge, C., "Single-sideband modulator in GaAs integrated optics for microwave frequency operation", in Integrated Photonics Research, OSA Technical Digest Series, 10, post-deadline paper PD-8 (1992).
- [37] Wale, M.J. and Birkmayer, W.S., "Coherent optical beamforming techniques", 23rd European Microwave Conf., Madrid, September 1993.
- [38] Mailloux, R., Phased array theory and technology", Proc. IEEE, 70, pp. 246-291 (1982).
- [39] Ng, W., Walston, A.A., Tangonan, G., Lee, J.J., Newberg, I.L. and Bernstein, N., "The first demonstration of an optically steered microwave phased array antenna using true time delay", J. Lightwave Technol., 9, pp. 1124-1131 (1991); Lee, J.J., Yen, H.W., Loo, R.Y., Walston, A.A. and Newberg, I.L., "System applications of photonics to phased arrays", SPIE, 1703B, pp. 490-501 (1992).

Michael Wale received the BA, MA and D Phil degrees from the University of Oxford, where he carried out research on spectroscopic remote sensing of the upper atmosphere. He joined GMMT (then Plessey Research Caswell) in 1982 to work on the development of guided-wave optical technology and he now heads the group responsible for semiconductor lasers, integrated optoelectronics and microwave optics at Caswell. Dr Wale is a member of IEEE and Optical Society of America.

Colin Edge graduated in Physics with Astrophysics from Leicester University in 1982 and obtained his MSc in Modern Optics from Reading University in the UK the following year. Since joining GMMT in 1983, he has worked on a variety of optoelectronic technologies, specialising in RF applications. As a senior principal scientist at GMMT, he is currently leading several microwave optical research projects and component developments.

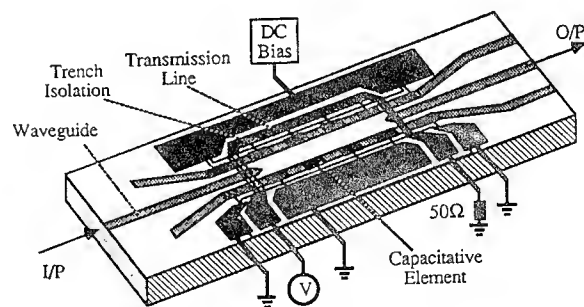


Fig. 1. Loaded-line travelling wave modulator in GaAs.

Author	Date	Type	Frequency GHz	Dynamic range dB Hz	SFDR dB Hz ^{2/3}	RF gain dB	NF dB	Ref.
Ackerman	1991	E	0.9±0.025	159	117	0	21	[20]
Ackerman	1992	D	12±0.4	139	99	-12.6	45	[22]
Betts	1989	E	0.042-0.072	159	111	+11	6	[23]
Betts	1990	E	16.8-22.0	157	108	-34	41	[24]
Cox	1990	E	0-0.580	165	113	-0.3	20	[25]
Glomb	1992	E	up to 0.5		107			[5]
Maignan	1992	D	3.6-4.2		97			[26]
Wanuga	1990	D	1.28±0.075	148	107	-1.8	31	[27]

Table 1. Recent reported results on microwave optical links.
Type = E (Externally modulated) or D (Direct laser modulation).

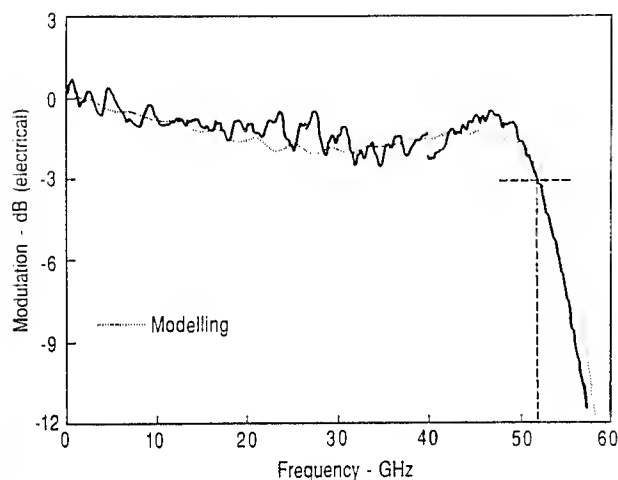


Fig. 2. Typical frequency response of a 50 GHz GaAs optical modulator.

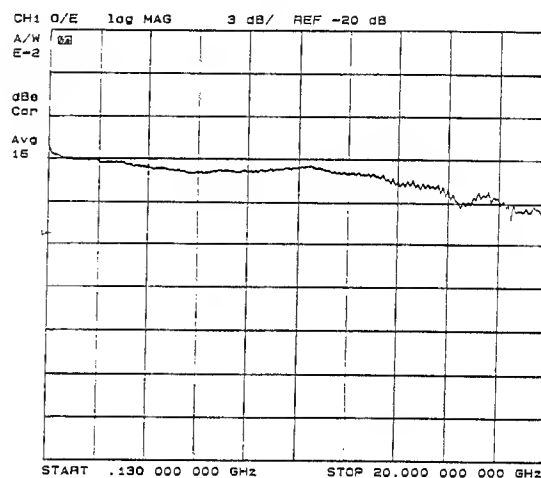


Fig. 3. Frequency response of a p-i-n InGaAs photodiode in a coplanar package. Horizontal scale: 0.13 to 20.0 GHz, vertical scale: 3 dB/division.

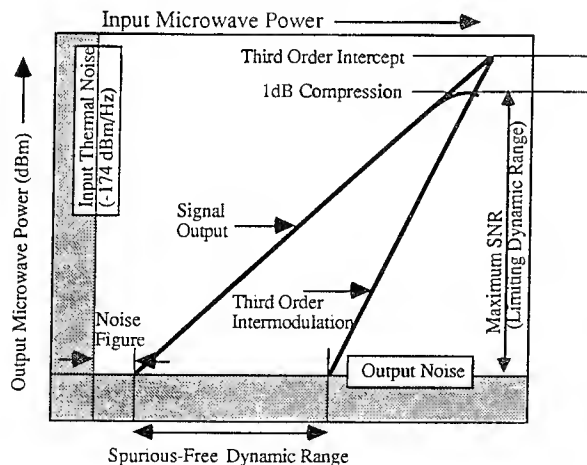


Fig. 4. Definition of terms describing microwave optical link characteristics.

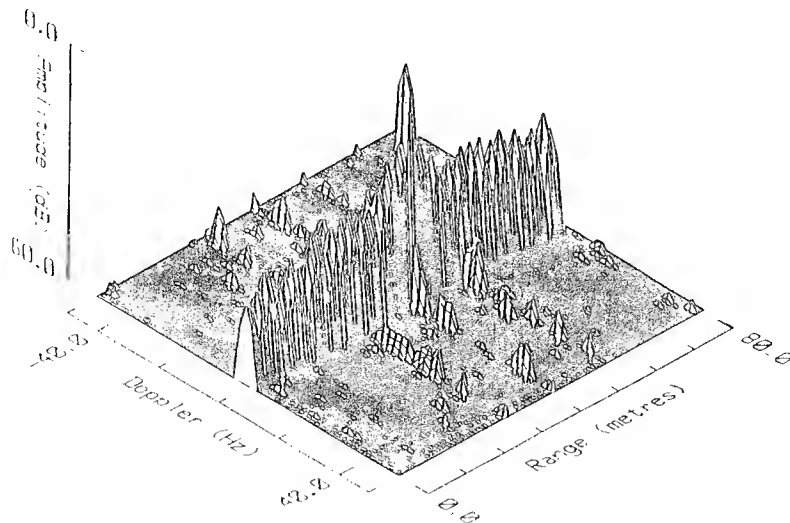


Fig. 5. Range doppler plot for an I-band radar with 270 MHz chirp bandwidth using a fibre optic delay line.

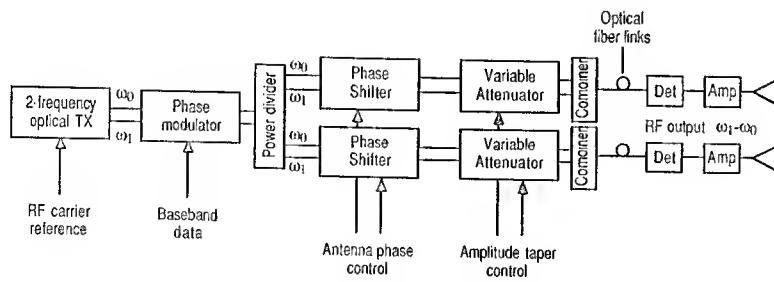


Fig. 6. A simple coherent optical system for RF signal generation, phase modulation and beam control.

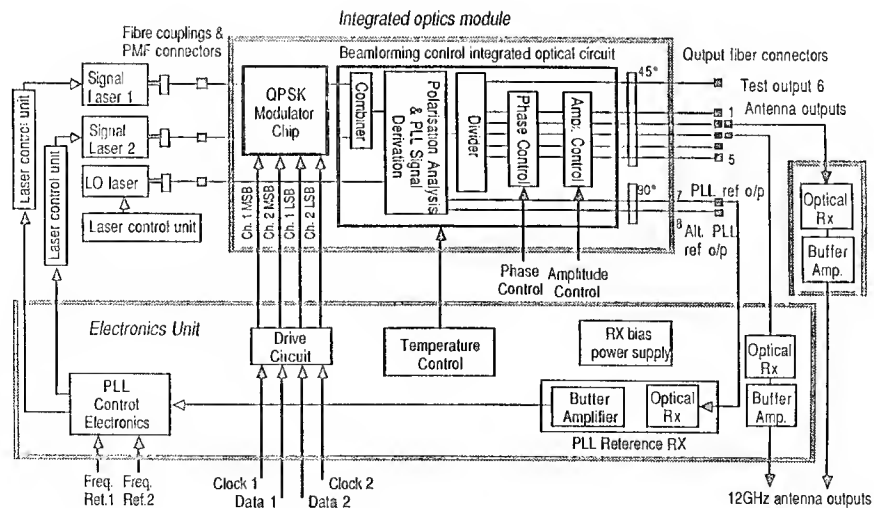


Fig. 7. Coherent optical beamforming network for transmit-mode phased array: proof of concept models (see references 15 and 37).

FUNDAMENTAL DESIGN OF INTEGRATED PHOTONIC SYSTEMS FOR PHASED ARRAY ANTENNA CONTROL

J. G. Wright, L. A. Coryell, W. H. Chang*, R. A. Lux*, T. J. Tayag**

U. S. Army Communications-Electronics Command, Fort Monmouth, NJ; *U.S. Army Research Laboratory, Electronics and Power Sources Directorate, Fort Monmouth, NJ; **U.S. Army Research Laboratory, Sensors, Signatures, Signal and Information Processing Directorate, Adelphi, MD

ABSTRACT

Research is underway at the Communications-Electronics Command (CECOM) and Army Research Laboratory (ARL) in the development of Integrated Photonic Subsystems (IPS) for use in the optical control of phased array antennas to be used in Army tactical systems for communications (COMM) on-the-move (OTM). This paper will describe Army needs, systems envisioned and IPS development work.

INTRODUCTION

The intensity and speed of Desert Storm highlighted the need for communications assets to keep up with highly mobile tactical commanders. Developments are underway at CECOM to develop technologies to support requirements for on-the-move satellite communications (SATCOM) ground terminals and on-the-move terrestrial communications links. Figure 1 provides examples of on-the-move communications applications on the future digital battlefield. The mobile Radio Access Point (RAP) provides connectivity between the backbone Mobile Subscriber Equipment (MSE) System generally used in the Division (Div) and Corps areas, and the highly mobile lower echelons. A high speed wireless Local Area Network (LAN) connects the vehicles comprising a Brigade Tactical Operations Center (TOC). Select vehicles might also support OTM high data rate SATCOM. Depending on the particular application, radio frequency (RF) carriers might vary from 6-58 Ghz with data rates from 2.4 Kb/s to 150 Mb/s. Survivability requirements, combined with a desire for a scalable, modular, frequency independent control system led to the need for an optically controlled phased array antenna¹.

INTEGRATED PHOTONIC SUBSYSTEM DEVELOPMENT

An analysis of the system applications envisioned leads to a number of conclusions effecting the control system design.

- A control system that is frequency independent allows use of the same basic subsystems for applications over a wide range of RF carriers.
- A control system that is modular and scalable allows use of the same basic subsystems for applications in which the required number of antenna elements might vary from hundreds to thousands.
- For continuous connectivity in a tactical environment, multibeam operation is required. A control system that readily supports this requirement is desired².

The fundamentals of a proposed approach, employing coherent optical techniques, are shown in Figure 2 (for simplification transmit direction only is shown). This high level look breaks out the functions of carrier generation, modulation, signal distribution and beamforming into a family of photonic chips. Two phase locked semiconductor lasers (IPS 1) are separated by f_c , the desired RF carrier. An optical modulator, fed by the system's data, imparts a phase shift on f_1 . Signals f_1 and f_2 are then combined (in orthogonal polarizations) for transmission to the antenna elements (IPS 4). IPS 2 provides the first level of signal splitting required to feed antennas which might vary from 100's of elements to 1000's of elements. Integral semiconductor amplifiers compensate for splitting loss. IPS 3 provides additional signal splitting, beam steering (via optical phase shifters) and shaping functions. Heterodyne detection at the photodetector at each element takes the optical phase shift and transfers it exactly to the RF carrier.

ARMY RESEARCH LABORATORY PROGRAMS

Two ARL Directorates, Electronics and Power Sources (EPS) and Sensors, Signatures, Signals and Information Processing (S³I) have efforts underway contributing to the underlying technology, and device development and assessment for the IPS.

EPS Directorate is located at Fort Monmouth, NJ and contains two divisions conducting research related to photonic control of phased array antennas. The Micro/Lightwave Division is concerned with optical

control of microwave devices, component development, device and circuit modeling, and integration of photonic and Monolithic Microwave Integrated Circuits (MMIC). The Electronic Devices Research Division is concerned with the design and fabrication of novel III-V semiconductor devices. It has molecular beam epitaxy capability for the production of AlGaInAs materials, etching and lithographic capability for the fabrication of prototype devices.

Research within EPS Directorate includes activities which would impact many of the major components of the proposed photonic control system. This includes development of Distributed Feedback Lasers (DFB) lasers at 1550 nm wavelength, with very narrow linewidth (IPS 1), development of 1:N splitters with an integrated gain element to recover the splitting loss (IPS 2), development of a birefringent III-V material optical phase shifter (producing a relative phase shift between horizontal and vertical polarizations) (IPS 3), and integrating a high speed photodiode with a MMIC RF amplifier (IPS 4).

Designs for quantum well birefringent phase shifters have been done for systems using various different wavelengths. The designs differ principally in the optical waveguide dimensions and in the semiconductor material system used to produce the quantum well and guiding layers. In this device a strained quantum well layer (lattice mismatched) is grown. Due to the strain, the absorption resonance is different for horizontal and vertical polarizations. By applying bias, the position of the absorption resonance can be shifted. The material layers and electronic band structure of this device is shown under positive and negative bias in Figure 3.

A proof of principle device designed for an operating wavelength of 980 nm was constructed using GaAs/AlGaAs layers. In this device a relative phase change of π was achieved with a 4 volt bias change. This sensitivity is ample for the control of a phase shifting array.

S³I Directorate, located at Adelphi, MD is developing optical power splitting devices to be used in IPS 2. Desired characteristics of a 1xN splitter for this application include a value for N of about 16, ability to split both the Transverse Electric (TE) and Transverse Magnetic (TM) modes, low cross talk between the 2 polarization modes, uniformity among the split channels, low throughput loss, compact size, and ease in manufacture. For N>4, fiber optic polarization preserving splitters are impracticable. Therefore, the splitting must be performed on an integrated optical substrate. Numerous passive integrated optical beam splitting techniques have been proposed and demonstrated. These include but are not limited to Y-junction branching waveguides³, evanescent field directional couplers⁴,

computer generated waveguide holograms⁵, symmetric mode mixers⁶, and radiative power splitters⁷. To achieve the desired device characteristics, the symmetric mode mixing approach holds the greatest promise.

The integrated optical power splitter based on symmetric mode mixing consists of a single mode waveguide (i.e. single mode in both the transverse and lateral dimensions) symmetrically feeding a multimode waveguide region (i.e. multimode in the lateral dimension only). A perspective view of a 1x4 waveguide beamsplitter is shown in Figure 4. If the sidewalls of the multimode region are highly reflecting, the diverging beam from the single mode input guide will form an interference pattern within the multimode region. This pattern results in the formation of multiple self-images of the input spot along the length of the multimode region. For a given width, W, of the multimode region, N images of the input spot are formed at a distance from the single mode input of

$$L = (n * W^2) / (N * \lambda_0), \quad (1)$$

where n is the mode index of the multimode region and λ_0 is the free space wavelength of light. The images at the output plane of the multimode region are equally spaced across the multimode guide with a pitch of W/N. This technique produces splitters with high accuracy and low throughput loss in a relatively short propagation length.

In order to realize the symmetric mode mixing technique in a variety of waveguide material systems, we developed a guide/antiguide beamsplitting structure. The guide/antiguide structure allows the fabrication of highly reflecting sidewalls in materials which are difficult to etch. Consider the mode index versus guide layer thickness plot of the asymmetric waveguide shown in the inset of Figure 5. For a guide layer thickness less than the fundamental mode cutoff thickness of 0.5 μm , no modes are supported by the guide. For incidence angles greater than the critical angle, a beam incident at the guide/antiguide interface will undergo total internal reflection (TIR)⁸. If the single mode rib waveguide input to the multimode region consists of the same structure as the multimode guide, then the incidence angle to the guide/antiguide sidewall will always be greater than the critical angle and thus be a TIR interface.

We have designed and fabricated 1xN symmetric mode beamsplitters for values of N between 4 and 17. An ion milling was used to fabricate the guide/antiguide structure in the GaAs/AlGaAs waveguide of Figure 5 (guide layer thickness is 1 μm). Figure 6 contains an image of the 1x16 splitter's output facet. The beamsplitting uniformity can be reliably fabricated to better than +1-5% and the polarization isolation has been measured to be better than 15 dB (this

measurement was limited by the dynamic range of the Charge Coupled Device (CCD) detector).

The guide/antiguide structure obviates the need for etching deep vertical sidewalls through the guiding layer of the waveguide structure. The symmetric mode mixing beamsplitter concept can therefore be applied to waveguide material systems, such as lithium niobate and lithium tantalate, in which it is difficult to etch deep vertical sidewalls⁹. Since a considerable portion of the throughput loss and mode conversion arise from scattering off sidewalls, the shallower etch depths required from the guide/antiguide structure decrease both throughput loss and polarization cross-talk.

CECOM-ELECTRONICS COMMAND PROGRAMS

Three CECOM programs supporting IPS development are described below.

Ongoing work with Princeton University is investigating design and modeling techniques and procedures for the growth and processing of monolithic photonic circuits containing diverse functions. The program will demonstrate a fully monolithic optical transmitter chip comprising a low threshold DFB multiple quantum well (MQW) laser integrated with a waveguide coupled MQW Mach-Zehnder modulator, a Y-junction coupler, and MQW optical amplifier (Figure 7). The modeling, design and fabrication techniques developed under this program will lead to the development of a fully integrated IPS 1.

Accompanying the above is an in-house CECOM effort to phase lock distributed feedback lasers at frequencies up to 44 GHz and beyond. This is critical to the development of cost effective monolithic transmitters with narrow linewidths, high power output and low relative intensity noise.

A new effort has just commenced which will demonstrate a fully monolithic IPS 3. A 16 channel, integrated phase and amplitude controller for two-dimensional control of a phased array antenna will be developed (Figure 8). The controller is based on using stages of Mach-Zehnder integrated optical interferometers as both phase shifters and attenuators. Tapered electrodes on the first two stages allow a single control voltage to control beam steering in each dimension. The third stage allows for correction of minor channel-to-channel phase errors, while the fourth provides for the desired beam amplitude taper for sidelobe control.

A sub-system demonstrator will also be developed. This will examine such important specifics as path and temperature tracking of the complete optical subsystem.

The final effort underway is examining system architecture details for COMM on-the-move applications

for vehicle-to-vehicle and vehicle-to-satellite communications.

REFERENCES

1. P. Sass and H. Wichansky, "Army Global Grid, the Last Mile," The 4th Biennial Department of Defense Fiber Optics and Photonics Conference, McLean, VA, March 22-24, 1994.
2. J. Wright, L. Coryell, A. Meshal, A. Paoletta, "Army Optically Controlled Phased Array Program," The Fourth Annual ARPA Symposium on Photonic Systems for Antenna Applications, Monterey, CA, 18-21 January 1994.
3. Y. Shani, U. Koren, B. I. Miller, M. G. Young, M. Oron, and R. Alferness, "Buried Rib Passive Waveguide Y Junctions with Sharp Vertex on InP," IEEE Photon. Tech. Lett., vol. 3, no. 3, pp. 210-212 (March 1991).
4. E. A. J. Marcatili, "Dielectric Rectangular Waveguide and Directional Coupler for Integrated Optics," Bell Syst. Tech. J., vol. 48, pp. 2071-2102 (September 1969).
5. J. Saarinen, J. Turunen, and J. Huttunen, "Volume Diffraction Effects in Computer-Generated Guided-Wave Holography," Appl. Opt., vol. 33, no. 6, pp. 1035-1043 (February 1994).
6. J. M. Heaton, R. M. Jenkins, D. R. Wight, J. T. Parker, J. C. H. Birbeck, and K. P. Hilton, "Novel 1-to-N Way Integrated Optical Beam Splitters Using Symmetric Mode Mixing in GaAs/AlGaAs Multimode Waveguides," Appl. Phys. Lett., vol. 61, no. 15, pp. 1754-1756 (October 1992).
7. M. Zirngibl, C. Dragone, C. H. Joyner, M. Kuznetsov, "Efficient 1x16 Optical Power Splitter Based on InP," Electron. Lett., vol. 28, no. 13, pp. 1212-1213 (June 1992).
8. R. Ulrich and R. J. Martin, "Geometrical Optics in Thin Film Light Guides," Appl. Opt., vol. 10, no. 9, pp. 2077-2085 (September 1971).
9. J. L. Jewel, R. E. Howard, E. L. Hu, and S. P. Lyman, "Reactive Ion Etching of LiNbO₃," Appl. Phys. Lett., vol. 38, no. 11, pp. 907-909 (June 1981).

ACKNOWLEDGMENTS

CECOM IPS development is supported by contract DAAB07-92-C-B007 with Princeton University (Cascadable, Monolithic Laser/Modulator/Amplifier Transmitter), DAAB07-94-C-D609 with GEC-Marconi Materials Corporation (Optical Techniques for MM-Wave Phased Array Communications Antennas), and DAAB07-94-C-D617 with Boeing Defense & Space Group

(Common Control Module for Photonically Controlled Phased Arrays).



James G. Wright is a member of the Fiber Optics Branch at CECOM. He is Project Engineer for programs supporting the development of photonics for the control of phased array antennas. Mr. Wright holds a BS in Electrical Engineering from Lafayette College and a MS in Electrical Engineering from Fairleigh Dickinson University. His employment with CECOM and its predecessors (starting in 1976) was interrupted by a two year tour (1989-1990) as Associate Science Advisor for U.S. Forces Korea/Eight U.S. Army, Seoul Korea.



Louis A. Coryell is the Chief of the Fiber Optics Branch in the Local Area Networks Division of the CECOM Space and Terrestrial Communications Directorate. He is responsible for the planning and execution of all Army tactical research and development programs in fiber optics. Mr. Coryell holds a BS in Electrical Engineering from Newark College of Engineering (1968) and MS degrees in Electrical Engineering (1972) and Business Administration (1985) from Fairleigh Dickinson University. He has been employed by CECOM and its predecessor Commands since 1968. Mr. Coryell is a member of the Armed Forces Communications-Electronics Association (AFCEA).

Mr. Wayne Chang received his MS degree in Ch. E. from University of Maryland in 1976. He worked at Comsat Laboratory and Siemens Corporation on compound semiconductor microwave devices, and material and processing technologies. In 1989, he joined the Army Research Laboratory, Fort Monmouth, NJ, where he is now a branch chief leading the research & development efforts in semiconductor optoelectronic devices.

Robert A. Lux
AB University of Chicago 1953
MS University of Chicago 1956
PhD University of Wisconsin 1963
From 1962 to 1967 with Radiation Effect Operation of General Electric Co. concerned with nuclear weapon radiation effects and electromagnetic pulse phenomena. Since 1967 with US Army at Fort Monmouth, NJ. Current interests are modeling and simulation of hetero-structure electronic and optoelectronic devices and diagnostic techniques for processing assessment. Holds eight patents and has published over seventy papers.



Tristan J. Tayag was born in Baltimore, MD in 1964. He earned the BSEE and MSE degrees from the Johns Hopkins University in 1986 and 1987, respectively and the PhD degree in electrical engineering from the University of Virginia in 1991. Since 1991, he has been with the Optical Processing Branch of the Army Research Laboratory where he conducts research in integrated optical processors for radar signal processing and communications applications.

Dr. Tayag is a member of Eta Kappa Nu, Tau Beta Pi, the Optical Society of America, and the IEEE.

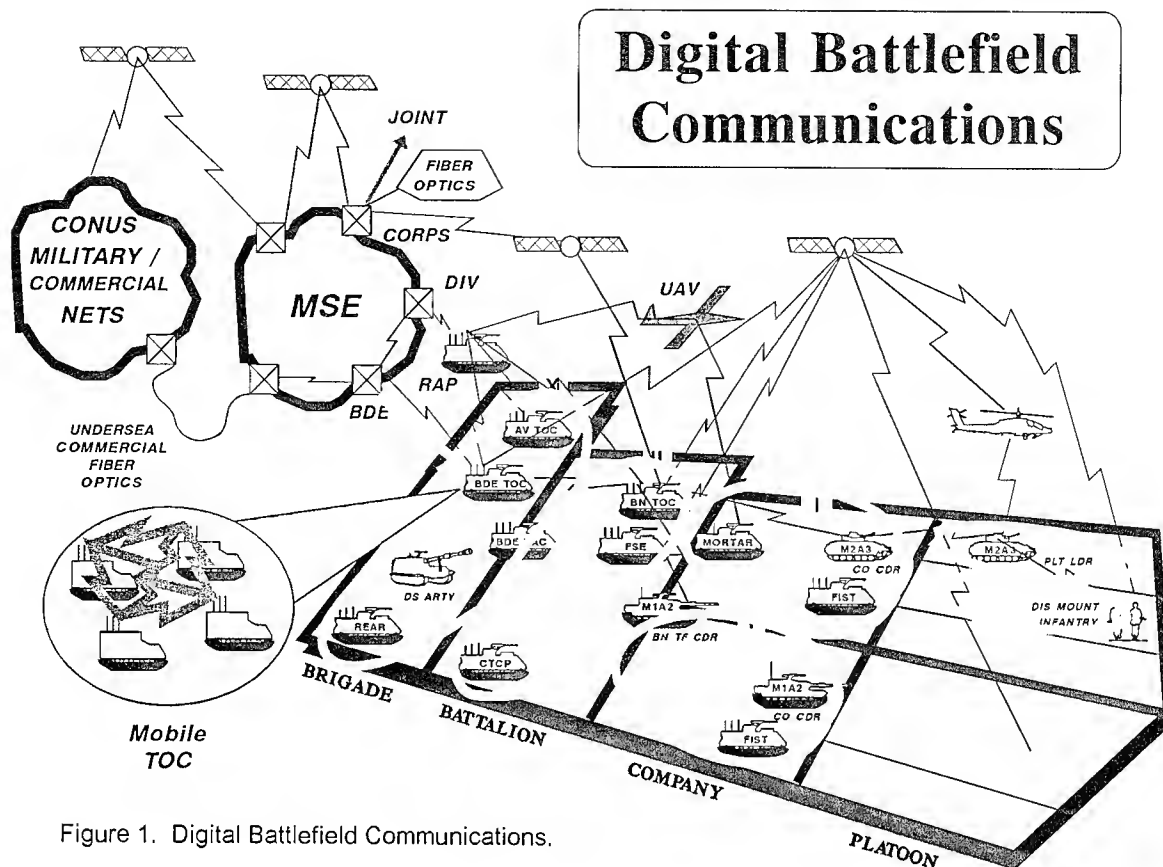


Figure 1. Digital Battlefield Communications.

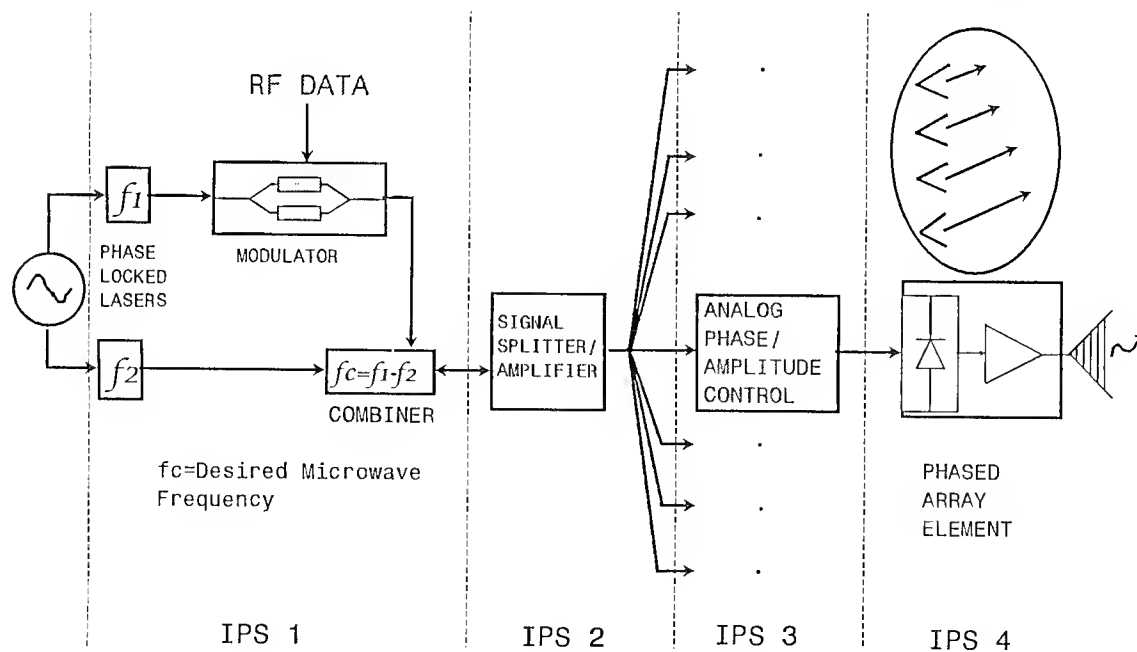


Figure 2. Integrated Photonic Subsystems.

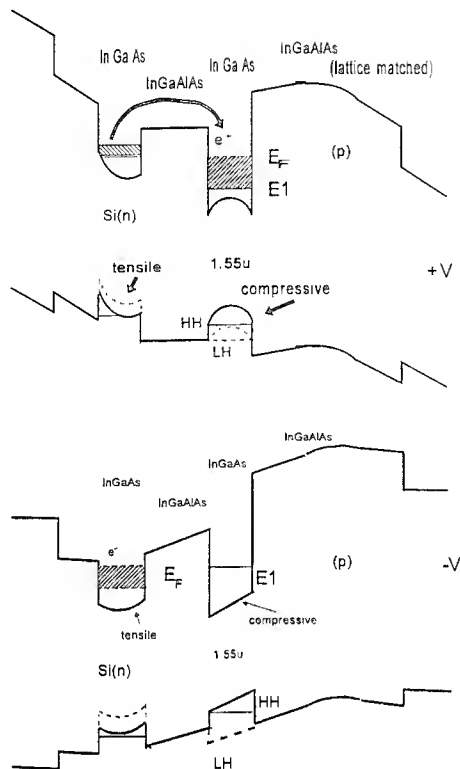


Figure 3. Band Structure of Strained Layer Birefringent Phase Shifter for 1550 nm Systems. Upper Figure with Positive Bias; Lower with Negative bias.

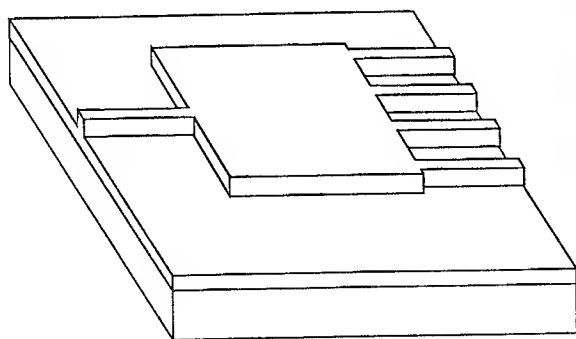


Figure 4. Perspective view of a 1x4 Symmetric Mode Mixing Beamsplitter.

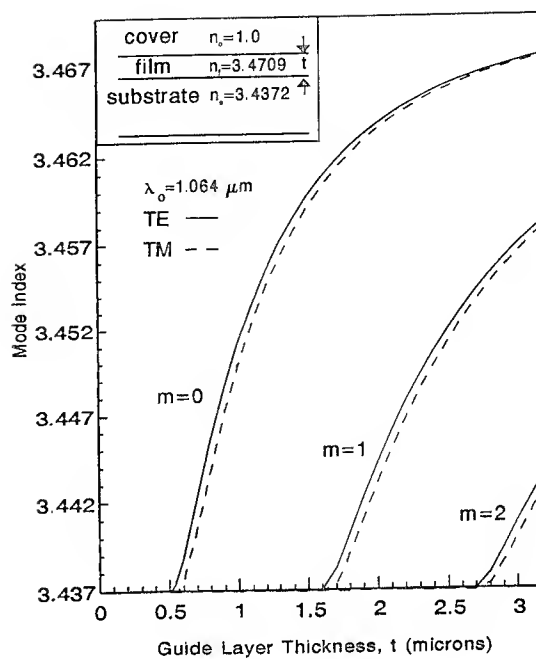


Figure 5. Mode Index Versus Guide Layer Thickness Plot of an Asymmetric Waveguide Structure.

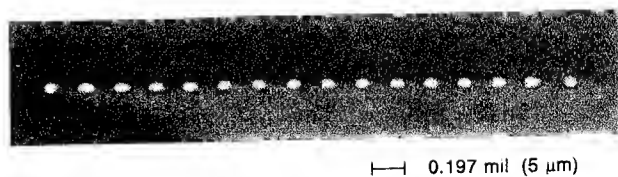


Figure 6. Imaged Output Facet of a 1x16 Beamsplitter for a TE Polarized Input Beam.

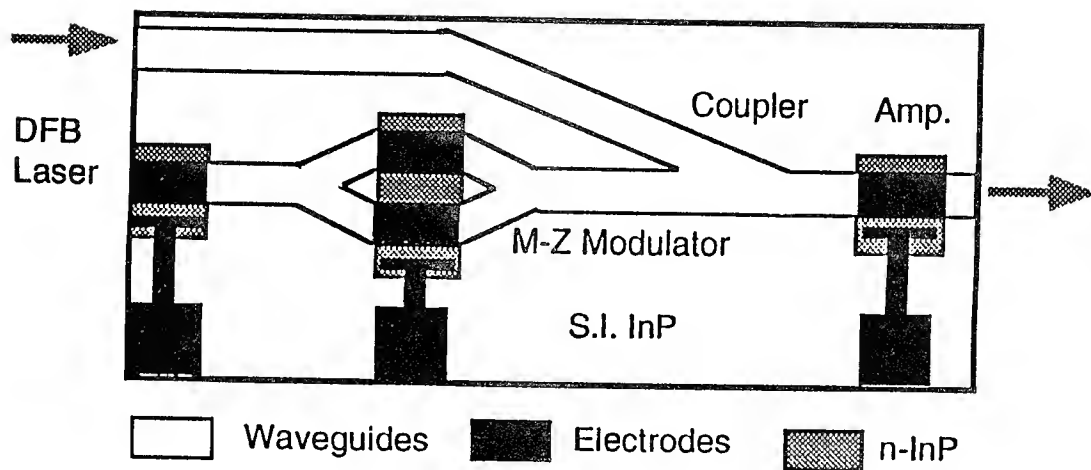


Figure 7. Cascadable, Monolithic Laser/Modulator/Amplifier Transmitter.

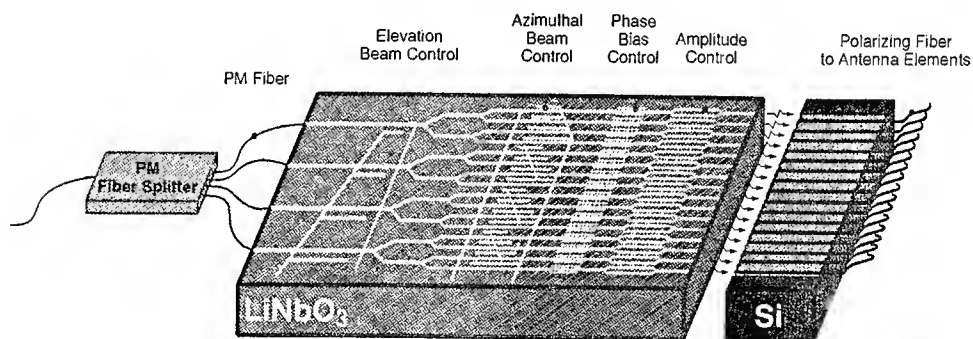


Figure 8. Integrated Phase and Amplitude Controller.

OPTICAL FIBER NETWORK CHARACTERIZATION :
WORK IN PROGRESS AT NATO PANEL IV,
RESEARCH STUDY GROUP 12

J. Isbert and J-M Maisonneuve

Abstract

The OTDR technique may solve the problems of characterizing and monitoring short-haul optical fiber networks with some limitations. We analyze these possibilities and these limitations in the frame of an inter-laboratory measurements comparison.

Experiments have been carried out on a basic short-haul multimode fiber network, with two types of apparatus. The first one detects the Rayleigh backscattering signal and the Fresnel reflections, the second one only detects the Fresnel reflections.

This work aiming at addressing the characterization of future networks, we propose recommendations concerning testing methods as well as we take into account their requirements in the design of the network.

I. Introduction

Optical fiber networks are likely to play an important role in data transmission in a large field of applications, especially in military field. Thanks to its performances (especially high data rate and low attenuation), this medium has been considered as the solution in telecommunication systems, replacing wire in long distance links and challenging it in local uses.

In this domain, after its new technology become usual, fiber will provide two more advantages : the dielectric material it is made of and the characteristics of the optical wave it guides. Concerning the first point, the network subscribers are electrically isolated from each other ; for the second one, the physical layer of the network can be tested simultaneously and regardless of the information transmitted through the fiber.

We are interested in this paper in passive optical short distance networks and in methods and procedures to test them. In this way we have considered the OTDR (optical time domain reflectometry) based on optical amplitude measurements, standing as a, but not unique, candidate to this kind of task.

II. Characterization requirements

An optical fiber transmission network needs, as any other system, (i) components to be characterized apart, in particular regarding their attenuation, (ii) network bearer to be tested after concatenation, (iii) ageing to be followed up, during network life time, taking into account the fault finding without disturbing the functioning.

These problems have to be addressed in the specific context of each application characterized by network topology, fiber length, components density, etc.. As an example, in the telecommunication domain, the test strategy for present-day networks is aimed to test the network that has just been installed in order to commission it, to find a fault when it is reported and, in a more longer term, to monitor the network [1]. The advantage of this third function is that it may detect faults before they affect the transmission of information.

As far as plenty of measurements are necessary to perform all these tasks, we, in NATO research study group, think that OTDR might be adapted to such a job, at least partly. Since we need to measure the attenuation of each component, or its variations, without to disconnect it from the network, and to localize a defect, a method which uses only one end of the network to check all the components is very attractive. However, we intuitively

make out that the signal from such a apparatus will not be easy to interpret, because of the multiple paths from the head-end.

In that way and anticipating this problem will become crucial for short distance optical fiber applications, we formed, in 1990 with NATO Panel IV RSG 12, a task group, the NTTG to address this problem and propose recommendations.

III. Work in progress in nato panel IV RSG 12

In the frame of NATO Defence Research Group (AC/243), Research Study Group number twelve (RSG 12) of Panel IV (optics and infrared) has carried out activities on fibre and associated optics technology, especially on nuclear and modal effects [2, 3]. In the above-mentioned context, a task group has been created in 1990 named NTTG, for Network Testing Task Group, in order to address the problem of testing and controlling the physical layer of the future optical fiber short distance networks.

Five countries joined this task group (see the list hereafter) and participated to an interlaboratory comparison in characterizing typical passive network breadboard by their own OTDR.

The aim of this research group was to analyze the needs and difficulties of characterizing optical fiber networks, to carry out some experiments on breadboards in an interlaboratory comparison in order to identify or define convenient apparatus, methods and procedures in particular in OTDR domain, and to propose recommendations to network designers and testers.

Its a priori limitations for this application come from the complexity of the signature formed with a high concentration of echoes from the many interfaces and the superimposed multiple reflections going back and forth between these interfaces. Moreover, due to the high power losses of such networks, the dynamic range of

the OTDR can lead to severe limitations in the use of this technology.

Two different types of OTDR, the characteristics of which are presented in Table1, are to be considered according to what they are able to detect, either the Rayleigh backscattering signal and the Fresnel reflections (type 1 : Rayleigh mode), or the Fresnel reflections only (type 2 : Fresnel mode). The main difference between them comes from the level of energy per pulse they launch into the fiber, which depends on the pulsewidth. With the present semiconductor laser diode technology, roughly speaking, pulsewidth below one nanosecond leads the OTDR only to detect the reflections ; if it is above that value, the apparatus can receive the Rayleigh scattering and the Fresnel reflections.

Apparatus type	Pulsewidth	Dynamic range	Wavelength
1 (Rayleigh)	2 - 3 ns	≈ 10 dB	0.8 - 1.6 μm
2 (Fresnel)	≈ 100 ps	≈ 40 dB	0.8 - 1.6 μm

Table 1 : Main characteristics of the OTDR's

Various apparatus of those two types were used to test two typical network breadboards described hereabove. The basic network architecture consists of three concatenated passive couplers, one outer port of the first coupler being linked to one inner port of the second one, and identically for the second and the third coupler.

The figure 1 herebelow shows the sketch of a network breadboard called EUNET, using 100/140 silica step index fibers and 4x4 torsion-fusion couplers, the fiber lengths being chosen to get separate reflections from the ends of the different paths. Different configurations of the network topology can be simulated by the fibers P1 to P4.

The second breadboard shown in the figure 2 is called USNET and is made

of 50/125 silica graded index fibers and 2x2 ion-exchange glass couplers. In this case $P1 = 10$ m, $P2 = 13$ m, $P3 = 16$ m, $P4 = 1.8$ m, and the fiber length from the outer port of a coupler to the inner port of the next one is 20 m.

For both breadboards, it has to be noticed that an inner port of the couplers is provided with a 20% reflection piece of mirror or silicon glued on the end of the fiber, to simulate a transmitter, and mode independent couplers and keyed connectors have been used to get rid off modal effect.

NTTG is now analysing the results of the round robin tests and preparing recommendations to design and test the optical fiber short distance networks.

The measurement procedure for each network described as follows :

1) Acquisition of the individual signature of the couplers

(see fig. 3).

2) Acquisition of the signature of the two concatenated couplers

(see fig. 4).

3) Acquisition of the signature of the three concatenated couplers

(see fig. 5, 6, 7).

4) Fracture localization : the fracture is simulated by a connector inserted in the special rig P4. It has to be connected in turn to F1, F2 and F3 respectively in place of P1, P2 and P3. Comparison of the obtained signatures with the basic network signature.

The following plots (fig. 3 - 7) show some results of the tests. Figure 3 shows a backscattered of I1, F1, P1 and O1. The signatures in the backscatter and in the Fresnel mode are shown (coupler C1 and coupler C2, figure 4). The locations of discontinuities indicated by the Fresnel mode (lower trace) can be attributed to the corresponding spatial positions in the broad saturation peaks and long dead zones in the backscatter traces (upper trace).

Figures 5 and 6 show a complete signature of the USNET and figure 7 a complete signature of the EUNET.

The following diagram (fig. 8) shows (USNET) the identification of discontinuities (connectors, end of fibers) concerning for most laboratories involved in this inter-comparison. Both apparatus (Rayleigh and Fresnel modes) are used for characterisation of the network.

Primary reflections due to index discontinuities at connectors and terminations can generally be located and identified from their temporal positions. Reflected intensities are roughly consistent with nominal network losses.

Distant reflections for the 3 coupler USNET were close to the sensitivity of the Rayleigh mode apparatus. The one - way loss of the network was approximately 10 dB. The complete EUNET is not matched for the test by Rayleigh mode apparatus (one - way loss ≈ 20 dB).

Both networks can be tested by Fresnel mode apparatus.

.Multi-pass reflections enormously complicate the interpretation of OTDR data.

.No information on the retrograde coupler ports was available directly.

.The multi-pass reflections can be greatly enhanced by installing a mirror on one of the forward terminations. This allows examination of the retrograde terminations using the same measurement setup. Each location of the mirror produces its own unique "footprint".

V. Discussion - Recommendations

Since NTTG ends its work only at the end of 94, these are preliminary recommendations.

The OTDR looks likely to be adapted to short distance network when only considering the amplitude and the localization of the reflections. The monitoring of the network while it is functioning is allowed by using a different wavelength from that of the signal. However the use of OTDR, which give directly access to attenuation measurements, and the interpretation of the signal in both cases can be facilitated, if one follows some rules which affect the topology as well as the components.

As regards the architecture of the network, it will be preferable to push the linear topologies opposed to star topologies, commonly called "buses", since it simplifies the OTDR signature and makes easy testing and monitoring, because OTDR is more adapted to serial events characterization than parallel one. Providing that an input is placed every 10 dB, it is allowed to use such an apparatus to measure directly the attenuation of each component of the network.

Concerning the components, it is essential to choose low reflection and dispersion ones. The first requirement consequences are low dead zones, low level of parasitic echoes and the possibility of using a high sensitivity measurement system to detect the faults in better situation.

The second requirement implies a higher sensitivity to detect a small variation of characteristics of components (attenuation, return loss coefficient).

In fact the ideal case is a bus (serie network) with an access every 10 dB path (dynamic of OTDR in high resolution mode) composed of monomode optical fiber components (low attenuation, low return loss and low dispersion).

Although a star topology is not suited, a part of a serie network could be implemented with this type of topology on condition that it must be integrated into a boundary area with easy access (of each branch of the star coupler).

Conclusion

These inter - laboratory measurements of network by OTDR technique allow to compare apparatus and methods.

After analysis of laboratory results we proposed some recommendations about architecture and components of optical fiber network for short haul applications.

This assessment of methods and OTDR apparatus will permit to develop automatic measurements in order to memorize a reference mapping of a network, and a periodic comparison, between reference and characteristics of a network, for monitoring and remote testing.

This basic laboratory comparison could contribute to the definition of apparatus and method to be integrated, as a remote fiber testing system. That should help improve the overall network reliability and maintainability while reducing operating and maintenance cost, which represent a critical parameter for telecommunication and aeronautical fields.

A future work could be in WDM filters (wavelength - division multiplexing) for testing the network (in service) with another wavelength than transmission signal, that heads to a 100 % surveillance of a network.

The second way could be in the study of an improvement (in time and space) of a network signature by the design of the architecture well matched to the OTDR technique and also by the insertion of a specific filters (Grating Bragg filters) in order to obtain, with a wavelength tunable OTDR, a signature without ambiguity (a specific reply for

each branch of an arborescent network).

Acknowledgements

We express our thanks to L.A. Coryell (CECOM, NJ, USA), Dr D.C. Johnson (CRC, Canada), M. LIZOT (DGA, DRET France), Dr J Maier (DASA, Germany), Ms A. Meshal (CECOM, NJ, USA), J.W. Ogle (LANL, NM, USA), Dr R. Payne (RL, MA, USA), G. Raimondi (CEAT, France), Dr U. Unrau (Tech. Uni. Braunschweig, Germany), D. Vidal (SCHLUMBERGER, France), Dr A. Zucchinali (SIRTI, Italy), for their participation in this task and the fruitfull discussions we had on that subject.

References

1. N. Lewis, P. Keeble, D. Ferguson, "Testing strategy for modern fibre network architectures", NIST Special Publication 839, Technical Digest, Symposium on Optical Fiber Measurements, 1992.
2. PanelIV RSG12 Nuclear Effects Task Group, "Interlaboratory comparison of the transient radiation-induced attenuation in optical fibres", NATO DRG Technical report AC/243(Panel4), 1993.
3. PanelIV RSG12 Modal Effects Task Group, "Modal effects in multimode optical fibre network", NATO DRG Technical report AC/243(Panel4), 1986.

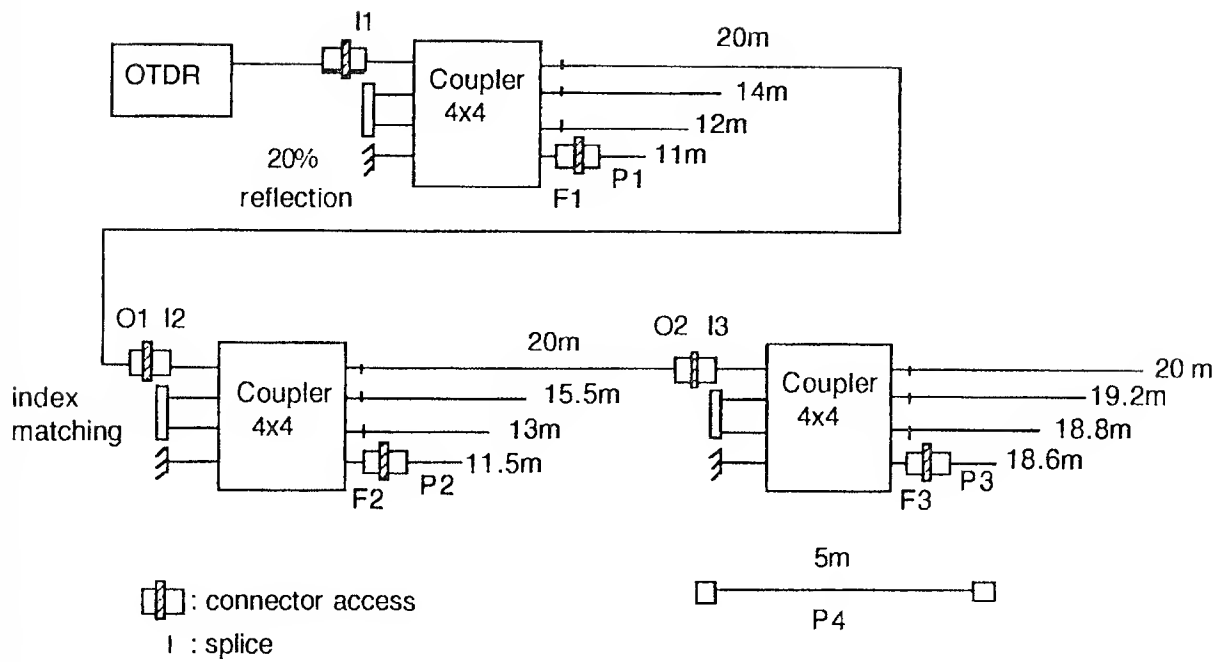


Fig. 1 : EUNET Network

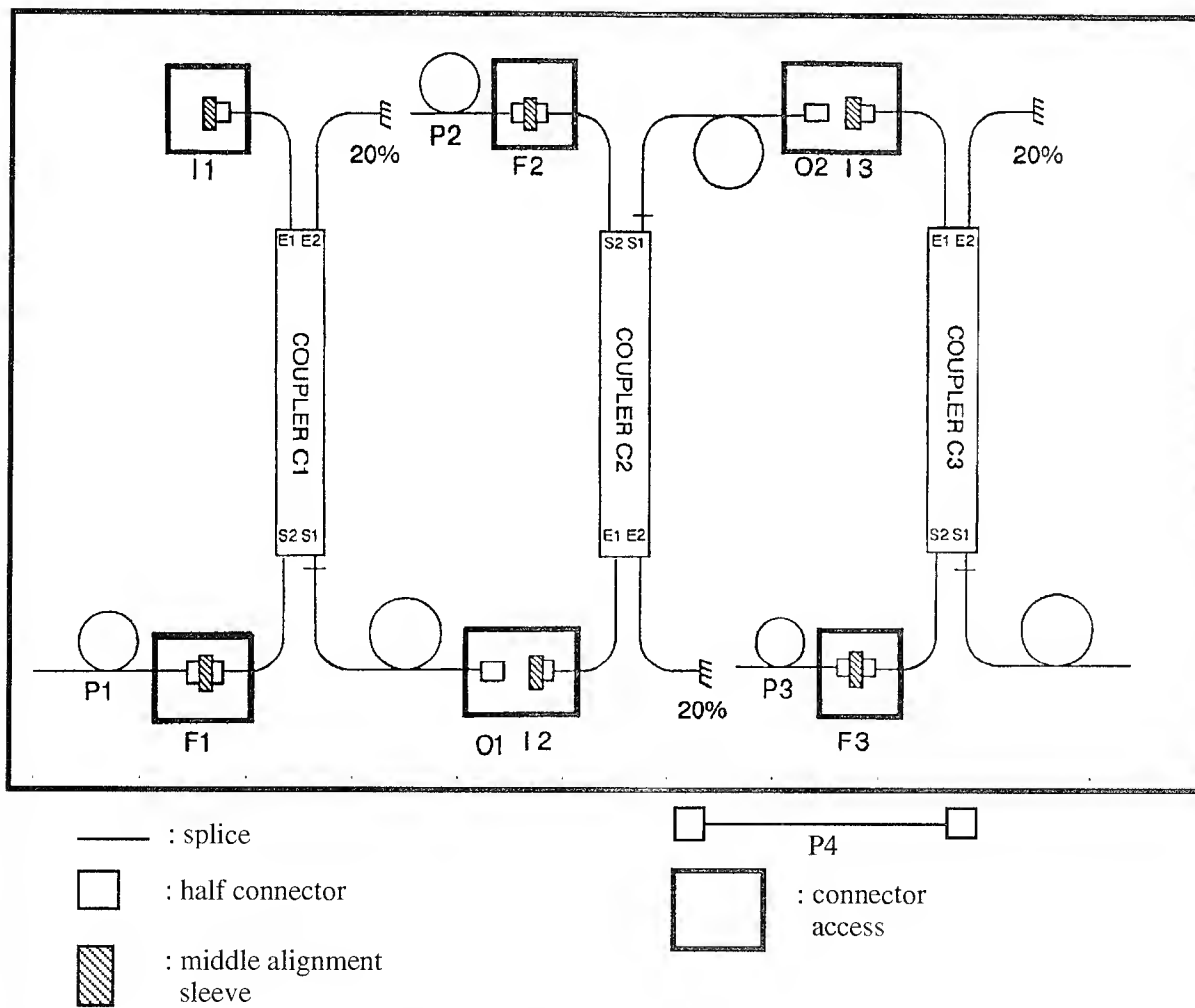


Fig. 2 : USNET Network

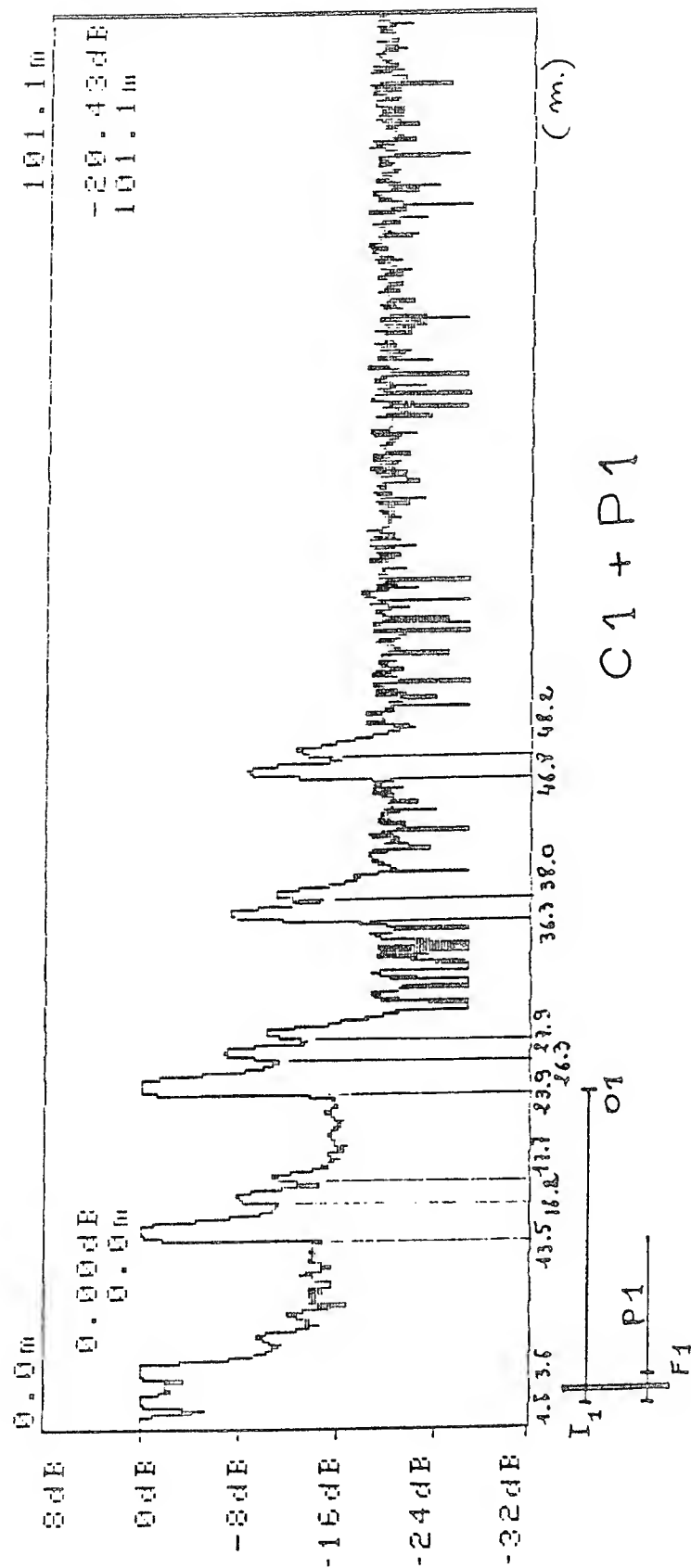


Fig. 3 - USNET 2 concatenated couplers.

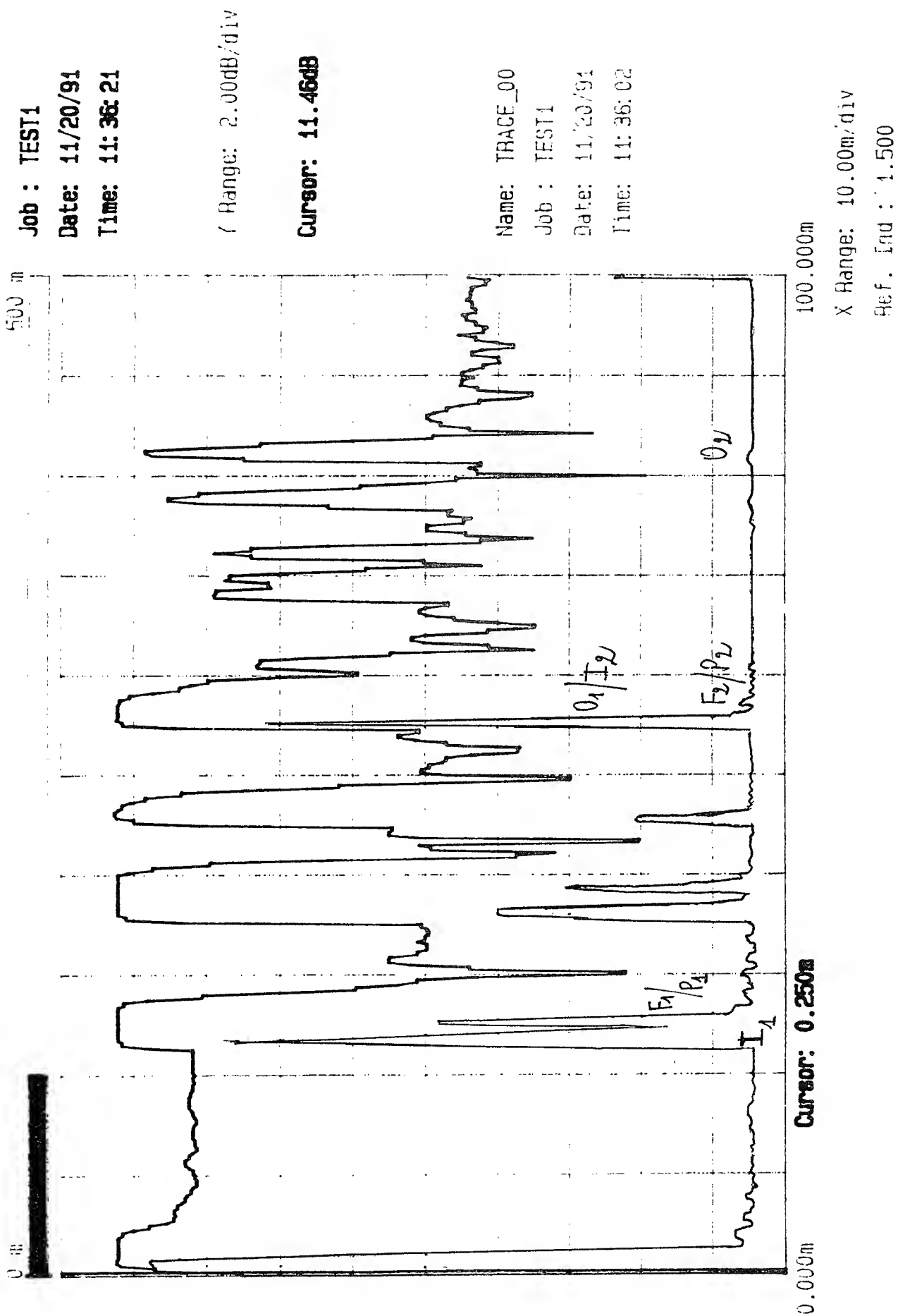


Fig. 4 - EUNET Rayleigh mode (upper trace) signature Fresnel mode (lower trace)

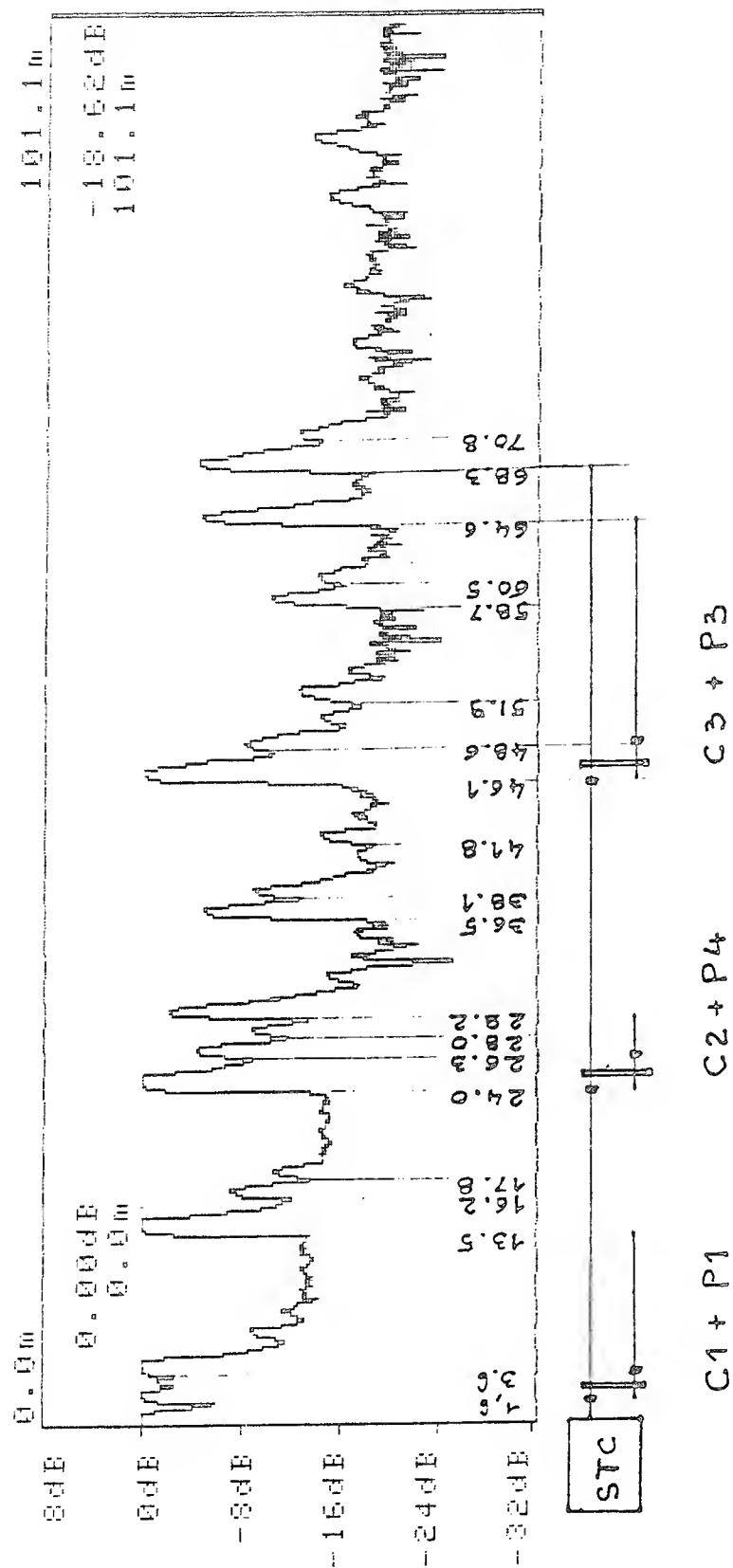


Fig. 5 - USNET 3 concatenated couplers

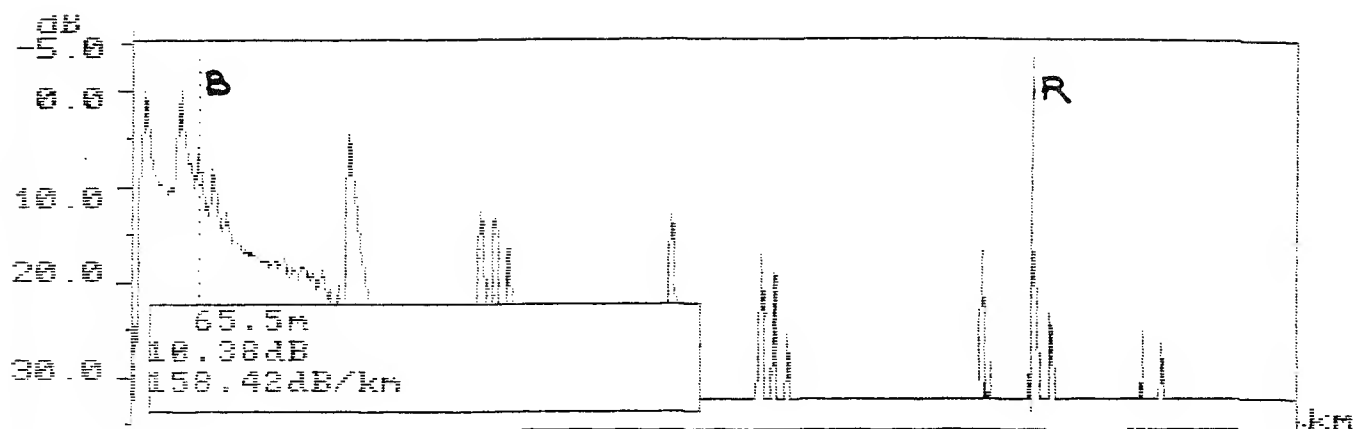


Fig. 6 - USNET : complete network

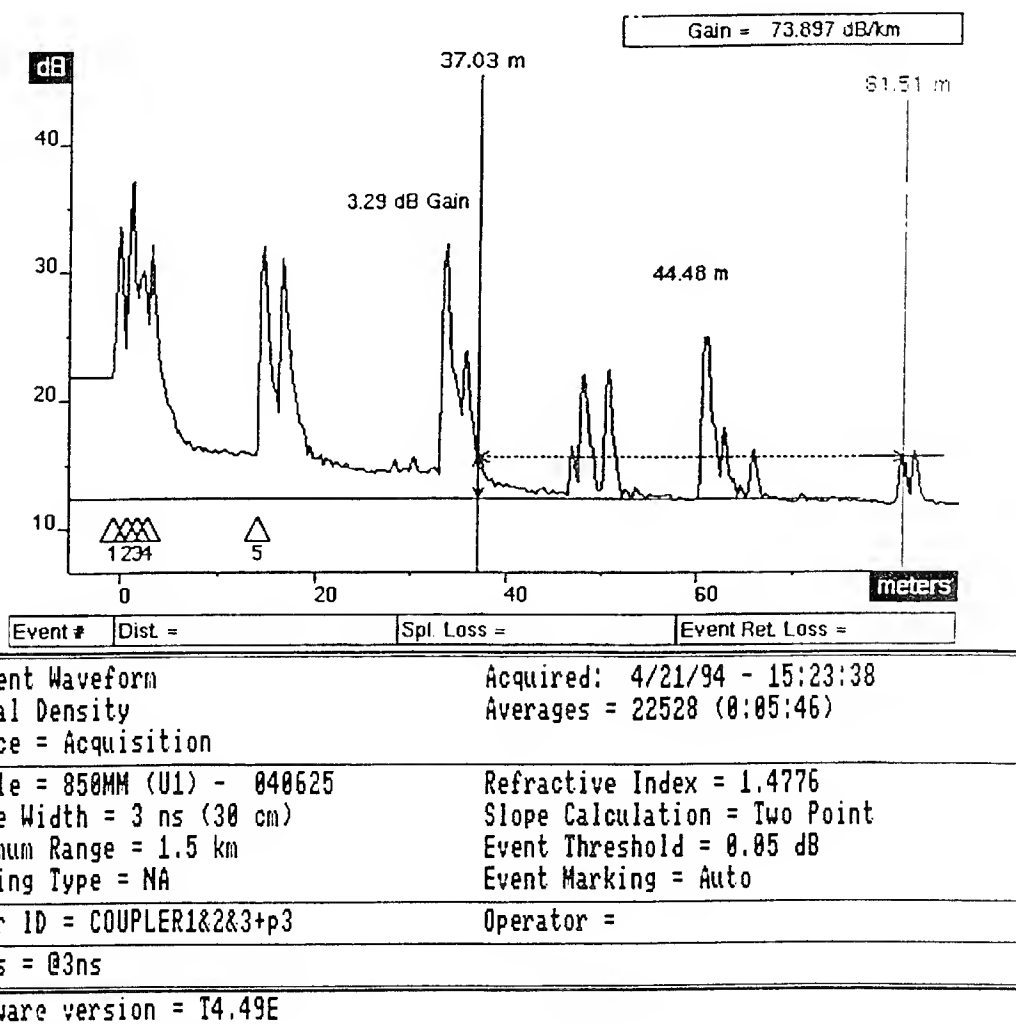
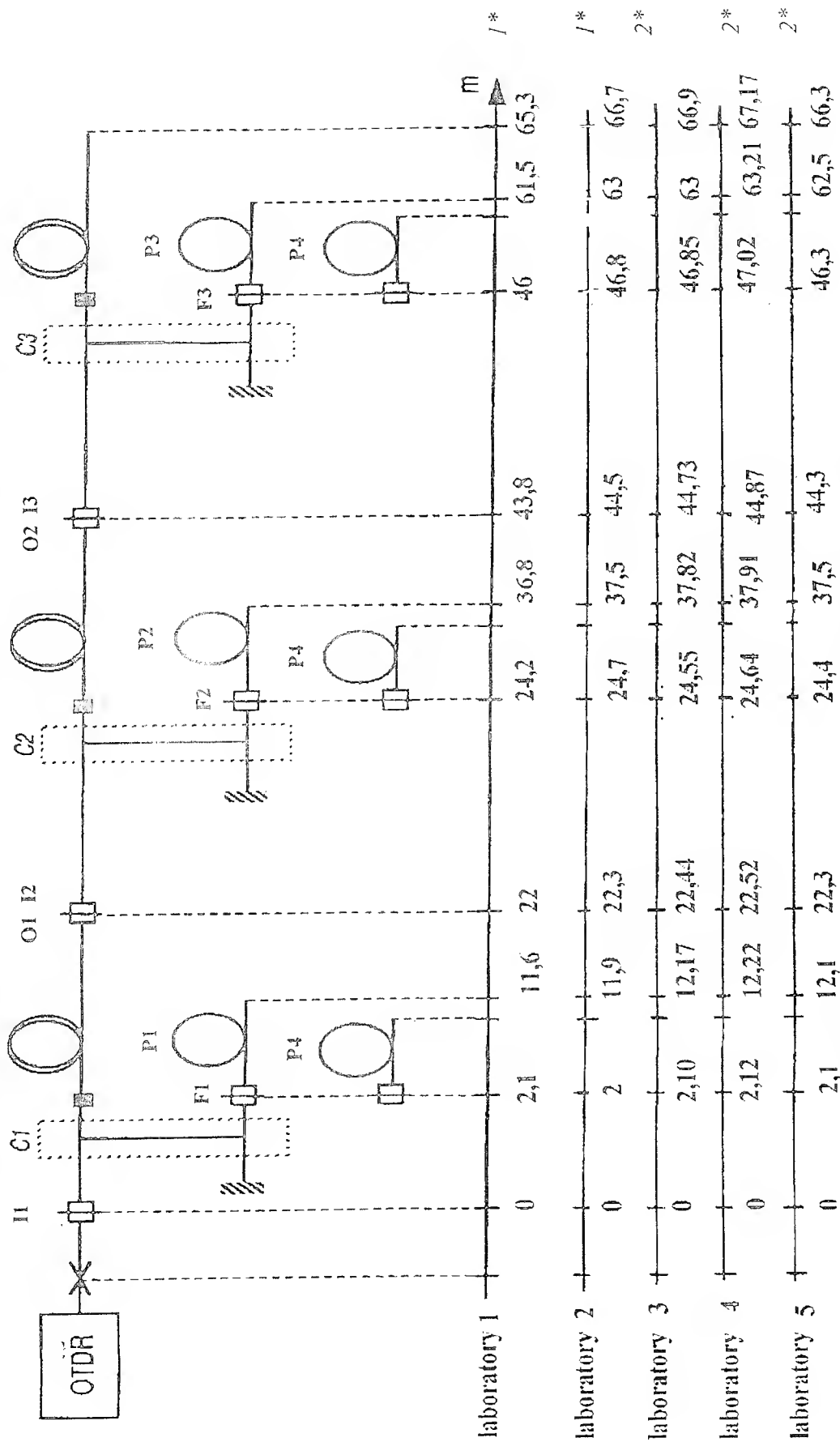


Fig. 7 - EUNET : complete network

Localization of Events by OTDR Method



1* : OTDR type 1 (Rayleigh and Fresnel measurement) 2* : OTDR type 2 (Fresnel measurement)

Fig. 8

Department of optics

Jean-Michel MAISONNEUVE and Jacques ISBERT are with Centre d'Etudes et
de Recherches de TOULOUSE F 31055 TOULOUSE France



MAISONNEUVE J



ISBERT J

DEVELOPMENT OF STANDARDIZED TEST PROCEDURES FOR RADIATION EFFECTS IN OPTICAL FIBERS BY THE NATO NUCLEAR EFFECTS TASK GROUP

E.J. Fricbele

Naval Research Laboratory, Washington, DC 20375

ABSTRACT

This paper summarizes the work of 17 laboratories in NATO Panel IV, Research Study Group 12, Nuclear Effects Task Group over a period of 8 years to obtain consistent measurements of the attenuation induced in optical fibers by steady state and transient radiation exposures. Consistent interlaboratory agreement has been obtained, and critical parameters for standardized testing have been identified. The results of the studies of fibers are being established as new test procedures, EIA FOTP-64 and FOTP-121.

INTRODUCTION

Since optical fiber data links and fiber sensors may be deployed in applications which might be exposed to radiation, it is important to determine the change in optical attenuation in the fiber induced by the radiation environment. Steady state environments include space, fallout, delayed gamma, nuclear reactors, medical applications, and hazardous waste monitoring, while potential transient radiation sources are pulsed fusion reactors, pulsed laboratory facilities, or military radiation environments. The incremental loss can be measured by conventional transmission or reflection techniques, but it is of the utmost importance that these measurements be standardized, that the parameters critical for consistent, reliable results be identified, and that values for these parameters be adequately specified.

In particular, measurement of the response of fibers to steady state environments addresses the growth of the incremental loss during exposure and the recovery following the irradiation, while transient measurements are primarily concerned with the recovery of the incremental loss following a high dose rate-pulsed radiation exposures of ≤ 100 ns duration. This paper will summarize the results of interlaboratory comparisons of the responses of fibers exposed to ^{60}Co steady state and various pulsed electron and x-ray radiation sources performed by members of NATO Panel IV, Research Study Group 12 Nuclear Effects Task Group. Three papers have been published summarizing steady state measurements[1,2] and transient results.[3]

Over the 8 year time period during which the comparisons were made, the tests have progressed from step

index silica core 100/140 multimode fibers at 0.85 μm to 1.3 μm , followed by measurements of graded index fibers at 1.3 μm , single mode waveguides at both 0.85 and 1.3 μm , and polarization-maintaining fibers at 1.3 μm . The 17 laboratories involved in the tests were: the Air Force Systems Command Weapons Laboratory (WL-now Phillips Laboratory), Air Force Air Logistics Command (SM-ALC), Aerospace Corporation, Boeing Aerospace Corporation, Commissariat à l'Energie Atomique (CEA) and Direction des Recherches, Etudes et Techniques-Etablissement Technique Central de l'Armement-Centre d'Etudes de Gramat (CEG) in France, EG&G Santa Barbara Operations, Fraunhofer-Institut für Naturwissenschaftlich-Technische Trendanalysen (FINT) and KFA in Germany, Harry Diamond Laboratories (HDL), the Jet Propulsion Laboratory (JPL), Lawrence Livermore National Laboratory (LLNL), Los Alamos National Laboratory (LANL), Messerschmidt-Bölkow-Blohm GmbH (MBB-now Deutsche Aerospace AG) in Germany, Naval Research Laboratory (NRL), and Royal Military College of Science (RMCS) and STC Technology Ltd. (STC) in the UK. Except as noted above, the laboratories were in the US.

RESULTS AND DISCUSSION

Steady State Transmission Measurements. Initial measurements carried out by the participating laboratories in 1984 using their own "standard" test conditions revealed a wide range of measured responses.[1] The first attempt at standardization was specification of 1 μW optical power in the fiber, a measurement wavelength near 0.85 μm , and specific combinations of dose rate and total dose shown in Table I. For the first set of measurements, the fibers were to

Table I Dose Rate and Total Dose Combinations Specified for Steady State Tests.		
Combination	Dose Rate (Gy/min)	Total Dose (Gy)
A	3	30
B	13	100
C	13	1000
D	100	10000

be irradiated using combination A, i.e. a dose rate of 3 Gy/min to a total dose of 30 Gy. (The Gray is the SI measure of absorbed ionizing dose = 100 rad = 10^4 erg/g). Fig. 1 shows the data reported by 4 laboratories who measured the 100/140 silica core fiber A nominally under the specified conditions. It is obvious that the agreement was not good--the average mean incremental loss at 20 Gy was 4.00 dB/km, but the standard deviation was 0.97 dB/km, i.e. approximately 25% of the induced loss. This wide variance was attributed in part to differences in source wavelengths from 0.828-0.850 μ m, optical powers from 0.75-1.0 μ W, dose rates from 1.92-3.04 Gy/min, sample coil diameters from 3.7-58 cm, and injection conditions.[1]

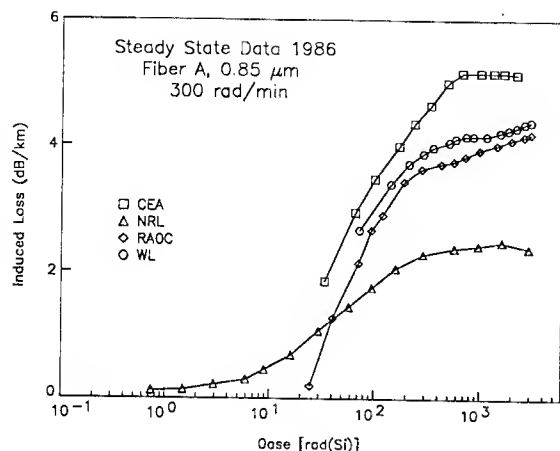


Figure 1. Growth of the radiation-induced optical absorption at 0.85 μ m in a 100/140 silica core multimode fiber during nominally 3 Gy/min steady state exposures to 30 Gy. The lines connect the data points. Note that 1 Gy = 100 rad.

Additional specification was thus implemented in later tests.[2] In particular, identical fiber-pigtailed LED's were distributed to participants, and a test protocol for assuring 1 μ W of injected power in the fibers was established. It was found that the presence or absence of mode scrambling and mode stripping had little effect on the measured loss, and an experiment conducted to compare the measured incremental loss using 70/70 limited phase space injection conditions[4,5] vs. simple fusion splicing demonstrated equivalent results.

Results typical of the improved agreement are shown in Fig. 2 for a 1.3 μ m silica core single mode fiber.[2] The mean peak incremental loss is 2.70 dB/km, and the standard deviation is only 0.35 dB/km. (The RMCS data were excluded from this calculation because they were obtained with an optical power level significantly lower than specification, which inhibited any photobleaching that occurred during exposure and made comparison with the other data meaningless.) Note that because of increased radiation hardness and longer wavelength of measurement, it was necessary to expose this fiber to dose-dose rate combination B to obtain sufficient induced loss for significant comparison. Under the tighter specifications, standard

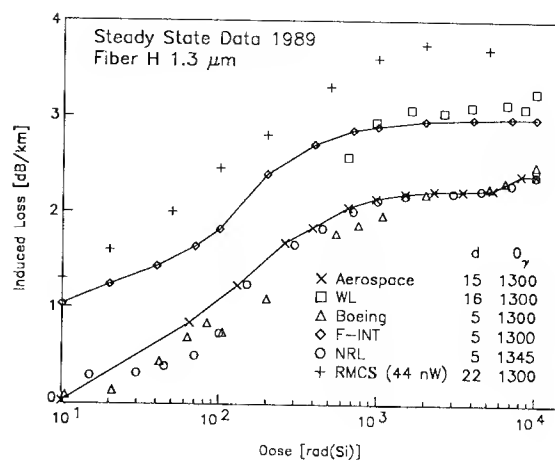


Figure 2. Growth of the radiation-induced optical absorption in a single mode silica core fiber during 13 Gy/min steady state exposures to 100 Gy. Note the different sample coil diameters d(cm) used by the laboratories. The two lines connect data sets of the two groups of laboratories reporting similar radiation responses (see ref. 2).

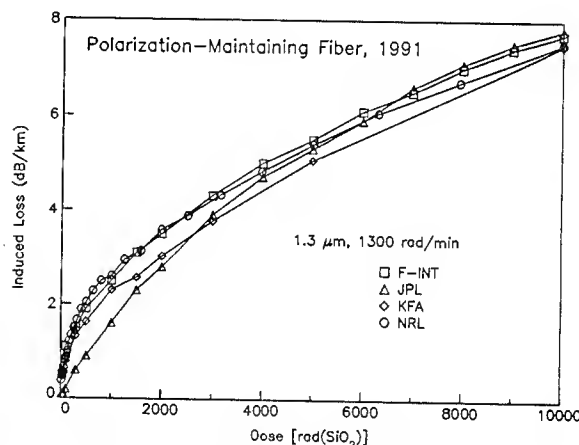


Figure 3. Growth of the radiation-induced loss in a 1.3 μ m polarization-maintaining fiber during steady state exposure.

Figure 3 contains the growth of the induced loss reported in 1992 on a rad-hard polarization-maintaining fiber during steady state ^{60}Co exposure. Four laboratories reported data at 1.3 μ m, and 2 of the 4 used dose rates close to the specified rate of 1.3 Gy/min (1300 rad/min). (Because the maximum rate attainable by KFA is 215 rad/min, the data plotted in Fig. 3 have been normalized by assuming that the fading effects are independent of dose rate and absolute induced loss. The measured induced loss during the 215 rad/min exposure was normalized to 1300 rad/min by dose and irradiation time.) As shown in Fig. 3, the agreement is quite good and that there is no apparent effect of variations in wavelength between 1.26 and 1.3 μ m or dose rate from 215 (normalized as described above) to 2120 rad/min in this fiber. For the 4 laboratories the average induced loss at 10^4 rad is 7.64 dB/km with a standard deviation of only 0.145 dB/km, i.e. 1.9%.

Figure 4 shows the growth of the radiation-induced attenuation reported on a 1.55 μm polarization-maintaining fiber during steady state ^{60}Co exposure. Three laboratories reported data for this fiber, two of which (Aerospace and F-INT) used dose rates approximating the specified 1300 rad/min and two of which (F-INT and NRL) used optical sources of nearly identical wavelength. The agreement in the growth data between F-INT and NRL is quite good, in spite of the larger dose rate used by NRL, while the loss reported by Aerospace is significantly less than that of the other two laboratories due to the fact that Aerospace was required to place the fiber spool close to the radiation source (13 cm), and there may be substantial dose nonuniformity across their 16 cm diameter fiber sample coil. Neglecting the Aerospace data, the average induced loss at 10^4 rad is 3.90 dB/km with a standard deviation of 0.07 dB/km, i.e. 1.8%. Although this is based on data from only two laboratories, it represents the best agreement yet obtained by the NETG for steady state measurements. It is also significant to note that this is the first measurement of any fiber at 1.55 μm by the NETG, and excellent agreement has been achieved in spite of the potential added complexity of measuring a polarization-maintaining fiber.

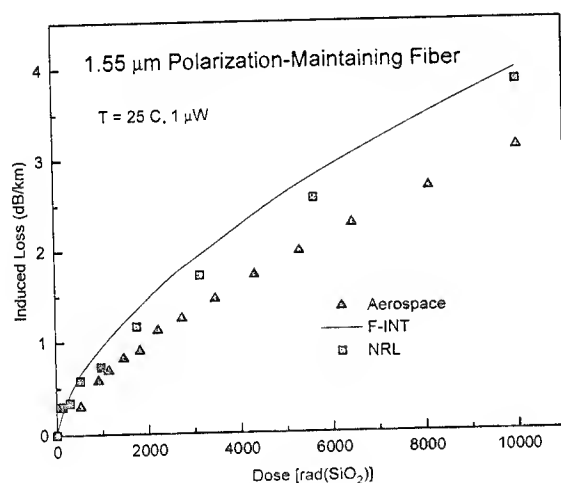


Figure 4. Growth of the incremental loss at 1.55 μm in a polarization maintaining fiber by steady state radiation exposure as measured by 3 laboratories.

OTDR vs. Transmission Measurements. Another activity of the NETG involved comparison of the radiation-induced loss measured by the *in-situ* transmission technique used above and by optical time domain reflectometry (OTDR). In some cases OTDR would be preferable because it requires access to only one end of the irradiated fiber, it is self-referencing if a length of unirradiated section precedes the test length, and it is not subject to long-term drift which typically degrades the measurement of incremental loss growth in low dose rate environments or recovery for long periods ($\geq 10^4$ sec). The fibers selected for measurement had been well-characterized in previous years, and both OTDR and transmission data are shown in Fig. 5. It is apparent that the

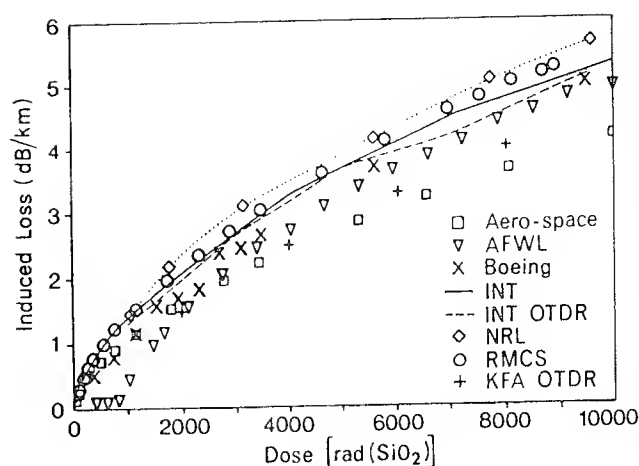


Figure 5. Comparison of the growth of the steady state incremental loss of a single mode fiber measured by transmission and OTDR techniques. Except as noted in the legend, data were obtained by transmission techniques.

OTDR data consistently falls within the range of transmission data reported for the different fibers. Note that in some cases, the OTDR data reported by a laboratory are actually in *better* agreement with the transmission data reported by the other laboratories than the original transmission data! In Fig. 5 there is excellent agreement of the F-INT OTDR data with the transmission data; the larger incremental loss measured at NRL by OTDR is likely due to the higher dose rate used in these tests.

In spite of the excellent agreement obtained in these tests, there are several factors[6] which need to be considered in using OTDR: 1) It is especially important to achieve an equilibrium mode distribution in multimode fibers through use of a lead-in, unirradiated section of the original fiber and to remove cladding modes; 2) One must be careful not to exceed the dynamic range for linear response of the OTDR instrument; 3) The type of OTDR head (i.e. single mode or multimode) must be matched to the fiber type under study; 4) An alternate optical source must be provided to maintain the required power (1 μW) injected into the fiber since the OTDR measurement is made periodically and adjustment of the OTDR power is not usually possible on commercial instruments; and 5) Because of the time required for an OTDR measurement, the technique is useful only when the optical attenuation is not rapidly changing, i.e. under low dose rate exposure or at long times following exposure.

These comparisons of steady state fiber responses have demonstrated that for consistent measurements it is essential to adhere to specified total dose-dose rate combinations and optical powers to minimize photobleaching differences, while variations in injection conditions do not appear to contribute significantly to variations in measured response. Although improvements have been achieved in interlaboratory results, there remain variances in reported measurements which may arise from factors such as differences in sample coil diameter, source spectrum due to

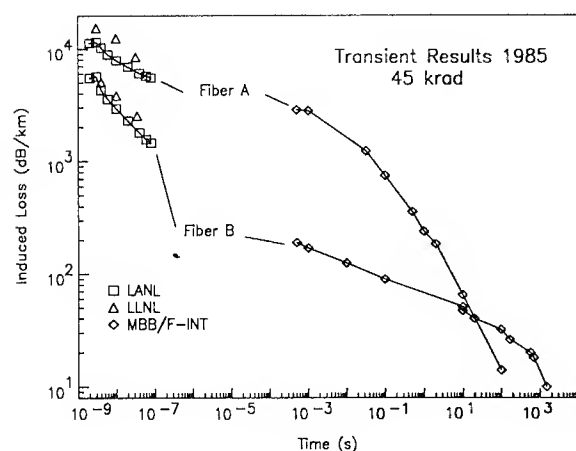


Figure 6. Transient radiation-induced absorption near 0.85 μm reported by 3 laboratories in 1985 on 100/140 low- and high-OH silica core fibers A and B, respectively. The lines connect the LANL and MBB/F-INT data sets.

moderation by either water or air between the source and sample, and the effect of dose buildup layers. Dose buildup occurs where the dose experienced by subsequent layers of fiber increases due to the enhanced stopping power for low energy electrons ionized from the air surrounding the fiber and the low energy component of the γ -ray source spectrum.

Transient Measurements. An example of the lack of agreement at the beginning of the study is shown in Fig. 6.[3] Since the 3 reporting laboratories used doses varying from 440 to 1200 Gy, the data have been normalized to 450 Gy. The LLNL spectral data were extrapolated to 0.84 μm , while LANL and MBB/F-INT used 0.84 μm LED's. Optical powers in the fiber varied from 0.2 to 300 μW . Note also the lack of temporal overlap between the data sets, precluding detailed comparisons.

To minimize the variations in test conditions among the laboratories, the level of specification of radiation and optical parameters was increased throughout the period.[3] Dose levels of 5, 100 and 1000 Gy were to be used, optical sources at 0.84 and 1.3 μm with powers of 1 μW were suggested, and significant efforts to improve dosimetry were undertaken.

An example of the excellent agreement obtained among 6 laboratories testing a silica core single mode fiber in 1989 is shown in Fig. 7.[3] The experimental parameters were quite consistent: almost all laboratories used a dose of 100 Gy; the optical source wavelengths varied only from 0.83-0.85 μm , and all but two laboratories used 1 μW optical power. This adherence to specified conditions, together with close attention to the dosimetry, resulted in excellent agreement in spite of significant differences in radiation source energy (0.5-25 MeV) and pulse length (1.5-9000 nsec) used by the laboratories.[3]

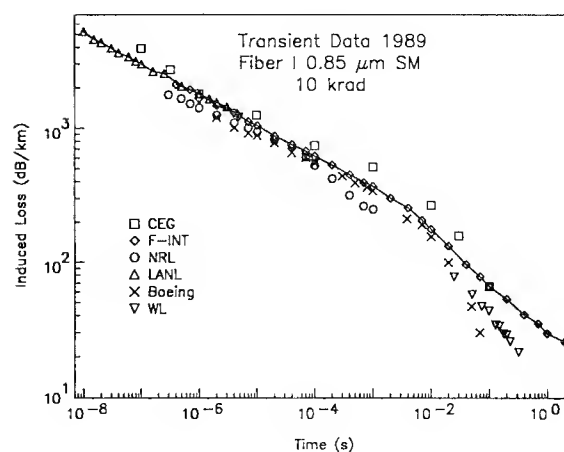


Figure 7. Transient radiation-induced absorption reported by 6 laboratories in 1989 on a silica core single mode fiber at 0.85 μm following an exposure of 100 Gy. A line has been drawn through the LANL and F-INT data sets to aid the eye.

CONCLUSIONS

The work of the NETG has demonstrated that consistent, standardized testing of the incremental loss induced in optical fibers by radiation exposure is achievable, provided the test parameters are properly specified and implemented.[2,3] As a result, an improved test procedure for measuring the response of optical fibers to environmental and adverse nuclear environments has been completed. This has been submitted to NATO and published as a technical report,[7] and it is also in the process of being adopted by EIA as FOTP-64. A derivative test procedure, FOTP-121, has been drafted for neutron effects on optical fibers.

It is clear that excellent interlaboratory agreement has been obtained in the measurement of a wide range of optical fiber types and wavelengths, and the critical test parameters have been identified. However, photonic systems comprise additional components which have not been thoroughly tested and for which test procedures have not been established; emphasis is now being shifted to these devices. In particular, the NETG has performed interlaboratory comparison studies of the radiation response of a 1 x 2 passive ceramic coupler, 1.3/1.55 μm and 0.98/1.55 μm wavelength-division multiplexing couplers, erbium-doped fiber amplifiers, and LiTaO_3 and LiNbO_3 integrated optic devices. Reasonable agreement has been obtained with these devices, and the parameters critical for good interlaboratory agreement are being refined.

There has also been a distinct shift in the world situation, which has impacted the future role of the NETG:

1. Continued support for NATO tactical and strategic applications; support for test procedures and specifications in NATO countries.

2. Applications of photonics for space environments, both natural and enhanced.
3. Investigate testing photonics for the nuclear industry; possible applications include continued support for UGT/AGT activities, nuclear waste cleanup and monitoring, nuclear process monitoring, power plant monitoring.
4. Support for scientific instrumentation in experiments in NATO countries where nuclear environments might degrade optical fibers and components, such as the International Thermonuclear Experimental Reactor (ITER) or the semiconducting supercollider.
5. Investigate the testing and qualification of optical fibers and photonics for medical applications, especially in nuclear medicine.
6. Investigate testing procedures for photonic sensors, e.g. fiber chemical sensors, fiber gyroscopes, and full systems, such as spacecraft fiber optic data buses, local area networks, etc.

The NETG is expanding the environments to which photonic components are exposed in order to be more responsive to system needs. Steady state ^{60}Co irradiations are continuing to be used, but low dose rate studies are considered for space applications. Likewise, both proton and electron, transient electron, x-ray and neutron, and neutron-gamma mixed field radiation environments are being studied to more fully address the applications listed above. Some applications require cryogenic temperatures and/or harsh chemical environments, and these are under consideration as well. Photonic devices to be tested include not only optical fibers, but integrated optic couplers and modulators, sources and detectors, lenses and bulk optics, organic films for holographic gratings and other applications, fiber optic lasers and amplifiers, and couplers and connectors.

REFERENCES

1. E.J. Friebele, E.W. Taylor, G. Turquet de Beauregard, J.A. Wall and C.E. Barnes, "Interlaboratory comparison of radiation-induced attenuation in optical fibers I. Steady state exposures," *J. Lightwave Tech.* **6** (1989) 165-171.
2. E.W. Taylor, E.J. Friebele, H. Henschel, R.H. West, J.A. Krinsky and C.E. Barnes, "Interlaboratory comparison of radiation-induced attenuation in optical fibers. Part II: Steady state exposures," *J. Lightwave Tech.* **8** (1990) 967-976.
3. E.J. Friebele, P.B. Lyons, J.C. Blackburn, H. Henschel, A. Johan, J.A. Krinsky, A. Robinson, W. Schneider, D. Smith, E.W. Taylor, G. Turquet de Beauregard, R.H. West, and P. Zagarino, "Interlaboratory comparison of radiation-induced attenuation in optical fibers. Part III: Transient exposures," *J. Lightwave Tech.* **8** (1990) 977-989.
4. P.R. Reitz, "Measuring optical waveguide attenuation: The LPS method," *Optical Spectra*, August 1981, pp. 48-52.
5. EIA-RS-455-FOTP 46: "Spectral attenuation measurement for long length, graded index optical fibers;" FOTP 50: "Light launch conditions for long length graded index optical fiber spectral attenuation measurements." Electronic Industries Association, Washington, DC.
6. R.H. West, H. Buker, E.J. Friebele, H. Henschel and P.B. Lyons, "The use of optical time domain reflectometers to measure radiation-induced losses in optical fibres," *J. Lightwave Tech.* **12** (1994) 614-620.
7. E.J. Friebele, P.B. Lyons, J.C. Blackburn, H. Henschel, A. Johan, J.A. Krinsky, A. Robinson, W. Schneider, D. Smith, E.W. Taylor, G. Turquet de Beauregard, R.H., "Interlaboratory comparison of the transient radiation-induced attenuation in optical fibers," NATO Technical Report AC/243 (Panel 4) TR/1, 1990.

A FOUR-FIBER TACTICAL FIBER-OPTIC CONNECTOR

Harold Muth
AT&T Network Cable Systems, Norcross, GA

Vasilios E. Kalomiris
CECOM, Space & Terrestrial Communications Directorate, Fort Monmouth, N.J.

ABSTRACT

A four-fiber tactical connector has been designed and its features and performance characteristics are presented. Both singlemode (SM) and multimode (MM) versions are hermaphroditic, sealed against casual water, and fit on 6.0-mm diameter cable. The connector employs closed zirconia alignment sleeves and zirconia 2.5-mm ferrules for fiber termination. Complementary bulkhead connectors have also been developed. Only singlemode performance is discussed. When subjected to thermal shock, high humidity, and thermal cycling, the prototype samples measured at the 1310 nm wavelength had an average insertion loss of 0.5 dB. Insertion loss at the 1550 nm wavelength after environmental testing was higher, indicating greater sensitivity to bending at that wavelength. Further development to control fiber bending within the connector shell should reduce this loss. Reflection averages at 1310 nm and 1550 nm were above 49 dB.

INTRODUCTION

For tactical as well as commercial fiber-optic systems, a four-fiber tactical connector family has been designed. Both MM and SM versions of the connector will accommodate 6.0-mm cables. The newly developed connector is similar to the existing, widely used, two-fiber connector associated with the Tactical Fiber-Optic Cable Assembly (TFOCA), except that the newer connector uses zirconia alignment sleeves and 2.5-mm domed ferrules for fiber termination. Testing of the connector indicates performance, that meets the 40 dB reflection level, in compliance with tactical requirements. This performance characteristic and four fibers make the connector ideal for intrusion-detection transmission systems as well as traditional tactical systems.

BACKGROUND

The requirement of information transmission protection in either voice, data, or video is placed on both military and commercial systems. In military systems, the use of encryption devices for radio or metallic cable links using keys and special codes

has been adapted to meet the requirement of information protection. However, with the adoption of fiber-optic links in long haul, short haul and networking, the need for information protection has been met with the development of the intrusion-detection optical communication system. This system operates on an interferometric principle which enables the system to detect a possible intruder immediately and cease transmitting. The intruder may be able to detect the amplitude of light with a tap, but without the ability to detect the phase changes, no real information can be regenerated.

This intrusion-detection optical communication system has been designed to protect FDDI links of 100 Mb/s, and it can achieve link lengths of 10 km with a cable assembly using the singlemode four-fiber tactical connector discussed here. Two of the four optical fibers are used for each direction of transmission. The fibers are terminated into zirconia ferrules which are mounted in a militarized hermaphroditic shell. Significant development was saved by adopting some of the developments of the earlier two-fiber TFOCA version. (1)

CONNECTOR DESIGN

The connector is shown in Figure 1a. It is 13.7-cm long, 4.2-cm in diameter and weighs 403 gm with its dust cover. The SM and MM connectors are the same physical size and weight and are true hermaphroditic connectors. The rear of the connector seals against water entry around the cable by compressing a compliant taper onto the cable sheath in much the same scheme employed in the earlier TFOCA design. The front of the connector is sealed when mated with another connector or its dust cover. Even without the dust cover, o-rings on the ferrule assemblies prevent water from entering the interior of the connector shell from the front. The dust covers seal against each other when mated and not in use. All of the alignment surfaces of the connector are accessible with a screwdriver for cleaning which eliminates the need for special tool kits. Each connector has a dust cover that is attached with a stainless-steel lanyard. A keying feature prevents inadvertent mating of SM and MM connectors, but within the same type, any connector end mates with any other end or with companion receptacle connectors.

The receptacle connector (flange mount) is shown in Figure 1b. A thread mounted version, not illustrated, has also been developed. Yellow hardware is used to visually distinguish SM connectors. The key alignment components of the connector are closed zirconia sleeves and 2.5-mm zirconia ferrules. Closed sleeves are used to withstand shock. The end faces of the ferrules are domed and are polished to minimize reflection. The cable-retention hardware is similar to existing TFOCA hardware with no adhesive used to grip the cable strength members. The connector geometry, material, and corrosion-resistant finish provide inherent strength and durability and the bulkhead connectors provide effective EMI shielding. These features make the connector resistant to the stringent environment typical of tactical military applications. The connector is repairable in a remote depot.

CABLE ASSEMBLY PERFORMANCE

Twelve cable assemblies were prepared with four-fiber connectors on one end and single fiber connectors on the other end. The single fiber connectors were added to facilitate connection to the test-set. This provided six mated, four-fiber, pairs (24 paths) that were environmentally tested. Abbreviated testing was conducted since many of the design features and materials of this connector are identical to those of previous proven designs. Tests were selected that would be likely predictors of tactical performance. Only singlemode test results are reported. The cable assemblies have been subjected to thermal shock, high humidity, and thermal cycling. Test conditions were as follows:

Thermal Shock (Mil Std 810C M503.1)

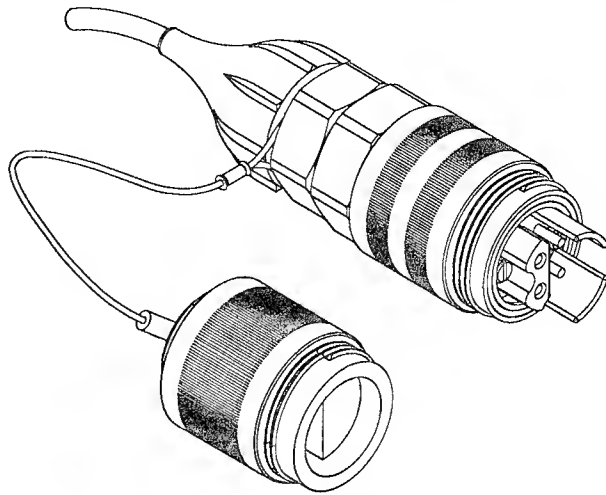
-55°C to +85°C (10 cycles)
30-minute dwell at each extreme
with less than 1-minute transition

High Humidity

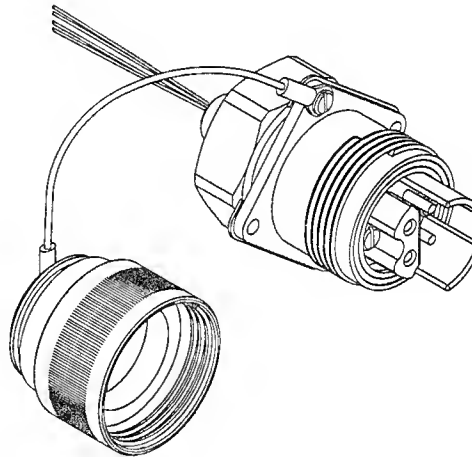
95% RH @ +75°C (14 days)
60-minute dwell at each extreme

Thermal Cycle

-40°C to +75°C (14 days)
60-minute dwell at each extreme



a) Connector and Dust Cover



(b) Receptacle and Dust Cover

Figure 1 - Four-Fiber Connector and Receptacle

Before exposure to environmental changes, insertion loss and reflection measurements were made at 1310-nm and 1550-nm wavelengths. The following means (\bar{x}) and standard deviations (s) are shown in Table 1.

TABLE 1

	1310 nm	1550 nm
Insertion Loss	$\bar{x} = 0.26$ dB $s = 0.22$	$\bar{x} = 0.26$ dB $s = 0.21$
Reflection*	$\bar{x} = 40.46$ dB $s = 4.22$	$\bar{x} = 40.89$ dB $s = 4.30$

*These values include the reflections from a single-fiber connector that was part of the test set up. The power reflected from the four-fiber connector alone is necessarily better; these values serve as an adequate baseline reference for change measurements.

Thermal Shock

Below is Table 2 showing before and after shock measurements of insertion loss at 1310 nm and 1550 nm. In all tables, the measurement sequence is preserved and corresponds to a particular channel.

TABLE 2

Insertion Loss (dB)			
<u>1310 nm</u>		<u>1550 nm</u>	
Before	After	Before	After
0.38	0.03	0.38	-0.10
0.14	0.15	0.14	0.27
0.21	0.14	0.21	0.25
0.59	0.14	0.56	0.02
0.14	0.84	0.20	0.84
0.47	0.27	0.48	0.33
0.31	0.27	0.36	0.30
0.32	0.76	0.31	0.78
0.54	0.58	0.53	0.66
0.04	0.27	0.06	0.38
-0.14	0.20	-0.17	-0.09
0.39	1.29	0.40	1.14
-0.18	0.25	-0.14	0.11
0.23	-0.06	0.19	0.20
0.34	0.19	0.28	0.34
0.34	0.01	0.27	-0.12
0.56	0.53	0.63	0.59
0.31	0.36	0.25	0.35
-0.12	0.01	-0.05	0.02
0.51	0.65	0.59	0.68
0.38	0.22	0.33	0.44
0.28	0.16	0.21	0.35
0.24	0.48	0.21	0.51
0.05	0.45	0.10	0.45
$\bar{x} = 0.26$		$\bar{x} = 0.26$	$\bar{x} = 0.36$
$s = 0.22$		$s = 0.21$	$s = 0.31$

The small negative insertion losses, shown in Table 2, relate to uncertainty and repeatability of the baseline reference or zero of the test configuration. Reflection

measurements were made at both wavelengths and generally improved during the test; numerical values are not reported because they include reflections and changes from the single fiber mentioned earlier. Following the thermal shock test, the undesirable extra connection was eliminated for subsequent tests by employing fusion splices.

High Humidity

The loss-measurement configuration during this test allowed the most accurate measurement of reflection from the four-fiber connector alone and should be most representative. The following is Table 3, the largest (worst) reflections measured during the humidity test.

TABLE 3

Largest Reflections (dB)	
<u>1310 nm</u>	<u>1550 nm</u>
45.0	39.0
49.5	36.5
42.4	37.0
47.9	38.3
45.9	40.9
44.4	41.9
50.1	38.3
44.9	37.2
48.1	39.7
48.8	38.0
45.1	35.8
47.4	37.5
54.3	34.5
48.0	38.2
46.1	40.4
50.8	41.5
47.2	39.0
41.8	36.0
50.0	37.5
44.6	37.3
43.4	35.7
35.5	30.5
46.6	40.5
46.8	40.7
$\bar{x} = 46.4$	$\bar{x} = 38.0$
$s = 3.7$	$s = 2.5$

Changes in individual reflections during humidity testing averaged 2.6 dB with a standard deviation of 1.3 dB at 1310 nm. The average change at 1550 nm was 2.0 dB with a standard deviation of 0.5 dB. Insertion losses changed an average of 0.09 dB and 0.31 dB at 1310 nm and 1550 nm, respectively. The corresponding standard deviations were 0.23 dB and 0.90 dB.

Thermal Cycle

The following is Table 4 showing the largest (worst) reflections measured during thermal cycling.

TABLE 4

Largest Reflections (dB)

1310 nm	1550 nm
44.9	38.8
49.3	36.0
42.1	36.4
47.3	37.6
44.6	40.3
44.2	41.1
49.5	37.7
44.6	36.9
47.7	39.1
48.6	37.5
44.9	35.4
46.4	36.9
60.7	34.1
47.9	37.6
45.9	39.8
50.5	40.8
47.0	38.5
41.7	35.4
50.0	36.8
44.4	36.8
43.6	35.4
35.6	30.3
46.0	39.9
46.2	40.0
x= 46.5	x= 37.5
s= 4.4	s= 2.5

Changes of individual reflections during thermal cycling averaged 3.3 dB with a standard deviation of 2.8 dB at 1310 nm. At 1550 nm the average individual change was 1.8 dB with a standard deviation of 0.8 dB.

Insertion losses changed an average of 0.03 dB with a standard deviation of 0.47 dB at 1310 nm and 0.03 dB with a standard deviation of 0.68 dB at 1550 nm.

After the three environmental tests above, final insertion loss and reflection measurements were made on four of the six mated four-fiber connections. The remaining mated pairs went directly to vibration testing. Insertion loss and reflection measurements were made to assess any lasting effects of the test program. The sample cable assemblies were fusion spliced into a test set cable, and the estimated splice losses were subtracted from measurements. Measurements were made at room temperature.

Below is Table 5 showing insertion losses at both wavelengths. The first two columns of measurements are with the connector as it is normally assembled. The last two columns are with the rear part of the connector unscrewed and the buffered fiber, normally stored, relaxed.

TABLE 5

Insertion Loss (dB)

1310 nm	1550 nm	Relaxed Fiber	
		1310 nm	1550 nm
0.60	2.48	0.47	0.77
-0.19	1.25	-0.08	0.05
0.45	3.83	0.21	0.27
1.72	2.30	1.17	1.11
0.05	1.06	0.04	0.22
0.01	0.70	-0.06	0.09
0.45	2.58	0.36	0.43
0.63	1.50	0.68	0.65
0.07	1.40	-0.07	0.18
0.47	4.16	0.16	0.27
-0.04	1.34	-0.08	0.03
0.38	2.34	0.18	0.43
2.17	5.74	1.16	1.34
0.05	3.23	0.34	-0.13
0.64	5.89	0.01	0.49
0.46	0.99	0.45	0.40
x= 0.50	2.55	0.27	0.41
s= 0.63	1.63	0.43	0.40

It was discovered during insertion loss testing at 1550 nm that the high loss was significantly reduced when the rear part of the connector was unscrewed and the buffered fibers were pulled out and allowed to relax. All of the cable samples were prepared with enough excess buffered fiber to allow two reterminations - one for manufacturing and one for the field. The most significant change occurred in insertion loss at 1550 nm; insertion loss at 1310 nm changed only slightly. The four connectors associated with the two highest losses were examined for end-face damage, fiber pull-back, and fiber cracks or breaks in the ferrule assemblies. Microscopic examination of the end faces at 300X revealed no end-face damage and good finishes. Interference fringes indicated no significant fiber pull-back. No cracks or breaks in the fiber were detected in the ferrule assemblies when they were examined with a high resolution Optical Time Domain Reflectometer (OTDR). To reduce the problem of permanent loss change at 1550 nm, the length of coiled fiber could be reduced, and a less severe method of storing it developed.

Reflections remained essentially the same at both wavelengths with or without the stored fiber relaxed. Below are the reflection averages and standard deviations.

Reflections (dB)

<u>1310 nm</u>	<u>1550 nm</u>
x= 49.7	51.9
s= 3.6	4.5
min 44.9	min 46.6

CONCLUSIONS

Based on tests to date, this four-fiber connector design should meet the requirements for a tactical connector when the loss associated with buffered fiber storage is reduced. The assembly is rugged, easy to handle, and to maintain.

ACKNOWLEDGEMENTS

The authors acknowledge Bruce Darden and J. M. Anderson for their guidance and consultation and Jim Elling, I. L. Pennington, R. L. Sweatt and Mary Wright for sample preparation and testing.

REFERENCES

1. Anderson, J. M., Darden, B. V., LeFevre, Kalomiris, V. E. "A Two-Fiber Tactical Fiber-Optic Connector," Proceedings of the 34th International Wire and Cable Symposium.



HAROLD MUTH is a member of Technical Staff at AT&T Network Cable Systems, Norcross, Georgia. He received a Bachelors degree in Electrical Engineering from Georgia Institute of Technology in 1968. He joined Western Electric in 1968 and has held various engineering assignments since. He began work in fiber-optic connector development in 1980 and is currently a member of the connector development group.



VASILIOS E. KALOMIRIS is Project Manager for Commercial Communications Technology Laboratory. Previously, he served as Chief Scientific Advisor for Local Area Network Division at CECOM's Space and Terrestrial Communications Directorate. He was the Branch Chief for Local Area Networks and Fiber Optics. He joined the U.S. Army CECOM 14 years ago. Prior to joining CECOM, he was employed by ITT-EOPD as a project engineer responsible for the design and development of various fiber optic cable systems. One of his projects was the design and development of the first air-layable fiber optic cable system. He also worked for General Cable Corporation R&D as a research engineer involved with the design, development, and manufacture of a prototype super-conductive power cable with flexible core. Vasilios holds three patents in fiber optic connector design.

Education: B.A. in Mathematics, B.S. in Electrical Engineering, and an M.S. in Electrical Engineering, all from the New York University, and an M.B.A. from Fairleigh Dickinson University. He is a member of AFCEA, IEEE, and the Technical Chamber of Greece (Society of Profession Engineers). He received the 3rd Annual Engineering Excellence Award for 1986 from CECOM; served for three years as chairman of the Tri-Service Group on fibers, cables, and connectors; currently is chairing the Fiber Optic Guided Vehicle Group.

Optimization of High Performance Unshielded Twisted Pair Media

Paul Z. Vanderlaan

Belden Inc., Richmond, IN

Abstract

This paper describes the development of enhanced performance pairs with the advantages they provide to the electrical parameters and the termination process. Terminating during the installation process can seriously affect the performance of the data link. The goal was to develop a robust cable as immune as possible to the installation process while maintaining transparency to the transmitted data. Stability in impedance and SRL were observed along with the virtual elimination of capacitance and DCR unbalance. Additionally, a reduction in sensitivity to termination process and improved crosstalk are discussed.

Introduction

Many articles have been written about the susceptibility of Category 5 cabling performance to a number of manufacturing and installation practices. Dimensional instabilities which lead to the degradation of various electrical properties have been well documented and almost accepted as inherent to the twisted pair construction. The installation process has also been identified as a Major influence on the potential link performance after the cable has been installed. Untwisting and severe kinking of the pairs has been linked to increased crosstalk reducing the effective bandwidth of the link.

The following chronicles the

definition of the problems associated with unshielded twisted pair cables, the development of an advanced twisted pair cable, and the various benefits which are provided by this enhanced design.

The Problem

Several problems can arise from the manufacture of standard category cables. Each step in the manufacturing process can introduce it's own problems into the final product. However, the first step, extrusion, is the most influential process to the manufacture of a quality cable.

Singles Extrusion

A well controlled extrusion process is the basis for the construction of a high performance cable. Several factors can influence the quality of the finished product. The ideal balanced pair appears below in Figure 1.



Perfect Pair

Figure 1

Each insulated conductor, or single has the exact same insulation and conductor diameter. Additionally, the conductors are perfectly centered within the insulation. Impedance stability is very dependent upon consistent center to center

dimensions. If the diameters and eccentricity are consistent throughout the cable, there would be no impedance variation around the nominal or characteristic impedance. During the extrusion process however, it is nearly impossible to maintain these perfect dimensions. Several types of dimensional variations affect the quality of the impedance at the finished products. Variations in the conductors eccentricity may result in an extruded single with an appearance similar to Figure 2.



Off Center Single

Figure 2

Additional inevitable variations in the insulation's diameter also have an effect upon impedance stability. When both singles, or insulated conductors, have these recurring periodic differences, impedance stability is compromised. Major abrupt impedance discontinuities are created by the periodic changes in center to center dimensions.

Twinning

Twinning, or the process of twisting two individual conductors together, can also create problems. A well twinned pair exhibits a perfect helical pattern. If the conductors were untwisted, they would be equal in length. When single wires are under unequal tensions during the twinning process, one wire is slightly twisted around another. This can cause several problems such as crosstalk failures, and unbalance in DCR and capacitance. When cross-sectional dimensions of paired singles with poor eccentricity and outer diameter variations are viewed, the conductors appear to periodically float in circular patterns causing

severe impedance mismatches (Figure 3). The resultant signal can be distorted by skew and noise.



Twinned Bad Pair

Figure 3

Installation

The installation process can cause several problems which limit link performance. When UTP cable is pulled, there can be significant effects on the input impedance. Such variations are thought to be the "opening" and "closing" of the twist in the cable core as it bends around the corners. When this occurs, the impedance may vary enough to cause SRL problems. This "opening" and "closing" is also believed to decrease the crosstalk performance in the 90 meter segment.

Final termination plays perhaps the largest part in the determination of the link crosstalk performance. The common rule for the installation of Category 5 cable is to untwist the pair no more than one half inch (13mm) to prevent crosstalk performance degradation. However, not all terminations can be visually inspected with the connector mounted in it's receptacle. When a connector is pulled for inspection, the pairs could be pulled taught, pulling the twist tighter, thereby giving the appearance of a proper termination. When the connector is reinserted, the tension is released and the pair are free to open up again. With the untwisting of the pairs the crosstalk performance declines and link performance is compromised. Improvements to the structural and electrical stability would help to provide a reliable cabling system with improved performance.

The Solution

In order to satisfy the previously mentioned problems, a new construction was required. The solution was a method to keep the conductor to conductor separation constant with minimal variations. The final result was the development of the adjoined, or webbed, singles. This development helped to virtually eliminate the problems associated with diameter and eccentricity variations commonly associated with separate singles or insulated conductors. The conductors are locked into place with the web to maintain the proper center to center spacing. The web also helps to keep a uniform helix during the twinning process. This also prevents the singles from excessively separating during the installation process.

The Results

Several benefits became apparent with this new construction. Improvements in impedance and SRL, capacitance unbalance, DCR unbalance, and crosstalk performance were all observed.

Improved Impedance and SRL

A dramatic improvement in impedance uniformity was noted. Unlike traditional unbonded insulated conductors which exhibit increasing impedance variation with higher frequencies, the impedance for the webbed pairs maintained its integrity well past 100 MHz. (Figure 4)

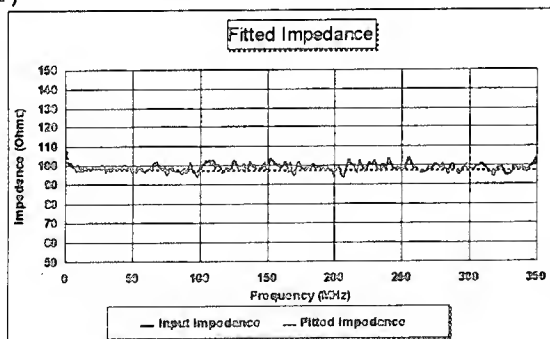


Figure 4

Typical input impedance variation for a 100 MHz bandwidth was reduced to ± 5 ohms (Figure 5).

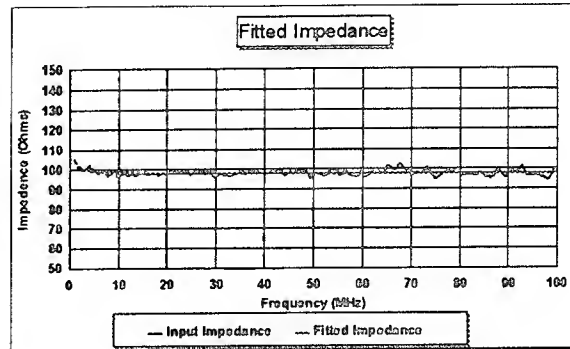


Figure 5

Because of this stability, SRL exhibited a dramatic improvement. The standard measured SRL now runs 30 dB (Figure 6) The calculated SRL based upon the fitting program is typically 35 dB (Figure 7).

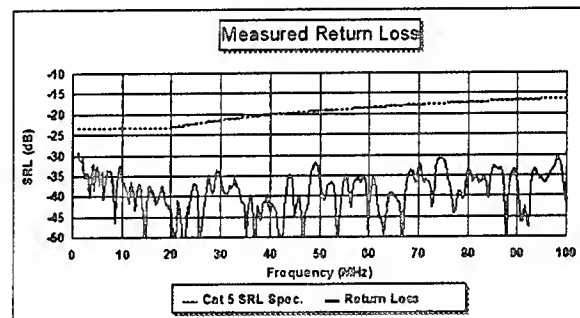


Figure 6

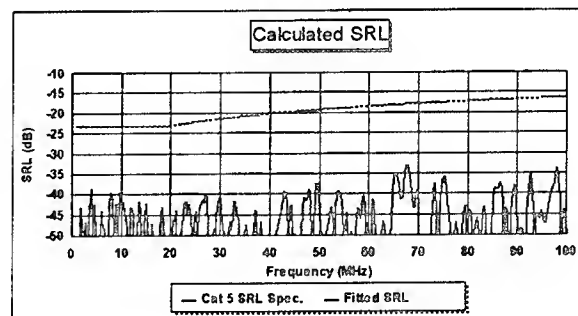


Figure 7

This reduction in SRL should have a corresponding reduction in jitter.

Improved DCR & Capacitance Unbalance

While preventing the uneven twisting of the insulated conductors, the webbed pair has virtually eliminated DCR and capacitance unbalance. Typical numbers for the DCR unbalance are below 1 percent while the capacitance unbalance normally runs below .1pf/ft.

Improved Electrical Stability During Installation

The installation process frequently determines the performance of the link. In the majority of situations, if there is a problem with crosstalk, it is due to the termination of the cable at the connector. This usually is the result of pairs, with the twist removed, radiating energy which is received by the other pairs. In order to test the new design, two different termination techniques were tested, one employing the recommended TIA/EIA termination technique, the other was not. Each test was performed to characterize the cable/connector interrelationship and gauge its success in achieving the desired goals. A similar common pair Category 5 cable was also tested as a benchmark reference.

Test Setup

Impedance and crosstalk measurements were performed with a 300 foot (91.4 meters) section of cable and the respective connector. A shorter length of 100 feet (30.5 meters) was used in order to prevent the masking the effect of the connector during the attenuation tests. Two types of connectors were used in the evaluation: a standard Category 5 110 punchdown block and a plug/jack combination. All measurements were performed using a network analyzer and 401 data points. The data was collected at the connector end of the setup where applicable. The TIA/EIA recommended termination involved removing as little jacket as possible and maintaining the twist up to the

connector. The non-compliant termination had 6 inches (152 mm) of jacket removed and 2 inches (50.8 mm) of twist removal. The bonded pairs were not separated and the single conductors of the common pair cable were left to "float" in a natural fashion.

Due to the limitation of the connectors, only data covering the bandwidth of .772 to 200 MHz is presented. Additionally, in the crosstalk comparison, the Category 5 specification was extended to calculate the limit line to 200 MHz.

Impedance Testing

The following tests represent typical pairs in their respective cables. The common pair is a standard Category 5 cable with twinned singles. The bonded pair is the enhanced Category 5 cable.

The following graphs represents the impedance of the unterminated cables.

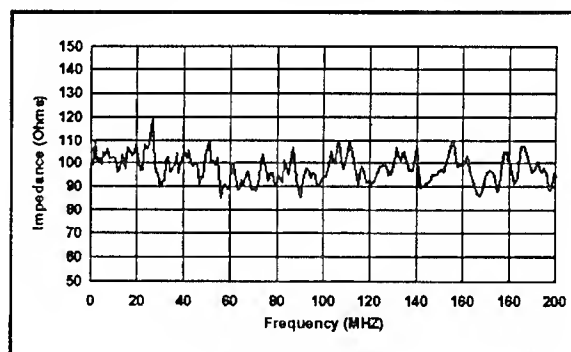


Figure 8
Impedance, Common Cat. 5 Pair
(300' cable)

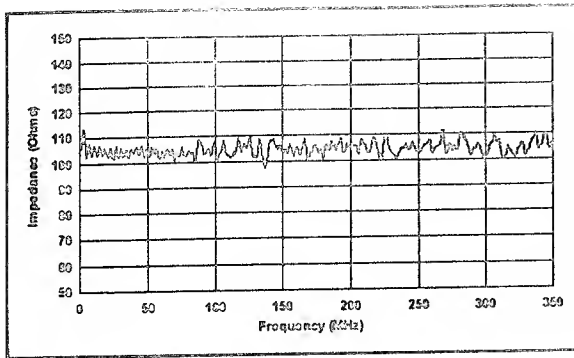


Figure 9
Impedance, Bonded Pair
(300' Cable)

The cables were then terminated in the RJ jack according to TIA/EIA recommendations. The results are shown in Figure 10 as the solid black line. Connector and termination techniques raised the characteristic impedance approximately 4 ohms. After 80 MHz the impedance shows a rise up to 150 ohms at 200 MHz.

The non-compliant termination, represented by the grey line, exhibited a much sharper increase starting at 50 MHz. Both traces exhibited an increase in the magnitude of the peak to peak values for the impedance when compared to the bulk cable.

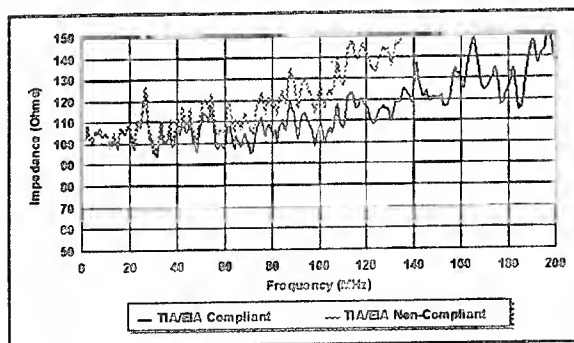


Figure 10
Impedance, Common Pair, 300' Cable,
Cat. 5 Jack

The bonded pair exhibited the same type of effects but to a lesser

degree. With the compliant termination, Figure 11, the increase in impedance began at 80 MHz and reached a maximum of 135 ohms at 200 MHz. The non-compliant termination, represented by the grey trace, revealed only a slight increase of a few ohms over the compliant termination with the gradual increase beginning at 50 MHz. Peak to peak impedance swings were also slightly increased, but not to the magnitude of the common Category 5 pairs.

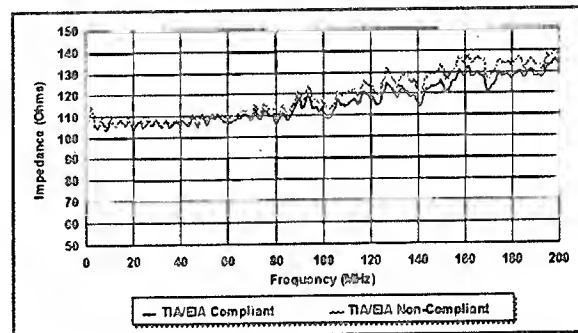


Figure 11
Impedance, Bonded Pair, 300' Cable,
Cat. 5 Jack

The Category 5 110 punchdown was tested in a similar fashion. Figure 12 depicts the impedance traces of the common pairs in both termination configurations. The impedance of the TIA/EIA configuration, represented by the solid black line, very closely resembles the cable alone out to 200 MHz.

The grey trace in Figure 12, representing the impedance performance of the non-compliant method, seemed consistent until 100 MHz where it started to rapidly increase in magnitude. However, the magnitude of the impedance spike at 27 MHz increased by ten ohms in comparison to the bulk cable. This would seem to indicate that major discontinuities are magnified to some extent by the combination of cable and connectors.

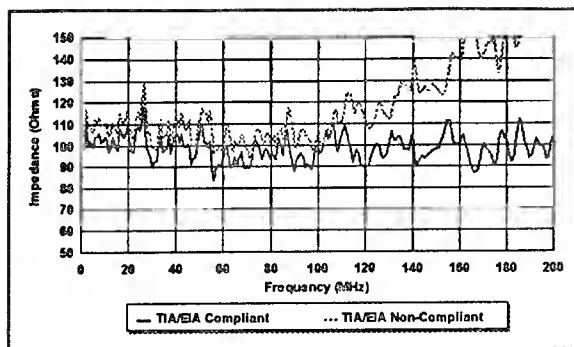


Figure 12
Impedance, Common Pair, 300' Cable,
Cat. 5 110 Punchdown,

When terminated to the 110 punchdown in the recommended format, the bonded pair exhibited the same stable characteristics as the cable alone out to 200 MHz. (Figure 13, solid black line.)

When terminated improperly, shown by the grey line, the impedance began to very slightly increase at 100 MHz, but leveled off for an average increase of 7 ohms out to 200 MHz.

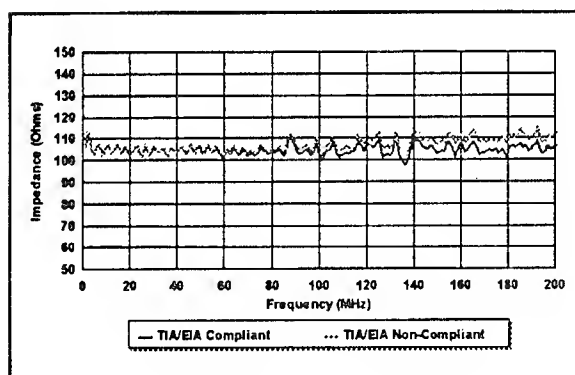


Figure 13
Impedance, Bonded Pairs, 300' Cable,
Cat. 5 110 Punchdown

The impedance of the bonded pairs was less susceptible to the termination process. The RJ connection seemed to impart a gradual increase in the impedance of all of the tests. However, the changes in peak to peak

impedance values were much greater in the common non-adjointed pair cable in comparison to the bonded cable. A cable which is near the SRL specification on the reel may have a substantially larger return loss once it is installed. This may cause problems with systems which are sensitive to the SRL in a given link.

Crosstalk Testing

Each of the following figures represents the worst case pair to pair crosstalk margin in each particular setup. The bandwidth from .770 to 200 MHz was divided into eight sections. The graphs were generated by obtaining the worst margin in the particular bandwidth and reporting that margin at the top of the bandwidth. All measurements were performed with the connector at the near end. The measurements were made under three conditions, which included the cable's performance alone, the cable terminated according to TIA/EIA, and the cable terminated with 6 inches (152 mm) of jacket removed and 2 inches (50.8 mm) of twist removed.

The cable under test in Figure 14 represents the common Category 5 cable.

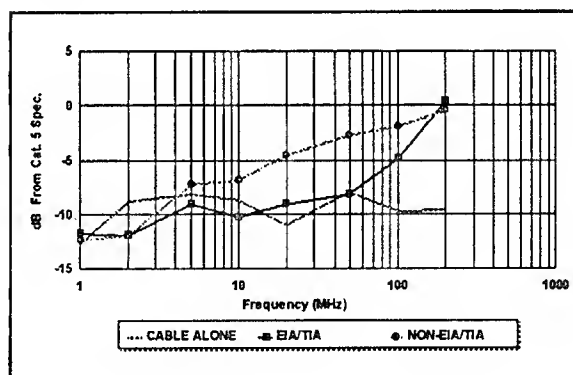


Figure 14
Common Pair NEXT Margin from Cat 5
Cable Spec., 300' Cable, Cat. 5 Jack

The margin of the non-compliant termination is substantially less

than that of the recommended configuration. However, the two traces converge at 200 MHz.

The bonded pair cable, Figure 15, exhibited less of a difference between the two test setups. The margin was reduced to approximately zero at 200 MHz again.

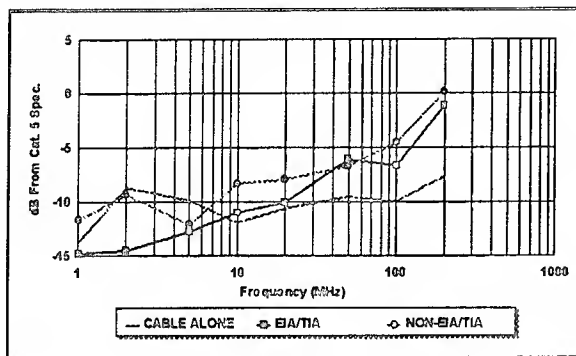


Figure 15

Bonded Pair NEXT margin from Cat. 5 Cable Spec., 300' Cable, Cat. 5 Jack

The Category 5 110 punchdown revealed some unexpected results. Once again the non-compliant common cable margin was substantially less than the compliant. (Figure 16) However, the margin for the non-compliant cable was still positive out to 200 MHz.

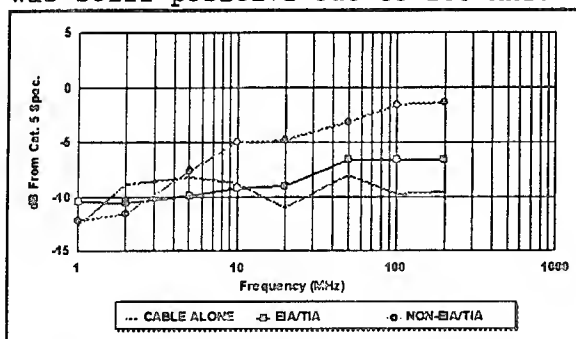


Figure 16

Common Pair NEXT Margin From Cat. 5 Cable Spec., 300' Cable, Cat. 5 110 Punchdown Block

The bonded pairs exhibited the same consistency in both configurations. Figure 17 shows a 7.5 dB margin from 50 to 100 MHz.

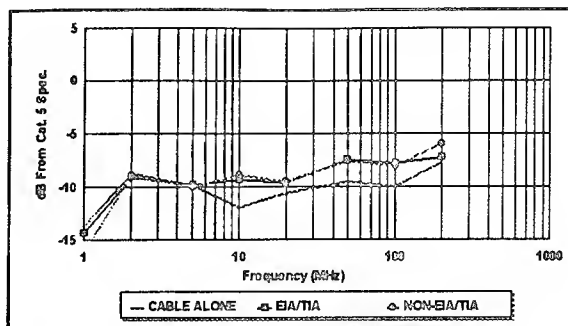


Figure 17

Bonded Pair Next Margin from Cat. 5 Cable Spec., 300' Cable, Cat. 5 110 Punchdown Block

From the first set of trials, it is apparent that the RJ connector was the weakest point in the link. The compliant 110 connections did not exhibit the rapid loss of margin at 200 MHz. Additionally, the 110 punchdown termination of the common pair never exceeded the specification. This is not meant to imply that cables do not have to be terminated in compliance since there was significant NEXT performance degradation. Finally, the data from the bonded pairs suggests that it is not the twist itself that prevents the crosstalk, rather, it is the consistent spacing of the conductors which prevents unwanted signal reception. The twist is merely the mechanism by which the conductors are kept together in a common pair. It may also follow that the unwanted transmission of information (e.g. emissions) is reduced as well.

Attenuation

The final test was an attempt to quantify the affect of termination method on attenuation. The attenuation of each setup was measured and compared to the attenuation of the cable alone to determine the additional loss. The following table lists the additional loss for each configuration.

Frequency @ 100 MHZ	TIA Compliant	Not TIA Compliant
RJ45 Jack		
Common	0.2 dB	0.7 dB
Bonded	0.2 dB	0.2 dB
110 Block		
Common	0.0 dB	0.5 dB
Bonded	0.0 dB	0.0 dB

With the compliant terminations, there was no discernable difference between the two cables. However, in the non-compliant tests, the common non-adjointed pairs had a reduction of .5 dB or more in performance. The bonded pair exhibited no such degradation between the termination methods.

Conclusion

The goal of an enhanced twisted pair was achieved through the development of the bonded pair technology. The impedance variation was reduced dramatically with a corresponding improvement in SRL. Additionally, the design exhibited reduced susceptibility to the installation process. Impedance traces showed a dramatic reduction in variation due to termination. NEXT performance degradation by improper termination was reduced by 4 to 5 dB from the common pair construction. Finally, attenuation degradation due to termination was virtually eliminated.

Acknowledgements

The author would like to thank the following people for their valuable assistance in developing and preparing the paper.

Mike Bertke, Product Development Engineer, Belden Inc., Richmond, IN.

Andrew Pluister, Product Engineer, Belden Inc., Richmond, IN.



Paul Vanderlaan is a Product Development Engineer at Belden Inc. He has been in the wire and cable industry for two years with primary responsibilities

in LAN cable development. He received his Bachelor of Science degree in Electrical Engineering in 1992 at Purdue University.

Performance Evaluation of Multiple Pair Category 5 Backbone Cable for High Speed Data Services

J.-H. Walling, M. Bélanger and B. Lord

Northern Telecom Canada, Ltd.
Transmissions and Components
Cable Group Technology

Abstract

Three 25 pair data grade cables have been categorized with respect to their design and electrical performance. Using these electrical performance characteristics we tried to predict their performance in actual LAN configurations. For this purpose the cables have been used for connecting multiple stations of a LAN test bed using different protocols, i.e. 10Base-T, 16 Mb/s Token-ring and 100 Mb/s TP-XDDI. These protocols were also used in a combined fashion, i.e. 10Base-T and Token-ring, TP-XDDI and 10Base-T or Token-ring, or all three using the same cable simultaneously.

These tests were carried out, connecting the cable following the structured wiring guidelines set forward by EIA/TIA-568 and by logically extending the scheme to higher pair counts. Consequently, six stations with four pairs each were used. But, to use the cables to their full capacity, 12 stations were also connected with 2 pairs each in a cross connected fashion. Under all conditions the maximum reach, under acceptable bit error rate conditions, has been determined.

The results indicate that cables designed only with the EIA/TIA SP-2840A Power Sum NEXT requirement in mind show relative poor FEXT crosstalk performance, which may impact upon the reach and more important upon the bit error rate susceptibility.

Introduction

Over the last couple of years the need for multiple pair data grade cables meeting Category 5 requirements for high speed data transmission, became more and more apparent. Therefore, the EIA/TIA Engineering Committee TR-41 is developing a standard to cover these cables. Though the standard is not yet finalized, the ANSI/EIA/TIA draft specification EIA/TIA SP-2840A serves as a basic guideline throughout the industry for the development of such cables. Following the requirements of this draft specification, several cable designs, finally, appeared in 1994 on the market.

It became mandatory to comparatively assess some of these designs with respect to their performance in an actual LAN environment, and, at the same time, to gather some indications upon the validity of the requirements as outlined in EIA/TIA SP-2840A.

Rationale

It is the objective of this paper to show that the performance of

data grade cables in high speed LANs is absolutely acceptable within the limiting constraints of reach according to EIA/TIA SP-2840A. Cables according to the EIA/TIA draft specification SP-2840A are designed towards the Power Sum NEXT requirements. It will be shown that the basic reach requirements are met with such cables. This will be done over a minimum length of at least 100 m. However, it will also be demonstrated that cables which are adequately designed and manufactured can substantially surpass the reach limitations, if the basic design criteria are extended beyond the EIA/TIA Power Sum NEXT requirements to cover also stringent Power Sum FEXT requirements.

To demonstrate this we have selected three cable designs. These cables were extensively tested with different configurations in mind, to establish their performance for high grade data transmission.

We established, furthermore, the maximum attainable reach for different LAN protocols. This has been done as follows. For each wiring scheme, i.e. for each LAN protocol and for the case of maximum utilization of all pairs in the cables, we computed the effective power sum crosstalk using the NEXT and FEXT matrices for the inside and the outside end of the cables respectively. All our measurements were based upon a minimum link length of 100 m. This is deviating from the link length of 90 m as specified in EIA/TIA SP-2840A. However, we tried to derive the cable performance characteristics out of their measured electrical data and these data are according to EIA/TIA SP-2840A measured on cables with a length of 100 m.

We determined the attenuation to crosstalk ratio (ACR) for the standard length of 100 m. We then calculated the margins with respect to the EIA/TIA SP-2840A requirements and derived the additional reach potential. We then compared these reach values with the practically obtained reach values under acceptable bit error rate conditions.

Cable No.	Insul. Wall [mil]	Insulation Material	Jacket Outside Dia. [inch]	Jacket Material
1	37.70	FRPE	0.460	PVC
2	37.00	PE/FRPE	0.500	PVC
3	37.70	FRPE	0.650	PVC

Table 1

Description of Cable Designs Investigated

Three cables were selected. All had a UL-CMR or UL-MPR

flammability listing. Two of the three cables are designed for horizontal distribution, whereas the last one is a data grade riser cable, having a corrugated aluminum shield of 0.008 inches thickness. All cables have 25 pairs of 24 AWG conductors. The basic design parameters are listed in Table I. The Cables # 1 and # 3 have solid FRPE insulation, whereas the cable # 2 has a PE-FRPE dual-layer insulation.

	Cable # 1		Cable # 2		Cable # 3	
	Min.	Max.	Min.	Max.	Min.	Max.
C. R. [Ohm/100 m]	8.56	9.18	8.50	8.99	8.48	9.09
C. R. U [%]	0.00	0.77	0.00	1.23	0.00	0.71
Mut. Cap. [nF/100 m]	4.76	5.57	4.66	5.37	4.45	5.60
C.U.P.G [pF/100 m]	2	70	1	67	2	119
C.U.P.P [pF/100 m]	0	2	0	0	0	4

Table II

The cables # 1 and # 3 were made by Northern Telecom. These are the NT-25 BDN Plus and the NT-25DGR Data Grade Riser Cable, respectively. They are characterized by having a single stranded core of 25 pairs with twist-lays below 1.0 inch. The cable # 2 has been purchased. This cable has 4 pair and 3 pair units. Some of the individually stranded units have identical twist-patterns. The 11 twist lays used range from 0.35 to 0.57 inches.

Hence forward only the cable numbers are used to refer to these cables.

Measurements and Methodology

Electrical Performance Characterization

Table II summarizes the wire resistance, the resistance unbalance, the mutual capacitance, the capacitance unbalance pair to ground and the capacitance unbalance pair to pair. Reported are the minima and maxima of the measurements. These measurements were made on a DCM test-set.

To assess the high frequency performance of the cables, frequency domain measurements were carried out to characterize the wires subject to sinusoidal signals. This has been done to measure the secondary transmission parameters and the near-end and far-end crosstalk for each pair combination. An HP-network analyzer in conjunction with an S-parameter test set, an impedance matrix switch-box and a Siemon balun matrix were used. The measurements were made in the frequency range of 0.3 to 100 MHz. For each measurement 401 points were recorded.

The network analyzer and the switch-box were controlled by a software package, programmed in MS-Visual Basic, specifically

developed by Northern Telecom.

All the measurements were carried out for both ends of the cable. Only the worst values were of interest. Therefore, both measurements were considered. This is the more justified, as the real traffic over the cable is also, inevitably, bi-directional.

The NEXT measurements were carried out and the power sums have been calculated for each pair. For the Power Sum NEXT a linear regression has been calculated over the entire population of measurements of a cable after a log-frequency transformation. The obtained regression line has then been shifted into the lowest point of all measurements, yielding the lower envelope of the measurements. The lower envelope of Power Sum NEXT definitely characterizes the most precisely the worst near-end crosstalk behaviour of any cable investigated. The utilization of the lower crosstalk envelope makes it mandatory to use swept frequency measurements.

This regression line has been, therefore, also used to calculate the attenuation to crosstalk ratio (ACR). The Category 5 requirements according to draft EIA/TIA SP-2840A have also been plotted (marked with an arrow).

The extreme points of the attenuations of all pairs, i.e. the upper and lower attenuation envelope have been determined. It is thought, that the upper envelope of attenuation best represents the worst case condition in a given cable. Therefore, the upper envelope of the attenuation has been used to determine the ACR.

Additionally, FEXT measurements were made. After compiling the Power Sum FEXT values for each pair, a lower envelope has been calculated. As FEXT is length dependent it is also dependent upon the attenuation. Hence, a linear log-transformed regression has been super-imposed to the regression indicated in EIA/TIA SP-2840A for the attenuation. Thus the regression used becomes:

$$FEXT = a + b \cdot \log(f) + c \cdot \sqrt{f} + d \cdot f + e \cdot \frac{1}{\sqrt{f}} \quad \dots(1)$$

In this context, it should be noted that the FEXT measurements depend upon the attenuations of disturbed and disturbing pair. In fact, more precisely, the FEXT depends upon the propagation constant, from which the attenuation is only the real part. According to [2] we get:

$$FEXT(l) = FEXT(l_o) - 20 \cdot \log\left(\frac{l}{l_o}\right) \quad \dots(2)$$

However, if the propagation constants are substantially different, we get:

$$FEXT(1) = FEXT(1_o)$$

$$- 20 \cdot \log \left\{ \frac{1}{I_o} \cdot \Re \left(\frac{\gamma}{\gamma_o} \right) \right\}$$

... (3)

The propagation constants are different for different pairs. This is due to the different twist-lays of the pairs, and the resulting helix length differences. Therefore, the FEXT values will also be different, i.e. $FEXT_i \neq FEXT_j$, hence the entire FEXT matrix can no longer be considered being symmetric. The same is also true for the NEXT measurements. According to [1] the NEXT values also depend upon the attenuation. Hence they are also different for each pair combination in the cables investigated here. Therefore, the obtained NEXT matrix is also asymmetric. These differences may be relatively small, but they may also attain values in the order of 2 dB. These values then have, definitely, an impact upon the calculated power sums.

It should be noted that the impedances of all pairs were measured and that the respective SRL values were derived. Both, measurements and derived values complied fully to the EIA/TIA SP-2840A requirements for all pairs in all the cables. They are, however, in the context of our prime objective, only of minor interest. Therefore, only the values of the impedances are reported here in Fig. 1 to Fig. 3. They show clearly the influence of the frequency shift of the extremes of the open and short circuit measurements due to different propagation modes in both types of measurement [3]. This has already been clearly observed [4]. In this context it is interesting to mention the latest Japanese contribution to IEC where it is proposed to use a modal decomposition method in conjunction with a network analyzer and an S-parameter test set. This method does not need the use of balanced-to-unbalanced conversion transformers (baluns) [5];[6]. Some advantages may be expected from this test method, provided that the impact of the grounding conditions upon the results can be controlled for unshielded twisted pairs.

Fig. 4 to 12 show the attenuation envelopes, the NEXT and FEXT power sum traces of all pairs and their lower envelopes. For the attenuation and the Power Sum NEXT the EIA/TIA limits are also indicated. These are marked in the Figures by an arrow.

In Table III are listed the pairs used for the different LAN protocols. In principle the 25 pair cable was used for 6 stations with 4 pairs dedicated to each station. This yields the highest LAN flexibility if, over time, different protocols are to be deployed.

Token-ring and TP-XDDI are fully compatible, i.e. they could be easily deployed maintaining the common structured wiring scheme to use the cable jointly. This requires only some straight cross-connection. 10Base-T and TP-XDDI are not directly pair to pair complementary with respect to the structured wiring scheme. A joint deployment requires, therefore, a shifted cross-connection. The joint use of the cable which allows the most economic pair utilization can be deployed only at the expense of increased installation difficulty.

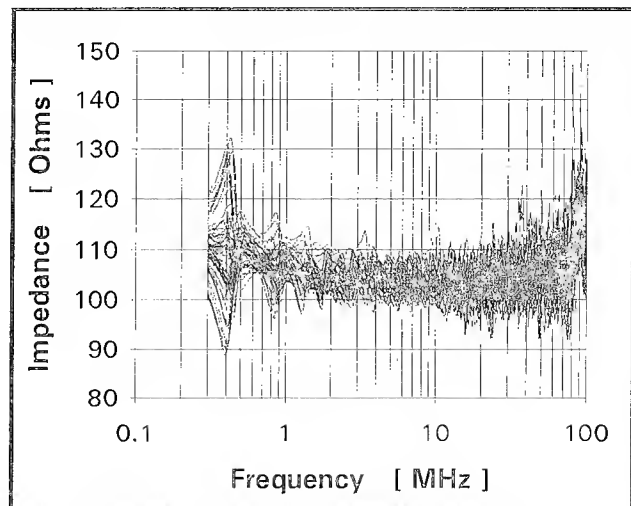


Fig. 1 : Impedance versus Frequency for the Cable # 1

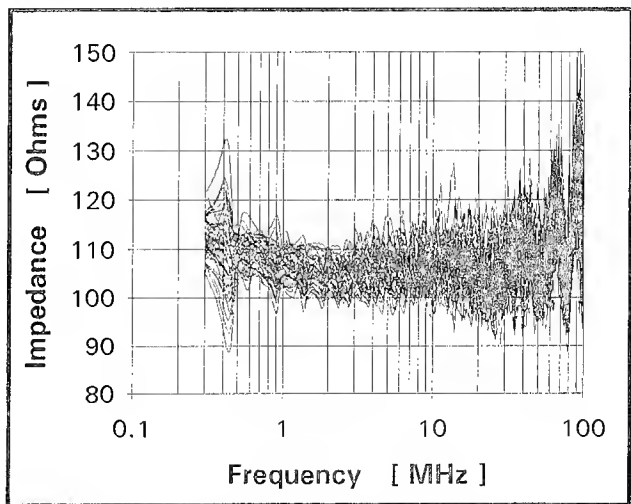


Fig. 2 : Impedance versus Frequency for the Cable # 2

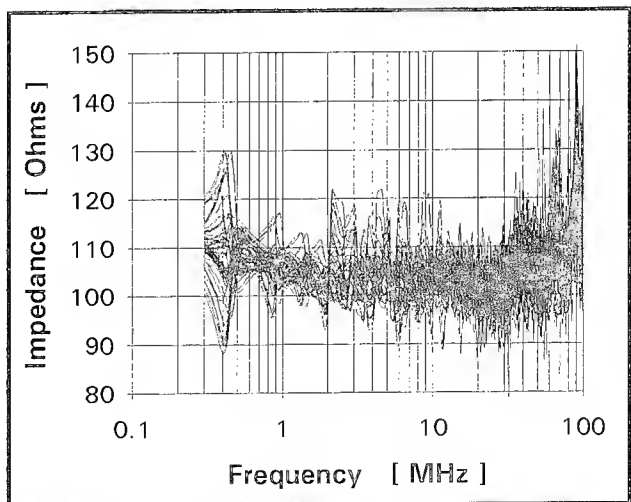


Fig. 3 : Impedance versus Frequency for the Cable # 3

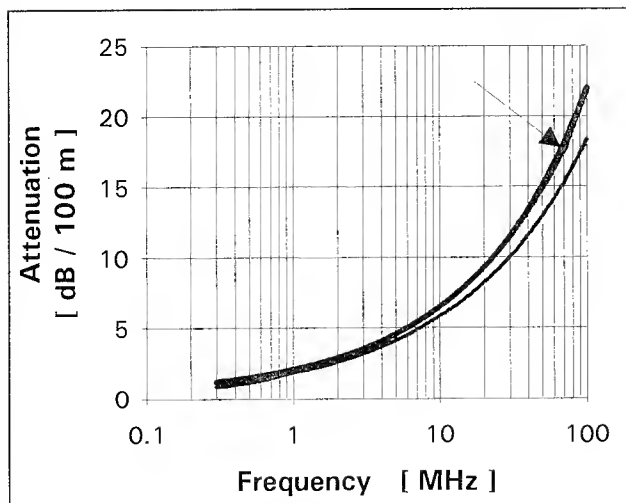


Fig. 4 : Attenuation versus Frequency for the Cable # 1

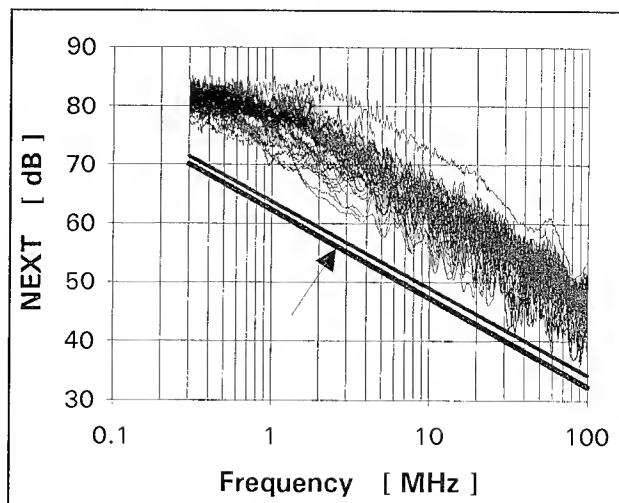


Fig. 7 : NEXT versus Frequency for the Cable # 1

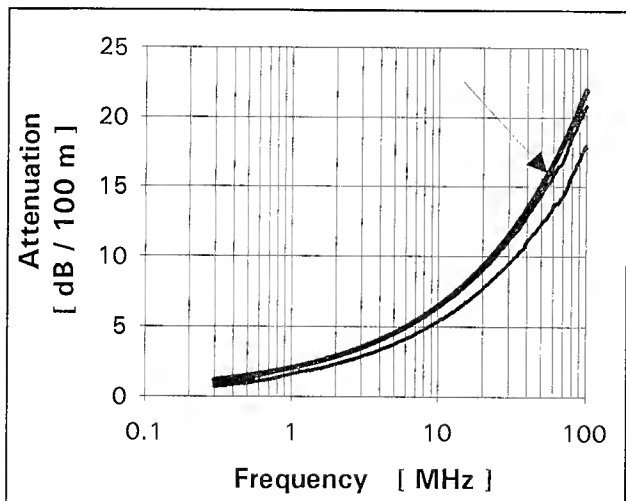


Fig. 5 : Attenuation versus Frequency for the Cable # 2

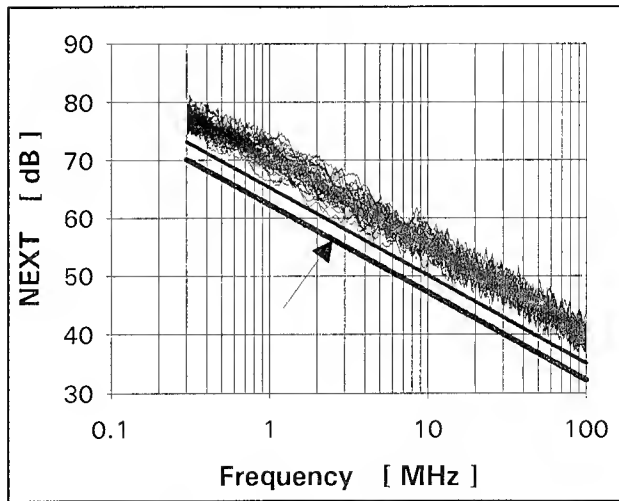


Fig. 8 : NEXT versus Frequency for the Cable # 2

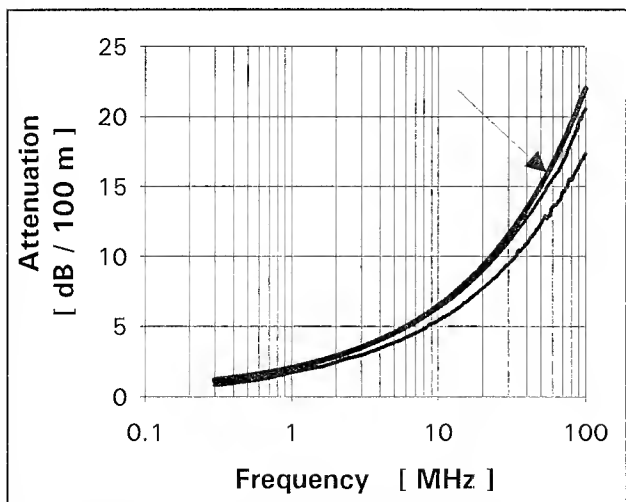


Fig. 6 : Attenuation versus Frequency for the Cable # 3

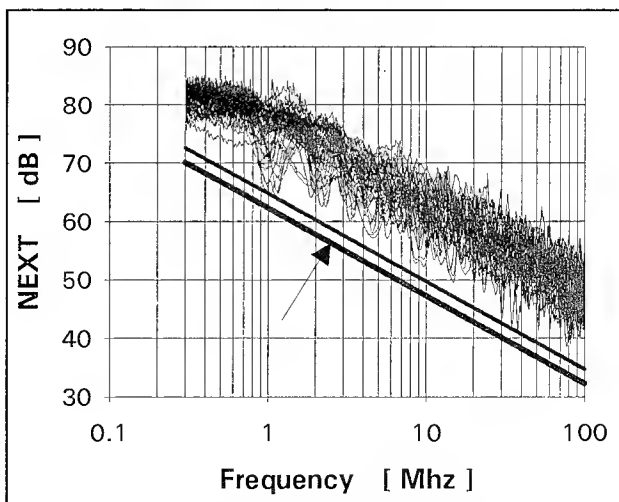


Fig. 9 : NEXT versus Frequency for the Cable # 3

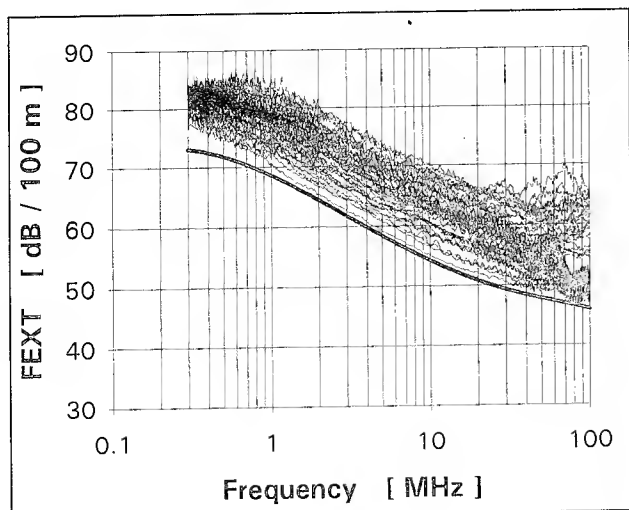


Fig. 10 : FEXT versus Frequency for the Cable # 1

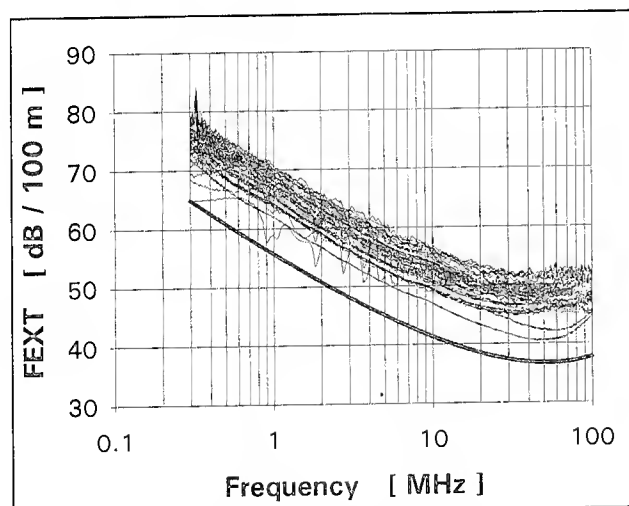


Fig. 11 : FEXT versus Frequency for the Cable # 2

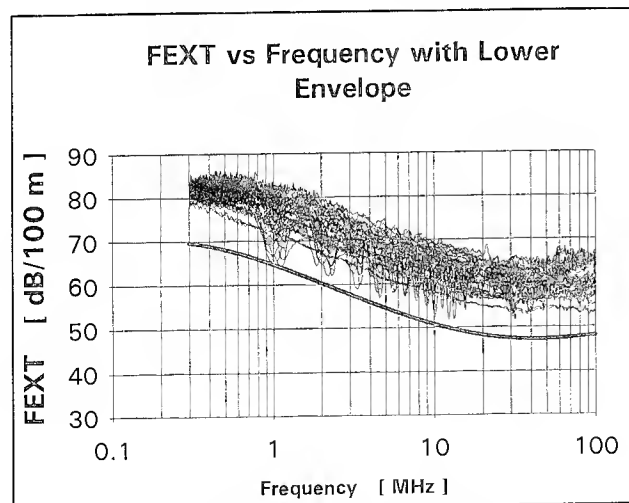


Fig. 12 : FEXT versus Frequency for the Cable # 3

Pair No.	TIP	RING	10Base-T	Token-ring	XDDI	12 Stations Running
6 Stations Running on Cable						
1	White	Blue		Receive		Receive
2	White	Orange	Receive	Transmit		Transmit
3	White	Green	Transmit		Transmit	Transmit
4	White	Brown			Receive	Receive
5	White	Slate		Receive		Receive
6	Red	Blue	Receive	Transmit		Transmit
7	Red	Orange	Transmit		Transmit	Transmit
8	Red	Green			Receive	Receive
9	Red	Brown		Receive		Receive
10	Red	Slate	Receive	Transmit		Transmit
11	Black	Blue	Transmit		Transmit	Transmit
12	Black	Orange			Receive	Receive
13	Black	Green		Receive		Receive
14	Black	Brown	Receive	Transmit		Transmit
15	Black	Slate	Transmit		Transmit	Transmit
16	Yellow	Blue			Receive	Receive
17	Yellow	Orange		Receive		Receive
18	Yellow	Green	Receive	Transmit		Transmit
19	Yellow	Brown	Transmit		Transmit	Transmit
20	Yellow	Slate			Receive	Receive
21	Violet	Blue		Receive		Receive
22	Violet	Orange	Receive	Transmit		Transmit
23	Violet	Green	Transmit		Transmit	Transmit
24	Violet	Brown			Receive	Receive
25	Violet	Slate	Spare Pair			

Table III

The cable is used to its full capacity if there are 12 transmit and 12 receive pairs at each end of the cable respectively, leaving one spare pair idle. Therefore, the crosstalk power sum of a receive pair was compounded from 12 near-end and 11 far-end disturbers (see for explanation Fig. 13, showing the second inside receive pair disturbed by three adjacent transmit and two far end transmit pairs).

Using both, the NEXT and FEXT matrices of all pairs, measured from the inside and the outside of the cable, the power sum crosstalk has been computed. Pair assignments have been selected assuming the cable is used to connect either 6 or 12 stations, i.e. using 12 or 24 pairs, respectively. The possible wiring schemes have been determined, and the transmit and receive pairs have been identified, as corresponding near-end and far-end crosstalk disturbers. For the six station usage, the three potential LAN protocols have been taken into account. Thus the effective power sum crosstalk is determined for the inside end of the cable using INEXT and IFEXT and for the outside of the cable using ONEXT and OFEXT. The calculation of the effective power sum crosstalk has been done using the equation (4).

The results obtained are given for all the cables in Fig. 14 to Fig. 19. These figures also show the calculated lower envelope and the EIA/TIA SP-2840A limit for the Power Sum NEXT (indicated by an arrow). Additionally, and for completeness sake only, the effective power sum crosstalk from the lower envelopes of the

Power Sum NEXT and FEXT populations has been calculated.

$$Ps\ X-Talk = 10 \cdot \log \left(\sum_{i=1}^{i=12} 10^{\frac{-NEXT_{2-i}(f)}{10}} + \sum_{i=1}^{i=12} 10^{\frac{-FEXT_{2-i-1}(f)}{10}} \right) \quad \dots(4)$$

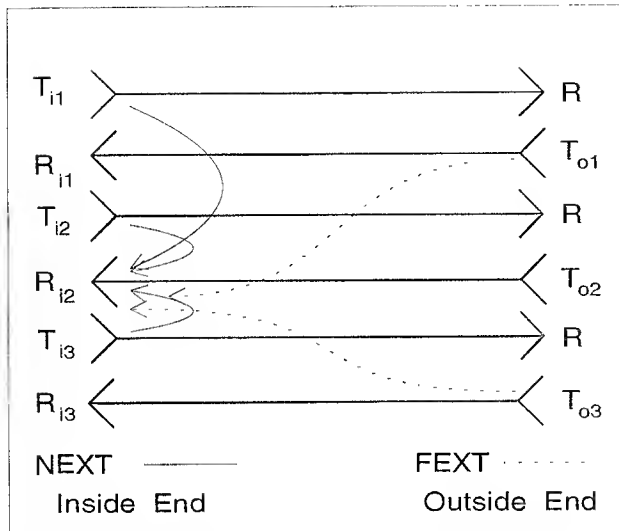


Fig. 13 : Schematics of NEXT and FEXT Disturbance on one Receive Pair

This has been done using the following formula, which takes all 25 pairs into account:

$$Ps\ X-Talk = 10 \cdot \log \left(\frac{12.5}{25} \cdot 10^{\frac{-NEXT(f)}{10}} + \frac{11.5}{25} \cdot 10^{\frac{-FEXT(f)}{10}} \right) \quad \dots(5)$$

All the characteristic power sum values are compiled in Fig. 20 to Fig. 22. Only the cable # 2 has power sum traces which are below the Power Sum NEXT requirement of EIA/TIA SP-2840A. This is due to the relatively poor FEXT crosstalk performance.

According to [1], both NEXT and FEXT are dependent upon a so called crosstalk-influence-function which allows to reduce not only NEXT, but also very substantially reduce the FEXT by properly selecting the twist-lay scheme. This crosstalk-influence-function depends upon the logarithm of the inter-axial pair spacing and is proportional to the inverted twist-lay differences :

$$CIF \approx \log_{10} \left(\frac{t_1 \cdot t_2}{t_1 - t_2} \right) \quad \dots(6)$$

The cable # 2 has some units having identical twist lay patterns. Therefore, primarily the FEXT values are negatively impacted upon as the CIF is not minimized sufficiently by selecting adequate twist-lays t_1 and t_2 . The very narrow grouping of the Power Sum NEXT values versus frequency of this cable

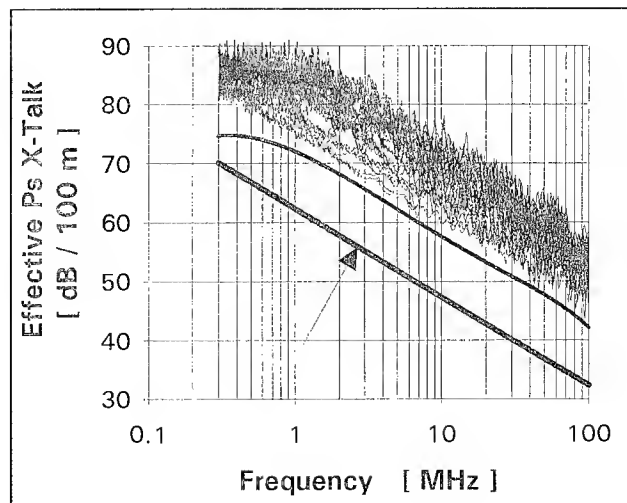


Fig. 14 : Effective Ps X-Talk vs Frequency for the Cable # 1 using 12 Pairs for 6 Stations

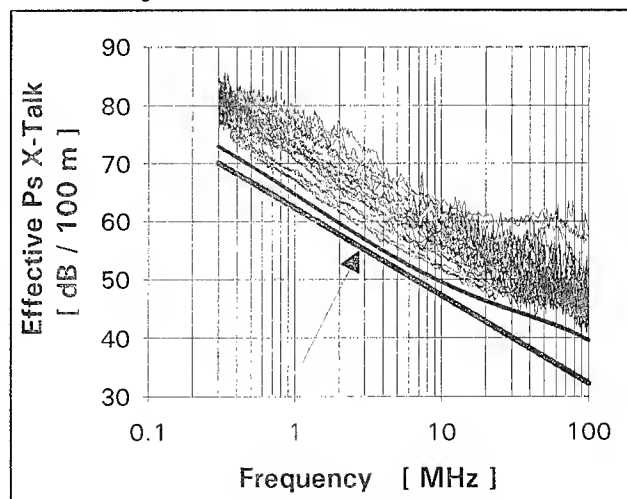


Fig. 15 : Effective Ps X-Talk vs Frequency for the Cable # 2 using 12 Pairs for 6 Stations

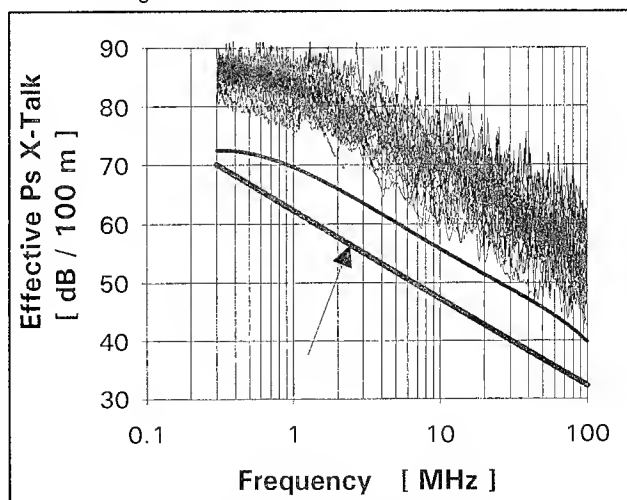


Fig. 16 : Effective Ps X-Talk vs Frequency for the Cable # 3 using 12 Pairs for 6 Stations

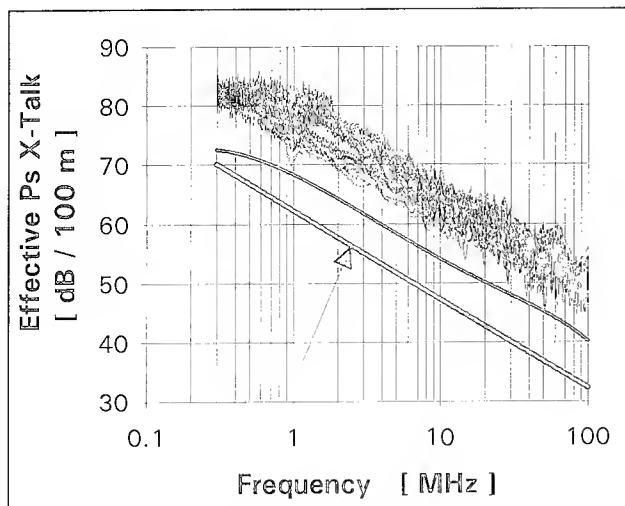


Fig. 17 : Effective Ps X-Talk vs Frequency for the Cable # 1 using 24 Pairs for 12 Stations

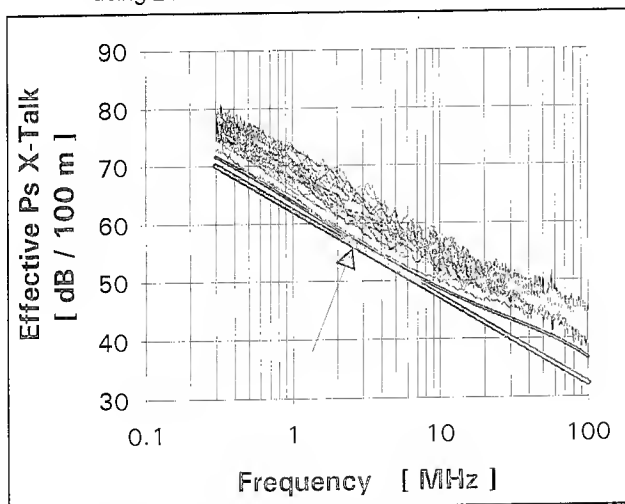


Fig. 18 : Effective Ps X-Talk vs Frequency for the Cable # 2 using 24 Pairs for 12 Stations

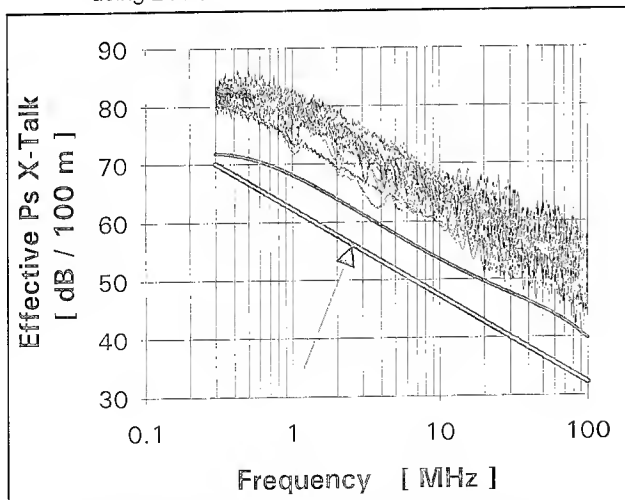


Fig. 19 : Effective Ps X-Talk vs Frequency for the Cable # 3 using 24 Pairs for 12 Stations

indicates, furthermore, that there are no frequency regions with marked crosstalk cancellation. In some frequency ranges an increasing crosstalk cancellation occurs if the twist-lays are further spaced apart.

Fig. 23 to 25 present the obtained attenuation to crosstalk values.

The ACR, i.e. the attenuation to crosstalk ratio has been calculated from the obtained upper attenuation envelope and the lower envelope of the Power Sum NEXT and the Effective Power Sum for 6 and 12 station usage. The EIA/TIA SP-2840A requirements for attenuation and Power Sum NEXT have been used to calculate ACR values over frequency, which correspond to a 100 m link. These values give a more detailed picture than the ACR values spelled out in IEEE 802.3, 802.5, 802.12 and ANSI X3T.9.5 for different protocols.

All cables show ACR values exceeding the minimum EIA/TIA SP-2840A requirements. Cable # 2, however, has ACR values which are exceeding the EIA/TIA requirement only by a very small margin. The difference between the cable specific ACR values and the EIA/TIA requirement yields an ACR margin. We can use this ACR margin to calculate an additional reach, i.e. a reach exceeding the basic specification length of 100 m. We obtain then the values shown in Fig. 26 to Fig. 28. These reach values indicate that we may expect an appreciable reach increase from the cables # 1 and # 3, whereas the additional reach margin for cable # 2 is very limited.

The Reach at LAN Frequencies

Method

To evaluate the cable performance at different bit-rates, three LANs with two servers have been set-up. One server has been used exclusively for TP-XDDI, whereas the second server has been equipped with 10Base-T and Token-ring cards, and was serving simultaneously both LANs respectively. The Token-ring has been used at a bit-rate of 16 Mb/s. A minimum of five to six stations were connected to each LAN. The cable was connected between two patch panels. The server was connected over a patch-cord of 4 feet via two pairs of the cable and another patch-cord of 4 feet to the hub (thus the total wiring length was approximately 102.5 m); the stations were connected in the same way through the cable to the hub. A schematic setup of the LAN and of the connection of the cable is shown in Fig. 29. It should be mentioned, however, that the link server-hub for 10Base-T and for Token-ring used also the entire cable length. As a result there were effectively only 5 stations connected. This was done because the signal density on this line is higher than on the line between the hub and any station. For the Token-ring we used a passive hub.

Traffic on the different LANs was generated by either swapping files or simply reading bit mapped files from the server. To follow the traffic in the LANs, protocol analyzers were connected to each of the different LANs. The protocol analyzers and also the Novell-LAN

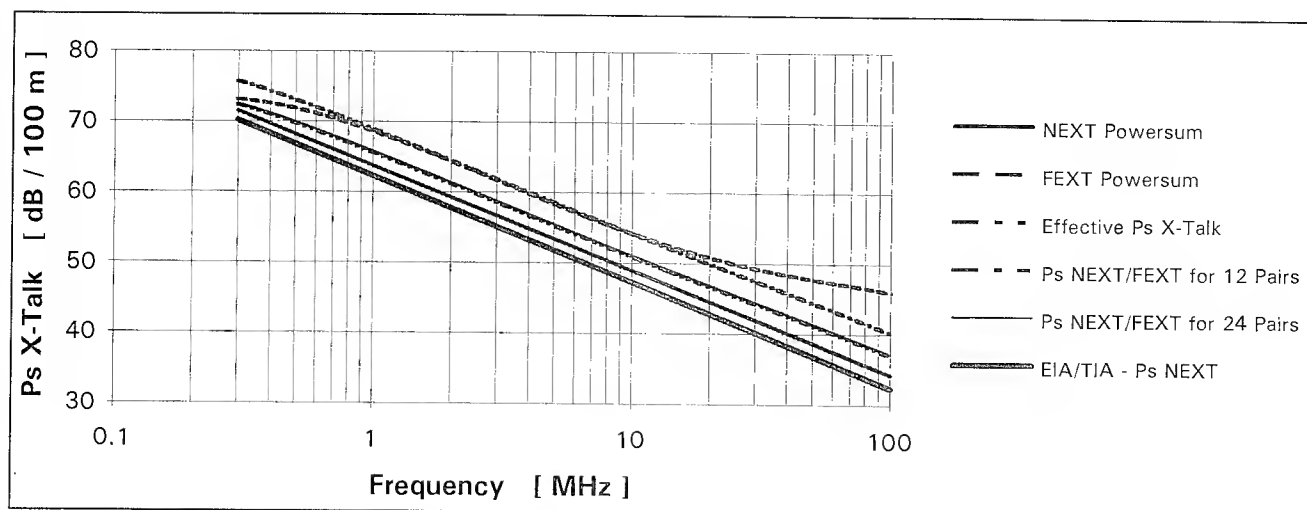


Fig. 20 : Ps X-Talk Envelope vs Frequency for the Cable # 1 including EIA/TIA Requirements

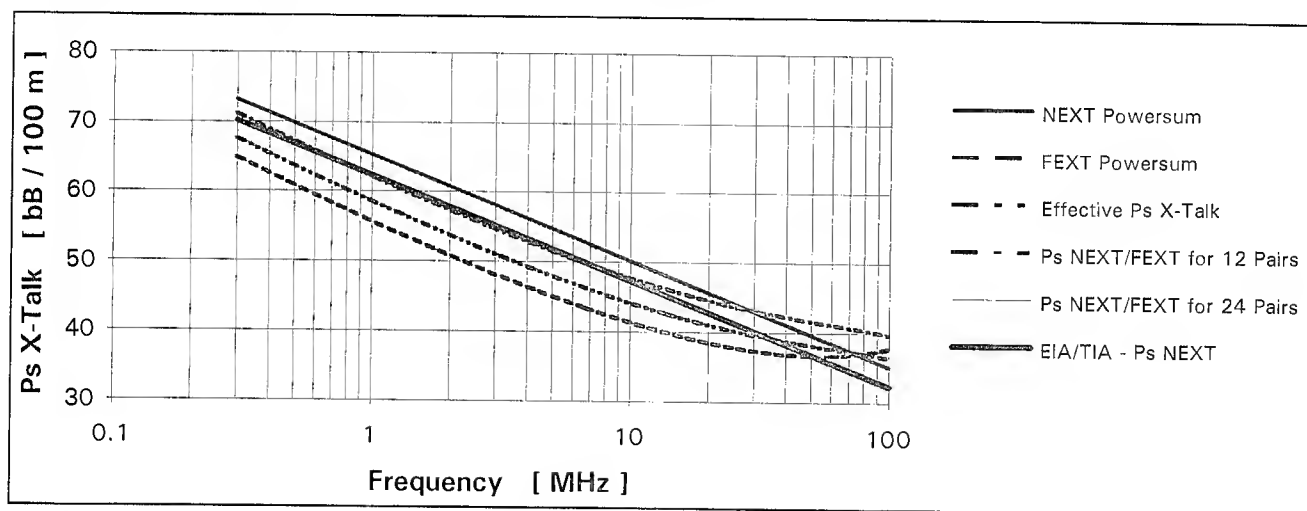


Fig. 21 : Effective Ps X-Talk vs Frequency for the Cable # 2 including EIA/TIA Requirements

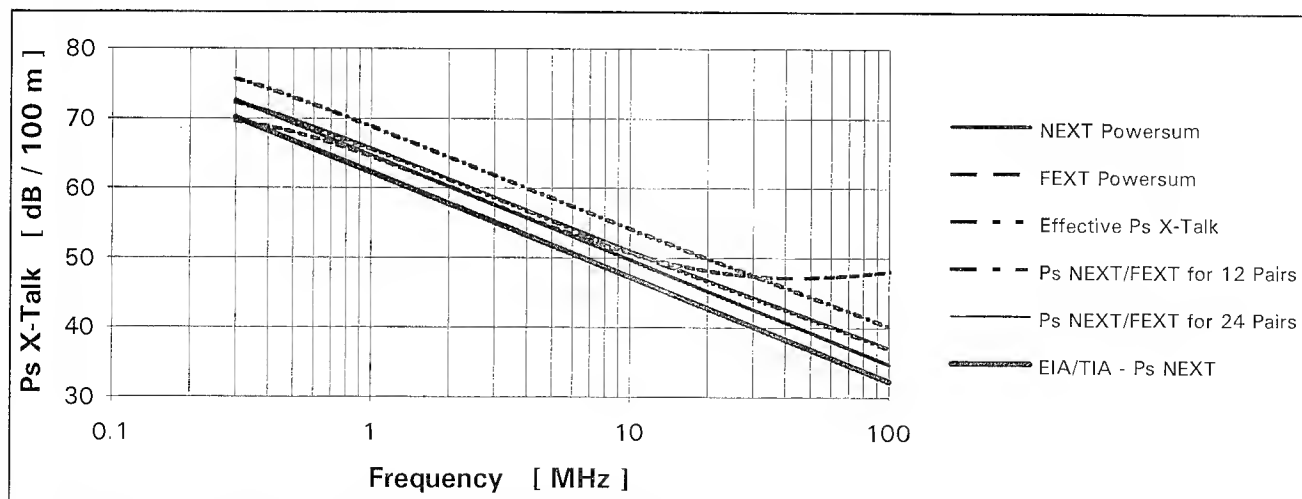


Fig. 22 : Effective Ps X-Talk vs Frequency for the Cable # 3 including EIA/TIA Requirements

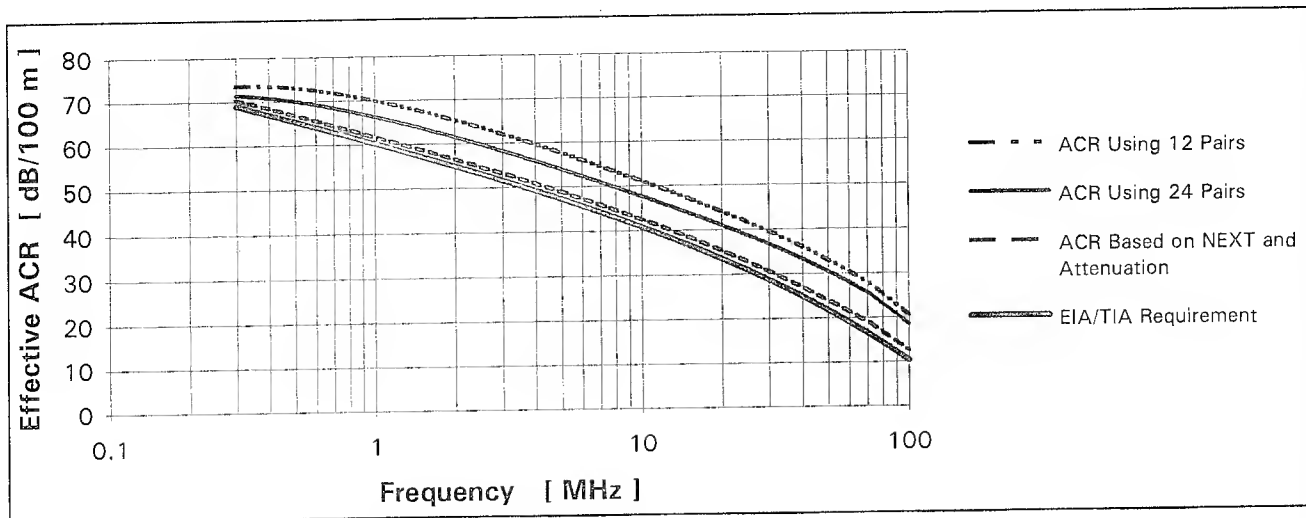


Fig. 23 : Effective ACR Values vs Frequency for the Cable # 1

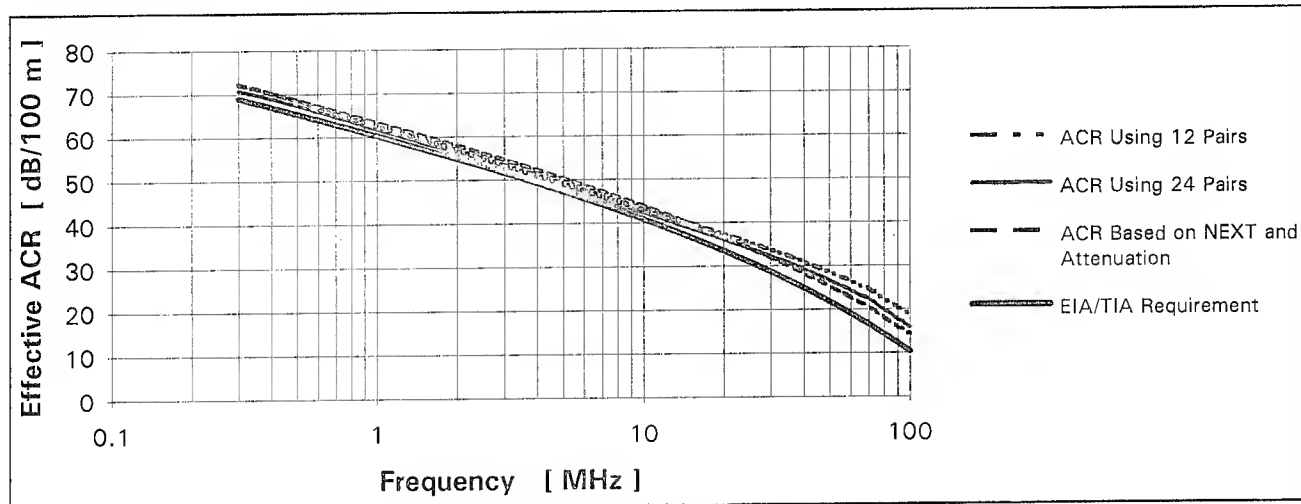


Fig. 24 : Effective ACR Values vs Frequency for the Cable # 2

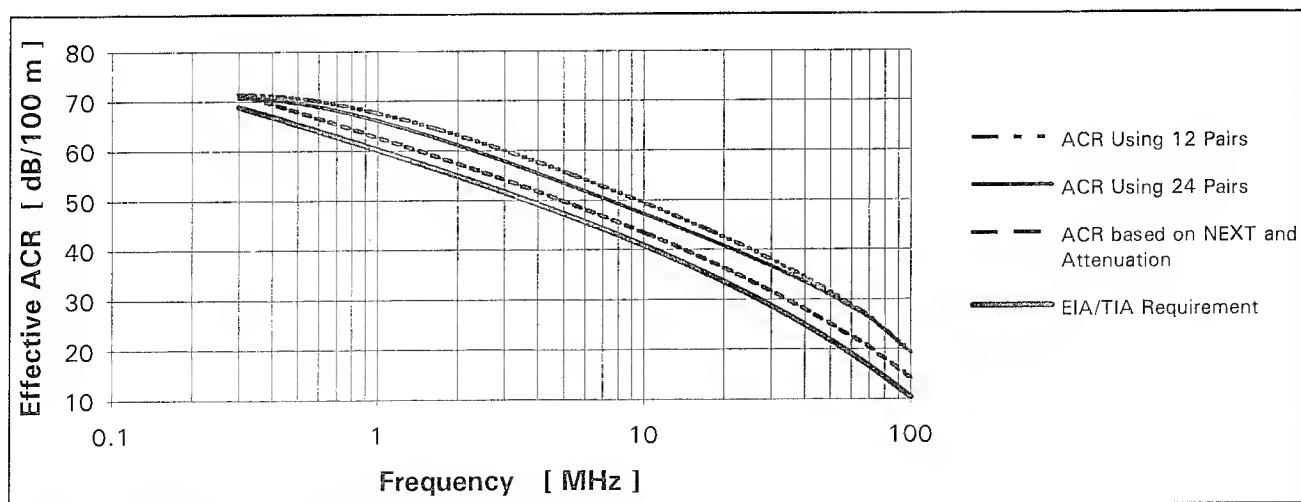


Fig. 25 : Effective ACR Values vs Frequency for the Cable # 3

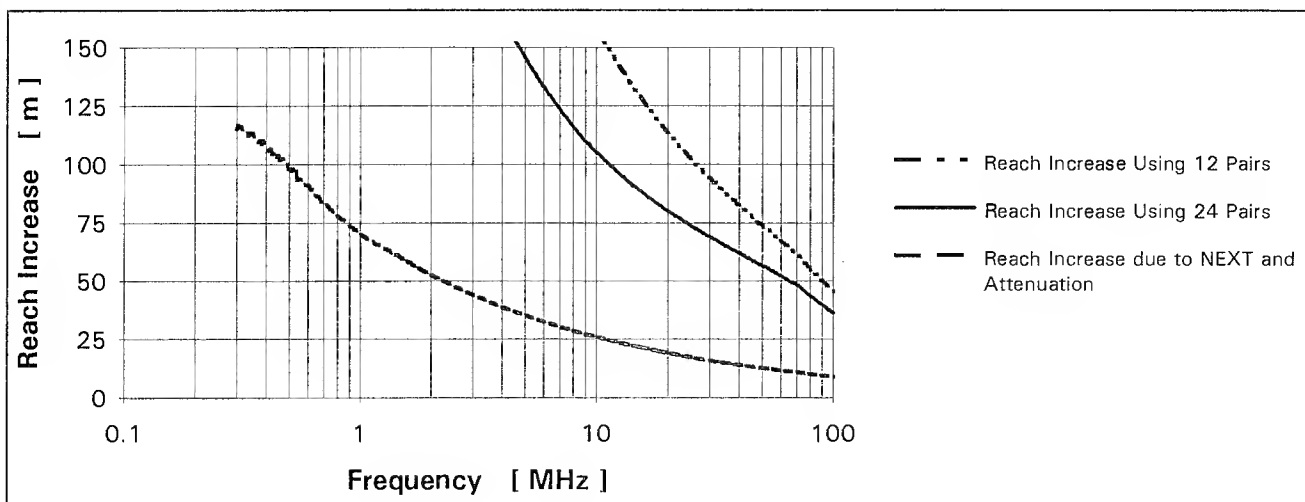


Fig. 26 : Additional Reach due to ACR Margin vs Frequency for the Cable # 1

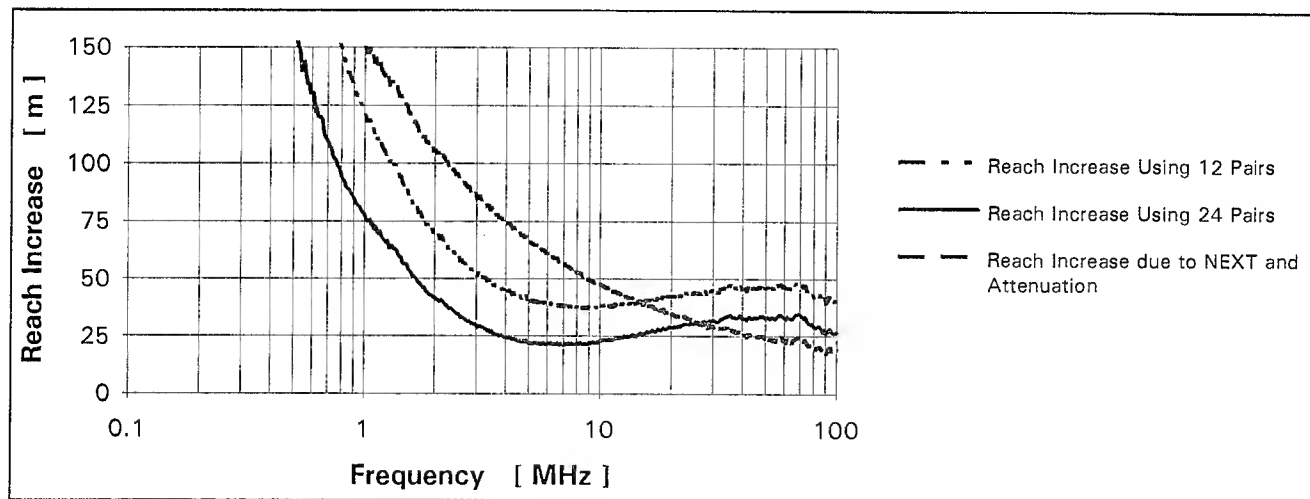


Fig. 27 : Additional Reach due to ACR Margin vs Frequency for the Cable # 2

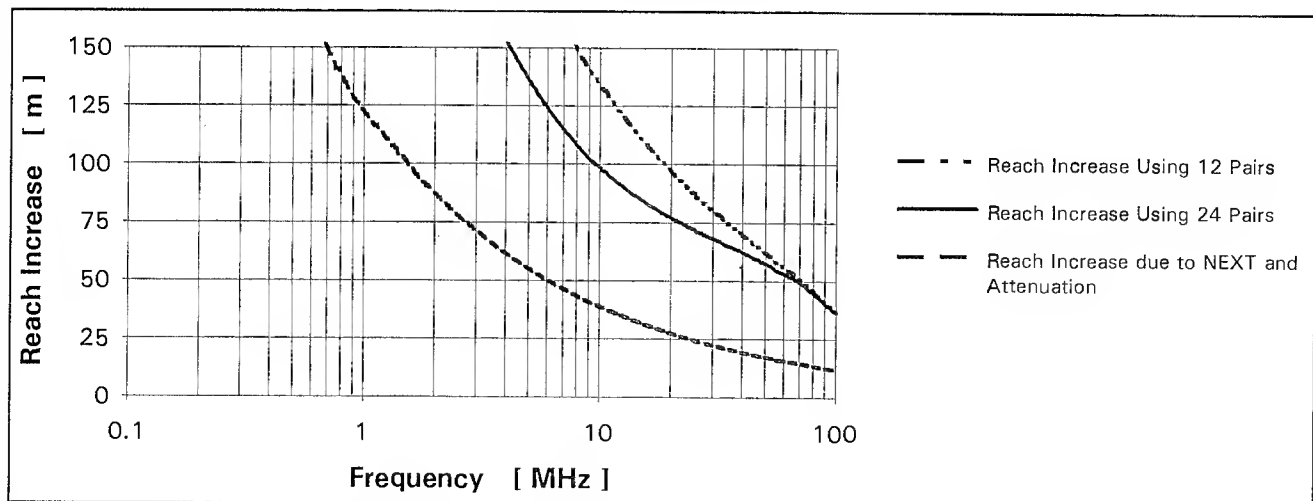


Fig. 28 : Additional Reach due to ACR Margin vs Frequency for the Cable # 3

managersoftware gave a full picture of the traffic levels in the LANs and on eventual error occurrences.

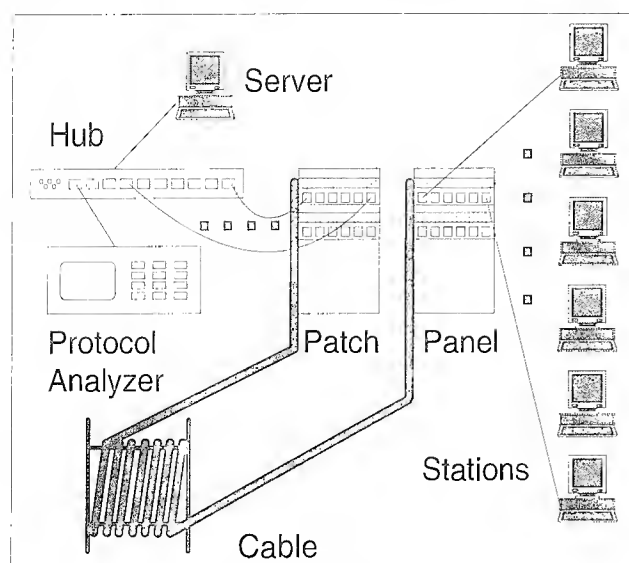


Fig. 29 : Schematic of the Test Setup

To establish the maximum reach under acceptable bit error rate conditions, the same LAN set-up has been used, but the cables were substantially longer. The cables were connected into the link with only two pairs to evaluate roughly the error behaviour or to determine if a link could be established. If this has been judged acceptable, then the entire cable was connected and the measurement were carried out. If the link could not be established or the obtained error rate was exceeding acceptable values ($BER \approx 10^{-9}$), the cable was shortened and the measurements carried out again. This has been repeated up to the time when the bit error rate was judged to be acceptable.

Bit - Error - Rates for a Standard 100 m Link			
	Cable # 1	Cable # 2	Cable # 3
10Base-T	1.6 e-10	-	-
Token-Ring	1.4 e-10	-	-
XDDI	1.4 e-10	-	-
10Base-T and Token-Ring	8.2 e-11 1.4 e-10	- -	- -
XDDI and 10Base-T	6.6 e-11 8.7 e-11	8.4 e-11 1.4 e-10	6.8 e-11 1.2 e-10
XDDI and Token Ring	8.4 e-11 6.5 e-10	6.2 e-11 1.1 e-10	6.3 e-11 1.2 e-10

Table IV

Results and Discussion

In Table IV the obtained bit error rates are compiled for the three different cables and for the different LAN

configurations.

Reach [m] \	Bit-Error-Rate for Different Links					
	Cable # 1		Cable # 2		Cable # 3	
10Base-T	215	1.5 e-9	180	-	215	1.7 e-8
Token-Ring	162	1.8 e-10	150	-	173	8.1 e-9
XDDI	125	2.7 e-10	130	1.0 e-10	134	1.1 e-10
XDDI &	125	4.1 e-11	128	1.2 e-10	134	1.4 e-10
10Base-T		1.4 e-10		1.7 e-10		2.2 e-10
XDDI &	125	1.2 e-10	128	1.4 e-10	134	1.4 e-10
Token-Ring		2.4 e-10		2.3 e-10		2.3 e-10

Table V

It is obvious that the utilization of the cable for a given LAN protocol will yield approximately the same bit error rates over a 100 m link. The same is also true for the joint utilization at relatively low bit error rates. The bit error rate measurements on the cable # 2 and the cable # 3 have, therefore, been omitted. Our results indicated, furthermore, that the high bit rate LAN protocol prevails with respect to the reach performance. We, therefore, omitted to report here the results for the utilization of the cable with three LAN protocols simultaneously.

Table V lists the obtained maximum reach values and the corresponding bit error rates that were obtained under these conditions. The results indicate that the maximum reach for the cables # 1 and # 3 under lower bit rate LAN protocols is higher than that of the cable # 2. The reach for the cable # 2 has been taken from an article [7]. At the high bit rate LAN protocol (TP-XDDI), the maximum reach falls slightly from cable # 1 to cable # 3, and this also occurs when the cable is fully utilized with TP-XDDI and either Token-ring or 10Base-T. However, also in this case the predominant influence is dictated by the high bit rate LAN protocol. To facilitate the assessment of reach due to the ACR margin, we indicated in Fig. 30 the primary lobes of the powerspectrum of the utilized LAN protocols. They were measured for each protocol at the transmit and the receive end. These power spectra indicate the main frequency range for each LAN protocol. These frequency ranges can be compared to the additional reach values versus frequency which are derived from the ACR margin.

These results were expected from the additional reach potentials derived from the ACR margins under different cable utilization configurations and taking the NEXT and FEXT measurements for the effective power sum into account (see also Fig. 26 to 28).

When supporting dissimilar high bit rate protocols like TP-XDDI, the upcoming 100Base-T and 155 Mb/s ATM, we anticipate that the maximum link length will have to be limited to approximately 100 to 110 m. We are planning some trials in this direction, though the 100Base-T (Fast-

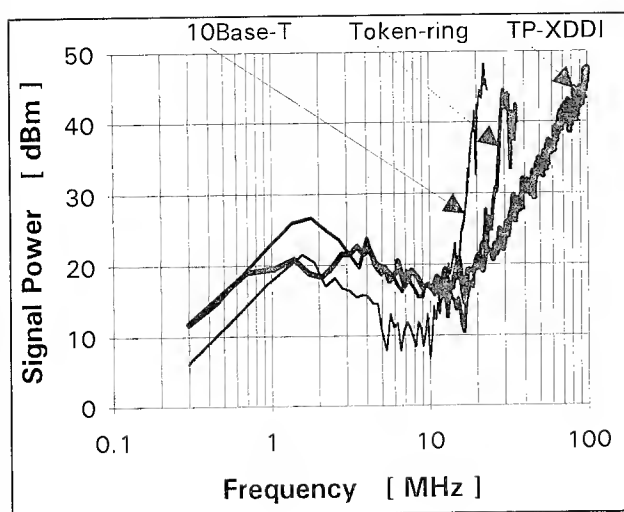


Fig. 30 : Primary Lobes of the Power Spectra of the used LAN Protocols

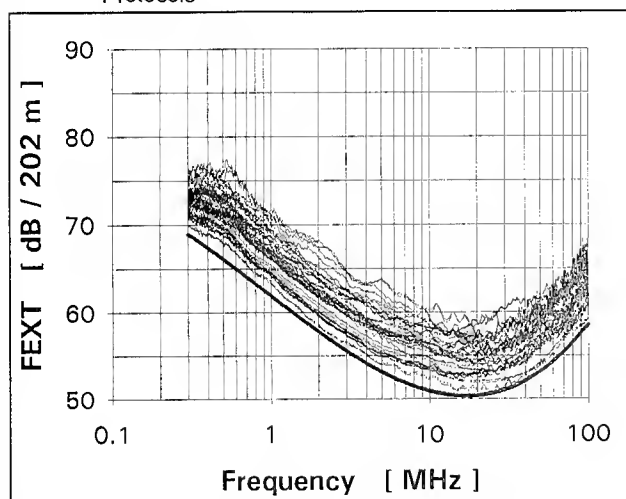


Fig. 31 : FEXT vs Frequency for the Cable # 2 with a Length of 202 m

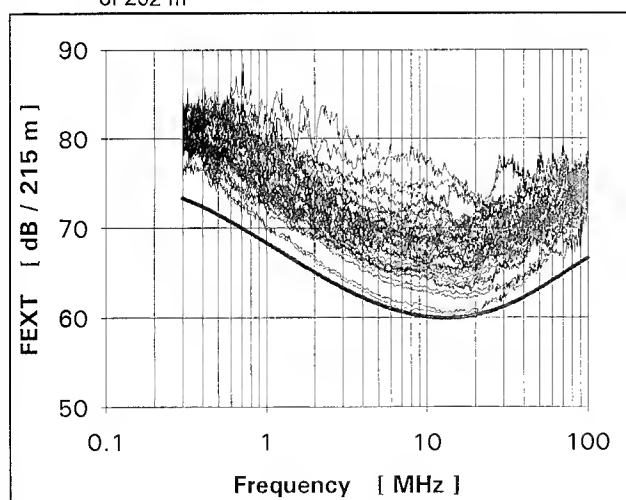


Fig. 32 : FEXT vs Frequency for the Cable # 3 with a Length of 215 m

Ethernet) protocols and the ATM Forum requirements are not yet finalized.

Conclusion

We can conclude from our measurements, that

- swept frequency measurements are required to safely assess the secondary transmission parameters and the crosstalk values.
- the lower envelopes for both NEXT and FEXT adequately describe the worst crosstalk condition provided they are based upon swept frequency measurements.
- the method to measure the impedance needs some refinement, in order to eliminate the fluctuations which are caused by a phase shift between open and short circuit measurements, and which deviate from 180°. These fluctuations are also falsely impacting upon the results of the SRL determination based upon the method described in the ASTM D 4565 Standard.
- for high bit rate LAN protocols the cable performance can be established correctly based upon the Power Sum NEXT requirements alone.
- additionally, FEXT measurements are required, if the cables are used for the lower bit-rate LAN protocols or for mixed protocols and this over length exceeding the basic 100 m link length. In fact, Fig. 31 and 32 show the minima for the Power Sum FEXT measurements for the cable # 2 at a length of 202 m and for the cable # 3 at a length of 215 m. These minima are falling right into the frequency range utilized for the low bit rate LAN protocols.
- if FEXT measurements are required the effective power sum crosstalk will have to be computed using the obtained NEXT and FEXT measurements, taking into account the applicable structured wiring scheme.
- the calculation of an additional reach beyond 100 m out of the ACR margin can yield a good indication for the obtainable reach increase, even if the change of the corresponding FEXT values, due to this length increase, are not yet taken into account.
- Correctly designed cables allow a installed cable length increases of 33% over the standard 90 m, even if they are used for high bit rate LAN protocols.

Literature

- [1] R.J. Oakley and R. Jaar: A Study into Paired Cable Crosstalk. IWCS 22(1973), p. 136-149

- [2] R. Jaar and R. L'Ecuyer: NEXT and FEXT Coupling Loss Variations with Length in Paired Telephone Cables. BNR-Technical Report TR-4090-71-09 (Internal Report)
- [3] R. Hoffmann and E. Stremmel: Error Correction of Characteristic Impedance Measurement of Twisted Pair Cables. IWCS 36(1987), p.504-508
- [4] J.-H. Walling et al: Transmission Performance of Quadded Wire and Cable for T1 and High Speed Data Services. IWCS 42(1993), p.283-295
- [5] K. Yanagawa, K. Yamanaka, T. Furukawa and A. Ishihara: A Measurement of Balanced Transmission Lines Using S-Parameters. Proposal to the IEC SC 46C/Wg7 in Paris on May 19-20, 1994. Also presented at the "10th Anniversary Instrumentation and Measurement Technology Conference", IEEE Instrumentation and Measurement Society, May 10-12, 1994
- [6] K. Yamanaka and K. Yanagawa: Balanced Parameter Measurement by Modal Decomposition. (Private Communication)
- [7] NN : Breaking the Power Sum Barrier. BICSI-News 14(1994), p. 6 ff.

Software Used

MS-Visual Basic 3.0
 Designer 3.0
 MS-Excel 4.0 & 5.0

Novell Netware 3.11
 WordPerfect 5.1 & 6.0
 MS-PowerPoint 3.0

Jörg-Hein (Jo) Walling received his diploma in Mechanical Engineering, Materials Technology in 1966 at the Technical University of Berlin. In 1974 he obtained a Doctor's degree (Dr.-Ing.) in Engineering, Material Science, at the same University. At the end of 74 he joined Northern Telecom



Canada Ltd. in the Research and Development Department. Since 1976 he is senior engineer at the Lachine Cable Plant. He is responsible for the Design of Outside Plant and Data Grade Wires and Cables.

Appendix

Equipment Used for Measurements

- 1 Compaq Deskpro 66M as Server with NT-XDDI-EISA-UX-F-Card
- 1 Compaq 486s/16 with 10Base-T and Token-ring Cards as second Server
- 5 Compaq Deskpro 386/25 with NT-XDDI-EISA-UX-F-Cards
- 6 Compaq 386/20 With 10Base-T and Token-ring Cards
- 1 TP-XDDI Hub NT-Lanmaximizer Mx-DE
- 1 10Base-T Hub Lannet SH-E16
- 1 Passive Token-ring Hub NT-HU 701601
- 1 Cybex Commander, 8-position Keyboard and Monitor Switch
- 1 Protocol-Analyzer Wandel & Goltermann, with 10Base-T, Token-ring and TP-XDDI cards
- 1 Protocol-Analyzer HP - Network Advisor Series 486 (This analyzer has been given on loan by Hewlett-Packard for the purpose of this investigation.)
- 2 Patch Panels QC BIX 46 DI with corresponding rackmount
- 50 Patch-cords, i.e. 25 ISDN and 25 TP-XDDI 4 feet long patch-cords respectively
- 1 HP - Network Analyzer HP-8753C
- 1 S-Parameter Test-Set HP-85047A
- 1 Impedance Switch Test Unit HP 3235 (a dual 32x32 matrix switch)
- 2 32 position balun matrix (The Siemon Company)
- 1 Compaq Deskpro XE 450 with Monitor 171FS
- 1 DCM-Testset and Fanning Fixture
- 1 Spectrum Analyzer Anritsu MS-2601A



Martin Bélanger is an electrical engineer. He received his B.E. in Electrical Engineering from the University of Sherbrooke. In 1992 he joined Northern Telecom Canada Limited, Cable Group Technology. He is actually working in the cable design group on high grade data cables and is

responsible for the development of electrical test methods and systems. He is also responsible to transfer newly developed data grade products into production.

Brenda Lord received her B.E. in Electrical Engineering from Concordia University in May 1994. At the University she held the position of chairperson of the student chapter of the IEEE. She recently joined Northern Telecom Canada Ltd. as an engineer in the Cable Group Technology department. She is actually working on high frequency system and component evaluation.



Analysis and Improvement of Crosstalk (NEXT & FEXT) for Multi-unit, Backbone UTP
Cable applied up to FDDI/ATM Data Speed

Shinji Hinoshita

Shinya Ishi

Kenji Ishii

Hitachi Cable, Ltd.

5 - 1 - 1, Hitaka - cho, Hitachi - shi, 319 - 14, Japan

ABSTRACT

For higher bit rate data transmission on paired cables, crosstalk (NEXT&FEXT) in multiple unit type backbone cables tend to be fundamental limitations. The purpose of this paper is to seek the indications of improvement of FEXT as well as NEXT through analyzing direct and indirect crosstalk paths.

For analysis purpose, basic crosstalk equivalent circuit model is proposed. Seven (7) crosstalk paths for each NEXT and FEXT are picked up through the solution of the input and output voltage formula derived from the partial differential equations and boundary conditions of transmission line equations of crosstalk model. For dominant crosstalk paths, statistical power sums of mean crosstalk formulas are obtained.

Through the above analysis, significant crosstalk improvement was achieved and guaranteed for Multi-Unit, Backbone UTP Cable applied up to FDDI/ATM speed by minimizing the standard deviation of unbalance coupling.

1. Introduction

Digital twisted pair cable has become preferable transmission media for building wiring in local area networks (LANs) because of easiness of joint and modification wiring within office environment. Improvement of the electrical performance upto FDDI data speed greatly contributes the decreasing LAN systems' cost. Crosstalk and electromagnetic interference (EMI) among electrical performance will be main features for unshielded twisted pair cable (UTP).

Crosstalk is picked up in this paper because improvement of crosstalk interference eliminates EMI problem.

Near-end crosstalk (NEXT) is basically dominant system feature and regulated in the specification for system guarantee convenience in open ended system. But far-end crosstalk (FEXT) is also considered in the paper whether FEXT becomes dominant in the point of view of the attenuation to crosstalk ratio (ACR) considered pair assignment of transmission directions of LAN link systems.

Through theoretical analysis of crosstalk (NEXT & FEXT), complete improvement of crosstalk attenuation of **Multi-Unit, Backbone UTP Cable** was achieved that guarantees upto ATM data speed (156 Mbit/s) transmission.

Cable Type Considered

Cable Type : Backbone UTP, 100 ohm
Construction : Multi-unit
Conductor size : 0.5mm
Number of pairs : 24 pairs or more

2. Crosstalk Equivalent Circuit Model

2.1 Five(5) conductor transmission line circuit^[1]

Five (5) conductor transmission line circuit is proposed in order to investigate crosstalk paths (Fig. 1). Conductor #1 and #2 are forming a real line circuit #r (disturbing pair), conductor #3 and #4 are forming a side circuit #s (disturbed pair) and conductor #5 consists of a bunch of conductors of rest of pairs.

2.3 Coupling function^[1]

Impedance unbalance and admittance unbalance are introduced in coupling function of equation (1) and (2) in order to estimate the crosstalk.

(1) Coupling function between real circuits (#r → #s)

$$K_{rs}^f(x) = \frac{Z_{0s}}{4} K_{rs} \mp \frac{M_{rs}}{Z_{0s}} \quad (3)$$

$$K_{rs} = Y_{13} - Y_{14} - Y_{23} + Y_{24} \approx j\omega k_{ss} \quad (4)$$

$$M_{rs} = Z_{13} - Z_{23} - Z_{14} + Z_{24} \approx j\omega m_{ss} \quad (5)$$

(2) Coupling function between real line circuit and tertiary line circuit (#r → #t)

$$K_{rt}^f(x) = \frac{Z_{0t}}{2} K_{rt} \mp \frac{M_{rt}}{2Z_{0r}} \quad (6)$$

$$K_{rp} = (Y_{13} + Y_{14} - Y_{23} - Y_{24}) + \frac{1}{2}(Y_{15} - Y_{25}) \approx j\omega k_{sp} \quad (7)$$

$$M_{rp} = (Z_{13} - Z_{23} + Z_{14} - Z_{24}) - (Z_{11} - Z_{22}) \approx j\omega m_{sp} \quad (8)$$

$$K_{rq} = (Y_{15} - Y_{25}) = j\omega k_{sE} \quad (9)$$

$$M_{rq} = (Z_{13} - Z_{23} + Z_{14} - Z_{24}) + (Z_{11} - Z_{22}) \approx j\omega m_{sE} \quad (10)$$

(3) Coupling function between tertiary line circuit and side line circuit (#t → #s)

$$K_{qs}^f(x) = \frac{Z_{0s}}{2} K_{qs} \mp \frac{1}{2Z_{0t}} M_{qs} \quad (11)$$

$$K_{qs} = Y_{35} - Y_{45} \approx j\omega k_{sE} \quad (12)$$

$$M_{qs} = (Z_{13} + Z_{23} - Z_{14} - Z_{24}) + (Z_{23} - Z_{44}) \approx j\omega m_{sE} \quad (12)$$

Where, Suffix letter on shoulder of K means ;

f : FEXT coupling function

n : NEXT coupling function

Z_{or}, Z_{os} & Z_{ot} : Characteristic impedance

Z, Y : Impedance and Admittance between conductors of transmission line.

Suffix numbers denote conductor number in Fig.2 to Fig. 4.

When, Series impedance unbalance (resistance and inductance) and Leakage conductance unbalance are neglected ;

k : Electrostatic coupling coefficient

m : Electromagnetic coupling coefficient

$\omega : 2\pi f$, f is frequency

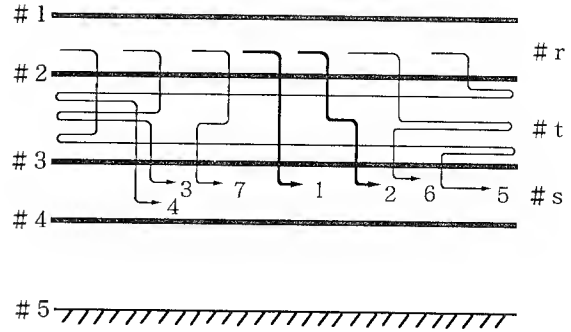


Fig. 2 FEXT paths #r to #s

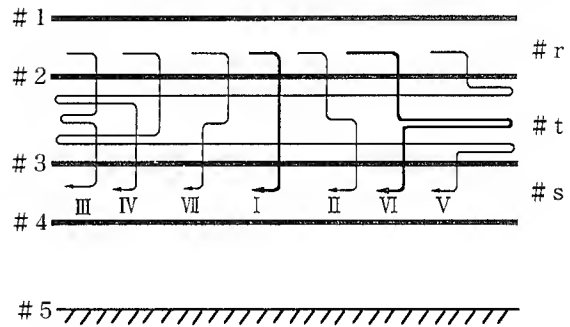


Fig. 3 NEXT paths #r to #s

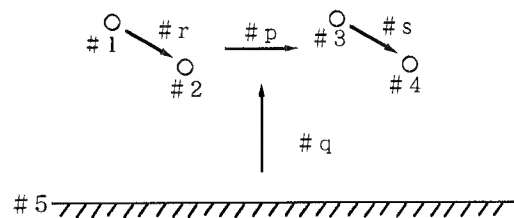


Fig. 4 Conductor number and line circuits formation

2.4 Calculation of crosstalk attenuation

In order to know whether equation (1) and (2) are useful, NEXT and FEXT are calculated with following conditions ;

- (1) Coupling function is uniform and constant along the cable length.
Cable length : 250 meter
- (2) Measured values are used for following parameters,
 k_{ss} , k_{sp} , k_{se} , m_{ss} , Z_0 and attenuation.
- (3) Assumed values are used from the measured values between real line circuit and unbalance line circuit of subjected pair,
 m_{sp} and m_{se} .
- (4) Phase constant is adjusted from the measured value to fit the resonance frequency of crosstalk frequency response. But for #r and #s, measured values are used.

2.4.1 Calculated value of FEXT

Comparison data of calculated FEXT and measured FEXT of length 250 meter cable is presented in Fig. 5.

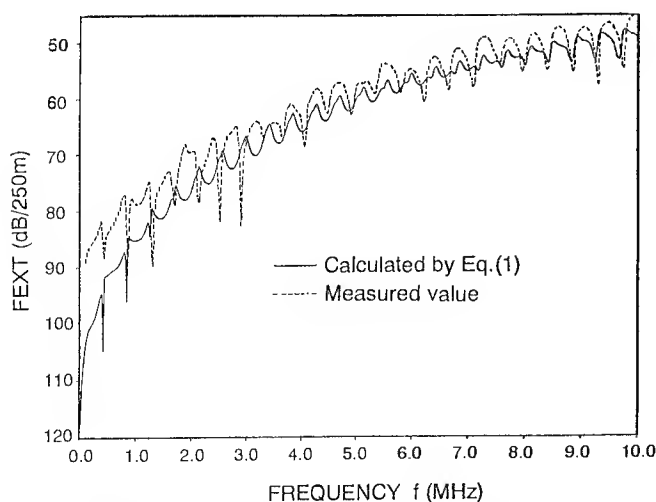


Fig. 5. Frequency response of FEXT

2.4.2 Calculated value of NEXT

Comparison data of calculated NEXT and measured NEXT of length 250 meter cable is presented in Fig. 6.

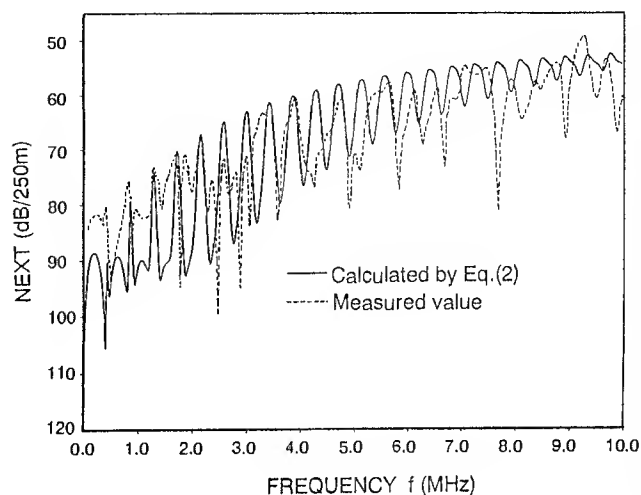


Fig. 6. Frequency response of FEXT

2.4.3 Dominant crosstalk path

Basic coincidence between calculated crosstalk data and measured crosstalk data is confirmed with level of frequency resonance response as shown in Fig. 5 and Fig. 6.

From the level comparison of calculated crosstalk paths (order of terms of equation (1) and (2) corresponds the crosstalk path number is Fig. 2 and Fig. 3), dominant crosstalk paths are obtained as follows.

FEXT ;

- Crosstalk path No. 1 : Direct FEXT (DFEXT)
- Crosstalk path No. 2 : Double FEXT (WFEXT)

NEXT ;

- Crosstalk path No. I : Direct NEXT (DNEXT)
- Crosstalk path No. VI: Farend - Refraction - Farend
NEXT (FRF - NEXT)

3. Statistical mean power of crosstalk

In order to seek major improvement parameters, statistical mean power of crosstalk is considered by introducing autocorrelation function on coupling functions for dominant crosstalk paths. Another purpose of following study is to find out frequency dependence and length dependence for dominant crosstalk paths.

3.1 Introduced autocorrelation function

Following autocorrelation functions of coupling functions are introduced under assumption that the coupling function has zero - mean and statistical random phenomenon.

3.1.1 Autocorrelation function of FEXT coupling function $(K_{sr}^f(\chi))$, NEXT coupling function $(K_{sr}^n(\chi))$, between #r and #s.

$$K_{sr}^f(\chi) = j\omega \left(\frac{Z_{0s} k_{ss}(\chi)}{4} + \frac{m_{ss}(\chi)}{Z_{0s}} \right) \quad (13)$$

$$= j\omega \kappa_{sr}^f(\chi)$$

$$\left\langle \kappa_{sr}^f(\chi) \kappa_{sr}^f(\chi + \delta) \right\rangle = \sigma_{sr}^2 e^{-\frac{|\delta|}{\delta_{sr}}} \cos S\delta \quad (14)$$

Where, $k_{ss}(\chi)$: Electrostatic coupling coefficient
 $m_{ss}(\chi)$: Electromagnetic coupling coefficient
 Z_{0r}, Z_{0s} : Characteristic Impedance of #r, #s
 δ_{sr} : Autocorrelation length
 σ_{sr} : Standard deviation of function $\kappa_{sr}^f(\chi)$

$$Sf = \frac{2\pi}{P_r} - \frac{2\pi}{P_s}$$

P_r, P_s : Lay length of #r, #s

3.1.2 Autocorrelation function of coupling function between real line circuit and tertiary line circuit

(a) #r \rightarrow #t

$$K_{rt}^f(\chi) = j\omega \left(\frac{Z_{0t} k_{rt}(\chi)}{2} - \frac{m_{rt}(\chi)}{Z_{0r}} \right) \quad (15)$$

$$= j\omega \kappa_{rt}^f(\chi)$$

$$\left\langle \kappa_{rt}^f(\chi) \kappa_{rt}^f(\chi + \delta) \right\rangle = \sigma_{rt}^2 e^{-\frac{|\delta|}{\delta_{rt}}} \quad (16)$$

(b) #t \rightarrow #s

$$K_{ts}^f = j\omega \left(\frac{Z_{0f} k_{st}(\chi)}{2} - \frac{m_{st}(\chi)}{Z_{0r}} \right) \quad (17)$$

$$= j\omega \kappa_{ts}^f(\chi)$$

$$\left\langle \kappa_{ts}^f(\chi) \kappa_{ts}^f(\chi + \delta) \right\rangle = \sigma_{st}^2 e^{-\frac{|\delta|}{\delta_{st}}} \quad (18)$$

(c) Mutual autocorrelation function of $K_{rt}^f(\chi)$ and $K_{ts}^f(\chi)$

$$\left\langle \kappa_{rt}^f(\chi) \kappa_{ts}^f(\chi + \delta) \right\rangle = \sigma_{rt} \sigma_{ts} e^{-\frac{|\delta|}{\delta_{12}}} \quad (19)$$

Where, $k_{rt}(\chi), k_{ts}(\chi)$: Electrostatic coupling function coefficient
 $m_{rt}(\chi), m_{ts}(\chi)$: Electromagnetic coupling function coefficient
 Z_{0r}, Z_{0s}, Z_{0t} : Characteristic impedance
 $\delta_{rt}, \delta_{ts}, \delta_{12}$: Correlation length
 σ_{rt}, σ_{ts} : Standard deviation of $\kappa_{rt}^f(\chi), \kappa_{ts}^f(\chi)$

3.2 Mean power of crosstalk

Mean power of crosstalk is calculated by conjugated complex integration method by introducing equation (14), (16), (18) and (19).

3.2.1 Mean Power of DFEXT ($\langle Fd^2 \rangle$)

$$\langle Fd^2 \rangle = \frac{\omega^2 \sigma_{rs}^2 \ell \delta_{rs}}{2(1 + (S^2 + \Delta\beta^2) \delta_{rs}^2)} \quad (20)$$

Where, $\Delta\beta$: Difference of phase constant between #r and #s.
 ℓ : length of cable

3.2.2 Mean Power of WFEXT ($\langle F_{ff}^2 \rangle$)

$$\langle F_{ff}^2 \rangle \approx \frac{1}{2} \omega^4 \sigma_{rt}^2 \sigma_{ts}^2 \ell^2 \delta_0^2 \quad (21)$$

Where, $\delta_{rt} = \delta_{ts} = \delta_0$

3.2.3 Mean Power of DNEXT ($\langle Nd^2 \rangle$)

$$\langle Nd^2 \rangle = \frac{\omega^2 \sigma_{rs}^2 \delta_{sr} (1 - e^{-4\alpha\ell})}{8\alpha(1 + (S^2 + 4\beta^2)\delta_{rs}^2)} \quad (22)$$

Where, α : Attenuation constant of #r, #s

β : Phase constant of #r, #s

3.2.4 Mean power of FRF-NEXT ($\langle N_{ff}^2 \rangle$)

$$\langle N_{ff}^2 \rangle = \frac{\omega^4 \sigma_{rt}^2 \sigma_{ts}^2 \ell^2}{4(e^{4\alpha_t\ell} + e^{2\alpha_t\ell} \cos\beta_{t\ell} - 1)(1 + \Delta\beta^2 \delta_0^2)^2} \quad (23)$$

Where, α_t : Attenuation of #t

β_t : Phase constant of #t

3.3 Frequency dependence and length dependence of dominant crosstalk paths

It is very important to know the feature of dominant crosstalk paths in order to design the extent of application (coverage area and frequency).

Frequency and length dependance of dominant crosstalk paths (Eq. (20), (21), (22) and (23)) are summarized in Table 1.

Table 1 Frequency and length dependance of dominant crosstalk paths

Crosstalk path	Frequency	Length
DFEXT (F_d)	$\propto f$	$\propto \sqrt{\ell}$
WFEXT (F_{ff})	$\propto f^2$	$\propto \ell$
DNEXT (N_d)	$\propto f^{\frac{3}{4}}$	$\propto \sqrt{1 - e^{-4\alpha\ell}}$
FRF-NEXT (N_{ff})	$\propto f^2 / e^{c\sqrt{f}}$	$\propto \ell / e^{2\alpha\ell}$

As conclusion of this clause, improvement WFEXT will greatly contributes to expand the application of area coverage and frequency range.

3.4 Method of improvement of crosstalk

Evident solution of crosstalk improvement is obtained from Eq. (20), (21), (22), and (23).

Diminishing of standard deviation and correlation length of coupling function will improve the crosstalk of four dominant crosstalk paths.

Measurement of coupling function is impracticable but step-pulse near-end crosstalk waveform^[3] substitutes coupling function for verification of this method.

3.4.1 Step-pulse near-end crosstalk response

Typical measured step-pulse near-end crosstalk waveform ($K'(x)$) are shown in Fig. 7.

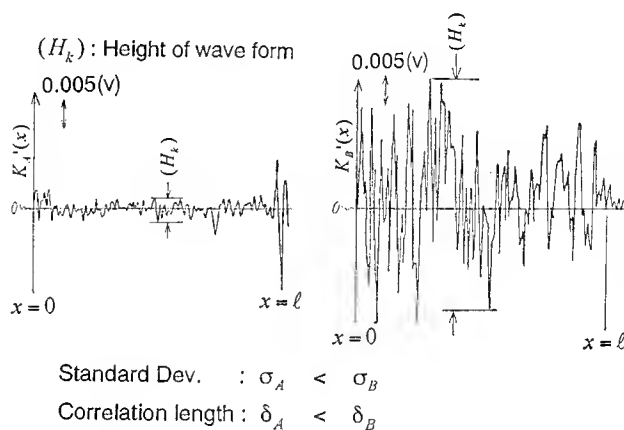


Fig. 7 Step-pulse near-end crosstalk waveform (11 volts-step balanced pulse, $\ell = 200$ meter)

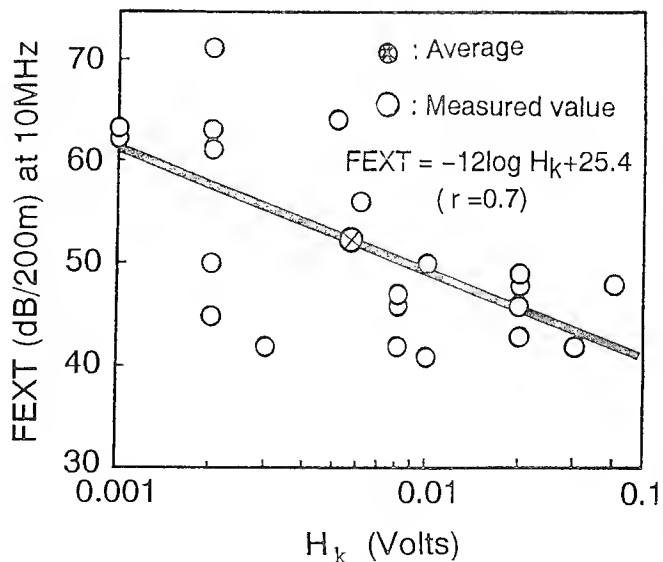


Fig. 8 Correlation analysis for FEXT & H_k

Height of wave form(Hk) may substitutes standard deviation of coupling function. FEXT may represents other crosstalk because FEXT can evaluate the value with per unit length. From correlation analysis between FEXT and Hk, correlation coefficient(r) is obtained 0.7 and formula is as follows. (See Fig. 8).

$$\text{FEXT (dB/200m/at 10MHz)} = -12\log Hk + 25.4 \quad (24)$$

It is verified that diminishing standard deviation of coupling function improves crosstalk.

3.4.2 Practical solution of crosstalk improvement

There are two ways of diminishing standard deviation of coupling function.

- (1) Decreasing the absolute value of lay length.

Half lay length promises half deviation from ideal geometry of pair and leads to 6 dB improvement.

Another decreasing lay length in half leads to 12 dB improvement in total, or

- (2) To use two plastic round string in quad formation when twisting a pair with ordinal

lay length and add close helical wrapping of plastic tape. This avoid the deviation from ideal geometry of pair.

- (3) Both two ways improvement show the same level of crosstalk performance that satisfies the requirement for bit rate above 100 Mbit/s.

4. Validation of mult - unit backbone UTP cable

In this clause, multi-unit backbone UTP cable developed by above technique verifies ACR of power sum crosstalk (P.S XT) performance in two(2) transmission case simulation.

Simulation (I) : Two(2) way transmission direction over one(1) cable.

Simulation (II) : Two(2) way transmission direction over two(2) cable.

4.1 Comparison between calculated value and measured value

Comparison data between calculated value by Eq. (1) and (2) and measured value of FEXT and NEXT over the frequency range 0.1 to 156MHz are presented in Fig. 9 and Fig. 10. Calculated condition is the same as that of clause 2.4.

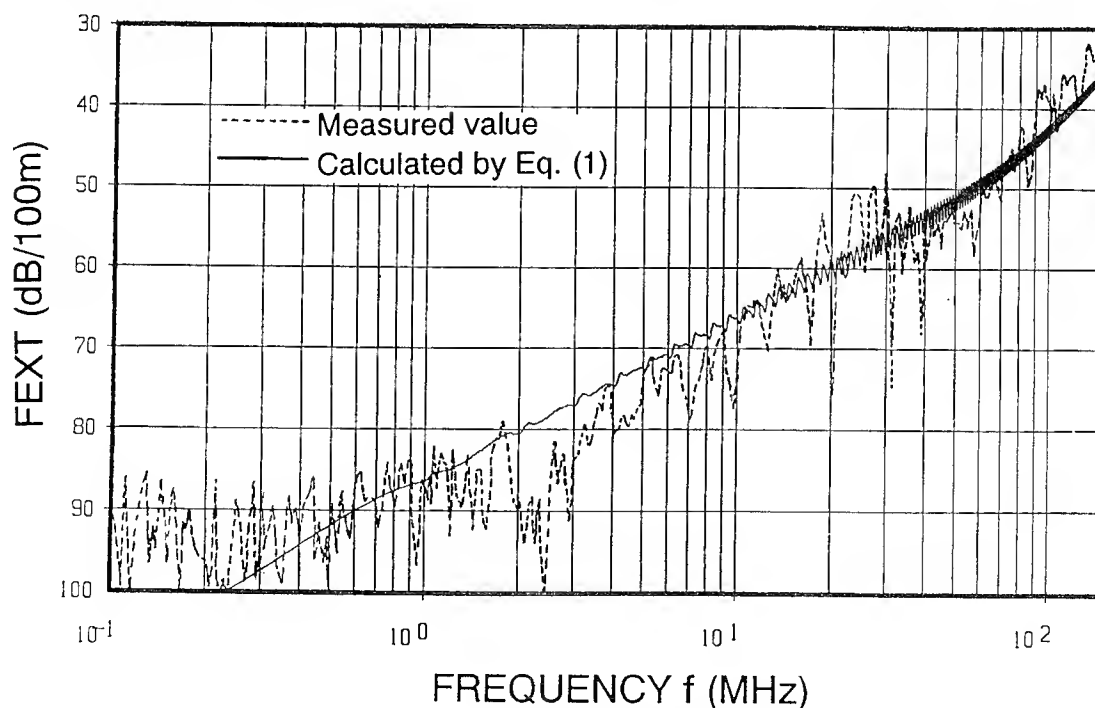


Fig. 9 Frequency response of FEXT

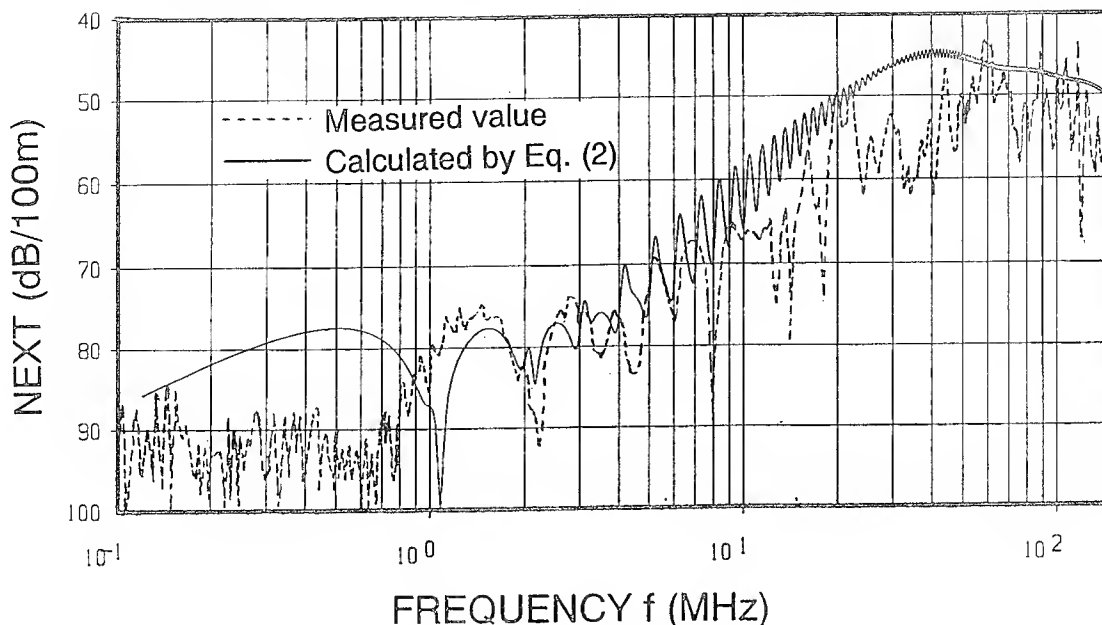


Fig. 10 Frequency response of NEXT

Equation (1) and (2) are useful when simulation data is required for different cable length to see the tendency of frequency response without cut in piece or joint for longer length.

4.2 ACR of power sum FEXT and NEXT

Power sum crosstalk requirement can not stipulate essentially as cable piece length requirement because number of disturbing pairs can not define without knowing transmission direction assignment for each pair especially for open end wiring system. However in this clause, ACR power sum crosstalk is considered in order to verify that the developed multi-unit backbone UTP cable meets the system requirement for two simulation case.

For verification, 0.5×25 pairs UTP (Category 5) cable, 100meter is used.

Another purpose of this simulation is to see which is dominant NEXT or FEXT in ACR of power sum performance over the frequency range 1 to 156 MHz.

4.2.1 Summarized data of 0.5×25 pairs UTP (Category 5) cable on FEXT and NEXT

Table. 2. Summarized data of ACR

100MHz, $\alpha = 20\text{dB}/100\text{m}$, Unit : dB/100meter

	Performance	Min.	Avg.	σ
F	FEXT	22	35	2.45
E	P.S. FEXT ¹⁾ n=24	18	20	1.38
X	Calculated ³⁾	-	20	-
T	P.S.FEXT (n=24)			
N	NEXT	42	48.2	1.72
E	P.S. FEXT ²⁾ n=24	33	34	0.64
X	Calculated ³⁾	-	34	-
T	P.S.FEXT (n=24)			
X	ACR P.S.XT ⁴⁾ n=24	13	14	-
T	ACR P.S. XT ³⁾ FEXT : n=11 NEXT : n=12	-	16	-

1) Simulation (II) : Two way/Two Cable System.

2) EIA/TIA 568 stipulation

n=24 is impractical in actual system

3) Simulation (I) : Two way/One Cable System

4) Simulation purpose, impractical in actual system because P.S. NEXT²⁾ value is used.

Note for Table 2

- 5) It is able to calculate when dB values are normal Gauss distribution with following formula.

$$P.S.XT = -10\log n + \text{Avg.} - 0.115 \sigma$$

σ : Standard deviation of Avg.

n : Number of disturbing pairs.

FEXT itself is ACR.

4.2.2 ACR P.S. NEXT and FEXT frequency dependance

Calculated ACR P.S. NEXT and FEXT value from measured value of 0.5×25 pairs UTP (Category 5) cable are presented over frequency range 1 to 156 MHz in Fig. 11.

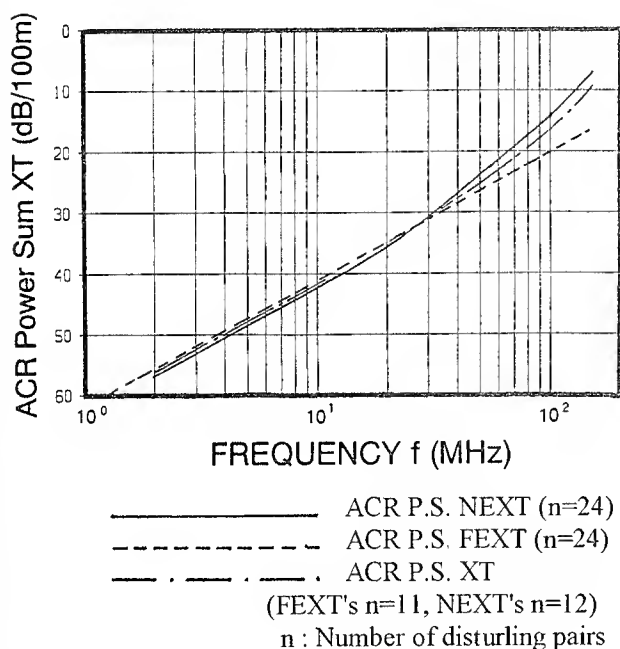


Fig. 11 ACR power sum XT frequency dependence

It is verified that the all ACR satisfy the requirement of EIA/TIA 568 (Standard Proposal No. 2840-A) and ISO/IEC 11801 (Draft stage No. ISO/IEC JTC 1/SC 25 WG3 N317).

System link length will be limited because of FEXT length dependance.

5 Conclusion

Through analysis of crosstalk and developing of multi-unit backbone UTP cable following conclusions are obtained.

- (1) Crosstalk model and its equations of crosstalk are useful to study length and frequency dependence without cut the cable.
- (2) Important parameter to improve crosstalk performance is to decrease the standard deviation of coupling function and practically, to avoid the deviation from the ideal geometry of pair.
- (3) It is proved that the power sum crosstalk can calculate with the average and standard deviation of crosstalk measured value when system integrated.
- (4) Newly developed multi - unit backbone UTP cable was validated on ACR requirement up to ATM data speed(156 Mbit/s).

REFERENCES

- [1] N.Kobayashi, "Telecommunication Line Transmission Theory", published by IEICJ, P146-152, 1971.
- [2] N.Holte, "A statistical model for calculation of crosstalk in a balanced pair cable", International Wire & Cable Symposium Proceedings, P25-31, 1976.
- [3] M.Yotsuya et al, "An approach to crosstalk coupling reduction of pair type cable", International Wire & Cable Symposium Proceeding, P182-193, 1974.



Shinji Hinoshita

Hitachi Cable, Ltd.

5-1-1, Hitaka-cho,
Hitachi-shi, 319-14
Japan

Mr. Hinoshita graduated in electrical engineering from Kure National College of Technology in 1970 and joined Hitachi Cable, Ltd and was engaged in research work for baseband PCM cable. He is currently responsible for design and development of optical fiber cables and telecommunication cables. He is now a senior engineer of the Telecommunication Design Department.



Kenji Ishii

Hitachi Cable, Ltd.

5-1-1, Hitaka-cho,
Hitachi-shi, 319-14
Japan

Mr. Ishii received the B.E. degree in mechanical engineering from Musashi Institute of Technology in 1973 and joined Hitachi Cable, Ltd. and is currently responsible for production engineering and development of digital data communication cables. He is now a deputy manager of Optical Fiber & Communication Cable Department.



Shinya Ishi

Hitachi cable, Ltd.

5-1-1, Hitaka-cho,
Hitachi-shi, 319-14
japan

Mr. Ishi received the B.E. degree in electrical engineering from Sibaura Institute of Technology in 1985 and joined Hitachi Cable, Ltd. and has been engaged in design and development of optical fiber cables and telecommunication cables. He is now a engineer of the Telecommunication Design Department.

100 Megabit per second LAN Utilizing Four and 25 Pair Unshielded Twisted Pair Media

Robert A. Wessels, Jr.

CommScope, Inc., Network Cable Division, Claremont, NC

ABSTRACT

Category 5 unshielded twisted pair (UTP) has become increasingly popular as a transmission media for high speed data. New applications are taxing the cables with higher frequencies and more stringent requirements. Since most Category 5 products currently installed have not yet been utilized past 16 Megabit per second (Mbit/s) applications there are questions about how actual installations perform at data transmission rates of 100 Mbit/s and faster. This paper reviews an actual installation on a large corporate campus that utilizes Category 5 UTP and multimode fiber to deliver Fiber Distributed Data Interface (FDDI) networking capability to over 10,000 users. In addition laboratory data is presented to illustrate the robustness of Category 5 applications.

INTRODUCTION

Category 5 UTP cable is a popular choice to support data applications ranging from Ethernet to FDDI and Asynchronous Transfer Mode (ATM). Tempering the enthusiasm for wide scale use of Category 5 UTP are concerns about performance in actual installations at data transmission rates of 100 megabits per second and higher. Until recently the availability of field data from these high speed applications has been limited.

This paper will present actual data from a campus wide installation at Microsoft's Redmond, Washington facility. Link performance after installation was measured for both 25 pair backbone and 4 pair applications running to the desktop. Bit error rate (BER) performance was monitored over a period of months to ensure consistent performance. In addition link performance measurements were conducted in the lab to establish the performance levels that could be expected in field installations.

Microsoft's Redmond Campus currently consists of 22 buildings. The Network must serve in excess of 20,000 computers that are used by the 12,000 employees employed at this location. All are networked together utilizing equipment based on the FDDI Standard. Per the proposed FDDI Twisted Pair Physical Layer Medium Dependant (TP-PMD)

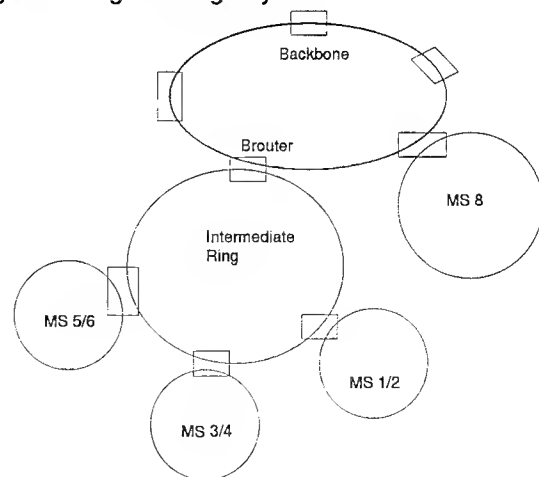
standard, MLT3 encoded signals are used to transmit data over the copper links.

FDDI was chosen to link the campus for many reasons. A major advantage to using FDDI is it's ability to support multiple protocols. In addition there are a wide variety of proven products on the market that will support both fiber and copper media choices for the migration from an existing Ethernet installation. Also the reliability of the network is enhanced by the built in redundancy of FDDI .

The Network is broken down into several components. A backbone ring serves two intermediate rings and twenty individual FDDI rings. Multimode fiber is utilized for all inter building applications on the campus. Within a building Category 5, four pair plenum rated UTP is run from the concentrator to the desktop. In addition over 1400 servers are linked to the main backbone using 25 pair, plenum rated Category 5 cable.

Microsoft's network engineers chose to use Category 5 hardware for these applications due to it's excellent electrical performance and significant cost savings over multi mode fiber. Purchase costs for the passive and active hardware components are significantly cheaper than for the fiber optic equivalent. Also, installers are more readily available and labor rates are lower than for fiber installations.

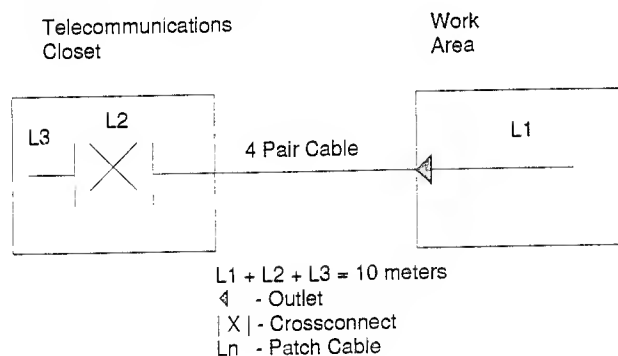
Figure 1: Logical Ring Layout



LABORATORY LINK TESTING

To simulate the actual link performance of the installed four pair Category 5 components two links were assembled under laboratory conditions. The links used 90 and 110 meters of plenum, FEP insulated, cable respectively. Patch cords were limited to 10 meters total following the draft TIA/EIA 568A guidelines. Although the 110 meter link fell outside of the standard's recommended maximum cable length of 90 meters, it represents a worst case example of what may occur in an actual installation. Attenuation and pair to pair Near End Crosstalk (NEXT) measurements were made from the wiring closet end of the link from .772 megahertz (MHZ) to 100 MHZ in frequency.

Figure 2, Lab Link Layout



A table showing the worst pair results for attenuation are shown in Figure 3. Figure 4 shows the worst pair combination NEXT for both links. The values are compared to guidelines listed in Annex E of the TIA/EIA 568A draft. Calculated attenuation to crosstalk ratios (ACR) are plotted in Figure 5. Even though the 110 meter link is 20 meters longer than recommended by the TIA/EIA 568A draft, the ACR for the link is within acceptable limits. The fundamental frequency for MLT3 encoded signal transmission is 31.25 MHZ. The worst case ACR at this frequency for the 110 meter link is approximately 25. Twelve is recommended as a minimum

for this application. Even exceeding the recommended link length by 20 meters there is significant margin available for the application.

The components used in the test are typical of the high quality Category 5 product currently available. They have significant margin for both NEXT and attenuation when compared to the Category 5 specification. Based on these results, similar field installations should perform well.

Figures 3/4/5

Table 3

Worst Case

90 meter Link

Freq. MHZ	Attenuation		NEXT		ACR
	Actual	Spec	Actual	Spec	
1	1.97	2.5	69.26	60.3	67.29
10	6.23	7.0	60.78	44.0	54.55
16	7.92	9.2	50.77	40.6	42.85
25	9.87	11.4	49.79	37.4	39.92
31.25	11.06	12.8	42.27	35.7	31.21
62.5	16.14	18.5	41.13	30.6	24.99
100	21.37	24.0	28.52	27.1	7.15

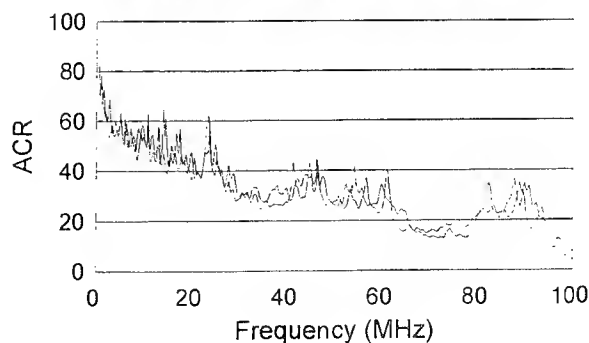
Table 4

Worst Case

110 meter Link

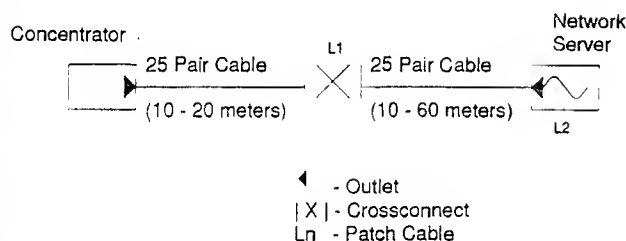
Freq. MHZ	Attenuation		NEXT		ACR
	Actual	Spec	Actual	Spec	
1	2.37	2.5	80.86	60.3	78.49
10	7.43	7.0	59.16	44.0	51.73
16	9.41	9.2	57.23	40.6	47.82
25	11.81	11.4	62.59	37.4	50.78
31.25	13.27	12.8	42.87	35.7	29.60
62.5	19.25	18.5	38.80	30.6	19.55
100	25.80	24.0	29.71	27.1	3.91

ACR 90/110 Meters



INSTALLED LINK PERFORMANCE

Figure 6, Link Model 25 Pair



Prior to turning up the new installatoin, all links were tested. At the time of the initial installations hand held testers capable of accurately measuring links to 100 MHZ in frequency were not available so a sampling of 100 MHZ tests were performed using a laboratory grade NetworkAnalyzer and S-Parameter. As previously stated there is not an established link specification so guidelines published in Annex E of the TIA/EIA draft specification were used to evaluate the link. All measurements were made from the equipment end of the link.

The 25 pair links connect the network servers through a 110 Type cross-connect to FDDI concentrators which are joined to the campus's main backbone. Plenum rated, FEP insulated, Category 5 cable was selected for this application. All pair combinations were swept tested at the factory from .772 to 100 MHZ for impedance, structural return loss, attenuation and power sum NEXT. A cross sectional view of the cable is shown in Figure 7.

Plugs and jacks were Category 5 rated however the 110 cross connect used was Category 4. Although by definition this lowers the link to a Category 4 rating, testing showed that the links all met the Category 5 guidelines for NEXT and attenuation. A typical NEXT graph is shown in Figure 8. Attenuation measurements were sampled and the results were well below the Annex E guidelines due to the relatively short twenty to seventy meter spans used in this application.

The four pair links tested used all Category 5 components and the results essentially matched those for the lab results discussed previously. All four pair links tested appeared to have adequate transmission characteristics to support TP-PMD applications.

Figure 7, Cross Section of 25 Pair Cable

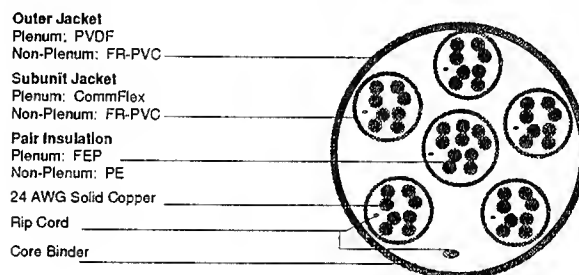
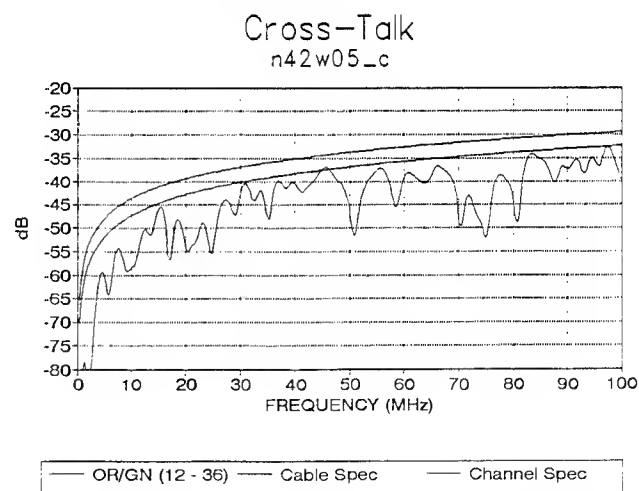


Figure 8, NEXT Results 25 Pair



BIT ERROR RATE PERFORMANCE

Even though the installed cable plant met all specified electrical guidelines, the real test is the performance of the network. There were also questions about how the electromagnetic fields (EMF) present in the environment would impact the data being transmitted.

The BER goal for FDDI systems is 1×10^{-12} with system failure occurring at 1×10^{-8} . Each concentrator monitors its transmissions for errors and provides a real time output showing link performance.

All links that have been converted to FDDI 100 Mbit/s operation have been operating with BER's between 1×10^{-12} and 1×10^{-15} . This includes all of the 25 pair links and approximately half of the 4 pair links. The 25 pair links have been operated at up to 95% of network capacity.

CONCLUSION

Laboratory measurements show that Category 5 UTP is a robust transmission media for TP-PMD 100 Mbit/s data applications. ACR values are within acceptable limits even when using links longer than the recommended 90 meters. As active devices become more bandwidth efficient, Category 5 cabling will support significantly higher data rates than are currently available.

A network consisting of Category 5, 100 ohm UTP and multimode fiber optics provides a reliable and efficient solution to large scale, high speed networking requirements. Applications such as 100 Mbit/s FDDI have been implemented in a campus environment using a fiber optic backbone and 4 and 25 pair UTP for horizontal cabling applications. Category 5 UTP media is not significantly effected by the levels of EMF found in a typical office building environment. After extended of operation, network BER performance is better than required for all TP-PMD applications currently operating.

ACKNOWLEDGMENT

The author would like to acknowledge the assistance of David Borkowski, Network Engineer for Microsoft Corporation in preparing this paper.

REFERENCES

1. EIA/TIA Standard for "Commercial Building Telecommunications Wiring Standard EIA/TIA-568 TSB 36", EIA/TIA, July 1991.
2. ANSI FDDI Twisted Pair Physical Layer Medium Dependent (TP-PMD), ANSI, March 1994.
3. TIA/EIA Standard for Commercial Building Telecommunications Wiring Standard TIA/EIA-568-A, March 1994.

BIOGRAPHY

Robert A. Wessels, Jr. received his Bachelors of Chemical Engineering degree from the Georgia Institute of Technology in 1982 and a Masters of Business Administration from Georgia State University in 1989. Rob is the Manager of Engineering for the CommScope General Instrument Network Division. He is also an active member of the TIA/EIA TR 41.8.1 committee that is writing the Commercial Building Wiring Standard, 568-A.



ENHANCED MULTI-PAIR CABLE DESIGNS: POWER SUM VALIDATIONS

William F. Reichert

Champlain Cable Corporation, Colchester, Vermont

Abstract

Enhanced multi-pair cable designs have evolved over the last several years to provide a more robust solution in local area network (LAN) applications. Although performance standards are evolving, field trials provide an important validation for LAN use. The rapid advancements in LAN technology will make Power Sum Near End Crosstalk (NEXT) important in multi-pair cable design, manufacture and end-use. Unlike the Worst Pair method, Power Sum NEXT is a measure of the cumulative energy in multi-pair cables. Requirements are close to being approval by the EIA/TIA Committee recognizing Power Sum cables in a Category 5 cable plant. Available performance data supports Power Sum NEXT capability. More importantly, OEM, lab and field data validates these robust designs and the Power Sum NEXT advantages. This paper will detail the findings of 25 pair Power Sum cable in actual network wiring applications.

Introduction

25 Pair backbone cables have evolved over time as a result of end user demand for high performance cabling. The majority of the cables are utilized in risers or plenums for closet-to-closet connections. Although issues still exist concerning performance and connectivity, designs have been tested to available requirements. Since there have been evolving draft performance standards concerning these high performance cables, development required tests and evaluations to Level 5 requirements which were available at the time. Testing was also performed by major OEM's interested in high performance, 25 pair cables in current and emerging LAN applications. These tests validate that Power Sum 25 pair cables successfully perform in network applications.

History

The dynamic LAN market necessitates that cable performance and designs are continuously improved. The history with 25 pair LAN cables began with Level 4 cable in 1991. Again, since there was no multi-pair standard at the time, the de facto standard became that of the existing "level" program and NEMA draft standards, which emphasized the Worst Pair method of crosstalk testing. Successful performance along with continuous improvements in design and manufacture led to the introduction of the first Level 5, 25 pair cable capable of performing at 100 Mbps.

As a result of the end-user/LAN community's interest in high performance, multi-pair cables, requirements are close to being approved by the EIA/TIA Committee which will recognize 25 pair backbone cabling in a Category 5 cable plant. The most significant impact of the acceptance is the requirement that multi-pair cables conform to Power Sum Near End (NEXT) Crosstalk. The difference will be that Power Sum values will reflect a total influence of pairs in the bundle versus simply finding the Worst Pair combination. A short review of each method will help clarify the differences.

Worst Pair Near End Crosstalk (NEXT) Method

A signal is applied to a pair (the disturbing pair). Crosstalk is the amount of the signal measured on another pair (the disturbed pair) at the near end of the cable. Each pair combination is tested at each frequency to determine which combination exhibits the worst crosstalk performance.

- It is assumed that all crosstalk on the disturbed pair is induced by the energy from the disturbing pair with no other pairs energized.
- This method determines the one worst pair combination from all the combinations tested.

While this is an acceptable method for bundles of 4 and fewer pairs, it does not account for the many interactions present in multi-pair cables, particularly in high speed LAN applications.

Power Sum NEXT Method

A signal is applied to a pair and measurements are made which simulate a fully active cable. The objective in this test is to determine the total amount of crosstalk present in the 25 pair bundle. In other words, beyond the Worst Pair combination, Power Sum is the cumulative effect on one pair given that the 24 other pairs exist in the bundle and are energized.

Because the power summing, in effect, is determined from combined Worst Pair measurements, cable performance is about 5 dB better when compared to Worst Pair values for the same cable. The higher the pair count, the more important the Power advantages. A 25 pair cable has 300 crosstalk pair interactions compared to 6 for a 4 pair cable!

The Power Sum method ensures compliance with Category 5 requirements using multi-pair cables in LAN applications. The validity of this method also allows the use of multi-pair cables in multiple signal applications.

Power Sum is the better parameter for revealing overall crosstalk tendency. It will show that two cables thought to have the same performance by the Worst Pair method actually do not when evaluated under the Power Sum method.

It is important to design and assemble multi-pair cables which optimize Power Sum crosstalk. It will become important for end-users to begin specifying quality, high performance cables. The advantages to be gained by Power Sum cables are:

- Category 5, latest revision, cable plant
- Cables tested which simulate fully energized pairs
- Better up-front interpretation of LAN operation
- Improved signal-to-noise ratios since NEXT will be improved
- Truer interpretation of cumulative crosstalk effects

Standards

EIA/TIA

The EIA/TIA 568A draft standard, SP-2840, for "Commercial Building Telecommunications Wiring" defines the standards for multi-pair cables. The standard defines performance for pair counts of 6 or more from Category 3 to Category 5. (Appendix 1 lists the electrical requirements for Category 3, 4 and 5 multi-pair cables.) The standard defines a wiring scheme which supports open architecture, multiple products and multiple vendors. The standard also defines both horizontal and backbone cabling. While the horizontal cable guidelines have long been established (EIA/TIA 568, TSB-36), the backbone guidelines are relatively new. Backbone cabling guidelines will allow the choice of intra-building backbone cable to be copper in designs of 6 pair and higher. Backbone cabling is specified as: connecting wire closets in the same building, from floor-to-floor or closet-to-closet. In the past, the choices for Category 5 were bundled 4 UTP cables. However, the choices are moving to Power Sum designs in 6 to 25 UTP cables.

UL LAN Cable Verification Program

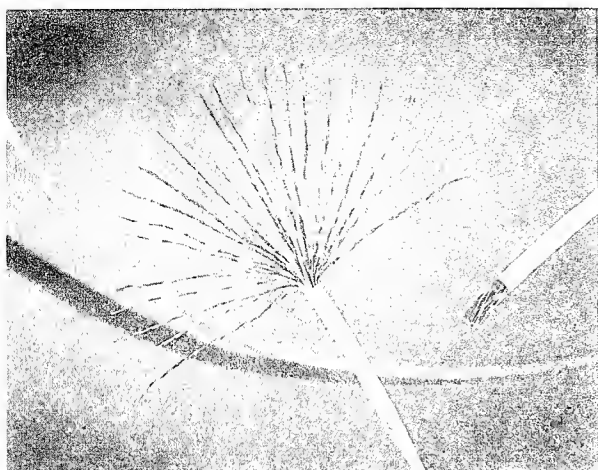
The UL program was established to support standards and provide evidence of satisfactory cable performance. Originally developed to verify Category 2 through 5, 4 pair cables, it is being expanded to include Power Sum verification on 6 pair and higher Category 3 through 5 cables. The UL program features independent verification, recognition of EIA/TIA standards, follow-up testing and quality support to monitor ongoing performance.

Design

Design

The most common multi-pair data cable in use is the 25 pair design, which is configured of 25 unshielded twisted pairs. Figure 1 is an illustration of a typical UTP design. The design considers the necessary electrical performance, as defined in Appendix 1, but also considers the needs of the installer and end-user. Multi-pair, and particularly 25 pair, cables should be designed so handling and flexibility are maximized. A couple of the design objectives to consider are easier cable management and installation.

Substitution of bundled 4 pair UTP cables with a 25 pair UTP cable should enable the installer to reduce installation costs while allowing a more manageable telecommunications closet.



Power Sum is a stringent method for determining NEXT. Previous designs were manufactured and tested to Worst Pair requirements. The issue with the Worst Pair design is it does not account for multi-pair interactions. On a 4 pair cable the majority of installations utilize 2 of the 4 pairs. Therefore, a worst pair approach is acceptable. Utilizing a multi-pair design is more complex due to the increased amount of pair interactions. Many of these cables have multiple signals running. As such, the relative energy in the cable is greater.

Multi-pair Power Sum, particularly 25 pair, cables therefore are designed with greater margin for NEXT than is typically seen. Generally, multi-pair Power Sum cable designs are about 5 dB better than past multi-pair cables designed for worst pair performance. (Appendix 2 illustrates a typical pair NEXT trace used in a 25 pair design.)

Cable Decisions

Power Sum NEXT performance is defined for 6 pair and higher on Category 3 through 5 cables. All of the different pair count designs satisfy the necessary requirements. The choice of which multi-pair cable to use depends on the particular LAN installation. Typical applications of Power Sum cables include horizontal and backbone installations. 25 pair cables are also being utilized in cable assembly applications.

It has been demonstrated that multi-pair Power Sum cables can support applications employing combinations of signals including multiple signals under one jacket. The following case studies validate multi-pair Power Sum use in LAN applications.

Applications

Case Study 1: 25 pair Power Sum UTP was trialed in a multiple signal application running 2 stations each of: 100 mbps FDDI, 16 Mbps Token Ring and 10 Mbps Ethernet. A 100 meter run of 25 pair was utilized between two prototype 50 pin connectors. Each 50 pin connector was then punched down to RJ-45 outlets via 2" (50mm), 4 pair Category 5 UTP leads. From the outlets, 4 pair UTP was utilized to connect to the hub and/or work stations. (Appendices 3, 4 and 5 illustrate the network set-up.) The goals of the tests were to:

- Determine bit error performance of one FDDI station over 90 meters of 25 pair Power Sum.
- Determine bit error performance of the same FDDI station while two Ethernet stations, two Token Ring stations and one additional FDDI station were energized—all under the same 25 pair Power Sum jacket.

4 pair UTP cable was also measured as baseline data and to quantify the 4 pair "patch" leads. (Appendix 6 graphically presents results.)

Bit Error Rate for FDDI Over
Category 5, 25 Pair Power Sum UTP

25 Pair FDDI Only 100 meters	-13 6.5 x 10
25 Pair Multi Topology 100 meters	-12 1.5 x 10
ANSI Standard BER for Cat.5	-12 1.0 x 10

The impact these BERs have on the network are shown in Appendix 7. The percentages represented for network overhead as a result of bit errors demonstrates very low overhead. Based on the results achieved, it is more likely to have other factors causing errors than cable.

Most installations would not have this worse case environment. Typically, 25 pair connections are punched down directly to 110 or 66 blocks on both ends. Additionally, cable is installed

straight out as opposed to coiled on a reel. This worst case set-up was done by design to determine worst possible performance. Actual installation performance would yield improved performance. Phase 2 of this study will utilize a 110 panel on each end with cable pulled off the reel.

Case Study 2:

The second illustration is from an installation at an insurance company. In this case, Power Sum was chosen as the solution for cable management and network operation. While standards are important and cables are designed to these standards, the true test of cable validity is if the network operates with no problems. This particular installation was experiencing problems with network performance utilizing a Category 5, 2 pair design as the interconnect cable. The design was such that each work station was dedicated to one 2 pair cable run. Since there were 200 work stations involved in the first phase, the closet contained many cables. Cable management, maintenance and shutdowns were problems.

The 2 pair design was chosen to isolate each run under its own sheath. Both 4 and 16 Mbps Token Ring were operating on the cable runs which averaged 45 feet. Contrary to what theoretically should happen, the 2 pair runs exhibited network shutdowns. Over the course of one year, network shutdown occurred 12 times or about one per month. Adding to the problem was the large amount of cables present in the closet. The existing cable plant was cluttered, cable plant maintenance was difficult and moves, adds, and changes were complicated and time consuming.

The solution was to install Category 5, 25 pair Power Sum as the replacement for the 2 pair cables. Each 25 pair bundle would be utilized to serve the work stations as before, only now the cable allowed the use of twelve 2 pairs under one sheath. This fully loaded the 25 pair cable, running signals on 12 pairs. Each end was still punched down on Category 5, 66 block, and the cable runs were maintained at 45 feet on the average. The 4 and 16 Mbps signals were run under separate cables, primarily due to their location in the building.

The results of utilizing Category 5, 25 pair Power Sum cable in a backbone environment were successful. The network shutdown problems were eliminated. As important, cable management was dramatically improved along with easier maintenance for adds, moves, and changes.

Conclusions

High performance, 25 pair, Power Sum UTP cables successfully support

applications in a backbone environment. The increased NEXT performance of these cable designs appears to account for the signal energy present in the single jacket cable bundle. These two case studies were chosen for their applicability to current LAN backbone cable questions:

1. Can multiple signals be supported under one jacket?
2. Will fully loaded cables support networks without shutdowns?

Both questions were answered with successful network operation. It still is important to select cable designs for particular LAN applications. While these case studies were successful, work still continues in areas of connectorization and standards approval.

In summary, 25 pair Power Sum cables:

1. Support multiple signals under a common sheath.
2. Perform successfully as a fully energized 16 Mbps Token Ring backbone cable.
3. Successfully support 100Mbps FDDI networks as a backbone cable.
4. Allow easier closet management and cable plant maintenance.

Acknowledgments

The authors would like to thank the following people and organizations for their valuable assistance in developing and preparing this paper:

John Curtis, The Tolly Group, Manasquan, New Jersey.

Don Aja, National Life Insurance Company of Vermont, Montpelier, Vermont.

Susan Maguire, Champlain Cable Corporation, Colchester, Vermont.

Katherine Prince, Champlain Cable Corporation, Colchester, Vermont.

Bibliography

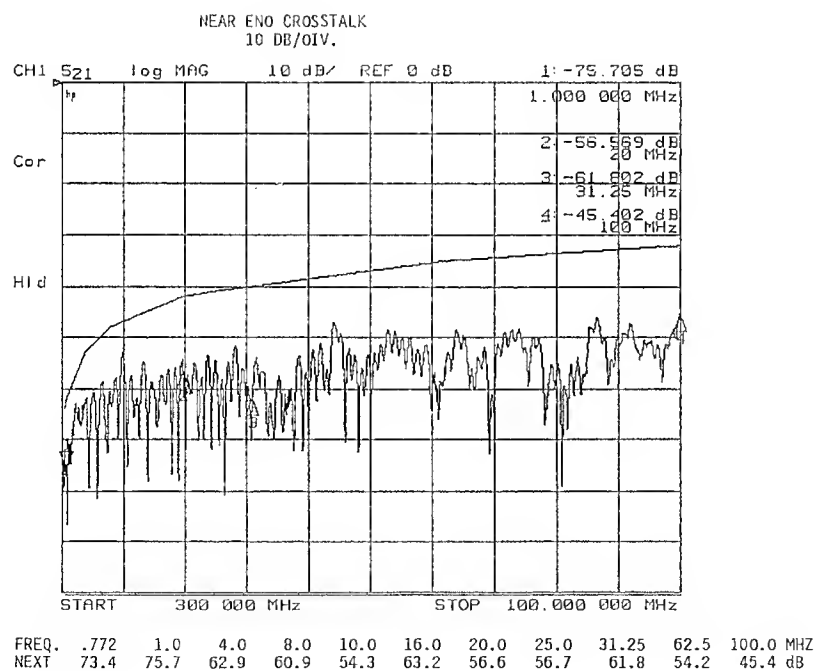
William Reichert

Bill Reichert is the LAN Market Manager at Champlain Cable Corporation in Colchester, Vermont. He has been in the wire and cable industry for 10 years, 5 of which have been in various operations and sales/marketing assignments with Champlain Cable. He was also instrumental in Champlain's ISO-9001 quality system registration. He received his Bachelor of Science degree in Chemistry in 1983, and his MBA in 1993, both from the University of Vermont.

APPENDIX 1

ELECTRICAL PROPERTY	FREQUENCY	CATEGORY 3	CATEGORY 4	CATEGORY 5
IMPEDANCE	1 - 16 MHz	100± 15		
(OHMS)	1 - 20 MHz		100± 15	
	1 - 100 MHz			100± 15
ATTENUATION	1 MHz	2.6	2.1	2.1
(dB/100m)	4 MHz	5.6	4.3	4.3
	10 MHz	9.8	7.2	6.6
	16 MHz	13.1	8.9	8.2
	20 MHz		10.2	9.2
	31.25 MHz			11.8
	62.50 MHz			17.1
	100 MHz			22.0
NEAR END CROSSTALK	1 MHz	-41	-56	-62
NEXT (dB)	4 MHz	-32	-47	-53
	10 MHz	-26	-41	-47
	16 MHz	-23	-38	-44
	20 MHz		-36	-42
	31.25 MHz			-39
	62.50 MHz			-35
	100 MHz			-32

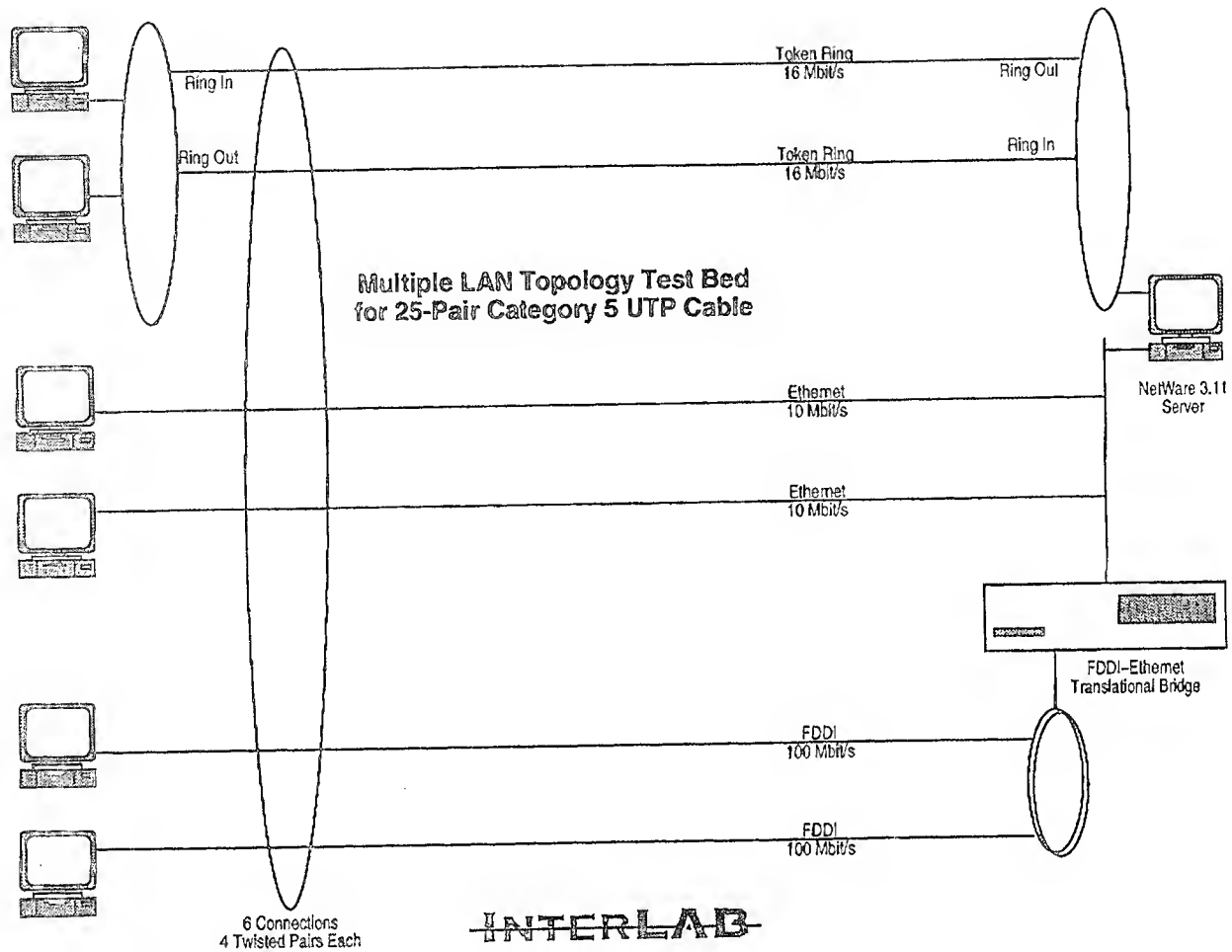
Appendix 2



CABLE IS ON THE RACK
PAIR 24 - 25
COLOR BRN/VIO - GRV/VIO
Note: POWER-SUM

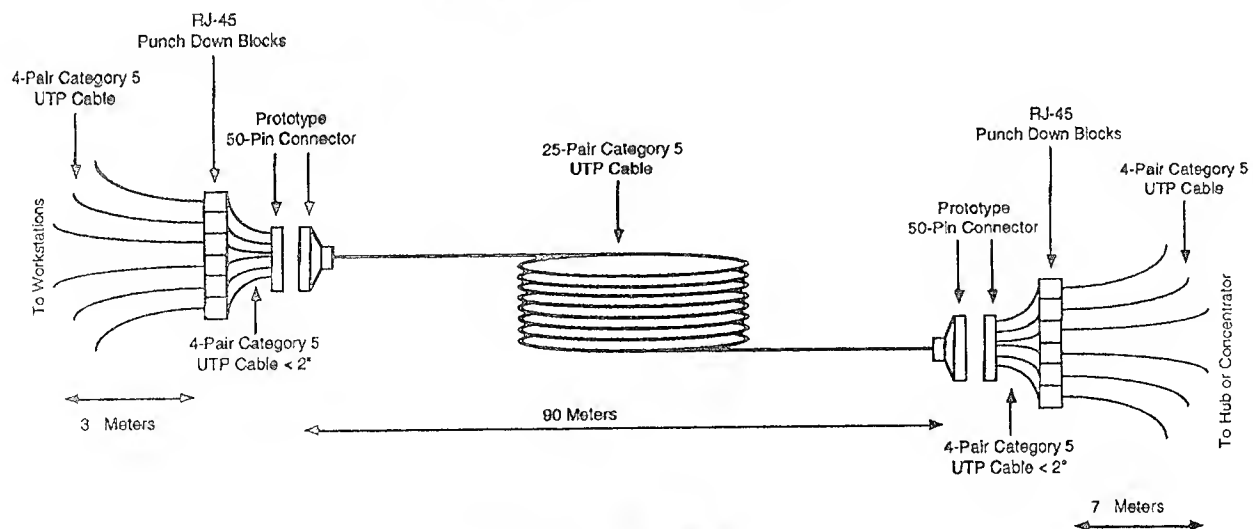
FOOTAGE= 328

Appendix 3



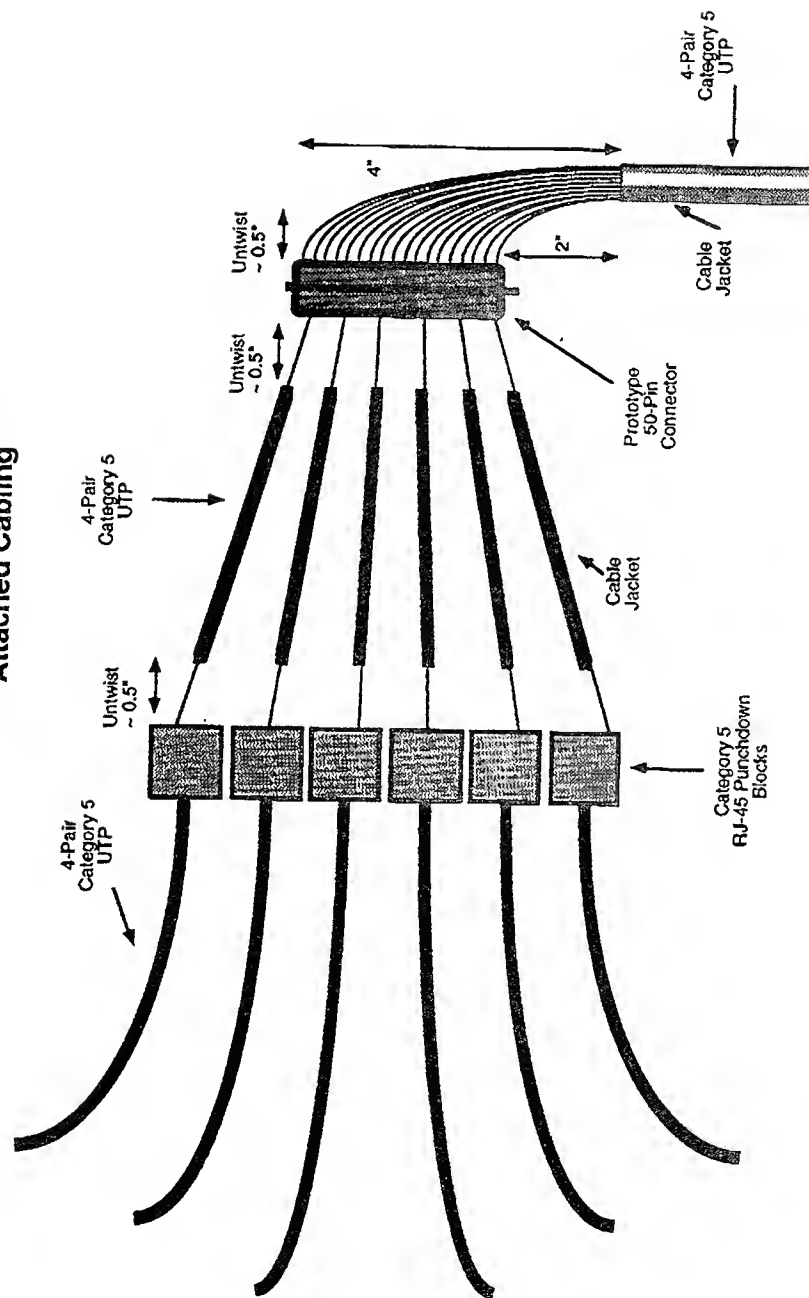
Appendix 4

Test Bed Cable Connections: 25-Pair Category 5 UTP Cable



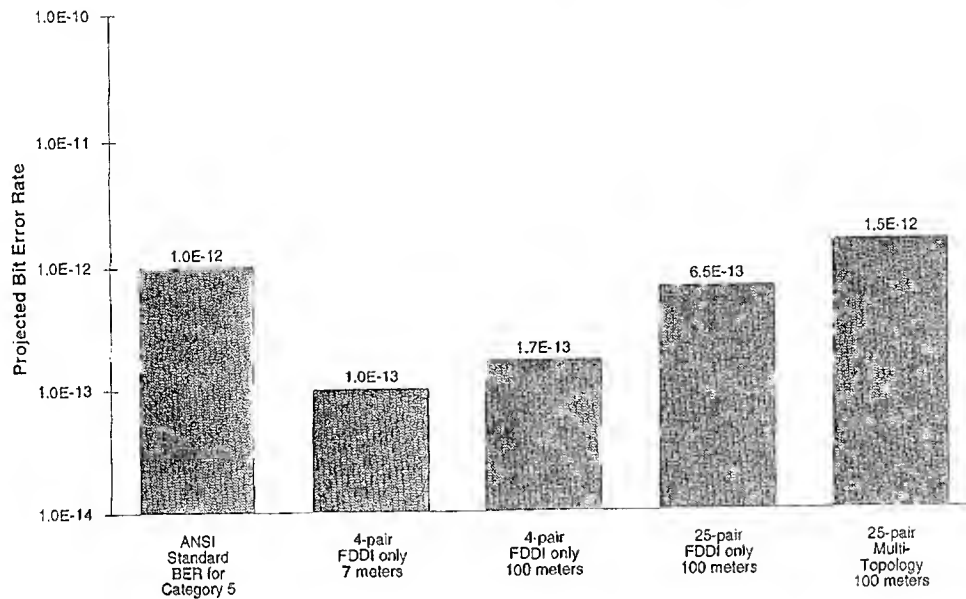
Appendix 5

**Detail of Prototype 50-Pin
Category 5 Connector and
Attached Cabling**



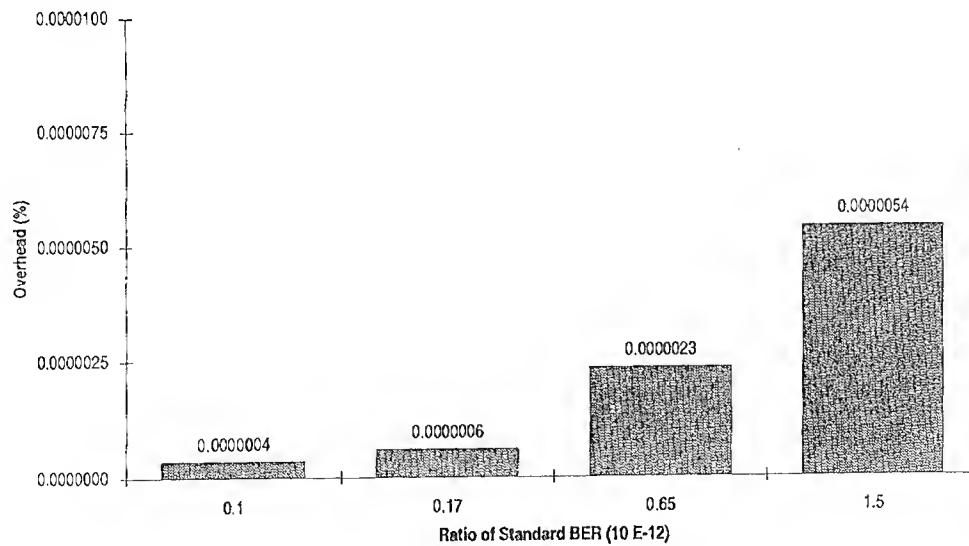
INTERLAB

Bit Error Rate for FDDI over Category 5 UTP Cable



© March 1994 InterLAB
CONFIDENTIAL: This document may not be reproduced.

Figure 4-1

Network Overhead
Caused by MLT-3 Bit Errors

Data cables and system components for the use up to 100 (300) MHz

Paul E. Gregor*, Toni Tholen*, Harald Knop**

* KABEL RHEYDT AG, Mönchengladbach, Germany

**BETEFA GmbH, Berlin, Germany

Abstract

The tendency towards higher data rates for advanced transmission systems is going on strongly. In order to improve economy of total links the necessary components have to be developed consequently.

This contribution describes a new cable technology using individual shielded pairs with respect to the basic intension for cable sharing. Cables have been tested up to 400 MHz. Regarding the most important electrical characteristics upon International Standard ISO/IEC DIS 11801 a comparison of test results and specified values has been performed up to 100 MHz. Furthermore it is stated that these cables can be applied for remarkable higher frequencies due to the achieved test results.

Additionally these cables have been combined with special shielded connecting hardware to erect a total link.

It has been expressed that there are certain measures to be taken into account during preparation of link in order to avoid mismatching. Moreover it should be pointed out that particular disadvantageful influence can occur by using lower quality of connecting hardware. This described cable and link concept opens possibilities for future application.

Introduction

The tendency towards higher data transmission rates for inhouse cabling systems is going on very clear worldwide. Based upon this background standardisation activities have been done accordingly. At present ISO IEC DIS 11801 is being under publishing as a very first international Standard for structured LAN networks including copper cables for the tertiary level. In that standard among various criteria characteristics for cables and connecting hardware for a cabling are specified up to a frequency of 100 MHz. However, a further strong increase of frequency range to be used for advanced transmission technologies occurs. Therefore design possibilities and properties of adequate data cables are to be investigated.

With respect to system requirements investigation of link behaviour as a combination of various components is necessary to be performed.

Design considerations of copper data cables

Generally cable design today has to be more than ever a certain compromise between high grade electrical transmission data and favourable mechanical features like diameter, pulling strength and bending behaviour for installation and economy aspects.

For the next cable generation pairs and star quads have been developed as stranding elements as given in the before mentioned international standard.

Bare and solid copper conductors are insulated with a special coloured polyethylene foam skin compound with respect to a low attenuation coefficient. Regarding the desired high transmission quality basically a high accuracy for homogeneity and symmetry of insulated conductors has been found as a clear presupposition to obtain that aim which can be realized by employment of most modern extrusion lines operating computer controlled.

Relatively short lay lengths are selected to be used for pair or quad twinning and stranding of cable core with respect to improved crosstalk attenuation and EMC considerations.

Stranding elements are shielded individually in order to increase crosstalk attenuation between transmission circuits essentially.

Normally 4 individually shielded pairs constitute a cable core which has been wrapped by plastic tapes helically and covered by shielding materials.

This common shield may be performed by using an aluminium tape applied longitudinally in combination with a tinned copper braiding considering a required favourable low transfer impedance.

As jacket material special halogenousfree flame retardant plastic compound has been extruded to fulfil requirements of IEC 332 respecting shaft oven (flame extension). Table 1 summarizes the most important design criteria of the tested cables with pairs:

type abbreviation: J-02YSCH 4x2x0,6 PiMF	
design component	dimension / comment
copper conductor diameter	0,6 mm
diameter over insulated conductor	1,5 mm
stranding element with individual shielding	pair
number of pairs	4
core shielding	aluminium coated plastic tape; tinned copper braiding, coverage approx. 70 %
jacket	halogenousfree flame retardent plastic compound
outer diameter of cable, nom.	8,8 mm
weight of cable	82 kg/km
fire load of cable	850 MJ/km
bending radius, min.	90 mm
pulling load, max.	140 N

table 1: design parameters of data cable

Figure 1 exhibits a sample of above described data cable.



figure 1: real data cable sample

Electrical characteristics of delivery length

DC and VF-characteristics

The electrical tests upon delivery lengths have been executed in a temperature range of 22°C up to 24°C. Test results for DC and VF criteria are put together in table 2:

characteristic at 20°C	requirement acc. to ISO/IEC DIS 11801 category 5	test result	test method IEC
			DIN VDE 0472
DC loop resistance of copper conductor	$\leq 192 \Omega/\text{km}$	$\leq 113,5 \Omega/\text{km}$	189-1 sub-cl. 5.1 part 501 item 2.1
DC insulation resistance 100 V, 60 s	$\geq 0,15 \text{ G}\Omega/\text{km}$	$\geq 112 \text{ G}\Omega/\text{km}$	189-1 sub-cl. 5.3 part 506
DC resistance unbalance	$\leq 3 \%$	$\leq 0,25 \%$	708-Am.3 cl. 24 part 501 item 2.2
dissipation factor at 800 Hz	not specified	$\leq 3 \times 10^{-3}$	part 505
mutual capacitance at 800 Hz	not specified	$\leq 45,0 \text{ nF}/\text{km}$	189-1 sub-cl. 5.4 part 504
capacitance unbalance between transmission circuits at 800 Hz	not specified	$\leq 15 \text{ pF}/\text{km}$	189-1 sub-cl. 5.5 part 502
dielectric strength cond. /cond. and cond. /shield	11 kV, 1 min } 2,5 kV, 2 sec }DC 700 V, 1 min } 1,7 kV, 2 sec } AC	passed	189-1 sub-cl. 5.2 part 509

table 2: DC and VF characteristics of data cables

HF-characteristics of data cables

Gencrally it shall be stated that regarding test procedures on the international level IEC still work in detail has to be done in order to get reproducible results.

Attenuation coefficient

The attenuation test has been carried out between 100 kHz and 400 MHz employing a network analyser, operating automatically (type HP 4396 A). The symmetry of the used matching transformer (type NH 13410) has 20 dB at 300 MHz. Since the recorded curve shows a continous shape upon the square root law the results seem to be acceptable.

In figure 2 typical obtained attenuation coefficients versus frequency up to 400 MHz has been drawn in comparison to the specified values within ISO/IEC DIS 11801 as far as applicable.

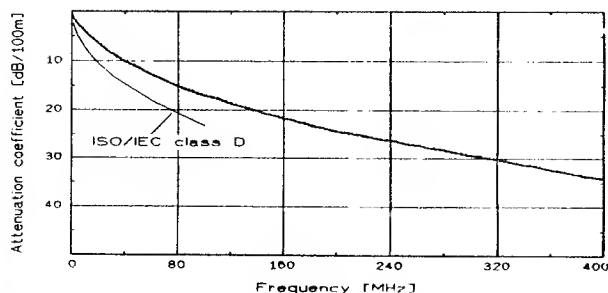


figure 2: attenuation coefficients of cable delivery lengths

Crosstalk attenuation

The crosstalk attenuation measurement has been carried out upon the above mentioned 4-pair cable between 100 kHz and 400 MHz using a network analyser, Type HP 4396 A. Consequently, 6 pair combinations apply for an individual cable. Pairs not being under test have been terminated with 100 Ω , too.

Since crosstalk attenuation is frequency dependent, the examination of this criteria has been done in intervals of 500 kHz. In figure 3 typical results of NEXT are shown up to 400 MHz compared to provisions in the international standard.

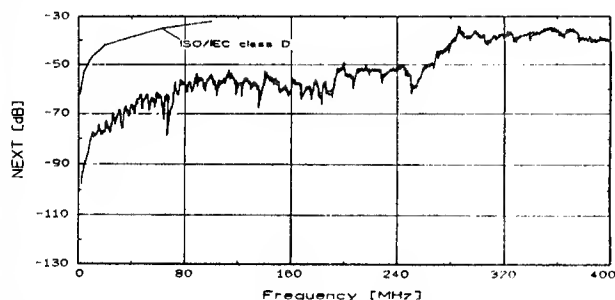


figure 3: Near end crosstalk of cable delivery lengths

Characteristic impedance

Typical test results have been taken into figure 4 respecting a frequency range up to 400 MHz together with the international specified limits

It is shown that even above international specified frequency limits the obtained Z-values maintain within the tolerances.

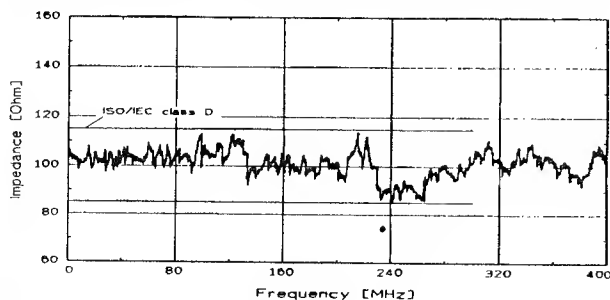


figure 4: characteristic impedance of cable delivery lengths

Phase velocity of propagation

Up to 300 MHz tests have been performed. As expressed in figure 5 the velocity level has been found almost constant corresponding to a value of 0,76c.

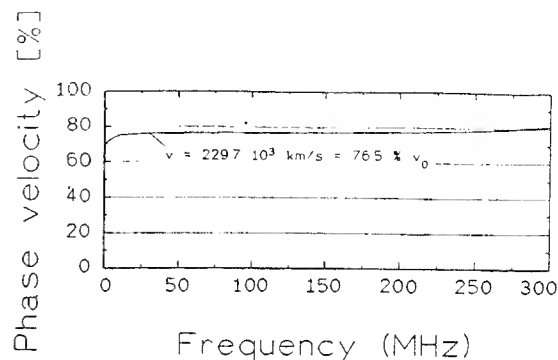


figure 5: phase velocity of cable delivery lengths

Transfer impedance

Based upon IEC 96-1, clause 18 tests have been done to give an indication compared to above mentioned standard. Results are listed up in table 3.

frequency MHz	1	5	10	12
transfer impedance m Ω /m	3,0	2,2	2,3	2,8

table 3: transfer impedance of data cable

Longitudinal conversion loss

The measurements have been carried out with a network analyser up to a frequency of 100 MHz. The achieved properties are sketched in figure 6. These LCL-values expresses the high homogeneity of this particular cable design.

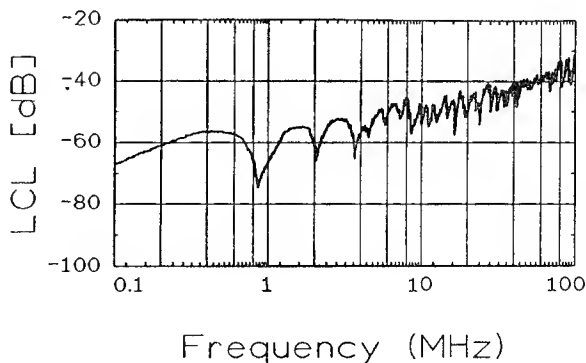


figure 6: longitudinal conversion loss of cable delivery lengths

Transmission characteristics of links

Although cables and their quality are obviously most important for a transmission line the other necessary components like connecting hardware can influence the total link essentially. Therefore tests upon link according to principle in figure 7 have been made.

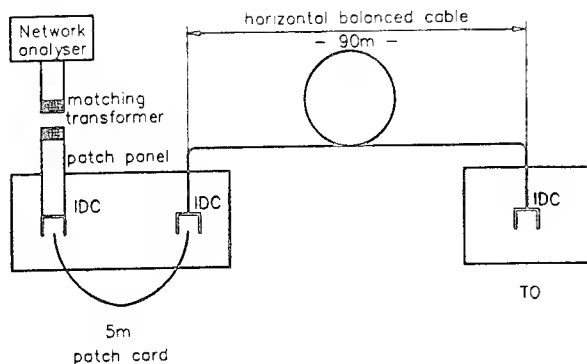


figure 7: link configuration

Following connecting hardware components have been used:

- KABEL RHEYDT patchpanel AVS 100, cat 5
- Hirose plug, level 5
- Molex Telecommunication outlet cat.5

Cable: J-02YSCY 4x2x0,6 PiMF

Test instrument: HP Spectrum Analyser

Matching transformer: North Hill NH 13410

Following test results have been gained:

Attenuation coefficient

In figure 8 results for a frequency range between 0,1 and 300 MHz have been recorded. The specified values according to ISO/IEC DIS 11801 are given as a comparison. It is shown that the tested link fulfils the standardized requirements sufficiently.

The test results achieved above 100 MHz up to 300 MHz exhibit a curve following an expected square root law.

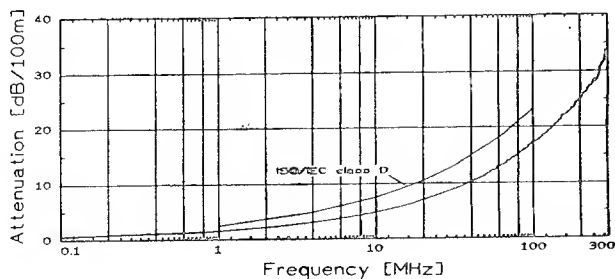


figure 8: attenuation coefficients of link

Near end crosstalk attenuation

NEXT measurement have been carried out up to 300 MHz from both ends of the link. The obtained values have been registered between 33 dB and 55 dB. In figure 9 results for the frequency range 0,1 MHz up to 300 MHz together with the provisions of International Standard up to 100 MHz are taken together. With regard to different qualities of link components test results may vary remarkable depending from selected end of link on which tests have been carried out.

As already stated in the section for cable delivery lengths a high number of frequency points should be tested in order to find all critical peaks within the whole bandwidth. Additionally particular importance should be placed upon the frequency range above 10 MHz accordingly.

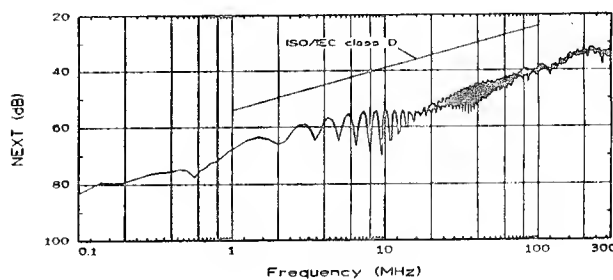


figure 9: Near end crosstalk attenuation for link

Characteristic impedance

In figure 10 a typical curve up to 300 MHz has been drawn. Compared to specified limits test results fulfil the requirements. It should be stated that the test results become incorrect if the test leads at the baluns are not short enough. Particular at frequencies above 100 MHz the total curve can be deviate by more than 50 % from the nominal value.

Additionally parasitical capacitances of unsymmetrical connecting hardware influences the results disadvantageful.

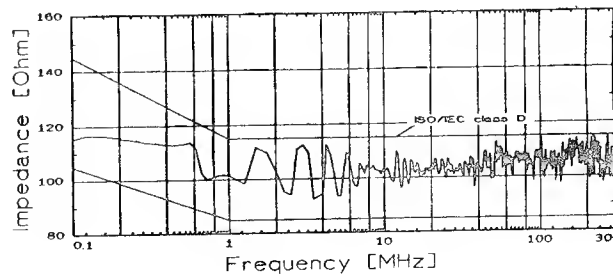


figure 10: characteric Impedance for link

Conclusion

These new designed advanced data cables with individual pair shielding are able to serve for future applications. Therefore cables have been tested up to 400 MHz.

Test results meet the international requirements within ISO/IEC DIS 11801 up to 100 MHz. It is proved by measurements that the properties attenuation coefficient and crosstalk attenuation follow the expected physical laws for frequencies up to 400 MHz, too. It became very clear that the link behaviour reacts extremely sensitive upon unsymmetrical connecting hardware and lower quality of patch cables at higher frequencies. Within measurement procedures it has to be made sure that test leads are kept as short as possible in order to get reproducible results. This data cable generation opens new aspects for future applications towards higher frequencies.

With respect to improved laying and mounting behaviour data cables should be designed with an increased pulling strength consisting of non metallic tensile strength elements in order to avoid any deterioration of electrical characteristics after installation procedures. Tests after erection of the cabling should be kept to a minimum in order to reduce the costs at site considerably.

Literature

- /1/ ISO/IEC DIS 11801: Generic cabling for Customer Premises
- /2/ Haag, H.; Hög, G.; Gregor, P.: Technical Review, Edition 3/86E; Optical Fibre/Copper Conductor Composite LAN Cable for Mining Application. Techn. Mit. Kabel Rheydt AG, 1986
- /3/ Haag, H.; Hög, G.; Lehan, K.; Gregor, P.; Zamzow, P.: Copper/Optical Fibre Hybrid Cable for LAN-Application. EFOC/LAN 1992
- /4/ Gregor, P.; Lehan, K.: Kupfer/Lichtwellenleiterkabel für Datennetze in großen Verwaltungsgebäuden; Signal und Draht 85 (1993) H.3
- /5/ Gregor, P.; Lehan, K.; Mühlen, H.: Normen für Meßmethoden an Kupfer- und Lichtwellenleiterkabeln
- /6/ DIN VDE 0472, Beiblatt 1, August 1992: Prüfungen an Kabeln und isolierten Leitungen; Verzeichnis der Normen der Reihe DIN VDE 0472. Berlin-Offenbach: VDE-Verlag
- /7/ Richter, S.; Lehan, K.: Copper cables for local area networks with very high bit rate data transmission
- /8/ IEC 793-1: Optical fibres; Part 1; Generic Specification: Berlin-Offenbach: VDE-Verlag
- /9/ IEC 794-1: Optical fibres cables; Part 1; Generic Specification: Berlin-Offenbach: VDE-Verlag



Paul. E. Gregor
KABEL RHEYDT AG
Mönchengladbach, Germany

Paul E. Gregor (52) is head of the Technical Sales Department for Telecommunications cables. He reached his Ing. from Ingenieurschule Duisburg in 1966 and joined Kabelwerk Duisburg, now a part of KABEL RHEYDT AG. After ten years activities in development department he took over the position as head of design branch for copper and optical fibre cables. Since 1989 he is engaged in his present position.

He is also a member of the standardisation bodies in DIN VDE AND ISO/IEC.

Harald Knop
Betefa GmbH
Berlin

Harald Knop (52) is the head of product engineering department for telecommunications and data cables. He finished his studies at Technical High-school Berlin in 1966.

Then he joined Betefa GmbH, a subsidiary company of KABEL RHEYDT AG. He has been responsible for design, testing and quality matters of low and high frequency data cables. Beginning from 1990 he is engaged in his present position.



Toni Tholen
KABEL RHEYDT AG
Mönchengladbach, Germany

Toni Tholen (36) is a member of Development Department for inhouse networks. He finished his studies at Technische Hochschule Aachen in 1981 as Dipl.-Ing.

Then he joined KABEL RHEYDT AG and was responsible for development of optical fibre cables and later on he was engaged for creating of testing equipments. In 1984 he went into his present position.

AERIAL FIBER OPTIC CABLE FOR RAILWAY APPLICATIONS METALLIC OR DIELECTRIC SOLUTIONS

J.P. BONICEL¹, O. TATAT¹, G. COUVRIE¹, L. RAPEBACH², P. ZAMZOW³, J. RAUCHS⁴, C. VERGEZ⁵

¹ ALCATEL CABLE - OFCCC, FRANCE - ² SNCF, FRANCE - ³ KABEL RHEYDT, GERMANY -
⁴ OPTICABLE, BELGIUM - ⁵ ALCATEL CONTRACTING, FRANCE

ABSTRACT

Today, aerial optical cables are well known and there are a lot of applications. However, in railways applications after utilization of «standard» aerial cable, different problems have been met due to different types of cable damage (bad climatic conditions, abrasion, shot gun, animal attacks). The optical cable in the railway sector is a «long distance» application and the lifetime is a basic problem, particularly because a low reliability may affect, in some cases, the passenger's safety or the transmission quality. To improve the reliability, different solutions have been investigated with different railway companies and particularly with SNCF, the French railway company, Belgian and German railway companies.

1. INTRODUCTION

Different solutions have been taken into account such as all dielectric self-supported (ADSS) cables or metallic cables. For the ADSS different solutions have been investigated, in some cases, by using a very high modulus, metal free cable to limit sag when the cable is submitted to the wind and / or ice effect ; and in other cases by using a metalfree cable with a special suspension technique. This special suspension technique is based on the fact that at pole distances of about 50 m a roll-bearing is used at each pole, allowing bracing fields of about 1000 m or more.

For these metal free cables, the shot gun resistance has been carefully investigated and test results are presented. The new solution for railway application that we have investigated is the introduction of optical fibers in a ground wire which is installed in most of the electrified railway lines. In fact, this kind of cable may be installed on poles of a new electrified line. It is easy to replace an old ground wire by a new optical ground wire.

This solution presents different advantages for the railway companies such as :

- no additional cables on the poles
- optical cable with similar mechanical and electrical

characteristics and outside diameter of a conventional ground wire
- similar accessories are used as for conventional ground wire

As a result of this study, the characteristics of these different metallic and metal free solutions, and taking into account their accessories, we present the advantages and drawbacks of the different solutions with particular attention to the reliability.

2. OPTICAL CABLES FOR RAILWAY APPLICATIONS

2.1. Aerial cable vs cables in concrete gutters

Most of the railway lines have generally different kinds of cables in parallel with the line and these cables are often laid in concrete gutters. In the same gutter it is possible to find up to 5 cables in line, but up to 150 cables near some of the technical stations. Figure 1 gives an example of the kind of gutter that it is possible to have with the different cables inside.

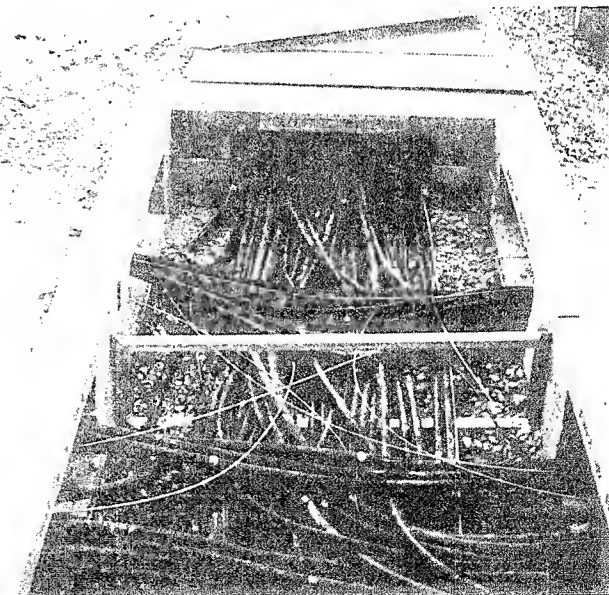


Fig 1 Concrete gutter with different cables inside.

When allowed by the type of ground, cables may be directly buried, with traditional means or with mechanical techniques.

Laying a new cable may sometimes lead to some technical problems (lack of space in the gutter, brittleness of optical cables compared to copper cables) or generate some substantial costs when it is necessary to install new gutters or to lay cable with a special technique.

Taking into account all the technical problems and installation difficulties, the alternative solution ; «aerial cable», seems to be very attractive, particularly when the railway company decides to use optical cable on an existing electrified line or when an old line is electrified.

2.2. Technical solutions for aerial cables

Two solutions have been investigated and both solutions are used : metal free cables and metallic cables. Both solutions have some advantages and drawbacks and are described here after. These solutions have been investigated by ALCATEL CABLE in relation with customers. Some of them currently use these solutions. Up to now the French Railway company (SNCF) is using optical cables directly buried or in gutters and has recently investigated the two solutions, aerial metallic and metal free cables. Similar situation may be found by other companies (DB, German Railway Company or SNCB, Belgian Railway Company...).

The needs are quite different in the cases of both kinds of cables :

- Dielectric cables, in case of an electrified line with an already installed ground cable, can be installed as a complement of another cable already laid in gutters or buried, but will be seen as a «foreign element» by people responsible for catenaries (overhead contact lines).

Perhaps it will be more interesting to install it on aerial existing lines, but this has yet to be investigated.

- The metallic aerial cable is more suitable in the case of a new electrification, which is the greatest potential market, or an electrified line with no ground cable installed. This type of cable and its laying technique are well known by the people responsible for catenary, only the splicing of the optical cable will be specific.

Improvement of fast laying may be interesting in the case of deregulation allowing a railway company to install flexible optical network in short time.

2.2.1. Metal free cables

Different experiences have already been presented on such cables (1) (2) (3). Here after 2 different cables and their associated characteristics are described.

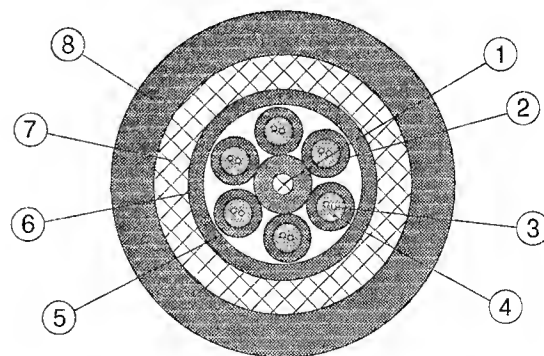
- cable supported by roll bearings and high fiber excess length

The cable must be designed to withstand extreme stresses, such as ice formation or falling trees without leading to excessive shock impact or fibre stretching that could affect transmission.

To protect the optical fiber against mechanical and temperature influences (-40° ... 80° C) a loose tube housing one or more fibres has been chosen for standard applications. The tubes are filled in both cases.

Specially for cable constructions needing a great fiber reserve (1 % to 2 %) the loose tube is most advantageous because the fiber is mechanically decoupled from the tube. Furthermore it is possible to easily produce a well defined fiber overlength, e.g. 2 %, by using an appropriate production technology. In principle, the cable construction can be realized as a stranded tube (Fig. 2).

The herein presented cable is made of stranded tubes because of the required fiber reserve of 1.2 % for the whole cable which is easier to fulfil with a stranded tube than with a central tube construction. The fiber reserve is the addition of the fiber overlength in the tube itself and the overlength given by the lay length.



- 1 : Buffered aramid cord
- 2 : Loose tube
- 3 : Optical fiber
- 4 : Filling compound
- 5 : Core wrappings
- 6 : 0.8 mm thick inner Pe jacket
- 7 : Glass rovings
- 8 : 2 mm thick LdPe outer jacket

Fig. 2 : Metal free optical fibre railway cable

The cable main characteristics are as follows :

- cable diameter : 15.5 mm
- cable weight : 204 kg/km
- cable cross section : 189.7 mm²
- calculated breaking load : 24 kN
- Young's modulus : 5.8 kN/mm²
(related on cross section)
- maximum permissible load : 10 kN
- thermal elongation coefficient : $11 \cdot 10^{-6}/^{\circ}\text{K}$
- maximum delivery length : 2/4 km
- temperature ranges :

transportation,	-40/+70°C
storage,	-40/+70°C
installation,	-5/+60°C
operation,	-40/+70°C

The cable must be designed to be able to support 10 kN without stress on fibers and with a cable elongation of 1.2 %. The figure 3 presents the stress / strain behaviour of such cable.

Accessories used to install the cable on poles are consisting of cable suspension pulleys with 150 mm diameter (figure 4) and aluminium dead-end spirals for the anchoring point (figure 5).

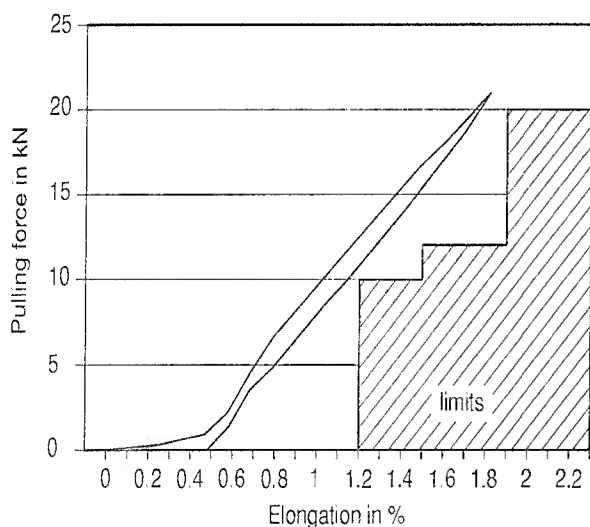


Fig 3 : Stress - strain behavior

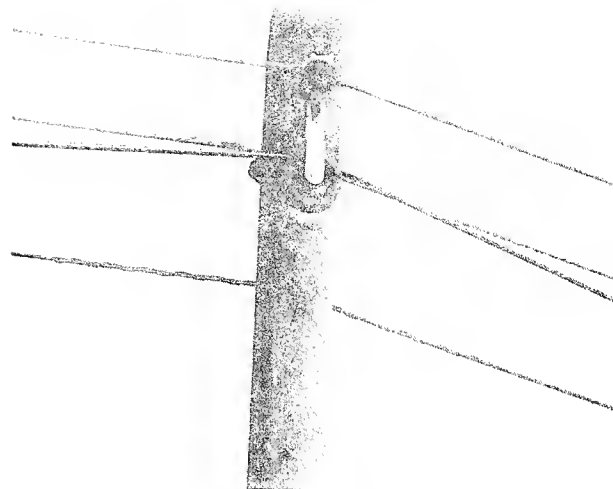


Fig 4 : Fixed pulley with cable

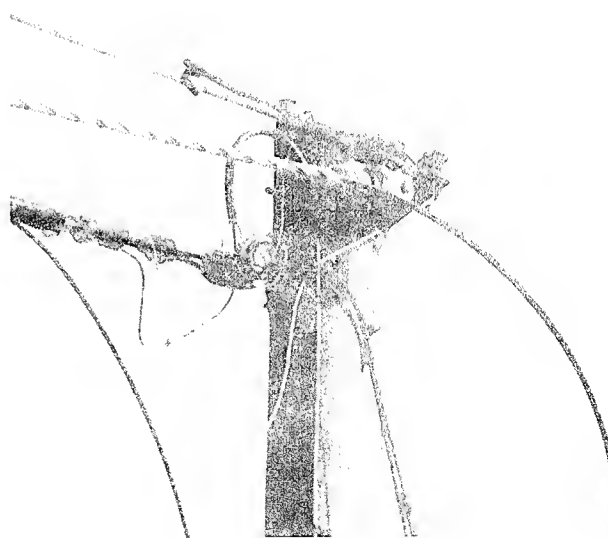


Fig. 5 : Dead-end spiral at one of the end poles

Presented aerial cable design is able to bear great pulling forces and elongations without influencing the optical transmission properties. To guarantee this ability a special tube with additional fiber reserve as well as special strength members have been used. This cable is able to work at 1300 and 1550 nm.

From all these considerations the German Railway Company (DB) decided to use only metal free cable constructions in the future. The specification for the cable and the accessories is now finished and in the future a part of the further installation of optical fibre cables will be replaced by this metal free aerial cable.

- Improvement of shot gun resistance of metal free cable

In some countries hunters are able to damage aerial cables and particularly metal free cable. Taking into account the work made on this subject (4) and when the customers requests antiballistic cable (eg : Belgian Railways) a new cable design has been developed. This cable is able to be used in aerial application, or may be directly buried. The figure 6 gives the cross section of such cable.

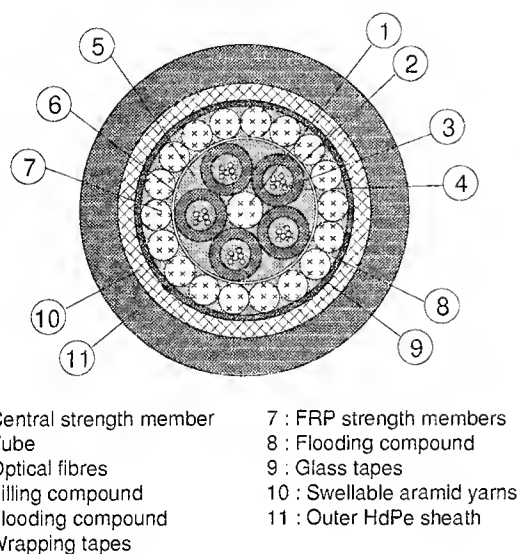


Fig. 6 : shot gun resistant metal free cable

This cable with such structure presents good performances in the pulling test and thermal test. The structure with different layers on the optical core gives good antiballistic performances.

Mechanical and thermal characteristics are presented in Figure 7 and shot gun resistance in Figure 8. For the shot gun test, a gauge 20 was used. The distance was 15 m. The lead pellets size was 6 (pellets diameter : 2.7 mm) and 4 (pellets diameter = 3 mm). Different cables have already been tested with the shot gun (3) and the present cables have a good resistance to such aggression.

- Cable diameter	13.4 mm
- Weight	113 kg/km
- Cross section	141 mm ²
- Young's modulus	17.6 kN/mm ²
- Calculated break load	35 kN
- Maximum permissible load	11 kN
- Minimum bending radius without tension	170 mm
- Minimum bending radius under tension	210 mm
- Compression (IEC-794-1-E4)	400 daN/10 cm
- Impacts (IEC-794-1-E4)	100 impacts of 5 N.m
- Operating temperature range (IEC-794-1-F1)	-30°C / +60°C
- Storage temperature range	-40°C / +70°C

Figure 7 : Mechanical and thermal performances

Cable pulling tension (daN)	190		540	
Pellet size (Ø mm)	6 (2.7)	4 (3.0)	6 (2.7)	4 (3.0)
Number of pellets in the cable	12	12	7	11
Status of first tape	no hole marks	no hole marks	no hole marks	no hole mark
Status of second tape	no hole no mark	no hole no mark	no hole no mark	no hole no mark
Status of optical modulus	no hole no mark	no hole no mark	no hole no mark	no hole no mark

Figure 8 : Shot gun resistance of metal free cable

2.2.2. Metallic cable for aerial railway application

In modern railway networks, railway lines are more and more electrified. Most of the 25 kV A. C. lines use an aerial metallic ground wire and the situation will be the same in the future for 1500 V lines. The main characteristics of standard metallic cable are given on figure 9. The advantages of this kind of cable are :

- grounding all metallic structures at the same potential
- reduction of induced voltage on other cables
- reduction of induced voltage on rails / ground
- improvement of the lightning protection

Characteristics	Unit	Value
Diameter		12.5
Weight	kg/km	437
Armor construction		7 steel + 12 A. Alloy
Armor cross section	mm ²	93.3
UTS	daN	4610
E modulus	daN/mm ²	13200
Coefficient of thermal expansion	°C·10 ⁻⁶	18
Electrical resistivity	Ω/km	0.30

Fig. 9 : Main characteristics of standard metallic wire (CDPA)

The cable must be able to support a short circuit current of 10 kA x 0.2 s and a permanent current of 150 A.

The SNCF's requests were to find a solution taking into account the following parameters :

- no addition of optical cable in gutters
- no other excess load on poles than the existing one
- cable easy to install (short time available for installation as the railway line is still busy)
- necessity to use the same accessories for the suspension clamp than the accessories already used for the standard metallic ground wire.
- high reliability (as good as or better than optical cables when they are laid in gutters)

After different investigations a metallic cable with an optical core derived from OPGW family cables (5, 6, 7), was proposed and tested to determine its compatibility with the aerial railway application and particularly the compatibility with the suspension clamp that induces a very high lateral pressure on the cable when the screw-bolt are very tight. The figure 10 presents the cross section and the main characteristics of the proposed cable named «CDPAO 59» are shown in figure 11. The cable was totally tested particularly for mechanical, thermal and aging characteristics. The cable was also tested at a very low temperature to find its limits. At -60°C, the change in attenuation was less than 0.1 dB/km at 1300 or 1550 nm. The increase in attenuation started at -70°C.

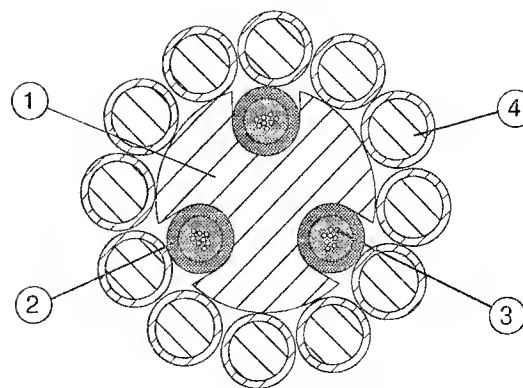


Fig. 10 : CDPAO 59 cable cross section

Characteristics	Units	Value
Diameter	mm	12.3
Weight	kg/km	476
Armor construction	wires	12 ACS Ø 2.5 mm
Armor cross section	mm ²	58.9
Aluminium alloy wire cross section	mm ²	0
ACS wires cross section	mm ²	58.9
UTS	daN	8,500
E modulus	daN/mm ²	18,570
Max. every day stress (EDS)	% UTS	20
Max. operating tension	% UTS	65
Min. static bending diameter	mm	450
Min. dynamic bending diameter	mm	450
Coefficient of thermal expansion	°C·10 ⁻⁶	14.6
Electrical resistivity	Ω/km	0.69
Operating temperature range	°C	-40/+70
Storage temperature range	°C	-40/+70
Installation temperature range	°C	-10/+45
Calculated short circuit I _{2t} for 160°C max. temp.	kA ² .s	41

Fig. 11 : Main characteristics of the CDPAO 59 cable

The cable was also submitted to a sheave test (3 sheaves of 450 mm diameter). It was tested under a tension of 20 % of UTS and with 60 sheaves movement. No change in attenuation and no deformation were found. The pulling test was made on 160 m and no change in attenuation and no stress on the fibers were found up to 70 % of UTS.

The figure 12 presents the suspension clamp used for the standard ground wire without fibers (CDPA) or for the new CDPAO 59 cable. Laboratory tests have been performed on a sample of cable with 28 looped single mode fibers. The screw of the suspension clamp were screwed down until the bolt broke (axial momentum with a couple ≥ 12 m/kg) and no attenuation was noted at 1300 or 1550 nm. No deformation was found on the aluminium slotted core.

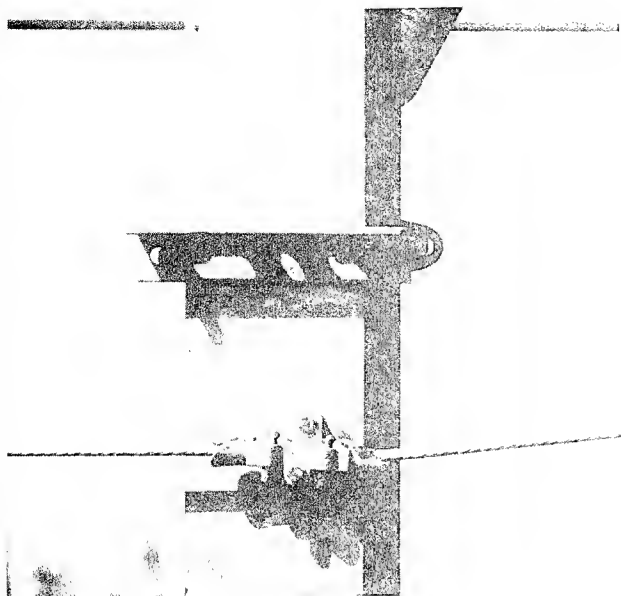


Fig. 12 : Suspension clamp with CDPAO 59.

The cable was also lightning tested according to the specification MIL STD 1757 A. The figure 13 gives the lightning parameters for the test and the cable was tested with 3 different levels (levels 1, 2 and 3).

For the 3 different levels no change in attenuation were found on the 28 single mode looped fibers. For the third level some armoring wires were damaged by the lightning impact and one wire was broken. However this third level is a high powering test.

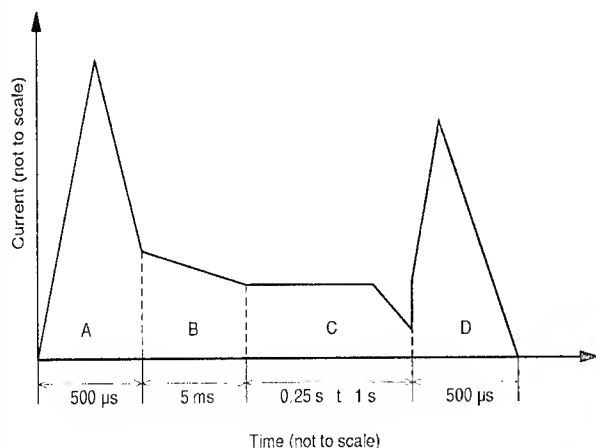


Figure 13a : Lightning test according MIL STD 1757A (current diagram)

COMPONENT A (initial stroke)
peak amplitude : $200 \text{ kA} \pm 10\%$
action integral : $2 \cdot 10^6 \text{ A}^2 \cdot \text{s} \pm 20\%$
time duration : $\leq 500 \mu\text{s}$

COMPONENT B (intermediate current)
maximum charge transfert : $10 \text{ C} \pm 20\%$
average amplitude : $2 \text{ kA} \pm 10\%$

COMPONENT C (continuing current)
charge transfert : $200 \text{ C} \pm 20\%$
amplitude : $200 - 800 \text{ A}$

COMPONENT D (restrike)
peak amplitude : $100 \text{ kA} \pm 10\%$
action integral : $0.25 \cdot 10^6 \text{ A}^2 \cdot \text{s} \pm 20\%$
time duration : $\leq 500 \mu\text{s}$

Level	Component A (A)	Component C (Coulombs)
1	30	15
2	100	100
3	200	200

Figure 13b : Lightning test according MIL STD 1757A (test conditions)

The figure 14 is a picture of accessories used to splice the cable and the complete splicing box is easily fixed on the metallic poles of the catenary line.

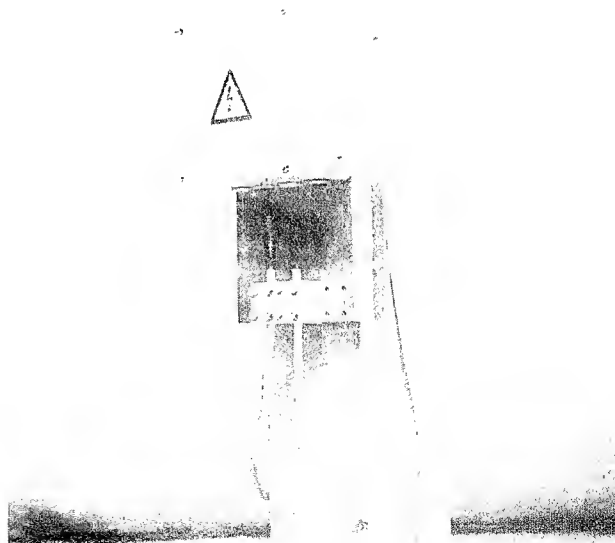


Figure 14 : CDPAO splicing system

3. CONCLUSION

The application of aerial optical fiber cable for railway applications has been carefully investigated taking into account the different customer requests. Different solutions are proposed based on metal free or metallic cable. In all cases, and because these telecommunication cables are used on railway lines where the passengers safety is the key point, our developments were driven by the «cable system reliability». In this way metalfree cables compatible with roller bearing supporting device, or metal free cable with an improved shot gun resistance, or very reliable and strong with small diameter metallic cable were developed and are now proposed for railway applications.

REFERENCES

- (1) F. FRAHN, N. LENGE, G. WECKERLE - ANT : Self-Supporting Optical Fiber Aerial with large Allowable elongation - IWCS Proceedings, 1991.
- (2) B. DIEHL, G. HÖG, KR : Lichtwellenleiter-Luftkabel mit nichtmetallinen Zugentlastungselementen für den Einsatz entlang von Bahnstrecken - Signal und Draht review.
- (3) A. BIDANGER, W. LYNEN and R. NEY : Design and operation of an aerial fiber - optic cable for railroad communications - IWCS Proceedings, 1991.
- (4) S. CAMARA and C. G. CORTINES - ACI : Evaluation of antiballistic sheathings for aerial fiber cables - IWCS Proceedings, 1991.
- (5) P. KOUTEYNIKOFF, M. de VECCHIS, JP. BONICEL : Single mode FOCGW using dispersion shifted fibers - EFOC/LAN 88 Amsterdam, 27 July to 1 August 1988.
- (6) P. KOUTEYNIKOFF, M. PAYS, Y. MOLLER, A. PANNIER, J.P. BONICEL, P. TROMBERT : Optical Fiber Telecommunications on the Electricity Transmission Network (Teleprotection, Teleoperation, Telecontrol) Equipment and Operating Experience - CIGRE 35-103/1990 session.
- (7) J. P. BONICEL, C. G. CORTINES, J.C. DELOMEL, G. HÖG, S. POUILLY, O. TATAT, P.E. ZAMZOW : Optical Ground Wire - A worldwide Technical Survey and Comparison - IWCS Proceedings, 1993.

AUTHORS

Jean-Pierre BONICEL - ALCATEL CABLE
35 rue Jean-Jaurès - 95871 Bezons, FRANCE

Jean-Pierre BONICEL was born in 1952. He received his engineering degree from the Institut des Sciences de l'Ingénieur de Montpellier (ISIM) in 1976. He joined Les Câbles de Lyon, now Alcatel Câble, in 1977 where he was in charge of material and mechanical problems for telecommunications cables. Now he is the head of the telecommunications cables laboratory, manager for the Alcatel Optical Fiber Cable Competence Center, and Technical Director for the Telecommunications Department.



Olivier TATAT - ALCATEL CABLE
35 rue Jean Jaurès 95871 Bezons, FRANCE

Olivier TATAT was born in 1959. He received his engineering degree from the Institut des Sciences de l'Ingénieur de Montpellier (ISIM) in 1982. He joined Les Câbles de Lyon in 1985 where he was in charge of material and mechanical problems for telecommunications cables. He is now working as project engineer in the Optical Fiber Cable Competence Center of Alcatel Cable.



Gérard COUVRIE - ALCATEL CABLE
35 rue Jean Jaurès 95871 Bezons, FRANCE

Gérard COUVRIE was born in 1949. He received his General Certificate of Education in 1968. After two years in Mathematics and Physics, he joined Les Câbles de Lyon Outside Plant Operations Department. He is now working on the development of OPGWs in the Optical Fiber Cable Competence Center of Alcatel Cable.



Peter E. ZAMZOW - KABEL RHEYDT AG
Mönchengladbach, GERMANY

Peter E. ZAMZOW (54) is director of the Telecommunication Division. After finishing his postgraduate studies in telecommunications in München and Graz as Dip.-Ing. he joined AEG KABEL in 1970. He has been engaged in development and production of telecommunications cables. In 1980 he became head of the fiber optic division at AEG KABEL and in 1982 he was nominated as a senior engineer. From 1992 on he was plant manager of the new Optical Fiber Cable Plant Rheydt. Since 01. July 1994 he is general manager for CATV activities worldwide.



Christian VERGEZ - ALCATEL CONTRACTING
30 rue des Chasses 92111 Clichy, FRANCE

Christian Vergez was born in Paris in 1952. He received the degree of Dipl. Ing. in Electronics Engineering in 1975 from «Ecole spéciale de Mécanique et d'Électricité, Paris. In 1977 he joined LTT outside plant Division. He is now at Alcatel Contracting Network Engineering and Installation Department in charge of the design and development of cables accessories.



Jean RAUCHS - OPTICABLE SA
Frameries, BELGIUM

Jean RAUCHS was born in 1965. He obtained his Dip. Ing. Degree in mechanics from the Faculté Polytechnique de Mons, Belgium, in 1989. He joined Opticable in August 1989 in the R&D department. He became in 1991 responsable for the Engineering department.



Lucien RAPEBACH - SNCF
Paris, FRANCE

Lucien RAPEBACH received his Engineer degree from École Nationale de Radio Électricité Appliquée, Paris. He joined the SNCF in 1974, where he is actually in charge of the «Infrastructure et équipements des réseaux supports» within the Telecommunications Railways Agency.



HIGH COUNT OPTICAL FIBER COMPOSITED GROUND WIRE (OPGW)

J. Sumita*, Y. Kashihara*, J. Ohta**, I. Sakabe**, T. Saito**

* The Kansai Electric Power Co., Inc.

** Sumitomo Electric Industries, Ltd.

1. Abstract

To meet the increasing demand of fiber optical telecommunication, a simplest solution is to use higher count cable. Generally increasing the optical fiber count increase the cable diameter. For the aerial cable which is used for long span such as OPGW, as larger cable diameter incurs the serious problems by wind and snow. We succeed the development of 48 fiber count OPGW which contains twice the optical fibers as conventional construction in the same diameter.

This paper will describe the design and the test result for newly developed OPGW.

2. Introduction

The Kansai Electric Power Co., Inc. has developed and applied the high count OPGW, up to 24 since 1982. To respond the demands for optical telecommunication which are becoming greater and getting various, it is necessary to develop the higher count OPGW. According to previous fiber count series, 6, 12 and 24, it is desirable that the count of newly developed OPGW is 48.

Since OPGW carries electrical current such as induction and short circuit, cable in itself is heated. For this reason, OPGW is required higher heat resistant property than commonly used optical fiber cable. Required heat resistant properties depend on the voltage of power line, cut off system of short circuit current and conductor cross section constituted OPGW.

Mainly the heat resistance of OPGW is restrict by the materials which make up optical sub-unit composite in OPGW. The conventional optical sub-units withstand 260°C aging for short term, 10 minute and 150°C aging for long term, 400 hour. In The Kansai Electric Power Co., Inc., however, the voltage of aerial power lines where OPGW is installed are mainly lower than 154kV. In such a line, required heat resistances are

120°C for short term, 8 hour and 90°C for long term, 400 hour. Therefore, to ease the heat resistance, we designed newly OPGW to make priority on the diameter and the composite fiber counts. This paper is described about the structure and the test result of newly developed OPGW.

3. OPGW design

The constructions of newly developed and former OPGW are shown in Fig. 1.

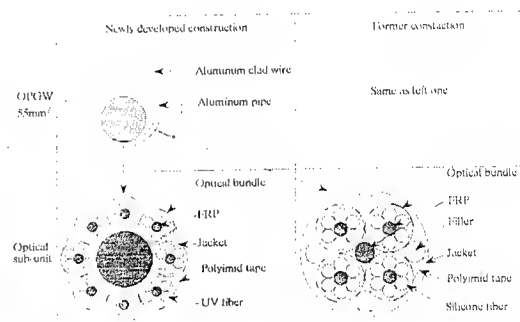


Fig.1 Construction of newly developed and former OPGW

For former construction, the 400 μ m diameter fiber coated by silicone resin (silicone fiber) is used to meet the severe heat resistant requirement. In case of using silicon fiber, maximum count is limited to 24 by the free space in OPGW. To composite 48 fiber, it is necessary to reduce the diameter of fiber to 270 μ m. In case of lower 270 μ m in diameter, however, a stiffness of silicone resin is very low, so the strength of fiber is weakened. On the other hand, the 250 μ m diameter fiber coated by UV curable urethane-acrylate resin (UV fiber) has stiff surface, so it is possible to avoid the problem of fiber strength. But UV fiber is more affected by microbend than silicone fiber. Microbend loss is sensitive to roughness and lateral force. For conventional construction, the source of roughness exist

on FRP surface shown in Photo 1, which is used for unit central member. To reduce roughness, we coated FRP surface by UV curable resin shown in Photo 2. And to minimize the effect of lateral force we examined the material and the extruding conditions for the jacket of optical bundle.

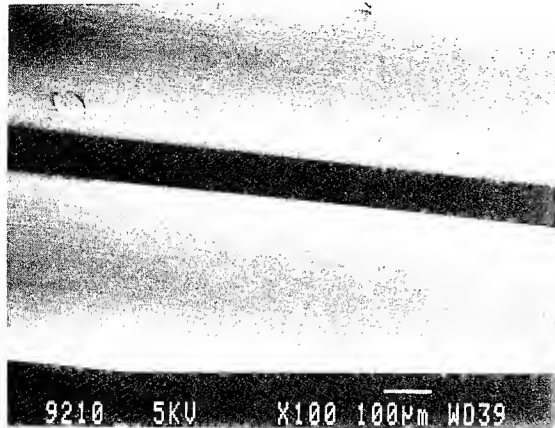


Photo1. Conventional FRP surface

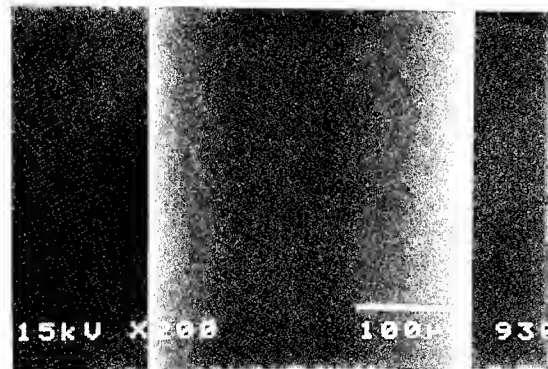


Photo2. FRP surface coated by UV curable resin

4. Optical characteristics

4-1. Attenuation change after cabling

This OPGW is used with a single mode fiber having the characteristics shown in Table 1. on condition of use $1.3\mu\text{m}$ band. The evaluated results of attenuation fluctuation through the manufacturing process for 1000 meter cable are shown in Fig.2. The attenuation fluctuation for the 48-core single mode fiber shows the very stable characteristics within the maximum 0.01 dB/km.

Table 1. Characteristics of fiber

Item	Characteristics
Fiber type	Single mode
Operating wavelength	$1.3\mu\text{m}$
Number of fiber	48
Attenuation ($1.3\mu\text{m}$)	$<0.4\text{dB/km}$
Cutoff wavelength	$1.17\sim1.29\mu\text{m}$
Mode field diameter ($1.3\mu\text{m}$)	$9.43\sim9.73\mu\text{m}$
Dispersion ($1.285\sim1.33\mu\text{m}$)	$<3.5\text{ps/nm/km}$
Coating diameter	$250\mu\text{m}$

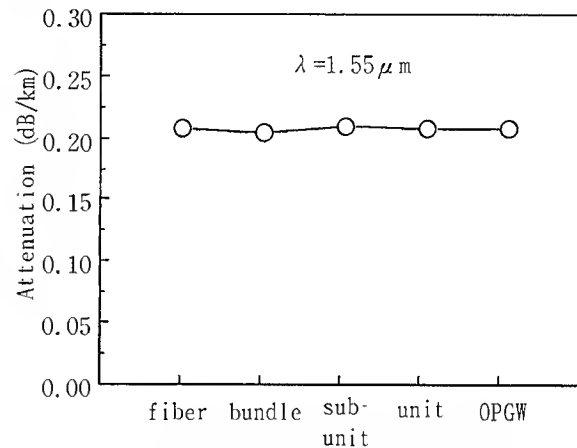


Fig.2 Attenuation of optical fibers in cable manufacturing

4-2. Short term aging

This test simulates the temperature rising by short circuit current. Therefore the aging temperature 120°C was set to maximum rising temperature when short circuit was occurred and the aging time 8 hour was chosen to the accumulation when temperature was over 40°C by short circuit during 36 year. We used the 500 meter length optical sub-unit which was loosely coiled in 280 millimeter diameter. The transmitted power fluctuation at $1.55\mu\text{m}$ was observed in condition of loop connection to the 6-core fiber. The results are shown in Fig.4. The power fluctuation was within 0.05 dB/km and any additional loss increase was not observed after aging.

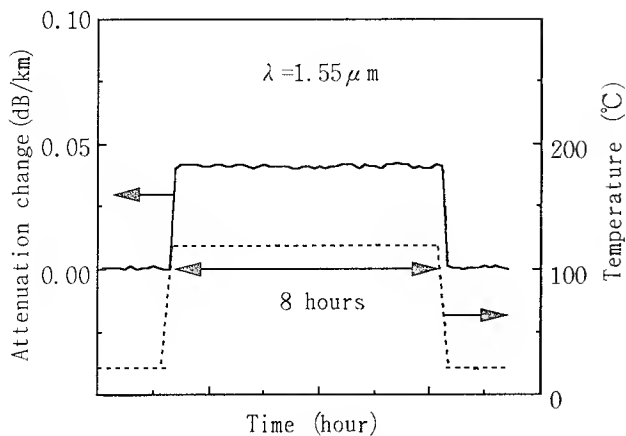


Fig. 3 Short term aging test

4-3. Long term aging

This test simulates the temperature rising when maximum induction was occurred in summer day. The aging temperature 90°C and the aging time 400 hour was chosen by the similar reason as the short term aging. The test sample and condition was same one as 4-2. The results are shown in Fig. 5. The power fluctuation at 1.55 μm was less than 0.01 dB/km and the additional loss increase was not observed after aging.

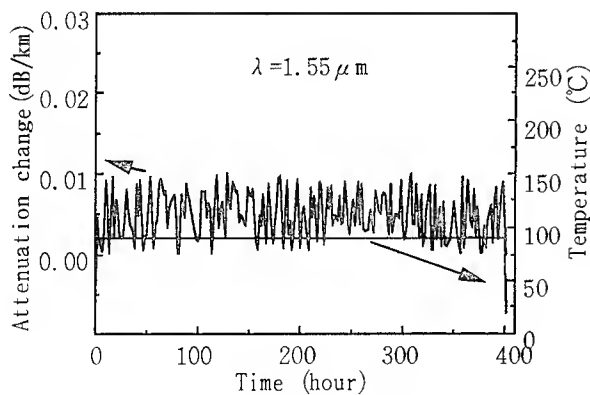


Fig. 4 Long term aging test

4-4. Temperature cycle

The power fluctuation at 1.55 μm due to temperature change within the range of -20°C to +90°C was evaluated. The test sample and condition was the same one as 4-2 and 4-3. The results are shown in Fig. 6. The power fluctuation in this temperature range was less than 0.04 dB/km.

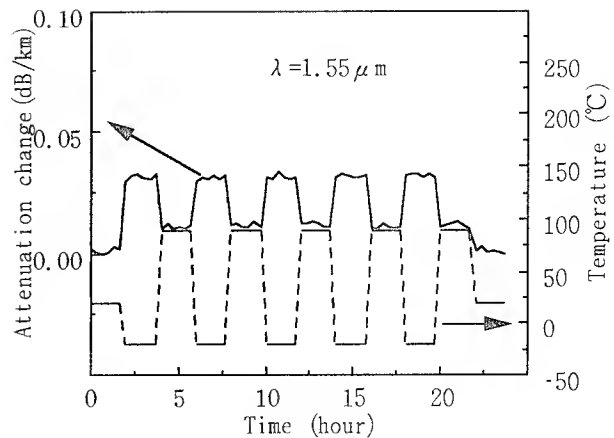


Fig. Temperature cycle test

4-5. Mechanical characteristics

We conducted many mechanical tests shown in table 2 for optical sub-unit, 55mm² OPGW and 70mm² OPGW. The results were all satisfactory for practical use.

Item	Sample	Result
Bend	Optical sub-unit	No attenuation change over ϕ 40mm bend at $\lambda = 1.55 \mu\text{m}$
Tensile strength	Optical sub-unit	No attenuation change under 1% elongation at $\lambda = 1.55 \mu\text{m}$
Crush resistance	Optical sub-unit	No attenuation change under 30kg/50mm load at $\lambda = 1.55 \mu\text{m}$
Squeeze	OPGW	No attenuation change over ϕ 450mm squeeze at $\lambda = 1.3 \mu\text{m}$
Tortion	OPGW	No attenuation change under 20 times/30m at $\lambda = 1.3 \mu\text{m}$
Crush resistance	OPGW	No attenuation change under 990kgf/50mm (55mm ² OPGW) 1280kgf/50mm (70mm ² OPGW) at $\lambda = 1.3 \mu\text{m}$

5. Conclusion

We have developed high density optical unit for OPGW which contains 48 optical fibers, the highest count published to date, and is accommodated in an existing OPGW. The developed OPGW shows excellent temperature stability and mechanical properties for practical application.

Jun-ichi Sumita
The Kansai Electric Power Co., Inc.
3-22, 3-chome, Nakanoshima, Kita-ku,
Osaka 530-70, Japan

Jun-ichi Sumita received the B.E. degree in electrical engineering from Kyoto University in 1972. He joined The Kansai Electric Power Co., Inc. He has mainly engaged in planning and designing of telecommunication systems. Presently he is responsible for regulating technical standards and supervising construction and education of telecommunication systems. He is a member of the Institute of Electronics and Communication Engineers of Japan.

Yoshinaga Kashiwara
The Kansai Electric Power Co., Inc.
3-22, 3-chome, Nakanoshima, Kita-ku,
Osaka 530-70, Japan

Yoshinaga Kashiwara received the B.E. degree in electrical engineering from Doshisha University in 1985. He joined The Kansai Electric Power Co., Inc. He has been engaged in designing of optical fiber telecommunication systems.



Jun-ichi Ohta
Sumitomo Electric Industries, Ltd.
1, Taya-cho, Sakae-ku,
Yokohama 244, Japan

Jun-ichi Ohta received the M.S. degree from Tokyo Institute of Technology in 1987. He joined Sumitomo Electric Industries, Ltd and has been engaged in research and development of optical fiber. He is now an engineer of Communication Cable Division.



Itaru Sakabe
Sumitomo Electric Industries, Ltd.
1, Taya-cho, Sakae-ku,
Yokohama 244, Japan

Itaru Sakabe received the M.E. degree in electronics and communication engineering from Electro-Communication University in 1993. He joined Sumitomo Electric Industries, Ltd and then has been engaged in the development and design of communication cable. He is now an engineer of Communication Cable Division.



Takashi Saito
Sumitomo Electric Industries, Ltd.
1, Taya-cho, Sakae-ku,
Yokohama 244, Japan

Takashi Saito received the B.E. degree in electronics engineering from Sendai Radio College of Technology in 1992. He joined Sumitomo Electric Industries, Ltd and then has been engaged in process development of communication cable. He is now an engineer of Communication Cable Division.



Jun-ichi Sumita



Yoshinaga Kashiwara

Optical Ground Wire and All Dielectric Self-Supporting Cable -A Technical Comparison-

Helmut G. Haag*, Georg Hög*, Ulrich Jansen*, Johann Schulte**, Peter E. Zamzow*

*KABELRHEYDT Aktiengesellschaft, Mönchengladbach, Germany

**Kabelmetal Electro GmbH, Hannover, Germany

1. Abstract

For the installation of optical fibre cables on high voltage overhead lines two basic cable technologies are used:

- Optical ground wire (OPGW)
- All dielectric aerial cable, self supporting or attached to the ground or phase wire

For OPGW applications especially in Germany, a change from fibres in plastic tube to fibres in metallic tube was done in the last 5 years. More than 50 % of the OPGW installations are done now by OPGW with fibres in stainless steel tubes. Also in other countries this market increases. Another market exists for all dielectric aerial cables world-wide in those cases where no ground wire exists or where new ground wires are newly installed without fibre optics. For these case dielectric self supporting aerial cables (ADSS) are used, normally on high voltage lines up to 150 kV.

The situation of these possibilities are described with regard to the cable constructions, accessories and environmental conditions.

2. Introduction

Aerial cables with telecommunication part (copper or fibre optics) are used by power utilities for around 25 years. Up to now these cables were used for internal requirements of the power utilities such as corporate telephony, data transmission and control purposes. With the deregulation of the telecom monopolies in many countries these aerial cables applications become more and more interesting for power utilities to build up their own telecom network with the existing infrastructure of the high voltage lines. For these applications a variety of aerial cable constructions, especially with higher fibre counts has to be realised. In most of the cases up to now cables with a maximum of 12 fibres are used. For the new situation in many countries the demand of cable constructions with more fibres (48 or even more) is growing.

One construction is the optical ground wire (OPGW), where telecommunication part and earthing functions are integrated in one cable /1, 2, 3, 4, 5, 6, 7/.

The second cable construction is a dielectric cable which can additionally be installed in the towers or is attached to the ground or phase wire /8, 9, 10, 11/.

The advantage of the dielectric cables is the relatively easy installation in existing lines, especially for the low weight. But for power lines with more than 150 kV the long time behaviour of the plastic sheath with regard to degradation is not quite clear.

In the case of OPGW with stainless steel tubes the problem does not occur, and these constructions are used for 400 kV and above.

Points to be considered in this comparison are:

- sag and wind behaviour (ice loading)
- temperature behaviour
- corrosion / degradation
- short circuit
- diameter/weight
- fibre count
- gun proofness /bird attacks
- life time reliability
- installation practice on new and existing lines
- suspension and dead end clamps/spirals
- costs for cables, accessories and installation

The principle for the installation of OPGW and ADSS are shown in figure 1.

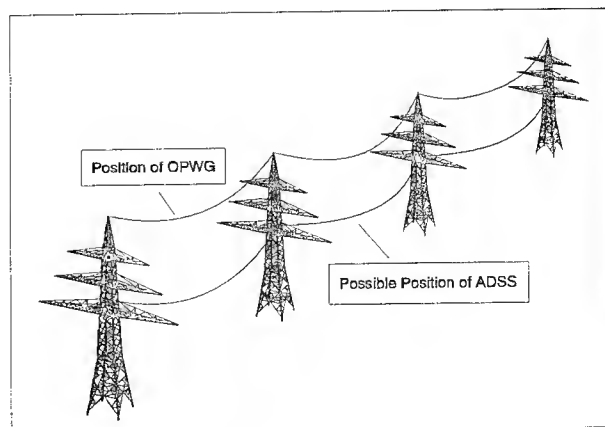


Fig.1: Installation of OPGW and ADSS

After an introduction phase of OPGW with fibres in metallic tube over 5 years, the actual situation of this OPGW family, especially for high fibre counts is compared with the dielectric cable solution. Various tests and their results are presented. Future aspects for power utilities using fibre optics in the various cable constructions are discussed. In this discussion as well as in the comparison the lashing and wrapping technique for light optical fibre cables is considered.

3. Self-Supporting Optical Aerial Construction

In aerial cables there will always be a tensile force in the installed cable, which causes cable elongation. This cable elongation is determined by the span length, the allowed sag, the weight and mechanical strength of the cable. The mechanical strength of a cable is determined by the product $A \cdot E$. E is the module of elasticity and A is the cross sectional area. E and A can be determined in reference to the cross section of the cable or to the cross section of the strength members in the cable. The cable elongation will change with temperature, wind and ice load. Over long time periods the tensile force in the cable will result in creep of the strength members, which adds to the cable elongation. Today computer programs exist, which take into account all these effects. Therefore, no detailed formula will be given here.

From the above it is obvious, that the user of an aerial cable first has to establish very well, which wind and ice loads and which minimum and maximum temperatures he expects. In some countries standards exist, that give some rules for the area covered. According to the local conditions the maximum allowed sag under worst case weather conditions has to be determined for each span. Taking into account all these conditions the applicability to a given cable can be calculated using its parameters: cable diameter, because the wind and ice load increase with cable diameters, cable weight, the $E \cdot A$ force in the cable. Some margin has to be left for cable creep. Fig. 2 gives an overview of OPGW and ADSS constructions.

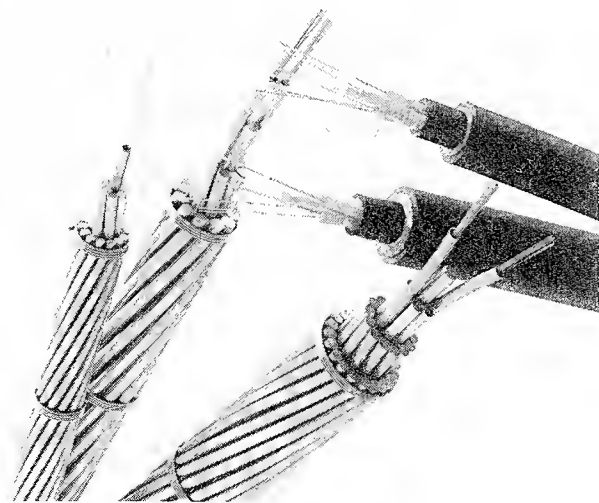


Fig 2: High Count OPGW and ADSS Types

3.1 All Dielectric Self-Supporting Cable (ADSS)

Cable design

It is obvious that the cable design should combine the highest mechanical strength with the smallest cable diameter and weight possible. At the same time the required number of fibres has to be inserted with a maximum of protection. Cable elongation must not result in stress on fibres. It is well-known that the loose tube construction, consisting of freely moving fibres in tubes stranded around a central element, gives maximum protection for the fibres and allows cable elongation without elongation of the fibres. Therefore, we have chosen this construction for the cable. An inner jacket is added in order to protect the cable core and to give a solid base for the strength members, stranded around this inner jacket. As strength members we have chosen aramid yarns because they combine a high module of elasticity with low specific mass and low long time creep. They are also very fatigue resistant and resilient to chemicals formed in the environment. Their thermal coefficient of expansion has a very low negative value.

A cable can be designed according to the requirements of the customer. For illustration Fig. 3 gives two designs for a smaller and larger maximum permissible load.

Type : A-D2Y(ZN)2Y 6x2E9/125 (16kN)		Type : A-D2Y(ZN)2Y 6x2E9/125 (35kN)	
1 - single mode fibre 9/125 0.38F3.5 2 - buffered tube 3 - central FRP element 4 - wrapping 5 - inner sheath 6 - aramid yarns 7 - wrapping 8 - outer sheath		1 - single mode fibre 9/125 0.38F3.5 2 - buffered tube 3 - central FRP element 4 - wrapping 5 - inner sheath 6 - aramid yarns 7 - wrapping 8 - outer sheath	
cable diameter	(mm)	14,3	16,6
cable weight	(kg/km)	165	215
number of fibres		up to 12	up to 12
max. permissible load	(kN)	16	35
calculated breaking load	(kN)	>48	>100
cable cross section	(mm ²)	161	217
young's modulus	(kN/mm ²)	14,5	23
(related to cable x-section)			
thermal elongation coefficient	(1/K)	3E ⁻⁶	1E ⁻⁶
operating temperature	(°C)	-40 .. +70	-40 .. +70

Fig.3: ADSS Types for 350m and 700m Span Length

A span length of 350m and 700m has been indicated for the two cables. This span length has been calculated using extra load according to VDE and limiting the maximum sag with extra loads to 4 %. Under different

conditions various spanlengths may be calculated. We assumed a maximum of 24 fibres, but cables with more fibres can of course be designed. The cable diameter ranges from 14,3 mm to 17,3 mm. Even thinner cables are feasible for shorter spans. Cable weight depends, whether the interstices between different tubes in the cable core are filled for water tightness and ranges from 155 kg/km to 235 kg/km only. Cable core filling for water tightness is considered necessary by some operators and not necessary by others. Up to loads of 16 kN and 35 kN respectively no fibre elongation will occur. At higher loads the fibre elongation will reduce fibre life time or the fibre may even break. The module of elasticity has been related to the cross sectional area of the cable, because this can directly be verified experimentally. If it is related to the aramid yarns only, values exceeding 100 kN/mm² are obtained. The breaking load of the two cables is at least 48 and 100 kN respectively. The breaking load is no parameter for the design of the cable spans, because the maximum permissible load must not be exceeded. The breaking load is nevertheless an indication of the amount of aramid yarns used and how uniformly they are applied to the cable. The thermal coefficient of expansion is mainly determined by the aramid yarns and is very small. These cables have been designed for a temperature range of operation from -40°C to 70°C.

Cable properties and tests

Tests of the optical fibre data have been performed according to IEC 793-1. They are the same as for other kind of optical cables and will not be discussed here. Mechanical tests are of special importance for aerial fibre optic cables and have been performed according to IEC794-1. Cable samples of various versions of the described design with maximum permissible load up to 35 kN have been tested.

Tensile performance has been tested according to IEC 794-1-E1. Here and in all further tests the cable was tested with the same dead-end spirals as used in field installation. The tested cable length was 100 m. Fig. 4 shows cable and fibre elongation together with attenuation for a cable specified for a maximum permissible load of 35 kN. Cable elongation increases linear with force from the beginning. This proves that all aramid yarns are uniformly stranded around the inner jacket. No fibre elongation or change of attenuation was observed up to 35 kN.

In a separate step 25 m of the cable sample were used to determine the breaking load. The calculated breaking load was 108 kN. The cable broke at 112 kN. These results together with results from other versions of this cable show that the theoretical calculation scheme is valid and that produced cables have the predicted tensile properties.

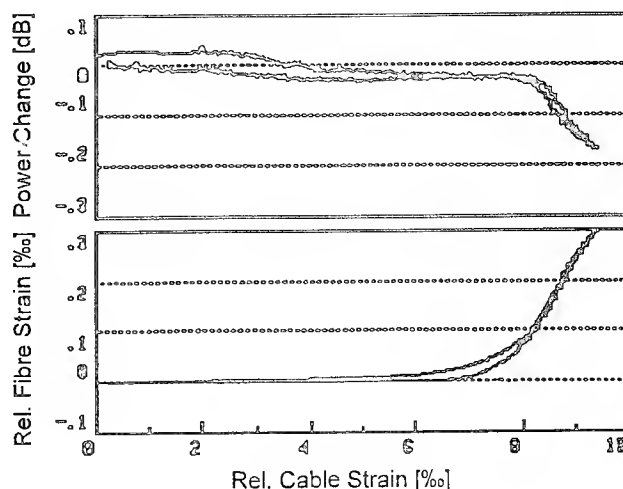


Fig.4: Fibre Strain in ADSS Construction

Cable creep has been measured using 20 m of cable. A constant load of 25 % of the breaking load was applied for 1000 h. This is much higher than every day load of the cable in operation. The measured elongation includes settling of the entire set-up. The initial period is dominated by the settling effect. Later cable creep is the main contribution. The measured cable creep was extrapolated for up to 10 years. Cable creep from 1 hour to 1 year was calculated to be $0,785 \cdot 10^{-3}$ and 1 hour to 10 years $1,28 \cdot 10^{-3}$. These values are very well in line with creep expected for aramid yarns /9/. From the creep behaviour of aramid yarns it can be concluded that the actual creep of the installed cable will be even lower and can be neglected in most cases.

Aeolian vibration performance was tested with a load typical for the every day load in an installation. A length of 44 m of cable was excited with 33 Hz for 10^8 cycles. All fibres were spliced in series and optical attenuation was monitored at 1550 nm. No change in attenuation was observed during or after the experiment. There was also no damage to the cable or the dead end spirals and no slippage between the cable and the spirals. Vibration damper of the Stockbridge type have been identified for the cables in self-damping experiments.

Results of further mechanical tests are summarised in table 1.

The cable is designed with homogenous dense layers of aramid yarns around the inner jacket. This assures the highest degree of resistance to shot-gun damage possible for metal free light weight aerial cable.

Mechanical characteristics			
Test	Test standard	Test conditions	Test results
Crush test	IEC 794 - 1/E3	L = 30m, $\lambda=1550\text{nm}$ $t=15\text{min}$, 1500N increase of attenuation $\leq 0,1\text{dB}$, no destruction of cable sheath	$\leq 0,01\text{dB meas.}$, no destruction of cable sheath
Impact test	IEC 794 - 1/E4	L = 30m, $\lambda=1550\text{nm}$ r = 10mm, load= 5Nm attenuation $\leq 0,1\text{dB}$, no destruction of cable sheath	$\leq 0,01\text{dB meas.}$, no destruction of cable sheath
Repeated bending	IEC 794 - 1/E6	L = 3m, 100 cycles, F=100N, $r=20\times\text{cable-}\phi$ no destruction of cable sheath and no fibre break	no destruction of cable sheath and no fibre break
Torsion	IEC 794 - 1/E7	L=1000mm, 5 cycles each $\pm 360^\circ$ F=100N, $\lambda=1550\text{nm}$ attenuation $\leq 0,1\text{dB}$, no destruction of cable sheath	$\leq 0,02\text{dB meas.}$, no destruction of cable sheath
Temperature cycling	IEC 794 - 1/F1	L > 1km, $\lambda=1310\text{nm}+1550\text{nm}$ temp.range: 20°C , -40°C , $+70^\circ\text{C}$, 20°C , change rate 1°C/min , variance of attenuation $\leq 0,1\text{dB/km}$ at 1310nm and 1550nm	attenuation variance 1310nm = $0,05\text{dB/km}$ 1550nm = $0,03\text{dB/km}$
Longitudinally watertightness	IEC 794 - 1/F5	L = 1m, water pressure 1m, duration = 24h no water drip	no water drip
Kink resistance	IEC 794 - 1/E10	L = 350mm, distance of sample ends = 100mm, no. of cycles = 5, loop diameter = 68mm, no kinking	no kinking

Table 1: Test Results for ADSS Cable Constructions

It has been reported that dielectric cables suspended in power lines with line voltage of 220 kV and above degrade and are finally destroyed through corona and tracking effects. These effects have widely been discussed in the literature [10]. The degradation effect in lines with these high voltages can be minimised or eliminated by placing the cable at a position where the coupled voltage has the lowest possible value and by using special jacket materials. Using a computer program we can calculate the electric field strengths in a given line and the optimum position of the tie points in the tower. We have also developed a tracking and corona resistant jacket material. However, in practical applications generally an OPGW will be chosen for line voltages of 220 kV and above. On the other hand for line voltages up to 150 kV dielectric cable constructions might be used without risks.

Installation

Cable parameters and accessories are chosen such, that every experienced installation company can install the cable using established techniques. The dead-end and suspension spirals and other fittings used are chosen from products available on the market. Initial sag has to be adjusted in a manner to make sure that there is enough clearance to ground and to the conductors under all load conditions. The effect of wind and ice has to be taken into account.

3.2 OPGW with Stainless Steel Tubes

About five years ago OPGW with stainless steel tubes were introduced into the market. Starting with a few in the beginning the amount of fibres was raised up to 12 fibres per tube. This was the mostly used number of fibres for OPGW in the early nineties.

The cable consist of two or more layers of stranded wires (mostly aluminium-clad steel and aluminium alloy) with one or more steel tubes placed in the first layer. With the right combination of tube dimensions, fibre count and pitch length it is easy to construct OPGW with 0,5 % excess length or more if wanted.

Two main tendencies were observed during the last two years. On the one hand the demand for thinner OPGW and on the other hand the demand for more fibres are growing.

The request for thin cables below 10 mm mostly results from weak tower constructions in order to minimise wind and ice loads. On the other hand the demand for a certain diameter in combination with a certain cross section often results from the earth rope that is to be replaced. For example one layer aluminium-clad steel conductors according to ASTM B416 are wide spread for use as earth and or shield wire.

To substitute for instance ASTM type 7 No. 8 AWG (7 ACS wires of diameter 3,26 mm) by an OPGW with stranded steel tube a two layer construction is compulsory in order to protect the tube. This causes small tube and wire sizes and is not the best. Another way is to place the steel tube in the centre of the OPGW. In this case the whole fibre excess length of the cable must be put into the tube. Fig. 5 shows a comparison of the above mentioned ASTM conductor and an OPGW of similar diameter with central steel tube. Also the sag behaviour including ice and wind loads is very similar as shown in Fig. 6. This thin OPGW is now available up to 12 fibres. The fibres excess length is at least 0,5 %.


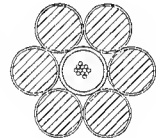
		
Mechanical Properties	ASTM	OPGW
Diameter [mm]	9,78	9,75
Cross Section [mm ²]	58,6	49,8
Weight [kg/m]	389,6	363
Breaking Strength [kN]	70,9	61,4
Resistance [Ω/km]	1,46	1,78

Fig.5: Comparison of ASTM 7 No.8AWG with Central Steel Tube OPGW

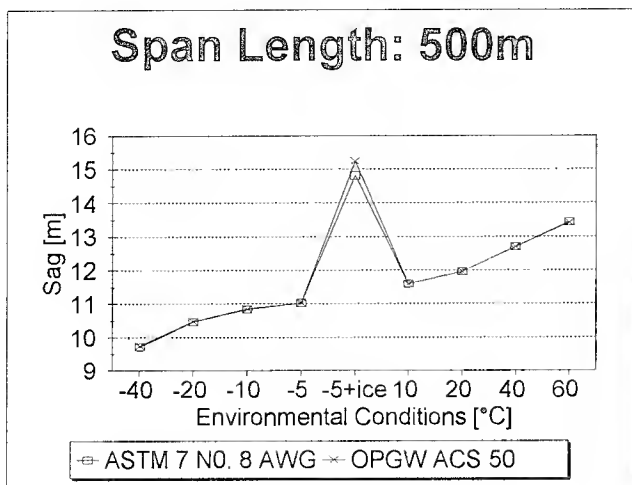


Fig.6: Sag Comparison for Span Length 500m

To increase the fibre count the steel tube technology offers two possibilities. On the one hand it is possible to place more than one tube in a cable and on the other hand it is possible to put more fibres into a tube. The number of fibres that can be put into a tube is limited by the remaining space which is necessary for having enough excess length. Table 2 shows the standard tube sizes with maximum fibre counts we are using at the moment.

Dimensions	Wall Thickness	Fibre Excess Length in Tube	Fibre Quantity
1,4/1,7mm	0,15mm	1 - 2‰	2 - 4
2,1/2,5mm	0,2mm	0 - 2‰ 6‰ (central)	2 - 15 2 - 6
2,3/2,7mm	0,2mm	0 - 2‰ 6‰ (central)	2 - 18 2 - 9
2,6/3,0mm	0,2mm	0 - 2‰ 6‰ (central)	2 - 24 2 - 12

Table 2: Steel Tube Types

For fibre counts in steel tube with more than 12 fibres, a special ring marking is used. With these standard tube sizes it is possible to create cable families (Fig. 7). The wires which are used in this cables have also standard sizes mostly in steps of 0,25 mm. An exception is the central wire which has special size in order to have less than 100 % of covering especially in the first layer. This prevents the steel tube from being squeezed between the wires. Coming from a standard type it is possible to create sub-families by replacing wires by steel tubes or by another kind of wire.

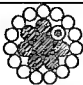




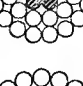
	ASLH-D(S)bb 1x24E9/125 (Ay/Aw 74/56-8,5) Diameter: 15,1 mm Short Time Current: 8,5 kA Ultimate Tensile Strength: 88,2 kN
	ASLH-D(S)bb 1x24E9/125 (Ay/Aw 83/56-9,4) Diameter: 15,6 mm Short Time Current: 9,4 kA Ultimate Tensile Strength: 91,0 kN
	ASLH-D(S)bb 1x24E9/125 (Ay/Aw 92/56-10,3) Diameter: 16,1 mm Short Time Current: 10,3 kA Ultimate Tensile Strength: 93,6 kN
	ASLH-D(S)bb 1x24E9/125 (Ay/Aw 121/56-13,1) Diameter: 17,6 mm Short Time Current: 13,1 kA Ultimate Tensile Strength: 102,3 kN
	ASLH-D(S)bbb 1x12E9/125 (Ay/Aw 226/56-23,3) Diameter: 22,1 mm Short Time Current: 23,3 kA Ultimate Tensile Strength: 133,1 kN
	ASLH-D(S)bbb 1x12E9/125 (Ay/Aw 279/56-28,4) Diameter: 24,1 mm Short Time Current: 28,4 kA Ultimate Tensile Strength: 148,6 kN

Fig.7: Cable Family with 2,6/3,0mm Steel Tube

Tests

To prove the reliability of OPGW with 24 fibres per tube a lot of tests were made. A type test was made with the cable construction shown in Fig. 8. The steel tube had an inner/outer diameter of 2.6/3.0 mm. The test procedures are described in the contribution we presented on IWCS 1991. In a traction test with measurement of pulling force, cable elongation, torque and fibre elongation it could be shown that the fibre excess length is > 0,5 %. Fig. 9 shows these results.

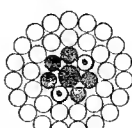
ASLH-D(S)bbb 2x24E9/125 (Ay/Aw 226/49-23,2)	
	Construction:
	Center: 4,1mm Aw-Wire
	1. Layer: 5 x 3mm Aw-Wire
	+ 2 Steel Tubes 2,6/3,0mm with 24 Fibres each
	2. Layer: 13 x 3,0mm Ay-Wire
	3. Layer: 19 x 3,0mm Ay-Wire
Technical Data:	
Diameter	: 22,1 mm
Weight	: 1010 kg/km
Supporting Cross-Section	: 274,7 mm²
Ultimate Tensile Strength	: 124,3 kN
Young's Module	: 75,6 kN/gm²
Thermal Elongation Coefficient	: 19,2 10 ⁻⁶ /K
DC-Resistance	: 0,140 Ω/km
Nominal Short Time Current	: 23,2 kA

Fig.8: OPGW with 48 Fibres

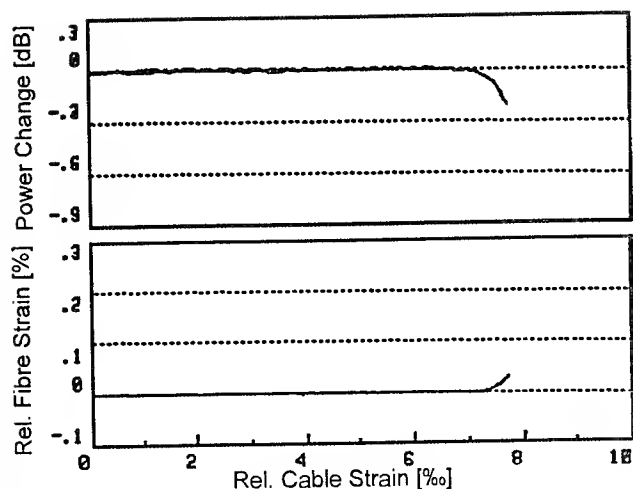


Fig.9: Fibre Strain for OPGW with 48 Fibres

In a short current test the cable was loaded with various currents and times. The short circuit current capacity $I^2 \cdot t$ was raised from nominal load up to more than 300 % of nominal load. Even at highest load there was only a very small rise in attenuation. First bird cages were registered at about 200 % of nominal load. So the optical transmission reliability in case of short circuit is better than the mechanical one (Fig. 10). A sheave test showed no deformation of the steel tube.

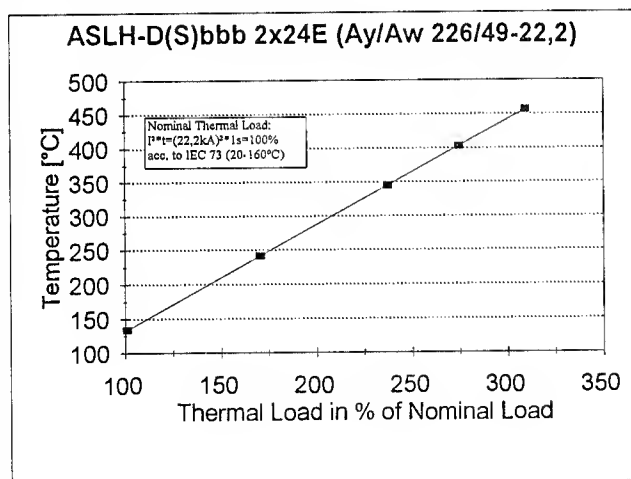


Fig.10: Short Time Current Test

Installation

For the installation of OPGW with stainless steel tubes well suited fittings must be used in order not to flatten the cable which could cause damage to the tube. Therefore the well-proved helical formed fittings should be used at tension and suspension points. To prevent damage and to increase life time The OPGW should be protected

from aeolin vibration with dampers. The right places and types of dampers can be calculated knowing the self-damping of the cable, span lengths and every day stresses.

The stringing of OPGW with steel tube is very similar to that of a bare ground wire. Special attention only has to be paid on the maximum installation forces and bending radii. For all these kinds of OPGW with two or more armour layers no anti-torque equipment is necessary. In long-time tests we could prove that the creep behaviour of OPGW is comparable to that of usual ropes with same or similar cross sections. Therefore, the adjustment of initial sags can be done as usual.

3.3 Wrapped Cable Constructions

The third technology to install fibre optic cables on high voltage lines is to use wrapped cables. In this case a fully dielectric and very thin cable (approx. 10 mm) is wrapped around the earth or phase conductor. Most of these wrapped systems are located on the earth conductor [11]. The wrapping cable technology has the advantage that no additional strength members in the cable are necessary, because the cable is supported by the ground or phase wire. On the other side the cable sheath has to be chosen to withstand bird attacks, so that special compounds must be used. A second problem is that the size and weight of the cable drum reduces the maximum cable length that can be installed in one piece. This problem does not occur in the case of OPGW and ADSS, where cable lengths of more than 5 km are normal. From these considerations the wrapping technology might be a good solution for "post" installations on new existing power lines, where it is not economical to replace the earth wire or to install an additional cable in the pole configuration.

4. Summary

It was shown that both aerial cable constructions - all dielectric or OPGW with stainless steel tube - meet the requirements for power utilities. The ADSS type should be used preferably for high voltage line up to 150 kV where the danger of degradation of the outer sheath is very low. The ADSS type can easily be used for high voltage lines where no ground wire exists or where it is not possible to replace the ground wire by an OPGW. However, in most of the cases, especially on new HV lines, the OPGW should be used. With some standard steel tube sizes it is easily possible to replace the bare ground wire by an OPGW with same mechanical and electrical behaviour. With this OPGW construction it is very easy to achieve high fibre counts up to 96 at present. In the near future stainless steel tubes will be available up to 36 fibres per tube, so that the maximum fibre counts in one cable will be 144.

	Standard Earth Rope	OPGW with Steel Tube	ADSS
Gun Proofness	very good	very good	good
Short Circuit Current	depends on cross section	similar as earth rope	-
Relative Cable Costs (without Fibres)	1	2	1,9
Relative Accessory Costs	1	3	3
Relative Installation Costs (without closures)	1	1,2	1,2
Sag Behaviour acc. to:			
temperature	normal	normal	around zero
ice load	normal	normal	higher
wind load	normal	normal	larger angle of decay tendency to galloping
Weight	depends on diameter and relation of cross sections (Al/St)	similar as for standard earth rope	very low
Corrosion/Degradation	normal	normal	corona and tracking effects can be prevented by placing the cable at the right position
Diameter	depends mainly on demanded short circuit current	similar as for standard earth rope	depends on span length and fibre count
Thermal Elongation Coefficient	depends on relation of cross sections ($11 < \alpha < 23 \{10^{-6}/K\}$)	similar as for standard earth rope	app. 0

Table 3: Comparison of Standard Earth Rope, OPGW and ADSS

5. References

1. Nakagaki, et al. 'Development of high-performance composite fibre-optic overhead ground wire', International Wire and Cable Symposium Proceedings, 1986, pp. 464 - 471
2. Russ, Misono, Okazato, Kobayashi 'Composite ground wire with optical fibres', International Wire and Cable Symposium Proceedings, 1986, pp. 484 - 489
3. Schneider, Schmelter, Herff 'Optical ground wire design with a minimum of dielectrics,' International Wire and Cable Symposium Proceedings, 1988, pp. 83 - 92
4. Haag, Hög, Zamzow 'New Generation of self-supporting optical fibre aerial cables,' 1989, pp. 575 - 582
5. Haag, Hög, et al. 'Self-supporting optical fibre aerial cable constructions and related fibre parameters for the transmission at $\lambda = 1550 \text{ nm}$ ', International Wire and Cable Symposium Proceedings, 1991, pp. 206 - 217

6. Bonicel, Cortinez, Hög, et al, 'Optical ground wire - a worldwide technical survey and comparison ', International Wire and Cable Symposium Proceedings, 1993, pp. 42 - 47
7. CIGRE SC35, 'Optical Fibre Planning Guide for Power Utilities'
8. Oestereich, Nassar ' Self-Supporting dielectric optic cables in high voltage lines', International Wire and Cable Symposium Proceedings, 1988, pp. 79 - 82
9. 'Kevlar for telecommunications cables', Technical Documentation, Du Pont de Nemours
10. Carter, Waldron, 'Mathematical model of dry-band arcing on self-supporting, all-dielectric, optical cable strung on overhead power lines', IEEE Proceedings s-c, vol. 139, No. 3, May 1992, pp. 185-196
11. Yoshida, et al, 'Winding of optical fibre cable on to existing ground wire', International Wire and Cable Symposium Proceedings,, 1986, pp. 42 - 47. G.

Authors

Helmut G. Haag
KABEL RHEYDT AG
Mönchengladbach, Germany

Helmut G. Haag (46) is Director of the Sales Division for Telecommunications. After reaching his Dipl.-Physiker-degree from the University of Stuttgart he joined KABELRHEYDT in 1975 for the development of coaxial cables. Later he has been also responsible for the development of optical cables. From 1980 to 1983 he built up the production plant for these cables. From 1984 to 1989 he has been responsible for the technical sales department. Since 1990 he took over his present position.



Georg Hög
KABEL RHEYDT AG
Mönchengladbach, Germany

Georg Hög was born in 1950. After studying electrotechnics at the Technische Hochschule Aachen he joined KABELRHEYDT as a development engineer for copper cables in 1977. In 1980 he became responsible for the development of symmetrical telecommunication cables. In this position he was also busy in the standardisation for copper cables for the German Telekom. In 1985 he became the head of the development for optical fiber cables. From 1987 to 1988 he was the head of the technique department of BETEFA (special cables for telecommunications). Since 1989, back to KABELRHEYDT, he is responsible for the development and construction department for optical fibre cables. He is also responsible for the standardisation for optical fibre cables for the DBP Telekom and a member in the standardisation bodies in VDE ETSI AND IEC for optical fibre cables.

Ulrich Jansen
KABEL RHEYDT AG
Mönchengladbach, Germany

Ulrich Jansen (30) received his Dipl.-Ing.-Degree from the University of Aachen in 1990. He joined KABELRHEYDT in the same year. As a member of the development department for optical fibre cables he is responsible for development of OPGW.



Johann Schulte
Kabelmetal Electro
Stadthagen

Johann Schulte received his physics degree in quantum optics in 1981 and his Ph. D. in engineering in 1986 from the "Technical University Hannover. After a research fellowship at IBM, Yorktown Heights, he joined Kabelmetal Electro in 1987, where he is currently in charge of cable engineering.



Peter E. Zamzow
KABEL RHEYDT AG
Mönchengladbach, Germany

Peter E. Zamzow (54) is director of the Telecommunication Division. After finishing his postgraduate studies in telecommunications in München and Graz as Dipl.-Ing. he joined AEG KABEL in 1970. He has been engaged in development and production of telecommunications cables. In 1980 he became head of the fiber optic division at AEG KABEL and in 1982 he was nominated as a senior engineer. From 1992 on he was plant manager of the new Optical Fiber Cable Plant Rheydt. Since 01. July 1994 he is general manager for CATV activities worldwide.



THE DEVELOPMENT OF A NEW SUBMARINE CABLE DESIGN FOR REPEATERLESS APPLICATION

Kaj Sjölin^{*}, Lennart Lidén^{*}, Nils-Erik Grip^{*}, Stig Lindohf^{**}, Jan Björkman^{**}

^{*} Ericsson Cables AB, 824 82 Hudiksvall, Sweden ^{**} Telia AB, 123 86 Farsta, Sweden

ABSTRACT

In order to meet new environmental and technical demands, a 48-fiber ribbon double armored lead-free submarine cable for repeaterless applications has been developed and tested for submersion down to 500 m.

A prototype cable and test cables have been made for verifying the mechanical properties and environmental reliability of the cable. Field trials and installation tests have also been carried out.

To be able to produce long cable lengths, a factory jointing method has been developed.

INTRODUCTION

Installing repeaterless submarine cable systems along the coasts of many countries (also called festooning) is frequently discussed. The reason for this is that a submarine cable system often is a very cost effective way to build up a telecommunication network. Distances up to 300 km can today be reached in one repeaterless length with commercially available end equipment.

But even with distances as short as a couple of kilometers it is often cheaper to submerge the cable rather than to bury it (if water is available of course).

The submarine cables used for transoceanic links are often overdimensioned for these types of applications, and also the number of fibers in these cables is low. New types of optimized cable designs are therefore an interesting development for repeaterless submarine systems.

Since Sweden is a country with more than a thousand lakes and with a coastline exceeding 2000 km, both power and telecommunication cables have been installed under water for more than one hundred years.

Most of the telecommunication submarine cables installed in Sweden up to now have contained a hermetic metal jacket of lead. The Swedish Environmental Protection Agency requests that submarine cables, used in Sweden, must not contain any lead as from January 1 1995.

Telia AB (formerly the Swedish Telecom, Televerket) has decided to stop all installation of lead cables from January 1 1994, one year earlier than requested.

This paper describes a new lead-free submarine cable design for repeaterless lengths, with high fiber count and for tough working conditions near the coast. The results from mechanical and environmental testing and the field trials are included.

CABLE REQUIREMENTS

With the recommendation from the Swedish authorities in mind, and with new cable demands from Telia AB, the cable development work started. The work was mainly carried out according to the following criteria:

- The cable shall contain a lead-free metallic sheath for water and hydrogen blocking.
- The fiber count shall be high. The cable shall contain 4-48 fibers in a ribbon design.
- The armoring shall be designed for a dynamic tensile strength of at least 100 kN, preferably as a double armoring.

- The self burrowing properties shall be good. Therefore the cable density to be at least 3kg/dm^3 .

- The cable is not intended to carry power feeding (repeaterless design).

- A jointing method is needed for the manufacturing of long cable lengths.

CABLE DESIGN

By June 1993 the new cable design was ready. Figure 1 shows the cable cross section. A design concept based on optical fiber ribbon technology has been used, allowing a higher fiber density.

Double Armored Submarine Cable

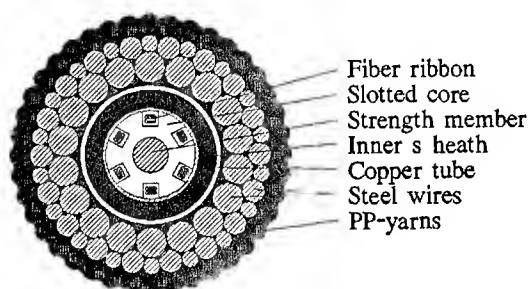


Fig.1

Cable core

The cable core consists of a slotted-core element made of high density polyethylene (HDPE) with a strength member of fiber reinforced plastic (FRP) in the center. Each slot can accommodate two 4-fiber ribbons. In total, there is room for 48 fibers in the cable. The slots are filled with a thixotropic gel to prevent axial water penetration. A wrapping tape on the outside of the core keeps the ribbon and gel in the slots. As an outer protection, a polyethylene (PE) sheath is used. The cable core design is of the same type as that used for ribbon duct cables installed in Sweden, and is known to be a reliable concept.

Hermetic sheath

Outside the cable core a sheath consisting of a copper tape is applied along the cable. This is formed to a tube around the cable core and seam welded into a hermetically tight tube by using TIG welding. Between the cable core and the copper tube a water blocking compound is applied. On top of the copper sheath a crepe paper layer is applied.

Armoring

The armoring is designed for tensile strength and for the maximum permissible fiber strain. Two layers of tightly packed steel wires have been used to give the cable a high density and good resistance to crush and impact. The galvanized armoring wires are impregnated with a corrosion-protective compound which also serves as a base for the outermost layer of polypropylene yarns.

Cable data

Cable diameter	29 mm
Weight	2.3 kg/m
Density	3.5 kg/dm^3
Tensile strength	100 kN

FACTORY JOINT

Due to limitations such as fiber length, strength member length, and drum size, long cable lengths have to be factory jointed.

The factory jointing concept is based on high strength fiber splicing and rebuilding of the cable core, with only a small diameter increase of the cable diameter. The jointing is performed before the cable core is supplied with the wire armoring.

The splicing of the optical fibers is carried out using the Ericsson High Strength Fiber Splicing method.

This method avoids touching or otherwise causing damage to the bare glass fiber surface during the splicing process.

After fusion splicing, the splice area is recoated and a tensile test of the splice is made to avoid low strength splices in the cable.

The restoration of the hermetic protection is performed by applying a copper tube (jointing tube) around the fibre splices and with a hermetic sealing around the cable ends (fig.-2a). A water-blocking compound is pumped into the jointing tube to allow the spliced fibers to move freely in the compound. This means that the fibers are stress free in the tube. The joint is completely integrated in the cable after armoring and not visible to the naked eye (fig.2b). The diameter increase over the joint is less than 2 mm

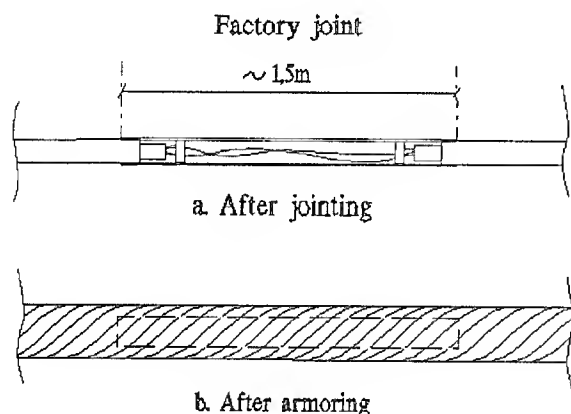


Fig.2

CABLE TESTING

General

All cable tests intend to simulate real situations when the cable is exposed to external "forces", during manufacturing, handling or installation.

The tests are performed in accordance with IEC 794-1, where applicable.

A two km long cable containing 36 fibers was produced and cut into relevant lengths for testing. The preparation of the test samples was mainly carried out as follows:

All fibers in the test sample were fusion spliced to form two separate loops for attenuation measurements at the wavelengths 1310 nm and 1550 nm. Each loop contained fiber from each ribbon. In the tensile tests three loops were used, the third loop was used for fiber strain measurements. The maximum permitted optical loss was 0.05 dB.

Hydrostatic pressure test

Two cable samples wound on two separate cable drums were placed in a pressure tank (fig.3).

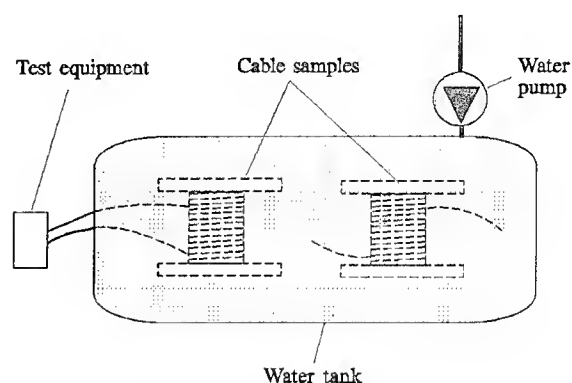


Fig.3

On one of the cables the ends were opened and exposed to the water. On the other cable the ends were taken out of the tank for attenuation measurements.

The tank was filled with water and the pressure was increased to 55 bar and held between 53 and 55 bar for 24 hours.

The fiber attenuation and the water pressure were continuously measured.

Results:

The cable ends were opened and the water ingress length was measured.

Table 1.

Cable end	Ingress length under the copper tube [m]	Ingress length in cable core [m]
inner	60	less than 5
outer	75	less than 5

No change in fiber attenuation exceeding 0.01 dB/km was observed. The graphs in fig.3 show the attenuation and the pressure change during the complete test period .

HYDROSTATIC PRESSURE TEST
Submarine cable: GASLMTV 48

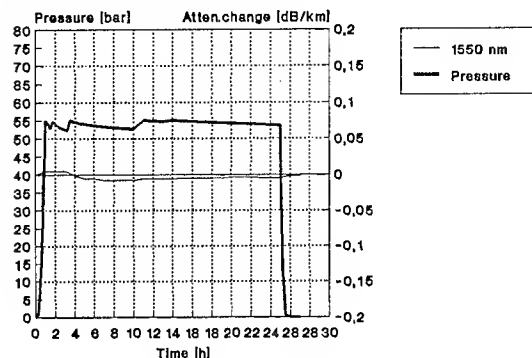


Fig.4

Temperature test

A one km cable length was wound on to a reel and placed in the temperature chamber. Ten temperature cycles were performed between -40°C and $+70^{\circ}\text{C}$. The attenuation at 1310 nm and 1550 nm was measured at each temperature.

Results:

No attenuation increase exceeding 0.05 dB/km was observed for any fiber during the test.

Hydrogen generation test

The test was carried out simultaneously with the temperature test. By monitoring the attenuation change at the hydrogen sensitive wavelength 1240 nm the hydrogen generation from materials inside the copper tube was observed. The fibers in slot no 1 (one ribbon) were fusion spliced and spectral attenuation measurements were made on six occasions.

Results: Table 2.

Measurement	Attenuation differences between 1240nm and 1310nm [dB/km]
Initial, room temp	0.164
cycle 1, $+70^{\circ}\text{C}$	0.160
cycle 2, $+70^{\circ}\text{C}$	0.160
cycle 6, $+70^{\circ}\text{C}$	0.167
cycle 10, room temp	0.168

No attenuation increase indicating hydrogen generation was observed. The difference between the initial and the end value, 0.004dB/km is within the uncertainty of the measurement.

Tensile test (dynamic)

A cable 100m long was tested, figure 5. At the middle of the length the cable was wound one turn around a moveable wheel with a radius of 1.25 m. The load was increased in steps of 10 kN up to 110 kN and back to zero. At each load the attenuation change, fibre strain and cable strain were measured.

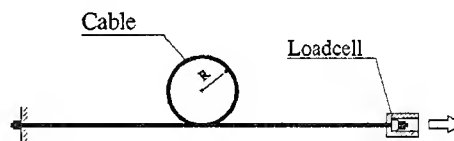


Fig.5

Results:

No change of attenuation was observed.

The fibre strain reached 0.24% at a tensile load of 100 kN. A remaining cable strain of 0.05% and a remaining fiber strain of 0.03% were observed after removing the loading from the cable from 110 kN.

Fiber and cable strain, as well as attenuation changes as a function of tensile load, are shown in fig. 6.

TENSILE TEST (dynamic)
Submarine Cable: GASLMTV 48

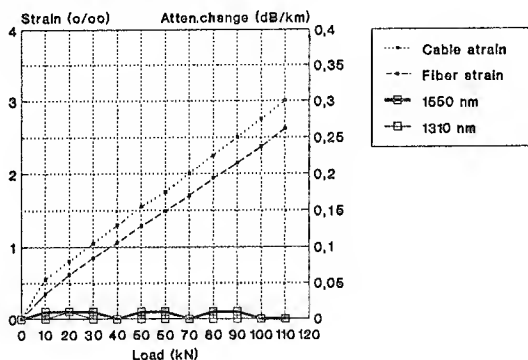


Fig.6

Tensile test (static)

The same setup as in the dynamic test was used. A static load of 5 kN was applied to the cable for 8 hours. Fiber attenuation and fiber strain were measured continuously.

Results:

No change of attenuation exceeding 0.05 dB/km was observed for a static load of 5 kN during 8 hours. Both cable strain and fiber strain were stable during the test. The fiber strain level was 0.15%. Fig.6 shows the test results.

TENSILE TEST (static)
Submarine Cable: GASLMTV 48

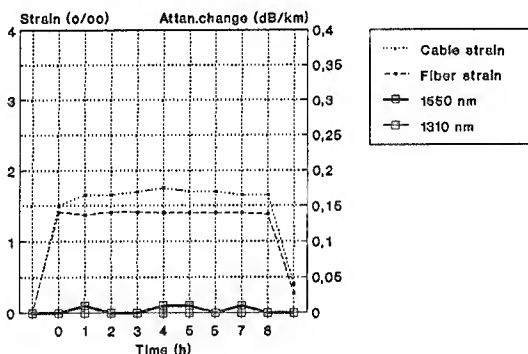


Fig.7

No damage to individual cable elements was observed after the tensile tests.

Crush test

The sample was placed between two parallel plates with the length of 100 mm. The load was gradually increased to 30 kN. The attenuation and cable deformation were measured continuously.

The test was performed at three different points on the cable, separated by at least 0.5 m.

Results:

The cable withstands loads up to 20 kN without any attenuation increase greater than 0.05 dB.

The cable deformation is 20% at a load of 5 kN.

CRUSH TEST
Submarine Cable: GASLMTV 48

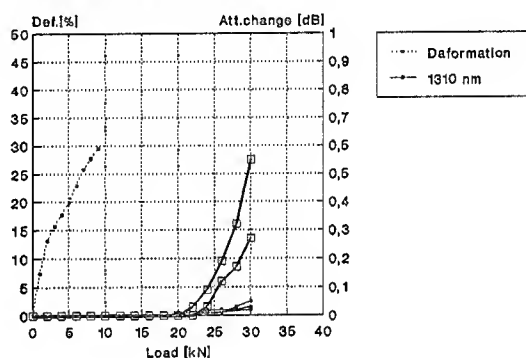


Fig.8

Impact test

Three impacts were made with the specified energy of 100 J. The impact energy was then increased.

Results:

The cable withstands impact energies up to 170 J without any attenuation increase or damage to the cable elements.

Table 3.

Test no.	Energy [J]	Att.change 1310nm [dB]	Att.change 1550nm [dB]
1	100	0.00	0.00
2	100	0.00	+0.02
3	100	0.00	-0.01
4	170	0.00	0.00
5	195	0.00	-0.21
6	215	-0.18	-0.32

Torsion test

A cable sample was twisted back and forth five times with a maximum torsion of one turn per 6 m of cable.

Results:

No change of attenuation or damage of the cable elements was observed.

Bend test

Bend tests both at room temperature and at -10°C were performed by using a bending radius of 0.5 m. The test was repeated five times at each temperature. The minimum bend diameter (one turn) at room temperature was tested by stepwise reducing the diameter.

Results:

No change of attenuation for bending at room temperature or at -10°C was observed. On completion of the tests the samples were opened. No damage to the copper tubes was observed.

Reducing the bending diameter to 300 mm produced no increase of attenuation.

Repeated bend test

A cable sample was bent through 180° ($\pm 90^\circ$) 25 times. The bend radius was 0.5 m.

Results:

No fiber breaks or damage to other cable elements was observed.

FIELD TESTS

Two test lengths were manufactured during August-September, 1993, for installation and testing. One of the lengths was used for testing the cable design to verify its mechanical properties and environmental reliability. The other length was used in a field test and was installed by Telia AB at the beginning of November 1993.

The results from these first two test cables were satisfactory, and production could begin in March 1994. A second field trial containing two cable lengths of 5 and 7 km, was carried out in April 1994. The first two field trials were

made by installing the cable from a raft.

The final field trial installation was made in August 1994, from the cable ship Plejel from Telia, Sweden. A cable length of 23 km was installed along the Swedish east coast.

Experience from these installations has been as follows.

·The winding and coiling properties are satisfactory.

The minimum winding and coiling diameter used was 1 and 2m respectively.

·The cable is easy to handle and work with. No kink or twist has been observed during handling or installation.

CONCLUSIONS

A new submarine cable design has been developed and tested.

The results from the design and field tests show that the cable fulfills all the initial technical, handling and environmental requirements of a lead free submarine cable.

A factory joint technique have been developed and can be used to facilitate the manufacture of long cable lengths.

AUTHOR'S ABSTRACT

Authors:



Mr Kaj Sjölin was born in Hudiksvall, Sweden 1953. He holds a M.Sc in technical physics. He joined Ericsson Cables Telecom Cables Division in 1987 and is now working with product development of optical cables.



Mr Lennart Lidén was born in Västervik, Sweden 1949. He joined Ericsson Cables Telecom Cables Division in 1991 and he is working with fiber optic installation and splicing technique.



Mr Nils Erik Grip joined Ericsson Cables Telecom Cables Division in 1982. He has been working as a process and production engineer and is at present working with product and process development and with special projects.



Mr Stig Lindohf was born in Stockholm, Sweden 1942. He holds a B.Sc. degree in civil engineering. He joined Telia in 1968 and is now a senior engineer at the Network Services Division and coordinator for submarine cable and offshore installation technology.



Mr Jan Björkman was born in Malmö, Sweden 1943. He has studied mathematics in Stockholm University and Polymer Science at the Royal Institute of Technology in Stockholm and he holds a degree in chemical engineering. He joined Telia in 1977. He is now a senior engineer at the Network Services Division and coordinator for optical fibres and cables.

NEXT GENERATION OF CABLE DESIGNS FOR OPTICALLY AMPLIFIED SYSTEMS

J.Power

C.Rochester

P.Worthington

STC Submarine Systems Limited, Southampton, England.
(A company of Alcatel Submarine Systems)

SUMMARY

Repeatered Submarine cable technology is undergoing a major transition from regenerative to optically amplified systems. The changes in repeater technology require enhanced optical characteristics and upgrades of the electrical performance of cables. These modifications, coupled with advances in materials, have led to the revision of the design of existing cables. Building on extensive previous experiences, the new design of cable uses the most effective optical fibres and packaging materials, optimised copper and steel components and improved electrical insulation materials. The cable has been developed and extensively tested both on land and at sea to demonstrate its suitability for use in depths down to 8km for the new generation of optically amplified systems.

1.0 INTRODUCTION

Long haul fibre optic systems installed in the last ten years have used "3R" type repeaters. The signal is retimed, reshaped and regenerated at each repeater using high speed electronics (up to 2.5 Gbits/s). The regeneration at each repeater means that tight control of the cable dispersion is not required. However, the next generation of systems using optical amplifiers require the dispersion to be more tightly controlled, as the absence of retiming and reshaping means that dispersion effects are additive along the whole length of the system. The changes in repeater technology have also led to revised electrical power requirements of systems such as higher line voltages, lower currents and higher cable resistance.

In order to optimise the cable design for these new requirements, a major design and development project has been undertaken by STC to achieve the best solutions for the next generation of optically amplified cables. The optical fibres with the necessary dispersion characteristics have been selected and the optical package material has been modified to reduce stress-induced birefringence in these fibres. The copper and steel cable elements have been optimised to achieve the higher cable electrical resistance compatible with the new repeater electronics. Considerable effort has been made to select an insulation material which maintains the highest reliability with increased line voltages to be used in future systems.

The chosen optimised cable design is NR cable. An extensive series of manufacturing trials and land and sea based tests have been conducted on NR cables to ensure that it is suitable for use in optically amplified systems in depths of 8km. The results of this testing have demonstrated conclusively that the performance required from the NR range of cables has been achieved.

2.0 REQUIREMENTS

2.1 Optical Requirements

For conventional repeatered systems the principal optical requirement for the cable is low and stable attenuation. Optical dispersion does not need to be tightly controlled as the signal is retimed at each regenerator. For optically amplified systems dispersion becomes a critical factor because of the higher bit rate and the absence of retiming at the repeaters.

Total dispersion is proportional to length and is a combination of chromatic dispersion (variation of propagation speed with wavelength) and polarisation mode dispersion (PMD) caused by the variation in propagation speed of the two orthogonal polarisation modes that are present.

It is necessary to operate close to the zero dispersion wavelength of the fibre to minimise chromatic dispersion. It is also essential to ensure that the polarisation mode dispersion is minimised, particularly for long-haul applications. Some tolerance in chromatic dispersion is permissible as the system can be equalised by inserting compensating fibre at intervals. However, polarisation mode dispersion is a random effect which increases as the square root of the length of the system and cannot be equalised. It must be controlled by careful selection of the fibres and by the design of the cable.

As for conventional systems, optically amplified systems require low and stable fibre attenuation. Ageing mechanisms in the cable need to be accurately quantified and minimised to maintain the system margins for the system design lifetime of 25 years.

2.2 Electrical Requirements

The cable must be capable of providing the required amount of electrical power to all the repeaters. The maximum span length of a system may be up to 10000 km and the nominal repeater spacing is in the range 35 to 100 km. The required electrical power can be achieved by applying a controlled voltage at each end of the system ensuring that a constant electrical current is passed down the cable. Some reduction in the conductor requirements of the cable can be accepted because of the reduced current of optically amplified systems. As the ends of the system can be up to ± 12 kV, the insulation of the cable must be designed to maintain the integrity of the power feed circuit for the 25 year design life of the system at such voltages.

2.3 Mechanical Requirements

In parallel with the optical and electrical developments taking place, developments on the mechanical and physical characteristics of the cable were made to optimise the cable design to best meet the new technological requirements, as well as specific requirements of customers. An extensive technical and marketing design study was carried out and a marketing requirement specification was defined. From this a list of the mechanical and physical requirements of the lightweight cable was compiled. This included the following:

- The cable should provide a robust optical environment compatible with any new optical package and/or fibres. The optical fibres must be protected from the potential optical loss increase due to hydrogen evolution or ingress.
- It should have sufficient tensile strength to be suitable for deployment and recovery in depths of 8km, withstanding radial pressures of up to 83 MPa, without compromising the optical, electrical or mechanical performance of the cable. The cable should be torsionally stable to resist excessive twist when under load.
- The cable should be resistant to abrasion which could be experienced during deployment or recovery or during service on the sea bed. It should resist crush loads and impact energies which could be encountered during storage, deployment, recovery or damage sustained during its service life.
- It should be capable of deployment, recovery and repair using conventional marine vessels and equipment and there should be adequate safety margins on cable performance to ensure safe operation.
- The cable should be suitable for jointing to existing cable designs of various suppliers using established jointing methods. The cable insulation should be suitable for moulding to maintain electrical insulation.
- In the event of damage at sea, water should penetrate by less than 1000m over 14 days.

- Each cable layer should have sufficient adhesion to the other layers to ensure there is adequate load transfer without slippage between the cable elements. The cable should be suitable for armouring for shallow water applications using galvanised steel wires over standard deep water lightweight cable and it should be suitable for burial in sand covered sea beds and for recovery from these areas.
- The cable should ensure a minimum design life of 25 years.

When these mechanical and physical requirements for the next generation optically amplified cable had been defined, a design study was carried out to achieve the optimum cable solution.

3.0 SOLUTIONS

3.1 Optical Solutions

3.1.1 Chromatic Dispersion

The first applications for the next generation of cables are likely to be for 5 Gbit/s operation with an operating wavelength close to 1560 nm. The average zero dispersion wavelength of the dispersion shifted fibre in operation on the sea bed must be controlled to be approximately 1-2 nm higher than the operating wavelength to minimise non-linear effects.

Dispersion is controlled by fibre selection prior to splicing to ensure that all fibres in a cable section have the same nominal dispersion.

A system is subdivided into a number of equalisation blocks (typically 500-1000 km of cable). The dispersion of each block is equalised by insertion of a short section of cable using non dispersion-shifted fibre with a higher dispersion at the operating wavelength. The length of the equalisation section is determined so that the overall dispersion of the block at the sea bed temperature will be close to zero.

3.1.2 Polarisation Mode Dispersion (PMD)

The primary cause of polarisation mode dispersion in single mode fibres is asymmetry in the core of the fibre. This may be geometrical asymmetry (core ovality) or asymmetry in the refractive index profile caused by stress. The effect of the asymmetry is to introduce local birefringence or different velocities of propagation of the two polarisation modes that can be present. The overall PMD is determined by the birefringence and by the coupling that takes place between the polarisation modes. This coupling can be characterised by a coupling length (ie. the average length over which power is transferred from one polarisation mode to the other). For a long length of fibre (ie. much longer than the coupling length) the PMD is given by:

$$\tau_{\text{pmd}} = \tau_b (L L_c)^{1/2}$$

where: τ_b = Birefringence (psec/km)
 L_c = Coupling length
 L = Fibre length

Hence PMD accumulates on a square root of length basis. Control of PMD can be achieved by control of τ_b , control of L_c , or both.

Fibres on shipping bobbins generally have low PMD because of the strong coupling (short coupling length) introduced by the winding. However, the same fibre in cable may show a much higher PMD as the coupling length is increased when the fibre is effectively laid out straight. STC NL cable (which has been in production since 1986) uses a fibre package in which the acrylic coated fibres are laid out straight and embedded in a thermoplastic elastomer. Investigation of PMD of the fibre in the elastomer package showed that the PMD was a result of the intrinsic fibre PMD plus additional birefringence caused by stress in the package. This stress is also the cause of PMD being affected by temperature change. An extensive series of trials was undertaken to investigate these effects and to provide a low PMD cable solution.

The optical package solution for the next generation cable is based on fibres with low intrinsic PMD and cabled with an optimised package.

3.2 Electrical Solutions

The NL cable has an electrical resistance of 0.65 ohm/km. The electrical power conducting requirements for optically amplified NR systems can be met with a cable resistance of 1.0 ohm/km. This is provided by a copper C-section and cladding formed around the package that is in contact with the steel strand wires. The majority of the power passes through the copper but there is a contribution to the conductivity from the strand. The strand wires are insulated from the sea using a layer of linear low density electrical grade polyethylene that will not degrade over the 25 year system life operating at the maximum system voltage of ± 12 kV. Electrical reliability tests have been conducted on the material and a Weibull plot of the performance is shown in figure 1. The characteristic voltage stress is 429 kV/mm compared with the maximum working stress of 2.3 kV/mm.

3.3 Mechanical Solutions

After consideration of the mechanical and physical requirements of the cable, the design solutions chosen were as follows:

- Around the optical package a tube is formed from a strip of copper tape. This tube or 'C-section' provides sufficient internal space for the optical package solution and has a suitable wall thickness to provide radial pressure resistance to depths of 8 km. The use of high conductivity copper as

C-section material allows it to contribute significantly to the power feed conductivity.

- A second copper tube using high conductivity copper is welded closed around the C-section and forms a hydrogen barrier around the optical area. This 'copper cladding' is of suitable size to provide the required electrical resistance of the cable, together with the copper C-section and the steel strand wires, of 1.0 ohm/km.

The welded composite copper tubes combine to form a rigid protective tube around the optical package core with a radial wall thickness of approximately 0.85mm. This provides significant protection from impact and crush loads.

- Two layers of steel wires are applied helically around the copper cladding in opposing directions of lay. The inner layer of larger wires has a left hand lay, the outer, smaller wires have a right hand lay. The wire numbers and sizes were chosen to provide sufficient strength to support the weight of the other cable elements and system components during deployment and recovery in depths down to 8 km, without exceeding the cable Nominal Transient Tensile Strength load ensuring a high survival probability of the optical fibres. The opposing lay directions of the wires results in a torsionally balanced cable design which exhibits minimal twist under load.

In order to best optimise the weight, strength and electrical conductivity of the metallic cable elements, several theoretical design iterations were made to reach the optimum solution.

- A linear low density polyethylene insulating sheath is extruded over the outer strand wires to produce an overall lightweight cable outer diameter of 21.5mm. The material is suitable for providing insulation to ± 12 kV on the power feed conductor and is a high purity submarine cable grade that ensures the maximum electrical stability of the cable over the required 25 year design life.

The sheath wall thickness is sufficient to provide the necessary electrical insulation with allowances for any material that may be removed by abrasion or damage. It also provides additional strength and stiffness to the cable. The linear low density material has a higher abrasion resistance than the non linear low density materials.

The material is suitable for moulding as well as extrusion which is important for the manufacture of joints.

- The water penetration along the cable is minimised by filling any gaps between the optical package, the C-section and the copper cladding with a high viscosity polybutene material resistant to water at high pressure. Gaps between the strand wires are filled with a curable silane terminated polyether material which again resists the flow of water.
- Adhesion between the outer strand wires and the polyethylene insulating sheath is aided by use of an ethyl vinyl acetate adhesive material, a thin layer of which is applied over the outer strand wires prior to the extrusion of the insulating sheath.

These components combine to provide a cable which meets the requirements for the next generation of optically amplified systems. Each cable element has been investigated extensively during the cable design study to ensure that the optimum solution has been achieved.

4.0 CABLE DESIGN SUMMARY

The cable design solution, the NR lightweight cable, is illustrated in figure 2. The performance characteristics of this cable are outlined in table 1.

Table 1 NR LW CABLE CHARACTERISTICS

	Units	
Electrical		
Conductor DC Resistance	ohm/km	1.0
Maximum Operating Voltage	kV	12
Optical		
Attenuation	dB/km	<0.21
Polarisation Mode Dispersion	psec/km ^{1/2}	<0.1
Physical		
Outer Diameter	mm	21.5
Weight in Air	T/km	0.798
Weight in Water	T/km	0.424
Ultimate Tensile Strength	kN	104
Tensile Stiffness	MN	11.6
Hydrodynamic Constant	degknot	53.9
Density	T/m ³	2.20
Hydrostatic Pressure Resistance	MPa	>83
Storage/Handling		
Temperature Range	°C	-40to60
Stowage Factor	m ³ /km	0.46
Minimum Bend Diameter (Storage)	m	1.8

A range of lightweight screened and armoured cables have been designed to provide a full range of next generation cable designs suitable for various applications. These cables use the NR lightweight cable as the core cable with additional layers applied as required.

A new cable-to-cable joint and cable termination have also been designed and optimised to efficiently joint NR cables.

5.0 CABLE TESTING

5.1 Optical Package Testing

5.1.1 Polarisation Mode Dispersion (PMD)

It was decided that the best approach for a low PMD cable was to use a cable process that minimised the external stress on the fibre and to use fibre selected to have low PMD when in a straight, unstressed condition.

A test was devised to measure the "intrinsic" PMD by laying out fibre in straight legs under slight tension (figure 3). PMD was measured using the Jones Matrix method ⁽¹⁾ which has a resolution of 0.005 psec or better or 0.01 psec/km^{1/2} on 250m lengths.

Fibres from several manufacturers were measured in this way. A very wide range of PMD values were obtained. It was found that a particular type of fibre had a consistently low PMD. It was also found that the PMD of fibres laid out straight could be reduced by introducing small amounts of twist in the centre of the straight legs (see figure 4). However, cabling trials using twisted fibre did not produce significantly lower PMD compared to untwisted fibre.

5.1.2 Birefringence

Further investigation was carried out to determine the effect of stress on the fibres and to investigate the sensitivity of different fibres and fibre coatings to applied stress. It was found that radial stress applied to a fibre will cause birefringence and thus PMD. This birefringence is given by ⁽²⁾:

$$\Delta\beta \cong \frac{8Cpk}{\pi d}$$

where: $\Delta\beta$ = Birefringence (radians/m)
 C = 3.44×10^{-11} m²/kg
 k = $2\pi/\lambda$
 d = Fibre diameter
 p = Radial Pressure

The fibres are protected to some extent by the acrylic coatings which attenuate the external stress. Two tests were devised to measure the change in acrylic coating diameter and to measure the birefringence caused by radial stress. Several different manufacturers' fibres were tested with different thicknesses of colour coatings. Generally the thicker the outer acrylic coating the smaller the diameter change and the smaller the observed PMD increase with radial loading. From this it is possible to modify stresses in the package to achieve low PMD. The amount of stress which the fibres could tolerate without inducing PMD was quantified and the optical package was modified accordingly. The optimised NR cable uses fibres with low intrinsic PMD and the manufacturing processes have been optimised to maintain low PMD in the finished product.

5.1.3 Attenuation Stability

The attenuation and ageing characteristics of NL cable using the standard elastomer with acrylic coated fibres has been extensively evaluated since the introduction of the design in 1986. For NR cable, the cabling increment with both dispersion-shifted and non dispersion-shifted fibres is zero and there is a system allowance for ageing effects of <0.001 dB/km in 25 years.

5.2 Land Based Cable Testing

A 10 km length of NR cable has been manufactured for an extensive prototype evaluation programme. The tests conducted cover cable, joints and repeater terminations.

The tests performed included:

Mechanical:	Ultimate Tensile Strength Load/Elongation NTTS, NOTS, Torsion, etc. Crush and Impact Radial Pressure Abrasion
Electrical:	HV Performance - Cable & Mouldings Electrical Resistance
Optical:	Pressure Coefficient Temperature Coefficient Strain Dispersion
Marine Handling:	Handling & Flex Around the Sheave. Bending Fatigue Water Penetration

These tests confirmed the theoretical cable performance characteristics and demonstrated that the cable can be deployed to and recovered from depths of 8km during worst case conditions without compromising its optical, electrical or mechanical performance or its design life of 25 years.

5.3 Deep Water Sea-Trial

A sea-trial has been completed on NR lightweight and lightweight screened cables, joints and terminations in order to complement the extensive series of land based testing carried out. A mini system was deployed, held and recovered in a 4 km water depth (see figure 5) in the Bay of Biscay off the west coast of France using the Cable and Wireless (Marine) Ltd. vessel, the C.S. Mercury. The 20 km system comprised NR lightweight and NR lightweight screened cables and contained four NR joints and one repeater. The system fibres were spliced together into loops for continuous optical loss and

strain monitoring of the entire system from the test end on board the ship. The PMD of the system was measured before deployment and after recovery and showed no change. The system was deployed over the stern using an 18 wheel pair linear cable engine, a stern to bow transfer was completed and after holding for 36 hours the system was recovered over the bow using a 4 metre diameter drum. During the entire operation the optical performance of the system remained stable, the system handled very well with all the ship's equipment, and creered smoothly back into the ship's tanks. On completion of the trial all the joints and terminations and samples of cable were high voltage tested and dissected. There were no electrical failures and no damage was found. Throughout the trial, both in the factory and on board the ship, the cable handled well without any difficulties. The trial clearly demonstrated that the NR product can be deployed and recovered in deep water.

6.0 CONCLUSION

NR cable has been developed as an optimised cable solution for the next generation of optically amplified submarine cable systems. NR has minimised polarisation mode dispersion, maintained low optical loss with zero cabling increment and optimised electrical performance required by the new optical amplifiers. The cable design has been subjected to a comprehensive series of tests, both on land and at sea which have confirmed its suitability for use in depths of 8km with optical amplifiers.

7.0 REFERENCES

- (1): B.L.Heffner
"Automated Measurement of Polarisation Mode Dispersion using Jones Matrix Eigen Analysis"
IEEE Photonics Technology Letters - September 1992
- (2): J.Sakai and T.Kimura
"Birefringence and Polarisation Characteristics of Single Mode Optical Fibres under Elastic Deformations"
IEEE Journal of Quantum Electronics - June 1981

8.0 FIGURES

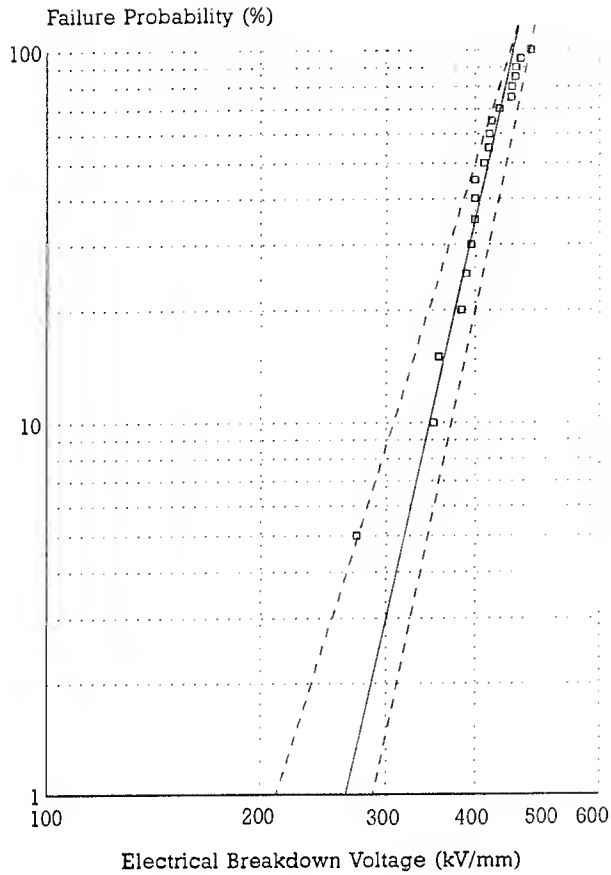


Figure 1 Weibull Plot of Electrical Breakdown Data from Linear Low Density Polyethylene

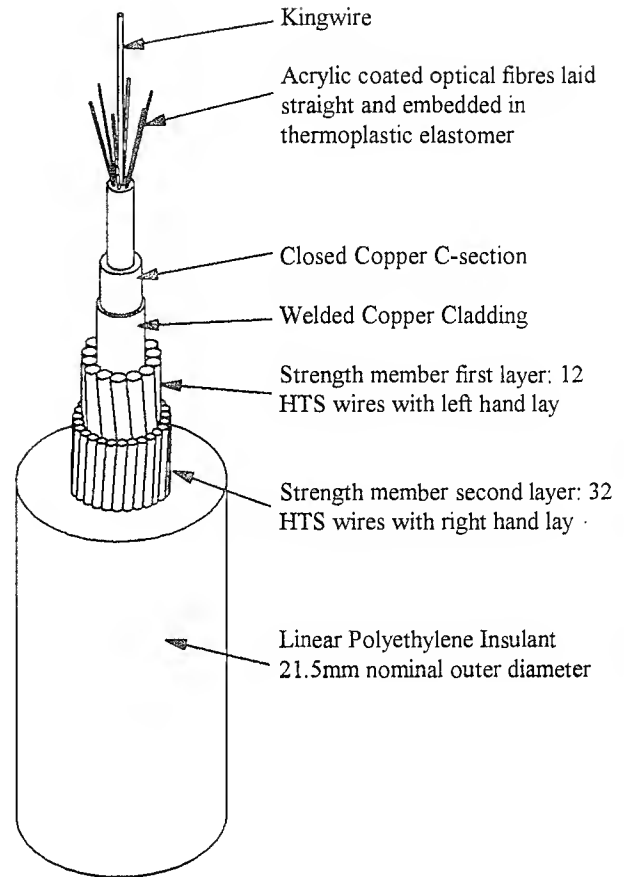


Figure 2 NR Lightweight Cable Diagram

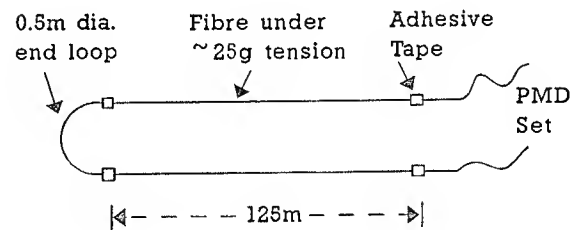


Figure 3 Measurement of "Intrinsic" Fibre PMD

9.0 BIOGRAPHIES

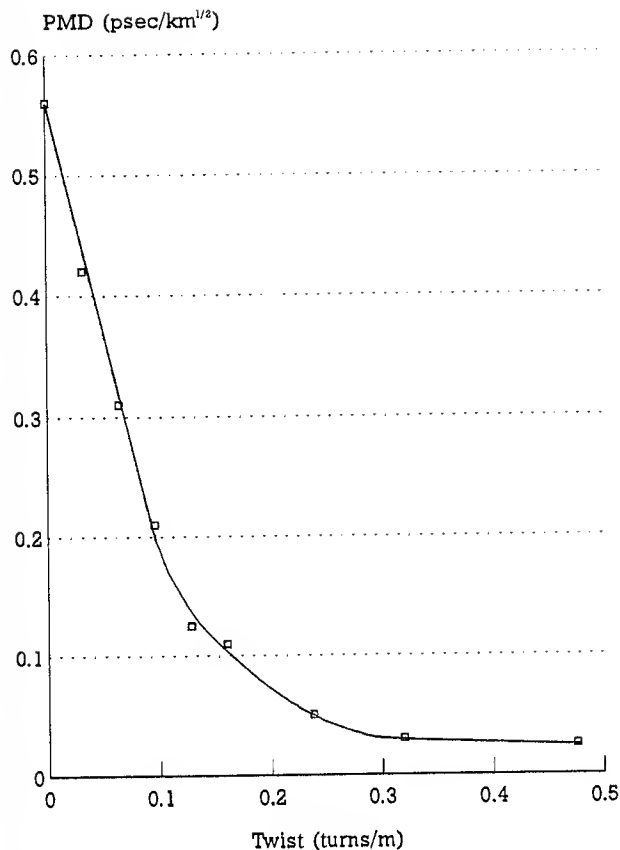


Figure 4 PMD vs. Twist
(fibres of high intrinsic PMD and long coupling lengths twisted in centre of each 125m leg)



James Power
STC Submarine Systems Ltd.
West Bay Road
Western Docks
Southampton
SO15 1DS
U.K.

James Power was born in Wexford, Ireland. He received a BSc(Hons) in Applied Physics from Dublin City University. He joined STC Submarine Systems in Southampton, England in 1991 as a New Product Development Engineer where he has been involved in the development of fibre optic submarine cables and joints.



Chris Rochester
STC Submarine Systems Ltd.
West Bay Road
Western Docks
Southampton
SO15 1DS
U.K.

Chris Rochester is the New Product Development Manager at STC Submarine Systems. He has a BSc in Chemistry and a PhD in Materials Science from the University of Sheffield. Since 1984 he has worked on optical fibres and since 1988 he has been involved in the development of fibre optic cables and joints for STC Submarine Systems.

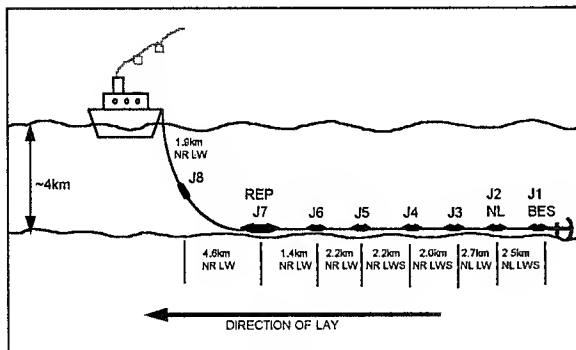


Figure 5 NR Deep Water Sea-Trial Line Diagram



Peter Worthington
STC Submarine Systems Ltd.
West Bay Road
Western Docks
Southampton
SO15 1DS
U.K.

Peter Worthington is a Development Engineer with STC Submarine Systems which he joined in 1974. He received a BSc in Electronics and Electrical Engineering from the University of Birmingham in 1971. Since 1977 he has been involved in the development of fibre optic cables for submarine systems.

Characteristics of Optical Fiber Submarine Cables for Long-haul Submarine Optical Amplifier Systems

Yoshihiro Yoshida, Naoki Norimatsu, Haruo Abe, and Hitoshi Yamamoto

Submarine Cable Systems Department
Kokusai Denshin Denwa Co. Ltd. (KDD)
2-3-2, Nishi-shinjuku, Shinjuku-ku Tokyo 163-03 JAPAN

Abstract

This paper provides a new design concept of optical fiber submarine cable for the long-haul optical amplifier submarine cable systems. Key parameters of the transmission fiber; optical loss, polarization mode dispersion (PMD), chromatic dispersion, and mode field diameter (MFD) are discussed in this paper. Based on the design concept, new dispersion shifted fiber cable called OS-A Cable with the same mechanical cable structure as the OS Cable was newly developed for the optical amplifier submarine cable systems such as TPC-5 Cable Network*. Some statistic data on these key parameters from actually manufactured cables are reported. Finally, this paper shows some environmental test data on optical loss and PMD changes with an ocean simulator and optical loss changes in an actual ocean trial at the ocean depth over 6000 m.

1. Introduction

In order to realize economical long-haul optical submarine cable systems with larger capacity and higher reliability, new optical submarine cable systems concatenated with erbium-doped fiber amplifiers (EDFAs) have been investigated^{[1][2]}. Compared with conventional regenerative optical submarine cable systems, the optical amplifier submarine cable systems have several advantages, such as larger capacity, lower cost and higher reliability. These advantages result from elimination of expensive high-speed electrical circuits for regeneration in the repeaters and from use of DC-operated pump laser diodes and passive optical components, such as erbium doped fibers and optical couplers. The price to pay for the elimination of regeneration in the repeaters is introduction of accumulated degradation along the system due to accumulated amplified spontaneous emission noise (ASE noise), chromatic dispersion, PMD, fiber non-linearity. This degradation mechanism requires a new design concept of transmission optical fibers, which are more sophisticated and different from the one for the conventional regenerative optical submarine cable systems. This paper discusses key parameters of the transmission optical fiber for the applications to long-haul optical amplifier

submarine cable systems; optical loss, PMD, chromatic dispersion, and MFD. We also report some data on these key parameters of the OS-A cable. Finally, this paper shows some environmental test data on optical loss and PMD changes with an ocean simulator and optical loss changes for various MFDs in an actual ocean trial over 6000 m depth.

2. Optical Loss

In the design of conventional optical submarine cable systems, lower optical loss of transmission optical fiber was always considered better since lower optical loss can provide longer repeater spacing^[3]. Therefore, the acceptable maximum optical loss is the principal specification for optical loss requirements. Naturally this parameter is still of great importance for optical amplifier systems. We have made intense efforts to decrease the optical loss of the dispersion-shifted fibers (DSFs) because DSFs inherently have somewhat higher optical loss than pure silica fibers.

In optical amplifier submarine cable systems, however, this is not enough to specify the loss requirements; the loss should reside within a certain range. Optical amplifier systems are designed to have the highest signal level and optical signal-to-noise ratio (SNR) at the operating signal wavelength. The change in span loss affect the system output level profile against wavelength (wavelength window), which may result in the signal level reduction and/or optical SNR degradation. This span-loss-dependence of wavelength window is due to the self-filtering characteristics^[4] of concatenated EDFAs. Unless the deviation of optical loss from the designed value is managed within small range, the wavelength range available for the system operation would be shifted away from the designed one, and the significant degradation of system performance could occur due to optical loss difference from its designed value on average in a total system. Fig. 1 illustrates how the span loss affects the wavelength window in the optical amplifier cable systems. Since the gain characteristic of an EDFA depends on the input power level, the change in span loss causes the change in gain slope of EDFAs. Therefore, to obtain the desired wavelength window as designed, the optical loss should be kept within a certain range.

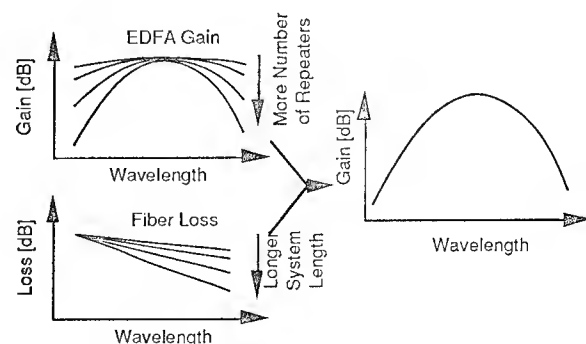


Fig. 1 Wavelength Window in System Concatenated with EDFAs

Fig. 2 shows the histograms on optical loss of DSF units and cables. As the average the optical loss of cables was 0.208 dB a year ago, we have expected that the average optical loss for the newly manufactured cables would be less than this figure a little. The optical loss of the manufactured cables was actually 0.206 dB on the average and was distributed within 0.008 dB without any significant loss increase during the cabling process. This indicates the control of optical loss is tight enough to avoid wavelength window error in the actual systems.

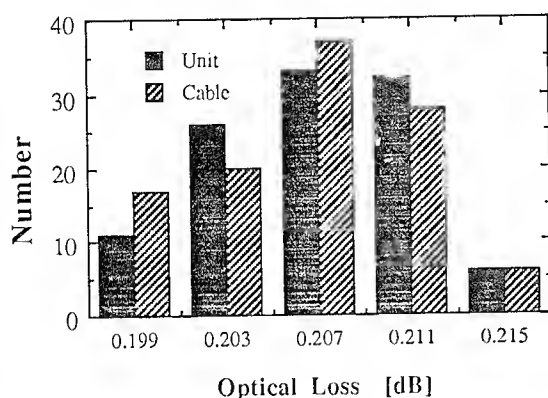


Fig. 2 Histogram of Optical loss of Units/Cables

3. Polarization Mode Dispersion (PMD)

PMD is the group velocity difference between the two orthogonal polarization components in the optical fiber due to fiber birefringence. Therefore, if the transmission fiber has a large PMD, a transmitted optical pulse may split into two pulses or suffer from significant waveform distortion. Fiber PMD is known to increase proportionally to the square root of cable length. In conventional regenerative systems, the possible PMD of concern with today's optical cables would be less than several ps since the regenerative span is less than a few hundred km.

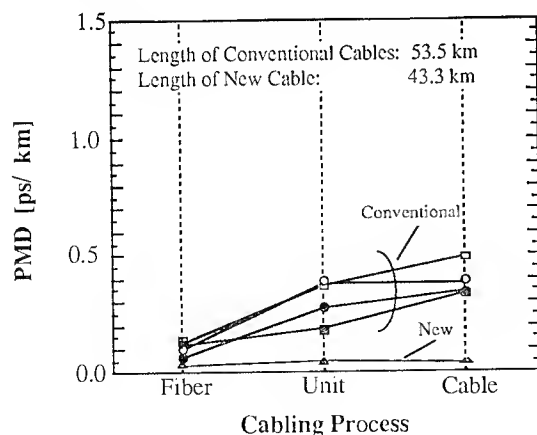


Fig. 3 Change in PMD during Cabling Process in Initial Development Stage

Fig. 3 shows an example of change in PMD during cabling process for the cables in the initial stage of the development^[5]. As the cabling process proceeded in the cables with conventional DSF fibers, the average PMD was approximately 0.5 ps/km for a lightweight cable. Even if such a cable is used for the conventional optical submarine cable systems, the PMD accumulated along a 150 km long repeater span will be just 6.1 ps. Such a value can be negligible for the bit-time-slot of a few hundreds of ps in multi-Gbit/s systems. Therefore, we did not have to pay any attention to it in regenerative cable systems.

In optical amplifier systems, the possible PMD of concern would be a few tens of ps or more since the regenerative span reaches about 10000 km. For example, if a 9000 km long submarine cable system is constructed by such cables, the average PMD accumulates to about 50 ps. Such a larger PMD is no longer negligible for the bit-time-slot in multi-Gbit/s systems and causes significant system performance degradation. Therefore, in optical amplifier submarine cable systems with a capacity over Gbit/s, the PMD must be specified to be as low as possible. Fig. 4 shows the

histograms on the PMD of the OS-A fiber units and cables. The PMD of the cables is almost constant and kept about one-tenth of the conventional DSF cables during and after the cabling process. This remarkable improvement was possible by improving the core non-circularity^[6] in the fiber manufacturing process.

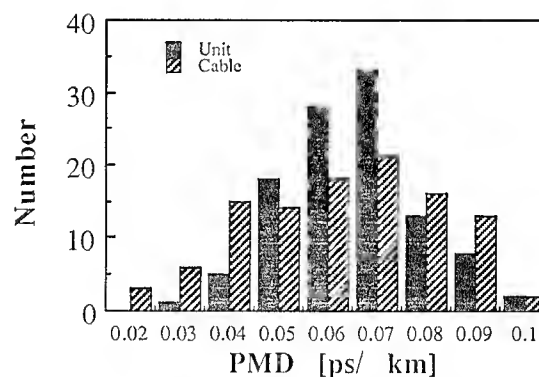


Fig. 4 Histogram of PMD of OS-A Units/Cables

4. Chromatic Dispersion Management

In regenerative systems, the amount of cumulative value in each repeater span was the only issue regarding fiber chromatic dispersion. In optical amplifier systems, as the optical pulses keeping high power are transmitted through multi-thousand km long optical fibers, the effect of fiber non-linearity causes the catastrophic optical pulse distortion. The pulse distortion due to fiber nonlinear effects is strongly affected by the chromatic dispersion characteristics of the transmission fibers. If most of the zero dispersion wavelengths of constituent transmission fibers coincides with the operating signal wavelength, the non-linear phenomenon called "Four-wave mixing" occurs greatly, resulting in significant signal spectrum broadening due to interactions between the signal and ASE noise. If most of the zero

dispersion wavelengths is shorter than the operating signal wavelength, the non-linear phenomena called "Self-phase modulation" and "modulation instability" devastate the transmitted optical signals^[7]. In order to alleviate these effects, most of the zero dispersion wavelengths of the constituent transmission fibers should well exceed the operating signal wavelength. Of course, the total chromatic dispersion should also be small to minimize linear signal wave-form distortion. Thus, the cumulative chromatic dispersion will be compensated by normal dispersion fibers. In long-haul systems, periodical compensation is preferred,

which requires "sawtooth" cumulative dispersion management along the system as shown in Fig. 5^[8]. Therefore, to minimize degradation due to both fiber non-linearity and linear distortions, precise dispersion management of the constituent fibers should be established.

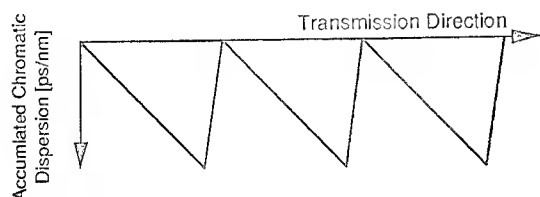


Fig. 5 An Concept of Chromatic Dispersion Management

The average zero dispersion wavelength of the new OS-A cable is 1562 nm whereas that of the conventional OS cable was 1550 nm. By slightly changing the profile of refractive index of the fiber, the average zero dispersion wavelength was shifted to around 1562 nm from 1550 nm. Fig. 6 shows the histogram of chromatic dispersion of the OS-A cable based on our chromatic dispersion management. The distribution profile of zero dispersion wavelength of the DSF cables is Gaussian-like. Most of the zero dispersion wavelengths are beyond the operating signal wavelength of 1558.5 nm within small deviation.

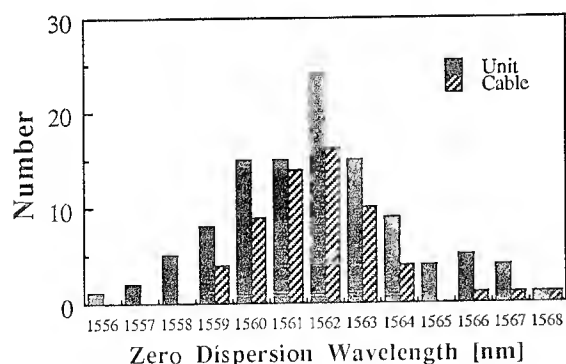


Fig. 6 Histogram of Zero Dispersion Wavelength of OS-A cable

5. Mode Field Diameter (MFD)

So far the smaller MFD has been considered better, unless causing larger splicing loss, since the smaller MFD provides the smaller bending loss. It is, however, no longer true for optical amplifier submarine systems. As was mentioned in Section 4, the DSFs with smaller MFD cause stronger fiber non-linearity because the optical intensity is inversely proportional to the square of MFD. To minimize transmission performance degradation due to the fiber non-linearity, a larger MFD is preferred. In addition, since the degradation due to fiber non-linearity increases with system length, the larger MFD will be required for the longer cable system. For example, a MFD of around $7.8 \mu\text{m}$ in average will be sufficient to realize the optical amplifier cable systems up to 4000 km system length, whereas the MFD over $8 \mu\text{m}$ will be required for the longer cable systems such as a direct link between the mainland of the United States and Japan without any degradation of cable loss characteristics. For such long-haul cable systems, the DSF fibers of larger MFDs than $8 \mu\text{m}$ with smaller fiber bending losses will be used for the OS-A cable. Since the larger MFD tends to cause the larger fiber bending loss which might be a reason of degradation of cable loss characteristics, it is very important to keep the fiber bending loss lower for larger MFDs and to confirm the loss characteristics of the cables accommodating larger MFD fibers under external stresses expected during the cable laying, holding and recovering (refer to Section 6.2).

6. Environmental Tests

6.1 Testing with Ocean Simulator

In order to confirm that the newly designed cables show no degradation under the sea, we measured the change in optical loss and PMD of the cables under the practical environments using an ocean simulator.

6.1.1 Optical Loss Optical loss change was measured with a 200 m long sample cable accommodating four DSF fibers. Fig. 8 shows the environmental test condition profile applied to this measurement. Under this condition, the change in optical loss was less than 0.001 dB/km for 18 hours. The results show that the optical loss of the cables will not increase under the actual ocean environment.

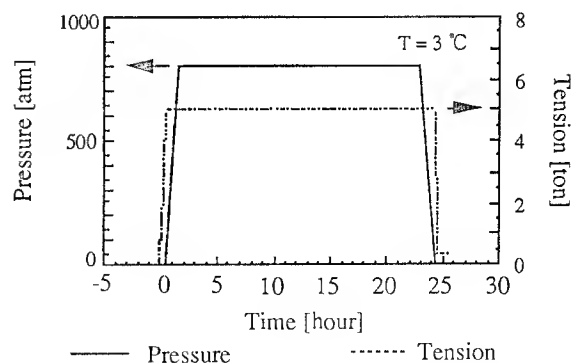
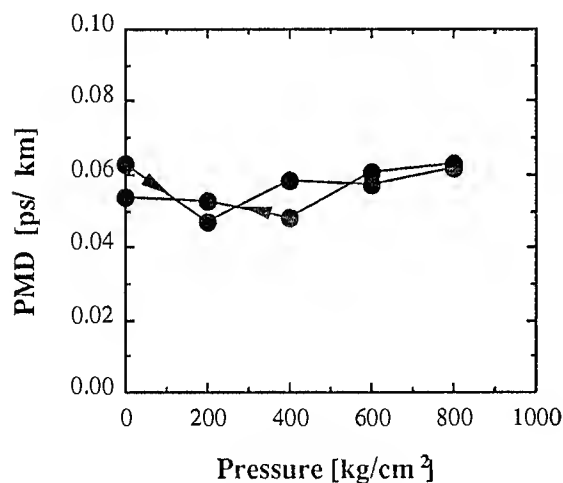


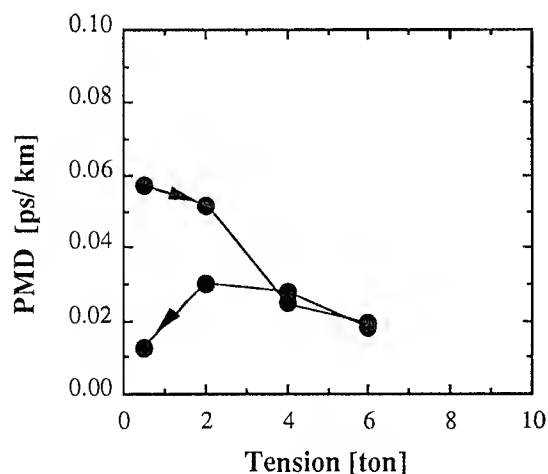
Fig. 8 Environmental Test Condition Profile in Ocean Simulator

6.1.2 PMD The change in PMD of the cable against possible pressure and tension was measured. The cable under test was the same as in the optical loss measurements. The test conditions were the same as in the Fig. 8.

Since the PMD of a 200m long DSF was too small to be measured, we spliced the four DSFs in the cable to make a 800m long DSF. The PMD measurement method adopted was the fixed analyzer method^[9]. Fig. 9 (1) and (2) show the changes in PMD against pressure and tension, respectively. As shown in Fig. 9 (1), no correlation was observed between the PMD and pressure. This is because the structure of the cable is designed to protect the inside fibers against the external stress. The change in PMD due to the applied tension was observed to be -0.04 ps/km and no PMD increase was observed. The change in tension is the severest while the cable is being laid. However, the PMD characteristic will be very stable after the laying since only a small constant residual tension will be exists under the sea. These results provide that the PMD of the cables will not increase and be kept low during construction, and will be quite stable in the sea bottom environment.



(1) Pressure



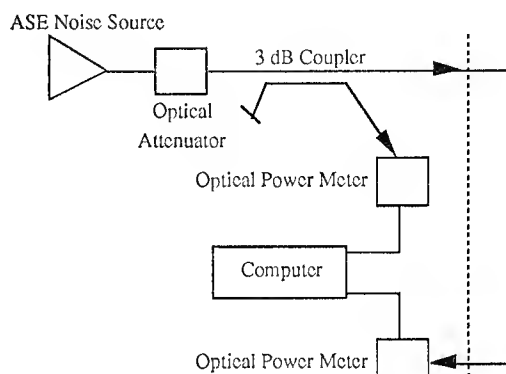
(2) Tension

Fig. 9 Change in PMD of OS-A Cable

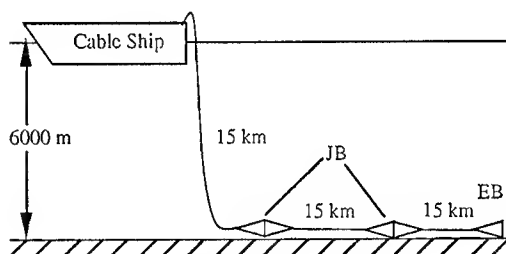
6.2 Deep Sea Trial

We have also conducted a deep sea trial at an ocean depth over 6000 m to evaluate the OS-A cable to confirm the loss stability of fibers of larger MFDs. Fig. 10 (1) and (2) show the test setup and the test cable configuration for the sea trial, respectively. The cable length under test was 45 km accommodating 6 DSF fibers with MFDs of 7.6 to 9.0 μ m.

Two fibers are spliced in the end box to have three sets of 90 km looped fibers. As in Fig. 10 (1), by using a EDF ASE noise source as a light source for the loss measurement, it became possible to monitor the loss changes of 0.001 dB for more than four days.



(1) A Block Diagram of Test Setup



(2) Configuration of Test Cable

Fig. 10 A Block Diagram of Deep Sea Trial

Fig. 11 shows the measured changes in optical transmission loss during cable laying, holding, recovering, and after recovering. The maximum tension applied to the cable was about 3.5 tons during laying, 4 tons during cable holding and 5.5 tons during recovery. The loss change during the laying was -0.1 dB, corresponding to -0.0011 dB/km, which was almost the same as the loss change due to temperature difference between the cable tank and sea bottom calculated by the temperature coefficient obtained in the factory temperature test. The offset loss of about 0.01 dB (0.0001 dB/km) between before the lay and after the recovery was also almost the same as loss change due to the temperature

difference of the cable tank atmosphere before the lay and after the recovery. The results show that the optical transmission loss of the OS-A cable is very stable against the tension and other external stresses for MFDs in the range of 7.6 to 9.0 μm .

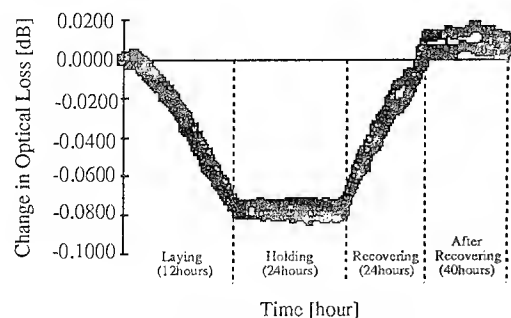


Fig. 11 Optical Loss Change of 90 km Fibers during Deep Sea Trial

7. Conclusions

The new design concept of optical submarine cable for optical amplifier cable systems was discussed. In the long-haul optical amplifier cable systems, the statistical management is required for all fiber parameters because the system performance can be determined by the average values of various parameters; optical loss, PMD, chromatic dispersion, and MFD. Based on this design concept, the OS-A optical submarine cable employing new dispersion-shifted fibers have been developed for the optical amplifier submarine cable systems. Various measurements have shown that the characteristics of the cable are better than required level and the parameters are able to be well-managed for the longer cable systems such as the direct trans-Pacific system, and furthermore they have excellent stability during laying and in the ocean environments.

8. Acknowledgment

The authors would like to thank Dr. Y. Niino, Mr. H. Wakabayashi, Mr. M. Tanaka, Mr. E. Nazuka, Dr. K. Goto, Mr. I. Marugome, Mr. T. Kawazawa, Mr. Y. Kurata, and the other member of KDD Submarine Cable Systems Department for their continued encouragement and valuable support. They also thank Mr. M. Nunokawa and Mr. M. Koike of KDD-SCS for their cooperation. Special thanks should be extended to Dr. S. Akiba, Dr. Y. Namiyama, Dr. S. Yamamoto, Mr. N. Edagawa of the KDD Laboratories for their fruitful discussions, and to members of the AT&T Bell Laboratories for the co-operation in the Joint Development.

They are grateful to Mr. K. Furusawa for his cooperation in the ocean simulator measurements.

Finally, the authors would like to extend their thanks to Furukawa Electric Co. Ltd., Sumitomo Electric Industries Co. Ltd., Fujikura Co. Ltd., and Ocean Cables Co. Ltd. for manufacturing the fibers and cables.

*TPC-5 Cable Network is being constructed by KDD-SCS and AT&T-SSI.

9. Reference

- [1] H. Taga, M. Suzuki, Y. Yoshida, H. Tanaka, S. Yamamoto, and H. Wakabayashi, "Characterization of chromatic dispersion effect on 5 Gbit/s ultra long-distance EDFA transmission using a circulating loop," in Technical digest, Optical Fiber communication Conference (Optical Society of America, San Jose), paper ThK2, 1992.
- [2] N. S. Bergano, C. R. Davidson, G. M. Homsey, D. J. Kalmus, P. R. Trischitta, J. Aspell, D. A. Gray, R. L. Maybach, S. Yamamoto, H. Taga, N. Edagawa, Y. Yoshida, Y. Horiuchi, T. Kawazawa, Y. Namiyama, and S. Akiba, "9000 km, 5 Gbit/s NRZ transmission experiment using 274 erbium-doped fiber-amplifiers," in Technical digest, Optical Amplifiers and Their Applications, Third Topical Meeting (Optical Society of America, Santa Fe), paper PD11, 1992.
- [3] I. Marugome, Y. Noguchi, N. Norimatsu, Y. Yamazaki, and H. Yamamoto, "Design and test result of OS-560M optical submarine cable," in Technical Digest, 2nd International Conference on Optical Fiber Submarine Telecommunications Systems, (Versailles) Paper 14.14, 1993.
- [4] J. P. Blondel, A. Pitel, J. F. Marcereau, and J. Augé, "Self-filtering features in transoceanic links," in Technical Digest, 2nd International Conference on Optical Fiber Submarine Telecommunications Systems, (Versailles) Paper S14.2, 1993.
- [5] Y. Namiyama, T. Kawazawa, and N. Norimatsu, "PMD reduction of optical fiber cables for transoceanic optical amplifier submarine cable systems," 42nd International Wire and Cable Symposium (International Wire and Cable Symposium Inc.), pp. 655-664, 1993.
- [6] Y. Suetsugu, et al., "Polarization mode dispersion in dispersion shifted single mode fiber," in Technical digest, European Conference Optical Communication (Moutroux), We 28, 1993.
- [7] D. Marcuse, "Single-channel operation in very long nonlinear fibers with optical amplifiers at zero dispersion," IEEE Lightwave Technol., vol. LT-9, pp. 356-361, 1991.
- [8] F. W. Kerfoot and S. M. Abbott, "Optical amplifier system technology," in Proc. Technical Digest, 2nd International Conference on Optical Fiber Submarine Telecommunications Systems, (Versailles) Paper 14.7, 1993.
- [9] Y. Namiyama, K. Nakajima, and T. Kawazawa, "Fully automated interferometric PMD measurements for active EDFAs, fiber optic devices and optical fibers," In Proceedings, Symposium on Optical Fiber Measurement (National Institute of Standards and Technology, Boulder) pp. 145, 1992.

BIOGRAPHY



Yoshihiro Yoshida

Submarine Cable
Systems Department

KDD
Tokyo, Japan

Yoshihiro Yoshida received both the B. S. and M. S. degrees in Electrical Engineering from Keio University, Tokyo, Japan, in 1987 and 1989, respectively. In 1989, he joined Kokusai Denshin Denwa (KDD) Meguro Research and Development Laboratories, Tokyo, Japan. He had been engaged in research on optical communication systems using optical amplifiers. From 1992, he has been in the submarine cable systems department at KDD headquarters. He has been engaged in the development of optical amplifier submarine cable systems.



Haruo Abe

Submarine Cable
Systems Department

KDD
Tokyo, Japan

Haruo Abe received his B. S. degree in 1977 and M. S. degree in 1979 in Electrical Engineering from Keio University, Japan. He joined KDD in 1979. He received M. S. degree in 1985 in E. E. (Applied Physics) from University of California (San Diego). He has been engaged in planning, development and engineering of fiber optic cable systems in KDD Head Office since 1984. He is currently a deputy manager of System Engineering Division, Submarine Cable Systems Department, KDD.



Naoki Norimatsu

Submarine Cable
Systems Department

KDD
Tokyo, Japan

Naoki Norimatsu received both the B. S. and M. S. degrees in Electrical Engineering from Kyusyu University, Fukuoka, Japan, in 1983 and 1985, respectively. In 1986, he joined Kokusai Denshin Denwa (KDD) Meguro Research and Development Laboratories, Tokyo, Japan. He was transferred to the submarine cable systems department at KDD headquarters in 1989. He has been engaged in the development and construction of optical fiber submarine cable systems.



Hitoshi Yamamoto

Submarine Cable
Systems Department

KDD
Tokyo, Japan

Hitoshi Yamamoto received the B. S. degree in 1971 and M. S. degree in 1973 in Communication Engineering from Osaka University, Osaka, Japan. He joined Kokusai Denshin Denwa (KDD) Research and Development Laboratories in 1973 and had been engaged in the development of optical fiber submarine cable system since 1977. He was transferred to KDD headquarters in 1983 and has been engaged in the construction of optical submarine cable systems such as TPC-3, TPC-4, and TPC-5 CN.

THE DEVELOPMENT OF A NEW LAND AND BEACH JOINT WITH POTENTIAL UNIVERSAL APPLICATIONS.

J. BISHOP

STC SUBMARINE SYSTEMS LTD.
SOUTHAMPTON, ENGLAND.
(A COMPANY OF ALCATEL SUBMARINE SYSTEMS)

ABSTRACT

A new land and beach joint has been developed for submarine cable systems with the aim of reducing the assembly time, reducing the amount of tooling required, and minimising the cost without compromising the reliability of the joints. This is achieved by using a commercially available joint housing and adding precision made components to suit the specific requirements of a submarine cable system.

An important aspect of the development of any high reliability product is the level of testing required to prove the performance of the product. Testing of the joints to simulate operation under the worst environmental conditions was a key aspect of the development programme. This paper covers the development of the joint from the initial design requirements, the testing programme, and demonstrates the flexibility of the joint by detailing the variants that have been incorporated to date, with specific reference to a joint that has been developed to enable two land cables to be independently connected to the same sea cable, the 'Beach Splitter Joint'.

1.0 INTRODUCTION

On submarine cable systems the submerged plant is connected to the transmission equipment, in the terminal building via several short lengths of land cable, which can either be directly buried or run through ducts. As the distance between the sea cable landing and the terminal can be tens of kilometres, there is a requirement to joint land cables as well as a transition joint (beach joint) between land and sea cable. Both land and beach joints must be assembled and installed quickly to avoid delay to the sea cable installation programme. Once installed, the sea cable deployment can be monitored from the terminal building. The joints often have to be installed under climatic extremes.

Thus, essential requirements for land and beach joints are ease of assembly, with minimal tooling and a low cost. However, this must not be achieved by compromising the reliability of the system over the predicted 25 year life. A new land and beach joint has been developed to meet these requirements, which is compatible with a large range of cables, for use on both powered and unpowered systems.

Simple modifications have been introduced to enable a power filter to be connected. Extra components such as Fibre Optic Couplers can also be incorporated, demonstrating the versatility of the joint design.

The need for reliability has resulted in an extensive testing programme to simulate the performance of the joint in the harshest of environments.

2.0 DESIGN REQUIREMENTS

Land and Beach Joints are usually installed either in a manhole on the cable route or by direct burial of the joint. A joint must be flexible enough to accommodate either option with the minimum of modification

The requirement for minimal tooling is a key requirement, as the joints can be installed anywhere in the world. Moving large amounts of specialist tooling around the globe is expensive, and any damages to the tooling that occur during transport cause extensive delays while replacements are being awaited. This requirement was central to the development of the joint.

The cost has been kept low by using a joint kit which is extensively used in the land cable industry, and customising it with a number of precision components.

On many submarine cable contracts, a requirement is to use locally sourced land cable. Consequently the joint design must be compatible with a whole range of land cables. The joint was specifically designed to be compatible with a virtually limitless range of fibre optic cable designs.

As the joints are an integral part of a submarine cable system, the level of reliability must be the same as for the submerged plant. Extensive testing under simulated environmental extremes ensures the joint is fit for purpose. Furthermore, as the installation sites are on or near coastlines, there is a tendency for the sites to regularly flood, and thus the water resistance properties need to be extensively examined. The testing programme was designed to determine the joint's ability to function for 25 years; a standard requirement in submarine cable systems.

3.0 BEACH JOINT DESIGN

Both the land and beach joints are based on the same commercially available housing. An additional feature of the beach joint is that insulated power wires can be taken out of the joint for connection to an external power filter, to minimise the effect of surge currents caused by lightning strikes in the vicinity of the terminal building.

At the centre of the joint is a commercially available, 12 fibre splice and fibre storage tray. The tray is secured to a central chassis plate, which includes studding to secure the cable clamps. The zinc coated cable clamps are fixed onto the chassis plate and secure strand wires, or central strength members of prepared cable ends. The clamps have a second purpose in that they are used for connection to the power supply. In a simple land joint on a powered system, the clamps are used to provide electrical continuity across the joint from one land cable to the other. In a beach joint where the power supply is to be filtered, a polyethylene insulated power cable is connected to each clamp, and taken outside the joint for connection to the filter.

Glanding of the cables is effected by drilling suitable holes in specifically selected end plates (or bulkheads) and using a combination of rubber tapes and resin to make a watertight seal around the cables and wires to the power filter.

Desiccant sachets are stored on the chassis plate, and the centre of the joint is then protected by an air tight inner PVC shell. A tough, stainless steel outer shell is used over the inner shell and creates a good seal around the end plates. Finally, the gap between the inner and outer shells is filled with a re-entenable resin to provide a durable seal, and to fill the interstices between the two shells. Figure 1 gives a 3 dimensional representation of a typical beach joint.

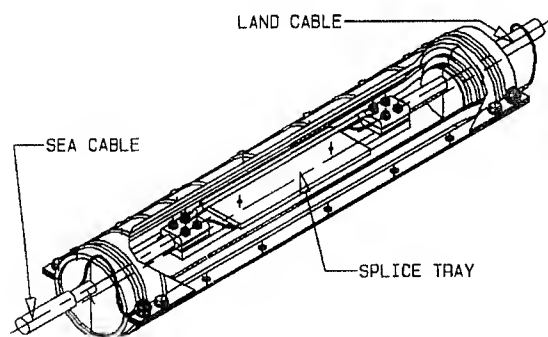


FIGURE 1 - Typical Beach Joint

4.0 TESTING PROGRAMME

The testing programme was established to evaluate the performance of the joint in three distinct areas. The testing philosophy was to subject a single sample to a range of tests. In some instances, individual tests have been carried out on a number of joints to give added confidence of the performance of the joint.

4.1 Mechanical and Environmental Tests

This range of tests were carried out to ensure that the joint performs to the expected standard when exposed to the extremes of conditions that may be encountered during installation or when in service. These tests were carried out on several joints, but always at least one fully optical conforming joint was subjected to each test.

4.1.1 Tensile Test

A full, optically conforming joint sample had a 10 kN load applied for 30 minutes. Optical monitoring was carried out throughout the test. No transient or residual losses greater than 0.03 dB (equivalent to 0.005 dB per fibre path) were recorded.

4.1.2 Torsion Test

A twist of 1 turn in 10 metres was applied to the sample and held for 10 minutes. The same degree of twist was applied in the other direction and held for 10 minutes. Optical monitoring was carried out throughout the test. No transient or residual losses greater than 0.03 dB (0.005 dB per fibre path) were recorded.

4.1.3 Temperature Cycling

The sample joint was placed inside an environmental chamber, with the test ends outside, and was subjected to 3 cycles of -20°C to $+60^{\circ}\text{C}$ with a 24 hour dwell at each temperature extreme. Small remote temperature and humidity dataloggers were placed inside the joint housing to monitor any changes in Relative Humidity (%RH) inside the joint during the test. Optical monitoring was carried out throughout. The monitored path showed a residual optical loss of 0.01 dB. The maximum % RH variation during the cycle was 5%.

4.1.4 Vibration Testing

A joint sample was placed on a vibrating test bed, and was subjected to a forced vibration of 10 Hz with a displacement of 0.7 mm for a period of 336 hours (14 days). The optical signal was measured before and after the test. There was no failure of the cable or clamping arrangements. The variance in optical signal between the start and finish of the test was typically 0.03 dB, although one fibre path recorded a change of 0.08 dB;— still less than the specified requirement of 0.1 dB per fibre path.

4.1.5 Flexural Test

With the joint secured, the cable was flexed through 30° around a radius of 300 mm, and repeated 50 times for each cable. The joint was examined for damage to the cable entry points. No damage was found.

4.1.6 Impact Test

A conical steel weight of 1 kg mass and with a 3 mm tip radius was dropped onto the joint sample from a height of 1 metre. The test was repeated at 90° intervals around the circumference of the joint. On completion of the impact tests, the joint was examined for any sign of cracking on the surface. None were found.

4.1.7 Water Ingress

The joint was immersed in 6 metres of water for a period of 336 hours (14 days). On completion of this test, the joint was examined for water ingress. There were no visible signs of water or moisture ingress. On subsequent dissection of the joint, the dataloggers were removed and the humidity and temperature data analysed. The dataloggers showed no signs of an increased level of humidity.

4.1.8 Dissection

On completion of the above tests, each joint was dissected paying particular attention to any water penetration or other factors which may influence the performance of the joint. In all of the joints dissected, no inconsistencies were found.

4.2 High Voltage Tests

4.2.1 High Voltage Ageing

In all powered systems the high voltage performance is of paramount importance. To fully ensure that the joint is capable of withstanding the service voltages for a period of 25 years, a range of joints are required to be tested.

It is common practice to use a 100 kV qualification test for a duration of 216 hours. This test is based on the Inverse Power Law, which is used to determine a test capable of simulating electrical ageing over 25 years at system voltages (10 kV):

$$tV^n = \text{constant} \dots \dots \dots (1)$$

(where t= time ; V= voltage and n = a constant)

The constant, n has traditionally been taken as 3 for submarine cable mouldings, which has been found to be pessimistic^①. Because these land and beach joints have air as the primary insulant, it is not feasible to test at 100 kV. Partial Discharge Characterisation methods were used to determine when damaging discharges began to initiate, and the test voltage was fixed below this level. It was found that new discharges

became significant above 45 kV, and so the test level was set at 40 kV.

The Inverse Power Law was used to predict the time at 40 kV which is equivalent to 25 years at 10 kV (using n = 3). The equivalent test found to be 40 kV for 141 days (3384 hours).

Three beach joints with filter connections and two land joints were subjected to this long term ageing test. All successfully completed the test without breakdown.

4.2.2 HV after High Humidity Assembly

The joints often have to be installed in warm, tropical climates, and thus there was a requirement to ensure that the presence of humidity inside the joint did not adversely affect the HV performance. A test was established which involved assembly of the joint at 30° C and at 70 % RH, followed by testing of the electrical characteristics (1000 Volt Insulation Resistance (IR) and Earth Leakage current at temperatures above and below the dew point of any moisture trapped inside the joint. This test did not show any significant changes in the IR or Earth Leakage at voltages up to 40 kV.

4.3 Assembly Tests.

All variants of the joint need to undergo an Assembly Trial with optical monitoring to ensure that the Assembly Specifications and list of components are valid for the joint design. The trial also demonstrates that following the documentation, correct assembly of the joint results in a joint with good optical performance. If a joint variant is to be introduced, this test is used to prove the performance of the joint, and is used as a final test of the joint design.

5.0 JOINT VARIANTS

5.1 Variants to the Basic Design

Since the introduction of the basic joint design, the design has been extended to incorporate a large range of cables. The cables that have been accommodated to date are given in Table 1.

Possibilities for further extending the range are great. This is made possible by the glanding arrangement for the cable at the end plates. Each bulkhead is individually drilled at the installation site depending on the cable diameter. To accept a different cable, the only change to the design required is a modification to the internal clamping arrangement. There are currently two types of clamp used for this joint. One is for cables with a central package (sea cables) and secures the strand wires and a heatshrink to keep the package in place. (See FIGURE 2).

CABLE TYPE	CABLE DIA (mm) .	No. OF FIBRES
Sea Cable (powered)	26.2*	4,6,8,12
Sea Cable (unpowered)	14.5*	4,6,8,12
Sea Cable (unpowered)	14.5*	24
Sea Cable (powered)	22.5*	4
Land Cable (powered)	20.0*	4,6,8,12
Land Cable (unpowered)	10.8	12
Land Cable (unpowered)	13.1	12
Land Cable (unpowered)	15.0	12
Land Cable (Unpowered)	15.0	12
Ruggedised Tails (unpowered)	15.0	24

* Single and Double Armoured variants of these cables have also been used.

NOTE: The powered variants have also been used in beach joints on unpowered systems.

TABLE 1 - CABLES USED IN NEW BEACH JOINT

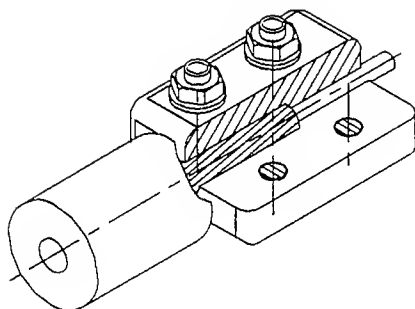


FIGURE 2 Typical Sea Cable Clamp

The other clamp design is primarily for use on land cables with a central strength member, anchoring the strength member in the clamp, while the fibres are routed out of the clamp. A typical clamp is shown in FIGURE 3.

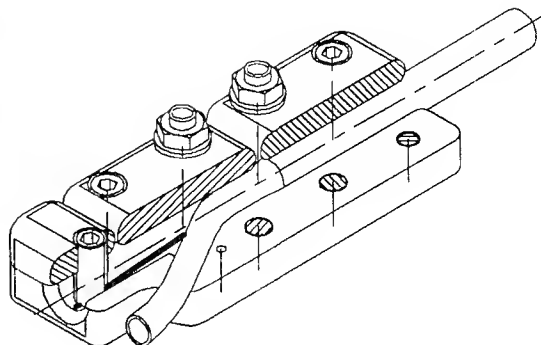


FIGURE 3 Typical Land Cable Clamp

Using this arrangement, a change in the cable diameter can be simply accommodated by altering the bore of the clamp.

5.2 24 Fibre Variant

A 24 fibre beach joint has been designed to splice two 24 fibre cables inside the joint for use on unpowered systems. This was carried out by the addition of an extra splice tray, which can easily be accommodated inside the joint

5.3 Beach Splitter Variant

The versatility of the joint design is best illustrated by Splitter Joint (See FIGURE 4). The splitter joint enables two land cables to be simultaneously connected to one sea cable. At the heart of the joint are four fibre optic couplers (one for each cable fibre). Three dispersion shifted fibres are used in each coupler; for splicing to each fibre in the two land cables and one sea cable. The coupler storage trays are modified splice trays, and each tray accommodates two couplers. Each splice tray is stowed vertically on either side of the central chassis plate.

A splice tray is fixed to the outside of each coupler tray, which is used to store the splices from the three cables to the four couplers. For four fibre land and sea cables, a total of twelve splices are required. See FIGURE 4.

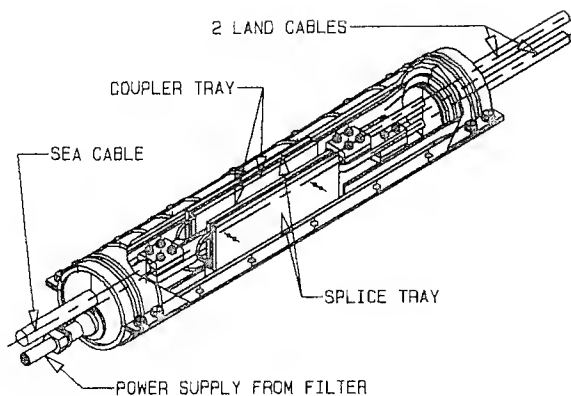


FIGURE 4 The Beach Splitter Joint

Prepared cables are secured into zinc plated steel split clamps. The clamps have 3 sections, a bell mouth to route the fibres, a section to clamp the fibre package, and a section to clamp the cable strand wires. The clamps also have a connection point to provide an electrical connection between the cable core and the wires to the power Filter. Where both land cables enter the joint, the clamps are in a staggered arrangement and on opposite sides of the central chassis plate. This arrangement provides suitable insulation to enable the two land cables to be powered independently, without any danger of current leakage from one cable to the other.

The power supply path is along the cable cores as far as the cable clamps. A polyethylene insulated conductor cable is secured into each cable clamp. The conductor cable is rated to 40 kV. The 3 conductors are then individually glanded at the joint end plate to prevent water ingress, and routed out of the joint. The conductors are fed into the remote Power Filter Unit via a length of conduit, secured onto the joint housing by a combination of a precision made flange and conduit connectors to make a waterproof seal. Using this arrangement, a switch in the Power Filter unit is used to switch power supply to the sea cable from one land route to the other

The final stages of the assembly of the joint is identical to the standard beach joint.

6.0 CONCLUSIONS

A new beach and land joint has been developed which can be rapidly assembled in the field, using a limited amount of tooling. The design has already proven to be versatile; and the joint is potentially compatible with a vast range of different land and sea cables.

A significant amount of testing has been carried out on the basic land and beach joint design and variants developed to date. The testing has demonstrated that the joints are extremely reliable under the type of conditions experienced during the service life of the joints. The success of the joint during the test programmes demonstrate the joint can be successfully installed and operated in the harshest of environments.

REFERENCES

- ① J. Bishop & A.E Davies 'The Application of Electric Stress Analysis and Breakdown Statistics to Inspection Criteria for Submarine Cable Systems',
Proc. 41st IWCS 1992.pp 356-61

Jim Bishop was born in London, England in 1965. After graduating in Chemistry with Polymer Science from Lancaster University in 1989, he had a brief spell as a Research Chemist, before joining STC Submarine Systems in 1990 to work on the High Voltage performance of cable systems. In 1993 he moved into the area of Project and Applications Engineering concentrating on various contract specific engineering projects.

EXPERIMENTAL INVESTIGATION OF THE MICROBENDING BEHAVIOR OF FIBER OPTICAL RIBBONS

Clemens Unger, Waldemar Stöcklein, Siegfried Unterberger, Walter Pfandl

SIEMENS AG, ÖN NK E K, Austr. 101, D-96465 Neustadt, Germany

Abstract

The microbending behavior of fiber optical ribbons with different designs was investigated with several test methods. It could be confirmed that the most important parameter is the microbending sensitivity of the single-mode fiber. A small loss increase due to microbendings can be achieved by selecting fibers with a low MAC-value and a coating of the fiber and ribbon as thick as possible with proper material combinations.

Introduction

To install future optical subscriber networks high fiber density cables are necessary. Based on the requirements of mass splicing and automatic measurement a construction is preferred in which fibers are fixed in a ribbon configuration. An important problem is the susceptibility of these cable designs to microbendings which can be improved by an optimization of the ribbon properties. Test methods to characterize the microbending sensitivity of these ribbons are essentially.

Typically used sandpaper or crush tests suffer from various disadvantages. As yet the influence of the bare fiber properties on the ribbon performance has not been analysed in detail.

We have investigated the microbending sensitivity of fiber optical ribbons with several methods: crush, winding, expandable drum, crepe paper and modified crepe paper test, temperature cycling and water immersion.

The properties of various ribbon designs with 4, 8, 12 and 16 fibers, with one or two coating layers and different combinations of materials were compared by the use of the above mentioned tests. The additional losses are very small for ribbons with a high thickness. 16 fiber ribbons with a reduced outer diameter of the fibers and minimized thickness of the ribbon are most microbending sensitive.

Experimental

General description

Several techniques can be used to organize the fibers in a parallel arrangement, called ribbon. We choose an encapsulated design (Fig. 1), which leads to a satisfactory planarity of the ribbon and a precise alignment of the fibers. Each fiber has its own UV-color to get an easy identification of each fiber. The ribbon consists of one or two coating layers to optimize the protection properties.

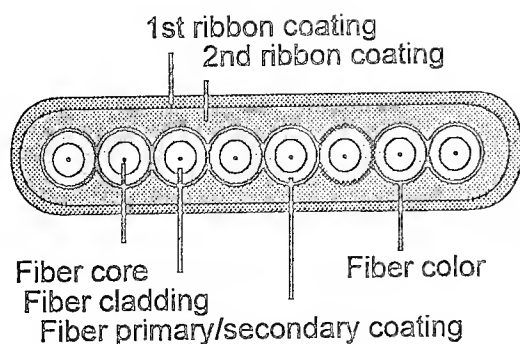


Fig. 1: Encapsulated ribbon design

Characterization of fibers and ribbons

We investigated different fibers listed in Table 1. The typical dimensions of the different ribbon types are indicated in Table 2.

Fiber type	Fiber Outer Diameter	Number of fibers in the ribbon
A	245 μm	2, 4, 8, 12
B	245 μm	2, 4, 8, 12
C	180 μm	16
E	200 μm	16
F	200 μm	16

Table 1 : Properties of investigated fibers

	a	b	c	d	e
I	4	245	1	340	1 070
II	4	245	2	390	1 100
III	12	245	1	300	3 000
IV	16	200	1	240	3 250
V	16	180	1	220	2 940
VI	16	180	2	250	3 200

Table 2 : Properties of investigated ribbons

- a) Number of fibers
- b) Fiber Diameter / μm
- c) Number of layers
- d) Thickness / μm
- e) Width / μm

Due to the reduction of the fiber diameter from the nominal value of 245 μm to 180 μm the 16 f. ribbon and the 12 f. ribbon have the same width. Thus, in comparison to 12 f. ribbons, the packing of ten 16 f. ribbons in a matrix configuration leads to an increase of 40 fibers per stack in an U-groove and 1000 fibers more in a cable. ¹

Micro- and macrobending

Due to the extreme fiber density in U-groove cables the bending properties, i.e., the susceptibility against micro- as well as macrobending, have to be investigated in detail. The different loss mechanisms lead to spectral attenuation curves shown in Fig. 2. Macrobending (in dB) can be identified by a relatively strong ascent of loss, whereas the typical behavior of microbending (in dB / km) is the gradual attenuation increase at shorter wavelengths.

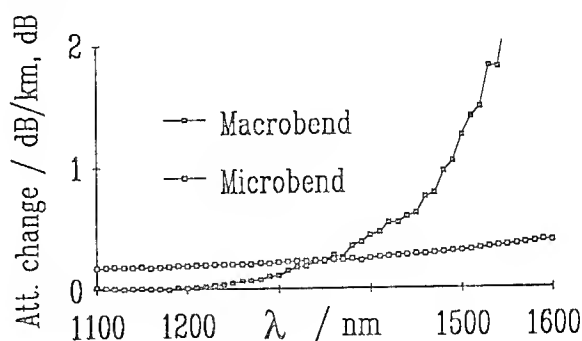


Fig. 2: Spectral change of attenuation of a ribbon due to macro- and microbending

The macrobending sensitivity of a ribbon is only determined by the bending radius and corresponds hence to the sensibility of the pure fiber which is well documented and understood. Serious difficulties arise from the practical determination and experimental simulation of the irregular curvature of a fiber in a cable and the characterization of its sensitivity to microbendings

which depends on the fiber refractive index profile, coating as well as ribbon coating and design.

In this paper, we report on systematic experiments with several tests to simulate the realistic conditions in real cables. Owing to the higher losses and a corresponding signal-to-noise ratio at longer wavelengths the examinations were performed only at 1550 nm.

Crush test

The crush test describes the lateral pressure characteristics of a ribbon (length 100 mm, Fig. 3). In this short length test a high linear pressure has to be applied to get a measurable loss increase. High quality ribbons should display no attenuation change at forces up to 1000 N.

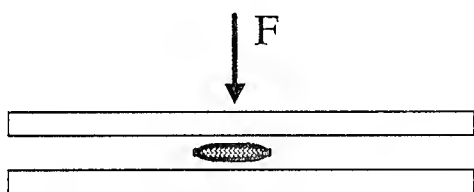


Fig. 3: Experimental set-up of the crush test

We investigated two 12 F. ribbons with a gap between fiber 5 and 6. This gap was caused by the use of fibers with an outer diameter much smaller than the nominal value of 245 μm (Fig. 4).

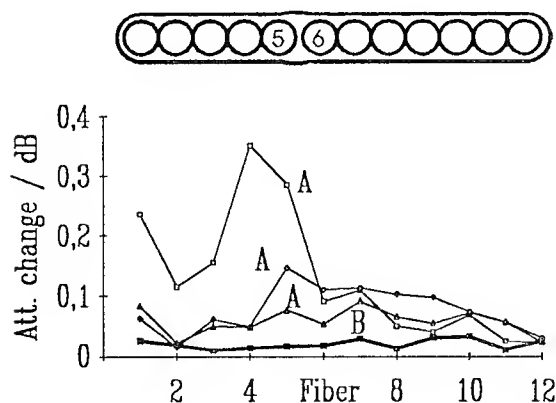


Fig. 4: Attenuation change during crush test of 12 f. ribbons (type III) with different fiber coatings (A, B)

We observed a strong influence of the fiber coating. However the results of 3 new samples with fibers of type A have a large scatter at forces of 16 000 N. The ribbon with fibers of type B showed almost no loss increase within a measurement uncertainty of 0.03 dB at 1550 nm at this extreme load of 16 000 N.

Due to the high load which is absolutely not realistic with regard to the application in cables and the poor repeatability the crush test can not be recommended.

Winding test

Experiments with a long ribbon length (several meters up to 1 km) result in a significant and reproducible excess loss at lower compression forces. The winding test (length 1 km, tension 100 cN) could be done as a routinely made manufacturing control to affirm the ribbon quality (fiber alignment, planarity, Fig. 5).

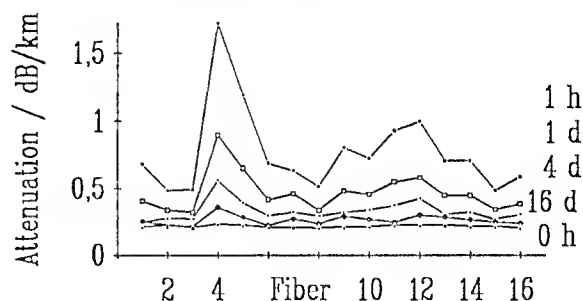
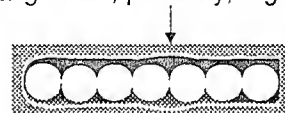


Fig. 5: Attenuation after winding of a 16 f. ribbon (type V) with imperfections

A significant drawback of this procedure is the effect, that the excess loss generally decreases with time (Fig. 5). The origin of this phenomenon (Fig. 6) could be a relaxation of mechanical stresses in the ribbon coating, but is not fully understood up to now.

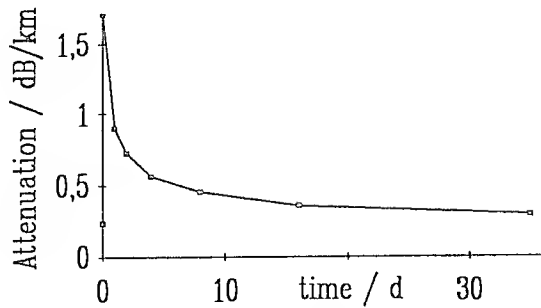


Fig. 6: Attenuation of fiber 4 of the 16 f. ribbon in Fig. 5 (at 23°C) as a function of time

Rewinding the ribbon on a shipping spool leads to an additional loss which decreases with different rates in dependence on the temperature (Fig. 7). On low temperature: low rate, on high temperature: high rate. The measurements in Fig. 7 were made at almost the same time intervals. After stress relaxation at room temperature or accelerated relaxation due to heating up to 60°C (near the glass transition temperature of the coating materials) the attenuation does not increase at -40°C.

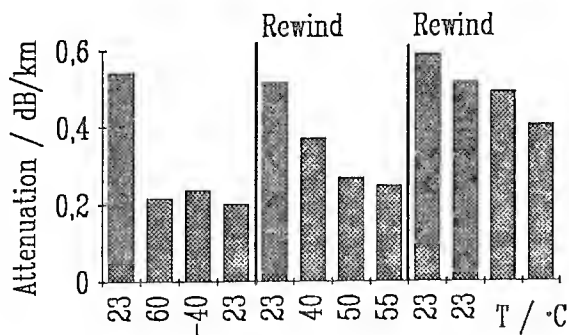


Fig. 7: Attenuation after winding and heating of a 16 f. ribbon (type V) with imperfections

Due to the uncertainty of the relaxation phenomenon and an unpredictable winding process (especially at the reversal points) we observed a large scatter of the attenuation values as a function of the MAC-value (mode-field diameter / effective cut-off wavelength, Fig. 8).

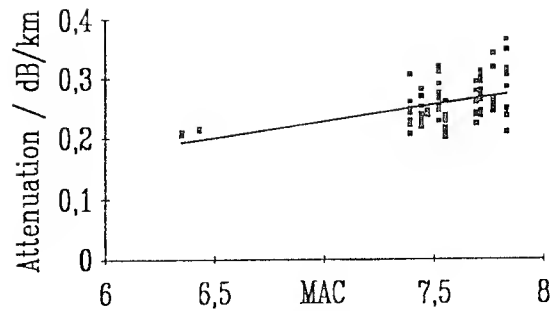


Fig. 8: Attenuation after winding of 16 f. ribbons (type V) on a shipping spool

Expandable drum test

According to an IEC recommendation of fibers the microbending sensitivity of ribbons was measured with an expandable drum (Fig. 9). The structure of sandpaper is expected to be much rougher than the inner surface of a cable. Consequently we used a polished aluminium drum (roughness 2 μm) without sandpaper and the ribbon coating itself is the source of microbends.

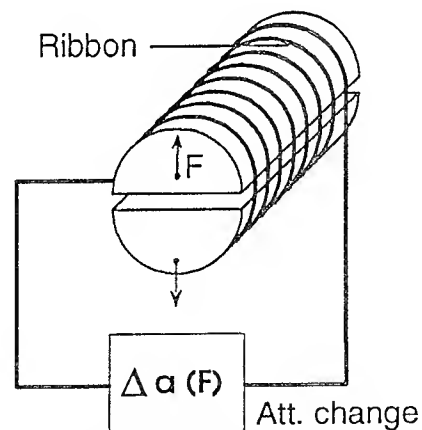


Fig. 9: Experimental set-up of expandable drum ($R = 0.11\text{m}$, Width = 0.3 m)

Typically 50 m ribbon were wound on the drum with zero tension, in a single layer and no crossovers. During expanding the drum the change of attenuation as a function of the pulling force F_{pull} was recorded (Fig. 10).

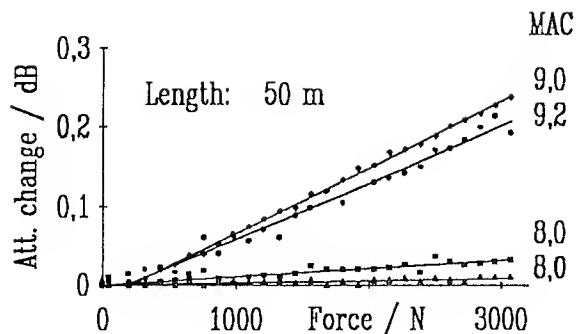


Fig. 10: Attenuation change of 4 fibers of a 12 f. ribbon (type III) during expanding of the drum

Because of the linear relationship of loss and F_{pull} the microbending sensitivity of ribbons can be characterized by the slope of this attenuation increase with pulling force. This outcome corresponds to the theoretical and experimental results 3, 5 of a linear increase of the fiber loss with increasing pressure.

The slope of the excess loss (normalized to the test length) as a function of F_{pull} (in dB/Nm) is shown in Fig. 11 for 4 different 4 f. ribbons in dependence of the MAC-value (= mode-field diameter at 1550 nm / effective cut-off wavelength).

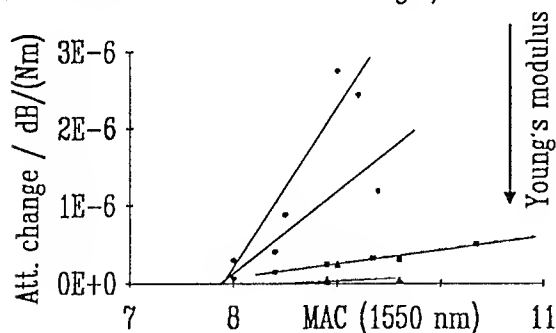


Fig. 11: Attenuation change during expandable drum test of four 4 f. ribbons (type II)

The experimental points are the average of at least 3 measurements.

It can be stated that fibers with a small MAC-value and ribbons with a low Young's modulus exhibited the best microbending performance.

The expandable drum test can also be used to detect the planarity of ribbons (Fig. 12). The ribbon with fibers of type A again shows a higher attenuation increase compared to those with B fibers.

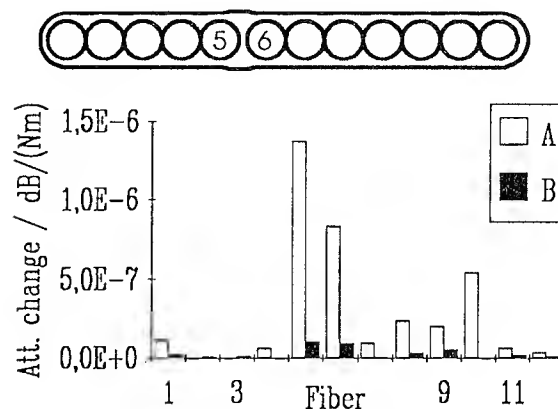


Fig. 12: Attenuation change of a 12 f. ribbon (type III) during expandable drum test

Consequently, the microbending behavior of cabled ribbons can be simulated with the expandable drum test.

Crepe paper test

We also investigated a short length (3 m) test, where a crepe paper (instead of the frequently used sandpaper) is applied to produce micro-deformations of the fiber axis (Fig. 13). Crepe paper is often used a swelling tape in cables and thus the curvature distribution of the microbends of the test is identical to that of a real cable.

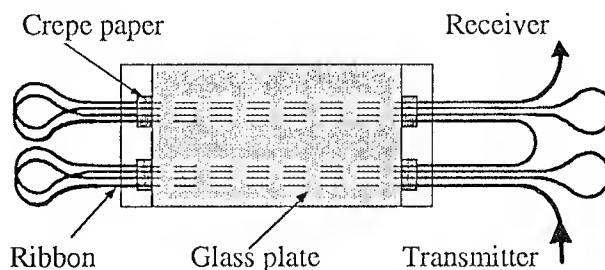


Fig. 13: Experimental set-up of crepe paper test

Under this circumstances no fiber break was observed and the repeatability of the test was within 10 %. Spectral scan measurements are made with the crepe paper pressed against the horizontal ribbon by different loads (Fig. 14).

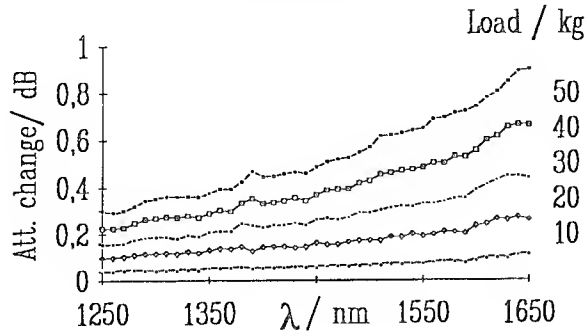


Fig. 14: Spectral change of attenuation of one fiber of a 16 f. ribbon in a ribbon during crepe paper test

The spectral curves exhibit the typical behavior of microbendings. An almost linear increase of attenuation change at a certain wavelength as a function of the weight was observed.

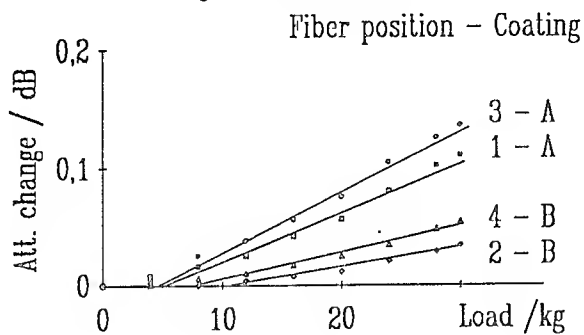


Fig. 15: Attenuation change during crepe paper test of a 4 f. ribbon with different fiber coatings

As well as for the expandable drum test, the microbending sensitivity of ribbons can hence be characterized by the slope of this increase.

The microbending performance of 4 f. ribbons, which are made of fiber coating A and B and different ribbon coating materials and layers (type I and II) was investigated by the crepe paper test (Fig. 15 and 16).

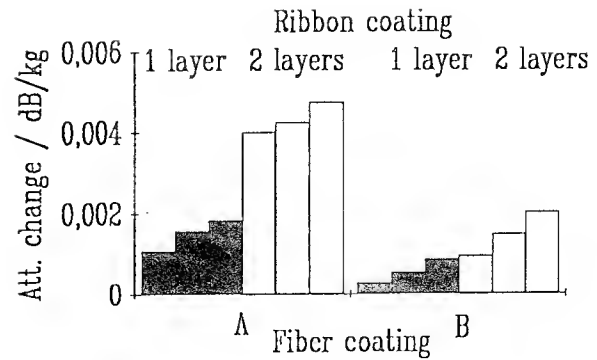


Fig. 16: Attenuation change during crepe paper test of six 4 f. ribbons with different fiber coatings (A, B) and ribbon coatings

A small microbending sensitivity of the ribbons can also be achieved by selecting fibers with a small MAC-value 5 (Fig. 17). Due to the smaller outer diameter of the C fibers and the thinner coatings in 16 f. ribbons the attenuation change is 2 - 3 times larger than for 4 f. ribbons.

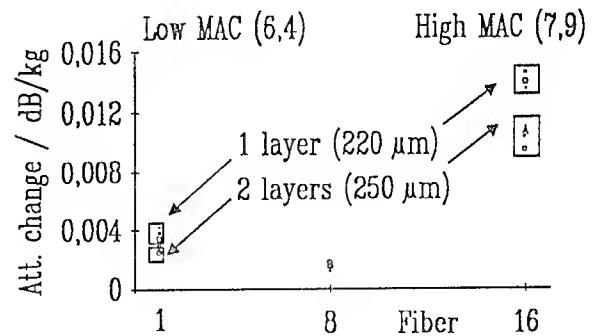


Fig. 17: Attenuation change during crepe paper test of ten 16 f. ribbons with different bending sensitive fibers (small and large MAC-value) and ribbon coatings and designs (type V and VI)

The microbending loss of 16 f. ribbons (type IV) can be reduced remarkably due to the optimization of the fiber coating (Fig. 18) according to fundamental investigations of Baldauf et. al.³

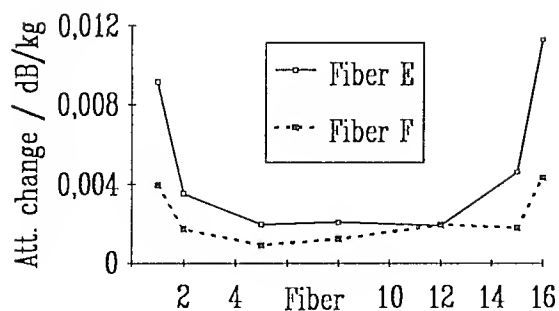


Fig. 18: Attenuation change during crepe paper test of 16 f. ribbons (type IV) with different fiber coatings (E, F)

It is also possible to inspect the ribbon quality (planarity) with the crepe paper test (Fig. 19).

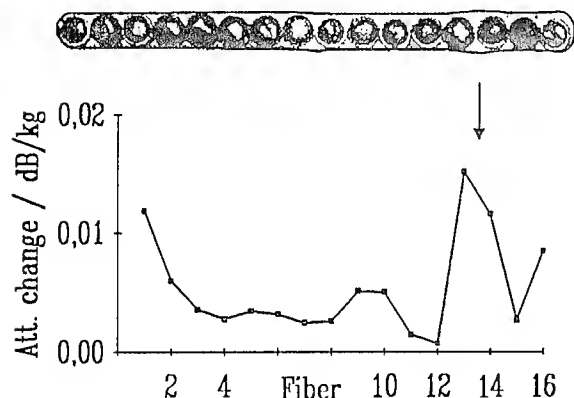


Fig. 19: Attenuation change during crepe paper test of a 16 f. ribbons (type V) with imperfections

The microbending behavior of a 16 f. ribbon was also investigated at different temperatures. We did not observe a noticeable change of the microbending sensitivity (Fig. 20). The most important point in temperature characteristics is the glass transition temperature of the coating materials. This value should preferably be outside of the used temperature range of the ribbon to ensure that the Young's moduli remain more or less constant.

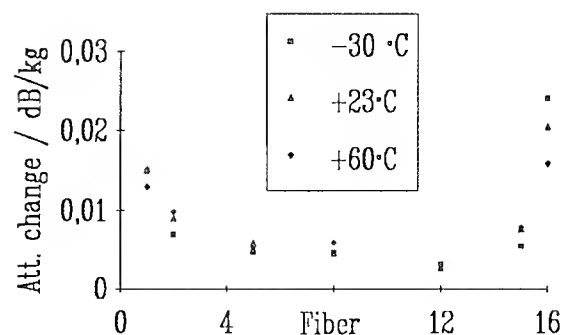


Fig. 20: Attenuation change during crepe paper test of a 16 f. ribbon (type V) at different temperatures

The results of all experiments with the crepe paper test indicate the strong influence of the microbending susceptibility of the optical fiber (MAC-value, coating materials, outer diameter) on the performance of the ribbon.

Modified crepe paper test

The above mentioned methods only studied the lateral pressure behaviour of a ribbon as typically done in literature. ⁴ The side pressure performance of ribbons is of special interest in U-groove cables where the whole ribbon stack can be pressed against the walls. 1, 2

We estimated the side pressure characteristics with the modified crepe paper test where 12 ribbons are located vertically in an aluminium U-groove. The attenuation increase is only measured of 10 ribbons at different loads to exclude the effect of the surface of the aluminium wall.

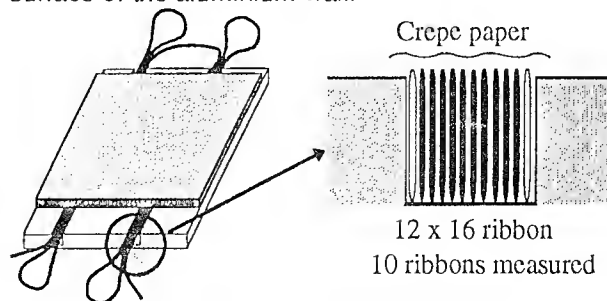


Fig. 21: Experimental set-up of vertical crepe paper test

The loss of the top and bottom fiber increases linearly with increasing load (Fig. 22). It is worth mentioning that the next but one top fiber demonstrates no additional losses up to a load of 10 kg. That means that the irregular surface of the crepe paper is smoothed by the top fiber and there is no deformation of next but one top fiber. Accordingly the attenuation in a ribbon stack of a U-groove is only increased at the edge positions. Therefore one solution of the problem could be a "dummy" ribbon which buffers the microbendings of the inner cable surface.

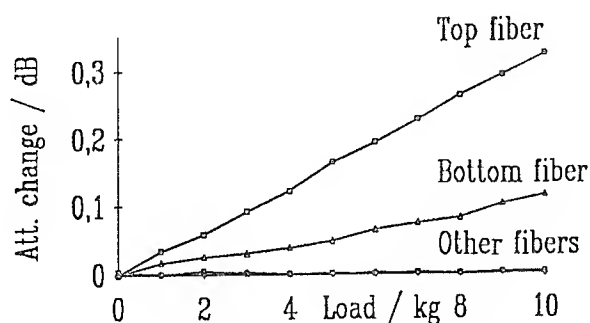


Fig. 22: Attenuation change during modified crepe paper test of a 16 f. ribbon (type V)

Temperature cycling

High quality ribbons do not change their attenuation over a typical temperature range from -30°C to $+60^{\circ}\text{C}$ (Fig. 23).

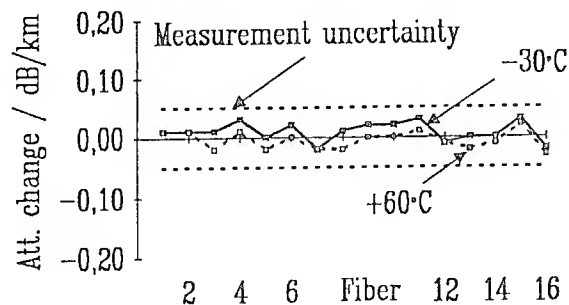


Fig. 23: Attenuation change during temperature cycling of a 16 f. ribbon (type V) in a loose coil

However imperfections (e.g. insufficient fiber alignment or non-planarity of the ribbon) can generate dramatic excess losses during temperature cycling (microbending curve of a 4 f. ribbon in Fig. 2).

Temperature tests of a 16 f. ribbon on a shipping spool or in a coil with many crossovers, as shown in Fig. 24, result in excess losses. The attenuation change strongly depends on the microbending sensitivity of the fiber, that means, the MAC-value.

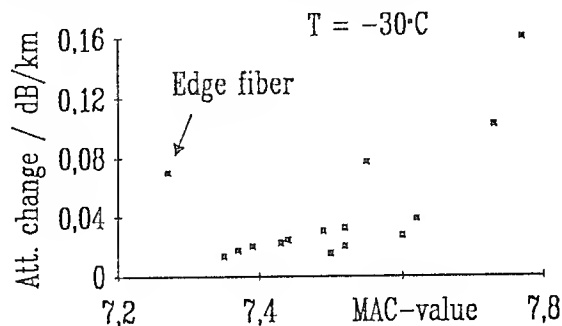


Fig. 24: Attenuation change during temperature cycling of a 16 f. ribbon (type V) in an imperfect coil

Water immersion

Water immersion of the ribbons usually leads to a swelling of the coating materials and consequently to additional microbending losses.

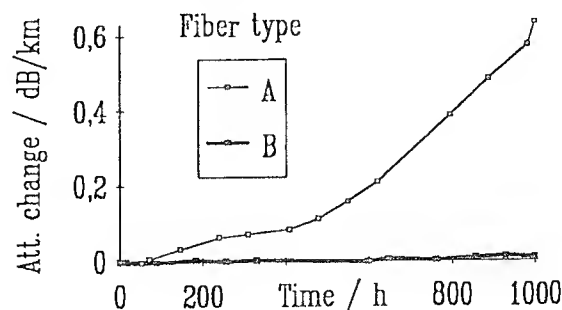


Fig. 25: Attenuation change during water immersion of 4 f. ribbons (type III) with different fiber coatings (type A and B)

The proper selection of the fiber coating (Fig. 25), the ribbon design and materials (Fig. 26) prevents a notable change of the attenuation for a long time, e.g. 1000 hours.

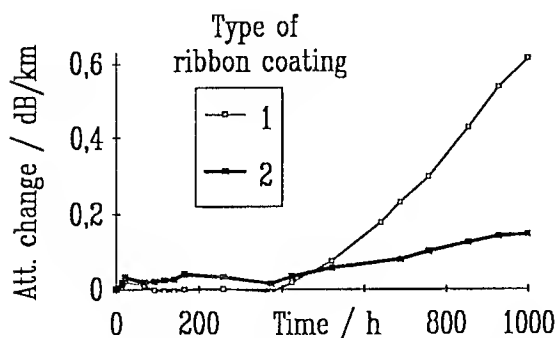


Fig. 26: Attenuation change during water immersion of 4 f. ribbons (type III) with different ribbon coatings

Advantageously, the ribbons with fibers of type A exhibit an excellent behavior during water immersion as well as a small microbending sensitivity in all performed tests (Fig. 4, 12 and 16).

Conclusion

The correct determination of the microbending properties of ribbons requires a suitable simulation of the conditions of a real cable, which can be verified with the spectral loss curves.

We have investigated various methods to predict the susceptibility of ribbons to rough structures and external forces. The long length tests with a significant and reproducible attenuation change at low compression forces can be suggested.

It could be confirmed in all experiments, including temperature cycling and water immersion, that the most important parameter is the microbending sensitivity of the single-mode fiber.

References

- 1 S. Tomita et. al.: "Preliminary research into ultra-high density and high count optical fiber cables", 40 th IWCS, 1991, pp. 8 - 15
- 2 S. Tomita et. al.: "Ultra high-density cable with thin coated fibers and multi-fiber connectors", 42th IWCS 1993, pp. 5 - 15
- 3 J. Baldauf et. al.: Relationship of mechanical characteristics of dual coated single mode optical fibers and microbending losses. IEICE Trans. Commun., E76-B (1993) S. 352-357
- 4 M. Saito et. al.: 16-fiber ribbon for ultra-high-density and high-count optical fiber cable. 42th IWCS 1993, pp. 16 - 19
- 5 C. Unger et. al.: Investigation of the microbending sensitivity of fibers. J. of Lightwave Technol., Vol. 12, No. 4, pp. 591-596

Authors:



Siemens AG ÖN NK E
Austr. 101
D-96465 Neustadt / Cbg
Germany

Fax: ++ +9568 93 2008

Clemens Unger was born in Blankenburg, Germany, in 1967. He received the degree in physics from the University of Jena, where he was working on fiber lasers and ultra short pulse generation. Now he is finishing his Ph.D. work about the micro- and macrobending behaviour of cabled fibers at the Siemens Fiber Optic Cable Development Department in Neustadt. Presently, his research interests are in transmission characteristics of single and multi-mode fibers for designing ribbons and optical cables, including the development of fiber optic test equipment.



Siemens AG ÖN NK E
Austr. 101
D-96465 Neustadt / Cbg
Germany

Fax: ++ +9568 93 2008

Walter Pfandl was born in Fürth, Germany, in 1950. He is the head of the Development Group for Optical Fiber and Copper Cables. He reached his Dipl.-Ing. degree in material sciences from the University of Erlangen / Nürnberg in 1976 and the Ph.D. degree in 1984. In 1985 he got the responsibility for a group at the Central Development Department of Siemens in Erlangen. Since 1993 he covers his present position.



Siemens AG ÖN NK E
Austr. 101
D-96465 Neustadt / Cbg
Germany

Fax: ++ +9568 93 2008

Waldemar Stöcklein was born in Coburg, Germany, in 1956. He attended the University of Bayreuth, where he studied physics and mathematics. In 1985, he received the Ph.D. degree in physics, for basic research in the field of magnetic resonance in "organic metals". From 1986 to 1987, he was an IBM Postdoctoral Research Fellow in the Almaden Research Center in San Jose, CA. In 1988, he joined the Fiber Optic Cable Development Department of Siemens in Neustadt / Coburg. He is involved in cable design, fiber characterization, and the development of fiber optic test equipment.



Siemens AG ÖN NK E
Austr. 101
D-96465 Neustadt / Cbg
Germany

Fax: ++ +9568 93 2008

Siegfried Unterberger was born in Stuttgart, Germany, in 1937. He studied mechanical engineering at the HTL in Graz. In 1962 he joined the development department for magnetic computer storage of the Siemens AG in München. Since 1970 he is working in the Siemens Fiber Optic Cable Development Department in Neustadt / Coburg. His current interests are the coloring of fibers and the ribbon design and manufacturing.

A STUDY OF 16-FIBER RIBBON FOR ULTRA HIGH DENSITY OPTICAL FIBER CABLE

T. Kakuta, K. Oishi, W. Katsurashima, H. Hongo, and Y. Matsuda

Sumitomo Electric Industries, Ltd.
1, Taya-cho, Sakae-ku, Yokohama, 244 Japan

Abstract

For the study to construct an ultra high count and high density optical fiber cable, 16-fiber ribbons with different coating structures were fabricated using thin coated fibers and their optical and mechanical characteristics were investigated. The optical characteristic against external force was evaluated with microbending loss under lateral force. It has been clarified that the optical characteristic of 16 fiber ribbon under lateral force depends on coating structure such as primary coating diameter, secondary coating thickness, Young's modulus of ribbon coating and ribbon thickness. The mechanical characteristic was also investigated from the view point of abrasion resistance. It has been proved that the abrasion resistance of the ribbon mainly depends on the total thickness of hard coatings, namely, secondary and ribbon coatings.

1. Introduction

On the basis of the fiber-to-the-home conception by NTT in Japan, the ultra-high-count optical fiber cable, which has several thousands of fibers and the almost same diameter as the high count conventional optical fiber cable, is recently discussed and studied[1]. In order to realize the cable with high optical fiber density, it is essential to develop the thin coated optical fiber and the multi-count fiber ribbon, and also to modify the cable construction. However, downsizing of the coated optical fiber and ribbon may cause deterioration of the optical performance and fiber strength during the manufacturing processes of the cable. Therefore, we investigated the characteristics of the thin coated multi-count optical fiber ribbon from the view point of the coating structure.

In this paper, the optical characteristics under lateral force and the abrasion resistance of thin coated 16-fiber ribbons are described and discussed.

2. 16-fiber ribbon

Using thin dual coated fibers with the diameter of 180 μ m or 200 μ m, 16-fiber ribbons(Fig.1) with different coating structures listed in Table 1 were prepared. The optical glass fiber is a normal single-mode type with a diameter of 125 μ m. UV curable resins were used as all coating materials.

Based on the recent studies of thin coated optical fibers [2][3], a primary coating material whose young's modulus is about a half lower than that of the conventional one and a secondary coating material whose young's modulus is about 2.5 times higher than that of the conventional one were used as the coating materials of the thin coated fiber for the 16-fiber ribbons.

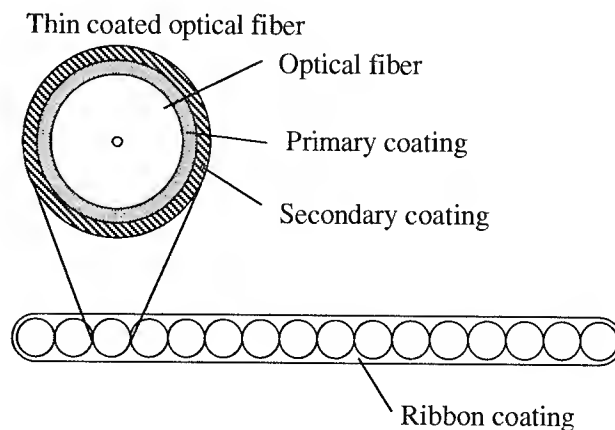


Fig.1 Structure of 16-fiber ribbon

3. Experimental

3.1 Optical characteristics under lateral force

3.1.1 Samples

In order to investigate the effect of coating structure of the 16-fiber ribbon for the optical characteristic, samples of No.1,5,9,10,14, and 15 in Table 1 were tested. Concerning the effects of Young's modulus and thickness of ribbon coating, samples of No.4,5,6, and 7 were tested.

3.1.2 Multi-layer winding test

Optical characteristics of 16-fiber ribbons under lateral force were investigated with the multi-layer winding test. The 16-fiber ribbon was wound on a reel whose diameter is 310mm at a spool tension of 150g and then was rewound on the smaller reel whose diameter is 150mm at the higher spool tension of 600g. Chromatic transmission loss spectrum in each winding condition was measured and we got loss-increase by the subtraction.

3.1.3 Presumed microbending loss

It is well known that microbending loss depends on the parameters of the optical fiber. Therefore, in the actual experiment, it is rather difficult to compare the detected loss-increase of the individual fiber with different parameters of fiber. To overcome this problem, we introduced presumed microbending loss (PML) method[2].

By fitting the measured data to microbending formula of Petermann[4], we get the correlation length L_c and the average bending radius R . These parameters are assumed to be inherent to the bending condition and not to be influenced by parameters of the fiber. Hence the effect of parameters of fiber on the induced loss increase is compensated. Substituting L_c and R again into the equation of a presuming standard fiber, we get the presumed microbending loss (PML).

Using this method, measured loss-increase at the multi-layer winding test of the 16-fiber ribbon was converted to the PML of a standard optical fiber whose mode field diameter is $9.5\mu\text{m}$ and effective cut-off wavelength is $1.25\mu\text{m}$.

3.2 Abrasion resistance

3.2.1 Samples

In order to investigate the effects of coating thickness of fiber, thickness of ribbon coating and Young's modulus of ribbon coating, samples of No.1,2,3,4,10,11,12 and 13 in Table 1 were tested.

Table 1 Coating structure of 16-fiber ribbon

Sample No.	Primary coating diameter(μm)	Secondary coating diameter(μm)	Ribbon thickness (mm)	Young's modulus of ribbon coating (kg/mm ²)
1	150	180	0.21	70
2	150	180	0.25	70
3	150	180	0.21	150
4	150	180	0.25	150
5	160	180	0.21	70
6	160	180	0.25	70
7	160	180	0.21	150
8	160	180	0.25	150
9	170	180	0.21	70
10	150	200	0.23	70
11	150	200	0.27	70
12	150	200	0.23	150
13	150	200	0.27	150
14	160	200	0.23	70
15	170	200	0.23	70

3.2.2 Abrasion resistance test

To investigate the contribution of coating structure to the protection from fiber breakage, abrasion resistance of the thin coated 16-fiber ribbon was evaluated with the abrasion resistance test as shown in Fig. 2. The 16-fiber ribbon was rewound through the pulleys wrapped with a sheet of abrasive paper at a tension of 1.2kg and then the frequency of fiber breakage which arose from the forced damage was observed with OTDR.

This examination was carried out using three kinds of abrasive papers with particles whose average diameters(D) are 11.5 μ m, 40 μ m, and 155 μ m.

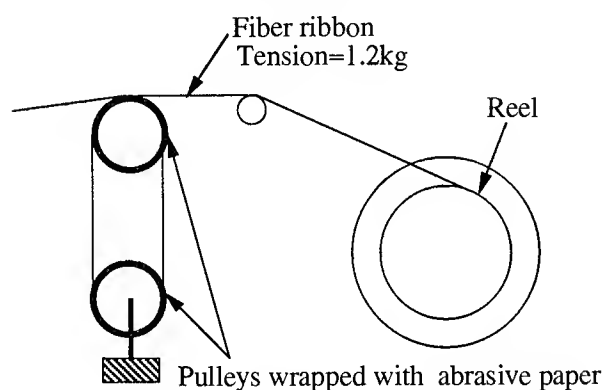


Fig.2 Abrasion resistance test

4. Results and Discussion

4.1 Optical characteristics under lateral force

4.1.1 Experimental results

Figure 3 shows the relationship between coating structure of fiber and PML at a wavelength of 1.55 μ m for 16-fiber ribbons with a constant thickness of ribbon coating. The PML of 16-fiber ribbon decreases as primary coating diameter increases for the both ribbons with coated fibers of 180 μ m diameter and 200 μ m diameter. While at the same primary coating diameter, thicker secondary coating reduces the PML. Figure 4 shows the relationship between coating structure and PML of the 16-fiber ribbons with coated fibers of 180 μ m diameter. It is recognized that higher Young's modulus of ribbon coating or thicker ribbon coating reduces PML.

4.1.2 Stress analysis by finite element method

The experimental results were compared with stress analysis of the fiber ribbon using finite element method(FEM).

Figure 5 shows the calculated stress on glass fiber in ribbons with coated fibers of 180 μ m diameter and 200 μ m diameter. It is interesting the stress shows the lowest at certain primary coating diameter for each ribbon. In the case of the ribbon with coated fibers of 200 μ m diameter, the calculated stress shows almost agreement with the experimental result. On the other hand in the case of the ribbon with coated fibers of 180 μ m diameter, the calculated stress is rather different from the experimental result, which may indicate that some other factors are required in the stress analysis.

At the same primary coating diameter in Fig.5, the thicker secondary coating gives the lower stress. This tendency in the stress analysis with FEM is in good agreement with that in the experimental result.

Figure 6 shows relationship between calculated stress on glass fiber in ribbon and structure of ribbon coating. The higher Young's modulus of ribbon coating or thicker ribbon coating reduces the stress on glass fiber. This tendency is also in good agreement with that in the experimental result.

From the experimental results and the stress analysis, thicker primary coating and higher Young's modulus of ribbon coating are desirable in order to improve optical characteristic of the 16-fiber ribbon under lateral force.

4.2 Abrasion resistance

In the 42nd IWCS, a study on the abrasion resistance of the thin coated optical fiber was reported and it was concluded that the abrasion resistance of the thin coated fiber mainly depended on the thickness of hard secondary coating[3]. The abrasion resistance of 16-fiber ribbon was also considered from the view points of hard coatings.

Figure 7 shows the relationship between the total thickness(T) of hard coatings, namely, secondary and ribbon coatings, and the frequency of fiber breakage in the 16-fiber ribbon. The frequency of fiber breakage almost reduces as the total thickness of hard coatings increases.

Figure 8 shows the relationship between Young's modulus of ribbon coating and the frequency of fiber breakage in the ribbon when the abrasion resistance test was carried out using the abrasion paper with particles whose average diameter is 155 μ m. The figure indicates that the higher Young's modulus of ribbon coating does not make more significant improvement for the abrasion resistance of the fiber ribbon than the thicker hard coatings. Therefore, the abrasion resistance of the 16-fiber ribbon mainly depends on total thickness of hard coatings in the ribbon. This result is in good agreement with the abrasion resistance of fiber itself [3].

Figure 9 shows the relationship between the ratio of average particle diameter(D) on the abrasive paper to the total thickness(T) of hard coatings and the frequency of fiber breakage. While thicker hard coating is necessary to improve the abrasion resistance of the 16-fiber ribbon, it is important to make the cleanliness of the environments into consideration when the ribbon is fabricated or used.

5. Conclusion

Using thin coated fibers, 16-fiber ribbons with different coating structures were fabricated. From the view point of coating structure, their optical characteristics under lateral force and abrasion resistance were studied.

It has been clarified the optical characteristic of the 16 fiber ribbon under lateral force depends on coating structures such as primary coating diameter, secondary coating thickness, Young's modulus of ribbon coating and ribbon thickness.

It has been also proved the abrasion resistance of the ribbon mainly depends on the total thickness of hard coatings, namely, secondary and ribbon coating.

References

- [1] T. Tomita et al. , "Ultra high-density optical fiber cable with thin coated fibers and multi-fiber connectors", proceedings of the 42nd IWCS(1993), pp 5-15.
- [2] W. Katsurashima et al. , "Microbending loss of thin coating single mode fiber for ultra-high-count cable", proceedings of the 41st IWCS(1992), pp 13-19.
- [3] K. Oishi et al. , "Coating design of thin coated fiber for ultra-high-count optical fiber cable", proceedings of the 42nd IWCS(1993), pp 687-693.
- [4] K. Petermann, AEU, 1986, 30, pp.337-342.

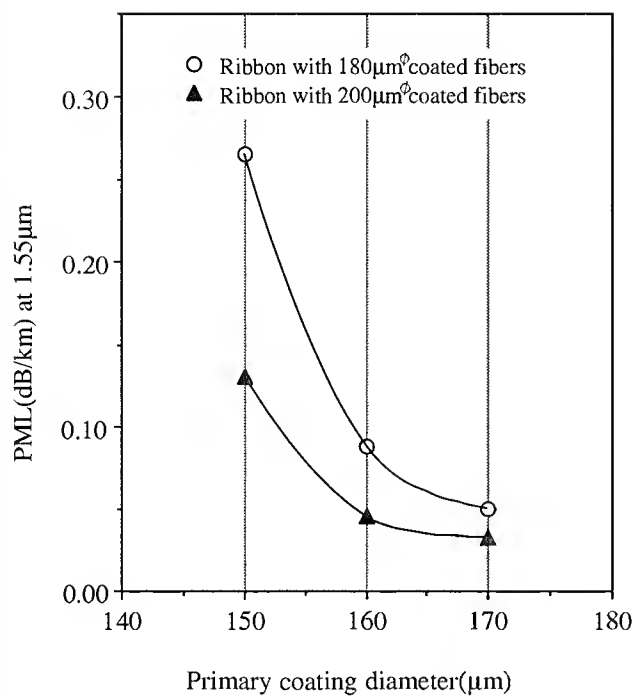


Fig.3 Relationship between structure of fiber coating and PML of 16-fiber ribbon

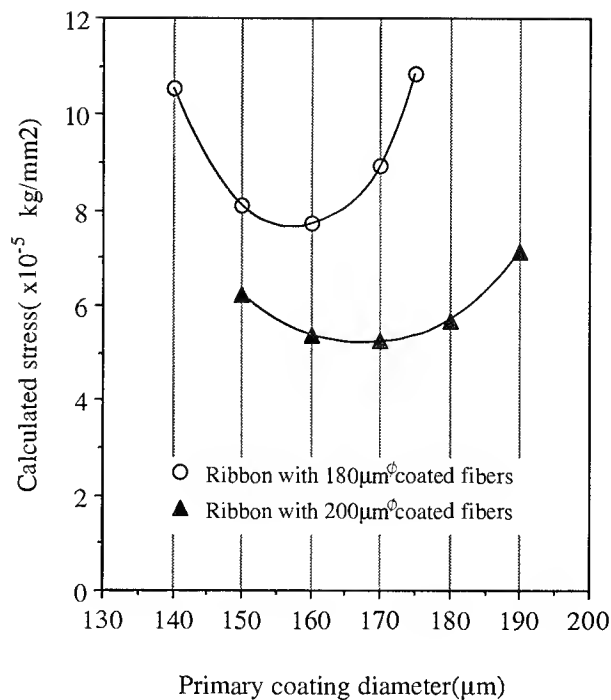


Fig.5 Calculated stress on glass fiber in ribbon for different structures of fiber coating

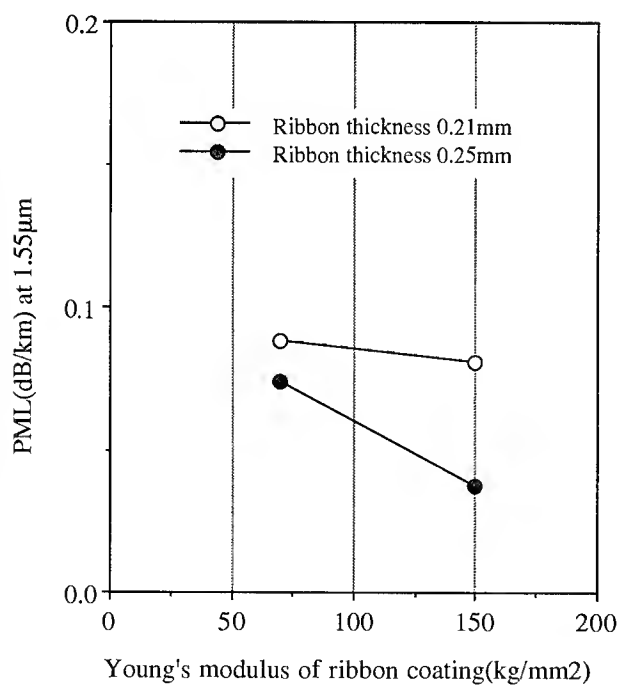


Fig.4 Relationship between structure of ribbon coating and PML of 16-fiber ribbon

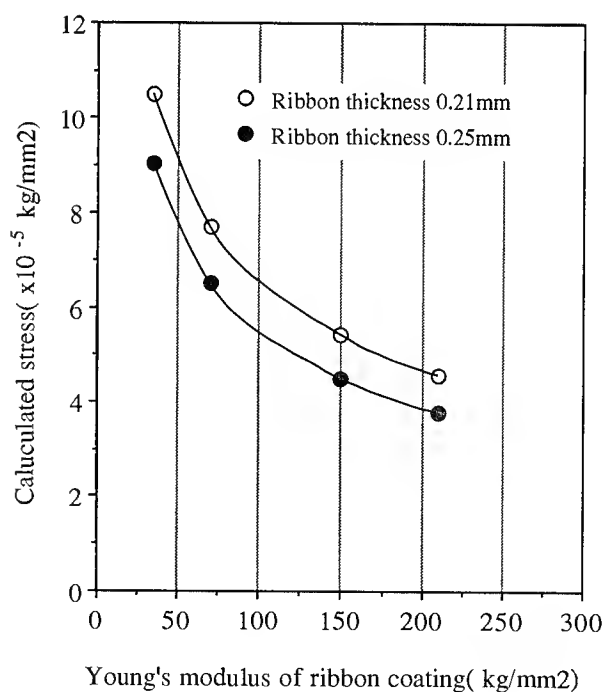


Fig.6 Calculated stress on glass fiber in ribbon for different structures of ribbon coating

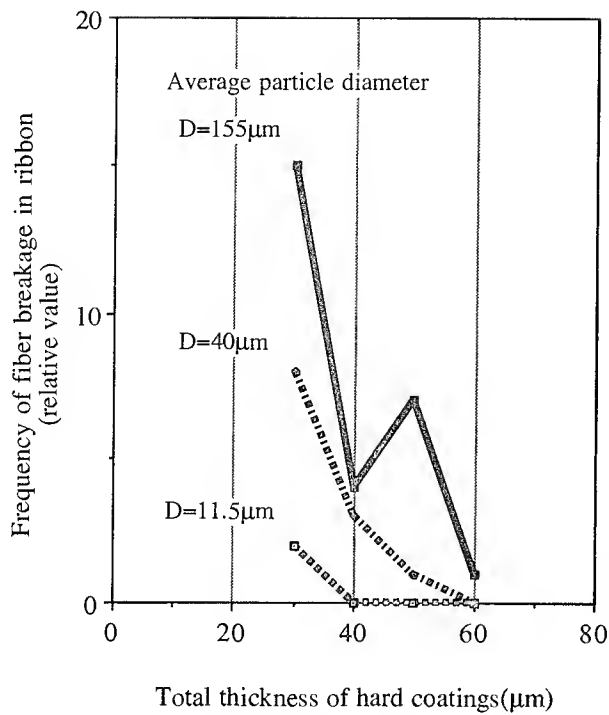


Fig.7 Relationship between total thickness of hard coatings and abrasion resistance of 16-fiber ribbon

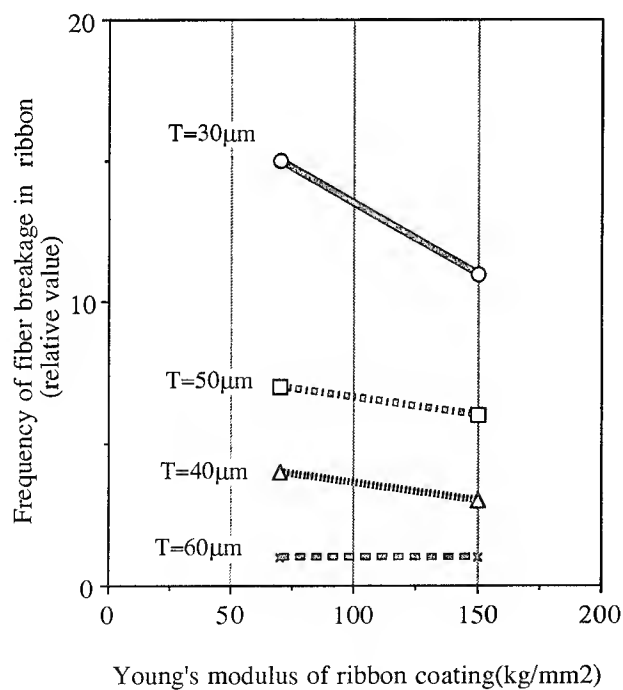


Fig.8 Young's modulus of ribbon coating and abrasion resistance of 16-fiber ribbon

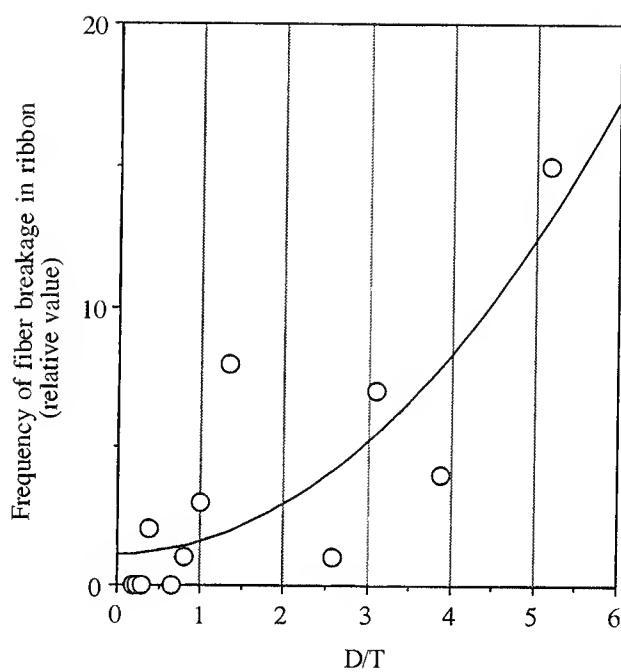


Fig.9 Relationship between D/T and abrasion resistance of 16-fiber ribbon



Tatsuya Kakuta

Sumitomo Electric
Industries, Ltd.

1, Taya-cho, Sakae-ku
Yokohama, Japan

Tatsuya Kakuta was born in 1960. He received his M.E. degree in Applied Chemistry from Osaka University in 1985 and joined Sumitomo Electric Industries, Ltd. He has been engaged in research and development of optical fibers and ribbons. He is a senior engineer of Transmission Media Department in Yokohama Laboratories.



Hiroyasu Hongo

Sumitomo Electric
Industries, Ltd.

1, Taya-cho, Sakae-ku
Yokohama, Japan

Hiroyasu Hongo received his M.E. degree from Tsukuba University in 1986 and joined Sumitomo Electric Industries, Ltd. He has been engaged in research and development of optical fibers. He is a member of Transmission Media Department in Yokohama Laboratories.



Kazumasa Oishi

Sumitomo Electric
Industries, Ltd.

1, Taya-cho, Sakae-ku
Yokohama, Japan

Kazumasa Oishi received his M.E. degree in Geochemistry from Tsukuba University in 1991 and joined Sumitomo Electric Industries, Ltd. He has been engaged in research and development of optical fibers. He is a member of Transmission Media Department in Yokohama Laboratories.



Yasuo Matsuda

Sumitomo Electric
Industries, Ltd.

1, Taya-cho, Sakae-ku
Yokohama, Japan

Yasuo Matsuda received his M.E. degree in Chemistry from Tokyo University in 1978 and joined Sumitomo Electric Industries, Ltd. He has been engaged in research and development of optical fibers and cables. He is a chief associate of Transmission Media Department in Yokohama Laboratories.



Wataru Katsurashima

Sumitomo Electric
Industries, Ltd.

1, Taya-cho, Sakae-ku
Yokohama, Japan

Wataru Katsurashima graduated from Tokyo University in 1987 and joined Sumitomo Electric Industries, Ltd. He has been engaged in research and development of optical fiber cables. He is a member of Communication Department in Yokohama Laboratories.

A COMPREHENSIVE APPROACH TO RIBBON DESIGN WITH A FOCUS ON MATERIALS

John R. Keesee and Gregory A. Lochkovic

Siecor Corporation
Hickory, North Carolina

David Smith and J. Richard Toler

Corning Incorporated
Corning, New York

ABSTRACT

Through the methods of experimental design, we have gained a broad scope understanding of ribbon performance characteristics and how they are affected by both fiber and ribbon matrix UV curable coating material properties. Reduced diameter fibers were used during this study which provided a most sensitive measure of performance. Ribbon performance characteristics studied include as-manufactured attenuation, winding under tension, lateral load crush, and strip testing. Following our ribbon testing, ribbons were tested in cables. As a result of our efforts, we have been successful in designing ribbons with reduced diameter fibers that can repeatedly achieve low fiber attenuation characteristics in both uncabled and cabled states. We present a discussion of our experimental method as well as the key properties of fiber and ribbon coating materials identified within the scope of the development effort.

INTRODUCTION

NTT (Nippon Telegraph and Telephone Corp.) is embarking on an aggressive plan which will greatly increase their fiber needs in communication and information routes. As plans begin to solidify, many unique requirements have surfaced. One highly visual requirement is the need for minimum diameter ultra-high fiber count cables [Tomita¹]. Cables containing up to 4000 fibers have been forecasted. This would benefit the cable development community because it requires the development of highly efficient optical cable configurations. With this as the prime objective, we initiated development of a cable, with an initial diameter target of less than or equal to 35 mm, capable of containing up to 4000 fibers while maintaining sound optical performance and long-term reliability. This paper deals with the fiber ribbonizing component of development.

Several key issues were addressed in our efforts to achieve a highly efficient packing density for the new cable. Two critical issues were fiber diameter and fiber

arrangement within the cable. Ribbonizing was chosen as the most efficient means of gaining fiber density within the cable. Loose tube packaging yields the highest theoretical packing density; however, practical packing densities are much lower if acceptable optical performance is to be attained. Ribbonizing, on the other hand, yields a lower theoretical limit of packing efficiency, but the theoretical limit is more closely achieved with acceptable optical performance due to the buffering effects of the ribbon structure [Jackson²]. Equally important to minimum cable diameter are the dimensions of the individual cable components; i.e., fiber diameter. As shown in Figure 1, the multiplicative effect of the fiber diameters is a major contributor to the final diameter of the 4000 fiber U-groove cable. As you will note in the figure, the line predicting the cable diameter is adjusted slightly upward from the original goal of 35 mm at the 180 μ m fiber diameter level. This is due to the cable development effort which indicated that the ribbons needed additional free space in order to provide a design which would consistently allow cable manufacture with minimal ribbonized fiber delta attenuation; thus, slightly increased cable diameters.

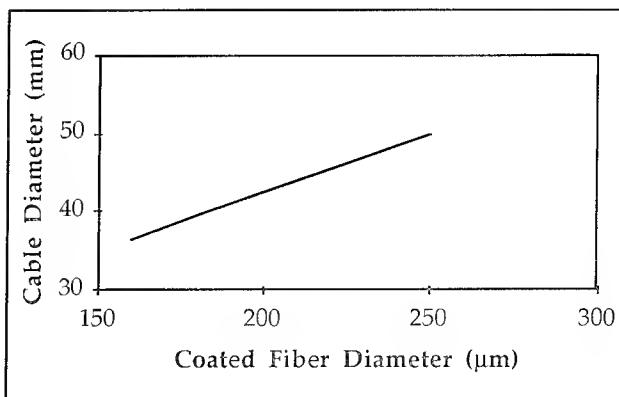


Figure 1 - U-groove Cable Diameter as a Function of Fiber Diameter

Due to the requirement for a small cable diameter, cable development utilizing fiber diameters of

approximately 180 μm dominated our efforts; however, further work demonstrated reliability issues with fibers of this size [Glaesemann³]. This concern with reliability initiated the decision directing development toward 200 μm diameter fibers. Notwithstanding, the majority of the development work reported in this paper deals with studies involving 180 μm diameter fibers.

Using reduced diameter fibers, the ribbon structure was investigated for key fiber and ribbon coating properties as well as the optimum levels (properties and/or dimensions) required to achieve minimal ribbonized fiber attenuation. This was accomplished using a logically planned series of designed experiments to first screen out the important properties, and then predict the best fiber and ribbon coating property and dimensional levels for optimum ribbon performance. This paper describes the experimental approach as well as the key fiber and ribbon UV curable coating properties identified during the investigation.

EXPERIMENTAL METHOD

A typical ribbon is a composite of several materials including the optical glass, fiber coating or coatings, and one to several layers of ribbon matrix coatings as shown in Figure 2.

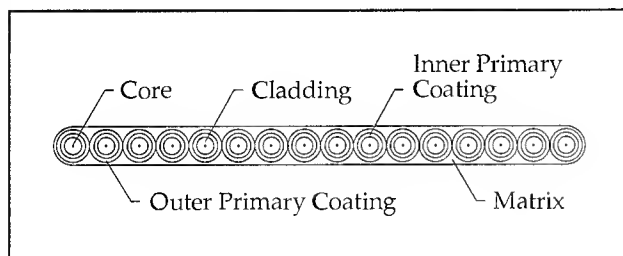


Figure 2 - Thin-Encapsulated Ribbon

The focus of our ultra-high fiber count cable development was performed using 180 μm coated diameter matched-clad fiber. This fiber design proved to be more sensitive to bending induced attenuations than standard 250 μm diameter fibers. This characteristic, predicted by Gloge⁴, is due to the reduced diameter as well as the thinner outer shell which both contribute to higher distortion losses. In our work with these bend sensitive fibers, we were able to see the effects of several ribbon design variables on attenuation characteristics that otherwise might have been missed. The general ribbon characteristics deployed in the initial investigation are shown in Table 1.

Optical Fiber (Matched Clad)		Petermann II MFD	9.20 - 9.50 μm
		λ_c	1.21 - 1.31 μm
Fiber Coating	Inner Primary	Modulus	1 - 4 MPa
	Outer Primary	Modulus	50 - 1600 MPa
Ribbon		Height	220 μm
		Modulus	30 - 1500 MPa

Table 1 - General Ribbon Characteristics in this Study

In order to comprehensively study the ribbon structure, an iterative approach to designed experiments was employed. An initial experiment was designed to allow determination of the critical variables (properties). This was followed by two experiments designed to focus on the optimum levels of those critical variables. From here, several additional experiments were performed to verify our results. All experiments were performed with uncolored, 16-fiber, thin-encapsulated ribbons in an uncabled state. Once the initial findings were verified, several additional experiments were performed in cable structures to ensure optimum performance in the 4000 fiber U-groove cable design.

Investigated Responses

Initial ribbon development efforts investigated responses that could be measured in ribbon-only form. This allowed us to simulate various cabled conditions and attain useful results at a much lower time and dollar cost than would have been possible through typical cabling experiments. Following are the key tests utilized during this phase of investigation.

- **Manufacturing Attenuation**
 - ≥ 900 m lengths of ribbon wound onto a 225 mm diameter drum at 110 g.
 - 1310 nm and 1550 nm OTDR measurement taken at 1 hour, 24 hours, and 2 weeks after manufacture.
- **Winding Under Tension Attenuation**
 - 500 meter lengths of ribbon wound onto a 225 mm diameter drum at 400 g.
 - 1310 nm and 1550 nm OTDR measurement taken at 1 hour after winding.
- **Parallel Plate Crush (Lateral Load) Attenuation**
 - Ribbon sample sandwiched between two 100 mm x 100 mm polished steel plates subsequently loaded to 400 N and 1000 N.
 - 1310 nm and 1550 nm attenuation characteristics measured at each load using a power meter.

- **Strip Cleanliness and Peak Strip Force**
 - Samples stripped at a rate of 100 mm/min with Fujikura thermal strippers set to 90 °C and the blade gap set to 150 µm.
 - Cleanliness graded on a subjective scale of 1 to 5 where 1 denotes a thoroughly clean strip with no residue, and 5 denotes a residue after stripping which cannot be removed with an alcohol wipe.
 - Strip force was monitored at 200 Hz, and the peak force recorded for each test.
- **Ribbon-to-Ribbon Coefficient of Friction** (see Figure 3 for test set-up)

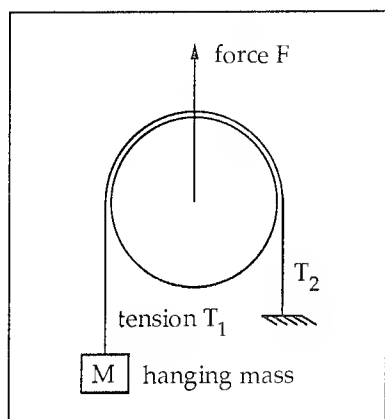


Figure 3 - Friction Test Set-up

- Ribbon sample wrapped around a 200 mm diameter mandrel, clamped in place, then another sample draped over the clamped sample. The draped sample is fixed at one end and a mass of 1600 g is attached to the free end with the entire assembly mounted in a tensile test machine.
- The draped ribbon is then pulled across the fixed ribbon at a rate of 25 mm/min while monitoring the load seen by the tensile tester.
- Using the basic principles of Statics, equation 1 was derived and used to determine the static coefficient of friction:

$$\mu = \frac{1}{\pi} \ln \left[\frac{F}{M \times g} - 1 \right] \quad (1)$$

where:

F = peak force generated (N)

M = hanging mass (kg)

g = acceleration of gravity (m/s²)

These responses were thought to be the critical parameters around which multi fiber ribbons could be evaluated for dry cable structures and handling in the

field. The time-based manufacturing attenuation allowed us to observe how the various designs would behave over time. Both the winding under tension and parallel plate crush testing allowed us to evaluate the bending sensitivity of each ribbon design.

It was proposed early on that high ribbon-to-ribbon mobility in a non-lubricated stack could add cable performance benefits due to reduced strains. We hypothesized that lower friction between ribbons in a stack would provide the mechanism that would allow lower strains. Therefore, we chose to generate information within this experiment on coefficient of friction with the various matrix materials.

Initial Experiment

The first experiment was a screening experiment with several variables chosen in order to identify the critical factors for optimum ribbonized fiber performance. This was a multilevel, multi variable, fractional factorial experiment. Table 2 details the coating properties addressed in this study.

Inner Primary	Outer Primary	Ribbon Matrix
Modulus	Modulus	Modulus
Elongation to Break	Elongation to Break	Elongation to Break
Adhesion to Glass		Glass Transition Temperature
		Coefficient of Friction

Table 2 - Coating Properties Addressed in the Study

It should be understood that some properties were not included based on prior knowledge and experience. For instance, we considered the need for a low glass transition temperature in inner primary coatings for optimum thermal performance to be well known, and not worth further investigation.

The inner primary, outer primary (or secondary), and ribbon matrix materials were considered to be the main variables within this experiment. Each main factor (inner primary, etc.) was given 4 standard levels. This allowed us to fashion the experiment in the form of a highly fractionated 4³ factorial. A simple model of the experiment is depicted in Figure 4. Additionally, center point levels, not shown in Figure 4, were chosen in an effort to more effectively cover the intended design space. The center points were not shown in order to maintain simplicity of the figure.

The levels (or values) for each factor (or property) were chosen based on nearest match to desired properties from readily available materials. We attempted to cover as wide a range of the properties as possible within and relative to each level in order to gain the maximum amount of information from our experimentation.

This was an experiment of "type" due to the chosen set-up. Since we chose each material type based on its specific properties, this allowed us to predict the critical properties and/or levels associated with each main factor. Additionally, we could determine the impact each main factor had on a ribbon structure relative to the other main factors. *An experiment of "type" typically employs factors with various kinds or types of materials or things; whereas, an experiment of level investigates measurable quantities of a given factor or factors.*

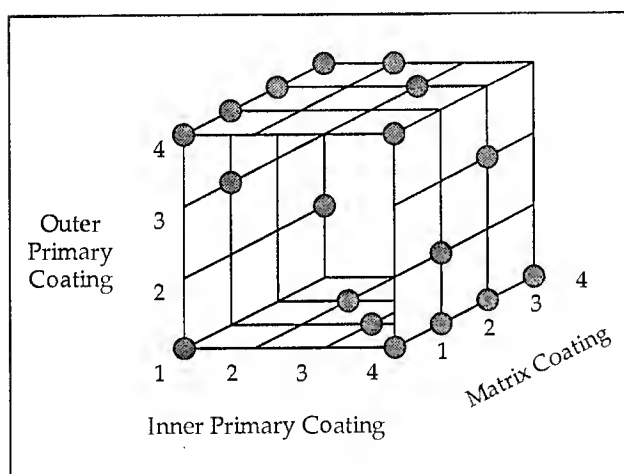


Figure 4 - Experimental Design Model

Statistical analysis of the data from the first experiment indicated that 96% of the variation in attenuation (*manufacturing, winding under tension, and crush*) could be attributed to material properties at a 95% level of confidence. This gave us confidence that our process was generating minimal variation in our test results.

Our data led us to the following general conclusions for reduced diameter fiber ribbons:

- The attenuation character of the ribbon design is most dependent upon the modulus of the ribbon matrix material, with lower modulus providing lower attenuation character at modulus levels above 100 MPa. There is also some indication that lower modulus outer primary materials provide

enhanced attenuation characteristics; though, not to the extent of matrix materials.

- The thermal strip characteristics of the ribbon design are most dependent upon two fiber inner primary material properties: adhesion to glass and elongation to break. Lower adhesions to glass yield predictably lower peak strip forces. Higher elongations to break yield enhanced strip cleanliness.

Iterative Experiments

Subsequent to the findings from our initial experiment, we were able to design and execute two additional ribbon-only experiments to focus on key areas brought to light in that experiment. While the initial experiment provided direction as to which components (inner, outer, and matrix coatings) and which properties of those components were important, the iterative experiments were designed to provide information about the optimum levels (values) of the critical properties for minimum attenuation. Additionally, the iterative experiments were designed to allow us to clear up some confusion in the analysis of the interactions from the first experiment. Again, we decided to focus on attenuation characteristics. Further work must be performed in the future to achieve acceptable thermal strip performance while maintaining minimal attenuation change.

Since we were able to reduce the number of variables for these experiments, we designed each experiment in the form of a 2^2 full factorial with centerpoints and replication of each combination. Centerpoints were included to give us an estimation of curvature if the system proved to be non-linear within the chosen limits of each property. In addition, replication of each combination was necessary in order to obtain a sound estimate of the manufacturing and testing variation, and therefore ensure that outlier data did not direct our decisions.

Both of the iterative experiments focused on matrix modulus; the factor with the largest attenuation impact from the initial experiment. One experiment varied inner primary modulus and matrix modulus while the other varied outer primary modulus and matrix modulus. Responses measured for the iterative experiments were the same as those for the initial experiment. The moduli ranges that were chosen for evaluation in these experiments are provided in Table 3.

A key discovery from these experiments was that ribbonized fiber attenuation changes could be minimized by using matrix materials with moduli between 100 and 400 MPa.

	Modulus (MPa)	
	Experiment #1	Experiment #2
Inner Primary	1	1 - 2
Outer Primary	300 - 600	1000
Matrix	50 - 400	50 - 400

Table 3 - Moduli Ranges for Coatings in Iterative Experiments

Other Experiments

With the key conclusions from the initial and iterative experiments in addition to several less statistically significant (yet interesting) trends, we performed other less rigid ribbon and cable experiments. In some cases, we investigated single variables, such as inner primary thickness, which did not require complex experimental layouts. Additionally, cabling experiments provided further information which we were previously unable to attain in our ribbon-only testing.

From accumulated information arising from the sum of the experiments, we have been able to identify critical properties associated with the inner primary, outer primary, and ribbon matrix coating materials as well as the optimum levels for each.

DEVELOPMENTAL RESULTS

The remainder of this paper will discuss the conclusions generated within the development work presented in the previous section. The key properties and their optimal levels for minimized cabled attenuation character are reviewed for each coating material in a thin-encapsulated ribbon design.

Inner Primary

It is clear that the glass to inner primary coating interface in a fiber is one of the most important parameters affecting the attenuation characteristics of a fiber. The glass should be in the lowest possible state of stress along its entire length in order to minimize the attenuation character of a given fiber. The optimum condition would be for the glass to be unsupported and suspended in the center of the outer primary coating without coming into contact with the inner surface. Obviously, this is not feasible; therefore, we initiated development efforts to attain an enhanced environment for minimal bending induced attenuation. This work allowed us to identify two key parameters of the inner primary coating material:

- Thickness
- Modulus

Other inner primary coating properties must be maintained, as defined in previous work [Overton⁵], in order to achieve critical fiber performance parameters (temperature cycling, thermal strip, etc.). However, thickness and modulus are critical toward achievement of the initial objective of acceptable room temperature performance in thin coated multi-fiber ribbons.

In his paper addressing the design of downsize coated fibers for minimal microbending loss, Hara⁶ discusses two useful prediction parameters, D (buffering effect) and H (stiffness), both previously derived by Gloge. Of particular importance for thin coated ribbon fibers is the buffering effect, D, defined as:

$$D = E_p + E_s \times \left[\frac{b}{R_s} \right]^3 \quad (2)$$

where E_p and E_s represent the inner and outer primary Young's moduli respectively, b represents the thickness of the outer primary, and R_s represents the radius of the outer primary.

In discussing his work, Hara notes that for fibers with diameters (d) less than or equal to 230 μm , a low b/R_s value results in lower microbending losses (he notes that the contrary is true when $d > 230 \mu\text{m}$). Generally, a lower value of D provides an enhanced buffering effect to the glass which results in a lower distortion loss (or bending induced attenuation). Therefore, given a fixed outer diameter (at less than or equal to 230 μm), the smaller the b value, the smaller the b/R_s value, resulting in lower microbending loss performance. Thus, the larger the inner primary thickness (implied by the smaller b value), the lower the microbending loss performance.

The positive buffering effect of a thicker inner primary can be seen in Figure 5.

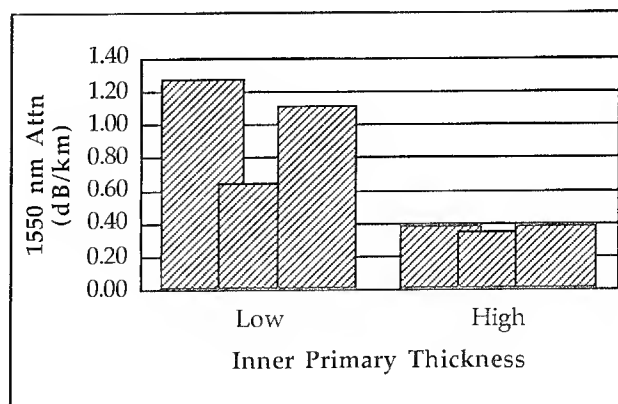


Figure 5 - Winding Under Tension Attenuation of 200 μm Fiber

Under tension wind testing, the high inner primary thickness fibers exhibited not only lower 1550 nm attenuation character but less variation from ribbon to ribbon than the fibers with the low inner primary thickness. These tests were performed on 200 μm ribbonized fibers with identical fiber and ribbon coating materials.

The use of the 200 μm fibers in this portion of the investigation was necessary in order to clearly see the effect of the inner primary thickness on ribbonized fiber attenuation characteristics. We wished to test a meaningful difference, and it was exceedingly difficult to manufacture 180 μm fibers with thicker inner primary coatings than our standard 180 μm fiber.

The modulus of the inner primary coating was also found to be important in attaining low attenuation character in ribbonized fibers; although, to a lesser degree than thickness. Referring to Figure 6, a significant trend was established in our experimentation showing that as the inner primary modulus is decreased, the ribbonized fiber attenuation decreases.

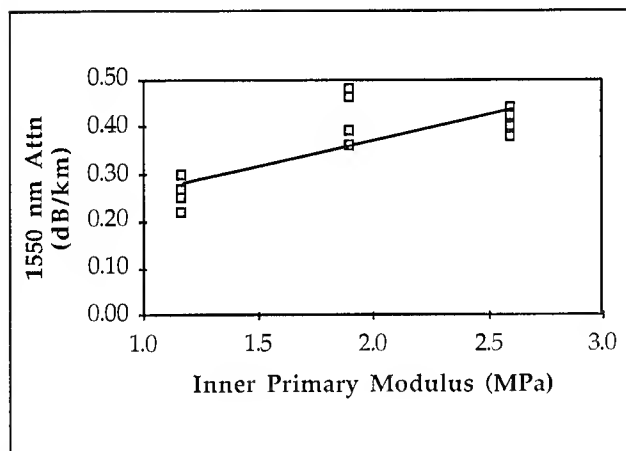


Figure 6 - Attenuation with Varying Inner Primary 180 μm Fiber

Hara previously identified this relationship, further noting that as the ratio of the outer primary thickness to outer primary radius increased (implying a thinner inner primary), the positive effect of low modulus inner primary materials on attenuation character became more pronounced. Referring to Figure 6, one would prefer to design ribbon fibers with inner primary materials possessing moduli as low as practically possible. We have found in numerous trial runs that enhanced microbending resistance can be achieved using fibers designed with progressively lower modulus inner primary materials.

Outer Primary

Within the scope of our development effort, we were somewhat restricted in varying the properties of the outer primary materials. This was largely due to the downsized diameters of the developmental fibers. While fiber break resistance is outside the scope of this paper, it is sufficient to say that we have found that some thin-coated fibers experience increased fiber break rates, as compared to 250 μm fibers, during processing. Additionally, their long-term reliability is reduced. Therefore, it was essential that higher modulus coatings be used in order to attain a higher degree of fiber protection [Glaesemann³].

It is well documented [Gloge⁴, Hara⁶, Saito⁷] that the thickness and modulus of the fiber outer primary coating can impact the attenuation character of a fiber design. Generally speaking, under lateral loading, the thicker the outer primary and the higher the modulus of this layer, the less bend sensitive the fiber due to increased stiffness of the outer shell. However, a balance must be obtained between the stiffness parameter, H , and the buffering parameter, D , to gain optimum ribbonized fiber attenuation performance.

Matrix Material

Given the rigid positioning of a fiber within a ribbon structure, the attenuation buffering properties of the matrix material which binds the fibers in a coplanar array must be considered. Other key matrix material considerations for which balance must be imposed are:

- Thermal performance.
- Ability to remove the individual fibers from the ribbon structure while leaving the original fiber coating/coatings intact with the fiber. (Breakout)
- Ability to handle and cable without ribbon structure degradation. (Toughness)
- Single or mass fiber strippability.

Of course, without acceptable initial room temperature attenuation performance, other key matrix material characteristics become unimportant. With this driving our experimentation, we performed tests focused toward low attenuation ribbons in the as-manufactured state, while noting other characteristics for future reference.

Our initial screening experiment (4³ fractional factorial) statistically demonstrated, at the 95% level of confidence, that 57% of the variation in bending induced attenuation for thin-coated fiber ribbons was accounted for by the matrix material. Further study of the data showed a strong correlation between matrix modulus and bending induced attenuation. As an example, through stepwise regression of the average 1-hour post-manufacturing 1550 nm attenuation data, a t -ratio of 8.44 was generated with respect to matrix modulus. With 29 degrees of freedom for the first

experiment, the critical t-ratio indicating significance at the 95% level of confidence is 1.699. Further studies holding the fiber type constant (similar fiber coating materials from one ribbon to the next) have repeatedly shown matrix modulus to be strongly correlated with average 1-hour 1550 nm attenuation character as shown in Figure 7.

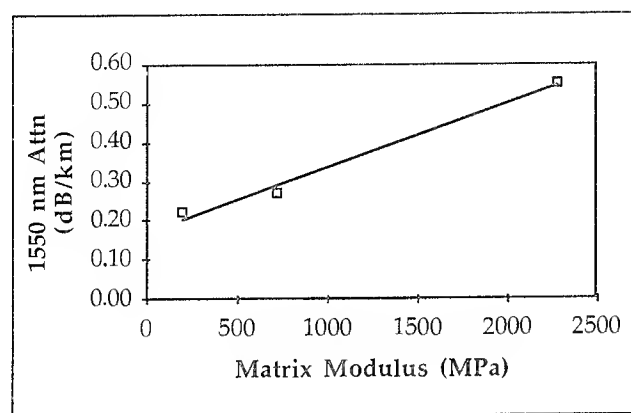


Figure 7 - Effect of Matrix Modulus on Attenuation of 180 μ m Fibers

Figure 7 clearly shows that higher modulus matrix materials provide less buffering effect to the small diameter fibers. This results in higher attenuations.

Data generated from the second series of experiments (2^2 factorials with centerpoints) support this correlation; however, an optimum region for modulus has been found between 100 and 400 MPa as shown in Figure 8.

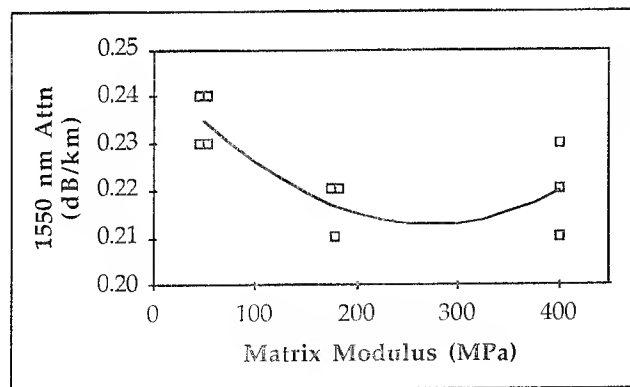


Figure 8 - Optimum Matrix Modulus Range (180 μ m Fibers)

Below 100 MPa, the attenuation buffering effect of the low modulus materials seems to diminish. The

reason for this has not been thoroughly investigated. We speculate that the blocking characteristics (cured material on cured material adhesion) and/or higher coefficients of friction associated with these materials cannot as easily accommodate subtle packaging anomalies experienced during winding. Thus, the ribbons cannot easily move to a lower strain. Similar behavior would be expected in a cabled environment.

Recall that these results were found using 180 μ m diameter matched clad fiber. We have since demonstrated that as the coated diameter of a fiber increases, the impact of the buffering effect of the matrix material diminishes. Notice in Figure 9 that, using 250 μ m fibers, the 1550 nm attenuation versus matrix modulus curve becomes essentially flat. This attribute is particularly evident as the inner primary coating diameter increases. Saito⁷ expressed this similar characteristic in terms of increasing ribbon height, and showed that the attenuation versus ribbon height curve substantially flattens at around a 0.25 mm ribbon height. The curve then becomes essentially flat at approximately 0.30 mm ribbon height regardless of the matrix material modulus.

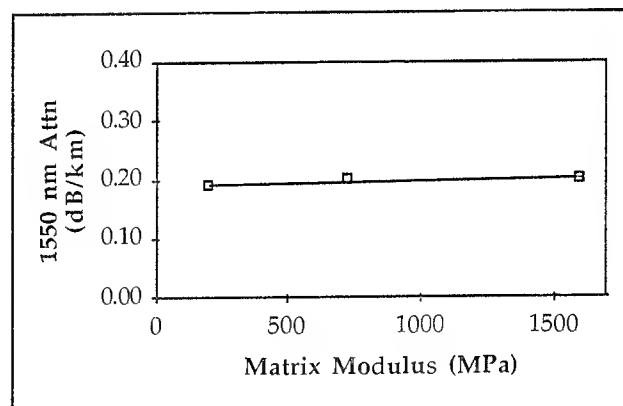


Figure 9 - Effect of Matrix Modulus on Attenuation of 250 μ m Diameter Fibers

Once we had successfully identified an optimum range of modulus for the matrix material, new materials were ordered per our new requirements from several suppliers. This exercise was performed in an effort to ensure that our predictions would hold true from one UV acrylate technology base to the next (across suppliers). Several ribbons were made in combination with each material and our sensitive (thin-coated) fibers, then checked for 1-hour manufacturing attenuation. In each case, we were able to achieve at or near fiber value attenuation characteristics; thus, confirming our predicted results - **the modulus range specified provides high level attenuation performance characteristics regardless of the material manufacturer.**

Results from the initial screening experiment clearly displayed the positive buffering effects of low modulus matrix materials. This led us to manufacture ribbons for cable prototypes to test our ribbon-based success. Closer inspection of the dry cable design (U-groove in this case) indicated that the low modulus matrix ribbons within a given stack may not easily slide over one another, as do those in a grease-filled cable design, when the matrix materials have high coefficients of friction or blocking characteristics. This would induce higher strains, most notably within the fibers of the top and bottom ribbons in a stack, leading to increased attenuation during handling and thermal cycling in the short term, unless strain relaxation could take place. Higher unresolved strains would subsequently result in long-term fiber reliability issues.

Unfortunately, the modulus of typical UV curable acrylate materials tends to decrease as the ribbon-to-ribbon coefficient of friction increases (within a given material type). We have tested cables with ribbons possessing ribbon-to-ribbon friction values ranging from approximately $\mu = 0.3$ to 1.1, and have found that optimum cabled results in U-groove cables are attained with ribbon-to-ribbon frictions at $\mu < 0.8$. Based on this observation, the use of low modulus matrix materials in dry cable designs did not seem feasible. However, realizing the potential positive benefits, we sought to develop a low modulus matrix material with lower frictional characteristics. To date, this has not been an industry standard. Therefore, we generated a new ribbon matrix coating specification list which included the low modulus and low friction combination, and sought suppliers who could develop a material meeting our requirements.

Using a newly developed low friction technology, we jointly worked with a supplier to develop an optimized ribbon matrix material possessing the key properties we identified. Table 4 shows the key mechanical properties of the optimized material as compared to a ribbon coating material more typically used in the ribbon market.

	Typical Ribbon Matrix	Optimized Ribbon Matrix
Modulus (MPa)	600 - 750	100 - 400
Ribbon-to-Ribbon Friction (μ)	≥ 0.8	0.3 - 0.4
Glass Transition Temperature ($^{\circ}\text{C}$)	40 - 50 w/sharp transition	40 - 50 w/subtle transition

Table 4 - Matrix Material Properties

The modulus of the new material is approximately 37% of that of typically deployed materials. The friction of the new material has been more than halved as compared to the typical ribbon matrix coating.

The development of a low modulus matrix material with a low friction character was a significant breakthrough in our development. This was a key which allowed us to achieve excellent cabled ribbon performance in room temperature as well as temperature cycling conditions.

Again referring to Table 4, it is particularly interesting to note the glass transition character of the optimized material. Referring to Figure 10, note the sharp tan delta peak and high low temperature modulus ($\sim 2,700$ MPa at -45°C) associated with typical ribbon matrix materials. In contrast to this, the optimized material has a very flat tan delta trace in combination with a lower relative modulus ($\sim 1,800$ MPa at -45°C) at low temperatures. The enhanced thermal character of the optimized material arises from the new backbone acrylate which exhibits a low thermal response over a broad temperature range due to a low degree of polar bonding between the molecular chains.

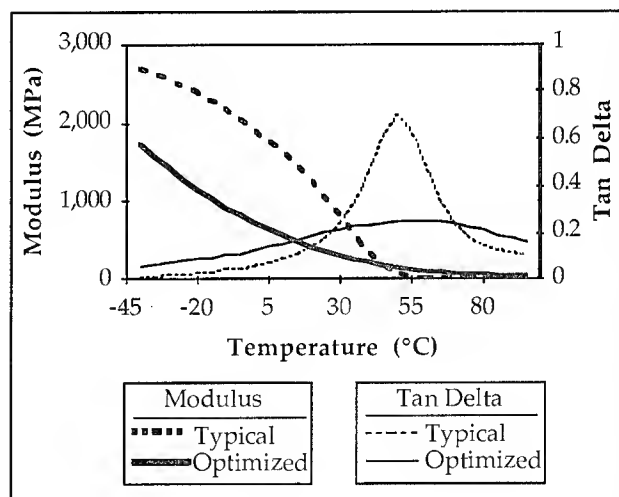


Figure 10 - Modulus and Tan Delta Curves for Typical and Optimized Matrix Materials

Ribbons were made and tested using the newly developed matrix material. We were able to manufacture ribbons with average 1-hour, post-manufacturing attenuation results consistently at 0.35 and 0.20 dB/km (equal to fiber values) at 1310 and 1550 nm respectively. Subsequently, U-groove cable designs were manufactured and tested that performed exceedingly well in all cable related testing. We

achieved temperature cycling performance to temperatures as low as -50 °C with less than or equal to 0.1 dB/km attenuation changes at both 1310 and 1550 nm. Additional tests performed in cable form [Wagman⁸] include winding and rewinding, figure 8'ing, and other performance and handling related tests.

CONCLUSION

Reduced diameter, or thin coated, fibers possess inherently higher sensitivity to bending induced attenuation than do standard 250 μ m diameter fibers. We have conducted development efforts on ribbons using these bend sensitive fibers as part of the development of ultra-high fiber count cables. As such, we were able to observe attenuation characteristics not typically noted with larger diameter fibers. This was accomplished through a series of iterative designed experiments for both fiber and ribbon UV curable coating materials. The development effort demonstrated that low modulus (100 - 400 MPa) ribbon coating materials having friction characteristics less than $\mu = 0.8$ provide greatly enhanced ribbonized fiber attenuation characteristics in thin-coated fiber ribbon structures. It was also shown that a higher thickness inner primary coating possessing a lower modulus provides a suitable environment in thin-coated fiber ribbon designs toward minimizing the ribbonized fiber delta attenuation characteristics. Using these concepts, in combination with a robust fiber outer primary coating, ribbons were manufactured that consistently exhibited low ribbonized fiber attenuation characteristics. Finally, reduced diameter fiber ribbons designed with materials possessing the key properties identified have been tested in high fiber count U-groove cable structures and exhibited performance to the level of standard diameter fibers.

ACKNOWLEDGEMENTS

The authors gratefully acknowledge the contributions of all technicians and engineers in the development teams at both Siecor RD&E and Corning R&D who so diligently worked to generate the valuable test results which allowed us to draw key conclusions in our development effort. The authors would also like to thank Clive Coady, Gregg Kuetemeyer, and David Szum of DSM Desotech Inc. for their valuable input and assistance in this project.

REFERENCES

1. Tomita, S., Matsumoto, M., Yabuta, T., & Uenoya, T., "Preliminary Research into Ultra High Density and High Count Optical Fiber Cables," *40th IWCS Proceedings*, St. Louis, MO, 1991, pp. 8 - 15.
2. Jackson, K.W., Santana, M.R., Sollenberger, N.W., Brown, R.J., Kroupa, K.M., & Webb, S.H., "A Modular Ribbon Design for Increased Packing Density of Fiber Optic Cable," *42nd IWCS Proceedings*, St. Louis, MO, 1993, pp. 20 - 27.
3. Glaesemann, G.S., "Process Handleability of Thin-coated Optical Fibers," *1994 Conference on Optical Fiber Communication Technical Digest*, Vol. 4, Feb. 20 - 25, 1994, pp. 243 - 244.
4. Gloge, D., "Optical-Fiber Packaging and Its Influence on Fiber Straightness and Loss," *The Bell System Technical Journal*, Vol. 54, No. 2, Feb. 1975, pp. 245 - 262.
5. Overton, R.J., Lopez, A.R., Michaud, H.M., Lasne, C., Sommer, R.G., "Designing An Optical Fiber Dual Coating System For Loose Tube And Ribbon Cable Long Line And Local Loop Applications," *42nd IWCS Proceedings*, St. Louis, MO, 1993, pp. 701 - 707.
6. Hara, M., Okagawa, S., Otake, A., "Design of Downsized Coated Optical Fibers To Minimize Microbending Loss," *41st IWCS Proceedings*, Reno, NV, 1992, pp. 20 - 24.
7. Saito, M., Okagawa, S., "16-Fiber Ribbon for Ultra-high Density and High-count Optical Fiber Cable," *42nd IWCS Proceedings*, St. Louis, MO, 1993, pp. 16 - 19.
8. Wagman, R.S., Bark, P.R., Cooke, H.G., Eoll, C.K., Livingston, R.O., Lochkovic, G.A., McAlpine, W.W., Sears, F.M., Sodhi, S.S., "Design Concepts for a 4000-Fiber Cable with Thin Coated 200 μ m OD Fiber," *43rd IWCS Proceedings*, Atlanta, GA, 1994.

AUTHORS



John R. Keesee
Siecor Corporation
489 Siecor Park (RD)
Hickory, NC 28603-0489
704-323-6267
siecor_rd@mike.lrc.edu
ATTN: John_Keesee

John R. Keesee received his bachelor's degree in Mechanical Engineering in 1991 from the Georgia Institute of Technology. He joined Siecor RD&E in 1991, and is currently working in the UV Development Group as a Product and Process Development Engineer. He is involved in the research and development of fiber optic ribbon cables.



David Smith
Corning Incorporated
SP-DV-02-4
Corning, NY 14831
607-974-3096
SMITH_DK@CORNING.COM

David Smith received a B.S. and an M.S. in Chemical Engineering from the University of Michigan, and an M.S. in Statistics from Rutgers University. He worked in R&D for DuPont from 1961 to 1972, and has been employed by Corning from 1972 to present. He specializes in statistical and reliability analysis, computer modeling, and optical fiber design in Corning's Math and Statistical Analysis Department.



Gregory A. Lochkovic
Siecor Corporation
489 Siecor Park (RD)
Hickory, NC 28603-0489
704-323-6224
siecor_rd@mike.lrc.edu
ATTN: Greg_Lochkovic

Gregory A. Lochkovic is the Supervisor for UV Development at Siecor RD&E in Hickory, NC. His responsibilities include the development of UV related products for both the domestic as well the Japanese markets. He has received a B.S.M.E. in 1985 from Purdue University and an M.S. in Manufacturing Systems from Clarkson University in 1993. He has worked in various areas of fiber optic cable product and process development since graduation in 1985, and has been with Siecor since 1991. He has been awarded 2 patents and has 2 publications.



J. Richard Toler
Corning Incorporated
SP-DV-01-8
Corning, NY 14831
607-974-3024
TOLER_JR@CORNING.COM

Dick Toler received his B.S. in Chemistry from Virginia Commonwealth University and his Ph.D degree in Organic Chemistry from the University of Virginia. He worked with Owens-Corning Fiberglas until 1986 when he joined Corning, Inc. He has worked on the development of coatings for optical fibers and optical fiber ribbons.

FUNDAMENTAL CHARACTERISTICS OF THE 500 kV XLPE CABLE

Masami Fukawa, Masato Asakawa

Tokyo Electric Power Company (Tokyo Japan)

T. Fukui, S. Fukunaga, H. Inoue, S. Osawa, K. Fudamoto, T. Hasegawa

Sumitomo Electric Industries, Ltd. (Osaka Japan)

Abstract

Problems for design, manufacture and installation of long distance 500 kV Cross linked polyethylene (XLPE) cable lines were depicted and evaluated. As a result, it was shown that XLPE cables with insulation thickness of 25 mm are applicable for 500 kV transmission lines. Extrusion molded joint (EMJ) was also demonstrated applicable for 500 kV lines.

1. Introduction

To meet the growing demand for electric power, introduction of a 500 kV trunk transmission system into the Tokyo metropolitan area is planned around 1998. XLPE cable technology is making steady progress and use at higher voltages is becoming possible through improvement in production process. It has already been applied to 275 kV long-distance transmission lines (insulation thickness 27 mm with joints).

Conventional extra-high voltage transmission lines mainly use oil-filled (OF) cable, however, it is expected that the 500 kV trunk lines will use XLPE cables for ease of maintenance and preservation of the environment (considering that XLPE cables are oil-free and applicable to long distances and complex terrains). The problems that had to be solved to achieve the goal above are as follows:

- 1) Reduction insulation thickness (25 to 27 mm) to make cable external diameter comparable with OF cable, and
- 2) Development joint with high reliability.

As 500 kV XLPE cables will be used at unprecedented electric stress (nearly twice that of 275 kV XLPE cables), we carried out basic research to investigate the characteristics of XLPE cables and joints required to realize 500 kV power transmission line system. The results of this research are reported in this paper.

2. XLPE Cable

2-1 Design of XLPE Cable Insulation

The thickness of the XLPE cable insulation is usually determined from the following Equations (1) and (2). These equations give the insulation thickness

needed to withstand AC voltage and lightning impulse voltage. Insulation thickness is determined from these values.

Insulation thickness needed for AC voltage (t_{AC}):

$$t_{AC} = \frac{V_{AC}}{E_{L(AC)}} \dots \dots \dots (1)$$

where:

V_{AC} : AC withstand voltage
 $= (V_0 / \sqrt{3}) \cdot k_1 \cdot k_2 \cdot k_3 \text{ (kV)}$

V_0 : Maximum line to line voltage(kV)

k_1 : Temperature coefficient

k_2 : Deterioration coefficient

k_3 : Allowance for uncertain factors

$E_{L(AC)}$: Design stress (kV/mm)

Insulation thickness needed for lightning impulse voltage (t_{imp}):

$$t_{imp} = \frac{V_{imp}}{E_{L(imp)}} \dots \dots \dots (2)$$

where:

V_{imp} : Lightning impulse withstand voltage
 $= BIL \cdot k'_1 \cdot k'_2 \cdot k'_3 \text{ (kV)}$

BIL: Basic impulse insulation level (Determined from the system insulation coordination) (kV)

k'_1 : Temperature coefficient

k'_2 : Deterioration coefficient against repetitive

k'_3 : Allowance for uncertain factors

$E_{L(imp)}$: Design stress (kV/mm)

The design stress $E_{L(AC)}$ and $E_{L(imp)}$ are obtained as follows. The cable insulation breakdown data conform to the Weibull distribution given by Equation (3), and the location parameter E_L is mathematically stress at which the breakdown probability $F(E)$ becomes zero. This parameter has been used for the design stress.

$$F(E) = 1 - \exp\left(-\left(\frac{E - E_L}{E_0}\right)^m\right) \dots \dots \dots (3)$$

Where,

$F(E)$: Probability of breakdown occur before stress E

E_L : Location parameter

E_0 : Scale parameter

m : Shape parameter

The deterioration coefficient for AC voltages, k_2 , is obtained as follows. The relationship between applied voltage and time until insulation breakdown is called the "V-t characteristics" and has the relationship shown in Fig. 1.⁽¹⁾

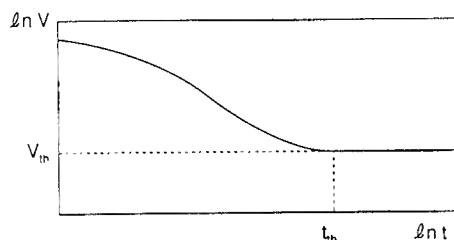


Fig. 1. General V-t curve

The characteristics in the high stress region are generally well described by the equation, $V^n \cdot t = \text{constant}$, where the lifetime exponent, "n", increases with decrease in applied voltage, and saturates ($n = \infty$) below a certain threshold voltage (V_{th}), where it may be considered that practically no deterioration of insulation occurs. However, there is no consensus regarding the threshold time (t_h) to V_{th} .

As an alternative, the following Equation (4) is used to determine k_2 that translates the operating voltage design lifetime of 30 years into 1-hour design AC voltage by using "n" and assuming $V^n \cdot t$ to be a constant:

$$k_2 = (30 \text{ years} \cdot 365 \text{ days} \cdot 24 \text{ hours} / 1 \text{ hour})^{1/n} \quad \dots \dots (4)$$

2.2 Evaluating the Reduction of Insulation Thickness

(1) Improvement of design stress E_L : The major factor governing the insulation performance of XLPE cables (when there is no external influence of moisture) is defects within the insulation, such as voids, impurities, and protrusions on semi-conductive layer. Electric tree are generated from these defects and propagate to cause insulation breakdown. Major improvements in manufacturing technique for XLPE cables of 66 kV or more, and resultant increases in E_L are shown in Table 1. Increase in E_L is due to improvements in manufacturing technology, such as eliminating harmful voids (by changing from steam cure process to a dry cure process) and reducing sizes of impurities in the insulation and protrusions on the semi-conductive layer (by more stringent control of material defects by resin manufacturers, use of finer screen meshes, advances in compound techniques, etc).

Recently, we developed a pre-breakdown partial discharge detection (PPD) method⁽²⁾ which makes it possible to locate defects that are the origin of insulation breakdown before these defects are burnt out. When this method was applied to a model cable (insulation thickness = 2 mm), it was revealed that impurities or protrusions on semiconductive layer were the origins of insulation breakdown, and that a smaller defect increased breakdown electric field stress (see

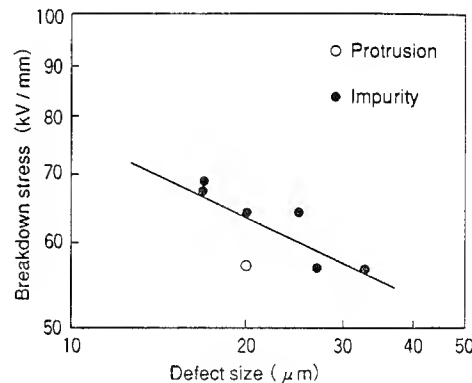


Fig. 2. Relation between defect size and the breakdown stress

Table 1. Improvement of manufacturing technology and E_L for over 66 kV XLPE cable

Defect	Manufacturing technology	'70	'71	'72	'73	'74	'75	'76	'77	'78	'79	'80	'81	'82	'83	'84	'85	'86	'87	'88	'89	'90	'91		
Void	Cure process	Steam		Dry (radiant curing process)																					
Impurity	Screen mesh size	Level I														Level II					Level III (275 kV class)				
	Clean level of extruding room	Level I																				Level II			
Protrusion	Screen mesh size	Level I														Level II									
$E_L^{(*)}$	(kV/mm)	$E_{L(AC)}$	20		30														35					40	
		$E_{L(imp)}$	50		80														90					100	

(Note) Obtained from the results of breakdown test for 66 & 77 kV XLPE cable

Fig. 2) ⁽³⁾. Since still greater reduction of impurities has been achieved in the latest ultra-high-voltage (UHV) XLPE cable manufacturing equipment, the E_L of UHV XLPE cables has been increased and reductions in the insulation thickness have been possible compared to conventional XLPE cables.

(2) Revaluation of lifetime exponent “n”: We have been using the value $n = 9$ for lifetime exponent assuming that deterioration was mainly due to partial discharge considering the results of experiments with samples containing artificial voids ⁽⁴⁾. This value was used because steam cured cable contains voids of larger than $10 \mu m$, thus it was safer to choose voids as the key factor affecting insulation performance rather than impurities or protrusions, and the effects of external moisture were not well understood. However, the voids contained in dry cured cables are so small that there is little probability of partial discharge. In addition, only impurities and protrusions can be assumed as the key factors affecting the insulation performance for UHV cables with metallic sheaths that prevent water penetration from the outside.

The lifetime exponent “n” obtained from the experiments so far on samples containing impurities and protrusions was sufficiently larger than 9, and as a result, it is possible to reduce AC withstand voltage, thereby reducing the insulation thickness. However, because of the high operating electric stress, it is important that the long-term influences on cable performance from bow-tie tree caused by the initial moisture contained in the insulation be identified.

(3) Selection of evaluation items: From (1) and (2) above, we decided to carry out optimal design of insulation for 500 kV XLPE cables using model cables prepared by the same manufacturing equipment and material control procedures as the UHV XLPE cables to evaluate the following:

- 1) Design stress E_L
- 2) Lifetime exponent “n”
- 3) Effect of initial moisture contained in insulation on long term performance of cables.

2-3 Evaluation of Design Stress E_L

The model cable (insulation thickness = 6 mm, conductor size = $150 mm^2$) used for testing had an inner to outer diameter (d/D) ratio comparable to that of the 500 kV cable with insulation thickness of 25 to 27 mm and conductor size of $2500 mm^2$. Figure 3 shows the results for the past three years of insulation breakdown

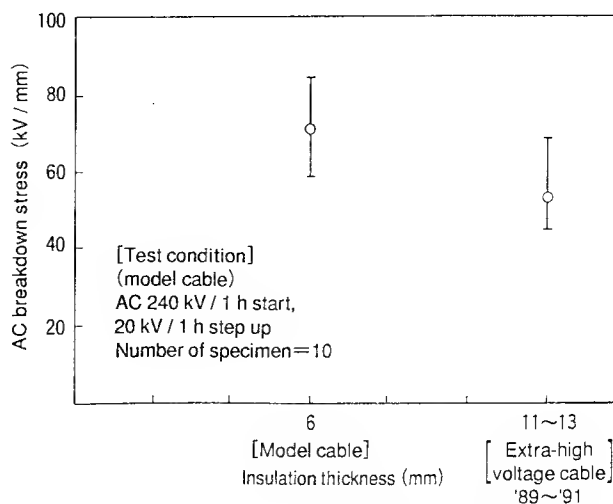


Fig. 3. Cable insulation thickness and the AC breakdown stress

tests for 66 & 77 kV class XLPE cables (extra-high voltage (EHV)). The breakdown stress determined from Equation (3) is $E_L = 43 kV/mm$ for the EHV XLPE cable and $E_L = 56 kV/mm$ for the model cable. It has been reported that E_L is dependent on insulation thickness according to the following Equation ⁽⁵⁾, although the reason for this is not well understood.

$$E_L = A \cdot t^{n-1} \quad \dots \dots \dots (5)$$

where,

t : Insulation thickness

A, n : Constants indicating dependence on insulation thickness

When E_L is calculated for 25 to 27 mm insulation using the value $n = 0.87$ from reference (5) and the results above, we get E_L values of 46.1 to 46.5 kV/mm for the model cable and of 38.2 to 39.5 kV/mm for EHV XLPE cables. Thus, even when we consider the dependence on the insulation thickness, it is clear that the value of E_L has improved for UHV XLPE cables compared to EHV XLPE cables. As a result it is possible to use $E_{L(AC)} = 40 kV/mm$ for insulation design of 500 kV XLPE cables. Further, although lightning impulse tests were not made this time, it is expected that $E_{L(imp)} = 80 kV/mm$ can be used for lightning impulse voltage based on the breakdown data of the present 275 kV XLPE cables and the $E_{L(AC)}/E_{L(imp)}$ ratio.

2-4 Evaluation of Lifetime Exponent n

Long term tests were conducted for aluminum sheathed cable with the same insulation thickness and conductor size as described above and with the aluminum sheath end portions sealed to prevent entry of moisture from outside.

(1) Test Conditions : Assuming the lifetime exponent to be $n > 15$, the following three levels for which insulation breakdown is expected to occur in 100, 1,000, and 3,000 hours respectively, were chosen (based on the relation ship, $V^n \cdot t = \text{constant}$, and with consideration of the initial breakdown voltage) :

- first step : 280 kV (46.7 kV/mm)
- second step : 250 kV (41.7 kV/mm)
- third step : 240 kV (40.0 kV/mm)
- Number of specimen : 5 points x 3 voltages
- Test temperature : Heat cycle (the current is applied for 8 hours until the conductor temperature reaches 90°C, and followed by 16 hours of natural cooling in air.)

(2) Test Result : Figure 4 shows the results of tests. A lifetime exponent of $n = 18.3$ was obtained by connecting the time plots at which the probability of insulation breakdown at the each test voltage determined from Equation (6) is 50%.

$$F(t) = 1 - \exp\left(-\left(\frac{t}{t_0}\right)^a\right) \dots\dots\dots (6)$$

Where,

$F(t)$: Probability of breakdown before time t

t_0 : Scale parameter

a : Shape parameter

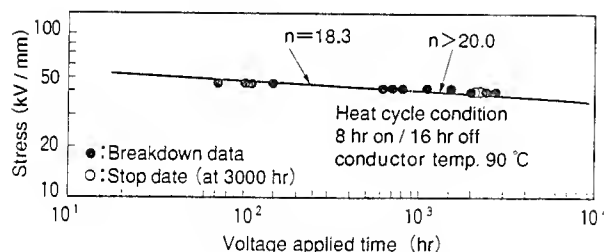


Fig. 4. V-t characteristics of XLPE cable

This result is far greater than the lifetime exponent obtained with the sample containing voids, and close to the value for the sample containing impurities or protrusions. This suggests that long-term performance of the cable is affected chiefly by impurities or protrusions, rather than voids. From this, it is considered safer to use a value of $n = 15$ for the lifetime exponent of the cable manufactured suppressing, as much as possible, the generation of voids and preventing effects from outside moisture.

2-5 Effect of Initial Insulation Moisture on Long Term Cable Performance

An aluminum-sheathed model cable with an insulation

thickness of 2 mm, and conductor size of 150 mm² was used for these tests. After the moisture contained in the insulation was modified through drying and humidification processes, the aluminum sheath end portion was sealed. The sample cables were classified by their moisture contents into normal cable (around 100 ppm), dry cable (below 50 ppm), and saturated cable (around 200 ppm). The dependence of bow-tie tree on the moisture content was then examined through long-term electric loading tests.

(1) Test Conditions :

<Initial test>

- Sample cables: 5 samples each
- Test temperature: Ambient
- Voltage elevation rate:

After 80 kV / 1hr applied, then 7 kV / 1hr step up

<Long-term test>

- Test voltage : Assuming a lifetime exponent of $n = 15$, a test voltage of 70 kV (35 kV/mm), at which insulation breakdown is expected in 500 hours, was chosen based on initial breakdown value.
- Voltage applied period: 50 and 500 hours and after the voltage is removed, the samples were tested for breakdown using the PPD method.
- Number of specimen : 5 specimens each x 2 voltage
- Test temperature: Heat cycle (the current is applied for 8 hours until the conductor temperature reaches 90°C and followed by 16 hours of natural cooling in air.)

(2) Test Results : While some humidified samples occurred the breakdown during the long-term test, all normal and dried samples survived the test. Figure 5 shows the breakdown test results after long-term test. The humidified samples show a slight decrease in insulation breakdown voltage while the values for dried and normal samples were almost the same as the

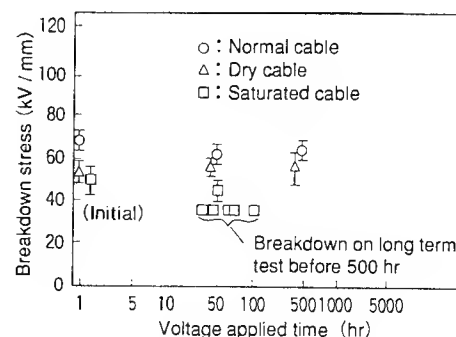


Fig. 5. Results of breakdown test after long term test

initial value. PPD succeeded for one dried 500 hour sample and one humidified 50 hour sample. For dried samples, electric tree origins was impurity and no bow-tie tree was observed (Fig. 6) For the humidified samples, electric tree origin was impurity generated bow-tie tree (Fig. 7). Microscopic examination revealed that bow-tie tree generated only in the humidified samples. Figure 8 shows the relationship between the sizes and the number of bow-tie tree. No significant difference exists in the numbers of bow-tie tree in the 50 and 500 hour samples.

This suggests that the growth of bow-tie tree is saturated between 50 and 500 hours. Since humidified cables during long-term tests and the breakdown values obtained were lower than the initial values, it is considered that the growth of bow tie tree influences



Fig. 6. Results of PPD method for dry cable

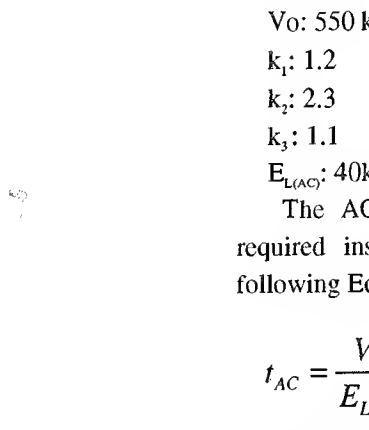


Fig. 7. Results of PPD method for saturated cable

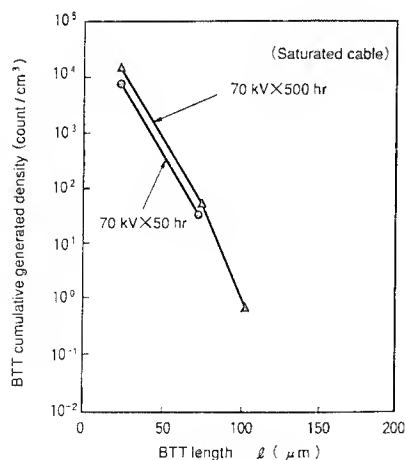


Fig. 8. Bow-tie tree N-I distribution

long term performance. However, even during initial tests, breakdown values are lower than for normal cables, thereby indicating that the humidifying process eliminates cross-linking byproducts such as acetophenone, etc. It was shown, meanwhile, that the moisture initially contained in the insulation does not affect the long-term performance since no bow-tie tree was observed with the normal and dried cables.

2-6 Insulation Thickness of 500 kV XLPE Cable

The insulation thickness for the 500 kV XLPE cable was calculated using the design stress (E_L) and the lifetime exponent "n" determined in the section above. The other design parameters were determined based on the past design values and the recent study.

Insulation thickness for AC voltage (t_{AC})

The following are the design constants used for calculation:

V_0 : 550 kV

k_1 : 1.2

k_2 : 2.3

k_3 : 1.1

$E_{L(AC)}$: 40 kV/mm

The AC withstand is thus $V_{AC} = 970$ kV. The required insulation thickness, t_{AC} , is given by the following Equation:

$$t_{AC} = \frac{V_{AC}}{E_{L(AC)}} = \frac{970}{40} = 24.3 \text{ mm}$$

Insulation thickness for lightning impulse voltage (t_{imp})

The following are the design constants:

BIL : 1425 kV

k'_1 : 1.25

k'_2 : 1.0

k'_3 : 1.1

$E_{L(imp)}$: 80 kV/mm

The lightning impulses withstand voltage is thus $V_{imp} = 1960$ kV. The required insulation thickness, t_{imp} , is given by the following Equation:

$$t_{imp} = \frac{V_{imp}}{E_{L(imp)}} = \frac{1960}{80} = 24.5 \text{ mm}$$

Choosing the larger insulation thickness from the values for AC and Imp. voltages, an insulation thickness of 25 mm can be used for the 500 kV XLPE cable.

3. Joint

Reliable joints are vital for realizing long-distance

transmission lines of 500 kV XLPE cables. At present, for 275 kV transmission lines with high operating voltages, extrusion molded joints (EMJs) manufactured with the same quality controls as the cables have been developed and are being used more widely. Since the operating electric stress in 500 kV EMJs is nearly double that of 275 kV EMJs, we investigated the feasibility of 500 kV EMJs by studying basic characteristics and performance of the crucial parts.

3-1 Selecting EMJ Parts for Performance Improvement

Figure 9 shows breakdown test data (collected since 1988) for the 275 kV EMJ⁽⁶⁾, classified by breakdown locations. This data shows that the breakdown locations are concentrated at the reinforcing insulation sleeve (location A) and insulation screen treated portion (location B). The electric stress at location A may be reduced by increasing the reinforcing insulation thickness, while the location B cannot be improved by structural design of the EMJ because electric stress G_{min} (near the insulation screen) is determined by the insulation thickness of the cable.

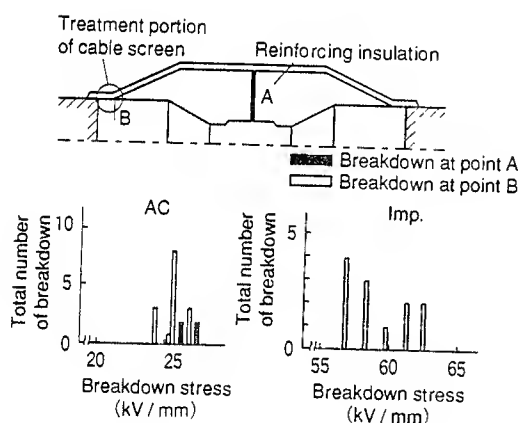


Fig. 9. Breakdown stress and breakdown location of 275 kV EMJ

The target performance for 500 kV EMJs are as listed in Table 2 and target performance for the insulation screen treatment portion have not been met according to measurements made (see Fig. 9) for 275 kV EMJs. We therefore decided to evaluate the possibility of realizing the performance target by identifying part defects and improving them. Note that the electric stress indicated in this table is calculated for a large sized conductor (which makes G_{min} large).

3-2 Investigation of EMJ Defects

The insulation of the 275 kV EMJ was cut and the defects causing breakdown were examined. We used a

Table 2. Required performance of 500 kV EMJ

	AC	Impulse
Withstand voltage	970kV/1hr	1960kV/3times
Withstand stress G_{min} (kV/mm)	30	60

Note: Insulation thickness of cable: 25mm

metallurgical microscope of 100X-400X to observe : sizes and numbers of protrusions, impurities and voids as shown in Table 3. The results of these investigations are shown in Fig. 10. The impurities and protrusions from the inner and outer semiconductive layers have higher amount of defects when compared with those of the cable. The protrusions on the treatment portion of the insulation screen have particularly high amount of defects compared to other parts. However, the size and number of voids for the EMJ is comparable to that of the cable, indicating that, similar to the cable, it is possible to control the size of voids by controlling the temperature and pressure in the extrusion and cross-linking processes. As a result, it is assumed that factors governing the performance of EMJs are impurities and protrusions, as for the cable itself. In particular, although the level of protrusions in the insulation

Table 3. Synopsis of method checked concerning defects

Item	Synopsis of method	Part checked	
		Reinforcing insulation portion	Treatment portion of insulation screen
Protrusions of semiconductive layer interface	100-to 400-power electron microscope observation of semiconductive layer interface and insulation (measurement of size/number)	○	○
Impurities and Voids in insulation		○	—

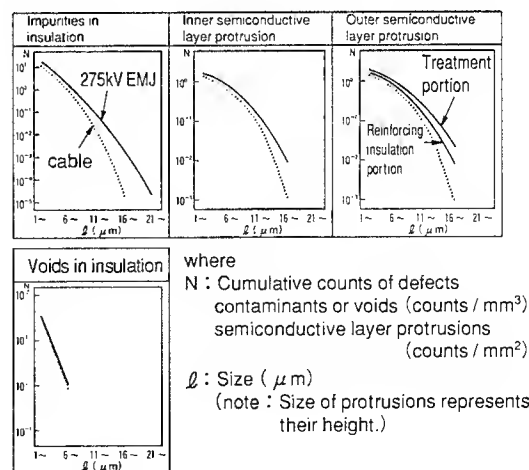
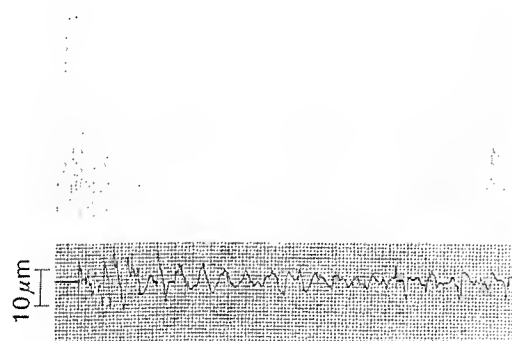


Fig. 10. Comparison of 275 kV EMJ and cable defects

screen treatment portion is high, this is probably because the insulation in that part is finished by manual operations with glass when making the connections and the surface roughness formed remains as projections when the outer insulation screen is fixed over them. Since the electric stress at this portion is determined by insulation thickness and cannot be controlled by design of the structure, this is a part that must be significantly improved to obtain better performance.

3-3 Performance Improvement Measures for the Treatment Portion of Insulation Screen

To evaluate if surface finishing really causes the Protrusions in the insulation screen treatment portion, the surface roughness of the insulation was measured after the insulation screen was scraped off with glass. Fig. 11 shows a sample measurement result. The level of surface roughness is 15 to 20 μm , which shows



(a) Surface finished with glass



(b) Surface finished with the new manufacturing method
Fig. 11. Example of measurement of the surface roughness

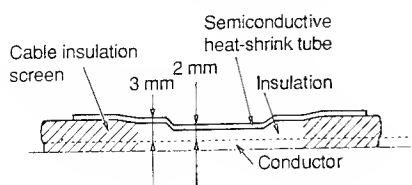


Fig. 12. Structure of model sample

good agreement with the measured size of the outer semiconductive layer protrusions shown in Fig. 10. It is likely that the roughness develop into protrusions. It was assumed that protrusions could be reduced by improving surface roughness after the outer semiconductive layer is scraped off. To improve surface smoothness, we employed a method of melting cable insulation and applying a heatshrink tube on the molten insulation to smooth the surface. Fig. 11 shows that surface roughness was significantly reduced to about 1 μm when this method was applied.

An electrical test was conducted to verify if the protrusions were the source of breakdown in the treated portion of the insulation screen. The model tested, as shown in Fig. 12, which consists of a insulation of 2 mm insulation thickness and a simulated treated portion of insulation screen. Defects were detected with the PPD test. An example of the protrusions detected in the PPD test is shown in Fig. 13. The test results in Table 4 indicate that the partial discharge stress level and the protrusion level have been improved with the new process. This is considered to contribute to the

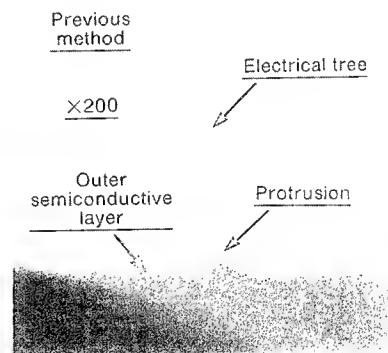


Fig. 13. Example of defect

Table 4. Results of PPD test

Finishing method	Stress detected pre-breakdown partial discharge: $G_{min}^{1)}$ (kV/mm)	Defect		Testing condition
		Kind of defect	Size (μm)	
Previous method (with glass)	71.2	Protrusion	20	AC 40 kV/ 10 min start → 10 kV/ 10 min step up
New manufacturing method (with heat-shrink tube)	80.3	Protrusion	10	

1) G_{min} is represented by average of 5 data.

improvement in the electrical characteristics. However, the level of projections is $20\ \mu\text{m}$ when the insulation screen is removed by glass. This is improved to about $1\ \mu\text{m}$ with the new polishing operation, and then is deteriorate to about $10\ \mu\text{m}$ when the insulation screen is applied again and cross-linking is carried out. This increase in the level of the protrusions is considered due to the recovery (to some extent) during cross-linking of the earlier smooth surface.

3-4 Evaluation of Performance Improvement on the Model EMJ

The new improved process was applied to the model EMJ shown in Fig. 14 and AC breakdown and impulse breakdown tests were conducted. The taper length in the new process has been doubled to reduce the stress in the axial direction. The test results in Table 5 confirm that the new process results in the improved performance of 10% for both the AC breakdown stress and the impulse breakdown stress. The results of investigating the protrusion level of the insulation screen treated portion are shown in Fig. 15.

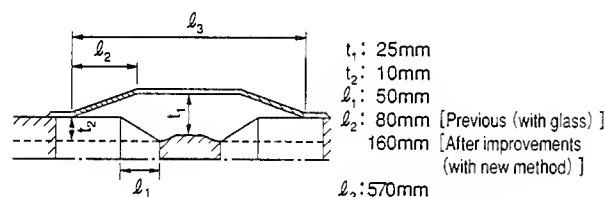


Fig. 14. Design dimensions of model EMJ

These show that there is a difference in the level (due to the finishing method), that agrees with the improvements in electrical performance. Next, the model EMJ prepared using the new process was subjected to long-term tests. The results of these tests in Table 6 indicate that the model EMJ had not broken down even after the specified time duration, thus confirming an equivalent life of over 30 years for the 500 kV EMJ. Following the long-term tests, breakdown

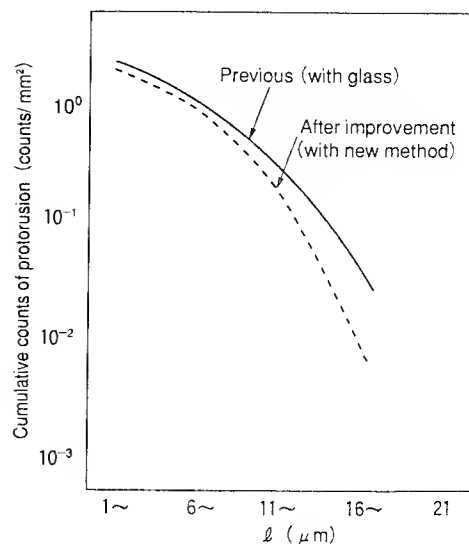


Fig. 15. Relation between the protrusion size and the cumulative counts

Table 6. Long-term test result

Synopsis of method		Test result
Number of specimen	2	3.1 months good
Applied voltage	190kV	
Test term	3 months	
Heat cycle	Conductor temp. 90°C 8hrs ON 16hrs OFF	

Table 7. Breakdown test result after long-term test

Breakdown voltage after long-term test ¹⁾		Breakdown voltage before long-term test ¹⁾		Testing condition
Breakdown voltage (kV)	Breakdown portion	Breakdown voltage (kV)	Site of breakdown	AC240kV/1hr → 30 kV/1hr step up
450	Treatment portion of insulation screen	498	Treatment portion of insulation screen	

Note 1) Breakdown voltage is represented by average.

Table 5. Test results of model EMJ

Finishing method	AC ¹⁾		Impulse ¹⁾		Breakdown portion	Testing condition
	Breakdown voltage (kV)	G_{min} (kV/mm)	Breakdown voltage (kV)	G_{min} (kV/mm)		
Previous method (with glass)	450	38.9	990	85.7	Treatment portion of cable screen	AC: 240kV/1hr start → 30kV/1hr step up Imp.: 600 kV/ 3shots → 30 kV/ 3shots step up
New manufacturing method (with heat shrinkable tube)	498	43.1	1092	94.4		
Breakdown voltage ratio	1.1		1.1			

Note 1) Breakdown voltage and G_{min} are represented by average.

tests were conducted. The results in Table 7 shows the same levels as initial breakdown stress.

3-5 Breakdown Stress Evaluation for Full-Size EMJ

One defect expected to cause deterioration of the EMJ performance is protrusions in the insulation screen treated portion. In the insulation screen treated portion protrusion level was improved using the model EMJ to improve performance. As the next step, the performance of a full-size EMJ designed for 500 kV cables was evaluated. The dimensions of the full-size EMJ are shown in Fig. 16. The thickness of cable insulation was designed at 25 mm as shown in Section 2-6 (to evaluate the electric stress on the insulation screen treated portion), and the cross-sectional area of the conductor was 2,500 mm². The test results, summarized in Table 8, confirm that the full-size EMJ is suitable for the use as a 500 kV EMJ.

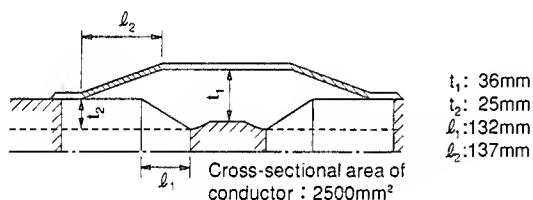


Fig. 16. Design dimension of actual EMJ

Table 8. Withstand voltage test results of actual EMJ

Kind of voltage	Test result	Required performance
AC	1190kV/1hr OK	970kV/1hr
Imp	2360kV/3shots OK	1960kV/3shots

4. Conclusions

Different aspects related to the design of the insulation required for application to long distance 500 kV XLPE cables were investigated. From the results of these studies it is possible to develop cables with an insulation thickness of 25 mm. Joints for such cables were investigated. EMJ has the capability to be used for joints at 500 kV and is practically applicable. In the future, we intend to solve the remaining problems and undertake extensive evaluation of this technology (including the thermomechanical stress effects expected in real transmission lines) as a part of development and field tests. We also plan to continue investigations to achieve higher reliability.

References

- (1) G. Bahder et al. IEEE Trans. PAS-101, P.1379 (1982).
- (2) K. Furukawa et al. "Analysis of insulation breakdown using PPD method" Sumitomo Electric Technical Review No. 139 (1991) (in Japanese).
- (3) T. Tanaka et al. JICABLE91 P.318 (1991).
- (4) Electric joint research association report Vol.34 No.1 (1978).
- (5) T. Kubota et al. 1992 IEEE National Convention No. 1460 (1992). (in Japanese).
- (6) H. Ishihara et al. "Improvement in reliability of extrusion molded joint for 275 kV XLPE cable" 1991 IEEE SM 513-2 PWRD.
- (7) Y. Takahashi et al. "Improvement of electrical performance of extrusion molded joint" 1992 Power and Energy Division National Conference of IEEE No.302 (1992) (in Japanese).

BIOGRAPHY

Masami Fukawa was born in Kanagawa Prefecture, Japan on March 20, 1950. He graduated from Yokosuka technical high school, Kanagawa, Japan, in 1968. He joined Tokyo Electric Power Co., Inc., in 1968 and has been engaged in underground transmission and transformation facilities and research and development of advanced power cables. Mr. Fukawa is a member of the IEEE.

Masato Asakawa was born in Chiba prefecture, Japan on November 12, 1961. He received the M.S. degree in electrical engineering from Nihon University, Japan in 1986. He joined Tokyo Electric Power Co., Inc., in 1986. He has recently been engaged in research and development of EHV cables and their accessories in Engineering Development Center of TEPCO. Mr. Asakawa is a member of the IEEE.

Takeshi Fukui was born in Nara Prefecture, Japan on July 26, 1945. He received the B. S. degree in Electrical Engineering from Kyoto University, Kyoto Japan, in 1968. In 1968 he joined Sumitomo Electric Industries, Ltd. and has been engaged in research and development on EHV power cables and their accessories. Mr. Fukui is a member of the IEEE.

Sadao Fukunaga was born in Tokushima Prefecture, Japan on April 10, 1949. He received the B. S. degree and M. S. degree in Electrical Engineering from Tokyo University, Tokyo Japan, in 1972 and 1974 respectively. In 1974 he joined Sumitomo Electric Industries, Ltd. and has been engaged in research and development on EHV power cables and their accessories. Mr. Fukunaga is a member of the IEEE.

Hitoshi Inoue was born in Osaka Prefecture, Japan on October 15, 1951. He received the B. S. degree in Electrical Engineering from Hiroshima University, Hiroshima Japan, in 1974. In 1974 he joined Sumitomo Electric Industries, Ltd. and has been engaged in research and development on EHV power cables and their accessories. Mr. Inoue is a member of the IEEEJ.

Shigeki Osawa was born in Aichi prefecture, Japan on October 28, 1949. He received the B.S. degree in Electrical Engineering from Waseda University, Tokyo Japan, in 1972. He joined Sumitomo Electric Industries, LTD in 1972 and has been engaged in design and development of power cables. Now he is a vice president of Sumitomo Electric USA Inc., and a member of IEEE and IEEEJ.

Koji Fudamoto was born in Ehime Prefecture, Japan on August 20, 1962. He received the B. S. degree and M. S. degree in Electrical Engineering from Okayama University, Okayama Japan, in 1985 and 1987 respectively. In 1987 he joined Sumitomo Electric Industries, Ltd. and has been engaged in research and development on the accessories for EHV power cables. Mr. Fudamoto is a member of the IEEEJ.

Takaaki Hasegawa was born in Hyogo Prefecture, Japan on December 27, 1963. He received a B. S. degree in electrical engineering from Kobe University, Hyogo Japan in 1988. In 1988 he joined Sumitomo Electric Industries, Ltd. and has been engaged in research and development on the accessories for EHV power cables.

EVALUATION OF SERVICE AGED EPR CABLES

Carlos Katz - Fellow IEEE
Cable Technology Laboratories, Inc.
New Brunswick, New Jersey

Michael Walker - Member IEEE
Houston Lighting & Power Company
Houston, Texas

ABSTRACT

Data is presented from laboratory evaluation of eighteen 15 kV and eleven 35 kV ethylene propylene rubber (EPR) insulated cables removed from field installations at Houston Lighting and Power Co. (HL&P), after being in service for up to twenty-two years. Of the twenty-nine cables in the study, sixty percent (60%) were manufactured by one company. The data on these is compared with similar data on the other cables, which were made by five manufacturers.

The results indicate that all cables, except some of the older ones, are aging at a slow rate. Extrapolation of the voltage breakdown data on cables up to eighteen years old indicate that they may remain in-service well in excess of thirty years. The cable voltage breakdown data was supplemented with measurement of physical, analytical and other electrical properties.

INTRODUCTION

Over a period of three years, Cable Technology Laboratories, Inc. (CTL) has been testing 15 and 35 kV EPR insulated feeder cables removed from service at the Houston, Texas metropolitan area. The evaluations have been made to establish the rate at which these cables age. In recent months an article,^[1] was presented which summarized findings on a portion of these cables made by one manufacturer that had been in service for up to twenty-two years. With one exception,^[2] the technical literature does not report on similar studies made on other EPR cables. The exception relates to a single, eighteen years in-service cable.

When [1] was presented, questions were raised as to how the data on the cables of this one manufacturer compare with the performance of other EPR cables with different formulations. Since cables made by six companies had been evaluated, and all had been removed from the same system, it was decided to expand on the article. It should be noted that of the six manufacturers, three have ceased to exist as independent organizations.

The aim of this paper, is to compare the aging characteristics of EPR cables made by different manufacturers, with different insulation and shielding compounds. It is recognized, that some of the manufacturers use proprietary compounds whose individual properties are quite different.

The results of many investigations have been published on the degradation of service aged polyethylene (PE) and crosslinked polyethylene XLPE cables.^[3,4,5,6] Polyethylene insulated, high voltage cables have been in utility service since the early 1940's, while XLPE and EPR insulated cables made their arrival in the early and mid 1960's, respectively. HL&P has been using EPR insulated cables since the late 1960's. Some of the older cables evaluated in this program, are among the earliest made. The service record of the EPR cables has been satisfactory.

While the analysis of performance of PE and XLPE cables is simplified by the fact that the insulations are translucent and most manufacturers have used the same type of compound over the years, these simplifications are not available with respect to mineral-filler-reinforced ethylene-propylene rubber (EPR) or ethylene-propylene-diene-terpolymer rubber (EPDM) where the materials are opaque and many manufacturers have their own formulation. Additionally, each formulation includes 10 or more ingredients. In the context of this paper both the EPR and the EPDM insulated cables are being referred to as EPR insulated cables.

The degradation of EPR cable has been studied for many years in the laboratory.^[7,8,9,10,11] However, with the named exceptions^[1,2] no information has been available on cables aged under service conditions. This article expands [1] by making available information on an additional fourteen cables and provides an estimation of expected life for the newer type of EPR cables (<18 years old).

CABLES EVALUATED

Both 15 and 35 kV, EPR insulated feeder cables are in use at Houston. HL&P removed in excess of 270 ft. (87 m) from each of twenty-nine sites and submitted them for evaluation to obtain an idea of the change in cable characteristics. Removal was facilitated by the fact that these cables are installed in ducts. Six different manufacturers were identified among the 29 sets of cables, with the bulk (18) having been supplied by one manufacturer. Three other manufacturers were represented by three cables each and two more by one cable each.

The manufacturer (A) of the eighteen cables provided information indicating that his five oldest cables (more than eighteen years old) had been made with a fully amorphous resin, incorporating carbon black as part of the filler system. The other thirteen cables had been made from a proprietary

TABLE 1. 15 kV EPR INSULATED CABLES FROM IN-SERVICE

Cable No.	Cable Service Years	Made by Manuf.	Conductor			Cond. Shield Type	Insulation			Insul. Shield Type*	Jacket Matl.
			Size		Matl.		Thickness		Color		
			kcmil	mm ²			mils	mm			
1	22	A	500	253	Cu	Tape	220	5.6	Black	Tape	Neop.
2	22	A	1000	507	Cu	Tape	220	5.6	Black	Tape	PVC
3	22	E	500	253	Cu	Extr	220	5.6	Black	Tape	Neop.
4	22	A	500	253	Cu	Tape	220	5.6	Black	Tape	PVC
5	20	F	750	380	Al	Extr.	175	4.4	Dk. Grey	Extr.	PVC
6	20	A	1,000	507	Al	Extr.	220	5.6	Black	Tape	PVC
7	19	A	750	380	Al	Extr.	175	4.4	Black	Extr.	PVC
8	18	F	750	380	Al	Extr.	175	4.4	Dk. Grey	Extr.	PVC
9	17	F	1,000	507	Al	Extr.	220	5.6	Dk. Grey	Extr.	PVC
10	13	A	750	380	Al	Extr.	175	4.4	Dk. Pink	Extr.	PVC
11	12	A	750	380	Al	Extr.	175	4.4	Dk. Pink	Extr.	PVC
12	12	A	750	380	Al	Extr.	175	4.4	Dk. Pink	Extr.	PVC
13	12	A	1,000	507	Al	Extr.	220	5.6	Dk. Pink	Extr.	PVC
14	10	D	750	380	Al	Extr.	175	4.4	Lt. Pink	Extr.	PVC
15	9	D	750	380	Al	Extr.	175	4.4	Lt. Pink	Extr.	PVC
16	8	A	1,000	507	Al	Extr.	220	5.6	Dk. Pink	Extr.	PVC
17	5	A	750	380	Al	Extr.	175	4.4	Dk. Pink	Extr.	PVC
18	2	A	1,000	507	Al	Extr.	220	5.6	Dk. Pink	Extr.	PVC

*Followed by Cu tape shield

*Followed by Cu tape shield

ethylene propylene copolymer, pink in color, which has a low level of crystallization. According to manufacturer A the same base polymer has been used over the last eighteen years. Other information indicated that changes had been introduced in the process of preparing the compound. It was understood that in the earlier years, the compound was mill-stripped, later it was pelletized. During the last ten to twelve years, the compound has incorporated a peroxide absorption system and continuous improvements have been made in screening out impurities and hard particles. The formulation of the semiconducting compound used by this manufacturer for conductor and insulation shielding, is based on EPR and the compound has changed very little over the last twenty years.

Little is known by the authors on the details of the insulation compounds used in the other cables. Manufacturers use proprietary EPR mixtures containing ethylene propylene copolymers denoted EPM or ethylene-propylene-diene-terpolymers, in the manufacture of medium voltage cables. These compounds are referred to as EP rubbers or EPR's. Information on crystallization, molecular weight distribution and other parameters, that define the nature and specific characteristics of the compounds, are rarely made public. The compounds used for semiconducting shields also are not known by the authors. It is known that some manufacturers use semiconducting XLPE for either the conductor or insulation shield or both. It is also known that all of these systems use a peroxide curing method, and that the cables are normally made in triple tandem extrusion processes, using steam as the heat transfer and pressurizing medium.

15 kV CABLES - These eighteen cables made by five different manufacturers, operated in service at 12.5 kV. Depending on age and conductor size (Table 1), they had 175 or 220 mils (4.4 or 5.6 mm) of insulation thickness. Except for some twenty-two and twenty year old cables, that had semiconducting fabric tape shields, all of the other cables

had extruded semiconducting shields. The dark gray color of the insulation is a variation of the black compound, having a lower content of carbon black. The dark gray cables in this group were all made by the same manufacturer. The non-metallic insulation shield was followed by a copper tape, applied helically and by a jacket. Except for cables 1 and 3, which had Neoprene, the other cables had all polyvinyl chloride (PVC) jackets. The use of copper as a conductor material was abandoned by HL&P about twenty years ago in favor of aluminum.

35 kV CABLES - These eleven cables were made by four different manufacturers and operated in service at 34.5 kV. All cables (Table 2) had the same size aluminum conductor and the same insulation thickness. The two older cables, made by manufacturer B, incorporated carbon black as part of the insulation. The extruded insulation shield in the three older cables was followed by copper tape, while in the rest it was followed by flat copper ribbons, 0.025 x 0.25

TABLE 2. 35 kV EPR INSULATED CABLES FROM IN-SERVICE*

Cable No.	Cable Service Years	Made By Manuf.	Insulation Color	Metallic Shield
1	19	B	Dk. Grey	Cu. Tape
2	17	B	Black	Cu. Tape
3	10	C	Lt. Pink	Cu. Tape**
4	10	A	Dk. Pink	Cu. Rib
5	9	A	Dk. Pink	Cu. Rib
6	8	B	Dk. Pink	Cu. Rib
7	7	A	Dk. Pink	Cu. Rib
8	7	A	Dk. Pink	Cu. Rib
9	6	D	Lt. Pink	Cu. Rib
10	4	A	Dk. Pink	Cu. Rib
11	2	A	Dk. Pink	Cu. Rib

* All cables had 1250 kcmil (633 mm²) stranded Al. conductor, extruded conductor and insulation shields, 345 mils (8.8 mm) of insulation and a PVC jacket

** Longitudinally corrugated

in. (0.635 x 6.35 mm), applied in parallel, in an open spiral. The cables had a PVC jacket overall. The time in-service and other design details are given in Table 2.

SERVICE ENVIRONMENT - All cables operated under similar environmental conditions. The cables had been installed in 6 in. (0.15 m) concrete encased PVC conduits; three cables in one conduit. The conduit system was filled with water the majority of the time, with the load on the cables being about 50% of their capacity and operating consistently at that level.

The service area of 5,000 sq. miles (13,000 km²) is flat. Approximately half of the service area is about 30 to 60 ft. (10 to 20 m) above sea level. The area has a very high lightning (isokeraunic) level. The average soil temperature, at the depth of the duct system, 4 ft. (1.2 m), is approximately 10°C with an average year round ambient mean temperature of approximately 28°C. The cable system is totally underground except where it enters substations. In the substations, the cables are protected by distribution class metal oxide arresters.

CHARACTERIZATION OF CABLES

Generalities - Immediately after the cables were removed from the ground, short sections of same were cut and submitted promptly to the laboratory for moisture content analysis. Cable ends were sealed. About 270 to 300 ft. (81 to 90 m) sections of each cable were submitted to the laboratory where they were stored inside a building. Because of equipment constraints and time required to execute the tests, it became necessary to store some of the cables for as long as six months. In each case, about three weeks prior to testing, the jacket and metallic coverings were removed and the cable cores placed in water containers. This procedure was used to restore moisture, which may have diffused out of the insulation system in the intervening time. Samples received for evaluation corresponded to two or three of the installed phases.

The short sections submitted immediately after cable removal from the ground and sections taken from the same cables just before initiating laboratory tests, were subjected to moisture analysis. Comparison of results indicated that the moisture in the outer part of the insulation, of both samples, was within 10% of each other. This provided assurance that the cables, as removed from the ground and as tested had about the same moisture content.

The long lengths of cable received at the laboratory were cut into shorter pieces just before testing. For a.c. and impulse voltage tests, samples approximately 27 to 30 ft. (8.1 to 9 m) in length were used. While the cables were in storage or in water, prior to testing, no voltage was applied. Evaluations were performed using current AEIC Specifications (AEIC CS6-87).^[12] Because testing of all cables was done over a period of three years, and initially not all tests had been scheduled, full characterization for all cables is not available. Some tables also present data for a recent new cable made by manufacturer A.

Visual Examination - The initial examination of each cable length consisted of inspecting the outside of the jackets to make sure that they did not contain breaks through which

water could have penetrated into the cable core. All jackets were found to be in satisfactory condition.

Inspection of the metallic shields revealed that most of them had corroded (Table 3). The degree of corrosion varied. In some of the older cables, the shield was in poor condition, it had become quite brittle, showing small holes and cracks. It is well known today that PVC jackets permit the permeation of moisture.

Most of the older cables (more than eight years old) had different degrees of corrosion of the conductor strands. There were some exceptions among the newer 35 kV cables where in spite of the thicker insulation wall, corrosion of the strands was observed. In the case of the Cu conductors, the corrosion was characterized by a darkish discoloration of the strand surface, while in the case of the Al conductors, the strands had developed a white coating characteristic of aluminum oxide. In some of the cables, moisture had entered into the conductor from the ends. In some other cables, it was obvious that the moisture had penetrated radially through the insulation wall, in these cables the outer strand layer was covered profusely with the aluminum oxide.

TABLE 3. VISUAL EXAMINATION OF CABLE COMPONENTS

Cable No.	Service Years and Manuf.	Corrosion		Voids		Contaminants	
		Cond. Strands	Copper Shield	No. per in. ² /cm ²	Max. Size mils/mm	No. per in. ² /cm ²	Max. Size mils/mm
15 kV Cables							
1	22 A	Yes	Yes	None	—	11/1.76	13/0.33
2	22 A	Yes	Yes	None	—	238/38.3	8/0.20
3	22 E	Yes	Yes	None	—	None	—
4	22 A	Yes	Yes	15/2.4	16/0.4	None	—
5	20 F	No	Yes	None	—	None	—
6	20 A	No	No	None	—	13/2.1	10/0.25
7	19 A	No	Yes	None	—	None	—
8	18 F	Yes	Yes	None	—	3/0.5	9/0.22
9	17 F	No	Yes	None	—	None	—
10	13 A	Yes	Yes	None	—	37/5.9	10/0.25
11	12 A	Yes	Yes	None	—	31/5.0	8/0.20
12	12 A	No	Yes	None	—	None	—
13	12 A	No	Yes	None	—	7/1.1	5/0.12
14	10 D	Yes	Yes	None	—	None	—
15	9 D	No	No	15/2.4	16/0.4	None	—
16	8 A	No	No	None	—	None	—
17	5 A	No	Yes	None	—	None	—
18	2 A	No	No	None	—	None	—
35 kV Cables							
1	19 B	No	Yes	None	—	6/1	9/0.22
2	17 B	Yes	Yes	None	—	150/24	7/0.18
3	10 C	Yes	Yes	None	—	None	—
4	10A	Yes	No	None	—	162/26	11/0.27
5	9 A	Yes	Yes	None	—	None	—
6	8 B	Yes	Yes	None	—	None	—
7	7 A	No	No	None	—	None	—
8	7 A	No	No	None	—	None	—
9	6 D	Yes	Yes	1/0.16	8/0.2	None	—
10	4 A	Yes	Yes	None	—	None	—
11	2 A	No	No	None	—	None	—

Microscopic Examination for Imperfections in the

Insulation - Microscopic examination of cross-sectional wafers of the insulation system (insulation plus non-metallic shields) were made. To cut the wafers, the conductors were dislodged by pushing out the strands. Since EPR compounds, in general, are quite elastic and the

semiconducting layers tend to smear, when cut at ambient temperature, the insulation was slowly frozen to about -20°C. The freezing imparted hardness to the insulation system. To assure proper cutting, very sharp knife blades were used. Slices were approximately 20 to 25 mils (0.5 - 0.6 mm) thick, with uniform, smooth surfaces. Microscopic examination of the slice surfaces were made for the presence of voids, protrusions from and into the insulation, contaminants and water tree formations.

Twenty cross-sectional slices from each of the cables, were used to establish the presence of voids, contaminants and protrusions, Table 3 provides the results of the examinations. Of the twenty-nine cables examined, only three had voids. Two of these were made by the same manufacturer. Ten cables were found to contain contaminants. All of these were ten years or older, providing certain assurance that improvements in compound processing are being achieved. In the context of this paper, contaminants are all elements (particles) which have a contrasting coloration with that of the insulation, even if these are poorly mixed ingredients of the compound. No protrusions, of any type, were found in the twenty-nine cables examined. It is to be noted, that cables which had an abundance of contaminants are the same ones which showed the greatest amount of water trees during subsequent examinations.

Stripping Strength - The adhesion of the semiconducting insulation shield to the insulation should be permanent over the life of the cable. It has been found that when the adhesion is lost, moisture collects at the interface and in time permeates the insulation in a concentrated manner. Water trees are found to be more numerous in cables having loose insulation shields. With three exceptions (Table 4) the adhesion of the insulation shield was found to meet present day AIEC specification requirements for this property. Two of the exceptions had very low adhesion. One of these was a cable with black insulation, the other, an eight year old cable that had water trees. It was not possible to establish if the low adhesion was a consequence of the passage of time or if the cables had been manufactured with this characteristic. The third exception was a 35 kV cable having excessive adhesion.

Physical Properties of the Insulation - Tensile strength and elongation of the insulation were measured in accordance with ASTM D412, on three thin specimens cut from close to the conductor shield. The values (Table 4) are the average of each set of tests. Retainage of tensile strength and elongation are related to characteristics of each compound and to the manner in which each ages. In general, for manufacturer A, the tensile strength of the black EPR insulation appears to be lower than that for the newer, pink EPR. It also appears that the tensile strength in the latter, changes very little over time, while elongation in these cables appears to drop somewhat. The compounds used by other manufacturers have higher tensile strength. With the exception of a 22 year old cable, the elongation of all other cables is in a relatively narrow range.

Moisture Content - Measurements of moisture in the insulation were performed on samples taken from the

TABLE 4. CHARACTERIZATION OF CABLE COMPONENTS

Cable No.	Service Years and Manuf.	Stripping Strength		Tensile Strength lb/in ² / kg/cm ²	Elongation %
		Min. lb/kg	Max. lb/kg		
15 kV Cables					
1	22 A	—	—	880/62	210
2	22 A	—	—	—	—
3	22 E	—	—	1010/71	560
4	22 A	—	—	—	—
5	20 F	11/5.0	12/5.4	1640/115	250
6	20 A	—	—	—	—
7	19 A	14/6.3	16/7.3	890/63	250
8	18 F	2/0.9	3/1.3	—	—
9	17 F	12/5.4	13/5.8	1700/119	250
10	13 A	8/3.6	9/4.1	1140/80	230
11	12 A	10/4.5	11/5.0	1100/77	230
12	12 A	7/3.2	8/3.6	—	—
13	12 A	11/5.0	12/5.4	1480/104	270
14	10 D	11/5.0	13/5.8	1830/128	290
15	9 D	12/5.4	13/5.8	—	—
16	8 A	12/5.4	13/5.8	1030/72	220
17	5 A	6/2.7	7/3.2	—	—
18	2 A	8/3.6	9/4.1	1370/96	290
35 kV Cables					
1	19 B	10/4.5	11/5.0	1070/75	250
2	17 B	2/0.9	4/1.8	—	—
3	10 C	9/4.0	10/4.5	1680/118	230
4	10 A	7/3.2	9/4.0	—	—
5	9 A	6/2.7	8/3.6	1360/96	280
6	8 B	25/11.2	27/12.1	1610/113	270
7	7 A	7/3.2	8/3.6	—	—
8	7 A	6/2.7	7/3.2	1230/86	250
9	6 D	20/9.0	21/9.4	1720/121	250
10	4 A	4/1.8	5/2.3	1200/84	250
11	2 A	8/3.6	9/4.1	1160/82	270
—	0 A	6/2.7*	8/3.6*	1130/79*	320*
*Typical values for cables of recent manufacture					

*Typical values for cables of recent manufacture

outermost and innermost 25% of the insulation wall of each cable. Tests were performed using an Automatic Titration Karl Fischer Moisture Analyzer (manufactured by Mitsubishi Model CA-05) Two to three tests were performed on each cable. The reported values (Table 5) are the average of each set of measurements. The individual results were within 10% of each other. For comparison purposes, Table 5 also provides moisture content on new cables (not exposed to soil moisture) made by manufacturer A. The results, regardless of manufacturer, indicate that older cables, containing carbon black particles, have a higher level of moisture. Most likely this is related to the affinity of carbon black for water. There is a higher moisture content towards the outside of the insulation wall and moisture content tends to increase with time. In addition it should be noted that: a) one of the black EPR cables had a moisture content twice as high as that of other EPR cables made at about the same time, b) the dark gray cables (made by manufacturer F) had a greater moisture content than cables from about the same age by manufacturer A, c) the cables from manufacturers C and D had a lower moisture content than that of similar age cables by manufacturer A, d) the moisture content of the insulation increases rather rapidly in the early years of aging.

Water Trees - Because of their dark color it was considered of no use to examine the insulation of the older

TABLE 5. MOISTURE IN CABLE INSULATION

Cable No.	Service Years and Manuf.	Moisture Content - ppm	
		Close to Insulation Shield	Close to Conductor Shield
15 kV Cables			
1	22 A	3.87	3.05
3	22 E	7.67	7.09
5	20 F	3.98	3.01
7	19 A	3.52	2.94
9	17 F	3.94	3.03
10	13 A	3.24	3.02
11	12 A	2.37	2.78
13	12 A	2.98	2.80
14	10 D	1.90	1.83
16	8 A	2.93	2.40
18	2 A	2.20	1.85
—	0 A	1.81*	1.58*
35 kV Cables			
1	19 B	3.32	2.98
3	10 C	2.13	2.03
5	9 A	2.65	2.31
6	8 B	2.83	1.91
8	7 A	2.74	2.34
9	6 D	2.14	1.72
10	4 A	2.89	2.78
11	2 A	2.64	2.05
—	0 A	1.64*	1.55*
*New cables as received from manufacturer			

*New cables as received from manufacturer

(more than seventeen years old) cables. With only a few exceptions, indicated in Table 6, water trees 2 to 50 mils (0.05 to 1.25 mm) in length, were found in the insulation of the cables, regardless of manufacturer.

Prior to microscopic examination the slices were subjected to staining of their surfaces. The method used is a modification of the technique used for methylene blue dyeing of crosslinked polyethylene insulation. Methods for examination for the presence of water trees in EPR

insulation have been described in the literature.^[5,13] The present method is somewhat similar to that described in [13]. The modification consists of subjecting the slices to multiple staining periods totaling about 20 hours. It should be noted that, in the case of EPR insulation, the visual examination has to be restricted to the surface and therefore, the observed water trees are being reported as trees per unit surface.

Most of the water trees started at the location of contaminants or voids in the bulk of the insulation. Table 6, summarizes the number of trees and their location on 30 slices examined, per cable length. Figure 1 illustrates some of the water trees found.

Dielectric Constant and Dissipation Factor - Table 7 provides results on these properties, measured at ambient temperature. The black compounds have higher dielectric constant and higher dissipation factor than the pink compounds, regardless of manufacturer. There are, however, substantial differences among individual compounds. The narrow range in dielectric constant and dissipation factor for cables less than 13 years old, appears to be indicative of the consistency of composition of the materials and also indicative of limited changes over time. In the case of manufacturer A, there is a slightly higher dissipation factor for the aged cables, possibly a consequence of moisture permeation and formation of water trees. It has been shown in [14], that both PE and XLPE cables having extensive water trees, have higher dissipation factor. This may also be the case with the EPR insulated cables. It should be noted, for example, that among the 15 kV cables made by manufacturer A, No. 12, which has the largest water trees, also has the highest dissipation factor.

Volume Resistivity of Shields - Present AEIC specification requirements allow for resistivities as high as 1000 ohm-m for the conductor shield and 500 ohm-m for the insulation shield. Except for the insulation shield of a 19

TABLE 6. WATER TREE ANALYSIS*

Cable No.	Service Years and Manuf.	Bow Tie Trees						Vented Trees					
		Number			Max. Length - mils			Number			Max. Length - mils		
		Ø1	Ø2	Ø3	Ø1	Ø2	Ø3	Ø1	Ø2	Ø3	Ø1	Ø2	Ø3
15 kV Cables													
10	13 A	18	16	22	35	30	50	0	0	0	—	—	—
11	12 A	11	12	16	30	30	30	0	0	0	—	—	—
12	12 A	7	8	—	38	40	—	1**	0	—	20	—	—
13	12 A	11	15	17	17	20	20	0	0	0	—	—	—
14	10 D	11	12	7	10	20	10	0	2**	0	—	5	—
15	9 D	0	0	—	—	—	—	0	0	—	—	—	—
16	8 A	6	8	12	18	20	20	0	0	0	—	—	—
17	5 A	0	2	—	—	20	—	0	0	—	—	—	—
35 kV Cables													
3	10 C	28	29	32	40	38	20	0	2**	3**	—	5	10
5	9 A	12	31	14	20	30	20	0	2**	0	—	10	—
6	8 B	14	16	15	20	20	30	0	0	0	—	—	—
7	7 A	0	0	0	—	—	—	0	0	0	—	—	—
8	7 A	5	6	8	15	10	15	0	0	0	—	—	—
9	6 D	24	24	30	35	20	20	0	5**	0	—	20	—
10	4 A	11	13	12	20	20	20	0	0	0	—	—	—
11	2 A	0	0	0	—	—	—	0	0	0	—	—	—
*Only trees larger than 2 mils (0.05 mm) considered;													
**Initiating from the conductor shield													

*Only trees larger than 2 mils (0.05 mm) considered;

**Initiating from the conductor shield

(a)

(b)

(c)

(d)

Figure 1 - Water Trees in EPR Insulated Cable - a and b in 12 Year Old, 15 kV (60X), c and d in 6 Year Old, 35 kV (40X)

TABLE 7. DIELECTRIC CONSTANT AND DISSIPATION FACTOR

Cable No.	Service Years and Manuf.	Dielectric Constant at V_0	Dissipation Factor - %		
			at 1.5 V_0	at 2.5 V_0	at 3 V_0
15 kV Cables					
1	22 A	3.87	1.09	1.17	—
3	22 E	3.28	1.22	1.29	1.43
4	22 A	—	0.59	0.61	0.67
5	20 F	3.02	0.31	0.32	0.33
7	19 A	3.59	1.06	1.18	—
8	18 F	—	0.37	0.43	0.49
9	17 F	3.02	0.56	0.58	0.62
10	13 A	2.80	0.40	0.41	0.42
11	12 A	2.84	0.35	0.36	0.37
12	12 A	—	0.50	0.60	0.67
13	12 A	2.92	0.36	0.37	0.38
14	10 D	2.85	0.30	0.30	0.32
15	9 D	—	0.24	0.26	0.32
16	8 A	2.94	0.36	0.38	0.42
17	5 A	—	0.34	0.39	0.44
18	2 A	2.97	0.34	0.36	0.41
35 kV Cables					
1	19 B	3.06	0.46	0.46	0.47
3	10 C	2.85	0.20	0.20	0.25
5	9 A	3.05	0.38	0.41	0.43
6	8 B	2.75	0.22	0.22	0.23
7	7 A	—	0.32	0.34	0.38
8	7 A	2.91	0.29	0.29	0.31
9	6 D	2.76	0.25	0.25	0.28
10	4 A	2.95	0.32	0.34	0.40
11	2 A	2.71	0.34	0.35	0.37

year old, 35 kV cable, all of the cables meet this requirement. Without having data on the cables as manufactured, it is not possible to establish if the shields have changed over time. It is assumed, because of the low resistivities measured, that this is not the case. It is to be noted, that the three cables having the highest volume resistivities were all made by the same manufacturer, no doubt, a characteristic of the compound used. It should also be noted that the two cables which have the highest volume resistivity of the insulation shield, have a high level of adhesion to the insulation, another characteristic of the same compound. The volume resistivity of the compounds used (by each manufacturer) appear to have been maintained relatively consistent, over time.

TABLE 8. VOLUME RESISTIVITY

Cable No.	Service Years and Manuf.	Volume Resistivity - ohm-m			
		Insulation Shield		Conductor Shield	
		at 90°C	at 110°C	at 90°C	at 130°C
15 kV Cables					
1	22 A	5.9	3.7	2.4	1.8
2	22 A	22.4	15.9	0.2	0.1
3	22 E	0.4	0.4	0.4	0.4
4	22 A	9.1	6.9	3.8	1.3
5	20 F	59.0	20.6	6.2	2.0
6	20 A	3.8	1.4	4.8	2.1
7	19 F	2.1	1.9	3.1	1.6
8	18 F	17.1	13.9	1.9	0.7
9	17 F	172.0	189.0	12.4	3.9
10	13 A	2.4	1.6	6.9	3.3
11	12 A	3.0	2.1	8.6	3.1
12	12 A	3.8	2.4	3.4	1.6
13	12 D	4.6	3.3	8.3	1.9
14	10 D	4.4	2.4	0.7	0.6
15	9 A	3.0	2.1	1.1	1.0
16	8 A	4.1	1.8	6.1	1.5
17	5 A	0.7	0.7	1.0	0.6
18	2 A	0.8	0.6	0.6	0.5
35 kV Cables					
1	19 B	4,300.0	3.020.0	87.0	106.0
2	17 B	4.2	2.3	720.0	590.0
3	10 C	2.7	1.3	0.9	0.7
4	10 A	2.6	1.6	3.1	1.7
5	9 A	2.0	1.5	2.1	1.3
6	8 B	216.0	138.0	0.9	0.8
7	7 A	1.5	1.2	2.6	1.1
8	7 A	0.7	0.5	2.5	1.1
9	6 D	17.0	5.1	1.4	1.0
10	4 A	0.4	0.4	1.9	0.9
11	2 A	3.2	2.0	1.5	0.8
—	0 A	1.7	1.3	0.8	0.6

A.C. Voltage Breakdown - The long lengths of cable submitted were cut into ten (10) individual sections. Five of the sections were used for a.c. voltage and five for impulse voltage testing to breakdown. For the a.c. voltage tests, about 10 ft. (3.0 m) of each cable section were used for terminations. The active test lengths were 17-20 ft. (5.2 - 6.1 m). Voltage was first applied at 20 kV and increased in steps of 10% of the last applied voltage, maintaining at each level for five minutes. The insulation thickness next to each failure was measured and the average breakdown voltage stress calculated. All tests were conducted at room temperature. The data points in Table 9 and in Figures 2

through 5 are the 63% probability of breakdown based on a Weibull distribution of five breakdowns. The two curves, in each of Figures 2 through 5, are the best fit for the breakdowns on the newer (pink color) EPR cables of manufacturer A only, and on all the pink cables combined.

Table 9, together with Figures 2 and 3, summarize the a.c. voltage breakdowns obtained on the cables tested. The clear outlined symbols represent the older cables, that had carbon black, while the dark symbols represent cables with pink insulation.

In comparing the older 15 kV cables it becomes clear that the cables from manufacturer F (dark gray color), are performing better than those from manufacturers A and E. As a matter of fact, these cables appear to approach the quality of the newer (pink color) EPR cables.

In the case of 35 kV cables, the black EPR cables also have lower breakdown voltage. However, in this case, the difference between the black and pink insulations is not as great. Assuming similar original breakdown levels, for the older (black) and the newer (pink) cables, there does not appear to be a significant difference in the rate at which these cables are aging, regardless of manufacturer.

Tests performed on new cables of various manufacturers indicate about the same average level of a.c.

TABLE 9.
A.C. AND IMPULSE VOLTAGE BREAKDOWN STRENGTH

Cable No.	Service Years and Manuf.	A.C.		Impulse	
		V/mil	kV/mm	V/mil	kV/mm
15 kV Cables					
1	22 A	170	6.7	560	22.0
2	22 A	220	8.7	800	31.5
3	22 E	220 ⁽¹⁾	8.7 ⁽¹⁾	700 ⁽¹⁾	27.6 ⁽¹⁾
4	22 A	120	4.7	525	20.7
5	20 F	360	14.2	930	36.6
6	20 A	165 ⁽¹⁾	6.5 ⁽¹⁾	—	—
7	19 A	140	5.5	680	26.8
8	18 F	345	13.6	980	38.6
9	17 F	310	12.2	845	33.3
10	13 A	405	15.9	1,020	40.2
11	12 A	450	17.7	1,200	47.2
12	12 A	360	14.2	980	38.6
13	12 A	440	17.3	1,140	44.9
14	10 D	570	22.4	1,320	52.0
15	9 D	500	19.7	1,410	55.5
16	8 A	295	11.6	1,110	43.7
17	5 A	480	18.9	1,360	53.5
18	2 A	750	29.5	1,400	55.1
—	0 A	800	31.5	1,900	78.5
35 kV Cables					
1	19 B	260	10.2	825	32.5
2	17 B	255	10.0	890	31.5
3	10 C	365	14.4	1,280 ⁽¹⁾	50.4 ⁽¹⁾
4	10 A	380	15.0	1,010	39.8
5	9 A	295	11.6	1,195	47.0
6	8 B	275	10.8	1,060	41.7
7	7 A	430	16.9	990	39.0
8	7 A	530 ⁽¹⁾	20.9 ⁽¹⁾	1,185 ⁽¹⁾	46.7 ⁽¹⁾
9	6 D	450	17.7	1,140	44.9
10	4 A	315	12.4	1,320	52.0
11	2 A	600	23.6	1,200	47.2
—	0 A	750	29.5	1,700	66.9

⁽¹⁾ 50% probability based on 3 tests only

⁽¹⁾ 50% probability based on 3 tests only

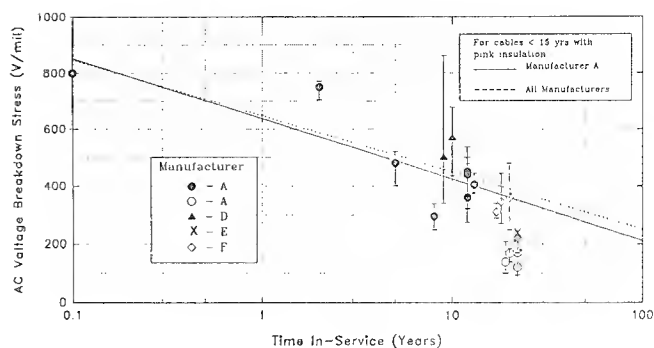


Figure 2 - AC Voltage Breakdown Strength of 15 kV EPR Insulated Cables

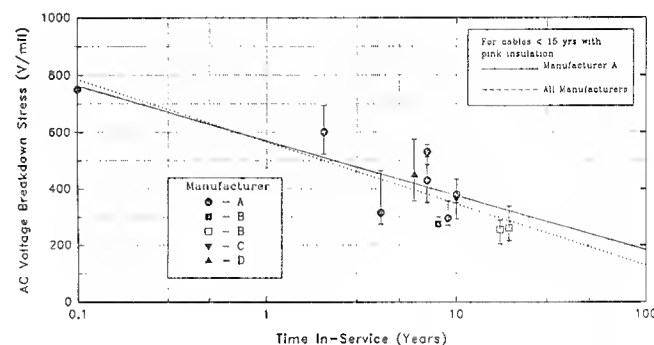


Figure 3 - AC Voltage Breakdown Strength of 35 kV EPR Insulated Cables

voltage breakdown, between 700 and 900 V/mil (28 - 36 kV/mm), justifying the use of the same base point, for results on new cables.

The range of results for individual cables, (presented in the graphs by the vertical lines) indicates that for most field aged cables, the variation in breakdown strength along the length is quite significant and that a comparison between cables of different vintage and manufacturer should be based on statistical analysis.

Comparison of the rate of degradation as established by the a.c. voltage breakdown indicates that both the 15 and 35 kV cables are degrading at about the same rate.

Impulse Voltage Breakdown - Five individual samples were tested for each cable. The tests were performed at room temperature in accordance with IEEE recommended guidelines. The individual tests were started at 75% of the Basic Impulse Level (BIL) followed by increases equivalent to 12.5% of BIL using a standard 1.5/40 μ s wave shape. After the first step, where three positive and three negative polarity impulses were applied, the tests were continued by applying three negative impulses at each voltage level, until breakdown. The average voltage stresses for each cable were used for preparing Weibull distributions. The 63% probability of impulse voltage breakdown obtained from these distributions are reported in Table 9. These same values were used to prepare Figures 4 and 5.

The data, for both the 15 and 35 kV cables, indicate

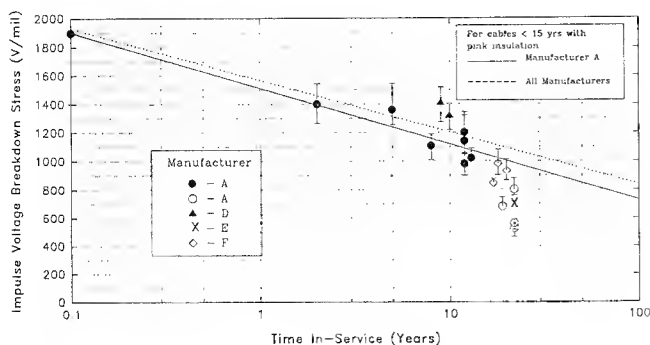


Figure 4 - Impulse Voltage Breakdown Strength of 15 kV EPR Insulated Cables

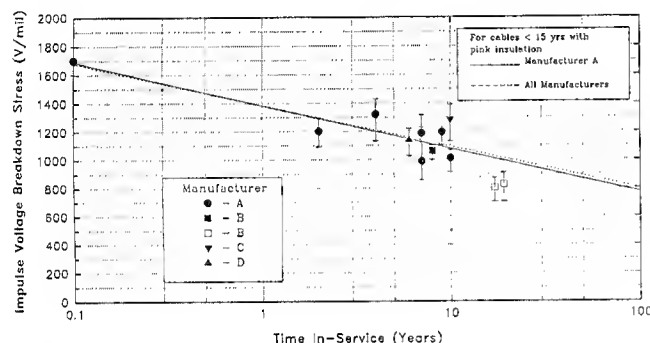


Figure 5 - Impulse Voltage Breakdown Strength of 35 kV EPR Insulated Cables

that the cables containing carbon black have lower impulse voltage breakdown strength. This may be due to a lower original breakdown when new or to faster degradation. For cables older than 15 years it is noted that the rate of aging of the dark gray EPR insulated cables falls in line with the rate of aging of the pink EPR insulated cables.

In reviewing the data for a.c. and the impulse voltage breakdown strength of all 15 kV cables, it appears that cables from manufacturer D have higher voltage breakdown strength than those from manufacturer A.

DISCUSSION

In extrapolating the voltage breakdown data presented in Figures 2 through 5 it becomes clear that some of the cables insulated with black compound will have a significantly shorter life, than cables made with newer gray and pink EPR compounds. This shorter service life appears to be due to the lower original voltage breakdown strength and faster deterioration of the older cables; no doubt related to the presence of a greater number of irregularities (voids, contaminants, protrusions), poorer mixing and larger size particles, all leading to greater localized voltage stress enhancement with consequent deterioration of the insulation.

It is of interest to note that in many cases voltage breakdown testing of older cables results in a larger range of individual values than in newer cables, a consequence of the presence of larger size imperfections and therefore greater

voltage enhancements leading to faster rates of degradation of the insulation. Differences in the level of moisture and shape, size and location of the imperfections in the insulation wall result in large differences in voltage breakdown strength. As voltage stress is enhanced, the insulation degrades at a faster rate. It is of interest to note that certain cables have an extremely high range of breakdown levels.

In reviewing the data for cables insulated with black EPR, it is noted that these cables exhibit lower tensile strength, higher moisture content, higher dielectric constant and dissipation factor and significantly lower a.c. and impulse voltage breakdown strength than cables made with pink EPR (≤ 15 years old) from the same manufacturer.

The three dark gray EPR insulated cables from manufacturer F appear to be aging at a slower rate than the black EPR insulated cables. The tensile strength of these cables appears to be significantly higher, while the dielectric constant and dissipation factor are lower, with consequent higher voltage breakdown levels. The rate of degradation appears to fall more in line with the pink than with the black compounds. It is of interest to note that while the 17 year old cable has the highest dissipation factor of the group, it also has the lowest a.c. and impulse voltage breakdown strength.

Reviewing the data, in particular for manufacturer A, for elongation, water trees, dissipation factor, a.c. and impulse voltage strength (Tables 4, 6, 7 and 9, respectively), it becomes clear that these characteristics of EPR cables deteriorate with time in service. As with PE and XLPE the deterioration appears to be the consequence of moisture permeating the insulation and water trees developing at the location of imperfections. The relatively high level of moisture permeation into EPR is well documented [2,7] and water trees have been observed by many investigators [1,2,13].

The higher moisture content at the outside of the cables is the consequence of the soaking period and the fact that during operation heat developed at the conductor drives moisture towards the outside. There is an exception in one of the 12 year old cables (Cable 13). This cable not only shows higher moisture in the inside part of the wall, it also shows corrosion of the conductor strands. It is quite possible that it had water at the conductor, at the time it was installed.

It is of interest to compare the slopes of the a.c. and impulse voltage breakdown strength curves, for cables of manufacturer A and for all cables combined. Because most of the cables are from manufacturer A, the curves for all the cables are heavily biased in the direction of manufacturer A. The closeness of the curves appears to indicate that all cables are aging at about the same rate.

One of the criteria for establishing the end of life for a cable in the field, is to relate voltage breakdown levels obtained during testing in the laboratory of severely deteriorated field aged cables with its operating voltage. Based on this knowledge and the rate of degradation of the present cables (Figures 2 through 5), it is possible to estimate that the newer type of EPR insulated cables (pink in color, ≤ 15 years old) will have service lives in excess of 30 years. It also appears that cables characterized by their dark gray

color and service ages up to 20 years, will have about the same service-life.

CONCLUSIONS

- 1) The present study, covering the evaluation of eighteen 15 kV and eleven 35 kV EPR insulated cables made by 6 different manufacturers, indicates that the newer cables (≤ 20 years), characterized by their pink or dark gray color insulation, are performing satisfactorily.
- 2) The older type of EPR insulated cables, characterized by their black color in service from 17 to 22 years, are not performing as well as the newer type.
- 3) All the newer type EPR cables, are aging at a relatively slow rate and can be considered as having somewhat uniform characteristics of degradation.
- 4) Aging of the EPR cables in this study can be characterized by an increase in moisture content, growth of water trees, drop in insulation elongation, increase in dissipation factor and decrease in a.e. and impulse voltage breakdown strength.
- 5) As judged by a.c. breakdown strength, the 15 kV cables in this study are aging at about the same rate as the 35 kV cables.
- 6) Based on extrapolation of the voltage-time curves (obtained from cables in service) it is estimated that the newer EPR cables in this study will have a useful service life in excess of 30 years, and the older black type will have a significantly shorter service life.

ACKNOWLEDGEMENT

The authors are indebted to HL&P for sponsoring this project and to several of their associates who have contributed to the removal of the cables, and to the laboratory investigation. In particular they wish to thank J. Dyndul for managing the performance of tests on the cables.

REFERENCES

1. Katz, C., Walker, M. "An Assessment of Field Aged 15 and 35 kV Ethylene Propylene Rubber Insulated Cables." Proceedings of the IEEE/PES Transmission and Distribution Conference, Chicago, IL, pp. 652-658, April 1994.
2. Barry E.P., Luther, E. "Evaluation of an In-service Aged Ethylene Propylene Rubber (EPR) Insulated Distribution Cable." IEEE Trans. PAS, Feb. 1983, pp. 448-453.
3. Bahder, G., Katz C., Lawson, J.H., Vahlstrom W., Jr. "Electrical and Electrochemical Treeing Effects in Polyethylene and Crosslinked Polyethylene Cables." IEEE Trans. PAS Vol. 93, May/June 1974, pp.977-986.
4. Thue, A.W., Bankoske, J.W., Burghardt, R.R. "Operating and Testing Experience on Solid Dielectric Cable. CIGRE 1980 Paper 21-10.
5. Steenis, E.F., Boone, W., Montfoort, A. "Water Treeing in Service Aged Cables, Experience and Evaluation Procedure." Trans. PWRD, Vol. 5, Jan.

1990, pp.40-46.

6. Bartnikas, R., Pelissou S., St-Onge, M. "A-C Breakdown Characteristics of In-Service Aged XLPE Distribution Cables." IEEE Trans. PWRD, Vol.3, April 1988, pp. 454-462.
7. Eichhorn, R.M. "A Critical Comparison of XLPE and EPR for Use as Electrical Insulation on Underground Power Cables." IEEE Trans. on EI-16. No. 6, 1981, pp. 469-482.
8. Brown, M. "Performance of Ethylene-Propylene Rubber Insulation in Medium and High Voltage Power Cable." IEEE Trans. PAS, Feb. 1983, pp. 373-381.
9. Farneti, F., Portinari, B., Bertani, E., Mosca, W. "Performance of EPR Insulated Cables Under Different Laying Conditions and Unusual Thermal Stresses. JICABLE 84, International Conference on Polymer Insulated Power Cables, Paris, 1984, pp. 56-62.
10. Walton, M.D., Bernstein, B.S., Smith III, J.T., Thue, W.A., Groeger, J.H. "Accelerated Cable Life Testing of EPR - Insulated Medium Voltage Distribution Cables." Trans PWRD, Vol. 9, July 1994, pp. 1195-1205.
11. Katz, C., Seman, G.W., Bernstein, B.S. "Low Temperature Aging of XLPE and EP Insulated Cables with Voltage Transients." Proceedings of the IEEE/PES Transmission and Distribution Conference, Chicago, IL, April 1994.
12. Association of Edison Illuminating Companies, "Specifications for Ethylene Propylene Rubber Insulated Shielded Power Cables Rated 5 through 69 kV," 5th Edition, New York, 1987 (AIEC CS 6-87).
13. Uematsu, T., Iwata, Z., Irie, S., Fugii, O. "Bow Tie Tree in EPR Cables After Accelerated Water Treeing Test." IEEE Trans. PWRD, Vol. 7, Oct. 1992, pp. 1667-1676.
14. Bahder, G., Katz, C., Eager, G.S., Jr., Leber, E., Chalmers, S.M., Jones, W.H., Mangrum, W.H., Jr. "Life Expectancy of Crosslinked Polyethylene Insulated Cables Rated 15 to 35 kV." IEEE Trans. PAS Vol. 100, April 1982, pp. 1581-1590.

BIOGRAPHIES



Carlos Katz (M'70-SM'78-F'87) Born in West Germany on August 18, 1934. Received an Electrical Engineering degree from Polytechnic Institute of Quito, Ecuador in 1961 and a MS degree from Stevens Institute of Technology, Hoboken, New Jersey in 1970.

From 1962 to 1971 he was associated with General Cable Corporation Research Center, and from 1971 to 1974 with the laboratories of Phelps Dodge Wire & Cable. In 1974 he became Assistant Director of

R&D at General Cable Corp. and later Technical Director Power and Control cables for General Cable International. He has been with Cable Technology Laboratories as Chief Research Engineer, since its founding in 1978. Mr. Katz's special field of activity is the investigation of extruded and laminar dielectric high voltage power cables, the manufacture and properties of such cables and the extension of service life of installed cables.

Mr. Katz is the author of 30 technical papers and holds 14 U.S. patents related to high voltage cables. He is an active member of ICC and CIGRE.



Michael L. Walter (M'-87)
Born in Madill, Oklahoma on August 31, 1952. Received an Associate in Electronics from South Oklahoma City Junior College in 1977 and a B.S. in Electrical Power Engineering Technology from Oklahoma State University in 1979.

From 1971 to 1974 he

served in the U.S. Army as a Specialist in Ground Surveillance and Electronic Warfare. Since 1979 he has worked for Houston Lighting & Power Company in Distribution Engineering. His expertise is in the utilization of overhead and underground cables for distribution applications, underground equipment and electrical conductor hardware.

Mr. Walker has authored or coauthored various technical papers related to power cables and their behavior on distribution systems. He is a voting member of the ICC, a member of the AEIC-Cable Engineering Section, and an industry advisor to EPRI on various cable projects.

MOISTURE CROSSLINKABLE POLYETHYLENE WITH IMPROVED PROCESSING AND CROSSLINKING PERFORMANCE

Bernt-Åke Sultan

Borealis Polyeten AB
Skills Centre Wire & Cable, Stenungsund, Sweden

ABSTRACT

This study shows that reactions, which lead to a marked increase in molecular weight, occur during the extrusion of moisture curable polyethylene. To avoid this problem, crosslinking catalysts of limited activity have to be used. Therefore, although not chemically involved in the crosslinking reaction, the processing window influences the crosslinking speed of cables insulated with moisture curable polyethylene. By using a compatible "scorch retardant additive" (SRA), the reactions which cause the increase in molecular weight during extrusion, can be prevented. As a result, more reactive catalysts have been developed, which reduce the crosslinking time at 60°C almost tenfold. The use of the SRA has made it possible to use the flexible but more scorch-sensitive terpolymer for commercial production of pipe, conduit and cables with excellent surface finish. We expect that the terpolymer will be useful in the future development of flame retardant cable materials for communications and power cable. Additional cable applications for this technology include crosslinked telephone cable jackets for steampath cable and over heat-sensitive thermoplastic insulation cores and thin insulations at high speeds. Other advantages of compounds containing the SRA are reduced die drool and simpler quicker tooling changes.

INTRODUCTION

Polyethylene was accidentally discovered in 1933¹. One of its major advantages was its nonpolar structure that resulted in outstanding dielectric properties. The good insulating properties made PE a key material in the development of radar during the second world war and was also early utilised in communication cables. For power cable insulation heat deformation properties as well as the dielectric properties are of great importance. Using thermoplastic Low Density Polyethylene (LDPE) or PVC the maximum operation temperature is limited to 70°C. By crosslinking LDPE a three dimensional molecular structure is formed which dramatically improves the heat deformation properties. This allows a maximum operation temperature of 90°C and increases the short circuit rating from 130 to 250°C. In addition to the improved heat deformation resistance several other properties such as abrasion-, chemical-, creep- and stress cracking resistance are improved. Impact- and tensile strength are increased, shrinkage decreased. Crosslinking also has a positive influence on the low-temperature properties.

The first crosslinked PE was produced by electron beam irradiation in the mid fifties². Irradiation crosslinking would probably have been more widely used today if the peroxide crosslinking process had not been invented a few years later³.

Today radical crosslinking by the use of peroxides has become the dominant technique for production of high and medium voltage cables. Cables up to 500 000 volt are today commercially produced by peroxide crosslinking. In spite of the excellent electrical and physical properties of peroxide crosslinked polyethylene its use for low voltage applications are rather limited. The high investment costs involved and the restriction in production speed limited by the cure rate and the demands for a certain residence time in the vulcanization tube make it economically difficult to compete with thermoplastic solutions.

With the introduction of the moisture crosslinkable silane grafting techniques, Sioplas^{®4} and Monosil^{®5} patented 1968 and 1974, respectively, more competitive crosslinking techniques for low voltage insulation were introduced. Besides these two grafting processes another silane crosslinking technique has become of increasing importance today, the silane copolymer process. By this process vinyl silane units, necessary for crosslinking, are introduced into the main chain by high pressure copolymerization with ethylene. This technique makes it possible to use existing PE and PVC-extrusion lines without any modification except for a feeder for addition of a catalyst masterbatch and preferably a dryer for colour and catalyst masterbatches.

In Europe, silane crosslinkable copolymers (Visico[®]) have been used in regular cable production since 1986. This paper will focus on describing these copolymers' thermal stability, extrusion and crosslinking performance. It will also present the introduction of the compatible "scorch retardant additive" (SRA) concept⁶ which is today dominating the European silane copolymer market.

MANUFACTURING PROCESSES

In the Sioplas[®] process, a vinyl silane, usually vinyl trimethoxy silane (VTMS), is compounded with Polyethylene (PE) and a small amount of peroxide (ROOR). The radicals formed by the peroxide abstract hydrogens from the PE forming alkyl radicals which readily react with the unsaturated silane, Fig. 1. In a subsequent extrusion step c:a 5 % of a catalyst masterbatch is added to the grafted compound. Normally an organo-tin derivative such as di-n-butyltin-dilaurate (DBTDL) is used as catalyst. The final product is immediately extruded. The curing is carried out subsequently by storage in hot water or in a steam cabinet at 60-90°C for 6-20 hours. The actual reaction scheme of the crosslinking is not known in detail. A simplified mechanism for the formation of the crosslinking point, the Si-O-Si bond, is given in Fig. 2. From the reaction scheme it can be concluded that one water molecule has to be added for every crosslinking point.

GRAFTING OF SILANE TO PE

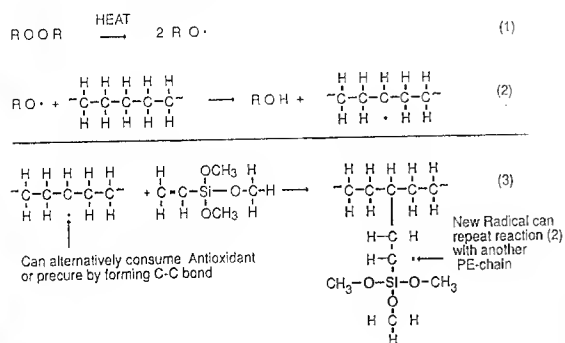


Figure 1. Grafting of vinyl silane to polyethylene - reaction scheme.

CROSSLINKING OF PE WITH SILANE

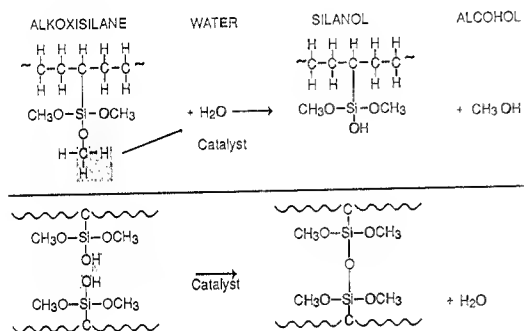


Figure 2. Silane crosslinking of polyethylene - simplified reaction scheme.

POLYMERISATION OF VINYL-SILANE - COPOLYMERS

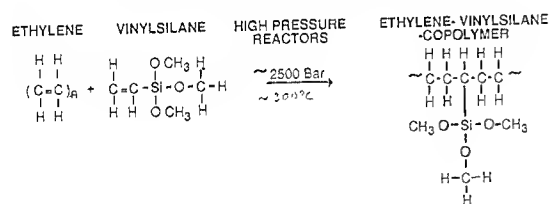


Figure 3. Polymerization of ethylene-vinyl silane copolymers.

Monosil® is a one step version of the Sioplas® process. All components, PE, peroxide, DBTDL and VTMS, are introduced in a special 30 L/D long extruder. Ethylene vinyl silane copolymers are produced in the same high pressure reactors as LDPE and other ethylene copolymers like ethylene vinyl acetate (EVA), ethylene ethyl acrylate (EEA), ethylene butyl acrylate (EBA) etc., Fig. 3. Moisture curable terpolymers consisting of vinyl silane and polar comonomer are also produced in this process.

The different processes discussed above are schematically described in Fig. 4.

SILANE CROSSLINKING

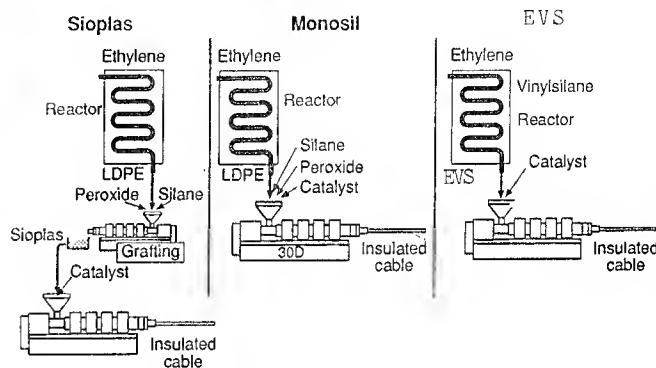


Figure 4. Common processes for production of moisture curable cables.

The copolymerization process has many advantages compared with the grafting processes;

A grafted compound has a rather limited shelf life as the crosslinking reactions proceed slowly, although without any addition of catalyst, due to the decomposition products from the grafting reaction acting as crosslinking agents. Furthermore a grafted VTMS polymer has a two carbons longer side branch than a copolymer thus increasing its reactivity, which also contributes to worse storage stability, see Fig 5.

STORAGE OF EVS AND GRAFTED COMPOUND

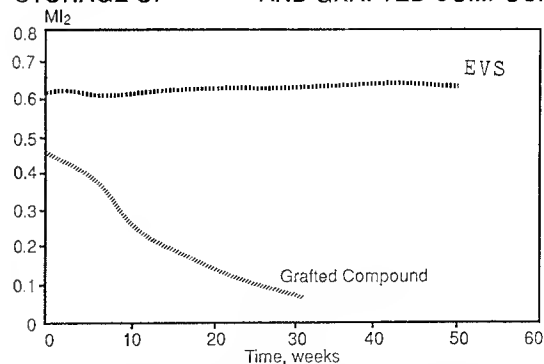


Figure 5. Storage stability test by measuring melt flow rate as a function of storage time. The grafted compound produced in accordance with the Sioplas® process. EVS-3 stored in a cardboard box and polyethylene liner. The Sioplas® material stored in presence of a drying agent in a steel drum and a polyethylene liner. Packages kept during ambient conditions.

- The grafting operation limits the choice of antioxidants, since many of them are effective radical scavengers and therefore inhibit the grafting reaction. Since aromatic amine stabilizers have a low tendency to "kill" these radicals, many of the Sioplas® and Monosil® compounds have a yellow colour due to the use of these additives.
- An increase in the viscosity of the PE melt is always seen during the grafting operation due to the fact that the reaction between the polymer and the unsaturated silane is non-terminating, see Fig. 1. Therefore the combination of alkyl radicals and other reactions results in a significant drop in viscosity and a broadening of the molecular weight distribution during the grafting step. Difficulties in controlling the grafting step results in variable final MFRs, silane yields and silane distributions.
- In a grafted compound the decomposition products of the peroxide as well as unreacted vinyl silane give the compound a strong odour. Our measurements indicate that in an optimized grafting process c:a 20% of the added vinyl silane is unreacted. In a copolymerization process unreacted silane is recovered in the gas purification system of the polymerization unit.

THERMAL STABILITY OF SILANE COPOLYMERS

Crosslinking reactions during extrusion can lead to formation of unmeltable particles, called scorch, that drastically reduce the breakdown strength and physical properties of an insulation as well as destroying its surface finish. All compounds containing crosslinking agents are more or less scorch sensitive, i.e. the problem is common also for peroxide crosslinkable compounds. Scorch properties are also of importance for production economics, as they determine the maximum production time for a given extruder set up.

Table 1. Data on polymers used for the thermal degradation studies.

	MFR ₂ g/10 min	Density kg/m ³	Cont. of Comonomer W-% VTMS BA	
EVS-1	0.7	923	1.6	0
EVS BA-2	4.0	928	2.3	20

In order to get an understanding of how a polymer will act during processing, isothermal degradation studies of different silane copolymers have been performed. The studies were made in an ultra pure nitrogen atmosphere as the oxygen levels during extrusion is small, c:a 0.3 %, and accordingly thermal reactions dominate⁷. The degradation experiments were performed on thin plastic films in a tubular oven. In order to keep the water content as low as possible, the films were kept in a desiccator for at least 10 hours before the heat treatment. In some of the studies the nitrogen was presaturated with water before entering the heated zones of the oven. The degradation procedure is described in more detail elsewhere^{8,9}.

Two fullscale produced polymers, one copolymer (EVS-1) and one more rubberlike terpolymer containing 20 w-% butylacrylate (EVS BA-2) were included in this investigation. The polymers are described in more detail in Table 1. The samples were degraded for 10 min. at temperatures up to 390°C.

Possible crosslinking reactions resulting in gel formation were followed by extraction of the degraded polymer in boiling decaline, basically following ASTM D 2765.

The results for the copolymer are summarized in Fig. 6. Hardly any gel (3-6%) is formed when the copolymer is heated in pure nitrogen. The same results are obtained for LDPE. Consequently the vinyl silane does not induce gel formation under pure thermal degradation. The experiments were continued by presaturating the nitrogen with water just before entering the heated zone of the oven. In the presence of water the amount of gel increased with temperature. At 360°C a gel content of 33% was obtained. The third curve in Fig. 6 represents the behaviour of EVS-1 containing a typical level, 0.05 w-%, of the commonly used crosslinking catalyst DBTDL and degraded in nitrogen presaturated with water. In this case the crosslinking started at a much lower temperature and proceeded at a higher rate. A maximum of c:a 75 % gel was formed after 10 min at temperatures above 250°C. In ordinary production, crosslinking is much slower, 75 % gel is formed after c:a 20 hours treatment in a water bath at 90°C.

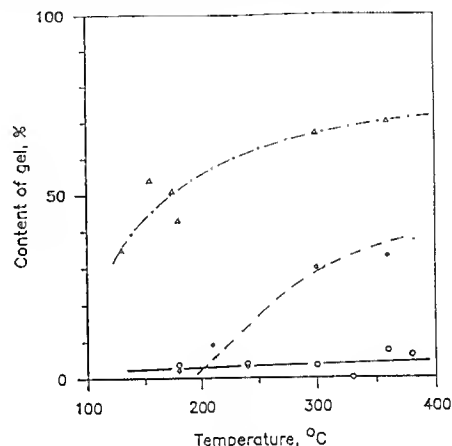


Figure 6. Gel content of EVS-1 after heat treatment for 10 min. under different conditions: (—○—) nitrogen; nitrogen presaturated with water (---○---); (- - -△- - -) nitrogen presaturated with water, crosslinking catalyst added.

In conclusion, the results obtained with EVS-1 show that the presence of water is necessary for the formation of gel in a silane copolymer. At temperatures below 200°C the rate of gelation is low if no catalyst is added. In practice, it is impossible to totally exclude moisture during processing. The oxygen levels are as indicated above low, but high enough to induce oxidation of the polymer and formation of water, which is one of the major decomposition products of the oxidation process¹⁰.

For the terpolymer a different degradation behaviour is observed, Fig. 7. Even in a dry nitrogen atmosphere and no presence of crosslinking catalyst, gel is formed. Up to somewhat below 300°C only a minor amount of gel was formed, but above that, the rate of crosslinking is increased markedly. At the highest temperature investigated, 360°C, as much as 70 % gel was formed, an alarming difference to what was found for EVS-1.

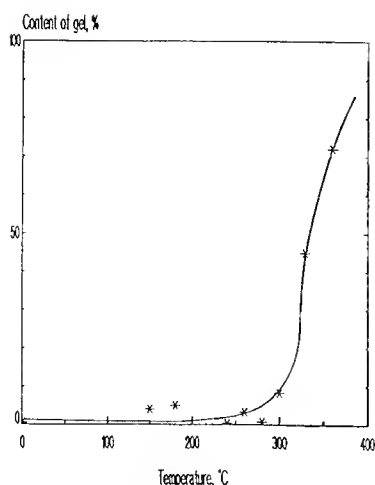


Figure 7. Gel content of EVS BA-2 treated in dry nitrogen for 10 min. at different temperatures.

One possible explanation for the big differences in crosslinking behaviour in pure nitrogen between the two polymers could be the presence of dissolved water which is considerably higher in the more polar EVS BA-1 than in EVS-1, 342 ppm and 135 ppm respectively. Calculations show, however, that the water content ought to be 3-4 times higher to account for the observed gel formation in EVS BA-2. The gel formation is more likely explained by the degradation of the butylacrylate (BA) group in the polymer. Earlier reported degradation studies of EBA^{11, 12, 13} have shown that the BA group start to degrade thermally at the temperature levels at which the gel formation of EVS BA-2 is observed. At these temperatures butene is split off and carboxylic groups remain in the polymer chain. The carboxylic acid groups are partly converted to anhydrides and water, Fig 8. Unchanged carboxylic acid groups will function as catalysts for the silane crosslinking reaction¹⁴. This explains the much higher gelation rate at temperatures above 300°C in the degradation of EVS BA-2 compared to uncatalyzed EVS-1 in the presence of water (compare Fig. 6 and 7).

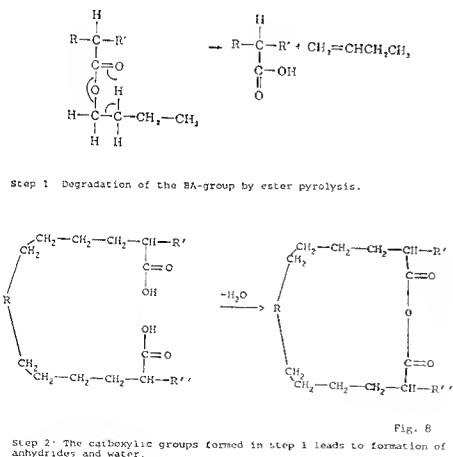


Figure 8. Thermal degradation reactions occurring in EBA.

EXTRUSION PROPERTIES OF SILANE COPOLYMERS

The results above show that when silane groups are introduced into a polyethylene chain its degradation behaviour at typical processing temperatures is dramatically changed in the presence of small amounts of water. Severe molecular enlargement reactions occur and gel is quickly formed. As mentioned above crosslinking reactions occurring during extrusion will narrow the processing window and increase the risk for scorch formation. In order to get an indirect value of the molecular enlargement reactions occurring in a real extrusion process the Melt Flow Rate at a weight of 21.6 N (MFR₂₁) of the extrudate has been measured at different temperature settings. Molecular weight increase will result in an increased viscosity of the melt, which will result in a decreased MFR₂₁ value. These studies have been performed on a 60 mm/20 L/D Troester extruder equipped with a PE-screw (compression ratio 3,3:1, 2D madock mixing section) and a 80/100/80 mesh screen. The extruder was run at 40 rpm at all temperature settings.

The extrusion studies were made on one co- and one terpolymer, EVS-3 and EVS BA-4 respectively. Both polymers contain VTMS as the crosslinking unit and the terpolymer has 17 w-% BA incorporated. Besides increasing the flexibility, the BA units improve the polymer's ability to carry fillers as well as its adhesion properties^{15, 16}. The polymer properties are described in more detail in Table 2.

Table 2. Properties of investigated polymers measured on crosslinked plaques. 5% CMB-A used as catalyst masterbatch.

	EVS-3	EVS BA-4	Unit	Test method
Butylacrylate content	0	17	w-%	Borealis 886
Melt flow rate (2.16)	0.9	4	g/10 min	ISO 1133 cond.4
Density	923	928		ISO 1872-2-B
Tensile strength	17	9	MPa	ISO 527
Elongation at break	350	350	%	ISO 527
Hot Set test (200°C, 0.2 MPa) ²	60	60	%	IEC 811-2-1
- Elongation under load	0	0	%	IEC 811-2-1
- Permanent set				
Durometer hardness	52	37	Shore D	ISO 868
Shelf life, (in unbroken package)	1	1	Year	
Dielectric constant (50 Hz)	2.3	-	-	IEC 250
Dissipation factor (50 Hz)	0.0005	-	-	IEC 250
DC volume resistivity	10 ¹⁶	-	Ω cm	IEC 93

In fig. 9 are the results for EVS-3 as well as a commercial Sioplas® material extruded with addition of 5% catalyst masterbatch presented. The MFR_{21} -values of the extrudate are plotted as a function of the exit melt temperature at the different temperature settings. In accordance with the isothermal degradation experiments the molecular weight increases, resulting in a drop in MFR_{21} , with increasing temperature both for the copolymer and the grafted compound produced by the Sioplas® process.

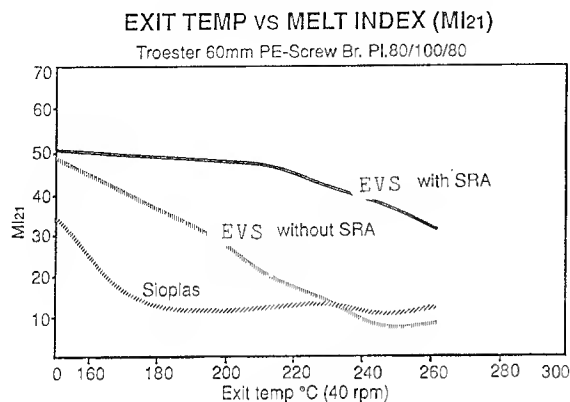


Figure 9. Processability test of silane crosslinkable compounds; 5 % catalyst masterbatch added. EVS = EVS-3/5% CMB- A. To the Sioplas® compound, 5 % masterbatch added in accordance with recommendations.

In order to increase the processing window of moisture crosslinkable polyethylene to a level more similar to that of thermoplastic compounds, intensive work to develop a compatible Scorch Retardant Additive (SRA), an additive that stops molecular enlargement reactions during extrusion, has been carried out⁶. As can be seen in Fig. 9, introduction of the SRA into the EVS-3/CMB-A system nearly stops the enlargement reactions at exit temperatures below 220°C and at higher temperatures a significant reduction is seen.

The SRA also makes the polymer more insensitive to residence time, a property which is of major importance when the screw speed is reduced to a minimum e.g. during tool changes and interruptions on the production line. In order to measure the residence time distribution of the melt in the Troester extruder a pellet of a titanium dioxide (TiO_2) containing PE masterbatch was introduced into the beginning of the feed section of the extruder. The content of TiO_2 in the extrudate was subsequently measured by X-ray fluorescence as a function of time. The results for three different screw speeds are presented in Fig 10. At 93, 50 and 5 rpm detectable amounts of TiO_2 were found after 4, 6 and 50 min. respectively. A residence time of 50 min. is a rather tough condition for a crosslinkable compound and without any SRA the surface finish quickly deteriorates and often it is impossible to get rid of formed gels without taking the extruder apart and cleaning it.

TROESTER PE-SCREW 60 MM

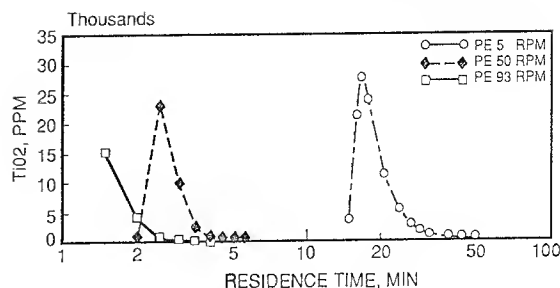


Figure 10. Residence time distributions at different screw speeds. (TiO_2 content measured by X-ray fluorescence).

In one of our standard tests in use for evaluating crosslinkable materials we produce a thin tape at a temperature of 210°C, 30 rpm, on a 19mm/20 L/D Brabender extruder equipped with a 3:1 compression screw. After 30 min extrusion, the extruder is stopped for 20 min.. Without SRA there is a large number of lumps in the extrudate when starting up the extruder and these cannot be removed without taking the extruder apart and cleaning it. With SRA containing compound excellent surface finish was obtained 2 min. after restarting the extruder.

With the SRA containing copolymer it is possible to produce very thin insulations at high speeds. A telephone wire consisting of a 0.4 mm copper conductor insulated with 0.2 mm EVS-3/5% CMB-C at a speed of 1650 m/min has e.g. been produced on a Nokia-Maillefer 60mm/30 L/D line.

As discussed above, the BA-containing terpolymer is more sensitive to high temperatures, as water is formed without the presence of oxygen. In Fig 11, processability of EVSBA-4/4436 is compared with EVS-3/CMB-A, both systems containing SRA. The terpolymer system does, indeed, show a more steep curve, indicating a higher sensitivity for processing. The MFRs for the extruded terpolymer system do, however, not drop to too dramatically low MFRs. The results indicate an acceptable processability, especially having in mind that EVSBA-4 has, compared to EVS-3, its optimal processing window at lower temperatures 150-180°C compared with 170-210°C for the copolymer. Due to the introduction of the SRA it has been possible to use terpolymers for production of cables and pipes with stable production conditions and excellent surface finish.

Exit Temp. vs Melt Flow Rate (MFR21)

Troester 60 mm PE-screw Br.PI. 80/100/80 (40 rpm)

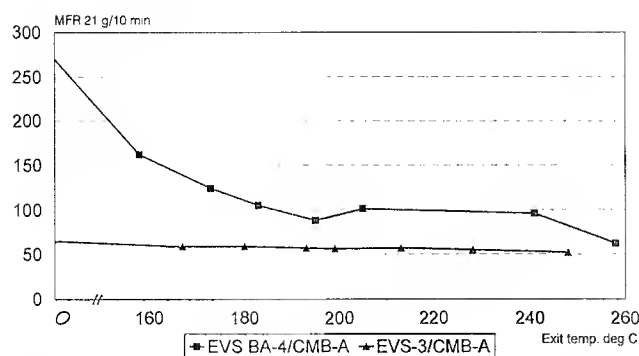


Figure 11. Comparison of the drop in MFR during extrusion for the BA-containing terpolymer, EVSBA-4 and the copolymer EVS-3. Both polymers extruded in presence of SRA and an addition 5 % catalyst masterbatch (CMB-A). The catalyst masterbatch not dried prior use, water content 360 ppm.

As seen above the essential difference in extruding crosslinkable PE compared to thermoplastic is that, for the former, molecular weight increase occurs already during extrusion. It is therefore essential to optimize the extrusion process in order to minimize these reactions i.e. minimize residence time and temperature. The residence time increases with screw cooling, with the mesh number of the screen pack and reduction of the screw speed. The extruder, screw and tool designs are also very important for the residence time distribution and for avoiding hot spots. Streamlined flow paths and the use of a conical screw top are of importance for making the residence time distribution more narrow. When extruding silane crosslinkable material it is essential to keep the moisture content as low as possible. Due to its nonpolar structure a silane copolymer absorbs low amounts of water, below 150 ppm, when stored at ambient conditions. The colour and catalyst masterbatches which contain a large amount of more polar chemicals will, however, quickly absorb high levels of water. An undried colour masterbatch will normally contain far over 1000 ppm water. It is recommended to dry all masterbatches to a water level below 200 ppm.

The introduction of the compatible SRA into the silane co-(EVS-3) and terpolymer (EVSBA-4), which were fully implemented in early 1990, has significantly widened the processing window and resulted in longer running times before cleaning. It makes it easier to make tool changes and makes it possible to extrude thin insulations at very high speeds and reduces the shrinkage of the insulation. It has also significantly reduced the die drool formation which is a common problem when extruding silane containing PE. Its introduction has resulted in a more forgiving compound that can be extruded on not fully optimized PE and PVC extruders as well as the long Monosil® machines.

CROSSLINKING PROPERTIES OF SILANE COPOLYMERS

The reason for the effectiveness of the SRA is that it reacts with water faster than the polymer itself during extrusion conditions. The concern is then, will it effect the crosslinking speed in the subsequent crosslinking step?

The crosslinking speed with and without SRA is compared in Fig. 12, where the gel content of a 1.8 mm thick tape was measured after crosslinking in water at 60 and 90°C for 1, 4, 8 and 20 hours. At 90°C no significant difference could be seen. At 60°C, there is a clear difference at the shortest crosslinking time, 1 hour. No gel at all is observed for the SRA containing compound while 30 % is achieved without. At the longer crosslinking times the same gel contents are obtained. The same behaviour would probably have been seen at 90°C, if gel at shorter crosslinking times had been measured.

COMPARISON CROSSLINKING SPEED with and without SRA

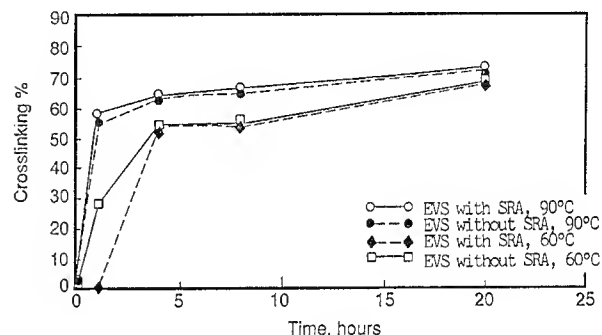


Figure 12. The effect of the scorch-retardant additive on the crosslinking speed: 1.8 mm thick extruded tape crosslinked in water at 60 and 90°C, respectively. EVS = EVS-3/5 % CMB-A.

In conclusion, the results obtained show that the SRA initially slows down the crosslinking reaction, but when it is consumed the crosslinking reactions goes faster than without the additive. The net effect is that the time to reach over 50 % gel content is the same as without the SRA. In practice, the observed difference is of minor importance as a crosslinking level over 50 % has to be reached in order to fulfil the demands on an insulation.

By the introduction of the SRA, the processing window has increased to such an extent that it has been possible to introduce more potent catalyst masterbatches. In table 2, the crosslinking speed of the recently introduced catalyst masterbatches, CMB-B and CMB-C, are compared with the original masterbatch CMB-A. As can be seen from table 3, the time to reach 60 % elongation in the hot-set test is dramatically reduced, especially at the lower crosslinking temperatures. At 60°C a close to tenfold decrease in crosslinking time for CMB-C is measured compared to the original catalyst masterbatch. At ambient conditions (22°C, 50 % relative humidity) we are approaching realistic crosslinking times for the most active masterbatch.

Table 3. Crosslinking speed of catalyst masterbatches of different activities, presented as time to reach 60% Hot Set measured according to IEC 811 (200°C, 0.2 MPa). Evaluation performed on 1.8 mm thick extruded tapes, 5% catalyst masterbatch added.

Catalyst MB	Year of introduction	Crosslinking conditions		
		90°C, H ₂ O, h.min	60°C, H ₂ O, h.min	Ambient ¹⁾ , days
CMB-A	1986	4.0	20	> 40
CMB-B	1993	1.50	9	15
CMB-C	1993	1.20	2.30	10

¹⁾ 55% Relative humidity, 22°C.

How the more active masterbatches effect the processability in comparison with CMB-A is shown in Fig. 13, where 5 % of the masterbatches is added to the SRA-containing silane copolymer EVS-3. The drop in MFR as a function of processing temperature increases with the activity of the masterbatches. In Fig. 14 the processability of EVS-3/ 5 % CMB-C containing SRA is compared with the traditional system EVS-3/5 % CMB- A extruded without any presence of SRA. In spite of the much higher activity of CMB-C safer processing is achieved due to the presence of the SRA.

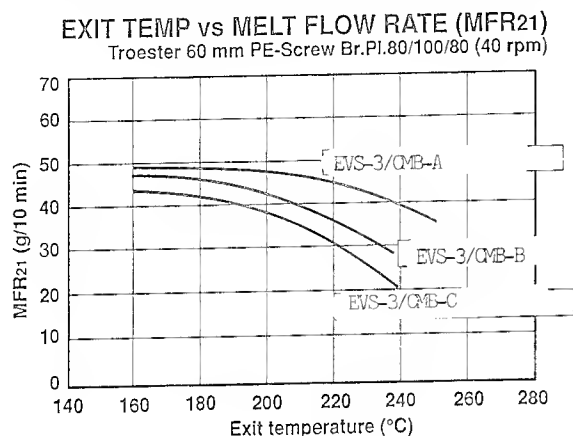


Figure 13. Processability of catalyst masterbatches with different activity in presence of scorch retardant additive. Masterbatches dried at 40°C over night prior extrusion, 5% masterbatch added.

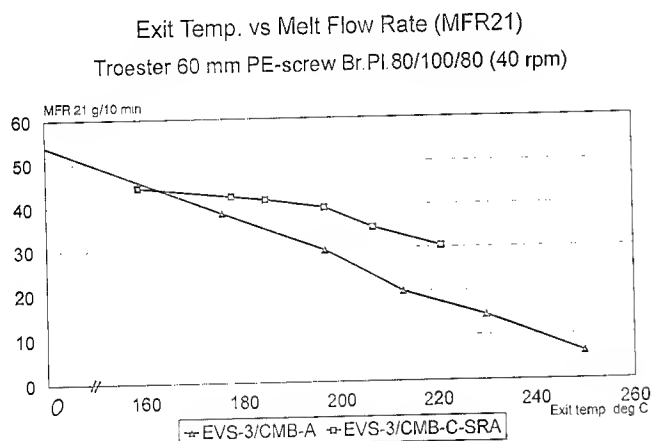


Figure 14. Processability of the traditional catalyst masterbatch CMB- A extruded without any presence of scorch retardant additive in comparison with the most active catalyst masterbatch, CMB-C, extruded in presence of scorch retardant additive.

SUMMARY

Isothermal degradation studies have shown that silane copolymers show a similar degradation behaviour as LDPE when degraded in dry Nitrogen. In the presence of small amounts of water a totally different degradation behaviour is observed, resulting in severe molecular enlargement. Ethylene(vinyl trimethoxy, n-butylacrylate) terpolymers show gelformation at temperatures above 300°C during pure thermal conditions. During this condition ester pyrolysis of the BA-group occur, resulting in formation of carboxylic groups in the polymer chain and subsequent anhydride formation. Butene and water are the decomposition products.

Due to the presence of small amounts of water and oxygen, a marked increase in molecular weight also occurs during extrusion. By introduction of SRA into the silane containing polymer systems these reactions are significantly reduced. Its introduction does not effect the time to reach necessary crosslinking levels in the subsequent crosslinking step. Instead the increased processing window has made it possible to use more active catalyst masterbatches resulting in a tenfold decreased crosslinking time at 60°C, H₂O. Introduction of the SRA into the more scorch sensitive terpolymer system has resulted in a commercial use of this flexible polymer for the production of cables and pipes.

Besides an increased processing window and improved surface finish the introduction of the SRA concept into moisture curable polymer system has resulted in reduced die drool formation and reduced shrinkage of the insulation as well as simplified routines when making tool changes on the extruder. It has also made it possible to produce thin insulations at high line speeds.

ACKNOWLEDGEMENTS

The author wish to thank Dr. Erling Sörvik and Prof. Thomas Hjertberg at the Department of Polymer Technology, Chalmers University of Technology, Gothenburg, Sweden for a fruitful cooperation in investigations of the thermal stability of ethylene copolymers.

REFERENCES

1. J.C. Swallow in Polyethylene, Second Edition, Ed. by A Renfrew and P. Morgan, Interscience Publishers Inc., New York, 1960.
2. B.J. Lyons, Polyethylenes 1933-1983 Conference, London, UK, 1983.
3. B.E. Roberts and S. Verne, Polyethylenes 1933-1983 Conference, London, UK, 1983.
4. U.S. Patent 3 646 155.
5. U.S. Patent 4 117 145.
6. US patent application 089418 (information of allowance received)
7. H.M. Quackenbos, Polym.Eng. Sci., 6, 117, 1966.
8. A. Holmström and E. Sörvik, J. Chromatogr., 53, 95 (1970).
9. B-Å Sultan and E. Sörvik, Thermal Degradation of EVA and EBA - A comparison, Changes in Unsaturation and Side Group Structure. Dept. of Pol. Techn. Chalmers Univ. of Techn. Göteborg, Sweden. A. Holmström and E. Sörvik, J. Chromatogr., 53, 95, (1970).
10. J.L. Bolland and G. Gee, Kinetic studies in the chemistry of rubber and related materials. KK. The kinetics of oxidation of unconjugated olefins. Trans. Farady Soc., 42 (1946) 236-43.
11. B-Å Sultan and E. Sörvik, Dept. of Pol. Techn., Chalmers University of Technology, Göteborg, Sweden. Thermal Degradation of EVA and EBA - A Comparison. I. Volatile Decomposition Products. Journal of Applied Polymer Science, Vol. 43, 1737-1745 (1991).
12. B-Å Sultan and E. Sörvik, Dept. of Pol. Techn., Chalmers University of Technology, Göteborg, Sweden. Thermal Degradation of EVA and EBA - A Comparison. II. Changes in Unsaturation and Side Group Structure. Journal of Applied Polymer Science, Vol. 43, 1747-1759 (1991).
13. B-Å Sultan and E. Sörvik, Dept. of Pol. Techn., Chalmers University of Technology, Göteborg, Sweden. Thermal Degradation of EVA and EBA - A Comparison. III. Molecular Weight Changes. Journal of Applied Polymer Science, Vol. 43, 1761-1771 (1991)
14. M. Andersson and I. Fransson, Diploma Work, Catalysts for Crosslinking of Ethylene Vinylsilane Copolymers, Chalmers University of Technology, Gothenburg, Sweden, 1990.
15. L. Ulrén and T. Hjertberg, Adhesion between aluminium and copolymers of ethylene and vinyltrimethoxysilane. J. Appl. Pol. Sci., 37 (1989) 1269.
16. L. Ulrén, T. Hjertberg and T. & H. Ishid, An FI-IR study on interfacial reactions in ethylene copolymers/aluminium laminates in relation to adhesion properties. J. Adhesion, 31 (1990) 117.

Bernt-Åke Sultan
Borealis Polyeten AB
S-44486 Stenungsund
Sweden



BIBLIOGRAPHY

Bernt-Åke Sultan was born 1957. He has a M. Sc degree in Chemical Engineering from Chalmers University of Technology. His Ph D is from the same university and dealt the stability and adhesion properties of ethylene copolymers. Since 1984 he has worked for Borealis (former Unifos and thereafter Neste), with development of polymers and compounds based on polyolefins intended primarily for cable applications. Today he is managing the group responsible for development and technical service of Borealis low voltage insulations and flame retardant cable materials. Dr. Sultan is author or co-author of 10 technical papers and 5 patents.

A NEW AUTOMATIC SYSTEM FOR INSTALLING AERIAL ROUND CABLE

Hiroshi Nakanishi, Kazuo Yamamoto

Access Network Systems Laboratories
Nippon Telegraph and Telephone Corporation
1-7-1 Hanabatake, Tsukuba-city, 305 Japan

Abstract

Lashing machines were once popular as a means of installing aerial round cable, but their use was discontinued due to problems with wind pressure oscillation. As a result, such cables are currently installed manually by technicians suspended from the suspension wire, to which they attach the aerial cable with cable rings.

To facilitate this task, we have developed a new cable ring and an automatic ring attachment machine that can install aerial round cable both safely and effectively, making it possible to automatically install cable from ground level at the work site.

1. Introduction

Aerial round cable was once installed by lashing, as shown in Fig. 1.



Fig. 1 Lashing Cable

However, the use of this technique was discontinued due to the serious oscillation that occurred in strong winds.[1][2][3] Today, only a few cables are attached in this way in Japan. Instead, the suspension wire and aerial cable are installed separately, and then joined together with regularly spaced cable rings, as shown in Fig. 2.

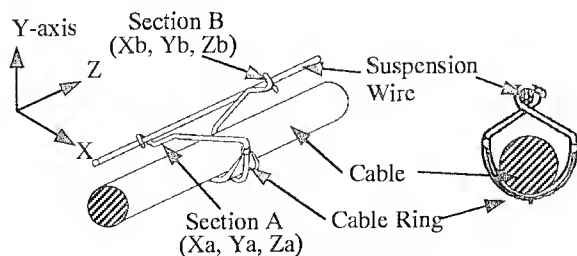


Fig. 2 Conventional Cable Ring

The use of cable rings has two advantages. First, the gap between the suspension wire and aerial cable reduces the dynamic lift forces acting on them, thus suppressing their

oscillatory behavior. Second, since the suspension wire and aerial cable are not tightly bound together, there is no failure of the aerial cable being heavily stressed due to thermal expansion of the suspension wire and aerial cable. The drawback of this method is that the cable rings must be attached manually by technicians inside a gondola suspended from the suspension wire. This is not only inherently dangerous, but also difficult and time-consuming work. To make things easier, we have developed a new cable ring and a new automatic ring attachment machine.

In this paper, we describe the results of an analysis of the current manual ring attachment method, and reflect these results in the development of a new installation system suited to mechanization. Then describe the new cable ring and automatic ring attachment machine, and describe the effectiveness and reliability of the system.

Finally, we describe a new installation system for aerial round cable using the new rings and the new machine.

2. The current method and its suitability for mechanization

Current cable rings prevent cable vibration and thermal stress. To ensure these characteristics are not lost, the new method should ensure the following requirements are met :

- (1) A clearance is established in the space between the suspension wire and aerial cable.
- (2) The rings should be tightly fixed to either the suspension wire or the aerial cable.
- (3) To reduce labor, the rings should be attached automatically at ground level at the work site.

Conventional rings are installed as shown in Fig. 2. First, section A of the ring is attached to the supporting cable at coordinates (X_a, Y_a, Z_a) . The aerial cable is then placed inside the ring, and finally section B of the ring is also attached to the suspension wire at coordinates (X_b, Y_b, Z_b) . Since the fixing of section A and B requires a degree of manual dexterity, the ring must be redesigned to enable mechanical attachment.

The manual installation of conventional rings can be broken down into four stages, as shown in Fig.3 : "transport", where the ring is brought to the cable ; "push", where force is applied to the ring to attach it to the suspension wire ; "see", where the ring position is visually confirmed ; and "hold", where the pressure is released.

We developed the new system based on these four stages and the requirements mentioned earlier.

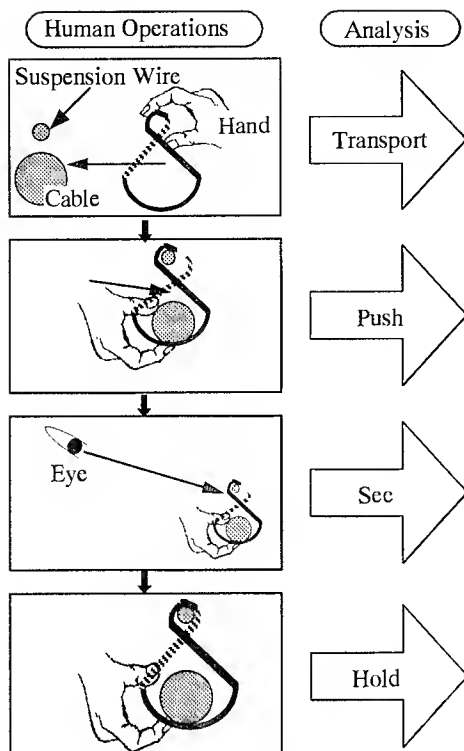


Fig. 3 Human Operations and Analysis

First we describe the configuration of a new ring that can be applied with a simple "push" operation. Next we describe equipment installing these rings automatically.

3. New Cable Ring

The rings are used to attach two cylindrical objects — the suspension wire and the aerial cable. To enable these two objects to be attached with a simple "push" operation, we developed the two shapes shown in Fig. 4.

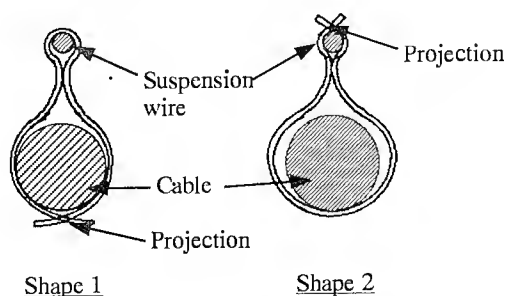


Fig. 4 Topology of New Cable Ring

These shapes feature projections at either the top or bottom of the ring. By pulling these projections apart, the ring can be fixed in a single movement; in shape 1 the ring is fixed to the aerial cable, while in shape 2 the ring is attached to the suspension wire. We tested rings of both shapes and conducted experiments to determine which is easier to install with a simple "push" operation, and found that the best results

were obtained with shape 1. This is because it is easier to tighten the ring around aerial cable, which has a large external diameter of 27.9-52.5 mm, than suspension wire, which has an external diameter of only 6.9-10.5 mm.

In addition, since the diameter of cables manufactured in Japan can vary by as much as 5 mm, we found through numerical calculations that tight connections to the aerial cable could be reliably achieved by incorporating six teeth into the cable ring to provide additional grip. Figure 5 shows a photo of the newly-developed cable ring.



Fig. 5 Photo of New Cable Ring

4. Automatic Ring Attachment Machine

Figure 6 shows how the four basic actions — "transport", "push", "sec" and "hold" — are incorporated into the operating principle of the automatic ring attachment device. First, a ring is transported from the ring supply to the attachment position using a gripper to replace human hands. Next, a decision is made regarding the attachment position where the ring will be fixed so as to connect the aerial cable and suspension wire. The machine then "pushes" on the two projections so as to open up the cable ring. To verify the attachment, human eyes are replaced by a sensor that measures the force applied while attaching the connecting ring. Once a specified force has been reached, the grip is released. The above procedure is repeated at regular intervals along the cable.

However, mistakes occurred with this method when the connecting rings were simply pushed apart. The reason for this was found to be as follows.

When the ring is pushed, the ring projections (i.e., the attachment positions) should theoretically follow circular paths in the x - y plane centered on the other end of the cable ring (point "0"), as indicated in Fig. 7. In practice, however, since the rings were made of stainless spring steel, they were prone to out-of-plane deformation by twisting. In other words, the trajectories of the ring projections become $u_1=f_1(x,y,z)$ and $u_2=f_2(x,y,z)$, which have components in all three dimensions.

Furthermore, due to manufacturing tolerances in the external diameter of the cable and the shape of the cable rings, the projections did not even follow symmetric paths. To account for these problems, we took steps to avoid out-of-plane distortion, and we theoretically investigated attachment

methods that could accommodate manufacturing variations.

To avoid out-of-plane distortion, we added a retaining mechanism to keep the sideways forces (i.e., Z-axis force) close to zero during the "push" stage of attachment. This made it possible to accurately control the motion of the ring and reduce the occurrence of attachment errors.

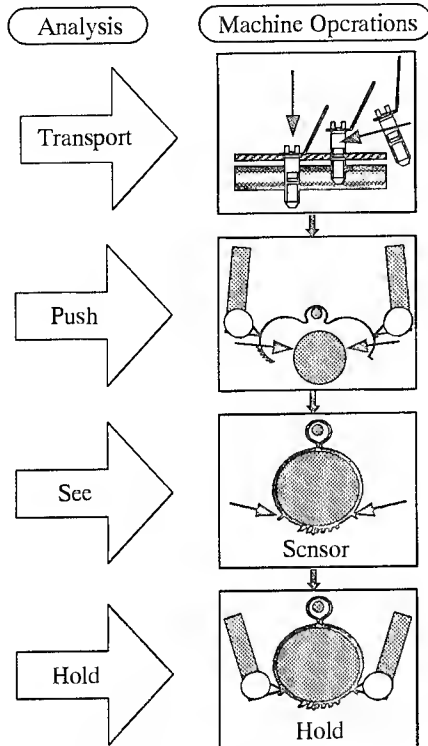


Fig. 6 Mechanical Operations of New Cable Ring

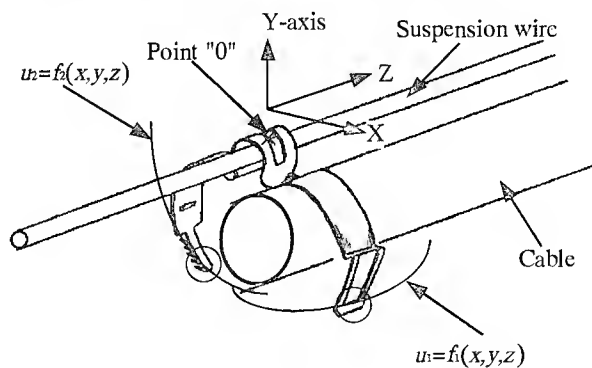


Fig. 7 Ring Attachment Theory

As for the manufacturing variations, we found that ring manufacturing tolerances were responsible for a gap of up to 1mm between the side of the ring containing the teeth and the side containing the projection. We compensated for this by fixing the trajectory of the projection side so that it intersected with that of the toothed side by rising up towards it, thereby closing up any gaps. From the results of a theoretical simulation, we arrived at the design shown in Fig.8. Assuring the teeth follow a circular path, the projection side is

made to follow a more highly curved path so that the ring can be attached in spite of the manufacturing tolerances.

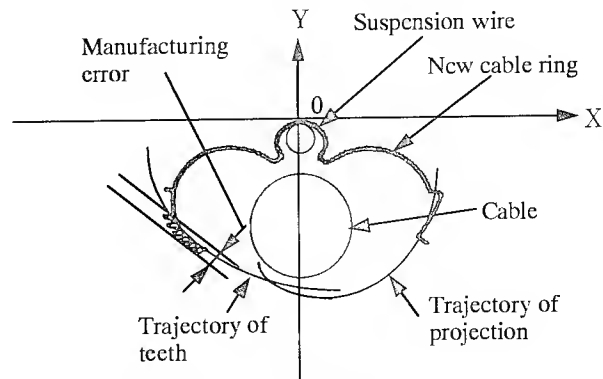


Fig. 8 Results of Theoretical Analysis

Figure 9(a) shows a block diagram of the equipment and Fig. 9(b) shows a timing diagram for a single ring attachment cycle.

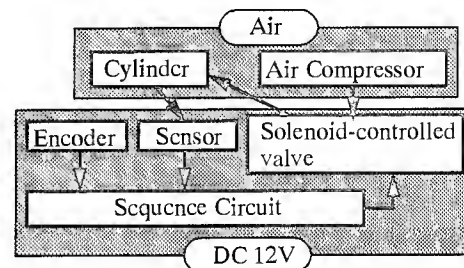


Fig. 9(a) Block Diagram

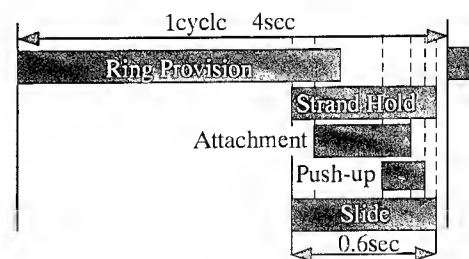


Fig. 9(b) Timing Chart

The ring attachment system also incorporates an encoder which measures the distances between attachment positions and automatically starts up the ring attachment process.

The newly-development ring attachment machine is shown in Fig. 10

6. The Installation System and The Equipment Employed

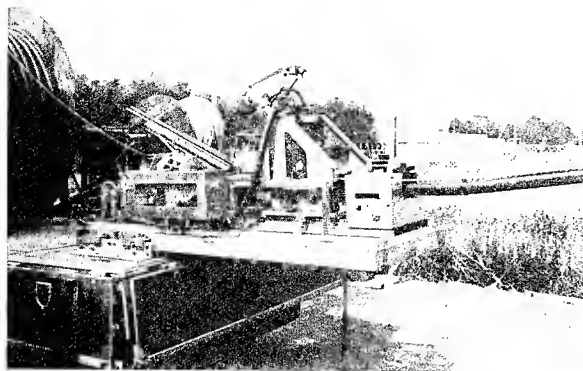


Fig. 10 Photo of New Ring Attachment Machine

5. Verification of Reliability

Using the experimental system shown in Fig. 11(a) we conducted vibration fatigue tests on a cable constructed outdoors using the proposed cable rings. The resulting strain of the cable sheath reached a maximum of only 150, as shown in Fig. 11(b), which is within the provided limits. No problems were found in the suspension wire or rings.

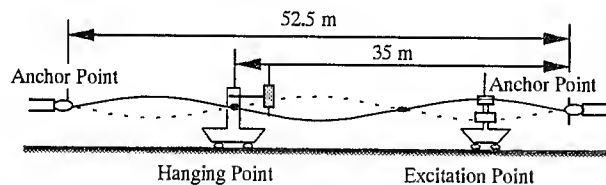


Fig. 11(a) Experimental Form

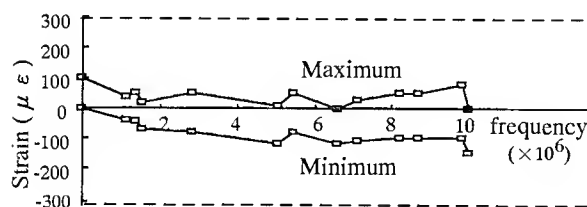


Fig. 11(b) Experimental Results

A cable constructed using the new cable rings is theoretically capable of reducing the tensile temperature stress in the cable. We used the proposed cable rings to construct 150 meters of cable in a temperature cycling facility and subjected it to thermal cycles between -20°C and 60°C . After these tests, the cable was still found to be functioning normally.

We also subjected cable made with these cable rings to temperatures ranging from -30°C to $+35^{\circ}\text{C}$ and peak wind speeds of over 20 m/s by running a three-year exposure test in northern Japan. Even after this treatment, wind oscillation and temperature changes were found to cause no problems.

These results confirm that cable mounted using the proposed cable rings is highly reliable.

When installing on site, this system utilizes a vehicle mounted cable drum, suspension wire drum and the new machine. With the addition of a simple mechanical device, the cable and suspension wire drums can be braked, enabling an unmanned series of movements. Heavy-duty cable presents suspension difficulties when the cable and suspension wire are installed simultaneously. In this instance, a messenger rope is used and line pullers deployed from the ground. In this way the difficulties are resolved. This system is shown in fig. 12.

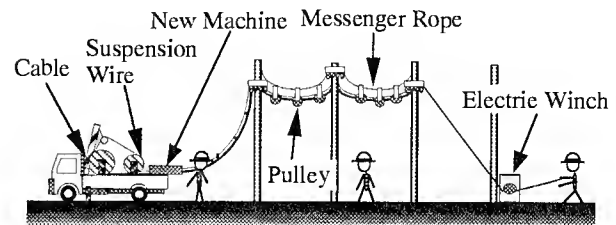


Fig. 12 New Installation System

7. Conclusion

A new cable ring and a new, automatic ring attachment machine has been developed to safely install aerial round cable in an effective manner. The new machine is a piece of equipment that automatically attaches new cable rings to moving suspension wire and cable at fixed intervals from ground level.

Through the new system that has been developed, it is now possible to automatically install cable from ground level at the work site.

References

- [1] Milos Novak : Aeroelastic Galloping of Prismatic Bodies, Proc. of ASCE, EM1, February 1969.
- [2] Ito, Fujino, and Yamaguchi : Wind study on galloping oscillations of suspend figure-8 telecommunication cables, Proc. of JSCE, Structural Eng./Earthquake Eng., Vol.1.2, No.1, pp.193s-201s, April 1985.
- [3] Tsuruta, I. : Aeroelastic Instability Oscillations of Suspend Figure-8 Telecommunication Cables, Master's Thesis, Dept. of Civil Eng., Univ. of Tokyo, 1983 (in Japanese).



Hiroshi Nakanishi

NTT Access Network
Systems Laboratories
1-7-1 Hanabatake, Tsukuba-city
305 Japan

Hiroshi Nakanishi is a senior engineer supervisor, in Access Network Systems Laboratories, Nippon Telegraph and Telephone Corporation (NTT). He received the B.S. degree in mechanical engineering from Tohoku University, Sendai, Japan, in 1977. He joined NTT in 1977. Currently he is responsible for development of robot system and mechatronics technologies for telecommunication cable construction.



Kazuo Yamamoto

NTT Access Network
Systems Laboratories
1-7-1 Hanabatake, Tsukuba-city
305 Japan

Kazuo Yamamoto received his B.S. degree in mechanical engineering from Hiroshima Institute of Technology in 1991. He joined NTT in 1991. He is engaged in the development of aerial cable installation technique.

Apparatus for Determining Condition of Cables Inside Plant

Toshiharu Hamade, Yukio Shimo* , Masao Sakata**, Koichi Sega***

NTT Hokuriku Construction Planning Center,
*NTT Hokuriku N.T.C, **NTT Fanet Systems Co., ***Sony Tektronix Co.

Abstract

This apparatus determines the status (active or dead) of both twisted pair cables connected to switching equipment and co-axial cables connected to transmission equipment. The key to its operation is a high performance current probe in the detection circuit. By simply clamping the ring shaped probe around a cable, the detector picks up any differential mode energy transmitted along the cable, whether noise from a switching power supply or an unbalanced twisted pair signal. Using this detector enables one to differentiate between active and dead cables. With this method it is no longer necessary to connect an oscillator to each cable, making it simpler for operators to accomplish their task. Furthermore, since no physical contact is made to the cable, detection can be made safely and without interference. Compared with traditional methods, this apparatus enables both improvements in the accuracy and efficiency of cable removal work.

1.Introduction

NTT is currently replacing analog equipment with digital equipment in its large telephone plants, it is important to have an efficient, accurate method for designating which co-axial and twisted pair cables should be removed from the multitudes of other cables. If one relies on visual inspection to determine the proper cables for removal, mistakes are often made which require more time to be spent for repairs. Another method involves attaching an oscillator to one end of a cable and picking up the signal at the other end with an antenna. However, when removing hundreds of cables this method is still not 100% efficient. The desire to improve the above methods drove the development of this new apparatus.

2.Cable types inside the plant

There are three basic types of cabling route for user circuits within a inside plant:

- 1-- Public lines
- 2-- Private lines
- 3-- Multiplexed transmission lines

These are described in figures 1 and 2 respectively. Table 1 shows what type of cabling is typically used for each route.

MDF* = Main Distribution Frame

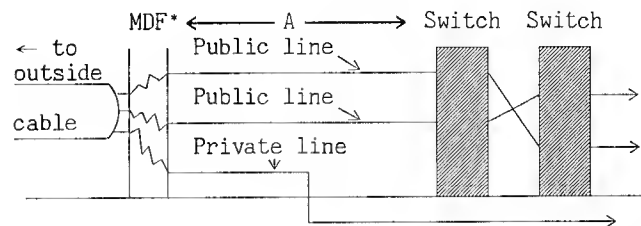


fig.1 cables between switching equipment and MDF

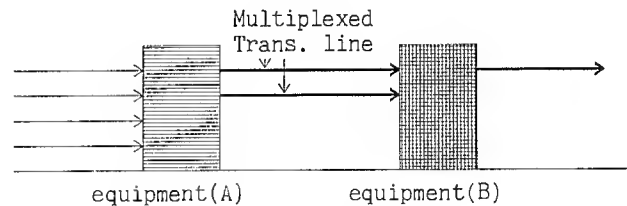


fig.2 cables between multiplexed transmission equipments

table 1 cabling used by line type

L i n e	Cable type
Public line	twisted pair cable
Private line	twisted pair cable
Multi. trans. line	co-axial cable

3.Procedure for replacing switching and other equipment

To replace an analog switches with a digital one for public lines, new cables must be connected between the MDF and digital switch. Because it is not necessary for private lines to be connected through the switching equipment, replacement is not necessary.

After having connected the new cables area "A" of figure 1 looks like photo 1 next page. This photograph is of a small scale plant. In large scale plants the number of cables can be over 100 times

greater. It is from this multitude of cables that the new unnecessary cables are then cut and removed. If one mistakenly cuts a "live" cable, communication over that cable is disrupted. This is especially a problem with private lines as they can be carrying critical information like signals to an airport control tower or financial exchange information between banks. When exchanging transmission equipment and equal amount of care must be taken as one live line cut affects a multiple number of communications.

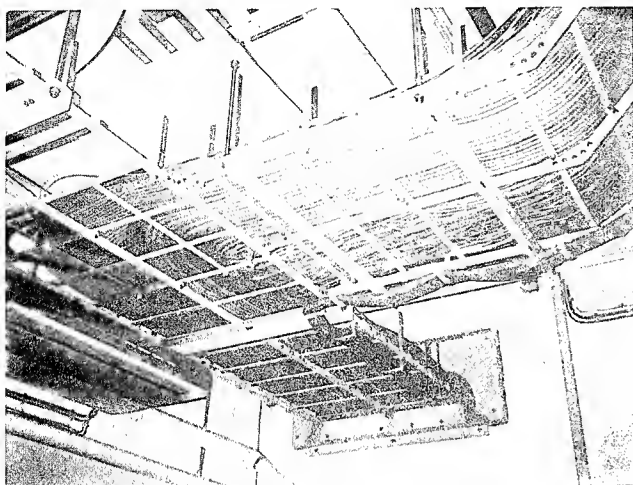


photo 1 cables inside plant

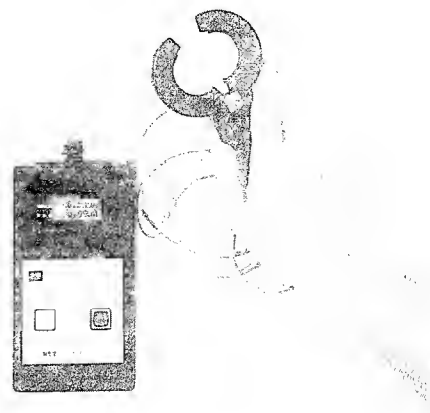


photo 2 apparatus developed

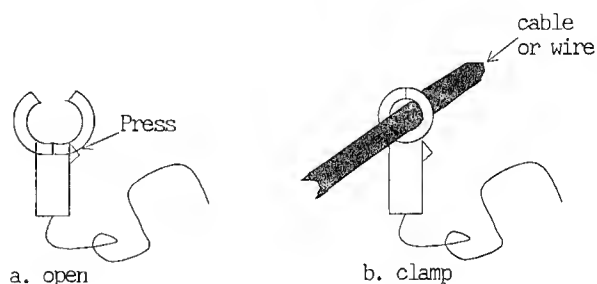


figure 5 method of use

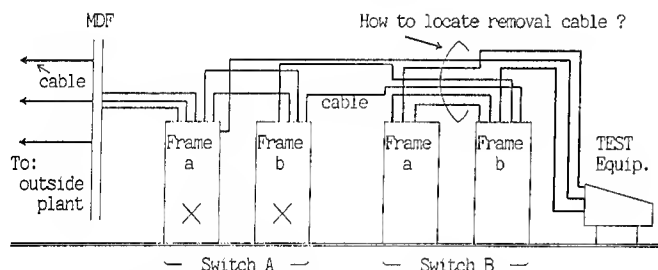


figure 3 example of removing switch A

4. Description of new apparatus

Figure, photo of apparatus developed (figure 4 , photo 2). Figure 5 shows its method of use.

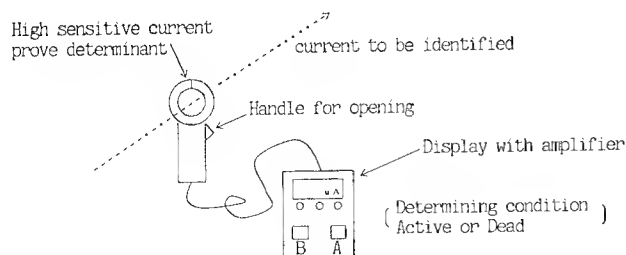


figure 4 an outline of apparatus

On active cables a current probe surrounding a cable can pick up rectifier circuit noise or switching equipment noise which is transmitted along the shield of a co-axial cable and twisted pair cable. It can also pick up any unbalanced signals along the twisted pair, some of which normally exists on an active twisted pair. For dead lines the probe will pick up a signal much closer to zero. By choosing an appropriate threshold it is possible to make an accurate distinction between active and dead cables. Because the noise and unbalanced signals used in the detection process are generally small amplitude signals with varied frequency characteristics, we had to develop a current probe which was highly insensitive to outer magnetic fields yet able to filter and amplify the signals of interest in an optimum manner. The development of this apparatus has allowed us to dramatically reduce the chance of communications interruptions due to cable removal errors. At the same time it has enabled a drastic improvement in work efficiency.

5. Principle of measurement

In twisted pair cables used for public lines, noise from many different sources is present. A few examples are rectifier circuit noise, switching noise and DC-DC converter noise. Figure 6 is an example of the noise spectrum from a twisted pair cable.

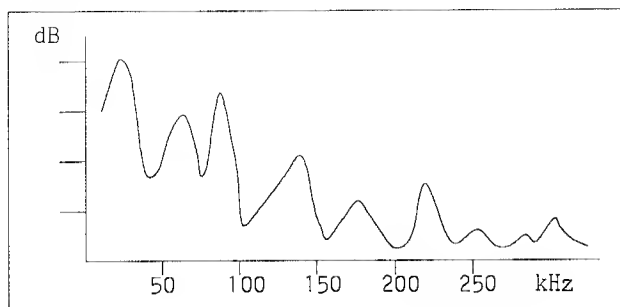


figure 6 Example of noise spectrum from a twisted pair cable

From the figure above it is apparent that noise levels are highest in the band from a few kHz to 100kHz. For this reason we designed the apparatus to have a sharp pick-up in this region through a careful filter design. For dead cables hardly any noise is present in this band. We are therefore able to use this difference to detect active and dead cables.

For private lines and multiplexed transmission lines we can make the same detection relying on leakage from the transmission carrier in the same band. Figure 7 shows a dead cable. Figure 8 shows an active public line twisted pair, figure 9 an active private line (9600bps), and figure 10 an active multiplexed transmission line (64kbps).

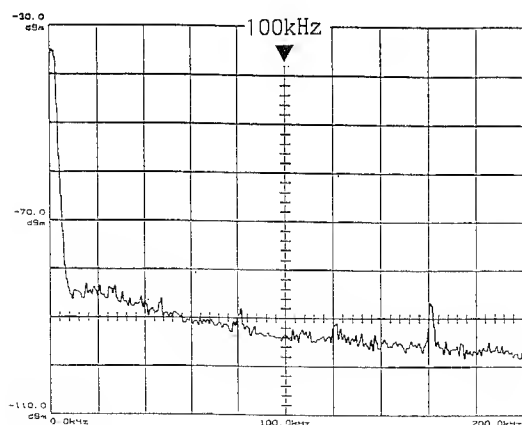


figure 7 spectrum from a dead cable (twisted pair cable)

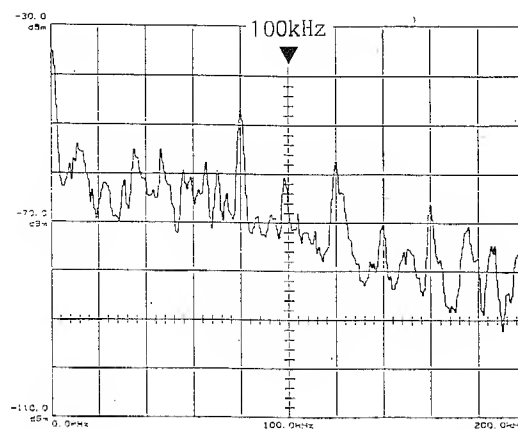


figure 8 spectrum from an active cable (twisted pair cable)

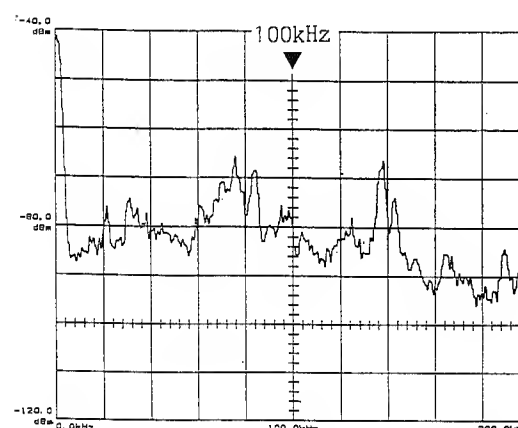


figure 9 spectrum from an active private line (jumpering wire at MDF) (9600bps)

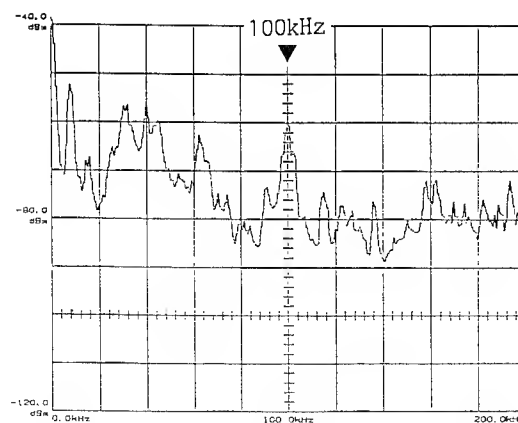


figure 10 an active multiplexed transmission line (co-axial cable)

Figure 9 and 10 was observed at MDF jumpering wire in NTT office.
 I'll also show you more detail principle of measurement. This apparatus catches the current that is flowing into the cable or wire. Therefore the value of result is displayed by unit "mA" or "uA". There are two current mode, cable or wire inside between equipments.
 The current of cable inside is mostly common mode

, however the one of wire inside is managed by differential mode if you clamp just 1 wire of twisted wire. Figure 11 shows current level on an active cable inside that is twisted pair cable and managed by common mode current if you clamp this cable around the sheath. Figure 13 shows similar current level on an active and a dead private line that is twisted wire at MDF. In this case, you should clamp just 1 wire.

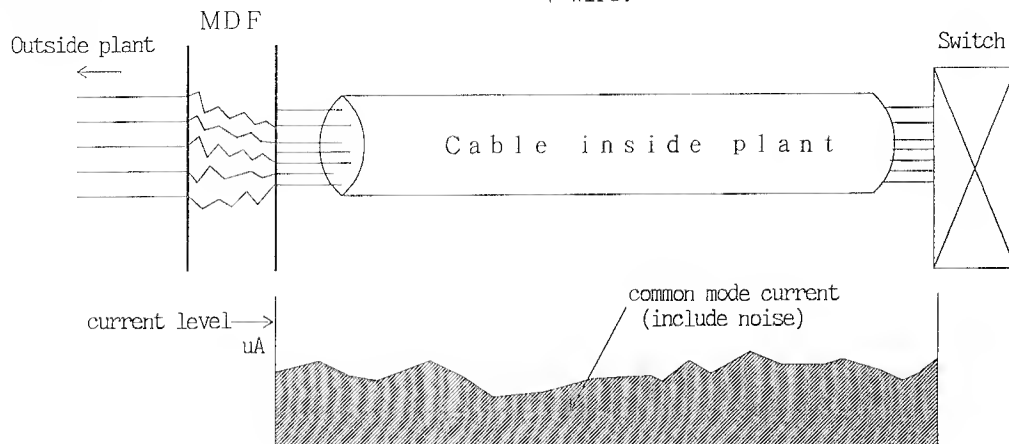


figure 11 current level on an active cable

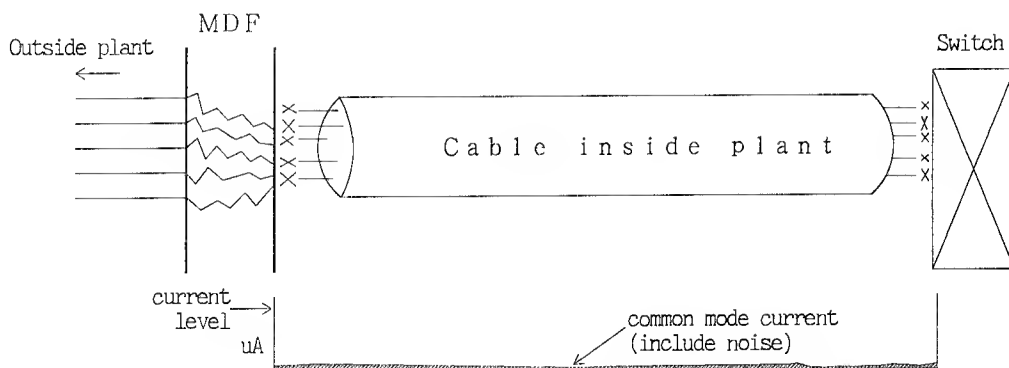


figure 12 current level on a dead cable

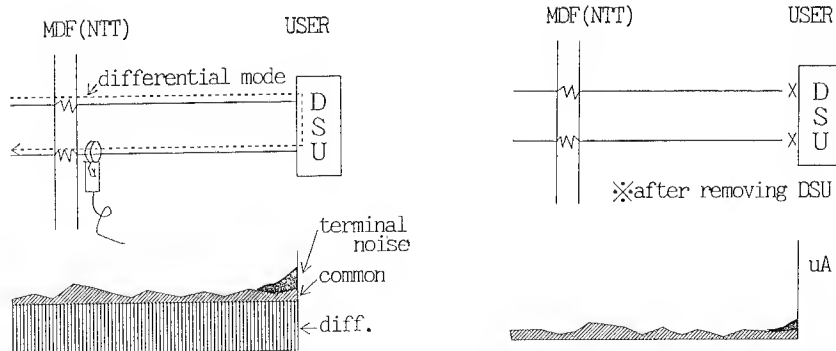


figure 13 private line
 (ISDN 64KBit/S , PACKET 9600Bit/S , On line system for BANK etc.)

6. Conclusions

In the past year, we have begun to study on differential mode energy transmitted along the cable as noise. Through this study, we have invented an apparatus for determining condition of cables that is dead or active in order to prevent cable removal accident.

Thus for we have clarified the following items.

- (1) The noise energy for public line cables has a comparatively large amplitude in the band ranging from a few kHz to 100kHz.
- (2) A similarly energy distribution is found on both private and multiplexed transmission lines.
- (3) The noise level of cables cut at both ends is extremely small, and therefore the difference on noise level as compared with (1) and (2) above is clear.

- (4) This apparatus was designed to make effective use if above facts.

The apparatus is small, lightweigh and can be operated by one person. Without extensive training one is still able to accurately determine an active or dead status through a buzzer and L.E.D.



Toshiharu Hamade

NTT Hokuriku construction planning center ,
1-43-1 Masuizumi
Kanazawa City, Ishikawa
921 Japan.

Toshiharu Hamade joined NTT in 1969 after graduating from Toyama Technical College. His research interests are in the area of

cable installation over long distances. He has developed a sealing method for preventing the flow of N_2 gas-filler out from cable connection point. He is now manager of quality administration section of constructive plants and a member of IEICE.



Yukio Shimo

NTT Hokuriku Network Technical Center,
4-1 Dewamachi,
Kanazawa City, Ishikawa
920 Japan.

Yukio Shimo joined NTT in 1965 after graduating from Hokuriku Technical High School.

He has been engaged in research and development of safe cable installation and sightseeing guide system using FM. He is now chief of cable setting section and a member of IEICE.



Masao Sakata

NTT FANET SYSTEMS Co.
NTT Ikegami Bldg 23-18,
Kugahara 2-Chome, Ohta-ku,
Tokyo 146 Japan

Masao Sakata was born on April 20, 1940 in Himeji, Hyogo, Japan. He received the B.E degree from Kobe University, Japan in 1964.

He joined NTT in 1964. He was engaged in the research and development of electronic switching system. He is now President of NTT FANET SYSTEMS Corporation.



Koichi Segal

Sony Tektronix Corporation,
9-31 Kitashinagawa 5-chome,
Shinagawa-ku,
Tokyo 141 Japan

Koichi Segal joined Sony Tektronix in 1984 after graduating from Tokyo Electric Engineering College.

He is currently engaged as product marketing for RF and wireless test equipment in Telecommunication Product Line. He is now manager of cable connection point. He is now manager of quality administration section of constructive plants and a member of IEICE.

Release of Lead from Lead-Sheathed Telecom Cables in Soil.

Sverker Forsberg
Swedish University of Agricultural Sciences.
S-750 07 Uppsala Sweden.

Jan Björkman
Telia AB.
S-123 86 Farsta Sweden.

Abstract

In order to establish if lead is released from lead-sheathed telecom cables, soil samples were taken above and beneath telecom cables on seven different sites, including four different soil types. The soils were three acidic sandy soils, two neutral heavy clay soils, one alkaline boulder clay soil and one acidic "gyttja" clay soil (acid sulphate soil). The cables were buried into the soil 30 to 45 years ago.

Background

In Swedish media Telia has been accused of creating environmental problems due to lead cables. The cables were said to leak enormous amounts of lead into the soil and could be a potential threat against the environment. In order to establish if lead is released from lead-sheathed telecom cables an investigation was made by order of Telia by the Swedish University of Agricultural Sciences, Department of Soil Science.

Sample preparation

The samples were taken from the following test sites :

- three sites with acidic sandy soil with a low pH-value, sample N1-N3.

- one site with neutral heavy clay soil , sample T1.
- two sites with alkaline boulder clay soil , sample M1 and M2.
- one site with acidic "gyttja" clay soil with a low pH-value, sample T2.

On every test site a 2 m long and about 1 m wide cavity was dug at about 0,5 m below the cable.

The samples were taken as shown below (figure 1) at both ends of the cavity.

Above the cable : 0-5; 5-10 cm

Below the cable : 0-5; 5-10; 10-15; 15-20; 20-30; 30-40 cm

Diagonally below the cable at both sides : 0-5; 5-10; 10-15; 15-20; 20-30 cm.

At a distance of approx. 1.5 m from the cables, in undisturbed soil, reference samples were taken at the following depths :

0-20; 20-40; 40-60; 60-80 cm.

The references at 40-60 and 60-80 cm were used for background correction of measured lead concentrations.

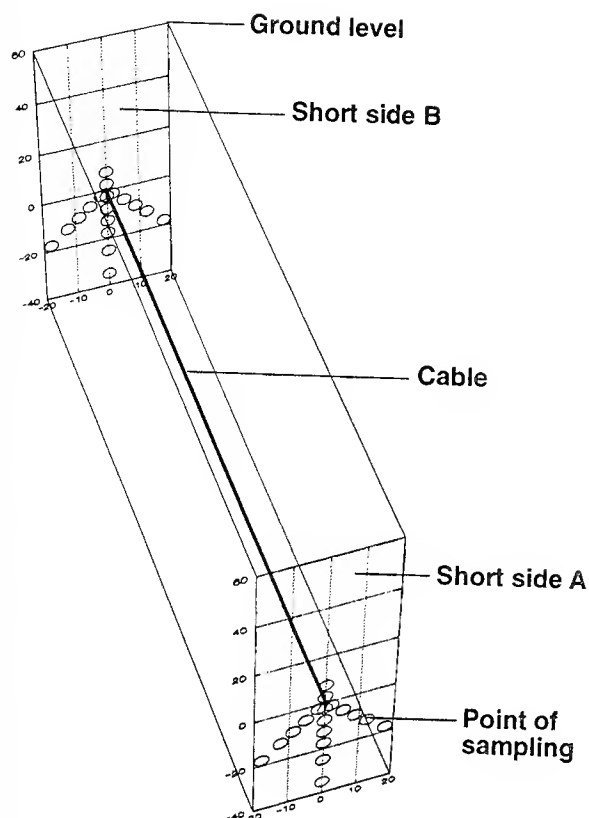


Figure 1.
Cavity dug around cable
for soil sampling (diagram).

Analysis

After air-drying and sieving, the soil samples were analysed for "total" lead by extraction with 2M HNO_3 for two hours at 100°C (figure 2-9)(1) and pH-value (table 1). Samples with high levels of lead were also analysed for easily exchangeable lead by extraction with NH_4OAc , pH 4.8, for eight hours in an end-over-end rotator (table 4)(1). Lead analyses were performed by ordinary AAS at 217 nm. A number of samples with low levels were analysed by flameless AAS at 283,3 nm. With both methods background correction was used.

The test sites T1 and T2 were assumed to contain substantial amounts of humus and sulphur and were analysed in accordance (table 2).

Test sites M1 and M2 were analysed for CaCO_3 (table 3).

All results are corrected for moisture content of air-dry soil.

Table 1

Close to the cable

Test site	pH-value
N1	4.8
N2	5.3
N3	5.7
M1	7.7
M2	8.0
T1	7.6
T2	4.3

Table 2

Close to the cable

Test site	Humus	Sulphur
T1	1.4 %	0.01 %
T2	28.0 %	0.39 %

Table 3

Close to the cable

Test site	carbonate
M1	<0.1 %
M2	16.5 %

Discussion

It may be concluded that some lead is released from telecom cables in soils, but in most soil types this will not become an environmental risk within the foreseeable future. The levels of lead in the soil immediately beneath the cables range from 100 to 4000 mg/kg soil. Between 83-98% of the released lead is retained within 5 cm from the cables. The highest levels and the largest amounts are found in acidic "gyttja" clay and one of the sandy soils. The lowest levels and smallest amounts are found in calcareous boulder clay.

Generally the amounts of lead in different soil types increase in the order :

calcareous clay<sandy soil<non-calcareous clay<"gyttja" clay.

Distribution of lead in nature

The total amount of non-corrosion protected lead cables in Telia is calculated to about 70 000 metric tons. The mean release from this lead cables is calculated to 7 metric tons annually.

The normal background levels in soil in Sweden vary between 2 and 200 ppm (2). In Swedish agricultural soil the lead content is around 16 ppm (3).

From the environmental point of view the most serious example of lead distribution during this century is as additive in petrol. In the southern third part of Sweden the deposition of lead is about 700 metric tons annually (4). This lead is atomized and is distributed as organic lead which makes it a direct health hazard and environmental problem.

Lead from skeet and trap shooting in Sweden is about 500 metric tons annually, and release of lead from hunting, about 70 metric tons annually (5).

References.

1. Andersson, A. 1976. On the determination of ecologically significant fractions of some heavy metals in soil. Swedish Journal of Agricultural Research 6, 19-25.
2. Lindsay W.L 1979. Chemical equilibria in soils. New York : John Wiley & sons
3. Andersson A 1977. Heavy metals in Swedish soils; On their Retention, Distribution and amounts. Swedish J.agric. Res. 7, 7-20.
4. Andersson A 1992. Trace elements in agricultural soils. Fluxes, balances and background values. Swedish Environmental Protection Agency report 4077.
5. Notter M, Moberg A & Andersson K. 1983 Blyhagelspridning och dess inverkan på mark och växtlighet. Swedish Environmental Protection Agency.

Sverker Forsberg was born 1968. He has a degree as agronomist from Swedish University of Agricultural Science in Uppsala Sweden. He is now making his PhD at the Radioecological Department in the same university.

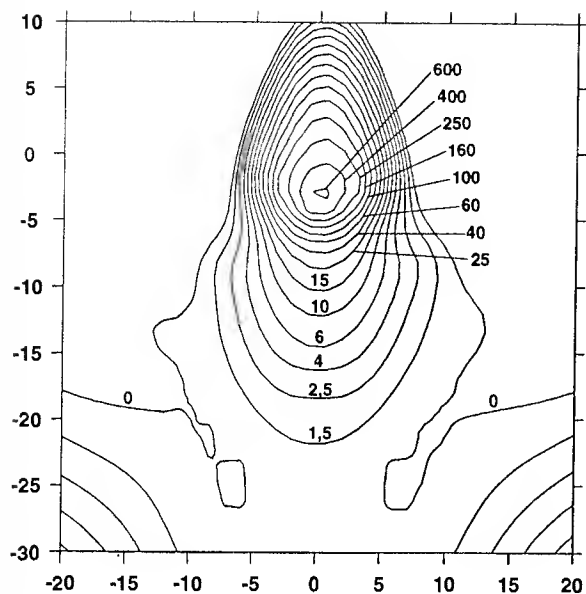


Jan Björkman was born in Malmö 1943. He joined Telia 1977. He is now a senior engineer at the Network Services Division and coordinator for optical fibres and cables. He holds a degree in chemical engineering from Malmö Technical School. He has studied mathematics in Stockholm University and Polymer Science at Royal Institute of Technology in Stockholm.

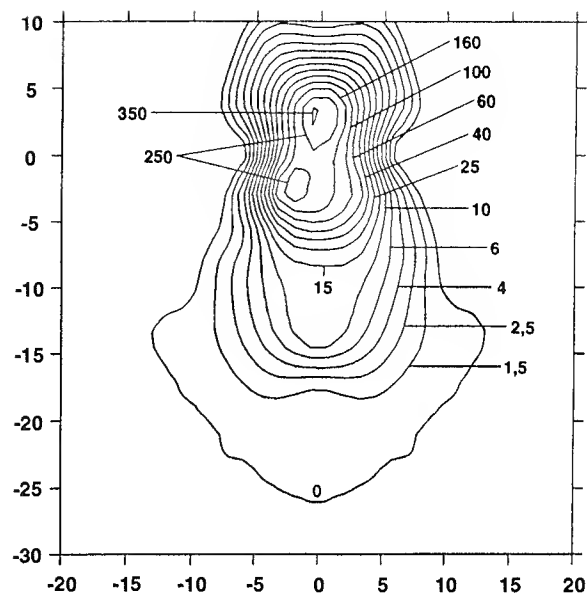
Table 4.

Content of easily exchangeable lead in ppm.

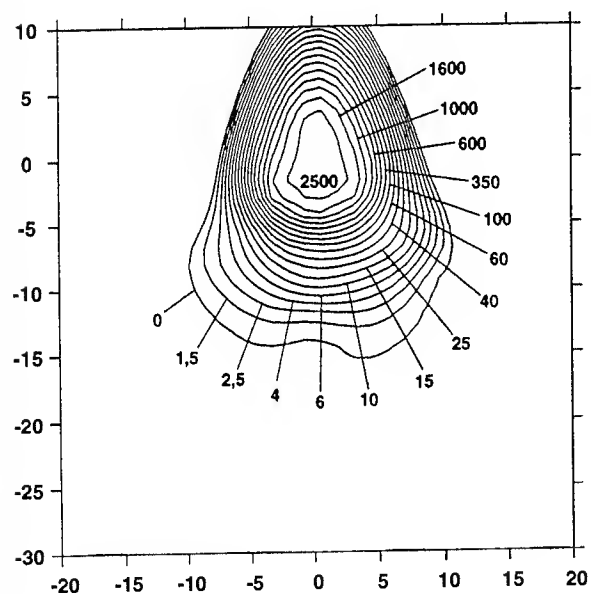
Test site	distance cm	above the cable	below the cable	diagonally left of the cable	diagonally right of the cable
N1	0-5	112	741	228	244
N1	5-10		54		
N1	10-15		36		
N2	5-10	70			
N2	0-5	2234	2380	1475	2046
N2	5-10				33
N3	0-5	349	261	360	86
N3	5-10		53		
T1	0-5	1243	1205	598	631
T1	5-10		4		13
T2	0-5	2175	2012	1703	2684
T2	5-10		38	29	52
T2	15-20		19	12	13
M1	0-5	67	65	23	36
M2	0-5	201	144	52	89



N1



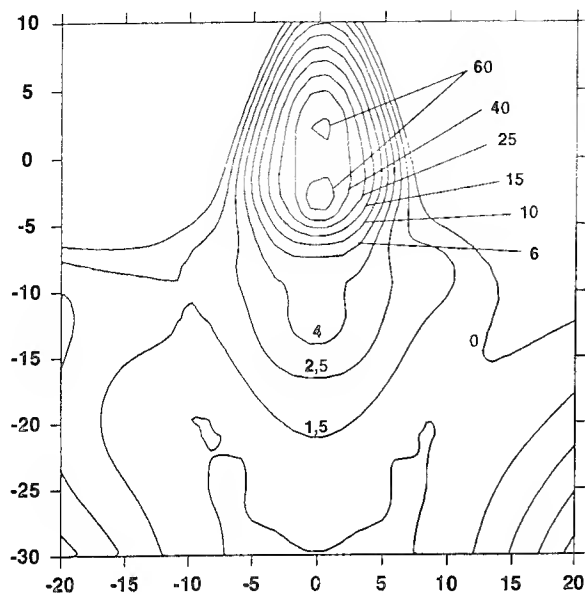
N3



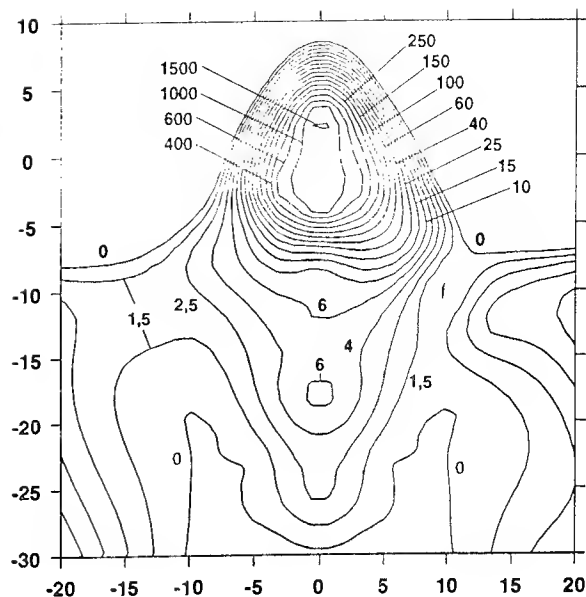
N2

Figure 4
Distribution of total lead at N3.

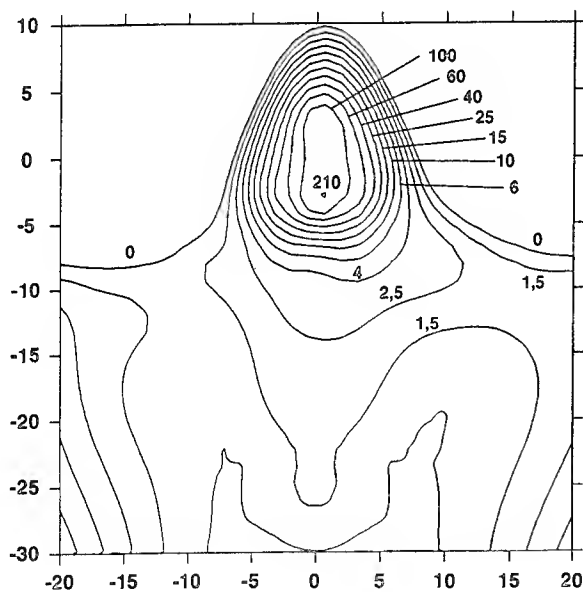
Figures 2 and 3
Distribution of total lead at N1 (top) and
N2 (bottom). The cable is located at 0; 0.



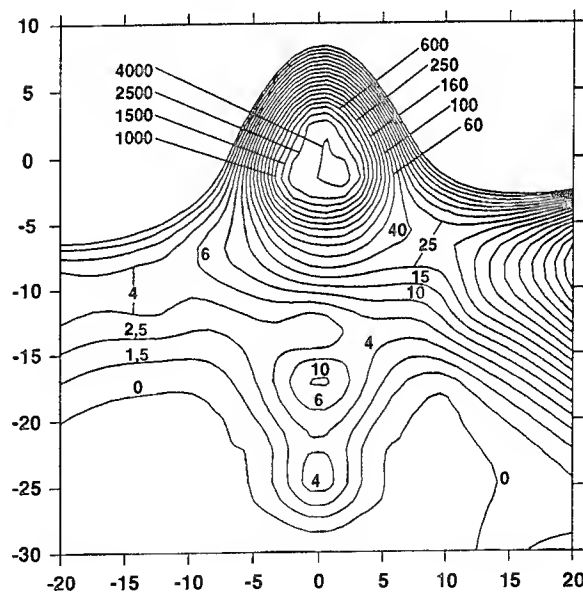
M1



T1



M2



T2

Figures 5 and 6
Distribution of total lead at M1 (top)
and M2 (bottom).

Figures 7 and 8
Distribution of total lead at T1 (top)
and T2 (bottom).

The Influence of Reflective Components in Lightwave AM-VSB CATV Systems Performance

*Tien-Jey Shen, Knaug-Yi Chen, Chih-Yih Wang,
Hung-Tn Chen, Fwu-Yuan Tsai, Wei-Shyan Chien,*

Telecommunication Labs, P.O. BOX 71 Chung-Li, Taiwan 32099, R.O.C.

Abstract

This paper discusses the influence between passive components and lightwave AM system performance. The lightwave AM system parameters were measured at different reflection on channel frequency 55.25MHz, 127.25MHz, 223.25MHz, and 319.25MHz.

The system parameters were measured by simulated method and actual passive component field test. No clear difference is observed between the simulated method and field test results.

1. Introduction

AM-VSB CATV systems now are very rapidly developed in Taiwan local area. Some CATV systems companies want to use subscriber optical fiber loop to transmit their video signals. There is lots of lightwave AM system parameters influence the quality of CATV systems.[1]-[3] Unlike digital systems, lightwave AM systems are very sensitive to small amounts of intensity noise. Such noise can significantly degrade lightwave AM system performance.[4] Reflectance in AM lightwave system can contribute intensity noise, multipath interference between reflective components can generate intensity noise which degrades the transmitted signal quality.[5]-[6]

What is the actual influence of the noise due to connectors, splitters, splicers, etc. between these passive components and system parameters? That is the more important thing we want to know. T.L. can get the test result to specify the quantity of those passive components used in the field.

In this paper, we discuss the influence between passive components and lightwave AM system performance theoretically in section 2. With regard to the impairments of carrier to noise ratio (CNR), and we also measured the CSO & CTB. We report test result and measured the CNR, CSO and CTB in section 3. In section 3, the setup for the analog measurements are described. Using such a laser module and measurement setup, experimental results are compared with theoretical results in section 3. Section 4 is the summary and conclusion.

2. Theoretical Result

It is reported that the analog performance of the system is impaired by fiber transmission, even though a spectrum light source such as a DFB laser is used. In this section, CNR degradation caused by Rayleigh backscattering and others parameter are theoretically investigated.

Every system has some theoretical calculate CNR which is a function of the double Rayleigh backscattering of the fiber, and the laser spectral width and the modulation depth. The equation of cavity CNR is expressed as

$$CNR_{cav} = 10 \log \left[\frac{\sqrt{2\pi} m^2 B_{fwhm}}{16 \sqrt{\ln 2} B_n R_{eq}} e^{2f^2 \frac{\ln 2}{B_{fwhm}^2}} \right] \quad (1)$$

where B_{fwhm} is the full width of half maximum of the laser spectrum under modulation. B_n is the noise bandwidth (4 MHz), and m is the modulation index of the laser. f is the measured frequency. R_{eq} is the equivalent reflectance of fiber Rayleigh

backscattering.

the Req is expressed as [4]

$$R_{eq} = \frac{S\alpha_s}{4\alpha} R_s \left[\left(1 - e^{-2\alpha l} \right) + \left(1 - e^{-2\alpha l} \right) \right] \quad (2)$$

where l is the fiber length. α is the total attenuation of the fiber. α_s is the fiber Rayleigh scattering coefficient = 0.076/km. S is the fraction of scattered light captured and guided by the fiber back to the source. The CNR of the system can then be

given as:[4]

$$CNR_{sys} = -10 \log \left[10^{-\frac{CNR_{base}}{10}} + 10^{-\frac{CNR_{cav}}{10}} \right] \quad (3)$$

where CNR_{sys} is the CNR of the system. CNR_{base} is the baseline CNR of the system.

The calculate results of Req, CNR_{cav} and CNR_{sys} are showing in table (1)-(4) with different measuring frequency.

3.Experimental Results

3.1 Test Setup

Diagrams of the experimental setup to evaluate the noise and distortion characteristics of the AM system are shown in Fig.1 The source consisted of a DFB laser driven by a multi-channel CATV generate which is set up with 40 channels from 55.25 MHz to 325.25 MHz. Angle FC/APC connectors or fusion splices with an optical reflection less then -60 dB are applied for the measurement. The link consisted of a test optical connector with different reflection loss from -55 dB to -20dB. RF signal generator is used Matrix SX-16 Distortion analyzer is Matrix R-75. CNR, CSO and CTB are measured under 40 channel modulation according to the NTSC frequency plan.

3.2 CNR Test Result

The lightwave AM system parameters CNR were measured trice and then average at each frequency.

Fig. 2(a) shows the CNR versus connectors with different reflection loss which locate in the middle distance of the test loop. The test frequency is 55.25 MHz (CH 2). There was a moderate degradation of the system CNR above connector reflection loss -40 dB. When the reflection loss was below -40 dB, degradation of the system CNR was not observed. And the maximum connector reflection loss increase from -40 dB to -30 dB, there is approximately 15 dB of degradation on CNR.

In Fig. 2(b) and Fig. 2(c), calculated CNR's using equation (3) are also plotted. The experimental results show good agreement with the theoretical values. Compare Fig. 2(a) to Fig 2(d), in Fig 2(a) shows the measured value is always below the theory calculate curve. But in Fig. 2(d) the measured value is always above the theoretical value. So the measured frequency may effect the degradation of system CNR. From Fig 2, the degradation caused by connector reflection become small as the frequency become higher.

3.3 CSO&CTB Test Result

Fig. 3 shows CTB as a function of connector reflection loss under 40 channel modulation. however, CTB is degraded by 2 dB after reflection loss is change from -40 dB to -30 dB. The measured frequency range was 55.25 MHz to 325.25 MHz, and the fiber total length was 4.4 Km.

Fig. 4 shows CSO as a function of connector reflection loss under 40 channel modulation. however, The measured frequency range was 55.25 MHz to 325.25 MHz, and the fiber total length was 4.4 Km. There is no clear degradation observed of the system CSO at the reflectance from -55 dB to -20 dB at channel frequency 55.25 MHz, 127.25 MHz, and 223.25 MHz. CSO is always within -52 dB from the reflection -55 dB TO -30 dB.

4. Summary and Conclusion

The lightwave AM system parameter characteristics are theoretically and experimentally investigated. From the theoretically calculated the each frequency CNR degradation compared with the experimental results. The experimental results agree well with the theory.

The lightwave AM system parameters were measured at different reflectance on channel frequency 55.25 MHz(CH 2), 127.25 MHz(CH 15), 223.25 MHz(CH 24), and 319.25 MHz(CH 40). We obtained the results that different channel frequency has a different curve, if we plot components' reflectance vs. system parameters' CNR, CSO, CTB, etc. When the average reflectance was below -40 dB, degradation of the system was not observed. When the reflectance increases from -40 dB to -30 dB there is approximately 15 dB of degradation on CNR. Lowest channel frequency is more degraded than highest channel frequency.

Other lightwave AM system parameters such as CTB and CSO are measured with reflectance from -55dB to -20dB. The reflectance increases from -40dB to -30dB, there is approximately 2dB of degradation on CTB. There is no clear degradation observed of the system CSO at the reflectance from -55dB to -20dB at channel frequency 55.25MHz, 127.25MHz and 223.25MHz. CSO is always within -52dB from the reflectance -55dB to -30dB.

Acknowledgments

The author would like to thank Dr. Yu-Whei Chen and Mr. Teng-Chih Feng for their encouragement. They also thanks Chia-Hsien Wu and Hsiu-Jung Chuang, C.C. Chu for their useful discussion.

Reference

- [1] Darcie, T.E. and G.E. Bodeep. "Fiber reflection-Induced Impairments in Lightwave AM-VSB CATV Systems." *Journal of Lightwave Technology*. Vol.9, No.8, 1991, pp 991-995
- [2] Judy, A.f. "Reflections and Fiber Video System." *Proceedings Southcon/91*. 1991, pp 181-188.
- [3] A.F. Judy, "Intensity noise from fiber Rayleigh backscatter and mechanical splices," in ECOC'89, 1989, PP 486-489.
- [4] M.J. Labiche, "Noise due to reflective components in fiber optic AM-VSB CATV systems" NCTA Conference Proceedings 1993 pp290-299.
- [5] T.J. Sheu, C.Y. Wang, etc. "Establish a test set for measurement the lightwave analog signals parameters" TL Technique Report 83-LL-048
- [6] T.J. Sheu, C.Y. Wang, etc. "The effect of connector return loss in lightwave AM-VSB CATV systems." TL Technique Report 83-LL-055

Return Loss (dB)	R_{eq} (dB)	CNR_{cav} (dB)	CNR_{base} (dB)	CNR_{sys} (dB)
20	48.79	34.76	46.90	34.49
25	53.79	39.76	46.90	38.99
30	58.79	44.76	46.90	42.68
35	63.79	49.76	46.90	45.08
40	68.79	54.76	46.90	46.24
45	73.79	59.76	46.90	46.68
50	78.79	64.76	46.90	46.83

Table 1.theoretical calculated results of R_{eq} , CNR_{cav} , CNR_{sys} versus different return loss on channel frequency 55.25MHz

Return Loss (dB)	R_{eq} (dB)	CNR_{cav} (dB)	CNR_{base} (dB)	CNR_{sys} (dB)
20	48.79	34.79	46.10	35.21
25	53.79	39.79	46.10	38.92
30	58.79	44.79	46.10	42.38
35	63.79	49.79	46.10	44.55
40	68.79	54.79	46.10	45.54
45	73.79	59.79	46.10	45.92
50	78.79	64.79	46.10	46.04

Table 2.theoretical calculated results of R_{eq} , CNR_{cav} , CNR_{sys} versus different return loss on channel frequency 127.25MHz

Return Loss (dB)	R_{eq} (dB)	CNR_{cav} (dB)	CNR_{base} (dB)	CNR_{sys} (dB)
20	48.79	35.81	46.70	35.47
25	53.79	40.81	46.70	38.81
30	58.79	45.81	46.70	43.22
35	63.79	50.81	46.70	45.27
40	68.79	55.81	46.70	46.19
45	73.79	60.81	46.70	46.53
50	78.79	65.81	46.70	46.65

Table 3.theoretical calculated results of R_{eq} , CNR_{cav} , CNR_{sys} versus different return loss on channel frequency 223.25MHz

Return Loss (dB)	R_{eq} (dB)	CNR_{cav} (dB)	CNR_{base} (dB)	CNR_{sys} (dB)
20	48.79	36.99	48.40	36.68
25	53.79	41.99	48.40	41.09
30	58.79	46.99	48.40	44.63
35	63.79	51.99	48.40	46.82
40	68.79	56.99	48.40	47.83
45	73.79	61.99	48.40	48.21
50	78.79	66.99	48.40	48.34

Table 4.theoretical calculated results of R_{eq} , CNR_{cav} , CNR_{sys} versus different return loss on channel frequency 319.25MHz

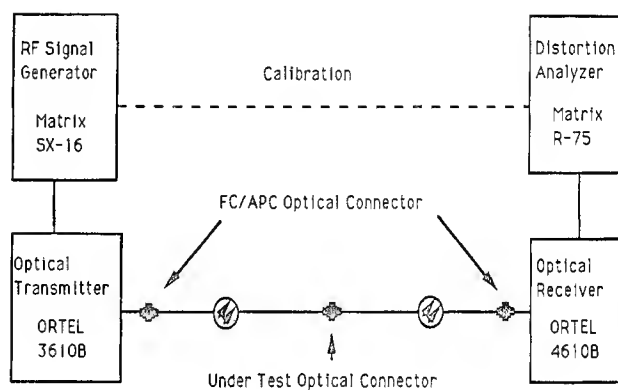


Fig. 1Schematic configuration of the lightwave AM-VSB CATV systems test set.

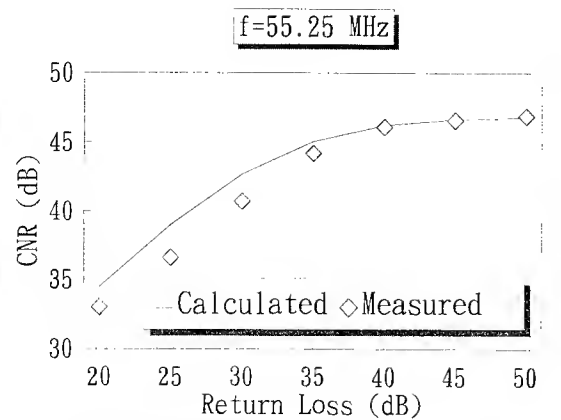


Fig. 2(a) Experimental results and predicted results of carrier-to-noise ratio CNRdegradation due to connector reflection on channel frequency 55.25 MHz.

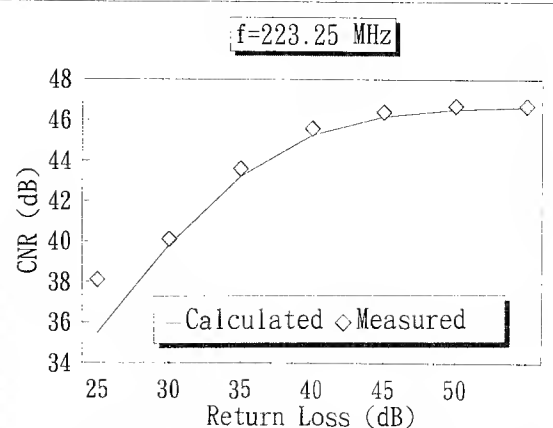


Fig. 2(c) Experimental results and predicted results of carrier-to-noise ratio CNRdegradation due to connector reflection on channel frequency 223.25 MHz.

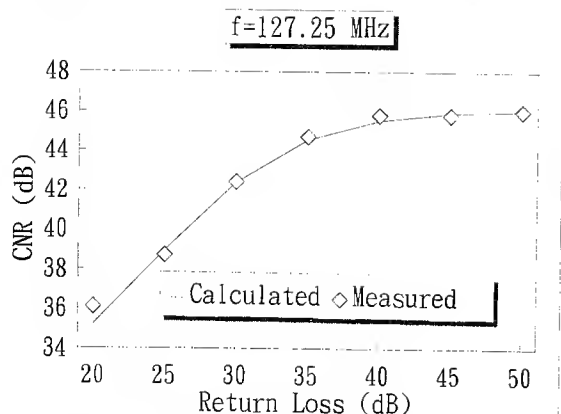


Fig. 2(b) Experimental results and predicted results of carrier-to-noise ratio CNRdegradation due to connector reflection on channel frequency 127.25 MHz.

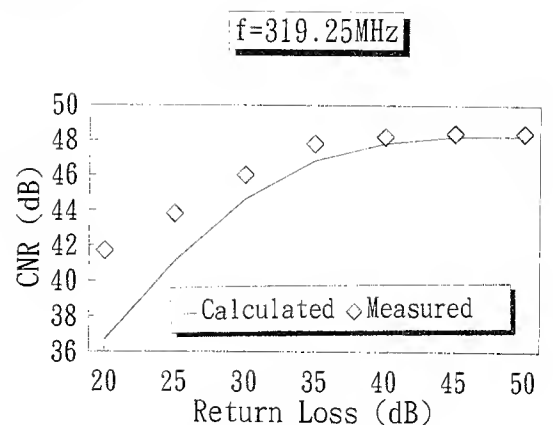


Fig. 2(d) Experimental results and predicted results of carrier-to-noise ratio CNRdegradation due to connector reflection on channel frequency 319.25 MHz.

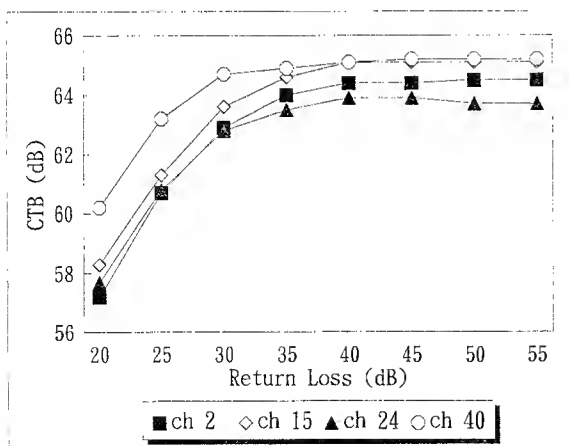


Fig. 3 Experimental results of CTB distortion due to different connector reflection on different channel frequency.

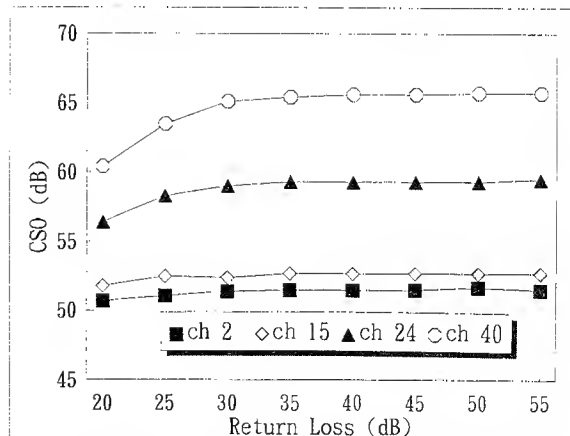


Fig. 4 Experimental results of CSO distortion due to different connector reflection on different channel frequency.

The effect of sulfate-reducing bacteria on the metallic corrosion in fiber optic cable

Jyh-Hwa Wang, Yaw-Tzong Horng, Hsi-Pai Hsh, Kuang-Yi Chen

Telecommunication Laboratories
P.O.Box 71, Chung-Li, Taiwan, R.O.C.

Abstract

The corrosion behaviors of various metals, used as the armored or shielding materials in fiber optic cable, were studied in a specific culture medium with and without sulfate-reducing bacteria(SRB). The metals employed in this study included carbon steel, 304 stainless steel, copper alloy and aluminum. Electrochemical measurements were conducted to assess the damages caused by microbiologically influenced corrosion. Besides the measurements of corrosion rate and the polarization curves, the electrochemical impedance technique has also been employed to continuously monitor the corrosion behavior of metals during exposure times to test media.

Introduction

Previous work has demonstrated that hydrogen increases attenuation of armored submarine cables [1-4]. The submarine cable is typically armored with one or more layers of armor wire to protect it from marine traffic as well as to provide sufficient weight for the cable to remain at the water bottom. The corroding armor wire was suspected to be the possible source for the hydrogen generation. An improved corrosion resistant design is therefore required for fiber optic cable in submarine environment.

SRB are likely found in the submarine environment and known to significantly increase the corrosion rate of many metals. In anaerobic environment, SRB use sulfate ions in place of oxygen as the terminal electron acceptor to produce hydrogen sulfide. The production of hydrogen sulfide could affect the fiber optic cable in two distinct forms: (1) stimulating the atomic hydrogen into materials by preventing its

recombination into hydrogen molecules[5] (2) promoting the corrosion of metallic components in cable. In the presence of sulfide, uncombined hydrogen atoms increase in number on the material surface, and the probability that they will diffuse into the materials also increases. Hydrogen sulfide produced by SRB therefore may stimulate the absorption of hydrogen into materials. SRB corrosion of steel is a well known phenomenon and an extensive literature exists on its possible mechanism[6-10]. Under anaerobic conditions, normal electrochemical corrosion is stifled because the cathode becomes polarized by the build-up of atomic hydrogen on the surface. SRB is thought to stimulate the normal electrochemical corrosion mechanisms by the removal of cathodic hydrogen. On the other hand, the biofilm on metal surface could produce an oxygen concentration cells and result in the localized corrosion. The biofilm produces an environment at the biofilm/metal interface that is radically different from that of the bulk in terms of dissolved oxygen, pH, organic and inorganic species. Consequently, the areas under biofilm become anodic and surrounding areas become cathodic. The differential aeration or oxygen concentration cells would be important in anaerobic corrosion.

Electrochemical techniques are increasingly being used in microbiologically influenced corrosion (MIC) studies to obtain a better understanding of the effects of microorganisms on the corrosion of metals. To avoid altering MIC processes by the analyses, the electrochemical impedance techniques that do not damage the biofilm are preferred. The advantage of the electrochemical impedance technique lies in its application of small amplitude signals, within the linear response range and generally 5 mV arc

applied. In fact, Franklin, et al. showed that the small current densities generated by impedance measurements did not damage the biofilm[11]. This study is concerned in using the electrochemical impedance technique and d.c. polarization measurements to investigate the influence of SRB on the corrosion behavior of metals.

Experimental

The metals used were carbon steel, 304 stainless steel, copper alloy and aluminum. The percentage average chemical composition is given in Table 1. The specimens were cut into 1 cm x 2 cm in dimension. Wires were soldered onto the specimens to provide the electrical connection. All specimens were finished with 600 grit silicone carbide paper. The specimens were ultrasonically cleaned with acetone and then rinsed with distilled water.

A SRB of *Desulfovibrio* species has obtained from the sludge in a drain and used in this study. The medium contained (per liter of deionized water) 7 g of sodium lactate, 1 g of yeast extract, 1 g of NH_4Cl , 0.5 g of KH_2PO_4 , 2 g of $\text{MgSO}_4 \cdot 7\text{H}_2\text{O}$, 1 g of CaSO_4 , 0.5 g of $\text{FeSO}_4 \cdot 7\text{H}_2\text{O}$, 0.1 g of ascorbate, 0.1 g of thioglycollate and 1 mg of resazurine. The pH of the medium was adjusted to 7.2 with NaOH. The medium was sterilized in an autoclave (121°C and 20 psi for 20 min) before being introduced to the test cells. Then, the active SRB culture was added to the medium. The medium was purged with N_2 to remove oxygen from the cell. The 14 ml flasks were used as test cells. The volume of medium in each flask was 8 ml. The flasks were sealed with rubber stoppers and draped with aluminum foil to prevent contamination. The test cell for the impedance measurements was a two electrode cell containing a working electrode and a Pt electrode. The typical three electrode cells, with a saturated calomel electrode (SCE) being introduced, were arranged for the polarization curve measurements. In all experiments the temperature was fixed at 28°C.

Potentiodynamic polarization experiments were carried out using a computerized corrosion measurement system (Model 273A, EG&G Princeton Applied Research, U.S.A.) and the scan rate was 1 mV/s. In addition, impedance measurements were

performed with an EG&G 273A potentiostat outfitted with option 92 and a Schlumberger 1255 frequency response analyzer (FRA). Sinusoidal potentials of 5 mV_{rms} around the open-circuit potential; ranging in frequency from 100 kHz to 5 mHz, were applied to the working electrode.

Results and Discussion

Figure 1 illustrates time dependence of the charge transfer resistance (R_{ct}) for the carbon steel in different test medium. In sterile medium, R_{ct} was nearly a constant value during the first 60 days of exposure and then decreased with the increase of exposure time. In SRB medium, R_{ct} decreased quickly in 20 days and then kept around a steady state value. For comparison at the same time, R_{ct} of carbon steel in SRB medium was noticed to be much lower than that in the sterile medium. This result indicates that SRB markedly promote the corrosion rate of carbon steel in the test medium. Figure 2 presents the results of potentiodynamic polarization experiments done on carbon steel after 14 days of exposure to sterile and SRB medium. Only a slight difference was observed between the anodic polarization curves. On the other hand, a significant increase in cathodic current density was noticed in the cathodic polarization measurements. Such behavior demonstrates that the primary effect of SRB on the corrosion of carbon steel is to affect the "depolarization" behavior on the cathode. The corrosion rate calculated on the basis of polarization curves in Fig 2 were 27.5 $\mu\text{A}/\text{cm}^2$ (in sterile medium) and 88.5 $\mu\text{A}/\text{cm}^2$ (in SRB medium). The results of polarization curve measurements is consistent with that of electrochemical impedance measurements.

Figure 3 presents the Bode-plots for 304 stainless steel after 155 days of exposure to different test media. The impedance of both are dominated by the capacitive component. No changes in the shape of the spectra were detected for 304 stainless steel in different test media. It was observed that only a slight decreases in impedance were caused by SRB. Figure 4 shows the polarization curves of 304 stainless steel after 120 days of exposure to test media. The pitting potential (E_{pit}) of 304 stainless steel in SRB medium was similar to that in sterile medium. Based on the results in Fig 3 and 4, it is

concluded that SRB would not significantly decrease the resistance of 304 stainless steel to pitting corrosion. In fact, there was no pitting corrosion observed for 304 stainless steel after 155 days of exposure to either sterile or SRB medium by morphological examinations.

The time dependence of R_{ct} for copper alloy in different test media is seen in Fig 5. The change of R_{ct} with time in sterile and SRB medium had the same general trend decreasing with time towards more negative values. However, the R_{ct} in SRB medium are much lower than that in sterile medium. Figure 6 shows the influence of SRB on the polarization curves for copper alloy after 75 days of exposure to test media. A significant increase in anodic current density was observed in the anodic polarization measurements. Changes in cathodic polarization curves were negligible in comparison with that in anodic polarization curves. The result in Fig.6 concludes that the influence of SRB on corrosion behavior of copper alloy is primarily to promote the anodic reaction, not the cathodic "depolarization" as occurred in carbon steel.

Figure 7 gives the time dependence of R_{ct} for aluminum in different test media. A dramatic decrease in R_{ct} for aluminum was seen after 80 days of exposure to sterile medium. Meanwhile, the R_{ct} of aluminum in SRB were always at very low values during the whole exposure time. Consequently, a much higher corrosion rate was expected for aluminum in SRB medium than that in sterile medium. The influence of SRB on the polarization curves for aluminum is shown in Fig.8. A passivation phenomenon in anodic region was observed in sterile medium, but not in SRB medium. Such result indicates that SRB could damage the passive film on aluminum and therefore decrease its resistance to localized corrosion.

Conclusions

1. Carbon steel, copper alloy and aluminum are highly susceptible to SRB attack in the specific culture medium.
2. SRB promote the corrosion rate of carbon steel through the cathodic "depolarization". For copper alloy and aluminum, the mechanism of SRB attack is to increase the anodic dissolution reaction.

Acknowledgments

The authors would like to thank Prof. Hsi-Hua Wang and Prof. Rucy-Shyang Hseu who belong to the Dept. of Agricultural Chemistry, National Taiwan University for their assistance in the cultivation of bacteria.

References

1. W.T. Anderson, A.J. Johnson, J.P. Kilmer, and R.M. Kanan, Proceedings of the 37 th International Wire and Cable Symposium, Reno, Nevada, November 15-17, 1988, pp.188-199.
2. W.T. Anderson, A.J. Johnson, and A. Devito, Proceedings of the 38 th International Wire and Cable Symposium, Atlanta, Georgia, November 14-16, 1989, pp.675-683.
3. N.E. Hardwick, III, L.C. Hotchkiss, J.J. Bless, and D.L. Philen, Proceedings of the 38th International Wire and Cable Symposium, Atlanta, Georgia, November 14-16, 1989, pp.689-695.
4. S. Hopland, Proceedings of the 38 th International Wire and Cable Symposium, Atlanta, Georgia, November 14-16, 1989, pp.684-688.
5. R.D. McCright, "Effects of environmental species and metallurgical structure on the hydrogen entry into steel" in Stress Corrosion Cracking and Hydrogen Embrittlement of Iron Base Alloys, National Association of Corrosion-Engineers, Houston, Texas, pp.306-325, 1977.
6. Von Wolzogen Kuhr, C.A.H. & I.S. Van der Vlugt, The graphitization of cast iron as an electrochemical process in anacrobic soils. Water, 18, 147-165 (1934).
7. G.H. Booth and A.K. Tiller, Corros. Sci; 3, 583 (1968).
8. L. Daniels, N. Bealey, B.S. Rajagopal and P. Weimer, Science 237, 509 (1987).
9. M. Eashwar, P. Chandrasekaran, G. Subramanian, K. Balakrishnan, Corrosion, Vol.49, No.2, pp.108-113 (1993).

10. Brenda Little, Patricia Wagner and Florian Mansfeld, *Electrochimica Acta*, Vol.37, No.12, pp.2185-2194 (1992).

11. Franklin, M.J. Nivens, D.E. Guckert, J.B. and White, D.C, *Corrosion* 79, 519-522 (1991).

Table 1. Chemical compositions of test metals

	Fe	C	Mn	Zn	Cu	Si	Mo	Cr	Ni	Al
carbon steel	bal	1.15	0.42	-	-	0.30	-	0.15	0.05	-
304 S.S.	bal	0.88	1.46	-	-	1.10	0.06	18.97	9.17	-
copper alloy	-	-	-	35.82	bal	-	-	-	0.05	-
aluminum	0.46	-	-	-	0.36	0.64	-	0.01	1.06	bal

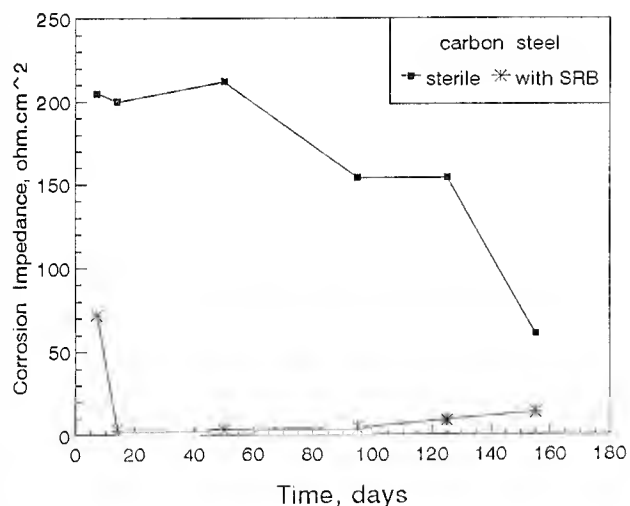


Figure 1 Impedance vs. time of carbon steel in two different test media.

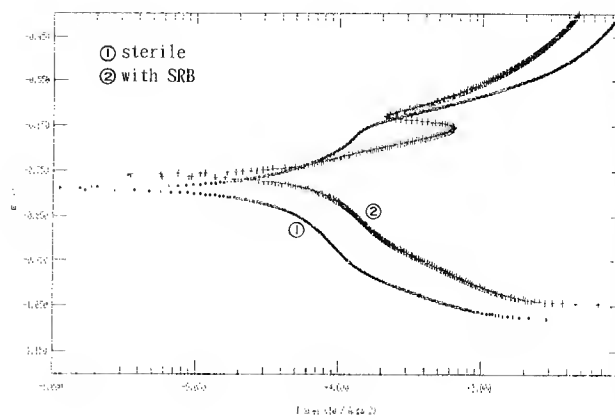


Figure 2 The polarization curves of carbon steel after 14 days of exposure in two different test media.

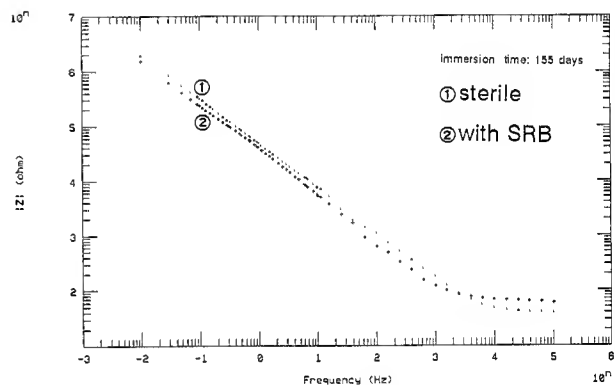


Figure 3 Impedance spectra of 304 stainless steel after 155 days of exposure in test media.

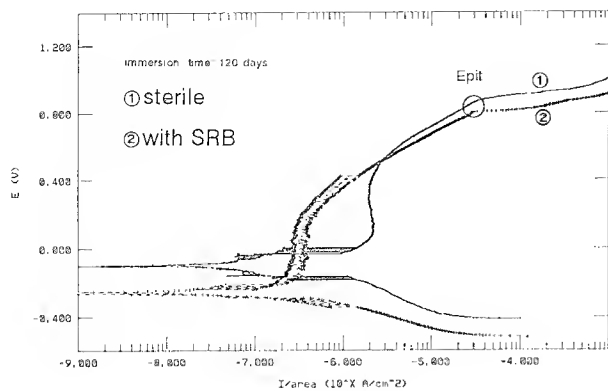


Figure 4 The polarization curves of 304 stainless steel after 120 days of exposure in test media.

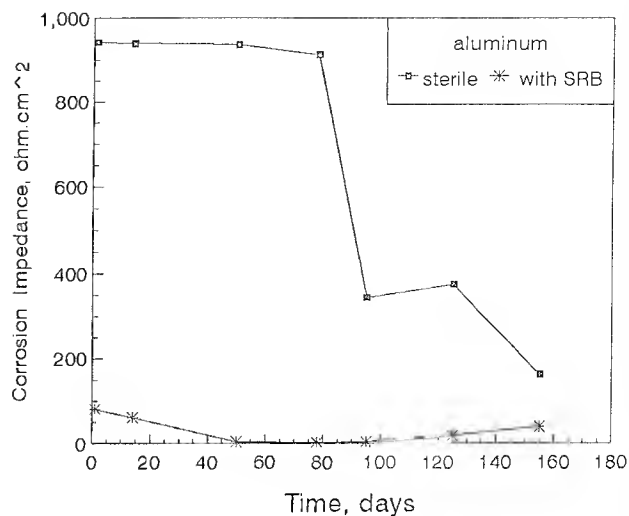


Figure 7 Impedance vs. time of aluminum.

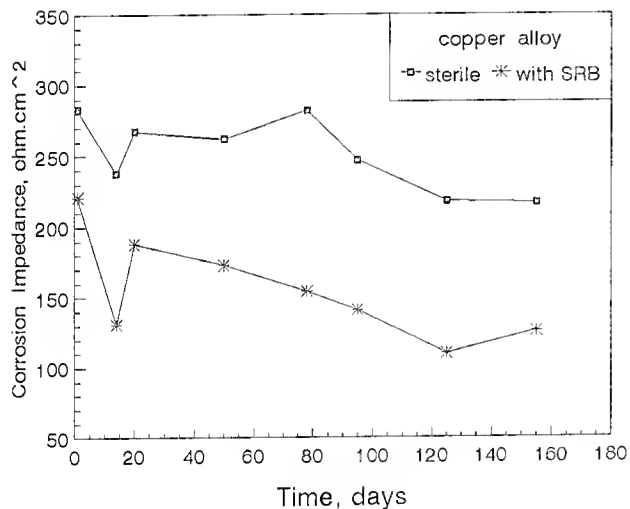


Figure 5 Impedance vs. time of copper alloy.

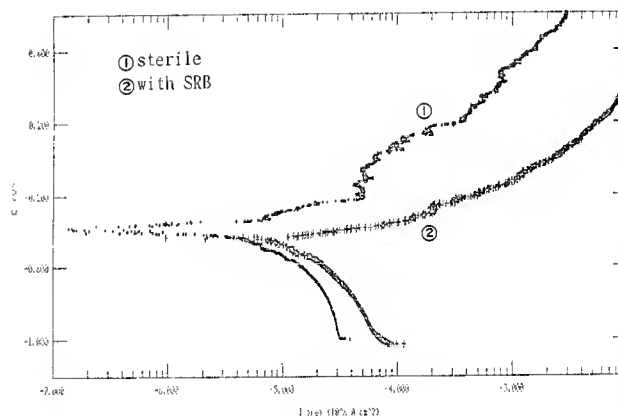


Figure 8 The polarization curves of aluminum after 120 days of exposure in two different test media.

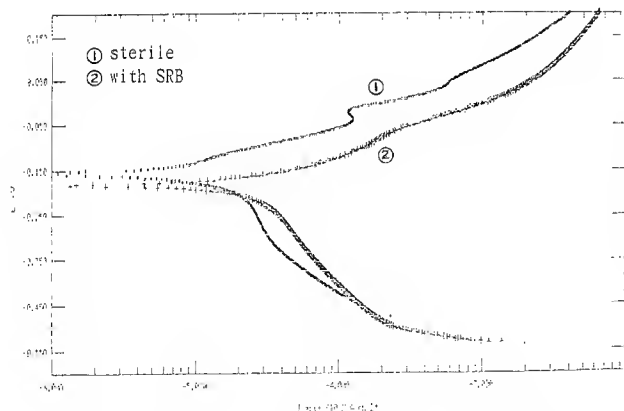


Figure 6 The polarization curves of copper alloy after 75 days of exposure in two different test media.

Jyh-Hwa Wang received his M.S.degree in Material Science from National Chong-Kung University. He joined T.L. in 1988 and has been engaged in Outside Plant technology.

Yaw-Tzong Horng received his M.S. degree in Electrochemistry in 1983 from National Taiwan Normal University. He joined T.L.in 1983 and has been engaged in Outside Plant technology. He is also a member of the Corrosion Engineering Association of R.O.C.

Hsi-Pai Hsu is currently a member of the material group of Loop and Outside Plant Laboratory, Telecommunication Labs.. He received his Ph.D degree in Chemistry in 1983 and has engaged in industrial materials research since then.

Kuang -Yi Chen was born in 1953 and received his Ph.D. degree in Electrooptics from National Central University in 1990. He has been engaged in research and development of optical fiber fabrication and communication technologies since 1977. He is currently the director of outside plant laboratory of Telecommunication Labs.

Optical Fiber Monitoring Systems for Passive Optical Networks

Chien-Chung Lee · Kuang-Yi Chen · Fwu-Yuan Tsai ·

Kuo-Hsiang Lai · Tay-Jang Liaw and Been-Huey Wann

Telecommunication Laboratory, Ministry of transportation and communication,
Taiwan, Republic of China.

Abstract:

Passive branching optical networks have difficulties in fiber monitoring and troubleshooting. This paper proposes two methods of fiber monitoring and troubleshooting for passive branching optical networks. Both methods can be used to build the fiber monitoring systems for passive optical networks(PONs).

1. Introduction

Optical splitters are used to construct passive branching optical networks(PONs) in fiber-in-the-loop(FITL) architecture. Host digital terminal transmits optical signal through PON to multiple optical network units(ONU). This point-to-multipoint architecture is different from the traditional point-to-point structure of conventional optical fiber feeder digital loop carrier system. Although techniques for the optical cable system of PON have been discussed in great details, the techniques for verifying optical cable system performance and locating faults have only recently been developed.

For the work of fiber troubleshooting and monitoring, the techniques in point-to-multipoint architecture are more difficult than that in point-to-point architecture, because optical time domain reflectometer(OTDR) is unable to recognize the individual optical backscattering signal of the branching fiber loop. In this paper, we propose two configurations, as shown in Fig.1 & Fig.2, for fiber troubleshooting and monitoring in PON. The basic considerations and calculations for these configurations are presented in section 2 & 3. The experimental results described in section 4 confirm the calculations.

2. Reflection-mode configuration

The reflection-mode configuration is shown in Fig.1. We use different time delay pulse waveforms to mark the individual branching fiber loops. The far-end reflective pulse height variation represents the loss variation of the individual branching fiber loop. When the pulse waveform reduces its pulse height or even disappears, we know that the loop loss is

increased or the loop line is broken. We can find out the fiber fault from the OTDR backscattering trace. Therefore we are able to troubleshoot and monitor fiber in PON by using this configuration. The basic considerations for this reflection-mode configuration are described as follows:

(a) Reflective pulse waveform resolution

If the reflective pulse waveform resolution becomes small, the needed fiber length difference among the loop fibers becomes small. The pulse waveform resolution is decided by the optical pulse width and the OTDR bandwidth. Theoretically, we can use event deadzone as the pulse waveform resolution; however, by considering noises and pulse waveform distortion, we recommend 0.5dB attenuation deadzone as the pulse waveform resolution. If we don't consider the OTDR receiver bandwidth, then the pulse waveform resolution (L_{res}) can be calculated as following formula.

$$L_{res} = 2 \times C \times t / n, \quad (1)$$

where C= speed of light,

t= pulse width in seconds,

n= refractive index of the fiber.

For N splitting fiber loops, the maximum fiber length difference (L_m) among the fiber loops can be calculated as follows:

$$L_m = (N - 1) \times L_{res}. \quad (2)$$

If we use 1ns pulse width probing light source, then the pulse waveform resolution is able to reach to 4 cm. For 32 splitting fiber loops, the maximum fiber length difference is only 1.24 m. By different fiber length deployment, we can easily detect the individual branching fiber loop.

(b) Fresnel reflection dynamic range and the fiber far-end return loss control

Fresnel reflection dynamic range and the fiber far-end return loss decide the pulse height on the OTDR trace. The pulse height (H_p) can be shown as follows:

$$H_p = DR_{4\%} - L_{system} - 0.5 \times (R - 14), \quad (3)$$

where L_{system} =optical fiber loop loss,

R=the branching fiber far-end return loss,

$DR_{4\%}$ =4% Fresnel reflection dynamic range.

And $DR_{4\%}$ can be calculated as following formula.

$$DR_{4\%} = DR_B + 0.5 \times (14 - BL), \quad (4)$$

where DR_B =backscattered dynamic range,

BL =backscattering level.

If we use 1ns pulse width probing light source to detect the fiber, $DR_{4\%}$ is about 37.5dB (not considering DR_B) and H_p is about 8.75dB for L_{system} =20dB. From Eq.(3), we can adjust return loss(R) to increase H_p and not needing to increase pulse width.

(c) Pulse height linearity and noise

When we use pulse height variation to detect fiber loop loss, the measurement errors come from pulse height linearity and receiver noise. According to Bellcore TR-NWT-000196, pulse height linearity should be less than $\pm 0.05\text{dB/dB}$. If we intend to detect 10 dB loss variation, the linear error will be less than 0.5 dB.

The pulse height noise (N_p) can be shown as the function of signal-to-noise-ratio(SNR) as follows:

$$N_p = 5 \log(10^{-\text{SNR}/5} + 1). \quad (5)$$

For 10dB pulse height, the pulse height noise is about 0.02dB. If the fiber loop loss increases 1dB, the possible maximum total detection error is about 0.07dB. Therefore, we can detect fiber loop loss variation precisely by proper pulse height value.

(d) Non-reflective and reflective fiber faults

If the non-reflective fiber fault happens in the branching fiber loop, the loss shown on OTDR trace will be different from direct power meter measurement. The loss(L_{OTDR}) measured by OTDR in N splitting fiber loop can be shown as the function of power meter measured loss(L_{PM}) as follows:

$$L_{\text{OTDR}} = -10 \log\left(\frac{N-1}{N} + \frac{1}{N} \cdot 10^{-L_{\text{PM}}/10}\right), \quad (6)$$

If 1XN splitter has unequal splitting ratio, L_{OTDR} will change Loss value to ($L_{\text{OTDR}} + dL_{\text{OTDR}}$) and dL_{OTDR} can be shown as following formula.

$$dL_{\text{OTDR}} = \frac{10}{\ln 10} \cdot 10^{-L_{\text{OTDR}}/10} \cdot \frac{(1 - 10^{-L_{\text{PM}}/10})}{N^2} \cdot dN, \quad (7)$$

where dN =ratio difference,

$dN = (10^{dU/10} - 1) \cdot N$,

dU =uniformity in dB.

If the branching fiber loop has 1dB bending loss, there is only 0.11dB loss shown on OTDR trace for 1x8 PON. Therefore it is difficult to find the small bending loss on multiple branching fiber loops. If the uniformity dU is 1.5dB, then dL_{OTDR} is about

0.04dB over 35% of above measured bending loss value.

3. Backscattering -mode configuration

The backscattering-mode configuration for fiber troubleshooting and monitoring in PON is shown in Fig.2. We use the optical reference reflector(reflectance>90%) to generate a opposite optical path, just as measuring the branching fiber loop from the far-end terminals. By using monitoring controller, we can switch the detected fiber to the fiber which we want to monitor. By using this method, we can test 、troubleshoot and monitor fibers in PON. The basic considerations for this configuration are as follows:

(a) Dynamic range and Noise consideration

The OTDR dynamic range needed in this configuration is calculated as the following:

$$DR = 1.5 \cdot (0.5 + 3.4 \log_2 N) + 2L\alpha + L_{\text{ref}}, \quad (8)$$

where N =splitting number,

L =fiber loop length in km,

α =fiber optical attenuation coefficient in dB/km,

L_{ref} =the optical loss of total reflector in dB.

For $N=8$ 、 $L=3\text{km}$ and $\alpha=0.35\text{ dB/km}$, DR should be larger than 18.6dB. It is no problem for today's commercial OTDR.

The noise on the OTDR trace is decided by SNR and can be calculated by Eq.(5). The higher accuracy we need, the higher SNR we have to design.

(b) The measurement for small fiber loss fault and large fiber loss

When using backscattering -mode configuration to monitor branching fiber loops, we can detect bi-direction OTDR traces. We use the opposite OTDR trace to detect small fiber loss fault and use near-end OTDR trace to detect large fiber loss fault.

(c) multi-reflection error

When we apply this configuration to monitor fibers in PON, the reflection pulses caused by other branching loops will generate noise on detected branching fiber trace. But if the fiber loop length is long enough, this error can be ignored.

4. Experimental results

We set up 1x4 and 1x8 experimental PONs. Their characteristics are shown in Table 1 and Table 2.

(a) Reflection-mode configuration

we use HP8146A/81465SL and Anritsu MW9040B OTDRs to implement this configuration, and select 5ns pulse width and 1310nm wavelength light source. We also choose the 1x8 PON in Table 1 as the experimental network. The experimental results are as follows:

(1) pulse waveform resolution

As shown in Fig.3, marked pulses can be distinguished by less than 12m fiber difference. In Fig.3, we mark 5 pulses by just using 60m maximum fiber length difference.

(2) pulse height linearity

Pulse height linearity is shown in Fig.4. When optical pulse

height is too high, the receiver of OTDR will be saturated and distort the linearity. From Fig.4, the pulse height linearity is within $\pm 0.1\text{dB}$ for 7dB variation and within $\pm 0.2\text{dB}$ for 10dB variation.

(3) pulse height noise

Testing the pulse height noise by varying SNR value, we obtain the relationship between noise and SNR, as shown in Fig.5. The testing result is very close to the calculated data. The noise becomes large when pulse height is small.

(4) pulse height long time stability

We measure the pulse height long time stability over 24 hours and record data for 15 minute interval. The pulse height long time stability as shown in Fig.6 is less than $\pm 0.2\text{dB}$. Therefore, we can use pulse height variation to detect the branching fiber loss variation which is larger than 0.4dB.

(5) Total error for pulse height

The total error E_t for pulse height can be calculated as following formula.

$$E_t = \sqrt{E_n^2 + E_l^2 + E_s^2}, \quad (9)$$

where E_n =pulse height error caused by receiver noise,

E_l =pulse height error caused by receiver linearity,

E_s =pulse height error caused by light source long time stability.

In our experiment, the total error E_t is about 0.22dB. We can detect the branching fiber loss variation which is larger than 0.5dB by using this experimental setup.

(6) Fiber monitoring and troubleshooting

We apply this configuration to the experimental 1x8 PON and monitor branching fiber loop by using 5ns pulse width probing light source. When fiber loop loss variation exceeds the alarm threshold value (3dB in our test), we use 2 μs optical pulse light source to locate the fiber fault. By using proper computer control and process, we can monitor and troubleshoot the fiber in PON. Loss variation detected by pulse height is shown in Fig.7a and Fig.7b. Fault location is as shown in Fig.8.

(b) Backscattering-mode configuration

We use Anritsu MW9040B OTDR to implement this configuration, and choose the 1x4 PON as the experimental network. We select 2 μs pulse width and 1310nm wavelength light source. The experimental results are as follows:

(1) The fault loss measured by OTDR in 1x4 PON

As we mention before, the fault loss measured by OTDR in 1x4 PON, is different with power meter measurement value. We measure several bending losses by OTDR and compare them with calculation values from Eq.(6). The results are shown in Fig.9. The bending loss value measured by OTDR is very close to the calculation value from Eq.(6). So we can use Eq.(6) to measure the fault loss in PON.

(2) The loss measured from far-end terminal vs. backscattering-mode configuration measurement

We compare far-end ONU terminal loss measurement with backscattering-mode configuration loss measurements. As

shown in Fig.10, the results show that we can measure the branching fiber loop loss by using backscattering-mode method.

(3) Fiber monitoring and troubleshooting

We apply this configuration to 1x4 experimental PON. This configuration can monitor individual fiber loop. When small loss fault happen in the branching fiber loop, we still can detect it by this architecture. As shown in Fig.11a, there is a 0.269dB bending loss in the branching fiber loop. By using this method, we can detect the fiber loop trace shown in Fig.11b, and find out the small bending loss is about 0.294dB. When branching fiber loop loss variation exceeds the alarm threshold value(3dB in our experimental setup), we can locate the fiber fault by tracing the near-end OTDR trace. Therefore we are able to monitor and troubleshoot the fiber in PON.

5. Conclusion

The two proposed configurations are both able to do the task of fiber monitoring and troubleshooting. The reflection-mode configuration can provide a reliable and cost-effective method to monitor and troubleshoot fiber in PON. If we need to know the OTDR trace of individual fiber loop, the backscattering-mode configuration will be a good method. By proper computer control and process, both configurations can do the fiber monitoring task for PON automatically. Therefore, these two configurations can solve the problem of fiber monitoring of PON ,and provide us to monitor and troubleshoot the fiber in PON.

References:

1. Ray Savich and Marvin D.Ashby," Testing and troubleshooting the passive branching plant",Lightwave, Oct. 1993.
2. OFred Scheu," Testing fiber in the loop",Lightwave,Oct. 1993.

Fig.1 The reflection-mode configuration for fiber testing , troubleshooting and monitoring in PON.

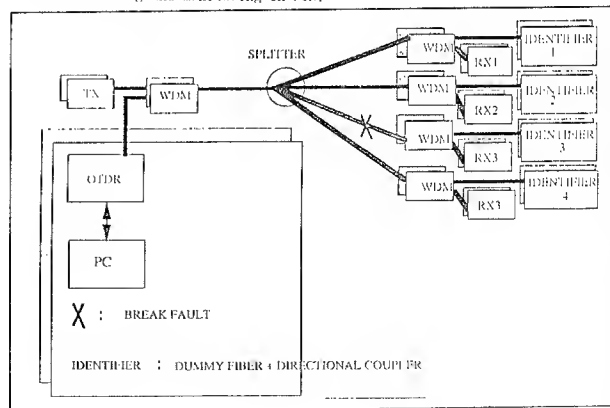


Fig.2 The Backscattering-mode configuration for fiber testing troubleshooting and monitoring in PON.

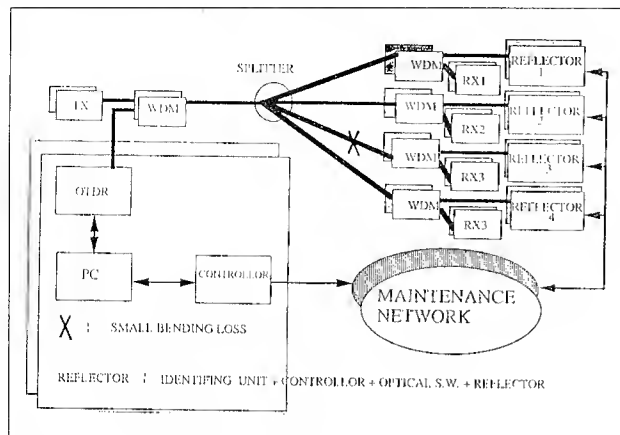


Fig.3 The 5 marked pulses waveform for PON.

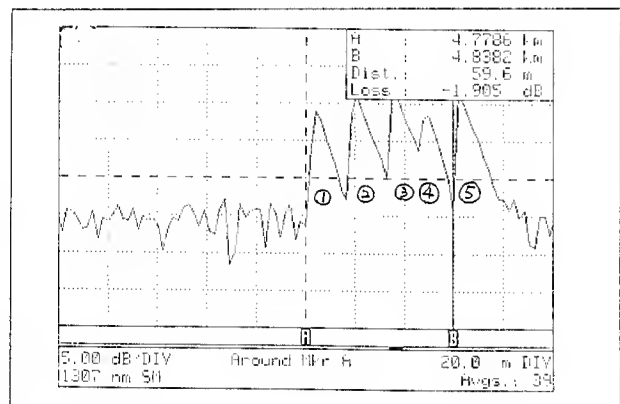


Fig.4 The linearity of the reflective pulse height variation.

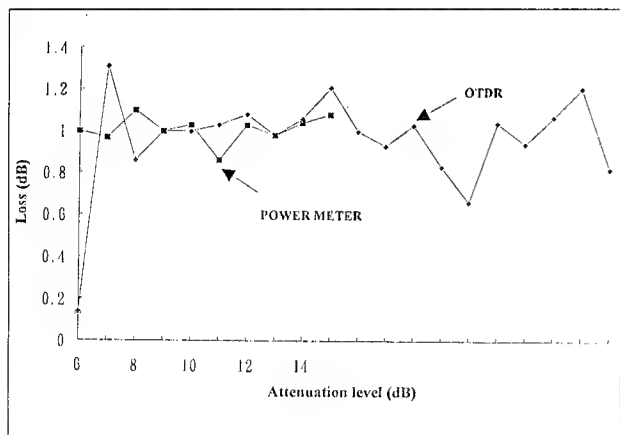


Fig.5 The relationship between reflective pulse height noise and SNR.

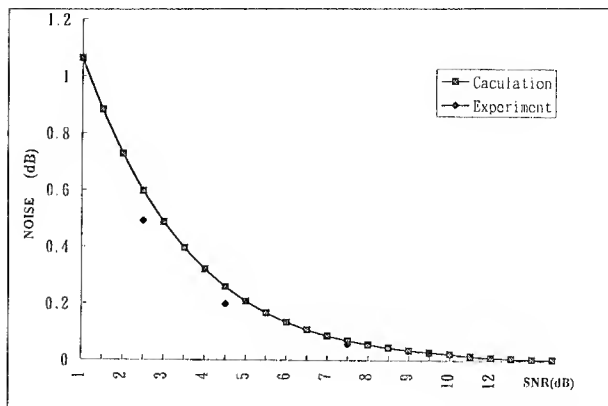


Fig.6 The long time stability of the reflective pulse height

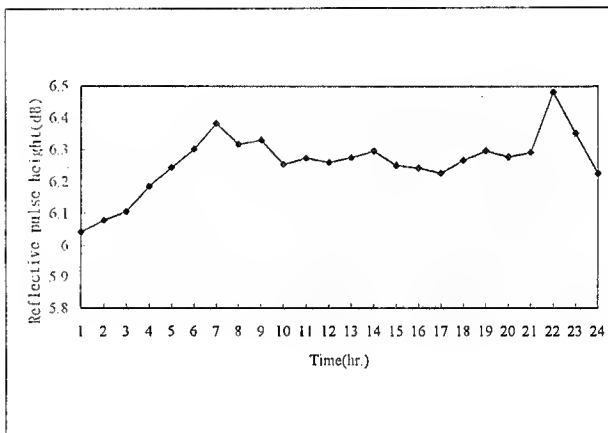


Fig.7a The reflective pulse waveform of the normal fiber loop.

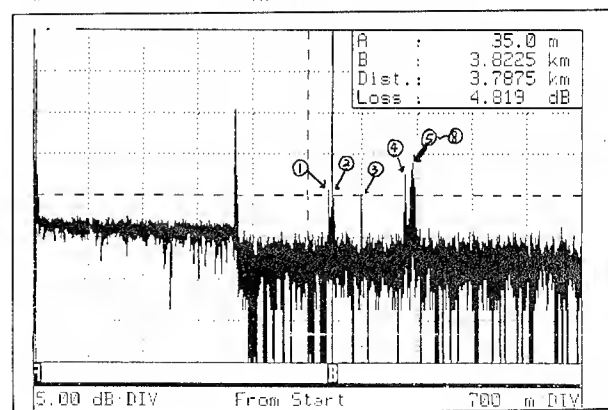


Fig.7b The reflective pulse waveform of the fiber loop with fault.

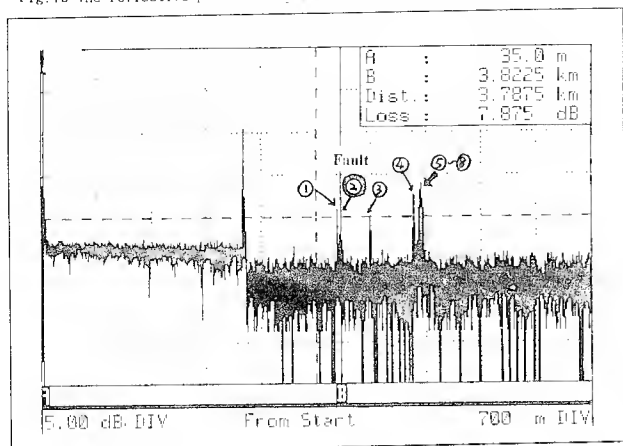


Fig.8 The fiber fault location of PON by using reflection mode configuration.

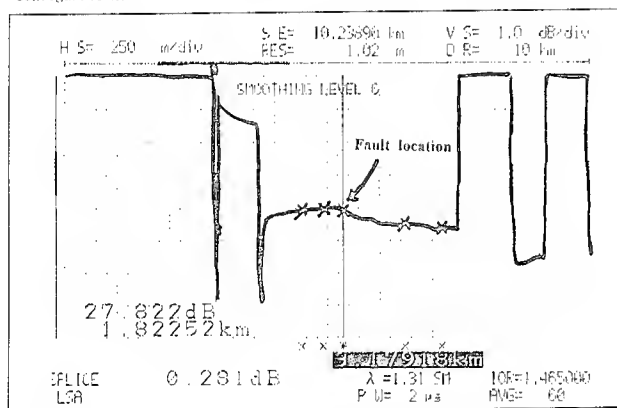


Fig.9 The bending loss measured by OTDR in 1x4 experimental PON.

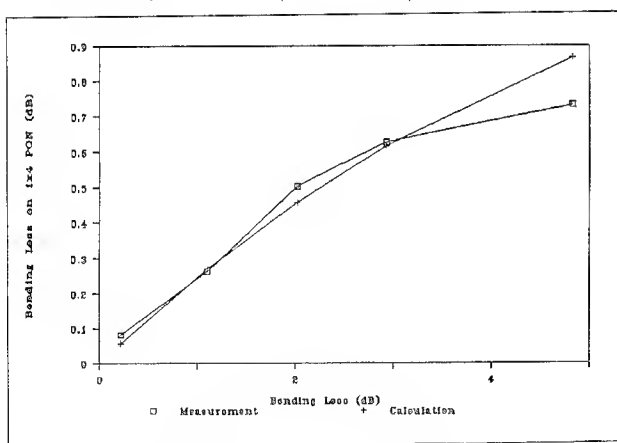


Table 1 The characteristics of 1x4 experimental PON.

LOOP CHARACTERISTICS	LOOP LENGTH (m)	LOOP LOSS (dB)
1	1538	8.98
2	1538	7.68
3	1538	7.4
4	1538	8.49

Fig.10 The comparison between far-end terminal OTDR measurement and backscattering-mode configuration measurement in 1x4 experimental PON.

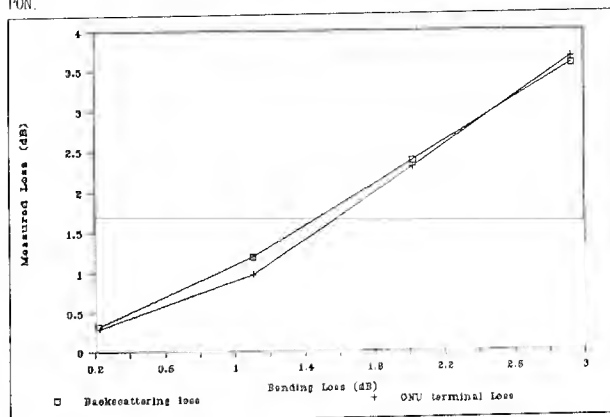


Fig.11a The terminal probing OTDR trace for 1x4 PON with a 0.269dB bending loss

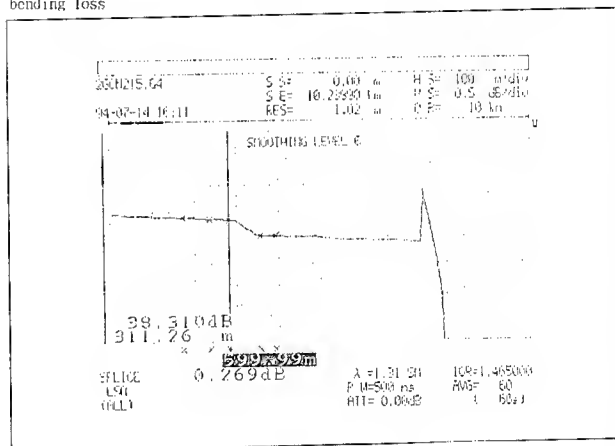


Fig.11b The OTDR trace measured by backscattering-mode configuration in 1x4 experimental PON with a 0.269dB bending loss

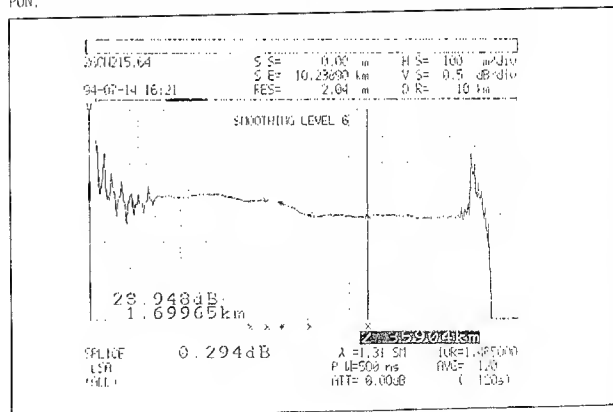


Table 2 The characteristics of 1x8 experimental PON.

LOOP CHARACTERISTICS	LOOP LENGTH (m)	LOOP LOSS (dB)
1	3763	16.97
2	3818	16.31
3	4181	19.39
4	4742	17.18
5	48070	17.63
6	4830	18.27
7	4840	17.57
8	4867	18.01

STUDY, MANUFACTURE AND TEST ON A S-Z STRANDED LOOSE TUBE OPTICAL FIBRE RIBBON CABLE WITH NO PRETWISTING AND NO FILLING COMPOUND

Luis Baguer, Pilar Blasco, Julio Cobo, Carlos D  a, Francisco Escribano

CABLES DE COMUNICACIONES, S.A.
ZARAGOZA - SPAIN
(BICC Group)

ABSTRACT

A new cable design for the subscriber loop has been studied, manufactured and tested.

The cable make-up is based on six loose tubes cabled around a dielectric central member. S-Z cabling was used. Inside each tube there are four ribbons with four optical fibres each one. No pretwisting was applied to the ribbons. No filling compound is present in the interstices between the tubes therefore we have a dry optical core. A polyethylene-aramid yarns-polyethylene sheath has been applied over the optical core, wrapped with a water-blocking tape.

The cable was successfully manufactured using standard fibre cable lines.

The cable was fully tested according to the latest international standards.

The results were fully satisfactory in every test and all of them are presented on this paper.

INTRODUCTION

New telecommunication projects have been announced in Spain. The main objective of these projects is to cable with fibre the subscriber loop. These new projects brought the need to have a new family of cables with a medium-high number of fibres, using four fibres ribbon in order to reduce installation costs and avoid if possible the use of a filling compound using instead a non-fluid element, in order to facilitate the installers day-by-day work and joint closures maintenance.

Customers preferences pointed out a design based on loose tube secondary protection with S-Z stranding in order to have the best tube accessibility. The fibre count with the greatest demand would be 96. Cable diameter should be near 18 mm and the thermal cycle to be accomplished by cable should be at least [-20  C, +70  C]. So the main objectives to be accomplished would be, first, try to put ribbons inside the secondary protection without pretwisting, in order to facilitate the manufacturing process, second, find a good lay length/length between S-Z changes relation in order to

achieve the customers requirements without detriment of the cable performance and, third, resolve the filling compound problem on optical cores trying to find a dry solution.

THEORETICAL POINTS

One of the key points in order to study the optical fibre performance in cable is to determine its curvature radius. In order to have a more accurate value of it, it is essential to take into account three components:

- Curvature (C_R) due to have the ribbon into the loose tube, with some length excess.
- Curvature (C_{tc}) due to have the loose tube cabled around a central reinforcement element.
- Curvature (C_c) due to have the cable curved with a certain curvature radius.

Curvature "C" is mathematically defined as:

$$C = \left| \frac{d^2 \vec{r}}{ds^2} \right| \quad [1]$$

being "r" the position vector and "s" the advancing path length.

So, we have that:

$$C_{to} = C_R + C_{tc} + C_c \quad [2]$$

Where $C = 1/R$, and R is the curvature radius. Equation [1] becomes:

$$1/R_{to} = 1/R_R + 1/R_{tc} + 1/R_c \quad [3]$$

R_{to} is the optical fibre curvature radius, and its value must be greater than the value of the minimum curvature radius, usually determined by the optical fibre manufacturer.

R_R is calculated from fibre excess into the loose tube (ϵ), tube inside diameter and ribbon bound

dimensions: $R_R = W/4 \cdot \epsilon$ [4]

where "W" is defined as tube-ribbon looseness. R_{tc} is calculated from tube cabling radius, lay length and number of turns between SZ reversings. For this purpose, instead of using the standard helix equation,

$$R_{talc} = R_{cabling} \left[1 + \frac{Step}{2\pi R_{cabling}} \right] \quad [5]$$

usually generalized for SZ cabling, we have developed from [1] an specific one where all the aforementioned variables are used and the minimum curvature radius is taken into account.

R_c is set to be 10 times the cable diameter.

While the first key point is related to cable dimensions, the second one refers to material properties. How to find an accurate cable thermal coefficient (α_c) is one of the most controversial points in cable designing. Cable thermal coefficient is defined as follows:

$$\alpha_c = \frac{\sum (E_i s_i \alpha_i)}{\sum (E_i s_i)} \quad [5]$$

However some corrections have to be made due to young modulus "E_i" and thermal coefficient "α_i" dependence with temperature, having the foresaid expression turned into:

$$\alpha_c = \frac{\sum (E_i k_{1i} s_i \alpha_i k_{2i})}{\sum (E_i k_{1i} s_i)} \quad [6]$$

where "E_i" is the Young modulus k_{1i} correction factor of the "i" material, and k_{2i} is the thermal coefficient "α_i" correction factor of the "i" material. A constant effective area "s_i" is supposed for each material.

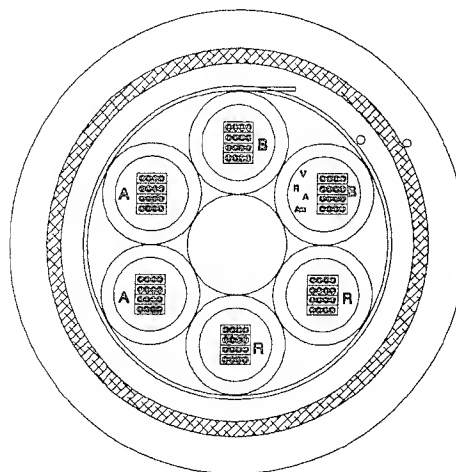
SETTING PARAMETERS

In order to set the different cable design variables, a software application was developed.

As said, cable structure is composed of six tubes with four four-fibre ribbons. These tubes are cabled around the central reinforcement element, forming cable core. Cable core is wrapped with an special water-blocking tape and after a polyethylene-aramid-polyethylene (both polyethy. sheaths low density polyethy.) is extruded over the wrapped cable core.

First of all, we have the curvature diameter of the fibre

to be at least 100 mm.



Cable Cross-section

Stack of ribbons is 1.52 mm height and 1.15 mm width, values determined by the type of ribbon used (0.38 mm height and 1.15 mm width, each). In the worst case we have a stack diameter of 1.9 mm.

Taking 18 mm as nominal value of cable diameter and knowing that closure dimensions limit the length between SZ reversings to 900 mm, we can determine easily tube dimensions, lay length and number of turns between SZ reversings by means of the developed software application.

As principal result can be lighted the need not to pretwist ribbons into the loose tube. Values for tube dimension have been obtained fully compatible with cable diameter required.

Theoretical thermal coefficients have been calculated for several minimum temperatures in thermal cycle test.

Values obtained are as follows:

MINIMUM T ^a SUPPORTED	MAXIMUM THERMAL COEFFICIENT
- 40°C	7.45 · 10 ⁻⁶ °C ⁻¹
- 30°C	8.94 · 10 ⁻⁶ °C ⁻¹
- 20°C	1.12 · 10 ⁻⁵ °C ⁻¹

As we are looking into a cable capable of supporting a temperature cycle of [-20°C, +70°C], our restrictive value will be the third of the foresaid list, in such a way we need to adjust the thermal coefficient of our cable

to have a value smaller than $1.12 \cdot 10^{-5} \text{ }^{\circ}\text{C}^{-1}$.

Cable thermal coefficient [6] was calculated and for the last and definitive design presented on this paper, a value of $8.5 \cdot 10^{-6} \text{ }^{\circ}\text{C}^{-1}$ was obtained once estimated k_{11} and k_{21} factors for each significative material of the cable, so the temperature cycle of $[-20^{\circ}\text{C}, +70^{\circ}\text{C}]$ was expected to be passed successfully.

The last point to be discussed was the suppression of the core filling compound. It was resolved by wrapping the cable core with an special water-blocking tape. The tape has an structure of sandwich with an hydrosoluble layer and synthetic crosslinked polymer which blocks water by swelling itself.

For this application a 110 g/m^2 weight tape was chosen. No problem was expected to appear at the manufacturing process.

TEST RESULTS

Cable was fully tested according to the latest international (IEC, EN) standards. Tensile performance, cable torsion, cable bend, impact, crush, temperature cycling and water penetration tests were carried off. Results are next presented.

Tensile performance.

The test was made according EN187000 Method 501 (IEC 794-1-E1). A sample length of approximately $90 \pm 2 \text{ m}$ was taken out from reel for testing. Maximum force applied on cable was 4000 N with a cable elongation of 0.25%. E*S of the cable was estimated to be 1600 kN. No attenuation increase larger than 0.05 dB was registered. An elongation/attenuation versus tensile graphic is presented in figure 1.

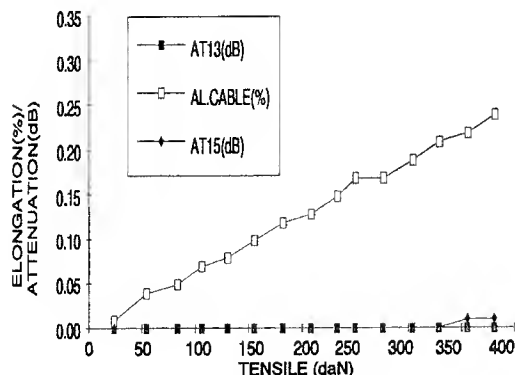


figure 1.

Cable torsion.

Torsion experiment was carried on per EN187000 Method 508 (IEC 794-1-E7). The test was made with a 2 metres cable sample. Ten cycles ($\pm 360^{\circ}$ each) were applied and no attenuation increase of more than 0.05 dB was recorded.

Cable bending.

Bending experiment was carried on per EN 187000 Method 513 (IEC 794-1-E11-Proc.1) with a forsaidd bending radius of ten times cable diameter. 10 turns per cycle and 10 cycles were applied. No attenuation increase ($\alpha \leq 0.05 \text{ dB}$) was detected.

Impact.

One hundred impacts were applied on cable sheath with an impact energy of 5 J. each, according EN187000 Method 505 (IEC 794-1-E3). No attenuation increase larger than 0.05 dB was recorded. Cable sheath presented no relevant damage after the test.

Crush.

Crush experiment was made per EN187000 Method 504 (IEC 794-1-E3). Cable supported 3000 N for 15 minutes with no attenuation change larger than 0.05 dB. Cable sheath presented no relevant damage after the test.

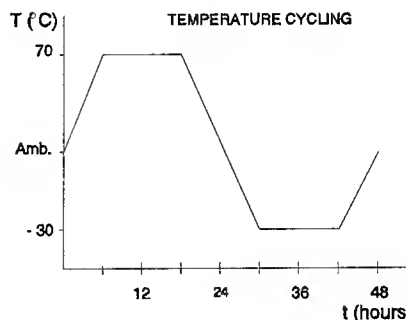


figure 2

Temperature cycling.

Temperature cycling test was made according EN187000 Method 601 (IEC 794-1-F1). A 1000 m cable length was introduced into the chamber for 48 hours with a temperature variation as indicated in figure 2. No attenuation increase was detected larger than 0.05 db/km. Figure 3 shows attenuation variation with temperature of each ribbon into one tube at 1330 nm and 1550 nm. All the fibres were tested and the results were similar to these shown in figure 3. As can be seen,

initial forecast at low temperature margin (-20°C) was improved (-30°C).

Water penetration.

Water penetration experiment was carried on per EN 187000 Method 513 (IEC 794-1-E11-Proc.1). As has been forecasted, desired results were not obtained when no special care was taken. After filling one metre the pressure column, flow was detected after 15 minutes. Therefore two experiments were made on two cable samples according with IEC.

At first attempt, special care was taken when inner and external sheaths were removed in order to not to damage the water-blocking tape overlap. Less than 5 ml were detected after 24 hours so test was passed successfully. Experiment was prolonged 24 hours more, and could be seen that tape had blocked water flow advance.

At the second attempt, moreover the foresaid at second trial, special care was taken filling little by little the pressure column during twenty minutes. No water was detected after 24 hours neither after 48 hours. Cable was examined and could be observed that water flow had stopped at 200 mm from opposite end.

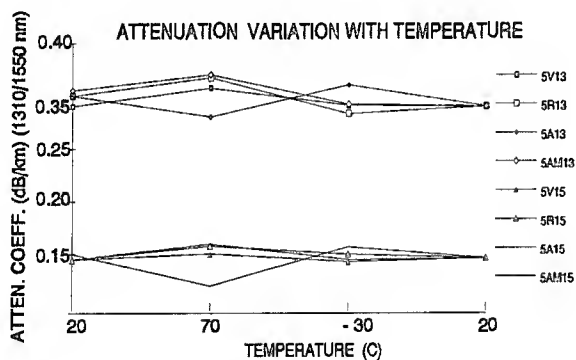


figure 3

CONCLUSION

A S-Z stranded loose tube ribbon fibre cable with no pretwisting of ribbons and no filling compound has been carried off. General requirements recommended by our main customers referred to mechanical performance, dimensional characteristics and so on, have been achieved successfully so we can say that all of them are technically achievable.

It is possible to design and manufacture a cable, with no pretwisting of ribbons inside the loose tube. This

conclusion is a very important one because implies that this kind of cable can be perfectly manufactured in a standard secondary protection extrusion line.

It is possible to find a good lay length/length between S-Z changes relation in order to achieve the customers requirements without detriment of the cable performance.

A mathematical model has been obtained to investigate this kind of cables. It has been checked with the values obtained from the tests.

It is possible to design and manufacture dry-core fibre cables avoiding the use of filling compounds. For this cable an special tape has been used to wrap the optical core. IEC test related to water penetration (IEC 794-1-F5) have been successfully passed but special care have to be taken when making it. So important benefits will be obtained using this cable, related to installation and hardware maintenance.

REFERENCES

Tatsuya Fuchigami, Yutaka Katsuyama, Masaaki Kawase.

"Optimum Clearance Design for a Loose Optical Fiber Cable Based on Suppression of Fiber Strain".

Journal of Lightwave Technology, vol. LT-3, NO. 1 FEBRUARY 1985

Masayoshi Yamanaka, Naoki Okada, Hiroyuki Sawano, Matsuhiro Miyamoto.

"A study on reverse lay stranding loose tube cable containing ribbon fibers".

I.W.C.S. Proceedings 1993.

Yutaka Kurosawa, Hiroyuki Sawano, Matsuhiro Miyamoto, Nobuyasu Sato.

"Development of ribbon loose tube cable for optical subscriber loop".

I.W.C.S. Proceedings 1992.

P.D. Patel, H.C. Chandan, D. Kalish.

"Failure probability of optical fibers in bending".

I.W.C.S. Proceedings 1981.

P. Neveux, W. Hatton.

"Designing compression resistance in loose tube cables".

I.W.C.S. Proceedings 1987.

P. Delage, R. Girbig, G. H g, M. Hoffart, H. Moers, P. Zamzow.

"A new cable family for the optical fiber subscriber network"

I.W.C.S. Proceedings 1992.

W. Lackas, J.M. Schneider.
"New fiber optic ribbon cable design"
I.W.C.S. Proceedings 1986.

Cortines, Bonicel, Kylen, Schulte, Paternostro,
Berthelsen, Lasne.

"An international development on ribbon technology
and evaluation of applicability to national specifications"
I.W.C.S. Proceedings 1992.

Luis Baguer Mor received the Master Degree in Telecommunications Engineering from Madrid Polytechnical University in 1972. He joined Cables de Comunicaciones in 1973 and at present is the Product Engineering Department Manager.



Carlos D a Navarro received the Bachelor Degree in Telecommunications Engineering from Engineering University of La Salle Barcelona in 1990. He joined Cables de Comunicaciones in 1990 and at present he is working in the Product Engineering Department.



Pilar Blasco Herranz received the Master Degree in Physics (Optic speciality) from Zaragoza University in 1989. She joined Cables de Comunicaciones in 1990 and at present she is working in the Optical Fibre and Cable Laboratories.



Francisco Escribano Garc a received the Master Degree in Telecommunications Engineering from Madrid Polytechnical University in 1982. He joined Cables de Comunicaciones in 1986 and at present he is working in the Cables Technology Area.



Julio Cobo Puente received the Bachelor Degree in Industrial Engineering from EUITI of Santander in 1969. He joined Cables de Comunicaciones in 1972 and at present is the Material Laboratories and Cable Technology Manager.



Evaluation of the environmental resistance of 900 μ m-jacket optical fibers using stripping profiles as a monitoring method

Hui-Fen Lin, Chi-Hsiang Hsieh, Shiow-Ing Wang, Y-C Lin, Kuang-Yi Chen

OSP, Telecommunication Labs.
P.O.Box 71, Chung-Li, Taiwan, R.O.C.

ABSTRACT

As optical fibers are increasingly deployed in the loop and customer premises, they are likely to be exposed to a wide variety of harsh environment. Therefore, the long term reliability of fiber is the most important item in the part of evaluating and choosing the fiber materials. Since the changes of tensile strength and strip force of fibers won't necessarily indicate the degree of degradation, the adhesion between glass and primary coating from a stripping profile is resolved and proposed as an additional indication of the degree of aging degradation. In addition, four types of 900 μ m fibers were aged in water, isopropanol, bleach solution, and ammonia water, and the changes of fiber surface, strip force, and adhesion between glass and primary coating were monitored. Results showed that the changes of adhesion between glass and primary coating are meaningful and reflect the actual extend of degradation.

INTRODUCTION

The 900 μ m optical fiber design is primary used for pigtails, jumper cables, and indoor cables. In considering their long term reliability, a particular concern is their resistance to common household chemicals. Generally, fiber samples are immersed into a certain chemical and their tensile strength and strip force are used to evaluate their resistance to that chemical. However, tensile testing was sometimes rendered impractical due to the fact that sample fibers were so much affected by the chemical that gripping the entire fiber became difficult. In the case of loose buffered 900 μ m optical fibers, tensile testing was also impossible because their loose buffered structure. Stripping test could performed on all

immersed samples, yet the peak strip force was more a function of the coating condition. It would be better to test also the glass condition of the immersed samples since there might be chemicals that could diffuse into the coating layer without disrupting the coating material much. A pull-out testing such as the one suggested by Overton [1] or Suhir [2] may provide some information about glass because the adhesive strength between glass and primary coating could be affected by chemicals. Another way of looking into this adhesive property may be the one described by Moses [3] utilizing the stripping profiles of 900 μ m optical fibers. In this paper, we tried to evaluate the resistance to household chemicals of 900 μ m fibers by peak strip force and the adhesive property elucidating from their stripping profiles.

EXPERIMENTAL

Material:

Four different commercial 900 μ m coated fiber products were used in this study. They were designated as A-, B-, C-, and D-fiber. The coating material and the structural characteristics of these samples are listed in Table 1.

Table 1 : The type and material of buffering layer of 900 μ m fiber sample

	A	B	C	D
type	loose buffered	loose buffered	tight buffered	tight buffered
material	PA-12	PVC	PVC	Hytrel

Aging:

Samples were cut to a length of about 25m, winding into circles, and were immersed in four different chemicals : distilled water, isopropanol, bleach solution(containing 5.25% of sodium hypochlorite) and 3.5% ammonia water. The aging

was done at ambient temperature. Two ends of the immersed fiber were left in the air. Specimens were periodically taken from the aging sample, wiped clean by paper towels, and conditioned at ambient condition for 24 hours before undergoing testing.

Testing:

Visual inspection of the fiber surface was helped by an Olympus stereo microscope. The testing method of EIA FOTP 178 [4] was followed to determine the stripping profile. The length of specimen was 300mm. Ten specimens were tested at a crosshead rate of 13mm/min, with a stripping length of 150mm. The stripping tool was Micro-strip from Micro Electronics Inc.. The glass transition temperature of the coating material was obtained by dynamic mechanical testing of the buffering layer of the sample fiber on a Polymer Laboratories' D.M.T.A.. Samples were tested in bending mode with an 1 Hz oscillation.

RESULTS AND DISCUSSION

Surface change:

Visually, the most obvious change occurred in the bleach solution. Both B- and C- fiber turned to brown after aging for 17 weeks in that medium, indicating the coating material, PVC, of these fibers was somewhat affected by this oxidizing environment. On closer look with the aid of a stereo microscope, these PVC coatings still retained their physical integrity and only minor surface roughness appeared after aged for 52 weeks. D-fiber showed a more damaging surface in the bleach solution under microscopic examination, though its color change was minor. Its surface roughened after the first week's immersion and cracks on the surface appeared after 17 weeks of aging. This result agrees well with Farro's [5] in that Hytrel, the coating material of D-fiber, is susceptible to bleach attack. A-fiber, with a PA coating material, seemed relatively immune to bleach solution. Only its coating turned opaque after being aged for 34 weeks and there was no change of the surface condition.

The other three chemicals, namely, water, isopropanol, and ammonia water, did not visually affect four fibers much. Ammonia water caused yellowing on Hytrel coated D-fiber and, to a lesser degree, on PVC coated B- and C-fiber. Isopropanol caused discoloring on D-fiber. However, none displayed any surface roughness as was seen in the samples

aged in the bleach solution. Water appears to be the more benign environment among the four tested since it caused no effect on the four fiber samples. Again, PA coated A-fiber seemed to be least effect by these three chemicals.

Although B- and C-fiber were not visually affected by isopropanol, they lose their flexibility after only aged for one week. In addition, B-fiber had its PVC coating shrunk significantly, while C-fiber also experienced a slight shrinkback of its coating. A check of the glass transition temperature(T_g) revealed that T_g of both PVC coatings were increased, indicating that isopropanol had extracted plasticizers out of the coating material and caused the stiffening and the dimension instability phenomena.

Stripping profiles:

The strippability of the fiber coating was tested as another way of evaluating the chemical resistance of sample fibers. Two parameters were extracted from the stripping profile of the 900 μ m coated fiber, the peak strip force and an adhesion indicator. The peak strip force is the maximum force encountered during the stripping process. The adhesion indicator is the slope of the region II of the stripping profile (see figure 1), which is considered to be an indication of the magnitude of adhesion between primary coating and glass [3] and has the same dimension factor of a dynamic friction coefficient. Table 2 lists the initial value of these two parameters for the four samples. The loose buffered fiber gave a quite different value from those of the tight buffered one. This difference may stem from the difference in their fiber structures, but it may also due to the fact that B-fiber being not a quality product.

Table 2 : The strip force and adhesion of four 900 μ m fiber samples.

	strip force (gf)	adhesion (gf/mm)
A	340.9 \pm 38.0	4.55
B	76.8 \pm 35.8	0.26
C	1154.2 \pm 283.6	21.16
D	1131.6 \pm 94.3	37.53

Figures 2 - 9 show graphically aging effects of four fibers caused by four chemical environments. The effect is represented by the change of the peak strip force and the adhesion indicator. Since the peak strip force depends on the ultimate tensile strength of the coating material and the static

friction force between coating and glass and the adhesion indicator depends on the dynamic friction force between coating and glass [3], retaining the value of both parameters is considered to reflect the ability of the coating material to resist the chemical attack itself and to prevent the chemical from reaching inside the coating.

Among four sample fibers, PA coated A-fiber (figure 2&3) appears to retain its peak strip force and adhesion indicator for the longest aging period. Only in isopropanol after 52 weeks' aging does the adhesion indicator of A-fiber drops to zero, conforming quite well with visual inspection results.

For Hytrel coated D-fiber (figure 4&5), the effect of bleach solution is detrimental. Here, changes of the adhesion indicator seem more sensitive and in better agreement with results obtained from microscopic examination than that of the peak strip forces. Ammonia water also causes the Hytrel coating to degrade after 52 weeks' attack on that material.

For PVC coated B- (figure 6&7) and C-(figure 8&9) fiber, the effect of isopropanol is obvious and agrees well with what has been observed visually. Meanwhile, ammonia water causes strong effect on the coating strippability despite the fact that there is no apparent visual changes of the coating. Bleach solution degrades the coating to a lesser degree, although both fibers turn brown visually. The difference in the resistance to bleach for the B- and C-fiber may be due to their different formulations.

SUMMARY

Besides visual inspections, stripping parameters such as peak strip force and the adhesion indicator (slope of the region II of the stripping profile) provide good indication in evaluating the chemical resistance of 900 μ m coated fibers. In some cases, the adhesion indicator seems to be a more sensitive parameter.

Among the coating material tested, polyamide seems to be more resisting to those household chemicals used in this study. PVC may also be a good coating material provided it is properly formulated.

REFERENCE

1. B. Overton and C. Taylor, Proc. SPE ANTEC 1988, p.392.
2. E. Suhir, J. Lightwave Tech., 11, 12, p.1905, 1993.

3. J. Moses and M. Sigmon, Proc. IWCS 1987, p.163.
4. EIA FOTP 178, "Measurement of strip force required for mechanically removing coating from optical fibers."
5. J. J. Farro, R. A. Frantz, J. P. Klimer, C. J. Wiczorek, and H. H. Yuce, Proc. IWCS 1991, p.693.

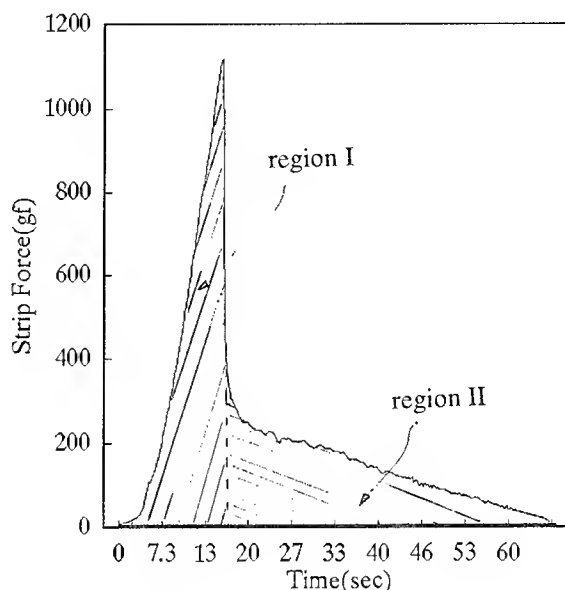


Fig. 1 A typical stripping profile of a 900 μ m coated optical fiber. This is C-fiber before aging.

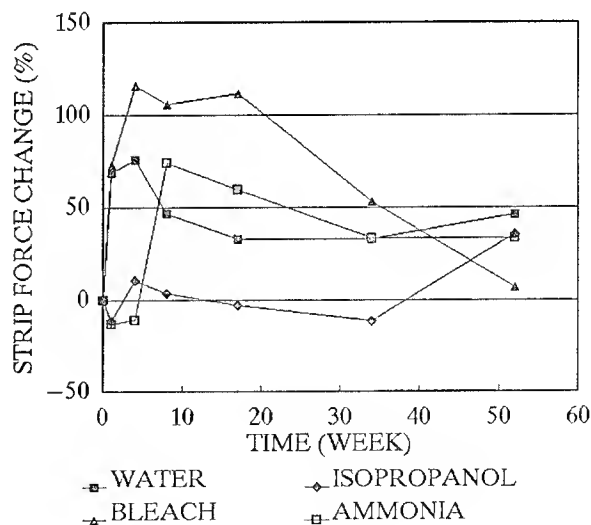


Fig. 2 The effect of four chemicals on the strip force of A-fiber.

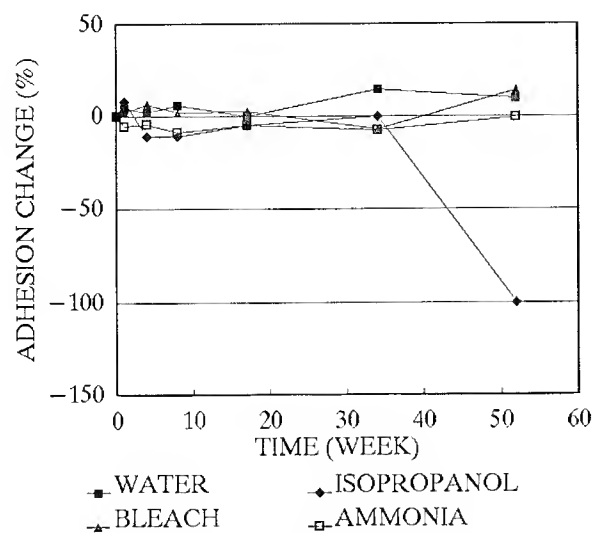


Fig. 3 The effect of four chemicals on the adhesion indicator of A-fiber.

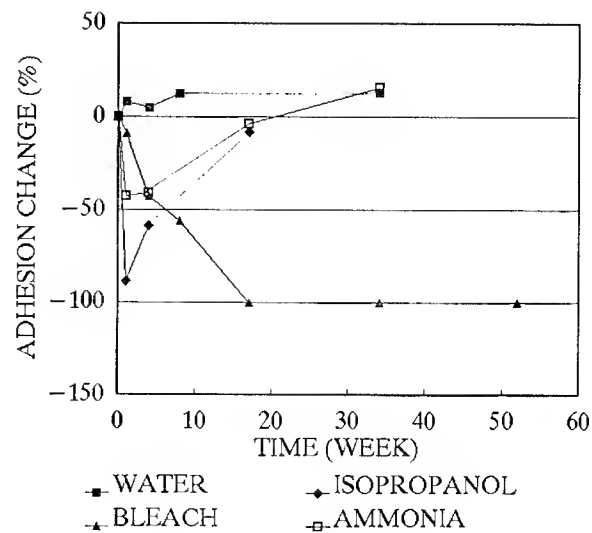


Fig. 5 The effect of four chemicals on the adhesion indicator of D-fiber.

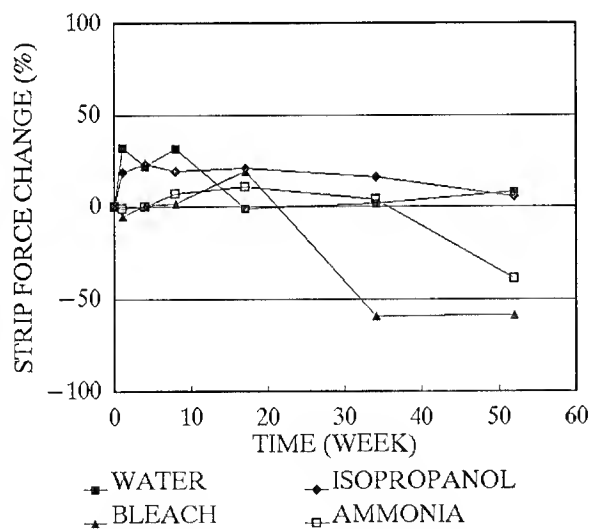


Fig. 4 The effect of four chemicals on the strip force of D-fiber.

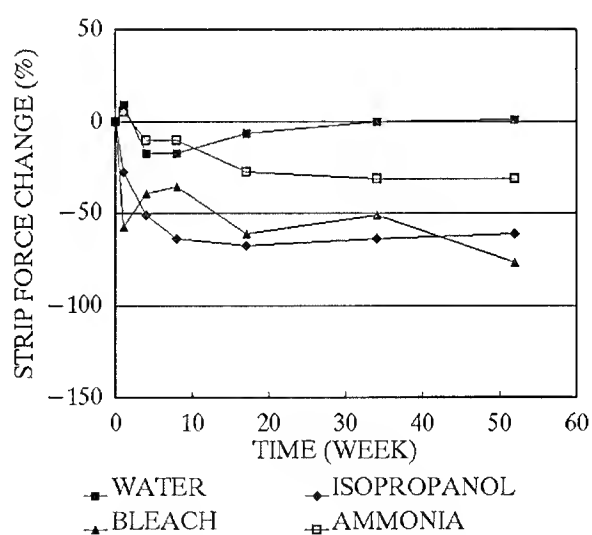


Fig. 6 The effect of four chemicals on the strip force of B-fiber.

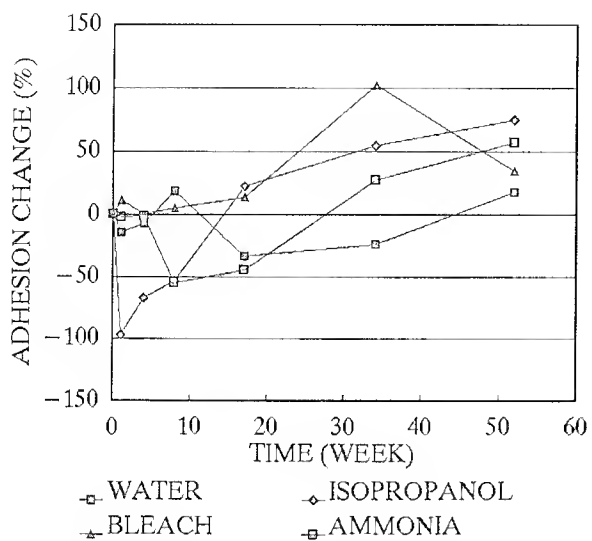


Fig. 7 The effect of four chemicals on the adhesion indicator of B-fiber.

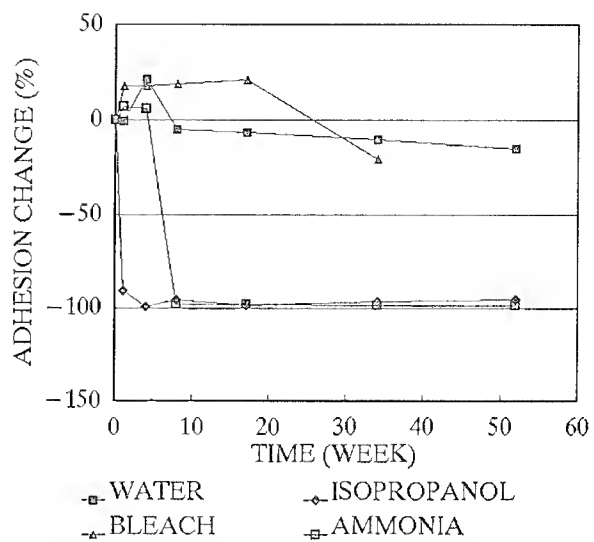


Fig. 9 The effect of four chemicals on the adhesion indicator of C-fiber.

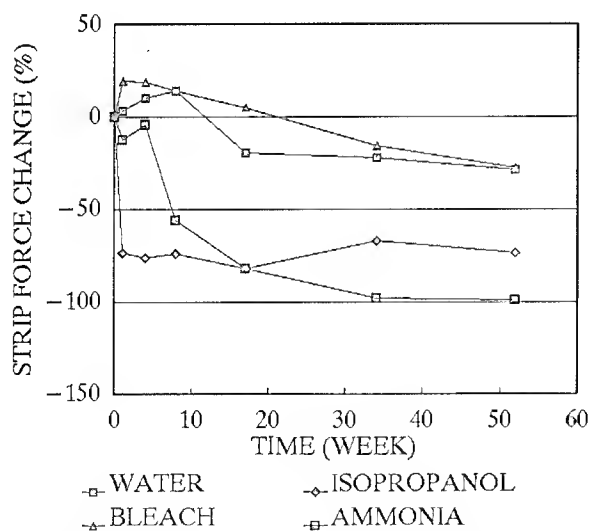


Fig. 8 The effect of four chemicals on the strip force of C-fiber.

A NEW, SEALED, HIGH CAPACITY UNIVERSAL FIBER OPTICS CLOSURE

Julian S. Mullaney, Thomas H. Wermke, William N. Beauchamp

Raychem Corporation, Telecom Division, Fuquay-Varina, North Carolina

Abstract

A universally applicable fiber optic splice closure has been designed for aerial, buried, and underground applications. To accomplish this, a new high-capacity splice-organizing system has been developed and enclosed within a rigid sealed container. A single technique for organizing single-fusion, mass-fusion, mass-mechanical, and a broad range of single fiber mechanical splices is discussed. The novel design allows a high degree of flexibility in terms of cables including dielectric, non-dielectric, single fiber, loose buffer tube, and ribbon construction. Such an organizing scheme allows very high fiber capacities with up to 576 single fusion splices or 1000 + mass fusion fiber splices and associated slack-storage in a single enclosure. The modular design of the components, especially fiber-splicing trays and individual splice-holders, allows a high degree of interchangeability and adaptability of the system to hold other accessories such as optical splitters and new types of splices.

Background and Introduction

Advances in fiber splicing technology have resulted in an ever-increasing array of fusion and, especially, mechanical splice types. Current technology now includes mass-fusion and mass-mechanical splicing of ribbon fiber. In addition, fiber-cable manufacturers are building higher capacity cables up to and in excess of 288 fibers.

The diversity of fiber network topologies available to a single telephone or cable television company can lead to the use of an array of different splices and cable constructions in certain situations. The economy of using mass-fusion splice techniques for high-density ribbon-fiber is very attractive, while mechanical single fiber connectors may be preferred for smaller cable sizes within the same splice enclosure.

The proliferation of new fiber optic cable construction designs and mechanical splice types has exceeded the ability of new splice closures and current organization techniques. The disadvantage of earlier fiber optics splice closures was their inability to easily accept a wide variety of splice type and cable constructions as they became available. Typically, a splice closure system would have

an internal organization and splice holding scheme for a specific cable and splice type. Having a high-capacity splice closure which could be used with any cable type and any splice type would represent a significant logistical advantage to the customer. The design of universal components able to handle a wide variety of splices and cable configurations would be very advantageous. In addition, using a modular design approach for the internal organization scheme allows the opportunity to exchange components and develop new components as new splice types and cable constructions become available.

In this paper, Raychem's FOSC 200 D fiber optics splice closure is disclosed which provides extensive versatility in terms of cable type and splicing method allowed, and also modularity of design as to allow for future adaptability.

Development Project Criteria

The design of the new product was based heavily on an older fiber optics splice closure, Raychem's FOSC 100 D. This existing closure had been developed for fusion splicing and was limited in capacity to 144 splices. The task of re-engineering the FOSC 100 D closure was undertaken primarily to increase fiber splicing capacity and to more easily accommodate newer cable types such as ribbon fiber. This resulted in a new product, the FOSC 200 D. All of the internal components were replaced with a new splicing and organization scheme, and were housed in the existing unchanged butt enclosure. A photograph of the product is shown in Figure 1.

Splice capacity was increased by designing a more compact, densely populated splice tray, and by changing other internal components such that additional trays could be fitted in the enclosure. The splicing and storage of high fiber count ribbon cable was taken into consideration in the new design, as was the complexity of organizing such large amounts of fiber in the closure before reaching the splice tray. The popular practice of "expressing" large amounts of un-cut ribbon fiber through a closure while splicing only a few ribbons present unusual difficulties that were considered in the design.

With the diversity of mechanical, fusion and mass fusion splices available to industry, it was impractical to provide tailor-made splice holders for each splice type. As a result, a single splice holder was produced capable of holding all single fusion, mass fusion, and most single mechanical splices currently in use. Subsequently, other specialized splice holders have been introduced for certain mass mechanical splices. A photograph of the splice holders is shown in Figure 2.

The need to maximize versatility and minimize design complication for cost reasons resulted in a closure with a modular design with very few fasteners. Most components were designed with snap fits such that interchange of components could be done in the field without tools. Furthermore, many components were designed to be interchangeable with the FOSC 200 D's predecessor, the FOSC 100 D.

The design of the splice trays, and other internal components of the closure are covered under U.S. Patent No. 5,323,480.

Components

Fundamental to the design is the splice holder module. Up to six modules, each holding six splices, may be attached to each of eight splice trays bringing the total individual splice capacity of the closure to 288. A populated splice module showing several installed splices is depicted in Figure 2. The splice holder module consists of three parts. A rigid outer shell provides support and serves as a means of attachment (snap fit) to the splice tray. Contained in the outer shell are two compliant polymeric splice holders molded to fit a wide range of splices. An important feature of the rubber splice holders is that they are hollow in design. Using this hollow molded technique allows the part to have a large amount of effective compliance, and accordingly conform to many different shapes of splices. The hollow cross section allows the rubber part to be molded with an otherwise impossible negative draft in the splice holding area. Thus splices are retained in the holder with positive snap retention rather than compressive force. A cross section view in Figure 3 illustrates the negative draft snap retention. With splices installed, the rubber splice holder is free of compressive loading. This feature was used to avoid inherent problems of long term compression set of polymeric materials and to avoid the danger of splices falling out of the splice holder after several years of use.

Splice holders may be removed or repositioned on the tray to allow flexibility of installation. Newer splice holders such as the mass mechanical splice holder in Figure 2 may be attached to the same tray.

A major concern in design of the tray on which the splice holders are fixed was to increase the internal dimensions of the tray without sacrificing rigidity or increasing outside dimensions. The internal height of the tray is large enough to route large amounts of ribbon fiber inside the tray, yet the exterior tray profile is small enough to allow a stack of eight trays to fit within the overall enclosure. This was accomplished by the use of high strength polycarbonate material and very thin wall thicknesses in the molding process. A populated tray is shown in Figure 4.

Passive splitters and other equipment may be stored in the closure by mounting on an unpopulated tray. Access to each of the trays is accomplished by hinging about the base as seen in Figure 1. Up to eight trays are held and may be removed from a molded plastic base with a simple snap fit. The hinging stacked tray configuration permits very economical storage of many splices and easy individual access.

For very high fiber count cables the complexity of internal routing, strength member retention, "express" storage, and electrical grounding present significant difficulties given a reasonable limit on outer closure dimensions. An internal organization scheme was designed to overcome such difficulties while using the existing outer closure shell. This is a conventional butt closure with six tubular cable entry ports. Un-cut fiber (i.e. "express") of ribbon or loose buffer tube construction is installed in the closure through the largest cable entry port. This port is oval in shape rather than round, so as to allow large bundles of fiber to pass through in a loop without excessive bending or kinking of buffer tubes. It is this "express" fiber that is stored in the slack fiber storage basket beneath the splicing trays in Figure 1. A full complement of 18 un-cut loose buffer tubes or 24 + un-cut ribbons may be coiled and stored in this space.

Routing of large amounts of spliced and expressed ribbon fiber using a ribbon distribution system is illustrated in Figure 5. Ribbon fiber deployment is popular in ring architectures where large fiber cables often pass through a closure with only one or two ribbons cut and spliced.

In this procedure all of the ribbons in the cable are initially routed to the slack fiber storage basket. This enables the easy storage of the express portion of the cable without tangling. Subsequently, the ribbons to be spliced are cut, separated from the express portion, and routed through the attached ribbon distribution organizer. The ribbons then are then directed via flexible tubes to the splicing trays. This ribbon distributor serves to secure the end of the flexible transport tubes and to control the bend radius of the ribbon between the tube and the cable. Such a procedure permits organizational flexibility in routing of ribbon fiber within the closure without the need for complex funnels and routing devices.

Conclusions

A re-enterable high-capacity fiber optic splice closure has been designed and developed and is capable of holding up to 576 single fiber splices and 1000 + mass fusion splices with the appropriate slack storage capabilities. The design of the splice trays and splice holders is highly modular, allowing future adaptability.

This internal organization scheme is contained in a re-enterable rigid outer housing which affords a pressure-tight and water-tight seal. The enclosure and cables are sealed by a thermally activated adhesive delivery system which is re-enterable and re-sealable. Adhesive seals are made between the cables and closure entry ports, and between the removable dome and base of the enclosure.

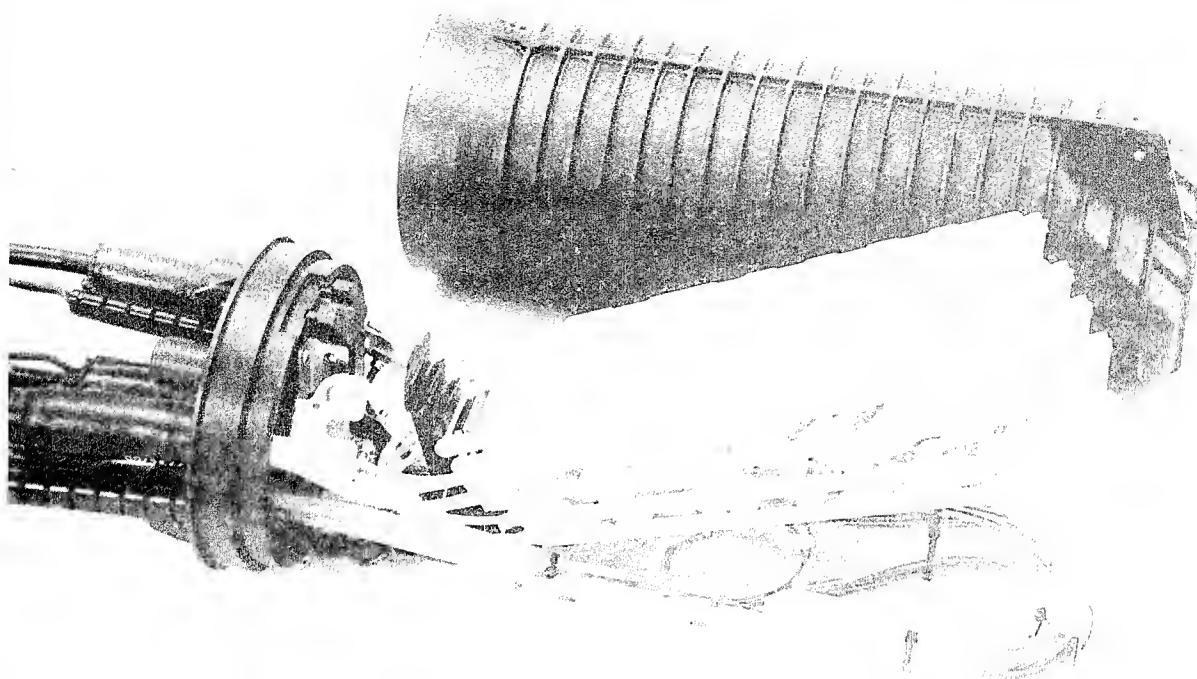


Figure 1. FOSC 200 D Closure

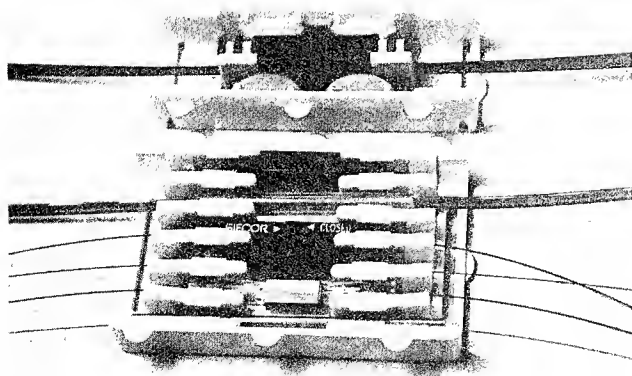


Figure 2. Splice Holder Module

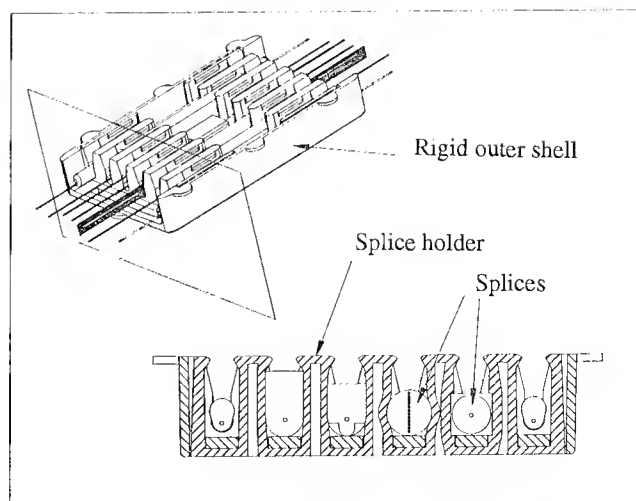


Figure 3. Splice Holder - Cross-section view

This product will serve the need for universally applicable high density fiber optics splice closures used in the trunking and distribution telecommunications networks. In the future, the basic design will adapt to house passive and active optical devices, new splicing techniques and new cable constructions.

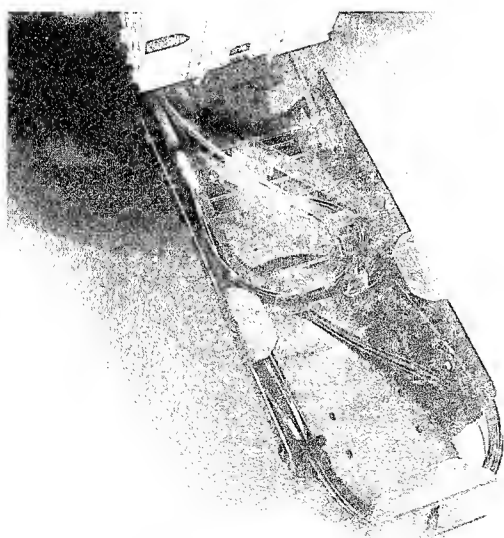
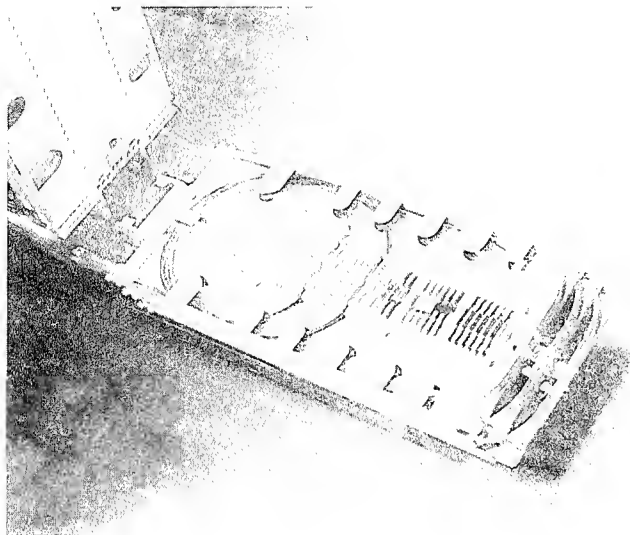


Figure 5. Ribbon Distribution System

Acknowledgments

The authors would like to acknowledge technical contributions to this work by Bill Curry, Bob Sember, Andy Webb, George Scalco, Bobby Bower, Bill Heisey, and John Kizis and development of the manuscript by Linda Taylor and Reed Reichardt.



Julian Mullaney is a fiber optic product development engineer at Raychem Corporation in Fuquay-Varina, North Carolina. Julian received a B.S.M.E. from North Carolina State University and joined Raychem in 1985 in the product development group. He has been involved in the design and development of sealed copper splice closures, sealed electrical devices, and sealed fiber optic closures. For the past two years he has been a project manager for development of new fiber optic cable closures.



Thomas Wermke has worked in the area of product development with Raychem Corporation for the past 4 years. His involvement has been primarily with design and development of fiber optics closures and sealed electrical terminals. He has a B.T. degree from S.U.N.Y.



Bill Beauchamp has worked in the area of product and machine design for 14 years. Since joining Raychem Corporation in 1989 he has worked on the design and development of several sealed copper splice closures, sealed electrical devices, and fiber optics splice closures.

Effect of superabsorbent materials on the performance of optical fiber ribbons

Y.-c. Lin, Ting-Chung Chang, Jye-meei Hsiao, Whei-Jen Chen, K-Y Chen

OSP, Telecommunication Labs, MOC, TAIWAN, ROC

Abstract

Two types of 4-fiber ribbons commonly used in dry-type optical cables designated as Ribbon-H and Ribbon-P are subjects to aging in superabsorbent material saturation solutions at 50, 70 and 85°C to understand the effect on the reliability. Bending strength measurements indicated that the strength of Ribbon-P dropped by 20% after 60 days aging. No apparent additional drops were observed for aging up to 180 days and the strength decrease was temperature independent. However, a dramatic drop of bending strength was seen for Ribbon-H and was temperature dependent. The strip force of Ribbon-P showed no apparent change when aging at 50°C for 180 days and decrease slightly when aging at 70 and 85°C. On the contrary, Ribbon-H dropped by as high as 36% when aging in 85°C for just 1 week. From the stereo microscope and AFM measurements, the matrix coating of Ribbon-H was swelling and roughness on fiber surface was observed. Results of strip forces' measurements echo the result of bending strength measurements as seen that the mechanical property of fiber ribbon is determined by the protective ability of matrix coating and coating materials characteristics, especially when the environments become harsh.

Introduction

For the purpose to reach the goal of "fiber in the loop", multi-fiber ribbons are chosen to incorporate into the design of optical cables to meet the high-count demand in the subscriber loop. Since the multi-fiber ribbon is the major expense within the

cost of a cable, together with the very high transmission capacity, it is important for any end-user or cables manufacturer to understand all the characteristics and its long-term reliability. The 4-fiber ribbons are usually used in slot type cables, which use water-block-tape (made from superabsorbent materials) for water blocking[1]. However, in cases of cable breaks or closure breaks, the water may enter the cables and soak the water block tape. Under such condition, the ribbons will be continually exposed to the soaked superabsorbent materials, and the long term reliability as well as the workability such as stripping of fiber ribbons becomes questions that needed to be addressed. Essentially, a ribbon is a collection of certain number of fibers that are bonded or encapsulated to form a ribbon. The only difference between fiber and ribbon is the matrix coating that is similar to the secondary coatings. However, problems have been complained by the installers during field-deployment, such as the abnormal high attenuation of certain fiber within a ribbon, geometry distortion of ribbon, difficulty of stripping and separating the adjacent fibers, unexpected breaks of certain fiber within an intact ribbon, and uncontrollable attenuation fluctuated with temperatures and sensitive to the ways of organizing the excess ribbon inside a splice closure. These complains suggest that the performance of the fiber in a ribbon is not as good as that inside the loose tube of a conventional cable even though they are basically the same fibers. Apparently, the matrix coating must have played an important role in affecting the individual fiber performance, especially when fatigue, environmental stress, and materials compatibility are issues to its long term reliability.

Experimental

Samples :

Two commercial available ribbons designated as Ribbon-P and Ribbon-H were chosen for tests. They are made from 4 single mode fibers ($125\text{ }\mu\text{m}$ of glass coated with dual coatings to a diameter of $250\text{ }\mu\text{m}$). The four fibers are encapsulated into a matrix coating to form the ribbon. The superabsorbent-aqueous-solution is prepared from dissolving the water-blocking-tape (contains the superabsorbent) in excessive distilled water inside beakers, and followed by removing the undissolved tapes and clear upper layer water to obtain a saturated solution after the beakers were left undisturbedly for a while.

Aging :

The ribbons were cut to numbers of samples at a length of ca. 1000 m. They were loosely wound as circles (diameter $\approx 300\text{ mm}$) and placed inside containers with the ends of ribbons leaving outside the containers. The stainless containers that contain the ribbons were then filled up with a saturated superabsorbent-aqueous-solution. The containers that contain the ribbons (immersing in superabsorbent solution) were brought to water baths and were stress free aged at 50, 70, and 85°C . The bath temperatures were arbitrarily selected and controlled within 2°C of variations. Sample of ribbons were removed from aging at period of time and the change of bending strength, strip force and bending loss were measured.

Bending Strength :

Minimum of 30 specimens for each sample were measured in a two-point bending machine equipped with an acoustic detector. Each specimen (ca. 30 mm) was placed inside two parallel plates separated by 10 mm. Using a step motor, one of the plate was driven toward the other plate by compressing the ribbon under a constant stress rate of 6 MPa/sec until the ribbon breaks. The distance between the two parallel plates at ribbon breaks is used to calculate the bending strength according to the equation derived by Matthewson and Kurkjian [2].

Testing conditions are under a laboratory ambient environment of 23°C and a relative humidity of 60%.

Strip Force :

Minimum of 10 specimens of each sample were measured in a customized stripping tensile testing machine mounted with a commercial 4-fiber stripping tool. The tool was pre-heat for 12 seconds using a DC power supply in a current output of 2.5 ampere to reach the temperature of $105 \pm 5^{\circ}\text{C}$ before stripping. The gage length is 100mm and stripping length is 15 mm with a stripping rate of 150 mm/min. Strip forces were collected through out the stripping process. Each sample datum was taken from the median of 10 tested specimens.

Result and Discussion

Changes of Strength

Fig. 1 and Fig. 2 show the changes of bending strengths of Ribbon-H and Ribbon-P aged in a superabsorbent solution respectively. Both the measured bending strengths and the aged strengths relative to the unaged initial strength shown as the residual strength are indicated. The strengths are obtained from the media of their corresponding Webull plots measured by 2-point bending methods. Both ribbons show : (a) A degradation of strength upon aging that similar to water immersion-stress-free-aging phenomena, (b) the strength dropped sharply at the initial aging stage and became less changeable after 60 days of aging., (c) competitive initial strengths of 4.682 and 4.732 GPa . In the meantime, obvious differences between Ribbon-H and Ribbon-P were seen as: (a) substantial higher degree of strength drops occurred on Ribbon-H. For example, aging at 85°C for 120 days, Ribbon-H dropped to 31% of its initial strength whereas Ribbon-P dropped to 80% of its initial strength. (b) Temperature-dependent drops of strength occurred on Ribbon-H whereas temperature-independent strength occurred on Ribbon-P. Ribbon-H showed a progressive increase of strength drops when aging temperature increased whereas Ribbon-P all gave a similar drop of strength at three aging temperatures.

Since the aging profiles are similar to that of a stress-free-aging, a method that plotting Log (strength) versus $t^{1/2}$ derived by J.J. Carr [3] was taken to examine the aging mechanism. Fig. 3 showed the plot according to the equation [3]:

$S(t)=S(0) \exp(-\alpha t^{1/2})$, where $S(t)$ is the aged strength, $S(0)$ is the initial strength, α is the aging parameter, and t is the aging time. The obtained α along with the values reported by Carr are listing in Table 1:

Table 1.

Aging parameters of Ribbon-H and Ribbon-P

	Ribbon-H	Ribbon-P	Fiber Carr
45°C			0.004
50°C	0.041	0.013	
65°C			0.047
70°C	0.043	0.011	
85°C	0.089	0.015	0.093

The aging parameters of Ribbon-H looks comparable to Carr's values, and it implies that the superabsorbent-solution immersion aging is similar to water-immersion stress-free-aging. However, this is only true when the Fig.3-plot-fitting is perfect and bending strength measurement can reflect the fiber strength just like tensile strength measurement does. The truth is that, from Fig.3, only the data of Ribbon-H aging at 85°C shows the best line fit at R square of 0.9651 and the rest of all showed less acceptable fitting. Apparently, the Carr's equation that describes the stress free aging of fiber may not exactly be applicable to the superabsorbent-solution-aging of ribbon here. Two possibilities may account for the deviation: (a) the function of superabsorbent solution exerting on the ribbon is not necessary as simple as that of the water exerting on the fiber during stress-free-aging, (b) the extra matrix coatings on the ribbons may serve as a significant barrier that protect fiber glass from corrosion factors (such as moisture). Since the superabsorbent solution has a PH value near 9, it is expected that it is more corrosive to glass fiber than distilled water is. However, the aging of ribbons here did not show worse of strength drop than that of fiber reported on stress-free-water-immersion agings[3]. It must be

due to the extra protection of matrix coating that offsets the corrosive superabsorbent solution. As a result, the extent of strength drops during aging is determined by the ability of matrix coating to serve as a corrosion barrier. In other words, the diffusion rate of corrosive factors (such as water molecules) through the coating will determine the degradation rate of fibers, and it will be temperature dependent if the water diffusion follows the Fick-type diffusion-sorption mechanism. Such as the case of 85 °C – aging of Ribbon-H in Fig. 3 shows a typical diffusion controlled degradation phenomenon. On the contrary, the coatings on Ribbon-P, actually, is harder and more crosslinked than that on Ribbon-H, and showing better resistance to the corrosive superabsorbent solution that it is hardly soaked by the solution. As a result, it shows only a 20% of drops and is temperatures independent. Also, in Fig. 3, the plots of Ribbon-H that aged at 50 and 70 °C look more like a curve than a linear fit, implying that other factors beside the water diffusion are also important to determine the strength drops. Such factors can contribute to the degradation of fiber describing as an independent term in the following equation: $S(t)=S(0)[\exp(-\alpha t^{1/2})+\exp(-\beta t^{1/2})]$, where α describes the normal stress-free-aging and β describes the other aging effect such as the corrosive effect of superabsorbent solution or the different diffusion effect occurring on the matrix coatings.

The strength degradation of Ribbon-H and Ribbon-P upon superabsorbent-solution aging, in fact, is due to the surface corrosion of fiber glass surface. Fig. 4 shows their AFM surface roughness measurements both before and after aging. The calculated mean roughness (Ra) and maximum height (Rmax) are tabled below:

Table 2. Mean Roughness (Ra)

Ribbon	unaged	50°C	70°C	85°C
H	0.916 nm	0.960 nm	1.181 nm	8.722 nm
P	1.022 nm			1.207 nm

Table 3. Maximum Height (Rmax)

Ribbon	unaged	50°C	70°C	85°C
H	8.8 nm	15.1 nm	25.0 nm	65.9 nm
P	8.8 nm			13.9 nm

The increase of roughness on the fiber surface is proportional to the extent of strength drops. Therefore, factors that corrode of glass surface is the major contribution of strength drops. Again, the results is consistent to the reality that the corrosion of fiber glass is controlled by the diffusion of corrosive factors through matrix coatings.

Strip force

Strip force usually directly reflects the workability of a ribbon and has the practical meaning of the coating protecting ability to the fiber glass. Table 4. shows the changes of strip forces of both ribbons aged in superabsorbent solution

Table 4. Strip forces of Ribbon-H and Ribbon-P aged in superabsorbent solution

Aging time, day	Strip Force (gram)					
	H- 50°C	H- 70°C	H- 85°C	P- 50°C	P- 70°C	P- 85°C
0	414	414	414	1146	1146	1146
7	283	143	87	1145	1022	1027
14	NA	NA	NA	862	870	872
30	NA	NA	NA	974	959	857
60	NA	NA	NA	1027	996	975
120	NA	NA	NA	1057	951	881
150	NA	NA	NA	878	1026	1095
180	NA	NA	NA	978	1056	1014

Unlike the comparable initial strength between two ribbons, the initial strip force of Ribbon-H is only 1/3 of that of Ribbon-P. During aging, the small strip force of Ribbon-H dropped so quickly that the strip forces were unable to measure when it had aged since day-7. The fiber became so fragile to the stripping tools that certain fibers within the ribbon always broke when stripping measurement was conducting. On the other hand, Ribbon-P showed a much higher initial strip force. Upon aging, a drop of

strip force was resulted. However, the drops reverse to increases when aging continues from day-30.

The strip force measurement echoes the result of bending strength measurements. Upon aging, the strength of Ribbon-H decrease quickly. When the residual strength reach 70% of original strength, it became difficult to strip. It seems that, with a initial strip force of only 414 gram, the fibers are less protected, and once the bending strength drops to 70% of initial strength, the ribbon will not be able to strip safely. The bending strength of Ribbon-P was never dropping below 80% of initial strength during aging, and it showed always strippable. Also, all three temperature-aging resulted in similar changes of strip forces in Ribbon-P, and is analogous to the temperature independent changes of bending strength.

In addition, when carefully examining the coating debris that were stripped from Ribbon-P, (as shown in Fig. 5), a trend that associated with the drop-increase profile of strip forces can be seen. In the force-dropping stage (before day-30 of aging), the debris showed clean cut and smooth debris surface, an indication of easy stripping to result in lower strip forces. However, when aging passed day-30, the stripped debris showed roughness with curling surface. Prolonged aging gave more serious curling of debris, an indication of the debris was not taken off effortlessly. As a result, an increase of strip force was obtained. The curling also indicates that the debris is harder and the matrix coating apparently has been undergone chemical changes caused by the aging effect of thermally hardening effect. In fact, the aging of ribbons in superabsorbent solution at elevated temperatures have resulted in permanent geometry distortion of ribbons that appear curl and twisted, and the distortion occurred on Ribbon-P appears to be more serious than that on Ribbon-H. Further observation of the cutting edge of stripped ribbons by SEM disclosed how the aged matrix coatings by the heat and superabsorbent solution have affected the ribbons geometry. As seen in Fig. 6, both unaged ribbons showed fibers with dual layers of coating that were well-aligned and encapsulated by

matrix coatings. After aging for 180 days at 85°C in superabsorbent solution, both matrix coating showed intact without any surface cracks. But at the cutting edges, Ribbon-H showed a still well-aligned fibers that seems, however, loosely included inside the matrix coating. No apparent geometry distortion was seen at the edge point. In the meantime, Ribbon-P showed disarranged fibers that seem being squeezed by the shrinking matrix coating. The geometry of Ribbon-P has changed from a flat ribbon to a round-ribbon. This confirmed the observed facts that (a) Ribbon-P is more tightly encapsulated, (b) Ribbon-P has more geometry distortions upon aging. (c) Ribbon-P is more protected by the matrix coating to give higher stripping forces and less degradation of bending strength. All of these can be accounted by the facts that the matrix coating of Ribbon-P has been hardened by aging effect. The hardened matrix coating will result in shrinking that will squeeze the fibers, and a tightly encapsulation is formed. If the shrink continues, the fibers will be squeezed out of alignments and a buckling ribbon is obtained. Also, harder coating will give higher strip force. All these aging results will lead to the difficulty in mass fusion. In addition, hardening of matrix coating will depreciate the ribbon's capability to macro or micro bending resistance. Apparently, hardening of matrix coating may be helpful in preserving the strength of ribbon, but shows all the disadvantage on the workability.

Conclusion

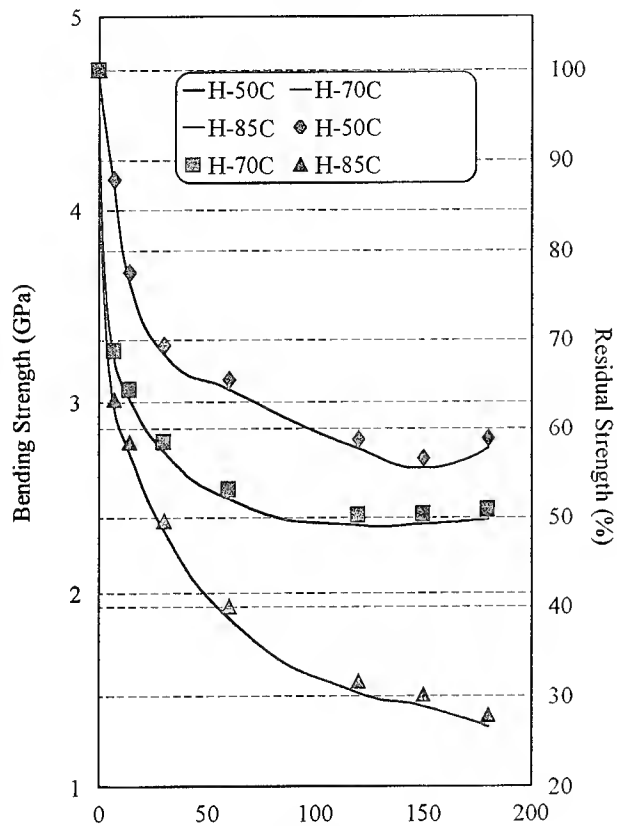
The aging of ribbons in superabsorbent solutions shows not as simple as a water-immersed-stress free aging. The more corrosive of superabsorbent solution and the better protecting ability of matrix coating are two factors that contribute to the deviation of this aging from stress free aging. In the case of here, the well-protected Ribbon-P only drops by 20% of bending strength upon aging, and is temperature independent. Whereas, Ribbon-H significantly drops by 70% of

bending strength after aging, and is temperature dependent. However, the coating that well-protects the ribbon strength shows all the disadvantages to the workability of ribbons. It may result in more geometry distortions of ribbon, misalignments of constituted fibers, shrinking of ribbon dimension, less capability to macro and micro-bending resistance, and higher strip forces. Nevertheless, ribbon with matrix coating less capable will be susceptible to environmental aging such as the superabsorbent solution, and the strength drops so quickly that the ribbon becomes untouchable. New coating materials that can fit to better protection while keeping less hardening upon aging at elevated temperatures is the hope to make ribbons that suitable for loop usage.

REFERENCE

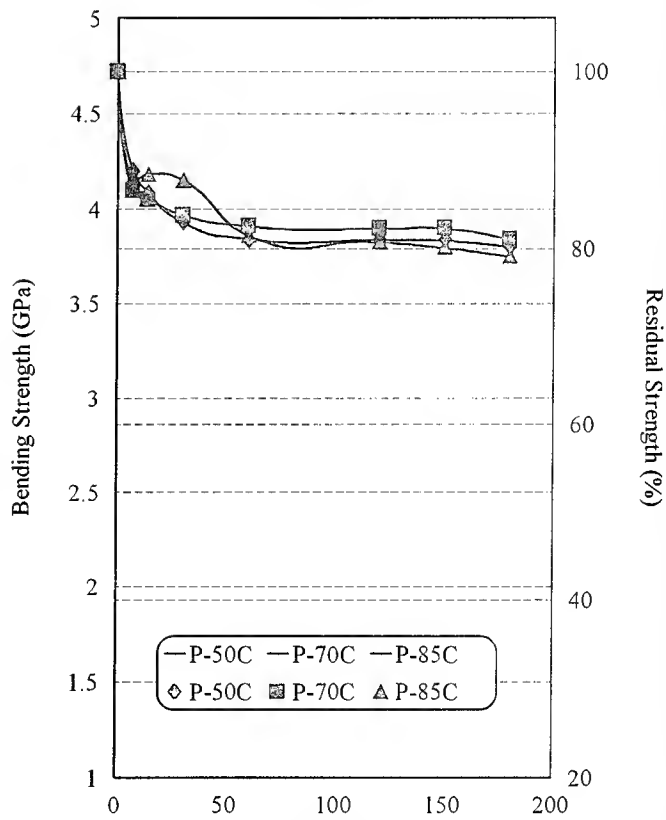
1. A.lino, M.Kuwabara, and K.kokura, J. Lightwave Technol. 8(11),p1675 (1990)
2. M.J. Matthewson and C.R. Kurkjian "Strength measurement of optical fiber by bending" J. Am. Ceram. Soc. 69(11), 815 (1986)
3. J.J. Carr "a zero-stress aging relationship for optical fiber" the 42nd IWCS, p394, 1993

Fig. 1
Changes of Bending strength of
Ribbon-H aged in superabsorbent
solution



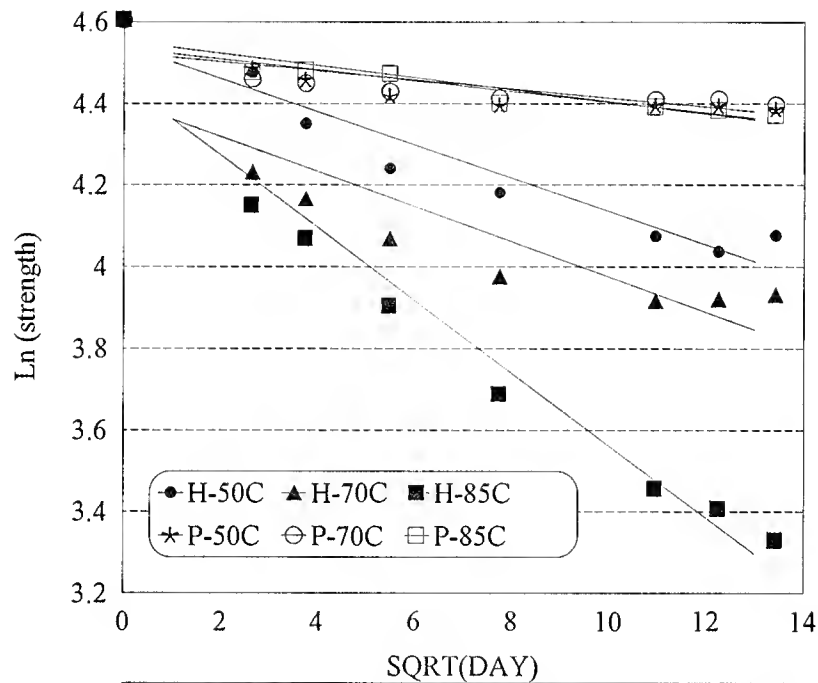
	Time (day)						
	0	7	14	30	60	120	180
H-50C	4.682	4.119	3.631	3.251	3.066	2.755	2.758
H-70C	4.682	3.221	3.017	2.739	2.493	2.354	2.386
H-85C	4.682	2.965	2.737	2.325	1.873	1.482	1.307
H-50C	100	87.9	77.6	69.4	65.5	58.8	58.9
H-70C	100	68.8	64.4	58.5	53.2	50.3	50.9
H-85C	100	63.3	58.5	49.7	40.1	31.7	27.9

Fig. 2
Changes of Bending strength of
Ribbon-P aged in superabsorbent
solution



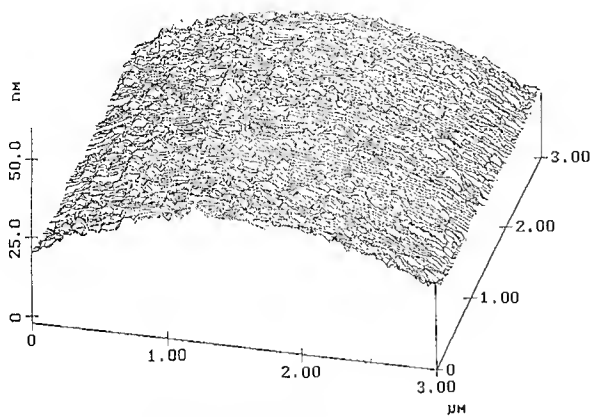
	Time (day)						
	0	7	14	30	60	120	180
P-50C	4.732	4.202	4.085	3.928	3.841	3.834	3.797
P-70C	4.732	4.097	4.05	3.967	3.909	3.894	3.837
P-85C	4.732	4.162	4.184	4.149	3.857	3.823	3.746
P-50C	100	88.8	86.3	83.1	81.1	81.1	80.2
P-70C	100	86.6	85.6	83.8	82.6	82.3	81.1
P-85C	100	88.1	88.4	87.7	81.5	80.8	79.2

Fig. 3
Plot of Ln (strength) vs. Square root time (Day)

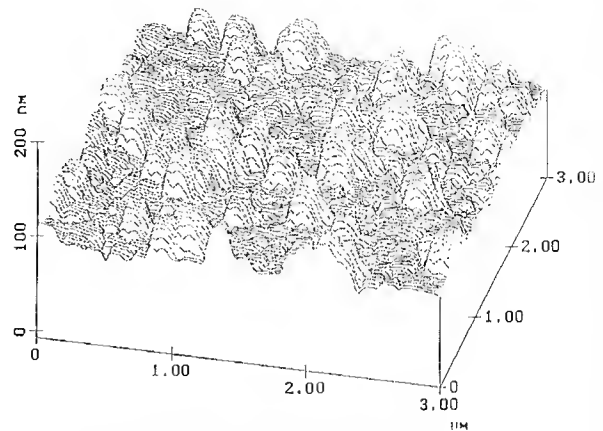


	0	2.6457	3.7417	5.4772	7.7459	10.9544	12.2474	13.4164
H-50C	4.60517	4.47715	4.35103	4.24037	4.18191	4.07479	4.03694	4.07557
H-70C	4.60517	4.23113	4.16567	4.06907	3.97473	3.91773	3.92095	3.93106
H-85C	4.60517	4.14829	4.06819	3.90499	3.68888	3.45504	3.40716	3.32918
P-50C	4.60517	4.48645	4.45831	4.41891	4.39625	4.39485	4.39414	4.38509
P-70C	4.60517	4.46112	4.44972	4.42889	4.41424	4.41029	4.41109	4.39558
P-85C	4.60517	4.47686	4.48203	4.47381	4.40085	4.39187	4.38391	4.37144

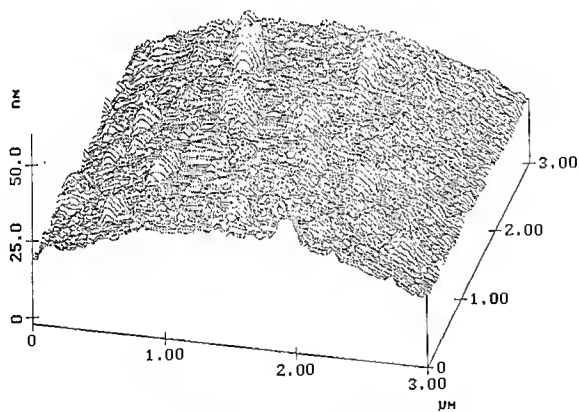
Fig. 4 AFM measurements of Ribbons aged in superabsorbent solution.



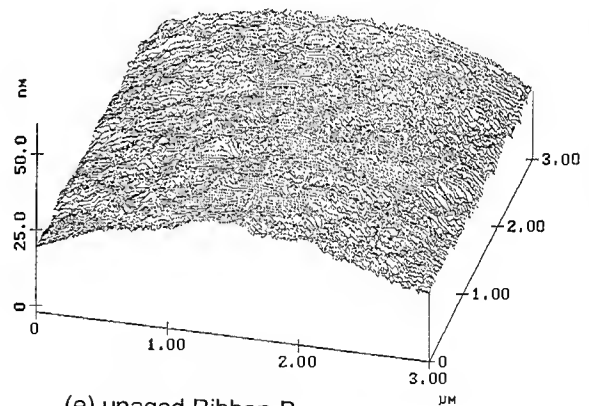
(a) Unaged Ribbon-H



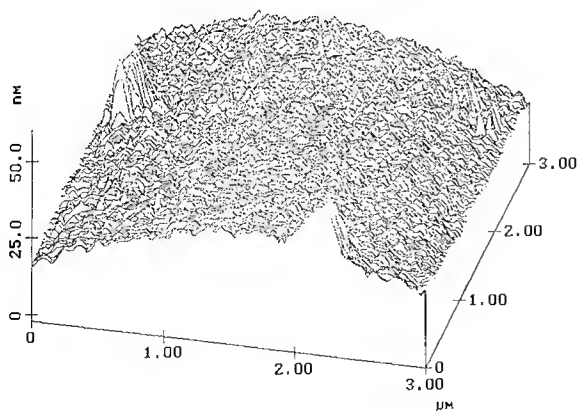
(d) aged Ribbon-H, 85°C, 180 days



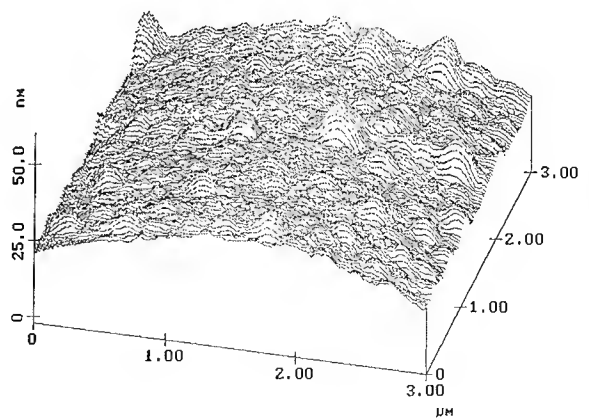
(b) aged Ribbon-H, 50°C, 180 days



(e) unaged Ribbon-P



(c) aged Ribbon-H, 70°C, 180 days



(f) aged Ribbon-P, 85°C, 180 days

Fig. 5 Stripping debris of Ribbon-P

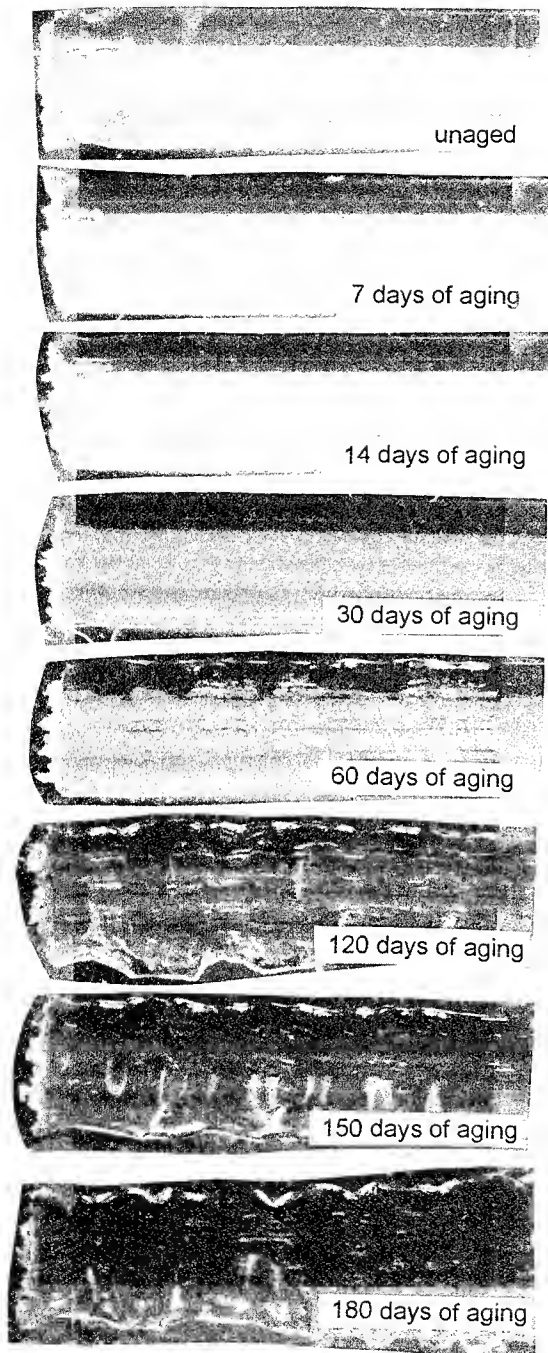
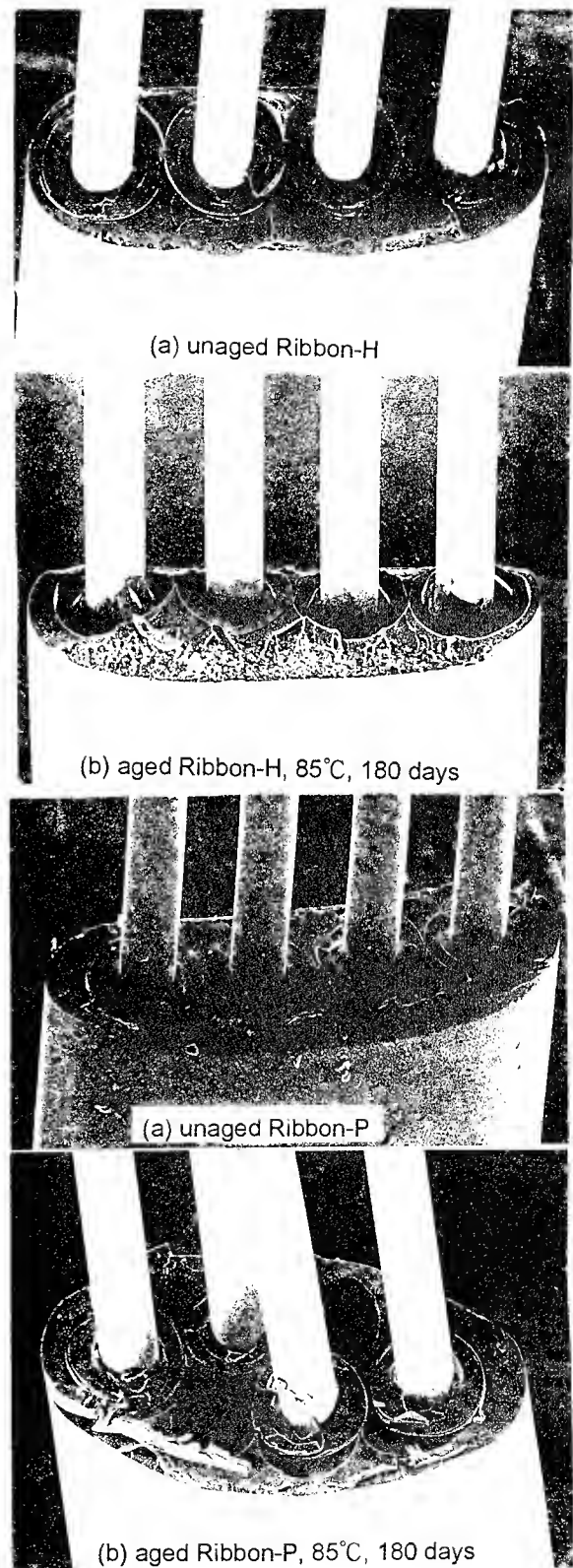


Fig. 6 SEM observations of the cutting edges of Ribbon-H and Ribbon-P



THE STABILITY OF OPTICAL FIBER COLOR CODES: EFFECTS OF MATERIAL CHOICES AND SERVICE ENVIRONMENTS

Barry J. Keon[†] and Rolf A. Frantz^{*}

[†]Telstra, Melbourne, Australia

^{*}Bellcore, Morristown, NJ

ABSTRACT

Optical fiber color codes must remain stable over the fiber service lifetime to facilitate rapid and positive identification of the fiber by craft personnel. Such stability obviously depends upon the characteristics of the ink used to color code the fiber. Less obvious, but nonetheless significant, are: (i) the effects of the manufacturing process, such as the uniformity with which the ink is applied to the fiber coating; (ii) the characteristics of the underlying fiber coating, such as its surface wettability and tendency to yellow during aging; and (iii) potential reactions with the different environments to which the fiber is exposed in service. We are presently examining a spectrum of commercial fibers, colored with both uv-cured and thermally-cured (solvent-based) inks. Film samples of typical coating inks enable us to separate the effects of the coating and the ink layers. The ink films also enable us to assess any nonuniformities in the pigment dispersions, while aging in a variety of environments helps identify potential color-change reactions. A standardized colorimetric measurement technique has been developed to quantify the color changes that occur, supplemented by visual observations as would be made by craft personnel.

INTRODUCTION

Cabled fibers, whether in ribbon or loose-tube arrangements, are visually identified in service by color codes. The discernibility and stability of the colors affect the ability of craft technicians to identify fibers in cables and splice enclosures. Prompt, correct identification is desirable to install new service efficiently; it is critical when working in crowded splice enclosures or restoring interrupted service—for example, after a cable break or dig-up. Quick and reliable identification and matching of fibers require that the colors used for such color-coding be consistent across the product lines from all cable manufacturers, be stable, and remain on the fiber throughout its service life.

Ink flaking and peeling may occur due to interactions with the environment—gel, air, humidity, contaminant liquids, etc. Ink retention is affected by the adhesion of the ink to the coating, which is influenced by the ability of the ink to wet the coating surface and by the ratio and properties of the ink binder resin. The uniformity of both the pigment dispersion and the method of ink application affect the color discernibility through non-uniformities in the ink layer. Wettability again plays a role, causing inks to “puddle” rather than evenly cover the coating surface. Visible color changes occur due to aging of the binder resin and discoloration of the coating. The latter is particularly noticeable in areas of thin pigment coverage. Interactions of the ink and coating with the environment (or with each other) can accelerate—or induce—color change reactions.

Colorimetric measurements provide a means of detecting small color changes before they are discernible by the human eye, enabling accurate tracking and prediction of color changes.^[1,2] The capability for measuring color differences precisely makes colorimeters useful for comparing nominally equivalent colors between suppliers or batch-to-batch variations for any single supplier, as well as the color changes that occur as the fiber ages.

We have begun a study of commercially-available fibers, color-coded with thermally-cured and uv-cured inks, and of films of typical inks. Examination of fiber and film samples helps quantify effects such as nonuniform surface coloration. Aging in a variety of environments causes color changes and enables us to assess the likelihood of ink flaking or peeling. In this paper, we describe both the development of a standard colorimetric measurement technique and the results of typical color change measurements.

SAMPLES AND AGING

We obtained samples of three commercially-available fibers, identified herein as fibers A, B, and C. Lengths of each fiber were color-coded with arbitrarily chosen colors of solvent-based (thermally-cured) inks (orange and blue) and uv-curable inks (rose and aqua). A length of fiber was also left natural (uninked). Additional samples of solvent- and uv-inked fibers and ink films were used in developing our measurement technique. We also obtained samples of the uv-curable and solvent-based inks that were used in color-coding the test fibers, as well as some typical optical fiber color-coding inks. We drew down and cured films of these materials on flat glass substrates; the uv-curable inks were cured using a conveyor belt system, while the thermal inks were cured in a 150 °C oven.

We aged fiber samples (as loose coils approximately 160 mm in diameter) in 65 °C and 85 °C deionized (DI) water and in 85% relative humidity (RH) at 65 °C and 85 °C. Color measurements were made of the unaged fiber and film samples and of fiber samples aged for 1, 7, and 28 days. All samples were conditioned at 23 °C/50 % RH for at least 24 hours after removal from the aging environment. Color changes were assessed visually by comparing aged and unaged samples and by matching to standard color reference chips.^[3] We also developed a standardized colorimetric measurement technique.

COLORIMETRIC MEASUREMENT TECHNIQUE

Color has three attributes: lightness (white or black), hue (red, green, blue, etc.), and chroma (saturation). Figure 1 illustrates how these attributes describe color space. The color names are from Munsell color notation, which has long been used for color description. The xyz axes form a three-dimensional coordinate

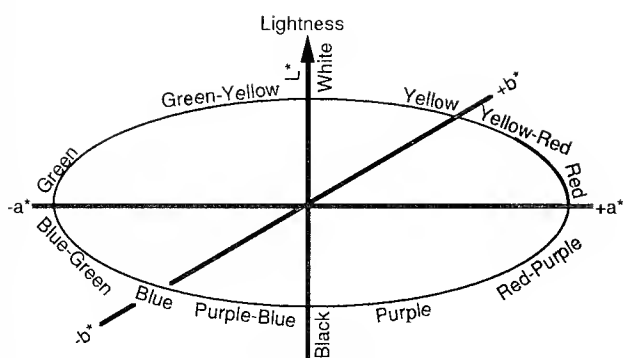


Figure 1. Three-Dimensional Descriptions of Color Space

system, called the $L^*a^*b^*$ system, which describes this same color space. It is particularly well-suited to calculating color differences, which are simple geometric distances. For this reason, we will use $L^*a^*b^*$ notation throughout this paper.

Colorimeters are either *tri-stimulus* (red-green-blue) meters or *spectrophotometers*; we used both types. The characteristics that affect a colorimeter's suitability for measuring fiber samples include the measurement aperture, the illumination/viewing geometry, and the ability to reference multiple colors. The measurement aperture defines the number of fibers required to form the sample. Large apertures require many fibers, which are difficult to arrange in a close-packed parallel array; small apertures measure only a few fibers and may not effectively average the sample color. Apertures 2–20 mm in diameter avoid these problems. Our colorimeters have either diffuse/8° or 45°/0° illumination/viewing geometry, both of which exclude specular reflection from the sample. With the 45°/0° geometry, the light illuminated the sample from all directions around the sensor to avoid a dependency on sample orientation; however, we found that some samples were still sensitive to alignment. Finally, colorimeters are particularly suitable for measuring color differences, and the ability to introduce reference standards for the twelve standard colors defined in EIA/TIA documents on color coding^[4,5] enables an accurate determination of the difference between the actual sample and the reference color.

For accurate color measurements, particularly of inks that are opaque only in thick sections, it is important to minimize the contribution of the background. A white background reflects most of the light reaching it through the sample, while a black background reflects little. The white background results in a stronger signal at the detector, artificially raising the L^* value,

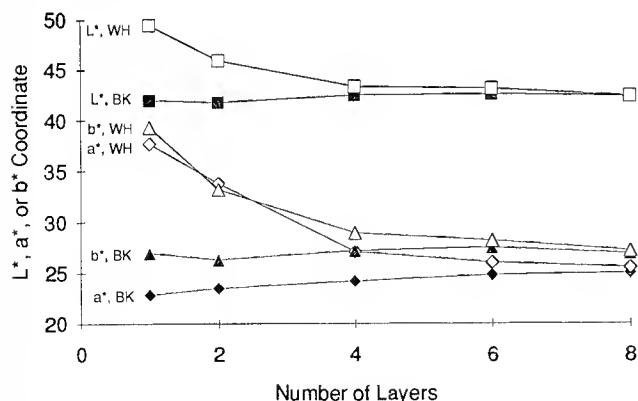


Figure 2. Masking of White (WH) and Black (BK) Background Differences by Layers of Orange Ink Film

while the weak signal from the black background lowers L^* and hinders the measurement of a^* and b^* . Colored backgrounds introduce bias in the form of a^* and b^* signals unrelated to the sample color. These effects diminish as the sample is made thicker and sufficiently opaque to mask the background. To learn how background effects varied with film thickness, we measured film samples of different thicknesses against white and black backgrounds. The results for 1–8 layers of a 13- μ m thick orange uv ink film are shown in Figure 2. Open symbols show the results with the white background, while filled symbols are the results for the black background. L^* , a^* , and b^* for the two backgrounds are all far apart for one film layer. With six film layers, however, the coordinates are nearly identical.

Some uv ink films exhibit a directional sensitivity in the 45°/0° colorimeter that correlates to the drawdown direction, even with circumferential illumination, because the pigment particles are dispersed throughout the film thickness. The meter sees not only the surface (as for an ink film deposited by solvent evaporation), but also the depth of the film, and thus is sensitive to any internal structure resulting from the unidirectional drawdown.

We typically use layers of short pieces as our fiber samples.^[2] Because this is time-consuming, we designed a small spool to wind continuous samples off and onto the storage spool without damage. Its small radius necessitated flat spots to eliminate curvature within the measurement aperture. We provided white and black backgrounds by wrapping the spool with a printing ink drawdown sheet, a standard paper form with white and black bars of specified gloss and reflectance used to determine the opacity of printing inks.^[6] The results for multiple layers of a blue uv-inked fiber layer-wound onto the spool are shown in Figure 3; L^* is plotted separately from a^* and b^* because of the difference in the scales. All three coordinates are quite different for one layer of fiber against the white and black backgrounds, but are very similar for four layers of fiber. Since a^* and b^* are both negative, the values for the black background lie closer to neutral, i.e., above those for the white background. Some fibers with uv inks exhibited a distinct directional sensitivity compared to solvent-inked fibers. This again illustrates that the pigment is dispersed through the thickness of the ink layer.

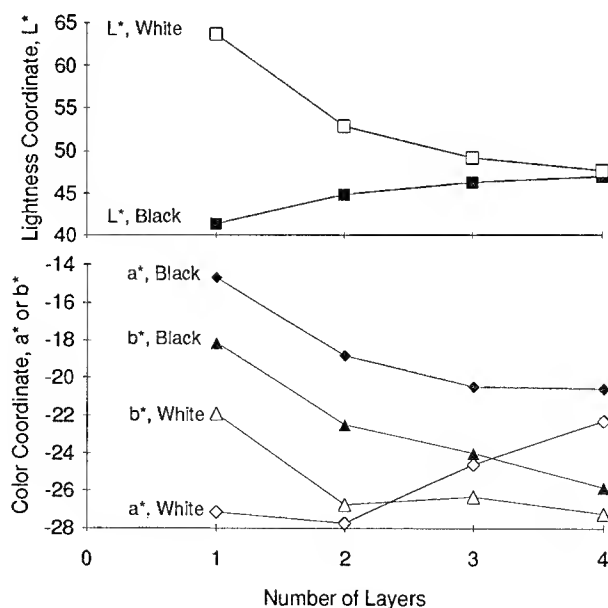


Figure 3. Masking of White and Black Background Differences by Layers of Blue Inked Fiber

Table 1. L*, a*, b* Coordinates of Color Coded Fibers and Ink Films against White Background

	Orange (Solvent)	Blue (Solvent)	Rose (UV)	Aqua (UV)
Fiber A	54.86, 54.88, 57.83	22.70, 11.82, -31.83	73.11, 29.65, 17.65	64.84, -24.84, -16.21
Fiber B	54.67, 52.01, 54.37	23.11, 10.06, -30.48	73.92, 28.99, 17.93	63.48, -23.21, -17.75
Fiber C	54.81, 52.87, 56.77	22.89, 10.13, -31.72	73.39, 30.14, 17.76	63.12, -23.17, -17.41
Ink Film	52.89, 60.71, 69.39	—	73.52, 29.28, 16.18	65.45, -25.55, -17.16

Measurements of single fiber layers, whether on the spool or as short pieces, were useful to assess any peeling or flaking of the ink that occurred during aging and handling. Comparisons of multiple-layer measurements provided a good indication of the extent of discoloration that occurred during aging.

RESULTS

Because we had limited lengths of each fiber, we used short fiber pieces for each color sample. The pieces were placed in a square U-shaped channel ~20 fibers in width. The channel bottom was lined with the white/black drawdown paper as a background. The aperture of our 45°/0° meter was equal to about seven fiber diameters, so we were able to take multiple readings against each background within the channel. Each reading averaged portions of seven fibers; three readings were averaged to get the mean value and standard deviation. The film measurements were made by cutting small samples from the cured sheets and placing them directly onto the drawdown paper background. All of the measurements reported here were made with the 45°/0° meter, but some measurements were confirmed using the diffuse/8° meter. We will report measurements for the white background because they show the layering effects better, while with sufficient layers, there is no white/black differential.

One factor that affects fiber identification and matching is whether the color-coded fibers meet the tolerances given in EIA/TIA standards 359-A and 598. Table 1 lists the measured L*a*b* coordinates for samples of fibers A, B, and C in the four color codes (blue and orange solvent inks and rose and aqua uv inks) used in this study. The coordinates for film samples of the inks are also reported. Comparing the color coordinates with the centroids and extended limits in the EIA/TIA standards indicates that all four colors are slightly dark (low values of L*), and that the orange and rose are both a bit too red (although they approach red from opposite sides). This is true for both the film and fiber samples.

Figure 4 shows the effects when one and four layers of a yellow ink film are superimposed on the white/black boundary of the drawdown background paper. Table 2 summarizes the L*a*b* coordinates for these three measurements. As expected, the differences between the measured colors on the two backgrounds decrease as the film layers increase. However, this particular ink was relatively transparent, so that even after four 15-μm thick layers were used, the white/black background differential was significant. For this ink, film thicknesses greater than 75–80 μm would be required to mask the background effect.

Figure 5 illustrates the relative opacity of the particular uv rose and solvent orange inks used in this study, which was the same for all fibers. Whereas two layers of rose-inked fiber were sufficient to effectively mask the white/black background effect, at least four layers of orange-inked fiber would be required for this same masking capability. One reason for this is the non-uniformity of the orange ink layer, which we discuss later.



Figure 4. Yellow Ink Film Layers on White/Black Background

Table 2. L*, a*, b* Values for Multiple Layers of Yellow Film

Number of Layers	White Background			Black Background		
0	93.61	-0.36	0.49	33.08	0.10	2.31
1	79.20	-9.93	114.27	46.98	-25.03	63.30
4	66.47	-5.47	94.30	54.89	-21.02	74.76

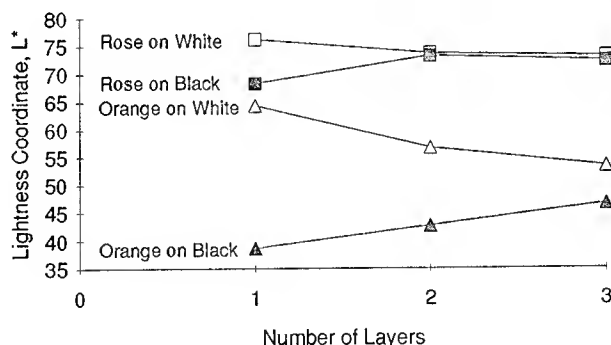


Figure 5. Lightness Coordinate of Multiple Layers of Inked Fibers on White and Black Backgrounds

Also, the uv ink layers are particularly thick on these fibers. An additional benefit of using multiple fiber (and film) layers not explicitly shown here is that the standard deviation in the measured value for each coordinate decreases to half or less of its one-layer value when three layers are used.

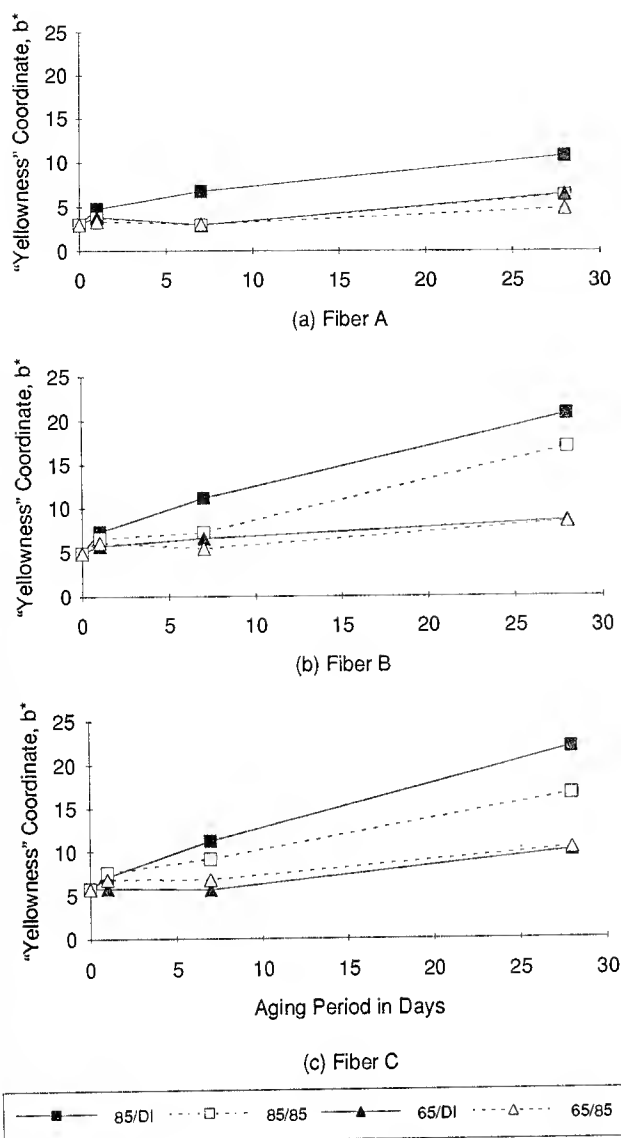


Figure 6. Effects of Aging on the Yellowness Coordinate of Three Layers of Uninked Fiber on White Background

The aging effects of the four environments, shown in Figure 6, support the perception that fiber coatings "yellow" with age. As shown in Figure 1, the color yellow lies along the $+b^*$ axis. In Figure 6 (a-c), b^* is plotted as a function of aging time for the natural (uninked) fibers A-C, respectively. The measurements are for three-layer samples against a white background; similar but lesser changes were seen with fewer layers and/or the black background. All three fiber coatings have a small $+b^*$ value before aging, but it is undetectable by eye. After aging, however, all of the fiber coatings had perceptibly yellowed, which is confirmed by the colorimeter measurements. Also, the samples aged in 85 °C DI water showed the greatest amount of discoloration. L^* decreased slightly as a consequence of the yellowing (darkening) of the fibers, while a^* stayed very near the neutral axis, indicating that the color change was very much a "yellowing" phenomenon. The changes in L^* and a^* were both smaller than the changes in b^* shown in Figure 6.

The effects of the fiber coating discoloration on aged three-layer samples of the color-coded fibers are shown in Figure 7. The orange solvent ink is much less effective than the rose uv ink in masking the color changes in the coating. This is again attributable to differences in thickness and uniformity between these two types of ink layers. The decrease in b^* shows that "yellowing" is a poor description for the color changes in the coating; "browning" is a better description for the discoloration defined by the lower L^* and moderate b^* values. It is this brown that, added to the orange ink color, gives the measured decrease in b^* . However, the thick rose ink prevents this brown from showing through. The 85 °C DI water aging environment again caused the greatest color change, and the effects of 85 °C aging in general were more pronounced than those at 65 °C.

DISCUSSION

Table 1 shows that the color of each ink varies depending on the fiber to which it is applied. The variations are small, however, as are the differences between the color of each ink film and the respective fibers. However, it is important to ensure that such measurements use a sample sufficiently thick to mask the background effects. Figure 8 shows the differences between the measured L^* value of single-layer film and fiber samples of the Aqua uv ink against both the white and black backgrounds. The differences between the two backgrounds are again evident; however, it is also evident that the differences between the film and some fibers are noticeably greater as well. The closeness of the multi-layer film and fiber results indicates that such film samples can be used in an incoming quality control inspection process with good predictability for the final inked fiber color.

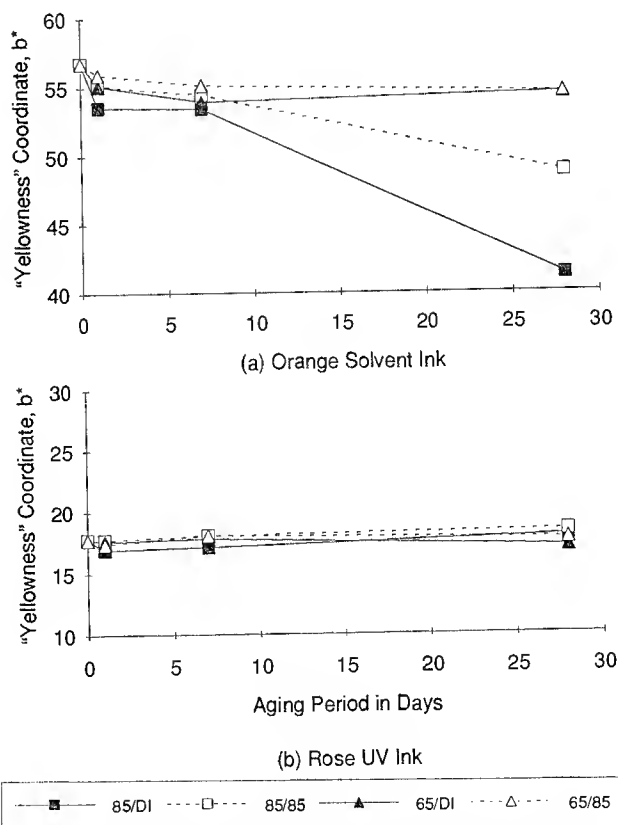


Figure 7. Effects of Aging on the Yellowness Coordinate of Three Layers of Inked Fiber on the White Background

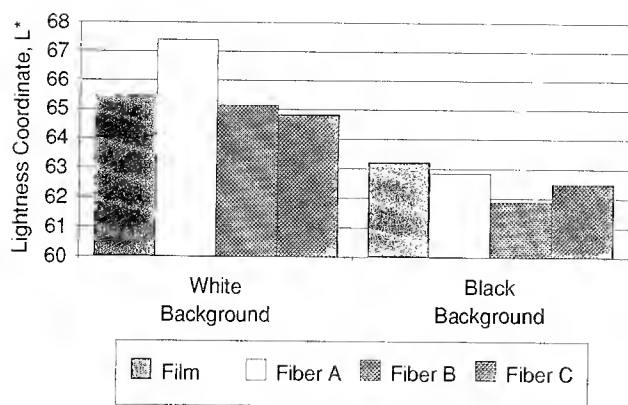


Figure 8. Lightness of Single-Layer Aqua UV Ink Film and Fiber Samples on White and Black Backgrounds

One issue that affects the use of ink films is the difficulty in obtaining uniform layering. Entrapped air bubbles seem to be unavoidable between film layers, causing different areas of the top layer of film to appear lighter or darker depending on the contact between the layers below; areas of poor contact should be avoided in measurements. The problem can be minimized by drawing thick films so that only two or three are needed to mask the background; these thicker films are also easier to handle, which minimizes the number of air bubbles. However, care must be taken to ensure proper cure throughout such thick films.

The multiple layers in fiber samples must stack so that any gaps between the fibers in one layer are covered by fibers in another layer to prevent the background from showing through. As the fiber ages, it develops a "set," even in the loose coils we used in our water tanks and humidity chambers. Short fiber pieces, which we used because of limited sample length, are difficult to stack uniformly, although our U-shaped holder minimizes the problem. Longer fiber samples can be wound onto a measuring spool as we described earlier, but the fiber stiffness (and, for extreme aging, brittleness) again causes handling problems.

Fiber samples appear to be preferable to film samples in that three to four layers of most fibers seem to mask the white/black background differential at least as effectively as 75–80 μm thick film layers. Several factors contribute to this: (i) each fiber adds the effective thickness of two ink layers, top and bottom, between the meter and the background; (ii) the fiber coating absorbs some light (especially when aged); and (iii) the interfaces (glass/inner primary/outer primary/ink/air) in the stacked fiber sample cause light reflection and refraction. These effects combine to increase the front surface reflection of the fiber sample and to minimize the amount of light that arrives at and is reflected from the background. Smaller changes occur in the measured color when multiple sample layers are added over the black background; the lower back reflection from this background means that there is less signal to be affected by the accumulation of sample layers.

As shown in Figure 5, the orange solvent ink was less effective than the rose uv ink in masking the background. One reason for this is the incomplete inking that was apparent on all three fibers. This is illustrated in Figure 9; the mottled light and dark pattern represents thin and thick spots in the ink, respectively. The unevenness is probably a result of the ink "puddling" on the surface owing to its inability to thoroughly wet the underlying

Figure 9. Uneven Coloring of Fiber by Orange Solvent Ink

coating. The difficulties we experienced in obtaining uniform pigment dispersion in film samples suggest that this could also contribute to these nonuniformities on the fibers. In addition, the orange ink showed a tendency to flake and peel off the aged fibers; this was slightly more noticeable for fiber A, and for fibers aged in DI water. Finally, this ink does not cover the circumference of the fiber completely; the application process apparently left a band along each fiber that was not adequately inked. If every length of fiber in the color sample could be positioned to orient the denser parts of the ink layer toward the meter, effective background masking might be possible with three fiber layers. However, the fact that the meter aperture averages the color for fibers with varied orientations does result in a more accurate representation of the perceived fiber color.

The larger changes in b^* for the orange ink (versus the rose ink) in Figure 7 are again evidence of these nonuniformities in the ink layer. These color changes measured for fiber C are effects of the coating discoloration showing through. Fibers A and B with the orange ink experienced smaller color changes, consistent with their smaller color changes in the natural state. In addition, the differences between the magnitudes of the color changes in the different aging environments are consistent between the orange-inked fibers and the natural fibers. These color changes reinforce the understanding that the most severe aging environments for fiber coatings (and inks, as is clear from the present work) are (i) high temperatures (85 $^{\circ}\text{C}$ is an adverse environment whether it is liquid, humid, or dry⁽²⁾) and (ii) liquid water (which is more degrading than high humidity).

SUMMARY

The identification of fibers by color necessitates that the colors be stable over time; this depends on the composite behavior of the fiber coating and ink in the service environment. Different fibers colored with the same ink exhibit different degrees of color change, depending on both the extent of the color change in the coating and the extent to which this discoloration shows through the ink layer. Different environments cause different extents of color change, with the aging temperature showing a greater effect than the difference between liquid water and high humidity environments. The inherent opacity of the ink layer, puddling of the ink due to its poor wetting of the coating surface, and nonuniform application of the ink during manufacturing all exacerbate the 'show-through' of the coating discoloration.

The development of a standardized test procedure enabled us to measure color changes accurately and reproducibly using a colorimeter. The technique described in this paper can serve as the model for an industry standard test method. Control of numerous parameters was found to be essential for reproducible measurements: the sample (fiber or film, number of layers, film or coating/ink layer thickness); the background (white or black of known color and reflectance); the presentation of the sample to the colorimeter (orientation, film smoothness); the meter characteristics (illumination/viewing geometry, light source); and the color reference(s) used for calibration.

ACKNOWLEDGMENTS

We gratefully acknowledge the efforts of Ed Beebe in making most of the color measurements reported here. The permission of the Director of Research, Telstra Corporation Limited, to publish and present this paper is also acknowledged.

REFERENCES

1. J.R. Petisce, M.D. Kinard, S. Siddiqui, and C. Taylor, "Effect of Environmental Aging on Optical Fiber Color Codings," *Proc. 42nd IWCS*, p. 552.
2. R.A. Frantz and I.M. Plitz, "The Effects of Aging on the Discernibility of the Color Identification of Optical Fibers," *Proc. 42nd IWCS*, p. 850.
3. *Munsell Book of Color*, Macbeth Division of Kollmorgen Instruments Corporation, Newburgh, NY.
4. ANSI/EIA/TIA-359-A, "EIA Standard Colors for Color Identification and Coding," Electronic Industries Association, Washington, DC 20006.
5. ANSI/EIA/TIA-598, "Color Coding of Fiber Optic Cables," Telecommunications Industry Association, Washington, DC 20006-1813.
6. Printing Ink Drawdown Sheet, Form 3NT-3, The Leneta Co., Mahwah, NJ.



Barry J. Keon is a Senior Materials Engineer in the Telecommunications Science and Technology Branch of the Telstra Research Laboratories in Melbourne, Australia. He holds a B.Sc. degree from Monash University, a post-graduate Diploma of Polymer Chemistry from Chisholm Institute of Technology, and a M.Eng.Sci. from Monash University. He has worked in the telecommunications industry since 1991, with responsibilities in the area of fiber reliability and cable materials performance. He is currently a Visiting Researcher in the Fiber Media and Component Reliability Group at Bellcore, working on reliability issues affecting optical fibers and cables.



Rolf A. Frantz is a Distinguished Member of Technical Staff in the Fiber Media and Component Reliability Group at Bellcore's Morristown, NJ facility. He earned his Bachelor's and Master's degrees in engineering from Cornell University and his Ph.D. in Engineering Mechanics from Brown University. For over a decade prior to the AT&T divestiture in 1983, he worked at Bell Laboratories, focusing on reliability issues related to electrically insulating materials. He continued to work in that area when he joined Bellcore at its founding in 1984. Since 1988, he has worked on optical fiber and component reliability, including coatings, inks, and materials compatibility issues.

FIBER CURL: A NEW MEASUREMENT METHOD AND A STATISTICAL PREDICTION OF THE INFLUENCE ON FIBER RIBBON SPLICE LOSSES

Mauro Bottanelli

SIRTI S. p. A., Cables and Optical Technologies - R&D Division
Via Manzoni 44, 20095 Cusano Milanino (MI), ITALY

Abstract

The aim of the work described in this paper was to analyze the impact of curl on multiple fusion splicing technique and to find a simple way for predicting ribbon splice losses with respect to the curl characteristic of the ribbon constituting fibers. In order to achieve this goal, a new optical method has been developed for measuring fiber curl, using a He-Ne laser gauge, scanning the whole length of the fiber under test instead of the sample end only. Moreover, by means of a statistical study of the influence of curl on fiber ribbon splice losses, a prediction formula for 4-fibre ribbon splice losses with respect to a given curl mean value has been found.

1. Introduction

The requirement of fast, high performance tools for durable, low-loss fiber optic multiple interconnections gave rise to the development of the modern multiple-fiber fusion splicers. The splice quality strictly depends on the fiber end face mechanical alignment, but in a multiple arc fusion splicer only an average alignment can be obtained. This is the reason of the recent interest [1, 2, 3, 4] about the so-called "fiber curl", i.e. the fiber natural tendency to take a particular curvature radius after the primary coating removal. In the case of a fiber wide and random-oriented deviation from the straight direction due to the curl (figure 1), problems may occur during splicing, from a strong increase of splices insertion losses up to the impossibility of correctly performing the splicing operation itself.

This paper describes a new method for curl measurement, and a statistical study of the acceptable curl level for low loss ribbon splices. The new measurement method is based on a helium-neon laser

scanning system considering the whole length of the fiber under test instead of the sample end only. The reproducibility is $\pm 0.1 \mu\text{m}$ with respect to the fiber deflection at 3 mm. The statistical study consists in a Montecarlo simulation of the curl deflection distribution and of the possible deflection combinations for three different fiber populations: by means of experimental data, theoretical and heuristic considerations, a prediction formula for 4-fibre ribbon splice losses with respect to curl deflections has been found.

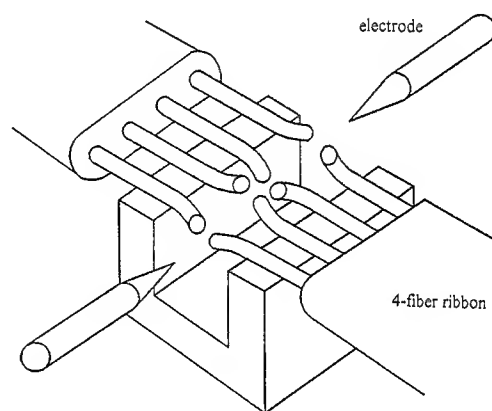


Fig. 1 - Curl effect on multiple fusion splicers

2. The origin of curl

During fiber drawing, the glass constituting the fiber is subject to a sudden temperature change. From the furnace to the take-up drum, the temperature of a fiber goes down from 1500 to 20 °C. But this is not the only force acting on the fiber. Immediately out of the furnace, in the case of a non uniform temperature distribution along the fiber cross-section, a stress is generated into the fiber glass, that, after the drawing process, gives rise to the curl. Let now R be the curl curvature radius, $T_1 - T_2$ the temperature difference

between two points in diametral opposition along the fiber cross-section, and α the silica thermal expansion coefficient. Let us consider the situation of figure 2, with a glass parallelepiped of limited length circumscribing the fibre, having two opposite faces at $T_1 > T_2$ steady heat condition and no temperature variation in z -direction. By applying the equations of equilibrium, the boundary condition and the compatibility conditions to the parallelepiped, after simple considerations [5] we obtain:

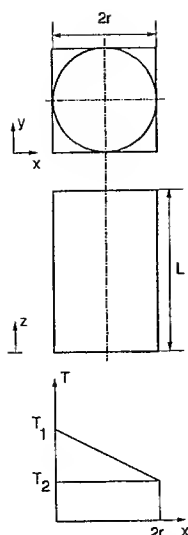


Fig. 2 - Boundary conditions for studying the origin of curl

$$(1) \quad R = 2r / [\alpha(T_1 - T_2)]$$

So, for instance, with the following assumptions:
 $r = 62.5 \mu\text{m}$, $T_1 - T_2 = 100 \text{ }^\circ\text{C}$, $\alpha = 5 \cdot 10^{-7} \text{ }^\circ\text{C}^{-1}$, we get a $R = 2500 \text{ mm}$ curl curvature radius.

3. A new curl measurement method

Traditional methods for measuring curl [1, 2, 3] refers to the geometrical situation of figure 3.

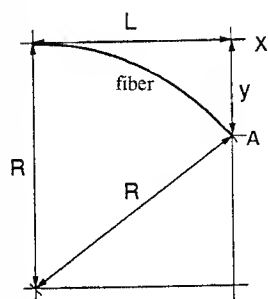


Fig. 3 - Geometry of curl

The relationship among the fiber length L , the deviation y and the curl curvature radius R is:

$$(2) \quad R = (L^2 + y^2) / (2y)$$

According to this formula, traditional methods make use of the rotation of the fiber around the x axis, measuring the displacement

of the point A through a camera placed in front of or sideways the fiber end face and evaluating the y deviation. Although this technique is referred as being fast, simple and "well working", nevertheless it can't be considered precise in the full sense of the word, at

least because of the following reasons: only one physical point of the fiber is considered and the other fiber end is inserted into a guiding element (usually a ferrule) directly influencing the measurement. We can summarize the previous considerations by saying that traditional methods don't perform a direct measurement of curl curvature radius. Let us consider now our new curl measurement method (figure 4). The fiber under test is inserted in the tight

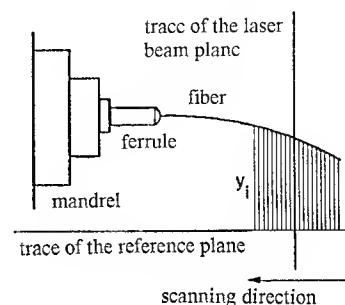


Fig. 4 - New curl measurement method

hole of a ferrule, leaning out of the free edge of the ferrule for about 40 mm. The ferrule itself is held by a precision mandrel and a He-Ne laser scanning gauge can transversally analyse the fiber by means of a linear and a rotative micropositioning motor. Only the first 20 mm of the fiber free edge are considered. The laser gauge can measure the local deviation y_i of the fiber with respect to a reference plane, the scanning step being adjustable according to the precision requirements. Finally, the curl curvature radius R is found as the radius of the circumference best fitting the experimental data by the least square method. Apart from other considerations, the portion of the fiber under test is completely free from any kind of constraint, with the exception of the action of the fiber weight. The deviation due to this action can be however calculated by means of a classic cantilever model, according to the formula:

$$(3) \quad y(x) = pL^4 \cdot [3 - x(4 - x^3)] / (24EI)$$

where $x \cdot L$ ($0 \leq x \leq 1$) is the horizontal co-ordinate ranging from the fiber free edge to the fixed one, L being the whole fiber length. With typical value, we get about $6.4 \mu\text{m}$ of deviation for the 20 mm length of the fiber under test, that is about $0.14 \mu\text{m}$ of deviation for the typical length (3 mm) of fiber leaning out of the fusion splicing machine holders.

This further deviation must obviously be subtracted from the measured one in order to obtain the correct curl value. Another problem concerns the orientation of the fiber under test with respect to the laser gauge beam: if the plane where the fiber lies is not perpendicular to the reference plane, the laser beam "sees" a lower curl curvature than the real one. So the fiber must be previously oriented; moreover (figure 5)

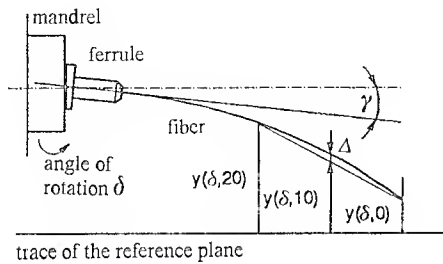


Fig. 5 - Compensation of orientation and mechanical errors

the orientation procedure have to neutralize the alignment errors due to the mechanical insertion of the ferrule into the mandrel (angle γ). The right orientation can be obtained by maximizing the quantity:

$$(4) \quad \Delta = y(\delta, 10 \text{ mm}) - [y(\delta, 0 \text{ mm}) + y(\delta, 20 \text{ mm})]/2$$

with respect to the angle of rotation δ . With a $\pm 10^\circ$ orientation step and a $0.250 \mu\text{m}$ scanning step, a $\pm 0.10 \mu\text{m}$ reproducibility for 3 mm curl deviation measurement has been obtained.

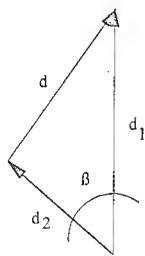
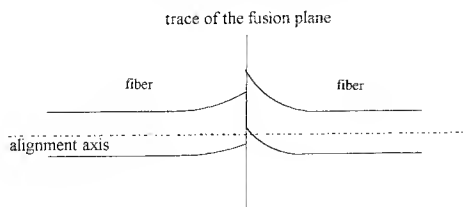


Fig. 6 - Curl deviations composition between fiber core centers in the fusion plane



4. Maximum curl allowable level with respect to a given splice loss value

The prediction of splice loss between two fibers in a joint can be obtained considering the situation of figure 6. Let the two vectors (having the same origin and plane) be the 3 mm curl deviations of the two fiber ends in the interconnection, d_1 and d_2 being their moduli. The offset between the fiber cores is then:

$$(5) \quad d = \sqrt{d_1^2 + d_2^2 - 2d_1d_2\cos\beta}$$

where β , d_1 e d_2 are random variables. In particular, β is uniformly distributed between 0° and 360° , while nothing can be a priori said about d_1 and d_2 . Figure 7 reports the experimental distributions of 3 mm curl deviations for three different SMR optical fiber populations.

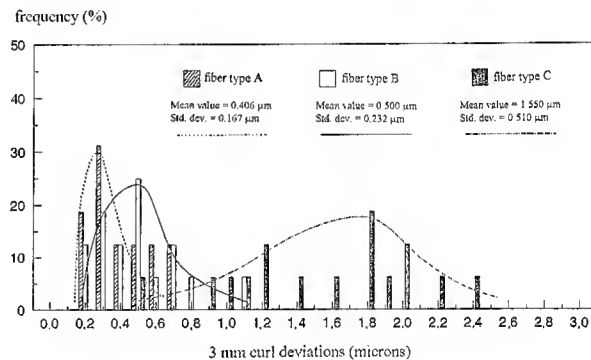


Fig. 7 - Experimental distributions of 3 mm curl deviations for three different fiber type populations

These three distributions can be represented through Rayleigh distributions, i.e. through the following probability density function:

$$(6) \quad f(x) = (x/\varepsilon^2) \cdot \exp(-x^2/2\varepsilon^2),$$

$$\text{mean value: } \varepsilon \cdot \sqrt{\pi/2}, \text{ variance: } \varepsilon^2 \cdot (2 - (\pi/2))$$

where ε can be chosen in order to have the best approximation of the real situation. Under these assumptions, the easiest way to calculate the distribution of d according to the (5) is a Montecarlo simulation. This can be done [6] by means of the formula:

$$(7) \quad x = \sqrt{-2\varepsilon^2 \ln(1 - k)}$$

giving a Rayleigh distribution of x , with the desired ε value, provided that k is a uniformly distributed random variable between 0 and 1. Following these considerations, we can calculate the distributions of the offsets d for the six possible combinations among the three different fiber populations (A-A, A-B, A-C, B-B, B-C, C-C). The problem is then to find a relationship between the calculated offset distributions and the splice loss distributions experimentally obtained by splicing the three different type of fiber ribbons. This formula must be based on the well-known formula for mechanical splice loss evaluation in the case of transverse offset between the fiber cores [7]:

$$(8) \quad \Gamma = 4.34 \cdot (d/W)^2 \text{ dB}$$

where W is the mode field radius (MFR) of the fibers. However, in the case of a fusion splice, a lower loss dependence from the transverse offset before fusion due to a little fiber MFR deformation and a natural tendency of the two fiber ends to approach one to the other during the fusion can be supposed. Following these considerations, we found the empirical formula:

$$(9) \quad \Gamma = 4.34 \cdot (d/W)^{1.9} \cdot \exp(-d^{0.55}) + 0.02 \text{ dB}$$

giving us the best correspondence between our theoretical calculations and experimental data (for the sake of brevity, we don't report the detailed calculated and experimental distributions in this paper).

Now, following the previous considerations, we want to focus our attention on the curl characteristic that a particular fiber population must have in order to ensure a given splice loss value. Under the assumption of a Rayleigh 3 mm curl deviation distribution, let us calculate, for instance, the ε value ensuring less than 0.07 dB splice loss in the 70 % of the cases and less than 0.13 dB splice loss in the 90 % of the cases (Italian PTT requirements). For a single curl deviation population we have:

$$(10) \quad d = d_1 \sqrt{2}$$

that is the core-to-core offset d is Rayleigh distributed too, but with a mean value (and ε parameter) multiplied by a factor $\sqrt{2}$. Then:

$$(11) \quad p(x \leq d) = 1 - \exp(-d^2/4\varepsilon^2) \leq P$$

is the probability of having an offset value lower or equal than d . By solving with respect to ε we obtain:

$$(12) \quad \varepsilon \leq (d/2) \cdot \sqrt{-1/\ln(1-P)}$$

Now, from the (9), a 0.07 dB splice loss corresponds to a 0.78 μm offset d , and a 0.13 dB splice loss corresponds to a 1.42 μm offset d . By substituting these values and their respective P values (70 % and 90 %) into the (12) we get:

$$(13) \quad \varepsilon \leq 0.355 \mu\text{m}, \quad \varepsilon \leq 0.468 \mu\text{m}$$

the first condition being the most restrictive. Consequently the fiber population must have (from equation (6)) a curl deviation mean value of 0.445 μm at 3 mm from the fiber end, i.e. about a 10 meters curl curvature radius.

5. Conclusions

In this paper we have reported the results of a study on fiber curl, from its origin to a new measurement method and a technique to calculate the maximum allowable curl level with respect to a given multiple splice loss. For example, more than 10 meters mean curl curvature radius are needed in order to have multiple splice loss below 0.07 dB for the 70 % of the splices.

References

- [1] A. L. Ingles
*AN AUTOMATED METHOD FOR MEASURING
THE RADIUS OF CURVATURE OF AN OPTICAL
FIBER*

Symposium on Optical Fiber Measurements - Boulder
(USA), September 1992 - NIST Special Publication
839, pp. 127 ÷ 130

- [2] K. Jonsson, A. Bjork
*COMPARATIVE MEASUREMENTS OF CURL AND
SPlice LOSS FOR AN OPTICAL 4-FIBRE RIBBON*
2nd Optical Fibre Measurement Conference - Turin,
September 1992 - Technical digest, pp. 73 ÷ 75

- [3] K. A. Eming
*A COMPARISON OF MANUAL AND AUTOMATED
FIBER CURL MEASUREMENTS SYSTEMS*
2nd Optical Fibre Measurement Conference - Turin,
September 1992 - Technical digest, pp. 85 ÷ 88

- [4] J. Schiestle, M. Stammer
*THE IMPACT OF FIBER CURL ON FIELD
SPlicing TECHNOLOGIES*
9th Annual National Fiber Optic Engineers Conference
San Antonio (USA), June 1993 - Book 4, pp. 89 ÷ 104

- [5] S.P. Timoshenko
THEORY OF ELASTICITY
McGraw-Hill 1982

- [6] A. Bjorck, G. Dahlquist
NUMERICAL METHODS
Prentice-Hall, New Jersey, 1974, p. 452

- [7] C.M. Miller
OPTICAL FIBER SPLICES AND CONNECTORS
Marcel Dekker 1986



Mauro Bottanelli

Cables and Optical
Technologies - R&D Division
SIRTI S.p.A.
Via Manzoni 44 - 20095
Cusano Milanino (MI) -
ITALY

Mauro Bottanelli was born in 1963. He received the Dr. Ing. degree in Nuclear Engineering from Politecnico of Milan. After a two years activity in the field of industrial automation, he joined SIRTI in 1990 as research engineer in the field of optical fiber cables and optical components measurement techniques. He is a member of the ITU-T 4/15 National Working Group on fibers, cables and optical components.

A COST-EFFECTIVE TECHNIQUE FOR THE GLANDING OF OPTICAL FIBRE BUNDLES INTO SUBMERGED REPEATERS

S. J. McManus, I. G. Watson, G. Waterworth.

STC Submarine Systems Limited. (A company of Alcatel Submarine Systems) London, England.

ABSTRACT

The advent of high bit-rate optoelectronics and, more recently optical amplifiers, has resulted in the domination of international communications by submarine fibre optic cables. At intervals these cables need to be glanded into a high pressure housing containing optical regenerators or amplifiers.

Hydrostatic pressure resistance is an obvious requirement for any such glanding system, but the less known and more stringent requirement is the prevention of hydrogen gas penetration into the repeater housing, (typically $<10^{-7}$ cms³ sec⁻¹ over the 25 year working lifetime.)

A new gland has been designed in which gas blocking of the critical fibre path is achieved using a low- permeability, high- viscosity liquid that is maintained in intimate contact with the fibres and gland internals, and is retained by a separate pressure resisting resin block.

The resultant gland has exceeded the requirements in gas, hydrostatic, electrical and optical performance. This new technology has been successfully implemented in CANTAT 3.

INTRODUCTION

Long and medium-haul underwater telecommunications cables require repeaters at intervals to regenerate or amplify the optical signals. These cables may need to operate in sea pressures of up to 12000 psi (83MPa) and in environments where as much as 10 atmospheres (1MPa) of hydrogen can be generated. Methods, therefore need to be devised to seal the repeaters, and in particular the cable entry glands, from these severe hydrostatic and gas pressures. After ten years working on such glanding systems a radical, effective and simple gland has been designed and implemented.

REQUIREMENTS OF SUBMARINE REPEATER CABLE GLANDING.

An optical repeater cable gland has to perform the following basic functions:

- Resist water penetration.
- Resist gas penetration .
- Provide a benign gas free passage into the repeater for the optical fibres.
- Carry an insulated power feed conductor into the repeater.
- Interface with the cable and repeater internals

Full details of these requirements are contained in Table 1.

In addition, it is desirable in the glanding design to minimise dimensions without compromising performance (most importantly reliability) and finally to keep production costs to a minimum.

MAIN DESIGN ROUTES FOR REPEATER GLANDING.

As repeater glanding is required to perform multiple functions, many designs have considered it necessary to separate these functions as much as possible. Traditional glanding methods were generally two stage: at the entry to the bulkhead a moulded polyethylene gland prevented water ingress, and beyond this up to nine separate hermetic glands were used to prevent gas entry to the repeater. The benefit of this technique is that a number of relatively low cost, individually testable, items are assembled to produce the overall glanding system. The arrangement performs well, but inevitably has the major disadvantage of requiring considerable additional space which is at a premium in undersea repeaters.

Alternatively, other designers have produced multi-function single glands, some of which have attempted to match the performance of multiple systems described above. These glands which require much less space, have tended to be of complex and expensive design although often of inferior performance to the multiple systems. However, as only one gland is used per bulkhead, the bulkhead can be simpler and therefore less expensive.

SPECIFIC DESIGN OBJECTIVES.

The challenge addressed in the gland described in this paper was to produce a composite single unit multi-function gland of simple low-cost design and of superior performance. As well as meeting the basic environmental requirements of the sub-sea repeater gland (contained in Table 1), the following additional objectives were targeted in the design:

- To design a glanding able to accommodate initially 12 and later up to 24 optical fibres and the power feed conductor in a single central repeater bulkhead penetrator.
- To increase the reliability of fibre glanding by the elimination of high risk solid interface technology.

The first requirement covered the maximum number of fibres in a cable at the time with a minimum of four spare , but looked towards future trends to increased cable fibre counts, some of which are now undergoing test.

The second requirement came about because to achieve hermeticity the nine glands (1 power feed gland and up to 8 metallised fibre glands per bulkhead) relied on the solid interface technology for the gas blocking function. In the case of the fibre glands this required the removal of the protective coatings to expose the fibre prior to metallisation and soldering. As a result of all the processes, considerable effort is required during manufacture to avoid fibre damage. This substantially increases manufacturing costs. The solid interface requires solutions to two major manufacturing problems:

- a) Due to differing thermal properties, temperature changes result in high mechanical stresses
- b) Handling of the fibre causes considerable difficulties due to the need for protective fibre coatings to be removed. In some instances this can lead to rework and extra manufacturing expense.

The gland described in this paper is a single unit that performs both water and gas blocking functions. In addition the design does not require fibre stripping and does not use a solid interface for the gas block.

GLAND DESIGN.

General

A detailed drawing of the gland is shown in Figure 1. A description of its design and components follows.

Gas Blocked Fibre Feed-Through.

The principal of the gland gas block is shown in Figure 2. In this design the gas blocking and pressure resisting functions of the fibre feed are separated.

For the gas blocking function, a low permeability, high viscosity liquid is used. The liquid is maintained in intimate contact with the coated fibres and internal surfaces of the gland body over a large effective length, irrespective of changes of temperature or pressure.

The gas blocking material is the highest viscosity variant of a range of polybutenes. Polybutenes have the following advantages:

- a) High viscosities are available up to 40×10^6 cPs at 20°C and these have the advantage of low creep at repeater service temperatures and hence are easily retained within the gland.
- b) They have a known low hydrogen permeability of $4 \times 10^{-8} \text{ cm}^3 \text{ cm}^{-2} \text{ sec}^{-1} \text{ atm}^{-1}$.
- c) They were already qualified and in use with the cabled fibre, hence they are easily obtainable from the cable factory.

The separate pressure resisting function is now a less critical item, as it is only required to seal against a high viscosity fluid rather than the small hydrogen gas molecule.

The pressure resisting resin block is sited at the low pressure end of the fibre feed-through tube and is required to maintain the polybutene within the tube.

During normal operation only very low pressures will be applied to the block and polybutene column. Calculations indicate a maximum of 10 atmospheres (1 MPa) of hydrogen gas pressure during system life. However, if the cable is severed or damaged close to a repeater then the cable core and termination may flood and apply sea pressure to the end of the gland fibre/tail tube within the termination. Under these conditions it is essential that the sea water should not be able to pass through the gland fibre tube into the repeater. The hydrostatic pressure is transmitted by the polybutene to the pressure resisting block and the block must resist this pressure until the repeater is lifted for system repair.

The pressure resisting block uses two resin materials to create a sealed plug round the fibres in the resin block body. See Figure 3.

A strong low expansion resin system with good adhesion properties is used as the load bearing section of the block. This rests on a step in the body forming a plug which also adheres well to the fibre coatings to prevent fibre extrusion.

For increased reliability and to give a positive seal, a secondary softer rubber resin system is injected into the high pressure end of the block body. The thin layer of rubber resin performs a function similar to an 'O' ring sealing round the fibres and to the body wall.

Conductor/Fibre Tube

The tube containing the fibres and gas block performs the additional function of power conductor which not only passes through the gland, but is extended to form a flexible tail tube between the repeater and the cable termination. The tube must, therefore, externally resist the full system hydrostatic pressure.

Polybutene Filling Adapter

The polybutene filling adapter is mounted on the low pressure end of the fibre tube using a hydraulic coupling. It performs the following functions:

- a) Housing for resin block and resin block body.
- b) Connection between the resin block body and the fibre / tail tube.
- c) Means of injecting polybutene into the fibre tube through a sealable port.

Internal Power Connection

The internal power connection provides a positive soldered joint between the fibre/power feed tube and the internal repeater power connection. It is soldered to the tube with a high melting point solder so that subsequent polyethylene moulding and soldering operations do not affect the joint.

High Voltage Insulation

The insulating function between the power conducting fibre tube and the earthed bulkhead / sea water combination is performed by the ceramic insulator and polyethylene mouldings. The polyethylene is in the form of an extruded tail tube sheath and an injection moulding in the gland body.

Hermeticity

The ceramic body not only insulates the power feed from the bulkhead it also forms part of the hermetic seal between the fibre tube and the bulkhead in addition to transferring hydrostatic load between the two.

Hermeticity is maintained by brazed metallised joints between the ceramic and nickel iron alloy components and soldered joints between the nickel iron alloy components and the fibre tube.

Gland Housing

A steel housing provides a water proof case over the interface between the ceramic and polyethylene as well as providing the primary water resistant termination of the tail tube polyethylene onto the gland. The rubber 'O' rings that provide the water seal to the bulkhead are also located in the gland housing.

Lead Seal

A lead seal is used to provide the final hermetic seal to the bulkhead, being mounted between this and the nickel iron flange brazed to the ceramic body. In order to provide a seal at the molecular level, stress raisers in the form of knife edges are machined on both sealing surfaces. These are forced into either side of the lead creating a friction seal.

Hydrostatic Load Path

The primary hydrostatic load on the gland is developed across the main 'O' seals. This load is transmitted via the outer bulk of the nickel iron flange to the lead seal and hence to the bulkhead. A secondary load path exists from the tail tube and polyethylene cross section and this load is partly transferred via the nickel iron end cap on the ceramic body through the ceramic body to the nickel iron flange and hence to the bulkhead. The other part load path is to the gland housing at the water seal and hence from here to the primary load path.

GLAND TEST PROGRAMME

The first system using the new gland design (CANTAT 3) has recently completed deployment and will begin service shortly. Before this stage was reached much individual component and complete gland testing was undertaken followed by a formal qualification programme.

Component Test Programme

The component test programme can conveniently be split into two forms of test:

Short term Test Programme This programme consisted of materials evaluation, component and electrical proof tests and in general was used to prove materials or bought in components fit for service. All materials or bought in components used in the gland were first subjected to an appropriate test programme.

Life Test Programme This programme was used to evaluate critical gland parts and sub-assemblies built in house. The critical parts and sub-assemblies tested and the test results are summarised in Table 2. It is of interest that most of these tests are continuing and no failures have been recorded on any test. All the assemblies and components used in the life tests are representative of the production product.

Complete Gland Test Programme

The gland test programme was divided into two phases dependant on where the glands were built:

Laboratory Built Glands As one would expect with any development programme a certain amount of evolution occurred during the laboratory build phase of the gland development. Build standards ranged from early prototype glands used for feasibility trials to final models as close to the proposed production build standard as is possible with laboratory facilities.

Testing was continuous during development culminating in a final laboratory batch of glands. Some of the earlier build and most of the final batch were subjected to a life test programme much of which is still ongoing. A summary of the life test programme and results are shown in Table: 3. As with the component life test programme no failures have occurred on any of the tests.

Factory Built Glands The aim of the factory build programme was firstly to prove manufacturability and then proceed to the qualification of the gland. The first factory build trials were made using as much of the production equipment, piece parts and processes as possible. The trials were also used to test and debug manufacturing equipment and to train operators.

Following these trials a production batch of glands together with some major separately testable sub-assemblies were produced to qualify the product. The build was entirely to production specifications, standards, and used 100% production personnel and equipment. Testing of the qualification glands was the most rigorous in the gland programme as it had to stand as proof to any potential customer that the whole gland concept was fit for the required 25 years service.

The programme had to fulfil the following requirements:

- a) To ensure that during all possible operating conditions the integrity of the power feed and optical path was maintained.
- b) To ensure that gas permeation was within design limits and that there was no water ingress.
- c) To ensure that the gland performed as designed under emergency conditions (eg cable or tail tube break).

The behaviour of the gland during the qualification programme under the various test conditions is summarised in Table 4 and showed excellent performance.

CONCLUSIONS

With the completion of the lay of the CANTAT 3 system the gland is about to go into full service. No problems have been encountered during the lay operation most of which is undertaken with the cable system powered.

The test record during development from the laboratory trials through to the qualification has been exemplary with no failures recorded in any test. The achieved gas leakage through the gland is four orders of magnitude better than required to maintain an acceptably low hydrogen concentration within the repeater, over the service life.

Production costs for repeater glanding has shown a marked cost-saving over previous gland designs both from actual manufacturing and component costs to the much improved yield.

ACKNOWLEDGEMENTS

The authors wish to thank the management of STC Submarine Systems for their support and permission to publish this paper.

REFERENCES

1. STC Patent : -90 301 449.6-2205.

1.0 General Requirements

- 1.1. Operational Life:- 25 years without repair or maintenance.
- 1.2. Storage Temperature Range:- -20°C to +40°C.
- 1.3. Operational Temperature Range:- 0°C to 30°C.
- 1.4. Hermeticity - Gland to Bulkhead - $< 1 \times 10^{-8} \text{ cms}^3 \text{ sec}^{-1}$ at 1MPa Hydrogen.
- 1.5. Hermeticity - Through Gland:- $< 0.8 \times 10^{-6} \text{ cms}^3 \text{ sec}^{-1}$ at 1MPa Hydrogen.
- 1.6. Hydraulic Operational:- 83MPa.
- 1.7. Hydraulic Cable Failure:- 83 MPa for 500 hours without visible signs of water ingress through gland.
- 1.8. Optical Loss:- $< 0.1 \text{ dB}$ at 1295 to 1570 nm. per fibre.

2.0 Operational Requirements : Electrical

- 2.1. Normal Operating Voltage:- 12kV DC.
- 2.2. Over Voltage:- 36kV DC.
- 2.3. Working Current:- 1.6 Amps maximum.
- 2.4. Leakage Current:- $< 10 \text{ nA}$ at 12kV DC.

3.0 Operational Requirements : Mechanical

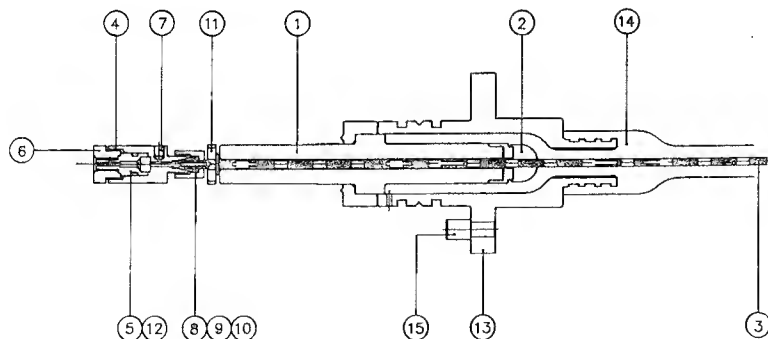
- 3.1. Tail Tube Bend:- 82° max.
- 3.2. Tail Tube Twist:- $\pm 60^\circ$.
- 3.3. Extension / Compression:- $\pm 115 \text{ mm}$.

TABLE 1 Requirements For Submarine Cable Gland

Component Tested	Number	Test Description	Cumulative Test Time
RESIN BLOCK	30	3000 Hours at 83MPa	96000 Hours (11 Years)
		Life Test at 100MPa	875000 Hours (100 Years)
RESIN BLOCK + HOUSING + FILLING PORT + HYDRAULIC FITTING + 660mm OF TUNGUM TUBE	18	Life Test at 83MPa	312000 Hours (35 Years)
AS ABOVE	5	Gas Test at 5MPa (Helium)	152000 Hours (17.4 Years) Leak Rate $< 1 \times 10^{-9} \text{ cms}^3 \text{ sec}^{-1}$
POLYETHYLENE SHEATH	10	12kV DC Ramp Life Test 100kV DC	100 x 1 hour Cycles 9 Days

Figures correct at: 9-3-94.

TABLE 2 Gland Test Programme - Component Life Test



ITEM	DESCRIPTION
1	GLAND SUB-ASSEMBLY
2	FLANGE
3	TAILTUBE
4	FILLING ADAPTOR
5	RESIN BLOCK BODY
6	RETAINING NUT
7	SEALING PLUG
8	UNION NUT
9	BACK FERRULE
10	FRONT FERRULE
11	HT CONNECTION
12	O' SEAL
13	GLAND HOUSING
14	P/E OVERMOULDING
15	LOCATING PIN

FIGURE 1. SECTION OF GLAND

Component Tested	Number	Test Description	Cumulative Test Time
COMPLETE GLANDS	4	Life test at 83MPa	111000 Hours (12.7 Years)
"	5	Life Test at 83MPa + 12kV DC	85000 Hours (9.7 Years)
"	3	Life Test at 83MPa + 36kV DC	58000 Hours (6.6 Years)
"	1	Life Test at 83MPa + Optical Monitor	11000 Hours (1.2 Years)

Figures correct at: 9-3-94.

TABLE 3 Gland Test Programme - Laboratory Built Glands

Group	Number	Test	Result
1	5 x Complete Glands	Bump & Vibration + Temperature Cycle + Optical Loss	Loss $< 0.074 \text{ dB}$ / Fibre
		Tail Tube Bend + Torsion + Extension + Compression + Optical Loss	Loss $< 0.01 \text{ dB}$ / Fibre
2	5 x Complete Glands	High Voltage Leakage 12kV " " 36kV " " Life Test 12kV	$< 1.8 \text{ nA}$ $< 14.7 \text{ nA}$ 2000 Hours No Failure
	3 x Complete Glands	Gas Life Test 5MPa Helium	$< 5 \times 10^{-10} \text{ cms}^3 \text{ sec}^{-1}$
	5 x Complete Glands	Optical Test at 83MPa	$< 0.01 \text{ dB}$ / Fibre
3	10 x Resin Blocks 5 x " "	Life Test 83MPa Fibre Twist & Pull	500 Hours No Failure $< 0.01 \text{ dB}$ / Fibre
4	25 x Lead Seals	Bump & Vibration + Temperature Cycle + a) Gas leakage life Test b) Hydraulic Test 83 MPa	$< 3.3 \times 10^{-10} \text{ cms}^3 \text{ sec}^{-1}$ 500 Hours No Leakage

TABLE 4 Gland Test Programme - Qualification Test Summary

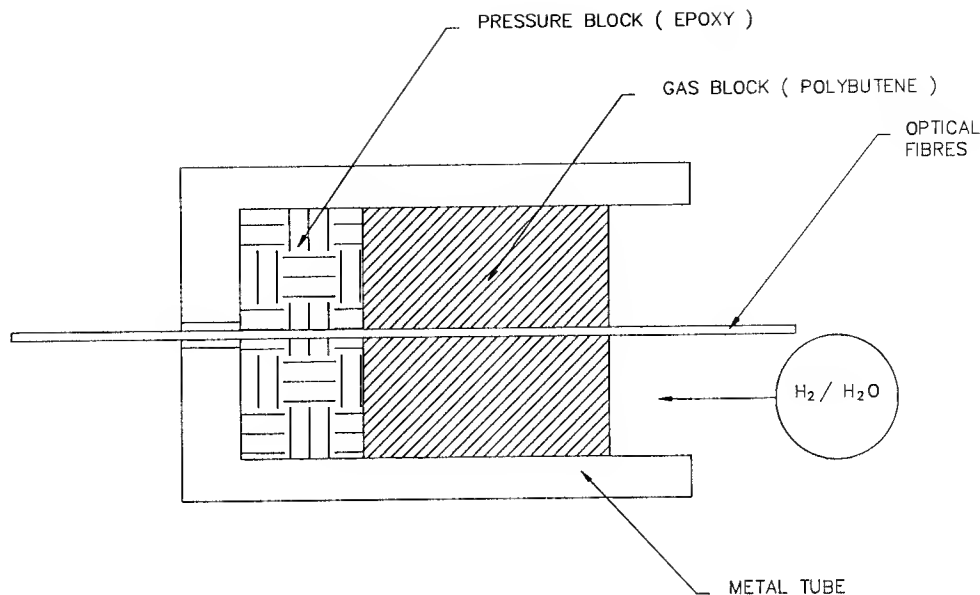


FIGURE2. PRINCIPAL OF THE GLAND GAS BLOCK

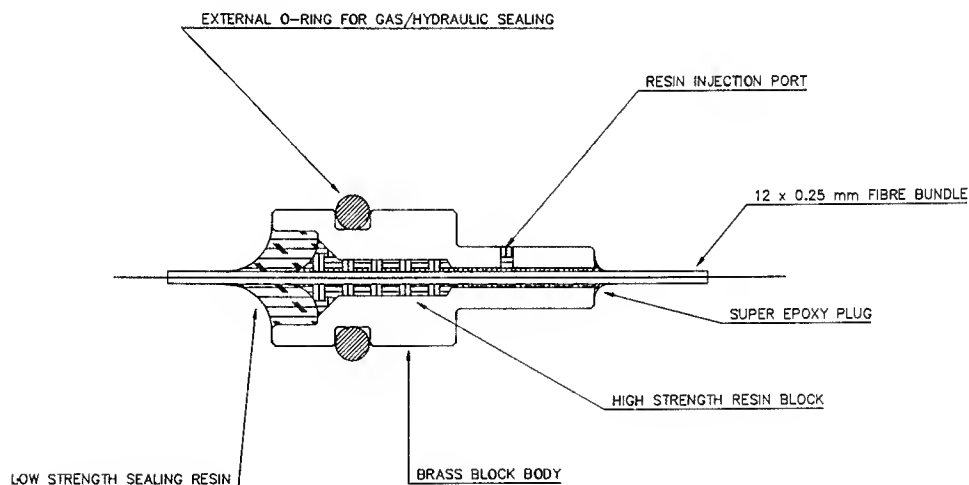


FIGURE3. PRESSURE RESISTING BLOCK

Stephen J. McManus was born in London, England. He joined STC Paignton in 1964 and received an HNC in Applied Physics and Electronics at the Northern Polytechnic, London in 1972. He has worked on a variety of projects including advanced capacitor materials, fluid bed deposition and electro-painting. He joined the Cable and Engineering group in 1983 working on the electrical, optical and mechanical aspects of submerged cable systems including cable glanding.

Gary Waterworth was born in London, England, he joined STC in 1979 as an apprentice. He was awarded a HNC in Mechanical Engineering in 1982 and a First Class Degree in Metallurgy and Materials in 1986. He has worked on a variety of projects including submarine cable jointing, installation, cable ships handling equipment and submerged plant design. As the Technical Manager for Mechanical Development Gary is also responsible for the introduction to manufacturing of all submerged equipment products at Greenwich.

Mr. Ian Watson, IEng, MIMechIE, was born in Sheffield, South Yorkshire, England. In 1984 he was awarded a HND in Mechanical Engineering at the Hatfield Polytechnic. In 1986 he joined the cable and mechanics department at STL, now BNR Europe, and now as part of the Design, Research and Development (DRD) Engineering Support Group has transferred to STC Submarine Systems in London.

As a Senior Mechanical Engineer Ian is currently working on many submerged plant mechanical development activities such as housing and glanding design and is currently involved in the design of fibre storage systems for underwater plant used by STC throughout the world.

PROPERTIES OF LOOSE TUBE OPTICAL CABLES CONTRIBUTING TO LOW-TEMPERATURE OPTICAL LOSS

M.J. Zammit, O.S. Gebizlioglu,* P.B. Grimado, G.D. Kiss

Bellcore

445 South Street, Morristown, New Jersey 07960

*331 Newman Springs Road, Red Bank, New Jersey 07701

ABSTRACT

Some loose tube fiber optic cables exhibited service-affecting transmission loss at low temperatures (-20 °C to -40 °C). These losses occurred predominantly at 1550 nm in aerial cables and were confined to the cable section adjacent to a splice closure. Optical loss measurements on commercial cables that were subjected to temperature cycling in an environmental chamber indicated that the thermal contraction of buffer tubes at low temperature was the major contributor to fiber bending-induced loss. Cables with an initially low ratio of fiber excess length-to-buffer tube inner diameter and strong buffer tube-to-central member coupling exhibited minimal loss. We demonstrated in the laboratory that cable termination hardware with proper mechanical sheath retention and central member clamps can be effectively utilized to prevent the low-temperature loss. However, we also found that five widely used commercial splice closures are ineffective in preventing loss-producing movement of cable components.

1. INTRODUCTION

Service affecting failures in loose tube fiber optic cables due to extreme low-temperature exposure have been well documented^(1,2). Failures have occurred primarily at 1550 nm in aerial single-mode fiber optic transmission lines. In some severe cases, however, losses have occurred at 1310 nm and in pedestal locations where long lengths of slack cable were available. In all cases, the optical losses were reversible in that they disappeared when the ambient temperature returned to moderate levels. However, the physical damage done to the cable as a result of thermal cycling was permanent. Cables exhibiting these losses would repeatedly fail whenever they were exposed to low temperature. Transmission lines exhibiting low-temperature loss could be remedied only by removing the affected length of cable and re-terminating the cable end.

The extent to which the low-temperature transmission loss has affected the existing telecommunications plant is grossly underestimated for two reasons. One reason is that the majority of transmission systems currently operate at 1310 nm. Studies⁽²⁾ have shown that only under the most severe

conditions and with highly susceptible cables will service-affecting losses be observed at 1310 nm. However, these same cables, under similar conditions, are much more likely to fail when transmission is at 1550 nm due to the heightened bend sensitivity of fiber at this wavelength. As fiber optic systems migrate toward 1550 nm to support higher bit-rate services on existing facilities, an increased frequency of field failures is expected. The second factor contributing to unreported instances of this phenomenon is that the losses are invariably mistaken as simple splice failures when diagnosed using common low-resolution optical time domain reflectometry (OTDR). Whether the splice is redone in a heated splice van or when ambient temperatures are more moderate, the problem is apparently corrected as the losses do not exist at these temperatures. This misjudgment is maintained until the ambient temperature once again drops below about -15°C and the losses reappear.

It is now understood that the losses observed are due to an increase in attenuation over a relatively short length of cable (3-10 meters) adjacent to the cable termination point at a splice closure. Laboratory experiments^(2,3) conducted in an environmental chamber have demonstrated that relative movements of cable core elements induce bending losses in optical fibers contained within the cable buffer tubes. The bending-induced loss results from an increase in the excess fiber length (EFL) within the buffer tubes beyond the design limits of the cable. Optical loss is further accentuated by a sharply increased modulus of the optical fiber coatings, particularly the inner primary coating, at low temperature. At temperatures below -10 °C, some inner primary coatings become as stiff as the outer primary layer and lose their ability to isolate the glass fiber from external mechanical loads.

In this report, we explore and identify cable structure/material parameters that determine the optical loss sensitivity of loose tube fiber optic cables in a low-temperature environment. We present a summary of optical measurements on sample cables exposed to temperature-cycling and relate these results to cable structure/material factors. Finally, in an attempt to accommodate the large embedded plant that may already be affected, we discuss cable rehabilitation and termination techniques aimed at preventing the onset of low-temperature-induced losses.

Copyright © 1994 Bellcore. All rights reserved.

2. CABLE CHARACTERISTICS and OPTICAL LOSS MEASUREMENTS

In general, loose tube cables consist of a bundle of elements stranded about a relatively rigid, dielectric central member (CM). Bundles of optical fibers are packaged inside polyester (PBT, poly(butylene terephthalate)) buffer tubes such that a specified amount of excess fiber length (EFL) is provided. This is done to ensure that individual fibers are not subjected to a strain when the cable is placed in tension, such as during installation. Buffer tubes are also filled with a gel compound that engulfs the fibers and inhibits water migration through the tube. Other elements that may be present in loose tube cables are filler rods, Aramid yarn filaments, and a plastic binder tape spirally-wrapped around the cable core. Prior to jacketing, the cable core is flooded with a cable filling compound aimed at inhibiting the migration of water between cable elements. The cable core is then jacketed using one or two layers of MDPE (Medium Density Poly(Ethylene)). A metallic layer of armor may also be added prior to the application of the outer jacket.

To identify the physical origin of optical loss in loose tube cables, we designed experiments to measure optical loss at low temperature. Seven cable samples from four manufacturers, approximately 21.3-m (70-ft) long each, were installed in an environmental chamber such that one end remained inside the chamber while the other end was terminated outside the chamber and maintained at a temperature of 23 °C. Inside the chamber, two fibers from separate buffer tubes were concatenated for an effective fiber length of 43 meters (141 feet). The cable end inside the chamber was left unterminated to simulate a worst-case installation environment. Clamping the cable sheath, such as is done inside a splice closure, is known to introduce a localized pinching force that tends to delay the onset of low-temperature-induced loss. Termination of the cable CM may also inhibit the movement of cable core elements depending on the particular hardware used. However, the intent of the experiments was to test cables to failure and conduct a comparative analysis of different cable constructions and configurations.

Table 1. A Summary of Cable Characteristics and 1550-nm Optical Loss at -40 °C

CABLE	1A	1B	2A	2B	3A	4A	4B
Jacket Thickness (mm)	MDPE 1.5 / 0.65	MDPE 3.25	MDPE 1.75	MDPE 1.45 / 0.45	MDPE 1.80	MDPE 1.45 / 0.8	MDPE 1.5
Corrugated Metallic Shield	Yes	No	No	Yes	No	Yes	No
Filler Tube MDPE	4	0	0	5	2	1	1
Buffer Tube PBT	2	8	6	13	4	5	5
Fibers / Tube	6	11	6	12	12	11	11
Buffer Tube ID / OD (mm)	1.5 / 2.4	1.7 / 3.0	1.4 / 2.4	1.85 / 2.95	1.6 / 2.7	2.15 / 2.95	2.15 / 2.95
Tube Thick. (mm)	0.45	0.65	0.48	0.55	0.55	0.4	0.4
Buffer Tube Gel	PIB Fumed Silica	PIB Fumed Silica	PIB Fumed Silica	PIB Fumed Silica	PIB Fumed Silica	PPG	PPG
CM	GRP	GRP Coated (MDPE/LDPE)	GRP Coated (LDPE)	GRP Coated (LDPE)	GRP	GRP Coated (LDPE)	GRP Coated (LDPE)
Excess Fiber Length to Tube ID Ratio (% / mm)	0.3 - 0.4	0.1 - 0.2	0.3	0.1	0.2 - 0.4	0.1	0.1
Optical Loss (dB) 1550 nm -40°C	11	0.15	7.8	0.03	26	0.03	0.1

Acronyms

MDPE	Medium Density Poly(Ethylene)	LDPE	Low Density Poly(Ethylene)
PBT	Poly(Butylene Terephthalate)	CM	Central Member
PIB	Poly(Isobutylene)	PPG	Poly(Propylene Glycol)
GRP	Glass Fiber-Reinforced Plastic		

Each cable was subjected to thermal cycling between -40 °C and 80 °C. Optical loss was measured at both 1550 nm and 1310 nm using an OTDR after reaching steady state at each temperature extreme. Figure 1 shows the response of a typical loose tube cable that is susceptible to low-temperature-induced loss. Increasing attenuation with the number of cycles suggests that temperature cycling aids to break down frictional coupling forces between cable elements. All cables subjected to thermal cycling did not show any loss at 80 °C. Table 1 presents a summary of the salient characteristics of each cable tested and the maximum loss measured at -40 °C.

2.1 Origin of Optical Loss in Loose Tube Cables

Having identified sample cables with high optical loss (cables 1A, 2A, and 3A) at 1550 nm and -40 °C, we designed a series of temperature-cycling experiments to investigate the contribution of individual cable elements to the low-temperature optical loss. Four samples of cable 1A, a high-loss cable, taken from the same reel were installed in an environmental chamber. Sample 1 was the unmodified cable. Sample 2 consisted of the core and inner jacket of the sample 1. In sample 3, we went one step further by removing the inner jacket from the sample 2 cable. Finally, sample 4 was the isolated buffer tube of the sample 1 (cable 1A).

Each cable was cycled as described above. A plot of attenuation change at -40 °C following each thermal cycle is shown in Figure 2. Measurements at 80 °C are not shown since in all cases the loss was zero. All samples showed the same temperature-dependent behavior. Losses appeared at low temperature and disappeared at high temperature. The isolated buffer tubes (sample 4) exhibited an increase in loss on the same order as the complete cable (sample 1). This critically important series of experiments suggested that the optical loss-producing motions originate from the buffer tube-fiber package and the major contributor to optical loss-producing motions in the cable is the buffer tube thermal contraction. However, a key difference in optical loss behavior between the complete cable (sample 1) and the isolated buffer tubes (sample 4) was that the losses in the isolated buffer tubes were observed during the first cycle whereas the complete cable required exposure to high temperature for optical loss to appear at low temperature. This result further indicated that the cable structure delays the onset of optical loss at low temperature. Repeated cycling of samples 1 through 3 gradually breaks down the coupling forces between cable elements allowing greater changes in the buffer tube length with each successive thermal cycle.

We conducted similar temperature cycling experiments on a low-loss cable, cable 1B (Schematic cross-sections of cables 1A and 1B are shown in Figure 3). In this experiment, only the complete cable and isolated buffer tubes were examined. Each sample was taken from the same reel of cable. The thermal cycling results are shown in Figure 4. In this case, the complete cable showed no sensitivity to low-temperature exposure. However, as with the high-loss cable 1A, the isolated buffer tubes did exhibit a substantial increase in attenuation. This finding confirmed that the buffer tubes themselves undergo

optical loss-producing thermal contraction. In addition, since no optical loss was observed in the complete cable, it could only be deduced that the cable structure prevents the optical losses from occurring. This conclusion, in turn, suggests that cable structure can be modified to reduce optical loss sensitivity of cables to low temperature.

2.2 Coupling Between Cable Elements

All of the elements making up a loose tube cable have different thermal expansivities (expressed by the coefficient of thermal expansion, CTE). For instance, the polymeric cable materials (jacket, buffer tubes and coatings) have thermal expansion coefficients that are three orders of magnitude larger ($2.5 \times 10^{-4} \text{ }^{\circ}\text{C}^{-1}$ for MDPE cable jacket, $1.3 \times 10^{-4} \text{ }^{\circ}\text{C}^{-1}$ for PBT buffer tubes, $1.0 \times 10^{-4} \text{ }^{\circ}\text{C}^{-1}$ for the outer primary coating, $1.3 \times 10^{-4} \text{ }^{\circ}\text{C}^{-1}$ for the inner primary coating, all at 25°C) than those of the glass fiber ($1.1 \times 10^{-7} \text{ }^{\circ}\text{C}^{-1}$) and the central member ($1.0 \times 10^{-6} \text{ }^{\circ}\text{C}^{-1}$). At low temperature, the polymeric cable materials undergo substantially larger thermal contraction than the glass fiber and the central member. For instance, the thermal expansion profile for a PBT buffer tube from cable 1A, shown in Figure 5, indicates that a temperature increase from -40 °C to 80 °C results in approximately two-percent displacement that is localized at the cable ends where frictional coupling between the cable elements is weak. As the buffer tubes contract within the cable core, the amount of fiber relative to the tube length increases since the optical fiber contraction is three-orders-of-magnitude smaller. At low temperatures, the dynamic viscosity of buffer tube gels rises sharply as shown in the dynamic viscosity profiles for both cable 1A and cable 1B buffer tube gels of Figure 6. Thus, during low temperature exposure, the fiber may not be able to reorient itself and relieve stress. Consequently, the contracting buffer tube may cause fibers to buckle and, ultimately, contact buffer tube wall. At temperatures below -10 °C, the modulus of the inner primary coating, shown in Figure 7, becomes too high to prevent the glass fiber from bending. For instance, at -40 °C, the storage modulus of the inner primary coating becomes equal to or exceeds the modulus of the outer primary layer, thereby greatly increasing the risk of generating random microscopic fiber axis perturbations. Therefore, under the conditions just described, one needs a strategy to arrest the optical loss-producing motions in the cable structure. We presented a cable coupling model in an earlier communication⁽³⁾ to implement one such strategy.

The components comprising a fiber optic cable are mechanically coupled by frictional forces that are either inadvertently or purposefully introduced during manufacturing. The stiffest element in a loose tube cable is the CM, and all other elements are packed around it. The cable fabrication process uses binder tapes and yarns to accomplish a tight packing. However, depending on the cable design and the fabrication process, cable structures allow different amounts of slipping and movement of cable elements relative to the CM. These movements are most pronounced at the cable ends near cable termination points such as splice closures. By considering mechanical equilibrium, one can define a slip region, measured from the cable end, over

which the relative movement occurs. The length of this slip region is inversely proportional to the frictional force between the cable elements as shown in Table 2.

The pull-out force refers to the force required to pull out the cable CM in 0.5-m cable samples. This table demonstrates a strong correlation between the low pull-out force (i.e. long slip region) and high optical loss at -40 °C. The CM protrusion was calculated from the cable coupling model as the difference between the displacement of the cable components at the cable end and the CM. According to this table, cables with a slip region longer than 3.6 m (11.8 ft) or a CM protrusion greater than 13 mm exhibit high optical loss at -40 °C. The CM protrusion observed in the temperature cycling tests and reported in the field failures agree with these findings.

We now re-examine the optical loss behavior of samples from cables 1A and 1B discussed in section 2.1. By stripping cables progressively from a complete cable to isolated buffer tubes, we had noted that cable 1A buffer tubes exhibited as much optical loss as the complete, high-loss cable. The isolated buffer tubes of cable 1B also showed high loss whereas the complete cable did not. For cables 1A and 1B, Table 1 indicates a significant difference in the excess fiber length-to-buffer tube ID (inner diameter) ratio. This ratio is an important parameter in determining the low-temperature loss resistance of loose tube cables as pointed out earlier by Fuchigami et al.⁽⁴⁾ The minimum cable strain to push the fiber into contact with the buffer tube wall depends on the excess fiber length and can be computed from the tube stranding parameters such as lay length and stranding radius.^(3,5) Table 3 presents a comparison of cables 1A and 1B.

Table 2. Cable Structure Tightness Parameters vs Optical Loss

CABLE	1A	1B	2A	2B	3A	4A	4B
Pull-out Force per Unit Length (Kg m⁻¹)	3.1	58.7	17.6	56.9	6.0	14.6	14.8
Slip Region Length (m)	7.2	1.5	2.2	0.25	5.9	1.5	1.8
CM Protrusion (mm)	53.6	11.4	16.5	1.8	43.7	11.2	13.2
Optical Loss (dB) 1550 nm -40°C	11	0.15	7.8	0.03	26	0.03	0.1

Table 3. Limiting Strain for Fiber-to-Tube Wall Contact

Cable	Lay Length (mm)	Stranding Radius (mm)	EFL-to-Tube ID Ratio (%)	Strain (%)
1A	83	2.6	0.3-0.4	-0.73
1B	114	4.4	0.1-0.2	-0.94

The strain gradient in cable 1B is much steeper than that in cable 1A as a result of tighter construction. The critical strain required to initiate fiber buckling within the tubes is exceeded for cable 1B over progressively longer lengths as resistance to buffer tube motion is removed by stripping the jacket and removing other cable core components.

3. CABLE TERMINATION and REHABILITATION

Low-temperature optical loss is observed only at the cable section adjacent to a splice closure. Therefore, we tested five commercial splice closures and an integrated cable sheath/CM clamp that we designed for cable termination effectiveness in

preventing the onset of low-temperature optical loss. The test closures were assembled per the manufacturers instructions using a known high-loss cable (cable 1A). As described earlier for the temperature-cycling experiments on the commercial cable samples, each cable used for the closure tests was 21.3-m (70-ft) long and two fibers from separate buffer tubes were concatenated for an effective fiber length of 43 m (141 ft). The cable end containing the closure was placed inside an environmental chamber while the other end of the cable was terminated outside the chamber and maintained at a temperature of 23 °C. Each closure was subjected to thermal cycling between -40 °C and 80 °C.

Figure 8 shows a plot of the low-temperature response of each

closure/cable combination. The high-temperature optical loss was zero in all cases. Although the low-temperature loss measured for each closure remained low relative to that for a free-end cable (i.e. cable with no end termination), it was unacceptably high in comparison to the optical loss measured with the integrated sheath/CM clamp. Throughout the entire temperature cycling experiment, the integrated sheath/CM clamp kept the optical loss to approximately 0.1dB or less.

Buckling of the cable CM was observed on closures 1, 2, 4 and 5 while closure 3 exhibited clamp failure resulting in unrestrained pistoning of the CM during thermal cycling. The cable central member buckles under the action of jacket shrinkage force. We measured this force by attaching a load cell to the end of a 21.3-m (70 ft) sample of cable 1A and subjecting the cable to thermal cycling. A maximum force of 36.4 kgs (80 lbs) was measured. Table 4 presents a summary of the optical losses measured for each closure/cable combination at 1550 nm. At the completion of the experiment, we removed the integrated sheath/CM clamp and measured the loss increase to show its effectiveness in suppressing loss-producing movement of cable components.

Table 4. Optical Loss Measured with Splice Closures

Closure #	Initial CM Length		Max. Loss (dB)	CM Slippage	Sheath Slippage	CM Bowing	Max. Loss CM Free
	(in)	(mm)					
1	2.38	60.33	0.97	NO	NO	YES	1.74
2	4.63	117.48	3.72	NO	NO	YES	8.00
3	1.25	31.75	6.49	YES	NO	NO	10.45
4	3.50	88.90	0.85	NO	NO	YES	2.34
5	2.56	65.02	0.75	NO	NO	YES	2.21
Sheath/CM Clamp	-----	-----	0.12	NO	NO	NO	N/A

4. SUMMARY and CONCLUSIONS

Some loose tube cables containing single-mode fibers exhibit service-affecting transmission loss at 1550 nm at low temperature (-20 °C to -40 °C). The loss occurs in the cable section adjacent to a splice closure, where the cable jacket is removed to expose fibers for splicing. The losses are observed when there is relative movement among cable core elements resulting in an increase in the excess fiber length (EFL) within the buffer tubes beyond the design limits of the cable. Optical loss is further accentuated by a sharply increased modulus of the fiber coatings, particularly the inner primary coating, at low temperature. At temperatures below -10°C, the inner primary coating becomes nearly as stiff as the outer primary layer and loses its ability to isolate the glass fiber from external mechanical loads.

Optical loss measurements during temperature cycling (from -40 °C to 80 °C) of cables from four manufacturers have shown that the major contributor to optical loss-producing motions in loose tube cables is the buffer tube thermal contraction. However, tightly structured cables with a low initial excess fiber length-to-buffer tube ID ratio can resist such thermally-induced loss-producing motion of the cable components. Tightly structured cables restrict relative motion of cable core components by coupling these elements to a relatively rigid central member.

Cable termination practices and splice closure termination hardware play an important role in preventing the low-temperature loss in optical cables that are subject to developing such losses. Mechanical sheath retention/central member clamps can be effectively utilized to prevent loss-producing

motions within the cable structure. Some widely used splice closures are neither robust enough to withstand thermal cycling nor effective in immobilizing cable elements to prevent optical loss at low temperatures.

ACKNOWLEDGMENTS

We thank I.M. Plitz for the analysis and identification of cable materials in the sample cables, and D. Unkel, G.T. Aich, R.M. Kanen and M.J. Kozlowski for performing cable tests.

REFERENCES

1. G. Kiss, "Self-Healing Failures in the Aerial Plant," *SPIE Boston Conference Proceedings*, (1993).
2. G. Kiss, M. Zammit, O. Gebizlioglu, P. Grimado, M. Hlavaty, C. Wiczorek, "Low-Temperature Reversible Splice Loss Accompanied by Cable CM Protrusion," *NFOEC Proceedings*, Vol. 2, p 411 (1994).
3. P.B. Grimado, O.S. Gebizlioglu, M.J. Zammit, G.D. Kiss, "Low-Temperature Transmission Loss in Loose Tube Fiber Optic Cables," *SPIE Annual Meeting Proceedings*, Vol. 2290 (1994).
4. T. Fuchigami, Y. Yokoo, K. Ugawa, M. Kawase, "Optical Loss Increase of SP-Optical Fiber Cable at Low Temperature," *The IEICE Transactions*, E 70, No. 4, p 282 (1987).
5. G. Mahlke, P. Gossing, "Fiber Optic Cables," John Wiley & Sons, Inc., New York, p 109 (1987).

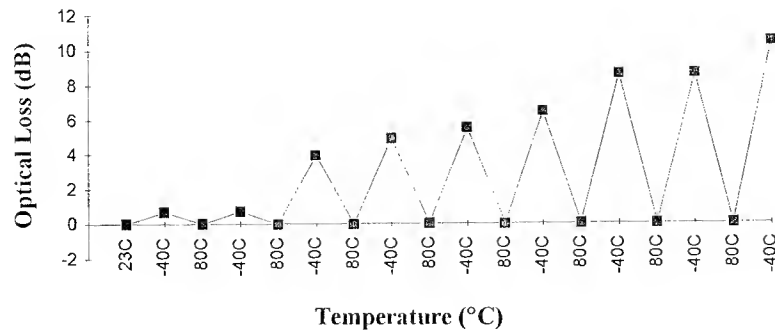


Figure 1. Optical loss versus the number of thermal cycles from -40 °C to 80 °C

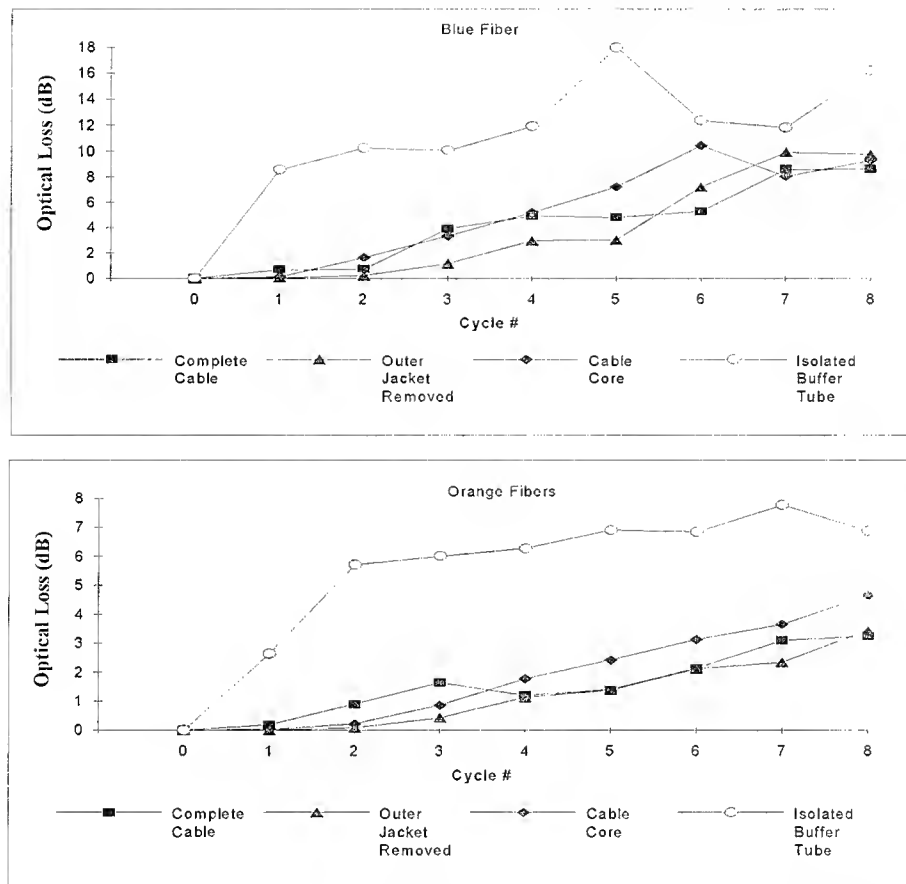


Figure 2. Optical loss profiles for cable 1A and cable 1A with stripped jacket/core components

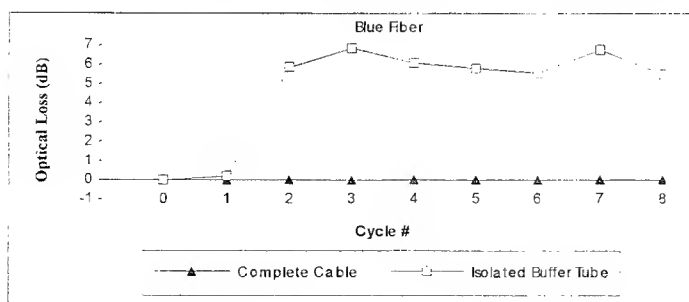


Figure 4. Optical loss profiles for cable 1B and cable 1B buffer tubes

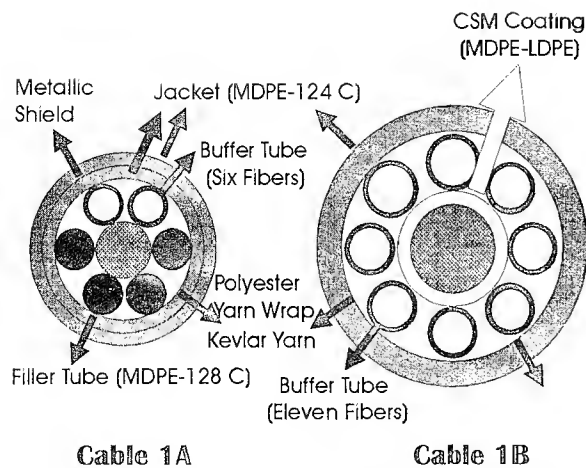


Figure 3. Schematic cross-sections of cables 1A and 1B

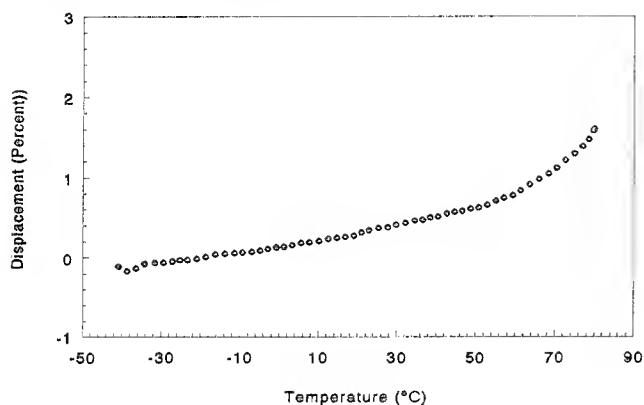


Figure 5. Thermal expansion profile of a cable 1A buffer tube

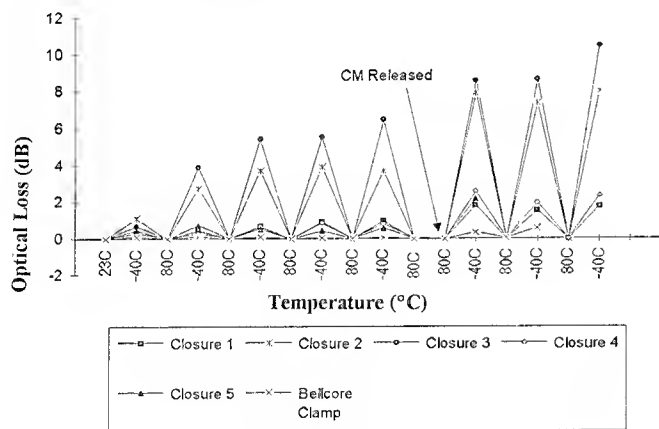


Figure 8. Low-temperature response of five splice closures with cable 1A

Osman S. Gebizlioglu is a Member of Technical Staff in the Metals & Plastics Technology Group at Bellcore. He holds B.S., M.S. (Middle East Tech. Univ., Ankara, Turkey) and Ph.D. (Princeton Univ., Princeton, New Jersey) degrees in Chemical Engineering. He was a Monsanto Research Fellow in Mechanical Engineering at MIT prior to joining Bellcore in 1987.

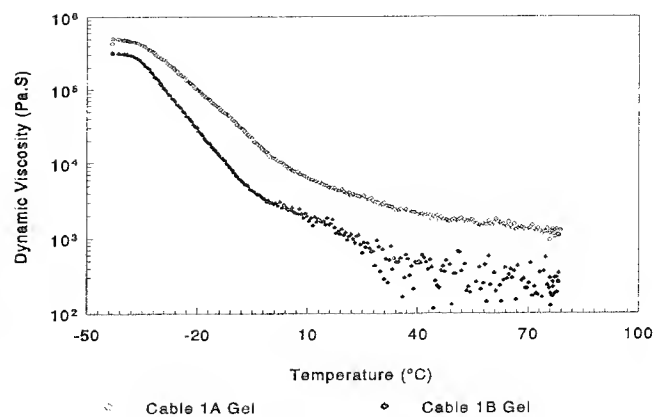


Figure 6. Dynamic viscosity profiles for buffer tube gels

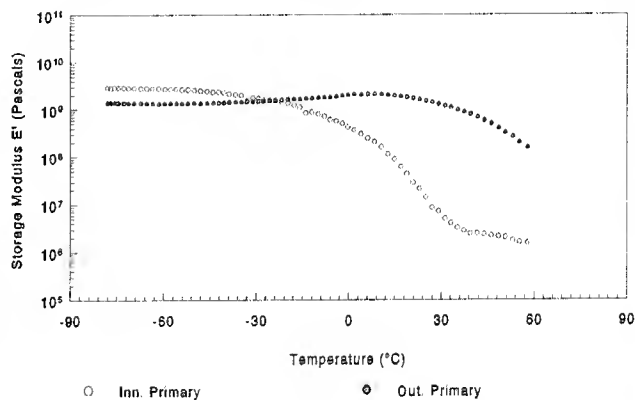


Figure 7. Storage modulus profiles for fiber coatings

Michael J. Zammit is a Member of Technical Staff in the Optical Cable & Component Technology Group at Bellcore. He holds B.S. (Columbia Univ., 1990) and M.S. (MIT) degrees in Mechanical Engineering. His responsibilities include the development of generic requirements, test procedures, and technical analyses for fiber optic splice closures, ONU (Optical Network Unit) enclosures, and innerduct. He is also involved in TIA standards development for splice closures.



Philip B. Grimado is a Member of Technical Staff in the Fiber Media & Component Reliability Group at Bellcore. He has a B.S. degree in Civil Engineering (City Univ. New York), and M.S. and Ph.D. degrees in Applied Mechanics (Columbia Univ.). He worked at Bell Laboratories from 1968 to 1983.



Gabor D. Kiss is a Member of Technical Staff in the Optical Cable & Component Technology Group at Bellcore. He holds B.S. (Case Western Reserve Univ.) and Ph.D. (Univ. of Massachusetts) degrees in Polymer Sci. & Engineering, and an M.S. degree in Computer Science (NJIT). He worked at Celanese Corp., Summit, NJ, from 1980 to 1985. His current responsibilities include generic requirements and performance analyses of fiber optic splices and connectors.



Long Term Environmental and Process Tests of On-Line Colored Fiber Optic Ribbons

Dr. Bertil Arvidsson, Ericsson Cables, Sweden

Mr. Mats Eriksson, Ericsson Cables, Sweden

Mr. Jukka Kohtala, Nokia-Maillefer, USA

Mr. Juha Tanskanen, Nokia-Maillefer, Finland

Abstract

In recent years the fiber optic ribbon technology and ribbon cable constructions have matured in several countries. The advantages such as mass fusion splicing and high fiber density in the cables are obvious. Furthermore, the productivity and efficiency are important features of fiber optic ribbon manufacturing. Ribbon process and type testing of ribbons have been widely studied. Despite good results and benefits of the ribbon have been achieved, the lack of experience and standards have caused delay in the employment of the ribbon cables.

This paper verifies the benefits of the tandemization of the coloring and ribbon processes. The paper also presents wide test results of these ribbons. Tandemization offers benefits like cost savings in intermediate storing and handling. It also gives flexibility for the production.

Introduction

The process tests are important to ensure quality in production and parameters as strippability and geometry of the ribbon, as well as the curl of the fiber must be checked to ensure good splicing. Additionally, separate fusion splicing and environmental tests especially water soaking with attenuation measurements are important parts of the quality control.

With this on-line coloring technique the coloring and ribboning are merged into one operation. By doing so, a higher total volume of ribbon production as well as savings in intermediate

storing and handling costs are achieved. With advanced line control and process testing, we show that continuous high quality can be achieved. Finally, test results of long term testing of ribbons produced from various fiber types verify the importance of material compatibility.

The rapid growth and expansion of the communication networks have increased the use of the fiber optic ribbon in all cabling applications. Two of the main cable structures - ribbons in tube and in slotted core - have presented several solutions to take advantage of ribbon benefits. The improvements of manufacturing, including materials and testing, and furthermore the development of the installation techniques, especially connecting and handling of the ribbon cables have also increased the demand for ribbon applications.¹

A large scale test program for encapsulated 4-fiber ribbons has been made to find the optimum processing conditions and to get long term results. To evaluate the behavior of different ribbons, four types of fibers were used for these tests. All of them were recommended for ribbon applications. The inks and the matrix materials were the same in all ribbons. So far, the fibers for ribbons are generally colored off-line. The ribbons tested here have been produced firstly by coloring the fibers in a separate process. And secondly the ribbons were produced by using on-line coloring technique.

Both in this and in our previous paper we have divided the ribbon testing into two different parts: type testing and process testing.² Type testing

include tests which are made after major modifications, material, dimensions etc. The process tests are executed daily and the main target is to ensure the best quality of the ribbon production.

Process tandemization

The fibers are paid off from the payoffs and after that lead to the multifiber coloring unit. All four fibers are colored at the same time with different colors. After coloring the ink is cured with UV lamps. Then colored fibers are lead into a ribbon coater and the ribbon form is also cured with UV lamps. The capstan defines the speed for the line and finally the ribbon is wound onto a take-up reel. All operations of the system are controlled by a control cabinet. The layout of the system is in figure 1.^{2,3}

Fiber Coloring

When coloring fibers the selection of the ink and determination of the right curing level is important. Fiber coloring for ribbon applications requires higher curing level and better surface curing than fibers in loose tube applications. The curing quality can also influence the transmission, strength and breakout properties.

For the reasons mentioned above the coloring lines are equipped with efficient UV curing and

nitrogen inert gas purge systems. The UV dose, including intensity and curing time, is important to reach highest possible curing level in high speed coloring.

Further, missing or unconcentric color layer can cause attenuation increase for the fiber and even more for the ribbon. Smooth color layer with high production speed can be achieved using pressurized coloring die assembly.

The temperature control keeps the temperature and the viscosity of the ink in the die system at optimum level. To prevent process problems in long length coloring dust and static electricity is removed before entering the coloring die.

Ribbon manufacturing

When paying off the fibers, constant tension and removal of static electricity are essential to achieve stable coating conditions. Dust is removed to prevent air bubble formation and attenuation increase of the ribbon. The compact coater construction offers easy handling and non-leaking operation. Good alignment of the fibers in the ribbons must be achieved especially for high production speeds. Viscosity of the liquid must be controllable to make the right shape and dimensions with narrow tolerances possible for the ribbon.

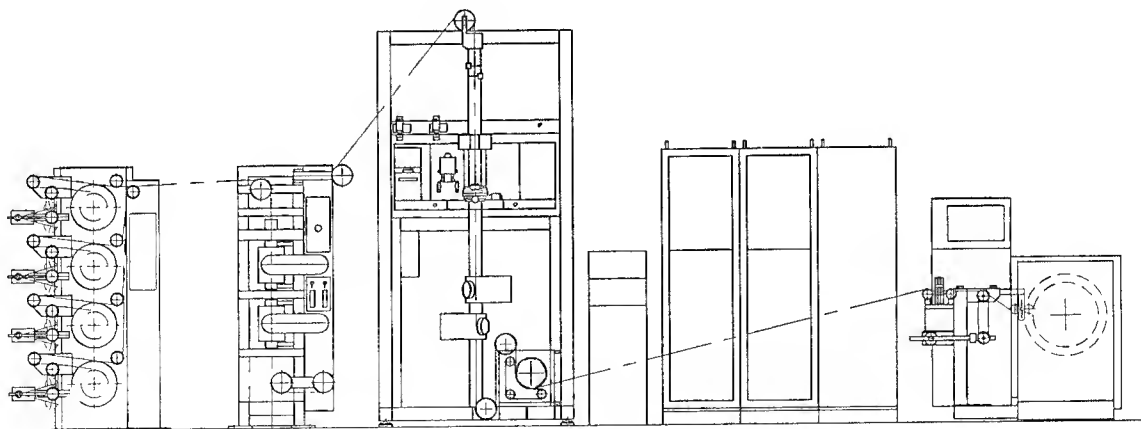


Figure 1. Fiber optic ribbon manufacturing system with on-line coloring.

Immediately after coating the ribbon is cured by using high intensity UV lamps together with nitrogen inert gas.

The use, preparation and start-up of the process and also short idle time are important when producing ribbons. The coater unit is designed to make ribbon manufacturing easy. Therefore no disassembling or adjusting is required between runs. Additionally two pressurized coating containers are used to minimize the waiting time for stabilizing the matrix materials. Wide operating range with speed, temperature and pressure control reserve is important to ensure good performance for the system also in the future.

For controlling the quality of the coloring process, the diameter of the fiber and thickness of the color layers are measured by means of a laser scanning system. With special software both the thickness of each color layer and the dimensions of the ribbon are measured. All tolerance violations are indicated.

The material selection for all layers of the ribbon is very important to be able to guarantee best possible properties of the ribbon. The other essential part of the ribbon manufacturing is to define right process parameters for the production.

For this particular study with on-line coloring the following processing parameters were used. The production speed was 200 m/min. Temperatures of the matrix material and coloring ink were 30°C and 29°C respectively. The nitrogen flow for four fibers was 30 l/min. The payoff tensions were adjusted in the base level of 60 grams. Two high intensity UV lamps were used to cure the inks and ribbon matrix material.

Characteristics for on-line coloring

Generally when coloring on-line one phase of production is avoided and additional benefits can be achieved. The intermediate storing, handling, coding and sorting of the different colored fibers are eliminated. Also the production scheduling and control is easier and further it offers additional flexibility for the production resulting in reduced labour costs.

In addition when optimizing color coding for four fiber ribbon, only one color must be changed when producing different ribbons.

The risks, e.g. the missing or too thin color layer, may ruin the whole ribbon. This can be avoided by using measuring systems. Other risks such as differences of color behaviour during coloring and thickness and viscosity of the color layer are similar as for an off-line coloring technique.

Test process conditions

For this study four different fiber coating materials (A, B, C and D) were chosen. The inks and ribbon matrix materials were the same in all cases.⁴ These materials are specially developed to meet stringent ribbon requirements. Other ribbon compatible fiber coatings, UV inks and matrix coatings are available on the market. The fiber coatings A, C and D, were all developed to meet both loose tube and ribbon fiber requirements. Fiber type B is specially used for ribbon applications.

An important parameter for colored fibers is the UV cure level of the inks. Because the MEK rubbing tests do not measure actual curing level, we used the standard FTIR method, where the degree of cure is calculated as percent reacted acrylate unsaturation (%RAU). It is important to have a high cure level to ensure a good performance of the ribbon.

Procedure to determine the degree of curing using FTIR

The degree of cure of the ink layer on the fiber is measured by using Fourier Transform Infrared (FTIR) Spectrophotometer, ATR crystal and ATR accessory. On the surface the degree of the curing is determined to the depth of 1-3 μm .

First the sample is prepared so that 10 x 100 mm area is covered on the crystal. After sample preparation the crystal with the colored fibers is mounted in the ATR accessory and fixed in the FTIR compartment. After that it is scanned with FTIR Spectrophotometer.⁴

After measuring of a specific net peak area of the ink and a reference, the results are compared. The degree of cure (percentage of reacted acrylate unsaturation) is then calculated by comparing the area ratio of the liquid ink and colored fiber with the following equation

$$\%RAU = \{(RL - RF) * 100\} / RL$$

where RL = area ratio of liquid
 RF = area ratio of colored fiber

The results of the degree of cure level of on-line colored fibers are presented in table 1. These data in combination with the test results of this study show that there is no remarkable difference of the curing when compared with off-line coloring. Most important is to achieve minimum curing level for each application.

SAMPLE	COLOR	DEGREE OF CURE (%RAU)	SPEED m/min
A1	white	95	100
A2	white	96	150
A3	white	94	200
A7	white	91	400
A11	white	89	600
B1	white	96	150
B2	white	96	200
B3	white	98	250
B6	white	92	400
B10	white	90	600
C1	blue	87	400
C3	blue	92	200
C4	blue	96	100
D1	red	87	400
D3	red	89	200
D4	red	94	100
F1	white	92	400
G2	white	95	200
G3	white	92	250
G6	white	90	400
G8	white	85	600
H2	red	87	200
H4	red	85	300
H6	red	84	400
H8	red	80	600

Table 1. The curing level of on-line colored fibers.

Test results of the on-line colored ribbon

In an on-going test program the ribbons are exposed to different requirements. In table 2 the relevant tests are summarized.^{2,5,6}

In this summary process and type testing have slightly different meanings. A transmission test as a process control means the OTDR 1550 nm measurement from one direction, while a full transmission test in a type test program includes all transmission parameters. The frequency of performing the different process tests can also vary. In the on-line coloring program it was logical to concentrate on tests #7, #11 and #12.

However, we would also like to devote some time on test #2, fiber curl, since it has been widely discussed for a few years.

It has been concluded in our internal investigations that fiber curl is inherent glass property, which has nothing to do with ribbon making. We have also found that curl should not be higher than 1.2 μ m on a 3 mm extension.⁶ Fiber curl could alternatively be expressed as a radius, see Table 3 for some different values. Curl has also to be related to the splice loss requirement, which in our case is max. 0.25 dB for any splice.

UV curing tests were discussed in the preceeding paragraph.

It was important to perform some environmental tests as well. In several earlier study programs water soak tests have been decisive. Our water tests consists of approximately 1000 m of ribbon put into a 'water bucket' with water kept at room temperature and measured daily with an OTDR at 1550 nm. Since we are interested in relative changes only, it was sufficient to measure from one end. In figures 2, 3, 4 and 5 we have collected our test results for the four different ribbon types A, B, C and D. Each type has been produced with both on-line and off-line coloring technique.

Test	Process test	Type test	This study
1. Geometry	*	*	*
2. Fiber curl	*	*	*
3. Transmission	*	*	*
4. Fusion splicing	*	*	*
5. Strippability	*	*	*
6. Compatibility		*	
7. Separability	*	*	*
8. Macrobend		*	
9. Crush		*	
10. Torsion		*	
11. Environmental	*	*	*
12. UV Curing	*	*	*

3mm extension (μm)	10mm extension (μm)	Radius (m)
2.25	25	2
1.2	13.3	3.75
0.8	8.9	5.6

Table 2. Ribbon tests.

Table 3. Fiber curl radius comparison.

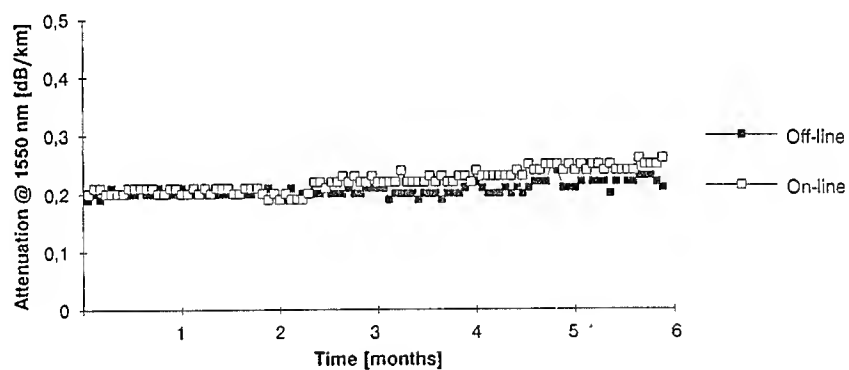


Figure 2. Ribbon type A.

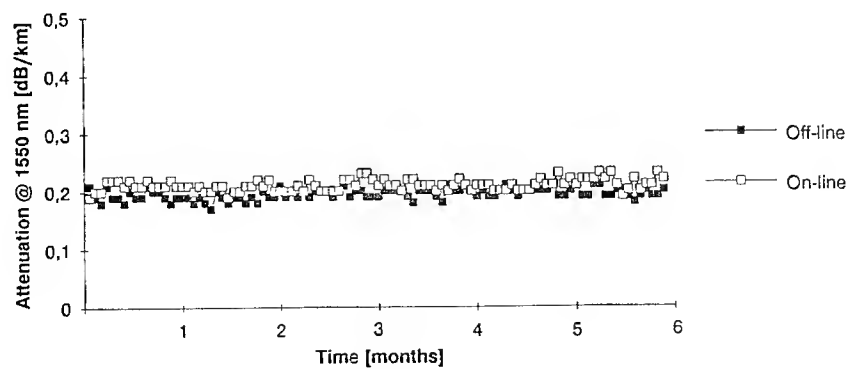


Figure 3. Ribbon type B.

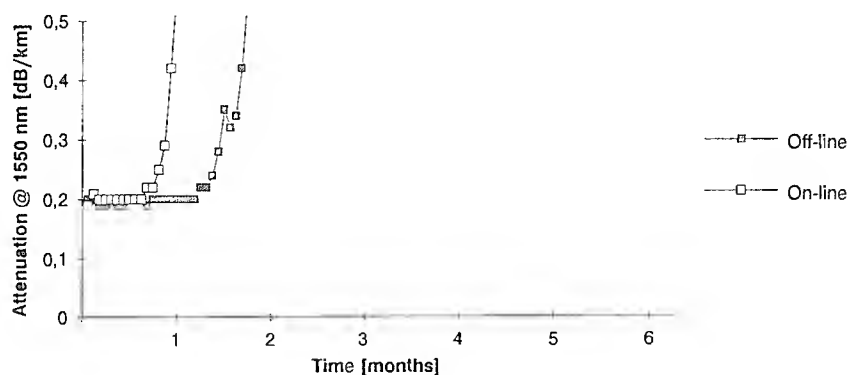


Figure 4. Ribbon type C.

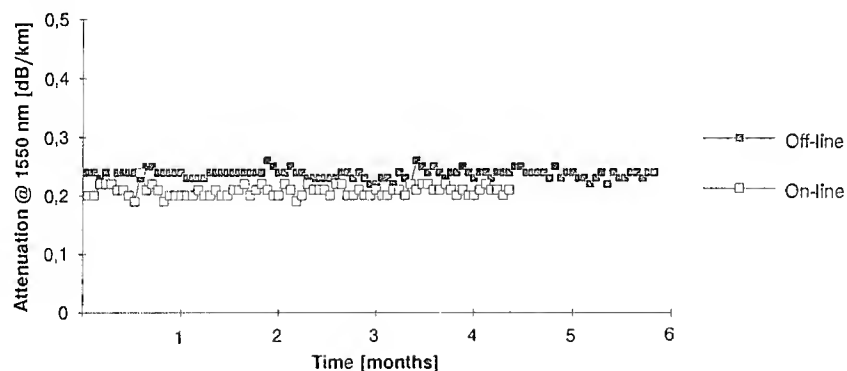


Figure 5. Ribbon type D.

Performing water soak tests at higher temperatures are also possible. In this case we have chosen to present the results for +20°C, since we believe they are the most relevant ones because of the general environmental requirements. Test results after 6 months water immersion are presented here. Types A, B and D are still continuing and two of them have now been in water more than one year.

Figure 4 shows the importance of material selection. Here the combination of different materials has given an increased attenuation after one or two months. Therefore type C is inadequate as a material used for a ribbon.

Conclusions

The long term testing of different materials shows

that material selection is an essential part of the ribbon manufacturing. Material improvements over the last couple of years show that it is possible to produce ribbons fulfilling present requirements.

We have also shown that the on-line coloring do not affect the properties of the fiber optic ribbon. The benefits of this tandemization technique have been analyzed.

Finally we have pointed out the necessity to divide the quality control into two groups: process testing and type testing.

Acknowledgement

We thank DSM Desotech bv for supplying the materials and valuable assistance in performing FTIR cure measurements.

References

1. F.Greco, A. Ragni, "High performance optical fiber ribbon by UV curing method," Wire Journal International, Dec. 1992.
2. B.Arvidsson, M.Eriksson, J.Kohtala, J.Tanskanen, "High Speed Manufacturing and Type Testing of Fiber Optic Ribbons," China FiberCom 94, Shanghai, 1994.
3. J.Kohtala, J. Tanskanen, P. Fickling, M. Eriksson, "A High Speed Coating Process for Optical Fibre Ribbon," IWCS, St Louis, 1991.
4. A.Abel, J.van Eekelen, "Dynamic water sensitivity of UV acrylate inks and matrix coating, and its relationship to the water soak performance of optical fiber ribbons", EFOC & N '93 11th annual conference, Hague, 1993.
5. B.Arvidsson, "An alternative test method for measuring ribbon geometry," OFMC, Torino, 1993.
6. K.Jonsson, A Björk, "Comparative measurements of curl and splice loss for an optical 4-fibre ribbon," OFMC, Torino, 1993.
7. C.-F. Cheng, J.A. Jay, "Technical Developments in Fiber Optics," China FiberCom 94, Shanghai, 1994.



Bertil Arvidsson,
Ericsson Cables,
S-824 82 Hudiksvall
Sweden

Bertil Arvidsson, manager of fiber and ribbon in Ericsson Cables, has been involved in optical fiber technique for several years. During recent years he has concentrated his work on fiber ribbon technology. He is active also in IEC with standardization regarding optical fibers and ribbon. Prior joining Ericsson 1990 he worked as a technical project manager in Sweden, United States and Switzerland. Before that he was a university lecturer in theoretical physics. He has a Ph.D. in Theoretical Physics from Uppsala, Sweden.



Mats Eriksson,
Ericsson Cables,
S-824 82 Hudiksvall
Sweden

Mats Eriksson received the engineers certificate in Machine Technique from Polhemsskolan, Gävle, Sweden in 1977. He joined Ericsson Cables same year first Ericsson Fiber Optic Center in Stockholm and then Hudiksvall in 1986. Currently he is responsible for developing and testing fiber and ribbon processes.



Jukka Kohtala,
Nokia-Maillfer Inc.,
1856 Corporate Drive
Norcross,
Georgia 30093
United States

Jukka Kohtala received the MSc degree in Physics from Turku University, Finland in 1983. After working two years with Nokia Cables as a research engineer he joined Nokia-Maillfer in 1990. He is currently responsible for Nokia-Maillfer fiber optics operations in America.



Juha Tanskanen
Nokia-Maillfer
P.O.Box 44
01511 Vantaa
Finland

Juha Tanskanen has B.Sc. degree of Mechanical Engineering from Wärtsilä Polytechnic, Finland in 1984 and the M.Sc. degree in Computer Engineering from Tampere University, Finland in 1991. He joined Nokia-Maillfer as a development engineer in 1990 and is currently working as a product manager for fiber coloring and ribbon lines.

PUSH IN MODULUS TEST FOR THE PRIMARY COATING OF DUAL-COATED FIBER

*Kazumasa OISHI, Nobuhiro AKASAKA, Tomoyuki HATTORI,
Tatsuya KAKUTA, and Yasuo MATSUDA*

SUMITOMO ELECTRIC INDUSTRIES, LTD.
1, Taya-cho, Sakae-ku, Yokohama, 244 JAPAN

ABSTRACT

The cure degree of the optical fiber coatings, especially the primary (inner) coating, determines the performance of the fiber, but can be difficult to be evaluated directly. We have developed the "Push In Modulus (PIM) Test" in order to evaluate the cure degree of the primary coating. Measuring the displacement of the glass fiber and the stress, while the glass fiber was being pressed axially, allowed us to determine the Young's modulus of the primary coating directly. The "PIM" test can evaluate the cure degree of the primary coating with high accuracy.

1. INTRODUCTION

Today's high-performance optical fibers heavily rely on polymer material engineering to achieve low-microbending susceptibility. The optical glass fibers are typically coated with two polymer coatings, a soft primary (inner layer) coating to cushion against microbending losses, and a hard secondary (outer layer) coating to provide abrasion resistance. Most commonly, UV curable urethan acrylate resins are used for the coating materials.

The protection afforded by coatings depends in part upon the cure degree of the coatings. Particularly, the cure degree of the primary coating is important, affecting properties such as

adhesion between the primary coating and the glass fiber, and fiber strength. Therefore, the cure degree of the primary coating must be controlled in a optimum range.

A search was being made for a method of determining the cure degree of the (primary) coating, which can be used for a process control. The followings are the conventional measurement techniques which we could apply :

- MEK Extraction Test (gel fraction)
- Tensile Modulus Test (Young's modulus)
- FT-IR ATR Method

The "MEK Extraction Test" ^{[1] [2] [3]} enables extraction of all the coating material which is not polymerized, so the cure degree of the primary coating alone can not be obtained with this test. The "Tensile Modulus Test" has been well known for determining the cure degree of coatings. But the secondary coating is about a thousand times as harder as the primary coating, so we can not evaluate the cure degree of the primary coating. The "FT-IR ATR Method" ^{[1] [2] [3] [4]} only measures the cure degree of the outer surface (about 3 μm thick) of the coatings. Therefore, we had no measurement techniques to evaluate the cure degree of the primary coating alone.

In AT&T Bell Laboratories, the "In Situ Modulus Test" ^{[5] [6]} had been developed for the primary

coating of the fiber. This was the only technique to evaluate the modulus of the primary coating directly. But this test was very difficult to prepare the test sample.

Therefore, it was necessary to develop a more convenient and accurate technique for evaluation the cure degree of the primary coating.

In this paper, the advantages of the "PIM" test are described for determining the cure degree of the primary coating, compared with other conventional techniques.

2. PUSH IN MODULUS TEST

2-1. SCHEME

The "Push In Modulus (PIM) Test" is based on isolating a section of the dual coating, bracing the hard secondary coating, and shearing the primary coating by applying a force to the glass fiber. This concept is illustrated in Figure 1. The applied stress, S (g), will produce a vertical (axial) displacement, Z (μm), of the glass fiber which depends on the shear modulus of the soft primary coating material. The hard secondary coating material, which is at least three orders of magnitude stiffer than the primary coating, will not contribute to Z . The stress-displacement relationship is

$$S = \left\{ 2\pi L G / \ln \left(\frac{D_p}{D_f} \right) \right\} Z \dots \dots \dots (1)$$

where L (mm) is the length of dual coated segment and G (kg/mm^2) is the shear modulus of the primary coating. The other terms are defined in Figure 1.

From measurements of the stress and the displacement, the shear modulus of the primary coating material can be determined from equation (1) as :

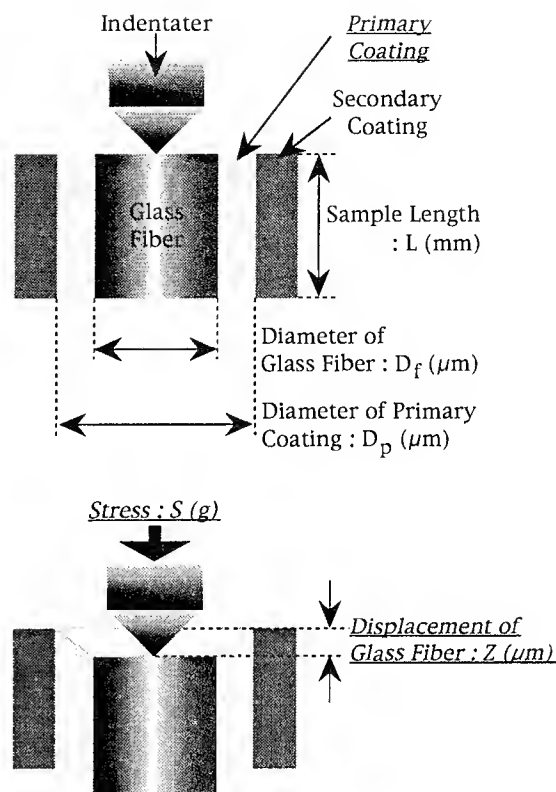


Figure 1 Scheme of PIM test

$$G = \frac{S}{2\pi L Z} \ln \left(\frac{D_p}{D_f} \right) \dots \dots \dots (2)$$

The equilibrium tensile modulus (Young's modulus), E (kg/mm^2), for a low modulus material is,

$$E = 2(1 + \nu) G \dots \dots \dots (3)$$

$$\therefore E = \frac{(1 + \nu) S}{\pi L Z} \ln \left(\frac{D_p}{D_f} \right) \dots \dots \dots (4)$$

where ν is poisson's ratio. Since past modulus results from the cured film of coating materials are reported as the tensile moduli, we calculate our results in terms of the tensile modulus from equation (4).

2-2. PROCEDURE

The procedure of the sample preparation is diagrammed in Figure 2. A bundle of dual coated

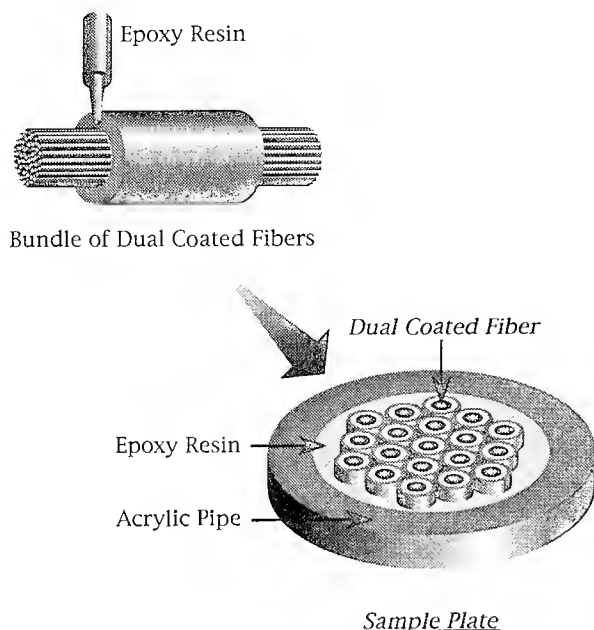


Figure 2 Diagram of sample plate
for PIM

fibers is inserted into acrylic pipe (inner diameter : 4mm ϕ , and outer diameter : 8mm ϕ) and settled using epoxy resin. The acrylic pipe with many dual coated fibers is sliced off in length of about 5mm and polished the both sections using the "Polishing Machine" (model PS-2000i, Polysys, Japan). In order to make each glass fiber free to move axially, the sample plate was kept off the ground and mounted on the "Dynamic Ultra Micro Hardness Tester (model DUH-50, Shimadzu, Japan)". The stress is axially exerted on the center of the glass fiber by indentater, see Figure 1. The tensile modulus is calculated by the equation (3) using the displacement of the glass fiber and the stress when the indentater presses the glass fiber axially.

3. EXPERIMENTAL

We tried to evaluate the cure degree of the coatings with the alternate conventional measurement techniques and the "PIM" test.

3-1. DESCRIPTION OF OTHER METHODS

• MEK Extraction Test

This is the oldest and most widely used technique in fiber industry, and is therefore regarded as a standard test method for comparison.

This test enables extraction of all the coating material which is not polymerized. About 0.15g of the coating material was weighed and extracted for 16hours with MEK (Methyl Ethyl Ketone) at 60°C. The gel fraction percentages (%GF) were calculated by the following equation :

$$\%GF = \frac{\text{weight (after extraction)}}{\text{weight (before extraction)}} \times 100 \dots (5)$$

• Tensile Modulus Test

For this measurement, we took the test specimens from the fibers directly. The tensile modulus was measured by a standard method (the modulus was defined by 2.5%-secant modulus). We performed this test at 1mm/min tensile speed using a 25mm gauge length for all sample.

• FT-IR Microscope Method

FT-IR measures the change in acrylate absorbance at 810cm⁻¹, which wavelength is characteristic of the reaction of functional groups like the double bond (-C=C-) in the monomer. In the polymerization reaction the double bond disappears and the absorbance at this specific wavelength changes. FT-IR measures the concentra-

tion of monomers that have not reacted. The measurement signal for the liquid coating material is set to 0% and that for a deliberately fully cured coating to 100%. We used FT-IR microscope (micro FT-IR) for measuring double bond content at the primary coating with 15 μ m thickness sliced primary coating.

• Strippability Test

This test is a measure of the stripping force of the coating materials from the glass fiber.

The coating was removed from the fiber with a stripping tool. The force required for this removal was measured with a tensile tester. We performed this test at 10mm/min stripping speed using a 10mm gauge length for all samples.

3-2. FILM PREPARATION

The film preparation was as follow : primary coating material is placed on a Poly Ethylene Terephthalate (PET) sheet. Coating material were then cured to different levels of UV dose. The UV dose was measured using the UV dose apparatus (model UV-M10, Orc, Japan). We obtained films that were uniformly cured as well as of uniform thickness (about 130 μ m).

3-3. FIBER PREPARATION

A few hundreds of the test fibers were drawn from one preform, at different speeds with the same number of UV curing ovens. The same primary and secondary coating materials were used for all fibers. Drawing and coating condition were maintained approximately constant for all test fibers.

4. RESULTS AND DISCUSSION

4-1. ADVANTAGE OF TENSILE MODULUS

We compared the tensile modulus test with the MEK extraction using the film of primary coating materials. The relationship between cure degree and UV dose was illustrated in Figure 3. The cure degree was then obtained:

$$\text{Cure degree (\%)} = \frac{\text{each value}}{\text{value}_{1000}} \times 100 \dots \dots \dots (6)$$

where value₁₀₀₀ is tensile modulus or gel fraction of film at 1000mJ/cm² UV dose.

The results with the films point to a constant extraction loss from 100mJ/cm² UV dose onwards, for our coating material and our application technique. This 100mJ/cm² UV dose point is therefore defined as the 100% cure point by the MEK extraction test.

On the other hands, with the tensile modulus test, the coating material seemed to be fully cured at 500mj/cm² UV dose, again for our coating material and application technique. This means that the tensile modulus test is more sensitive to cure state than the MEK extraction test.

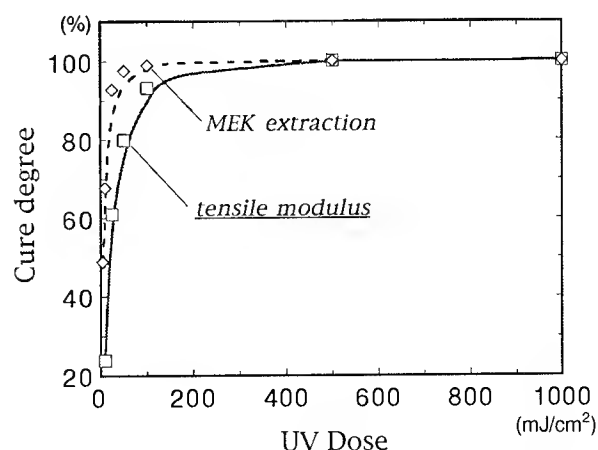


Figure 3 Cure degree with tensile modulus and MEK extraction

Furthermore, the MEK extraction test itself takes about one days, which is too long for process control in production. The tensile modulus measurement is preferable to the MEK extraction.

4-2. ADVANTAGE OF PIM TEST

The various measurement techniques were conducted to ensure the sensitivity of the PIM test using the test fibers. The relationship between cure degree and relative draw speed was shown in Figure 4 and Table 1. The cure degree was then obtained :

$$\text{Cure degree (\%)} = \frac{\text{each value}}{\text{value}_1} \times 100 \dots \dots \dots (7)$$

where value₁ is the value with each measurement for fiber coatings at one relative draw speed.

The precision was then obtained :

$$\text{Precision} = \frac{\text{standard deviation}}{\text{each value}} \times 100 \dots \dots \dots (8)$$

At over a wide range of draw speed, the MEK extraction and the FT-IR microscope showed little variation (nearly 100% cure area), for our coating material and our application technique. On the other hand, the strippability, the "PIM" and the tensile modulus (by conventional method) varied dramatically. This means that strippability, the

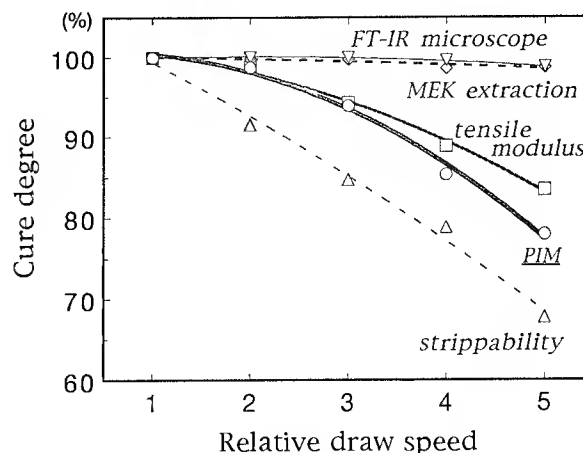


Figure 4 Comparison of the cure degree with various measurement techniques

"PIM" and the tensile modulus should allow more meaningful interpretation at near 100% cure area by the MEK extraction test. In the FT-IR microscope method, the resolving power of IR absorbance spectrum is extremely low, because of the small double bond contents of the primary coating material and the noisy IR spectrum due to the small measurement area.

As stated before, the tensile modulus (by conventional method) only measures the cure degree of the secondary coating (the secondary coating is at least three orders of magnitude stiffer than

Table 1 Summary of the cure degree with various measurement techniques

relative draw speed	MEK Extraction	Tensile Modulus	FT-IR Microscope	Strippability	Push In Modulus
1	100.0%	100.0%	100.0%	100.0%	100.0%
2	99.82%	98.89%	100.0%	91.53%	98.78%
3	99.76%	94.28%	100.0%	84.75%	93.90%
4	98.63%	88.87%	99.59%	78.93%	85.37%
5	98.75%	83.48%	98.79%	67.80%	78.05%
<i>precision_{max}</i>	0.9%	6.3%	73%	10%	5.0%

* *precision_{max}* is the maximum value of each precision obtained from five fibers drawn at different speeds

the primary coating). The strippability is affected by not only modulus of the primary coating but also modulus of the secondary coating and adhesion between the primary coating and the glass fiber.

For these reasons, the "PIM" test is the only technique to evaluate the modulus of the primary coating directly, and should allow evaluating of more slight difference of the cure degree.

The "PIM" test gives us simple and quick measurement using "Dynamic Ultra Micro Hardness Tester", computer analysis system and sample plate.

5. CONCLUSION

We have developed the "Push In Modulus (PIM) Test" to measure the tensile modulus of the primary coating material on a dual coated optical fiber directly. The results of the "PIM" test for the test fibers showed the reasonable draw speed dependence with better sensitivity and reproducibility than conventional measurement techniques. We are confident that the "PIM" test has led to the convenient, accurate in-process evaluation technique for the cure degree of the primary coating.

6. REFERENCES

- [1] R. A. Frantz, et al., "Evaluation of Techniques for Determining The Extent of Cure of Optical Fiber Coatings", Proceeding of the 40th IWCS, p134-p140, 1991.
- [2] H. Marsman, et al., "Coating Stripping Force Measurement : A New and Quick Test Method for The Determination of The Degree of Curing for Optical Fiber Coating", Proceeding of the 40th IWCS, p815-p818, 1991.
- [3] E. Cressman, et al., "The Effects of Environment on Ultra-Violet Curable Optical Fiber Coatings", Proceeding of the 42nd IWCS, p843-p849, 1993.
- [4] A. Mizutani, et al., "Application of FT-IR to The Cure Degree Measurement of UV Curable Optical Fiber Coating", Proceeding of the 41st IWCS, p249-p252, 1992.
- [5] C. R. Taylor, "In Situ Mechanical Measurements of Optical Fiber Coatings", Meeting Digest of OFC '85, p20-p21, 1985.
- [6] J. W. Shea, et al., "Characterization of Critical Properties of Optical Fiber Coatings", Mat. Res. Soc. Symp. Proc., Vol 244, 1992.



Kazumasa OISHI

*Sumitomo Electric
Industries, Ltd.*

*1, Taya-cho, Sakae-ku
Yokohama, JAPAN*

Kazumasa Oishi received his M.S. degree in Geochemistry from Tsukuba University in 1991. He joined Sumitomo Electric Industries, Ltd. in 1991, and has been engaged in research and development of optical fiber and cables. He is a member of Transmission Media Department in Yokohama Research Laboratories.



Tatsuya KAKUTA

*Sumitomo Electric
Industries, Ltd.*

*1, Taya-cho, Sakae-ku
Yokohama, JAPAN*

Tatsuya Kakuta received his M.E. degree in Applied Chemistry from Osaka University in 1985. He joined Sumitomo Electric Industries, Ltd. in 1985, and has been engaged in research and development of optical fiber and cables. He is a senior engineer of Transmission Media Department in Yokohama Research Laboratories and a member of Institute of Electronics and Communication Engineers of Japan.



Nobuhiro AKASAKA

*Sumitomo Electric
Industries, Ltd.*

*1, Taya-cho, Sakae-ku
Yokohama, JAPAN*

Nobuhiro Akasaka received his M.E. degree in Chemical Engineering from Tokyo University in 1983. He joined Sumitomo Electric Industries, Ltd. in 1983, and has been engaged in research and development of optical fiber and cables. He is a senior engineer of Transmission Media Department in Yokohama Research Laboratories.



Yasuo MATSUDA

*Sumitomo Electric
Industries, Ltd.*

*1, Taya-cho, Sakae-ku
Yokohama, JAPAN*

Yasuo Matsuda received his M.E. degree in Chemistry from Tokyo University in 1978. He joined Sumitomo Electric Industries, Ltd. in 1978, and has been engaged in research and development of optical fiber and cables. He is a chief research associate of Transmission Media Department in Yokohama Research Laboratories.



Tomoyuki HATTORI

*Sumitomo Electric
Industries, Ltd.*

*1, Taya-cho, Sakae-ku
Yokohama, JAPAN*

Tomoyuki Hattori received his M.E. degree in Chemistry from Kyoto University in 1987. He joined Sumitomo Electric Industries, Ltd. in 1987, and has been engaged in research and development of optical fiber and cables. He is a member of Transmission Media Department in Yokohama Research Laboratories and a member of Institute of Electronics and Communication Engineers of Japan.

REDUCING TOXIC AIR EMISSIONS BY REPLACING METHYL ETHYL KETONE INKS AND SOLVENTS WITH AQUEOUS INKS FOR MARKING PVC INSULATED CONDUCTORS

Bruce M. Brokke
AT&T Network Cable Systems
Phoenix, AZ

John E. Bosak
AT&T Network Cable Systems
Phoenix, AZ

Tony Davidow
Toncee, Inc.
Smyrna, GA

Abstract

A primary environmental goal of the AT&T Phoenix Works was to completely eliminate toxic air emissions by 1994. To achieve this goal methyl ethyl ketone (MEK), the major contributor used in the manufacturing process of marking polyvinyl-chloride insulated conductors had to be eliminated. This was accomplished by substituting acrylic aqueous inks for the MEK inks resulting in a higher quality product with substantial savings in disposal, cleaning, and labor costs.

INTRODUCTION

AT&T is committed to a leadership position in environmental protection and has world-wide goals of zero toxic air emissions for all major manufacturing facilities by the year 2000. The goal of Network Cable System's Phoenix Works was to reduce toxic air emissions to zero by 1994. To achieve this goal, all contributors of toxic air emissions had to be either eliminated or replaced with an environmentally friendly substitute. The major contributor of toxic emissions at the Phoenix Works was MEK inks and MEK solvent. MEK was used in the manufacturing and cleaning processes for marking PVC insulated conductors as shown in Figure 1. The proposed MEK substitute was an acrylic latex aqueous ink, jointly developed by AT&T and Toncee.

PROBLEM STATEMENT

To accomplish zero toxic emissions, the Phoenix Works and Toncee needed to develop an environmentally friendly substitute for MEK inks and solvents that would satisfy the following conditions:

DESIGN CRITERIA

1. Maintain and/or improve the color definition of the ink mark applied on PVC insulated conductors.
2. Maintain and/or improve the abrasion

resistance of the mark throughout the manufacturing process.

3. Maintain and/or improve the manufacturing line speeds and batch load running times with minimal changes to the existing application and delivery system to accommodate the new ink.
4. Maintain and/or reduce the labor required to service the ink application system and cleaning services.

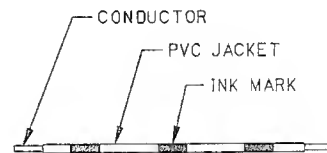


FIGURE 1: PVC INSULATED CONDUCTOR

THE APPLICATION PROCESS

The diagram in Figure 2 identifies the delivery and application system for marking insulated conductors. The purpose of the ink application system is to supply a constant amount of ink to the coder disks. In addition, the motor/pump must provide agitation of the ink to keep the ingredients in suspension. The ink is pumped through the prefilter assembly up to the distributor manifold assembly, where it is distributed to the two rotary unions, and then into each coder disk. Each disk contains a filter similar to the prefilter to prohibit small particles from plugging the small coder disk holes. In order to produce high quality marks, these holes must be kept free of contamination.

The serving head contains the ink spray, as well as routing the ink overspray away from the wire as it passes through the serving head. Improper drainage will result in ink drops falling onto the wire, and therefore, improper marks on the wire. The serving head also collects the additional ink and returns it to the bucket

via the drain where it is again mixed in solution.

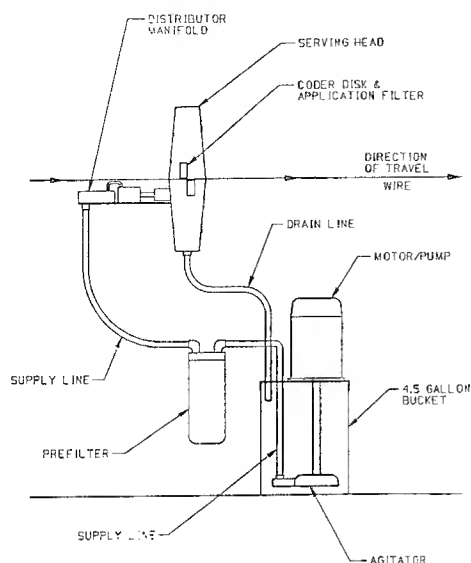


FIGURE 2: INK APPLICATION SYSTEM

THE COLOR DEFINITION

Maintaining the correct viscosity of the MEK inks during the manufacturing process was critical for good color definition. The high evaporation rate of MEK created problems in maintaining the proper viscosity during the manufacturing process. The continual evaporation of the MEK ink was especially significant in warm environments. Color code definition is directly related to viscosity. Therefore the definition of the mark will vary with the viscosity. Evaporation increases the viscosity of the MEK ink, causing both the prefilter and coder disk to begin to plug. The restricting flow of ink results in poor quality marks in both coverage and spacing. Correcting the high viscosity problem by adding MEK was subject to human error. Operator over-adjustments cause too low a viscosity, resulting in a poor quality, light colored mark. This battle to maintain the correct viscosity to produce high quality marks consumes valuable time of both the line operators and the ink coding operator. The maintenance of the proper viscosity in the aqueous inks during the manufacturing process was critical for success. This viscosity concern was addressed AND COMPLETELY CORRECTED IN THE DEVELOPMENT OF THE AQUEOUS INKS. The new aqueous inks maintain constant viscosity during the entire manufacturing process. This improvement greatly reduced plugging of both the prefilter and coding disk during the manufacturing process. (Improvement was realized using new filters - See section on Follow Up And Control) A typical manufacturing run will usually last 12 hours, consuming about 5 gallons of ink. The new aqueous ink can be added to the reservoir without

affecting the viscosity, thereby extending production runs of the same color. The viscosity of aqueous inks remain stable well beyond 48 hours. This stability is a requirement for reusing leftover ink at a later date.

Stable viscosities throughout the manufacturing process produce very uniform coatings. This is the result of the slower drying speeds of the aqueous inks. The ink exiting the coder disk delivers a very uniform coat because vaporization and drying is minimal prior to contacting the .350" PVC jacket. This was not the case with MEK inks because of its low flash point. The aqueous inks produced a higher quality uniform coverage which increased the overall color brightness of the mark.

ABRASION RESISTANCE

The abrasion resistance of MEK ink on the PVC jacket was generally acceptable. The major benefit of its fast drying characteristics was the minimal bleed-off upon hitting the cooling trough after the application head. Still, MEK's abrasion resistance did not fully pass all the manufacturing operations unscathed. Persistent problems of residue build up would occur in the next operation of twisting the insulator conductors together. Build up would occur on the twister bows over a period of weeks. This shortcoming was addressed in the development of the aqueous inks. It was determined that the selection of the acrylic emulsion in the aqueous inks would have to be a high molecular weight to improve toughness and abrasion. For added toughness, additives were selected to improve the adhesion to the PVC jacket and abrasion, thereby increasing its abrasion resistance. As a result, the aqueous inks have proven superior in their abrasion resistance throughout the manufacturing process. Machine downtime in the Twist operation due to residue build is nonexistent.

MAINTAINING THE MANUFACTURING ENVIRONMENT

Financial considerations played a significant role in the design criteria. The need to maintain the manufacturing environment with the existing process equipment in the conversion to aqueous inks was crucial for success. Major modifications to the applicator, coder tooling, and delivery system would prove time consuming and very expensive, because it would require extensive training for both operators and maintenance personnel. In converting to aqueous inks, the existing line speeds and color batch sizes had to be maintained.

The process for accomplishing the above was very complex. Applying aqueous inks with the same process and on the same equipment presented a multitude of problems. The MEK inks have a PVC medium molecular

weight co-polymer resin as the vehicle for pigments. MEK re-solubilizes any dried ink in the delivery process, thus eliminating the problems of skinning and build-up. MEK inks evaporate very rapidly, therefore drying is not a problem. Since the MEK inks do not foam in the manufacturing process where aqueous inks do, modifications were required to process the aqueous inks.

Applying the aqueous inks with the same delivery equipment required process and handling modifications for successful substitution. The high molecular weight acrylic aqueous emulsions did not have an affinity to PVC, requiring additives to be added to the emulsion to improve adhesion. These additives caused foaming during the application process. To correct the foaming problem, a defoamer was added which sustained consistency for 100 hours without affecting the adhesion of the ink. Foaming was also reduced by selecting the correct type and amount of dispersant used for dispersing the pigment. Various additives were evaluated and added for improvement of the abrasion characteristics, without causing incompatibility or foaming. The use of additives and solvents contributed to controlling the skinning of the ink, while improving its drying characteristics. All the above, achieved the desired results of a simple changeover to aqueous inks.

IMPLEMENTATION OF THE AQUEOUS INKS

After various prove-in trials, the transition to the aqueous inks began in January of 1993. The long term introduction of the aqueous inks in the manufacturing process presented problems in two areas: 1) The ink application system, and 2) The cleaning facility required to service the application equipment. Both situations were interlinked and serious. The quality of the ink marks were better than anticipated, but the line operators and coding operators were struggling to use the new ink with the existing process equipment.

The main problem with the ink application system was premature blockage of the coder disk, coder filter, and the delivery system's prefilter. This would occur at various times between the three components throughout the shift. The blockage occurred because the reusable stainless steel mesh filters inside the coder disk and prefilter originally designed for MEK inks caused problems with the aqueous inks. The problem was magnified by the existing set-up procedure used for cleaning the filters.

The original cleaning facility proved inefficient for the transition to aqueous inks. When using MEK inks, the mesh filters could be cleaned thoroughly with MEK. This was not the case with the aqueous inks. Additionally, there were no environmentally friendly thinners or cleaners for the aqueous inks which cleaned

the mesh filters. The adhesion of the aqueous inks to the mesh filters proved impossible to clean thoroughly after three manufacturing applications. This, coupled with the ink buildup on leftover residue, aggravated the problem even further. The situation was potentially a financial disaster, considering the average replacement cost of the stainless steel prefilter was nearly \$40 each.

The solution to the blockage and cleaning problems was to replace the reusable mesh filters with disposable polypropylene filters. The selection of the filter's micron rating was based on maximizing the running time of the coder disk. The mechanical modification was simple and cheap. Installing the new polypropylene prefilter housings on all the delivery systems cost only \$1500, and was completed in less than a week. Also, the installation required no machine downtime or operator training. The costs of the new disposal filter are a \$1.50 each. More importantly, it was this particular modification to the manufacturing line that removed any doubts that operating personnel had with using the new aqueous inks.

The solution to improve the cleaning process was slightly more complicated. Engineering required that operating minimize their use of clean water, as well as recycling process water in the cleaning process. To accomplish this, engineering installed a closed-loop cleaning system as shown in Figure 3. Engineering also removed all drains from the cleaning room to discourage operators from dumping unprocessed waste water into the plant's reclaim system.

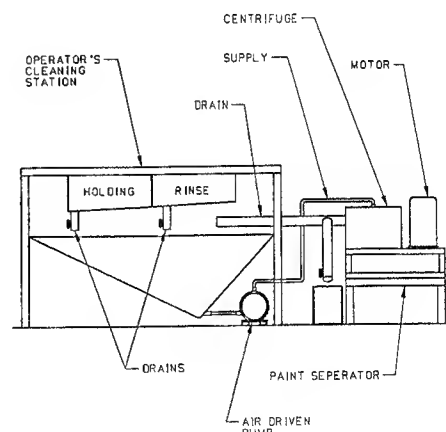


FIGURE 3: CLEANING CLOSE-LOOP SYSTEM

The cleaning process itself was greatly simplified by the addition of the disposable filters. The process consisted mainly of cleaning the prefilter housing, coder disk, and flushing of the pumps at the end of the week. All of this was accomplished by incorporating a paint separator in the closed-loop cleaning facility shown in Figure 3. The

paint separator is simply a high speed centrifuge, continuously separating liquids and solids. An air-driven pump supplies process water to the separator, which then drains back to the reservoir. The aqueous pigment is deposited to the walls of the separator, and must be manually cleaned once a day. Once an acceptable amount of pigment has been removed, the excess water can be deposited and reused in the trough reservoirs of the production lines.

FINANCIAL BENEFITS OF AQUEOUS INKS

The financial benefit of eliminating MEK ink and solvents from the manufacturing process is substantial. Hazardous waste disposal costs were completely eliminated. The disposal costs for MEK in Phoenix is listed in Table 1.

Table 1: MEK Disposal Costs

Year	Wt (lbs)	Costs (\$)
1993	13,000	\$ 9200*
1992	12,980	\$ 9100
1991	13,840	\$ 9700
1990	21,300	\$ 14900
1989	20,480	\$ 14400

*Estimated savings, costs not incurred

There weren't any disposal costs generated in 1993. The estimated savings disposal costs incurred is \$9,200. This, coupled with the fact that MEK was no longer required in the cleaning or thinning processes provided additional savings as well. Estimated savings in costs not incurred for MEK was \$18,100 for 1993. The usage of MEK as a solvent is listed in Table 2.

Table 2: MEK Solvent Use

Year	Wt (lbs)	Cost (\$)
1993	33,000	\$ 18,100*
1992	36,100	\$ 19,900
1991	48,100	\$ 26,500
1990	70,700	\$ 38,900
1989	58,020	\$ 31,900

*Estimated savings, costs not incurred

Operating also realized substantial labor savings with the new aqueous inks. With the MEK inks, the Operating department required at least one coder operator for every four lines in service. For eight production lines, three operators were required with the third dedicated to the cleaning facility. This all changed with the introduction of aqueous inks and the disposable filter. Coder operators were no longer required to monitor viscosity levels, or clean stainless steel mesh filters. The simplicity of the modified delivery system allowed the line operators to change the disposable prefilters themselves, relieving the pressures on the coder

operators. Today, one coder operator can successfully manage up to eight production lines, as well as the cleaning facility.

CONCLUSIONS

In 1993, the Phoenix Works successfully replaced MEK inks and solvents with aqueous inks in the manufacturing process of marking PVC insulated conductors. The color definition quality of the the aqueous mark is better than the previous MEK inks. The abrasion resistance of the aqueous ink mark is superior to MEK. The transition to aqueous inks did not effect manufacturing line speeds, or include large mechanical changes. The manufacturing batch size and production running time using aqueous ink, increased with the advent of the disposable polypropylene filters. The cleaning facility was improved with the aqueous inks by using a closed-loop cleaning process. Substantial savings were realized by eliminating MEK disposal and cleaning costs.

ACKNOWLEDGMENTS

Chuck Cantrell
Environment Health & Safety
AT&T Network Cable Systems

Jerry Obertynick
Mechanical Designer
Butler Services

BIOGRAPHIES



Tony Davidow, President of Toncee, Inc. in Smyrna, GA has a B.S. from Rutgers University, and has been involved in the technical aspects of the vinyl industry for more than 30 years. Toncee, founded by Mr. Davidow in 1981, develops and manufactures specialty colorants and coatings for applications in the following industries: wire and cable, automotive, wallcoverings, defense, shoes, handbags, and outdoor furniture. Toncee is a recipient of AT&T's "Partners in Quality" award, and is a certified vendor to AT&T.



Bruce M. Brokke received a Bachelor of Science degree in Industrial Engineering from North Dakota State University in 1961. He is currently a Member of Technical Staff for AT&T Network Cable Systems at Phoenix, Az. He has worked in the Plastic Insulate area for twenty five years. Mr. Brokke has been awarded a patent for an Insulate Transfer Mechanism, has authored two previous articles, and is an active member of the Society of Plastics Engineers.



John Bosak is a Member of Technical staff for AT&T Network Cable Systems in Phoenix, Arizona. He received his B.S. in Mechanical Engineering from Northern Arizona University. John joined AT&T in 1988, and has worked primarily in Plant and Factory Engineering.

MECHANICAL PROPERTIES OF AGED FIBER COATINGS BY DYNAMIC MECHANICAL ANALYSIS OF OPTICAL FIBERS

O.S.Gebizlioglu*, I.M. Plitz*, R.A. Frantz**

Belcore

*331 Newman Springs Rd.
Red Bank, New Jersey 07701

**445 South Street
Morristown, New Jersey 07962

ABSTRACT

A dynamic mechanical analysis (DMA) technique, commonly used for polymeric materials, was adapted to optical fibers for direct measurements of storage modulus (E')/loss tangent ($\tan \delta$) - temperature profiles of coatings. This technique involved testing a parallel array of optical fibers in single cantilever bending. The measured E' and $\tan \delta$ profiles for unaged dual-coated fibers showed an inner primary glass transition temperature (T_g) at about 29 °C and an outer primary T_g at 60 °C. While the DMA spectra for fibers aged for 30 days at 85 °C with uncontrolled humidity indicated some cross-linking, samples aged for 30 days in 85 °C deionized (DI) water exhibited a 6 °C rise in T_g and a 4% volume shrinkage. This substantial rise in T_g and up to a 40 % increase in the optical fiber E' for both humidity and DI-water aged fibers suggest that some degradation of the dual-layer coating structure accompanies the loss of water-extractable coating components.

INTRODUCTION

Polymer coatings are essential in isolating the glass fiber from the environment and in protecting against mechanical stresses during the handling and installation of optical cables. These materials are applied as a liquid mixture to the glass fiber and cured by exposure to ultraviolet (UV) light. During the curing process, an extensive three-dimensional network structure develops by the cross-linking reactions. The key properties of this cross-linked material include the extent of cross-linking (or the degree of cure) expressed by the cross-link density (number of cross-linkages per unit volume), the modulus (a measure of deformation resistance or

stiffness), and the glass transition temperature (T_g). The modulus of the coating, in particular, exhibits strong time and temperature dependence. Hence, the relationship of the long-term mechanical behavior of fiber coatings to the reliability of optical fibers has attracted considerable attention.⁽¹⁻⁷⁾

Despite the widespread interest in the long-term performance of fiber coatings, measurements of the coating mechanical properties remained limited to dynamic mechanical analysis (DMA) of free-standing coating films tested in tension. In an earlier report,⁽⁸⁾ we showed that DMA in single cantilever bending can be applied to optical fibers to directly assess the time- and temperature-dependent coating mechanical properties. This technique was developed for a parallel array of about one-inch lengths of optical fibers subjected to single cantilever bending. In this communication, we demonstrate that the DMA of aged optical fibers can identify the effects of different aging environments on the coating materials. Fundamentals of the DMA technique were presented earlier⁽⁸⁾ and reproduced in Appendix A. Also included in this Appendix is the derivation of the geometry factor used in the calculation of the optical fiber storage modulus for a parallel array of optical fibers tested in single cantilever bending.

EXPERIMENTAL MATERIALS AND METHODS

The dual-coated optical fiber used in this study was drawn in an approximately 2.5-kilometer length from a standard fused silica preform.⁽⁷⁾ While one portion of

Copyright © 1994 Bellcore. All rights reserved.

this fiber was tested in the unaged condition, the remaining lengths were exposed to three aging environments:

- In an oven at 85 °C with uncontrolled humidity (Aging Condition 1). The temperature control was within ± 1 °C, and the relative humidity was below 30%.
- In an environmental chamber operated at 85 °C and 85% RH (Relative Humidity) (Aging Cond. 2). The humidity was controlled to within ± 4 %.
- In 85 °C deionized water (Aging Condition 3). The temperature was controlled to within ± 0.5 °C. The pH of the water was maintained at 7.0 ± 0.5 using a buffer solution.

The fiber samples were exposed to these three aging environments as loose coils. In this report, we will limit our discussion to the 30-day aging effects on the fiber coatings.

For dynamic mechanical analysis, we used a Polymer Laboratories DMTA (Dynamic Mechanical Thermal Analyzer) Mark III. To maximize signal-to-noise ratio and reproducibility in the fiber measurements, the optimum test configuration was a parallel array of non-contacting optical fibers placed in a modified film clamp as shown schematically in Figure 1. The clamp faces for both the stationary and drive (moving) clamps were machined to have twelve V-grooves. Nineteen-millimeter (three quarters of an inch) long fibers were mounted into these grooves with a small spot of a cyanoacrylate adhesive. The fiber free length (or cantilever length) was 2 millimeters. The temperature range for the DMTA scans was from -100 °C to 100 °C, and the thermal scan rate was 2 °C per minute. The measurement frequency was 1 Hertz (Hz). Optical fiber diameters were measured with an Anritsu laser micrometer.

RESULTS AND DISCUSSION

Figures 2a and 2b present DMA spectra for the storage modulus and loss tangent, respectively. These figures compare the dynamic mechanical spectra for fibers exposed to the three aging conditions described in the preceding section. In the storage modulus spectra of Figure 2a, we see two distinct regions. On the far left (the glassy region) and far right (the rubbery plateau region), the storage moduli are independent of temperature. Over the temperature range from about

20 °C to 50 °C, the storage modulus profiles drop with temperature by nearly an order of magnitude and go through an inflection. Over the same temperature range, the loss tangent ($\tan \delta$) profiles of Figure 2b show maxima. These $\tan \delta$ maxima signify the glass transition temperatures of the coating layers on the optical fiber. Before discussing the magnitude of aging-related changes in the DMA spectra, we first address the appearance of one major and broad glass transition region in the DMA spectra obtained in single cantilever bending.

In an earlier publication,⁽⁸⁾ we showed that the modulus drop and the $\tan \delta$ peak in the DMA spectrum of a dual-coated optical fiber originate from the dual-layer coating. When tested in tension, a free-standing film of each coating layer gives distinct modulus and loss tangent spectra as shown in Figures 3a and 3b. The modulus spectra reveal that the inner and outer primary coating layers are comparable at low temperatures, but that they differ greatly at temperatures above about 0 °C. Figures 3a and 3b show an inner primary coating T_g at 29 °C and an outer primary T_g at 59 °C, respectively. In Figure 4, we present the DMA spectra for a free-standing dual-layer (composite) coating film. This figure shows one major T_g located close to the T_g region of the outer primary coating. A $\tan \delta$ peak value of about 0.4 further indicates that the DMA response of this composite coating film is dominated by that of the outer primary coating. We computed the composite modulus of an optical fiber by adding the product of E' (storage modulus) and I (area moment of inertia about the fiber centroidal axis) for the glass fiber and the inner and outer primary coatings. In Figure 5, we compare the optical fiber modulus calculated from component moduli measured by DMA with the optical fiber modulus measured in single cantilever bending. The inflection points on both modulus traces are located near 33 °C, i.e., closer to the inner primary T_g . Of the two coating layers, the inner primary exhibits more than twice as much mechanical loss (indicated by the $\tan \delta$ peak value) as the outer primary. Furthermore, the $\tan \delta$ spectrum for the unaged fiber in Figure 2b shows a shoulder located at about 60 °C with a $\tan \delta$ peak value of 0.06. This shoulder is reminiscent of the outer primary coating glass transition peak. The peak value of 0.06 is about half the $\tan \delta$ peak value for the major peak at 33 °C.

Focussing our attention on the $\tan \delta$ profiles of the aged coatings in Figure 2b, we note that the $\tan \delta$ peak temperature rises to 33 °C for aging condition 1 (85 °C with uncontrolled humidity), 34 °C for aging condition 2 (85 °C / 85% RH), and 35 °C for aging condition 3 (85 °C DI water). The distinct 60 °C shoulder present in the unaged $\tan \delta$ profile seems to have disappeared for the aged fiber profiles. However, a closer examination reveals that significant peak broadening due to aging would cover any peaks in the 60 °C region. Moreover, the DI-water aging gives rise to a secondary $\tan \delta$ peak of 0.06 at about 88 °C. In Table 1, we present a summary of the aged fiber characteristics, namely, fiber diameters, glass transition temperatures, and $\tan \delta$ peak values from the DMA spectra of Figure 2b. This table shows that the aging media can be ranked in the increasing severity of changes shown in the $\tan \delta$ profiles as follows: 1) 85 °C with uncontrolled humidity, 2) 85 °C / 85% RH, 3) 85 °C DI water (The T_g , $\tan \delta$ peak value, and the volumetric change upon 30-day aging are the highest). In cross-linked polymers, an upward trend in T_g is normally associated with a significant increase in the cross-link density in the absence of other mechanisms such as the loss by extraction or leaching of low molecular weight fractions and additives that are not incorporated into the network structure. In both cross-linking and the loss of small molecular components, the $\tan \delta$ peak value would decrease. Contrary to the $\tan \delta$ trend expected from these processes, Table 1 indicates that the $\tan \delta$ peak value increases with the volumetric shrinkage upon aging. We note that the $\tan \delta$ peak value did not change during aging condition 1 while the T_g increased by 5 °C and the sample shrank volumetrically by 1.6 %. If these changes resulted from thermally-driven cross-linking, one would expect to see some increase in the rubbery plateau modulus to the right of the T_g region in the modulus profiles of Figure 2a. To reveal changes in the fiber moduli more clearly, we present in Figure 6 modulus profiles normalized to the modulus profile of the unaged sample. The normalized modulus profile for aging condition 1 remains close to 1, suggesting that the storage modulus of the aged sample did not change appreciably from that of the unaged fiber. This observation, in turn, points out that 1.6 % by volume shrinkage may have resulted from small-scale cross-linking (and/or the loss of some components) that might not significantly affect the composite fiber modulus. Therefore, the changes summarized in

Table 1 for aging conditions 2 and 3 clearly indicate the added effect of humidity or liquid water at 85 °C. The normalized modulus profiles for aging conditions 2 and 3 with the volumetric shrinkage figures in Table 1 suggest that a combination of water-induced degradation and extraction of component materials from the coatings may have taken place with or without cross-linking, thereby supporting similar conclusions drawn in earlier investigations.^(6,9)

SUMMARY AND CONCLUSIONS

We applied dynamic mechanical analysis to optical fibers to directly measure storage modulus (E') / loss tangent ($\tan \delta$) - temperature profiles of fiber coatings. The optimum deformation mode for DMA of optical fibers was single cantilever bending. We used a special set of clamps that contained a parallel array of V-grooves on the clamp faces to hold the optical fibers. The storage modulus and loss tangent profiles of the unaged fibers exhibited a major glass transition near 29 °C with a $\tan \delta$ peak value of 0.12 and shoulder at 60 °C with a $\tan \delta$ peak value of about 0.6. The major transition appeared near the T_g of a free-standing inner primary film measured in tension while the shoulder was close to the T_g of the outer primary coating film. Aging for 30 days at 85 °C resulted in a 1.6 % by volume shrinkage and 5 °C rise in T_g , thereby suggesting some cross-linking and/or the loss of low molecular weight coating components. However, the extent of this cross-linking was not large enough to raise the rubbery plateau modulus of the composite coating. The most severe aging environment was DI water at 85 °C. A 4.1% shrinkage accompanied a 40 % increase in the fiber composite modulus and represented primarily the loss of coating components by extraction and/or some water-induced degradation.

REFERENCES

1. J.T. Krause, *J.Non-Cryst. Solids*, **38 & 39**, 497 (1980).
2. T. Wei, *Adv. Ceram. Mater.*, **1**, 237 (1986).
3. J.E. Ritter, T.H. Service, K.Jakus, *J. Amer. Ceram. Soc.*, **71(11)**, 988 (1988).
4. T. Wei, B.J. Skutnik, *J. Non-Cryst. Solids*, **102**, 100 (1988).
5. K.E. Lu, G.S. Glaesemann, R.V. Vandewoestine, G. Kar, *J. Lightwave Tech.*, **6(2)**, 240 (1988).

6. R.A. Frantz, I.M. Plitz, H.H. Yuce, O.S. Gebizlioglu, *IWCS Proc.*, **41**, 279 (1992).
7. H.H. Yuce, R.A. Frantz, O.S. Gebizlioglu, I.M. Plitz, T.T. Volotinen, *IWCS Proc.*, **42**, 857 (1993).
8. O.S. Gebizlioglu, P.B. Grimado, I.M. Plitz, R.A. Frantz, *SPIE Proceedings*, Vol. 2290, (1994).
9. J. Julian, C.P. Chawla, *RadTech '92 N. Amer. UV/EB Conf. Proc.*, p 315 (1992).
10. R.J. Roark and W.C. Young, "Formulas for Stress and Strain, 5th Ed.," McGraw-Hill, New York, p 91 (1982).
11. R.J. Roark and W.C. Young, "Formulas for Stress and Strain, 5th Ed.," McGraw-Hill, New York, p 96 (1982).

APPENDIX

DYNAMIC MECHANICAL ANALYSIS

For a polymeric material, a sinusoidally varying strain leads to a cyclic stress that lags behind the strain as shown in the following expressions

$$\varepsilon = \varepsilon_0 \sin \omega t \quad (1)$$

$$\sigma = \sigma_0 \sin(\omega t + \delta) \quad (2)$$

where δ is the phase angle or phase lag describing the relative angular displacement of stress and strain shown in Figure 7. Expanding Eq. 2 for stress gives

$$\sigma = \sigma_0 \cos \delta \sin \omega t + \sigma_0 \sin \delta \cos \omega t \quad (3)$$

The stress in Eq. 3 is resolved into two components: the first term on the right gives the stress component in phase with the strain, and the second term is the 90° out-of-phase component. Hence, we define two dynamic moduli; E' and E'' designate the in-phase modulus and out-of phase modulus, respectively.

$$E' = \frac{\sigma_0}{\varepsilon_0} \cos \delta \quad E'' = \frac{\sigma_0}{\varepsilon_0} \sin \delta$$

Eq. 3 can be rewritten as follows

$$\sigma = \varepsilon_0 E' \sin \omega t + \varepsilon_0 E'' \cos \omega t \quad (4)$$

The phase angle δ is defined as

$$\tan \delta = \frac{E''}{E'}$$

Rewriting Equations 1 and 2 in complex notation

$$\begin{aligned} \varepsilon &= \varepsilon_0 \exp(i\omega t) \\ \sigma &= \sigma_0 \exp[i(\omega t + \delta)] \end{aligned} \quad (5)$$

we arrive at the following expression for the complex modulus E^*

$$E^* = E' + iE''$$

E' and E'' are called the storage modulus (real part of the complex modulus) and loss modulus (imaginary part of the complex modulus), respectively. While E' signifies the elastic character (stored portion of the mechanical energy input), E'' indicates the energy dissipated through molecular flow processes. Experimentally, E' and E'' can be measured in tension, compression, bending (Figure 7 schematically depicts DMA in the single cantilever bending mode), and shear deformation modes (torsion for solids and parallel plates for fluids and gels). In tension, compression and bending, one obtains the tensile modulus designated by E while the shear deformation mode gives the shear modulus G .

Dynamic Mechanical Analysis of Optical Fibers

Typical DMA specimens are rectangular bars with a cross-sectional area of the order of a square millimeter. The cylindrical symmetry and the small diameter of an optical fiber present clamping and measurement challenges in dynamic mechanical analysis. Preliminary analysis of single and multiple fibers showed that a parallel array of optical fibers can be tested in the single cantilever bending mode as depicted in Figure 7. In this figure, the following boundary conditions apply to the elastic deformation of a beam of circular cross-section:

- 1) One end of the fiber is fixed to the stationary clamp.
- 2) The other end is guided by the moving clamp.
- 3) The fiber slope is zero at both the guided end and the fixed end.

The general differential equation for (linear elastic) bending of an optical fiber is⁽¹⁰⁾

$$EI \frac{d^2 y}{dx^2} = M \quad (6)$$

where E is the modulus of elasticity, I is the area moment of inertia about the beam centroidal axis, and x and y refer to the coordinate along the beam axis and the deflection of the beam measured perpendicular to the beam axis, respectively. The solution of this equation for the maximum deflection y_{\max} in single cantilever bending of an optical fiber yields the following expression⁽¹¹⁾

$$y_{\max} = \frac{-Wl^3}{12EI} \quad (7)$$

where W and l refer to the concentrated load at the guided end of the beam and the beam length, respectively. In the single cantilever bending mode, DMA is conducted by imposing a constant strain amplitude and measuring the dynamic force. Hence, collecting the deflection, y_{\max} , and the load, W, on one side in the Eq. 7 above, we obtain

$$\frac{-W}{y_{\max}} = \frac{12EI}{l^3} \quad (8)$$

On the right-hand side of this expression, all quantities except E refer to the beam geometry. Therefore, we define a geometry factor k

$$k = \frac{12I}{l^3} \quad (9)$$

For a circular beam of radius R, the area moment of inertia, I, is

$$I = \frac{\pi R^4}{4}$$

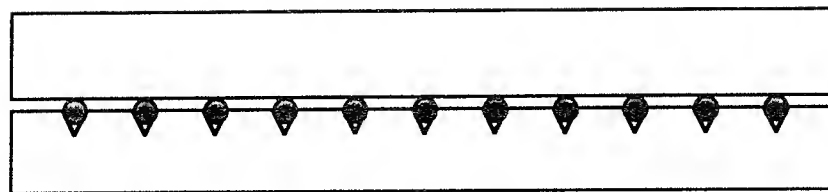
Substituting for I into Eq. 9, we obtain the following expression for the geometry factor for an optical fiber,

$$k = \frac{3\pi R^4}{l^3} \quad (10)$$

For a parallel array of n fibers, the geometry factor k is multiplied by n to arrive at the compound geometry factor for the array.

Table 1
Aged Fiber Characteristics

Aging Condition	Unaged	1 85 °C Uncontrolled Humidity	2 85 °C 85 % RH	3 85 °C DI Water
Tg (°C)	29	33	34	35
Tan δ Peak Value	0.12	0.12	0.13	0.15
Fiber Diameter (μm)	242	240	239	237
Volumetric Change Upon Aging (%)	0	-1.6	-2.5	-4.1



Edge View

Figure 1. Special clamp for cantilever bending of optical fibers

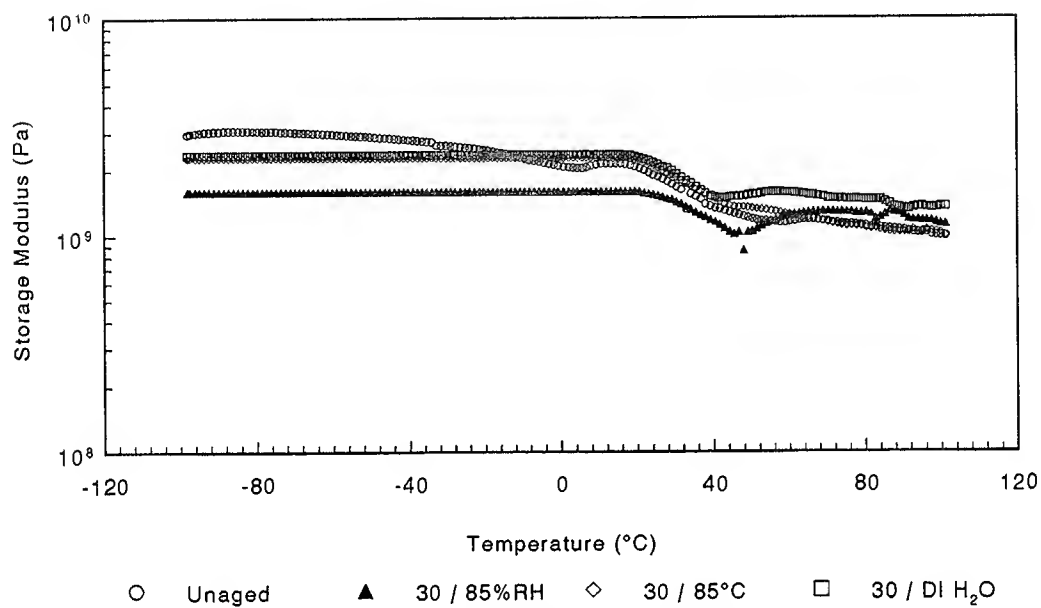


Figure 2a. Storage modulus profiles for the unaged and aged fibers

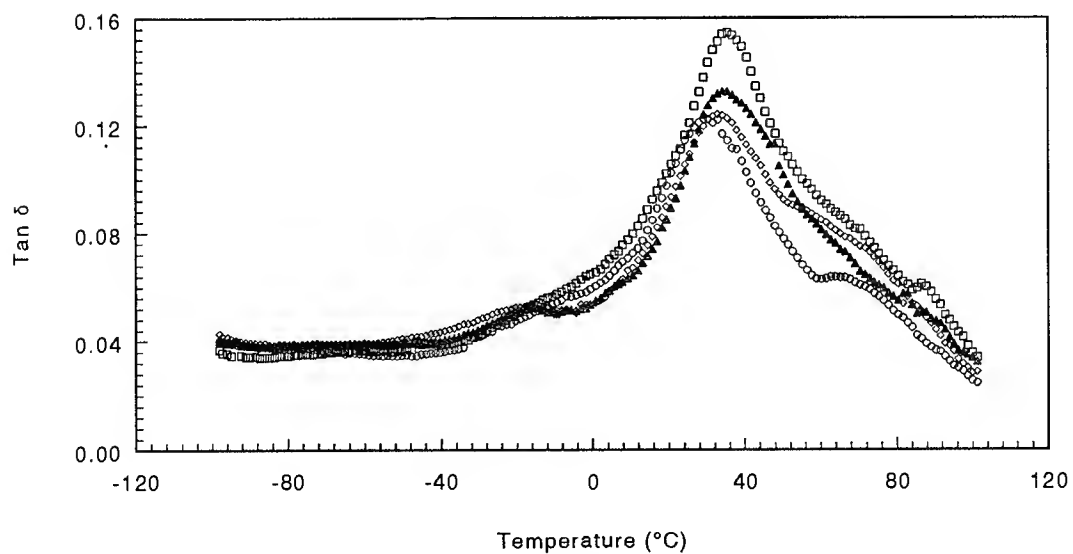


Figure 2b. Loss tangent profiles for the unaged and aged fibers

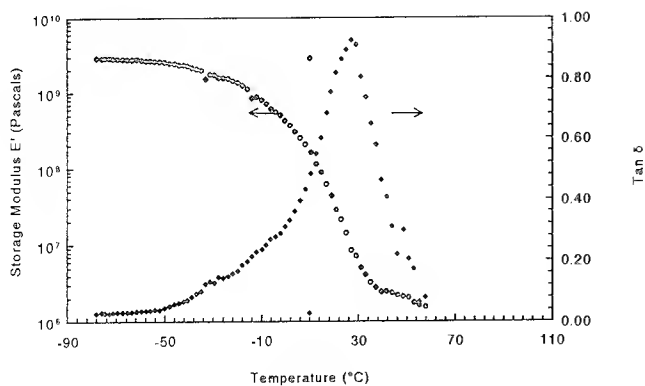


Figure 3a. Dynamic mechanical properties of an inner primary coating

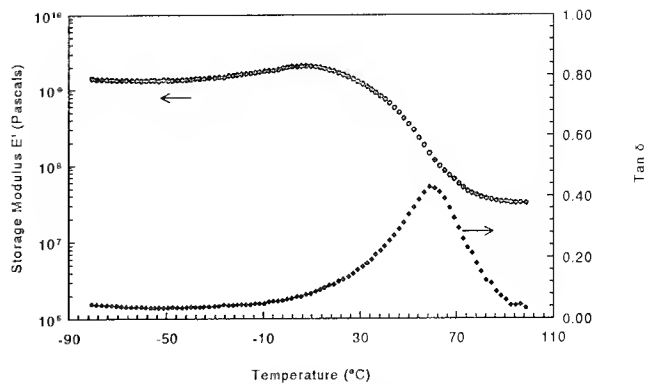


Figure 3b. Dynamic mechanical properties of an outer primary coating

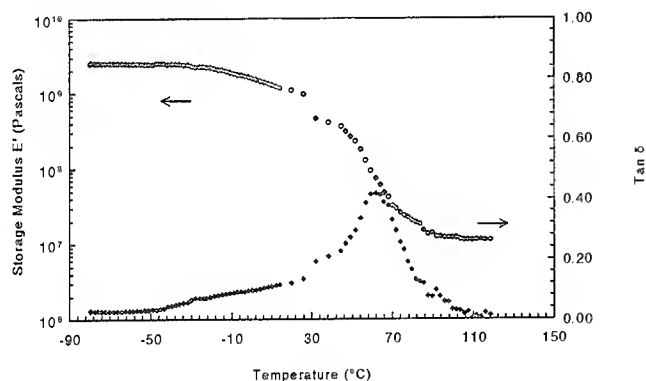


Figure 4. Dynamic mechanical properties of a dual coating film tested in tension

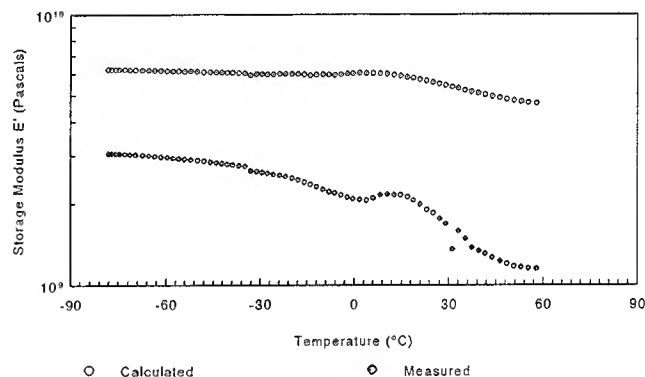


Figure 5. A comparison of calculated and measured fiber modulus profiles

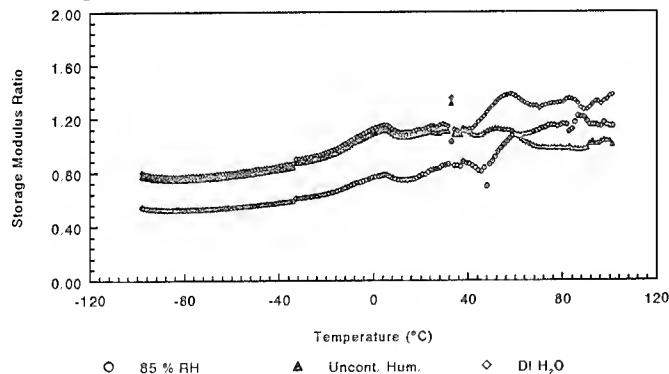


Figure 6. Normalized storage modulus profiles for fibers aged 30 days at 85 °C

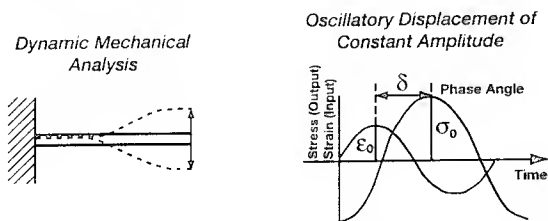


Figure 7. Dynamic mechanical analysis in cantilever bending

Osman S. Gebizlioglu is a Member of Technical Staff in the Metals & Plastics Technology Group at Bellcore. He holds B.Sc., M.Sc. (Middle East Tech. Univ., Ankara, Turkey), and Ph.D. (Princeton Univ., Princeton, NJ) degrees in Chemical Engineering. He was a Monsanto Research Fellow in Mechanical Engineering at MIT prior to joining Bellcore in 1987.

Irene M. Plitz is a Member of Technical Staff in the Metals & Plastics Technology Group at Bellcore. She holds a BS degree in Chemistry. She worked for Bell Laboratories and joined Bellcore in 1983. Her research interests have been in the degradation, characterization, and reliability of polymeric materials in telecommunications applications.

Rolf A. Frantz is a Distinguished Member of Technical Staff in the Fiber Media & Component Reliability Group at Bellcore. He holds BS and MS degrees in Engineering from Cornell Univ., and Ph.D. in Engineering Mechanics from Brown Univ. He worked at Bell Laboratories on the reliability of electrically insulating materials. He joined Bellcore in 1984. Since 1988, he has been working on optical fiber and component reliability.



ECONOMICAL FIBER MIGRATION IN THE LOCAL LOOP: NEW TECHNOLOGIES AND CONCEPTS CUT INTO THE CABLE PLANT

W. Liese, W. Wenski and H. Schönfeld

Kabelmetal Electro GmbH
Postfach 260
30002 Hannover, Germany

Summary.

New services and applications from a broad customer base generate demands for economical transmission and distribution of more information and at higher transmission rates over FITL networks. Fiber optic technology, advances in encoding and data compression, digitalization and the introduction of SDH, STM and ATM standards have placed new equipment into the networks to address this need. This increases the flexibility of today's networks and permits the installation of new structures in the access cable plant with increased distances between the CO and the customer. New enhanced PON and AON systems provide very high utilization of the access line plant. This also applies to rural areas where there are 5 lines per sq. km. The fiber length, per subscriber, is drastically reduced to between 20 and 200 m.

Introduction.

Current political, technical and commercial efforts in telecommunications focus on one issue: how to bring powerful services, such as video on demand, multimedia and fast data exchange economically to the customer. Today, fiber optic data highways provide the long-distance communications links. However, the key to these services lies within the access network. In communications networks the cost of the access networks amounts up to 50%. It requires the most economical implementation, such as overlay, rehabilitation or newly-built networks. The investment also calls for immediate return from the services, while maintaining strong growth potential for future services. Present FITL installations have become cost-competitive with copper networks¹ although they are challenged by copper pair and coax as well as by radio-based services. In the planning of the FITL networks the long service lifetime must be considered. This implies changes in customers and services, in transmission and switching technologies with new systems and complete network structures^{2 to 8}.

An evaluation of today's FITL cable plants must take these future trends into consideration.

Service Demands and Technology of Access Networks

For our analysis we take a network design approach (Fig. 1): we review customer service demands, review requirements for the technologies of switching, transmission and the cable plant and finally consider their impact on the network structure, cable plant and installed fiber plant.

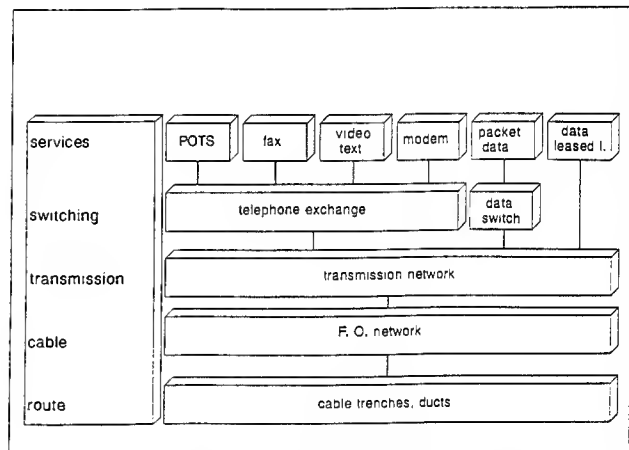


Fig. 1 Services and Information Transport in a Network

Customers and Services.

The sophistication of services differs widely from residential to large business customers (Fig. 2). For industrialized European countries like Germany, the following, although idealized, profile may apply:

Residential Customers and small Businesses. Residential customers and "family type" small businesses represent the majority of from 80 to 90% of the subscribers with demand for one to two lines per subscriber and narrow bandwidth. Traffic for family type businesses is heavier than

for residential users. The line density for residential areas is low, especially if detached houses are served. In areas of residential blocks the line density increases significantly. However, the bandwidth requirement is lower than for business areas of similar density.

customer type	residential	business small medium large	mobile
customer number	very high	medium	low
turnover for operator	high decreasing 60 - 40%	high increasing 40 - 60%	small/ growing 10 - 20%
network demands	full area coverage	overlay	overlay
service requirements	less sophisticated, low traffic	traffic and bandwidth medium to high	less sophisticated

Fig. 2 Customer Groups and Services

Today's service requirements are unsophisticated, consisting usually of POTS and CATV. Future services, such as advanced video games, teleshopping/banking applications and video services in various forms are the driving factors for fiber introduction. Family type businesses will also utilize on-line data bases, multimedia video conferencing and business data bases.

This group requires complete coverage of the CO area of urban, residential and rural settings. Revenue from this group represents over 50% of the total revenue for the operator. Although this group will show increasing growth over the next years, its share of the total revenue will drop below 50% due to stronger growth in the business and large business sectors.

Medium-size Businesses. This sector contributes 5% to 10% to the customer base and requires upwards of 3 lines per subscriber. Today's services incorporate all previously mentioned services, including data exchange and leased lines. The customer utilizes some switching services (e.g.: switchboard) and may use LAN system approaches. Future services include ISDN, low bit rate videophone, multimedia and business services. This group is a potential target for "teleworking" (e.g.: the ability to exercise one's profession remotely from home). Its broadband demands can be satisfied with low to medium Mbit/s channels. Aggregated bandwidth for a customer with 10 to 30 lines frequently justifies dedicated fiber lines². Strong annual growth will bring its revenue to well above 50% of the total.

Large Businesses and Systems Users. This group represents only a few tenths of one percent of the customer base. However, the number of installed lines per customer typically exceeds 50.

Present service requirements range from POTS with switchboard, fax, LANs, MANs over leased private lines for high-speed data and LAN services to video conferencing. Selected customers have a requirement for virtual private networks (VPN) and global networks. The service mix is similar to that of the medium business but it requires higher bandwidth in both switched (ISDN) or leased line services. Traffic volume is frequently heavy enough to justify the installation of customer-dedicated fibers, independent of FITL programs. This group contributes a few percent to the total revenue of the operator.

The combination of business and systems users of the average and large business groups can be served through fiber from a single overlay network connected to the data highway.

Mobile and Radio Links. The mobile and radio penetration rate varies largely from one country to another. In Germany the penetration of mobile terminals is approximately 10% of the total with strong growth potential. Expectations are that by the year 2000 30% of all terminals will be linked by radio. Services include POTS and mobile data transmission. The revenue contribution of this group is increasing.

Key considerations for the economical installation of fiber in the loop are: return on investment per customer group and the service requirements. These are expressed in transmission rates and aggregated rates for narrow and broadband services, the distinction between symmetrical and asymmetrical services and switching requirements in the network.

Transmission and Switching.

For the technical implementation of services such as multimedia, the information must be encoded for transmission, signaling and switching. Information, counted in bits, is transmitted as bit rates over the transmission path (e.g.: cables or radio links). The ultimate physical constraint is the bandwidth, measured in Hz. The efficiency of this task can be expressed in bits/Hz.

Encoding of information has reduced transmission rates for voice and video applications. Analog transmission of voice requires a dedicated copper pair per customer, operating over the voice frequency spectrum between 300 and 3,400 Hz.

The digital pulse code modulation (PCM) technique permits simultaneous operation of 30 voice channels over two copper pairs.

Higher utilization of the copper pairs is possible. While the current ITU recommendations for digital voice transmission call for 64 kbit/s (compatible with ISDN) today's technology permits a nearly identical quality to be transmitted at 16 kbit/s and acceptable quality at 4 kbit/s. Future developments aim at 2 kbit/s (Fig.3)⁵. Video and TV transmission show similar spectacular results^{8,9}. A combination of picture processing and encoding techniques provides for about 10 to 100 times lower transmission rates than for raw pictures (Table 1). Video and digital TV require between 1.5 and 10 Mbit/s. HDTV, the current stepchild of the high end of TV quality, needs between 30 and 34 Mbit/s. Depending on the level of encoding, from 1 to 5 bits/Hz are used with 1 bit/Hz dominating. 10 bits/Hz have been achieved experimentally. Data from different services have distinct synchronization requirements and provide barriers for the encoding.

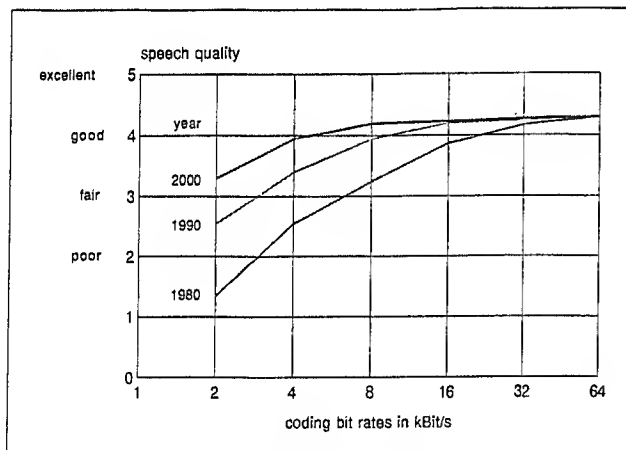


Fig. 3 The Evolution of Voice Encoding reduces the Transmission Rate Requirements.

Compression of voice and video signals is regarded as the major precondition for handling, storage, retrieval and transmission of multimedia data⁴, helping to make multimedia for the residential user a reality. In the long run, this application will require significantly more bandwidth.

Future services can be allocated into three groups according to their transmission rates (Fig. 4): the low end requires $n \times 64$ kbit/s for POTS, fax, low resolution videophone and data applications, including multimedia. The medium range, with enhanced service characteristics, operates

with $n \times 2$ Mbit/s, including the 30 Mbit/s range. The third group provides high-end professional services with dedicated lines STM 1 and higher. It may be worthwhile to note that the potential bandwidth of fiber, in the THz range, permits considerably higher potential for bit rates with enhanced multiplex schemes. Indications are that this potential will be tapped already for rates above 10 to 20 Gbit/s³ with wavelength multiplexing around the year 2000.

PICTURE CODING STANDARDS		DATA RATES in bit/s
PAL	864 x 625 pixels, 50 frames/s	
NTSC	858 x 525 pixels, 60 frames/s	
VIDEO STANDARDS	APPLICATION	
G.721	highest quality video transmission	140 M
G.723	TV production	34 M
MPEG 2	all applications of picture coding	2-15 M
H.261	mainly video conferencing	46 k to 2 M
MPEG 1	video codec	1,5 M
	FUTURE STANDARDS (in process)	
H.26P	for stand-alone equipment and PCs	8k/14,4k
MPEG 4	improved picture quality at unchanged data rates	

Table 1 Video Standards

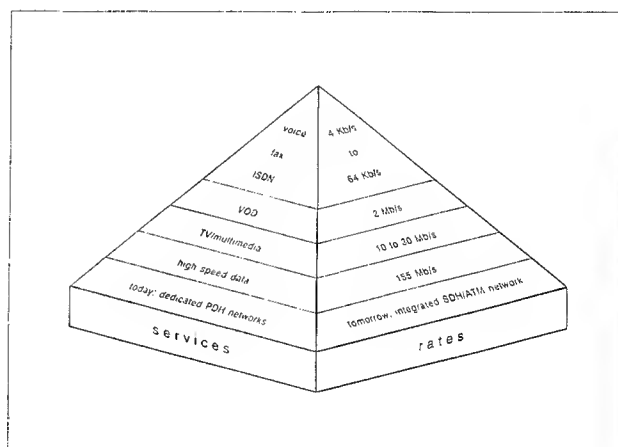


Fig. 4 Services and Transmission Rates

Miniaturization of electronics, an economical alternative, led to digitalization of the networks. Introduction of SDH protocols permits easy mux/demux and cross-connect operations⁷ located in the central office or distributed in remote terminals (RT). These developments are corner stones for ring architectures, for enhanced sharing of fiber and radio links and they increase the network reliability. In addition, they permit the implementation of larger size COs.

SDH cross-connects and dynamic channel allocation provide for flexible management of transmission paths which are tailored to current needs. In the future, ATM switching will further increase flexibility by allocating paths for single data packets instead of fixed transmission time slots. This results in enhanced throughput of information over the same fiber or radio link. In addition, data streams from different services can be integrated into a single network, leading to further savings on investments for the cable plant.

The new equipment generation permits to envision a network with few levels and substantially higher traffic concentration, resulting in improved economics. The cable plants provide reliably a fixed bandwidth which can be exploited further through upgrading of the transmission rates where and when required. This presupposes that sufficient base capacity (number of fibers or copper pairs) has initially been installed. Alternately, cables can be pulled into existing ducts as long as they were initially provided in the network construction.

Broadband services like CATV are currently distributed as analog broadcast services. In FITL networks analog optical amplifiers are used economically. Additional digital schemes for efficient use of existing bandwidth make possible Video-on-Demand (VOD) and Near-Video-on-Demand (NVOD) services. Upon subscriber request, over a slow channel, the high bit rate services may be transmitted to the subscriber. These asymmetrical services effectively remove the switch from the TV set to the CO and save bandwidth.

Radio links and mobile applications benefit from the efficient utilization through encoding, SDH and ATM technology. Point-to-point links via radio are now expanding into the access and local networks where they compete with cable. Alternative service providers consider this as a route to independence. The strong growth in the mobile sector is partly in competition with cable-based networks.

Today's services are provided through a mix of technologies and networks. POTS services are transmitted generally over standard symmetrical copper pair or coax cables as analog or digital signals. CATV is offered over a dedicated coax analog network. High-speed data and video conferencing are distributed via dedicated coax or fiber networks. Current FITL networks in Germany deliver interactive services in channels up to 2 Mbit/s. Distributive broadband services like CATV are provided via a separate fiber network which utilizes the existing infrastructure (cables,

trenches, distribution points, etc.) of the narrow and interactive network. Since the revamping of a major network using new technology takes on the order of 10 years, old and new technologies will continue to coexist.

Cable Plant Technology

The cable plant provides the physical link for the transmission of information. Efficiency and economics in the cable plant translate into sharing of trench routes among several cables with many fibers, coax cables, pairs or quads. The key considerations are cable plant architecture, line density and CO size. The latter depends also on the transmission and switching equipment which creates, through fixed or allottable channels or packets, a temporary logical transmission line path for the cable plant. The maximum number of lines per cable is determined by the transmission rate and cable bandwidth.

Cables. The cable plant is defined by bandwidth and range without repeaters. Fig.5 reviews typical applications for various cable types. The operating distance of the cable depends of course on the equipment, encoding, etc.

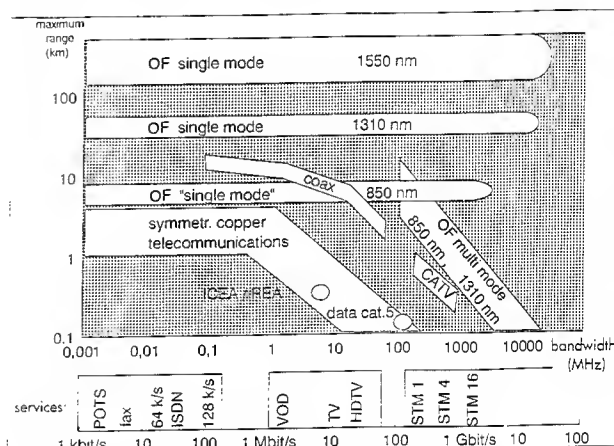


Fig.5 Typical Range and Bandwidth of Cables

Standard optical fiber cables for single mode operation at 1500 or 1300 nm span distances in excess of 150 km and 30 km, respectively. The upper limit of accessible bandwidth is usually determined by dispersion effects.

If operated at 850 nm in the first optical window, a standard single mode cable has a reduced range of 3 - 5 km and some reduced bandwidth. The option to deploy standard single-mode fiber for operation at 850 nm today and for future upgrade to 1300 or 1550 nm is provided for in LANs and FITL networks.

Multimode fibers have a somewhat lower range and bandwidth. They are used mainly in LANs.

Coax cables for long distance communications have a repeater length of up to 10 km. Bandwidth and range are strongly interrelated. Typical CATV cables have a span length of few hundred meters for bandwidth up to 1 GHz. In actual networks high-end transmission rates of about 650 Mbit/s in the transport and 750 Mbit/s in the drop network have been reported. Operators are evaluating the possibility of running some 100 digital TV channels and POTS over the existing CATV cable plant, in addition to their analog TV programs.

Symmetrical copper pairs or quads form the basis of the POTS network. Typical span length is 2 to 4 km for conductors of .4 mm (#26 AWG) diameter. A maximum of 18 km can be achieved with .8 mm (#20 AWG) dia. Although designed for low bandwidth services they support higher bandwidths at reduced range. For example, ICEA / REA Standards¹⁰ for local copper cables specify performance levels at 6 MHz and 300 m; level 5 data cables are specified for 100 MHz and 90 m. Current telecommunications copper pair cables were recently evaluated up to 20 MHz^{11,12}. At frequencies above 10 MHz, unshielded cables are increasingly susceptible to EMI; screening becomes important.

Major efforts in equipment development aim to enhance the transmission rates and range of the existing copper pair/quad line plant. ADSL, HDSL and VHDSL techniques⁸ are used to extend the range up to 5 km at rates of 2 Mbit/s with a goal of reaching up to 34 Mbit/s. Usually more than one copper pair per channel is required.

Cable Plant Architecture. Up to the 1980s, conventional copper access networks were of star configuration with a dedicated copper pair from the CO to the subscriber. For CATV and special services separate networks were installed.

With the arrival of fiber optic cables unlimited bandwidth, longer range and a new network approach became possible. Uncompressed TV/video services in the early 1980s suggested to supply each subscriber with 140 Mbit/s to 565 Mbit/s channels. The network approach consisted of a passive star configuration with dedicated fibers and optoelectronics in optical network units (ONUs) in each home (FTTH). However, early pilot projects confirmed that costs of electronics and fiber would delay an economical introduction for the network applications "newly built", "overlay" or "fiber reinforcement".

Other configurations were considered, focusing on equipment and fiber sharing. Fiber to the building/block (FTTB) and fiber to the curb (FTTC) are approaches for such passive networks (PON). Key to these systems is the transmission of services for all subscribers over a single feeder fiber, a passive splitter and individual drops to the ONUs. Allocation of time slots for each subscriber provides logical separation. Typically 10 to 30 ONUs share the feeder fibers. Due to the limited power which can be fed into standard single-mode fiber, the splitting ratios in PONs are fixed to a maximum of about 1:32. The range of the PON is about 20 km. Pilot installations around the end of the 1980s/early 1990s used this approach and most of the present equipment is developed for this PON concept. Enhanced PON systems with active components show added flexibility and increased range, as described further below.

For maximum utilization of equipment and feeder fibers a free choice of splitting ratio and distribution point location is needed, as provided for in active optical networks (AON). A high traffic feeder from the CO to an active distribution point covers most of the distance to the subscriber. Secondary distribution lines in fiber (or copper, if desired) with lower traffic run short distances to the ONUs in curbs or blocks, as in the PON configuration. Larger distances can be covered, independent of the splitting ratio. The theoretical limit for the splitting ratio of the active splitters is given by the ratio between the transmission rate of feeder and drop line. Equipment for STM 1 to 4 feeders with 155 to 640 Mbit/s and the highest narrow band rate E1 of 2 Mbit/s permit a ratio of 1:60 and 1:250. The active distribution point provides flexibility for new network planning, rehabilitation of the existing copper plant with fiber overlays or utilization of selected sections of the copper network. Cascading of distribution points boosts the range to over 90 km. This also renders rural areas accessible for fiber in the loop.

Planning of Subscriber Distance. In the OPAL '93 FITL networks civil works contributed 25 to 70% to total network costs, excluding electronics, whereby the cable costs amounted to only 5%¹. Cable trenches become a significant cost element for "newly built" installations. However, there is little choice in the selection of the line plant configuration as it must follow the streets. To provide insight into the dynamics of network design, the following reasoning will derive some scaling rules for star and double star configurations.

For simplification we shall consider areas of uniform line density N/A , where N is the number of lines and A the area of the CO.

Planning of single Star Networks. In single star configurations fiber length L is increasing proportional to the square root of the area A to be served (Fig. 6). It decreases with the square root of the line density.

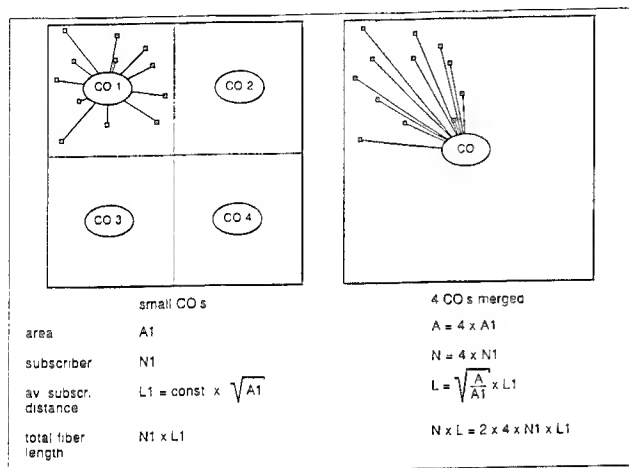


Fig. 6 Cable Plant Increases through Merging of CO Areas

Merging several COs of given service areas into one large CO increases the average line length to the subscriber as well as the total line plant length. For example, merging four COs in our model from 25,000 lines into one of 100,000 lines increases the average line length by a factor of two.

Double Star and Tree Networks. Double stars and trees have a branch-out point for the cable trenches or fibers in the network. They reach identical points but with dedicated fiber in the tree and a common feeder in the double star. When the feeder line can be shared among tens or hundreds of drop lines the feeder length becomes small in comparison to the drop network. Splitters with high ratios close to the subscribers are a cornerstone of efficient network architecture. The actual geometry of the feeder (ring or star) is then no longer a concern for fiber length.

Ring vs. Star Configuration. Simple geometric considerations show that rings provide efficient feeder configurations with respect to fiber length if several distribution points have to be served. They are increasingly used in today's long-distance, regional, urban and LAN network structures.

State-of-the-Art Networks, Systems and Cable Plant Inventories

Networks.

Conventional local copper networks for POTS are part of a four-level national structure with separate dedicated networks for CATV and high speed data transmission (Fig. 7).

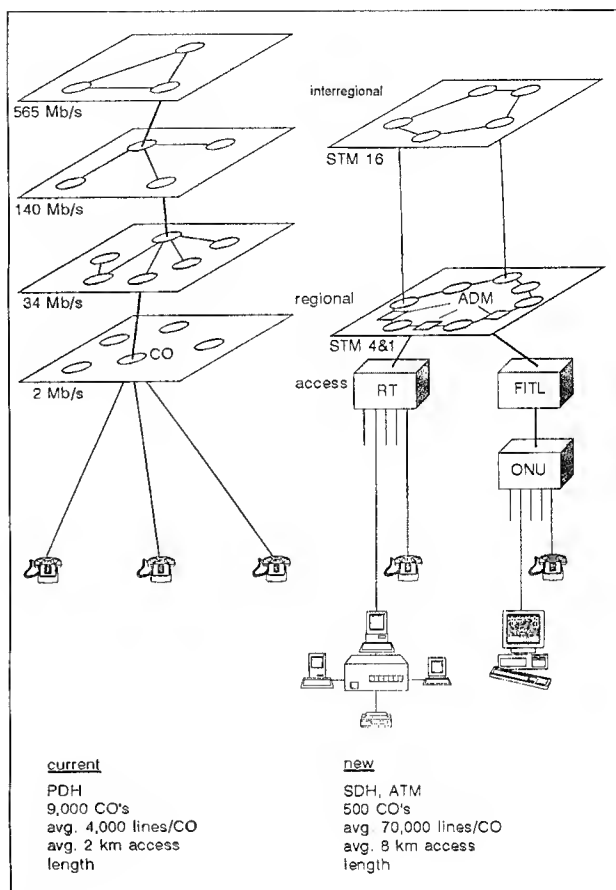


Fig. 7 New Technologies stimulate lean Network Structures

Digitalization, the introduction of SDH and fiber signal the advent of drastic changes to the network structures. Currently the German network is undergoing a restructuring program which evolves 9,000 local COs to about 500 regional offices. At present, four network levels will be merged into one interregional and one regional network level⁷. The access network consists of a combination of feeder and distribution network. The reduction in network levels is accompanied by an upgrade of transmission capabilities by a factor of 4 in all levels. A maximum of 2.4 Gbit/s transmission rate is reached in the interregional network. Currently, various PDH layers below STM 1 are still used.

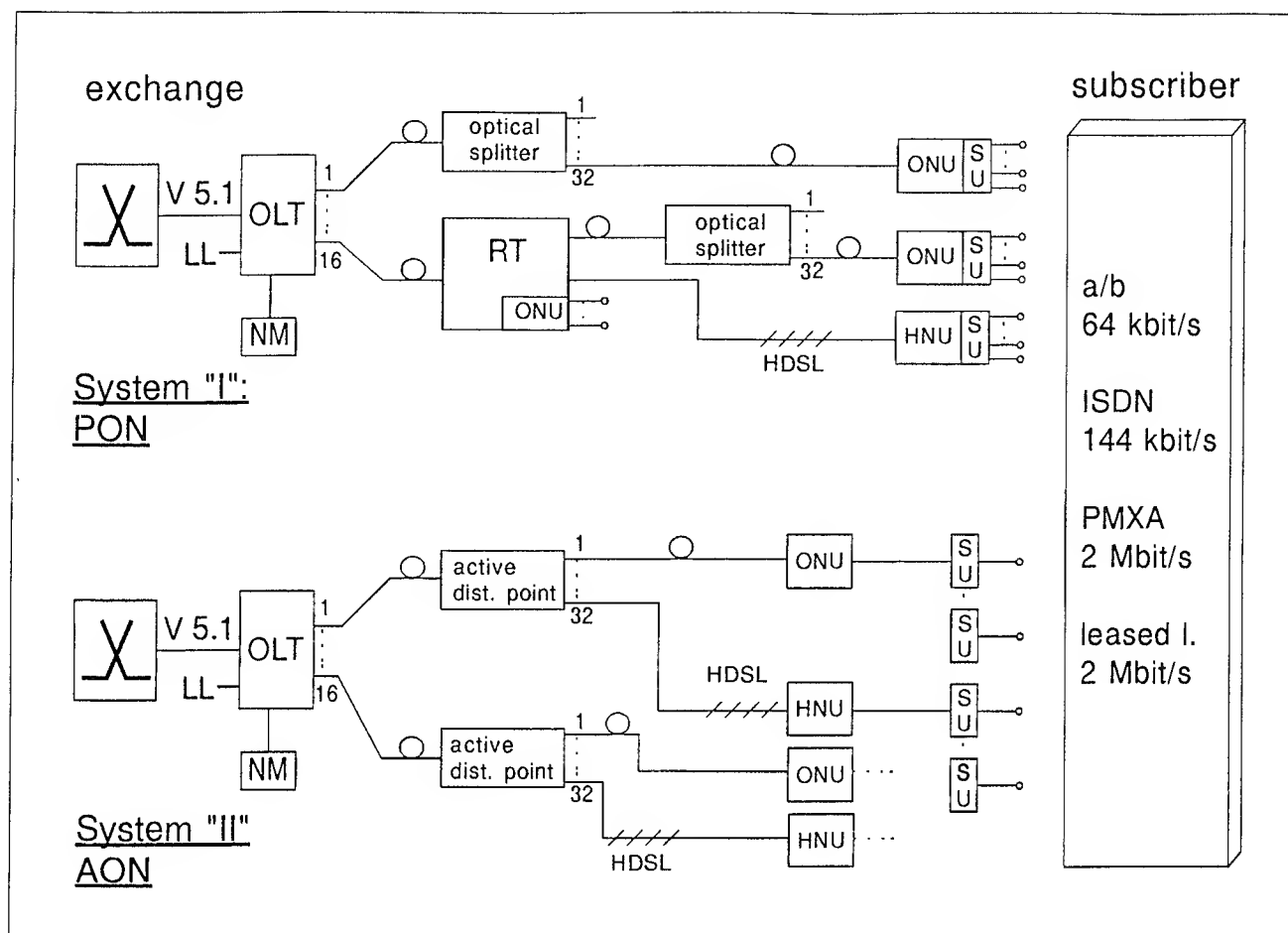


Fig. 8 Enhanced PON and AON Systems provide Flexibility in the FITL Network

In the future, the only acceptable PDH rate will be 2 Mbit/s, thus making the network homogeneous, more flexible and ATM-oriented.

Restructuring of the network results in larger COs with increased switching capabilities for improved economics. Statistically, the average CO increases in Germany range from some 4,000 access lines to 70,000 lines plus reserve. The actual size can range up to 120,000 lines. The average distance from the CO to the subscriber increases thereby from 2 km to more than 8 km with actual maximum line lengths exceeding 60 km. The network is enhanced between regional COs through remote active elements such as: add/drop multiplexers and cross-connects, which provide higher utilization and traffic concentration in the cable plant. Fiber optic feeder cables to the conventional distribution points appear to be economical. For the anticipated German DBP Telekom 1995 version of the FITL program, "OPAL '95" fiber is integrated into the existing access networks through a V5.x interface.

Systems.

Today's interactive systems for the access network exceed the demands set forth by DBP-Telekom for flexibility of services, range and introduction of fiber into existing copper plants. Two examples may illustrate the network topology in the fiber access loop (Fig. 8). Both systems are compatible with ring network structures. Capacities with 1,500 to 2,000 x 64 kbit/s equivalent channels at the CO represent the base configuration. They offer a mix of a/b 64 kbit/s and leased lines (LL), 2 Mbit/s PMXA and leased lines and base ISDN. The systems offer flexible introduction of fiber into the loop, utilizing the existing copper distribution lines up to 3.5 km wherever economically justified. Through introduction of active remote network elements a range exceeding 60 km can be achieved. A wide selection of ONUs provides from 4 to >200 x 64 kbit/s and up to 8 x 2 Mbit/s channels. Therefore "newly built", "refurbishing" and "overlay" projects can be addressed with a high degree of flexibility in urban, residential and even in rural settings.

System "I" is based on PONs. Up to 16 PONs are served from the CO, each serving ONUs in outdoor or indoor locations over splitters (up to 1:32). The range of the PONs is 20 km. A remote indoor/outdoor terminal (RT) extends the range of the PONs by up to 40 km. The existing copper network can be utilized via HDSL on lines to the network interface (HNU). Another option connects nearby customers directly from ONUs in the RT.

System "II" is based on AONs. Up to 16 AONs are served from the CO over active distribution points in outdoor cabinets with splitting ratios up to 1:32. They serve ONUs in indoor or outdoor locations. The HDSL technique utilizes the existing copper plant up to the HNUs. Relocating the service units (SU) from the ONU/HNU into the subscriber's home provides service advantages and reduces the ONU/HNU to a briefcase-size miniature curb unit (Fig.9). These units can be hidden away in a well-protected, underground housing system of novel design. It provides access to the line plant and to the power lines through a closure system (Fig. 10).



Fig. 9 Compact Underground Housing System renders active Components of Minicurbs accessible

The cable plant for the enhanced AON- and PON-based networks is expected to be quite similar. The choice of equipment options of these systems in the CO, distribution points and ONUs permits FITL installations approaching the minimum of fiber length per subscriber in cities. This minimum is achieved if equipment technology is eliminated as the limiting factor in network planning, thus permitting high

fiber sharing in the feeder parts of the network. The last drop length which is shared only between a few subscribers, depends critically on the distance between subscribers. This is given by the property size.

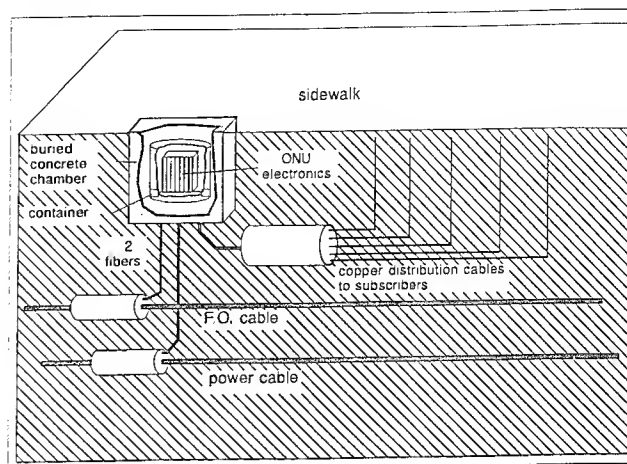


Fig. 10 Minicurb Installation. Schematic Representation of Underground Housing and Closure System

device:	lines per device	splitting ratio	area per device sq. km	lines per device area 1 / sq. km	popul. per device area 1 / sq. km	cable length m / subscr.
subscriber	1	1 : 25	0.005	200	600	160 (Cu)
curb-ONU	25	1 : 20	0.125	200	600	80 (OF)
distr. point	500	1 : 10	3.75	130	400	70 (OF)
CO	5000		1100	4.5	13	

CO traffic split:

1900 x 64 kbit/s line equivalent capacity and a traffic load of 12 % result in the following service split for the rural model area:

service:	provided	lines simult. operating
64 kbit POTS	5000	600
2 Mbit/s	340	40

Table 2 FITL in rural Areas with 4.5 lines/sq.km. Parameters of simulated Plant Layout and Cable Length per Subscriber

Based on our experience in building the first AON turnkey networks for DBP-Telekom's program OPAL'93¹ we have simulated a network layout for interactive services for the toughest condition: a rural setting with an average line density of only 4.5 lines per sq.km. This is the equivalent of a population density of 13 inhabitants per sq.km! This corresponds to the most lightly populated regions in Germany or elsewhere.

Guided by real data we assumed 10 villages spread over 1,100 sq.km with 5,000 lines to be connected to one CO. It is assumed that dynamic channel allocation permits the simultaneous operation of 12 % of the subscriber lines. Other parameters of this rural model are listed in Table 2. By assuming the use of two fibers from the CO to the distribution points and Curb-ONUs we obtain a maximum fiber share of only 150 m per subscriber and a 160 m copper drop. It suggests that fiber can be an economical choice even in this situation. For this network the CO could provide 5,000 subscribers with 64 kbit/s and, in addition, 340 customers with 2 Mbit/s service.

Similar simulations for high density urban regions show that the fiber length per subscriber can drop to 20 - 50 m.

Installed Cable Plant.

Today's and tomorrow's cable plant are presented in Fig. 11. Approximate averages for Germany's long distance and local networks are indicated as well as the cable breakdown for a current regional network serving 500,000 subscribers. In addition, a local network of a densely populated Berlin suburb is shown. The cable plant per subscriber declines as expected with increasing subscriber density. FITL networks with FTTH would require between 2 and 10 km per subscriber in copper-equivalent lay-outs.

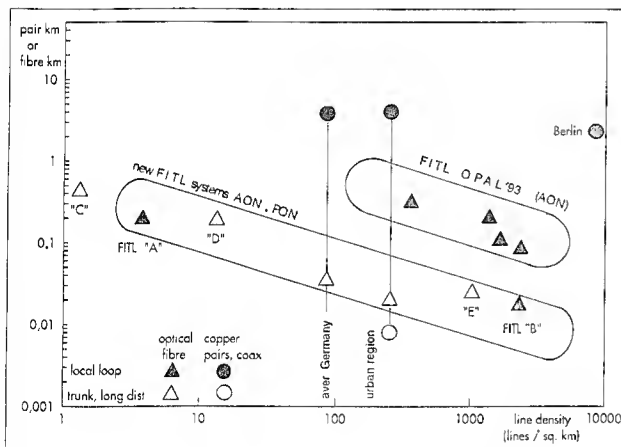


Fig. 11 Cable Length per Subscriber

The OPAL'93 project was the first large-scale fiber deployment for both CATV and POTS services worldwide, using conventional copper topology in the network. The new technology vintage for PON and AON provides for still higher savings in available fiber deployment: down to 150 m in most sparsely populated rural areas (A) and 10 to 50 m per subscriber in urban (B) areas. Examples (C) and (D) represent

fiber lay-outs for networks recently planned in republics of the former Soviet Union and (E) for a major city in the Far East. From this we draw the conclusion that technology permits the successful deployment of fiber, also in rural areas. The fiber plant, per subscriber, of today's access networks is as low as that of regional trunk networks if low reserves are installed. Future services in the residential market, like multimedia, will again call for higher fiber capacity.

Such a network requires longer, high-quality cables for feeder applications. Fiber count for these cables ranges from some ten to several hundred fibers per cable. It differs greatly from the technology required for FTTH via dedicated fibers which have fiber counts of hundreds to thousands of fibers. The accompanying cable accessories (splicing, connecting) can be different and does not mandate ribbon technology. Branching of the cables becomes more important.

Conclusions.

In reviewing the factors affecting the cable plant we find the following trends:

- The demand is broken down into four customer groups:

- Residential and Small Business;
- Medium Business;
- Large Business and
- Mobile.

Their service requirements can be met with low, medium and high transmission rates as multiples of 64 kbit/s, 2 Mbit/s or 155 Mbit/s.

- Data processing permits video transmission as $n \times 64$ kbit/s or, for greater quality, at $n \times 2$ Mbit/s data streams. The existing POTS copper access plant can be used for these rates. It makes the medium transmission rates an attractive alternative, also for residential services.

- The advent of digital technology, SDH/STM-based networks and other technological progress permits the implementation of lean national network structures of increased flexibility. They consist of only two network levels and few COs, supported by remote terminals. ATM will further increase the efficiency along with higher utilization of the cable plant.

Although larger COs increase the average link length to the subscriber, very efficient utilization of the access cable plant reduces the required fiber per subscriber. This calls for implementation of feeder and distribution structures with high splitting ratios, as currently introduced in Germany. A new generation of PON and AON systems is available to address these trends.

In the course of a network planning exercise we tested the newest 1995 generation of enhanced FITL systems with respect to the required fiber length. For these systems, only 20 to 200 m of fiber per subscriber are needed in urban and low-density rural regions. This result is in sharp contrast with the 2 to 10 km length required for FTTH with dedicated fibers. If the existing copper network is utilized, the result will improve even further. Cost savings can now be used to incorporate spare fibers for future growth. The cable plant structure is compatible with later FTTH upgrades. FITL can be started today with conventional low to medium count fiber optic cable technology. The outlined strategy permits a flexible and economical evolution for FITL.

Acknowledgments.

The authors wish to express their gratitude to Mr. D. Stein and Mr. H. Hofheimer of Cable Consultants Corporation, Larchmont NY, for their comments and valuable assistance in the preparation of this paper. We also like to thank Dr. Chahabadi from KE Kommunikationselektronik, Hannover for numerous stimulating discussions. Further we like to thank our partners from DBP-Telekom, Alcatel SEL and Alcatel Contracting for contributing their experiences in systems installations.

Acronyms used in this Paper

ADSL	Asymmetrical Digital Subscriber Line
AON	Active Optical Network
ATM	Asynchronous Transfer Mode
CO	Central Office
FITL	Fiber in the Loop
FTTB	Fiber to the Building
FTTC	Fiber to the Curb
FTTH	Fiber to the Home
HDSL	High Speed Digital Subscriber Line
HNU	HDSL-Network Unit
ISDN	Integrated Services Digital Network
LAN	Local Area Network
LL	Leased Lines
MAN	Metropolitan Area Network
NVOD	Near Video on Demand
ONU	Optical Network Unit
PCM	Pulse Code Modulation
PDH	Plesiochronous Digital Hierarchy
PON	Passive Optical Network
POTS	Plain Old Telephone Service
RT	Remote Terminal
SDH	Synchronous Digital Hierarchy (SONET)
STM	Synchronous Transfer Mode
SU	Service Unit
VHDSL	Very High Speed Digital Subscriber Line
VOD	Video on Demand
VPN	Virtual Private Network

References.

1. "First large scale FITL installation: Experience from OPAL'93"; W.Wenski, H.Dominik, W.Liese, H.Schönfeld; Proceedings of the 42nd International Wire and Cable Symposium, St. Louis MO, Nov. 15 - 18, 1993
2. "A review of the technical options for evolving FITL to support small business and residential services", P.J. Dyke; D.B. Waters; Journ. Lightw. Techn. Vol. 12, no. 2 (1994) pp. 376 - 381.
3. "Optical communication network trends" P. Kaiser (editor) in: Optical Communications Network Trends, Special Issue; Proc. IEEE, Vol. 81, No.11 (1993) pp.1543 - 1547.
4. "Emerging residential broadband Telecommunications", D.S. Burpee; P.W. Shumate; Proc. IEEE, Vol. 82, No.4 (1994) pp.604 - 614.
5. "Technologies for multimedia communications", J.L. Flanagan, Proc. IEEE, Vol. 82, No.4 (1994) pp.590 - 603
6. "Local loop evolution - emerging technologies", G.L.Sparks; Proc. IWCS 1993, pp.329 - 338.
7. "Übertragungstechnik und Netzmanagement in Deutschland"; K.D.Schenkel in: Proceedings of 35. Post- und Fernmeldetechnische Fachtagung des VDI der Post- und Telekomunikation e.V.: - Europäische Telekommunikation - eine Standortbestimmung; Verband Deutscher Post-Ingenieure; Hannover, Germany, March 16-17, 1994, pp. 4.1 - 4.17.
8. "Live Wires"; J. Williamson; Global Telephony, Intertec Publ., Chicago; July 1994, pp. 20 - 26.
9. "Towards global information networking", S.Personick; Proc. IEEE, Vol. 81, no.11, 1993 pp. 1549-1557.
10. ICEA Publication S-84-608-1988, ICEA-Inc., PO Box 440, South Yarmouth MA 02664, May 1989 and "REA - Specification for filled telephone cables with expanded insulation", 7CFR, Part 1755.890, RIN 0572-AA56.
11. "Performance of current local cable designs in high bit rate applications", G.D.Maltz, Ch. Chojetzki, J.Schulte, G.Verdenhalven, K.Verlande; Proceedings of the 42nd International Wire and Cable Symposium, St. Louis MO, Nov 15-18, 1993; pp. 270-282.

Wolfgang Liese
Kabelmetal Electro GmbH
P.O. Box 260
30002 Hannover
Germany



Wolfgang Liese received his Ph.D. degree in physics from the University of Hannover in 1977. From 1978 to 1991 he occupied technical positions in Canada, including head of the optics group at Seastar Optics, Sidney BC and manager of the fiber research group at Northern Telecom. Upon returning to Germany he joined Kabelmetal where he is currently manager of marketing in the Telecommunications Division.

Hans Schönfeld
Kabelmetal Electro GmbH
P.O. Box 260
30002 Hannover
Germany



Hans Schönfeld was born in 1941. After graduating from the Ohm Polytechnikum in Nürnberg he joined Kabelmetal in 1966, where he has been engaged in the field of telecommunications cables development and marketing. Currently he assumes the position of senior engineer for telecom cable plant installations. He is working on OSP planning and introduction of FITL networks.

Wolfgang Wenski
Kabelmetal Electro GmbH
P.O. Box 260
30002 Hannover
Germany



Wolfgang Wenski received his electrical engineering degree from the University of Braunschweig in 1984. After developing electronic circuits for laser and LED modules he joined Kabelmetal in 1986. As group leader he was responsible for the development of telecommunications cables and, especially, for fiber optic cables. In 1990-91 he was general manager of a cable plant before managing the FITL program and the OPAL '93 Project for Kabelmetal. He is now head of the product group "Turnkey and Services".

Optical Power Measuring System for High Count Fiber Ribbons

T.Takashima Y.Unami T.Yamada K.C.Au(*)

Fujikura Ltd. Chiba, Japan

* Fujikura Asia Ltd. Singapore

Abstract

It is necessary to measure the power loss of optical fibers during installation and maintenance of optical cables. As high fiber count optical cables and optical connectors are commonly used in modern communication systems, their loss measuring is laborious and complicated. Currently, there is no efficient measuring system to perform this task.

We have developed an innovative optical power measuring system for the efficient measurement of high fiber count optical cables and high density SM fiber connectors. The system can measure optical power of 80 fibers in 45.5 seconds.

1. Introduction

Increasing the applications of high fiber count optical system such as subscriber optical fiber system, their installation and maintenance has become increasingly complicated. In particular, the efficient measurement of high count fibers and high density fiber connectors¹⁾ is an urgent requirement. We have already developed and put into practical use an optical power measuring system²⁾ for optical fiber ribbons utilizing an instantaneous stabilizing light source unit. However, its present performance has not been sufficient for the high count fiber sys-

tem, so a new optical power measuring system suitable for high fiber count system applications is required. Consequently, we focus on the following target functions to meet market demands:

- [1] Automatic simultaneous optical power measuring of multiple optical fiber ribbons (16 fibers x five sets) and high density fiber connectors (80-fiber connector)
- [2] Provision of a sufficiently practicable dynamic range (more than 20 dB)

A prototype system based on the above functions was designed and evaluated successfully. This paper describes the principles and performances of this new optical power measuring system.

2. System Configuration

Fig. 1 shows the configuration of the new optical power measuring system and Fig. 2 shows the appearance of this system. The system consists of a light source unit, an optical division unit, and an optical power meter, each of which has the features described below:

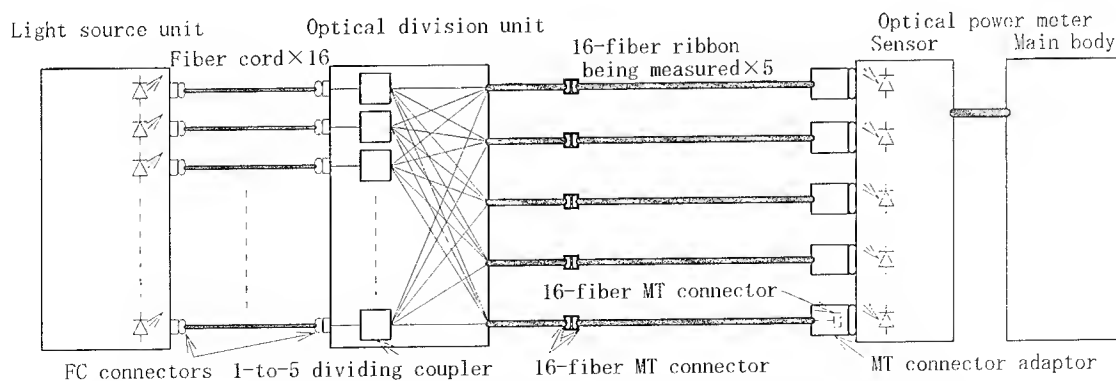


Fig.1 Block Diagram of the Optical Power Measuring System

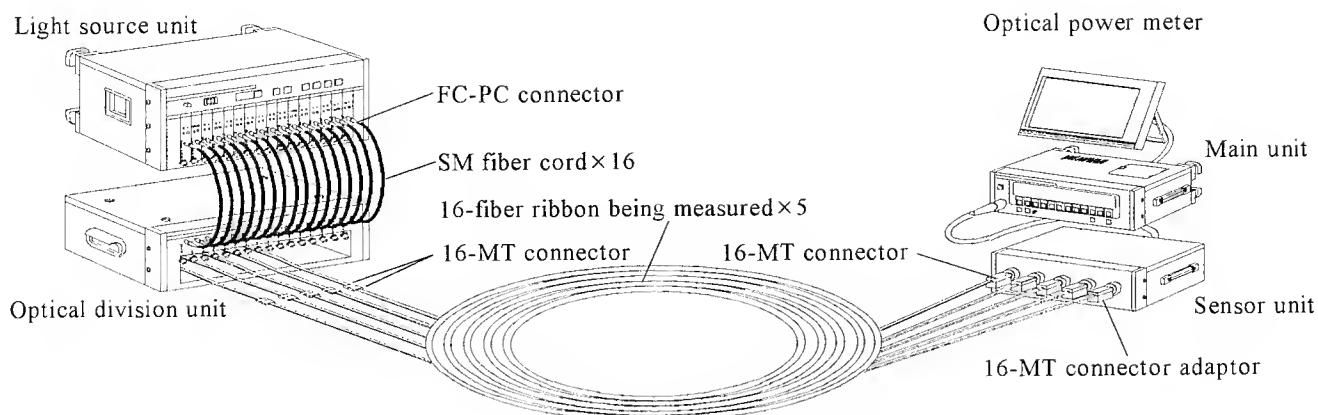


Fig. 2 Appearance of the Optical Power Measuring System

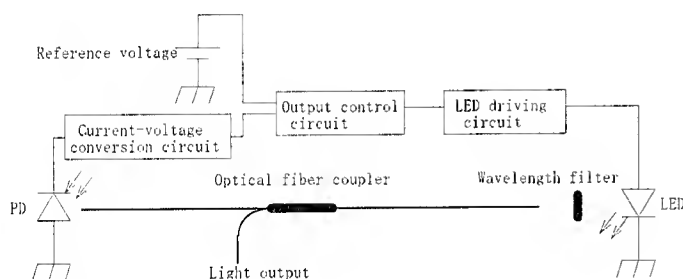


Fig. 3 Forward Light Feedback Method

2.1 Light Source Unit (LSU)

The LSU has sixteen 1.31 μm LED light sources, and the optical output of each is stabilized by the forward light feedback (FFB) method³⁾. The FFB method is configured as shown in Fig. 3. The optical power from the LED is divided by an optical fiber coupler into the stabilized optical power used as the light output and the light used to monitor LED emission power. The latter is converted by a photo diode (PD) into a current signal, which is then converted into a voltage signal by a current-voltage conversion circuit. This voltage signal is compared with the reference voltage at the output control circuit to control an LED driving current.

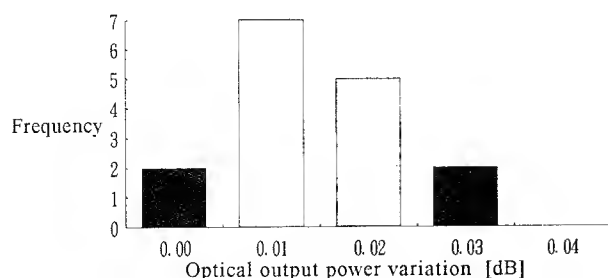


Fig. 4 Stability of the LSU's Power

The FFB method directly monitors part of the optical output of the light source unit to perform feedback control, stable emission power is instantaneously attained when the power supply is turned on. Fig. 4 shows the optical output power variation for two hours from power is turned on. It is restricted to 0.03 dB or less. The power variation is also very stable within ± 0.02 dB in a temperature range of 0°C to 40°C. Moreover, the installation of a wavelength filter in the feedback loop allows the emission center wavelength to become as stable as 1310 ± 10 nm and spectrum full width half maximum to be as stable as 20 nm or less.

2.2 Optical Division Unit (ODU)

The ODU divides the input of the 16-channel light into five sets of 16-fiber ribbons outputs. The ODU has 16 FC-connector receptacles on the light input side and five sets of 16-fiber MT connectors on the light output side, and incorporates sixteen 1-to-5 dividing optical star couplers between the light input side and the light output side. As shown in Fig. 5, a 1-to-5 star coupler consists of four optical fiber couplers with a different coupling ratio. The total loss between a part of the input side and five parts of output side is calculated as following:

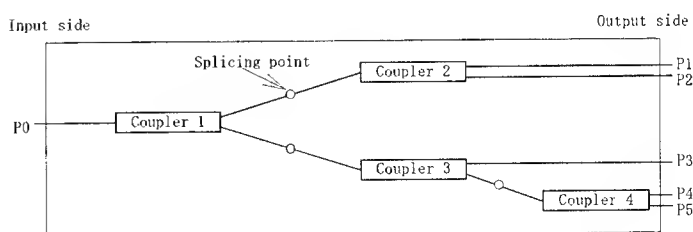


Fig. 5 1 to 5 dividing Optical Coupler

The P0-to-Pi total loss is T_{0i} ($i=1,2,3,4,5$),

The coupling ratio of Coupler 1 $C_1 = 40 \pm 3$ [%],

The coupling ratio of Coupler 2 $C_2 = 50 \pm 3$ [%],

The coupling ratio of Coupler 3 $C_3 = 33 \pm 3$ [%],

The coupling ratio of Coupler 4 $C_4 = 50 \pm 3$ [%],

The excess loss of coupler k $T_{Ek} \leq 0.3$ [dB] ($k=1,2,3,4$),

The insertion loss of a splicing point $T_s \leq 0.1$ [dB]

$$\begin{aligned} T_{01} &= C_1 (1 - T_{E1}) C_2 (1 - T_{E2}) (1 - T_s) \\ &= 6.42 \text{ to } 8.30 \text{ [dB]} \end{aligned}$$

$$\begin{aligned} T_{02} &= C_1 (1 - T_{E1}) (1 - C_2) (1 - T_{E2}) (1 - T_s) \\ &= 6.42 \text{ to } 8.30 \text{ [dB]} \end{aligned}$$

$$\begin{aligned} T_{03} &= (1 - C_1) (1 - T_{E1}) C_3 (1 - T_{E3}) (1 - T_s) \\ &= 6.44 \text{ to } 8.37 \text{ [dB]} \end{aligned}$$

$$\begin{aligned} T_{04} &= (1 - C_1) (1 - T_{E1}) (1 - C_3) (1 - T_{E2}) C_4 (1 - T_{E4}) (1 - T_s)^2 \\ &= 6.31 \text{ to } 8.76 \text{ [dB]} \end{aligned}$$

$$\begin{aligned} T_{05} &= (1 - C_1) (1 - T_{E1}) (1 - C_3) (1 - T_{E2}) (1 - C_4) (1 - T_{E4}) (1 - T_s)^2 \\ &= 6.31 \text{ to } 8.76 \text{ [dB]} \end{aligned}$$

The variation of total loss of each port of the ODU is shown in Fig. 6. These results indicate that each output of a star coupler has nearly equivalent optical power divided from the input optical power. The optical powers from the outputs of the star couplers are led into the five sets of 16-fiber ribbons corresponding the input channel to the same channel of output 16-fiber ribbons. Finally, the divided optical power is put into a target fiber to be measured through the 16-fiber MT connectors.

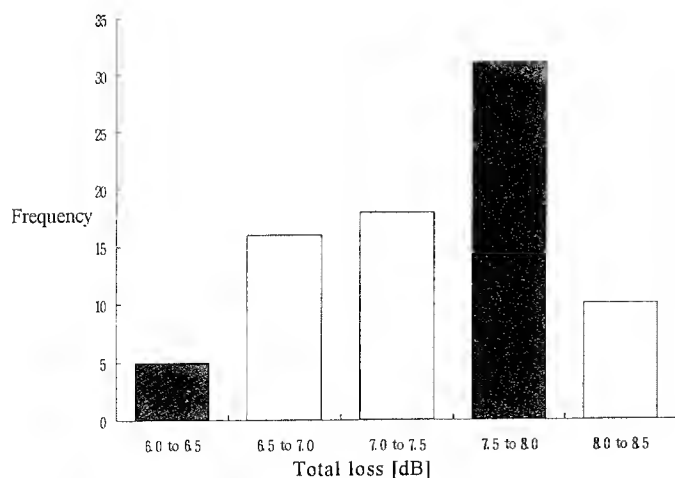


Fig.6 Total Loss Variation of the ODU

2.3 Optical Power Meter (OPM)

The OPM consists of two units: the main unit and the sensor unit, which are connected to each other through a sensor cable.

The sensor has five large-diameter photo diodes (PDs) which directly detects the power from the 16-fiber ribbons, and a built-in microprocessor independently measures each optical power detected by each PD. The microprocessor uses PD wavelength sensitivity data that is pre-stored in the memory to correct the wavelength sensitivity of the measured values. This enabled highly precise measurements at the wavelength of 0.75 um to 1.75 um.

The main unit of the OPM has a large LCD and also enables the connection of an external CRT so that a large volume of data can be collectively displayed at the same time. Moreover, it has a calendar function, memory with a backup function, a printer, and GP-IB interface connections for convenient operations.

Several important technical items on detecting power from optical fiber ribbon are described below:

2.3.1 Reflection of OPM PD

In the optical power measurement, it is a problem that part of the light injected into the sensor from the fiber ribbons being measured is reflected by the optical power meter PDs and returns to the fiber ribbons.

The reflection power coupled fiber is sufficiently restricted small in comparison with the Frenel reflection at the end face of the fiber by following two solutions:

- 1] The eight-degree angled PD surface with the fiber incident axis.
- 2] The 2 mm distance from the end face of fiber to the PD.

2.3.2 Detection Diameter of the OPM PD

The cost of the PDs increases with an increase in the PD's detection diameter. Consequently, we considered the minimum detection diameter that will allow sufficient light detection.

The distance between the end faces of the 16-fiber ribbon is determined from the expanse of light beam from the end face of the 16-fiber ribbon and the fiber pitch of the 16-fiber ribbon. Using PD of a 5 mm detection diameter, the distance between the end faces of the 16-fiber ribbon and the PD should be less than 4 mm. According to the result of section 2.3.1 above, the distance range is determined from 2 mm to 4 mm.

2.3.3 Type of OPM PD

The optical power coupled to the fiber ribbon being measured is less than that of the direct coupling from the LSU by the amount of loss at the ODU. To secure a sufficient dynamic range, the conventional Ge-PD is replaced by InGaAs-PD which has low dark current and a large internal resistance. This results in significant improvements in the signal-to-noise ratio in the conversion from optical power to current, and the minimum detection level of the OPM improved from -59 dBm to -81 dBm for 270 Hz modulated light.

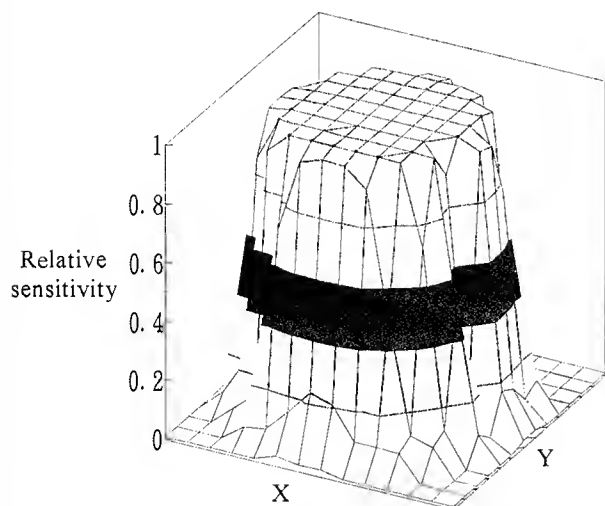


Fig. 7 PD Surface Sensitivity Distribution

2.3.4 Surface Sensitivity Ununiformity of the OPM PD

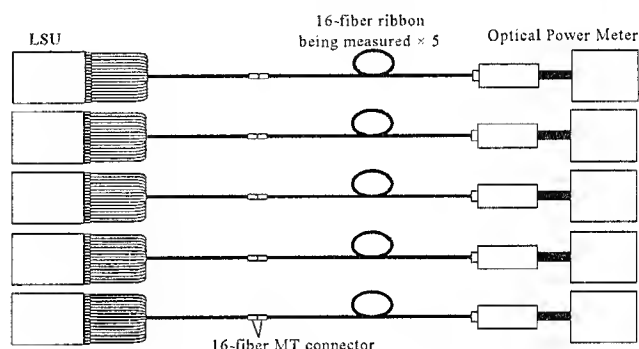
When a large-diameter PD receives optical power from each core of the fiber ribbons, PD surface sensitivity ununiformity appears directly as measurement errors. Especially with a larger-diameter PD, the surface sensitivity ununiformity tends to be larger. Fig. 7 shows the sensitivity distribution on the PD surface used in the experiment. This data shows that variations in the measured values caused by the sensitivity distribution on the PD surface were as small as 0.03 dB or less. For optical power measurements with a higher accuracy, involving both the reference optical power and relative optical power, matching the fiber in the same position relative to the PD allows the effects of the surface sensitivity ununiformity of PD to be greatly reduced.

3. Advantage of System

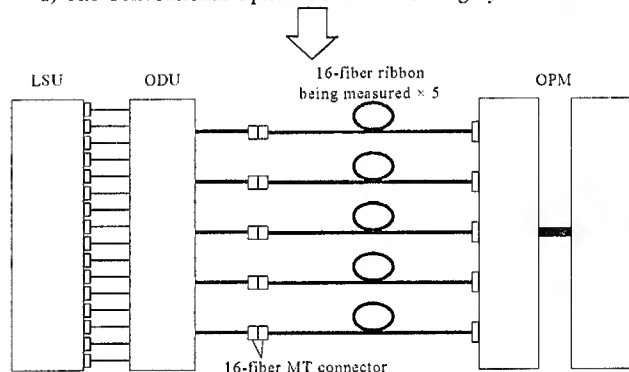
Lights emitted from 16 LED light sources in the LSU enter the ODU through fiber cords. The ODU divides all lights into five parts, which then are launched into the five sets of 16-fiber

ribbons. Therefore, the light source side is functionally equal to five sets of 16-channel light sources with an emission power level approximately 1/5 that of the light directly emitted from the LED. The detection side is equivalent to five sets of optical power meters, since five PDs are independently controlled. Consequently, when considered in terms of the overall system, the optical power measuring system simultaneously measures the optical power of five sets of 16-fiber ribbons (Fig. 8). This is more advantageous in terms of cost and size than the conventional system.

Fig. 9 shows the improved optical power measuring method



a) The Conventional Optical Power Measuring System x 5 set



b) The New Optical Power Measuring System

Fig. 8 Advantage of the New System

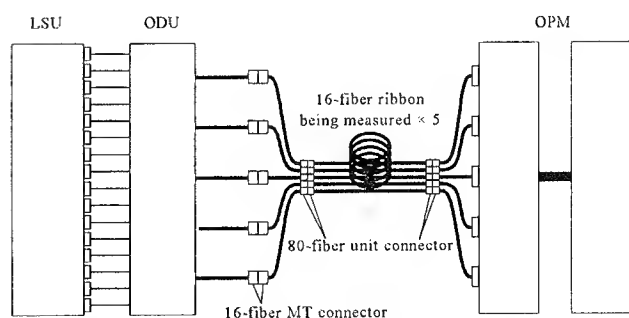


Fig. 9 Improved Use of the New System

using the new system, which has an operation of optical power measuring suitable for use of the 80-fiber unit connector¹⁾.

4. Measuring Method

For automatic measuring, one PD must be capable of individually measuring the optical power of 16 fibers. To achieve this, we adopt a time-division power measuring method for high count fibers that causes each light source to emit light in turn in order to measure the optical power of each channel.

The LSU turns the optical power on and off at the pulse timings shown in Fig. 10. This causes light from 16 channels to be collectively incident on each PD in the OPM, and the OPM detector observes the optical pulses as shown in Fig. 11. When light emission is on continuously for 2.5 seconds, the OPM identifies it as the starting signal. After that, the OPM measures the optical power detected at each PD by identifying no emission interval of 0.5 seconds as well as each channel emission of 2.0 seconds. When the continuous light emission of 2.5 seconds appears again, the OPM completes the measurement of a single cycle. Moreover, the OPM has a threshold of -81 dBm used to identify the presence or absence of light, and this threshold power determines for example whether the fiber is broken according to whether the power is above or below the threshold.

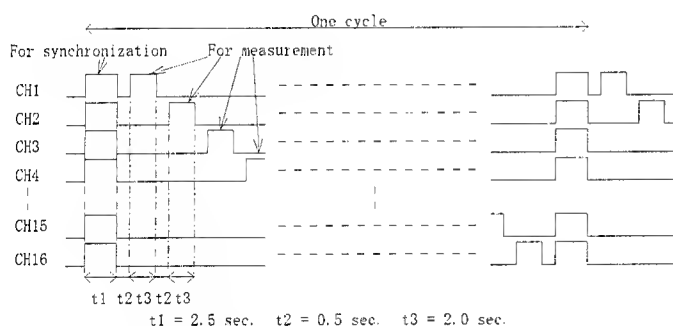


Fig.10 Optical Pulse Timing of the LSU

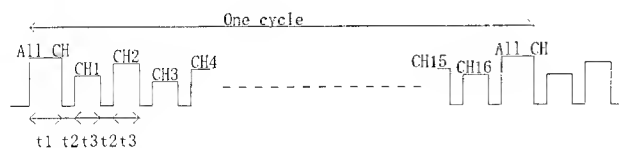


Fig.11 Waveform Detected by the OPM Detector

5. Prototype System Characteristics and Conclusions

Tables 1 to 3 show the characteristics determined by the prototype system, and Tables 4 and 5 show values obtained through comparison with the conventional power measuring system.

When optical power through 12 fibers was detected and measured using the conventional power measuring system²⁾, the measuring time was 35.5 seconds. On the other hand, the prototype optical power measuring system requires 45.5 seconds to measure the optical power emitted through 80 fibers. In other words, the measuring time per fiber is reduced from 2.96 seconds to 0.569 seconds, improving the measuring efficiency by about five times.

The ODU has an insertion loss of approximately 7 dB, reducing the optical power coupled to the fibers being measured by that amount. However, because InGaAs-PD is changed instead of conventional Ge-PD, the minimum detection level has improved from -59 dBm to -81 dBm, and the overall system dynamic range increased by 12 dB.

These results verify that the new optical power measuring system is effective in measuring the optical power of high fiber count system.

References:

- 1) S. Tomita, M. Matsumoto, S. Nagasawa, and T. Tanifuji, "Ultra High-Density Optical Fiber Cable with Thin Coated Fibers and Multi-Fiber Connectors", 42nd IWCS, 1993
- 2) Y. Unami, M. Tanaka and T. Yamada, "Optical Power Measuring System for Fiber Ribbon", 39th IWCS, 1990
- 3) Y. Unami, M. Tanaka and T. Yamada, "Evaluation of Light Sources with Forward Light Feedback Method", IEICE of Japan, B-735, 1990

Table 1 Characteristics of the LSU

Item	Description	Remarks
Stabilizing method	FFB method	
Light emitting device	InGaAs-LED	Edge emitting type
Light detection device	InGaAs-PD	
Optical division device	Optical fiber coupler	
Number of channels	16 channels	
Connector type	FC - PC	
Output light waveform	270Hz modulated light / CW light	Modulated light is 50% of square waves
Fiber coupled power	-31dBm or more	Upon SM10/125, CW light
Center wavelength	1310±10nm	
FWHM	25nm or less	
Temperature characteristics	Within ±0.02dB	Maximum fluctuation at 0 to 40°C
Stability	0.03dB or less	Maximum fluctuation between the level just after switch-on and that after 2 hours
Repeatability	0.02dB or less	Maximum fluctuation at 100 cycles of 10 seconds ON and 20 seconds OFF
Dimensions	470W×326D×210H mm	
Weight	14kg	
Power supply	100V AC	

Table 2 Characteristics of the ODU

Item	Description
Optical dividing device	fiber fused coupler
Number of channels on the input side	16 channels
Input connector type	FC - PC
Number of channels on the output side	16×5 channels
Output connector type	16-fiber MT connector
Insertion loss	6.0 dB to 8.5 dB
Dimensions	470W×360D×150H mm
Weight	8.5kg

Table 3 Characteristics of the OPM

Main Unit

Item	Description	Remarks
Waveform of the light to be measured	Normal measurement 270Hz modulated light / CW light Optical power measurement for high-count fibers 270Hz modulated light only	Modulated light is 50% of square waves
Number of channels to be measured	16 fibers × 5 channels maximum	
Resolution	For [dBm]display 0.01dB For [W]display 0.1 to 1%	
Data memory function	Normal measurement data 100 files or more Optical power measurement data of a high-count fiber 20 files or more	
Interface	GP-IB	Compliant with IEEE Std. 488-1978
Operating temperature	0°C to 40°C	
Dimensions	300W×215D×94H mm	
Weight	4kg	
Power supply	100V AC	

Sensor Unit

Item	Description	Remarks
Number of channels to be measured	16 fibers × 5 channels maximum	
Detecting Device	5mmφ InGaAs-PD	
Optical power measurement range	Modulated light 0 to -81dBm CW light 0 to -51dBm	Upon measurement at 1300nm
Accuracy	±0.3dB	at 25°C, 1300nm, -30dBm
Wavelength measurement range	750 to 1750nm	
Operating temperature	0°C to 40°C	
Dimensions	300W×255D×94H mm	
Weight	6kg	

Table 4 Comparison of Measurement Efficiency

	Conventional optical power measurement system	New optical power measurement system
Number of channels to be measured	12	16×5 (80)
Measurement time	35.5seconds	45.5seconds
Measurement time per fiber	2.96seconds	0.569seconds

Table 5 Comparison of Dynamic Range

	Conventional optical power measurement system	New optical power measurement system
Fiber coupled power	-34dBm or more	-44dBm or more
Minimum detection level (Light detecting device)	-59dBm (Ge-PD)	-81dBm (InGaAs-PD)
Dynamic range	25dB or more	37dB or more

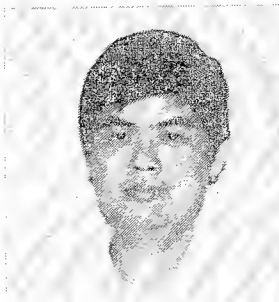


Tetsu Takashima

Fujikura Ltd.

1440, Mutsuzaki, Sakura,
Chiba, 285, Japan

Tetsu Takashima was born in 1966. He joined Fujikura Ltd. after his graduation from Chiba University with the B.E. degree 1989 and has been engaged in research and development of optical systems. He is now an engineer of optical communication system section and a member of IEICE of Japan.



Kum Chuen Au

Fujikura Asia Ltd.

460, Alexandria Road #22-02
PSA Building Singapore 0511

Kum Chuen Au was born in 1963. He joined Fujikura Asia Ltd. after his graduation from Nanyang Technological Institute with the B.E. degree 1991 and has been engaged in research and development of optical systems. He is now an engineer of optical communication system section.



Yoshiharu Unami

Fujikura Ltd.

1440, Mutsuzaki, Sakura,
Chiba, 285, Japan

Yoshiharu Unami was born in 1961. He joined Fujikura Ltd. after his graduation from Chiba University with the B.E. degree 1982 and has been engaged in research and development of optical systems. He is now a chief engineer of optical communication system section and a member of IEICE of Japan.



Takeshi Yamada

Fujikura Ltd.

1440, Mutsuzaki, Sakura,
Chiba, 285, Japan

Takeshi Yamada was born in 1950. He joined Fujikura Ltd. after his graduation from Waseda University with the B.E. degree 1973 and has been engaged in research and development of optical systems. He is now a vice general manager of optical system R&D department and a member of IEICE of Japan.

RESTORATION OF THE MECHANICAL STRENGTH OF AGED OPTICAL FIBER

Göran Ljungqvist, Magnus Johansson and Leif Stensland

Ericsson Cables AB
Optical Network Research Center
S-172 87 Sundbyberg, Sweden

ABSTRACT

The mechanical strength of aged, brittle optical fibers was studied before and after heat treatment. The treatment restored the mechanical strength of the fibers to approximately their original values. These fibers had been aged in water at a temperature of 85°C for several months. After ageing, the bare fibers (the acrylate coating had been removed) had an average strength of 1-2 GPa, measured by the two point bending method. The restoration was carried out by heating short pieces of the bare fibers to their softening point in a CO₂-laser beam. The process significantly reduces the number of flaws and corrosion pits, which otherwise could act as crack initializations. The attenuation increase in the treated fibers is small.

INTRODUCTION

The mechanical reliability of optical fibers is a major concern as more and more fiber cables are installed in the field. The influence of water combined with applied stress is well known to cause a degradation of fiber strength¹⁻³. The corroded fiber surface shows a large number of pits and cracks, where the fiber tends to break when stressed⁴⁻⁵. Aged fibers, buried in cables, have sometimes degraded in mechanical strength to a point where they are difficult to handle during splicing in a repair or rerouting situation.

2 GPa is considered a minimum mechanical strength for fibers in field use⁶. This value is sufficient for the fiber to withstand all the stress applying processes; stripping the coating, cleaning and cleaving the fiber, splicing, and installing of protection sleeves. A lot of the present work on fiber reliability is undertaken with the aim of ensuring that this minimum strength is maintained during the fiber lifetime. However, the handling problems of old and brittle fibers already in the field have to be overcome to allow safe splicing operations.

Here we present a new method to restore the mechanical strength of aged, brittle fibers. The method relies on the use of a CO₂-laser to heat the fiber to its softening point. This reshapes the fiber surface. After treatment it is possible to handle and splice the fiber end in a normal way. The restoring method is briefly described below, followed by our experimental results.

EXPERIMENTAL

A standard commercial silica SM-fiber with a diameter of 125 µm and a dual-layer acrylate coating of 250 µm was used throughout the testing series. Continuous lengths of fiber were each wrapped on plastic spools with a diameter of 8.5 cm. These spools were kept in a glass container, filled with deionized water. During the preparation, the glass container was kept in an oven, at a temperature of 85-90°C. The water was refilled approximately each two weeks. One spool of fiber, which was designated as the control or reference specimen, was maintained at normal room temperature and humidity. At different times after the start of the ageing process, the fiber strength was tested using the two point bending method.

From the resulting fiber spools samples of 20 cm lengths were cut, and the coating was removed chemically in order to avoid any damaging of the fiber surface caused by mechanical stripping operations. To hold the samples during treatment, the fibers were placed in V-groove fiber clamps, allowing 5 cm of the bare fiber to be heated. The experimental set-up is shown in fig. 1.

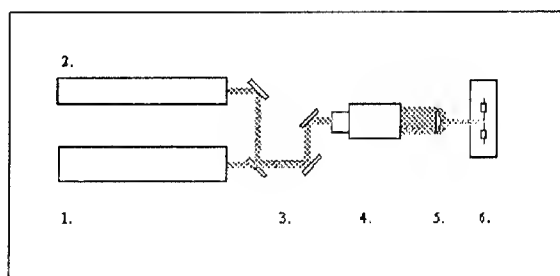


Figure 1. Experimental set-up used to treat aged fiber samples.

1. CO₂-laser
2. Alignment HeNe-laser
3. Mirrors and beam selector
4. Beam expander
5. Focusing lens
6. Fiber sample in clamps, movable with step motor.

The carbon dioxide laser beam was set perpendicular to and focused close to the fiber. The fiber was moved back and forth in the beam focus (2 mm/s) using a step motor. The process results in a heat treatment of the fiber in pieces of 5 cm length. Fiber strength was then tested with the two point bending method⁷. The fiber strength was calculated using⁸

$$\epsilon = 2.396 \frac{r}{D-d}$$

and

$$\sigma = E\epsilon$$

where r is the radius of the bare fiber, D is the plate separation in the two point bending apparatus at fiber breaking point and d is the overall fiber diameter. E is the assumed Youngs modulus for fused silica (71.7 GPa), and ϵ is the strain.

The result σ gives the maximum tensile stress in GPa.

After treatment a sufficient part of fiber had recovered its mechanical strength, well enough to allow safe cleaving and splicing operations.

RESULTS

Figure 2 and 3 show the mechanical strength of the fiber samples before and after treatment. Figure 2 shows the successive decrease of the strength of the fibers aged in water, compared to the restored samples.

In figure 3 the treatment result for one of the fibers is shown.

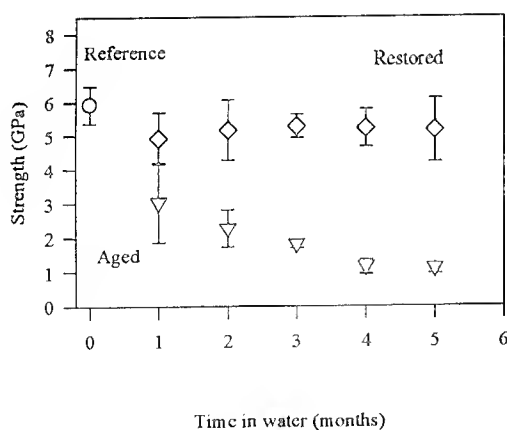


Figure 2. Maximum tensile strength. Results from two point bending test. Samples from reference fiber, fibers aged during one to five months and restored fiber.

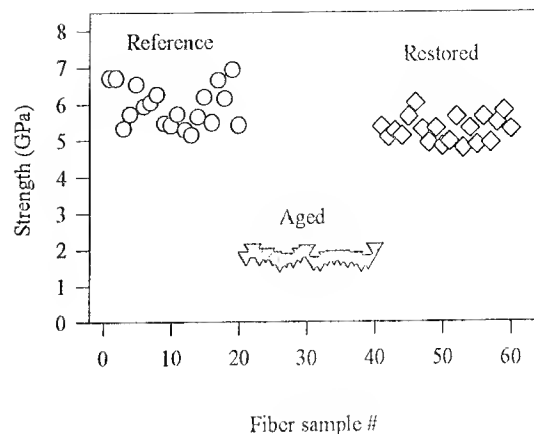


Figure 3. Maximum tensile strength. Results from two point bending test. Samples from reference fiber, fiber aged during three months, and restored fiber.

In all our cases of aged fiber samples the results show an initial degradation in strength compared to the reference fiber that was kept at normal room temperature and humidity. As an example (fig. 3), the strength had deteriorated to a mean value of 1.8 GPa after three months. After treatment the fiber strength increased to a mean value of 5.4 GPa.

The restoration process was repeated with a fiber of other manufacture, with the result of increasing fiber strength from about 1 GPa to 6 GPa as shown in fig.4

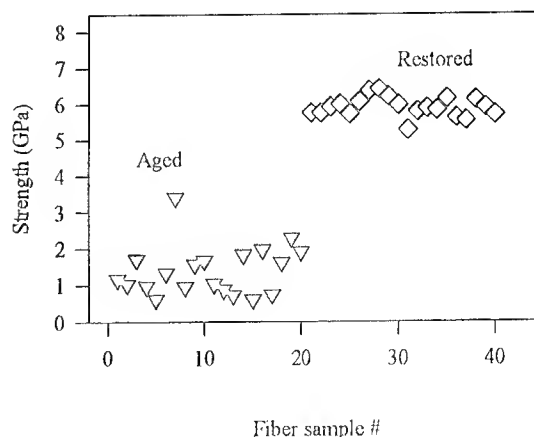


Figure 4. Restoration of fiber strength for a different fiber brand. The fiber had been aged in water at a temperature of 90 °C for 9 months.

Fiber surfaces before and after the restoration process were studied using an atomic force microscope (AFM). The results, fig. 5-6, show a significant decrease in the ruggedness of the surface. The number of corrosion pits and surface flaws, acting as crack initializers, were thus considerably reduced by heating the fiber to its softening point.

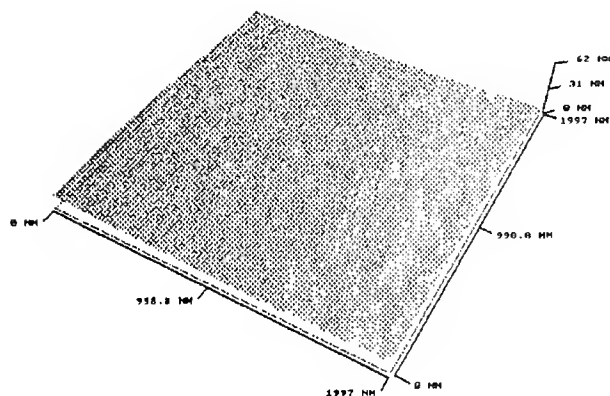
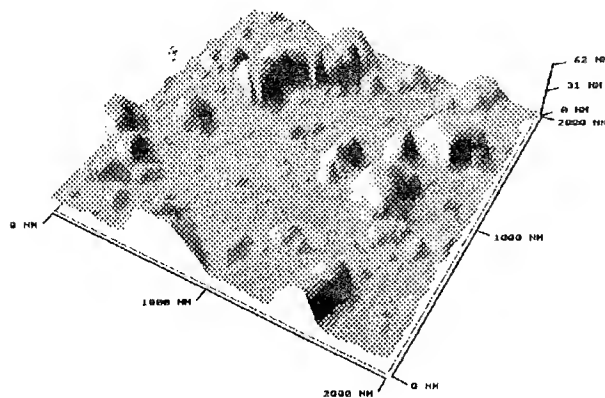


Figure 5-6. Typical AFM-pictures of aged, corroded fiber surface (above) and fiber surface after the restoration process (below). Fiber samples were aged for 3 months in 85°C water.

By optical time domain reflectometer measurements the loss when splicing a treated fiber sample to an unaged SM-fiber, was determined.

Aged and thereafter restored fiber samples were spliced between two standard SM-fibers. The splice-losses were estimated in the used Ericsson FSU 905 splicer. Total loss measurement, achieved with OTDR, includes the loss in the transition zone between treated and untreated aged fiber.

See figure 7.

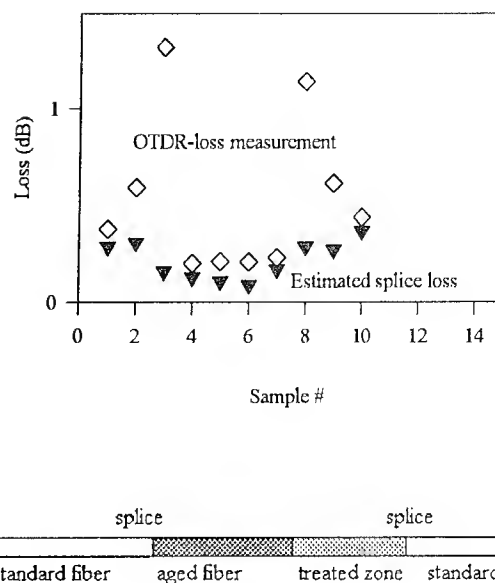


Figure 7. Splice losses between new fibers and treated, aged fiber sample.

There seems to be a loss increase in the transition between treated and untreated fiber. This loss is a few tenths of a dB. The increase, comparable to the loss in one or two splices, should be acceptable if the choice is to exchange the whole aged fiber link.

CONCLUSIONS AND DISCUSSION

We have here reported a novel method to increase the strength of aged, brittle fibers. This restoration is shown to increase fiber strength from below 2 GPa to, and above, 5 GPa - to the region of original as-manufactured fiber strength. The treatment significantly reduces the number of surface corrosion pits and cracks that otherwise could act as breaking points when the fiber is stressed. After the process it is possible to handle and splice weak fiber ends. The physical process, in combination with an inserted protection sleeve covering the splice and the resting bare part of the brittle fiber, can make it possible to overcome the problem with degraded mechanical strength in the repair or rerouting of an aged fiber link.

Further studies are needed to find solutions to the problems with aged fiber coatings. Further interesting work is the possibility of making the treatment process applicable to field use.

ACKNOWLEDGEMENTS

The authors wish to thank Merja Herranen from the Institute of Chemistry, Uppsala University, for her valuable help with the AFM-studies.

REFERENCES

1. P. Hasloev, K. Bundgaard Jensen and N. Skovgaard
"Degradation Study for Stressed Optical Fibres in Water. New Worst Case Lifetime Estimation Model"
Proceedings 41th Int. Wire and Cable Symposium, pp. 423-427 (1992)
2. W. Griffioen
"Ageing of Optical Fibres in Water"
Proceedings 41th Int. Wire and Cable Symposium, pp. 622-628 (1992)
3. W. Griffioen, W. Ahn, A. De Boer and G. Segers
"Stress-induced and stress-free ageing of optical fibres in water"
Proceedings 40th Int. Wire and Cable Symposium, p. 673 (1991)
4. T. Volotinen, H. Yuce and R. Frantz
"Aging behaviour of fibers"
Proceedings SPIE 1993, Vol 1973, pp. 161-174
5. R. Robinson, H. Yuce
"Scanning Tunneling Microscopy of Optical Fiber Corrosion: Surface Roughness Contribution to Zero-Stress Aging"
J. Am. Ceram. Society, 74, pp. 814-818 (1991)
6. T. Volotinen, H. Yucc, N. Bonnano, R. Frantz and S. Duffy
"Splicing of aged fibers"
Proceedings SPIE 1993, Vol 1973, pp. 186-192
7. J. B. Murgatroyd
"The Strength of Glass Fibers. Part II. The Effect of Heat Treatment on Strength"
J. Soc. Glass Technology, 28, pp. 388-405 (1944)
8. M. Matthewson, C. Kurkijan and S. Gulati
"Strength Measurement of Optical Fibers by Bending"
J. Am. Ceram. Society, 69, pp. 815-821 (1986)



Göran Ljungqvist received his M.Sc. degree in Engineering Physics from the Royal Institute of Technology, Stockholm, in 1992. He has since then worked at the Optical Network Research Center.



Magnus Johansson received his M.Sc. degree in Engineering Physics from the Lund Institute of Technology in 1993. He has since worked at the Optical Network Research Center and has been engaged in the fields of erbium doped fiber amplifiers and ageing behaviour of optical fibers. He is a member of the Swedish Optical Society.



Leif Stensland received the degree licentiate in technology in optical physics from the Royal Institute of Technology, Stockholm, Sweden in 1971. Until 1982 he was with the Institute of Optical Research in Stockholm heading a group in fiber and integrated optics. He joined Ericsson Cables in 1982 as the manager for fiber and optical cable developments. His present position is manager of the Optical Network Research Center, at which studies and developments of specialty fibers are performed.

MEASUREMENT OF DISTRIBUTED STRAIN IN FROZEN CABLES AND ITS POTENTIAL FOR USE IN PREDICTING CABLE FAILURE

Toshio Kurashima*, Kazuo Hogari*, Satoshi Matsushashi**, Tsuneo Horiguchi*,
Yahei Koyamada*, Yutaka Wakui** and Hiroshi Hirano***

NTT Access Network Systems Laboratories*, **
Tokai-mura, Naka-gun, Ibaraki-ken, 319-11 Japan*
1-7-1 Hanabatake, Tsukuba-shi, Ibaraki-ken, 305 Japan**
NTT Technical Assistance & Support Center***
3-9-11 Midori-cho, Musashino-shi, Tokyo, 180 Japan

ABSTRACT

Distributed strain in an optical fiber cable frozen in a conduit was measured for the first time using Brillouin optical-fiber time domain analysis. Experimental results reveal that slotted-core type single-mode optical fiber cable suffered from the intense compressive force induced as the water in a conduit freezes along the cable. The compressed optical cable buckled and optical fibers in the cable broke. In addition, the experimental results show that the strain measurement has the potential for use in predicting cable failure due to water freezing in a conduit.

1. INTRODUCTION

When water freezes in a conduit in which an optical fiber cable is installed, the cable is subjected to very intense pressure, which is generated by the expanding volume of ice. To date, the optical loss increase has been examined for a twenty-four-fiber unit type multi-mode optical fiber cable in frozen water in a 3 m conduit [1]. The results revealed that the optical loss increase occurred due to the radial deformation of the cable caused by the lateral freezing pressure. However, little is known about the relationship between optical loss and the strain along the cable length caused by the pressure in frozen cables, especially when the cable has a realistic length of more than 100 m.

We have prepared a 135 m conduit in a long refrigerated room to simulate a frozen cable on a realistic scale in the field. This makes it possible to measure the distributed strain and loss in the frozen cable by using Brillouin optical-fiber time domain analysis (BOTDA) [2] and optical time domain reflectometry (OTDR) [3], respectively. This paper describes these experimental results and discusses the mechanism of cable failure resulting from frozen water in a conduit.

2. BOTDA MEASUREMENT TECHNIQUE

BOTDA [2] can be used to measure local changes in longitudinal strain along the length of a optical single-mode fiber. The method is based on the Brillouin interaction between the pulsed pump lights and the continuous-wave (CW) probe lights counterpropagating in optical fibers, as shown in Fig. 1. When the optical frequency difference $\Delta\nu$ between two lasers coincides with the Brillouin frequency shift ν_B at

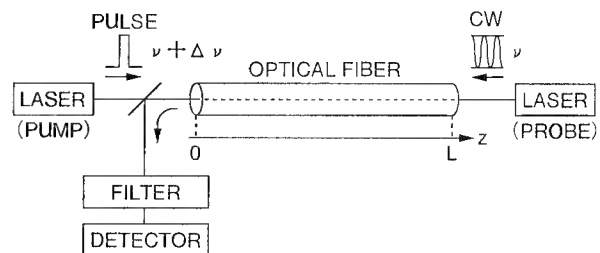


Fig. 1 Basic configuration of BOTDA.

some point in the fiber, the CW light is amplified [4] by the pulsed light. The amplified CW light is passed through an optical frequency filter at the fiber end into which the pulsed light is launched, and is detected by time-resolved measurement. The filter allows only the CW light to pass and rejects light at other frequencies including backscattered Rayleigh scattering and the Fresnel reflection of the pulsed light. Therefore, ν_B distribution can be determined by repeated measurement of the time dependent CW light power for various $\Delta\nu_s$, at which the amplified CW light power is maximized. It is known that ν_B increases in proportion to the strain induced in the fiber [5]. The strain coefficient of ν_B , $\partial\nu_B/\partial\epsilon$, at a wavelength of $1.55\ \mu\text{m}$, is given by [6]

$$\partial\nu_B/\partial\epsilon = 493\ \text{MHz}/1\% \quad (1).$$

Thus, spatially distributed strain is evaluated by measuring the ν_B distribution. The spatial resolution in BOTDA depends on the pulsed light width, as with conventional OTDR.

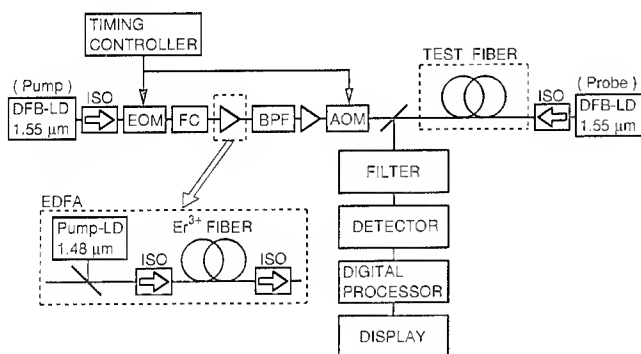


Fig. 2 Block diagram of BOTDA.

Figure 2 shows the configuration of the BOTDA system which we used to measure the distributed strain along a test optical fiber. Two laser beams, a pulsed light and a CW light, counterpropagate in the test fiber so that they interact through stimulated Brillouin scattering. Two frequency tunable distributed feedback laser diodes (DFB-LDs) operating at a wavelength of $1.55\ \mu\text{m}$, are used as light

sources. A pump pulsed light with a duration of 100 ns, which allows a 10 m spatial resolution, is generated from the DFB-LD by means of an electro-optical modulator (EOM). The pulsed light is amplified with two erbium-doped fiber amplifiers (EDFAs) consisting of an erbium-doped single-mode fiber pumped with a laser diode (Pump-LD) at a wavelength of $1.48\ \mu\text{m}$. An optical bandpass filter (BPF) and an acousto-optical modulator (AOM) are used to suppress the amplified spontaneous emission noise from the EDFAs in the frequency and the time domain, respectively. The timing of the AOM is synchronized with that of the EOM by using a timing controller. To eliminate the signal fluctuation due to the polarization dependence of Brillouin gain [7], the polarization states of the pulsed light are averaged by rotating the polarization of the pulsed light with a Faraday cell (FC). The temporal change in the probe CW light power is measured at the fiber end nearest the pulsed light source. These signals are then averaged by integrating them 2^{11} times using a digital-processing system. The Brillouin gain spectra along the fiber length are measured by varying the frequency difference between the two DFB-LDs, with a frequency interval of 10 MHz around the ν_B of approximately 11 GHz. The ν_B s along the fiber length are determined as the center frequency of the Brillouin gain spectra. Then, the ν_B distribution can be identified as the strain distribution along the fiber, by using the strain coefficient of ν_B in Eq. (1).

3. TEST CABLE

3.1 CABLE STRUCTURE

The distributed strain in a frozen cable was measured using a nonmetallic water-blocking (WB) optical fiber cable [8], whose length, outer diameter and weight were 160 m, 12 mm and 0.115 kg/m, respectively.

The WB cable structure is shown in Fig. 3. The cable is composed of six fiber ribbons, a

slotted-rod, a strength member made of Kevlar-FRP, water-blocking tapes [9] and a polyethylene (PE) sheath. Each ribbon contains four dispersion-shifted single-mode optical fibers. Two ribbons are stacked closely at the bottom of each slot. Thus, there were twenty-four optical fibers in the test cable. The water-blocking tape is wrapped around the slotted-rod.

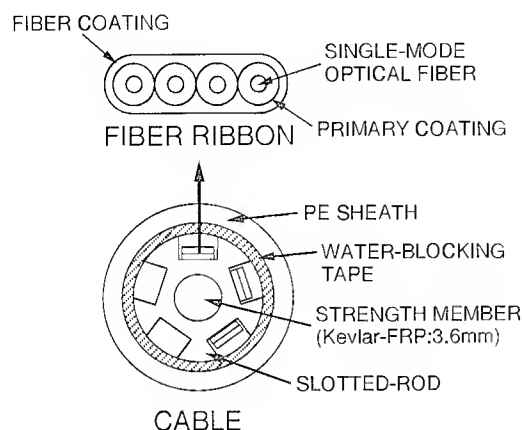


Fig. 3 Optical fiber cable structure.

3.2 THERMAL CHARACTERISTICS

When the strain distribution in the refrigerated cable was measured, the ν_B change due to temperature change must be corrected. The temperature dependence of ν_B and the measured thermal characteristics of the cable are given below.

Changes in both strain and temperature result in variations in the ν_B value in single-mode optical fibers [10]. Therefore, temperature change ΔT induces strain measurement error ε_1 in BOTDA. In addition, temperature change induces additional strain ε_2 due to the thermal expansion of the material surrounding the fiber, if the thermal expansion coefficient of the surrounding material differs greatly from that of the fiber and if the fiber is tightly stacked against the surrounding material of the cable. Temperature change ΔT , therefore, induces strain measurement error $\Delta\varepsilon$, which is given by

$$\Delta\varepsilon = \varepsilon_1 + \varepsilon_2, \quad (2)$$

$$\varepsilon_1 = (\partial\nu_B/\partial T) \times \Delta T / (\partial\nu_B/\partial\varepsilon) \quad (3)$$

$$\varepsilon_2 = \alpha \times \Delta T \quad (4),$$

where $\partial\nu_B/\partial T$, $\partial\nu_B/\partial\varepsilon$, and α are, respectively, the temperature coefficient of ν_B for bare fibers, the strain coefficient of ν_B , and the test cable thermal expansion coefficient. $\partial\nu_B/\partial T$ at a wavelength of $\lambda=1.55 \mu\text{m}$ is given by [10]

$$\partial\nu_B/\partial T = 1.00 \text{ MHz/}^\circ\text{C} \quad (5),$$

assuming ν_B varies as λ^{-1} [11]. Calculations with Eqs. (1) and (5) give an ε_1 value due to ΔT of about 0.002 %/ $^\circ\text{C}$. From Eq. (5), the error in the strain measurement caused by $\Delta T=5^\circ\text{C}$ is almost the same as the strain measurement accuracy of 0.01 % [2]. Therefore, temperature effects can be ignored for most applications. For accurate strain measurements, however, we must take into account the temperature effects given by Eqs. (2)-(5). Therefore, we measured the thermal characteristics of the test optical fiber cable.

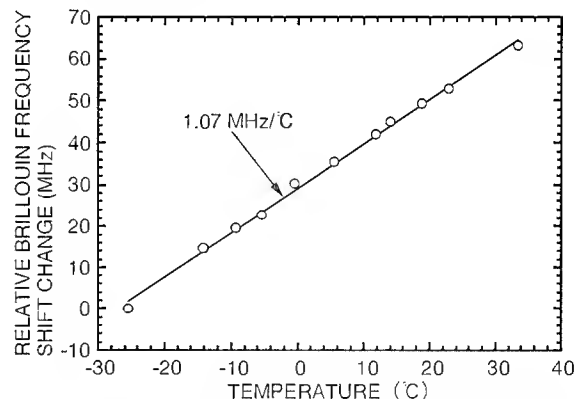


Fig. 4 Temperature dependence of the Brillouin frequency shift of the fiber in the test cable.

We prepared a test cable approximately 100 m in length to examine the ν_B change induced by ΔT . The test cable was coiled with a diameter of 4 m and placed in a thermostatic chamber. Care was taken to ensure that no additional mechanical stress was applied to the cable. The ν_B in eight sample fibers (Ribbons

No. 1 and 2) in the test cable were measured using BOTDA with a spatial resolution of 10 m, at temperatures ranging from -25 to +35 °C. Brillouin frequency shift ν_B as a function of temperature T is shown in Fig. 4. The ν_B values plotted in Fig. 4 were obtained from the average ν_B of the eight measured fibers. Figure 4 shows that the change in ν_B is proportional to the change in T , with a slope of 1.07 MHz/°C. The slope is in good agreement with the previously reported value for bare fibers [10], which is given by Eq. (5). This result indicates that the thermal expansion coefficient of the test cable is not in the -25 to +35 °C temperature range. This means that the thermal stress ε_2 due to the difference in the thermal expansion coefficients in the fiber and surrounding material can be ignored. In the strain measurements described below, the strain error has been corrected by using the coefficient of 1.07 MHz/°C.

4. EXPERIMENT

Figure 5 shows the experimental configuration of the measurement apparatus and the test cable. The test cable was first installed in a steel conduit, whose respective length and inner diameter were 135 m and 80 mm. This was located in a 150 m long refrigerated room, and then the conduit was filled with water. The conduit was cooled from room temperature to -20 °C and was kept constant for six days. A 30 m long heat insulator made of glass wool 0.1 m thick, was wrapped around the mid-section (section BC) of the conduit in order to simulate temporal and

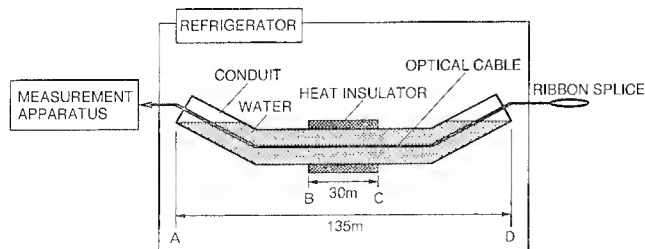


Fig. 5 Optical fiber cable and conduit configuration.

local changes in temperature in field-installed optical fiber cables. In order to investigate the mechanism which causes optical fiber cable failure as a result of water freezing in the conduit, we measured both the distributed strain and loss along the cable length using BOTDA and OTDR, respectively, with a spatial resolution of 10 m. In addition, optical transmission loss was also measured using both a CW light source at a wavelength of 1.55 μm and a power meter. The measurement was carried out in eight fibers to measure even a slight loss change. The ribbons accommodated in the different slots in the cable were spliced in series at both ends of the cable to investigate the strain and the optical loss characteristics of the test cable. The temperature of the conduit surface with and without the heat insulator was also measured by two thermocouples.

In addition to the experiment mentioned above, we performed the same experiment but without the heat insulator to examine the behavior of the frozen cable without temporal and local changes in temperature along the conduit.

5. RESULTS

5.1 TEMPERATURE MEASUREMENT

In the experiment, the water-filled conduit is cooled from room temperature to -20 °C for six days. In Fig. 6, the solid and broken lines show the temperature of the conduit surface with and without the heat insulator, respectively. To in Fig. 6 denotes the time at which the water in the mid-section (section BC) starts to freeze, since the temperature of the conduit surface in the center of section BC fell to 0 °C at time T_0 . While the temperature of the conduit surface in both section AB and section CD without the heat insulator, was about -20 °C at time T_0 . This means the water in these regions has already frozen. Thus, it is confirmed that the water in the mid-section of the conduit began to freeze

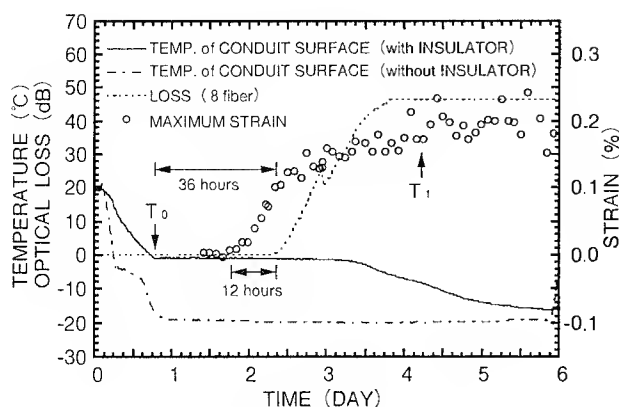


Fig. 6 Optical loss and maximum strain change.

when both ends of the section were tightly sealed with frozen water, namely the ice in section AB and section CD.

5.2 OPTICAL LOSS MEASUREMENT

The dashed line in Fig. 6 shows the change in optical transmission loss of eight fibers spliced in series, in the experiment with the insulator. Figure 6 shows that the optical loss began to increase 36 hours after time T_0 . As described in chapter 5.3 below, there was a gradual increase in the strain along the cable as well as in the optical loss. The optical loss finally exceeded the measurement limit of about 46 dB. The optical loss per fiber can be estimated at more than 5 dB ($\cong 46 \text{ dB}/8 \text{ fiber}$). OTDR is a technique used for locating faults in optical fibers. Figure 7 shows the backscattered

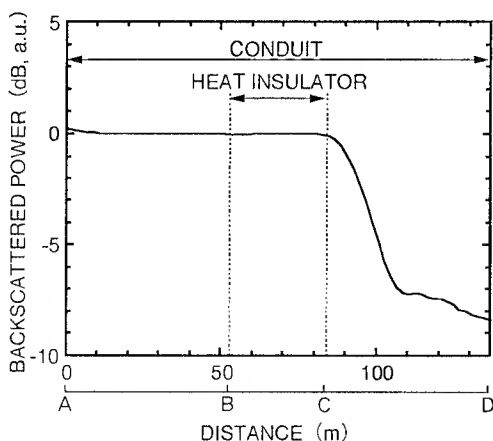


Fig. 7 Backscattered waveform obtained from OTDR.

waveform obtained using OTDR at time T_1 . The optical loss increased near point C, which was one end of the mid-section (section BC). However, no optical loss increase was observed at point B under the same conditions as point C. This difference between points B and C with regard to optical loss increase, is discussed in section 6. In another experiment performed under the same conditions, the optical fiber loss gradually increased and all the fiber ribbons in the test cable finally broke because the cable buckled near one end of the mid-section. This behavior of the frozen cable in the conduit will also be discussed in section 6.

No optical loss increase was observed in the experiment without the heat insulator.

5.3 STRAIN MEASUREMENT

The circles in Fig. 6 show the maximum tensile strain changes along the test cable in the mid-section with the heat insulator. Figure 6 shows that the strain increase along the test optical cable was first observed 24 hours after time T_0 in the mid-section of the conduit. The strain gradually increased to approximately 0.2 % about four days later. It is noted that the tensile strain along fiber length began to increase 12 hours before the optical loss began to increase. The measured strain distribution in the test fiber at time T_1 , shown in Fig. 6, is given in Fig. 8. From Fig. 8, we can see that a large amount of tensile strain (about 0.2 %) was

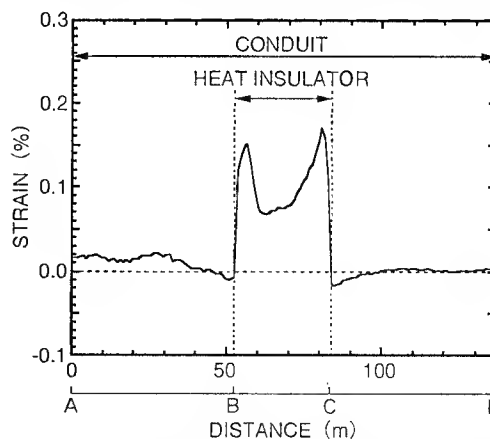


Fig. 8 Strain distribution obtained from BOTDA.

induced in section BC, especially near its ends. Then, slight compressive strain was observed just beyond the two ends of section BC. However, the optical loss increase was only observed at one end of the mid-section, as described in chapter 5.2. The reason for this will be discussed in section 6.

There was no change in the strain along the fiber in the experiment without the heat insulator.

5. 4 OUTER APPEARANCE INVESTIGATION

After completing the freezing experiment in the long refrigerated room, the test cable was pulled out of the conduit, and the cable sheath, the slotted-rod and the optical fiber ribbons were examined.

Oval holes and slight buckling were found in the cable sheath 1 m from the two ends of the mid-section. The holes may have been formed when the ice increased in volume in the conduit and the cable was pressed and dragged to the hollows on the inside wall of the conduit. The hollows are at the joints of the 5.5 m long conduit, and are 15 mm wide. Their depth corresponds to the conduit thickness of 4 mm. Thus, we can see that the optical loss in the hollow increases due to the cable buckling, which is induced by very intense pressure. In addition to this, we found from the shapes of the oval holes that the cable near both ends of the mid-section had moved, due to water freezing in the conduit. The movement was in the direction from the mid-section towards the conduit ends. There was also no damage to the optical fiber ribbons, although there was a slight deformation of the slotted-rod. In another experiment performed under the same conditions, the cable was buckled as described in chapter 5.2. Figure 9 shows a buckled slotted-rod and broken optical fiber ribbons. The buckling is observed in the test cable approximately 0.4 m from point C in the direction towards the conduit end (point D), although the cable did not buckle near point B.



Fig. 9 Damaged slotted-rod and optical fiber ribbons.

No deformation was observed in the test cable as a results of water freezing in the conduit in the experiment without the heat insulator.

6. DISCUSSION

This section discusses the mechanism of the cable failure as a result of water freezing in a conduit.

From Figs. 6-8 and an investigation of the appearance of the test cable, the following results were obtained : (a) the optical loss began to increase 12 hours after an increase in the strain, (b) tensile strain occurred in the mid-section (section BC) of the conduit, (c) the optical loss near point C increased due to cable buckling, (d) compressive strain occurred near both ends of section BC, and (e) the cable near points B and C moved towards the conduit ends, points A and D, respectively.

On the basis of these experimental results, let us consider the mechanism of the cable failure.

We believe that the water in the conduit gradually freezes from the inside wall of the conduit towards its center axis. Assuming the water freezes uniformly along the conduit, the water near the axis of the conduit is pushed out from the conduit ends, since the volume of ice near the inside wall of the conduit expands. Then, the intense pressure caused when water freezes does not occur, and the frozen cable will not fail. In our experiment, the cable did not fail without the insulator.

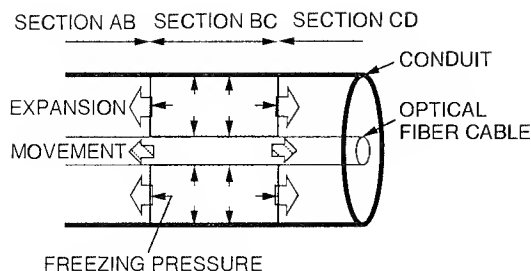


Fig. 10 Mechanism of the cable buckling in a conduit.

Now, let us consider cable behavior when there is a temperature distribution along the conduit. Figure 10 is a schematic side view of a water-filled conduit in which an optical fiber cable is installed. We assume that the water in Section BC begins to freeze after that in Sections AB and CD has frozen. Since the water expands as it freezes, very intense freezing pressure occurs in Section BC. The ice in Section BC may expand towards Sections AB and CD, provided that conduit expansion can be ignored. Then, tensile strain is induced in the cable in Section BC, because the cable is elongated as the volume of ice increases. Compressive strain is induced in the cable adjoining Section BC, because the cable near Section BC is compressed by the elongated cable in the same Section. Thus, the frozen cable in the conduit is buckled due to longitudinal compressive stress near both ends of Section BC. We can therefore expect that the optical loss will gradually increase and finally the fiber will break. The experimental results mentioned earlier support these assumptions and expectations.

Finally, we would like to focus attention on an analysis of our experimental optical loss distribution measurements. From Fig. 7, we can see that the optical loss increased only near point C. In another experiment performed under the same conditions, the optical fiber ribbon broke near point C. However, compressive strain occurred near both ends of section BC, as shown in Fig. 8. This discrepancy between the strain and loss distribution measurements

may have resulted from a slight temperature unevenness along the conduit in the refrigerated room. As far as the cooling speed in the refrigerated room is concerned, we confirmed that the temperature near point B inside the room fell to -20°C earlier than that near point C. Therefore, it is likely that the cable in section BC was lengthened much further, due to the expanding volume of ice in the conduit, in the point C direction than in the point B direction. Therefore, we consider that greater longitudinal compressive stress occurred near point C, and this induced the cable buckling and optical loss increase at that point.

7. CONCLUSION

We conclude from these experimental results that the optical loss in slotted-core type single-mode optical fiber cable frozen in a conduit increases because of cable buckling resulting from longitudinal compressive stress rather than because of bending caused by lateral pressure. The compressive stress is induced by the pressure of the water as it freezes along the cable. Another important conclusion is that distributed strain measurement using BOTDA makes it possible to predict the fiber failure caused by water freezing in the conduit, because the strain begins to occur much earlier than the optical fiber loss.

ACKNOWLEDGMENT

The authors are grateful to K. Ishihara and T. Morimitsu for their helpful suggestions and comments.

REFERENCES

- [1] M. Tanaka, T. Kobayashi, Y. Sugawara, K. Inada, C. Tanaka, Y. Katsuyama, and Y. Ishida, "Optical-cable properties under frozen water in a conduit and a suitable method for

prevention of degradation", *Electron. Lett.*, Vol. 17, No. 21, pp. 796-798, 1981.

[2] T. Horiguchi, T. Kurashima, and Y. Koyamada, "Measurement of temperature and strain distribution by Brillouin frequency shift in silica optical fibers", *Technical Digest of SPIE, Distributed and Multiplexed Fiber Optic Sensor II*, pp. 1-13, 1992.

[3] M. K. Barnoski and S. M. Jensen, "A novel technique for investigating attenuation characteristics", *Appl. Opt.*, Vol. 15, No. 9, pp. 2112-2115, 1976.

[4] N. A. Olsson and J. P. van der Ziel, "Cancellation of fiber loss by semiconductor laser pumped Brillouin amplification at 1.5 μm ", *Appl. Phys. Lett.*, Vol. 48, No. 20, pp. 1329-1330, 1986.

[5] T. Horiguchi, T. Kurashima, and M. Tateda, "Tensile strain dependence of Brillouin frequency shift in silica optical fibers", *IEEE Photon. Tech. Lett.*, Vol. 1, No. 5, pp. 107-108, 1989.

[6] T. Kurashima, T. Horiguchi, M. Tateda, and Y. Koyamada, "Large extension of dynamic range in distributed fiber strain measurement by using Brillouin spectroscopy", *Technical Digest of CLEO, CThN5*, pp. 416-4117, 1991.

[7] R. H. Stolen, "Polarization effects in fiber Raman and Brillouin lasers", *IEEE Quantum Electron.*, Vol. QE-15, No. 10, 1157-1160, 1979.

[8] F. Ashiya, K. Hogari, and K. Omoto, "A water-blocking optical fiber cable system for subscriber networks", *NTT Rev.*, Vol. 3, No. 1, pp. 110-116, 1991.

[9] S. Kukita, T. Nakai, A. Hayashi, and H. Koga, "Design and performance of nonmetallic waterproof optical fiber cable using water-absorbent polymer", *IEEE J. Lightwave Tech.*, Vol. LT-7, No. 4, pp. 740-746, 1989.

[10] T. Kurashima, T. Horiguchi, and M. Tateda, "Thermal effects on the Brillouin frequency shift in jacketed optical silica fibers", *Appl. Opt.*, Vol. 29, No. 15, pp. 2219-2222, 1990.

[11] D. Cotter, "Stimulated Brillouin scattering in monomode optical fiber", *J. Opt. Commun.*, Vol. 4, No. 1, pp. 10-19, 1983.



Toshio Kurashima
NTT Access Network
Systems Laboratories
Tokai-mura, Naka-gun,
Ibaraki-ken, 319-11
Japan

Toshio Kurashima was born in Nagano, Japan, on June 16, 1961. He received B. S. and M. S. degrees in electronic engineering from the University of Electro-Communications, Tokyo, Japan, in 1986 and 1988, respectively. He joined NTT Transmission Systems Laboratories in 1988. He has been engaged in research on optical fiber distributed sensing techniques. Since 1994, he has been engaged in research at the NTT Access Network Systems Laboratories. Mr. Kurashima is a member of the Institute of Electronics, Information and Communication Engineers (IEICE) of Japan and the Japan Society of Applied Physics. He received the IEICE Excellent Paper Award and Young Engineer Award in 1991 and 1992, respectively.



Kazuo Hogari
NTT Access Network
Systems Laboratories
Tokai-mura, Naka-gun,
Ibaraki-Ken, 319-11
Japan

Kazuo Hogari was born in Ibaraki, Japan, on February 28, 1959. He received a B. S. degree in electrical engineering from Ibaraki University in 1981. He joined the NTT Electrical Communications Laboratories in 1981, where has been engaged in the research and development of high-fiber-count and high-density optical fiber cables. His current interests include premises distribution systems. Mr. Hogari is a member of the IEEE, and the Institute of Electronics, Information and Communication Engineers of Japan.



Satoshi Matsuhashi
NTT Access Network
Systems Laboratories
1-7-1 Hanabatake,
Tsukuba-shi,
Ibaraki-ken, 305 Japan

Satoshi Matsuhashi is a Senior Engineer at NTT Access Network Systems Laboratories. He received his B. E. degree in electronic engineering from Hokkaido University in 1981. He joined NTT in 1981. He is engaged in the development of aerial cable installation and cable splicing techniques. He is a member of the Institute of Electronics, Information and Communication Engineers of Japan.



Yahei Koyamada
NTT Access Network
Systems Laboratories
Tokai-mura, Naka-gun,
Ibaraki-ken, 319-11
Japan

Yahei Koyamada was born in Mie, Japan, on September 15, 1947. He received B. E., M. E., and D. E. degrees, all in electrical engineering from Osaka University, in 1970, 1972 and 1978, respectively. He joined the NTT Electrical Communication Laboratories in 1972. From 1972 to 1977, he was engaged in research on surface acoustic wave device. Since 1978 he has been engaged in development research on optical fiber cables and related measurement techniques. He is now Executive Manager of the Optical Transmission Line Systems Laboratory, NTT Access Network Systems Laboratories, Ibaraki, Japan. Dr. Koyamada is a member of the IEEE and the Institute of Electronics, Information and Communication Engineers of Japan.



Tsuneo Horiguchi
NTT Access Network
Systems Laboratories
Tokai-mura, Naka-gun,
Ibaraki-ken, 319-11
Japan

Tsuneo Horiguchi was born in Tokyo, Japan, on June 5, 1953. He received B. E. and Dr. Eng. degrees from the University of Tokyo, Tokyo, Japan, in 1976 and 1988, respectively. In 1976, he joined the Ibaraki Electrical Communication Laboratory, NTT, Ibaraki, Japan, where he worked on the measurement technology of the transmission characteristics of optical fiber cable. Since 1988, he has worked in the field of optical fiber distributed sensing. He is presently a Senior Research Engineer, Supervisor of NTT Access Network Systems Laboratories. Dr. Horiguchi received the IEICE Excellent Paper Award in 1991. He is a member of the IEEE, the Optical Society of America, and the Optical Society of Japan.



Yutaka Wakui
NTT Access Network
Systems Laboratories
1-7-1 Hanabatake,
Tsukuba-shi,
Ibaraki-ken, 305 Japan

Yutaka Wakui was born in Tokyo, Japan, on March 21, 1943. He received a B. S. degree in electronics and communication engineering from Waseda University in 1966. He joined the Nippon Telegraph and Telephone Public Corporation in 1966 to work on outside plant planning and telephone office management. He was Executive Manager of the Facility Planning and Coordination Division in the Technical Planning Bureau from 1986 to 1989, and Vice President of Tokai Branch Office from 1989 to 1991. He is currently Director of NTT Access Network Systems Laboratories. Mr. Wakui is a member of the Institute of Electronics, Information and Communication Engineers of Japan.



Hiroshi Hirano
Technical Assistance &
Support Center
3-9-11 Midori-cho,
Musashino-shi,
Tokyo, 180 Japan

Hiroshi Hirano was born in 1960 and received a B. E. degree in architectural engineering from Toyo University in 1982. He joined Nippon Telegraph and Telephone Public Corporation in 1982. He was mainly engaged in system engineering and maintenance for metallic and optical fiber cables in telecommunication networks. Since 1992, at the Technical Assistance & Support Center, he has been active as a technical consultant and in the development of outside plant and line engineering in telecommunication systems.

EFFECT OF PARAMETER DIFFERENCES ON THE FIBER SPLICE LOSS AND EASY BIDIRECTIONAL OTDR MEASUREMENT IN THE FIELD INSTALLATION

Zhang Wanchun

Dalian Vastone Communication Cable Corp., Dalian, P.R. China

Risheng Yang, Ferdi Schank

Siecor GmbH & Co.KG, F.R.Germany

ABSTRACT

This work reports on fiber splice results from the world's longest aerial optic cable. The effect of fiber manufacturing process, mode field diameter (MFD)- and refractive index mismatch on splice loss have been studied both theoretically and experimentally. Furthermore, a "return circuit" method has been proposed for easy bidirectional OTDR measurements of splice loss in field installations. Using this method, the mean splice loss at 1,310 nm of 1,500 splices along a distance of 346 km is 0.037 dB.

INTRODUCTION

An important part of any installed optical fiber cable is the fiber splice, which has a great influence on the transmission quality. Splice losses can be divided into extrinsic and intrinsic ones. Extrinsic losses are related to the techniques used to splice fibers and are caused by parameters such as transverse offset between the fiber cores, fiber end separation, axial tilt, and fiber cleaving angle. Intrinsic losses are related to the properties of fibers and are caused by MFD mismatch, circularity and concentricity of core and cladding diameters. MFD mismatch is the major contributor to intrinsic splice losses.

This work reports on a part of the fiber splice results of a 4,700-kilometer-long optic cable line, which today is the longest aerial cable in the world. The trunkline connects Beijing with China's southern-most Hainan Island. Considering the large quantity of fibers involved, more than one manufacturer was needed. In this paper the influence of fiber manufacturing process, MFD- and refractive index mismatch on splice losses have been studied both theoretically and experimentally. Furthermore, a "return circuit" method has been proposed for easy bidirectional OTDR measurements of splice losses in the field installation.

OTDR TRUE AND APPARENT SPLICE LOSSES

OTDR is now commonly used to estimate splice losses for single-mode fibers in the field installation. In view of some misunderstanding and misuse regarding measurement by OTDR, the OTDR true and apparent splice losses will be discussed.

According to /1/, the backscattered power detected by OTDR from a point immediately preceding the splice is given by

$$P_1 = P_0 S_1 \exp(-2\alpha_1 L_1) \quad (1)$$

where P_0 is the initial power level, L_1 the fiber length, α_1 the attenuation coefficient, and S_1 the capture fraction, the latter being given by /2/

$$S_1 = 0.038 \left(\frac{\lambda}{n_1 w_1} \right)^2 \quad (2)$$

where λ is the wavelength, w_1 and n_1 the MFD and core refractive index, respectively. The subscript 1 refers to the input fiber.

The backscattered power detected by OTDR from a point immediately following the splice is given by /1/

$$P_2 = P_0 S_2 T_{12} T_{21} \exp(-2\alpha_1 L_1) \quad (3)$$

where T_{12} is the splice transmission value in the forward direction, and T_{21} the corresponding quantity in the reverse direction. S_2 is given by

$$S_2 = 0.038 \left(\frac{\lambda}{n_2 w_2} \right)^2 \quad (4)$$

where the subscript 2 refers to the output fiber.

The one-way OTDR splice result is determined from the ratio of these two power levels

$$\alpha_{12} = 20 \log \left[\frac{1}{2} \left(\frac{w_1}{w_2} + \frac{w_2}{w_1} \right) \right] + 10 \log \frac{w_2}{w_1} + 10 \log \frac{n_2}{n_1} \quad (5)$$

In Eq.(5) the first term describes the true splice loss caused by MFD mismatch, the second and third terms imply the apparent losses due to MFD- and refractive index mismatch of the two fibers, respectively.

From Eq.(5), the one-way splice loss obtained via OTDR technique is equal to the true splice loss plus two apparent losses. Therein the contribution of the third term can be neglected because of its much smaller value compared to that of the second term. As the absolute value of the second term may be much larger than the true splice loss, a one-way OTDR result may exceed the true splice loss by far, or even turn into an apparent gain!

Similarly, the one-way OTDR value when measuring from the opposite direction is given by

$$\alpha_{21} = 20 \log \left[\frac{1}{2} \left(\frac{W_1}{W_2} + \frac{W_2}{W_1} \right) \right] + 10 \log \frac{W_1}{W_2} + 10 \log \frac{n_1}{n_2} \quad (6)$$

Obviously, the true splice loss is obtained by averaging Eqs. (5) and (6):

$$\alpha_s = 20 \log \left[\frac{1}{2} \left(\frac{W_1}{W_2} + \frac{W_2}{W_1} \right) \right] \quad (7)$$

The double and the single lines in Figure 1 show the true and apparent splice losses, respectively, as a function of the MFD mismatch. As shown in Figure 1, a 10% MFD mismatch contributes approximately 0.45 dB to the one-way results, but only 0.05 dB to the true splice loss, which, as just mentioned, is determined by the average value of the OTDR measurements from both directions.

The single one-way OTDR value does not provide true splice loss but only an apparent loss because of fiber backscatter parameter variations. In the field installation one-way values up to 0.6 dB may be accepted. To check the theoretical results, we spliced a series of fibers with different MFDs, and measured the splice loss at 1310 nm by cutback as well as one-way and two-way OTDR methods. Measured results for both one-way and bidirectionally averaged results are also shown in Figure 1. The measured values agree with the calculated ones. Figure 2 shows the correlation between measured cutback losses and OTDR average losses. The difference between splice losses measured by both methods is only 0.003 dB with a standard deviation of 0.012 dB.

APPARENT LOSS DUE TO THE REFRACTIVE INDEX MISMATCH

From Eq.(5), the additional apparent loss due to the refractive index mismatch of the two fibers with the same MFDs is given by

$$\alpha_i = 10 \log \frac{n_2}{n_1} \approx 10 \log \frac{1 + \Delta_2}{1 + \Delta_1} \quad (8)$$

where Δ_2 and Δ_1 are the relative refractive index differences of the input and output fibers, respectively. Figure 3 shows the additional apparent loss versus the mismatch of the relative refractive index difference. As shown in Figure 3, a mismatch of refractive index difference has little influence on both apparent as well as true OTDR splice loss as long as MFD remains the same.

INFLUENCE OF THE MANUFACTURING PROCESS ON SPLICE LOSS

To study the influence of the manufacturing process, matched clad fibers produced by four different suppliers were chosen. Three of the suppliers used the OVD method, one used MCVD technique. The mean splice losses at 1,310 nm between OVD fibers from different suppliers and between OVD and MCVD fibers are 0.04 dB and 0.06 dB, respectively. Figure 4 shows the distribution of the splice losses between OVD and MCVD fibers. These results show that telephone companies can use a fusion splicer for joining the matched clad fibers from different suppliers, regardless of the manufacturing process.

ACTUAL SPLICE RESULTS IN THE FIELD INSTALLATION

For accurate determination of splice loss with an OTDR, measurements taken from both directions through a fiber are necessary. In the field installation, however, a two-way measurement is time consuming and in certain cases difficult to carry out. During construction of the splices for the Beijing - Hainan line one-way OTDR values were commonly used to estimate the true splice loss. The entire repeater spacing was reviewed by two-way OTDR method immediately after completion of each repeater spacing construction. The corresponding flow chart is shown in Figure 5. In the following we present the fiber splice results of the 1,034 km long Beijing-Xinyang route, which belongs to the north section of the Beijing-Hainan Island line, and which is installed in Hebei and Henan provinces of China. Table 1 shows the statistical results of splice losses, which are based on the data for the Beijing-Xinyang route with 6,348 measured splice losses. It is shown that with the quality of the fusion splicer available today, a mean splice loss of less than 0.07 dB can be reached, fol-

lowing the flow chart in Figure 5 and using one-way OTDR values in the field installation.

In some cases, as for a longer repeater spacing, a much tighter splice loss of, for example, less than 0.05 dB may be required; then it is not sufficient using one-way OTDR values to estimate the true splice loss. In order to be able to splice single-mode fibers with a mean splice loss of less than 0.05 dB in the field installation, a "return circuit" method is proposed. Figure 6 shows the basic configuration for this method. The cabled fibers 1 and 2, for example, are concatenated to form a continuous loop for the splice measurement. At first the OTDR signal is launched into fiber 1, and one-way OTDR values for both splice 1 and splice 2 are obtained. Then the signal is launched into fiber 2, and one-way values for splice 1 and splice 2 are obtained from the opposite direction. Thus, with one single OTDR and one fusion splicer we are able to carry out bidirectional OTDR measurements in the field installation quite easily. Using the "return circuit" method, we were successful in preparing all the splices in the 364 km long Xian-Yanan route with 1,500 splices. The thereby obtained statistical results and distribution of splice losses are shown in Table 1 and in Figure 7, respectively. From Table 1, the mean true loss of the 1,500 splices is 0.037 dB.

CONCLUSION

The effect of different fiber manufacturing processes as well as MFD- and refractive index mismatch on splice losses have been studied both theoretically and experimentally. A 10% MFD mismatch contributes approximately 0.45 dB to the one-way OTDR values, but only 0.05 dB to the true splice loss. In the field installation one way values up to 0.6 dB may be accepted. The manufacturing process has only a limited influence on the splice loss, and telephone companies can therefore splice together the matched clad fibers from different suppliers, regardless of the manufacturing process. Using one-way OTDR measurement values to estimate roughly the true splice loss, a mean splice loss of less than 0.07 dB was obtained in the field installation. For much tighter splice loss requirements, a "return circuit" method has been proposed. Using this method, along a distance of 346 km a mean splice loss of 0.037 dB has been obtained for 1,500 splices.

ACKNOWLEDGEMENTS

The authors would like to acknowledge W. Renken for his encouragement and support. They would also like to thank S. Uebelhack for her kindful help with manuscript preparation.

REFERENCES

- /1/ C.M.Miller, S.C.Metter and I.A.White, Optical Fiber Splices and Connectors, Marcel Dekker Inc., New York and Basel, 1986, pp. 217
- /2/ E.-G.Neumann, Single-Mode Fibers, Springer-Verlag, 1988, pp. 353

	Beijing-Xinyang Route	Xian-Yanan Route
Total Length (km)	1,034	364
Number of Values	6,348	1,500
Average Values (dB)	0.069	0.037
Minimum Values (dB)	0	0
Maximum Values (dB)	0.490	0.336
Percentage of Values greater than 0.1 dB (%)	20.4	0.47

Table 1: Splice Results of the Beijing-Xinyang Route and the Xian-Yanan Route

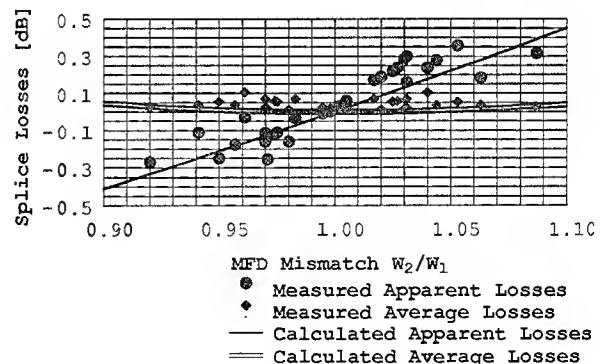


Fig. 1: OTDR Apparent and Average Splice Losses vs. MFD Mismatch

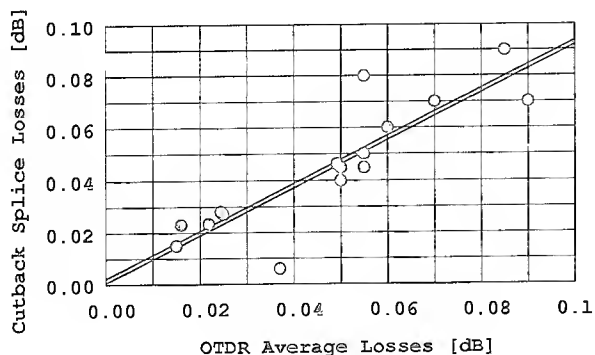


Fig. 2: Correlation between Splice Losses measured by Cutback- and Two-Way OTDR Methods

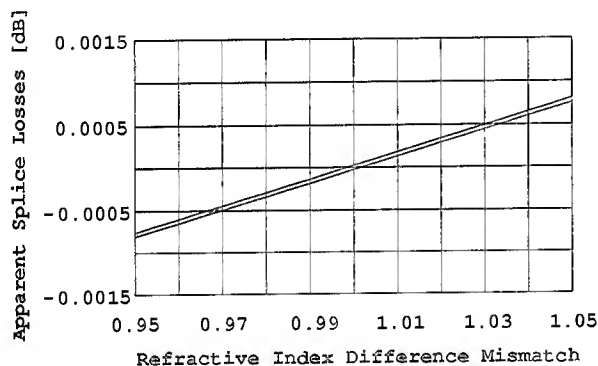


Fig. 3: OTDR Apparent Splice Losses vs. Relative Refractive Index Difference Mismatch

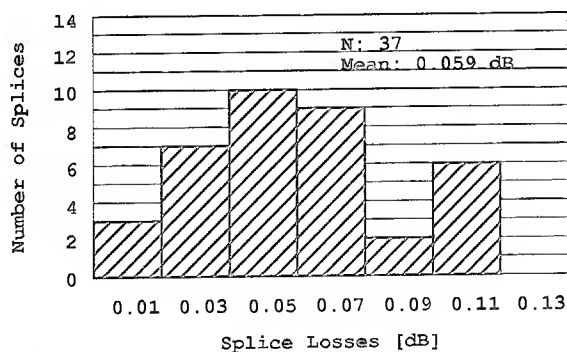


Fig. 4: Splice Losses between OVD- and MCVD Fibers

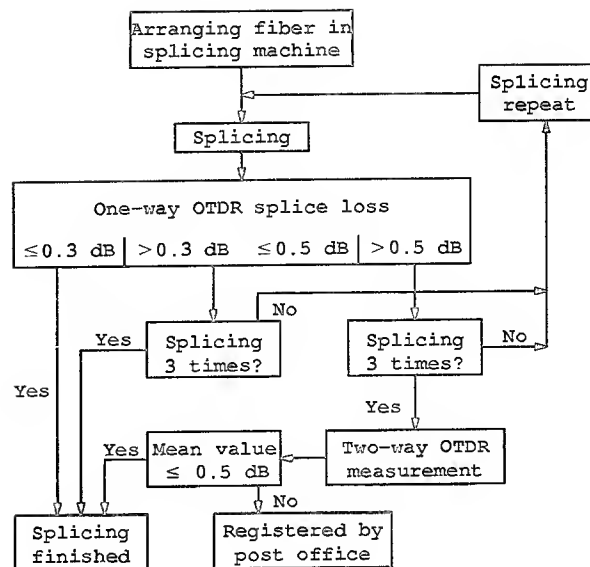


Fig. 5: Flow Chart for Splicing during Field Installation

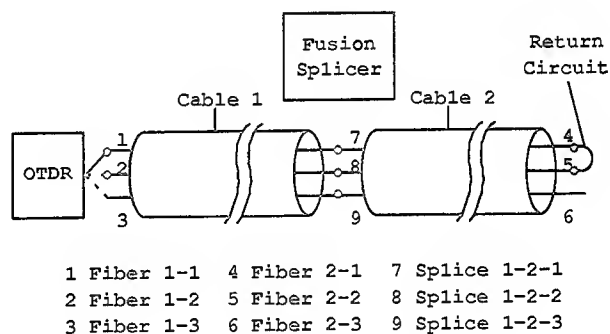


Fig. 6: Basic Configuration for "Return Circuit" Method

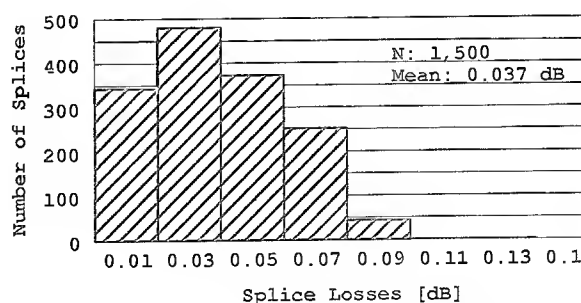


Fig. 7: Distribution of Splice Losses for a 364 km long Route



Zhang Wanchun
Dalian Vastone Communication
Cable Corp.
Dalian, P.R. China

Zhang Wanchun graduated from Radio Engineering Department of Beijing Institute of Posts and Telecommunications, China, in 1968. From 1985 to 1987 he was a Visiting Scholar at Institute of Electrical Communications, Northeast University, Japan. He used to be the Chief of Technology Section, Senior Engineer of the Houma Cable Factory, and now he is acting as the Chief Engineer of Dalian Vastone Communication Cable Corp., Fiber Optic Cable Plant.

Dr. rer. nat. degree from the Universität des Saarlandes for contributions to the field of nonlinear physics in 1984 and 1990, respectively. In 1991, he joined Siecor GmbH & Co.KG as a Product and Application Engineer for fiber optics. Dr. Schank is a member of the German Physical Society.



Risheng Yang
Siecor GmbH & Co.KG
Neustadt/Coburg, Germany

Risheng Yang graduated from Physics Department of Tsinghua University, China, in 1968. He received the M. Sc. degree from Chengdu Institute of Radio Engineering, China, in 1981 and Ph. D. degree from the Technical University of Braunschweig, Germany, in 1988, both in electrical engineering. Since 1984 he has continually worked in the area of optical fibers. He joined Siecor GmbH & Co.KG in 1991 after prior employment at AEG Kabel. Dr. Yang is a member of the Optical Society of America and SPIE.



Ferdi Schank
Siecor GmbH & Co.KG
Neustadt/Coburg, Germany

Ferdi Schank was born in Völklingen, Germany, in 1960. He received the Dipl. Phys. degree and the

Remote Optical-fiber Testing System For Unrepeatered Long-span Optical-fiber Trunk lines

Shinji GOTO*, Izumi SANKAWA**, Tsuneo HORIGUCHI***, and Naoyuki ATOBE*

*NTT Network Systems Development Department

**NTT Technology Research Department

***NTT Access Network Systems Laboratories

Abstract

This paper proposes a testing method that suppresses fluctuations in the test light caused by stimulated Raman scattering. The key feature of this method is that the direction of the test light is made the same as that of the communication light. Since the test light wavelength is $1.65\ \mu\text{m}$, it is possible to monitor the characteristics of an in-service dispersion-shifted fiber whose communication-light wavelength is $1.55\ \mu\text{m}$. A high-power communication light ($1.55\ \mu\text{m}$) produces a peak of stimulated Raman scattering in the $1.65\text{-}\mu\text{m}$ band. According to the establishment of function for detecting the communication light direction, the measurement error caused by stimulated Raman scattering was suppressed.

1. Introduction

To increase the cost-effectiveness of optical repeater lines, NTT is using optical-fiber amplifier technology to double the maximum spacing between repeaters along its DSF (Dispersion Shift Fiber) cables (whose communication wavelength is $1.55\ \mu\text{m}$) from 80 to 160 km. To handle this increased spacing, we have also increased the effective length of the FITAS (Fiber Transfer and Test System)⁽¹⁾⁽²⁾ used to maintain and transfer these optical repeater lines. The FITAS system structure is shown in Fig. 1.

FITAS is an operational system that supports the construction and maintenance of optical-fiber trunk line and junction transmission lines. The main functions provided by this system are automatic testing of optical fibers and the remote transfer of optical fibers, which is enabled by the use of transfer connectors. In the regular testing of optical repeater

paths a loss tester is used to measure the loss of optical-fiber lines. In DSF cables, testing is done using the $1.31\text{-}\mu\text{m}$ light that does not interrupt data transmission. However the increasing length of optical repeater paths has made it impossible to monitor the test light because the maximum cable length is 160 km. Consequently, the $1.65\text{-}\mu\text{m}$ light was chosen for test.

The high-power level communication light ($\lambda = 1.55\ \mu\text{m}$) affects the test light by stimulated Raman scattering in the silica optical fiber.

We therefore considered the theoretical effects of stimulated Raman scattering on the test light and transmitted the optimum testing method for the FITAS. This paper describes a practical new testing method for FITAS.

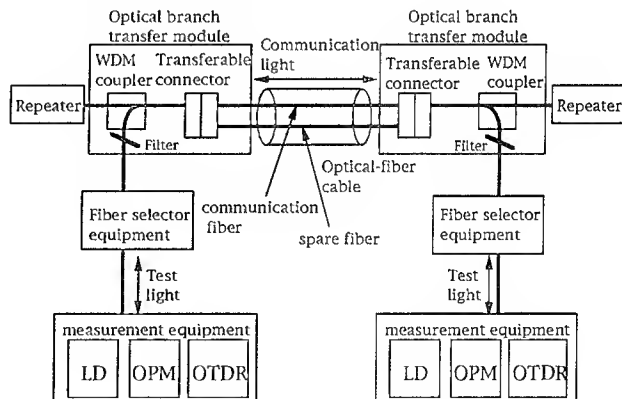


Figure 1. Structure of FITAS

2. Effect of Stimulated Raman scattering on test light

Stimulated Raman scattering is a stimulated phenomenon whereby the frequency of strode light is shifted by nonlinear optical effects due to interaction between light waves and phonons.⁽³⁾

The long-wavelength shifted light is called "Stokes shifted", and the short-wavelength shifted light is called "anti-Stokes shifted". The frequency shift is 13 THz in the silica optical fiber. When the wavelength of the transmitted light is 1.55 μm , the center wavelengths of Stokes and anti-Stokes shifted lights are 1.65 μm and 1.45 μm respectively. The Stokes-shifted light is approximately five orders of magnitude more intense than the anti-Stokes light at normal temperatures.

When the test light wavelength is 1.65 μm , it is affected by stimulated Raman scattering of the communication light. The theoretical effect of stimulated Raman scattering and the results of experiments using FITAS are shown below.

2-1. The theoretical effect of stimulated Raman scattering

When a high-power communication light enters the optical fiber, stimulated Raman scattering occurs. The wavelength of stimulated Raman scattering (Stokes) is the same as the wavelength of the test light. When we measure the optical-fiber loss, the stimulated Raman scattering becomes noise light. The stimulated Raman scattering travels both backward and forward, as given by the following expressions:

$$P_F / P_{in} = a \times (\exp(-\alpha_2 L) - \exp(-\alpha_1 L)) / (\alpha_1 - \alpha_2) \quad (1)$$

$$P_B / P_{in} = a \times (1 - \exp(-(\alpha_1 + \alpha_2)L)) / (\alpha_1 + \alpha_2) \quad (2)$$

where P_F (W) is the optical power level of forward stimulated Raman scattering and P_B (W) is optical power level of backward stimulated Raman scattering. P_{in} is the average optical power level of the communication light. a is the scattering coefficient of the optical fiber per unit length, α_1 is the loss coefficient of the communication light in the optical fiber, and α_2 is the loss coefficient of the optical fiber due to stimulated Raman scattering. Assuming $\alpha_1 = 7.03 \times 10^{-5}$ neper/m, and $\alpha_2 = 8.08 \times 10^{-5}$ neper/m, we calculated the optical power level of stimulated Raman scattering using $a = 6.9 \times 10^{-10}$ (m^{-1}).

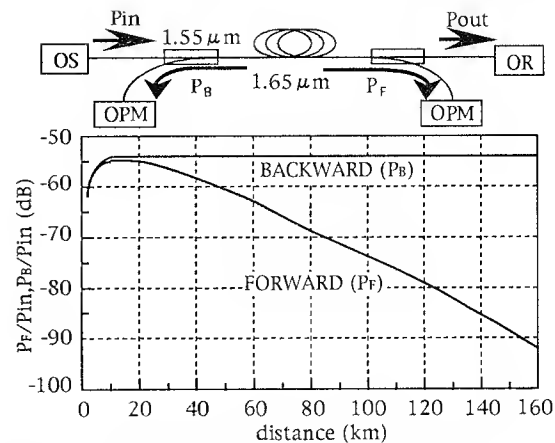


Figure 2. Stimulated Raman scattering by communication light ($\lambda = 1.55 \mu\text{m}$)

The calculated results (P_F and P_B) are shown in Fig. 2. As can be seen, the longer the optical fiber, the less the optical power level of forward stimulated Raman scattering at lengths of over 20 km.

But the optical power level of backward stimulated Raman scattering remains constant at optical-fiber lengths of over 20 km. The 1.65- μm test light is used in experiments with long-span optical fibers of over 80 km. The backward scattering power had the greatest effect on the optical power level of the test light at 160 km, while the forward scattering power had the greatest effect at 80 km. We thus calculated the optical power levels of stimulated Raman scattering at 160 km and 80 km. Assuming that the optical power level of the communication light (P_{in}) is 18 dBm,

$$P_F = -51 \text{ dBm}, P_B = -35 \text{ dBm at } 80 \text{ km}$$

$$P_F = -74 \text{ dBm}, P_B = -35 \text{ dBm at } 160 \text{ km}$$

On the other hand, assuming that the transmitted optical power level of the test light is -15 dBm, the optical power level of the output light is -43 dBm at 80 km and -71 dBm at 160 km.

When the test light and the communication light travel through an optical-fiber cable in opposite directions, the optical power level of the noise light is 8 dB higher than the optical power level of the test light at 80 km, and exceeds the optical power level of the test light by 36 dB at 160 km.

When the test light and the communication light travel through an optical-fiber cable in the same direction, the optical power level of the test light exceeds the optical power level of the noise light by 8 dB at 80 km, and exceeds the optical power level of the noise light by 3 dB at 160 km. Therefore, it is possible to make measurements when the test light and the communication light travel through the optical fiber in the same direction.

2-2. The examinations

We carried out an examination to confirm the effect of stimulated Raman scattering. The optical power level of forward scattering over a short distance is theoretically higher than that of forward scattering over a long distance. We therefore examined the optical power level of forward scattering over a short distance (86 km). The test conditions are shown in Fig. 3. In this figure, OS is the optical source of the communication light and OR is the optical receiver of the communication light. Measurements were made with the test light and communication light traveling in the same direction and opposite directions. The results are shown in Fig. 4.

When the communication light and the test light traveled in opposite directions, the optical power level is almost constant because the optical power level of backward scattering is higher than the optical power level of the test light. On the other hand, when the communication light and the test light travel in the same direction, the measurements are not affected by the optical power level of backward scattering. Because the test light was modulated at 270 Hz and stimulated Raman scattering was almost isolated by a band-pass filter. As a result, the measurement value is better than the theoretical value. On the other hand, when both lights traveled in the same direction, the measurement error caused by stimulated Raman scattering was small.

Therefore the communication light and the test light must be transmitted in the same direction to minimize the effects of stimulated Raman scattering.

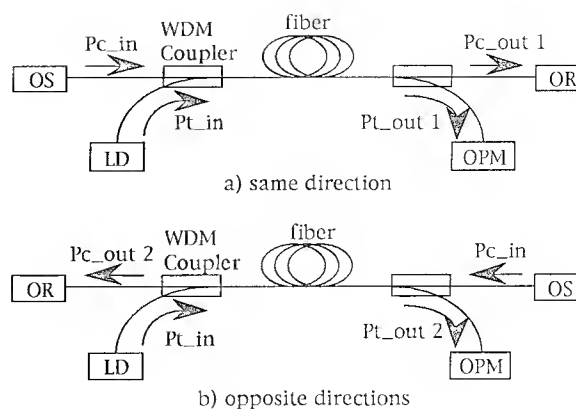


Figure 3. Measurement conditions of stimulated Raman scattering

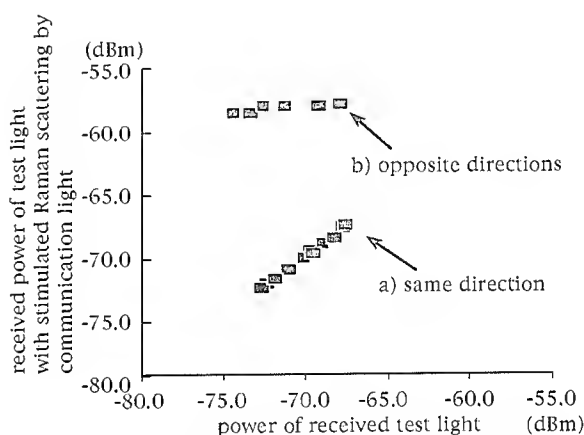


Figure 4. The effect of stimulated Raman scattering on the test light

3. The testing method

The communication light and the test light must be transmitted in the same direction in order to test long-span optical fiber lines. For this purpose, we need to know the direction of the communication light, i.e. the location of the OS (optical source of communication light). We carried out a study to distinguish the directional propagation of communication light with an optical power meter using FITAS.

3-1. Stimulated Raman scattering in 1.65- μ m band

In FITAS, an optical-filter is put between the optical-fiber cable and the optical-power meter to isolate the communication light. The directional pro-

pagation of the communication light cannot reliably measure the optical power level of the communication light. However, when the high-power communication light ($\lambda = 1.55 \mu\text{m}$ band) enters the optical fiber, a small part of the communication light's energy is transferred from $1.55 \mu\text{m}$ to $1.65 \mu\text{m}$ by stimulated Raman scattering.

Therefore we studied the possibility of confirming the propagation direction of communication light using this stimulated Raman scattering. When the communication light and the test light travel in the same direction, the optical power level of stimulated Raman scattering decreases as the optical-fiber length increases above 20 km. However, when the lights travel in opposite directions, the optical power level of stimulated Raman scattering remains uniform at lengths above 20 km.

3-2. The received optical power level of optical power meter

The directional propagation of stimulated Raman scattering is shown in Fig. 5. The stimulated Raman scattering is received by optical power meters at both sides because it propagates in both directions in the optical fiber.

To distinguish the direction of the communication light, we measured stimulated Raman scattering produced by a high-power communication light at both ends of transmission sections; the results are shown in Fig. 6. The fiber lengths used in these measurements are 86 km and 133 km. In the 86-km fiber, the difference in optical power levels of the OS side and the OR side was more than 10 dB.

Therefore we can determine the direction of light propagation in an optical fiber by measuring the optical power level (at $\lambda = 1.65 \mu\text{m}$) of stimulated Raman scattering.

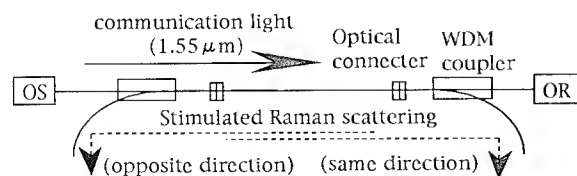


Figure 5. The directional propagation of stimulated Raman scattering

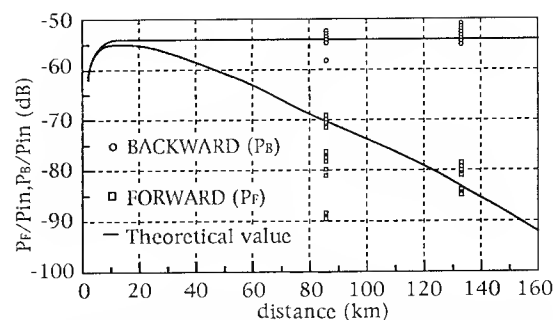


Figure 6. Stimulated Raman scattering ($\lambda = 1.65 \mu\text{m}$) by communication light ($\lambda = 1.55 \mu\text{m}$)

4. The optimum structure of FITAS

NTT is using optical-fiber amplifier technology to double the maximum spacing between repeaters from 80 km to 160 km in optical repeater lines. To handle this increased spacing, we have also increased the effective length of the FITAS. Table 1 summarizes these improvements. To measure the line loss of the 160-km repeater span, the wavelength of the test light was changed from $1.31 \mu\text{m}$ to $1.65 \mu\text{m}$ and the loss testers were replaced. The optical couplers and filters corresponded to a wavelength of $1.65 \mu\text{m}$ inside the optical branching and transfer module to input or output test lights mixed with the communication light. In order to increase repeater spacing, we improved our test meters and optical branching and transfer modules. Also according to the establishment of a function for detecting the direction of communication lights, it is possible to test fibers without degradation due to stimulated Raman scattering.

Table 1. Primary improvements to FITAS (Along DSF Cable)

Device	Improvement Made	Conventional	Long-Span
	Distance	80 km	160 km
Loss testing Equipment	Test wavelength	$1.31 \mu\text{m}$	$1.65 \mu\text{m}$
Optical Branch Transfer Module	Coupler (WDM)	$1.31/1.55 \mu\text{m}$	$1.65/1.55 \mu\text{m}$
	Filter	$1.31/1.55 \mu\text{m}^*$	$1.65/1.55 \mu\text{m}^*$

*: allowable wavelength / cut-off wavelength

5. Conclusion

In order to increase the repeater spacing in optical fiber lines, we changed the test light wavelength to $1.65\ \mu\text{m}$ and increased the communication light power. The increased spacing leads to move severe stimulated Raman scattering. Therefore, to avoid the effects of stimulated Raman scattering, we made the communication light and the test light travel in the same direction. Also, to determine the direction in which the test light should be transmitted, we established a new method for detecting the propagating direction of the communication light. We plan to apply this technology from September 1994 at FITAS to handle increased repeater spacing.

Acknowledgements

The authors thank N.Nakao and H.Matamoto for useful discussions. The authors gratefully thank Y. Yuuki and O.Yamauchi for their encouragement.

References

- (1) H. Matamoto et al. , "Cable Transfer and Supervisory System for Trunk Optical Fiber Cables" 40th IWCS, 1991.
- (2) K. Yoshioka et al. , "High Count Trunk Optical Fiber Cable and Related Technology Development" 41th IWCS, 1992.
- (3) R. H. Stolen, in "Optical Fiber Telecommunications", edited by S. E. Miller and A. G. Chynoweth, Academic, New York, 1979.



Shinji Goto

NTT Network Systems
Development
Chiba, Japan

Shinji Goto is a Engineer, Access Networks Project Group in Network Systems Development Department of NTT. He received his B.S. degree from Yamagata University in 1989. He joined NTT in 1989.



Izumi Sankawa

NTT Technology Research
Department
Tokyo, Japan

Izumi Sankawa received the B.S. and D.E. degrees in electrical engineering from Waseda University in 1979 and 1991, respectively. He joined NTT in 1979. He was engaged in the development of optical fiber measuring technologies and optical fiber surveillance systems from 1987 to 1993. He is a manager in NTT Technology Research Department. He is a member of the Institute of Electronics, Information and Communication Engineers of Japan who presented him with the 1985 Young Engineer Award.



Tsunco Horiguchi

NTT Access Network
Systems Laboratories
Ibaraki, Japan

Tsuneo Horiguchi received B.S. and Dr. Eng. degrees from the University of Tokyo, Tokyo, Japan, in 1976 and 1988, respectively. In 1985, He joined the Ibaraki, Japan, where he worked on the measurement technology of the transmission characteristics of optical fiber cable. Since 1988, he has worked in the field of optical fiber distributed sensing. He is presently a Senior Research Engineer, Supervisor of NTT Access Network Systems Laboratories. Dr. Horiguchi received the IEICE Excellent Paper Award in 1991. He is a member of the IEEE, the Optical Society of America, and the Optical Society of Japan.



Naoyuki Atobe

NTT Network Systems
Development
Chiba, Japan

Naoyuki Atobe received the B.S. degree in electrical engineering from Kyushu University in 1979. After joining the Engineering Bureau, Nippon Telegram Telephone Public Corporation, in 1979, he worked on research and development of communication cables and splicing technologies. He had worked on planning and investment of telecommunication plants at Hokuriku regional head quarter in 1986. He is a Senior Manager, supervisor in the Access Networks Project Group in NTT Network Systems Development Department, and is currently engaged in development of testing system for fiber optics network systems, and fiber termination systems.

Mr. Atobe is a member of the institute of electronics, information and communication engineers of Japan.

80-Fiber Connector

Hiroyuki Yanagase, Takashi Shigematsu, Jun Yamakawa, Ken Kanai

The Furukawa Electric Co.,Ltd.
6, Yawata-Kaigandori, Ichihara, Chiba, 290, Japan

Abstract

Two types of an 80-fiber connector have been developed, in an attempt to reduce the cable-to-cable connection working hours and make the connector compact in size. One of them is "a stacked type" in which five 16-fiber connectors are piled up. Its structure allows to take out and bring back one of the five 16-fiber connectors while keeping all fiber connection. Insertion loss is the same as when a single 16-fiber connector is connected : about 0.2dB. The other is "a unit type" that employs only one connector to include 80 fibers. Because of large ferrule, it is difficult to mold. But it is compact in size and fiber density is higher than that of stacked type connector. It features mean insertion loss of about 0.4dB.

1. Introduction

Along with expansion of the optical telecommunication networks, cables are designed to have increasing number of fibers. In an attempt to introduce the optical fiber to the entire subscriber networks, a great effort has been made to develop a 4000-fiber cable⁽¹⁾. As for the connection technology, it is important to reduce cable-to-cable connection working hours and to make the connector compact in size. In order to overcome these problems, the high speed and high count connecting technique has been developed.⁽²⁾ This paper presents two types of an 80-fiber connector.

The stacked type connector can be partially disassembled as necessary while keeping all fiber connection. This feature makes it possible to replace or repair a malfunctioning 16-fiber connector individually. The stacked type connector is required to minimize

deterioration of performance that is induced by piling up 16-fiber connectors. It is also expected to be almost as small as five 16-fiber connectors in size. The stacked type connector is designed to two-dimensionally arrange fibers : 16 fibers x 5 tiers. On the other hand, a unit type connector is designed to arrange 80 fibers laterally. A unit type connector is about 2/3 of the stacked type connector in volume. The remainder of this article describes configuration and characteristics of these two connectors.

2. Stacked type 80-fiber connector

2-1 Structure of the connector

Figure 1 shows a 16-fiber connector⁽³⁾⁽⁴⁾ which functions as a unit connector. The 16-fiber connector is entirely made by high precision plastic molding technique. It is designed to have 16 fibers arranged in its center of ferrule. Guide pins are inserted to guide holes

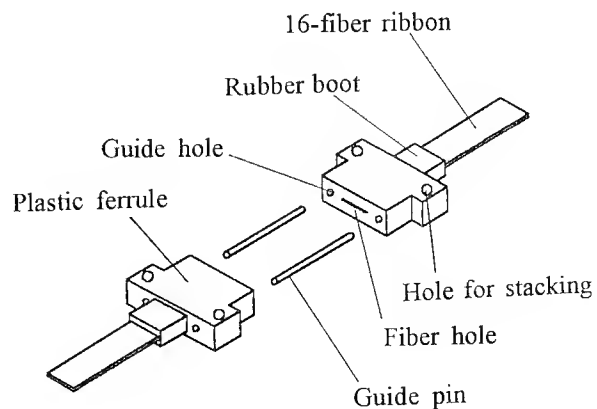


Fig.1 16-fiber connector

located on the both sides of the fibers to securely fix the connector. The 16-fiber ferrule has two holes which run from its one end to the other in vertical direction to the fibers. Binding pins are inserted to these holes, when five 16-fiber connectors are stacked up, to make the stacked structure stably fixed. (See Figure 2.)

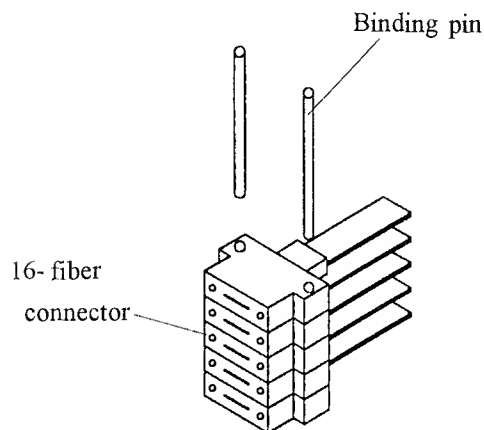


Fig.2 The structure of stacked 80-fiber connector

Figure 3(a) shows five 16-fiber connectors securely and completely piled up. Ten guide pins are used to fix these connectors. Five clamp springs are integrated on a binding plate so that they can be mounted onto the connectors at one time. This stacked type connector can be partially disassembled while keeping all fiber connection. Figure 3(b) shows how to take out one of the 16-fiber connectors while keeping the stacked type body connected. Its structure allows one malfunctioning 16-fiber connector to be replaced while keeping all fiber connection. Binding pins and pin holes are designed to have appropriate clearance, that realizes floating structure to allow each stacked 16-fiber connector to feature some freedom. Figure 4 shows how floating amount is determined. Insufficient clearance makes the 16-fiber connectors interfere each other, that may lead to increase of insertion loss. when clearance is too much, on the other hand, it may take longer time to assemble the stacked type 80-fiber connector, which deteriorates one of advantageous characteristics of this structure. These factors need to be studied to determine optimum clearance.

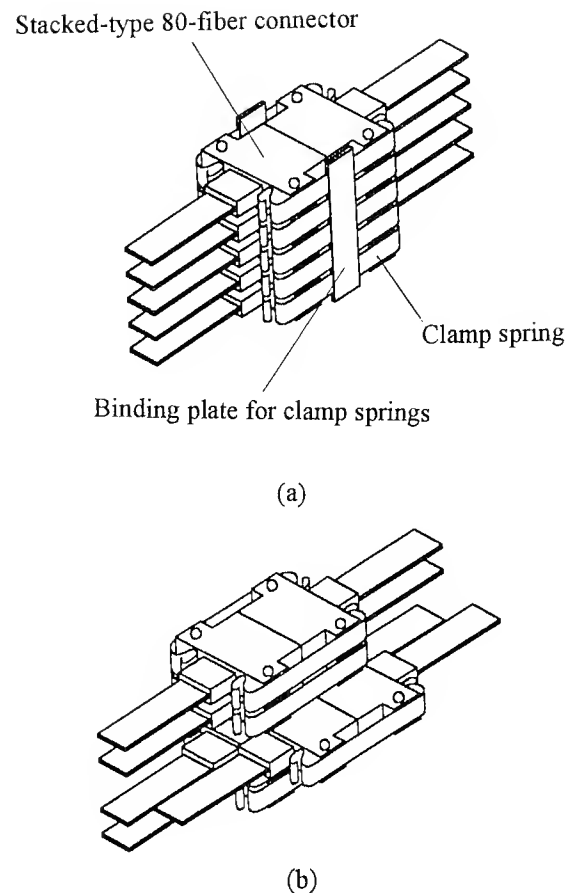


Fig.3 (a) The completely assembled stacked type 80-fiber connector
(b) How to take out a 16-fiber connector independently

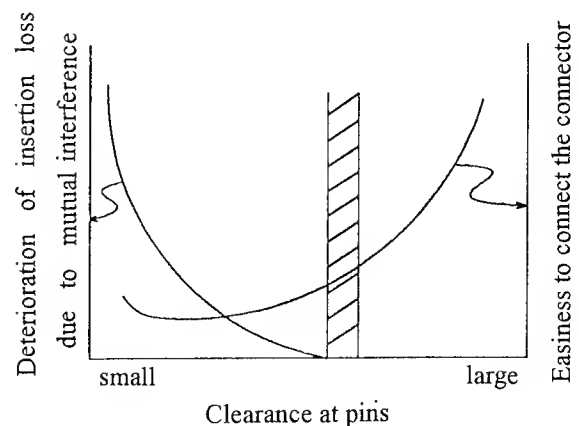


Fig.4 How to determine floating amount

2-2 Characteristics

(1) Insertion loss

Figure 5 shows insertion loss measured in the experiment. Mean insertion loss is 0.19dB. Insertion loss is found 0.18dB when a single 16-fiber connector is connected.(See Figure 6.)These measurement results demonstrate that the stacked type 80-fiber connector features no deterioration of insertion loss.

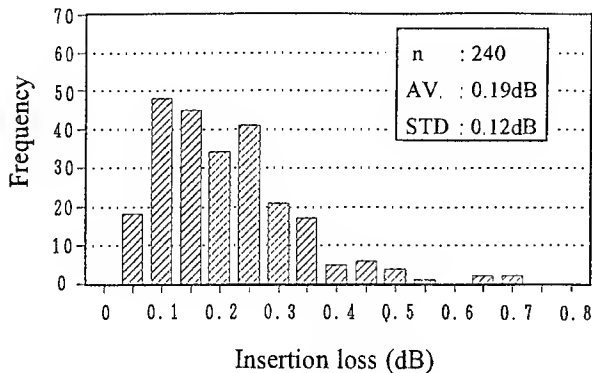


Fig.5 Insertion loss histogram of stacked-type 80-fiber connector

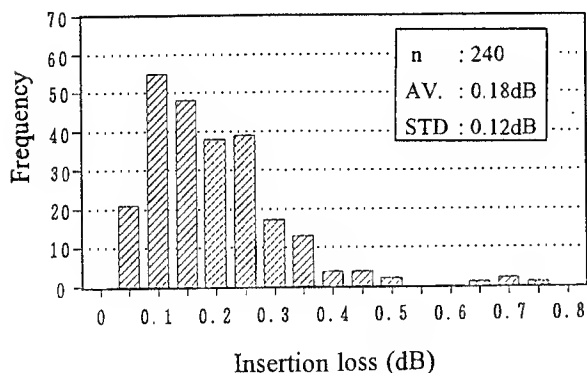


Fig.6 Insertion loss histogram of 16-fiber connector

(2) Temperature cycling test

temperature condition : -40°C to +70°C

duration : 7 days (4 cycles / day)

Figure 7 shows fluctuation of insertion loss. It is revealed insertion loss increases at a low temperature and that it decreases at a high temperature. This fluctuation is considered to be caused by the changes in

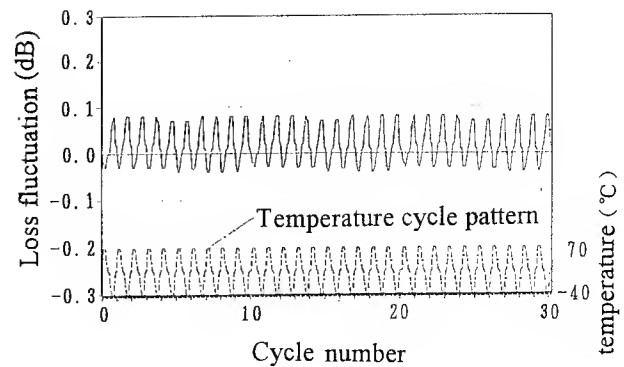


Fig.7 Fluctuation of insertion loss for temperature cycling test of stacked-type 80-fiber connector

smoothness of matching oil and pressure of clamp springs. Fluctuation, however, is favorably limited within ± 0.2 dB.

(3) Reconnecting test

The stacked type fiber connector is connected and disconnected 100 times. Fluctuation of insertion loss is found limited within ± 0.2 dB.

(4) Time required to complete connection working hours

- ① to insert guide pins
- ② to clean the face of connectors
- ③ to apply index matching oil
- ④ to connect two sets of the stacked type 80-fiber connectors at one time
- ⑤ to mount clamp springs

It takes about 4 minutes to complete these five steps.

3. Unit type 80-fiber connector

3-1 Configuration

Figure 8 shows configuration of a unit type 80-fiber connector. It is designed to arrange 80 fibers laterally. five 16-fiber ribbons are inserted. In order to ensure that each tape is inserted appropriately, a partitions is set at every 16 fibers where fibers are inserted. A unit type 80-fiber connector is compared with the 8-fiber MT (Mechanical Transferable) connector⁽⁵⁾ in terms of fiber density. (The 8-fiber MT connector features the highest fiber density at present.)

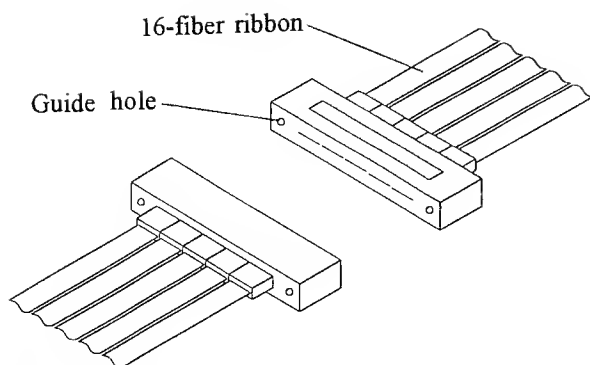


Fig.8 The structure of a unit-type 80-fiber connector

8-fiber MT connector : $21\text{mm}^3/\text{fiber}$
 80-fiber connector : $7.5\text{mm}^3/\text{fiber}$

A unit type 80-fiber connector features 3 times higher fiber density than the 8-fiber MT connector.

3-2 Orientation of construction

In the case of the stacked type 80-fiber connector, some combinations of the connectors do not allow strict fiber number matching. It is required, therefore, to control fiber number in construction. As a unit type 80-fiber connector is designed to arrange fibers laterally, connection is always possible even without controlling fiber number. It is possible for a unit type 80-fiber connector to eliminate complex fiber number control.

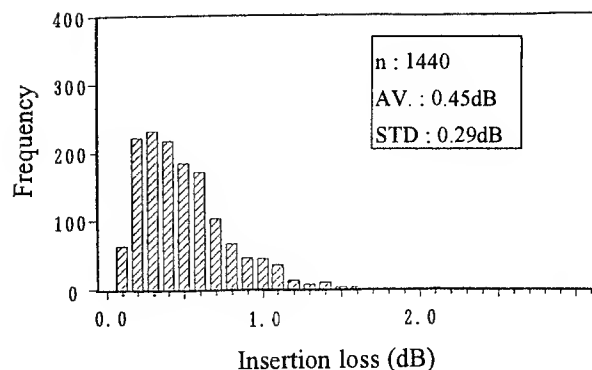
3-3 Characteristics

(1) Insertion loss

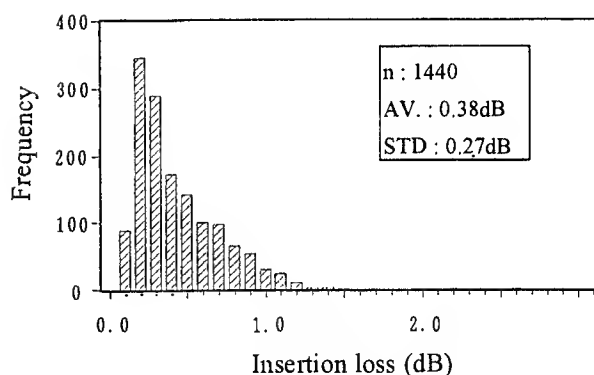
Figure 9 shows insertion loss measured in the experiment. Mean insertion loss is found about 0.4dB. At insertion loss characteristics, inverse connection features better than normal connection. This is considered because fiber holes are located slightly off along Y direction as shown in Figure 10.

(2) Reconnecting test

A unit type 80-fiber connector is connected and disconnected 50 times to evaluate fluctuation of insertion loss. Fluctuation is found limited within $\pm 0.4\text{dB}$.



(a) Normal connection



(b) Inverse connection

Fig.9 Insertion loss histogram of a unit-type 80-fiber connector

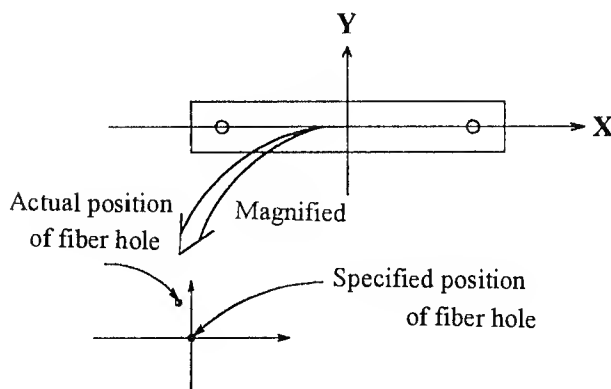


Fig.10 Actual position of fiber holes of the stacked type 80-fiber connector

4. Conclusion

Two types of the 80-fiber optical connector are developed and evaluated in an attempt to establish the advanced high speed and high count connecting technique. The stacked type 80-fiber connector is designed to allow a 16-fiber connector to be independently taken out and brought back. No characteristics are deteriorated by piling up the connectors. Mean insertion loss is found about 0.19dB. Fluctuation of insertion loss is limited within ± 0.2 dB in the temperature cycling test and the reconnecting test. In the case of a unit type 80-fiber connector, mean insertion loss is found about 0.4dB. Insertion loss is considered to be improved by regulating fiber holes of ferrules. Both types of the 80-fiber connectors have reduced size and connection working hours.

5. References

- (1) T.Haibara, S.Tomita, M.Matsumoto, T.Yabuta "High-Speed, Low-Loss Connection Techniques for High-Count Pre-Connectorized Cables" 40th IWCS, pp.296-302, 1991
- (2) S.Tomita, M.Matsumoto, S.Nagasawa, T.Tanifuji "Ultra High-Density Optical Fiber Cable with Thin Coated Fibers and Multi-Fiber Connectors" 42nd IWCS, pp.5-15, 1993
- (3) S.Nagasawa, T.Tanifuji, M.Matsumoto, M.Kawase, "Single-Mode Multifiber Connectors for Future Large Scale Subscriber Networks" ECOC'93, pp.29-32, 1993
- (4) J.Yamakawa, H.Yamada, T.Shigematsu, H.Yanagase, K.Kanai "16-Fiber Optical Connector" 42nd IWCS, pp.225-230, 1993
- (5) T.Ohta, Y.Kihara, T.Shigematsu, "High Quality Multiple-Fiber Connector" FURUKAWA ELECTRIC REVIEW. No.89, pp.9-14, December. 1991



Hiroyuki Yanagase

The Furukawa Electric Co.,Ltd

6, Yawata-kaigandori,
Ichihara, Chiba, 290, Japan

Hiroyuki Yanagase was born in Niigata, Japan, in 1966. He received the M.E. degree in electrical engineering from Niigata University, Niigata, Japan, in 1991. He joined The Furukawa Electric Company, in 1991. Since then he has been engaged in R&D on optical component.



Takashi Shigematsu

The Furukawa Electric Co.,Ltd

6, Yawata-kaigandori,
Ichihara, Chiba, 290, Japan

Takashi Shigematsu was born in Shizuoka, Japan, in 1963. He received the B.E. degree in precision engineering from Yamagata University, Yamagata, Japan, in 1986. He joined The Furukawa Electric Company, in 1986. Since then he has been engaged in R&D on plant and facilities Div.



Jun Yamakawa

The Furukawa Electric
Co.,Ltd

6, Yawata-kaigandori,
Ichihara, Chiba, 290, Japan

Jun Yamakawa was born in Hokkaido, Japan, in 1965. He received the B.E. degree in applied electronic engineering from University of Electro- Communications, Tokyo, Japan, in 1989.

He joined The Furukawa Electric Company, in 1989. Since then he has been engaged in R&D on optical component.



Ken Kanai

The Furukawa Electric
Co.,Ltd

6, Yawata-kaigandori,
Ichihara, Chiba, 290, Japan

Ken Kanai was born in Niigata, Japan, in 1967. He received the M.E. degree in applied chemical engineering from Keio University, Kanagawa, Japan, in 1992.

He joined The Furukawa Electric Company, in 1992. Since then he has been engaged in R&D on optical component.

PRECISION-LENGTH OBLIQUE CLEAVING OF RIBBON FIBERS FOR HIGH-PERFORMANCE MECHANICAL SPLICES

R. J. Ferina, Jr.
Radiall, Inc.
Stratford, Connecticut

H. B. Yin
Radiall S.A.
Voreppe, France

ABSTRACT

A new technique has been developed to cleave optical fibers of a ribbon both obliquely and to a precise length. The technique, which appears to be better suited for ribbon fibers than traditional torsion methods, employs transverse displacement to produce uniformly-oriented oblique cleaves. Precision-length oblique cleaving is attractive for achieving low-reflectance, low-insertion loss mechanical splice performance. Splice plugs prepared in a 4-step oblique cleaving tool yielded a mean insertion loss of 0.16 dB and minimum return loss greater than 55 dB in mating trials using a prototype 6-fiber remateable ribbon splice. In this paper, test results of oblique cleaving and splicing performance are presented following theoretical description of the transverse-displacement cleaving technique.

INTRODUCTION

Multiple fiber cables and mass termination techniques have been used to reduce installation and maintenance unit-costs of optical transmission networks. Fusion splicing technology, for example, has been successfully adapted to provide reliable, cost-effective permanent joints of ribbon fibers. Remateable ribbon fiber connectors now available offer the advantage of reconfiguration flexibility for multi-fiber optical networks. However, costs associated with these polished connectors remain high, especially for low-reflectance versions.

Recently high return loss has become an increasingly important and widespread requirement for components throughout optical fiber networks because of the transparency to future evolution it may offer them. For example, some components such as distributed feedback laser sources exhibit sensitivity to back-reflected optical power. Low-cost mechanical

splices offering remateability and low reflectance, therefore, may prove to be a viable alternative to ribbon fiber connectors at network points requiring branching flexibility.

This paper describes a new technique of oblique cleaving developed in conjunction with a remateable ribbon fiber splice. The splice is being designed to offer limited mating endurance at a low cost. Cleaving was selected because it has long been used as a quick, simple and cost-effective method of preparing suitable fiber mating faces. Oblique cleaves with core angles in the range of 5° to 10° should provide adequate return loss when used with index-matching material, although lower angles may suffice for cleaved, as compared to polished, surfaces [1]. The new technique utilizes transverse displacement rather than torsion and hence is potentially easier to implement in ribbon fibers.

TRANSVERSE DISPLACEMENT OBLIQUE CLEAVING

Oblique Cleaving

Commercially-available oblique cleaving tools often employ torsion in combination with separately-applied axial tension to produce angled optical fiber end faces. The normal-section shear stress distribution associated with this torsion results in principal tensile stresses that are inclined with respect to the fiber axis. Because brittle, isotropic materials tend to cleave along a gradient perpendicular to the local principal tensile stress, the resulting torsion-influenced cleaves are angled with respect to a normal section of the fiber.* In contrast, flat or perpendicular

* Neglecting material property differences due to doping of the fiber core, theory predicts a helical cleaved surface with a minimal gradient at the exact center of fibers cleaved with torsion.

cleaves are obtained when the direction of the principal tensile stress is uniformly parallel to the fiber axis, which is the case when no shear conditions are present.

Shear stress to bias the direction of the principal stress may also be realized by transversely displacing one clamped end of a fiber relative to the other. Deviation from the initially straight fiber trajectory intrinsically creates axial tension in addition to the shear stress because of the elongation induced. By carefully selecting the span length and the axial position of the cleave, oblique cleaves may be produced using a single movement.

Transverse Displacement Cleaving Theory

Figure 1 depicts a fiber clamped at both ends and subjected to a small transverse displacement y of one of its ends. For simplicity, linear beam analysis leads to the theoretical deflection curve v as a function of axial distance z from the fixed clamp, expressed as

$$v(y, z) = \left(3 - 2\frac{z}{L}\right)\left(\frac{z}{L}\right)^2 y \quad (1)$$

where L is the span length of the clamped fiber segment. The internal shear force V developed in the beam,

$$V(y, z) = EI \frac{d^3}{dz^3} [v(y, z)] = -12EI \frac{y}{L^3} = V(y), \quad (2)$$

is constant with respect to axial position z . Here E is the elastic modulus and I is the moment of inertia of the fiber. For a span length constantly maintained, the axial elongation δL (due to the change in fiber trajectory) varies parabolically with small displacements y :

$$\delta L(y, z) = \frac{1}{2} \int_0^L \left\{ \frac{d}{dz} [v(y, z)] \right\}^2 dz = \frac{3}{5} \frac{y^2}{L} = \delta L(y). \quad (3)$$

The elongational stress is given by Hooke's Law, $\sigma_e = E \delta L / L$. The bending stress also acts in the axial direction and influences cleaving conditions. It is given by the flexure formula, $\sigma_b = -M \rho / I$, in which ρ is the distance from the neutral surface of the fiber and $M = M(y, z) = EI d^2/dz^2 [v(y, z)]$ is the bending moment associated with transverse displacement y .

Superposing the two stresses gives the total axial stress σ which may be expressed as

$$\begin{aligned} \sigma(y, z, \rho) &= \sigma_e(y) + \sigma_b(y, z, \rho) \\ &= 3E \frac{y}{L} \left[\frac{1}{5} \frac{y}{L} + 2 \frac{\rho}{L} \left(2 \frac{z}{L} - 1 \right) \right]. \end{aligned} \quad (4)$$

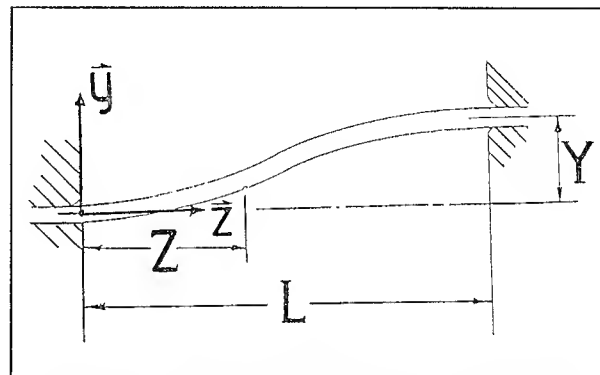


Figure 1: Transverse displacement (exaggerated) of a fiber clamped at both ends.

To calculate the shearing stress in a normal section of a fiber of radius R , an approximation is used in which the horizontal (x -) components are neglected [2]. The obtained magnitude of the shearing stress in the core region of the fiber is accurate to within 5% of the exact solution [3]. The shearing stress distribution $\tau(y, \rho)$ along the vertical (y -) axis of the fiber thus found varies parabolically with ρ :

$$\tau(y, \rho) = -4E \frac{y}{L^3} (R^2 - \rho^2). \quad (5)$$

Note that the shearing stress τ , like the shear force V , is independent of axial position away from the clamped ends ($z=0$, $z=L$).

As previously noted, the cleaved-surface gradient is perpendicular at each point to the principal tensile stress at the instant of cleavage. Then the angle at each point of the cleaved surface with respect to a normal section is equivalent to the angle α that the principal tensile stress makes with the fiber axis at the instant of cleavage. In this case the local angle is given by

$$\alpha(y, z, \rho) = \frac{1}{2} \tan^{-1} \left(2 \frac{\tau(y, \rho)}{\sigma(y, z, \rho)} \right). \quad (6)$$

The cleaved angle α_0 at the fiber core ($x=p=0$) simplifies to

$$\alpha_0(y) = \alpha(y, z, 0) = \frac{1}{2} \tan^{-1} \left(-\frac{40 R^2}{3 L y} \right), \quad (7)$$

where the z -terms have been eliminated due to $p=0$.

The theoretical form of the profile cleaved along the y -axis of the longitudinal cross-section is given by

$$P(y, z, \rho) = \frac{1}{2} \int_{-R}^R [\alpha(y, z, \rho)]^2 d\rho \quad (8)$$

which entails inaccuracies associated with the approximate shear distribution (5).

Equation (7) indicates that the angle of obliqueness at the fiber core depends uniquely on and inversely with the span length L and the magnitude y of transverse displacement (at the instant of cleavage), and that it is independent of the axial position $z=Z$ of the cleave. However, to optimize cleaving, the score position Z must be carefully selected due to the interaction of the bending moment, which varies linearly along the fiber axis. In particular, the bending stress must be taken into account to avoid formation of lip and hackle on the cleaved end face [4] (influenced by choice of Z) and breakage at the fiber clamps where it attains its extreme values (influenced by choice of L). Figure 2 shows how the bending stress in a normal section slightly distorts the otherwise purely sinusoidal cleaved profile, as predicted by equation (8) for cleaving parameters yielding a theoretical $\alpha_0=8.2^\circ$. The maximum surface gradient occurs slightly above the fiber core ($p>0$) in this case.

As compared with axial torsion methods, the transverse displacement technique of oblique cleaving develops all necessary stresses with one uniform movement, which simplifies mechanical conception of a cleaving tool. However, the interdependence of all three types of stress (shear, tensile, and bending) necessitates careful selection and precise setting of cleaving parameters.

A potential advantage of the transverse displacement method is that it is conceptually well-adapted to oblique cleaving of multiple fibers deployed in a

planar configuration such as is found in fiber ribbons. The traditional torsion method of oblique cleaving requires rotation about each individual fiber axis which appears more difficult to achieve for ribbon fibers because of their close spacing. However, Boitel *et al* [5] reported success with the torsion method on ribbon fibers whose diameters were selected to allow for effective clamping [6].

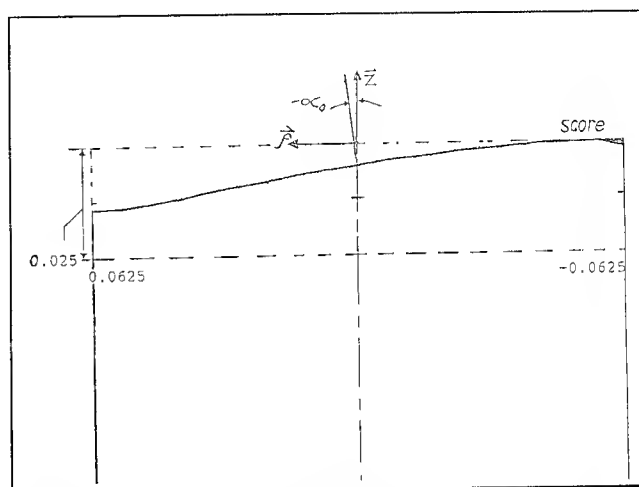


Figure 2: Scaled theoretical profile of a 125 μm diameter fiber cleaved by transverse displacement ($\alpha_0=8.2^\circ$). The profile is calculated along the longitudinal cross-section ($x=0$).

Another potential benefit of the transverse displacement method especially relevant for ribbon fibers is that the principal gradient of the cleaved surface is systematically oriented parallel to the displacement. The gradients of each cleaved fiber of a ribbon, therefore, are parallel to one another and perpendicular to the plane defined by the ribbon. In splicing applications this may be exploited to systematically achieve parallel orientation of mated oblique end faces. Moreover, the sinusoidal profile obtained with transverse displacement may be preferable to the theoretically helical surface of a torsion-cleaved fiber.

Ribbon Fiber Oblique Cleaving Tool

Figure 3 is a photograph of a prototype tool designed to obliquely cleave ribbon fibers by transverse displacement to a precise length. The tool was developed in conjunction with a prototype remateable 6-fiber ribbon splice. To minimize insertion loss extremely precise fiber lengths are required, implying highly repetitive positioning of the plug in the tool and of the score sites on the fibers relative to the plug.

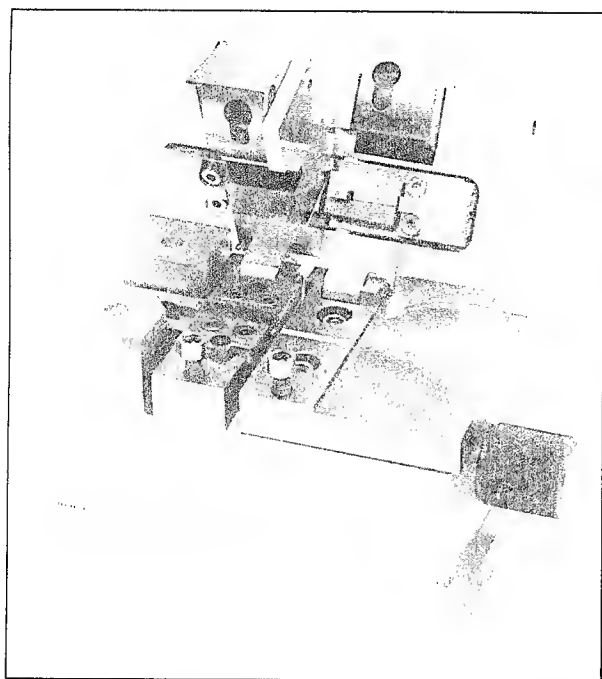


Figure 3: Photograph of the prototype ribbon-fiber oblique cleaving tool.

Cleaving with the tool occurs in four steps following insertion of a prepared splice plug into the tool's passive alignment guide. The first step consists of closing and locking a specially designed mechanical clamp which immobilizes ribbon fibers of non-identical diameters without introducing torsion. Next a straight diamond blade is raised via a highly repetitive mechanism against the fibers to score them simultaneously. This method of scoring was chosen because of geometrical constraints of the plug and adaptor designs. After the next step of closing and locking the second fiber clamp, it is transversely displaced vertically upward until all fibers have cleaved.

EXPERIMENTAL RESULTS AND DISCUSSION

Oblique Cleaving Test Results

Angle Measurements. Core angle of Corning SMF-28 single mode fiber was measured with an estimated accuracy of 1° on a test set-up based on the visible-beam deflection technique described in Bellcore specifications [7]. Results for 30 single-fiber oblique cleaves are presented in Figure 4 both independently of and as a function of way or track on the cleaving tool.

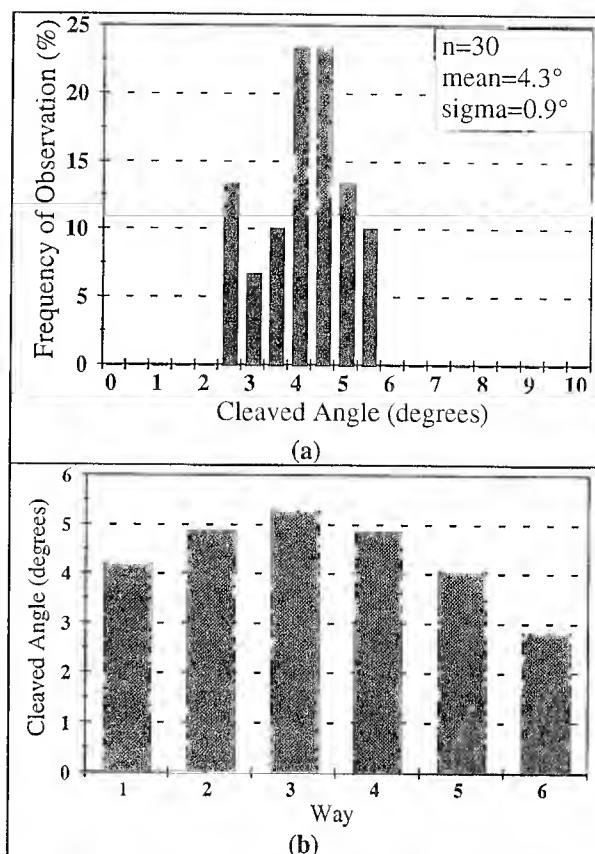


Figure 4: (a) Histogram of cleaved angle independent of way. (b) Bar graph of mean cleaved angle for each way.

The measured overall mean cleaved angle of 4.3° , weighted by way, is misleading because of the significant differences observed in the means of individual ways. Fabrication imperfections in the prototype tool create variation between ways in effective cleaving parameters, notably in L and in Z , which may account for these differences. Despite these differences, the total dispersion for the 30 cleaves was limited to 3.2° .

The measurement results associated with ways 2, 3, and 4 have a combined mean cleaved angle of 5.0° with a standard deviation of 0.6° , which is probably more indicative of the tool's capability. Although this mean value meets the tool's minimum design goal, it is significantly lower than the value $\alpha_0=7.4^\circ$ theoretically predicted for the nominal parameters L and Z used in setting the tool. This discrepancy between theory and experiment may be partially attributed to measurement uncertainty associated with the actual position of the boundary condition on the fixed fiber support guide. Due to slight rounding of

the upper clamp surface, the actual values of L and Z are most likely larger than the nominal values measured from the edge of the fiber support guide as indicated in Figure 1. Adding a positional offset of 200 μm , for example, yields a theoretical cleaved angle value in excellent agreement with the results for these ways.

Cleaved Length Measurements. Cleave quality was monitored and cleaved length was measured using a high-magnification self-collimating lens system in which a target image was focused on the cores of plug-mounted ribbon fibers. The parameter measured was the position of each cleaved end face (at the fiber core) relative to a reference on the prototype splice plugs. The measurement uncertainty was estimated as 2 μm .

The distribution of cleaved end face position for 29 oblique cleaves of 6-fiber plugs is plotted independently of way as a histogram in Figure 5(a). The standard deviation in cleaved length of all 174 fibers measured was 3.4 μm without accounting for differences between ways of the tool. The mean absolute position as a function of way is graphed in Figure 5(b). These data are indicative of the axial separation expected between end faces mated in the prototype splice, described below. Although slight differences in the means are present, the mean intra-ribbon dispersion in cleaved length was 3.3 μm for 6 fibers. These results tend to confirm the alignment setting of the tool and the repetitiveness of plug positioning relative to the tool's scoring blade.

Visual inspection of the 174 oblique cleaves revealed no unacceptable irregularities such as lips, cracks, etc., except for occasional harmless traces of hackle. Furthermore, the shape of the theoretically-predicted profile shown in Figure 2 was qualitatively confirmed.

Prototype 6-Fiber Ribbon Splice

Several duplicates of a prototype mechanical splice were fabricated to mate plug-mounted ribbon fibers in machined V-grooves. The plugs are positioned by passive alignment in each splice adaptor, which contains index-matching material. Figure 6 is a photograph of a typical splice plug for which the fibers have been obliquely cleaved so that the end faces are slightly recessed with respect to the plug's reference surface. For two mated plugs, insertion loss due to the small resulting axial gap between end faces thus depends directly on the accuracy and precision in

cleaved length of the tool. Return loss performance is linked primarily to the obliqueness of the cleaved end face in the core region. Mated oblique end faces were oriented so that they were parallel to each other in the splice.

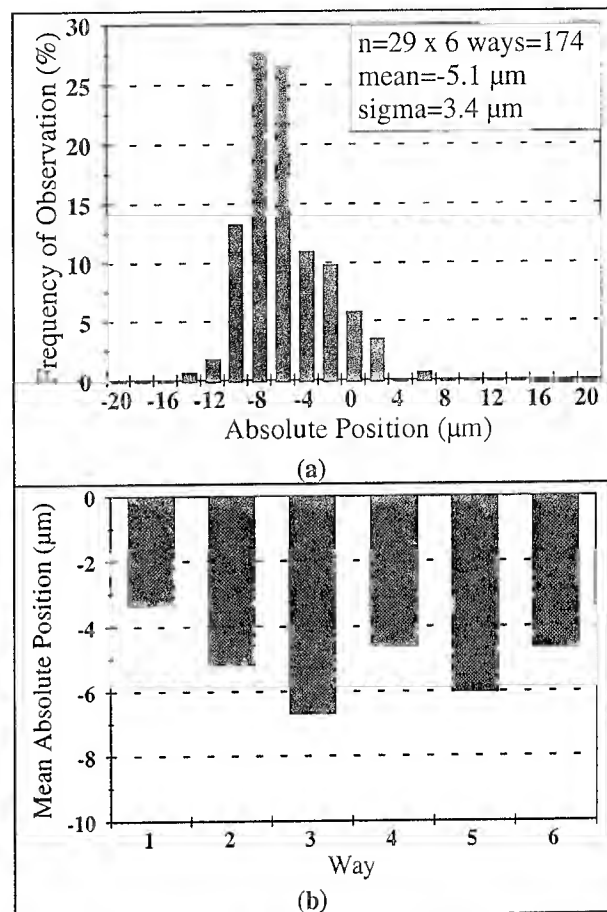


Figure 5: (a) Histogram of cleaved length independent of way. (b) Bar graph of mean absolute cleaved position as a function of way.

Optical Performance Results

Insertion Loss. Optical loss was evaluated by inserting the splice in an Acome 6-fiber ribbon cable after initial power throughput measurement for each way at the single mode wavelength of 1300 nm. Figure 7(a) shows a histogram of first-mating insertion loss values independent of way for 14 connections, four of which were measured with an optical time domain reflectometer (OTDR). The insertion loss, which had a mean of 0.16 dB, varied with a standard deviation of 0.11 dB for all 84 values.

Analysis of the data graphed by way in Figure 7(b) indicates rough correlation between insertion loss and cleaved length with the exception of way 4. The lack

of a strong correlation may be attributed to various factors such as fabrication differences between adaptor and plug prototypes. Five plugs (cleaved 21 times) were mated in five different adaptors for these trials.

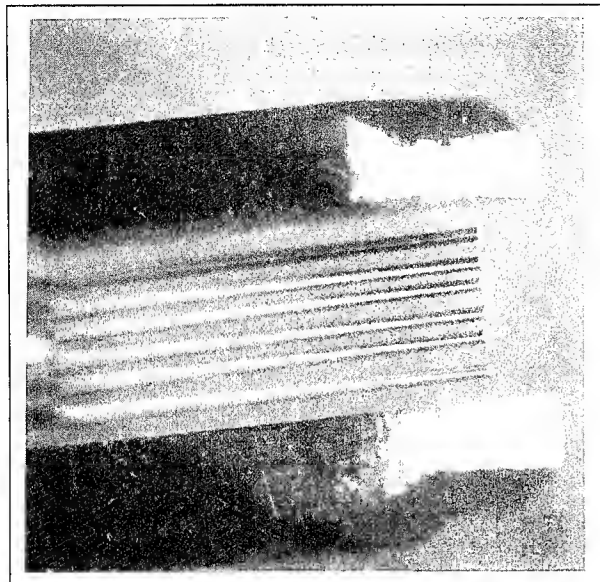


Figure 6: Photograph of a 6-fiber ribbon obliquely cleaved in a splice plug.

Return Loss. Return loss was calculated from the average back-reflected power as measured for both transmission directions with an OTDR. The minimum return loss value measured in 4 mated pairs of 6-fiber plugs was 55.5 dB. For each of the 4 connections of the prototype splice, the minimum return loss was recorded for way 6 for which the cleaved angle was also a minimum.

Discussion

Although measured core angle was lower than the theoretical prediction, the return loss performance for all ways of the prototype 6-fiber ribbon splice was still acceptable for most anticipated splicing applications. Despite the discrepancy in measured versus predicted angle, which is most likely due to imprecise measurement of cleaving parameters, results confirm that the transverse displacement technique is an effective method of obliquely cleaving ribbon fibers.

Analysis of the overall results indicates qualitative correlation between cleaved length and insertion loss and between core angle and return loss. Improved fabrication techniques of both the cleaving tool and

splice prototypes should lead to more uniform results between ways as well as stronger correlations between the parameters mentioned above. Although non-negligible way-to-way differences were observed, the combination of precise fiber lengths with oblique cleaves was successfully demonstrated on ribbon fibers using the new cleaving technique, as the overall insertion loss and reflection performance suggests.

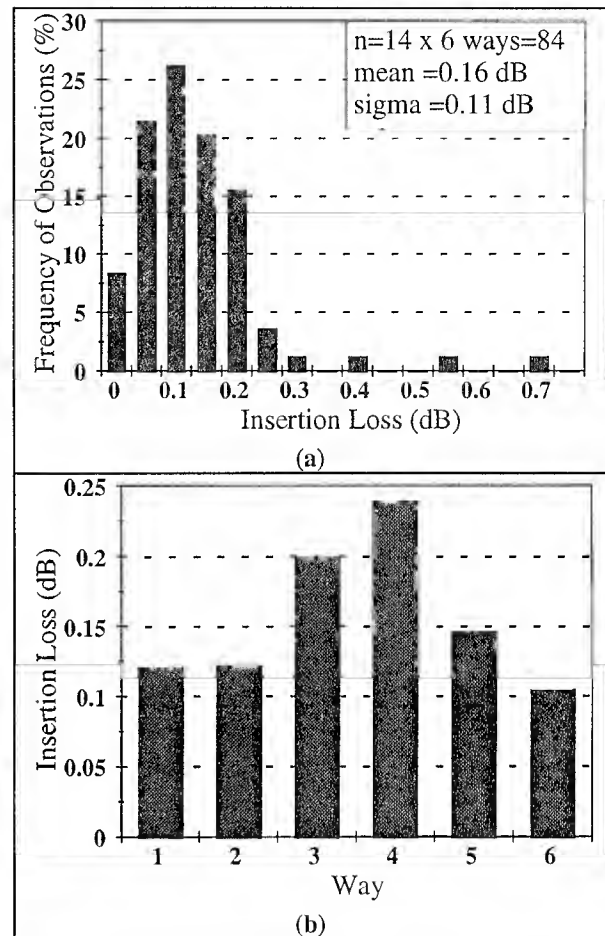


Figure 7: (a) Histogram of first-mating insertion loss independent of way. (b) Bar graph of mean loss by way.

CONCLUSIONS

A new method of oblique cleaving has been demonstrated to be effective in achieving low reflection performance in ribbon fiber mechanical splicing applications. The measured mean cleaved angle of 4.3° , which appears low compared with the cleaving tool's potential ability, resulted in a minimum return loss greater than 55 dB in a developmental 6-fiber splice. The prototype tool

based on the new technique was successfully designed to yield precise fiber lengths (standard deviation of 3.4 μm), which resulted in a mean insertion loss of 0.16 dB in the ribbon fiber splice.

ACKNOWLEDGEMENTS

This research has been partially funded by a grant from France Telecom.

The authors gratefully acknowledge the experimental and design work contributed by Jacques Lenuzza, Pierre Royer, Norbert Valade, and Elie Zajac.

REFERENCES

[1] V. Shah, L. Curtis, and W.C. Young, "Transmitted Power Variations in Single-Mode Fiber Joints with Obliquely Polished Endfaces," *Journal of Lightwave Technology*, Vol. 7, pp. 1478-1483, 1989.

[2] E. P. Popov, *Mechanics of Materials* (2nd ed.), Englewood Cliffs, N.J.: Prentice-Hall, 1976.

[3] A. E. H. Love, *Mathematical Theory of Elasticity* (4th ed.), New York: Dover, 1944, as cited in [2].

[4] C. M. Miller, S. C. Mettler and I. A. White, *Optical Fiber Splices and Connectors: Theory and Methods*, New York: Marcel Dekker, 1986.

[5] M. Boitel, J. M. Cailleaux, D. Crespel, T. Mahe and Y. Ruello, "Fracture en biais du câble ruban," OPTO '93, Paris, 1993, pp. 418-419.

[6] As communicated at a conference presentation, "Fracture en biais du câble ruban," OPTO '93, Paris, 1993.

[7] "Generic requirements for optical fiber cleavers," *Technical Reference TR-NWT-000 264*, Issue 2, Bellcore, December 1993.



R. J. Ferina, Jr.
Radiall, Inc.
150 Long Beach Blvd.
Stratford, CT 06497
U.S.A.

Robert J. Ferina, Jr. earned the B.A. degree in Physics from Colgate University in 1987 and then attended Rutgers University, where he conducted research in fiber optic sensors leading to the M.S. degree in Mechanical Engineering. He joined Radiall's Fiber Optic Division near Paris, France, in 1990 as an engineer involved in research and development of optical fiber splices and cleaving. In 1994 he moved back to the U.S.A. where he is currently working for Radiall, Inc.

H. B. Yin
Radiall S.A.
642, rue Emile Romanet
38340 Voreppe
France

H. B. Yin was born in Tchong King, China, in 1944. He received his university degree in Physics in 1966 from the Hang Tcheou University in China and the doctoral degree in Physics in 1985 from the University of Franche-Comté (Besançon) in France. He joined Radiall in 1983 as an engineer and was engaged in the research and development of fiber optic passive components. In 1988 he was appointed R & D Manager of the Fiber Optic Division. He has recently been transferred to the company's Voreppe location for a new project.

High Fiber Count Push-on Pull-off Connector

Y. KIKUCHI, H. FURUKAWA, Y. NOMURA and H. YOKOSUKA

OPTO-ELECTRONICS LABORATORY, FUJIKURA LTD.
1440, MUTSUZAKI, SAKURA-SHI, CHIBA, 285, JAPAN

Abstract

High-fiber-count optical connectors have become important components in subscriber cable networks, because they can reduce the connection time and save a space at the interconnection between equipment terminals.

In this paper, we describe the development of a single mode push-on type 16-fiber connector using oblique and end face contact between plastic ferrules. The connector has a mean connection loss of 0.25 dB and a return loss of higher than 50 dB without index matching materials.

1. Introduction

In recent years, large quantities of single mode fibers and SM fiber connectors have been used to build low cost, high quality subscriber networks[1]. Very high count single mode cables and connectors are needed to construct future FTTH (Fiber To The Home) networks[2]. A high fiber count connector with a low connection loss is a key component of the system.

In the 42nd IWCS, a 16-fiber connector with the mean connection loss of less than 0.2 dB using a high precision plastic molding technique has been discussed[3]. Furthermore, a multi-fiber push-on type and backpanel connector have been proposed to the interconnection of distribution frames and equipment terminals in advanced subscriber network[4].

In this paper, we present the development of 16-fiber push-on type connector for use in fiber ribbon distribution frames and equipment terminals.

2. Design criteria

For connectors used to the fiber distribution frames and equipment terminals in advanced subscriber network, the following requirements should be taken into account.

- 1) High packaging density
- 2) Ease of operation and cleaning
- 3) Low insertion loss
- 4) Low reflection
- 5) Low cost

As the reply to above requirements, a single-mode multifiber push-on type connector up to 8-fiber ribbon, has been already developed and in commercial use[5][6]. Typical insertion loss of the connector is 0.5 dB on an average without index matching materials. Return loss of higher than 50 dB is achieved by using oblique and direct end face contact between plastic ferrules.

In designing the 16-fiber push-on connector, the following should be insured against increasing fibers.

- 1) Connector size should be same as that of MPO connector, considering high packaging density.
- 2) High-precision plastic ferrule molding technique for the guide pin holes with highly accurate dimensions.
- 3) Angle polished end face with a slight fiber protrusion to enable direct fiber end face contact.

We have refined existing MT connector manufacturing technology to obtain a 16-fiber push-on type connector with low connection loss and high return loss.

We have conducted various performance tests and reliability tests on this newly developed connector and verified its consistency. The tests confirmed that the connector can be successfully used in the field.

3. 16-fiber push-on connector

3.1 Connector Structure

The structure of a 16-fiber connector is shown in Fig. 1. The connector consists of two plastic ferrules and two guide pins. Sixteen fibers are fixed in fiber-holes that are aligned by two guide holes. The ferrule is designed to compact with a width of 8 mm and height of 2.5 mm. The pitch of the fiber holes is less than 200 μm and nominal pitch between the two guide holes is 5.6 mm. The structure of an angle polished 16-fiber connector is also shown in Fig. 1. A 16-fiber ferrule end face is diagonally polished so as to make the fiber tips protrude. Therefore, the fibers can be connected directly resulting in a high return loss. The effects of Fresnel reflection can be eliminated by polishing the end face at an angle of 8° . The connector can be connected in a dry state without the use of index matching material. This contributes to easy installation and subsequent reconnection.

The structure of the developed push-on 16-fiber connector is shown in Fig. 2. The basic structure is similar to that of conventional multi-fiber push-on pull-off connector. The housing is designed to apply pressure on the ferrule from behind by mean of a coil spring. It however allows the ferrule a certain degree of movement during insertion and extraction. This structure enables the ferrule end faces to be connected securely with a low insertion loss. As the end faces are constantly kept under a certain pressure by the spring, the connector is stable against environmental changes. The plug and adaptor are engaged by fitting a pair of elastic hooks into the corresponding grooves.

The structure of a backpanel type connector is shown in Fig. 3. The connector comprises two of the push-on type plugs above, a printed board housing and a backpanel housing. Basic technologies are the same that realize a low-loss connection and high return loss in push-on type and backpanel type connector.

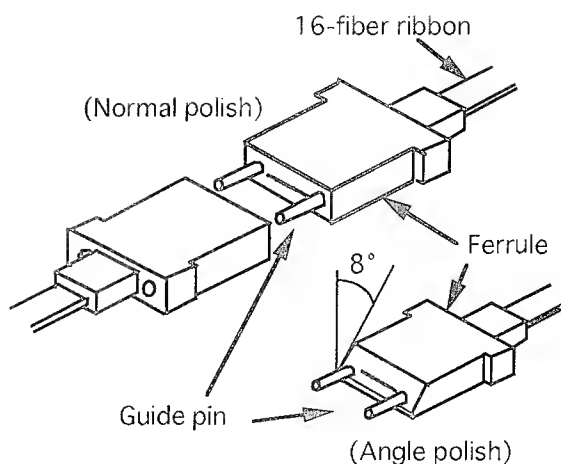


Fig. 1 16-fiber connector

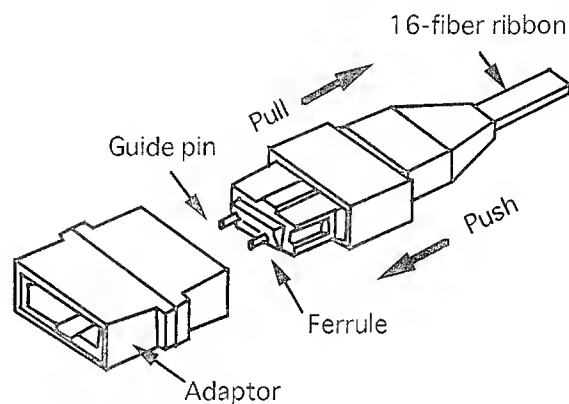


Fig. 2. Push on type 16-fiber connector

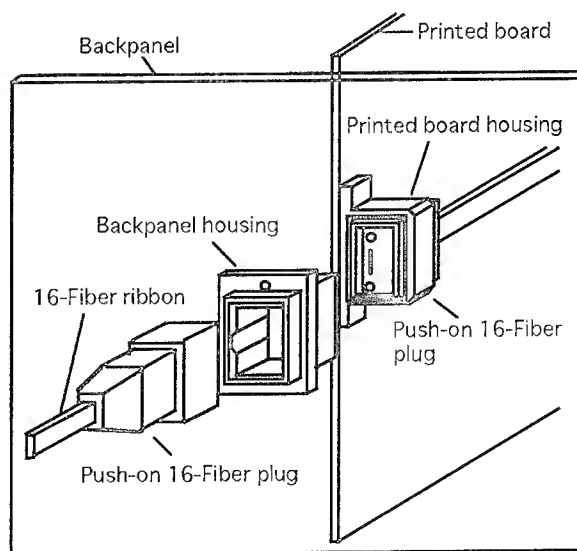


Fig. 3 Backpanel type 16-fiber connector

3.2 Low-loss connection

An angle polished connector has an advantage of high return loss. However, achieving a low-loss connection, additional transverse offsets related with angle polishing should be suppressed.

As is well known, the splicing loss components in single mode fiber connection are transverse offset, angular tilt and end separation[7]. Generally, transverse offset is the most serious factor. The offset causes the loss as[1].

$$L = -10 \log \{ \exp -(d/w)^2 \} \quad (1)$$

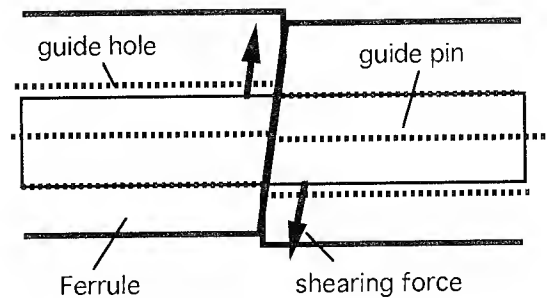
where L = connection loss (dB)
 d = transverse offset
 w = mold field radius

For standard single-mode fibers, a transverse offset of 1 or 2 μm causes a connection loss of 0.19 dB or 0.77 dB.

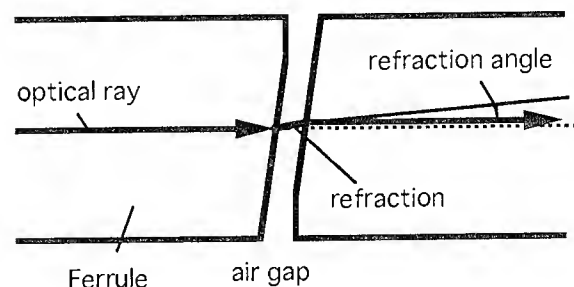
Additional factors of transverse offset in an angle polished connectors are shown in Fig. 4. The first offset is concerned with the shearing stress at the angle polished mating face. As shown in Fig.4, the clearance between guide pin and guide hole is directly related to offset. Therefore, the dimensional tolerances for the guide pins and their holes should be suppressed less than 1 μm . The precision molding technique for ferrules, which is the key technology in reducing the connection loss of the angle polished 16-fiber connector.

Second offset is related with that the refracted light pass is differ from the fiber axis. When fiber end face separates 10 μm each other, additional offset becomes to 0.7 μm , in the case of 8 degree angle polished connector at a dry condition. Direct fiber end face contact is enough solution to suppress this offset.

For the precision molding of ferrules, it is necessary to use a molding resin having a low shrinkage, dimensional stability under varying environments, and high mechanical strength for repetitive connection. Silica filler size in the resin also affects on the yield of physical contact in the 16-fiber connector plugs because of their small pitches. We succeeded in enhancing the dimensional accuracy of the 16-fiber connector ferrule by using the micro-silica filled thermosetting epoxy resin.



(a) Offset by shearing stress



(b) Offset by fiber end separation

Fig. 4 Additional offsets in an angle polished connector

3.3 Ferrule end face

As ferrule end faces are abutted against each other, they must have high degree of flatness and angular precision. In order to minimize fluctuation in insertion loss caused by attachment/detachment as well as environmental factors, the fibers should be abutted too. It is known that the insertion loss increases due to Fresnel reflection as the adhesive applied between ferrules contracts at high temperatures leading fibers being pulled back to widen the interstice between the fiber end faces of a ferrule.

To eliminate this, we refined a novel polishing technique to make the fibers project from the ferrule end face by 1 μm . A new high precision polishing machine was developed and is capable of achieving an end face flatness of 1 μm with an angular precision of $\pm 0.1^\circ$.

Typical values of the end face evaluation are summarized in Table 1.

Table 1 Typical data of angle polished 16-fiber connector end faces

Item	Results
Nominal oblique angle	8°
Angular precision	$< \pm 0.1^\circ$
Flatness of mating face	$< 1\mu\text{m}$
Nominal fiber protrusion	0.5 μm

4. Characteristics

The optical characteristics of the connector were verified. The results are shown in section below.

4.1 Insertion Loss

A 16-fiber connector was assembled, using a 16-fiber ribbon in which the core eccentricity in a fiber is less than 0.5 μm and the clearance between fiber and fiber hole in the ferrule less than 1 μm . The connection losses of the push-on type 16-fiber connector, measured with a master plug, are given in Fig. 5. Measurements were taken at a wavelength of 1.3 μm , without index matching materials. The mean connection loss was 0.25 dB and the maximum value was less than 1 dB.

4.2 Repeatability

Fig. 6 shows the results of the repeatability measurement test. The insertion loss was measured repeatedly attaching and detaching the connector 100 times.

On the basis of on these tests, we have verified that the connector has stable connection characteristics and has a low insertion loss for a push-on type 16-fiber connector.

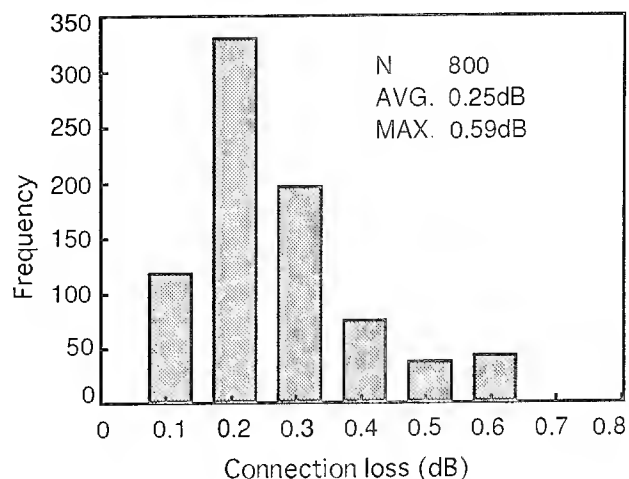


Fig. 5 Histogram of connection loss of 16-fiber push-on connector

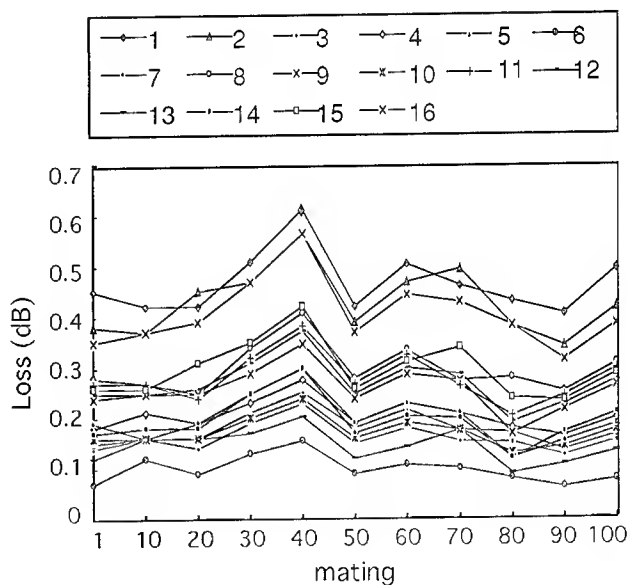


Fig. 6 Insertion loss change at 1.3 μm for typical connector pair during durability test.

4.3 Return Loss

The return loss was measured with the connector mated with a master connector. The histogram of the results of the test is given in Fig. 7. The return loss was higher than 50 dB for the case of a push-on type 16-fiber ribbon connector.

4.4 Heat cycle characteristics

The insertion loss fluctuation of the connector was measured repeating a 6 hour cycle of -25°C to 70°C ten times. The results of the measurement are shown in Fig. 8. The loss fluctuation was within ± 0.1 dB.

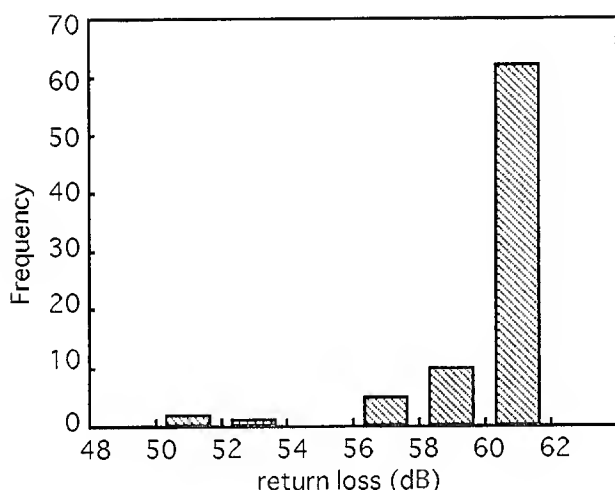


Fig. 7 Histogram of the return-loss

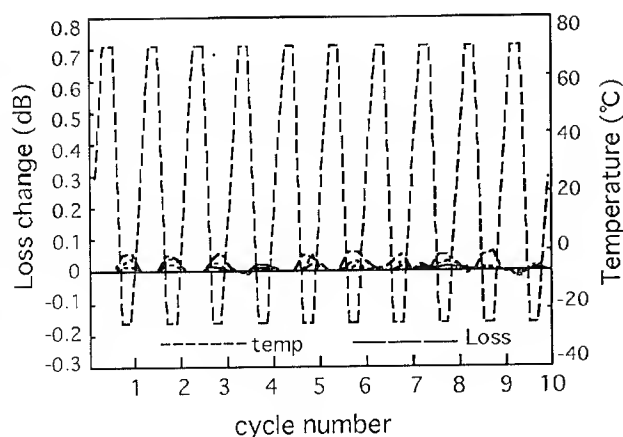


Fig. 8 heat cycle test results

5. Conclusion

A single mode push-on type 16-fiber connector using oblique and end face contact between plastic ferrules has been developed. The connector has a mean connection loss of 0.25 dB and a return loss of higher than 50 dB without index matching materials.

For future FTTH applications, we intend to continue investigations of high-count fiber connector and its application for the possibilities of attaining lower losses, shorter connection time, and greater ease of connection.

References

- [1] T.Satake, S.Nagasawa and R.Arioka, "A New Type of Demountable Plastic-molded Single-mode Multifiber Connector" *J. of Lightwave Technology*, Vol.L4, No.8, August, 1986.
- [2] S.Tomita, M.Matsumoto and S.Nagasawa, "Preliminary research into High-Count Pre-Connectorized Optical Fiber Cable", 41st IWCS 1992.
- [3] Y.Kikuchi, Y.Nomura, H.Hirao and H.Yokosuka, "High Fiber Count Optical Connectors", 42nd IWCS 1993.
- [4] S.Nagasawa, T.Tanifuji, M.Matsumoto and M.Kawase, "Single-Mode Multifiber Connectors for Future Large Scale Subscriber Networks" ECOC'93, MoP1.5, PP29-32, 1993.
- [5] S.Nagasawa, Y.Yokoyama, F.Ashiya and T. Satake, "A Single-Mode Multifiber Push-on Type Connector with Low Insertion- and High Return-Losses" ECOC/IOOC'91, MoB1-7, pp.49-52, 1991.
- [6] Y.Nomura, Y.Kikuchi and H.Hirao "Push-on Pull-off Multi-Fiber Connector", 41st IWCS 1992.
- [7] D.Marcuse, "Loss analysis of single-mode fiber splices", *Bell Syst. Tech.J.*, Vol.56, No.5, 1977.



Yoshio KIKUCHI

Fujikura Ltd.

1440 Mutsuzaki
Sakura, Chiba, 285,
Japan

Yoshio Kikuchi was born in 1955. He joined Fujikura Ltd. after his graduation from Tohoku University with a M.E. degree in 1980. He has been involved in research and development of optical fibers, cables and accessories. He is now a manager in Fiber and Cable Accessory Department within Opto-Electronics Laboratory and a member of the IEICE of Japan.



Hiroshi YOKOSUKA

Fujikura Ltd.

1440, Mutsuzaki
Sakura, Chiba, 285,
Japan

Hiroshi Yokosuka graduated in mechanical engineering from Tokyo Metropolitan Technical Junior College in 1967. He has been engaged in development of telecommunication cables and accessories. He is now a manager of the Fiber and Cable Accessory Department within Opto-Electronics Laboratory and a member of IEICE of Japan.



Hiroshi FURUKAWA

Fujikura Ltd.

1440, Mutsuzaki
Sakura, Chiba, 285,
Japan.

Hiroshi Furukawa was born in 1959. He graduated from Chiba university in 1984.

He joined Fujikura Ltd., and has been engaged in research and development in the Fiber and Cable Accessory Section. He is a member of the IEICE of Japan.



Yoshikazu NOMURA

Fujikura Ltd.

1440 Mutsuzaki
Sakura, Chiba, 285,
Japan

Nomura was born in 1951. He graduated in mechanical engineering from Shinsyu University. He has been engaged in the research and development of telecommunication cables and accessories. He is presently a manager in the Fiber and Cable Accessory Department within Opto- Electronics Laboratory.

INTEGRAL MULTI-FIBER MANAGEMENT FOR ECONOMIC MASS-FUSION SPLICING

M. Loch, Siemens AG, 81359 Munich, Germany

G. Boscher, RXS Schrumpftechnik-Garnituren GmbH, 58093 Hagen, Germany

Abstract

The expanding demand for information necessitates a well designed multi-fiber topology. Therefore, an integral multi-fiber management system consisting of all practically feasible configurations for networks/communication systems will be discussed in detail in this paper. New components such as an improved multi-fiber handling/protection and splicing system and a "hyper-ribbonizer", necessary for pragmatic installation are presented. This innovative concept reveals opportunities for the verification of area networks. Consequently, the envisioned breakthrough of multi-fiber technology is achieved.

Introduction

The permanent and increasing demand for broadband data communication and the growing dependence of industry as well as national, international and private commerce can only be controlled by complex and interlaced networks. Additional networks as well as the extension of existing communication systems and the arrangement of supplementary local distribution networks dictate the installation of high fiber count cables. Therefore, a multi-fiber/ribbon technology is economically and fundamentally justified. Until now, the advantages of the multi-fiber technique could not be realized because peripheral problems have been widely neglected. Mass fusion splicing itself has been perfected. However, the ease in handling and the clearly arranged organization of the completed splices experienced in the single-fiber technology are not practically feasible in multi-fiber structures.

This paper investigates the actual situation that occurs in the multi-fiber technology. Beginning with mass-fusion splicing we discuss integral multi-fiber management which includes novel and important components and configurations such as the transition from ribbon to sub-ribbons.

Mass-fusion organizing

Low count ribbon splicing:

Cost and time expenditure for the splicing process can be minimized essentially by using a reliable and easy to operate splicing technique. Therefore an adequate technique is available, today: low loss mass-fusion splicing of multi-fiber/ribbon structures. So, there are small fusion splicers designed for fusing up to 4 individual fibers or 4-fold ribbons, respectively. These machines - like the RXS types X74-4 and X75-4 - are based on fixed V-groove positioning procedure with or without control of realized splice loss. However, in these machines there is no really intelligent system for minimizing the splice loss.

High count ribbon splicing:

Therefore, other multi-fiber fusion splicers (like the RXS X120 type) have been developed working fully automatically with integrated x- and y-positioning, designed for up to 12 fibers in multi-fiber/ribbon structure. Using three dimensional positioning, the maximum splice loss can be reduced significantly as proven in extensive tests. By the development of an intelligent multi-fiber LID system [1,2] the main advantage of the LID technology known in the single-fiber splicing technique could be transferred to the multi-fiber structure. Thus, a fiber-selective measurement of transmitted power is possible by using a galvanometer scanner with the operating wavelength of 1300 nm. Specifically, an automatic control and consequently an optimization of the fusion process or the fusion time, respectively, is possible. This is prerequisite for minimizing the maximum splice loss as well as the average loss within the multi-fiber structure. Furthermore, the inherent intelligence of this system facilitates the handling and improves the reliability of this technique because of its large user-independence.

Fig. 1 shows a histogram of measured splice loss. Using the LID technology to control the splicing process of different ribbons, the average splice loss could be reduced from 0.12 dB to 0.07 dB corresponding to an increased splice yield of about 6 %. So, the splicing of ribbons with up to 12 fibers will be state of the art.

Handling and protection of the multi-fiber splice:

After finishing the splicing process, the multi-fiber splice has to be taken from the fusion splicer in order to protect it and to place it into the splice tray. However, the ribbon ends and the multi-fiber splice are very sensitive concerning external stresses, i.e. twisting and bending, etc. So, until now, the handling of the unprotected multi-fiber splice is more critical than that of single-fiber splices. Therefore, an improved handling system, eliminating any mechanical stress, is necessary. We developed a new multi-functional system for the multi-fiber splice designed for all types of multi-fiber/ribbon structures up to 12 individual fibers (Fig. 2). Prior to the stripping and cleaving process, "one-way" adapters are attached at the multi-fiber structures near to the ends to be spliced. Then, the multi-fiber/ribbon structures are inserted into the handling adapters as usual. Before opening these handling adapters after the fusion process to remove the multi-fiber splice from the splicer, a stable support module is put on the "one-way" adapters, which are still attached on both sides of the multi-fiber splice. This support module is provided with an easy to handle "click mechanism" to connect both "one-way" adapters. Now, the spliced multi-fiber unit can be removed from the splicer easily without any risk to damage any of the individual fibers within the multi-fiber splice by uncontrolled twisting, bending, compressing, etc. of the fibers and without any risk of inducing additional losses. A strong parallel alignment of the fibers as provided during the splicing process is maintained during the handling.

In a very comfortable way, the support module also serves as the fundamental part of the splice protection unit consisting of a bottom as its lower part and a cover as its upper part with a protective elastical adhesive in between. In comparison to the normally used shrinking procedure, which requires up to two minutes for the shrinking process, the use of this new handling/protection system is less time-consuming and easier to handle because of its multi-functionality.

Multi-fiber topology

From the technical point of view, ribbons with all different numbers of fibers are conceivable and also partly available, today: e.g. two, three, four ... up to 12 or 18 fibers per ribbon. For the near future, however, the maximum is expected to be 12 fibers within the ribbon structure. With regard to different optical telecommunication network structures discussed and planned in many countries at present, a multi-fiber structure based on the "four-fibered" system seems to be the most preferred one. For example, Taiwan, Korea, Italy, Switzerland, Japan ...

Consequently, multi-fiber structures with 4, 8 or 12 fibers, respectively, are very interesting concerning the handling, the fusion technique and the organization of the splices. In addition, the two-fiber ribbon might be taken into consideration as the smallest unit connecting the subscriber directly to the distribution network. In our opinion, the other ribbon structures - the 6-/10-fold structures as well as ribbons with any odd number of fibers - do not have any substantial practical significance or are negligible, respectively.

Furthermore, for transition from overlay ring structures to smaller distribution networks, the coupling/splitting of high fiber count ribbons to several low fiber count ribbons is indispensable and very important for the break-through of the multi-fiber technology. Listing all theoretical combinations of different fiber counts - there are 18 possible combinations for the 12-fold ribbon structure - and analyzing these with regard to their estimated practical significance, the number of their combinations can be reduced dramatically to only some configurations satisfying the requirements of practical interest. In the "four-fibered" system there are only three important combinations to be regarded. These standard splitting ratios are:

- splitting of 12-fold ribbon to 3x4-fold ribbons,
- splitting of 8-fold ribbon to 2x4-fold ribbons,
- splitting of 4-fold ribbon to 2x2-fold ribbons.

Accepting two further splices, also more complicated configurations, e.g. the splitting of a 12-fold ribbon to one 8-fold and one 4-fold ribbon can be accomplished by the simple serial connection of the standard splitting ratios.

Finally, to bring the fiber to the subscriber, the transition from ribbon structure to individual fibers is also necessary. To reduce installation time and to improve efficiency working with existent high fiber count cable systems based on bundle technology, the simultaneous splicing of individual fibers is very important. Utilizing a ribbonizer for the correct arrangement of up to 12 individual fibers, the splicing procedure itself is comparable to that of ribbons.

So, a small number of multi-fiber structures and their combinations satisfies all practical requirements as discussed. Most of these combinations being found in complicated future network topologies can be realized without any problems, today. However, up to now, there is no possibility of realizing connections from ribbon to sub-ribbons - meaning low fiber count ribbons - with the conventionally used ribbon design. Due to different outside geometry/ dimensions of the ribbon structure, the simple arrangement of several ribbons side by side is not possible. So, at first, we developed an improved ribbonizing system - a "hyper-ribbonizer" - which allows the organization and the handling of several individual low fiber count ribbons independent of their actual fiber number. All inherent individual fibers are arranged equidistantly within the handling system. That is possible by a clever arrangement of the individual ribbons and/or a special preparation procedure for adapting the outer ribbon geometry to guarantee the correct position of the fibers. Now, the simultaneous handling of several ribbons and the easy production of splitting modules are possible in the field using a technology similar to the handling of individual fibers prepared for the mass-fusion process.

Furthermore, for standard splitting ratios factory-made ribbon splitting modules are available, which are placed in specially designed organizer trays with one high fiber count incoming ribbon and several (up to three) low fiber count outgoing ribbons. These modules could be incorporated into distribution networks by simple splicing of the particular ribbons. For re-splicing, an extra ribbon length of about 4 ft is stored within the tray. For example, Fig. 3a shows a splitting module with the ribbon splitting ratio 1:3, Fig. 3b demonstrates the transition from ribbon to individual fibers in bundle technology.

Organizer trays and closures

When joining high fiber count cables, a clearly arranged organization of the protected splices within special trays must allow the removal of individual splices without any risk of damaging other fibers. We propose a new universal organizer tray system which is applicable for the single-fiber as well as for the multi-fiber/ribbon technology. Depending on the actual operating range and the fiber topology, the new organization can be fitted to all conceivable splice combinations: one tray can hold several splices of single-fiber, multi-fiber structures/ ribbons or the combination of these. The system is also suitable for the "ribbon to sub-ribbon" splitting. Depending on the multi-fiber structure, up to 60 splice joints are placed within one tray. For re-splicing an additional fiber/ribbon length is stored within the tray:

Several trays could be connected to a pivoting block as shown in Fig. 4. Below, there is room to house un-cut bundle/ribbons and additional length of cut bundles/ribbons enough to bring the organizer tray to the fusion splicer.

Upon completion of the splicing process and placement of the splices into organizer trays, special consideration must be given to protect these multi-fiber splices from environmental stresses, to shield the splices from cable pull-out stresses, to secure and/or ground the cable central strength member in order to avoid future problems as known in the single-fiber technology. This can be accomplished by utilizing special splice closures [3].

The UCNP (Fig. 5) is a hermetically sealed splice closure which provides the necessary protection for single-fiber as well as for multi-fiber splices in underground, buried and aerial environments. This closure allows 6 cables to enter each side of the closure (12 in total) and can be utilized in both in-line and butt configurations. Each end cap can accommodate 2 un-cut fiber optic cables as well as 4 cut cables. Additional cable installation does not affect existing cable seals. In a spacious slack box up to 180 ft of fiber buffer/fiber ribbon can be housed. In order to eliminate cable pull-out/push-in stresses which may occur due to laying conditions and temperature changes, each cable is secured inside the closure to a user-friendly strain relief bracket. To prevent future movement of the central strength member into the closure, a system to captivate the central strength member has also been incorporated into the strain relief bracket. Core blocking can be provided. The smallest closure size can accommodate in one bank up to 12 splice trays allowing individual tray access.

The UCNP is equipped with permanent reusable sealing gaskets and is closed via plastic clamping bars. This allows the closure to be sealed and/or re-entered quickly and easily, minimizes cost and labor associated with removal and replacement of sealing materials. The UCNP Closure System has an all plastic exterior which eliminates corrosion concerns and is supplied with all components necessary for installation in all types of fiber optic networks.

Conclusion

We discussed an integral multi-fiber management for an overall economic application of multi-fiber technology in data communication systems, feeder and distribution networks. This includes mass-fusion splicing - taking the advantage of intelligent LID systems and three dimensional positioning to reduce maximum as well as average splice loss in combination with most easiest handling - new multi-fiber splice handling/protection system and new multi-functional organizer trays - designed for all multi-fiber configurations being of practical interest - and closures. Novel components which are indispensable for a multi-fiber topology applicable to differently structured networks have been presented. Therefore, providing reliable economic advantages, the break-through of multi-fiber technology is irresistible.

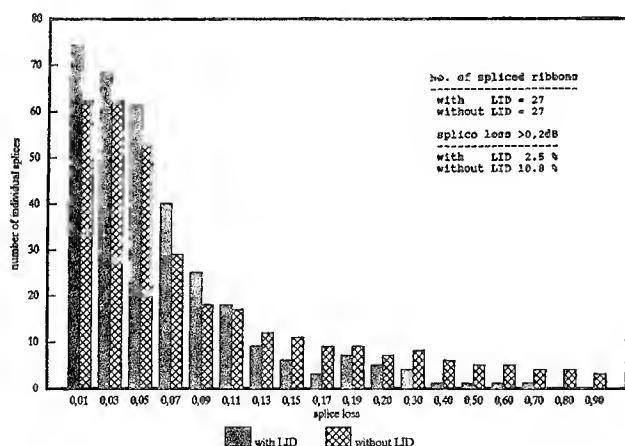


Fig. 1: Splicing of different fiber ribbons with/without multi-fiber LID system (RXS X120); increase of splice yield from 90 % to 96 % by using the LID system

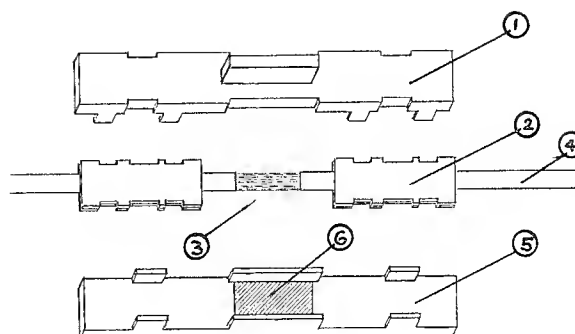


Fig. 2: Multi-fiber handling/protection module: 1 support module; 2 "one-way" adapters attached to 4 multi-fiber/ribbon structure; 3 multi-fiber splice; 5 lower part (bottom) of protection unit; 6 elastical adhesive

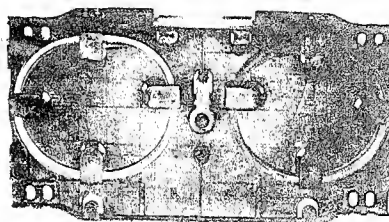


Fig. 3a: Ribbon splitting module: splitting of high fiber count (12 fibers) ribbon to three low fiber count (4 fibers) ribbons

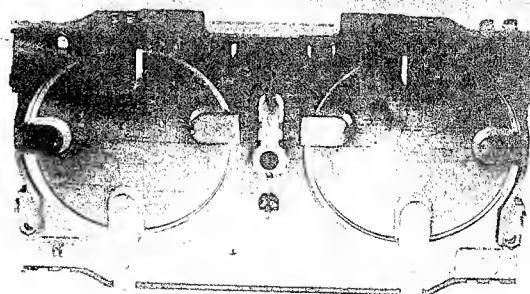


Fig. 3b: Transition from ribbon (4 fibers) to individual fibers in bundle technology

Biography of authors

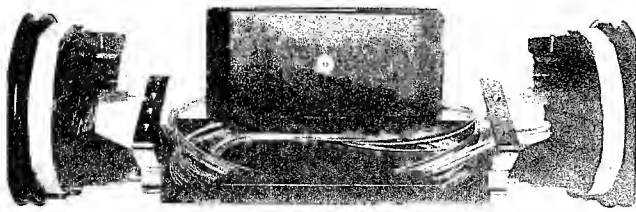


Fig. 4: Fiber optic splice closure with pivoting trays

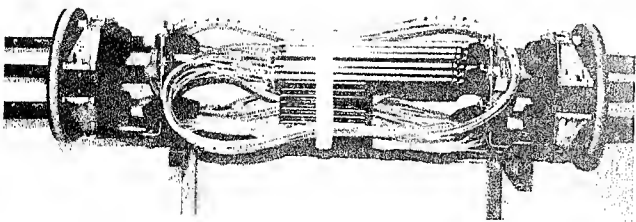


Fig. 5: Hermetical sealed splice closure UCNP



Manfred Loch received his diploma degree and Ph.D. degree in electrical engineering from the University of Kaiserslautern, Germany in 1983 and 1989 respectively. He was concerned with refractive-index profile measurements and characteristics of birefringent fibers. Since 1989 he has been employed at Siemens AG, Munich, Germany. He is responsible for the development of fusion splicing equipment and optical measurement systems.



Georg Boscher received his diploma degree in physics from the University of Munich, Germany in 1967. He joined Siemens AG and worked for several departments. In 1970 he became responsible for the development and testing of accessories in the Telecommunications Cable Division. Since 1985 he has been working as a deputy director and head of Marketing and Product Management of RXS Schrumpftechnik-Garnituren GmbH, a fully-owned subsidiary of Siemens AG. RXS manufactures and markets accessories for telecommunication and power cables.

Acknowledgement

The authors would like to thank Messrs. Finzel and Glaser for their valuable discussions and cooperation.

References

- /1/ M. Loch, R. Kossat, G. Ruegenberg, G. Boscher: Intelligent LID systems in the multi-fiber technology. Proceedings of 41st IWCS, Nov. 1992, pp. 126-131
- /2/ M. Loch, G. Boscher: Multiple LID system: the modern approach to ribbon splicing and measuring. Proceedings of OPTO, May 1993, pp. 420-425
- /3/ D. Kunze, J. Rost, E. Bachel, G. Boscher, L. Mendat: A new universal splice closure system. Proceedings of 36th IWCS, Nov. 1987, pp. 699-704

IMPROVED SPLICE LOSS OF OPTICAL FIBER RIBBON AT ALTITUDES

Masahiro Hamada, Toru Yanagi, Yoichi Okamoto
Tsutomu Watanabe, Keiji Osaka, Tetuya Taguchi

Optomechatronics systems R&D Dept., Yokohama Research Labs.,
Sumitomo Electric Industries, LTD.

Abstract

Even if fusion conditions were optimized at a factory around the sea level, the splice loss may increase to above 1.0dB at higher altitude due to discharge power change. The properties of discharge under various altitudes were analyzed and reducing method of splice loss at each altitude was investigated. An appropriate discharge current, which is different depending on fiber count and altitude, was obtained. A method was proposed employing an automatic discharge current correction by the aid of an atmospheric pressure sensor. This method was proved to lower splice loss to 0.05dB on the average for every ribbons of up to 12-fiber at even the high altitude of 4,000m.

1. Introduction

Recently, high-count, high-density optical fiber cables were introduced into subscriber networks. Mainly for such application, mass-fusion splicing technologies have been developed for the purpose of joining optical fiber ribbon quickly and economically. It was reported that an automatic fusion splicer was developed capable of mass-splicing up to 12-fiber ribbons with the splice loss lower than 0.1dB.[1][2] It is one-body, light-weight and portable to any environment. The splice loss was, however, very susceptible to the surroundings of the field.

In this paper, firstly a problem of fusion splicing under the field usage is clarified. Next the experimental results concerning the influence of the altitude on the discharge is indicated. Lastly a method of automatic discharge current correction is proposed and the remarkable improvement of splice loss under the altitude changes is reported.

2. Problem of fusion splicing on field

In the conventional fusion splicing procedure of optical fiber cables, after jacket removing and cleaving, bare fibers are placed face to face on a V-groove and fusion spliced with an electric discharge (Figure 1).

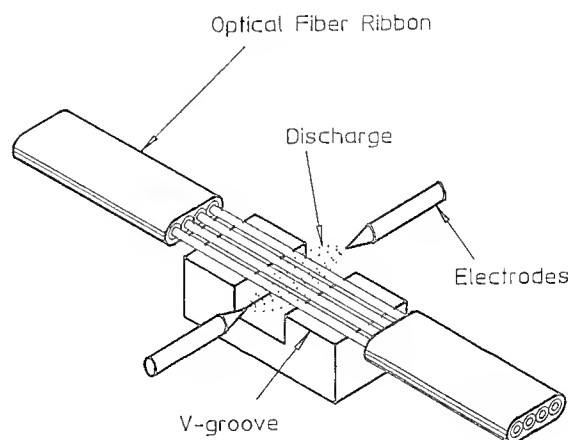


Fig.1 Schematic View of
Fusion splicing

When the optical fibers are fusion spliced, the main fusion splicing conditions which affect splice loss are as follows:

- 1) End face gap
- 2) pre fusion duration
- 3) fusion duration
- 4) stuffing stroke
- 5) stuffing speed
- 6) discharge power

In case of the automatic fusion splicer using the electric discharge, the CPU (Central Processing Unit) and the memory are installed in the body. Therefore the above fusion conditions are optimized through the experiment and memorized in the factory so as to obtain low splice loss. These conditions are controlled with high reproducibility at the field. However the discharge power, which is the most sensitive condition for splice loss, is influenced by the change of the some environments on the field, especially by the altitude. We considered the reason of this phenomenon as the following.

The discharge power (P_d), which is applied to the fibers, is expressed as the function of the product of the voltage (E_d) and the discharge current (I_d) between two electrodes as Eq.(1).

$$P_d = f (E_d \cdot I_d) \quad (1)$$

Then the voltage is also a function of the atmospheric pressure (Paschen's law) as following Eq.(2).

$$E_d = f (p \cdot d) \quad (2)$$

where p is the atmospheric pressure of the working place and d is the distance between electrodes. Therefore, When the fusion splicing is performed at the high altitude, the decrease of atmospheric pressure causes the reduction of discharge voltage. Therefore it is supposed that the high altitude considerably makes the discharge power weaker and results in higher splice loss.

3. Experiment of discharge

3-1. Experimental apparatus

We tried to verify the above supposition experimentally. Figure 2 shows the experimental apparatus for the measurement of the discharge voltage and current, which consists of:

1)a discharge circuit, which can precisely control the discharge current; 2)a pair of electrodes; 3)an ammeter, which measures the current; 4)an oscilloscope with a probe, which are to measure the voltage. Impedance of the probe is very high in order not to change the state of discharge between the electrodes; 5)a chamber, which can control the atmospheric pressure corresponding to the altitudes from 0m to 4,000m using a vacuum pump.

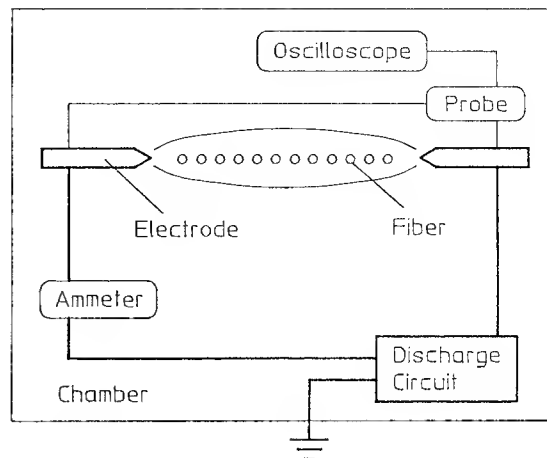


Fig.2 Experimental apparatus

3-2. Experimental results

Firstly we measured the discharge voltage between electrodes at each altitude without the optical fiber on the V-groove. Figure 3 shows the relationship between the altitude and the voltage. The voltage decreases in proportion to the altitude under the condition that the discharge current (I_d) is constant. It was found that the voltage at the altitude of 4,000m are reduced to 90% of the value on the sea level.

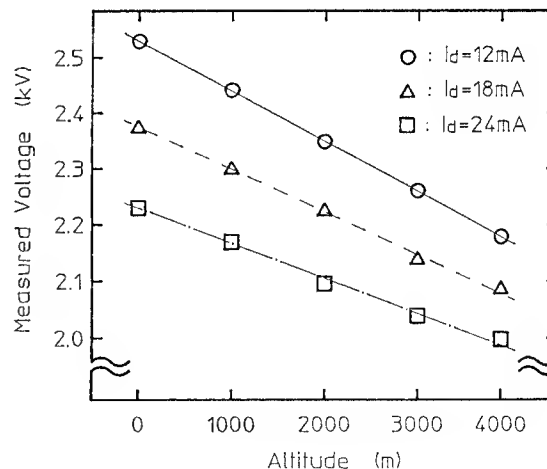
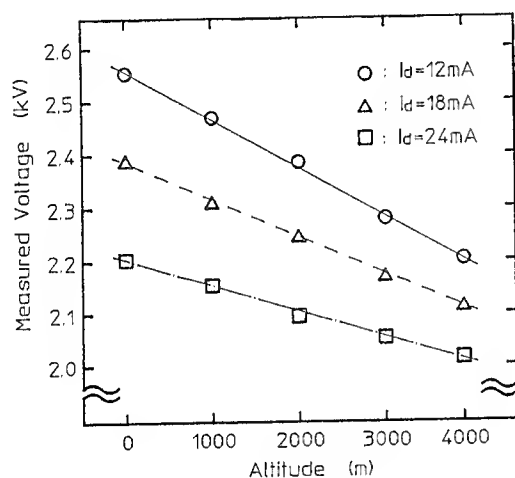
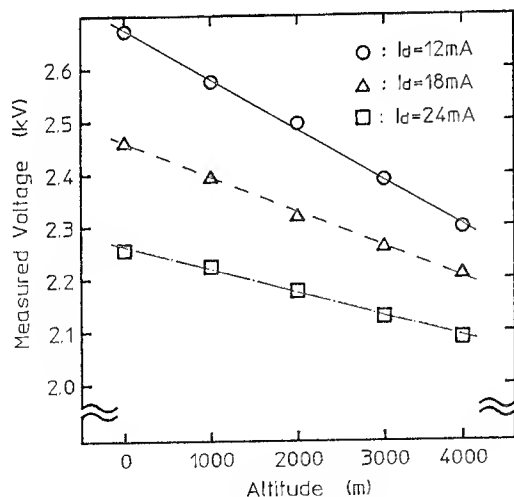


Fig.3 Measured voltage between electrodes without fibers

Next we measured the discharge voltage between electrodes for each altitude with some kind of fibers on the V-groove in order to investigate the influence of the state around the electrodes. Figure 4 shows the relationship between the altitude and the voltage in case non-carbon coated fibers and carbon coated fibers are set on the V-groove. When the fibers are set on the V-groove, especially carbon coated fibers, the voltage tends to become high. However, the tendency of the voltage decreasing for the altitude are very similar for some states around electrodes. The influence of the altitude on the discharge power was proved clearly.



(1) Non carbon-coated fiber

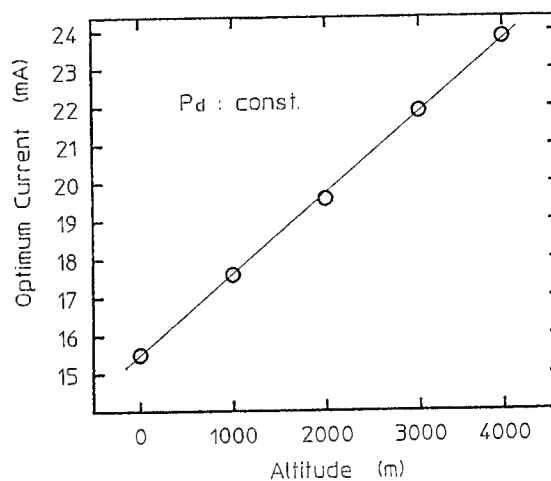


(2) Carbon-coated fiber

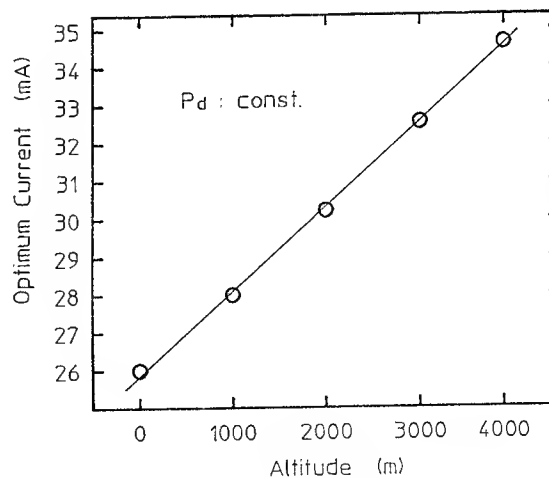
Fig.4 Measured voltage between electrodes with fibers

4. Correction of discharge power

It was found that the voltage happens to change for the altitude. However it is difficult to detect and control actually the voltage as high as 2kV between the electrodes inside the fusion splicer at the field. Therefore the voltage change must be compensated practically by the discharge current which can be closely controlled by the feedback circuit in the fusion splicer.



(1) 4-fiber ribbon



(2) 12-fiber ribbon

Fig.5 Optimum discharge current at each altitude

On the other hand, the optimum discharge current at each altitude, which is needed to maintain the equivalent discharge power (P_d) to that of the sea level, was obtained by the experiment applying the method of monitoring discharge power using an image processing [3]. Figure 5 shows the optimum current at each altitude in case of 4-fiber ribbon and 12-fiber ribbon. The optimum discharge current increased in proportion to the altitude. The discharge current at the altitude of 4,000m must be corrected adding about 9mA compared with that at the sea level for both fiber ribbon.

5. Improvement of splice loss

We propose a method of automatic discharge power correction using an EEPROM (Electric Erasable Read Only Memory) and an atmospheric pressure sensor. The correct current (ΔI_d) is obtained from the relationship between the optimum current and the atmospheric pressure corresponding to each altitude (Figure 5) as Eq.(3).

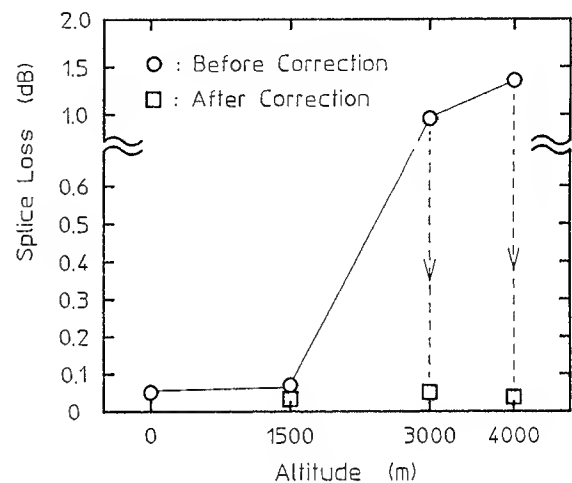
$$\Delta I_d = f(p) \quad (3)$$

Figure 6 shows an algorithm of automatic discharge power correction of our fusion splicer.

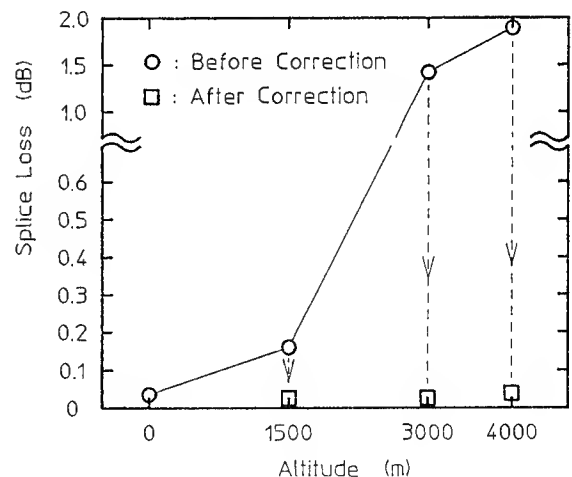
- 1) Input optimum discharge current and atmospheric pressure at the sea level into an EEPROM
- 2) Measurement of pressure at the altitude of the working field
- 3) Calculation of a correct current for the specific altitude using Eq.(3)
- 4) Input a new appropriate discharge current into the EEPROM

Fig.6 Algorithm of automatic discharge power correction

Figure 7 indicates the measured splice loss for 4-fiber ribbon and 12-fiber ribbon before and after the correction of discharge current using the above method at each altitude of the field actually. The splice loss lower than 0.05dB on the average for 4-fiber ribbon and 12-fiber ribbon at even altitude of 4,000m were achieved by using automatic discharge power correction method.



(1) 4-fiber ribbon



(2) 12-fiber ribbon

Fig.7 Splice loss at each altitude before and after correction of Discharge Current

6. Conclusion

When conventional fusion splicer is used at the altitude more than 3,000m, the splice loss increased to above 1.0dB on the average under the optimum fusion conditions of the sea level. By investigating the influence of the altitude to the discharge phenomena between electrodes, the splice loss reduction have been tried on the basis of the experimental results. The main results were as follows:

- (1) It was clarified that the voltage between two electrodes decreases in proportion to the altitude in case the current is constant.
- (2) The discharge current correction was effective in order to match the optimum discharge power and lower the splice loss.
- (3) The method of the discharge power correction automatically using the atmospheric pressure sensor and EEPROM was proposed on the basis of the experimental results.
- (4) It was confirmed that the splice loss were reduced to less than 0.05dB at even high altitude of 4,000m using the proposed correction method.

References

- [1] Osaka et al., Sumitomo Electric Tech. Review, No.29, p85, 1990
- [2] Hamada et al., 40nd IWCS, pp.309-315, 1991
- [3] Morooka et al., 42nd IWCS, pp.212-217, 1993



Masahiro Hamada

Sumitomo Electric
Industries, Ltd.

1, Taya-cho, Sakae-ku
Yokohama, Japan

Masahiro Hamada was born in 1962 and received his M.S. degree in electronic engineering from Shizuoka University in 1987. He joined Sumitomo Electric Industries the same years and has been engaged in the research and development of fusion splicing technologies for optical fibers. He is a member of the Institute of Electronics, Information and Communication Engineering of Japan.



Toru Yanagi

Sumitomo Electric
Industries, Ltd.

1, Taya-cho, Sakae-ku
Yokohama, Japan

Toru Yanagi was born in 1939. He joined Sumitomo Electric Industries in 1964 and has been engaged in the research and development of fusion splicing technologies for optical fibers. He is a member of the Institute of Electronics, Information and Communication Engineering of Japan.



Yoichi Okamoto

Sumitomo Electric
Industries, Ltd.

1, Taya-cho, Sakae-ku
Yokohama, Japan

Yoichi Okamoto was born in 1965. He joined Sumitomo Electric Industries in 1983 and has been engaged in the research and development of fusion splicing and mechanical switching technologies for optical fibers.



Tsutomu Watanabe

Sumitomo Electric
Industries, Ltd.

1, Taya-cho, Sakae-ku
Yokohama, Japan

Tsutomu Watanabe was born in 1964 and received his B.S. degree in mechanical engineering from Tokyo University in 1987. He joined Sumitomo Electric Industries the same year and has been engaged in research and development of fusion splicing technologies and mechanical switching technologies for optical fibers. He is a member of Japan Society of Mechanical Engineers and the Institute of Electronics, Information and Communication Engineering of Japan.



Keiji Osaka

Sumitomo Electric
Industries, Ltd.

1, Taya-cho, Sakae-ku
Yokohama, Japan

Keiji Osaka was born in 1955 and received his M.S. degree in precision mechanical engineering from Kyoto University in 1981. He joined Sumitomo Electric Industries the same year and has been engaged in research and development of high NA optical fiber fabrication and fusion splicing technologies for optical fibers. He is now a chief research associate of Optomechatronics Systems R&D Dept. Yokohama Research Laboratories and a member of Electronics, Information and Communication Engineering of Japan.



Tetsuya Taguchi

Sumitomo Electric
Industries, Ltd.

1, Taya-cho, Sakae-ku
Yokohama, Japan

Tetsuya Taguchi was born in 1955 and received his M.S. degree in electronic engineering from Osaka University in 1980. He joined Sumitomo Electric Industries the same year and has been engaged in research and development of video signal processing technologies and fusion splicing technologies for optical fibers. He is now a chief research associate of Optomechatronics Systems R&D Dept. Yokohama Research Laboratories.

STRUCTURES AND CHARACTERISTICS OF CARBON FILMS ON OPTICAL FIBERS

Motonori Nakamura, Akira Urano, Haruhiko Aikawa, Hiroki Ishikawa, and Toshio Danzuka

Sumitomo Electric Industries, Ltd.

1, Taya-cho, Sakae-ku, Yokohama City, 244

1. Abstract

We tried several analytic methods (AFM, AES, and so on) for carbon-coated optical fibers to know characteristics of the carbon films on carbon-coated optical fibers. This time we adopted the electron spin resonance spectroscopy to directly investigate the structure. We can get the ESR spectra of them and estimate carbon layers are made of graphite. These analyses tell us that the hermeticity of carbon films are dependent on the sizes of graphite particle of the films.

2. Introduction

It is known that the absorption of moisture into optical fiber promotes mechanical fatigue and that the entrance of hydrogen into fiber core increases transmission loss. In order to prevent these problems, carbon coating is usually put on the surface of optical fiber^{(1),(2),(3)} and we can improve their long-term reliability. Carbon-coated optical fiber has high hermeticity against hydrogen and fatigue characteristics because of the high hermeticity of carbon coating itself. So we can estimate the hermeticity is dependent on the structure of carbon layer. However it is not clear what kind of carbon structure on the fiber causes high hermeticity. It is difficult to analyze the structure because of the thin and curved carbon layer on the fiber. In this

study, we manufactured several carbon-coated optical fibers that have different characteristics and investigated the hydrogen permeability and fatigue property with each of them. Moreover we measured the ESR (Electron Spin Resonance)^{(4),(5)} spectra of carbon-coated optical fibers to get the information of the structure of the carbon on the fiber.

3. Apparatus

Germanium-doped silica core single mode fibers were used in this study. Figure 1 shows the schematic diagram of apparatus for carbon coating on the fiber. Preforms were heated in the furnace and drawn to 0.125 mm in diameter. Then fibers were immediately fed into the reactor which was filled with material gas such as the hydrocarbon. Then the fiber was coated with thin carbon film by thermal chemical

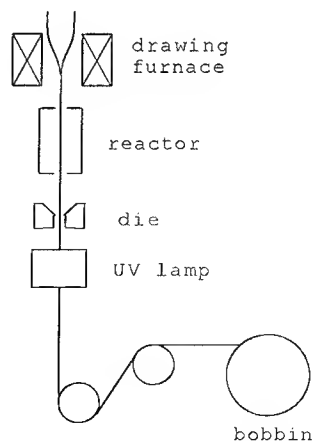


Figure 1. Schematic diagram of apparatus of carbon-coating on fiber

vapor deposition (CVD) method. Its own heat causes the material gas to start reacting on the fiber. The carbon film grew thicker and thicker as the chain reaction of reactant continues, then the thickness of carbon film became about 40 nm. After that, bare carbon-coated optical fiber is also coated with UV-cured resin and then 0.25mm carbon-coated optical fiber can be obtained. A cross-sectional view of carbon-coated optical fiber is shown in figure 2.

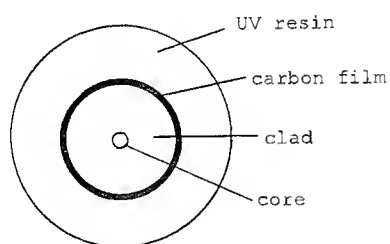


Figure 2. Structure of a carbon-coated optical fiber

4. Previous analysis

We have already investigated carbon-coated optical fibers by using Scanning Electron Microscope (SEM), Atomic Force Microscope (AFM), and Auger Electron Spectroscopy (AES)⁶⁾.

We can prepare carbon-coated optical fibers which have various permeabilities. Although their hermeticities are different, the thickness of carbon layers which was measured by SEM are almost the same (about 40nm). Then we tried to know the structure of carbon layer and explore the surface of the carbon. Auger electron spectra tell us that the film which has low permeability indicates the signal of Si-C bonding at 260eV or so. Moreover the detected intensity profiles of C and Si were also measured. While the surfaces of carbon films were sputtering. This result shows that wider area where carbon and silica

coexist causes higher hermeticity. We recognized the roughness of the carbon-coated optical fibers are different from each other by AFM. From these analyses, we can roughly estimate the relation between the structure and the characteristics of carbon films. However they did not concern the structure of carbon but interface between carbon and silica or the surface of the fiber. The difference among permeability of carbon-coated optical fibers is dependent on the structure of carbon layer. In order to find out the structure of carbon layers, we tried other spectroscopy than the above.

5. Experimental

Three kinds of carbon-coated optical fibers were manufactured under several conditions. These fibers were broken into pieces of 2cm and only fifteen pieces were set in the sample tube for ESR spectrometer in order to avoid detecting the signal from E'-center of the silica in the fiber. We used an ordinary X-band ESR spectrometer for measuring ESR spectra of carbon-coated optical fibers.⁴⁾ In addition, we measured their fatigue coefficient, their hydrogen permeability, and the distribution of carbon particles in the reaction tube.

6. Results and Discussion

Table 1 shows loss increases at 1.24 μ m after hydrogen treatment ($\Delta\alpha_{1.24}$) which was performed in hydrogen partial pressure of 10 atm at the temperature of 100°C for 50 hours. These results are expressed as the values divided by saturated loss increases ($\Delta\alpha_{1.24,\infty}$) at 100°C. Fiber C has excellently high hermeticity against hydrogen diffusion, while there is little

hermeticity for fiber A. The fatigue coefficient which was obtained by dynamic fatigue test is also shown in Table 1. Fiber A has smaller fatigue coefficient than fibers B and C. This means that fiber A has higher permeability of water molecules than others, because water molecules attack the surface of the fiber and promote fatigue of it.

We measured ESR spectra of these carbon-coated optical fiber in order to investigate the structures of carbon layer. At first, we measured the ESR spectrum of the fiber without carbon coating. The result is shown in Figure 3. The two sharp peaks are the ESR signals of Mn^{2+} ions. (reference standard) If plenty amount of the E'-center of silica are there, we can get the ESR signal of it between these two Mn^{2+} signals. Usually much more pieces of fibers are necessary to obtain ESR spectrum of E'-center of them at least. In this study, we are not necessary to pay attention to the E'-center.

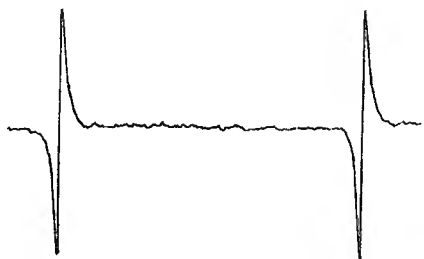


Figure 3. ESR spectrum of bare optical fiber

Figure 4 shows ESR spectra of fibers A, B, and C. In the spectrum of fiber A, only Mn^{2+} signals appear and no carbon signal can be seen between them. This means that

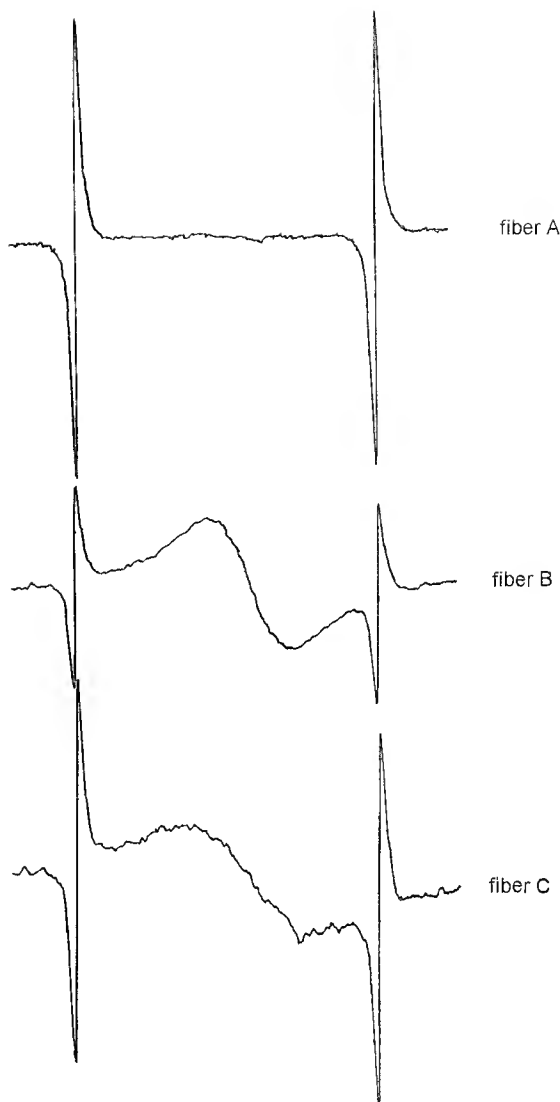


Figure 4. ESR spectra of carbon-coated optical fibers

carbon film of fiber A is made of amorphous and minute carbon that has little hermeticity. Amorphous carbon is ESR inactive. In the spectra of fibers B and C, the ESR spectra of fiber B and C are shown. Broad signals due to the carbon film on the optical fibers were measured

Table 1. Properties of carbon-coated optical fibers

	fiber A	fiber B	fiber C
$\Delta\alpha_{1,24}/\Delta\alpha_{\infty}$	1	1×10^{-2}	1×10^{-4}
n-value	50	>100	>100
linewidth(mT)	-	2.5	3.2

in the center. It is suggested that the carbon films of fiber B and C are not made from amorphous carbon, have similar structure to each other and are different from that of fiber A.

We tried to get the ESR spectra of the carbon to know what structure of the carbon coating is made from. Figure 5 shows the measurement results of graphite polycrystal which indicates anisotropic



Figure 5. ESR spectrum of graphite polycrystal

ESR spectrum. This ESR spectrum are indicated by the conduction electrons in the graphite polycrystal. In general, small crystal particles do not show anisotropic ESR spectrum but show the isotropic one, because crystal particles spatially turn to all directions and anisotropic signal is canceled. In this case, the polycrystal are made of large particles enough to show anisotropy. Moreover we measured ESR spectrum of carbon powder which was made by breaking graphite polycrystal into pieces. The spectrum is shown in figure 6. We cannot see anisotropic spectra any more and only broad signal was detected. Because

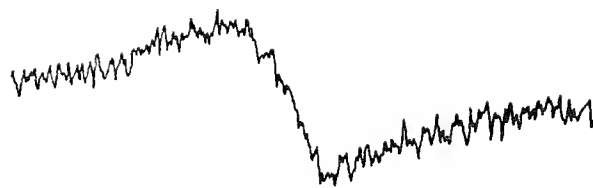


Figure 6. ESR spectrum of graphite powder

graphite polycrystal was crushed into small pieces, which don't show the anisotropy.

There are several kinds of carbons, however, almost all of them are ESR inactive except diamond structure. The carbon of diamond structure shows ESR by the impurity in it, which is usually nitrogen atom. ^{14}N has nuclear spin at 1. Therefore ESR signal is split into three lines.

Only isotropic peaks are seen in ESR spectra of fiber B and C and we cannot recognize the splitting peaks by nitrogen or so. This means that those carbon films are made of graphite crystal and the sizes of carbon layers are small enough not to indicate anisotropy because the thickness of carbon layer is only 40 nm or so. There is a small difference between ESR spectra of fiber B and C, we will discuss that point next.

Carefully comparison of these two tells us the difference between the spectra of fibers B and C. We can see the linewidths are different from each other. The linewidths of the spectra of fibers B and C are also shown in table 1. Fiber B shows narrower ESR spectrum than fiber C.

In general, the lineshape $g(x)$ of ESR spectrum is represented as follows:

$$g(x) = \frac{T_2/\pi}{1+T_2^2(x-x_0)^2} \quad (1)$$

where T_2 is spin-spin relaxation time.

According to equation 1, we can easily calculate width at half power ($x_{1/2}$) :

$$x_{1/2} = 1/T_2 \quad (2)$$

Therefore linewidth of ESR spectrum is a function of the spin-spin interaction between unpaired electrons. If stronger interaction are there between electrons in the sample, the linewidth will be narrower. In other words, the linewidth will be narrow when the orbits of two spins can overlap each other and influence local magnetic field of others. At that time, the distance between unpaired electron, and other electron or nuclear in the carbon layer is relatively short, that is, the range that the conduction electron can move is spatially definite.

We can estimate the structure of carbon layer as follows:

The carbon layer consists of graphitelike parts and amorphouslike parts. They are not separate from each other but continuous. Figure 7 shows model of carbon layer. The carbon layer which

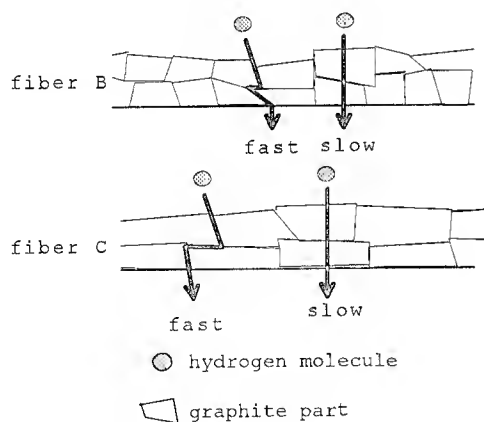


Figure 7. Model of structure of the carbon coatings

has relatively high hermeticity has graphite structure in carbon. Then the hermeticity is dependent on the extent of graphitelike part. In other words, graphite itself has very high hermeticity and the hydrogen molecule permeates the structure except graphite such as diamond or amorphous structure.

When the structures of carbon particles that adhered to reaction tube resemble that of the carbon on the optical fiber, it is useful to investigate the distribution of carbon particles in the reaction tube to evaluate the size of graphite extents on carbon-coated optical fiber. The measured results are shown in the Table 2. This means that those carbon particles of fiber C are larger than those of fiber B. These two (fiber B and C) have the same structure of carbon but the sizes of their carbon particles are different. These results tell that larger graphite extent prevents the hydrogen from permeating into the core of the optical fiber and that smaller particle have low hermeticity against hydrogen. This also suggests that larger extent of graphite achieves lower permeability.

7. Conclusion

Three kinds of carbon-coated optical fibers that have different characteristics in hydrogen diffusion and fatigue coefficient were manufactured. We measured ESR spectra of these fibers and found the peaks of two carbon-coated optical fibers which have high hermeticity. Investigating the spectra in detail, we found there is

Table 2. Distribution of the particle sizes

	fiber B	fiber C
Mode(μm)	0.15	0.54
Average(μm)	0.23	0.32

obvious difference between the ESR spectra of fiber B and C. The linewidths of ESR spectrum of fibers B and C are quite different. This shows they have a difference in the extent of graphite structure. Furthermore, we studied the distribution of the sizes of carbon particles in the reaction tube of those two. The carbon particles with high hermeticity is larger than that of lower hermeticity. This is also suggested by ESR measurement carbon layer made by the condition in which large carbon particles grow in the reaction tube have low hydrogen permeability. More investigation is necessary for clearing the structure of the carbon layer.

References

- 1) R.G.Huff, F.V.Dimarcello and A.C.Hart, "Amorphous Carbon Hermetically Coated Optical Fibers", Technical Digest for OFC, TUG-2, 1988.
- 2) K.E.Lu, M.T.Lee, D.R.Powers and G.S.Glaczmann, "Hermetically Coated Optical Fibers", Technical Digest for OFC, PD1-1, 1988.
- 3) N.Yoshizawa and Y.Katsuyama, "High-Strength Carbon-Coated Optical Fibers", Electron Lett., 25, No.21, 1429-1431, 1989
- 4) G. Wagoner, Physical Review, 118, 647, 1960
- 5) C.P.Slichter, "Principles of Magnetic Resonance", Springer-Verlag, 1989
- 6) H.Aikawa et al. "Characteristics of Carbon-coated Optical Fibers and Structural Analysis of the Carbon Films", Proceeding for the 42nd IWCS, 1993



Motonori Nakamura

Sumitomo Electric Industries, Ltd.

1, Taya-cho, Sakae-ku
Yokohama, Japan

Motonori Nakamura was born in 1968 and received his M.S. degree in physical chemistry from Osaka University in 1992. He joined Sumitomo Electric Industries, Ltd. the same year and has been engaged in the research and development of industrial technology for optical fibers. He is an engineer of Transmission Media R&D Dept. in Yokohama Research Labs.



Akira Urano

Sumitomo Electric Industries, Ltd.

1, Taya-cho, Sakae-ku
Yokohama, Japan

Akira Urano received his B.S. degree in material science from University of Tsukuba in 1984. He joined Sumitomo Electric Industries, Ltd. in 1984 and has been engaged in research and development of optical fiber. He is a member of Analytical Characterization Center in R&D Group, and a member of the Japan Society of Applied Physics.



Haruhiko Aikawa

Sumitomo Electric
Industries, Ltd.

1, Taya-cho, Sakae-ku
Yokohama, Japan

Haruhiko Aikawa was born in 1964. He received his M.S. degree from Tohoku University in 1989. He joined Sumitomo Electric Industries, Ltd. the same year and has been engaged in the industrial technology for optical fibers. He is an engineer of Fiber Optics Division.

received his M.S. degree in mechanical engineering Science from Tokyo Institute of Technology in 1982. He joined Sumitomo Electric Industries, Ltd. the same year and has been engaged in the research and development of industrial technology for optical fibers. He is a senior engineer of Transmission Media R&D Dept. in Yokohama Research Labs. and a member of the Institute of Electronics, Information and Communication Engineers of Japan.



Hiroki Ishikawa

Sumitomo Electric
Industries, Ltd.

1, Taya-cho, Sakae-ku
Yokohama, Japan

Hiroki Ishikawa was born in 1965 and received his M.S. degree in applied physics from Tohoku University in 1990. He joined Sumitomo Electric Industries, Ltd. the same year and has been engaged in the research and development of fiber-optic cables. He is an engineer of Communication R&D Dept. in Yokohama Research Labs.



Toshio Danzuka

Sumitomo Electric
Industries, Ltd.

1, Taya-cho, Sakae-ku
Yokohama, Japan

Toshio Danzuka was born in 1956 and

In-Line Methods of Assuring the Characteristics of Hermetically Carbon-Coated Optical Fibers

T. Shimomichi , K. Oohashi , S. Araki, and T. Maruoka

Fujikura, Ltd., Opto-Electronics Laboratory
1440 Mutuzaki, Sakura, Chiba, 285, Japan

Abstract

We examined the microwave and laser-beam methods as means of assuring carbon layer characteristics throughout the entire length of hermetically carbon-coated optical fibers. In this study, we monitored the carbon layers of 1,000 carbon-coated fibers when fuel gas of a static composition was present. The frequency of errors that occurred in judging whether the carbon-coated fiber was satisfactory, using a judgment threshold with a 5% safety margin on the standard value of the carbon coating properties, was 0% for the microwave method and 0.5% for the laser-beam method. When fuel gas composition is kept constant, the microwave method enables highly accurate judgments. Using the microwave and laser-beam methods simultaneously makes it possible to more accurately monitor changes in the carbon layer quality.

1. Introduction

The excellent properties inherent in carbon-coated fibers have made it possible to use the fibers in submarine cables. Other uses have also been examined. Because carbon-coated fibers are nearly always used under adverse conditions, it is important to develop a method for confirming their characteristics. Various methods have been proposed, including the eddy-current method (1,2,3), the laser-beam method (4), and the microwave method (5). However very few reports have been made on the reliability or the results of statistical examinations of these methods.

In this study, the reliability of the microwave and scanning-laser-beam methods of evaluation were examined using 1,000

sample fibers. We also examined various ways of enhancing the reliability of these methods.

2. Measurement Systems

2.1 Microwave method

Fig. 1 shows an overview of the microwave-method measurement system. This measurement system consists of a microwave oscillator, analyzer, recorder, and computer.

A wave guide is installed above the primary UV curable resin coater as a carbon-layer detector, and the fiber is threaded through a space 6mm in diameter located between the wave guides, as shown in the schematic diagram in Fig. 2. Based on the microwave reflection level of bare optical fibers, 125

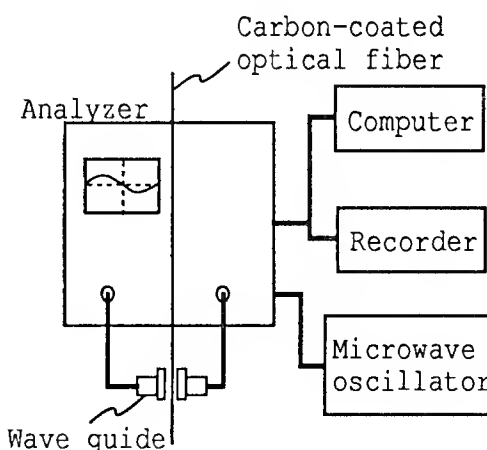


Fig.1 Schematic diagram of a microwave-method measurement system

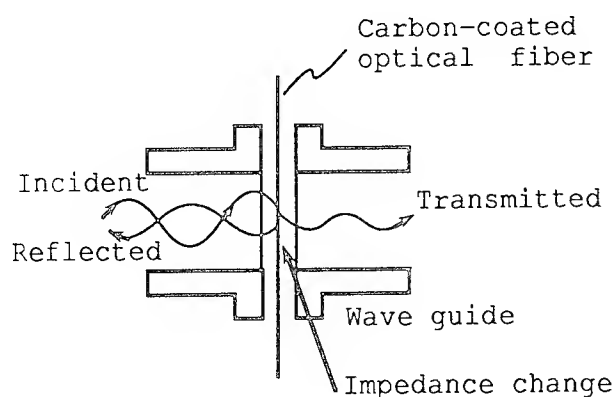


Fig.2 Cross section of the wave guide

μm in diameter, we measured changes in the intensity of waves reflected by the carbon-coated fibers of the S-parameter method.

The magnetic characteristics of the carbon layer change according to the quality and the quantity of its carbon coating. The quality of the carbon layer depends on its structure, orientation status, and coadunation of microcrystalline. When the microwave method was used, microwaves were irradiated to the carbon-coated fiber and the amount of deposition and quality of the carbon layer were monitored based on changes in the microwave reflection intensity.

2.2 Scanning-laser-beam method

Fig. 3 shows an overview of the scanning-laser-beam-method measurement system. This measurement system consists of a detector and monitor, and has the same configuration as a laser outer-diameter measurement system. The system sends the measurement results to the same recorder and computer used in the microwave-method measurement system. A detector is installed on an outer-fiber-diameter measurement unit with an automatic follow-up function.

The transmission attenuation of the laser against the carbon layer is correlated to the thickness of the carbon layer. There-

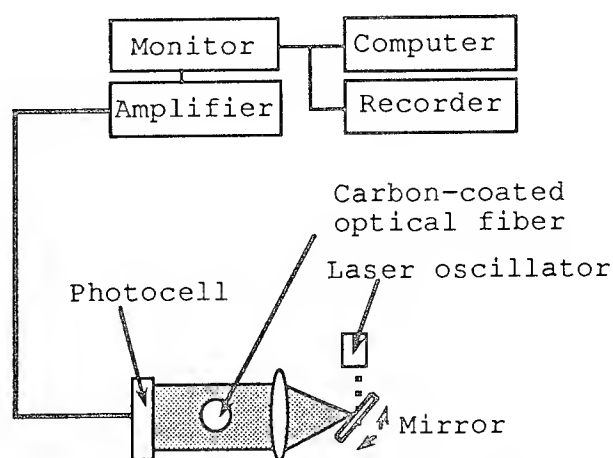


Fig.3 Schematic diagram of the scanning-laser-beam-method measurement system.

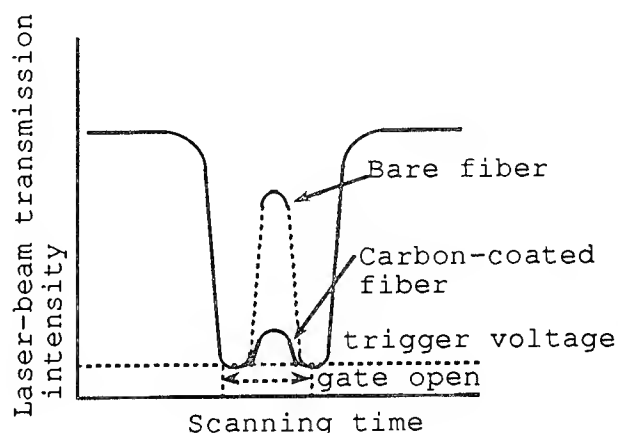


Fig.4 Laser-beam transmission intensity change

fore, when we used the laser-beam method, we scanned the beam at 90-degree angle to the carbon-coated fiber and measured the amount of transmission attenuation (see Fig. 4). In this way, we were able to monitor the thickness of the carbon layer. We successfully measured the thickness of the carbon layer by comparing the transmission attenuation rate of the laser beam and the measured thickness of the carbon layer using SEM.

Fig. 5 shows the relationship between the thickness of the carbon layer and the monitoring results of the scanning-laser-beam method.

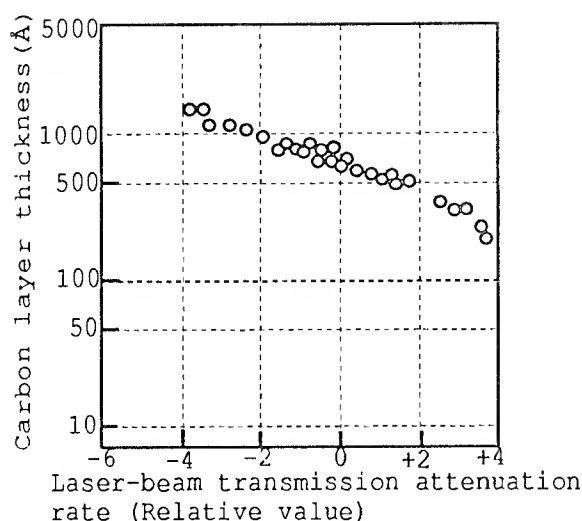


Fig. 5 Relationship between the thickness of the carbon layer and the change in the transmission attenuation rate of the laser-beam, based on the transmission level of standard carbon-coated fibers

3. Measurement Results of Each Monitoring Method

We changed the CVD conditions (including fuel-gas composition, reaction temperature, and drawing speed) to produce carbon-coated fiber samples of different layer qualities and layer thicknesses, and we measured these samples using the micro-

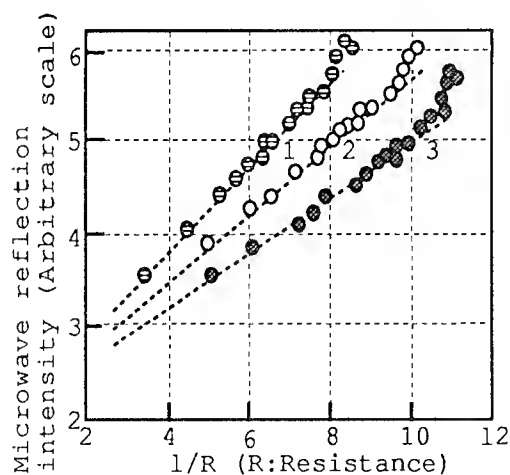


Fig. 6a Relationship between carbon-layer electrical resistance and the results of on-line carbon layer monitoring by the microwave method for fuel-gas composition types 1, 2, and 3

wave and scanning-laser-beam methods. Fig. 6 shows the comparison between the electrical resistance of the carbon layer and the measured results yielded by the two monitoring methods. We measured the electrical resistance of the carbon layer according to a four-wire electrical resistance measurement method using a multimeter and 4-cm carbon-coated fibers. For fuel gas compositions types 1, 2 and 3, Figs. 6a and 6b show the relationship between carbon-layer electrical resistance and the results of on-line carbon-layer monitoring of the carbon-coated optical fiber samples by the microwave and scanning-laser-beam methods. For Fig. 6, only the reaction temperature was changed, while the other CVD conditions remained unchanged. In the case of changes in the other conditions, the relationship between carbon-layer electrical resistance and the monitoring results shows a similar tendency except for a change in the fuel-gas composition. In each case, with the constant fuel-gas composition, changes in both the intensity of the microwaves reflected by the coated-carbon layer and the laser transmission rate of the carbon layer show an almost straight-line relationship

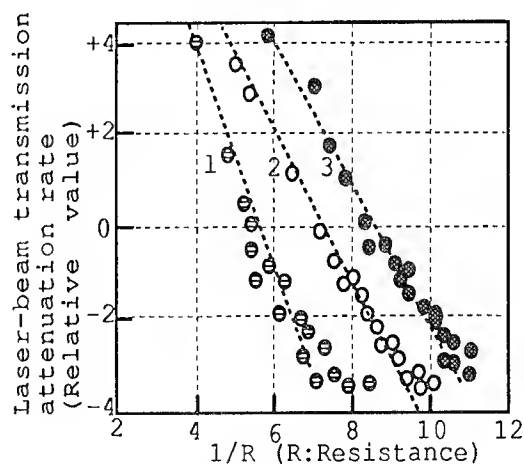


Fig. 6b Relationship between carbon-layer electrical resistance and the results of on-line carbon layer monitoring by the scanning laser-beam method for fuel-gas composition types 1, 2, and 3

within a certain range, with the inverse of the carbon-layer electrical resistance. This result reveals that only the thickness of the carbon layer changes, while the quality of the carbon layer remains constant within that range. Moreover, comparative data shows that changing the fuel-gas compositions causes the quality of the carbon layer to change.

In this study, when the fuel-gas composition remained unchanged, variations in the carbon-layer electrical resistances measured by the microwave method were revealed to be $\sigma=2\text{k}\Omega/\text{cm}$, while variations in the electrical resistance measured by the scanning-laser-beam method were found to be $\sigma=8\text{k}\Omega/\text{cm}$.

Figs. 7a and 7b show the relationship between the results obtained by the microwave and scanning-laser-beam methods and the results of a hydrogen resistance test for fuel-gas-composition types 1, 2, and 3. In the hydrogen resistance test, we used 2,000-m optical fiber samples and measured the increase in transmission loss at a

wavelength of $1.24\text{ }\mu\text{m}$, after 24 hours, under a partial hydrogen pressure of 1 atm and at a temperature of 80°C . The figures reveal that the threshold for quality assurance in monitoring the carbon layer varied as the fuel-gas compositions changed.

4. Reliability of the microwave and scanning laser-beam methods

We monitored the carbon layers of 1,000 carbon-coated fibers when fuel gas of a static composition was present. Fig. 8 shows the distribution of increased hydrogen loss for the 1,000 monitored samples. Based on the results shown in Fig. 7, we determined the judgment threshold for each monitoring method. We used a judgment threshold with a 5% safety margin on the standard value of the carbon coating properties. The frequency of errors that occurred in judging whether the carbon-coated fiber was satisfactory, was 0% for the microwave method and 0.5% for the scanning-laser-beam method. When the fuel gas composition does not change, the microwave

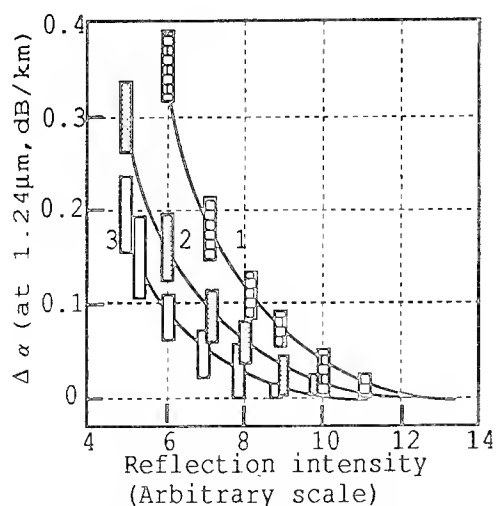


Fig.7a Relationship between changes in the reflection intensity of microwaves and the increase in loss resulting from the hydrogen gas (80°C , 1atm, after 24 hours) for fuel-gas composition types 1, 2, and 3

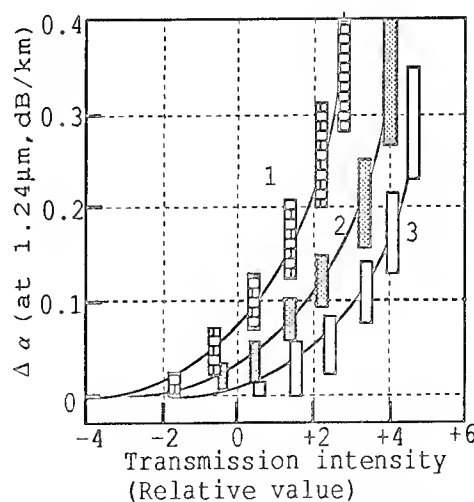


Fig.7b Relationship between changes in the transmission intensity of laser beams and the increase in loss resulting from the hydrogen gas (80°C , 1atm, after 24hours) for fuel-gas composition types 1, 2, and 3

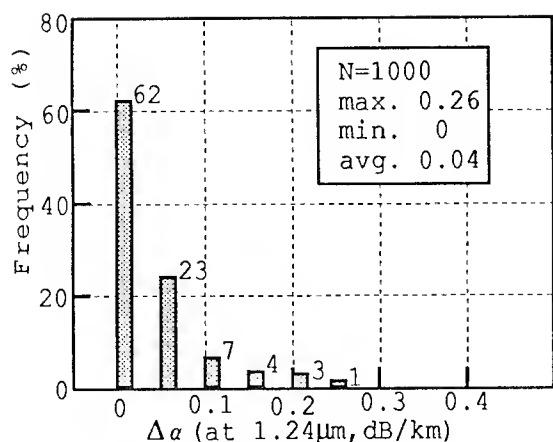


Fig.8 Frequency distribution of the loss increases induced by the hydrogen gas for the monitored samples

method enables highly accurate judgments.

The test results in Figs. 6 and 7 reveal that varying the fuel-gas compositions causes the quality of the carbon layer to change significantly. This indicates that the properties of the carbon-coated fibers are different even if the monitoring results are the same. In other words, both the microwave and scanning-laser-beam methods feature the disadvantage of being unable to simultaneously monitor changes in the quality and thickness of the carbon layer.

Based on the results shown in Fig. 6, Fig. 9 compares the results of measurement using the microwave method with those using the scanning-laser-beam method. Since an almost straight-line relationship exists between these evaluation methods when the fuel-gas compositions remain unchanged, using the microwave and scanning-laser-beam methods together and then comparing the monitoring results may allow individual monitoring of carbon-layer quality and thickness. Fig. 10 is a histogram of the loss increases induced by the hydrogen gas for the sieved samples. In the case of distribution 1, the judgment threshold was maintained to the value of fuel-gas composition type 2. In the case of distribution

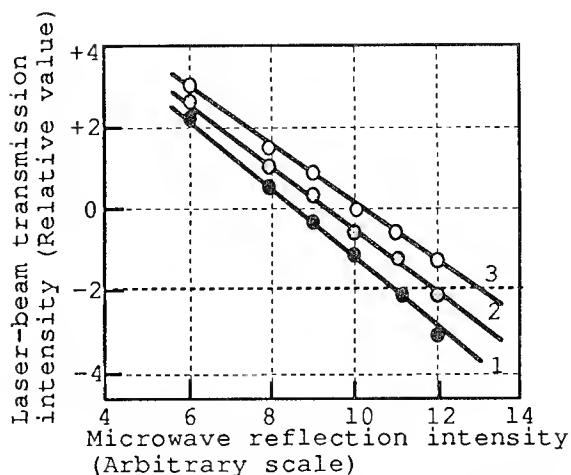


Fig.9 Relationship between changes the reflection intensity of the microwaves and changes in the transmission intensity of laser beams for fuel-gas composition types 1, 2, and 3

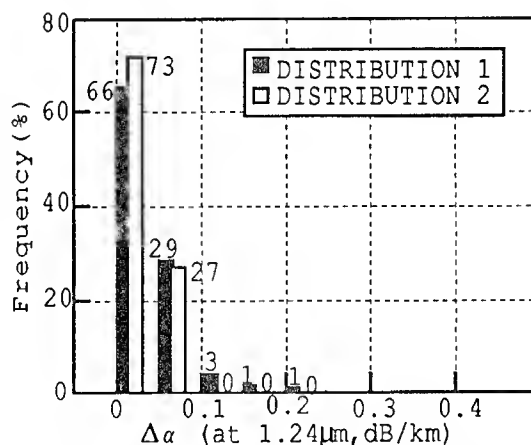


Fig.10 Frequency distribution of the loss increases induced by the hydrogen gas for the sieved samples

2, the threshold was determined by using both the microwave and scanning-laser-beam methods and comparing the results. These fiber samples can be produced using fuel-gas composition types 1, 2, or 3. When the fuel-gas flow rate is controlled to maintain a constant fuel-gas composition, the microwave method was found to be sufficiently reliable in assuring the carbon-layer properties. However, we found that

using the scanning-laser-beam and microwave methods together and then comparing the results yielded even greater reliability.

5. Conclusion

(1) The measurement results of the microwave and scanning-laser-beam methods under varying CVD conditions were compared with the loss increase of the carbon-coated fibers due to hydrogen gas. The microwave reflection intensity of the carbon layer and the laser-beam transmission amount were correlated to the loss increase due to hydrogen gas.

(2) The carbon layers of the 1,000 carbon-coated fibers in the presence of fuel gas of a static composition were monitored. The frequency of errors that occurred in judging whether the carbon-coated fiber was satisfactory, using a judgment threshold with a 5% safety margin on the standard value of the carbon-coating properties, was 0% for the microwave method and 0.5% for the scanning-laser-beam method. When the fuel gas composition does not change, the microwave method enables highly accurate judgments.

(3) Each method has its own particular disadvantage: the microwave method lacks the capacity to measure the thickness of the carbon layer, while the scanning-laser-beam method is unable to monitor changes in the quality of the carbon layer. These drawbacks make it impossible to simultaneously detect changes in both the thickness and quality of the carbon layer when the composition of the fuel gas changes significantly. However, using microwave and scanning-laser-beam methods concurrently enables an accurate judgment.

(4) Simultaneously use of the microwave and scanning-laser-beam methods makes it possible to monitor changes in the quality of carbon layers more accurately.

References

- (1) C.M.G. Jochem et al, OFC 1989 PD8
- (2) F.V. Di Marcello et al, OFC 1990 TH H5
- (3) M. Koguchi et al, OFC 1990 TH H6
- (4) D.H. Smithgall et al, OFC 1991 TH G3
- (5) J.Y. Boniort et al, ECOC 1991, pp.37-40



Tsuyosi Shimomichi

Opto-Electronics
Laboratory
Fujikura Ltd.

1440, Mutsuzaki,
Sakura-shi, Chiba,
285, Japan

Mr. Shimomichi, who was born in 1960, joined Fujikura Ltd. after graduating from Nagasaki University in 1986 with an M.E. degree. He has been engaged in research and development of optical fibers and optical fiber coatings. He is now an engineer for the Telecommunication Cable Material Section and a member of IEICE of Japan.



Shinji Araki

Opto-Electronics
Laboratory
Fujikura Ltd.

1440, Mutsuzaki,
Sakura-shi, Chiba,
285, Japan

Mr. Araki, who was born in 1950, joined Fujikura Ltd. after graduating from Tokyo Metropolitan University in 1974 with a B.E. degree. He has been engaged in research and development of optical fibers and optical fiber coatings. He is now chief of the Telecommunication Cable Material Section and a member of IEICE of Japan.



Keiji Oohashi

Opto-Electronics
Laboratory
Fujikura Ltd.

1440, Mutsuzaki,
Sakura-shi, Chiba,
285, Japan

Mr. Oohashi, who was born in 1956, graduated from the Tokyo Institute of Technology in 1980 with a B.E. degree. After eight years of work as an engineer in materials for motor vehicles, he joined Fujikura Ltd. and has been engaged in research and development of optical cables. He is now assistant chief of the Telecommunication Cable Material Section and a member of IEICE of Japan.



Toshikuni Maruoka

Opto-Electronics
Laboratory
Fujikura Ltd.

1440, Mutsuzaki,
Sakura-shi, Chiba,
285, Japan

Mr. Maruoka, who was born in 1943, joined Fujikura Ltd. after his graduating from Tokyo University in 1967 with a B.E. degree. He has been engaged in design, research, and development of transmission cables. He is now the manager of Transmission Line Department and a member of IEICE of Japan.

IMPROVED PMD STABILITY IN OPTICAL FIBERS AND CABLES

Arthur F. Judy
AT&T Bell Laboratories
2000 Northeast Expressway
Norcross, GA 30071
404-798-2761
afj@akguc.att.com

ABSTRACT

We report on the performance of optical fibers made with a new technique that creates not only very low, but also highly stable Polarization Mode Dispersion (PMD). By introducing oscillatory spin within the fiber, PMD variability from handling or temperature is greatly reduced. This allows the PMD of installed cabled fibers to be reliably predicted from factory measurements on reeled cables or even spooled fiber. Also, because variations in mode-coupling are greatly reduced, these fibers allows the detection of small, average changes in birefringence from such factors as differences in winding tension.

INTRODUCTION AND THEORY

PMD is the length scaled differential group delay ($\Delta\tau$) between the principle polarization modes in a fiber. For long optical fibers PMD is determined by a complex interplay of intrinsic fiber parameters and external perturbations. Normally, the intrinsic properties of geometric ovality and material stress asymmetries determine the inherent fiber birefringence ($\Delta\beta$). If there were no external stresses or internal length variations, PMD would just be the frequency derivative, $\Delta\beta'$. Because this state usually can only occur for a few meters, $\Delta\beta'$ is often called the short-length PMD. Over long lengths, not only do fiber parameters vary, but also external stresses and geometric deformations are introduced by spooling, cabling or installation. These create random couplings between the polarization modes and PMD becomes a

stochastic quantity which can be characterized only by its statistics.

For example, if an otherwise uniform fiber with a known $\Delta\beta$ experiences random perturbations, the root-mean-square $\Delta\tau$ is given by:^{1,2}

$$\begin{aligned} \langle \Delta\tau^2 \rangle^{1/2} &= \Delta\beta' \left(\frac{\exp(-2hz) - 1 + 2hz}{2h^2} \right)^{1/2} \\ &\cong \Delta\beta' \left(\frac{z}{h} \right)^{1/2} \dots \left[z \gg h^{-1} \right], \end{aligned} \quad (1)$$

where $\langle \dots \rangle$ denotes the expected value, z is the length and the parameter h is the inverse of the mean mode-coupling length.

In most cases, equation.(1) is useful only for predicting general length dependency, but not precise PMD. One reason is that variables such as $\Delta\beta'$ will not necessarily be length independent. More fundamentally, h is usually unknown since it is determined by the mechanical perturbations which can also vary with z as well as with fiber configuration or deployment conditions. So in practice PMD is usually not predictable but must be measured.

Even then a serious further complication occurs for standard fibers. Typically, a spooled fiber will have a much lower PMD than the same fiber in a cable because the spooling induces a large amount of mode-coupling. Likewise a cabled fiber on a reel will often have a different value than the same fiber off-reel. Thus large differences in PMD can occur and it

becomes problematic predicting the PMD of an installed fiber system from measurements in the factory.

This paper discusses the performance of fibers made with a method for substantially reducing this difficulty. By introducing oscillatory twist during preform draw, one can reduce the relative effect of external perturbations.³ This is accomplished by adding a variable, oscillatory spin to the fiber core during preform draw. This changes the orientation of the fiber with respect to external perturbations and tends to reduce their impact. This also results in a reduction in the total PMD and, we believe, is an important development in the fiber manufacturing technology.

EFFECTS OF A CONSTANT TWIST ON PMD

Some of the advantages of oscillatory spinning can be appreciated by investigating a similar process of mechanically twisting a fiber. Several studies have analyzed the effect of twist on a uniform fiber with no external perturbations. These show that twist reduces the short-length PMD by:^{4,5}

$$\Delta\beta'_{tw} = \frac{\Delta\beta'}{\sqrt{1 + 4(\theta/\Delta\beta')^2}} \quad (2)$$

where θ is the effective twist rate. For mechanical twist, the effective twist is reduced from the actual twist by $(1-g)$ where g (≈ 0.08) accounts for the photoelastic effect which counters the mechanical twist by inducing circular birefringence in the opposite direction.⁶

Theory also shows that a twisted fiber with random mode coupling also has a PMD length dependence given by equation (1), but not necessarily with the same h value.⁴ There are apparently no studies of whether twist changes h or, more importantly, whether twist improves the stability of h and consequently PMD.

To investigate this we performed the following experiment. Six 4-km dispersion-shifted fibers were selected to have an unusually large range of $\Delta\beta'$ values, ranging from 2 to 22 ps/km as measured on 16-m end samples. Each fiber was divided into four 1-km segments which were wound to have twists of 0, 2, 4 or 6 turns per meter. The resulting 24 fibers were cabled into a central-tube cable and measured for PMD while on a 75 cm diameter reel. The cable was then unreeled, laid out and remeasured. In both cases, PMD is measured by the wavelength scanning method from 1525 to 1575 nm.⁷ PMD stability was measured by calculating the ratio of off-reel to on-reel PMD. Figure 1 plots this ratio for each fiber and twist.

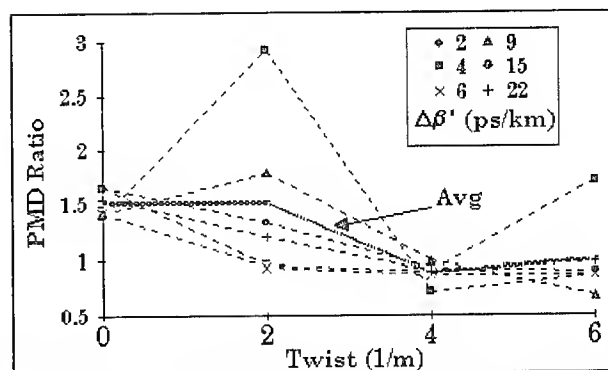


Figure 1. Ratio of off-reel/on-reel PMD as function of twist.

Although there is much fluctuation in this data especially for the low $\Delta\beta'$ fibers where PMD measurement accuracy is more limited,⁸ the trend is that indeed PMD stability improves with twist. For the fibers with no twist, the PMD ratio averaged 1.6. At 6 turns/m, this decreased to 1.0. For all fibers, the ratio was smaller at 4 than at 0 turns/meter.

We also estimated h from:

$$h = (\Delta\beta'_{tw}/\text{PMD})^2$$

where PMD is measured on the off-reel cable as described above, and $\Delta\beta'_{tw}$ is calculated from Equation (2) using values of $\Delta\beta'$ as the average of the two short-length PMDs measured on 16-

m samples from each fiber end (measured from 1300 to 1650 nm), and $\Delta\beta$ is assumed equal to $\Delta\beta'/\omega$ where ω is the optical frequency.

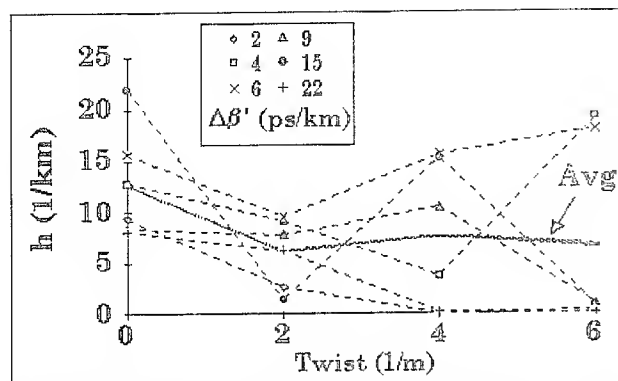


Figure 2. Estimated h parameter for mechanically twisted fibers.

Figure 2 shows that no trend is obvious when h is plotted versus twist. Since it appears that the average h does not vary with twist, the improvement in PMD stability arising from a stabilization in mode-coupling rather than an improvement in it. It should be cautioned that the accuracy in estimating h is not high because of uncertainties in measuring the various parameters, and also the likelihood that for these special fibers $\Delta\beta'$ is varying with distance.

SPUN FIBERS

Although the above experiment showed some of the advantages we seek, there are a number of reasons why the process of mechanically twisting fiber is not desirable. It is complicated to perform in a factory. It leaves an inherent torque in the fiber which can complicate color-coding and cabling. The added torque leaves stress in the fiber which limits the amount of twist one can safely apply. And the stress-optic effect counters the twist and reduces the effective twist applied.

These disadvantages can be eliminated by forming the twist into the fiber as the fiber is drawn. This was first accomplished by spinning the preform during draw.⁹ But preform spinning is a daunting engineering challenge at high draw speeds. For example, a draw speed of 10 m/s requires a preform spin rate of 2400 rpm just to attain 4 turns/m. A recent development is the method of introducing an oscillatory twist by varying the torque on the fiber during draw.³ Initially introduced as a proprietary process in 1991, this has been implemented on a large scale production basis and has resulted in consistent, low PMD fibers.^{10,11} It was also observed that fibers produced with this method appeared to have improved PMD stability.¹¹ We present here further evidence of this PMD stability under normal conditions and also a stability limit when these, or any fibers, are subjected to high transverse stress.

PMD STABILITY OF SPUN FIBERS WITH WINDING TENSION

To gauge the PMD stability of spun fibers we repeatedly respooled eleven 25-km dispersion-shifted fibers with different winding tensions. After each respooling, the average PMD was measured using the wavelength scanning method between 1400 and 1600 nm. To prevent any hysteresis, the following winding sequence was used: 13 gm, 45 gm, re-measure of 45 gm after 30 days, 35 gm, 40 gm and 25 gm.

The box plots in Figure 3 show the data and statistics. It is seen that PMD is constant below 40 gm indicating little variation in mode-coupling, but it increases at 40 gms and above. It is unlikely that this increase is caused by mode coupling effects since higher tensions should, if anything, increase mode coupling and decrease PMD.

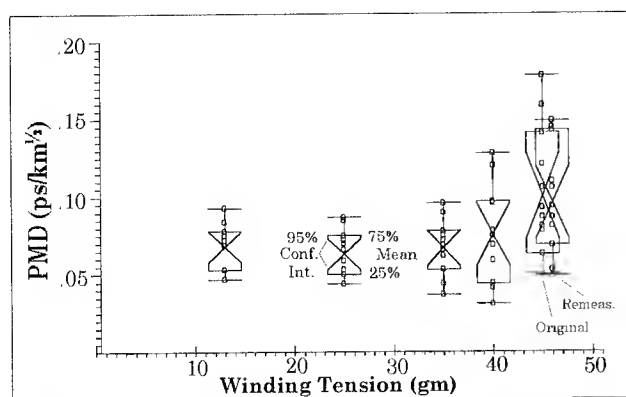


Figure 3. PMD variation with winding tension for eleven 25-km spools of dispersion-shifted fiber.

Rather, the PMD increase indicates that stress-induced birefringence is being created. That is, it is known that birefringence, and hence PMD, can be generated in a perfectly circular, stress-free fiber by applying asymmetric transverse pressure^{12,13}. The functional relation is:

$$\Delta\beta' = \frac{8 C P}{c \pi d} [1 + f(V, a, d)], \quad (3)$$

where C is the net photo elastic constant ($3.36 \times 10^{-10} \text{ cm}^2 / \text{gm-weight}$), P is the linear pressure in (gm-weight/cm), c the light velocity, and d the fiber cladding diameter. The function $f(V, a, d)$ incorporates the interaction of mode-field size and differential stress in the fiber core, but for wavelengths between 1.3 and 1.6 μm , $f(V, a, d) < 0.005 \ll 1$ and is negligible. For a nominal fiber with $d=125 \mu\text{m}$, equation (3) is: $\Delta\beta' (\text{ps/km}) = 0.234 P (\text{gm/cm})$.

If a fiber is wound with tension, T , on a frictionless drum of radius, R , then $P=T/R$. Thus the above fibers wound at 40 grams tension on a 8-cm spool, will experience 5 gm/cm of transverse pressure. Equation (3) predicts that this would induce 1.2 ps/km of PMD (assuming equal loading on both sides of the fiber). Note that this is of the same order of magnitude as the inherent PMD in the untwisted fibers used in the mechanical twist experiment. Thus this mechanism is large

enough at high tensions to cause the observed added PMD. At low tensions the effect is not apparent for a combination of probable reasons. Friction between the fibers and the spool will reduce the effective longitudinal tension. The coating will buffer more of the transverse pressure. And measurement uncertainty will obscure and small PMD increase.

PMD STABILITY OF SPUN AND STANDARD FIBERS

We evaluated PMD stability with a cable containing an equal number of spun and standard fibers. The fibers, all dispersion-shifted, were obtained from two sources: the spun fibers from our own production, the standard fibers from a commercial vendor. Both fiber types were intermixed within binder groups and cabled into a 5-km, 52-fiber, central-tube cable. The fibers were measured before and after cabling, and then at various points during a two-week Bellcore-type temperature cycle. To maximize measurement precision and minimize measurement time, pairs of same-type fibers in the cable were spliced together to form 10-km loops.

PMD Change From Spool To Cable

Average PMD was measured from 1200 to 1600 nm using wavelength scanning for both spools and cable. The resulting PMD statistics at room temperature are shown in the box plots in Figure 4.

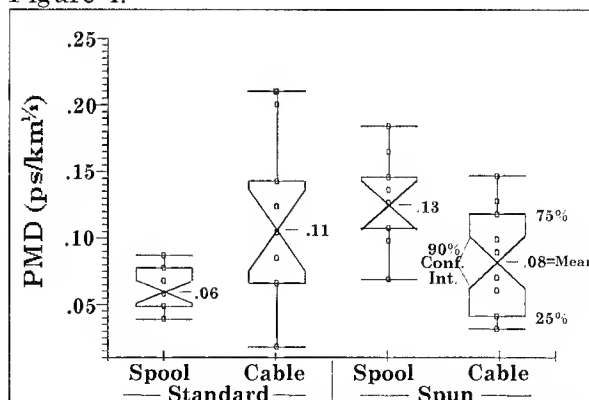


Figure 4. PMD change from spool to cable for standard and spun fibers in same cable.

The two types of fiber performed quite differently. The standard fibers increased by $0.05 \text{ ps/km}^{1/2}$, almost doubling their spooled PMD, while the spun fibers decreased by $0.05 \text{ ps/km}^{1/2}$.

In Figure 5, the same data is shown by comparing each 10-km cable loop to the root-sum-square spooled PMD of the two constituent fibers. This shows the results are remarkably consistent with no spun fibers increasing in value and only two standard fibers decreasing.

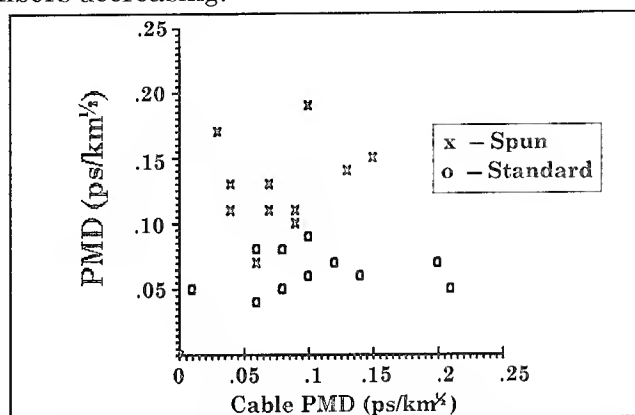


Figure 5. Path by path PMD comparison of fibers on spools and in cable.

The reasons for the dramatic difference between the two fiber types was established in the introduction. That is, for the standard fibers mode-coupling is very sensitive to packaging, as was seen above for the untwisted fibers in the mechanical twist experiment. So the standard fibers' on-spool mode-coupling is high, and the PMD is artificially reduced, because of perturbations from the multiple layers of fibers. In contrast, the cable, which is designed to minimize extrinsic stresses, reduces the mode-coupling and the PMD approaches its intrinsic value. It is even possible that a further increase would occur if the cable were unreeled. In contrast, the spun fibers are far less dependent on extrinsic mode-coupling and less able to have their intrinsic PMD masked. But they had been wound in the factory at high tension, so their spooled PMD was increased by the added lateral stress, which disappeared upon cabling.

In a previous paper we reported no PMD change from spools to cable for two 90 fiber cables.¹¹ The fibers in that data were also spun fibers but they were production lengths that had been wound at lower tension. So spooling induced PMD was not apparent and no significant change from spool to cable was measured. Together, both experiments illustrate the control that is possible with spun fibers. If winding tensions are kept low, cable PMD will be very close the spooled values. If higher tensions are necessary, for example for shipping purposes, the additional stress induced PMD can be estimated, and it is still possible to predict final PMD in a cable. Even if winding conditions are unknown, spun fibers are still advantageous because, unlike standard fiber, cable PMD will not increase.

PMD Stability With Temperature

We evaluated PMD stability of this cable by varying temperature and measuring PMD after the various dwells.

Temp(*C)	23	55	-40	55	55	-40	23	-40	23
Dwell (days)	>7	2.5	1.5	1	4	2.5	1	1	1
Spun	.081	.079	.095	.081	.081	.099	.083	.097	.079
Standard	.100	.092	.155	.095	.096	.160	.100	.150	.101

Table 1. Temperature, dwell time and average PMD ($\text{ps/km}^{1/2}$) results for spun and standard fibers.

The results (Figure 6 and Table 1), again show the spun fiber is more stable. This is especially apparent at -40°C where the cable structure is most likely to contract and the modulus of the cable filling compound to increase. Either effect will tend to induce extrinsic stress in the fibers and change PMD. If the average PMD of the six measurements above -40°C is compared to the average of the three reading at -40°C , it is seen that the standard fibers increased by 60% from 0.097 to 0.155 $\text{ps/km}^{1/2}$, while the spun fibers changed only by 20% from 0.081 to 0.097.

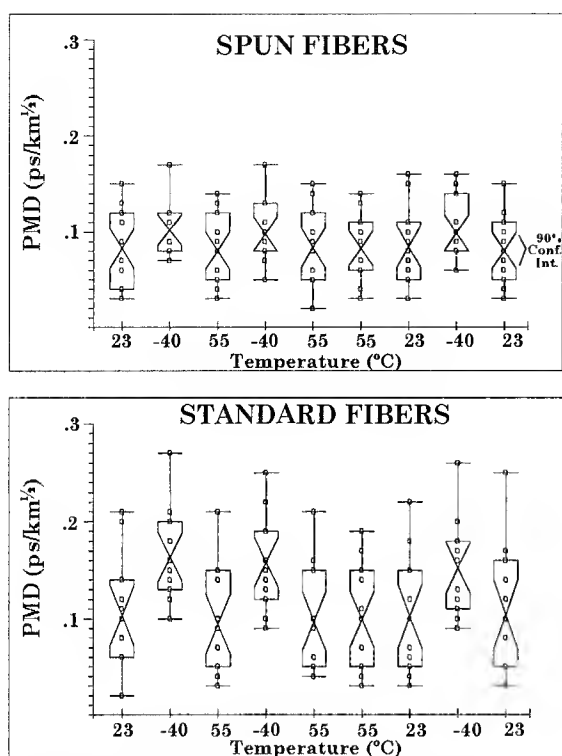


Figure 6 Cable PMD stability with temperature for standard and spun fibers.

PMD OF INSTALLED CABLE

Finally, it is necessary to verify that in fact little change occurs when cables with spun fibers are installed in the field. We recently measured a 130-km route containing over 12×10^6 fiber-meters of dispersion-shifted fiber in 96-fiber cables. Average PMD was measured by wavelength scanning between 1460 and 1560 nm using a tunable laser source for dynamic range. The results for the 96 paths is shown in Figure 7.

Although the PMD of these specific cables was not measured before shipping, the results can be compared to our previous reports of typical PMD values¹¹ which showed average and median PMDs of 0.08 and 0.08 ps/km^{1/2}, respectively, for 113 spools measured in the factory. The excellent agreement to the above data again illustrates the robustness of spun fibers.

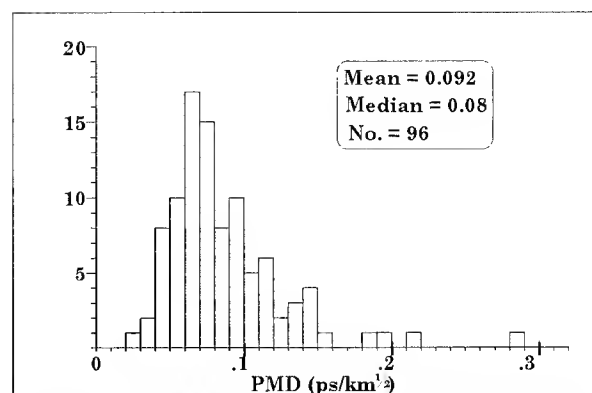


Figure 7. PMD of installed cable route.

CONCLUSIONS

The recent introduction of oscillatory spinning in optical fibers creates a fiber with both low and stable PMD. This allows much more predictability and control of PMD at various stages in the manufacturing process. It also enables reliable predictions of installed system PMD from factory measurements of completed cables, or even fiber spools.

ACKNOWLEDGMENTS

I gratefully acknowledge the contributions of R. G. Albrecht, J. S. Breffle, R. J. Brown, J. A. Edmonston, D. V. McJunkin, and F. A. Rotoloni for the work reported in this paper.

BIOGRAPHY



Arthur F. Judy is a Distinguished Member of the Technical Staff in the Lightguide Systems and Applications

Engineering Group. In his 26 years at AT&T Bell Labs he has worked on the theory, modeling and measurement of optical fibers as well metallic media. He has a BSEE from the University of Maryland, a MSEE from the University of Michigan, a MS in Physics from Georgia Tech and is currently pursuing a PhD in non-linear optical physics.

REFERENCES

1. C. D. Poole, Optics Letters, **13**, 687 (1988).
2. N. Gisin, J. Lightwave Tech., **9**, 821 (1991).
3. Hart-Huff-Walker, U.S Patent 52980047, March 29, 1994..
4. M. Monerie and L. Jeunhomme, Optical and Quantum Electronics, **12**, 449 (1980).
5. G. J. Foschini and C. D. Poole, J. Lightwave Tech., **9**, 1439 (1991).
6. R. Ulrich and A. Simon, Applied Optics, **18**, 2241, (1979).
7. EIA Standards Proposal No. 3152, (To be EIA/TIA-455-113), FOTP-113
8. C. D. Poole and D. L. Favin, J. of Lightwave.Tech., **12**, 917, (1994).
9. A. J. Barlow, J. J. Ramskov-Hansne, and D. N. Payne, Applied Optics, **20**, 2962, (1981).
10. A. F. Judy, J. B. Haber, W. T. Greene, A. J. Ritger, K. L. Walker, OFC'93, Postdeadline Papers, PD20-1, (1993).
11. A. F. Judy, W. T. Greene and J. B. Haber, Proceeding of 42nd IWCS, 630, (1993).
12. J. Sakai and T. Kimura, IEEE J.Q.E., **QE-17**, 1041, (1981).
13. N. Imota, et.al. IEEE J.Q.E., **QE-16**, 1267, (1980).

Bending Induced Polarization Mode Dispersion with Random Mode Coupling

T.Sekito, Y.Suetsugu, Y.Yamazaki, and Y.Saito

Sumitomo Electric Industries, Ltd.

Abstract

This paper describes bending induced Polarization mode dispersion (PMD) with random mode couplings in long length of fibers. By using three fibers, dispersion unshifted SM fiber (SMF), dispersion shifted fiber (DSF) and pure silica core fiber (PSCF), with different coatings, we confirmed that the bending induced PMD with random mode coupling was independent of refractive index profiles. It was confirmed experimentally by using the interferometric method that the bending induced PMD with random mode coupling was governed by a mean coupling length. Required conditions for keeping PMD of $250\mu\text{m}$ ϕ coated fiber low, specifically in the fibers on bobbins, was examined taking the bending effect into account in this paper.

1. Introduction

In recent years, polarization mode dispersion (PMD) has become an important parameter which determines performance of optical systems for not only digital transoceanic applications but also for analog CATV applications^[1] and PMD properties of SMF and PSCF as well as those of DSF are drawing much attention. Fiber bend causes additional PMD, even in fibers with perfect circular symmetry. Fibers usually experience different levels of bending at every inspection process after fiber drawing and cabling. So it is essential to characterize the bending induced PMD, however, a theoretical model of the bending induced PMD with mode coupling in long length of fibers has not yet been clarified.

In this paper, the bending induced PMD in long length fibers is discussed.

2. Test Samples

Measurements on PMD were conducted in three kinds of fibers and two levels of coating diameters; SMF with $250\mu\text{m}$ coating, PSCF with $250\mu\text{m}$ coating, DSFs with $250\mu\text{m}$ coating and with $400\mu\text{m}$ coating. Fig.1 shows refractive index profiles and coating structures of the fibers.

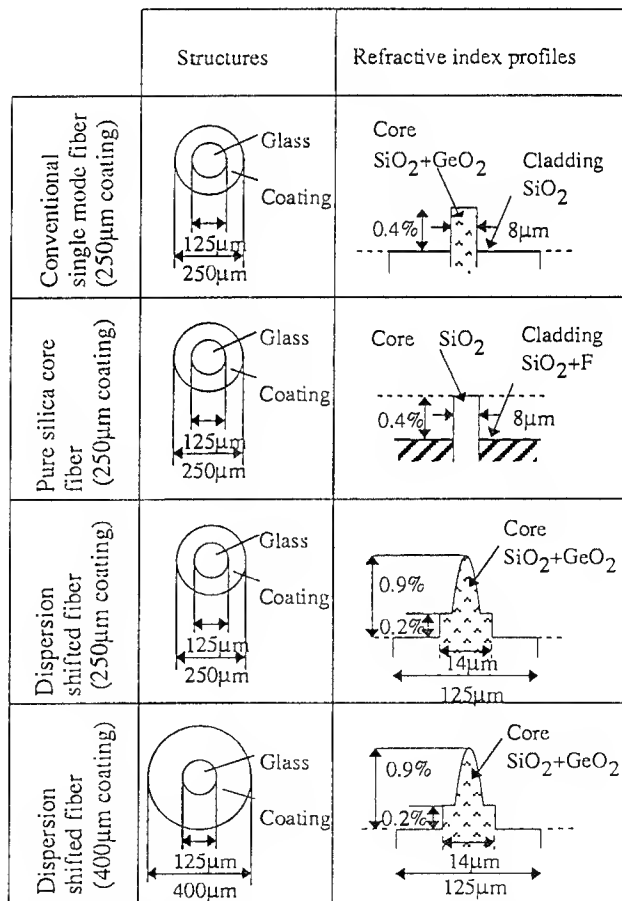


Fig.1 Structures and refractive index profiles of test fibers

3. Inherent PMD of Fiber [3]

In order to make a clear comparison, it was important to use fibers whose inherent PMD were low enough to evaluate the bending induced PMD in the experiment. Because of the random mode coupling caused by fiber coating, PMD of coated fiber is expected to be smaller than the inherent PMD, which could be determined by measuring the PMD with bare fiber [3]. Loosely coiled 100m fibers were soaked in concentrated sulfuric acid to completely remove the fiber coating as shown in Fig.2. Then measurement of the inherent PMD was conducted for the bare fibers using the interferometric method[4]. Coil diameter was 280mm, which gave an only negligible small bending induced PMD of less than 0.008 ps/100m as described in section 5.

All of the fibers used in this experiment had quite small inherent PMD less than 0.005 ps/100m.

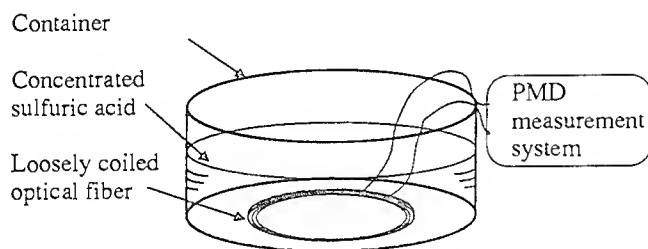


Fig. 2 Experimental set up for measuring the inherent PMD

4. The effect of lateral pressure

It is extremely important in cable design to evaluate the effect of lateral pressure on PMD. We have evaluated it by changing the level of the taking-up tension of reel, since lateral pressure onto the fiber on a reel shall be in proportion to tensile stress. The DSFs with the two coating sizes were also evaluated.

Actual test conditions are as follows;

Coating diameter	:250 μ m and 400 μ m
Fiber length	:14500m
Taking-up tension	:30g, 40g, 60g, 100g, 150g, 200g
Reel diameter	:152mm
PMD measurement method	:Fixed analyzer method

Measured PMD vs. taking-up tension is shown in Fig.3.

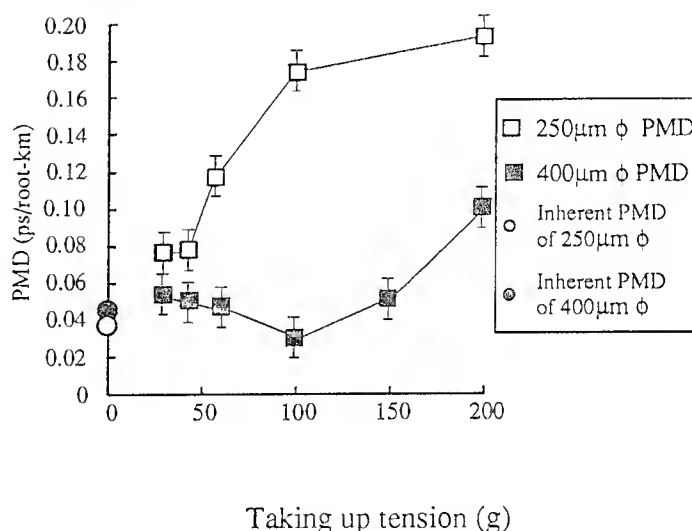


Fig.3 PMD vs. Taking up tension

As shown in Fig.3, the PMD of DSF with 250 μ m coating increased in tension above 60 grams, while DSF with 400 μ m coating exhibited very little change up to 150 grams tension. The influence of coating thickness between 400 μ m and 250 μ m on PMD was less than 0.02ps/ \sqrt km under the condition of low tension up to 40 grams. Because thick coating provided well protection against a lateral pressure, as it was confirmed in Fig. 3, 400 μ m coating fiber showed much better stability in PMD over 150 grams tension.

In order to minimize the influence of lateral pressure at a PMD measurement on a reel it was appropriate to apply a winding tension of less than 40 grams.

5. Bending Induced PMD

5.1 Bending Induced PMD without mode coupling

Bending induced birefringence, $\Delta\beta$, is expressed by equation(1) in Reference[2]

$$\Delta\beta = 0.25kn^3(p_{11}-p_{12})(1+\nu)(d/D)^2, (1)$$

where n is refractive index of fiber core, p is the strain-optic coefficient, ν is Poisson's ratio, d is the fiber diameter(=0.125mm) and D is a bending diameter.

Without mode coupling, bending induced PMD (τ) is described by equation(2)

$$\tau = (\Delta\beta / k)(L / c), (2)$$

where k is the wave number, c is the light velocity in vacuum and L is a fiber length. It should be noted that the induced PMD is almost independent of refractive index profiles and is proportional to $(1/D)^2$. In order to confirm that, PMD vs. bending diameter was measured with a dispersion unshifted SM fiber, a dispersion shifted SM fiber and a Pure Silica Core fiber.

2 meter sections of the fibers were loosely coiled with diameters from 20 mm to 60 mm and PMD was measured by the interferometric method. Measured PMD of the three kinds of fibers are shown as a function of the bending diameter in Fig.4. From Fig.4, it is concluded that the measured bending induced PMD was almost independent of the index profile and exactly followed Eq.2.

5.2 Bending induced PMD with random mode coupling

In order to describe the bending induced PMD with random mode coupling, a mean coupling length, h , has been introduced. When L is shorter than h , because of negligible mode coupling, PMD increases linearly with a fiber length L . When L is longer than h , PMD increases with a square-root of L due to random mode coupling. Bending induced PMD with random mode coupling were calculated using the h -parameter and the existing theory by Eq.2 for the case of no mode coupling.

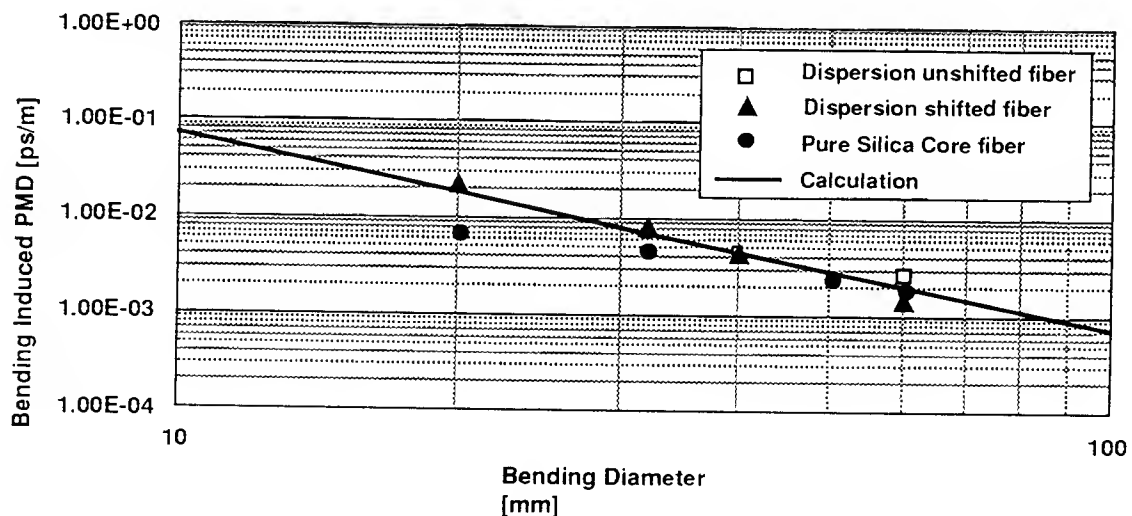
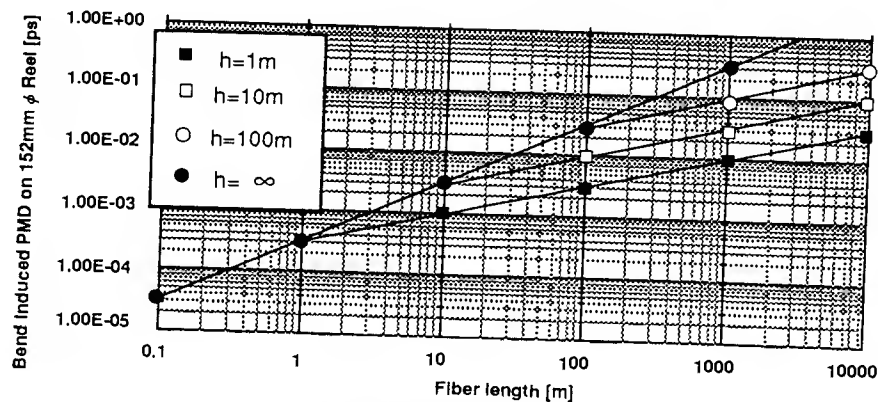


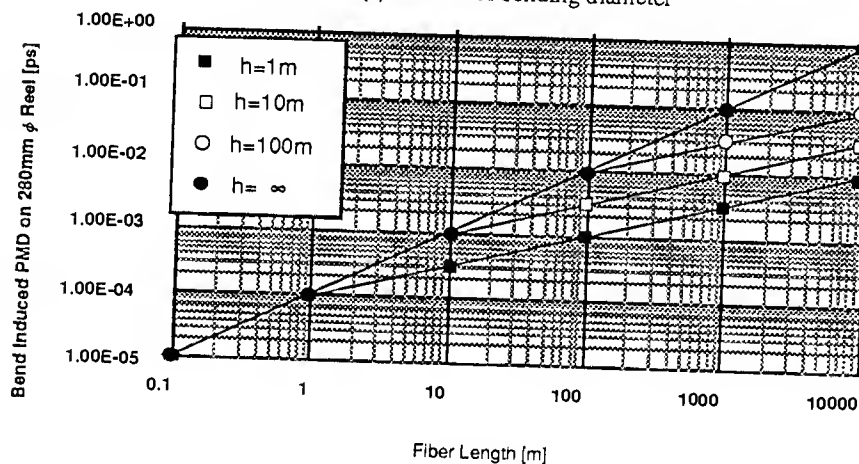
Fig.4 Bending induced PMD without mode coupling

Fig. 5 shows the bending induced PMD vs. fiber length with random mode coupling. Figures 5 (a) and (b) show the cases of 152 mm and 280 mm winding diameters, respectively.

A diagram for the bending induced PMD with random mode coupling was also developed as a function of the bending diameter as shown in Fig. 6. The bending-induced PMD with random mode coupling was also shown to be proportional to $(1/D)^2$.



(a) 152mm of bending diameter



(b) 280mm of bending diameter

Fig.5 Induced PMD dependent on fiber length

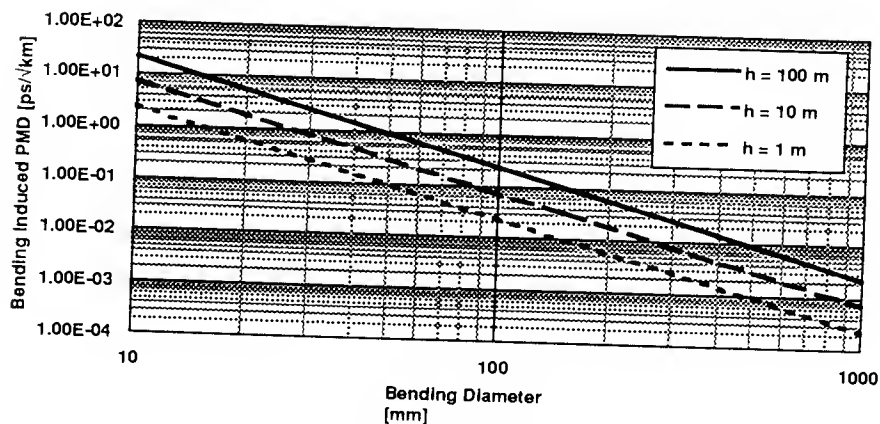


Fig.6 Bending induced PMD with random mode coupling in long length of fibers

Measurement of the bending induced PMD was then conducted for DSFs with 250 μ m coating with lengths between 2.2 km and 22.4 km. The fibers were taken-up on bobbins at two levels of winding diameters, 152 mm and 280 mm with minimal tension of 40 grams, to avoid additional birefringence due to lateral force. PMD was measured by the fixed analyzer method. Figure.7 shows the measured bending induced PMD of long DSFs and PSCFs with the two levels of winding diameters. From Fig.7, the bending induced PMD in long length of DSFs and PSCFs apparently showed the square-root dependence on fiber length.

And the induced PMD in the DSFs and the PSCFs were the same independent of index profile and glass compositions.

These test results are plotted as a function of the bending diameter in Fig.8, together with the theoretical calculation. It is shown that winding on 152 mm bobbins resulted larger bending induced PMD by 0.09ps/ $\sqrt{\text{km}}$ on the average than on 280 mm bobbins. The results agreed well with the calculation at $h=180\text{m}$. 10km of PSCF fiber showed a similar tendency to have random mode coupling with $h=180\text{m}$.

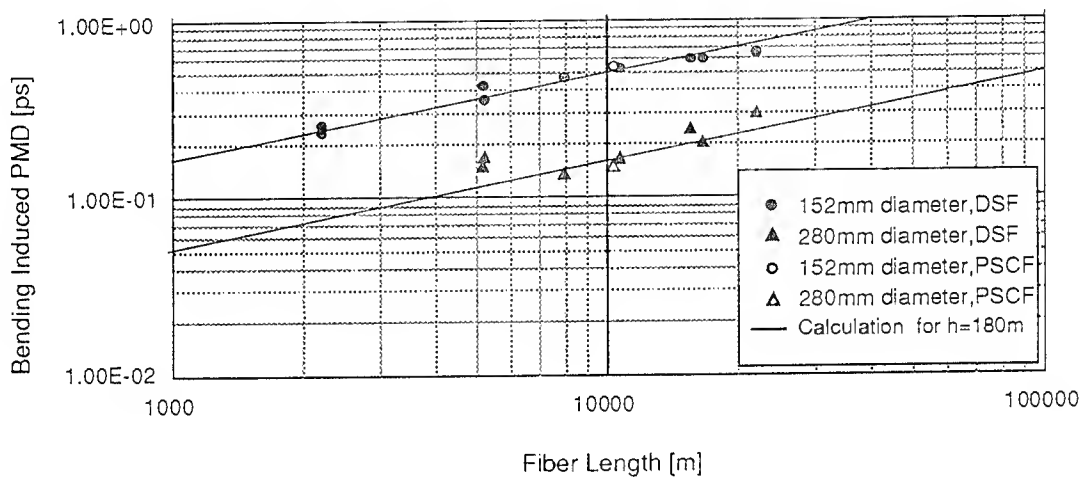


Fig7 Fiber length vs. Bending induced PMD

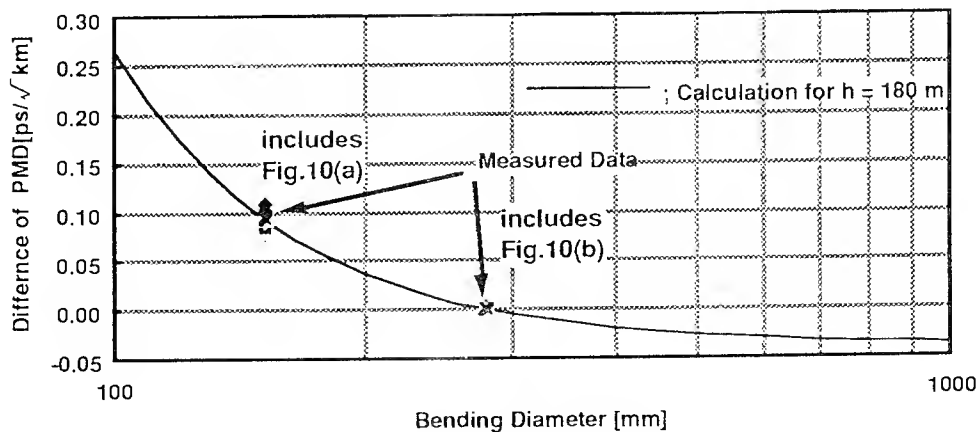
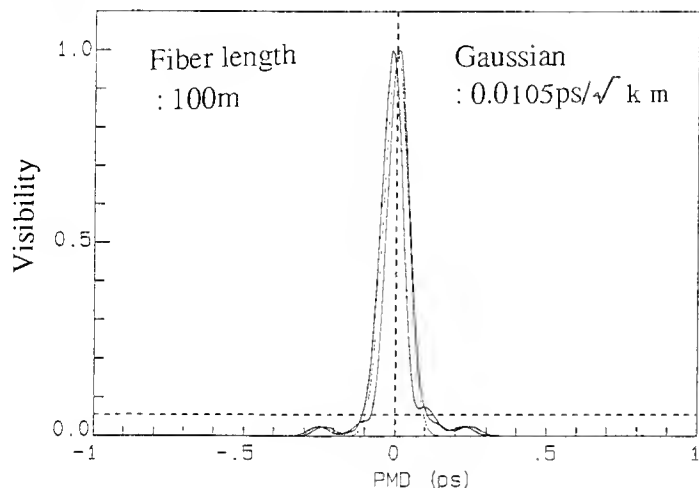


Fig.8 Measured bending induced PMD in long length fibers

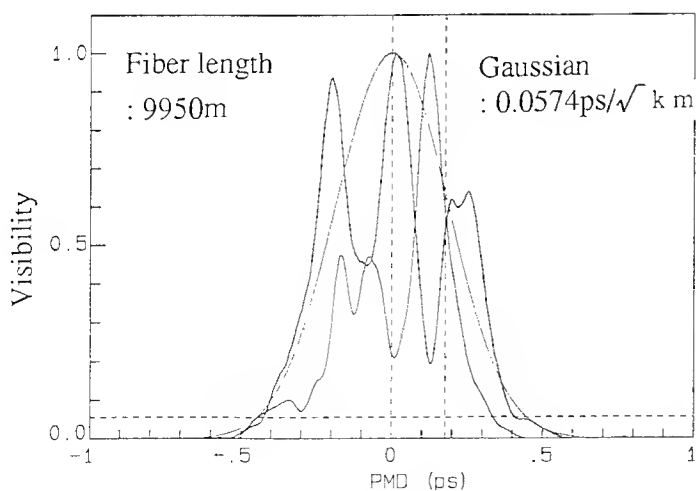
In order to visualize the random mode coupling in long length of fibers and the negligible mode coupling in short length of fibers, PMD was measured for 100 m and 9950 m of DSFs wound on 280 mm bobbin by the interferometric method.

Fig. 9 (a) and (b) show the interfered fringe envelopes in 100 m and in 9950 m of DSF on 280 mm bobbin.

Clearly negligible mode coupling is seen in 100 m of the DSF whose length is shorter than the obtained mean - coupling length h (≈ 180 m) and extensive mode coupling, on the other hand, is observed in 9950 m of the long DSF whose length is much larger than the h .



(a) Bending induced PMD (length : 100m)



(b) Bending induced PMD (length : 9950m)

Fig.9 Interferometric PMD measurement results

Conclusion

The bending induced PMD of three kinds of SM fibers have been investigated.

(1)Winding fibers on bobbins caused PMD to increase. To minimize the effect of winding, thicker coating, lower winding tension and larger bobbin size are preferred.

(2)Bending induced PMD with and without mode coupling is independent of the refractive index profile and glass compositions. Dispersion shifted fiber, conventional SMF and pure silica core fiber, showed the same results and agreed well with the calculation.

This study gives one possible way to estimate bending induced PMD even in long length of fibers with random mode coupling.

Reference

- [1] A. F. Judy et al., "PMD characterization of production cables for evolving lightwave systems," OFC'93, PD20, 1993.
- [2] R. Urich et al., Optics Lett., "Bending induced birefringence in single-mode fibers," Vol.5, p273 (1980)
- [3] Y. Suetsugu et al., " Polarization mode dispersion in dispersion shifted single mode fiber, "ECOC'93, Montreux, Switzerland, We28, 1993.
- [4]Y. Namihira and J. Maeda, "Polarization mode dispersion measurements in optical fibers", Proceeding of SOFM,Invited paper , Boulder, USA, Sep.1992.



Toshimi Sekito

Sumitomo Electric
Industries, Ltd.

1, Taya-tyo, Sakae-ku
Yokohama, 244, Japan

Toshimi Sekito graduated from Tokyo Science University in 1992. She joined Sumitomo Electric Industries, Ltd in 1992 and has engaged in design and development of optical fiber.



Yasunori Saito

Sumitomo Electric
Industries, Ltd

1, Taya cho, Sakae-ku
Yokohama, Japan

Yasunori Saito received his B.S. degree in Electrical Communication Engineering from Tohoku Univ. in 1969. He then joined Sumitomo Electric Industries and has been engaged in research and development of optical fiber cable. Mr. Saito is a manager of Fiber Engineering Department, Fiber Optics Division. He is member of Institute of Electronics and Communication Engineers of Japan.



Yoshiyuki Suetsugu

Sumitomo Electric
Industries, Ltd.

1, Taya-cho, Sakae-ku
Yokohama, Japan

Yoshiyuki Suetsugu was born in 1961 and received the B.S. degree from Tsukuba University in 1984. He joined the Sumitomo Electric Industries Ltd. in 1984, and has been engaged in research and development of optical fibers and cables in Yokohama Research and Laboratories. He is a member of Institute of Electronics and Communication Engineers of Japan.



Yosuke Yamazaki

Sumitomo Electric
Industries, Ltd.

1, Taya-cho, Sakae-ku
Yokohama, Japan

Yosuke Yamazaki graduated from Tokyo Institute of Technology in 1983 with a B.S. in mechanical engineering. He then joined Sumitomo Electric Industries, Ltd., where he is a cable design engineer in the Fiber Optics Division.

THERMAL CHARACTERISTICS OF THE PROPAGATION DELAY FOR BARE AND CABLED SINGLE MODE OVD FIBERS

Wang Shou Jia, Tian He Chen
Chengdu Cable Plant of P & T Ministry, PR China

Risheng Yang, Eduard Baumann, Armin Landers
Siecor GmbH & Co.KG, Germany

ABSTRACT

This work reports experimental studies concerning temperature dependence of the group delay for both bare and cabled OVD fibers. Measurement results show that the delay change does not increase linearly with temperature. At low temperatures the delay changes more rapidly. The average increasing rates at 1300 nm for bare and cabled fibers are 40 and 48 ps/km/°C for a temperature range from -60 °C to +80 °C, respectively. Based on the thermal characteristics of the delay, fiber strain and group index dependence on temperatures have been determined, thereby taking into account the contribution of secondary coating. Furthermore, the additional stress induced by the cabling process has been calculated. It is based on the delay increase in cabled fibers compared to bare fiber results. The delay change in cabled fiber at -60°C has decreased by 847 ps/km which indicates an additional compression of 16 MPa/km.

INTRODUCTION

Optical cables are subject to a variety of different temperatures during operation. For buried and duct cables only relatively small variations in environmental temperatures are to be expected; for aerial cables they would be much greater. For the specified temperature range for each cable type the transmission properties of the optical fibers may change only within a limited range. Thermal characteristics of optical attenuation in cables have been investigated intensively. There have been only a few studies on the thermal characteristics of the propagation delay in optical cables. Thermal characteristics of the delay are important factors when the cables are used as transmission line in a long-distance trunk covering districts with large temperature differences /1/. For example, according to the specification for the Beijing-Wuhan-Guangzhou optic cable line of China, the delay change should be less than 40 ps/km/°C for temperature range from -20 to +40°C.

In addition, based on the thermal characteristics of the delay, the fiber strain as well as the group index dependence on temperatures can be determined. In this paper the thermal characteristics of the delay, fiber strain and group index change for both bare fibers and fibers in central core tube cables were investigated intensively. Furthermore, a method was proposed to determine the additional stress induced by the cabling process. It is based on the delay increase in cabled fibers compared to bare fiber results.

EXPERIMENTAL RESULTS FOR BARE FIBERS

Temperature dependence of the delay change

For the measurement of the delay change with temperature in bare fibers, eight standard unshifted OVD fiber samples with different mode field diameters (MFD) and cutoff wavelengths were selected. The fibers were loosely coiled and placed in a temperature-controlled chamber. Care was taken to ensure that no additional stresses were applied to the fibers. Initial measurements were performed at room temperature (23°C). The chamber was cycled from -60 to +85°C in approximately 20 degree increments. The duration of each temperature, where the measurements were performed, was taken to be 100 minutes in order to reach a thermal stabilization of the fibers. The delay changes with the temperature at 1300 nm were measured by a differential phase shift based measurement system, which gives very accurate and reliable results. Figure 1 shows the temperature dependence of the delay change relative to the delay at 23°C. In contrast to results in most publications /2/ - /3/, the delay change does not increase linearly with temperature. At low temperatures the delay changes more rapidly. The average increasing rates at 1300 nm are 36.7 and 40.2 ps/km/°C for temperature ranges from -20 to +40°C and from -60 to +85°C, respectively. Previous work on the delay versus temperature resulted in a slope of 42.7/km/°C /2/. The delay change depends slightly on MFD. When MFD increases from 9.0 to 9.5 micron, the average delay change increases

about 1.4 ps/km/°C for a temperature range from -20 to +40°C, which is shown in Figure 2. Measurement results show that the delay change is independent from the cutoff wavelength.

Temperature dependence of the fiber strain

For a fiber coated by two layers of UV-cured acrylate resins, the effective thermal expansion coefficient K_{eff} is given by /4/

$$K_{eff} = \frac{K_f A_f E_f + K_p A_p E_p + K_s A_s E_s}{A_f E_f + A_p E_p + A_s E_s} \quad (1)$$

where A, E and K denote the cross-sectional area, Young's modulus and thermal expansion coefficient, respectively, and subscript f, p and s refer to fiber, primary and secondary coating, respectively. Young's modulus and thermal expansion coefficient for fused silica glass are 72900 MPa and $5.5 \cdot 10^{-7}/^\circ\text{C}$ /5/, respectively, and are considered to be independent from the temperature. The contribution of the primary coating can be neglected because of its much smaller Young's modulus compared to that of the fiber and the secondary coating. Thus, the effective thermal expansion coefficient is given by

$$K_{eff} = \frac{K_f A_f E_f + K_s A_s E_s}{A_f E_f + A_s E_s} \quad (2)$$

Since Young's modulus E_s and thermal expansion coefficient K_s of secondary coating change with temperature, the strain at temperature T is given by

$$\Delta \varepsilon = \int_{T_0}^T K_{eff} dT \quad (3)$$

where T_0 is the initial temperature. From /6/, Young's moduli for secondary coating are 1932, 690 and 345 MPa at temperatures of -60, +23 and +80°C, and the thermal expansion coefficients K_s are 0.00021 and 0.00091/°C in temperature ranges from -60 to +23°C and from +23 to +80°C, respectively. The calculated strain for fibers is also shown in Figure 3, using the values of E_f , K_f , $E_s(T)$ and $K_s(T)$.

Temperature dependence of the group index

The delay change with temperature T in a fiber of length L is given by /7/

$$\frac{\Delta \tau}{\Delta T} = \frac{1}{c} \left(L \frac{\Delta N}{\Delta T} + N \frac{\Delta L}{\Delta T} \right) \quad (4)$$

where τ is the delay, c the speed of light in vacuum and N the group index, which is approxi-

mately 1.47 at room temperature. The first term on the right-hand side implies a thermal dependence of the group index, and the second term describes the influence of the linear thermal expansion coefficient.

The group index change versus temperature is given by integrating Eq. (4) with respect to T

$$\Delta N = \frac{c}{L} \Delta \tau - N \Delta \varepsilon \quad (5)$$

The calculated group index change versus temperature is shown in Figure 4, using the delay and strain changes in Figures 1 and 3, respectively. The average increasing rate of the group index at 1300 nm is 0.000006/°C for a temperature range from -60 to +80°C. Previous work /2/ on temperature dependence of the group index for OVD fibers resulted in a rate of change of 0.00001/°C. The result in this paper is even smaller. The discrepancy may be caused by the temperature dependences of Young's modulus and of the thermal expansion coefficient for the secondary coating. In the present work the contribution of the secondary coating has been considered. At -60°C the decrease in group index is 0.00063. If the 23°C group index would be taken for the OTDR, this would cause an error of -43 cm per kilometer in the length measurement.

EXPERIMENTAL RESULTS FOR CABLED FIBERS

The thermal effect on cabled fibers is expected to be larger than that on bare fibers. Central core tube cables containing 4- and 8-OVD fiber bundles were measured for temperature dependence of the delay. Figure 5 shows a typical basic structure of such a cable. Samples of 250 m length were placed in a chamber whose temperature could be controlled over the range of -60 to +80°C to within 1°C. The measurement was performed with a commercial system, based on the phase shift technique. The resulting temperature dependences of the delay change relative to the delay at 23°C for fibers in 4- and 8-fiber-bundle central core tube cables are shown in Figure 6. Additionally, the nonlinear behavior of the delay change can be seen. The average increasing rates of the delay at 1300 nm in both loose structure types are 38.6 and 48.4 ps/km/°C for temperature ranges from -20 to +40°C and from -60 to +80°C, respectively. Almost the same delay changes in 4- and 8-fiber types indicate that the fiber number in the bundle central core tube type has only a limited influence on the delay change with temperature.

ADDITIONAL STRESS BY CABLING PROCESS

The thermal effect on cabled fibers is larger than that on bare fibers. Figure 7 shows the increased delay change versus temperature in cen-

tral core tube cables compared to that in bare fibers. Comparing the delay change in cables to that in bare fibers, the additional stress due to the filling compound can be determined as a function of temperature.

The delay change with stress in a fiber of length L is given by /7/

$$\frac{\Delta\tau}{\Delta\sigma} = \frac{1}{c} \left(L \frac{\Delta N}{\Delta\sigma} + N \frac{\Delta L}{\Delta\sigma} \right) \quad (6)$$

where σ is the stress on the fibers. The delay change caused by stress is divided into two terms. The first term is due to changes in the group index. In Eq.(6), the value of $\Delta N/\Delta\sigma$ for OVD fiber is reported to be $-0.348 \cdot 10^{-5}/\text{MPa}$ /2/. The second term results from changes in the length of fibers under stress.

According to /5/ the stress is given by

$$\Delta\sigma = E_{\text{eff}} \frac{\Delta L}{L} \quad (7)$$

where E_{eff} is the effective Young's modulus for a fiber, which is obtained by

$$E_{\text{eff}} = \frac{A_f E_f + A_c E_c}{A_f} \quad (8)$$

In Eq.(8), the contribution of the primary coating is neglected. Substituting Eqs.(7)-(8) into (6), we have

$$\Delta\sigma = \frac{c\Delta\tau}{\left(N \frac{L}{E_{\text{eff}}} + L \frac{\Delta N}{\Delta\sigma} \right)} \quad (9)$$

Based on the increased delay change shown in Figure 7 and on the effective Young's modulus according to Eq.(8), the additional stress versus temperature has been calculated. Figure 8 shows the temperature dependence of the additional stress on fibers in central core tube cables. The negative sign in Figure 8 indicates a fiber compression. It has been found that the delay change in cabled fiber at -60°C had decreased by 847 ps/km indicating an additional compressive stress of 16 MPa/km!

CONCLUSION

The thermal characteristics of the delay for both bare fibers and fibers in 4- and 8-fiber bundle central core tube cables were investigated intensively. In contrast to results in many publications, the delay change does not increase linearly with temperature. At low temperatures the delay changes more rapidly. The average increasing rates at 1300 nm for bare and cabled fiber are 40 and 48 ps/km/ $^\circ\text{C}$ for a tem-

perature range from -60°C to $+80^\circ\text{C}$, respectively. Based on the thermal characteristics of the delay, the fiber strain as well as the group index dependence on the temperature have been determined. In calculating the fiber strain and group index changes the contribution of the secondary coating has been taken into account. The average increasing rate of the group index at 1300 nm is $0.000006/^\circ\text{C}$ for a temperature range from -60 to $+80^\circ\text{C}$. Previous work /2/ on the group index versus temperature for OVD fibers resulted in a rate of change of $0.00001/^\circ\text{C}$. The smaller result in this paper may be caused by the contribution of the secondary coating. At -60°C the decrease in group index is 0.00063. This will cause an error of -43 cm per kilometer in the length measurement when the 23°C group index is taken for the OTDR. Furthermore, the additional stress induced by the cabling process has been determined. It is based on the delay increase in cabled fibers compared to bare fiber results. It has been found that the delay change in cabled fiber at -60°C decreased by 847 ps/km corresponding to an additional compressive stress of 16 MPa/km.

ACKNOWLEDGEMENT

The authors would like to acknowledge W. Renken for his encouragement and support. They would also like to thank S. Uebelhack for her kindful help with manuscript preparation.

REFERENCES

- /1/ Specification for aerial cable installed in Beijing-Wuhan- Guangzhou Trunk, Ministry of Posts and Telecommunications, PR China, 1992, pp. 29-30
- /2/ D.B.Williams et al., "Single-mode optical fiber index of refraction dependence on product parameters, tensile and temperature", IWCS Proc., 1990, pp. 726-729
- /3/ L.G. Cohen et al., "Effect of temperature on transmission in lightguides", BSTJ 58, 1979, pp. 945-951
- /4/ N.Shibata et al., "Thermal characteristics of optical pulse transit time delay and fiber strain in a single-mode optical fiber cable", Applied Optics, Vol.22, 1983, pp. 979-984
- /5/ G.Mahlke et al., Fiber optic cables, 2nd, revised edition, 1993, pp. 31
- /6/ private communication
- /7/ A.H.Hartog et al., "Variation of pulse delay with stress and temperature in jacketed and un-jacketed optical fibres", Optical and Quantum II, 1979, pp. 265-273

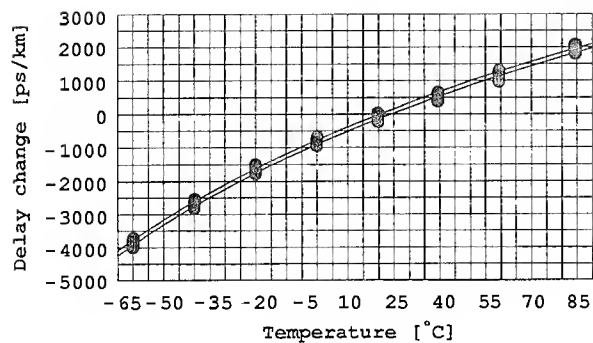


Fig. 1: Delay change at 1300 nm vs. temperature for bare fibers

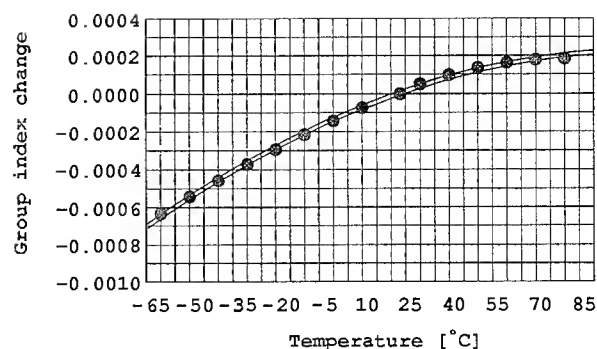


Fig. 4: Group index change at 1300 nm vs. temperature for bare fibers

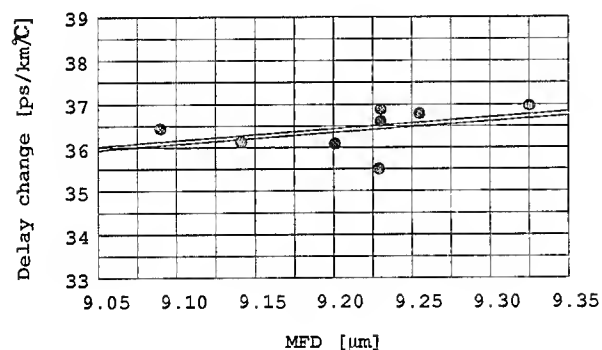


Fig. 2: Delay change at 1300 nm vs. MFD

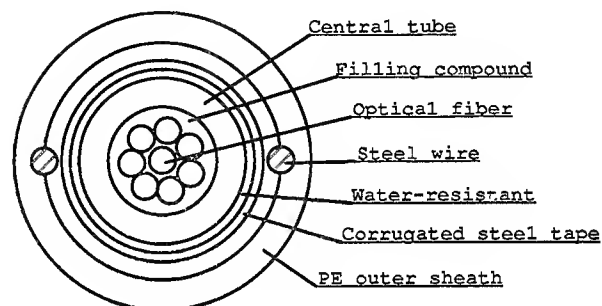


Fig. 5: 8-fiber bundle central core tube cable

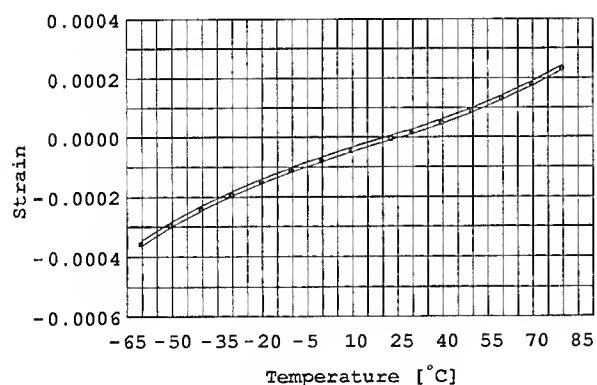


Fig. 3: Fiber strain vs. temperature for bare fibers

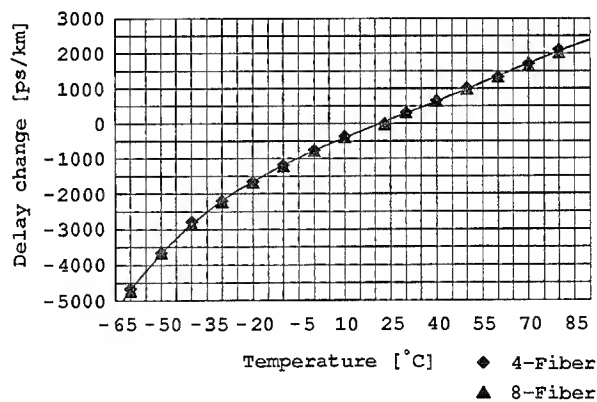


Fig. 6: Delay change at 1300 nm vs. temperature for fibers in 4- and 8-fiber cables

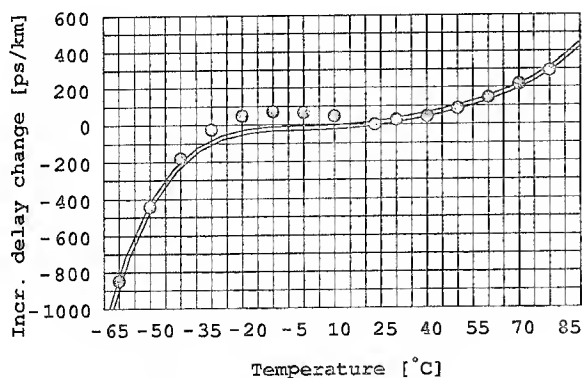


Fig. 7: Increased delay change in cabled fibers

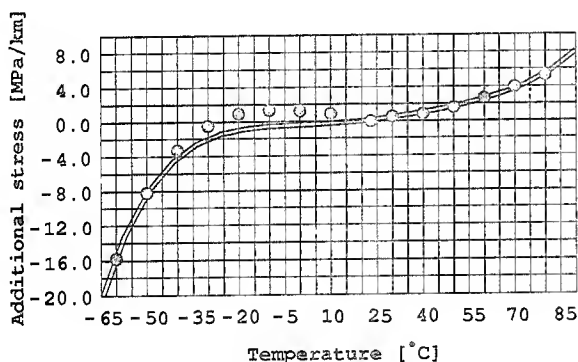


Fig. 8: Additional stress vs. temperature for fibers in central core tube cable



Wang Shou Jia
Chengdu Cable Plant
Chengdu, China

Wang Shou Jia was born in 1964 and received his M. Sc. degree in laser physics from Sichuan Normal University in 1988, majoring in laser scattering. In the same year he joined Chengdu Cable Plant of P & T Ministry, China, where he is currently engaged in the research and development of optical fiber cables, especially, in the study of the reliability of optical fiber cables.



Tian He Chen
Chengdu Cable Plant
Chengdu, China

Tian He Chen was born in 1937 and graduated from Electrical Engineering Department of Xian Jiao Tong University in 1961, majoring in electric insulation and cable technology. He joined Chengdu Cable Plant in the same year. In 1991, he was awarded the title of National Expert for his outstanding contributions to the development of telecommunication technology in China. He is now Deputy Chief Engineer, senior engineer of the plant, and is in charge of the research and development of optical fiber cables and materials.



Risheng Yang
Siecor GmbH & Co.KG
Neustadt/Coburg, Germany

Risheng Yang graduated from Physics Department of Tsinghua University, China, in 1968. He received the M. Sc. degree from Chengdu Institute of Radio Engineering, China, in 1981 and Ph. D. degree from the Technical University of Braunschweig, Germany, in 1988, both in electrical engineering. Since 1984 he has continually worked in the area of optical fibers. He joined Siecor GmbH & Co.KG in 1991 after prior employment at AEG Kabel. Dr. Yang is a member of the Optical Society of America and SPIE.



Eduard Baumann
Siecor GmbH & Co.KG
Neustadt/Coburg, Germany

Dr. Eduard Baumann was born in Daber/Poland in 1959. He received his physics degree in 1987 and his Ph. D. in Fluid Dynamic in 1990 from the University of Göttingen, Germany. He joined Siecor GmbH & Co.KG in Neustadt/Coburg, Germany in 1991 and is an Application Engineer.



Armin Landers
Siecor GmbH & Co.KG
Neustadt/Coburg, Germany

Armin Landers was born in Oberhausen, Germany, in 1954. He received his Dipl.-Ing. degree in chemistry from Fachhochschule Niederrhein in 1985. He joined Siecor GmbH & Co.KG in 1986 and is an Application Engineer.

PHOTO-ELASTIC CORRECTION FACTOR FOR FIBER STRAIN MEASUREMENTS IN A CABLE UNDER TENSILE LOAD

K. Abe*, K. Yoshida**, O. Daneshvar***, and J. J. Carr****

*i/FO Technologies, 60 Robert St., Ottawa, Ontario, Canada, K2P 1G4

**Phillips-Fitel Inc., 300 Consillium Place, Bureau 200, Scarborough, Ontario, Canada, M1H 3G2

***ATT-Fitel Inc., 201 Adamson Ind. Blvd., Carrollton, GA 30117

****Corning Inc., Corning, NY 14831

ABSTRACT

There has been a large variation among reported values for photo-elastic correction factor (K). The non-linearity of group index vs. strain plot was demonstrated to be the cause of the inconsistency. Based on this finding, it is concluded that the K value should be in the range of 1.26-1.30 when the fiber strain is less than 0.6 %, and 1.22-1.24 when the strain is in the range of 2-3 % regardless of fiber types and measurement wavelengths. As a practical example of strain measurements, a test result for an OPGW was described. Applying the tensile load of 127 kN over the time duration of 96 hours, it has been confirmed that the cable withstands the load without exceeding the fiber strain of 0.5 % which was the design target of the cable.

INTRODUCTION

For the purpose of estimating fiber strain in cable, it has been a common practice to measure either the time delay or the phase shift of the modulated optical signal which is transmitted through the fiber. The "optical strain" measured in this manner has to be converted to actual "mechanical strain" taking into account the fact that the group velocity of the optical signal increases as the fiber is elongated, due to the stress-optic or photo-elastic effect.

The photo-elastic correction factor has been known to be in the range of 1.2-1.3.^{1,2,3,4,7} In other words, the mechanical strain is larger than the optically measured strain by 20-30 %. In spite of the fact that most cable manufacturers are equipped with their own calibration facilities to determine the value of this correction factor, there have been relatively few reports on the variation (or consistency) of the values for different types of fibers and light sources used for the measurements. Table 1 lists some of the reported values. It should be noted that currently there is no standard for the definition of the parameter. In order to generate Table 1, the reported experimental data had to be converted to a parameter with a consistent definition, sometimes using certain assumptions. The correction factor (K) listed in Table 1 ranges from 1.20 to 1.40. This indicates a need of more accurate value for qualification tests of cables. Furthermore, the values in the table have been generated for a wide variety of fiber types and measurement

conditions, e.g. wavelength. The objective of this report is to critically assess experimental data and to generate more accurate value for the photo-elastic correction factor which can be utilized for qualification tests of single-mode fiber cables.

DEFINITION OF PARAMETERS

The following equations define relevant parameters assuming that the time delay method is used for the measurement. However, the ratio (the change of time delay due to strain)/(absolute time delay for the gauge length) should be considered as optical strain. Therefore, the same equation can be used for the phase shift method as well, provided that the experimental data are expressed as optical strain.

The time delay (t) of a pulsed optical signal when it travels over the fiber length L is given by

$$t = N \cdot \frac{L}{c}, \quad (1)$$

where N is the group index defined as

$$N = n - \lambda \cdot \frac{dn}{d\lambda}, \quad (2)$$

n is the refractive index, and λ is the wavelength. In practice, the experimental N value which is relevant to the current investigation may slightly deviate from the group index of the above definition due to the waveguide dispersion and the higher order mode(s) when the wavelength of the strain measurement is below the cutoff wavelength of the single-mode fiber. Under zero strain,

$$t_0 = N_0 \cdot \frac{L_0}{c}. \quad (3)$$

From equation (1), a small change of time delay can be expressed as

$$dt \approx dN \cdot \frac{L_0}{c} + N_0 \cdot \frac{dL}{c}. \quad (4)$$

Our objective is to determine the following correction factor K :

$$\frac{dL}{L_0} = K \cdot \frac{dt}{t_0}, \quad (5)$$

where, dL/L_0 and dt/t_0 are the mechanical and optical strain, respectively.

Calibration tests to determine the K value involve measurements for the change of time delay (dt) as a function of elongation (dL) for a known length of fiber (L_0). Often the calibration test results are plotted on the dL vs. dt scale and the slope S is determined:

$$S = \frac{dL}{dt} \quad (6)$$

From equation (5),
$$K = \frac{dL}{dt} \cdot \frac{t_0}{L_0} = \frac{dL}{dt} \cdot \frac{N_0}{c} \quad (7)$$

Therefore,
$$K = S \cdot \frac{t_0}{L_0} = S \cdot \frac{N_0}{c} \quad (8)$$

Alternatively, the same calibration test results can be plotted on the N vs. strain scale. If the plot is linear, the results can be fitted to

$$N = N_0 \left(1 + X \frac{dL}{L_0}\right) \quad (9)$$

Then, the K value is determined by

$$K = \frac{1}{1 + X} \quad (10)$$

Equation (10) was derived from equations (4) and (7).

The following equation can be found in one of the documents issued by the EIA standard committee,⁵

$$\varepsilon_f = (t_{\text{stress}} - t_{\text{ref}}) \frac{c}{LN} \cdot \frac{1}{k} \quad (11)$$

where, ε_f is the mechanical strain, $t_{\text{stress}} - t_{\text{ref}} = dt$, and $1/k = K$. Therefore, this equation is equivalent to equation (5).

CALIBRATION MEASUREMENTS TO DETERMINE K

Fig. 1 illustrates an example of dL vs. dt plot. The calibration test was performed for a matched clad dispersion shifted (MDS) fiber with a test set operating at 850 nm using time-of-flight measurement technique. A mandrel mode stripper was used to attenuate the higher order modes. The measurements were performed by using a high resolution optical time domain reflectometer (OTDR). Two test results are illustrated in the plot: one for the gauge length of 12.71 m and the other for 1.34 m. Least squares fitting the data to equation (6) and using equation (8), the K values of 1.30 and 1.24 were obtained for the gauge lengths of 12.71 and 1.34 m, respectively. The cause of this discrepancy is evident in Fig. 2 when the same test results are plotted on the N vs. strain scale. The observed deviations from the linear assumption could be partly due to experimental errors which were exaggerated when the short gauge length was used, and also partly due to the inherent property of fiber as will be described later. As indicated in Fig. 2, the slopes of the two test results (short and long gauge lengths) agree well at the low strain region, i.e. $<1\%$. Considering that the objective of this paper is to determine a reliable K value for cable qualification

tests, where the typical strain of interest is 0.5 %, the K value determined by using the gauge length of 12.71 m with a maximum strain of 0.3 % is more appropriate for the current objective than that determined by the short gauge length measurement which extends to the maximum strain of 3 %. Similarly, the K values were determined for other types of fibers using the same 850 nm test-set, and the results are listed in Table 2.

Previously, it was reported that the N vs. stress plot was not linear.⁴ Knowing that the Young's modulus of silica is a function of strain,⁶ the same test results were plotted as a function of strain which was recorded during the previous measurements. The results shown in Fig. 3 for a matched clad single-mode (MSM) fiber which was measured at 1295 and 1532 nm indicate that the nonlinear trend of the plot is less than that of the N vs. stress plot but it still exists, confirming the previous observation at 850 nm.

Considering the facts, that the N vs. strain plot is not linear and that the range of strain we are interested in is the region of 0.5 %, the test data up to the maximum strain of 0.6 % were used and least squares fitted to equation (9) as indicated in Fig. 3 with straight lines. Then, the K value was calculated using equation (10). The result was a slightly larger K value of 1.26 as compared to the previous 1.22-1.23 (reference 4 and Table 1) which was obtained by force fitting all the data to a linear slope. The same analysis was repeated for a MDS fiber measured at the wavelengths of 1532 nm. The values for the correction factor K are summarized in Table 2.

For practical applications of the above mentioned calibration results, it is more convenient to describe the K value as a function of optical strain. From equations (4) and (5),

$$K = 1 - \frac{t_0}{N_0} \cdot \frac{dN}{dt} \quad (12)$$

If the N vs. optical strain plot can be fitted to a quadratic equation, equation (12) implies that the K vs. optical strain plot should be linear. Because some of the calibration test results were compiled as N vs. mechanical strain, the following equation derived from (1) and (3) was used to convert to optical strain,

$$\frac{dt}{t_0} = \frac{N}{N_0} \left(1 + \frac{dL}{L_0}\right) - 1 \quad (13)$$

The results are shown in Fig. 4. The erratic results in the extreme low strain region are due to the difficulty in measuring the mechanical length accurately. In practice, the raw experimental data of calibration tests are dt , t_0 , dL and L_0 . Therefore, the K vs. optical strain plot could be generated simply by using equation (8).

Among the K values listed in Table 2, those measured at 850 nm appear to be mostly larger than the ones measured at 1300 and 1550 nm. On the other hand, the stress-optic coefficients reported in reference 7 have indicated that the wavelength dependence of the K value should be negligibly small suggesting

that the discrepancies are not due to the inherent wavelength dependence of the parameter. The causes of this small discrepancy could be the higher order mode(s) at 850 nm or the waveguide dispersion which has been ignored for the current investigation. In practice, the above mentioned small inconsistency is not a concern for cable testing provided that the K value is calibrated for the specific test-set covering the strain region of interest and corrected for possible measurement errors which may be unique to the test-set and/or the test method. However, the current investigation has indicated that the physics of stress or strain induced change of group index has not been fully examined.

In conclusion, the most reasonable K value is in the range of 1.26-1.30 when a small fiber strain (<0.6 %) has to be measured, and 1.22-1.24 when the strain ranges from 2 to 3 %.

CABLE LOADING TEST

With a heavy cable, the fiber strain measurement in a loaded cable can become cumbersome, and the measurement can not always follow the approach described in the previous sections. As an example, a test which was performed for an optical ground wire (OPGW) is described in this section in order to illustrate an actual cable test method and the interpretation of the test results.

An OPGW sample with the approximate length of 69 m was laid in the field and the load was applied to the middle section of the cable as shown in Fig. 5. The cable construction is illustrated in Fig. 6. When the cable was visually straightened at the load of 2.5 kN (255 kg-f), the distance between the clamps were measured mechanically as 29.35 m, and the total fiber length (for the full cable length of about 69 m) was measured optically by using an OTDR operating at 850 nm. The fibers in the cable were MDS fiber. At the time of this cable test, the group index N was set at 1.457 for the OTDR test-set. The reading of the OTDR in length can be described as an "apparent optical fiber length". While this apparent optical fiber length was being monitored, the load on the cable was increased to 127 kN (13,000 kg-f) and the cable was subjected to the load over the time duration of 96 hours. After the 96 hour test, the load was reduced for a short time period and it was increased to 127 kN again.

From the changes of the apparent optical fiber length and the mechanical cable length between the clamps, the optical strain and the actual mechanical strain were calculated as follows: First, the change of the apparent optical fiber length (dl) was converted to the change of the time delay using 1.457 for the group index,

$$dt = 1.457 \cdot \frac{dl}{c}. \quad (14)$$

Assuming that the mechanical cable length between the clamps are the mechanical fiber length for the section where it was strained, and using the correct group index of 1.4728 for MDS fiber at 850 nm (see Table 2), the time delay under zero stress

for the loaded section length was estimated as

$$t_0 = 1.4728 \cdot \frac{29.35}{c}. \quad (15)$$

Actual mechanical strain dL/L_0 can be given by the following equation using the photo-elastic correction factor of 1.30 for the fiber type and the test wavelength,

$$\frac{dL}{L_0} = K \cdot \frac{dt}{t_0} = 1.30 \cdot \frac{1.457}{1.4728} \cdot \frac{dl}{29.35} = 0.04382 \cdot dl. \quad (16)$$

Because the OTDR test-set, which was used for the cable loading test, was not available for calibration test, the largest K value obtained for the same type of test-set and fiber was used for equation (16).

The test results are summarized as the fiber strain as a function of time as the loading level on the cable is changed (Fig. 7) and also as the fiber strain as a function of the loading level (Fig. 8). Note that the fiber strain did not exceed the 0.5 % design target for this cable at the sustained cable loading of 127 kN (13,000 kg-f) over 96 hours. The hysteresis effect shown in Fig. 8 is primarily due to the tightening of the stranded aluminum-clad steel and aluminum-alloy wires (see Fig. 6) under the maximum load and the subsequent cable elongation.

CONCLUSIONS

Previously reported values for the photo-elastic correction factor (K) range from 1.20 to 1.40. It has been demonstrated that the non-linear trends of the group index vs. strain plots are the major cause for the variation of K values. Taking the non-linearity into consideration, it has been concluded that the K value should be in the range of 1.26-1.30 when the fiber strain of less than 0.6 % has to be monitored and 1.22-1.24 when the strain is in the range of 2-3 %. In practice, the remaining small inconsistency does not impose any problem provided that the specific test-set is calibrated for the strain region of interest and corrected for possible measurement errors which may be unique to the test-set and/or the test method. However, the current investigation suggests the need for a better grasp of the physics of stress-optic and photo-elastic effects in optical fiber.

Lastly, a fiber strain measurement in a loaded OPGW was described in order to illustrate an application of the test methodology to a practical case. The tensile load of 127 kN (13,000 kg-f) was applied to the cable over the time duration of 96 hours while the fiber strain was being monitored. It has been confirmed that the cable withstands the load without exceeding the fiber strain of 0.5 % which was the design target for the cable.

ACKNOWLEDGMENT

The authors would like to thank Hydro Quebec for providing us with their test results and for drawing our attention to this topic, and also Ontario Hydro who provided the facilities for the cable loading test.

REFERENCES

1. M. Johnson and R. Ulrich, "Fibre-optical strain gauge", Electron. Lett. vol.14, pp. 432-433, 1978.
2. K. Matsui, S. Tanaka, and M. Hoshikawa, "Precise measurement of optical fiber breaking elongation", NBS Symposium on Optical Fiber Measurements, NBS Special Publication #641, pp. 51-54, 1982.
3. K. H. Hafemeister, T. A. Clarke, and E. J. Buonopane, "Automated differential fiber strain measurement system for single and multimode fiber", NBS Symposium on Optical Fiber Measurements, NBS Special Publication #683, pp. 81-84, 1984.
4. J. J. Carr, S. L. Saikkonen, and D. H. Williams, "Refractive index measurements on single-mode fiber as functions of product parameters, tensile stress and temperature", Symposium on Optical Fiber Measurements, NIST Special Publication #792, pp. 59-62, 1990.
5. "Measurement of fiber strain in cables under tensile load", Proposed EIA/TIA Standard, FOTP-38
6. F. P. Mallinder and B. A. Proctor, "Elastic constants of fused silica as a function of large tensile strain", Physics and Chemistry of Glasses, vol. 5, No. 4, pp. 91-103, 1964.
7. A. J. Barlow and D. N. Payne, "The stress-optic effect in optical fibers", IEEE J. Quantum Electron., QE-19, No. 5, pp. 834-839, 1983.
8. I. H. Malitson, "Inter specimen comparison of the refractive index of fused silica", J. Opt. Soc. Amer., vol. 55, pp. 1205-1209, 1965.
9. Private communication from Hydro Quebec.

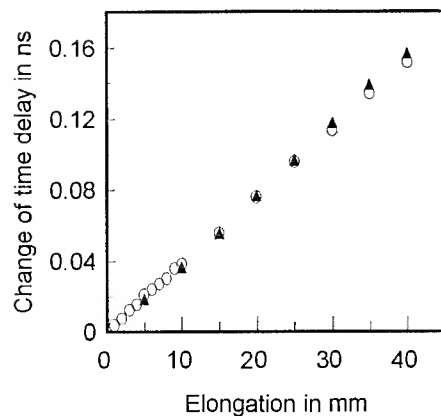


Fig. 1: dt vs. dL ; matched clad dispersion shifted fiber measured at 850 nm. \blacktriangle ; gauge length 1.34 m, \circ ; gauge length 12.71 m.

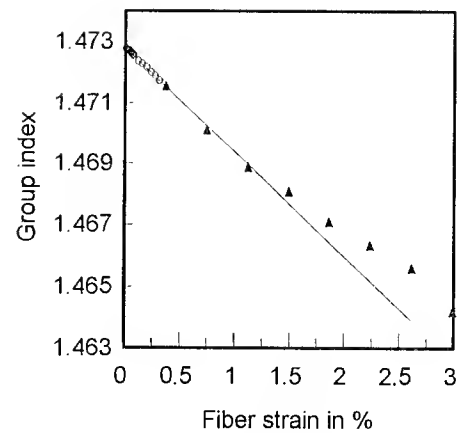


Fig. 2: N vs. strain; matched clad dispersion shifted fiber measured at 850 nm. \blacktriangle ; gauge length 1.34 m, \circ ; gauge length 12.71 m, —; linear fit to 0-0.3 % strain.

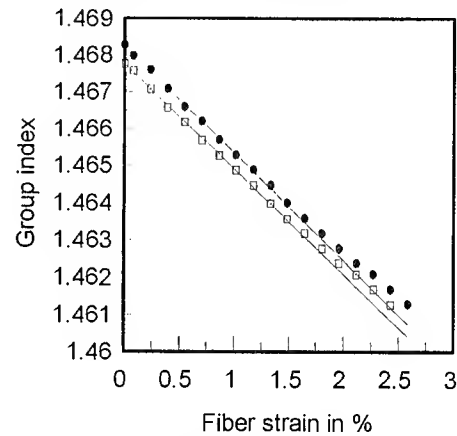


Fig. 3: N vs. strain; matched clad single-mode fiber measured at 1295 and 1532 nm. \square ; 1295 nm, \bullet ; 1532 nm, —; linear fit to 0-1 % strain.

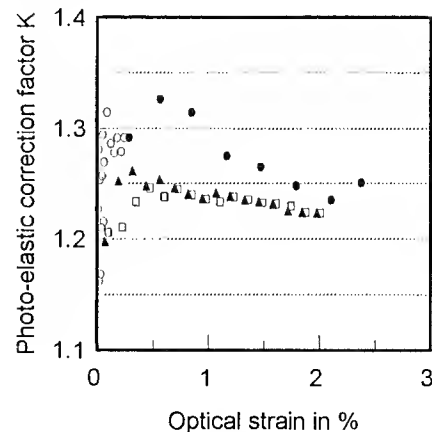


Fig. 4: K vs. optical strain. \circ ; depressed clad dispersion shifted fiber measured at 850 nm using the gauge length of 12.71 m. \bullet ; same as above except the gauge length of 1.34 m. \blacktriangle ; matched clad single-mode fiber measured at 1295 m. \square ; same as above except measured at 1532 nm.

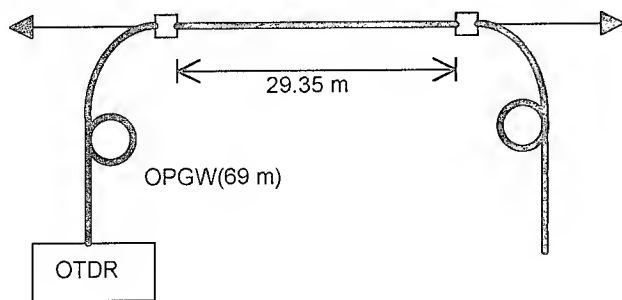


Fig. 5: Set-up for cable loading test

OPGW

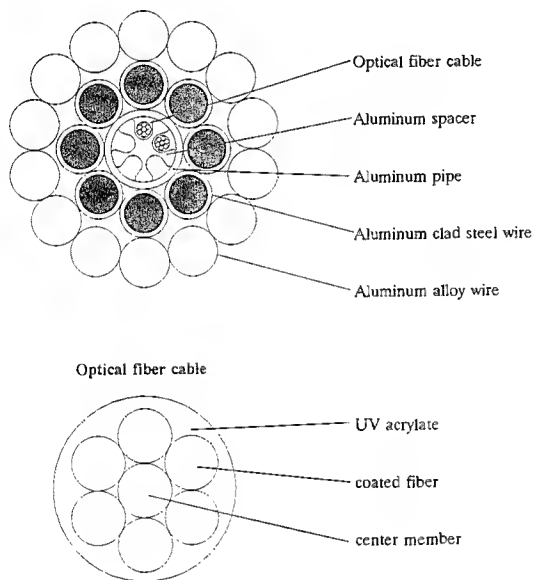


Fig. 6: Cross section of OPGW

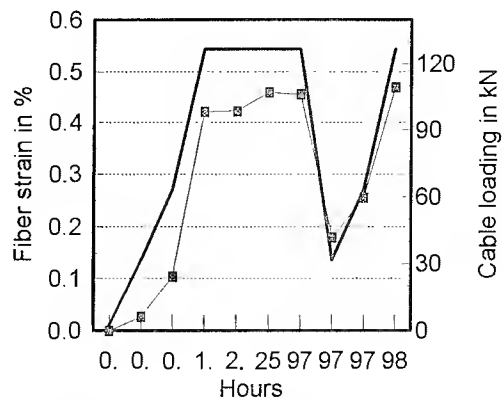


Fig. 7: Cable load and fiber strain; time evolution over 98 hours. —■—; fiber strain, —; cable loading

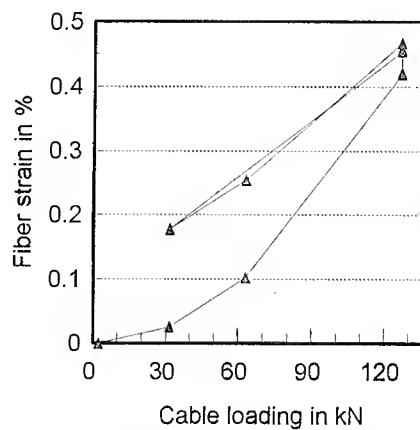


Fig. 8: Fiber strain vs. cable load

Table 1: Reported photo-elastic correction factor (K) for optical fibers

K	Fiber	Wavelength	Comment
1.33	MM	820 nm	Time delay method. Reference 1.
1.26	MM	?	Phase shift method, $N_o=1.48$ (assumed). Reference 2.
1.20	SM	846/1200	Time delay method. Reference 3.
1.22-1.23	SM/DS	1295/1532	Time delay method. Reference 4.
1.21	SM	1000-1300	Calculated from stress-optic coefficients. Reference 7.
1.40	DS	1550	Phase shift method. Reference 9.

Note: Fiber types MM, SM and DS designate multimode, single-mode and dispersion shifted fiber, respectively.

Table 2: Photo-elastic correction factor (K) and group index (N_0)

K	N_0	Fiber type	Wave-length	Gauge length	Max. strain
1.30	1.4728	MDS	850 nm	12.71 m	0.3 %
1.28	1.474	MSM	850	12.71	0.3
1.24	1.4663	DDS	850	12.71	0.3
1.30	1.460	DSM	850	12.71	0.3
1.26	1.4706	MDS	1532	50	0.60
1.26	1.4678	MSM	1295	50	0.55
1.26	1.4683	MSM	1532	50	0.55
1.23	1.4706	MDS	1532	50	2.6
1.22	1.4678	MSM	1295	50	2.4
1.23	1.4683	MSM	1532	50	2.6

Note: The designation of the fiber types is the following: MDS (matched clad dispersion shifted), MSM (matched clad single-mode), DDS (depressed clad dispersion shifted), and DSM (depressed clad single-mode). "Max. strain" is the maximum strain which was used to determine the K value.

AUTHORS



Koichi Abe
i/FO Technologies,
Ottawa, Ontario, Canada

He received Ph.D. degree in Chemistry in 1970 from the University of Tokyo, Japan. His involvement in fiber optics technologies started in 1974 when he joined Bell-Northern Research. He worked for Northern Telecom, Nokia Cables, and the National Optics Institute. Since 1992, he has been a consultant for the government of Canada and various industries who are involved in fiber optics and photonics technologies.



Koji Yoshida
Phillips-Fitel Inc.,
Scarborough, Ontario,
Canada

In 1969, he received B.Sc. degree in Electrical Engineering from Yokohama National University, Japan. In the same year, he joined The Furukawa Electric Co. Ltd. and worked on overhead transmission lines in the R&D division. In 1980, he was transferred to Bare Conductor Engineering Division and worked on the design, fabrication and characterization of wide

varieties of overhead conductors including OPGW. Since 1992, he has been with Phillips-Fitel Inc. as the VP Technology.



Omid Daneshvar
AT&T Fitel Co.
Carrollton, GA

Omid Daneshvar is R&D Manager at AT&T-Fitel Co. He holds B.S. and M.S. degree in Electrical Engineering from Georgia Institute of Technology. He joined AT&T-Fitel in 1985 and has since had responsibilities in the development of fiber optic

cables and measurement systems.



Jim Carr
Corning Inc.
Corning, N.Y.

Jim Carr received B.S. and M.A. degrees in physics from the State Univ. of New York in 1976 and 1979. He was Assistant Professor in the Dept. of Engineering and Physics at Monroe Community College, Rochester. In 1985 he joined Corning Inc. as a Senior Product Engineer working on qualification and specification of optical fiber products. In 1990 he moved to the Center for Fiber-Optics Testing as a Project Team Leader where he developed a laboratory for mechanical reliability testing and experimentation with mechanical effects on the optical performance of fiber.

LONG-TERM OPERATING EXPERIENCE OF LARGE DIAMETER FLEXIBLE COAXIAL CABLE IN HIGH-POWER BROADCASTING STATIONS.

Manfred Franz
Kabelmetal Electro GmbH
Postfach 260, 30002 Hannover, Germany

Gerhard Schweiger
German Bundespost TELEKOM
Am Kavalleriesand 3, 64295 Darmstadt, Germany

Dimitri R. Stein
Cable Consultants Corp.
7 Woodland Avenue, Larchmont NY 10538

Summary.

This paper reviews the operating experience of coaxial cables designed for the transmission of large amounts of high-frequency power (with outer diameters up to 12 in.). The cable consists of a welded and corrugated inner conductor, dielectric spacers and a welded and corrugated outer conductor. The major advantage of this design lies in its flexibility and in the fact that it can be produced in long continuous lengths, limited only by the reel capacity. Since the early 1970s over 400 km of this cable have been put into service for broadcast and TV stations operating in frequency ranges up to 900 MHz. Mechanical and electrical design specifications are reviewed and the operating experience analyzed.

Introduction.

A review of the high-frequency power of broadcast transmitters over the past several decades shows a steady increase until about 1970. Since then the power output (Table 1) has not increased significantly.

Frequency Range:	Max. Transmitter Power:
Long wave band (LF) 150 - 285 kHz	2,000 kW carrier power
Broadcast band (MF) 525 - 1605 kHz	1,000 kW carrier power
Short wave band (HF) 5.95 - 26.1 MHz	500 kW carrier power
Television (VHF/UHF) 174 - 960 MHz	2 x 40 kW sync. peak power

Table 1 High-Frequency Power of the most powerful Broadcast Transmitters around the Year 1970

The increase in the transmitter power rendered necessary the development of low-loss high-power antenna feed cables. A new kind of high-frequency coaxial cable was developed during the 1950s as an outgrowth of the family of power and communications cables, based on the "Wellmantel" (welded and corrugated sheath) technique. The outer conductors (in the case of larger dimensions also the inner conductors) of these cables were fabricated from thin-walled, longitudinally-welded, corrugated tubes. These new cable types started to replace existing, conventional cables as well as cables built from short sections of rigid lines. The latter exhibited the typical disadvantages associated with this type of cable (numerous connections, thermal expansion problems due to temperature changes, problems with imperviousness, costly installation).

A technology related to the multi-section rigid coaxial line concept was recently described in a paper presented at the 1993 IWCS ¹. It deals with a semi-flexible high-frequency transmission line built up of many 11.58 m (38 ft.) sections using corrugated instead of rigid tubes. By contrast, the cable described in this paper can be made in long continuous lengths, limited only by the capacity of the take-up reel at the end of the manufacturing line or by the size restrictions for the transport of the cable reel.

For the new cable design a number of technical parameters had to be considered in addition to low attenuation and high structural uniformity to meet the transmission requirements. Other factors, such as thermal problems (losses and heat dissipation) and electrical problems (voltage strength, partial discharge, leakage currents) had to be taken into

account in increasing measure. Moreover, since the transmission lines were operated at substantial internal pressures, mechanical strength and gas tightness were of paramount importance.

To meet these requirements novel approaches had to be developed both with regard to the basic cable design as well as to the materials used and the manufacturing techniques employed. This work culminated about 1970 in the development of a high-power coaxial cable with an outer diameter of 312 mm (12.28 in.)².

An overall consideration was to ensure that the proven long-term reliability of existing cables would be equal to that of the newer high-frequency cables with increased power rating. The reliability of this high-power cable has proven itself in the field: in excess of 400 km (249 miles) in the 6 in., 8 in. and 9 in. dia. dimensions have been in operation for the last dozens of years.

A purpose of this paper is to document the long-term behavior of high-frequency power cables. A typical case study is represented by the HF9'-S AL cable type at the Wertachtal transmitting Center of the German Telekom. This is a particularly good example because of the unusually large scale of this installation, operating at a very high transmitted power rating which called for a rather unconventional cable design. Last but not least we should mention that this installation has been in operation in excess of 20 years.

We shall describe the transmitter before presenting the high-frequency cable installation. In so doing we shall dwell in greater detail on the cable for the benefit of the operational experience gained along with the inherent reliability concept on which this development was based.

The Wertachtal Broadcast Transmitting Center.

The Wertachtal Transmitting Center was erected by the German Bundespost during 1969 - 1972 in the foothills of the German Alps, 40 km southwest of Augsburg. This new transmitting center became necessary because the other existing centers of the "German Welle" (Worldwide Broadcast Service of the German Federal Republic) were no longer adequate.

When it was commissioned, the Wertachtal Transmitting Center included the following ancillary systems:

- 12 shortwave transmitters (5.9-26.1 MHz) with 500 kW carrier power;
- 74 antennas, mostly directional curtain antennas with fixtures for shifting the main beam direction by $\pm 30^\circ$.
- 53 km (33 miles) type HF9'-S AL high-frequency power cable

in addition to an antenna matrix switch unit with 12 inputs and 76 outputs that permitted coupling each transmitter to each antenna. This makes the Wertachtal Center the largest broadcasting center in the Western world. Fig. 1 illustrates the general transmitting center concept.

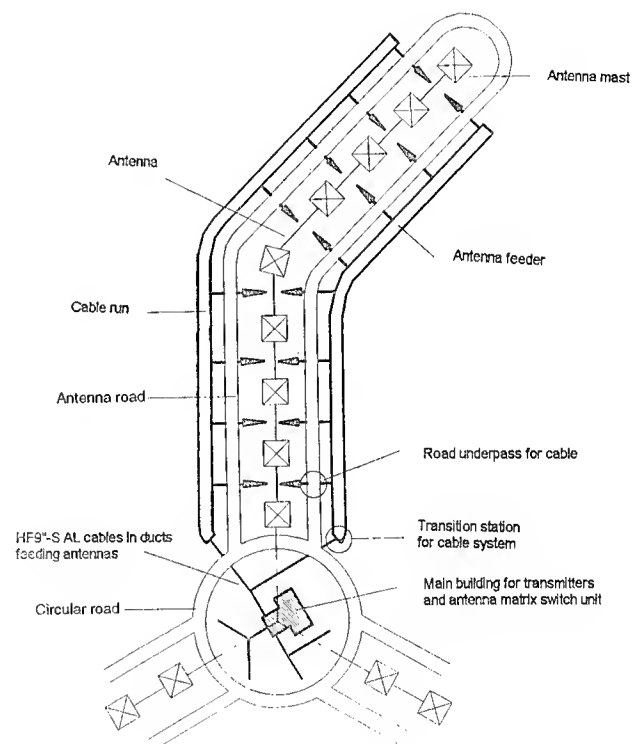


Fig. 1 Schematic Representation of the Wertachtal Transmitting Center.

The main building is located in the center of the complex. It houses the transmitters and the antenna matrix switch unit. The cables to the individual antennas originate from here.

The antennas are arranged in the field on each side of a three-pointed star. The antenna walls which are located at a 120° angle with respect to each other have a length of about 1.9 km (1.2 miles). They feature a bend along their path (Fig. 1). For a detailed description of the Wertachtal transmitter we refer to ³.

Properties:	Values:
Characteristic Impedance	50±1 ohms
VSWR [1.9 km (1.2 mi.) cable @ 5.9 - 26.1 MHz]	≤ 1.1
Max. Operating Frequency	26.1 MHz
Carrier Power	500 kW
VSWR (Antenna connected)	
continuous	≤ 2
intermittent	2.2
Modulation factor	
average, continuous	60%
intermittent	105%
Max. environmental Temperature	35°C

Table 2 Specified Properties and operational Requirements of the High-Frequency Power Cable.

The High-Frequency Cable System of the Wertachtal Transmitting Center.

The High-Frequency Power Cable, its Specifications and Design.

The requirements for the high-frequency power cable were based on the specified properties and operational requirements of the German Bundespost (Table 2).

The figures given in Table 2 reflect, under worst-case conditions, the following load on the cable:

$$P(\max) = 1,180 \text{ kW at } V(\max) = 21.5 \text{ kV} \quad (1)$$

wherein:

$P(\max)$ is the average power within a local current peak (a measure of the heat build-up in the cable);

$V(\max)$ is the peak voltage value at a local voltage maximum with maximum modulation.

(For a description of the general relations between cable design, operational conditions and load capacity of high-frequency power cables we refer to ².)

High-frequency cables for such demanding requirements did not exist anywhere at the time. This led to the development of a new, especially designed cable for this project. Foremost consideration during all stages of design, planning, production and installation of these cables was the goal to achieve for long-term, reliable and failure-free operation.

An important step toward this goal was the decision to avoid, as much as possible, the introduction of components that could become possible sources of failure, such as mechanical contacts and seals. Therefore, a welding technique instead of the conventional clamping technique was implemented. This was also a reason for maintaining the cable diameter as small as possible: the smaller the diameter, the greater the length of cable that could be accommodated on a shipping reel of a given size. In order to enhance the heat loss dissipation while maintaining the voltage strength, it became necessary to increase the operating temperature and internal over-pressure of the cable. We selected Teflon® as insulating material for the spacer which centers the inner conductor. The material for the outer conductor was a 2.5 mm (.098 in.) thick AlMn strip.

Fig. 2 illustrates the cable design. The three Teflon® support arms of a spacer are mounted on an open metallic spring-loaded ring. This feature enabled us to reduce to a strict minimum the quantity of the required insulating material needed for centering the inner conductor.

The main technical characteristics of this cable are listed in Table 3.

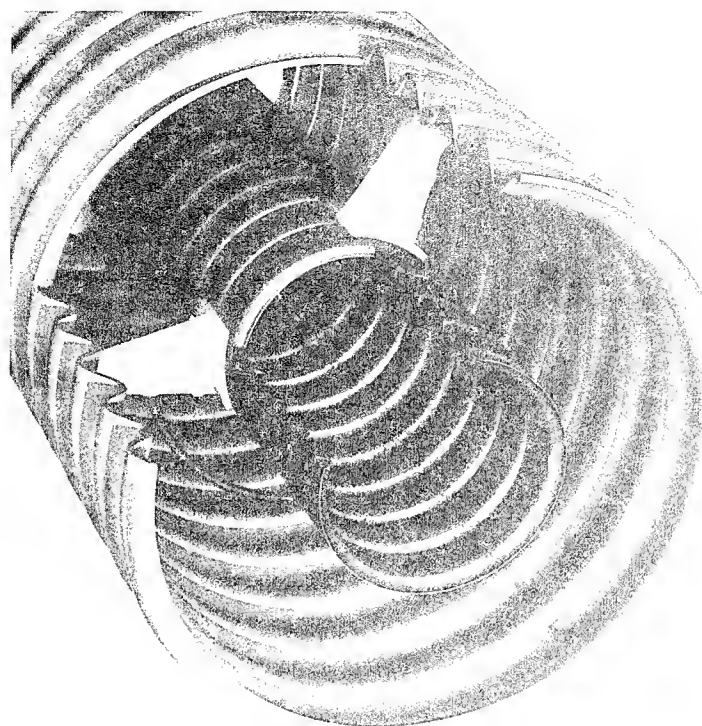


Fig. 2 Cable Type HF9"-S AL

Parts or Properties	Dimensions or Values
Cable Design	
Inner Conductor: corrugated copper tube	99 mm (3.9 in.) dia.
Spacer Material: Teflon®	217 mm (8.54 in.) dia.
Outer Conductor: corrugated aluminum tube	246 mm (9.7 in.) dia.
Outer Protection: protective coating (applied after installation)	
Mechanical Properties	
Max. admissible Overpressure	5 bar
Max. recommended Filling Pressure	4 bar
Minimum Bending Radius	3,000 mm (118 in.)
Electrical Properties	
Characteristic Impedance	50±0.5 ohms
Attenuation (@ 26.1 MHz, 20°C)	0.77 dB/km
Max. admissible High-Frequency Voltage	24 kV (@ 1.0 bar) 42 kV (@ 2.4 bar Absolute filling pressure in actual operation)
Max. admissible Input Power	
	1,230 kW (@ 26.1 MHz/40°C/1.0 bar) 1,600 kW (@ 26.1 MHz/40°C/2.4 bar)

Table 3 Technical Characteristics of Cable Type HF9"-S AL

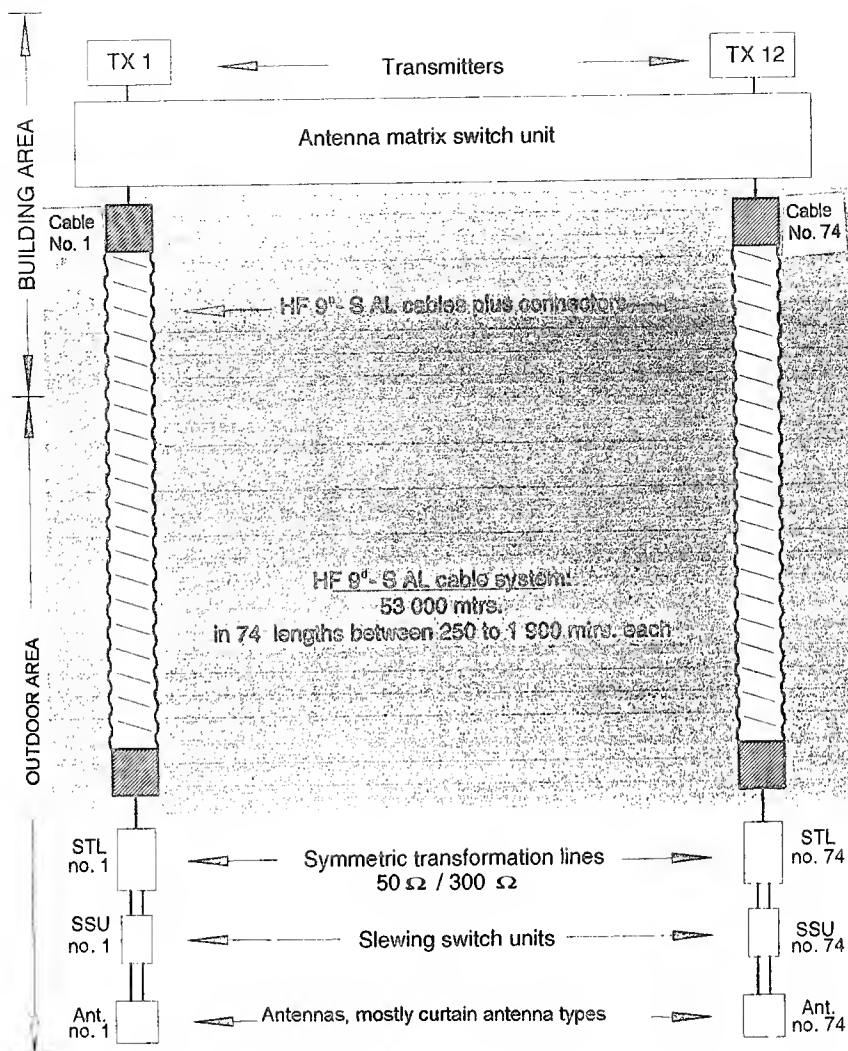


Fig. 3 Schematic Layout of Wertachtal HF9"-S AL Cable System

Installation of the High-Frequency Power Cables.

The overall cable length of the system at commissioning time was 53 km (33 miles) in individual lengths of 180 m (590 ft.). These were assembled into 74 runs of 1,900 m (6,234 ft.) max. length (Fig. 3). Individual cable lengths were shipped on reels with 3 m (9.84 ft.) core dia. and 4.5 m (14.76 ft.) flange dia. During installation the inner and outer conductors of adjoining cable sections were welded together in an inert gas atmosphere. Special weld couplings were developed for this application (Fig. 4). The same welding technique was equally used for the terminations of the 74 individual runs. The only seals required were located at the ceramic spacers of these connectors.

The individual cable runs are routed out of the basement from underneath the antenna matrix switch unit through six underground walk-through channels (Fig. 5) to transition stations. From here on the cables are run outside in parallel, about 0.7 m (2.3 ft.) above ground, on both sides of the antenna walls. They leave the common route, one after the other, in open ducts to terminate at the symmetric transformation lines of their respective antennas (Figs. 5 and 6). Over the length of their exterior run the cables are covered with concrete plates for protection against icing and direct exposure to the sun.



Fig. 4 View of a Cable Coupling for Type HF9"-S AL Cable during Installation

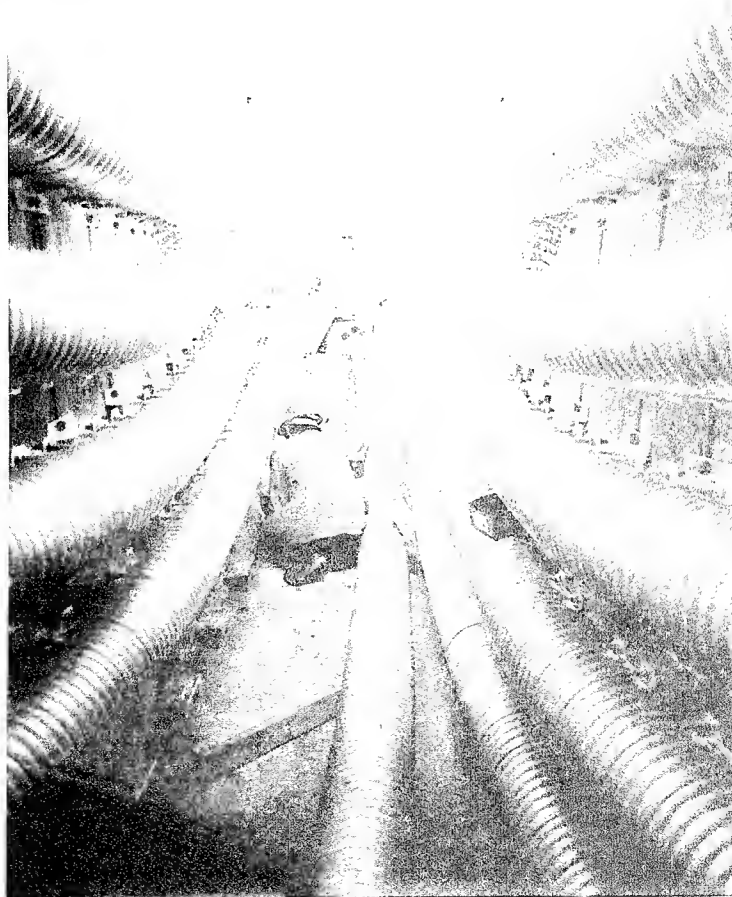


Fig. 5 Transition of HF9"-S AL Cables from vertical to horizontal Runs

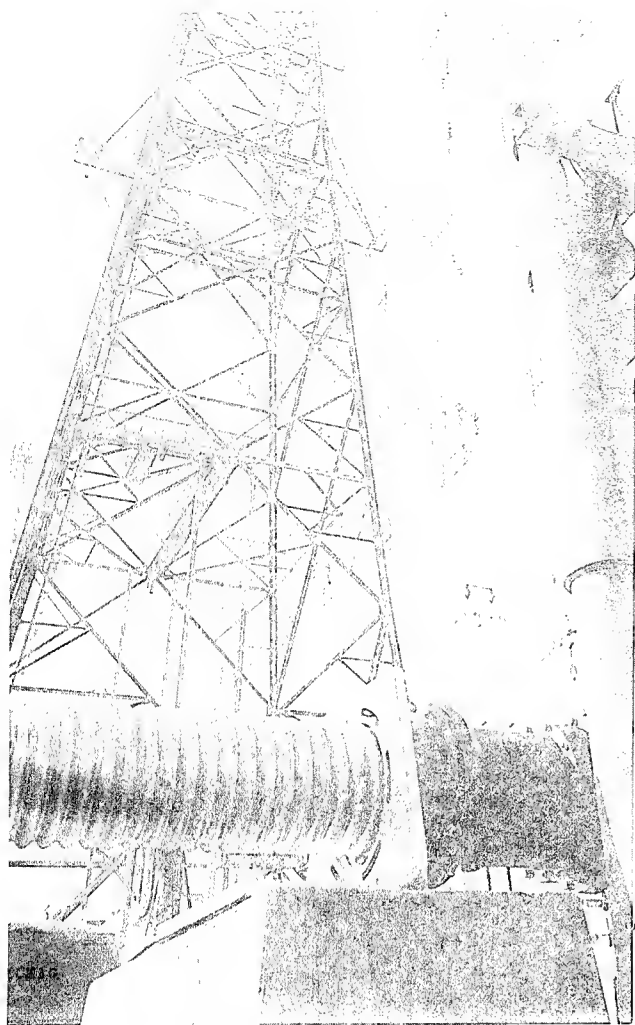


Fig. 6 HF9"-S AL type Cable connected to Coaxial/Symmetric Transformation Line.

Compressed Air Supply.

Dry air is used as the pressurized gas for increasing the power rating and for monitoring the integrity of the cable runs. The compressor is located in the basement under the antenna matrix switch unit. Its capacity is 88 Nm³/h which meets the requirements of the Bundespost: max. 4 hrs. fill time for a 1.5 km (.93 mi.) long cable run.

To ensure the long-term operational life of the cables it is important that all traces of humidity, oil, dust or other foreign matter be reduced to the absolute minimum. This is a significant requirement which was carefully considered in the planning of the compressor station. Thus, for example, the dew point of the compressed air lies at -40°C. The dew point is monitored by the computer of the station.

Each individual cable run has its own monitor which includes a cut-off valve, a magnetic valve, a flow regulator, a spring-loaded check valve and a safety valve. In case the monitor detects a pressure drop in excess of 0.2 bar with respect to the nominal operating pressure, it will automatically supply a limited air flow into the cable until the nominal pressure is once again attained.

The incident and its duration are recorded by the station computer so that irregularities that may lead to later problems may be recognized in time. In the event of substantial leakage if the pressure drops even further, the transmitter turns itself off once the minimum required pressure is reached. It is possible to bypass the flow regulator for the purpose of a rapid fill.

Operating Experience.

The Wertachtal Transmitting Center has already exceeded two decades of operation. This corresponds to the equivalent expected life time of a cable. What can we say about the behavior of the cables? The following influences and properties which are significant for the long-term reliability, such as fatigue or aging effects, will be considered:

- Overall operating time;
- Mechanical and thermal load factors;
- Corrosion;
- VSWR;
- Voltage strength;
- Attenuation;
- Gas tightness;
- External factors, miscellaneous effects.

Overall Operating Time.

Table 4 reflects excerpts from the statistics for the years 1993/94 of the broadcast station. These may be considered to be representative for the total operating life.

Mechanical and Thermal Load Factors.

We describe here the basic load factor which is modulated by a variable load factor (as a function of operating cycles and environmental temperature variations). This is particularly important for the effect of the internal over-pressure on the weld seams in the cables and on the spacers in the connectors that terminate the individual cable runs. No destructive changes to these parts have been noticed. The effects on the leak rate are described further below.

Operating Experience per Cable Run (over a 22-yr. Period):	Minimum:	Average:	Maximum:
Operating time (years)	0.6	4.1	16.6
Switching frequency (cycles)	8,000	21,700	56,200

Table 4 Operating Statistics of Cable Runs, excerpted from the Operating Records of the Wertachtal Transmitting Center.

The spacers are subjected to temperature cycling. It is possible for the surface temperature of the inner conductor to reach 140°C. Any change of the Teflon® spacers due to aging which could result in the inability of the springs to maintain their concentric position could have serious consequences (voltage breakdown - see further down).

An additional mechanical load is exerted on those of the approx. 200,000 spacers which are located in cable bends. These must resist radial forces in order to maintain the inner conductor in its centered position. Any weakening of the insulating spacers under the effect of these forces would cause the inner conductor to approach the outer conductor, risking a short-circuit.

Finally, it is possible for the outer surface of the cable to rub against its retainers (i.e.: clamps) in such fashion that the protective coating may locally be rubbed off. This could lead to corrosion of the aluminum outer conductor.

Corrosion.

Aluminum which is exposed to the elements without protection will corrode. For this reason (and for improved heat exchange) all cables have been covered with a double layer of protective coating. The externally-located part of a cable run which was exposed to the elements revealed weathering and peeling off of the coating. A new coating will be applied. We did not observe any corrosion damage to the outer conductors.

VSWR.

Changes in the geometry of the cable (conductor warpage, shifting of the spacers, excursion of the inner conductors from their centered position in cable bends) affect the characteristic impedance and VSWR of the cable. The VSWR of the cable runs was measured prior to commissioning. A typical example of the VSWR in the 5.9 to 26.1 MHz frequency range is shown in the acceptance test report of a long cable run (Fig. 7).

In principle, it is possible to establish any changes in VSWR through a renewed measurement. Since there was no reason up to now to go through this trouble (the cables would have to be disconnected at both ends) these data are not available. On the other hand, we can state that during operation the monitoring of the VSWR of the cables connected to the antennas have not revealed any abnormalities that could have pointed to changes in the cables. We therefore draw the conclusion that no noticeable variation of the characteristic impedance in the cables has occurred.

Voltage Strength.

Maintaining the voltage strength is of particular importance for the operational safety of the transmitter. Should a flash-over occur during operation, the cable would certainly be destroyed in the vicinity of the flash-over point, requiring the replacement of a short cable section.

The individual cable runs were tested prior to commissioning with 1 bar pressure at 40 kV DC. This corresponds to about twice the value of $V(\max)$, the peak value of the highest expected voltage stress. The pressure during operation is 2.4 bar. This permits an increase of the allowable operating voltage by a factor of 1.75 (Table 3). We therefore achieve a safety factor of about 2 with respect to $V(\max)$.

According to reports from the operating staff, the system has not experienced any flash-over in a cable up to this time. Also, no defects in a cable have been detected nor has there been any flash-over in a cable as a result of emergency shutdowns following arc-overs in an antenna - a potential cause for voltage surges.

This positive experience confirms the validity of the design, considered rather revolutionary at the time, which called for the inclusion of a metallic spring within the high-voltage field between two conductors to connect the three support elements of a spacer.

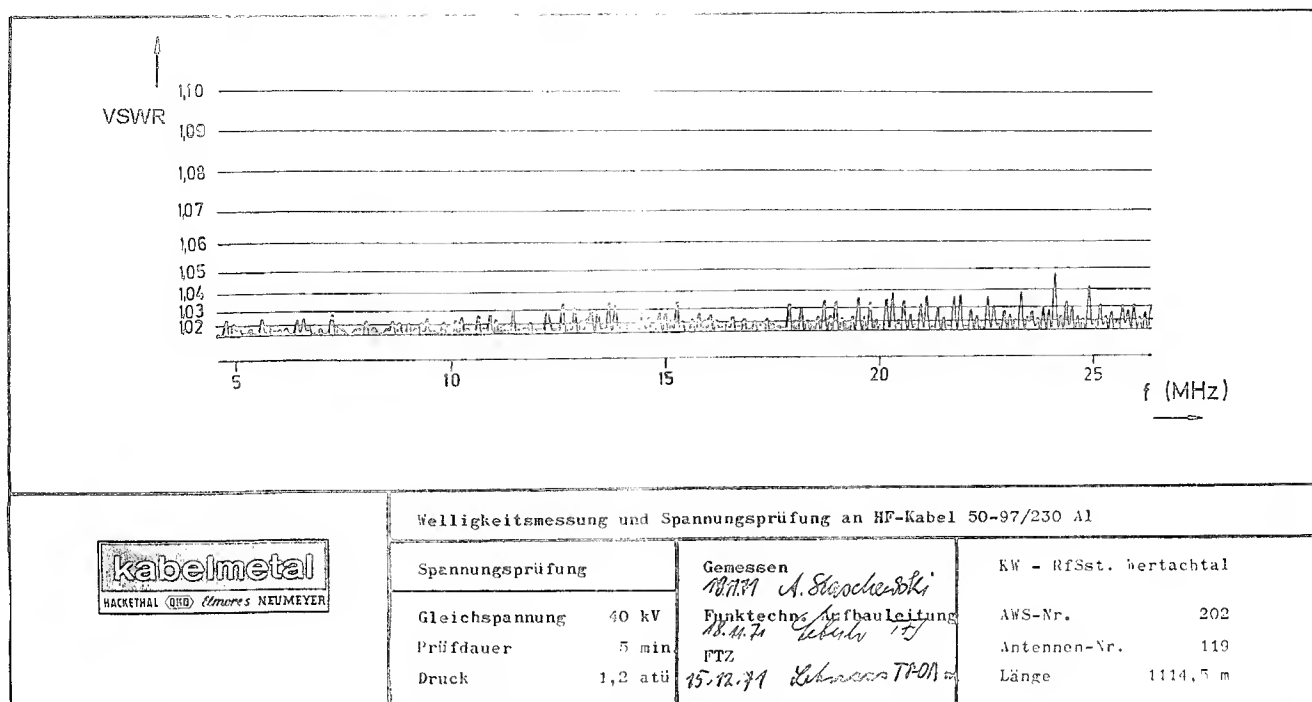


Fig. 7 VSWR Measurement and High Voltage Test on a Type HF9"-S AL Cable

Attenuation.

Increased attenuation would be indicative of aging of the insulation material of the spacers. The only information available for attenuation is the result of prototype testing. No additional measurements were made. We therefore have no further data.

Gas tightness.

Complete and permanent gas tightness of the cables was a basic consideration for setting pressure level thresholds in the monitors. The following events are programmed:

- transmitter power interruption;
- gas backfeed occurrence;
- gas backfeed interruption;
- max. operating pressure occurrence;
- safety valve actuation.

The pressure levels are attuned to each other in such a fashion that the safety valves will not actuate or that the pressure drop will reach a level that will cause the transmitter to be disconnected, even under extreme conditions. Any and all noticeable air consumption is a reliable indicator of leakage under these conditions. According to the transmitter operating staff, no consumption of air due to leakage has ever been recorded in their entire operating experience.

Of course, repeated demands are made on the compressor unit during maintenance and repair work. This requires disconnecting cable runs with subsequent rinsing and filling. Another occasion was the enlargement of the transmitter facility in 1990. During the course of this kind of activity which required separating the connection between cable and STL (Fig. 6) we noticed, in a few cases, minor damage to the spacer disks in the connectors. We assume that this was the result of the mentioned intervention and we replaced the spacer disks as a precautionary measure. Of course, this required bleeding the air in the cables and refilling them.

External Factors, Miscellaneous Effects.

There were only two incidents during the entire operational life of this installation, as far as we could determine, in which cables were damaged during construction work. In one case, a concrete plate, while being raised, fell on a cable. This caused the outer conductor to be deformed to the point where repair became necessary. For the repair the cable was cut at the point of failure and both ends were joined with a welded coupling. Provided that the required tools, spare parts and expert technical personnel are on hand, this kind of repair can be carried out in one day.

In the second case, several adjoining cables were damaged by a backhoe. The resulting damage, however, was less severe than in the first case. Repair of the damage was not necessary; the cables continue in operation.

Conclusion.

The advent of broadcast transmitters with ever-increasing power throughout the world required the availability of high-frequency cables of increased dimension and higher load capacity for feeding the transmitting antennas. This development was essentially concluded in the years after 1970.

After two decades of operating experience with this unique design combining features of communications and high-voltage cables, it is instructive to review the performance record of the cables. The Wertachtal Broadcast Station of German Telekom is a perfect test case for this purpose.

The Wertachtal transmitter was commissioned in 1972 with 12 ea. 500 kW short-wave stations, 74 antennas connected by 53 km (33 mi.) of the type HF9"-A AL high-frequency power cable. This paper reports on the considerations given to the design and planning of the cable system with a view to operational safety and long-term operating reliability and how these factors have proven themselves over the years.

The information gained from this large-scale installation confirms its reliability and the soundness of the cable design meeting all technical and maintenance requirements. The installation continues to function properly. There is no end in sight for the economic and technical viability of the system. Here is a rare instance in cable technology where a high-power high-frequency cable developed in the 1970s still today represents the state-of-the-art.

References.

1. "A new High-Power Segmented semi-flexible Coaxial Transmission Line for use at HF". H. R. Nudd. Proc. International Wire & Cable Symposium 1993.
2. "High-Power Radio-Frequency Coaxial Cables; Their Design and Rating". H. Martin. Proc. International Wire & Cable Symposium 1973.
3. "Die Kurzwellen-Rundfunkstelle im Wertachtal". H. Krath, B. Alt, W. Burckhardsmaier, P. Bruger, G. Langel, E. Ossendorf. Jahrbuch des elektrischen Fernmeldewesens 1973.



Manfred Franz
Kabelmetal Electro GmbH
Postfach 260
30002 Hannover, Germany

Manfred Franz was born in 1934. In 1959 he graduated from the Technical University, Berlin, with a degree in communications engineering (Dipl.-Ing.). He joined Kabelmetal Electro in 1966. Since that time he has worked in the Kabelmetal Radio Frequency Division. When the Wertachtal Project was launched in 1970, he was appointed special project manager. Subsequently, he occupied the position of sales manager responsible for both domestic and export sales. Currently, he is senior sales manager for special programs.



Gerhard Schweiger
Deutsche Bundespost Telekom
Am Kavalleriesand 3
64295 Darmstadt, Germany

Gerhard Schweiger received his masters degree in electrical engineering from the Technical University, Munich in 1957. He joined Deutsche Bundespost Telekom in 1958. Since 1966 he has been located in the Technical Engineering Center (FTZ) in Darmstadt. He is currently the head of the Outside Plant Division.



Dimitri R. Stein
Cable Consultants Corp.
7 Woodland Avenue
Larchmont NY 10538

Dimitri Stein is a director of Kabelmetal Electro GmbH, Hannover, Germany and, since 1962, president of Cable Consultants Corp., Larchmont NY. He holds a graduate degree in electrical engineering from the Technical University, Berlin, Germany. He is the author or co-author of numerous papers on cables and cable technology and a senior life member of the IEEE.

Shielding Effectiveness of Coaxial Drop Cable and Simulated Aging by Flexure

By: Joe Elko, Terry McAlister, and Kevin Gantt

CommScope, Inc
General Instrument Corporation

Abstract

The electrical property that enables RF signals to propagate through coaxial cables unaffected by outside interference is shielding. The effectiveness of a shield is completely dependent on the outer conductor. In drop cables this consists of a multi-layered conductive tape in conjunction with a metallic wire braid. Most of the high frequency shielding is achieved as a result of the conductive tape. Over time, stresses induced by flexure cause this tape to develop radial cracks that decrease the shielding effectiveness of the cable. Because of this, simulation in the laboratory is necessary to predict, thus anticipate this change. The device used to simulate flexure must be severe, and apply equal stress to the entire perimeter of the cable. When considering shielding effectiveness values, data taken after flexing should be evaluated.

Introduction

Many changes are in store for the telecommunications industry. From interactive video services to telephony, the information highway is under construction. Full service networks using digital compression are already being evaluated in test trials. Along with these new services comes additional concerns for system performance. Digital transmissions are very tolerant of noise, but if affected, the result can be catastrophic signal loss. This is in contrast to analog signals where noise causes distortion

but the signal is not lost. The original function for coaxial drop cable was to carry television video and audio. While interrupted service was not welcome, it was not life threatening. At most it was a nuisance. Now that many new system designs are planning to offer full service, including telephony with 911 service, system reliability will be paramount.

The final link of most all proposed broadband multimedia network architecture's is the drop cable. This cable must be flexible, durable, yet maintain the desired electrical performance over time.

In the field, cables experience an environment of wide temperature variations, wind and ice loading, and stress inducing movements caused by the wind. When properly installed the drop cable will maintain all of the electrical characteristics, with the exception of shielding effectiveness. Field studies have shown that shielding effectiveness degrades over time on cables that have been installed aerially.⁽¹⁾

The field samples used for this report were messenger and non-messengered cables that were installed aerially. Installing non-messenger cable aerially is not a recommended practice, but one that occurs regularly. In terms of shielding effectiveness, a non-messengered cable installed aerially may represent the worst case scenario. A field study was completed to obtain a basic view of shielding effectiveness in aged cables. A more detailed characterization of shielding

effectiveness degradation that examines the many variables present in aerial drop cable spans is necessary.

Several techniques for accelerating fatigue by mechanical flexure have been used in the cable industry. This paper focuses on the rotary flexer as it has been shown to produce shielding effectiveness degradation similar to that observed in the field. A direct correlation of shielding effectiveness degradation induced by simulated aging, to actual field aging, is not practical without more data. It is however, a very useful tool for cable to cable comparisons and for material and process variations.

Drop Cable Design

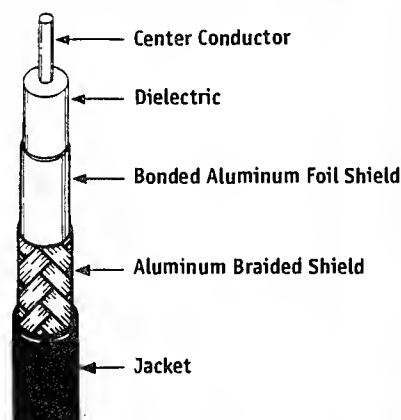
Coaxial drop cables are manufactured in various standardized sizes, each size having several construction variations. They range in size from approximately 0.240 inches (6.096 mm), to 0.405 inches (10.287 mm) in outside diameter. The major advantage gained with increased size is lower attenuation values.

The general construction of coaxial drop cable is a center conductor, usually surrounded by a foamed polyethylene dielectric. The center conductor is usually coated with a precoat material to aid in corrosion prevention, and to insure complete and easy removal of the dielectric material when preparing the cable for a connector. The foamed dielectric is then surrounded by a laminated shielding tape. This tape is generally comprised of two layers of aluminum foil laminated to a strength member. This first shield is usually bonded to the dielectric to better withstand the fatigue of the foil tape associated with flexing. This is followed by a conductive braid, generally made of aluminum, to aid in electrical shielding and to add structural support. The braided core is then covered with a PVC or PE jacket for protection. All of these variations are also

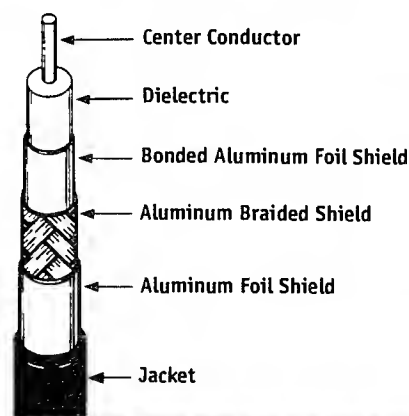
available with steel messenger wires for aerial applications.

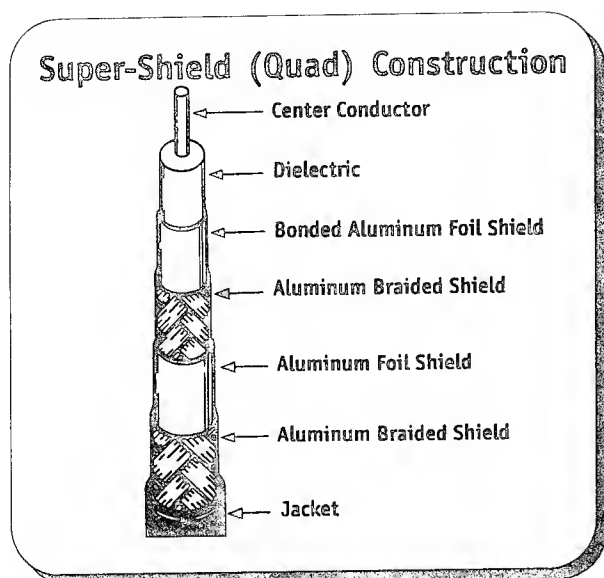
The major variations within cable sizes are found in the shielding configuration. Standard shielded cables have one layer of laminated tape and one layer of braided wire. Still within the realm of standard cable construction, the braiding variations are typically available from 60% to 95% coverage. The advantages of larger braid coverages are electrical shielding, mechanical strength, and lower DC resistance. Tri and quad shield variations are also available with various braid coverage's. Tri-shield cables have a second laminated shielding tape over the braid, and the quad-shield cables have a second layer of braid over the second tape.

Standard Shield Construction



Tri-Shield Construction





The various construction differences offer a tradeoff between flexibility, cost, and electrical performance. The end result is to produce a cable that is flexible and durable, yet possesses and maintains the desired electrical performance.

Aerial installation

Aerial drops are typically messenger cables, installed by attaching the messenger wire at the pole and at the house using various types of hardware designed for this purpose. In this case, the weight and tension of the cable is largely supported by the messenger wire. Although aerial installation without a messenger is not recommended, many drops have been installed in this manner. There are several clamping devices that are designed to support non-messenger cables. In these instances the stress from some types of these cable clamps have been noticed to cause deformations in the dielectric and the outer conductor that result in impedance discontinuities. Drop cable spans generally vary in length from 50 to 150 feet. Variables like tension, span length, climate, exposure to wind, installation practices, and other environmental

factors, make it impractical to predict with any certainty, shielding degradation over time.

Effects of Environment

It can be shown that under certain conditions as in NESC heavy loading districts, drop cables can experience strain from 0.25 to 0.50 percent.⁽²⁾ Most of this strain is from the effects of ice and wind loading. These forces were derived under static conditions, however it can also be shown that aerial drop cables are not static but will sway and flex in the wind. Samples of drop cable collected from aerial installations in the field exhibited small radial cracks in the aluminum shielding tape. The decrease in shielding effectiveness of the aged samples can be linked to these small radial cracks. The cracks can terminate current densities and scatter electromagnetic energy.

Shielding Effectiveness Study

A field study was conducted. Several samples of F59 with 67% braid coverage drop cable were obtained from a system in North Carolina. The age of the samples were approximately 10 years old. The messengered samples were F6 and F59 and were obtained from a system in Florida. The age of the messengered samples were approximated at 5 to 10 years old. The shielding effectiveness of the samples was determined using a triaxial transfer impedance chamber.

Methods of measuring transfer impedance have been adequately treated in several papers, thus a simple generalization will be offered here.⁽³⁾ The triaxial transfer impedance method is a technique that measures longitudinal currents on the outer surface of the shield induced by currents on the inside surface of the shield. This method produces a dB value that represents the difference

between the energy propagating inside the cable and the energy received by a probe positioned on the outside of the cable's outer shield. This value is a direct result of the outer shield's ability to contain electromagnetic energy.

A wide range of shielding effectiveness was noticed in the non-messengered field samples. They ranged from 100 to 60.7 dB in shielding effectiveness. This is understandable when one considers the many variables involved with cables installed in the field.

Some of the variables are as follows. The triaxial chamber used to measure the shielding effectiveness is only one meter in length. The section cable being measured may have been from the center of the span, or near the hangers and experienced much less movement. Many other variables exist from span to span including length, temperature, orientation to prevalent wind direction, tension, and other factors.

The shielding effectiveness of the messenger samples are listed in Table 1 below.

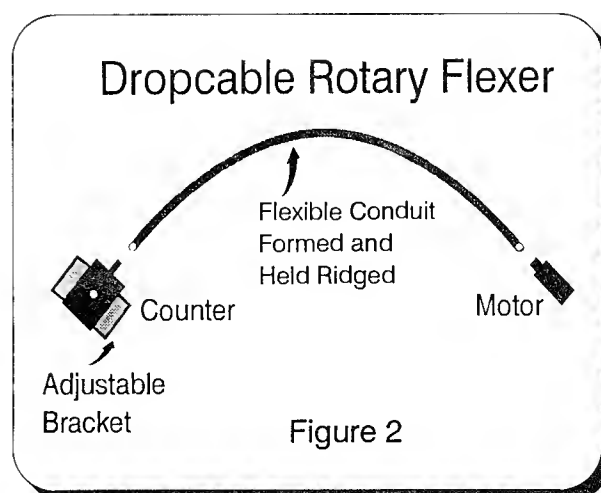
Shielding Effectiveness of Messenger Samples		
Description	Braid Coverage	Average dB
F 59 Messenger	67%	80.5
F 6 Messenger	60%	79.6
F 6 Messenger	60%	82.1

Table 1

Shielding effectiveness measurements of various typical drop cable shield configurations were made using the triaxial transfer impedance method and are listed in Table 2. The flex fatigue was achieved using the rotary method described in Figure 2.

Typical Drop Cable Shielding Effectiveness Range		
Description	Unflexed dB	Flexed 10K Revolutions
59 Series 40% Braid	65-75	55-65
59 Series 67% Braid	90-100	80-90
59 Series 95% Braid	95-105	85-95
59 Series Tri-shield	100-110	90-100
59 Series 77% Tri- Shield	105-115	90-100
59 Series Quad-Shield	105-115	100-110
6 Series 40% Braid	65-75	55-65
6 Series 60% Braid	80-90	70-80
6 Series 90% Braid	85-95	75-85
6 Series Tri-Shield	105-115	80-90
6 Series Tri-Shield 77 %	105-115	85-95
6 Series B Shorting Fold	105-115	85-95
6 Series DFBO	105-115	90-100
6 Series Quad-Shield	110-120	95-105
7 Series 60% braid	70-80	55-65
7 Series Tri-Shield	100-105	60-70
7 Series Quad-Shield	105-115	75-85
11 Series 60% Braid	80-90	45-55
11 Series 90% Braid	90-100	70-80
11 Series Quad-Shield	100-115	80-90

Table 2



Simulated Fatigue Flexing

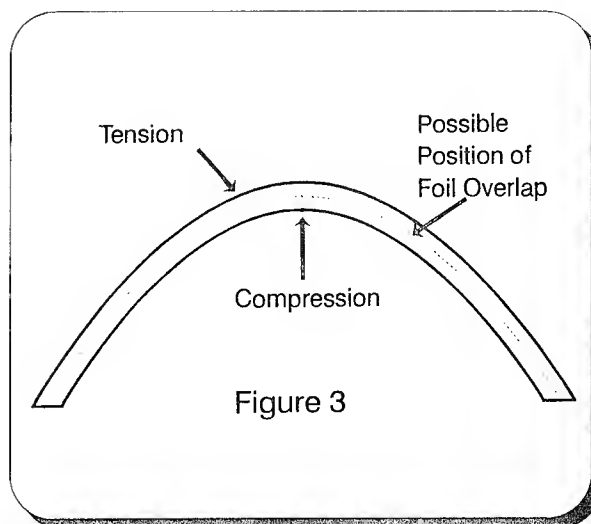
Several flexing techniques were considered to simulate the cyclic stress created by the environment. The simulator had to severely stress cables. It was also deemed necessary to subject the entire perimeter of the cable to flexure equally. The simulator also had to induce shielding effectiveness degradation similar to that observed in the field. One way to achieve these objectives was to bend a piece of conduit, as if over a mandrel, hold it steady, then rotate a cable that was inserted into the conduit. See Figure 2.

With this method the sample undergoes expansion and compression around the entire circumference. In order to evaluate all samples equally regardless of the construction, flexure had to be equal around the entire perimeter of the cable. This is necessary since the shielding tape is a flat tape longitudinally wrapped around the cable. This creates an overlap in the foil. This overlap section makes the tape two layers thick for the overlapped portion of the cables perimeter.

In the field, aerial cables can be shown to sway back and forth about an arc. The motion of the rotary flexer was designed to continue that arc through 360 degrees of rotation. This insures that the sample will be flexed around the entire perimeter.

Flexing cables has not been shown to seriously degrade the structure of the braid. The damage is mostly confined to the laminated shielding tape. Small radial cracks have been observed in the foil laminate tape in aerial samples taken from the field. These cracks are similar in appearance to the cracks visible on the samples that underwent accelerated flexure fatigue using the rotary flex method.

Other flexers considered, subjected samples to flexing in only one plane, similar to the back and



forth motion of a reverse bend test. Since various cable designs have different bonding and overlap characteristics of the laminated shielding tape, this type of flexer was considered inadequate. For instance, if a sample had a weak bond at the overlap, but was positioned so the overlap was 90 degrees to the direction of the motion, the overlap will not receive the full punishment of compression and stress. See Figure 3.

Conclusion

A necessary characteristic of coaxial drop cable is flexibility. To achieve this flexibility, the basic outer conductor designs consist of a laminated foil shielding tape in conjunction with a flexible conductive wire braid. While this design offers flexibility along with a high degree of shielding effectiveness, there is a trade-off, flexibility for shielding effectiveness.

When comparing coaxial drop cables for shielding configurations it is important to use the values obtained after flexure. It has been shown that the shielding effectiveness of new drop cables will in many cases degrade with time when installed aurally.

Drop cables installed aerially are subjected to stress from several sources. The major sources are wind and ice loading, and constant flexure from movements caused by the wind. It has been shown that the shielding effectiveness in samples from the field, can degrade. At high frequencies this degradation is most likely due in part from small radial cracks induced in the laminated shielding tape.

Accelerated flex fatigue, using the rotary type flexer induces small radial cracks that are similar in appearance to the cracks observed in the field samples. The decline in shielding effectiveness noticed in the field study was consistent with the results achieved using the rotary flexer to accelerate the fatigue of laboratory samples. A more detailed characterization of shielding effectiveness degradation that examines the many variables present in aerial drop cable spans is necessary.

REFERENCES

1. K.L. Smith "Drop Cable Leakage Throughout 20 Years of Service," *NCTA Technical Papers*, 21 (1981).
2. **National Electric Safety Code**, The Institute of Electrical and Electronics Engineers, Inc, (1993).
3. Schelkunoff, S.A., "Electromagnetic Theory of Coaxial Lines and Cylindrical Shields," *Bell System Technical Journal*, Volume 13, (1934).

Biographies

Terry McAlister is currently the Drop Cable Engineering Manager and has held several other positions including Engineering Manager, Applications Manager, and Product Manager over 27 years with CommScope. He is a 15 year member of the SCTE serving on various committees including the Interface Practices Sub Committee for Drop Cable. He has four years electronics experience with the Navy and holds associate degrees in both Electronics and Business Administration.



Joseph S Elko is a member of the Product Engineering Group at CommScope. He graduated in Electronic Engineering Technology from Catawba Valley Technical College and is currently enrolled at Lenoir Rhyne College in the Physics Program. He has been employed in the cable industry with CommScope, Cablewave Systems, and Prodelin since 1979.



Kevin Gantt has 17 years of experience in the cable industry, and is a national member of the Society of Cable Television Engineers. He received an Electronics Engineering Technology degree in 1990 while working in Product Development. Since 1991 he has worked as a Product Engineering Specialist.



ELECTRICAL PROPERTIES OF THERMOPLASTIC POLYIMIDE INSULATED COAXIAL CABLE FOR USE AT HIGH TEMPERATURE AND UNDER RADIOACTIVE CONDITION

Shigeaki SUDO, Shinichi ONO, Masataka USHIKI, Tomotaka MURASE, Yoshimi SATO, Takeo SHIONO
Hisayasu MITSUI *

Showa Electric Wire & Cable Co., Ltd.

* Toshiba Corporation

1. Abstract

Thermoplastic polyimide insulated coaxial cable for use under high temperature and radioactive conditions was developed and its electrical and mechanical properties were evaluated in comparison with cable insulated with polyetheretherketone which is known for its superior heat and radiation resistant characteristics. According to experiments, the electrical properties of thermoplastic polyimide insulated cable are stable over a wider temperature range in comparison with polyetheretherketone insulated cable even after 1.2 MGy of γ -ray irradiation and 6-months heat aging at 220°C, indicating that thermoplastic polyimide is superior for use as a heat- and radiation-resistant cable covering material. The electrical properties of TPI cable observed, were within actual use requirements, even under γ -ray irradiation up to 1,000 Gy/h.

2. Introduction

Polyimide (PI) is known as a resin which has superior heat and radiation resistant characteristics among engineering plastics which are used for many applications. Conventional PI, however, is not suitable for extrusion covering, and it could be only

applied by varnishing or taping to electric wires. It is difficult to form a uniform and thick insulation layer by such methods, and application of PI-insulated electric wire has been limited. Thermoplastic polyimide (TPI) with properties shown in Table 1 has been developed lately, which allows a thick insulation layer to be formed, and TPI insulated electric wires have been developed for a variety of applications.

Electrical and mechanical properties of cable insulated and sheathed with TPI (which is referred to, hereinafter, as TPI cable) are investigated in this study over the temperature range of room temperature to 220°C. Electrical and mechanical properties of TPI cable and the effects of γ -ray irradiation and long-term heat aging are described first, and then they are compared with the properties of coaxial cable (PEEK cable) insulated and sheathed with polyetheretherketone (PEEK)⁽¹⁾ known, like PI, as a heat- and radiation-resistant resin. Electrical properties measured under γ -ray irradiation are also described.

Table 1 General Properties of TPI and PEEK

Item	TPI	PEEK
Melting point (°C)	388	334
Glass transition temperature (°C)	250	143
Heat distortion (°C)	238	152
Specific gravity	1.33	1.30
Water absorption (%)	0.34	0.14
Permittivity 1 kHz	3.2	3.4
Flammability rating UL-94	V-0	V-0

3. Sample Cables

All sample cables, having coaxial cable construction as shown in Fig. 1, were prepared using TPI or PEEK as insulation and sheath and silver-covered annealed copper wires as inner and outer conductors. The insulation thickness was determined so that the characteristic impedance was $50\ \Omega$ at room temperature. The cable construction and electrical properties of the original cables (i.e., cables before γ -ray irradiation and/or heating) at room temperature are shown in Table 2.

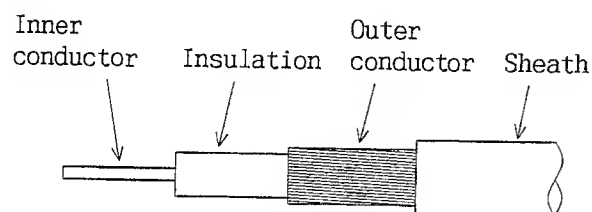


Fig. 1 Cable construction

4. Tests

4.1 Deterioration Test

Sample cables were subjected to γ -ray irradiation of 1.2 MGy, and then to heat aging of 220°C for 6 months. The γ -ray irradiation was conducted on two sample cables at a dose rate of about 10 kGy/h in the air at room temperature. One of the two irradiated cables was subjected to heat aging in the air and the other in nitrogen. Non-irradiated samples were also subjected to heat aging for comparison.

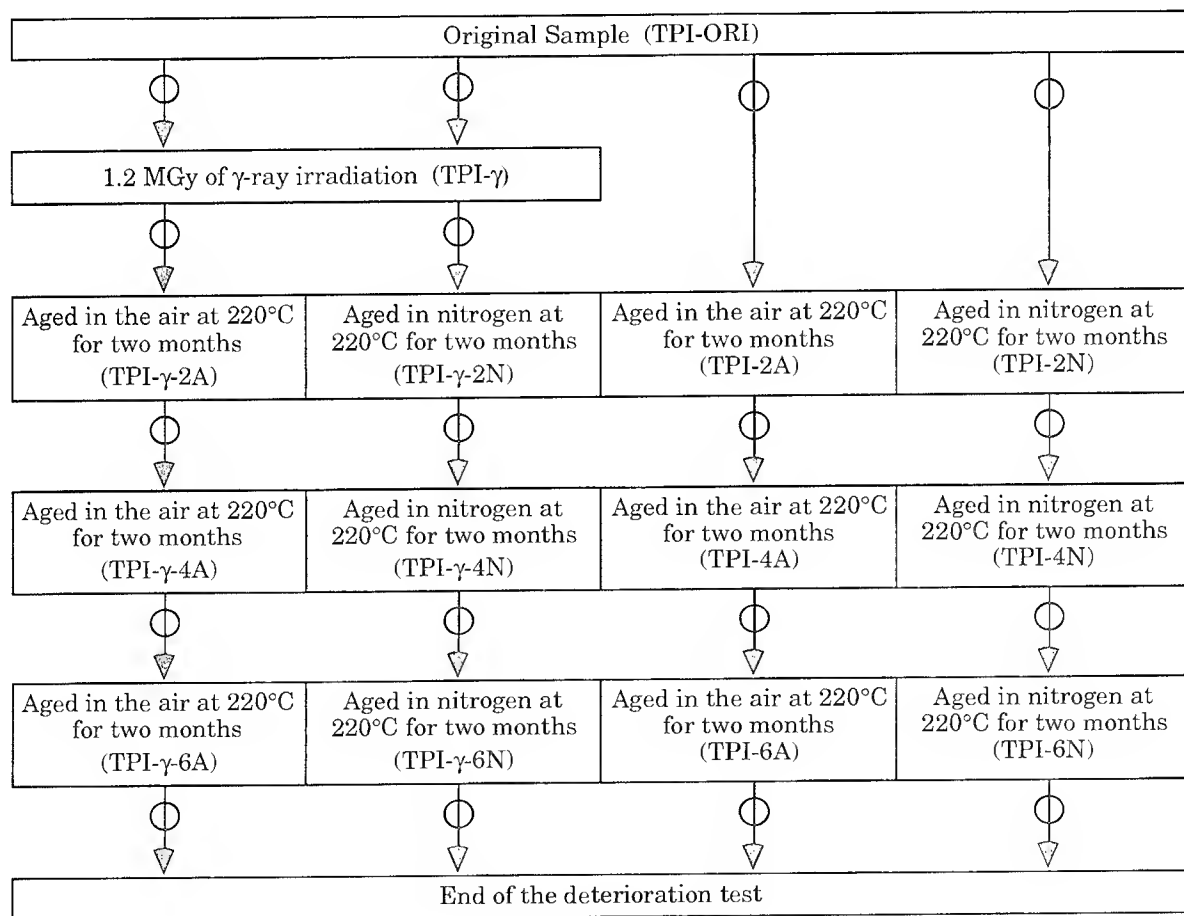
Measurements and tests shown in Table 3 were carried out before the deterioration test, after γ -ray irradiation, during heat aging (every two months) and after heat aging as indicated in Fig. 2. TPI cables at respective stages of the test are referred to, in the rest of this paper, by symbols given in parentheses in Fig. 2, and PEEK cables are also referred in a similar manner.

Table 2 Cable Construction and Electrical Properties at Room Temperature

Item			TPI cable	PEEK cable
Cable construction	Inner conductor	Material	Solid Ag-covered copper wire	Stranded Ag-covered copper wire
		Construction	1 no. / 0.26 mm	7 no. / 0.10 mm
	Insulation	Material	TPI	PEEK
		Thickness	Approx. 0.4 mm	Approx. 0.4 mm
	Outer conductor	Material	Ag-covered copper wire	Ag-covered copper wire
Electrical properties	Outer conductor	Construction	Whipping shield	Whipping shield
		Material	TPI	PEEK
	Outer diameter		Approx. 1.7 mm	Approx. 1.6 mm
	Characteristic impedance (10 MHz)		50.4 Ω	50.3 Ω
	Insulation resistance		$1.2 \times 10^6\ \text{M}\Omega\ \text{km}$	$1.0 \times 10^6\ \text{M}\Omega\ \text{km}$
	Attenuation	3 MHz	66.8 dB/km	78.4 dB/km
		5 MHz	87.3 dB/km	103.0 dB/km
		10 MHz	124.0 dB/km	145.0 dB/km
	Capacitance (1 kHz)		120.5 nF/km	122.2 nF/km

Table 3 Measurement Items

Item		Measurement / test temperature
Electrical properties	Attenuation (3-10 MHz)	Room temperature to 220°C
	Insulation resistance	
	Capacitance (1kHz)	
Mechanical properties	Tensile strength and elongation	220°C
	Flexibility test	23°C



○ : Measurement / test

Fig. 2 Deterioration test procedure

4.2 Electrical Properties during γ -ray Irradiation

Electrical properties of sample cables during γ -ray irradiation were measured as following :

- (1) Lead cables (polyethylene-insulated coaxial cable) are extended into the irradiation facility, and electrical properties only of the lead cables are measured.
- (2) Sample cables and the lead cables are connected, and electrical properties of the connected cables are measured.
- (3) Electrical properties only of the sample cables are calculated from results obtained in steps (1) and (2) above.

5. Results

5.1 Properties of TPI Cable

5.1.1 Electrical Properties

(1) Effects of deterioration test

Results of electrical tests made on samples subjected to γ -ray irradiation and then heat aging in the air at 220°C are shown in Figs. 3 to 5.

Fig. 3 shows the results of insulation resistance measurement. The insulation resistance of TPI-ORI decreases gradually as the temperature rises, and the slope increases at temperatures over 100°C. Such samples as TPI- γ and TPI- γ -6A show a temperature dependence of insulation resistance similar to that of

TPI-ORI. The insulation resistance did not decrease but rather tended to increase a little for the conditions of this deterioration test.

Results of attenuation measured at 3 and 10 MHz are shown in Fig. 4. The attenuation of TPI-ORI increases gradually from room temperature to 220°C. The attenuation was affected little by the deterioration test, indicating that dielectric characteristics (permittivity and loss tangent) of TPI are not greatly affected by the deterioration test.

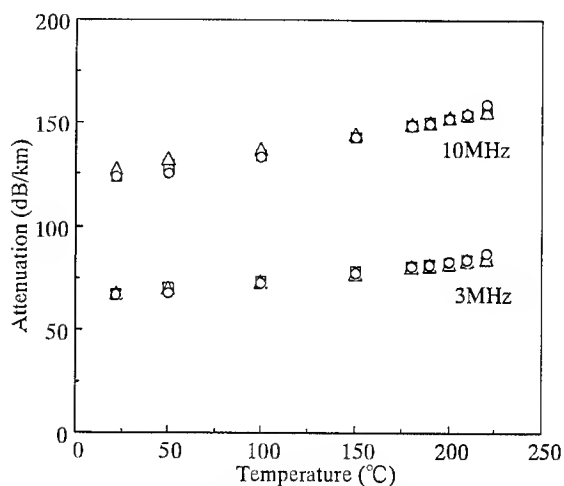


Fig.4 Relationship between attenuation and temperature. (TPI cable irradiated to γ -ray and aged in air at 220°C)

□ : TPI - ORI Δ : TPI - γ \circ : TPI - γ - 6A

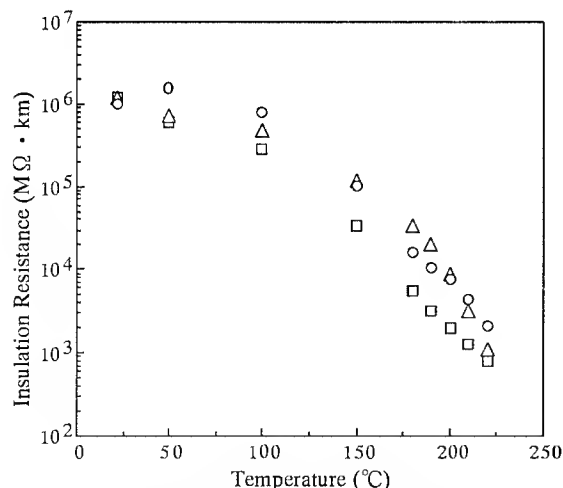


Fig.3 Relationship between insulation resistance and temperature. (TPI cable irradiated to γ -ray and aged in air at 220°C)

□ : TPI - ORI Δ : TPI - γ \circ : TPI - γ - 6A

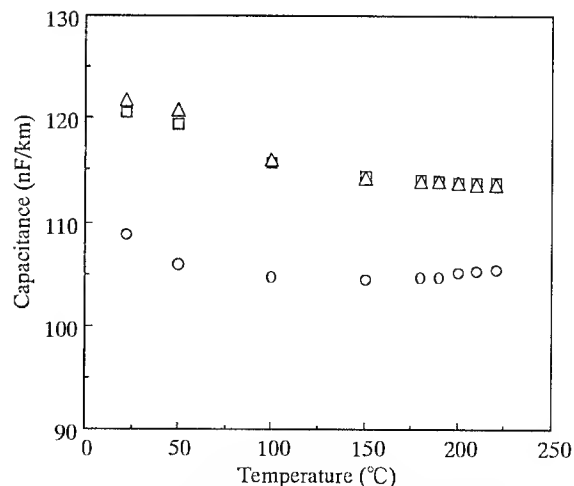


Fig.5 Relationship between capacitance at 1kHz and temperature. (TPI cable irradiated to γ -ray and aged in air at 220°C)

□ : TPI - ORI Δ : TPI - γ \circ : TPI - γ - 6A

Results of capacitance measured at 1 kHz are shown in Fig. 5. The capacitance of TPI-ORI decreases gradually as the temperature rises to 220°C. The slope changes also near 100°C, but, contrary to the case of insulation resistance, the capacitance changes only slightly at temperatures over 100°C. The capacitance of TPI- γ shows a temperature dependence similar to that of TPI-ORI, but the capacitance of TPI- γ -6A is lower. The capacitance of TPI-6A is also lower, and it can be said that such low capacitance was brought about only by the heat aging and the γ -ray irradiation had no effect on it.

(2) Effects of aging atmosphere

Electrical properties of the sample heat aged in a nitrogen atmosphere, after the γ -ray irradiation, are compared with those of the sample heat aged in an air atmosphere in Figs. 6 to 8.

Fig. 6 compares the insulation resistance. The changes in insulation resistance of TPI- γ -6N from that of TPI-ORI are similar to the case where the sample is heat aged in the air, indicating that the aging atmosphere has little effect on insulation resistance. This result suggests that the decrease of insulation resistance by carbonization does not occur in TPI.

Fig. 7 compares the attenuation. The attenuation of heat aged samples changed little from that of TPI-ORI, irrespective of the aging atmosphere.

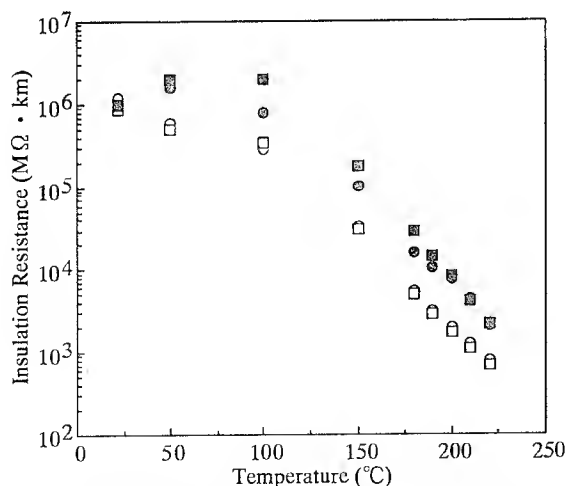


Fig.6 Relationship between insulation resistance and temperature (TPI cable irradiated to γ -ray and aged in air or N₂ at 220°C)

○ : TPI - ORI (To be aged in air) ● : TPI - γ - 6A
□ : TPI - ORI (To be aged in N₂) ■ : TPI - γ - 6N

Fig. 8 compares the capacitance. The capacitance of TPI- γ -6A is lower as described above, but that of TPI- γ -6N changes little from that of TPI-ORI, indicating that oxygen plays some role in the change in capacitance by heat aging.

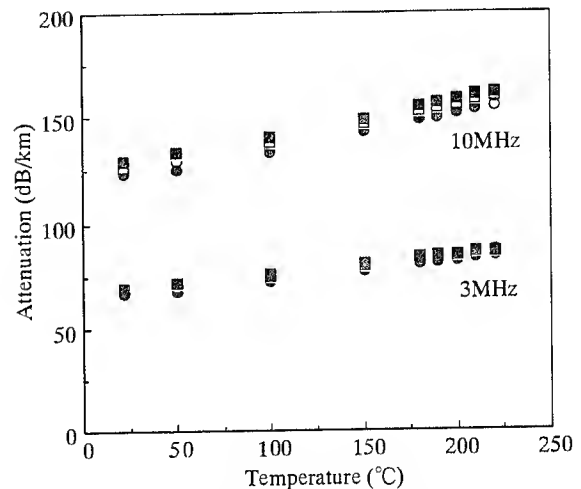


Fig.7 Relationship between attenuation and temperature. (TPI cable irradiated to γ -ray and aged in air or N₂ at 220°C)

○ : TPI - ORI (To be aged in air) ● : TPI - γ - 6A
□ : TPI - ORI (To be aged in N₂) ■ : TPI - γ - 6N

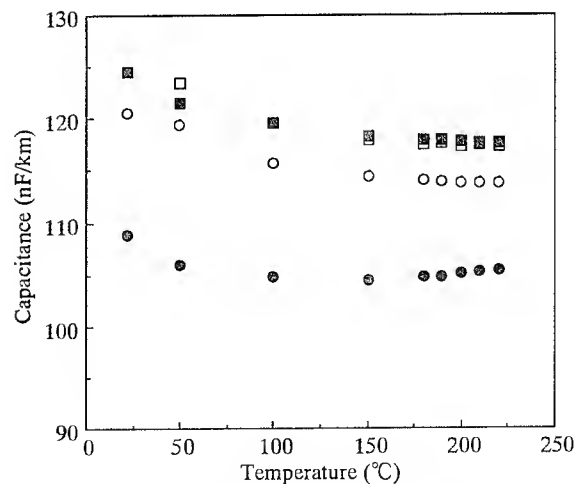


Fig.8 Relationship between capacitance at 1kHz and temperature (TPI cable irradiated to γ -ray and aged in air or N₂ at 220°C)

○ : TPI - ORI (To be aged in air) ● : TPI - γ - 6A
□ : TPI - ORI (To be aged in N₂) ■ : TPI - γ - 6N

5.1.2 Mechanical Properties

(1) Tensile test

The tensile strength and elongation of TPI-ORI and TPI- γ during the 6-months heat aging at 220°C in the air and nitrogen are compared in Figs. 9 and 10.

As seen in Fig. 9, the tensile strength is slightly increased due to γ -ray irradiation. By heat aging in the air, the tensile strength decreases slightly and

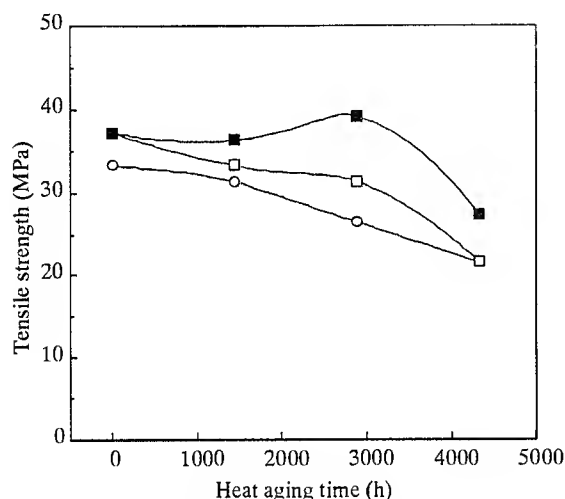


Fig.9 Relationship between tensile strength at 220°C and heat aging time at 220°C.

○ : Non-irradiated TPI cable aged in air.
□ : Irradiated TPI cable aged in air.
■ : Irradiated TPI cable aged in N₂.

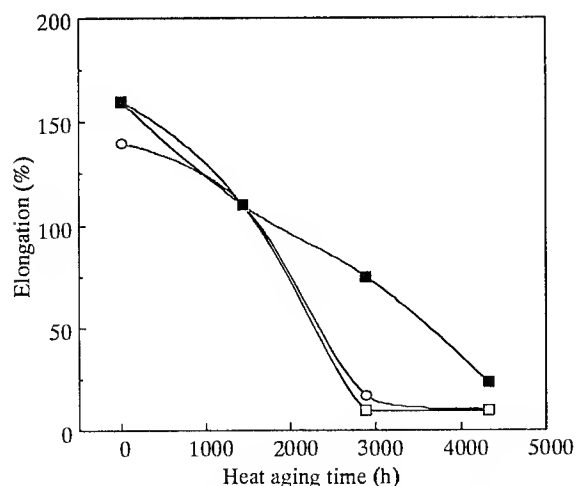


Fig.10 Relationship between elongation at 220°C and heat aging time at 220°C.

○ : Non-irradiated TPI cable aged in air.
□ : Irradiated TPI cable aged in air.
■ : Irradiated TPI cable aged in N₂.

the elongation decrease greatly, irrespective of application of γ -ray irradiation. As for samples heat aged in nitrogen, on the other hand, the decrease in tensile strength or elongation was smaller in comparison to the case where samples were heat aged in the air. It can be said therefore that oxidative deterioration must also play some roles in changes of physical characteristics in TPI during the heat aging.

(2) Flexibility (Winding test on a mandrel with the same diameter to the cable)

Results of winding test on a mandrel with the same diameter to the cable are shown in Table 4. Not only TPI-ORI but also TPI- γ shows adequate flexibility. In heat aging of TPI- γ , the sample heat aged in the air showed cracks in the sheath after two months of heat aging, but the sample heat aged in nitrogen showed no cracks even after six months of heat aging.

Heat aged TPI-ORI also showed results similar to heat aged TPI- γ , indicating that 1.2 MGy of γ -ray irradiation has little effect on cable flexibility.

Table 4 Results of Winding Test

Sample		Results	
TPI-ORI		○	
TPI- γ		○	
TPI- γ -2A	TPI- γ -2N	×	○
TPI- γ -4A	TPI- γ -4N	×	○
TPI- γ -6A	TPI- γ -6N	×	○

○ : No cracking × : Cracking occurred

5.2 Comparison of TPI and PEEK Cables

Electrical properties of TPI and PEEK cables measured after γ -ray irradiation and heat aging in the air at 220°C are compared in Figs. 11 to 13.

Fig. 11 compares the temperature dependence of insulation resistance. The insulation resistance of PEEK cable decreases rapidly at temperatures above 143°C, the glass transition temperature (T_g) of PEEK, whereas insulation resistance of TPI cable decreases gradually up to 220°C reflecting the T_g of TPI of 250°C. Insulation resistance of PEEK-ORI decreases by the order of 10^8 when the temperature rises from room temperature to 220°C, while that of TPI-ORI

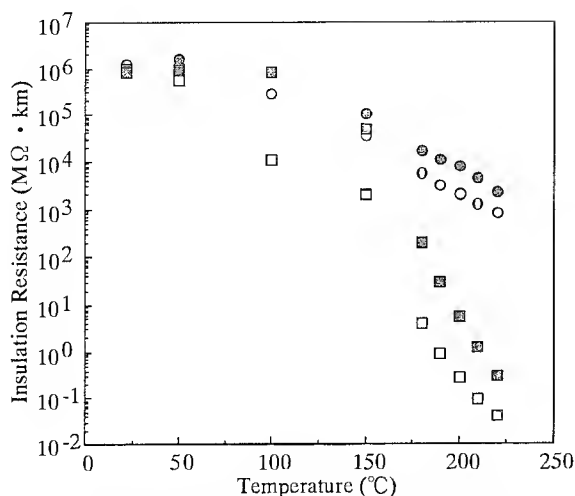


Fig.11 Relationship between insulation resistance and temperature. (TPI cable and PEEK cable irradiated to γ -ray and aged in air at 220°C)
 ○ : TPI - ORI ● : TPI - γ - 6A
 □ : PEEK - ORI ■ : PEEK - γ - 6A

decreases only by the order of 10^3 . In addition, the insulation resistance of either cable does not decrease by the γ -ray irradiation or the heat aging.

Fig. 12 shows temperature dependence of attenuation measured at 3 and 10 MHz. Their absolute values cannot be compared due to the difference in cable construction, but, as a trend, the attenuation in the TPI cable increases gradually up to 220°C while that in the PEEK cable increases gradually up to about the Tg of PEEK and then more rapidly at temperatures above that temperature. These results suggest that dielectric characteristics (i.e., permittivity and loss tangent) of TPI are stable at temperatures from room temperature to 220°C while those of PEEK change greatly from a temperature range just below its Tg. In addition, the deterioration test had not much effect on attenuation in either cable except the temperatures greater than 200°C where slight effects were noticed in the PEEK cable.

Fig. 13 shows temperature dependence of capacitance at 1 kHz. The capacitance of TPI cable gradually decreases up to 220°C, while that of PEEK cable decreases gradually up to about the Tg of PEEK and decreases rapidly above that temperature. The γ -ray irradiation showed little effect on capacitance of either cable, but the heat aging affected the cables differently. The capacitance of heat aged TPI cable decreased at all points of measurement, but that of heat aged PEEK cable decreased only in the temperature range above the Tg.

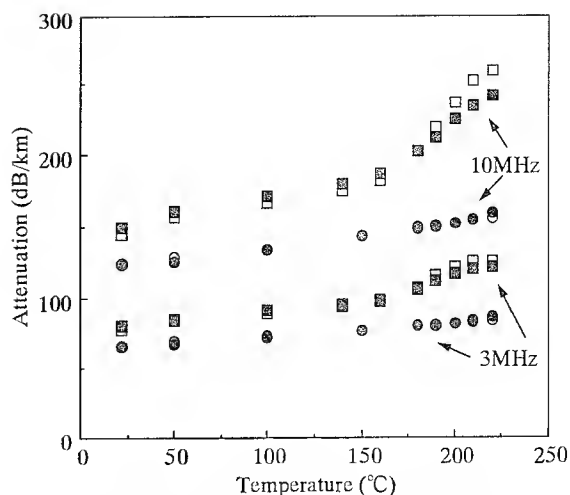


Fig.12 Relationship between attenuation and temperature. (TPI cable and PEEK cable irradiated to γ -ray and aged in air at 220°C)
 ○ : TPI - ORI ● : TPI - γ - 6A
 □ : PEEK - ORI ■ : PEEK - γ - 6A

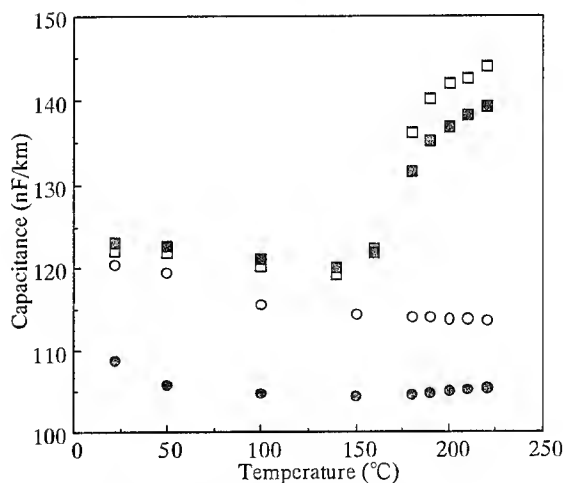


Fig.13 Relationship between capacitance at 1kHz and temperature. (TPI cable and PEEK cable irradiated to γ -ray and aged in air at 220°C)
 ○ : TPI - ORI ● : TPI - γ - 6A
 □ : PEEK - ORI ■ : PEEK - γ - 6A

5.3 Electrical Properties during γ -ray Irradiation

Electrical properties of TPI-ORI and PEEK-ORI were measured on room temperature to 220°C under γ -ray irradiation dose rate of 0 to 1,000 Gy/h in air.

Results of insulation resistance measurement are shown in Fig. 14. The effect of γ -ray irradiation is clearly visible in insulation resistance measured at room temperature, where the insulation resistance decreases as the dose rate increases. The effect of γ -ray irradiation decreases at high temperatures where the insulation resistance itself is lower.

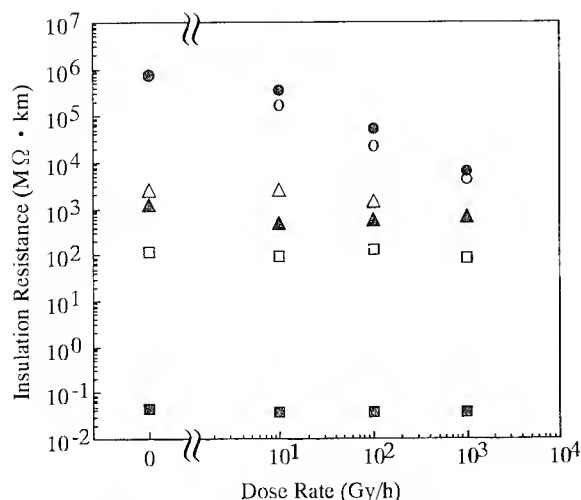


Fig.14 Relationship between insulation resistance and dose rate for TPI cable and PEEK cable.

TPI cable ○ : Room Temp. △ : 160°C □ : 220°C
PEEK cable ● : Room Temp. ▲ : 160°C ■ : 220°C

The γ -ray irradiation showed little effect on other electrical properties such as attenuation and capacitance which are measured using alternating current.

6. Discussion

Various methods such as, dynamic viscoelasticity, infrared absorption (FT-IR) and differential scanning calorimetry (DSC) were carried out to study the occurrence of crosslinking caused by the γ -ray irradiation, occurrence of chemical changes and changes in the crystallographic state of the material, respectively, in order to identify causes of changes in mechanical properties by the deterioration test.

The dynamic viscoelasticity of TPI-ORI and TPI- γ was also measured. The temperature dependence of $\tan\delta$ is shown in Fig. 15. The peak appearing at about 250°C is referred as to the β -peak. The rapid increase in $\tan\delta$ visible in the temperature range of the β -peak comes from the three dimensional motion of the principal chains associated with the glass transition. Fig. 15 shows, in addition, that the β -peak of TPI- γ (at glass transition temperature T_g) appears at a temperature a little higher than that of TPI-ORI, suggesting crosslinking caused by the γ -ray irradiation.⁽²⁾ It is judged therefore that the increase in tensile strength after the γ -ray irradiation is associated with crosslinking caused by the γ -ray irradiation.

Infrared absorption of TPI-ORI and TPI- γ -6A was measured, but little difference was observed between their absorption spectra, suggesting that no remarkable changes in chemical construction occurred in TPI due to the deterioration test used in this study.

Results of DSC measurement made on TPI-ORI, TPI- γ , TPI- γ -6A and TPI- γ -6N are shown in Fig. 16.

The DSC curve of TPI-ORI shows a change due to the glass transition temperature at about 250°C, an exothermic peak at about 300°C (T_c) and an endothermic peak due to melting of crystal at about the melting point (mp) of 388°C. The presence of the exothermic peak indicates occurrence of crystallization during the temperature rising process of the DSC measurement. The DSC curve of TPI- γ shows trends, in comparison with that of TPI-ORI,

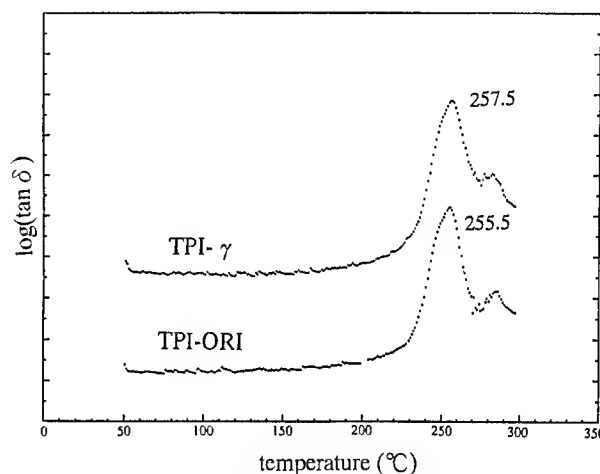


Fig.15 Effect of γ -ray on $\tan\delta$

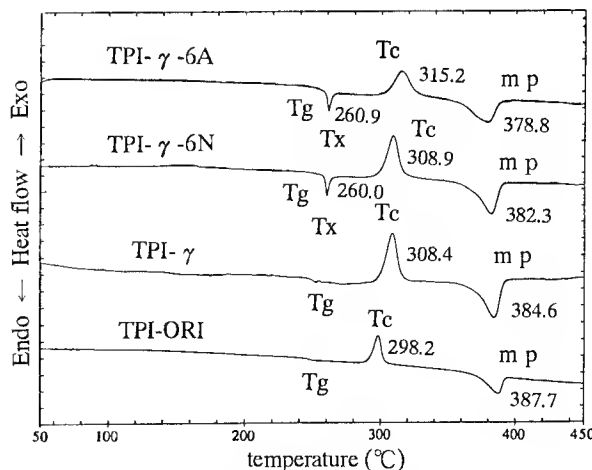


Fig.16 DSC curve of TPI

that the T_c is higher and the mp is lower. It is judged that the lower mp of TPI- γ comes from lower molecular weight caused by scission of principal chains in TPI by the γ -ray irradiation.

As for the samples heat aged at 220°C (i.e., TPI- γ -6A and TPI- γ -6N), an endothermic peak (T_x) appeared at about 260°C, and their mps were lower than that of TPI- γ . The presence of the endothermic peak at T_x suggests occurrence of a change in crystallographic state by the heat aging made after the γ -ray irradiation.⁽³⁾ In addition, the lower mp is judged to come from lower molecular weight also due to the scission of principal chains because the lower mp was more marked in the sample heat aged in the air.

It can be said, from above discussions, that changes in mechanical properties observed after the deterioration test come from scission of principal chains and crosslinking by the γ -ray irradiation and crystallographic changes and scission of principal chains by the heat aging.

7. Conclusions

Changes in electrical and mechanical properties of TPI cable were studied after a deterioration test comprising a 1.2 MGy of γ -ray irradiation and 6-months heat aging at 220°C. It is clear from this study that the electrical properties of TPI are stable in a wider temperature range in comparison with PEEK, and change little by the deterioration test. On the other hand, as for the mechanical properties of TPI, little change is caused by the γ -ray irradiation but they deteriorate due to heat aging. Elongation deteriorated greatly, but samples heat aged in nitrogen atmosphere showed no trouble in the winding test even after the 6-months heat aging, and retained adequate flexibility as cables.

Even under γ -ray irradiation up to 1,000 Gy/h, electrical properties of TPI cable did not show any troubles, which might be a problem in actual use.

It was demonstrated from this study that the TPI cable is usable at high temperatures and under highly radioactive condition by selecting its operating atmosphere.

8. References

- (1) ICI Literature, Lit Ref. VK2/0785
- (2) T. Hirade, Y. Hama, T. Sasuga, and T. Seguchi, *POLYMER*, **32**(14), 2499-2504 (1991)
- (3) Z. Wu, R. Yokota, M. Kochi, and H. Kambe, *Kobunshi Ronbunshu*, **38**(9), 601-606 (1981)



Shigeaki Sudo

Showa Electric Wire & Cable Co., Ltd., 4-1-1 Minamihashimoto, Sagamihara, Japan

S. Sudo received his B.E. degree from Yokohama National University in 1989. He joined Showa Electric Wire & Cable Co., Ltd. in 1989. He is an engineer of the Engineering Sec. 2 of the Optics & Communications Engineering Dept.



Shinichi Ono

Showa Electric Wire & Cable Co., Ltd., 4-1-1 Minamihashimoto, Sagamihara, Japan

S. Ono received his M.E. degree from Muroran Institute of Technology in 1991. He joined Showa Electric Wire & Cable Co., Ltd. in 1992. He is an engineer of the Engineering Sec. 2 of the Optics & Communications Engineering Dept.



Masataka Ushiki

Showa Electric Wire & Cable Co., Ltd., 4-1-1 Minamihashimoto, Sagamihara, Japan

M. Ushiki received his B.E. degree from The University of Electro-Communications in 1977. He joined Showa Electric Wire & Cable Co., Ltd. in 1977. He is the manager of the Engineering Sec. 2 of the Optics & Communications Engineering Dept.



Tomotaka Murase

Showa Electric Wire & Cable Co., Ltd., 4-1-1, Minamihashimoto, Sagamihara, Japan

T. Murase received his B.E. degree in Kanagawa University in 1993. He joined Showa Electric Wire & Cable Co., Ltd. in 1993. He is an engineer of the Material Research Division of Telecommunication R&D Dept.



Hisayasu Mitsui

Toshiba Corporation, 2-4 Suehiro, Tsurumi, Yokohama, Japan

H. Mitsui received his B.S. degree from Nagoya Institute of Technology in 1965 and the Dr. Eng. Degree in Electrical Engineering from Nagoya University in 1985. Since joining Toshiba Corp. in 1965, he has been engaged in the research and development of electrical insulating materials and insulation systems for heavy apparatus. He is now a Chief Specialist in the Heavy Apparatus Eng. Laboratory of Toshiba Corp. He is a Senior Member of IEEE, and a Member of Japan Consulting Engineers Association.



Yoshimi Sato

Showa Electric Wire & Cable Co., Ltd., 2-1-1 Odasakae, Kawasaki, Japan

Y. Sato received her B.E. degree from Tokai University in 1991. She joined Showa Electric Wire & Cable Co., Ltd. in 1991. She is an engineer of the Materials Research Laboratory.



Takeo Shiono

Showa Electric Wire & Cable Co., Ltd., 4-1-1 Minamihashimoto, Sagamihara, Japan

T. Shiono received his Ph.D. degree in Chemical Engineering from the University of Tokyo in 1979. He joined Showa Electric Wire & Cable Co., Ltd. in 1979 and works in the development of telecommunication cable's materials. He is the manager of the Material Research Division of Telecommunication R&D Dept.

Optimized VARIO Leaky Feeders for 900 and 1800 MHz Frequency Bands with Optical Fibers integrated in the Inner Conductor for Use in Mobile Radio Communication Systems in Tunnels and Buildings

G. Brambilla ¹⁾, H. G. Haag ²⁾, K. Schulze-Buxloh ³⁾, A. Weiss ²⁾

¹⁾ Sirti S.p.A., Milano, Italy

²⁾ Kabel Rheydt AG, Mönchengladbach, Germany

³⁾ RFS, Hannover, Division of kabelmetal electro GmbH, Germany

Abstract

The technical standards GSM and DECT for wireless communication are used in more and more countries worldwide, in order to expand the outside coverage into confined areas. A combined radiating and fiber optic transmission system is presented in this paper with respect to optimized sections of the system configuration.

Leaky coaxial cables using the VARIO-concept for compensation of the influence of the longitudinal attenuation of the cable on radio communication systems performance have been optimized and tested successfully in the GSM (900 Mhz). Integrating the optical fibers into the inner conductor tube of a leaky coaxial cable parts of the costs for fiber optic track cable and mounting thereof can be avoided.

Therefor VARIO leaky feeders with compensated longitudinal attenuation and which contain optical fibers integrated in the inner conductor combine the advantages of both:

- nearly constant signal level distribution along the leaky cable in the confined area,
- fiber optic signal transport along the track without separat cable.

Introduction

The increasing demand for mobile communications is being satisfied by several wireless networks (D1- and C-net of German PTT, D2-net of Mannesmann Mobilfunk and E-net of e-plus) in Germany, and many other countries worldwide have also adopted GSM- and DECT-standards for their networks. The coverage and the subscriber capacity are being increased more and more by implementing more and more base stations. So in future there will be "total" coverage except in confined areas such as tunnels, parkings, buildings, airports, railway stations, etc..

There has been a number of system proposals for the extension of the outdoor coverage into confined areas and great efforts have been made in optimizing the different approaches. Also the radiating elements like antennas and leaky coaxial cables have been investigated intensively. One of the most promising system solution optimized for GSM applications will be presented here.

System Performance

There are 2 different approaches in order to connect a base-station to a mobile subscriber in a confined area as for example a tunnel:

- extension of the outdoor base station coverage using a repeater-amplifier ("cell-extender"- concept),
- placing an extra base-station inside the tunnel ("dedicated cell" concept).

For the cell extender concept some advantages have been evaluated within the DRIVE research program sponsored by the European Community /1/:

- no handover problems,
- low price,
- easy planning and optimization.

A favorable system configuration especially suited for long tunnels is shown schematically in fig. 1, 2.

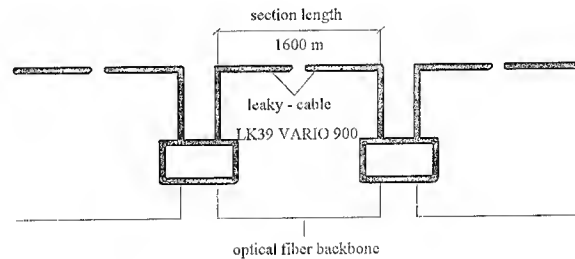


figure 1: section scheme of the conventional system in the tunnel:
leaky feeder and optical fiber backbone separated (2 different cables)

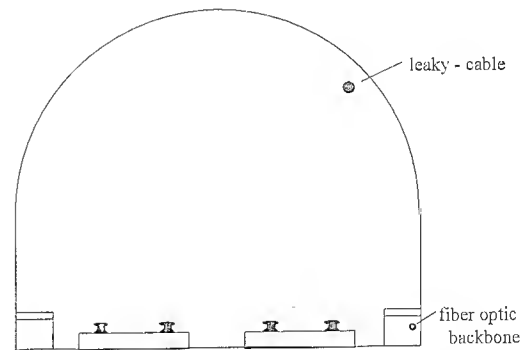


figure 2: tunnel cross section with leaky cable and fiber optic backbone cable

Two radiating cables are being fed from one common central point, the far cable ends are terminated with the specific impedance (50Ω). The signals to and from the feed in point are transported via a backbone cable system which can be coaxial but preferably uses fiber optic cables. So the advantages of low attenuation and broadband transmission are exploited. The opto-electric conversion takes place at the central feed-in point.

For a long tunnel many of these installations of two radiating cables with central feed can be obtained and interconnected by the fiber optic "backbone" system. The number of feed-in points inside a given tunnel length depends on the largest frequency of the system, because the maximum length of the radiating cable is limited by its longitudinal attenuation /2/. It has been deduced, that the maximum radiating cable length depends on the maximum allowable system loss (= sum of longitudinal and coupling loss) and simultaneously on the signal dynamics received by a mobile antenna along the entire radiating cable length (= difference between strongest and weakest signal level). The results of the measurements are given in fig. 3, 4.

figure 3: measurement of received signal level
in 14 km tunnel, 467.5 MHz

Date: 19-04-94
Place: Prato-Tires-Tunnel, Bolzano, Italy
Transmitter power: 17 dBm
Antenna Type: quarter wavelength antenna
Distance antenna-cable: 3 m
Frequency: 467.5 MHz

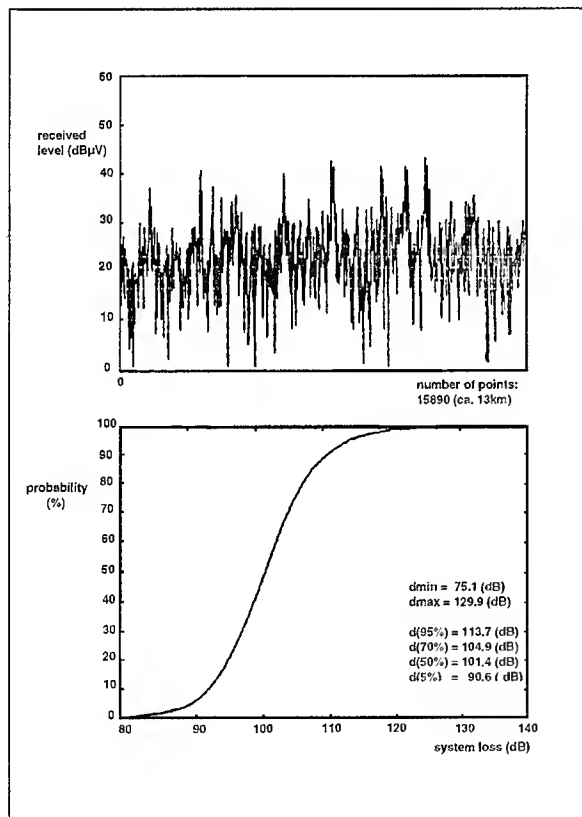
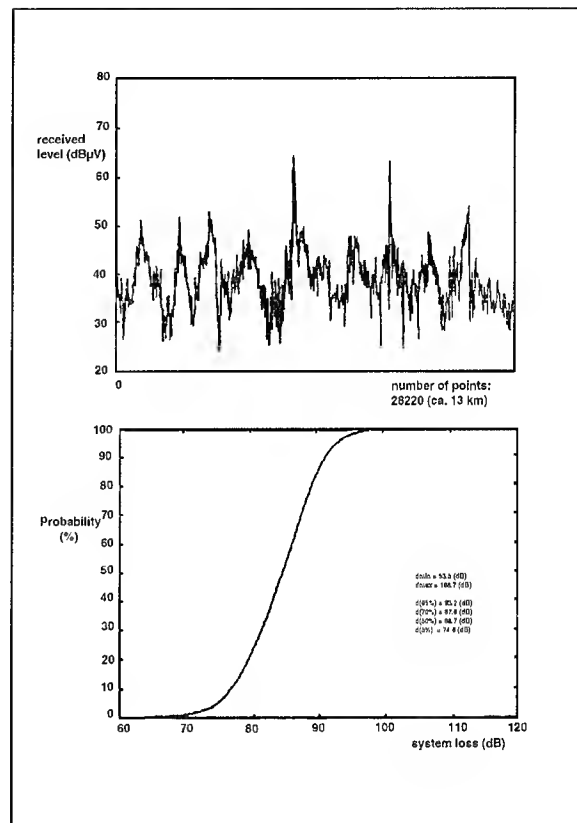


figure 4: measurement of received signal level
in 14 km tunnel, 947.6 MHz

Date: 20-04-94
Place: Prato-Tires-Tunnel, Bolzano, Italy
Transmitter power: 16 dBm
Antenna Type: quarter wavelength antenna
Distance antenna-cable: 2 m
Frequency: 947.6 MHz



The VARIO-concept has proven itself as the optimum solution, because it enables considerably longer radiating cable sections compared to standard radiating cables only because of a clever distribution of the radiating apertures along the VARIO cable length. By this the influence of the longitudinal attenuation on the received signal along the cable is compensated by reducing radiation of the VARIO cable at the feed-in part and increasing it at the termination part of the VARIO cable. By using VARIO cables the number of feed-in points is minimized. As an application example we report on a long railway tunnel in the Alps.

The Italian Railways are building several tunnels along the "Passo Brennero" route between Bolzano and the Austrian border. The new high speed railway link will solve many snow and avalanche problems which have severely affected the old track. So Italy will be connected to the European High Speed Train Network.

The new tunnels will be equipped with a specific railway wireless communication system called RRRP (= Réseau Radio Resource Partage) which has been established as an international standard by UIC (= Union International des Chemins de Fer): RRRP is very similar to GSM. A prototype system installation was tested in one of the new tunnels under realistic conditions for the first time worldwide. For RRRP frequencies between 870 and 890 MHz a conventional radiating cable length of approx. 500m is the maximum because of the allowable maximum signal level dynamics between signal at the feed-in part of the radiating coaxial cable and the weak signal at the termination of the cable because of the longitudinal attenuation. The new VARIO concept (grading of the coupling factor in order to compensate the influence of the longitudinal attenuation) allows up to 800m cable length. So the number of feed-in points which feed 2 radiating coaxial cables in a T-configuration can be divided by a factor of approx. 1,6. This important cost reduction is achieved only by a clever distribution of radiating apertures along the VARIO cable. In the case of the "Prato-Tires" tunnel with a length of 14 km only 9 feed-in points with 18 VARIO cables of approx. 800m length instead of 14 feed-in points with 28 conventional cables of 500m are necessary.

The VARIO leaky feeder system was under normal operation and transmitted among others at the frequencies 947.6 MHz and 467.5 MHz. A small van transported the receiving equipment along the tunnel so that the distribution of the received signal level along the tunnel was recorded and evaluated statistically.

Fiber Optic Integration

A further improvement for such a system was the use of a hybrid cable construction combining the advantages of both, the leaky coaxial cable and the fiber optic cable. Here, the backbone cable can be installed at the same time as the leaky cable. The optical backbone will be connected by joints along the tunnel length (figure 5).

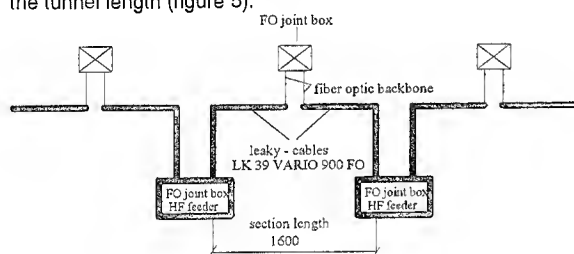


figure 5: section scheme of the system in the tunnel: leaky feeder and optical fiber backbone integrated in one single cable

Cable Construction

The cable combines and keeps the original properties of a leaky cable and a fiber optic backbone cable without any changes to the transmission properties of the single cable types. For the optical fibers a loose steel tube is used, as it is known and common from the OPGW. The steel tube has an outer diameter of 3.0 mm. The number of fibers in the tube can be

varied in a range of 2 to 24; for special applications a further increase is possible. The color code for the fibers allows an individual curing for at least up to 30 fibers.

Such a steel tube is the central element in a standard leaky cable, type LK 39 VARIO 900 (figure 4). The tube gets an electrical insulation toward the inner conductor. The exact distance between inner conductor and the outer, radiating conductor is made by PE disks, covered by a PE tube (bamboo type dielectric). As outer jacket a halogenfree, flame retardant material is used to reduce the flame propagation of the cable.

The steel tube is the best solution for protecting optical fibers against strong mechanical forces like by crush or by impact. Furtheron it gives a good protection in case of fire, which is important to keep the system running in all sections not influenced by the fire.

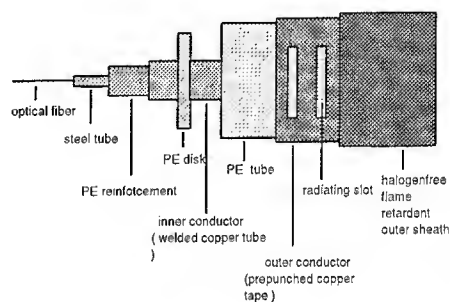


figure 6: cable cross section (cable type LK39 VARIO 900 FO)

Connector

A new cable connector was developed (figure 7) to guide the optical fibers out of the leaky cable to a joint. The main requirement for the plug was not to disturb the RF-transmission at the implementation of the fibers. Here, only non-metallic constructions are possible; the steel tube leading outside would give a short circuit.

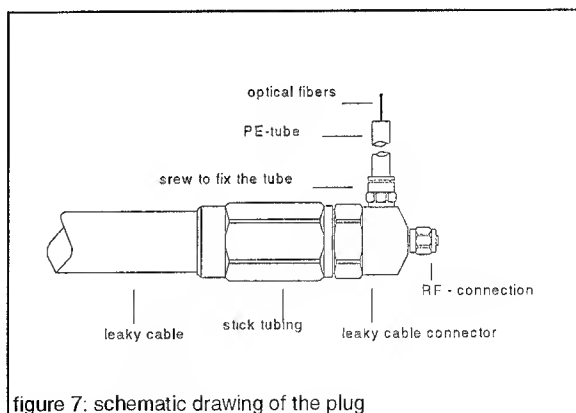
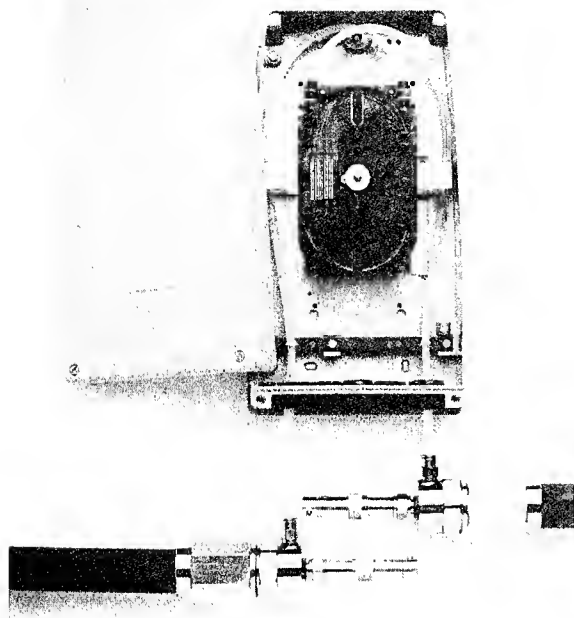


figure 7: schematic drawing of the plug

The connection is made by guiding the fibers in a plastic tube to the joint box (figure 8). To guarantee the watertightness the tube will be filled with a loose tube filling material. The additional fit is located at the side of the plug; here a joint box can be installed easily. The bending radius of the fiber passing the plug is similar to the one in the joint. Changes in optical attenuation are avoided. The distance between plug and joint box can be up to some meters; as it is required by the tunnel installation. Figure 8 shows a sample for a joint box, including the splice box with the fibers. The cable ends are terminated in matched loads.



Testing of the plugs showed that in fact the RF-transmission is not disturbed. The behavior of the pass is like one of the PE-disks in the cable.

Operational Characteristics

Flame retardance tests

Low smoke emission test

The test has been carried out according to IEC 1034. The specification demands a light transmission $> 60\%$. The measurement gave a value of 86% for the cable. The excellent high value is due to the materials of the cable, only PE and the halogenfree, flame retardent outer jacket (FRNC jacket). The steel tube filling compound is also halogenfree.

Flame propagation test

The test has been carried out according to IEC 332/3. In this test 7 samples are fixed vertically in the oven, in a distance of 20 cm between each other.

The cable sheath protected the cable until the polyethylene was molten and began to drop out. After catching fire, the polyethylene burnt down completely. The last cable element being destroyed is the steel tube. To ensure its function even longer a flame retardent filling compound can be used. The fibers can be protected against the heat by using a fiber coating stable up to 180°C (normal fibers: 110°C).

It was remarkable that although the cable burnt down during the test the steel tube was able to protect the fibers against mechanical damages. Increasing the heat during the test will also destroy the fiber coating and the filling compound completely.

In a tunnel the cable is installed horizontally; in this case the fibers are lying without any mechanical stress in the steel tube. The transmission in case of fire will be working until a mechanical stress will occur at the "naked" fibers. So the steel tube can protect the fibers for a long time and ensures the function of the system in every section being not affected by the fire.

Mechanical Tests

Crush-Test

The test has been carried out according to EN 187000, 504. The plate had an area of $10 \times 10 \text{ cm}^2$. The sample is lying on a flat underground.

The crush resistance was tested up to 5 tons of load. No damage to the steel tube could be found. The cable was only crushed very slightly. Increasing the load up to 10 tons will crush the cable without damaging the steel tube.

The RF-transmission is not affected as long as the cable is crushed slightly. Such a crush results in a little higher attenuation, which will not avoid radiation of signals. The optical transmission was not affected anyhow.

Impact-Test

The test has been carried out according to EN 187000, 505. For the test an anvil of 1 cm^2 was used, the weight had 5 kg, the falling height was 25 cm.

This impact of 12.5 Nm caused no significant damage to the cable, the steel tube was not affected at all. Until the steel tube gets damaged an impact of at least 50 Nm is necessary.

Results

The results are showing that the cable can guarantee a high security level for a tunnel application. It is stable against high mechanical forces like crush and impact and is very suitable in case of fire with low environmental pollution. The steel tube as central element is very well protected against environmental influences, therefore the system allows maintaining of the services also in case of fire and mechanical damages for a long time. The optical transmission will be working further, even when the outer cable elements are completely destroyed.

Especially the reliability in case of fire results in a reliable tunnel communication system, whose sections keep working, except the burnt part.

The cable is completely halogenfree. Therefore no hazardous and/or corrosive gases will be emitted in case of fire. The damage to the tunnel and its technical installations will be limited to the area of the fire.

The replacement of a damaged cable of the system can be done very quickly, because only the cable has to be replaced by a new one. No duct has to be opened; the cable is installed at the tunnel wall.

Conclusion

A VARIO leaky cable offers, in comparison to normal leaky cables, the possibility to realize big sections lengths; about 60% longer. The system installation is much cheaper, because the number of feeders decreases about 55% and the installation time is cut down in the same way.

The next step in optimizing a tunnel system is to build up systems with hybrid cables, type LK 39 VARIO 900 FO. This cable type allows to install only 1 cable in the tunnel line; the fiber optic backbone cable is no longer necessary. Especially the installation is simplified, because only 1 cable has to be installed; the costly installation of the fiber optic backbone in the duct will be avoided completely.

A significant increase in reliability and safety can be obtained with these cables, especially in case of fire. The systems can be planned and build up much cheaper and in shorter times.

All in all it can be stated that the advantages of the VARIO cable concerning reach and signal quality have successfully been combined with the fiber optic backbone cable by integrating it into one single hybrid cable.

Literature

1. Heddebaut, M. Klingler, W. Pirad, M. Szélag, Technological Solutions for the transmission of the GSM signals in confined areas, DRIVE Technical Days 1993, Konsortium V2014-ICAR
2. Coraiola, H. Haag, K. Schulze-Buxloh, G. Thönneßen, Leaky Coaxial Cables with length independent antenna receiving level, IWCS 1992, pp 748-756
3. Becker, K. Schulze-Buxloh, GSM-Paramettermessungen im Düsseldorfer "Rheinallee"-Tunnel unter Verwendung eines "Repeater"-Verstärkers und eines optimierten strahlenden Kabels (VARIO 450/900), ITG Fachtagung "Antennen '94", Dresden, Antennentag 1994 pp 309-314

Gioio Brambilla

Director

Sirti S. p.A., Milano, Italy

G. Brambilla is technical director in the transmission systems division of Sirti S. p. A., Milano.



Helmut Haag (speaker)

KABELRHEYDT AG

Director

Mönchengladbach, Germany

Helmut G. Haag (46) is Director and head of the Product Group Telecommunication Cables. After reaching his Dipl.-Physiker-degree from the University of Stuttgart he joined AEG Kabel (previous name of KABELRHEYDT) in 1975 for the development of coaxial cables. Later he has been also responsible for the development of optical fiber cables. From 1980 to 1983 he built up the production plant for these cables. From 1984 to 1989 he has been responsible for the technical Sales Department and took over the Sales Division in 1990. He holds his present position since 1993.



Karl Schulze-Buxloh

RFS Hannover

Division of kabelmetal electro GmbH

Sales Department

Project Sales Engineer

Hannover, Germany

Karl Schulze-Buxloh (38) finished his studies at the Ruhr University Bochum in 1986 as Dipl. Ing. In the same year he joined Kabelrheydt. Since this time he is engaged in the development and sale of Leaky Coaxial Cables. In May 1994 he left KABELRHEYDT to join RFS, Hannover, a division of kabelmetal Hannover where he occupies the position of a project sales engineer in the field of distributed communication systems and RF-transmission lines.



Alexander Weiss

KABELRHEYDT AG

Development Telecommunication Cables

Mönchengladbach, Germany

Dr. Weiss (33) is head of the development department for Optical Fiber Cables since 1992. He finished his studies of chemistry at the University of Tübingen in 1990 as a graduate chemist. In the same year he joined Kabelrheydt.

Design of VHF-UHF super-wideband leaky coaxial cable(LCX)

I.Sakabe, K.Aihara, S.Hisano, Y.Sakata, S.Suzuki

Sumitomo Electric Industries, Ltd.
1 Taya-cho, Skae-ku, Yokohama 244, Japan

Abstract

Leaky coaxial cable (LCX) is a feeder provided with antenna functions to radiate electric wave with less field fluctuation along the cable. The increased use of the wide-frequency band by FM radio broadcasting (80 MHz) to portable digital phones (1900 MHz) is making it necessary to expand the band. The new LCX demonstrated good radiation characteristics over a frequency band by 80 to 2600 MHz, much wider than the widest conventional LCX covering the frequency band by 80 to 900 MHz through the following two modifications.

The first modification was to minimize the field fluctuation range of the multi-mode radiation band by optimizing the slot length through strict control of radiation directivity from the slot.

The second modification was to form a dummy slot, unrelated to radiation, in each half slot-group pitch to reduce impedance mismatch causing reflection.

1. Introduction

The leaky coaxial cable (LCX) is mainly used for mobile radio communication in the blind zone, such as tunnels and underground shopping areas. In Japan, it is applied to FM broadcasting (80 MHz), civil services such as law enforcement and firefighting (150 and 400 MHz), and business use services such as railroad radio (400, 900 MHz). In the past, LCX was laid individually for each frequency band. In 1992, we developed and put in practical use LCX applicable to an ultra-wide band of 80 to 900 MHz with one, and reported on it at the 41th IWCS¹⁾.

Mobile radio communication is growing rapidly as, in addition to the above services, the demand for telecommunication services such as pagers (280 MHz) and mobile personal phones (900 and 1500 MHz) is increasing. LCX used for these telecommunication services covers the 280 to 1500 MHz band with one.

LCX is now being studied for use in digital personal handy phone services requiring a much higher frequency band (1900 MHz).

Conventionally, several cables had to be laid to cover all of the above frequency bands shown in Fig. 1. We therefore developed LCX that covers the VHF-UHF super wide-band from 80 to 2600 MHz including the above whole bands, using one cable only.

The design concept and cable features are detailed in the sections that follow.

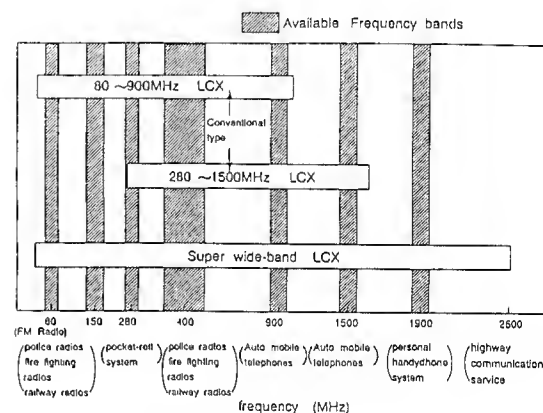


Fig. 1 Zone of available frequency

2. LCX cable structure

Fig. 2 shows the structural drawing of LCX. A hole called a "slot" in the outer conductor of LCX is foamed for radio wave radiation. This slot determines LCX radiation characteristics. The LCX diameter is about 52 mm. Aluminum pipe 17.3 mm in diameter is the inner conductor. Corrugated aluminum or copper tape is used as the outer conductor. Glass tape may be used to meet heat resistance specifications.

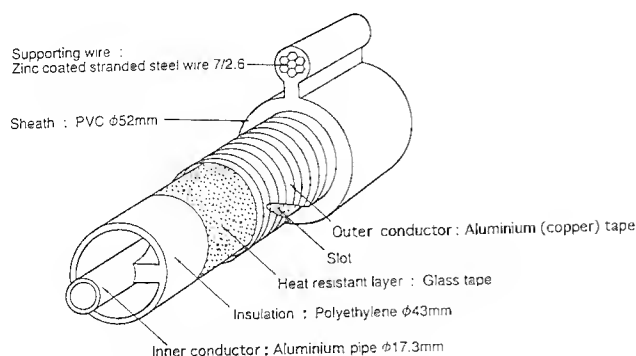


Fig. 2. Construction and size of super wideband LCX

3. Technical problems

3-1. Conventional LCX radiation principle

LCX uses the principle of the slot array antenna, having a slot group for radio wave radiation on the outer conductor. This slot group is formed in a predetermined cycle so that field strength is distributed as a sine wave. Since this slot group has an array antenna property, cutoff frequency is generated where the phase constant along the z axis is zero. The surface wave is obtained at frequencies below this cutoff frequency and the radiation wave at frequencies above it. LCX is mainly used for radiation band where radio waves must reach a distant destination. This radiation band can be divided into two zones -- the single-mode radiation zone where field fluctuation is small and the multimode radiation zone where field fluctuation is large (Fig.3). Conventional LCX is used only in the single-mode radiation zone.

This single-mode radiation zone was expanded two to three times by Nakahara et al. of SEI,²⁾ three to seven times by Kurauchi, Yoshida et al. of SEI,³⁾ and seven to 15 times by Aihara et al. of SEI.¹⁾ This single-mode band is restricted, however, by the complex dielectric constant of the insulation separating the outer and inner conductors, making it difficult to expand the band further due to the relationship with other vibration characteristics, for example.

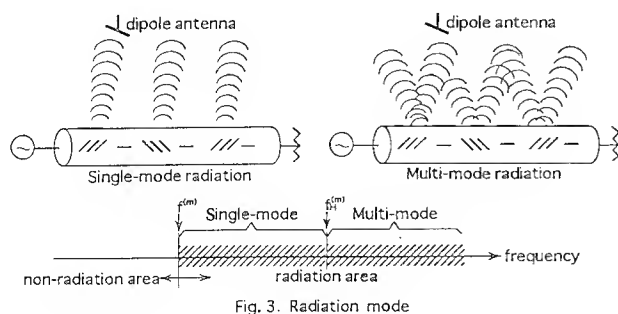


Fig. 3. Radiation mode

3-2. Frequency band expansion

3-2-1. Wideband radiation characteristics

To cover a wider available frequency band, we used the multi-mode radiation band, previously unused because its field fluctuation is large compared to that of the single-mode radiation band. When the slot length is elected most suitably, however, the directivity of the electric wave radiated from the slot is also optimized, reducing the radiation interference. Field fluctuation can be reduced to a level for communication even in multi-mode band where field fluctuation is large, and the frequency band can be greatly widened.

3-2-2. Reduction of resonance value

Resonance frequency had to be eliminated from the available frequency band because it increased transmission loss and noise, even in the single-mode radiation band. The progressive wideband implementation in available frequencies has made it impossible to eliminate such resonance frequency. We focused on the fact that resonance frequency is generated by slot reflection, and found that forming a superimposed slot (we call it "dummy" slot) unrelated to radiation for each half slot-group pitch reduces the resonance value. The use of almost all available frequencies, including resonance frequency in which communication was not possible in conventional slot design, thus became possible.

4. Theoretical considerations

The wideband radiation characteristics and reduction of resonance value, which were mentioned in Section 3, are detailed in this section.

4-1. Wideband radiation characteristics

Slots are arranged cyclically in the outer LCX conductor. This slot acquires susceptance, and progressive wave flowing in LCX is modulated spatially based on the periodic structure of this slot. It acquires spatial harmonics having a slot pitch cycle. When the phase constant along the z axis is assumed

$$\beta_n, \quad \beta_n = \beta + 2\pi n/p, \quad \beta = k/K_\lambda \quad (4.1.1)$$

where $n = 0, \pm 1, \pm 2, \dots$

p : one slot-group pitch

K_λ : wavelength compression rate in cable

k : free-space wave number

The radius component of the propagation constant β_n shown in equation (4.1.2) must be a real number for the radio wave leaked from the slot to become a radiation wave.

$$\beta_m = \text{Sqrt}(k^2 - \beta_n^2) \quad (4.1.2)$$

When β_m is a real number, the radiation area is as follows,

$$-n \times c / p / (1/K_\lambda + 1) < f < -n \times c / p / (1/K_\lambda - 1) \quad (4.1.3)$$

where c : light velocity

The radiation area can be divided into the following three frequency bands based on the interference of radio waves leaked from multiple slots:

- (1) Frequency band where β_m is an imaginary number and becomes the surface wave mode
- (2) Frequency band where β_m is a real number and consists of single-mode radiation only
- (3) Frequency band where β_m is a real number and consists of multi-mode radiation.

Standard LCX uses the single-mode radiation only. It is difficult for one cable using the single-mode radiation to cover the whole band from FM (80 MHz) to PHP (1900 MHz) because the frequency band ratio of the single-mode, f_H/f_L , is restricted to about 17 times, as shown in equation (4.1.4), on the assumption that the wavelength compression rate, K_λ , of the insulating material between the outer and inner conductors is 0.885:

$$f_H/f_L = (1 + K_\lambda) / (1 - K_\lambda) \approx 17 \quad (4.1.4)$$

This band ratio for the single-mode radiation, f_H/f_L , is less than that of the demanded band; $1900 \text{ MHz}/80 \text{ MHz} = 24$. Therefore, we focused on frequency bands for both (2) and (3). The frequency band for (3) was considered inappropriate for communication in the past because field fluctuation is increased by multimode radiation. Field strength leaked from the slot is expressed by equation (4.1.5),

$$E_\phi = \sum_{\{n, -\infty, \infty\}} j/4 J_{mn} \beta_n H_1^{(2)} \exp \{-j \beta_n z\} \times 2 \sin \{kl \sin \{\arctan(z/h)\} / k \sin \{\arctan(z/h)\}\} \quad (4.1.5)$$

where

J_{mn} : magnetic current distribution in slot section

$H_1^{(2)}$: Hankel function

l : slot length

z : distance from cable end along z axis

h : vertical distance between antenna and cable

j : imaginary number

The directivity of the electric wave leaked from the slot changes with the relationship between the slot length and available wavelength as shown by the sin term in equation (4.1.5). Fig. 4 shows the calculated field strength leaked from one slot, where the slot length is a parameter.

Field strength actually changes with the slot length, but all maximum field strengths are standardized at 0 dB so that directivity can be compared more easily.

Fig. 5 shows the theoretical computed results for the field strength fluctuation width in radiation from multiple slots using radiation characteristics of one slot in Fig. 4.

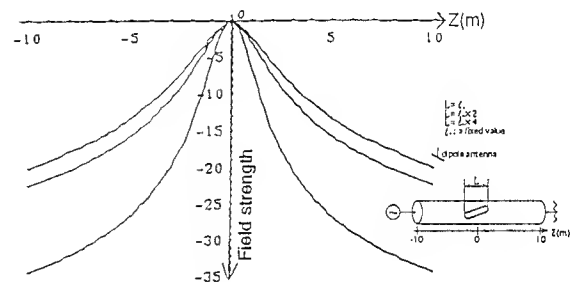


Fig. 4. Theoretical computed results of the field strength radiated from one slot

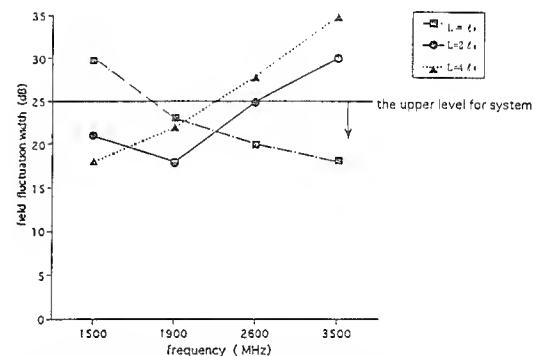


Fig. 5. Theoretical computed results for the field strength where slot length is a variable

Since the variation of field fluctuation width by slot length in the single-mode radiation band is small, Fig. 5 shows only the field fluctuation width in the multimode radiation band. In the implemented wideband frequencies of 1500 MHz and 1900 MHz the slot length with the lowest fluctuation is $2l_0$ and this $2l_0$ is understood to be the optimum slot length. Since the allowable field fluctuation width in the standard system is below 25 dB, the upper frequency limit will be 2600 MHz. That is, the frequency band ratio, f_H/f_L , is understood to be extended from the conventional 17 times to 32 times ($2600 \text{ MHz}/80 \text{ MHz} = 32$).

4-2. Reduction of resonance point

The voltage standing wave ratio (VSWR) is an index showing reflected wave intensity, and is defined as shown in equation (4.2.1):

$$\text{VSWR} = (1 + \Gamma) / (1 - \Gamma) \quad (4.2.1)$$

The reflection coefficient, Γ , is a sum of electrical power reflected from impedance mismatch and expressed in equation (4.2.2),

$$\Gamma = -2j \Gamma_0 \sum_{\{n, l, N\}} \sum_{\{m, l, M-1\}} \times \sin(kl/2) \times \exp\{jkp(m/M+n)\} \quad (4.2.2)$$

$$\Gamma_0 = Z' / Z \\ = j \{ \beta l^3 \sin^2(\theta) \} / \{ b^2 \text{Log}(b/a) \} \\ \times \{ \text{Log}(4l/w) - 1 \} + w/2\pi b \} \quad (4.2.3)$$

where

Z' : characteristic impedance in slot section

Z : characteristic impedance in non-slot section

l : slot length

w : slot width

b : inside diameter of outer conductor

a : outside diameter of inner conductor

In the conventional sineously slotted LCX, slots were arranged so that the wave resource intensity of the E_ϕ component was distributed as a sine wave. Slots were not opened to reduce transmission loss in the region that the E_ϕ component is zero. Therefore, impedance mismatch along the cable occurred in each half slot-group pitch. Since the resonance point causing trouble in communication appears at integral multiple frequencies (f_r) equivalent to the same wavelength as the impedance mismatch cycle, it was not possible to eliminate the resonance point from the frequency band if the available frequency band increased:

$$f_r = c \times K_\lambda / p \times n \quad (4.3.3)$$

A dummy slot was formed to eliminate impedance mismatch in each half slot-group pitch. This is equivalent to the sum, m , of equation (4.2.2) taken up to M .

In the slot configuration (Fig. 6), a dummy slot is formed for each half slot-group pitch in addition to the conventional slots. If the dummy slot is configured so that the characteristic impedance of each slot section is almost equal, the VSWR value shall be reduced.

Fig. 7 shows an example of VSWR calculation with and without dummy slots in Fig. 6.

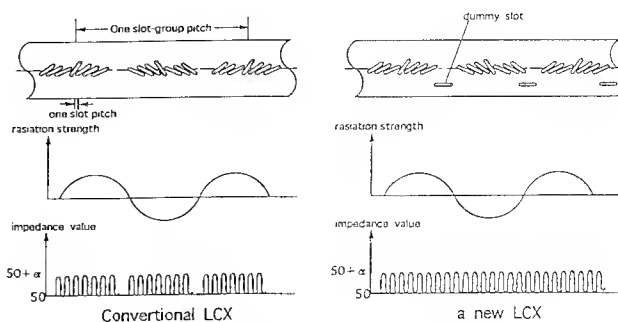


Fig. 6. Slots arrangement on a outer conductor

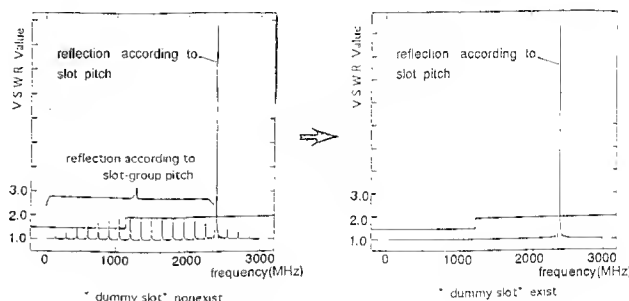


Fig. 7. Theoretical computed results for the VSWR characteristic

5. Experimental considerations

LCX with a slot pattern (Fig. 6) was fabricated and the coupling loss, transmission loss, and VSWR characteristic measured.

5-1. Coupling loss

Fig. 8 shows the frequency characteristics of the fabricated cable's coupling loss. The cable was laid straightly on the concrete and the distance between the cable and the dipole antenna was maintained at 1.5 meters, then the receiving level over the cable length (about 50 m) was consecutively measured. The mean value in the figure is a 50% accumulated value of level fluctuation and the fluctuation width is a peak-to-peak value. Frequency here is a representative value used for mobile radio communications in Japan.

The 50% accumulated value of coupling loss increases in proportion to frequency but, at frequencies above 1000 MHz, the receiving level drop due to multiple radiation interference. However, even at frequencies where the receiving level drops, the receiving level is over -85 dB required for the normal system.

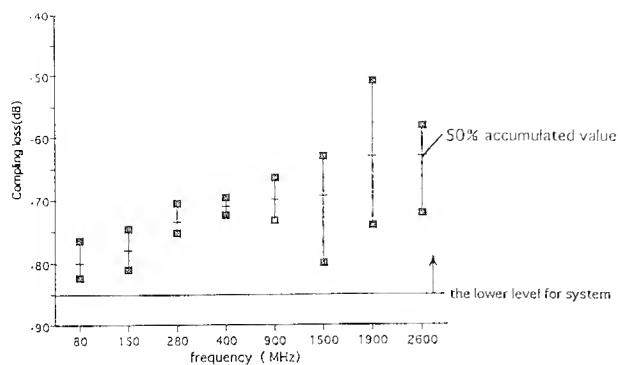


Fig. 8. Experimental results coupling loss

5-2. Transmission loss

Fig. 9 shows the frequency characteristics of transmission loss.

The allowable attenuation factor for the standard LCX is up to about 10 dB. The distance for 10 dB attenuation at a frequency of 1900 MHz is 100 meters. If the service area of the personal hand phone base station in Japan has a zone of about 100 meters, the fabricated LCX can cover this area without a amplifier. Transmission loss increases around 2400 MHz due to resonance in slots.

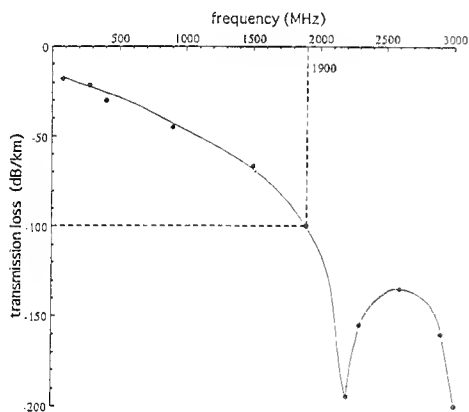


Fig. 9. Experimental results of transmission loss

5-3. VSWR

Fig. 10 shows the VSWR frequency characteristics of the fabricated cable after measurement each 1.87 MHz from 300 kHz to 3000 MHz. No resonance point appears except around 2400 MHz due to impedance mismatch for each slot.

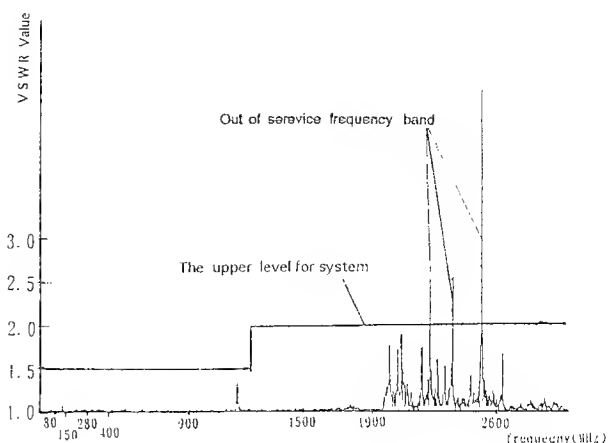


Fig. 10. Experimental results of VSWR characteristics

6. Conclusion

We studied the implementation of wideband leaky coaxial cable in theory and experimentally by clarifying two points:

- (1) Field fluctuation must be reduced so that radio directivity can be well controlled, even in the multimode radiation frequency band, by optimizing the slot length.
- (2) The formation of a dummy slot for each half slot-group pitch eliminates the large peak of impedance mismatch along the cable axis and reduces the resonance value.

We therefore suggest that LCX be used in communication systems both at conventional 80 - 900 MHz and at frequency bands of 1500 and 1900 MHz

7. References

- 1) K. Aihara et al., Ultra-High-Bandwidth Heat-Resistant Leaky Coaxial Cable, International Wire and Cable Symposium, Vol. 41, 1992
- 2) T. Nakahara et al., Leaky coaxial cable with slot array, IEEE Symposium on Antenna and Propagation, Boston, USA, Sept. 1968
- 3) N. Kurauchi, K. Yoshida et al., Wideband Leaky Coaxial Cable, Electronics and Communication in Japan, Vol. 54-B, No. 11, 1971

Itaru Sakabe
Sumitomo Electric
Industries, Ltd.
1, Taya-cho
Sakae-ku
Yokohama 244
Japan



Itaru Sakabe received the M.E. degree in electronics and communication engineering from Electro Communication University in 1993. He joined Sumitomo Electric Industries, Ltd. and then has been engaged in the development and design of communication cables. He is now an engineer of Communications Cable Division.

Yasuo Sakata
Sumitomo Electric
Industries, Ltd.
1, Taya-cho
Sakae-ku
Yokohama 244
Japan



Yasuo Sakata received the B.E. degree in electronics and communication engineering from Osaka University in 1974. He joined Sumitomo Electric Industries, Ltd. and worked on the development of the low loss unbalanced type cables. Thereafter, he concentrated on the development of coaxial cables and optical fiber cables. He is now Manager of Communications Cable Division.

Katsuyuki Aihara
Sumitomo Electric
Industries, Ltd.
1, Taya-cho
Sakae-ku
Yokohama 244
Japan



Katsuyuki Aihara received the B.E. degree in Physics from Tsuba University in 1987. He joined Sumitomo Electric Industries, Ltd. and then has been engaged in the development and design of communication cables. He is now an engineer of Communications Cable Division.

Shuzo Suzuki
Sumitomo Electric
Industries, Ltd.
1, Taya-cho
Sakae-ku
Yokohama 244
Japan



Shuzo Suzuki received the M.S. degree from Tokyo University in 1972. He joined Sumitomo Electric Industries, Ltd. in 1972, and has been engaged in research and development of optical fiber, cable and joining technologies. He is now Manager of Communications Division.

Satoshi Hisano
Sumitomo Electric
Industries, Ltd.
1, Taya-cho
Sakae-ku
Yokohama 244
Japan



Satoshi Hisano received the B.E. degree in electronics engineering from Shizuoka University in 1983. He joined Sumitomo Electric Industries, Ltd. and then has engaged in the development and design of communication cables. He is now a senior engineer of Communications Cable Division.

THE CLOSE-COUPPLING RADIO (CCR) SYSTEM

T.Ando, T.Watari

Hitachi Cable Ltd., Hitachi, JAPAN

Abstract

Automated rail-guided carrying vehicles require a reliable and high-rate data transmission system between a host computer and the vehicles when used for a high speed and large scaled system. Up to the present, common method is to use contact wires and collector brushes or optical laser communication system. However, the former has had frequent transmission error problems due to momentary contact breaks that happen as the vehicle travels, especially at high running speed. And the latter has been impossible to communicate on a non-linear route.

To solve these problems, a non-contact transmission system named "The Close-Coupling Radio(CCR) System" was recently developed. A twisted-pair leaky cable and coupler antenna are the fundamentals of the system.

This system can transmit carrier frequencies modulated by data and video, and audio signal.

Introduction

Automated rail-guided carrying vehicles(VEHICLES) system, as illustrated in Fig.1, is becoming common among plants due to the development of factory automation. These VEHICLES are suspended from the monorail and installed along transportation route. Many VEHICLES are located on the same line. Therefore, safety and high efficiency are required for the host computer(HOST) to control VEHICLES traffic via information correspondence between the host computer and the VEHICLES.

The twisted-pair cable and coupler (composed of small loop antennas and signal feeding circuit) were developed as a powerful communication means for the VEHICLES system. This new system has a stable transmission performance even in an environment with high electromagnetic noise. The radio system needs generally a radiating device such as an

antenna or a leaky cable. The CCR System may be classified as a kind of leaky feeder system, but it rarely radiates electromagnetic energy. Therefore, this system can be applied as a license-free low-power radio.

This paper describes development details, the functions, and applications of the CCR System.

The first investigation

When we communicate with mobiles, the radio communication method is frequently used. But generally, the communication method of VEHICLES system is to use the contact wires or optical laser. Because radio system has some transmission troubles by obstacles(for example, wall, machinery noise, etc.). And if it is used, the user must be licensed to use radio wave.

Therefore we had started to develop a new low-power radio system using leaky cable, to meet demands (license-free, large service length along the VEHICLE's route).

The most general leaky cable is a leaky coaxial cable, whose outer conductor has some slots to radiate radio wave. First, this cable was investigated. But the following problems were left.

- (1)An antenna, such as a half wavelength dipole antenna, on VEHICLE radiates too high electromagnetic field.
- (2)Both this cable and an antenna receive noise as much as required carrier.

So we had to develop a leaky cable with a new concept to solve these problems.

The CCR cable and a coupler

Selection of frequency band

It is not too much to say that selection of frequency band decides characteristic of radio system.

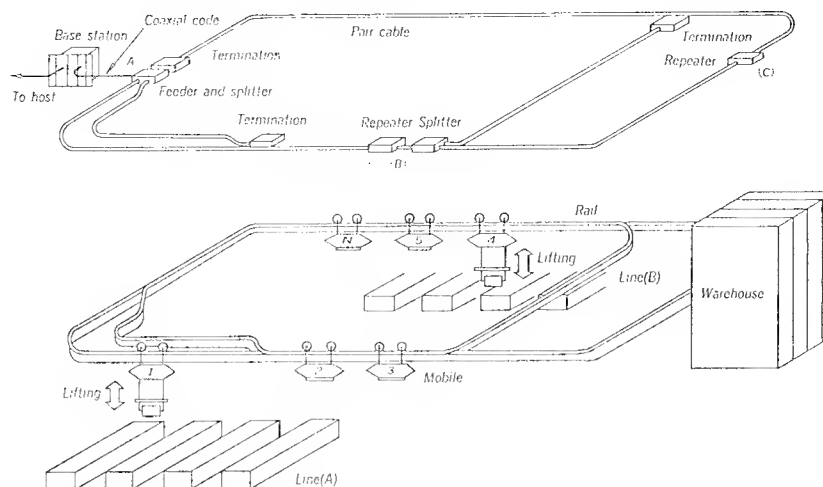
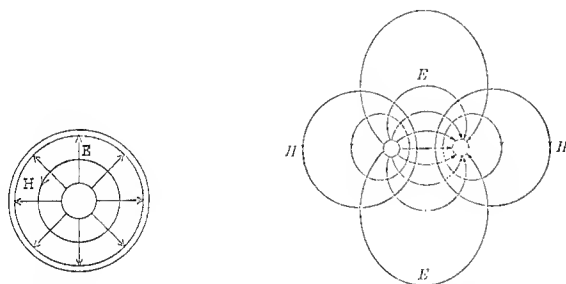


Fig.1 - Monorail VEHICLES and a CCR System
Monorail VEHICLES run on a rail route along a transportation line in plant. Carrier signals transmit between a HOST and the VEHICLES through a CCR Cable.

VHF band was selected because the transmission loss is not too much and the electromagnetic noise at VHF band is low.

The CCR Cable

Common feeders for VHF band are a coaxial cable and a non-twisted bifilar line. These transmission modes are shown in Fig.2.



(a) Unbalance Mode (b) Balance Mode

Fig.2 - Transmission Mode

The noteworthy point in Fig.2 is that an electromagnetic field distributes widely around a bifilar line. An inductive radio system, one of the applications of this line, utilized effectively electromagnetic field.

Therefore we investigated if a bifilar line can be applied at VHF band as an inductive radio system. But the electromagnetic field of this cable can be easily converted to an unbalance mode or radiation mode. When we construct license-free low-power radio system, electromagnetic power to supply to a leaky

cable or an antenna must be much small. Such means goes against to keep long service length.

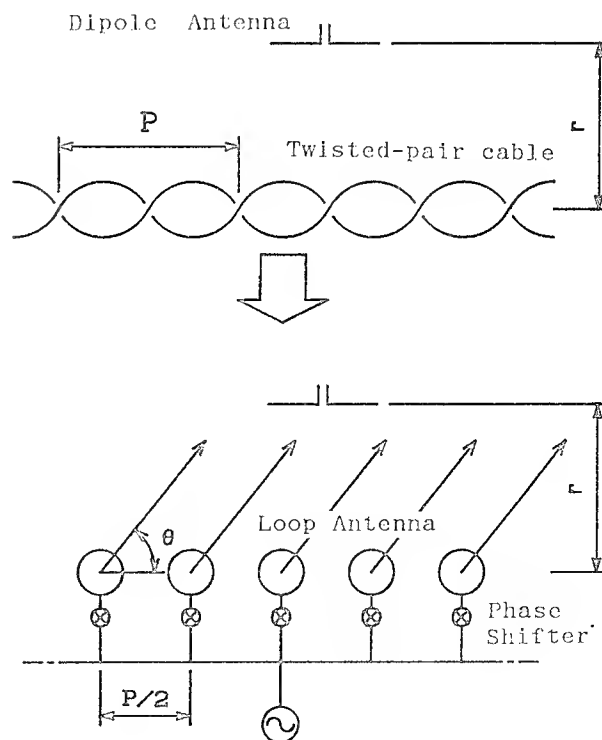


Fig.3 - Radiating Model
For investigating easily, twisted-pair cable is replaced with the array antenna.
 P : Lay Length
 r : Distance between the cable and the antenna
 θ : Radiating Angle

Then, we paid attention to a twisted-pair cable. To analyze an electromagnetic field from this cable, it can be replaced with loop antennas as shown in Fig.3. A power source feeds signal to each antenna through a phase shifter. A phase difference is decided by lay length (P). Therefore, the component magnetic field (H_0), which each antenna leaks, is shown in Formula (1) at a long distance from the cable.

$$H = \sum_{n=1}^N e^{-jkr} H_0 e^{-j\phi} \quad (1)$$

$$\left[\phi = k_0 n \frac{P}{2} \cos \theta - n \pi \left(\frac{P}{\lambda} + 1 \right) \right]$$

H_0 : Magnetic Field
 k_0 : Phase Speed in free space
 k : Phase Speed
 P : Lay Length
 θ : Radiating Angle
 λ : Wavelength
 r : Distance between cable and Antenna

When lay length is equal to wavelength and radiating angle is equal to 90 degree, $|H_0|$ becomes maximum as shown in Formula (2).

$$|H| = NH_0 \quad (2)$$

When lay length is sufficiently shorter compared with the wavelength, ϕ is nearly equal to $n\pi$, and $|H_0|$ becomes minimum as shown in Formula (3).

$$|H| = 0 \quad (3)$$

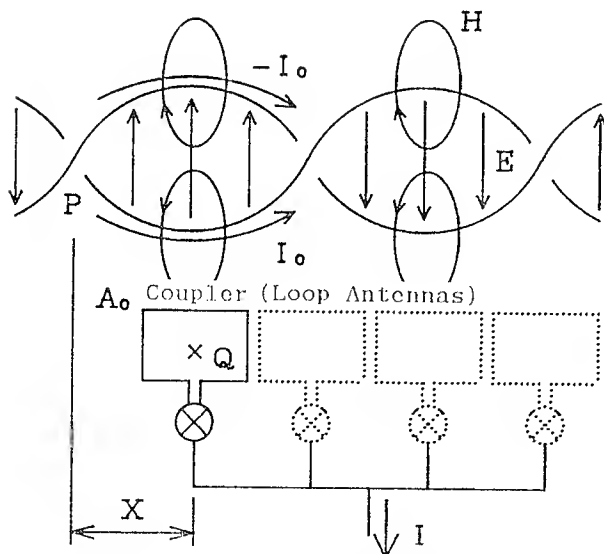


Fig.4 - Transmission Mode of The CCR Cable and Coupler

I_0 : Electric current
 E : Electric Field
 H : Magnetic Field
 A_0 : Coupling loss
 X : Length between P and Q

By applying this theory, we developed the CCR cable which restricts radiation.

Fig.4 shows a coupler as an antenna and the electromagnetic field of the CCR cable.

Coupler

As mentioned above, the CCR cable as shown in Fig.5 is a specially designed leaky cable, which distributes electromagnetic field close to this cable as shown in Fig.4. It is clear that an common antenna, such as a half wavelength dipole antenna, can not pick up this electromagnetic field.

Then we developed an array antenna constructed by small loop antennas.

In Fig.4, electromagnetic field can be replaced with an electric current I_0 . An output current I , which is received by one loop antenna, is shown in Formula (4). A_0 is a constant to mean minimum coupling loss.

$$I = A_0 \sin \left(\frac{2\pi}{P_0} X \right) I_0 e^{j\omega t} \quad (4)$$

A_0 : Coupling Loss
 P_0 : Lay Length
 I_0 : Electric Current
 ω : Angle Speed

This formula shows that an output current by one loop antenna fluctuates frequently.

Then, when two loop antennas are arranged in half of lay length, an output current I , which combined with 180 degree phase difference, as shown in Formula (5).

$$I = A_0 I_0 e^{j\omega t} \left[\sin \left(\frac{2\pi}{P_0} X \right) + \sin \left(\frac{2\pi}{P_0} X + \pi \right) e^{j\pi} \right] \\ = 2 A_0 I_0 e^{j\omega t} \sin \left(\frac{2\pi}{P_0} X \right) \quad (5)$$

This formula shows that even two loop antennas can not prevent frequent fluctuation.

When four loop antennas are arranged in quarter of lay length and fed with 90 degree phase difference, output current I is shown in Formula (6). This formula shows zero fluctuation.

$$I = A_0 I_0 e^{j\omega t} \left[\sin \left(\frac{2\pi}{P_0} X \right) + \sin \left(\frac{2\pi}{P_0} X + \frac{\pi}{2} \right) e^{j\frac{\pi}{2}} \right. \\ \left. + \sin \left(\frac{2\pi}{P_0} X + \pi \right) e^{j\pi} + \sin \left(\frac{2\pi}{P_0} X + \frac{3\pi}{2} \right) e^{j\frac{3\pi}{2}} \right] \\ = A_0 I_0 e^{j\omega t} \left[2 \sin \left(\frac{2\pi}{P_0} X \right) + j 2 \cos \left(\frac{2\pi}{P_0} X \right) \right] \\ = A_0 I_0 \exp \left\{ j \left(\omega t + \frac{2\pi}{P_0} X + \frac{\pi}{2} \right) \right\} \quad (6)$$

A coupler is shown in Fig.6.

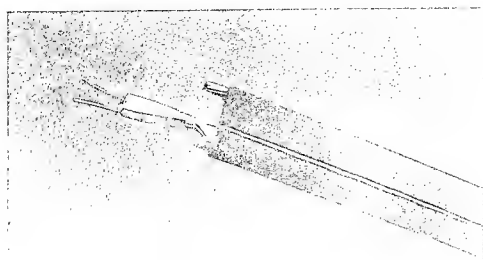


Fig.5 - CCR Cable

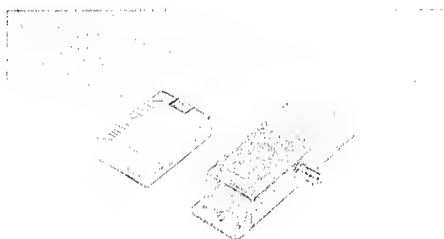


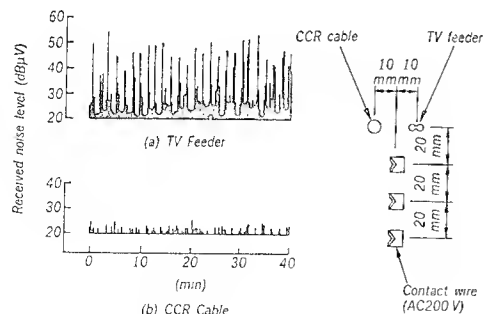
Fig.6 - Coupler

Received Noise Level

It is already explained that the CCR cable rarely radiates radio waves. In the other word, the CCR Cable rarely receives a noise from machines or other radio system.

Fig.7 shows carrier noise levels from power feeding contact wires that located very close to the CCR Cable.

Noise levels on a TV feeder (a non-twisted bifilar line selected as an example) and on the CCR Cable were compared. The noise level on the CCR Cable is 20 to 30 dB less than on the TV feeder.



Note: Quasi-peak value at 150 MHz

Fig.7 - Received Noise Level
Noise level on a CCR Cable is 20 to 30 dB less than a TV feeder.

Level Diagram

A Formula (7) shows a level calculation of the CCR System. Fig.8 is an example calculation at the (A)-(B)-(C)-(A) shown in Fig.1. This route maintains a minimum value of 48dBμV by repeaters installed at points (B) and (C). When a route length is longer than normal or a route split is added, a repeater compensates the loss and maintains the minimum required level.

$$\begin{aligned} \text{Received voltage} &= \text{Output power}(113\text{dB}\mu\text{V}) \\ &- \text{Attenuation}(4.8\text{dB}) \\ &\div \text{Amplitude of repeater}(15\text{dB}) \\ &- \text{Attenuation of the CCR Cable} \\ &\quad (0.06\text{dB/m}) \\ &- \text{Coupling loss}(50\text{dB}) \end{aligned} \quad (7)$$

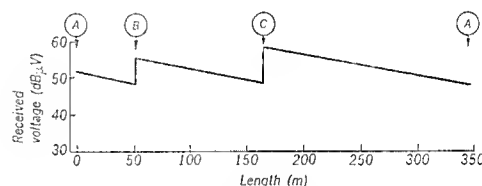


Fig.8 - Level Diagram
Repeaters are strategically to maintain a minimum received voltage of 48dBμV.

Requirement For Communication

VEHICLES move on command from the HOST. For example, when the HOST demands the VEHICLES to carry a certain package from the production line to specified automatic warehouse, a CPU on the VEHICLE, gives servo-devices sequential orders to complete the transportation movement. The HOST controls VEHICLE traffic depending on status information generated from each VEHICLE.

The data communication system between the HOST and VEHICLES should operate accurately under any VEHICLE conditions: speed, running route, number of VEHICLES and so on.

Electromagnetic compatibility(EMC) and stable transmission should be assured for this purpose.

Furthermore, when this communication system is applied to a plant-use monitoring system, video and sound transmission should also be available in the system.

Transmission Concept

According to the requirements above.

- (1) Data transmission speed is available up to 19.2 kbps.
- (2) Frequency range covers video and sound signal.

- (3) Data must be transmitted from the HOST to the VEHICLES within 0.3 seconds.
- (4) Communication must be correct and clear regardless of background noise from power feeding contact wires or other machinery nearby.

The VEHICLES System Application

Component of this system

Actual plants require various configurations in rail routing. The CCR System must have flexible construction ability to suit any required rail route. Components as shown in Table 1 accommodate this demand. Fig.9 illustrates the base station, the vehicle station, and the coupler.

Communication Protocol

The HOST controls vehicular stations to switch transmission in order when plural vehicular MODEMs simultaneously transmit carriers on same frequency.

Transmission time is one of the important factors in the VEHICLES System. Switching creates unstable time which decreases transmission capacity, even if the bit rate of a radio MODEM is high.

Table 1 - Specifications of CCR System Components.

Using a splitter and a repeater, various roots can be composed.

	Items	Specification
Data transmission	System	Full duplex Asynchronous
	Modulation	FSK
	Carrier	2 frequencies at VHF
	Bit rate	19.2 kbps
	Controller for base	16 bit CPU Max. 576 kbytes RAM/ROM
	Controller for vehicle	8 bit CPU Max. 64 kbytes RAM/ROM
Video transmission	Modulation	FM
	Carrier	VHF
	Video signal	NTSC, 1 V _{p-p}
Audio transmission	Modulation	FM
	Carrier	VHF
CCR cable	Impedance	180 ohm nominal
	Attenuation	6.0 dB/100m
	Diameter	12.5 mm
Jamper cable	Impedance	180 ohm nominal
	Attenuation	30 dB/100m
	Diameter	10 mm
Coupler	Coupling loss	50 dB at 10 mm gap
	Impedance	50 ohm
Feeder	Power feeding	DC +12 V
	Attenuation	0.5 dB at VHF
	Impedance	50 ohm
	Balanced terminal	180 ohm
Splitter	Attenuation	3.5 dB at VHF
	Impedance	180 ohm nominal
Repeater	Gain	10 to 15 dB at VHF
	Impedance	180 ohm nominal
Termination	Impedance	180 ohm nominal



(a) Base Station



(b) Vehicular Station

Fig.9 - Based Station and Vehicular Station

An ordinary MODEM has an unstable time of hundreds milliseconds. Polling, as shown in Fig.10(a), has been applied generally. A high-speed polling system was developed for the VEHICLES System (Fig.10(b)). In this paper, the former is referred to as low-speed polling.

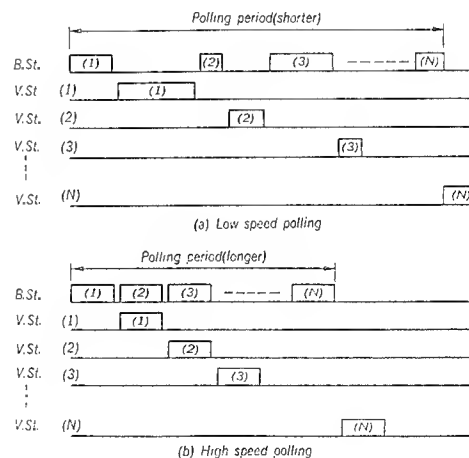


Fig.10 - Transmission Procedure
Data length is variable for low-speed polling and constant for high-speed polling. Polling period is shorter on the latter than the former.
B.St. : Based Station
V.St. : Vehicular Station

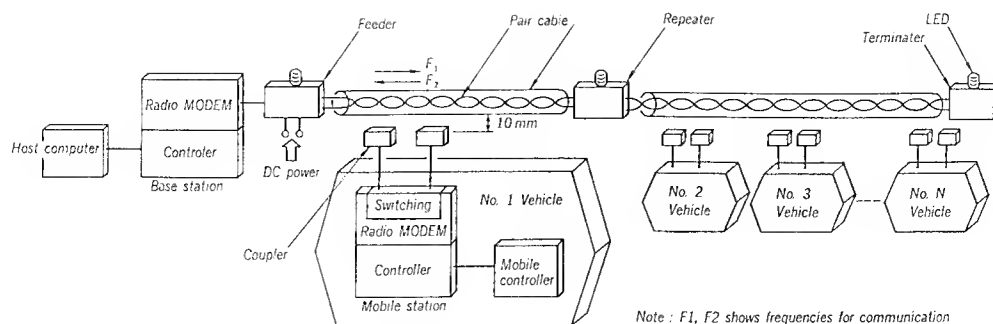


Fig.11 - Communication of CCR System
VHF signal transmit between a CCR cable and a coupler.
Two coupler are used for diversity.

An ordinary MODEM has an unstable time of hundreds milliseconds. Polling, as shown in Fig.10(a), has been applied generally. A high-speed polling system was developed for the VEHICLES System (Fig.10(b)). In this paper, the former is referred to as low-speed polling.

In this system, the HOST selects low-speed polling for non-work and high-speed polling for work. As a result, a polling period of 0.3 sec. was accomplished when the HOST communicates 2 bytes of data with 32 VEHICLES.

Fig.11 shows constitution of the CCR system for VEHICLES System.

The Patrol Robot Application

Fig.12 shows an automated patrol robot used at a hydroelectric power plant. Generally, large hydroelectric power plants that are located in remote areas, are planned to be unmanned. For this purpose, many types of automaton are applicable. A patrol robot is one automated system used to detect visible and audible trouble in the plant. This robot is useful for monitoring plant operations and acts according to directions from a remote control center in case of emergency.

A patrol robot requires the following transmission performance functions:

- (1) Clear image information under bad electromagnetic circumstance.
- (2) Reliable transmission under bad condition.

The CCR System is appropriate for these requirements due to its stable coupling and restrained noise at carrier frequency.

Table 2 shows the patrol robot specification. This robot is patrolling in Kurobe-gawa Daiyon Power Plant from 1992.

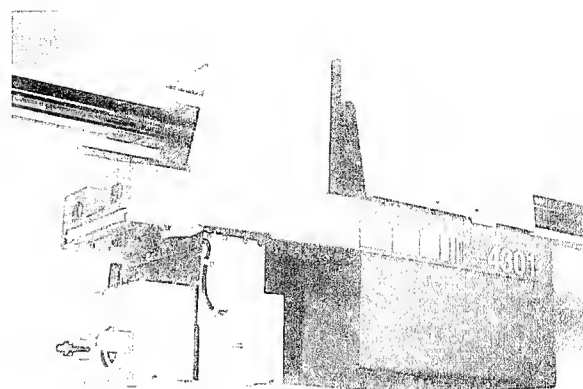


Fig.12 - Patrol Robot
This robot patrols in Kurobe-gawa Daiyon Power Plant.

Table 2 - Specifications of Patrol Robot
There are two ways to operate a robot. Remote manual operation (for emergency), and remote automatic operation (for regular conditions).

Items	Specification
(1) Sensor	ITV camera with zoom lens, Thermo-sensor, Microphone
(2) Max. speed	About 40 m/min.
(3) Transmission	Data, Audio, Video Data transmission speed 9600 bps Image S/N > 30 dB
(4) Operation	1) Remote manual operation 2) remote automatic operation
(5) Option	Image processing system

Conclusions

Development of the CCR System and its application to VEHICLES System and a patrol robot was described.

This system accomplished high-speed operation of the VEHICLE and patrol robot with high reliability and clear video and sound transmission. This is economical because it requires less VEHICLES thanks to highly efficient transportation.

Reference

(1) T. Ando, T. Watari: "A Close-Coupling Radio (CCR) System for Monorail Vehicles" Hitachi Cable Review, 1991.



Toshiyuki Ando

Communication System
Design Dept.
Hitachi Cable, Ltd.

5-1-1 Hitaka-cho,
Hitachi-shi Ibaraki-ken
JAPAN

Currently engaged in the radio system and antenna cable development and engineering. Received B.E. degree in information science from the University of Tsukuba, 1990.



Toru Watari

Communication System
Design Dept.
Hitachi Cable, Ltd.

5-1-1 Hitaka-cho,
Hitachi-shi Ibaraki-ken
JAPAN

Currently engaged in the radio system and antenna cable development and engineering. Graduated from Miyagi Technical College, 1968.

OPTICAL FIBER STRENGTH, FATIGUE AND HANDLEABILITY AFTER AGING IN A CABLE

Anurag Dwivedi*, G.S. Glaesemann* and C.K. Eoll**

*Corning Incorporated, Corning, NY 14831. (607) 974-3543

**Siecor Corporation, Hickory, NC 28603. (704) 323-6218

Abstract

A recent publication clearly shows that the primary cause of mechanical failure for fiber-optic cable in the field is digups.¹ To repair the cable, it is important that the fiber be handleable, even after exposure to extreme natural environments. In the present work we study the effectiveness of cable and optical fiber coatings in maintaining the handleability of fibers contained in a cable exposed to severe environments.

Optical fibers were removed from a cable that was severely aged in the laboratory and stored outside without a thermal barrier. The strength was not degraded and the peak strip force was found to be within the acceptable handleability limits.

Introduction

Handleability of optical fibers pertains to the ability to strip, clean, cleave, terminate and connectorize short lengths of fiber during installation or re-entry. The combined bending and tensile stress applied to short fiber lengths during termination or splicing can be on the order of 200 to 300 kpsi (1.4-2.1GPa).² For example, it is believed that applied stresses on this order can be generated during stripping and that the peak strip force is simply a reflection of this. Therefore, in addition to such external factors as damage from the stripping tool and stripping technique, the fiber brings two key handleability properties; namely, fiber strength and peak strip force. Sufficient strength over short lengths ensures survival of the handling event and a peak strip force within established limits keeps the applied stress below the fiber strength during stripping.

Strength testing and peak strip force testing are two ways in which the handleability of cabled fiber can be assessed. These tests can be performed on as-drawn or as-cabled fibers to examine handling during installation. To determine the handleability of fiber for eventual re-entry one would clearly prefer to test fiber in the aged state. Whereas there is an abundance of strength data on short fiber lengths after laboratory aging, there are only a few publications that examine the strength of fiber in the field aged state.^{3,4} The purpose of this study is to examine the handleability of fiber aged in a cable and to reflect on the significance of the results as they pertain to handleability of fibers during cable repair.

Aging of pristine optical fiber surfaces is a process whereby extreme temperature and humidity conditions in the laboratory may introduce microscopic flaws onto the surface of optical fiber. The introduction of these flaws is known to reduce fiber strength of short lengths from near intrinsic levels. For example, Figure 1 shows a dramatic decrease in fiber strength, as measured in 2-pt bending, as a function of time in 100°C water.⁵ Like the data in Figure 1, nearly all aging studies have been performed on short lengths of optical fiber in the as-drawn condition and in unrealistic aging environments. Consequently, some have suggested that aging is a life-limiting phenomenon for installed optical fiber.^{6,7,8} However, for most fiber applications, one can show that the flaws of greatest strength related reliability risk are not those on pristine fiber surfaces. Rather, it is flaws near the proof stress that pose the greatest risk.⁹ Thus, the aging of relatively large flaws receives the bulk of our reliability concern and the aging of pristine surfaces receives the bulk of our handleability

concern. The aging and fatigue of relatively large flaws in optical fiber has been addressed in a recent publication.¹⁰

Due to the susceptibility of the silica optical glass fiber to subcritical crack growth, cables are designed to minimize the applied tensile stress on the fiber. To the authors' knowledge, no field failure has been attributed to strength degradation from fiber fatigue. The effect of either coatings or the cable components during aging on the fatigue resistance of silica fiber is also studied in the present work by testing the dynamic fatigue of cable-aged fibers.

The Cable Design

A schematic of the design of cable used in the present study is shown in Figure 2. The fibers in the cable consisted of nine standard silica-clad fibers and one commercial titania-doped-silica-clad fiber. All fibers were coated with a dual layer acrylate coating and an overcoating of a thin layer of solvent based colored ink.

These fibers are contained within a buffer tube filled with fill compound. Kevlar strength members flooded with a water blocking compound are arranged around the buffer tube. This assembly is enclosed within a steel armor which is not hermetically sealed. Finally, an outer polyethylene jacket surrounds all the components. The basic components surrounding the fiber are labeled in Figure 2.

Aging Conditions

The deliberate aging tests performed on this cable are given below.

Accelerated aging:

- ≈15 days at 70°C during Temperature Cycling.
- 7 days at 80°C Heat Soak.
- 5 weeks at 80°C and 94% RH Heat/Moisture Aging.

Storage: The cable was stored on a wooden reel and left outside the building from August 20, 1990 until December 3, 1992. There was no thermal wrap covering the cable. The combined effect of laboratory aging and natural environment was severe enough that the original cable reel disintegrated and the cable had to be transferred onto another reel before testing.

Experimental Testing

In this study we focus primarily on fibers from the outermost wrap of the original reel since this portion of the cable was directly exposed to the aging environment.

Removing fibers from the cable:

Approximately two meters of cable was cut from the cable reel and fibers were carefully pulled out without touching the prospective gauge length portion of the fibers. The filling compound was removed from individual fibers by soaking a Kimwipe cloth with D-Gel and carefully sliding the fiber through the cloth. After cleaning, fibers were hung vertically by attaching their ends to double-sided sticking tape mounted on the wall. All specimens were prepared in a controlled environment of 45% RH and 23°C.

Strength Testing:

Strength testing was performed on a universal testing machine.[†] The gauge length was 0.5 meters and the cross head speed was 500 mm/min which corresponds to a strain rate of approximately 70%/min. Fibers were attached to the testing machine by wrapping fiber a minimum of two times around 2" diameter seamless Tygon tubing capstans at either end of the gauge length. The fiber is finally held in place by securing the ends under an elastomeric band. The test environment was maintained at 45% RH and 23°C. Approximately 15 specimens were tested for each color.

[†] Instron Corp., Canton Ma.

Strip Force Testing:

Strip force testing was performed using the industry accepted TIA test method FOTP-178.¹¹ Peak strip force results were obtained using a data acquisition rate of 5 Hz. The effect of coloring ink on peak strip force was studied. Also, the peak strip force was measured as a function of preconditioning time in ambient environment.

Dynamic Fatigue Testing:

In addition to examining fiber handleability, it is convenient to perform fatigue testing as well. Specimens were removed from the cable, cleaned, and stored in ambient conditions for two months. All specimens were preconditioned in the test environment of 100% RH and 23°C before testing. Fibers were tested using four strain rates ranging from 25%/min. to 0.025%/min. Fifteen specimens per rate were tested for silica-clad fibers, whereas, only five specimens per strain rate were used for the titania-doped-silica clad fiber.

It is important to note that the functional implications from fatigue results obtained on short fiber lengths tested at fast rates has been questioned. Fatigue tests on longer lengths using slower stressing rates provide more functional n parameter since the fatigue of the largest flaw under static loading condition controls the mechanical reliability of fibers in the field installed cables. In the present study, however, tests were performed on shorter lengths due to the difficulty in removing long length fibers from the cable. For this reason, the fatigue results of short length cable aged fibers from this study are compared with those obtained on as-drawn fibers.

Results and Discussion

The Aging Environment:

Though accelerated aging is convenient for commercial purposes, it is recognized that models translating experimental results from accelerated aging studies to actual in-service environments are limited. Without a predictive model for translating accelerated test environments to equivalent in-service

environments, one can either wait 10 to 20 years and test actual field installed cables or choose accelerated tests that are far worse than expected for the in-service environment. The first option requires an unacceptable amount of patience for cable developers while the latter, used for this study, runs the risk of being too conservative.

Strength Experiments.

Several specimens were tested for strength immediately after preconditioning in 23°C/45%RH for one week. The strength values are shown in Figure 3 and Table 1 for fibers of different color. The results indicate that there is little dependence of strength on ink color. More importantly, the measured silica-clad fiber strength distribution with a median value of 775 kpsi (5.35GPa) is the same as the as-drawn fiber strength distribution for this fiber shown in Figure 4. Similarly, the strength of the aged titania-doped-silica-clad fiber of 715 kpsi (4.93GPa) is typical for this fiber in the as-drawn condition.¹² It is concluded that the aging of this cable has not degraded the strength distribution of the fibers contained within. The strength of these fibers is sufficient for common field handling scenarios during cable repair even after the severe aging.

Strip Force Experiments:

Strip force measurements were performed on each of the colored silica-clad fibers immediately after removal from the cable. The strip force results of aged colored fibers are summarized in Table 2 where the standard deviation for five test specimens is reported. The results show that there is little or no dependence of strip force on ink and that the peak strip force is approximately 0.53 lbf for silica-clad fibers. Furthermore, the strip force values for aged silica-clad and titania-doped-silica-clad fibers (Table 2) are typical of as-drawn values of the respective fiber/coating systems.

To better understand the effect of time after removal from the cable on the handleability of the fiber, peak strip force was measured as a function of drying time after removal from the cable. A total of 20 specimens were tested in the as-removed condition and five

specimens were tested for each subsequent drying time. During the time between removal from the cable and testing, the fibers were stored in laboratory ambient conditions of 23°C and relative humidity ranging from 25 to 35%. The results from this testing are summarized in Figure 5 and show a small increase in peak strip force for both fiber types. This increase is believed to be due to the removal of residual moisture from the coatings. All fibers show strip force appropriate for good handleability of the fibers.¹³

Dynamic Fatigue of Aged Fibers:

Dynamic fatigue testing of these fibers did not yield any unusual results. The n value for silica-clad fibers and titania-doped-silica-clad fibers was measured to be 22.6 and 26.9, respectively. The dynamic fatigue plots are given in Figures 6 and 7 respectively. Dynamic fatigue of the aged fibers is not statistically different from that of as-received fibers tested in the same manner. This indicates that the fatigue behavior of the fibers was not degraded by aging in the cable.

Summary

Severe aging of a fiber-optic cable did not degrade the handleability or fatigue behavior of the fibers contained within it. The peak strip force of aged fibers is the same as the typical peak strip force of unaged fibers and is considered appropriate for handleability. In addition, the strength of aged fibers is not degraded due to severe cable aging. It can be concluded from these studies that zero-stress-aging is not a reliability concern for fibers aged in fill compound and other cable components because no strength degradation was observed after severe cable aging.

This work also suggests that the cable components do what they are designed to, which is protect the fiber even in events such as severe aging. This suggestion is also supported by the recent work published by Hoslov where strength and static fatigue resistance of fiber is found to be better in cable environment than in uncabled form.⁸ In conclusion, the cable-aged fibers are handleable for cable repair and the aged coating and cable components did not create

an environment where accelerated fatigue or aging of the fibers occurred.

Table 1. Fiber Strength and Fatigue after Aging in Cable

Fiber Type	Color	Mean Strength kpsi (GPa)	Weibull Slope m	Fatigue suscep- tibility parameter (nd)
Silica-clad	Blue	783 (5.40)	63	23
Silica-clad	Green	791 (5.46)	73	
Silica-clad	Orange	782 (5.39)	54	
Silica-clad	Brown	767 (5.29)	62	
Titania- doped- silica-clad	Red	712 (4.91)	47	27

Table 2. Fiber Peak Strip Force after Aging in Cable

Fiber Type	Color	Mean Strip Force, lbf (N)	Typical Strip Force of As-Drawn Fibers, lbf (N)
Silica-clad	Blue	0.55 ± 0.07 (2.45 ± 0.31)	0.55 ± 0.04 (2.45 ± 0.18)
Silica-clad	Green	0.54 ± 0.10 (2.40 ± 0.45)	
Silica-clad	Orange	0.50 ± 0.05 (2.22 ± 0.22)	
Silica-clad	Brown	0.54 ± 0.08 (2.40 ± 0.36)	
Titania- doped- silica-clad	Red	1.05 ± 0.29 (4.67 ± 1.29)	1.05 ± 0.15 (4.67 ± 0.68)

Acknowledgements

The authors thank D.W. Hill, P.T. Garvey, D.A. Clark and D.J. Walter for their technical advice and experimental assistance. They also thank R. S. Wagman for his help.

References

1. S.V. Lisle, "The History, Prevention, and Impact of Fiber Optic Cable Failures," pp. 223-235 in Proceedings of the 1993 National Fiber Optic Engineers Conference (NFOEC '93) in San Antonio, Tx, June 14-17, 1993.
2. N.J. Bonanno et al., "Handling Behavior of Aged and Unaged Fibers During Splicing Operation", pp. 241-244 in Proceedings of the 1993 National Fiber Optic Engineers Conference (NFOEC '93) in San Antonio, TX, June 14-17, 1993.
3. H. Yuce, et al., "Effects of the Environment on an Unprotected Reel of Optical Fiber," Proceedings 40th International Wire and Cable Symposium, pp. 700-706 (1991).
4. H.H. Yuce et al., "Fiber Reliability Study of Field Aged Optical Cables," pp. 705-708 in proceedings of the 41st International Wire and Cable Symposium, November 16-19, Reno, Nevada, 1992.
5. M.J. Matthewson and C.R. Kurkjian, "Environmental Effects on the Static fatigue of Silica Optical Fiber," J. Am. Ceram. Soc., 71 [3], pp. 177-83 (1988).
6. Kurkjian, SPIE Berlin, 1993 to be published.
7. P. Haslov, K.B. Jensen, and N.H. Skovgaard, "Degradation Study for Stressed Optical Fibers in Water. New Worst Case Life Time Estimation Model," pp. 423-427 in proceedings of the 41st International Wire and Cable Symposium, Reno Nevada, 1992.
8. P. Haslov, K.B. Jensen, and N.H. Skovgaard, "Degradation of Stressed Optical Fibers in Water: New Worst-Case Lifetime Estimation Model," J. Amer. Cer. Soc., 77 [6], pp. 1531-1536, 1994.
9. G.S. Glaesemann, "Optical Fiber Failure Probability Predictions from Long-Length Strength Distributions," pp. 819-825 in proceedings of the 40th International Wire and Cable Symposium, St. Louis, Mo., 1991.
10. G.S. Glaesemann, "The Mechanical Behavior of Large Flaws in Optical Fiber and Their Role in Reliability Predictions," pp. 698-704 in proceedings of the 41st International Wire and Cable Symposium, Reno Nevada, 1992.
11. TIA Fiber Optic Test Procedures (FOTP) 178 and 76.
12. S.T. Gulati, J.D. Helfinstine, G.S. Glaesemann, D. R. Roberts, E. Cuellar, and L.M. Middleman, "Improvements in Optical Fiber Reliability via High Fatigue Resistant Composition," in Fiber Optics Reliability: Benign and Adverse Environments, Proceedings of SPIE 842, pp. 22-31 (1987).
13. Bellcore TR-NWT-000020, issue 5.

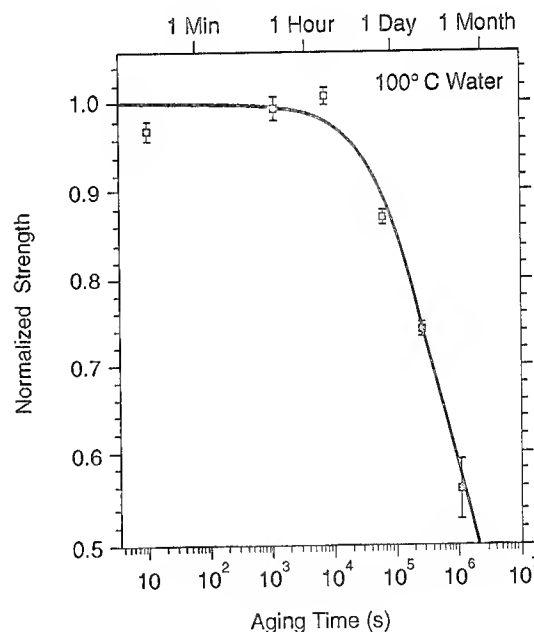


Figure 1. Fiber Strength After Aging in 100°C Water (ref. 5)

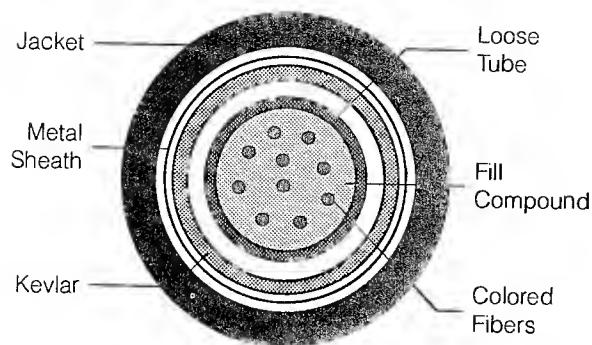


Figure 2. Schematic of the Cable Design

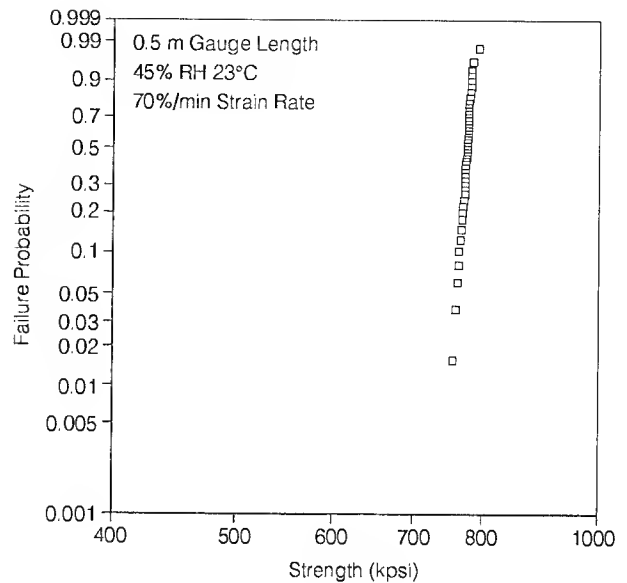


Figure 4. Typical Strength Distribution of As-Drawn Silica-Clad Fibers.

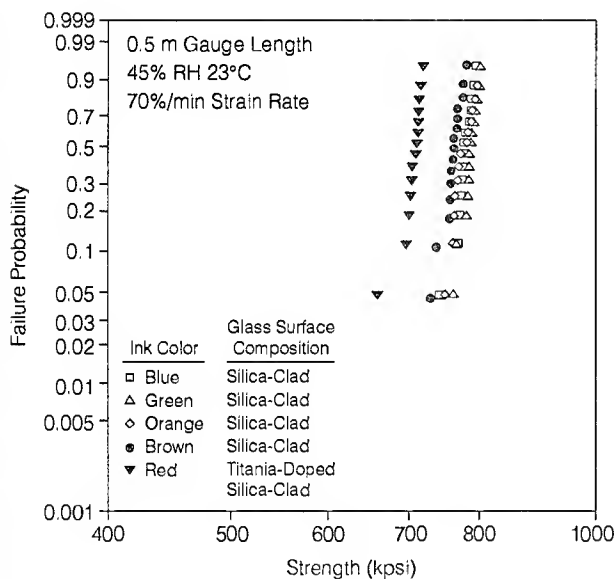


Figure 3. Strength Distribution of Fibers Removed From Cable.

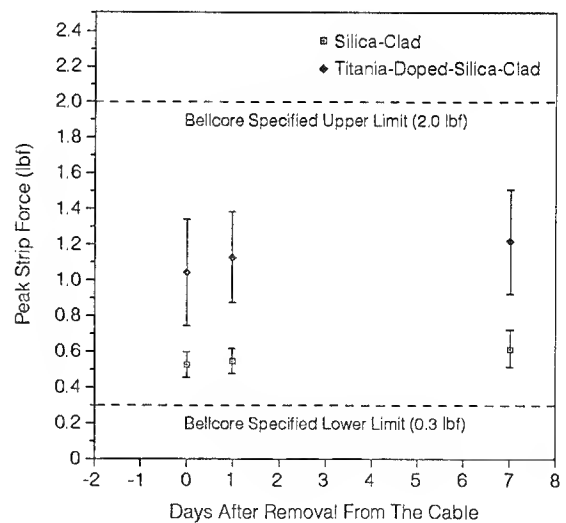


Figure 5. Peak Strip Force as a Function of Drying Time.

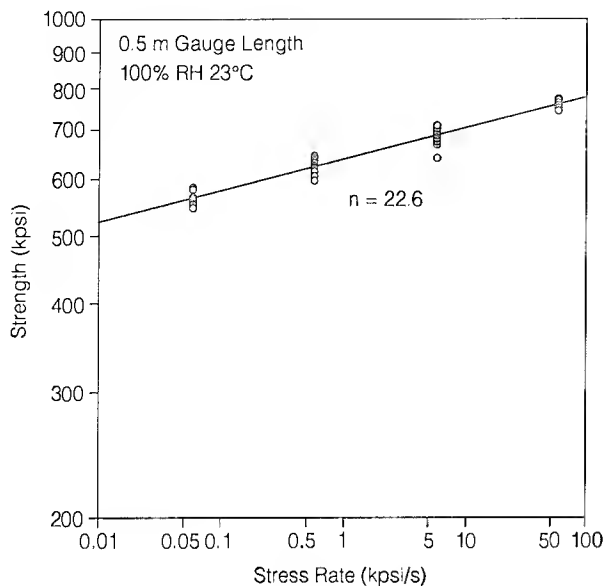


Figure 6. Dynamic Fatigue of Silica-Clad Fibers.

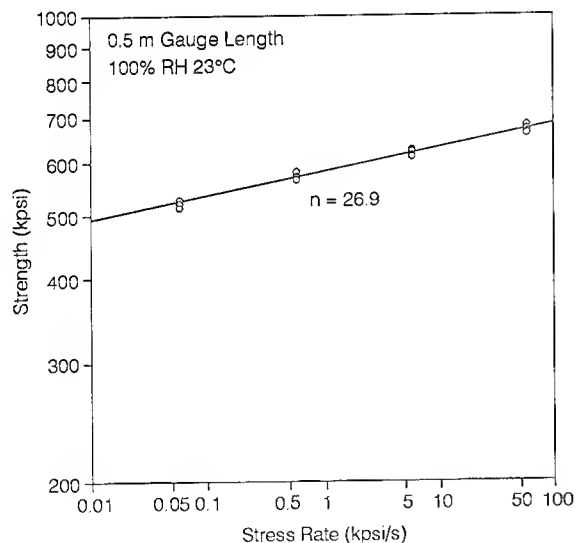
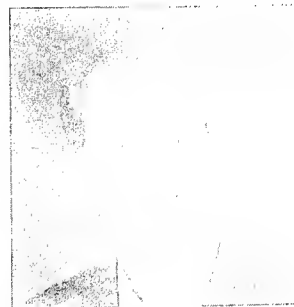


Figure 7. Dynamic Fatigue of Titania-Doped-Silica-Clad Fibers.



Anurag Dwivedi is a Senior Engineer at the Center for Fiber-Optic Testing (CFT), Corning Incorporated, Corning NY. Currently he is responsible for leading the ribbon and strip force testing team at CFT. He joined Corning in 1992 as a Senior Product Engineer. From 1991-1992 he was employed by Alfred University, Alfred, NY as a post-doctoral research associate.

Anurag received a Ph.D. in ceramics in 1991 and M.S. in ceramic Engineering in 1988 from Alfred University and a B.S. in ceramic engineering in 1986 from the Institute of Technology, Benaras Hindu University, Varanasi, India.



G. Scott Glaeseman, SP-DV-01-8, Corning Inc., Corning, NY 14831. Glaesemann is a Senior Development Engineer responsible for the optical fiber strength laboratory at Corning. His research focuses on the mechanical properties and reliability of optical fiber. He has been employed by Corning for eight years at the Sullivan Park technology facility. Glaesemann received his master's degree and Ph.D. in mechanical engineering from the University of Massachusetts and a B.S. in mechanical engineering from North Dakota State University.



Christopher K. Eoll was born in Thunder Bay, Ont., Canada in 1940. He received a B.Sc. in physics and an M.Sc. in theoretical physics from Queen's University in Kingston, Ont., Canada in 1961 and 1964, respectively. In 1967, he was granted a Ph.D. in mathematical physics by the University of Toronto in Toronto, Ont., Canada. Subsequently, he spent two years as a Postdoctoral Fellow at the University of Sussex in Brighton, England and the International Center for Theoretical Physics in Trieste, Italy.

From 1969 to 1977, he was employed by Canada Wire and Cable Ltd., where his final position was Product Development Manager for the Communications Products Division. He joined Superior Cable Corp. in 1977 as Technical Director. At present, he holds the position of scientist in the Research, Development & Engineering Dept. of Siecor Corp. He has recently been focusing on aspects of optical cable design, material properties and light transmission.

STRESS ASSISTED CORROSION MECHANISM OF PRISTINE AND CORRODED SILICA GLASS FIBERS

D. Inniss, Q. Zhong, and C. R. Kurkjian

AT&T Bell Laboratories, Murray Hill, New Jersey 07974

ABSTRACT

Mechanical reliability assessments of silica optical fibers are based on the assumptions that the strength controlling flaws of pristine silica are sharp and that the failure time from stress assisted corrosion (i.e., fatigue) is a function of the propagation rate of these flaws. However, there are a number of environmental conditions which do not influence crack growth rate in silica glass but affect failure times of silica glass fibers, suggesting that the rate limiting step of fiber fatigue is not crack propagation. Recently, the inert strength of corroded silica glass fibers was shown to be controlled by partially embedded hemispherical flaws. Preliminary results suggest that corroded and pristine silica fibers fatigue similarly, via a mechanism different from crack propagation. It is, therefore, proposed that the strength controlling flaws of pristine silica are not sharp. In addition, we propose that the fatigue rate limiting step is determined by the time necessary to form flaws which are sufficiently sharp to propagate. This fatigue model is based on the chemical kinetics mechanism proposed earlier, but generalized by incorporating the effect of flaw curvature on the reaction rate.

INTRODUCTION

Strength degradation of silica glass fiber has been the subject of numerous reports because it impacts long term mechanical reliability of telecommunication optical fibers. While it is generally accepted that the strength of glass fibers is controlled by the size and shape of surface flaws and residual stresses, and that these flaws grow at rates dependent on the chemical environment and the applied stress, little emphasis has been placed on the flaw growth mechanisms. This is because, in part, crack growth has been studied extensively for the propagation of sharp flaws in bulk silica, and is considered to be well understood. Wiederhorn et. al.¹ applied the thermodynamic description of reaction rate theory to model the crack growth process. Eqn.1,

$$v = v_0 \exp \frac{-E^* + bK_I}{RT}, \quad (1)$$

illustrates the empirical expression, where v is the crack growth rate, v_0 is the pre-exponential factor, E^* is the activation energy, b - an experimentally determined constant - is a function of the activation volume and the crack tip radius, K_I is the stress intensity factor, R is the gas constant and T is temperature. Since sharp flaws are necessary for crack propagation, the stress intensity factor, following Griffith², is usually defined as

$$K_I = Y \sigma_a c^{1/2} \quad (2)$$

where Y is a geometric factor, σ_a is the applied stress and c is the crack length.

A similar approach has been applied to predict failure time of pristine silica fibers. Because of the small fiber size (typically 125 μm diameter for telecommunication fiber) and its high inert strength (12-14 GPa), neither the initial flaw or its propagation has been directly observed. The strength controlling flaws are assumed to be sharp and the stress intensity factor is taken as shown in Eqn. 2. The crack velocity is expressed as a function of the stress intensity factor,

$$v = \frac{dc}{dt} = f(K_I) \quad (3)$$

where c is the crack length, t is time and $f(K_I)$ is a function with respect to the stress intensity factor, K_I . The catastrophic failure time from the crack propagation mechanism, t_p , is predicted to occur when the stress intensity factor increases to the fracture toughness, K_{IC} , of the glass (Eqn. 4).

$$t_p = \int_{K_{I_0}}^{K_{IC}} \frac{dc}{f(K_I)} \quad (4)$$

All currently used mechanical reliability assessments are based on the above treatment. However, there has been considerable controversy over the correct mathematical expression, $f(K_I)$, used to predict failure times. None of the currently considered models accurately describe the performance of pristine silica fiber. The problem is complex because the

geometry of the strength controlling flaw is not known; therefore, K_{II} may not be accurately defined. Thus failure times may not be accurately predicted from Eqn. 4 because either $f(K_I)$ or K_{II} is not well defined. Moreover, the implicit assumption of applying Eqn. 4 to predict lifetimes is that the rate limiting step for stress assisted corrosion (i.e., fatigue) of silica fibers is crack propagation. There are numerous examples where the environment does not affect the rate of crack growth in silica, but it does influence the failure time of fibers (see ref. 3 for a summary). These results suggest that the rate determining step of failure of fibers is not slow crack growth.

In this paper, the fatigue mechanism of pristine and corroded silica fiber is proposed. Although it is not necessary to characterize the strength determining feature to predict the fatigue mechanism, it does provide insight. First, the fatigue of corroded fibers are considered, since aging pristine silica fibers in the vapor of hydrofluoric acid produces partially embedded hemispherical flaws.⁴ The rate determining step leading to catastrophic failure of silica containing these flaws is questioned. Formation of a flaw sufficiently sharp to propagate is considered the rate determining step. The failure time expression is based on application of chemical kinetics - as previously done for the fatigue of pristine silica fiber⁵ - to the fracture process. The result is, therefore, more general than previously reported, in that the effect of curvature is considered. Furthermore, we show that pristine and corroded silica fatigue via the same mechanism, but apparently different from that of crack propagation. These results suggest that the strength controlling flaws in pristine silica are not sharp.

STRENGTH-FLAW RELATIONSHIP OF CORRODED SILICA GLASS FIBERS

There have been numerous attempts to directly quantify the relationship of fiber strength and flaw size and geometry for corroded pristine silica fibers. Fibers were aged at high temperatures in water or at high relative humidities and the resultant glass topography was characterized with either a scanning tunneling microscope (STM)^{6,7} or an atomic force microscope (AFM)^{8,9}. These results have not produced good characterization of the flaw-strength relationship, in part, because the fibers were corroded everywhere, making it difficult to identify the flaw characteristic of the largest stress intensity factor.

In a recent report⁴, we demonstrated that well defined, spatially resolved flaws could be produced on the surface of a pristine silica fiber after its exposure to the vapor of hydrofluoric acid (HF). In this model system,

standard 125 μm diameter fused silica glass (Amersil TO8) fibers are exposed to the vapor of 1 vol % HF. This treatment results in mechanical strength degradation, and the development of well defined, spatially resolved flaws, as determined by an AFM.

A comparison of the surface topography of these fibers is illustrated in Fig. 1. AFM images of an unaged

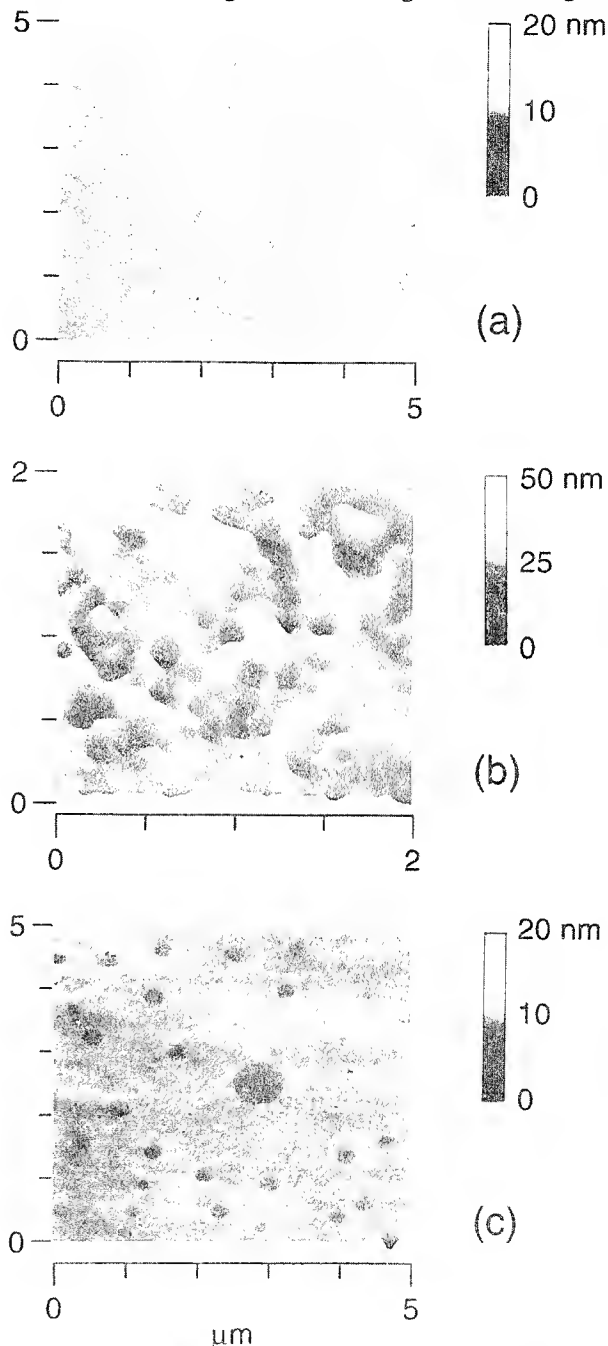


Figure 1. AFM images showing the surface topography of a) an as received silica fiber, b) a fiber corroded in 90°C water and c) a fiber aged in HF vapor.

fiber, a fiber aged in water and one aged in the vapor

of HF are shown. The unaged sample appears smooth (i.e., the RMS is 0.2-0.4 nm) with no distinguishing features. The surface of the sample aged in water is corroded everywhere with hills and pits of varying dimensions. In contrast, the sample aged in HF contains distinct etched pits, some much wider than others. The surface next to these pits appears smooth, especially when compared to samples aged in water.

To quantify the strength-flaw relationship, the flaws are modeled as partially embedded hemispheres. The stress concentrator, β , is defined by Roach and Cooper¹⁰ as

$$\beta = \frac{1}{1.62} \left[\frac{1}{0.27} \frac{c}{\rho} \right]^{0.85} \quad (5)$$

where c is as define previously and ρ is the radius of curvature of an assumed hemispherical flaw. It can be calculated based on the measured c and a (i.e., a is the half width of the flaw opening) as follows,

$$\rho = \frac{c^2 + a^2}{2c} \quad (6)$$

The measured strength vs flaw is compared to the calculated by applying Eqn. 5 to the formalism of Inglis¹¹,

$$\beta = \frac{\sigma_{th}}{\sigma_a} - 1, \quad (7)$$

where σ_{th} is the inert strength of pristine silica at the crack tip (~12.5 GPa for pristine silica in liquid nitrogen) and σ_a is the applied stress. The solid curve in Fig. 2 represents the calculated strength-flaw size

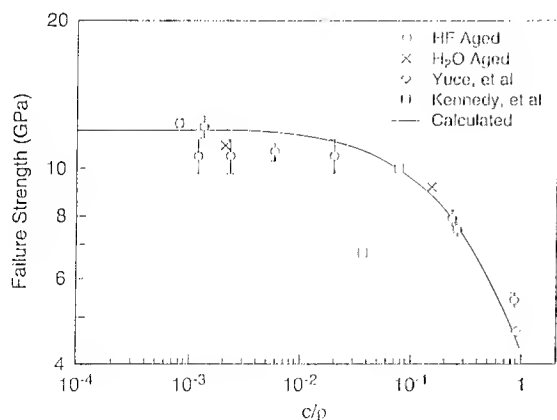


Figure 2. The maximum flaw concentrator, c/ρ , is plotted vs. the measured inert strength. The data are compared to the blunt flaw theory (solid line) as predicted by a partially embedded hemisphere.

relationship, and is compared to that of the measured inert strength (i.e., measured in liquid nitrogen) and

the maximum stress concentrator; a good agreement is observed.

FATIGUE OF CORRODED SILICA

FIBERS WITH BLUNT FLAWS

Han and Tomozawa¹² studied fatigue of blunt and sharp flaws in silica rods. Sharp flaws were created by mechanically abrading the rods and blunt flaws were formed by soaking the abraded rods in hot water. Both the inert strength and the stress corrosion parameter (i.e., $n = -\partial \ln t_f / \partial \ln \sigma$) increased after treating the rods in hot water. The authors attributed the decrease in the fatigue rate as a consequence of the fatigue mechanism. The sharp flaws fatigue via slow crack growth; while for the blunt flaws it is necessary to first initiate a sharp flaw prior to the slow crack growth. Initiation of a sharp flaw was shown to control the failure time of the rods with blunt flaws. The transformation of a blunt to a sharp flaw by stress assisted corrosion was studied by Hillig and Charles.¹³ Application of a stress causes crack tip sharpening at the site of the maximum stress concentration. Slow crack growth commences when the flaw is sufficiently sharp; the radius of curvature remains constant, but the crack tip advances (see Fig. 3).

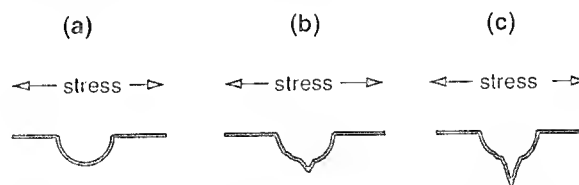


Figure 3. Schematic illustrating the transformation of a blunt (a) to a sharp (b) flaw followed by crack propagation (c).

Consider a partially embedded hemispherical flaw in silica: application of a stress lowers the effective activation energy and it can cause flaw tip sharpening. The crack tip sharpening rate, dN_s/dt , where N is the number of broken siloxane bonds necessary to form a crack sufficiently sharp to propagate, is controlled by chemical kinetics. In Eqn. 8,

$$\frac{dN_s}{dt} = \frac{\kappa kT}{h} \exp \left(\frac{-\Delta G^\ddagger}{RT} \right), \quad (8)$$

the thermodynamic formulation of reaction rate theory is illustrated where t is time, κ is the transmission coefficient - usually taken as one, k is Boltzmann's constant, T is temperature, h is Planck's constant, ΔG^\ddagger is the change in the Gibbs free energy and R is the gas constant. Since the equilibrium under investigation is the activity of the transition state and the product of the activity of the silica surface and water (see ref. 5), ΔG^\ddagger is the difference of the standard Gibbs free

energy of the transition state and the initial state. The free energy, accounting for the surface curvature as previously described by Wiederhorn et. al.¹, is

$$\Delta G^\ddagger = -T\Delta S^\ddagger + \Delta E^\ddagger - P\Delta V^\ddagger - \frac{(\gamma^\ddagger V^\ddagger - \gamma V)}{r} \quad (9)$$

where ΔS^\ddagger is the entropy change, ΔE^\ddagger is the change of the zero stress activation energy, P is the pressure or the applied stress, ΔV^\ddagger is the change of the activation volume, γ is the surface energy, V is the partial molar volume and r is the crack-tip radius.

Consider at a given stress the number of broken bonds to produce a sharp flaw, dN_s , is constant (i.e., $dN_s = c(\sigma)$). Since dt represents the time between application of the stress and failure, Eqn. 8 can be rewritten as

$$t_i = t_0 \exp \frac{\Delta E^\ddagger - P\Delta V^\ddagger - \frac{(\gamma^\ddagger V^\ddagger - \gamma V)}{r}}{RT} \quad (10)$$

where

$$t_0 = \frac{c(\sigma)h}{\kappa kT} \exp \frac{-\Delta S^\ddagger}{R}. \quad (11)$$

Eqn. 10 describes the time it takes to create a flaw that is sufficiently sharp to propagate. The effective activation energy (ΔE_a),

$$\Delta E_a = \Delta E^\ddagger - P\Delta V^\ddagger - \frac{(\gamma^\ddagger V^\ddagger - \gamma V)}{r}, \quad (12)$$

and t_i are decreased by the application of a stress and by increasing the curvature. The failure time of a corroded silica fiber can be considered to be the sum of the crack initiation, i.e., t_i , and propagation, i.e., t_p processes. As reported by Han and Tomozawa¹² for blunt flaws in silica, $t_f = t_i$ and $t_i \gg t_p$. Similarly, for blunt flaws in a corroded pristine silica fiber, crack propagation is probably not a significant contributor to the rate determining step of fatigue, and therefore, $t_f = t_i$.

FATIGUE OF PRISTINE SILICA FIBER

There are a number of examples which suggest that pristine silica fiber fatigues via a different mechanism from that of the slow crack growth. The rate of crack growth in NaCl and other salts in solution is reported to be independent of the electrolytes present in comparison to water.¹⁴ In contrast, pristine silica fibers are sensitive to these electrolytes.¹⁵ Furthermore, slow crack growth in bulk silica is independent of the type of cations in MOH solutions¹⁶ while the fatigue of pristine silica fiber is sensitive to the cation type¹⁷. These results suggest a different fatigue mechanism for pristine silica fiber. This is probably because the geometry of the strength defining flaw is not sharp so

that the accessibility of reagents is not restricted.

Figure 4 contains Weibull¹⁸ strength distributions of

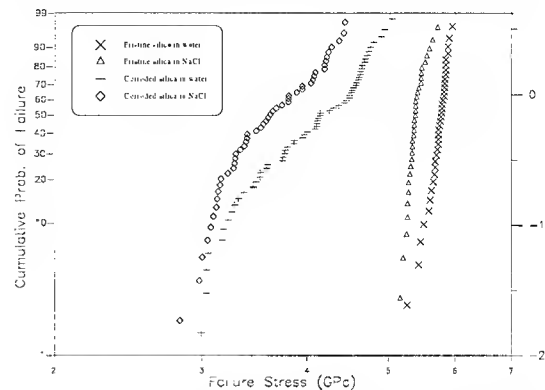


Figure 4. Weibull strength distributions of pristine and corroded silica fibers fractured in deionized water and in a 1 molar NaCl solution.

corroded fibers fractured in water as compared to those in a 1 molar NaCl solution. The fibers were aged at room temperature in the vapor of 1 vol % HF for 20 minutes and fractured at room temperature in two point bending. The failure stress was determined as previously described.⁴ This comparison illustrates fracture stresses lower in aqueous NaCl (3.36 ± 0.07 GPa) than in water (3.63 ± 0.08 GPa), similar to that reported for pristine silica and suggests that blunt flaws and pristine silica fatigue similarly.

In the above section we postulated that the chemical kinetics model best describes fatigue of a blunt flaw. The same model has been applied to the fatigue of pristine silica. From Eqn. 10, assuming the surface of pristine silica is flaw free (i.e., $r = \infty$), valuable information has been provided to describe the fatigue mechanism for pristine fibers. In references 5, 15, and 19-20 details of the systems studied and results are presented. In aqueous NaCl¹⁵ and NaOH¹⁹ the reaction order is the same as reported for the dissolution kinetics of silica. In MOH¹⁷, where M is an alkali cation, the strength of pristine silica is shown to follow the reverse trend as that of the dissolution rate of silica. The fibers are weakest in KOH and the dissolution rate is greatest relative to the other MOH's. These observations suggest that the rate limiting step of the fatigue of pristine silica involves similar rate limiting reactions which control dissolution of the glass. Therefore, Eqn. 10, which describes the failure rate as a function of chemical kinetics, best describes fatigue of pristine and corroded silica.

SUMMARY

The stress assisted corrosion mechanism of pristine and corroded silica fiber is proposed to consist of crack initiation and propagation steps. The

contribution of crack propagation to the failure time is considered small. This is based on comparison of the environmental dependence of crack propagation in bulk silica to fatigue of fibers. The results suggest a different stress assisted corrosion mechanism for both pristine and corroded fibers. It is proposed that the crack initiation step involves chemical reactions which break bonds regiospecifically and, therefore, leads to the formation of a sharp crack. For corroded silica fibers, where the initial flaws are characterized as partially embedded hemispherical pits, the effective activation energy of hydrolysis of silica, and hence the failure time, is lowered by increasing the local stress and/or the curvature. This result further generalizes the chemical kinetics model previously describe for the fatigue of pristine silica, in which case, the radius of curvature is infinite.

Mechanical reliability assessments of optical fibers are all based on the assumption that the strength controlling flaws are sharp and that crack propagation is the rate determining step. The model described herein is, however, not necessarily applicable to all fiber surface conditions. Certainly there are cases where the flaws are sharp and the fatigue rate limiting step may be crack propagation. Furthermore, we did not attempt to describe the anomalies in the stress corrosion parameter between crack propagation and those reported for the fatigue of silica fibers,²¹ although these differences may be intrinsic to the mechanism.

REFERENCES

1. S. M. Wiederhorn, E. R. Fuller, Jr. and R. Thomson, *Met. Sci.*, 450-58 (1980).
2. A. A. Griffith, *Philos. Trans. Roy. Soc., London*, A221, 163 (1920).
3. D. Inniss, D. L. Brownlow and C. R. Kurkjian, *SPIE Proceedings*, 1791, 2-6 (1992).
4. D. Inniss, Q. Zhong and C. R. Kurkjian, *J. Am. Ceram. Soc.*, in press (1993).
5. D. Inniss, C. R. Kurkjian and D. L. Brownlow, *Ceram. Trans.*, 28, 569-78 (1992).
6. R. S. Robinson and H. H. Yuce, *J. Am. Ceram. Soc.*, 74[4], 814-818 (1991).
7. W. Griffioen, G. Segers and E. Van Loenen, *Proc. Int. Wire. and Cable Symp.*, 386-372 (1990).
8. H. H. Yuce, J. P. Varachi, Jr., J. P. Kilmer, C. R. Kurkjian and M. J. Matthewson, Optical Fiber Communication Conference, Post-Deadline Papers, OSA, Washington, DC (1992) PD-21.
9. M. T. Kennedy, E. Cuellar and D. R. Roberts, *SPIE Proceedings*, 1580, 152-162 (1991), and M. T. Kennedy, E. Cuellar, D. R. Roberts and M. M. Stipek, *SPIE Proceedings*, 1791, 67-79 (1991).
10. D. H. Roach and A. P. Cooper, in *Strength of Inorganic Glass*, C. R. Kurkjian ed., New York, Plenum, (1985).
11. C. E. Inglis, *Trans. Inst. Nav. Archit.*, 55, 219-30 (1913).
12. W. Han and M. Tomozawa, *J. Non-Cryst. Solids*, 122, 90-100 (1990).
13. W. B. Hillig and R. J. Charles, in *High Strength Materials*, ed. V. Zackay, Wiley, NY 1965, p. 682-705.
14. S. M. Wiederhorn and H. Johnson, *J. Am. Ceram. Soc.*, 58[7-8], 342 (1973).
15. D. Inniss, D. L. Brownlow and C. R. Kurkjian, *J. Am. Ceram. Soc.*, 75, 364-68 (1992).
16. G. S. White, S. W. Freiman, S. M. Wiederhorn and T. D. Coyle, *J. Am. Ceram. Soc.*, 70[12], 891-895 (1987).
17. V. V. Rondinella, M. J. Matthewson and B. Lin, *Ceram. Trans.*, 20, 171-83 (1991).
18. W. Weibull, *J. Appl. Mech.*, 8, 293 (1951).
19. D. Inniss, D. L. Brownlow, C. R. Kurkjian and L. R. Borges, *MRS Symp. Proc.*, 244, 91-95 (1992).
20. D. Inniss, C. R. Kurkjian and D. L. Brownlow, *J. Am. Ceram. Soc.*, 75[12], 3485-86 (1992).
21. T. A. Michalske, W. L. Smith and B. C. Bunker, *J. Am. Ceram. Soc.*, 74[8], 1993-96 (1991).



D. Inniss
AT&T BELL
LABORATORIES
600 Mountain Avenue
Murray Hill, NJ 07974



Charles R. Kurjian
AT&T BELL
LABORATORIES
600 Mountain Avenue
Murray Hill, NJ 07974

Daryl Inniss is a member of the technical staff of the Optical Fiber Research Department at AT&T Bell Laboratories. He joined Bell Laboratories in 1988 and is currently studying the microstructure of silica fibers to understand its influence on corrosion, adhesion, and light propagation. Dr. Inniss was educated at Princeton University, Princeton, NJ, where he received a A.B. in chemistry in 1983. He subsequently attended the University of California at Los Angeles and received a Ph.D in Chemistry in 1988.

Charles R. Kurjian received a BSc. degree in Ceramics from Rutgers in 1952 and the ScD. degree in Ceramics from M.I.T. in 1955. After postdoctoral work at M.I.T. and the University of Sheffield, England, he joined AT&T Bell Labs in 1959. He is a member of the National Academy of Engineering, and the Academy of Ceramics, and a Fellow of the American Ceramic Society of Glass Technology.



Qian Zhong
AT&T BELL
LABORATORIES
600 Mountain Avenue
Murray Hill, NJ 07974

Qian Zhong is currently a Member of Technical Staff at AT&T Bell Laboratories. He joined Bell Labs in 1992 as a postdoctoral member of technical staff in the optical fiber research department. His current responsibilities include material aspects of submarine cables and systems. He holds B.S. and Ph.D. degrees, both in materials science and engineering, from Shanghai Jiao Tong University, China and the University of Pennsylvania, respectively. He is a member of Materials Research Society.

THE EFFECTS OF OPTICAL FIBER COATING AND INK MATERIALS ON THE CORROSION OF THE GLASS SURFACE

Rolf A. Frantz*, Barry J. Keon†, Eva M. Vogel*, Trevor N. Bowmer^, and Hakan H. Yuce*

*Bellcore, Morristown, NJ

†Telstra, Melbourne, Australia

^Bellcore, Red Bank, NJ

ABSTRACT

Surface corrosion of glass optical fibers degrades their strength and increases their susceptibility to in-service failures. Previous work has shown that the protective polymer coating can affect the rate of such corrosion. Fibers with low extents of coating cure experience significantly greater corrosion during aging. Fibers with different coatings also experience corrosion at different rates. In addition, coating-related properties (e.g., strip force) change at different rates for different coating systems; a subsequent loss of adhesion of the coating to the glass can also adversely affect the fiber reliability. Previous studies, however, have not reported on the local environment at the glass surface, nor investigated the separate contributions of the inner and outer primary coatings, color-coding ink layer, and service environment to the aging process. We have undertaken a systematic study to analyze these contributions; this paper represents a progress report on the work to date.

INTRODUCTION

The long-term reliability of optical fibers can be compromised if the fiber strength degrades due to corrosion of the glass surface. One function of the protective polymer coating applied to the fiber during the drawing process should be to protect against such corrosion. However, previous work has shown that the coating can significantly affect the rate of corrosion and that a loss of adhesion of the coating to the glass can affect the long-term reliability. In one investigation, reducing the extent of cure of the coating led to faster and more severe corrosion of the glass during aging in water and high-humidity environments.^[1] In another study, different extents of corrosion were found to occur on similar fibers that had different coatings.^[2] While these studies thoroughly characterized the mechanical properties and surface morphology of the glass, they did not examine the local chemical environment at the glass-coating interface. Also, the effects on coating-related properties such as strip force, pull-out force, and coating delamination from the glass have not been systematically examined as functions of different coating formulations, the presence or absence (and type) of color-coding inks, and interactions with the aging environments.

We have initiated a systematic program to investigate the contributions of fiber coating materials to the glass corrosion and to changes in their own mechanical characteristics. We are addressing the complete optical fiber system:

glass fiber
+
inner and outer primary coatings
+
color-coding ink
+
service environment

where the service environment may be a surrounding buffer tube gel, the air in a splice case or pedestal (including ambient humidity), or the chemical species introduced, for example, in a flooded vault or manhole. Mechanical characterization, optical and atomic force microscopy, and chromatography are among the techniques included in our investigation. We are seeking to understand how the changes in coating-related fiber properties correlate with the individual coating and ink materials used on specific fibers. We also seek to understand the chemistry and interactions at the glass/coating interface—specifically, what contributions the coatings, color-coding inks, and service environments make to the conditions at this interface. Finally, we wish to determine the extent to which the interface environment affects the surface corrosion of the glass fiber.

In the following sections, we describe the samples and aging environments, test procedures, and typical results from our studies to date, and examine correlations among the test results.

SAMPLES, AGING, AND CONDITIONING

We obtained samples of three commercially-available optical fibers (identified as fibers X, Y, and Z), each of which was divided into three equal lengths. The first length was left in the natural (uninked) state. The second length was color-coded using a solvent-based ink, while the third length was color-coded with a uv-curable ink. Loose coils approximately 160 mm in diameter were prepared from each of the resulting nine samples for aging in the environments described below. Each coil was identified by a stainless steel tag label (denoting its source fiber, aging environment, and exposure time).

We chose four aging environments: deionized (DI) water at 85 °C and 65 °C, and 85% relative humidity (RH) at 85 °C and 65 °C. The fiber samples were aged as loose coils that were supported on specially-designed stainless steel frames in the water baths or laid on the shelves of the temperature/humidity chambers.

Each of the samples was aged for a predetermined amount of time (e.g., 1, 7, or 28 days). Upon removal from the aging environment, the samples were divided into two lots and were post-conditioned for a minimum of 24 hours at 23 °C in DI water (if aged in water) or in 85% RH (if aged in 85% RH).

EXPERIMENTAL TECHNIQUES

Strip Force

We measured the strip force according to Telecommunications Industry Association Fiber Optic Test Procedure FOTP-178 except that the testing machine limited the crosshead speed to 125 mm/min (instead of 500 mm/min). The stripping tool had a circular aperture 160 µm in diameter. After aging, the samples

Copyright © 1994 Bellcore. All rights reserved.

were conditioned as described above and tested in a 23 °C/50% RH controlled ambient immediately after removal from the conditioning environment.

Pull-Out Force

The pull-out force was measured using the procedure of proposed FOTP-105 but with a constant crosshead speed of 5 mm/min (instead of a force build-up of 1 N/sec) owing to the limitations of the testing machine. The samples were conditioned as described above and bonded to cardboard tabs with cyanoacrylate adhesive. A chemical accelerator was used to cure the adhesive. The fibers were cut to the 10 mm gage length with a razor blade, but the cardboard mounting tab was not bent because the breaking of the fiber was clearly audible during cutting. The end opposite that at which pull-out occurred was placed in masking tape, which was then clamped in rubber-faced jaws to apply the force. The testing was again performed in a 23 °C/50% RH controlled environment. Sample mounting went quickly, and the test was typically started within 1 minute after the sample was removed from conditioning.

Two-Point Bending

We measured the fiber strength in dynamic two-point bending using a modified version of method 1 of FOTP-90. The samples were conditioned and tested in 23 °C DI water. A total of either 11 or 21 samples were tested. All calculations were based on the nominal glass and coating diameters of 125 µm and 250 µm, respectively. The initial jaw spacing was 10 mm and the platen velocity was 10 µm/sec.

Optical Microscopy

We used an optical microscope to examine and photograph 5 cm long pieces of each fiber after each aging interval. The samples were immersed in an index-matching oil; care was taken to ensure that the fiber ends were kept out of the oil. The fibers were examined immediately after removal from the appropriate conditioning environment described above. It was possible to locate the core/cladding, glass/inner primary, and inner/outer primary interfaces in most fibers using transmitted light illumination; the exceptions were the uv-inked fibers, for which the thickness of the ink layer obscured any internal details.

Atomic Force Microscopy

An atomic force microscope (AFM) was used to study the surface morphology of the fibers with sub-nanometer resolution. The control system varied the voltage to keep the cantilever deflection nearly constant as the probe was scanned over the sample surface in a raster pattern. Variations in the voltage translated directly into variations in the height of the surface. The fibers were scanned in air after chemically stripping the coating using 200 °C sulfuric acid and then rinsing them with acetone. To ensure representative results, several samples of each fiber were scanned. Each sample was also examined with at least two different AFM tips to minimize the possibility of misinterpreting any tip-induced artifacts in the images.

Gas Chromatography/Mass Spectrometry

Lengths of fiber were inserted into the GC/MS injection port with the port temperature held below 50 °C and the oven/column temperature set at -20 °C. At these low temperatures, any volatile compounds from the fiber sample were initially trapped at the head of the column. After equilibrium was re-established in the gas flow, the injection port was heated to 100 °C and the scan was begun. The column was heated at 8 °C/min to 240 °C and then held at 240 °C for an additional 20 minutes or so.

RESULTS

Strip Force

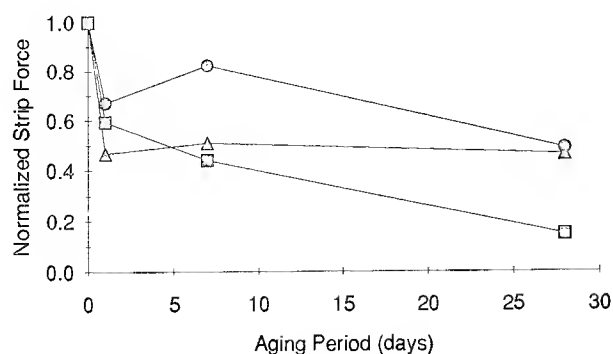
Typical strip force results for fibers X and Z are plotted in Figures 1 and 2, respectively. All values have been normalized to the maximum strip force of the respective unaged sample. No plots are shown for fiber Y because it behaved similarly to fiber Z. Only the results in the 85 °C DI water environment, the most severe aging environment that we used, are plotted; the changes seen in the other environments were smaller than those shown here. It is worth noting that for fibers Y and Z, the DI water environments (65 °C and 85 °C) were more severe than the 85% RH environments, while for fiber X, the 85 °C environments (DI water and 85% RH) were more severe than those at 65 °C. Figures 1(a) and 2(a) show the 'maximum'—the peak value of strip force recorded during the test. Figures 1(b) and 2(b) show the 'average,' which is a visual estimate that attempts to average the multiple peaks and valleys of typical a strip force record. Comparing the maximum and average values indicates that the uv ink resulted in more uniform stripping behavior, with the average noticeably closer to the maximum value. The maximum strip force varied considerably among the different aging environments, suggesting that it may be affected by differences in the equilibrium moisture content in the outer primary and ink layers. In contrast, the average value was relatively consistent among all environments and correlated with the tendency for the coating to slide off as a tube, implying a loss of adhesion at the coating/glass interface. Finally, it is apparent that where significant reductions in strip force took place, they occurred during the first few days of aging.

Pull-Out Force

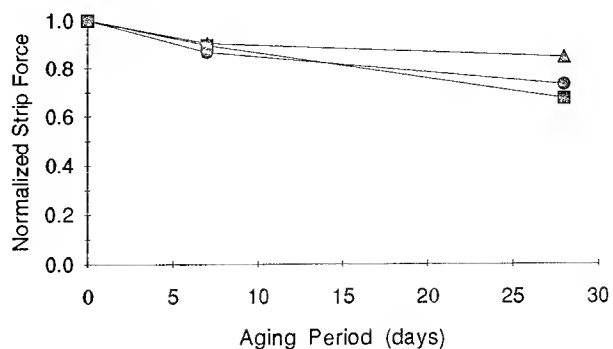
Figures 3 and 4 show the results of the pull-out tests for fibers X and Z, respectively. Again, all values have been normalized to the maximum pull-out force of the respective unaged sample. Also, fiber Y again behaved similarly to fiber Z. These results are plotted for the 65 °C/85% RH environment, the least severe of those we used, but the one in which we typically found the largest changes in pull-out force to occur. In the pull-out test, any effects of aging temperature (as seen in the strip force data for fiber X) were masked by the differences between the DI water and 85% RH environments. Figures 3(a) and 4(a) show the peak pull-out force, which usually is reached shortly after the start of the test. Figures 3(b) and 4(b) show the value recorded after 0.5 mm of fiber has been pulled out beyond the peak value. A comparison of the peak and post-peak values shows that, particularly for fiber X, a high peak pull-out force can be followed by a low residual force; in some cases, the glass simply slides effortlessly out of the coating. Comparing the curves within any of the figures, it can be seen that both the solvent ink and the uv ink affect the pull-out force. The effect can be an increase or a decrease; however, the uv ink typically has a more significant effect than the solvent ink. In some cases, the effect of the ink was that it debonded from the coating, in which case the coated fiber pulled out of the ink layer; these instances are not included in any of the force calculations. The increase in the pull-out force for fibers Y and Z at 65 °C/85% RH may be due to the relatively mild environment: absorption of moisture by the coating can be expected to cause swelling, which will increase the mechanical friction at the coating/glass interface; in more severe environments, this effect would be counteracted by other mechanisms that degrade the coating/glass bond.

Two-Point Bending

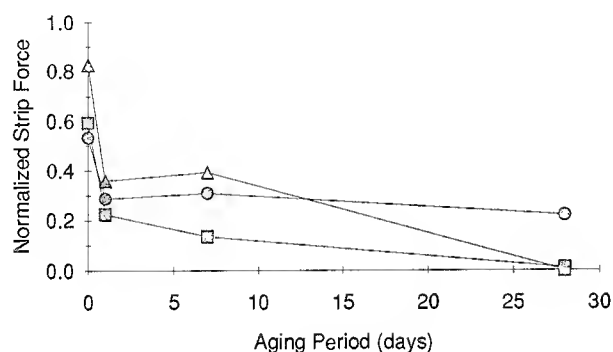
The two-point bending results are presented in Table 1. We have summarized the *median* strengths for the sets of samples tested; the *mean* values are in all cases very close to the median values



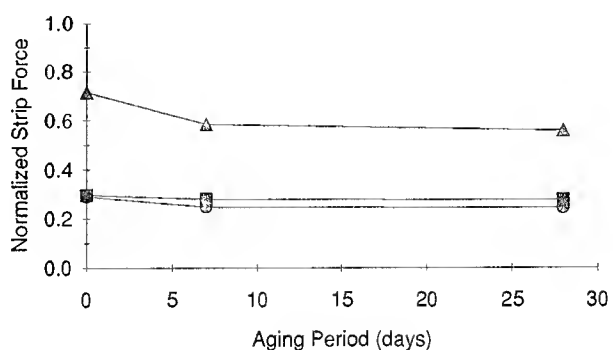
(a) Maximum



(a) Maximum



(b) Average



(b) Average

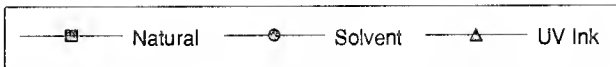
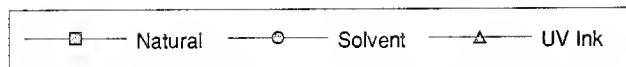


Figure 1. Strip Force for Fiber X Aged in 85 °C Deionized Water
(a) Maximum Value (b) Average Value

Figure 2. Strip Force for Fiber Z Aged in 85 °C Deionized Water
(a) Maximum Value (b) Average Value

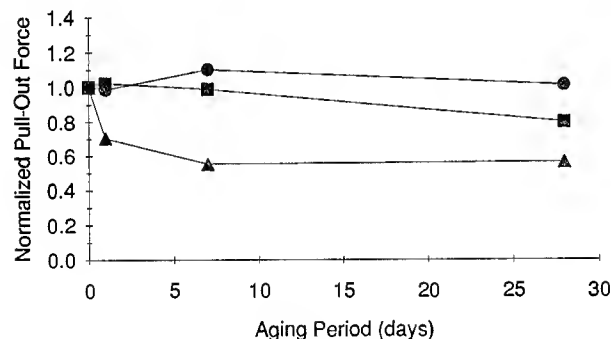
Table 1. Normalized Median Two-Point Bending Strength Results

	Unaged	65 °C/85% RH			65 °C DI Water			85 °C/85% RH			85 °C DI Water		
Days:	0	1	7	28	1	7	28	1	7	28	1	7	28
X Natural	1.00	0.99	1.06	1.14	1.01	0.80	0.90	0.99	1.04	1.16	0.78	0.61	0.49
X Solvent	1.00	0.99	1.05	1.14	1.06	1.04	1.06	0.97	1.09	1.17	1.09	1.02	0.69
X UV-Ink	1.00	1.01	1.05	1.08	1.05	1.05	1.00	1.03	1.06	1.13	0.97	0.96	0.97
Y Natural	1.00	—	0.94	0.93	—	0.90	0.91	—	0.90	0.91	—	0.95	0.92
Y Solvent	1.00	—	0.97	0.95	—	0.93	0.94	—	0.93	0.94	—	1.01	0.97
Y UV-Ink	1.00	—	0.91	0.93	—	0.85	0.90	—	0.85	0.90	—	0.96	0.96
Z Natural	1.00	—	1.08	1.19	—	1.12	1.22	—	1.09	1.20	—	1.16	1.00
Z Solvent	1.00	—	1.07	1.15	—	1.06	1.18	—	1.09	1.16	—	1.14	1.19
Z UV-Ink	1.00	—	1.04	1.11	—	1.07	1.15	—	1.06	1.17	—	1.10	1.18

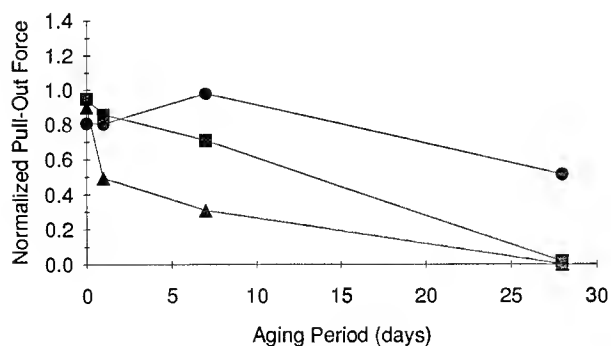
listed. All of the values have been normalized to the bending strength of the respective unaged sample. Two trends are noticeable. For almost all combinations of base fiber, inking condition, and aging environment, the strength either remained essentially unchanged or increased slowly with aging time. Such gradual increases in strength are typically evidence of blunting of the strength-limiting surface cracks over time due to the action of the aging environment. However, for the situations where this was not true—fiber X, either natural (uninked) or solvent-inked, aged in DI water—the decrease in strength was substantial. This was also apparent in handling the natural fiber while preparing samples for measurement: it was quite brittle and weak, and required extra care to provide an adequate number of samples for testing.

Optical Microscopy

Figures 5(a) and 5(b) are typical microscope photographs of fibers Y and Z, respectively. They represent natural (uninked) fibers after aging for 28 days in 65 °C DI water. Fiber Y shows virtually no effects of this aging, while fiber Z has developed voids or delaminated areas at the glass/coating interface. Fiber X behaved similarly to fiber Z, but with noticeably more voids or delaminated areas. These same behaviors were observed to a greater or lesser degree after aging in the other environments or for shorter times. Figure 6 shows a solvent-inked fiber after one day of aging in 85 °C DI water; the surface “bubbles” indicate debonding of the ink layer; this illustrates the problem that occurred in those pull-out tests in which the coated fiber pulled out of the ink, rather than the glass pulling out of the coating.



(a) Peak Value



(b) 0.5 mm Past Peak



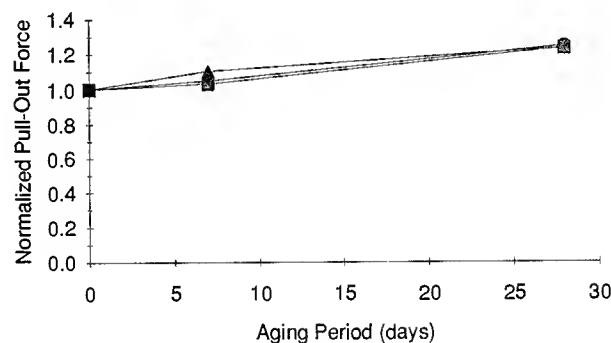
Figure 3. Pull-Out Force for Fiber X Aged in 65 °C/85% RH
(a) Peak Value (b) 0.5 mm Past Peak

Atomic Force Microscopy

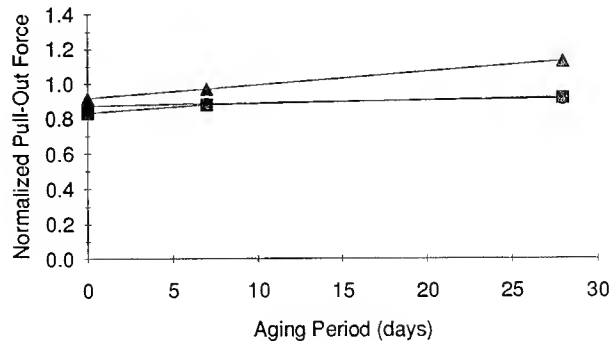
AFM scans of various aged fibers are shown in Figures 7 and 8 for ~2000 nm-square areas on the glass fiber surfaces. Note that the vertical scale is about one-hundred times as sensitive as the horizontal scale. Figure 7 shows that the aging in 85 °C DI water for 28 days had the largest effect on Fiber X in the (a) natural (uninked) condition; the roughening is much less for (b) the solvent-inked and (c) the uv-inked samples of this fiber after this same aging history. The maximum roughness depth, R_{max} , for these three scans is 4.2 nm, 2.6 nm, and 1.9 nm, respectively. These results suggest that the ink layer, whether solvent or uv curable, provided added protection against water permeation into the coating and penetration to the glass surface. The increase in roughness of this natural fiber was the largest we found for any fiber under any aging condition up to 28 days of exposure. In contrast, Figure 8 shows that fiber X experienced essentially no surface roughening after 28 days of aging in the 85 °C/85% RH environment. Such minimal surface roughening was typically observed for all three fibers in their natural, solvent-inked and uv-inked conditions after all aging times in all other aging environments. However, the DI water environments did cause *marginally* more corrosion than the 85% RH environments.

Gas Chromatography/Mass Spectrometry

Between five and ten different compounds were found in the GC/MS trace for each fiber sample. The major constituents volatilized appear to be residual photoinitiators and byproducts,



(a) Peak Value



(b) 0.5 mm Past Peak



Figure 4. Pull-Out Force for Fiber Z Aged in 65 °C/85% RH
(a) Peak Value (b) 0.5 mm Past Peak

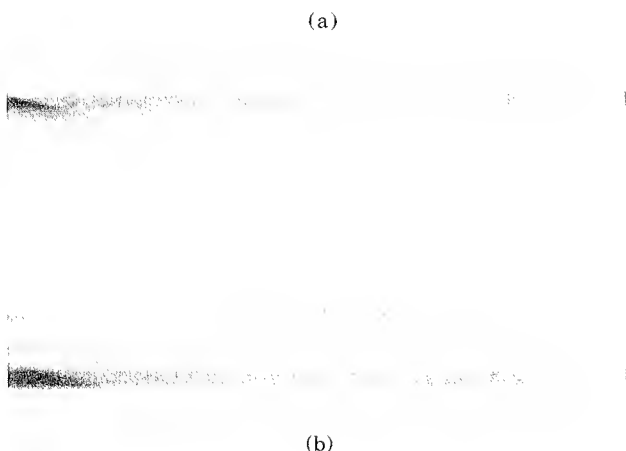


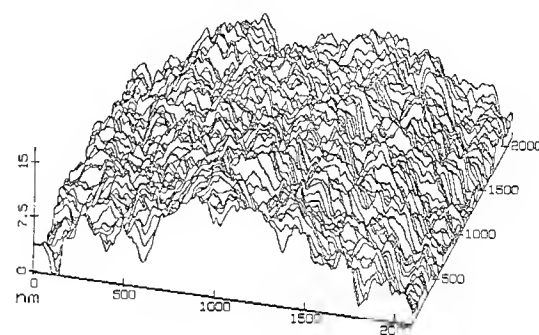
Figure 5. Photographs of Fibers Aged 28 Days in 65 °C/85% RH
(a) Fiber Y (b) Fiber Z

although solvents, anti-oxidant stabilizers, and some urethane-acrylate fragments from the polymer matrix were also present. As shown in Figure 9, fibers X, Y, and Z can be clearly distinguished by characteristic peaks on their GC/MS traces. Also, as shown in Figure 10, the uv-inked fibers can be clearly identified by the presence of the peak at 20–21 minutes; the three fibers can still be distinguished by their characteristic peaks, although these are reduced in amplitude. The solvent-inked fibers have less-pronounced added peaks than the uv-inked fibers but are also identifiable, and they again remain distinguishable by their residual characteristic peaks. Using both sectioned fibers and lengths of coatings removed from the glass, we established that the volatile compounds are derived equally from both the inner and outer primary coatings. The traces for fibers aged for 7 days in either 85 °C DI water or 85 °C/85% RH showed that over 95% of these volatile compounds were extracted by such aging conditions. It has previously been reported that photoinitiator, in particular, is susceptible to extraction during water aging.^[3] Thus, our results suggest that under these aging conditions, water is likely to be permeating into and through the coatings and reaching the glass surface.

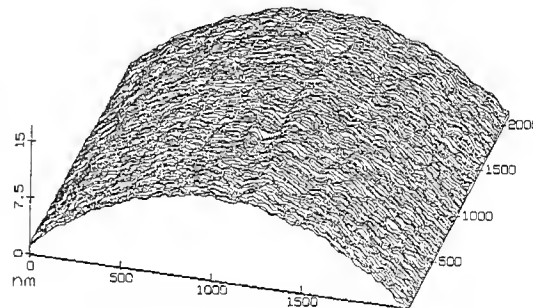
DISCUSSION

The results just presented can be separated into two categories: coating-related properties (strip force, pull-out, visible changes, and GC/MS traces), and glass strength-related measurements (two-point bending and AFM scans). Our results suggested no correlations between changes in either the strip force or pull-out force of the coating and the strength or corrosion of the glass.

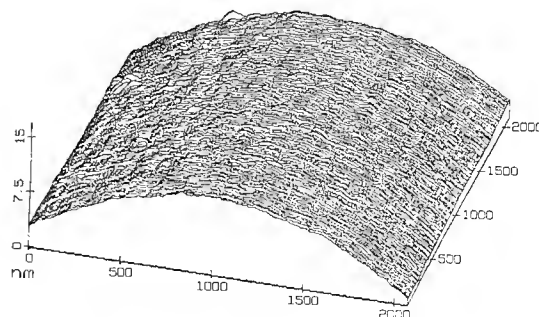
Figure 6. Ink Layer Delamination of Solvent-Inked Fiber after Aging 1 Day in 85 °C/85% RH



(a)



(b)



(c)

Figure 7. AFM Scans of Glass Surface of Fiber X Samples Aged 28 Days in 85 °C Deionized Water

(a) Natural (b) Solvent-Inked (c) UV Inked

The strip force and pull-out force results do show a clear correlation for all fibers and in all environments. Both measurements provide comparable evidence that the coating on fiber X is adversely affected in the aging environments, more so than the coatings on fibers Y and Z. The strip force and pull-out data appear to correlate with the GC/MS results. The bulk of the changes in strip force and pull-out force typically occur within the first 7 days of aging, while the GC/MS results indicate that most of the volatile materials are extracted from the coatings within that same time frame. Finally, there is a distinct association between the strip force/pull-out force and the optical microscope observations: for those fiber samples with low strip or pull-out forces, significant void formation or delamination was observed at the coating/glass interface.

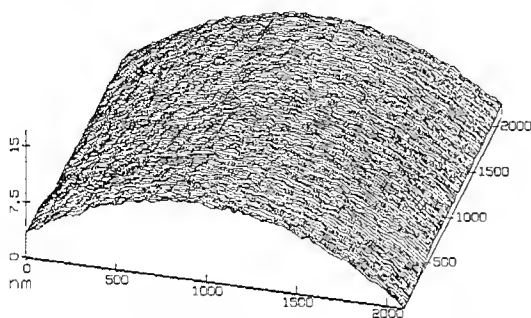


Figure 8. AFM Scan of Glass Surface of Fiber X (Natural) Aged 28 Days in 85 °C/85% RH

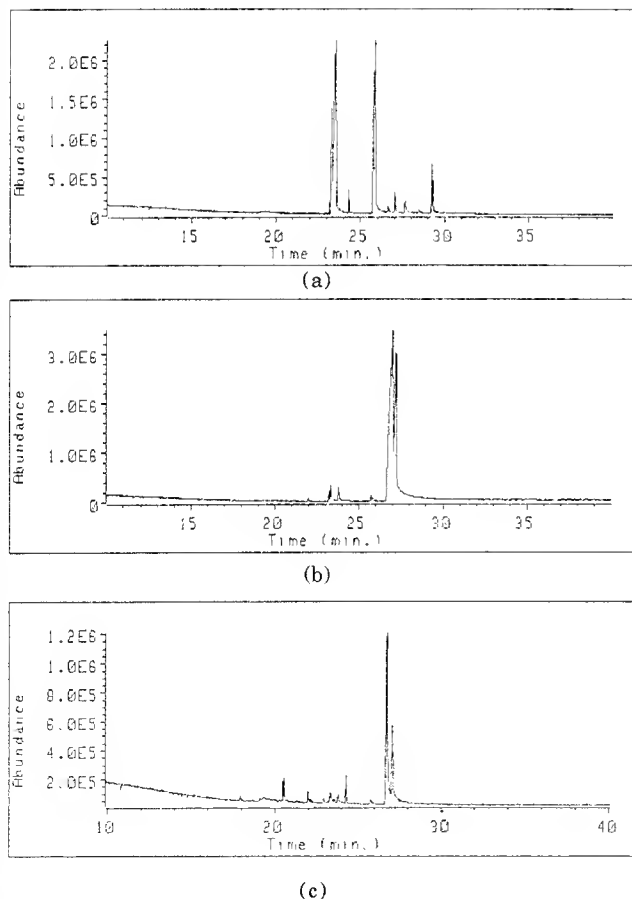


Figure 9. GC/MS Traces for Unaged, Uninked Fibers
(a) Fiber X (b) Fiber Y (c) Fiber Z

In all environments except the 85 °C DI water, the two-point bending strength of all fiber samples was essentially unchanged. This is consistent with the AFM scans, which show no significant change in glass surface roughness for any of these samples. In the 85 °C/DI water environment, however, the strength of fiber X in its natural (uninked) condition decreased significantly, starting on the first day of aging (Table I). This correlates well with Figure 7a, where the surface roughness of this fiber after 28 days of aging is much greater than that of any other sample we measured. The correlation between strength and surface roughness has previously been established.^[4] Note, however, that both of the inked fibers show significantly less surface roughening and strength degradation. After 28 days, the solvent-inked fiber is just beginning to roughen, while its strength has fallen by about one-third. The uv-inked fiber shows neither surface roughening nor strength degradation, indicating an even higher level of protection than that added by the solvent ink layer.

The strength and surface roughening behaviors are consistent with the GC/MS results. After the additional processing step of solvent inking, the levels of the volatile compounds, shown in Figure 9 as characteristic of the individual fibers, are reduced. The reduction in volatiles content after uv inking, shown in Figure 10, is even more pronounced. In the only instance where a significant strength loss and surface roughening occurred (fiber X in 85 °C DI water), a much longer aging period was required before the onset of these degradations in the solvent-inked fiber, as compared to the natural fiber. In addition, the uv-

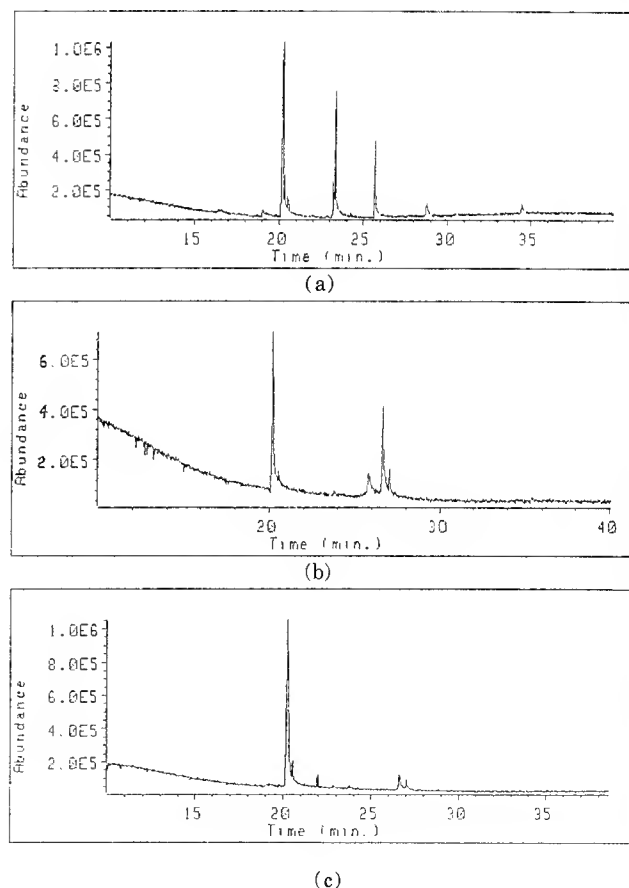


Figure 10. GC/MS Traces for Unaged UV-Inked Fibers
(a) Fiber X (b) Fiber Y (c) Fiber Z

inked fiber has shown no degradation of either kind, even after 28 days of aging. This potential correlation needs to be further studied (i) through longer aging times and possibly additional environments and (ii) through additional analytical methods. The former will focus on identifying other conditions under which strength and surface roughness changes occur. The latter will focus on a better understanding of the surface chemistry at the coating/glass interface. We have, in fact, obtained some preliminary FTIR reflectance spectra for fibers and for individual inner and outer primary coatings that were peeled apart under a microscope. However, it is premature to make any judgment other than that this technique appears to be promising for examining the various interfaces in the fiber structure.

FUTURE WORK

As noted earlier, this paper constitutes an interim report on work in progress. There remain some combinations of fiber/ink/environment/time for which testing is necessary to form a complete picture of the various effects. Future work will also include aging samples for longer time periods in at least some of the environments to determine more precisely the rates of degradation and/or stabilization. Additional fiber samples, as well as coating and ink materials, have been obtained to examine combinations not included in the present tests. These samples will also enable us to expand our list of measurement techniques to obtain additional specific characterizations where suggested by our present results. Among the techniques we have begun to apply is Dynamic Mechanical Thermal Analysis, by which we are able to investigate changes in the coating thermo-mechanical properties during aging.^[5]

CONCLUSIONS

The coating-related properties (strip force and pull-out), bending strength, and surface corrosion of glass optical fibers all depend to some degree on the nature of the coating materials and their reactions in the specific aging environment. Among the factors affecting the changes in these properties are:

- the presence and type of any color coding ink (which may form an additional protective layer);
- the conditions at the coating/glass interface, such as the adhesion (or delamination) of the coating to the glass;
- the nature and volatility (or extractability) of the constituent materials in the fiber coatings; and
- any physical or chemical reactions between the coating (or ink layer) and the immediate environment.

ACKNOWLEDGMENTS

We gratefully acknowledge the efforts of Chris Burpee, Mario Dellafera, Frank DeRosa, and Mike Kozlowski in performing many of the tests described herein and of Barry Vaning in designing and fabricating various test fixtures. The permission of the Director of Research, Telstra Corporation Limited, to publish and present this paper is also acknowledged.

REFERENCES

1. H.H. Yuce, et al., "The Mechanical Performance of Aged Dual-Coated Fibers with Varying Extents of Coating Cure," *Proc. 42nd IWCS*, 1993, p. 857.
2. H.H. Yuce, T.T. Volotinen, and R.A. Frantz, "Effects of Glass Preparation on the Surface Corrosion of Fused Silica Optical Fibers," *Proc. SPIE 2074*, 1993, p. 83.
3. J. Julian and C.P. Chawla, "Spectroscopic Analysis of Water Sensitivity of UV Curable Optical Fiber Coatings," *RadTech '92* (Proc. No. Amer. UV/EB Conf.), 1992, p. 315.
4. H.H. Yuce, et al., "Optical fiber corrosion: coating contribution to zero-stress aging," *OFC '92 Tech. Digest*, 1992, post-deadline paper PD21.
5. O.S. Gebizlioglu, I.M. Plitz, R.A. Frantz, and P.B. Grimado, "Mechanical Properties of Aged Fiber Coatings by Dynamic Mechanical Analysis of Optical Fibers," *Proc. 43rd IWCS*, 1994.



Rolf A. Frantz is a Distinguished Member of Technical Staff in the Fiber Media and Component Reliability Group at Bellcore's Morristown, NJ facility. He earned his Bachelor's and Master's degrees in engineering from Cornell University and his Ph.D. in Engineering Mechanics from Brown University. For over a decade prior to the AT&T divestiture in 1983, he worked at Bell Laboratories, focusing on reliability issues related to electrically insulating materials. He continued to work in that

area when he joined Bellcore at its founding in 1984. Since 1988, he has worked on optical fiber and component reliability, including coatings, inks, and materials compatibility issues.



Trevor N. Bowmer is a Member of Technical Staff in the Metals and Plastics Technology group at Bellcore in Red Bank, NJ. He received his Ph.D. from the University of Queensland, Australia, where he studied the radiation chemistry of polymers. He joined Bell Laboratories in 1980, where his work was directed toward the applications of radiation cured materials and lithographic materials. He joined Bellcore at its inception in 1984, and since that time has worked

extensively in the areas of degradation mechanisms and of the mechanical characterization of polymeric materials used in copper, coaxial, and fiber cables for telecommunications applications.



Barry J. Keon is a Senior Materials Engineer in the Telecommunications Science and Technology Branch of the Telstra Research Laboratories in Melbourne, Australia. He holds a B.Sc. degree from Monash University, a post-graduate Diploma of Polymer Chemistry from Chisholm Institute of Technology, and a M.Eng.Sci. from Monash University. He has worked in the telecommunications industry since 1991, with responsibilities in the area of fiber reliability and cable materials

performance. He is currently a Visiting Researcher in the Fiber Media and Component Reliability Group at Bellcore, working on reliability issues affecting optical fibers and cables.



Hakan H Yuce is the Director of Bellcore's Fiber Media and Component Reliability group based in Morristown, NJ. He has a B.S. degree from the Technical University in Istanbul, an M.S. from MIT (both in Mechanical Engineering), and earned a Ph.D. in Mechanical Engineering and Materials Science from Stanford University. He leads Bellcore's research program in the areas of optical fiber and fiber optic component reliability. He also plays an active role in the establishment of US and international standards for optical fiber test procedures to assure long-term reliability. He was a 1992 recipient of *Telephony* magazine's Ray Blain Outside Plant Achievement Award.



Eva M. Vogel is a Member of Technical Staff in the Fiber Media and Component Reliability Group at Bellcore, Morristown, NJ. She received her Dipl. Chem Eng. and Ph.D. degree in Ceramic Engineering from Slovak Technical University, Bratislava, Slovakia. She joined Bellcore in 1984 after working at Bell Telephone Laboratories since 1970. Her research at Bellcore has focused on novel properties of electronic and optical materials such as oxide glasses for

photonic switching and optical amplifiers. She is currently working in the areas of optical component and fiber reliability. She is a Fellow of The American Ceramic Society.

OPTICAL FIBER INERT STRENGTH AND B-VALUE

Willem Griffioen*, Torbjörn Svensson⁺, Bob Friderich*

*PTT Research, St. Paulusstraat 4, NL-2264 XZ Leidschendam, The Netherlands

⁺Telia Research AB, S-136 80 Haninge, Sweden

Abstract

To avoid weak-flaw statistics, a "Minimum-Life" model is used for optical fiber lifetime estimations. This model requires measurements of the initial strength, usually performed in vacuum, liquid nitrogen, or at high-speed. A 2-point bending "guillotine" has been developed, capable to fracture fibers at extremely high stress rates. The measurements indicate a strength increase with stress rate in the "guillotine", well beyond the region where leveling occurs in high-speed pulling experiments. The existence of two types of initial strength is proposed: S_1 in vacuum, and S_{1h} in "humid" environment, the latter measured with high-speed techniques and at low temperatures. The value in vacuum, typically 16 GPa, must be used, per definition, in the Minimum-Life model. But then much more conservative lifetime estimates are obtained than when statistics-based lifetime models are used. Using the B -value from high-speed techniques, much higher stresses are allowed in service, without making larger errors than from the unavoidable effect of proof-test unloading.

Introduction

An important failure mechanism of an optical fiber is fracture caused by stress enhanced crack growth. This mechanism is the basis for several models used to estimate the lifetime of the fibers. Models based on the so-called stress corrosion susceptibility parameter, n , can be split into two groups. The first group uses weak flaw statistics, obtained from destructive testing of long lengths of fibers, or from proof testing. In a COST-218 study¹ this group was condensed to two models, one basic, and one alternative for use with on-line proof testing.

The second group does not require the hard-to-obtain weak flaw statistics. Instead the proof-test level is used for a minimum strength approach.¹ The simple-to-use models from the second group, however, make use of the so called B -value on which no international agreement is yet achieved.

In order to obtain the B -value it is necessary to measure the optical fiber's initial¹ strength.² Three techniques have been used for this: vacuum², low temperature³ and high-speed⁴ dynamic measurements. The initial strength values from vacuum and liquid nitrogen experiments are about 16 GPa.^{2,3} Note that a temperature dependence of initial strength is found at low temperatures.⁵ The value of

about 7 GPa from high speed pulling experiments^{4,6}, where a leveling of the strength appeared just at the highest speed, is a factor of (more than) 2 lower. As a consequence B -values and lifetime estimates may differ over a range of five decades.^{2,3,4,5,6,7}

In this paper results are given, obtained with a new high speed technique. This technique uses a "guillotine" applied on 2-point bending of the fiber, which enables us to reach a stress rate of 1.6×10^4 GPa/s. This is an increase by more than an order of magnitude compared with high speed pulling.⁴ Experimental results with the latter techniques are given for the same fiber. The results are compared with those from other techniques. The technique dependent values for the initial strength are discussed. An environment dependent definition of the initial strength is given. It is argued how to apply the value of the initial strength in the second group of lifetime models.

Theory

Optical fibers are made from silica glass which consists of ring structures of Si-O tetrahedra.⁸ The mechanical strength of the tetrahedral bonds gives a maximum stress value of 20 GPa, but fracture of the fibers usually occurs at a lower value, due to stress concentration. The stress concentration at crack-tips is characterized by the stress-intensity factor K_I which is given by:⁹

$$K_I = Y\sigma\sqrt{a} \quad (1)$$

where Y is a geometrical factor (1.24 for an elliptical crack), a the depth of the crack and σ the applied stress. Fracture occurs when K_I reaches the critical value K_{Ic} of $8 \cdot 10^5$ N/m^{3/2} (where catastrophic failure occurs).¹⁰ At that moment, the stress σ is equal to the current strength S . From this it follows:

$$S = \frac{K_{Ic}}{Y\sqrt{a}} \quad (2a)$$

An expression for the initial strength S_1 , at $t = 0$, where $a = a_1$, is also given:

$$S_1 = \frac{K_{Ic}}{Y\sqrt{a_1}} \quad (2b)$$

The usually observed time-dependence of the strength of optical fibers, can be explained by crack-growth due to a stress-enhanced chemical reaction (stress corrosion) breaking the bonds. This crack growth is influenced by the environmental conditions, especially humidity. Stress corrosion of silica is usually modeled using a power law, so that crack-growth is given by:⁹

$$\frac{da}{dt} = AK_1^n \quad (3)$$

¹In literature the initial strength is often called inert strength. Measurements of initial strength are carried out in an environment which is inert, or effectively inert, i.e. under such conditions that the environment does not influence the strength of the fiber.

with A a scale factor for the speed of crack-growth and n the corrosion susceptibility factor. For dynamic fatigue experiments with $\sigma = d\sigma/dt \cdot t$, where the stress rate $d\sigma/dt$ is constant, this equation can be integrated, using (1) and (2):

$$S_I^{n-2} = \frac{\sigma_d^{n+1}}{B(n+1)d\sigma/dt} + \sigma_d^{n-2} \quad B = \frac{2}{AY^2(n-2)K_{Ic}^{n-2}} \quad (4)$$

with σ_d the dynamic failure stress, the value of the stress σ when σ and S become equal, and catastrophic failure occurs. In Figure 1 the relation between σ_d and $d\sigma/dt$ is given for typical values of n , S_I and B for vacuum and high-speed experiments. When measurements can be fitted by a sloped straight line, which is usually the case, the n -value is found with (4), neglecting the right hand term σ_d^{n-2} . Note that the sloped straight line is the same for both combinations of S_I and B , since the products BS_I^{n-2} are equal. As a consequence the B -values cannot be obtained separately. In lifetime models with the minimum strength approach, in which a crack that corresponds with the proof test level grows until fracture, this B -value is needed.¹ Therefore additional initial-strength measurements must be performed, to obtain the B -value. The initial strengths can be recognized as a horizontal leveling of the lines in Figure 1.

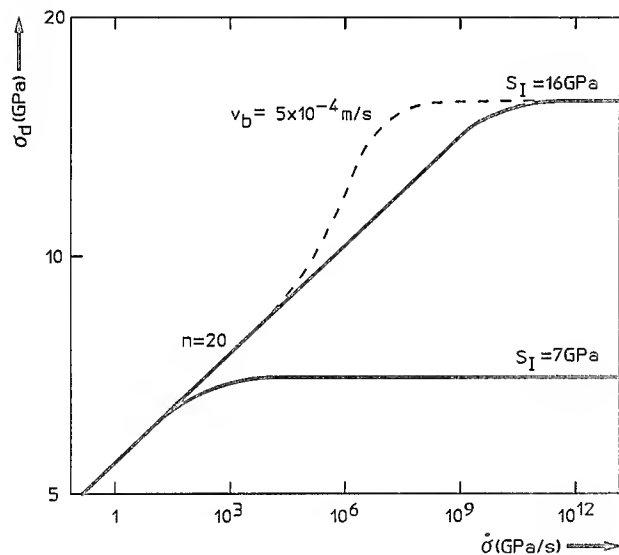


Figure 1 Dynamic failure stress σ_d as a function of stress rate $d\sigma/dt$ according to (4) with typical values of the corrosion susceptibility n of 20 and initial strength S_I of 16 GPa (B -value of 2×10^{-8} GPa²s), typical for vacuum.² A line for $S_I = 7$ GPa ($B = 0.06$ GPa²s), reported from high-speed measurements⁴, is also drawn. The dashed line is calculated including the constant crack growth speed v_b of 5×10^{-4} m/s in region II.

Stress corrosion cannot be modeled by a power law above a critical value v_b of the crack velocity.⁹ The behavior is trimodal as can be seen when plotting the crack velocity v as a function of the stress intensity K_I (Figure 2). Region I, which is modeled by the power law, results from stress corrosion caused by moisture in the environment. At the critical speed v_b the limiting rate of water diffusion to the region of the crack tip results in region II behavior,

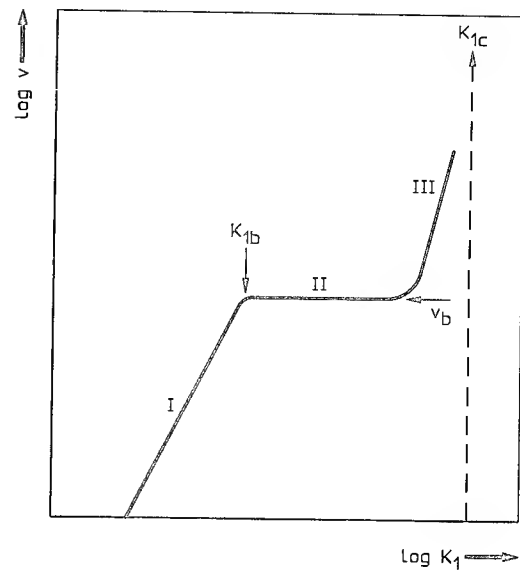


Figure 2 Schematic representation of the effect of stress intensity K_I on crack velocity v during slow crack growth.

where the crack velocity is determined by this diffusion and does not further increase with stress intensity. The value of v_b depends on the relative humidity (RH) and temperature, and is about 5×10^{-4} m/s for fused silica in ambient environment (75% RH, 20°C) and drops to much lower values for lower RH.¹¹ Region III, just before catastrophic failure occurs at K_{Ic} , is independent of environment. When moisture is eliminated, such as in vacuum experiments², region II shifts down and region III will be followed for a large portion.

From (1) and (2) it follows that the strength S_b at the moment that region II is entered can be written as $S_b = \sigma_b K_{Ic} / K_{Ib}$ with σ_b the value of the applied stress and K_{Ib} the stress intensity at that moment. For dynamic measurements it follows with (4):

$$S_I^{n-2} = \frac{\sigma_b^{n+1}}{B(n+1)d\sigma/dt} + \left(\frac{K_{Ic}}{K_{Ib}} \right)^{n-2} \sigma_b^{n-2} \quad (5)$$

In region II the crack-growth velocity is constant: $da/dt = v_b$. This can be written with S , using (2), and integrated. At fracture, when S and σ_d become equal, this gives:

$$\sigma_d^{-2} = \left(\frac{K_{Ic}}{K_{Ib}} \right)^{-2} \sigma_b^{-2} + \frac{Y^2 v_b}{d\sigma/dt \cdot K_{Ic}^2} (\sigma_d - \sigma_b) \quad (6)$$

Usually region I behavior is sufficient to describe stress corrosion and the dynamic failure stress from (4) is accurate. When the stress rate becomes very high, region II behavior becomes important. Now (5) and (6) must be used, the latter solved numerically. This is done for $v_b = 5 \times 10^{-4}$ m/s in Figure 1, shown by the dashed line. Note that in the case that $S_I = 7$ GPa such a behavior does not occur, because the crack velocity remains below v_b . This means that the parameters from high speed experiments⁴ do not match with the v against K_I plot, measured on bulk silica.¹¹ In the Section about the definition of initial strength it is argued that immediate catastrophic failure after the first bond rupture can be the cause for this anomalous behavior.

Reported Initial Strengths

In order to measure the optical fiber's initial strength, stress-corrosion assisted growth of cracks must be prevented. Three techniques have been used for this: low humidity^{2,10}, low temperature³ and high speed⁴ dynamic "fatigue" measurements. These techniques and their resulting values for the initial strength will be discussed below:

Low Humidity Measurements Here moisture is taken away which reduces the reaction speed, and hence the crack velocity. Tensile pulling measurements under a -40°C bone-dry-grade CO₂ environment¹⁰ resulted in an initial strength of 6.76 GPa. In a later 2-point bending experiment under vacuum conditions it has been shown, however, that extremely long pumping times of 5 days are needed to obtain correct values of the initial strength.² Taking this into account an initial strength of 16 GPa was found (this value has been obtained from the reported strain using a nonlinear relation between stress and strain)¹².

Low Temperature Measurements Here the bond-rupture (reaction) speed is reduced by lowering the temperature. Experiments at temperatures from -196°C (liquid nitrogen) to 100°C resulted in dynamic (2-point bending) strengths from 18 to 4 GPa, respectively³ (these values have been obtained using Ref.12 again). The authors interpreted this variation in strength as a variation in water availability because the saturated vapor pressure of water (dew point) decreases with decreasing temperature. It is, however, the water content at the fiber surface, and not the water content in the surrounding air that determines the crack growth. Only during the time that the fiber is hotter than the liquid in which it is cooled, a small amount of moisture will diffuse into the liquid. Because this time is very short compared with the 5 days needed to eliminate enough moisture to measure initial strength² (even more time is needed at lower temperatures) it is concluded that it is the temperature, and not the availability of water, that is responsible for the increase of measured strengths (these assumptions were also made in Ref.2 and Ref.14). The reported value of 18 GPa for the initial strength, is close to the vacuum value of 16 GPa. However, a significant temperature dependency of the initial strengths of weak flaws is found⁵, a 30% increase from -120 to -180°C. In Ref.15 even a further increase is found for fused silica, when cooling down to the temperature of -269°C of liquid helium. According to the previous study, the "liquid nitrogen value" of the initial strength, extrapolated to ambient temperatures, is not equal to the "vacuum value". It is suggested that the extrapolated liquid-nitrogen strength is equal to the strength, obtained with high-speed techniques.⁵

High Speed Measurements Here the reaction speed remains constant, but fracture is intended to occur faster than crack growth. With a special high-speed pulling technique a value for the initial strength of 7 GPa has been extrapolated from experiments where a leveling of the measured strength just started.⁴ In this paper a newly developed 2-point bending "guillotine" has been applied, in order to get experimental information beyond the leveling of measured strength. The experimental work in this paper focuses on the high speed technique.

Measurements

Samples The tests have been performed on the same fiber "B", as used in a previous study.² The fiber is a commercial silica optical fiber, double-coated with uv-cured acrylate (CPC3).

2-Point Bending Guillotine A special fiber tester, the 2-point bending guillotine, has been developed and is shown in Figure 3. A sample fiber is positioned in a vertical "D-shape" in a slot, using a groove in the anvil and another groove in a movable bender. The bender has a low weight, sufficient to bend the fiber, but low enough to avoid fracture, and even crack growth. A falling "axe" can be placed at an adjustable elevation. A weight can be mounted on this axe. When the axe is released, it falls down (without friction), and reaches a speed v_{axe} when arriving at the bender, depending on the elevation h :

$$v_{axe} = \sqrt{2gh} \quad (7)$$

with g the acceleration of gravity. The maximum stress σ , at the apex of the bent fiber, is given by:^{12,16}

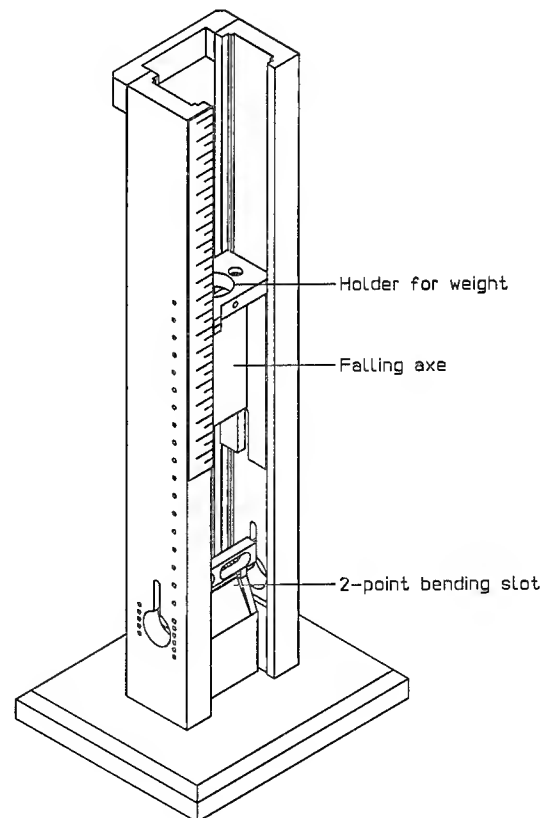


Figure 3 The 2-point bending guillotine.

$$\sigma = E_0 \varepsilon \left(1 + \frac{\alpha'''}{2} \varepsilon \right) \quad \varepsilon = \frac{1.2 d_f}{d_{plate}} \quad (8)$$

with E_0 the Young's modulus of fused silica, α''' a constant for its non-linear elastic behavior (4.25 for 2-point bending)¹², ε the maximum strain at the apex of the bent fiber, d_f the diameter of the uncoated fiber, and d_{plate} the effective distance between the plates, corrected for groove and fiber diameter. From (8) it follows, with $d_{plate} = d_0 - \nu_{axe} t$:

$$d\sigma/dt = \frac{\nu_{axe} \sigma_d^2}{1.2 d_f E_0} \quad (9)$$

Note that the terms for non-linear elasticity cancel. For the maximum elevation h of 20 cm, the speed ν_{axe} is 2 m/s, resulting in a stress rate of 1.6×10^4 GPa/s.

Fracture of the fiber in the 2-point bending guillotine is detected by means of a high-speed video. This video is capable to make 12000 exposures per second. An example of 6 subsequent exposures is shown in Figure 4. In the 4th exposure the separation of the broken fiber is obvious, but in the 3th recording it can be seen that the fiber was fractured also during a part of the shutter time (which is just $1/12000$ s).

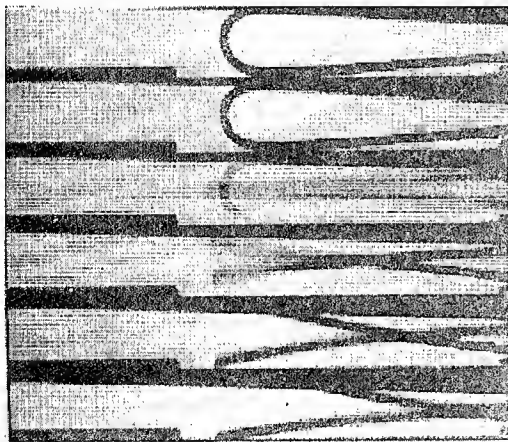


Figure 4 Example of high speed recording of a fracturing fiber in the 2-point bending guillotine, at a speed of 1 m/s. The frame rate of the video is 12000 s^{-1} .

The equipment was calibrated first with the help of spacers of 0.6 and 1 mm. The measurements were analyzed by plotting the plate distances for 6 subsequent recordings. Then a line was drawn through these points, giving information about the speed of the axe. At the highest speed of 2 m/s, the difference of the plate distance between two exposures is $1/6$ mm. The resolution is improved by a factor of 4, interpolating the fracture between exposures, by estimating the part that has fractured during the last recording where the fiber was in its "D-shape" (see Figure 4). The resolution in time, together with the screen resolution, result in an accuracy of 3% for the highest speed (plate distance around 1.5 mm). The resolution is better for lower speeds. Also the median value of 10 points has a higher accuracy.

Measurements were made under ambient (23°C , 50-70%RH), but non-controlled, conditions. The results are shown in the Weibull plot of Figure 5, for speeds ν_{axe} of 0.33, 0.5, 0.89 and 1.95 m/s. The lowest speed was obtained

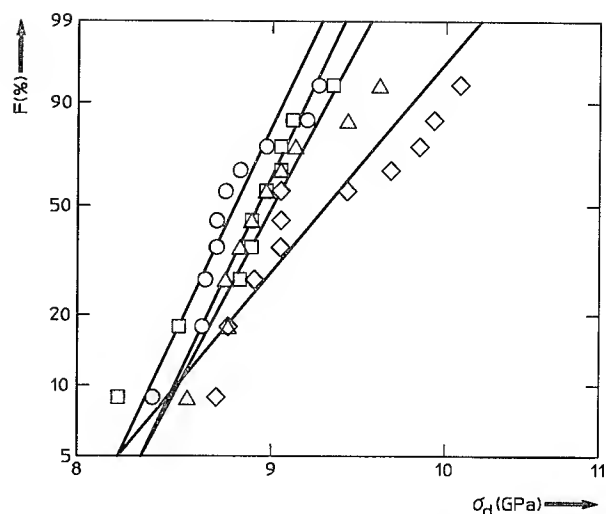


Figure 5 Weibull plot of dynamic failure stress from 2-point bending guillotine, for different speeds.

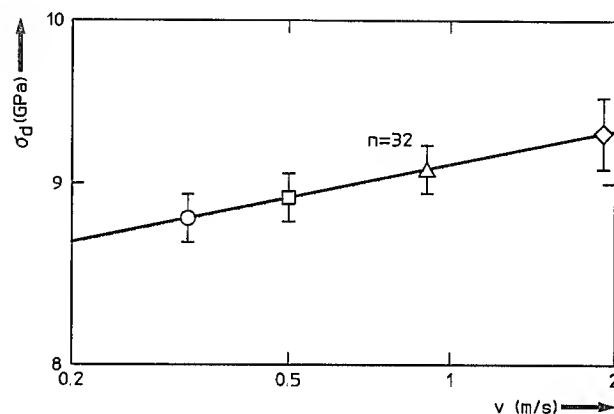


Figure 6 Median dynamic failure stress, obtained from Figure 5, as a function of speed. The symbols correspond to the ones in Figure 5.

for low weight and elevation, where the reaction force of the fiber is able to decrease the speed a little below the value of (7). Due to the limitations of the high speed recording the spread in results (Weibull parameter¹⁷ m from 20 to 40) is higher than the natural spread of this fiber (m values from 50 to 100)². The median values from Figure 5 are plotted as a function of speed ν_{axe} in Figure 6. They are also given as a function of stress rate in Figure 9, where a comparison is made with results from other techniques.

Although inaccurate, the estimate of the n -value of 32, from Figure 6, agrees well with the measured value of 30 from Ref.2, for the same fiber. More clear is the fact that the strength of the fiber continues to increase (up to 9.33 GPa), at stress rates well above those of high-speed pulling⁴. A calibration with tin-coated fibers²², which are expected to show a speed independent strength, has also been performed. When these fibers fracture in 2-point bending, usually the tin layer remains intact. Because of this, the increase in resolution by estimating the part that has fractured in one exposure, cannot be made. Detection of fracture is, however, still possible. The strengths, found

in 2-point bending (10 fibers per speed), are 12.3 ± 0.5 and 12.2 ± 1.5 GPa (better accuracy for median) for speeds of 0.33 and 1.95 m/s, respectively. No dependency of strength on speed is found, as expected, within accuracy. This accuracy is, however, very low.

High-Speed Pulling The fiber, which was measured with the guillotine equipment, has also been tested with the high-speed pulling technique, described in Ref.4. For each stress rate (0.010, 14, 140 and 1400 GPa/s), 30 fiber spec-

imens (gage length of 50 cm) were randomly taken from the reel. The measurements were performed in a conditioned room at 23°C and 50%RH. The fracture data are shown in Figure 7. The Weibull parameter m varies from 61 to 85, with an average around 70. From Figure 7 the median values have been determined, which are given as a function of stress rate in Figure 8. In this Figure also a fit like in Ref.4 is drawn, using (4) in its full form. Here the n -value is around 26. the initial strength S_1 is 7.1 GPa and the B -value is 0.016 GPa²/s.

Comparison In order to compare high-speed pulling experiments (test length 50 cm) with 2-point bending (effective test length around 10 μ m, for an m -value of 70), a correction for the test length must be performed.¹⁶ It was shown in earlier work of Breuls¹⁸, that the techniques of 2-point bending and tensile testing match, when such a correction is done. In Figure 9 the results of both techniques are plotted on a 2-point bending scale, using an m -value of 70 for the length correction of the tensile pulling data. The 2-point bending data from previous work on the same fiber² B are also plotted for comparison. The fit is the same as the straight part of Figure 8. The n -value of 26 differs from the values of 30 and 32 for 2-point bending, but the mismatch in Figure 9 is small, especially when considering the large error for the 2-point bending guillotine. A clear effect, however, is that the guillotine experiments show a further increase in strength, well beyond the region where leveling occurs in the high-speed pulling experiments. This cannot be explained by inertia effects (calculated from experiments). An attempt was made to check the equipment with a tin-coated fiber²², which is expected to show a speed independent strength. Unfortunately, the strength variations between the specimens, for the gage lengths used with high-speed pulling, were too large for a reliable check.

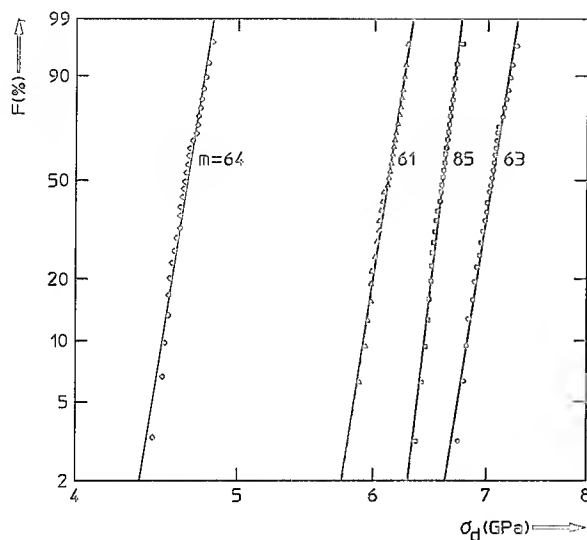


Figure 7 Weibull plot of dynamic failure stress from high-speed pulling (gage length of 50 cm), for stress rates of 0.010, 14, 140 and 1400 GPa/s (from left to right).

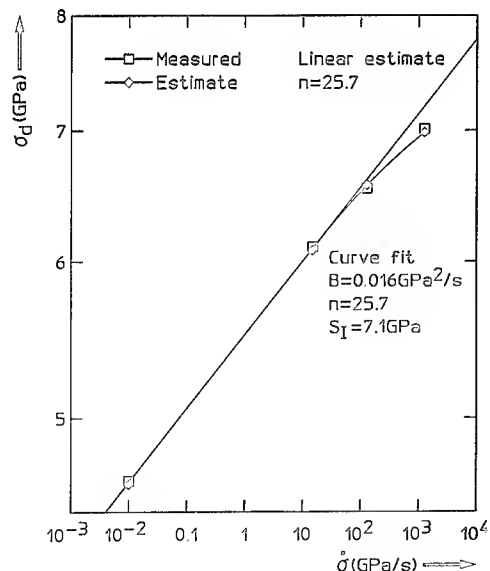


Figure 8 Median dynamic failure stress, obtained from Figure 7, as a function of stress rate. A fit like in Ref.4 is drawn, using (4) in its full form.

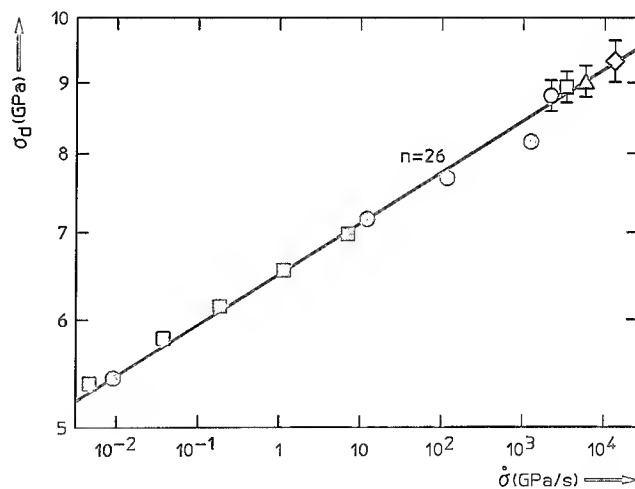


Figure 9 Median dynamic failure stress as a function of stress rate. The 2-point bending guillotine measurements appear in the upper part (open symbols). In the lower part, 2-point bending data from previous work² on the same fiber are shown (solid squares). The results of high-speed pulling experiments from this work, corrected for the different test length¹⁶, are also pasted in this figure (solid circles).

Lifetime model

In literature some models appear which are based on a "minimum life" approach. They are summarized in ¹, where the Minimum-Life model was suggested as the most suitable, because of its simplicity. In this model it is assumed that always a crack exists, that corresponds to the proof-test level σ_p , no matter what the considered fiber length is. The allowable stress σ_a during a service life t_a follows with (1), (2) and (3):¹⁹

$$\sigma_a = \sigma_p \left(\frac{B}{\sigma_p^2 t_a} \right)^{1/n} \quad (10)$$

It must be borne in mind that this lifetime model assumes that the weak flaws, that cause failure in practice, are sharp. Because this assumption has never been verified, the other extreme situation, where these flaws are blunt, must also be considered. The theory for blunt flaws has been developed in Ref.20. From this a Minimum-Life model for blunt flaws can be derived:

$$\sigma_a = \sigma_p \left(\frac{B}{S_{fb}^2 t_a} \right)^{1/n} \quad (11)$$

with S_{fb} the local initial strength at the bottom of the flaw. This bottom is considered the same as the surface of fibers in the high strength mode. Therefore the same value can be taken for S_{fb} as the initial strength S_i , discussed in this paper.

Definition of initial strength

Use of the Power Law The value of the initial strength is necessary, in order to obtain the B -value, appearing in minimum-life approach models. This B -value is defined by the power law (3). It is generally accepted that an exponential description of crack growth is more physically realistic, although not always better fits of experimental data are obtained.¹³ The exponential law, originated from chemical kinetic theory, is given by:

$$\frac{da}{dt} = v_0 \exp \left(\frac{-E_a + bK_I}{RT} \right) \quad (12)$$

with v_0 a scale factor for the crack growth velocity, R the gas constant (8.31 J/K), T the temperature, E_a the zero-stress activation energy and b a constant.²¹ With the exponential law, the onset of initial strength will deviate: the dashed line in Figure 1 will first bend below the solid "power law" line, before it bends up again. The level of the initial strength is, however, the same.

The power law description is more widely used, because it is mathematically better tractable. Although the power law fit is only correct for a certain window, no extrapolation errors occur when transforming fatigue experiments on high-strength fibers to service lifetime of weak flaws. This is because the stress intensity and crack velocity are comparable in both situations.²³

It was noted by Kurkjian and Inniss¹³, that very large differences between extrapolations with power law and exponential law to shorter times, in the neighborhood of the initial strength, are present. This is illustrated by the predicted limiting times of 10^{-8} and 10^{-14} s, respectively. However, the initial strength is not influenced by fatigue, so neither the power law nor the exponential law must be applied for analysis of the measured initial strength.

Principally, the measured initial strength can be directly used to distil a detached B -value from the product BS_i^{n-2} , measured in fatigue experiments.

Different Definitions for Initial Strength The exponential law will be used now to give a better understanding of Region I, II and III crack growth in Figure 2. It is reasonable to assume that the zero-stress activation energy E_a in this law, which describes an energy barrier between bound and dissociate state²⁴, depends on the environment. In Figure 10 the exponential law is shown for two values of E_a . The left curve, with $v_0 = 3.83$ m/s, $b = 3.25 \times 10^8$ JGPa⁻¹m^{-1/2} and $E_a = 131.5$ kJ, represents Region I, which determines the behavior in fatigue measurements. The mentioned parameters agree with those presented by Bouten et al.²¹, and also with measurements of crack velocities in bulk silica in Region I (and II and III).¹¹ The crack growth velocities, that are followed in fatigue measurements on fibers, are much lower than those for crack growth velocity measurements in bulk silica. This explains the difference in measured n -values, 20 and 40, respectively (the n -values follow by the slopes in Figure 10).

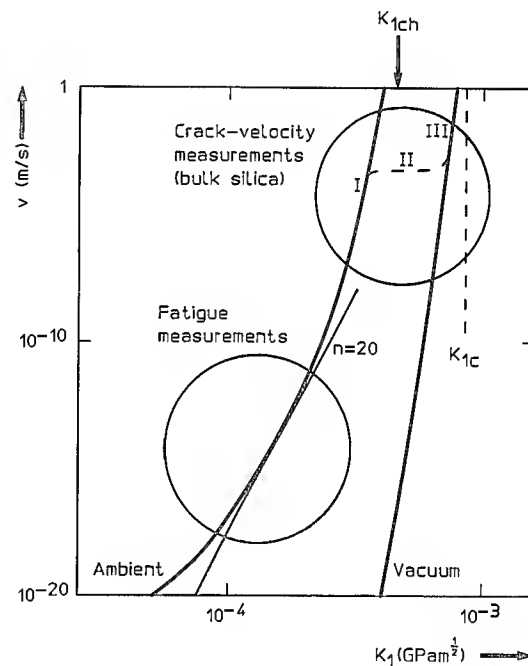


Figure 10 Schematic representation of the effect of stress intensity K_I on crack velocity v . The upper part is that of Figure 1, for which bulk silica data exist of Regions I, II and III. The lower part represent stress intensities and crack velocities, that occur in optical fibers. A fit with the exponential law through Region I, explains the n -value of 20 for optical fibers and of 40 for bulk silica. Another exponential-law fit, with another value E_a , can be drawn through Region III.

The right curve is an exponential fit through Region III (which is followed in vacuum), with the same parameters as for the left curve, only now with an activation energy E_a of 250 kJ. It becomes clear that the part of Region III is so steep now (it corresponds well with measurements in Ref.11), that an experimental distinction between this behavior and catastrophic failure cannot be made anymore. Therefore the conclusion is that the stress intensity that

is approached by the exponential law, in vacuum, at high crack growth velocities, is almost equal to the critical stress intensity K_{Ic} . It is also concluded that for ambient (humid) environment, described by Region I, another critical stress intensity, K_{Ich} , and according to (2b) another initial strength, S_{Ih} , follows than for vacuum (K_{Ic} and S_I , respectively). The value of low-temperature initial strength (extrapolated to room temperature) will also be K_{Ich} . Because $K_{Ich} > K_{Ib}$ and K_{Ib}/K_{Ic} has a value of 0.64 to 0.76 (when bulk measurements apply for optical fiber)^{11,27}, a "high-speed" value of initial strength between 10 and 16 GPa is expected.

In practical situations the crack growth follows Regions I, II and III, before it fractures. Catastrophic failure always occurs in a vacuum-like environment, no matter how you test it, because in regions II and III the transport of humidity does not keep pace with the crack growth anymore. It all becomes different, however, for high-speed measurements on fibers, when they are assumed to be flaw free. In this case the very first bond rupture determines the strength. After this rupture the strength would drop by a factor of 2, according to Inglis²⁵, and the stress intensity (which, at high speed, is already very high for the first bond rupture) "hops" beyond K_{Ic} (note that $K_{Ib}/K_{Ic} = 0.64$ to 0.76 for 20°C and $75\%\text{RH}$)^{11,27}. This means that now the initial strength of the fiber depends on the critical stress intensity, K_{Ich} , in the ambient environment, the exponential extrapolation of Region I. In this case it can be understood that the behavior of high-speed pulling experiments may differ from the dashed line in Figure 1. The exact shape of the strength versus stress rate is difficult to obtain because the transition from dynamic to inert behavior is a transition from region I to II and III and also from continuous to discrete behavior (in the latter, not the speed of crack growth, but probability of bond rupture, describes fracture.²⁶

Which Definition for Minimum-Life Model? In the previous paragraphs, two definitions of critical stress intensities and (proportional) initial strength were used, the old definition (region III) K_{Ic} and S_I , and the new definition (region I) K_{Ich} and S_{Ih} , the latter for ambient environment (with humidity). In vacuum S_I is measured, in liquid nitrogen (extrapolated to room temperature) and at high speed, S_{Ih} is measured.

Crack growth in an environment with some humidity, like in n -value measurements, in proof testing, or in service, is described by the power law (region I), given by (3). The parameters A and n depend on environment, but not on initial strength. The initial strength S_I appears only after the solution of (3) for failure condition, e.g. (4) for dynamic fatigue. The B -value is, unlike A , not only dependent on environment, but also on the definition of S_I (and K_{Ic}). For usual stress rates, the right-hand term in the left formula in (4) is negligible small, so that only n and the product BS_I^{n-2} are measured. The latter product can be written, using (2b), as:

$$BS_I^{n-2} = \frac{2}{AY^2(n-2)} \left(\frac{1}{Y\sqrt{a_I}} \right)^{n-2} \quad (13)$$

All terms on the right-hand side of (13) do not depend on the definition of K_{Ic} or, via (2b), on the definition of S_I . This means that also the solution (4) of (3), for usual stress rates, does not depend on the definition the initial strength, even though it's value appears in the formula. This can be understood easily. For usual stress rates, the slow crack growth behavior in Region I determines failure.

As soon as crack velocities become high, which is certainly true in Regions II and III, fracture occurs almost instantaneously. The regions with high crack velocities have no effect. The location of K_{Ic} is not "seen". Therefore the choice is free which B , S_I or K_{Ic} values are to be used, as long as the same definition is maintained. The latter two parameters are linearly related by (2b). The values of S_I , B and K_{Ic} become only important when a comparison with a certain stress level is made. Examples are the proof-test level in the Minimum-Life model, or weakening due to proof-testing unloading. An illustration will be given below.

Consider a description, which is defined in humid environment. This will be used in the Minimum-Life model (10), which describes crack growth for a flaw that just survived the proof test. When the proof test is not performed on-line, this crack growth occurs under fatigue. That means that regions I, II and III are followed for a crack that just fails. Now it becomes clear that the guaranteed minimum strength, equal to the proof-test level, is S_I and not S_{Ih} . Therefore the substitution $S_{Ih} = \sigma_p \times S_{Ih}/S_I = \sigma_p \times K_{Ich}/K_{Ic}$ must be made in the solution of (1), (2) and (3), to obtain a Minimum-Life model equivalent to (10). In this model also B_h must be used instead of B :

$$\sigma_a = \sigma_p \frac{K_{Ich}}{K_{Ic}} \left(\frac{B_h}{\sigma_p^2 t_a \times K_{Ich}^2 / K_{Ic}^2} \right)^{1/n} \quad (14)$$

B_h can be written as $B \times (K_{Ic}/K_{Ich})^{n-2}$. When this is substituted in (13), exactly the same formula as (10) appears.

It is also possible to use the definitions for vacuum from the start. In that case, no correction for the guaranteed initial strength is needed, and (10) is obtained directly. It is concluded that the initial strength value that must be used to obtain B -values for Minimum-Life models, is the strength in vacuum, and not in liquid nitrogen (extrapolated to room temperature) or at high speed. A typical B -value for vacuum is 2×10^{-8} GPa²s, for n -values of 20. For a proof-test level σ_p of 0.5 GPa, and a lifetime t_a of 30 years, the Minimum-Life model gives allowable stresses of $0.16 \times \sigma_p$ and $0.12 \times \sigma_p$, for sharp and blunt weak flaws, respectively. This means that the Minimum-Life model is more conservative than models which are based on weak-flaw statistics.¹

The reason that the the Minimum-Life model is too conservative, is the fact that the probability to find a crack after proof test, with $S_I = \sigma_p$, is extremely small. The probability to find a crack that just stopped growing at the end of proof test, with a state somewhere on region II or III (i.e. between K_{Ib} and K_{Ic} in Figure 2), will be estimated. Immediate unloading of the proof test is assumed. From (1) and (2), equations like (5) and (6) can be derived for a static proof test. These formulas are given in Ref.27, resulting in:

$$S_I^{n-2} = \frac{\sigma_p^n t_p}{B} + \left(\frac{K_{Ic}}{K_{Ib}} \right)^{n-2} \sigma_p^{n-2} \quad (15a)$$

when reaching K_{Ib} , and:

$$S_I^{n-2} = \frac{\sigma_p^n t_p}{B} + \left(\frac{K_{Ic}}{K_{Ib}} \right)^{n-2} \sigma_p^{n-2} - \frac{(K_{Ic}^2 - K_{Ib}^2) \sigma_p^{n-2}}{BY^2 v_b} \quad (15b)$$

for fracture. For the parameters used in this paper, with the low B -value for correct description, it follows that a crack with an initial strength value, S_I , of 1.2394 GPa, will just fracture, while a crack with a slightly higher

value of 1.2395 GPa, just reaches K_{Ib} .

The probability, F_{rr} , to find a crack in this "risky region", follows from Weibull statistics:¹⁷

$$\ln(1-F_{rr}) = \ln(1-F_p) \times \left(1-N_p/N_b\right) \quad LN(S_i) = \frac{L}{L_0} \left(\frac{S_i}{S_0}\right)^m \quad (16)$$

with F_p the failure probability at proof test, and N_p and N_b the failure number, and the number that reaches K_{Ib} , respectively. It follows, for a proof test failure of 0.02 km⁻¹ and a Weibull parameter m of 2⁻¹, that the probability to find a crack in the "risky region" is less than 3×10^{-6} .

The probability to find a crack in the "risky region" between K_{Ib} and K_{Ic} is comparable with the probability to have a crack in the "risky region", that corresponds with weakening below the proof-test level during proof-test unloading, without fracturing.²⁷ The unloading makes 100% guarantee Minimum-Life estimations impossible. Even when the proof-test level is raised by orders of magnitude, still weakening below practical values like 0.5 GPa can occur²⁷ (note that also for this estimation the low B -value for vacuum must be used). Therefore a Minimum-Life estimation, based on a B -value that is found with high-speed techniques (K_{Ic} is higher than K_{Ib}), is practical, not giving larger errors than from the unavoidable proof-test unloading.

It is also possible to find B -values for abraded fibers⁵, which might show slightly different behavior. Also here the initial strength shall be measured in vacuum. Another technique, proposed by Hanson⁷, is to assess the B -value by numerically fitting the measured distribution of weak flaws. This looks paradoxical. For the high strength mode it is necessary to measure the inert strength to find the B -value. It is under study if it is possible to obtain the B -value from the more difficult to measure weak-flaw distribution, with it's more difficult statistics (because of the proof-test effects), while in all steps normal fatigue occurs.

Conclusions

A 2-point bending "guillotine" has been developed. With this equipment, considerably higher stress rates have been applied than with high-speed pulling techniques. The experimental results are compared with the ones from the latter technique, and with 2-point bending techniques at lower speeds. The results are comparable, but the strength continues to increase in the "guillotine" experiment (up to 9.33 GPa), well beyond the region where leveling occurs in the high-speed pulling experiments. An explanation is not found.

It is reasonable to assume that two types of initial strength exist, S_i in vacuum, and S_{ih} in ambient (humid) environment. The latter is measured with high-speed techniques and in liquid nitrogen (extrapolated to room temperature). The value in vacuum, typically 16 GPa, can be applied for Minimum-Life models according to their 100%-guarantee definition. This corresponds with a typical B -value of 2×10^{-8} GPa²s, for an n -value of 20. For 30 years lifetime, the Minimum-Life model gives a maximum stress level of 0.16 and 0.12 times the proof-test level, for sharp and blunt weak flaws, respectively. This is more conservative than results of lifetime models that are based on weak-flaw statistics. Using the B -value from high-speed techniques in the Minimum-Life model, much higher stresses are allowed in service (almost factor of 2), without making a larger error than that, which is caused by the unavoidable effect of proof-test unloading.


References

- 1 W. Griffioen, T. Breuls, G. Cocito, S. Dodd, G. Ferri, P. Haslov, L. Oksanen, D. Stockton, T. Svensson, "COST 218 evaluation of optical fibre lifetime models", *Proc. SPIE* Vol.1791 (1992) 190.
- 2 W. Griffioen, G. Segers, E. van Loenen, "Two-point bending apparatus, fracturing optical fibres at different speeds in one run; measurements in standard and vacuum environment", *Proc. 39th IWCS* (1990) 368.
- 3 W.J. Duncan, P.W. France, K.J. Beales, "Effect of service environment on prooftesting of optical fibres", *Proc. 7th ECOC* (1981) 4.5.
- 4 T. Svensson, "High strain-rate testing of optical fibres", *Proc. 37th IWCS* (1988) 217.
- 5 G.S. Glaesemann, J.D. Helfinstine, "Measuring the inert strength of large flaws in optical fiber", *SPIE* Vol.2074 (1992) 95.
- 6 T. Svensson, L. Sundeman, E. Sundberg, "Methods and studies on fibre reliability at Swedish Telecom", *Proc. SPIE*, Vol.1973 (1993) 180.
- 7 T.A. Hanson, "Analysis of the proof test with power law assumptions", *Proc. SPIE*, Vol.2074 (1992) 108.
- 8 T.A. Michalske, B.C. Bunker, "The fracturing of glass", *Scientific American*, december (1987) 78.
- 9 A.G. Evans, S.M. Wiederhorn, "Prooftesting of ceramic materials- an analytical basis for failure prediction", *Int. J. of Fracture* 10 (1974) 379.
- 10 D. Kalish, B.K. Tariyal, "Static and dynamic fatigue of a polymer-coated fused silica optical fiber", *J. Am. Ceram. Soc.* 61 (1981) 518.
- 11 S. Sakaguchi, Y. Sawaki, Y. Abe, T. Kawasaki, "Delayed failure in silica glass", *J. Mat. Sci.*, Vol.17 (1982) 2878.
- 12 W. Griffioen, "Effect of nonlinear elasticity on measured fatigue data and lifetime estimations of optical fibers", *J. Am. Ceram. Soc.* 75 [10] (1992) 2692.
- 13 C.R. Kurkjian, D. Inniss, "Understanding mechanical properties of lightguides: a commentary", *Opt. Eng.*, Vol.30, No.6 (1991) 681.
- 14 C.R. Kurkjian, D. Inniss, "Strength and fatigue of silica glass", *Proc. 7th Int. Conf. on Phys. of Non-Crystalline Solids*, Cambridge (UK) (1991) 649-653, Ed. L.D. Pye, W.L. La Course and H.J. Stevens, Taylor and Francis, London, 1992.
- 15 B.A. Proctor, I. Whitney, J.W. Johnson, "The strength of fused silica", *Proc. R. Soc. London, A*, 297 (1967) 534.
- 16 M.J. Matthewson, C.R. Kurkjian, S.T. Gulati, "Strength measurement of optical fibers by bending", *J. A. Ceram. Soc.*, Vol.69, No.11 (1986) 815.
- 17 W.B. Weibull, "A statistical distribution function of wide applicability", *J. Appl. Mech.* (1951) 293.
- 18 A. Breuls, "A COST 218 comparison of n -values obtained with different techniques", *Proc. 2nd Opt. Fib. Meas. Conf.*, Turin (1993) 9.
- 19 A.G. Evans, S.M. Wiederhorn, "Prooftesting of ceramic materials- an analytical basis for failure prediction", *Int. J. of Fracture*, Vol.10 (1974) 379.
- 20 W. Griffioen, "Mechanical lifetime model for optical fibers in water", *Proc. SPIE*, Vol.2074 (1993) 2.
- 21 P.C.P. Bouten, G. de With, "Crack nucleation at the surface of stressed fibers", *J. Appl. Phys.*, Vol.64, No.8 (1988) 3890.
- 22 M.M. Bubnov and S.L. Semjonov from the Russian Academy of Science (Moscow) kindly supplied us with tin-coated fibers. See e.g. M.M. Bubnov, E.M. Dianov, S.L. Semjonov, "Maximum values of strength and fatigue pa-

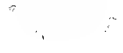
- parameter n for hermetically coated optical fibers", Proc. 41st IWCS (1992) 629.
- 23 W. Griffioen, "Effects influencing measurements of optical fibre corrosion susceptibility", Proc. 2nd *Opt. Fib. Meas. Conf.*, Turin, (1993) 13.
 - 24 K.Abe, G.S. Glaesemann, S.T. Gulati, T.A. Hanson "Application of a phenomenological fatigue model to optical fibers", *Opt. Eng.*, Vol.30, No.6 (1991) 728.
 - 25 C.E. Inglis, "Stresses due to the presence of cracks and sharp corners", Proc. *Inst. Naval Architects*, March (1913) 219.
 - 26 W. Griffioen, "Discrete modeling of crack growth in optical fibers", Proc. *SPIE*, Vol.2290, paper 07 (1994).
 - 27 W. Griffioen, "Evaluation of optical fiber lifetime models based on the power law", *Opt. Eng.*, Vol.33, No.2 (1994) 488.

Biographies

Willem Griffioen received his MS degree in physics and mathematics from the University of Leiden, The Netherlands, in 1980, where he also worked until 1984. In 1984 he joined PTT Research, The Netherlands. He started there with research and development of optical cables and installation techniques. He was responsible for the development of the blowing technique, to install cables for the trunk network in underground ducts. Currently his main responsibility is reliability of optical fibers. From September 1991 until March 1992 he worked at Ericsson Cables AB, Hudiksvall, Sweden, as part of an exchange project. For the current paper, which is a joint project between PTT Research and Telia Research, he stayed three weeks in Stockholm.



Torbjörn Svensson received his MS and Ph.D. from the Royal Institute of Technology, Stockholm. In 1976 he joined the Dept of Physical Metallurgy at RIT where he worked on mechanisms of plastic deformation. In 1979 he joined the Dept of Materials at the National Defence Research Institute of Sweden, essentially working on high-strain-rate effects in solids. During his employment at the Swedish Telecom Technology Dept, in 1985-91, and later at the Networks Outside Plant Division, he has been engaged in quality assurance and techniques for testing fibers and cables. Dr. Svensson holds a number of patents, being the inventor of fiber optical test methods as the high-speed tensile test, the expander, the tube test, and the distributed strain technique. His present employment is at Telia Research AB, Sweden, where he is responsible for fiber mechanics and splicing technology.



Bob Friderich was born in Rotterdam in 1942. He finished the secondary technical school, the Christiaan Huygens school, in 1962, in the field of fine-mechanical engineering. After this school he followed courses in cybernetics. In the same year he joined PTT Research, where he started his work in engineering works, later as a designer. He continued these activities in the department Mail Systems. Currently he is a laboratory associate in the department Automated Mail Systems.

Distributed Strain Technique, Verified by Applying Slant Two-Point Bending of Optical Fibres

Torbjörn Svensson

Telia Research AB, Systems Research
S-136 80 HANINGE

Abstract

Recent findings have indicated that the fatigue parameter "n" of optical fibres is available by monitoring a series of fibre fractures, in fact without a specific knowledge of the applied stress causing failure. This curious procedure, the "distributed strain technique" now has been verified experimentally.

In order to do this, a method, "slant two-point bending" (STB) was developed. Except for the fibre fixture, the only equipment needed for the test is an anvil, a piezoelectric transducer and an event logger. Being surprisingly easy to perform, compared with other tests used in order to determine the value of n, the STB is probably the most efficient method available today.

The value of n obtained by the STB is shown to agree well with corresponding data from regular testing methods. In this respect, it may replace two-point bending- and mandrel tests in routine testing applications. This will result in a manifold reduction of the rate of working.

Introduction

The lifetime of optical fibers under stress may be predicted by the use of different models¹. A limitation of lifetime due to regular stress corrosion is usually described by the parameter n, which is defined by the time-to-failure, t_s , as a function of applied static stress, σ , according to

$$\frac{d \log(\sigma)}{d \log(t_s)} = -\frac{1}{n}$$

Most models take into account the occurrence of weak flaws either by worst case assumptions, or by applying screen test statistics. A precise knowledge of the failure frequency and fatigue behaviour of weak flaws will certainly require elaborate test methods, involving the testing of large fibre lengths², or specially prepared fibre³.

On the other hand, the STB test described in this paper will be confined to a short length of fibre, and will therefore suite similar applications as commonly applied two-point bending- and mandrel tests. The most significant result from such tests is the n-value, which normally is requested by customers as an indication of fibre quality, and also being used for lifetime estimation.

The major advantage of the STB test, compared with regular testing, is that several test series can be replaced by just one, from which the value of n is evaluated directly. During

manufacture, a considerable reduction of work on routine testing is desirable. As a research tool, the STB enables a quick and extensive study on the effect of various coatings, treatment, and environments on the n-value of silica fibres.

Theory

Theoretically has been shown that a linearly increasing distribution of static stress along a fiber will lead to a series of failure events which are simply correlated to the range of applied stress, R, and the n-parameter. A curious feature is, that no specific knowledge of the value of applied stress is required. Even the number of failures may be omitted in a completed test. This feature is most apparent in the relation

$$n = \frac{\Delta \ln(t_s)}{\ln(R)} \quad \text{.. (1)}$$

where $\Delta \ln(t_s)$ is the effective time interval of failures, given below. For practical purposes, equation (2) is normally used.

By monitoring the events, and assigning them their ordinal number and time-to-failure, this data can be used in order to estimate of the n-value defined above. This procedure, the "distributed strain technique" has been previously described⁴.

In the study was found that, when properly assigning two constants to the test, N, and R, a correlation will appear between the the value of the n-parameter, and the ratio of increasing number of failures versus the natural logarithm of time. This is accomplished for by the formula,

$$n = \frac{N}{\left(\frac{dk}{d \ln(t_s)}\right) \cdot \ln(R)} \quad \text{.. (2)}$$

in which

k =

N =

$\ln(t_s) =$

$R = \sigma_{\max}/\sigma_{\min}$

$dk/d \ln(t_s) =$

ordinal number of failure.

maximum number of failures. A design parameter

natural logarithm of the time-to-failure under static stress. To be monitored.

ratio between the maximum and minimum load on fiber, the load increasing linearly from one end of the fiber to the other. A design parameter.

the slope of a linear curve fit to data.

By introducing an effective time interval of the test, $\Delta \ln(t_s) = N/(dk/d \ln(t_s))$, equation (1) is readily obtained.

The application of the distributed strain technique has been discussed theoretically, in terms of interference from weak flaws, and limitations due to a variable n -value⁵.

For commercial fibres an occurrence of weak flaws will not affect the evaluation of n . Premature failures due to weak flaws can be readily discerned, and the value of N is just to be reduced by the number of truncated flaws. Finally, applied on short lengths as in the STB test, weak flaws are exceedingly rare.

If a proper ratio R is used, a variation in the value of n will not affect the average value typical for the time interval of measurement, $\Delta \ln(t_s)$.

Design

The basic idea of the distributed strain technique is to apply the strain such that the load gradually increases from one end of the fiber to the other. In this paper, the same principle has been verified by using a method closely similar to regular two-point bending, though a significant difference is that the static load is different for all bends of the fibre.

A procedure which has been proven useful, is to wind a coil of fibre on a substrate, and to apply the load on the coil using two slant plates and an anvil. Due to the geometry of the test, and the bending load on fibre, the name "slant two-point bending" (STB) has been used here. See Figure 1.

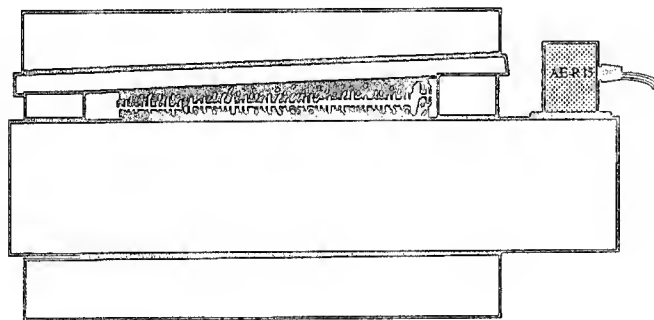


Figure 1. Design of the STB test. Schematic.

Some practical aspects concerning the performance of the test is given under the chapter "STB test". In short, a procedure to assign STB design parameters for most commercial silica fibres is as follows:

1) In order to keep the test period within reasonable limits, a suitable value of minimum load on fiber must be assigned to the test, as a first step. Generally, it is advised to estimate the plate distance which would cause complete failure of the fibre coil after less than one week in a regular two-point bending test. A useful assumption is, that under ambient conditions this will occur at about 4.3 mm. This value is assigned the plate distance at the widest part of the deformed fibre coil.

2) Then the maximum stress, at the tightest part of the coil is to be determined. A design ratio R between 1.15-1.35 is preferred when testing ordinary silica fibre. If a wide spread of failure times is requested, the higher the chosen value of R must be. This implies that the value of n will be averaged during a longer period of time. A positive effect of choosing a higher R -value is that the precision of measurement increases, but this is counteracted by variations in the n -parameter with

time. The value of n may vary significantly depending on the range of stress applied⁶.

3) A permanent angle and length of the slant plate arrangement may be chosen, for instance corresponding to an upper value of $R=1.5$. The value of R applied during test is adjusted by the length of the coil, and the minimum stress adjusted by positioning the coil along the plates. By changing the length of a coil having a constant pitch, the value of N in equation (2) will change. However, this will not influence the estimated value of n ⁴.

4) In principle, a knowledge of values of applied stress is not required for the test, according to item (3).

Experiments

A commercial grade, acrylate coated silica fibre was chosen for the test. The glass diameter was 125 μm , and the total diameter was 250 μm . All tests were made in 23°C, 50% RH.

In Figure 2 below, some examples of STB tests are shown, for the values of $R = 1.244, 1.243$, and 1.330 . The minimum stress corresponding to these values can be calculated from the maximum plate distance, 4.040, 4.077, and 4.358 mm.

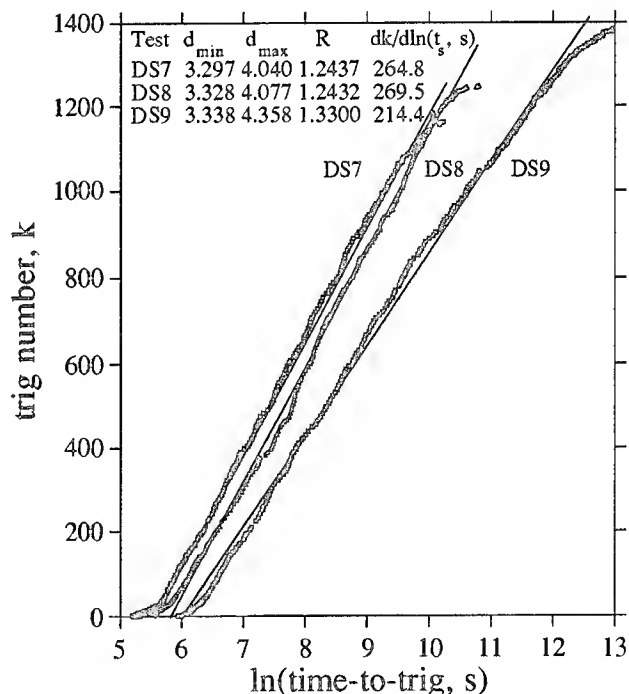


Figure 2. Slant two-point bending test of optical fiber.

STB test

A single-layer fibre coil was tightly wound in a lathe, using a 150x16 mm tube of stiff plastics on which a substrate (a thin paper) was slightly attached. The number of turns were counted automatically in a slow winding process, in which a small winding tension was applied to the fibre. After completion of the desired number, the lathe was automatically shut off. The ends of the coil were secured by rapid glue, on portions to be in contact with the plates during test. The coil-on-paper was carefully twisted/pulled from the tube, so that the fibre spacing and the length of coil was not disturbed.

The specimen, containing 400 turns of fibre, was then positioned between the plates, on a thin string of double adhesive tape. Firmly adhered gauge blocks defined the angle between plates. A piezoelectric transducer was mounted on the lower plate, an aluminium profile having high stiffness and a smooth surface. The upper plate was a 150x50x6 mm ground steel plate. The plates were mounted in an anvil, which was properly tightened in order not to bend the plates, and to eliminate any clearance between the plates and the gauge blocks. During compression, the substrate bended inwards, releasing the fibre from any tensile stress.

After having activated the specimen, the transducer output was fed into a data logger. All trig events were monitored, and studied after completion of the test, according to Figure 2.

An undesirable effect has been the occurrence of separate trig events, a first from the fracture of glass, the second from the final rupture of the coating. However, this has not severely influenced the evaluation of the n -parameter from the tests. The original procedure could be readily applied, by taking into account the observed ratio between the number of observed trig events and the constant value of N .

The value of the other design parameter, R , was calculated from the position and length of the fibre coil.

The number of turns were exactly 400 in all cases, thus the maximum number of fractures is limited to $N = 800$, since each turn corresponds to two bends. Trig events in excess of this number are due to the mentioned effects of separate glass- and coating ruptures.

A curiosum which can be observed in Figure 1, is a small but characteristic irregularity superposed on all curves. This irregularity is caused by the rough surface of the upper plate, a quite coarsely ground steel plate. Due to the averaging procedure during evaluation, this effect will not significantly influence the estimated value of n .

From equation (2) and Figure 2 can be calculated the values of n , being $n = 20.1$ (DS7), 21.3 (DS8), and 22.7 (DS9). Because of excessive trigs due to the tough coating these tests have been evaluated by replacing the geometrically defined number N ($= 800$) with the maximum number of monitored trig events, N_{trig} . Since all the bends had failed, the substitution made will not influence the estimated value of n . In fact, by the use of equation (1) no value of N is necessary. Corresponding test data are

Test	R	N_{trig}	$\frac{dk}{d\ln(t_s, s)}$	$\frac{N_{\text{trig}}}{dk/d\ln(t_s) \cdot \ln(R)}$
DS7	1.2437	1,160	264.8	20.086
DS8	1.2432	1,247	269.5	21.256
DS9	1.330	1,385	214.4	22.652

By modifying the sensor arrangement it should be possible to monitor just one event per bend failure. In that case, the test can be interrupted after 75% of the events, and the n -parameter be evaluated by a linear estimate applied on the interval between 25% - 75% of failures. The value of N shall also be reduced 50%. Numerical simulations have shown that the

value of n will be the same as when all failures are included (this is also apparent from the symmetry of Figure 4).

The reduced number implies further improvement when considering that waiting for the last 25% of failures will take half the time of a completed test.

Two-point bending test

A regular two-point bending test was made on the same fibre as in the previous tests, in the same environment. The loading mode was constant strain rate. 40 specimens were tested at each rate, 0.03, 0.3, 3.0, and 30%/min. The failure stress as a function of strain rate is shown in Figure 3.

The maximally achievable time-to-failure was about 13,000 s, which corresponds to an effective static loading time of 680 s. This is considerably less than the average times-to-failure in the STB tests, and the n -value should expectedly be smaller. A value of $n \approx 19.5$ was also found which agrees well the range of slightly higher values, $n = 20.1 - 22.7$, found in the previous STB tests. The median time-to-failure in these tests varied between 2,100-7,700 s.

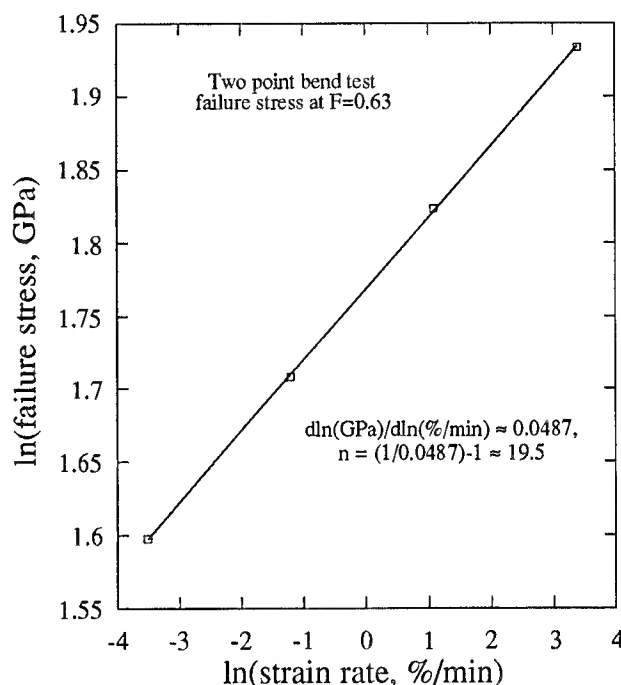


Figure 3. Dynamic two-point bending test, 4 stress rates

STB test simulation

In order to estimate the expected repeatability and accuracy of an ideal STB test, the test DS7 was simulated numerically. In this way an average result could be used for comparison with the real test (though being just a single measurement).

This test was characterized by the design parameters $N = 800$, and $R = 1.2437$. The value $n = 20$ was also taken from test DS7. A maximum stress about 3.80 GPa, was calculated from the minimum plate distance.

An initial distribution of strength was assumed, based on the maximum strength S_{max} , and the Weibull modulus m ,

$$S_i = S_{\text{max}} \cdot (k/N)^{1/m}$$

where S_{max} is assumed to be 7.5 GPa. The value of the Weibull modulus estimated in a two-point bend test was used,

$m = 80$. This value is not crucial⁴. The ordinal number of increasing strength is $k = 1, \dots, N$.

A number of 800 strength values were assigned. These values were randomly distributed along a "fibre" on which a load was applied, increasing from 3.80/1.2437 (σ_{\max}/R), in equal steps between each site, up to 3.80 GPa (σ_{\max}). By experience and some trial-and-error a set of data was found, which well reproduces the test DS7. These values are $B = 0.02 \text{ GPa}^2\text{s}$, and $\text{Si}_{\max} = 7.5 \text{ GPa}$.

The results from ten simulations are shown below,

Simul.	$dk/d\ln(t_s)$	n
1	179.16	20.474
2	182.00	20.155
3	179.94	20.386
4	180.13	20.364
5	179.63	20.421
6	181.11	20.254
7	180.40	20.334
8	181.20	20.244
9	179.94	20.386
10	181.31	20.232

Statistics of estimated n -values:

Minimum	20.155
Maximum	20.474
Mean	20.325
Median	20.349
Std Deviation	0.0998

Somewhat higher values than from the real test were obtained from the simulations, $n \approx 20.32 \pm 0.10$. Owing to a high repeatability, the scatter is less than the systematic deviation from the assigned value, about 0.3 units. The assigned value was $n=20.00$.

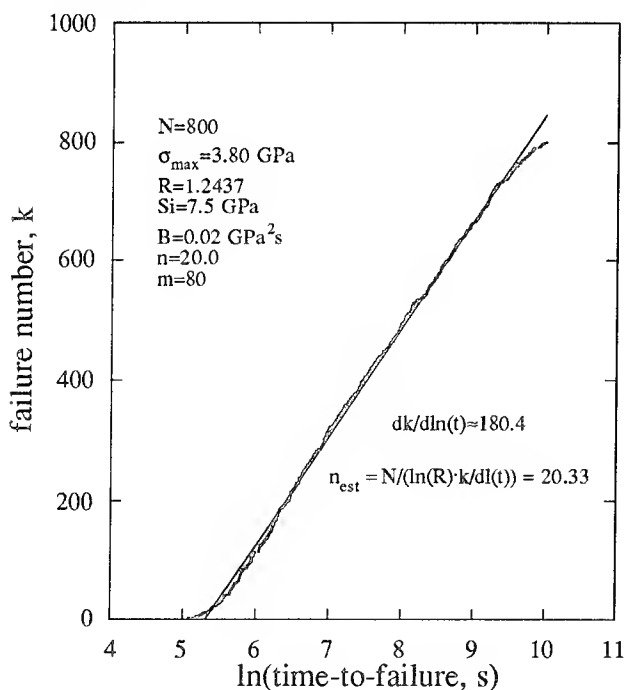


Figure 4. Simulation of test DS7

A typical simulation is shown in Figure 4 above. The curve features are in high accordance with the test DS7 in Figure 2.

Summary

Experimentally, and theoretically has been proven, that the n -parameter of optical fibre can be evaluated from the equations

$$n = \frac{N}{\left(\frac{dk}{d\ln(t_s)}\right) \cdot \ln(R)} = \frac{\Delta \ln(t_s)}{\ln(R)}$$

A method, "slant two-point bending", STB has been described in detail. The significant test equipment, and the procedure of testing have been demonstrated, and the results have been discussed.

A commercial grade acrylate coated silica fibre was tested in 23°C, 50%RH. In a comparative dynamic two-point bend test $n = 19.5$ was obtained for effectively static times from about 1 to 680 s.

In the STB test values of $n = 20.1-22.7$ were found, for static loading times from about 200 to 270,000 s. Higher values were obtained within a wider range of failure time. The value of the n -parameter increased systematically with an increasing average time of load, in accordance with other studies on comparable fibres.

The conclusion is, that the STB may replace the established two-point bending- and mandrel tests in applications where a cost- and time-effective evaluation of the n -parameter is necessary. It will serve as an efficient tool in future testing of optical fibre, in routine applications as well as fibre research.

References

1. W. Griffioen et al., "COST 218 evaluation of optical fibre lifetime models", *SPIE Vol 1791*, p 190 (1992)
2. S. Glaesemann and D. J. Walter, "Method for obtaining long-length strength distributions for reliability prediction", *Opt. Eng.* 30 (6) p 746, ISSN 0091-3286 (1991)
3. T. Svensson and A. Breuls, "Strength and fatigue of different kind of weak spots from the manufacture of optical glass fibres", *SPIE Vol 2290* (1994)
4. T. Svensson, "Distributed strain- a rational test of fiber fatigue", *Proc. of the 41st IWCS*, p 725 (1992)
5. T. Svensson, "New technique for measurement of static fatigue of optical fibres", *SPIE Vol 1973*, p 175 (1993)
6. A. Breuls, "A COST 218 comparison of n -values obtained with different techniques", *Proc. 2nd OFMC*, 9 (1993)

Biography

A biography of the author is given in the paper "The Tube Test.." in this proceedings.

The Tube Test. A Small-Size Sturdy Specimen for Static Fatigue of Long Optical Fibres under Uniaxial Stress

*Torbjörn Svensson
Per-Olov Karlsson*

Telia Research AB, Systems Research
S-136 80 HANINGE

Abstract

The tube test for static loading of optical fibres opens up new ways to the study of long-term fatigue of optical fibres, in uniaxial tension. Though having a handy size, 10x10 cm, it accommodates a considerable length of fibre, about 40-60 m. Accordingly, a large number of failures will be accessed in each test, also weak precursors can be studied. The tube test has been shown applicable also in hot water. Owing to the rigid structure of the tube test specimen, active samples have been sent between laboratories, in "blind" tests.

In this paper, some data from tube tests are shown, including testing in hot water. The design of the tube test specimen and a working concept for activating the specimens are presented.

Introduction

An important factor when mechanically testing optical fibre is the volume of fibre under full stress. A quite large volume is required in order to monitor weak spots¹ and failure precursors, i.e. premature weak spots on fibre, which may develop during fatigue and ageing. The volume involved in a uniaxial tensile test vastly exceeds that in the two-point bending- and mandrel tests usually applied in static testing, about 3-5 orders of magnitude. However, static testing of medium lengths of fibres has been relying upon extensive use of weights and instruments.

Recently, the efficiency of uniaxial testing has been greatly improved by the development of the pilot expander² and, based on the same principles, the tube test^{3,4}. A tube specimen of the size 90x100 mm has the capacity of at least 40 m fibre, with an outcome of a hundred fractures monitored in one series during the test.

The small size of the tube, and the easiness of data acquisition enable the parallel running of several tests in limited physical environments, e.g. small climate chambers. Accordingly, a detailed picture of the strain-dependent time-to-failure in different environments, and also of different fibre types, may be accessed within the same test period, by employing a number of tubes in parallel tests.

The equipment needed for mechanical activation of samples is quite limited. By shearing this facility, the initial costs of testing can be further reduced, since only a number of

piezoelectric sensors and a data logging equipment is applied during the monitoring of tests.

These features of the tube test probably makes it the ultimate technique for static testing of fibre in uniaxial stress.

Design

The function of a tube test is based on the static straining of a fibre, wound directly on a metal tube, which is permanently deformed in a quick operation using hydraulics. The requested level of strain is applied to the fibre by pulling a tool of proper diameter through the metal tube. See Figure 1 and 2.

In the present study, on each metal tube of 100 mm length, a continuous length of 40 m fibre was wound along 50 mm of the central portion of the tube, in order to avoid effects from tube barrelling. The winding was done at a fibre tension of 50 gf, using a modified lathe. Three turns of EPDM rubber sheath of the size 840x80x0.48 mm was wrapped outside the fibre. The metal tube was lubricated inside, and the arrangement was placed in a tube of plastics, according to Figure 1.

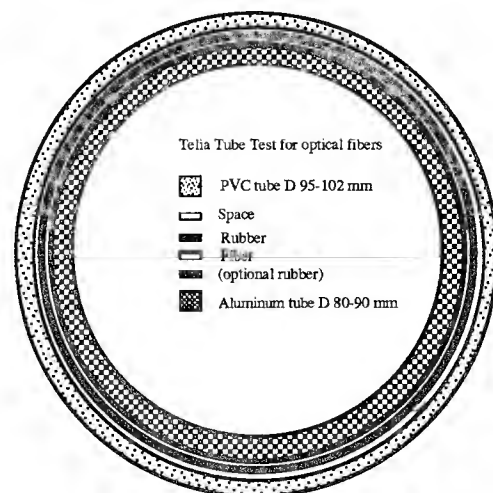


Figure 1. Cross section of a tube test specimen.

Finally, a tool of suitable diameter was pulled through the metal tube. The initial diameters of the metal tube, D_{i0} and

D_{y0} , and the diameter of the tool, $\approx D_i$ determines the hoop strain of the fibre, ε , according to

$$\varepsilon = 0.5 \cdot \ln \left\{ \left(\frac{D_i}{D_{y0}} \right)^2 + \frac{L_0}{L} \cdot \left[1 - \left(\frac{D_{i0}}{D_{y0}} \right)^2 \right] \right\} \quad ..(1)$$

This formula takes into account the shortening of metal tubes caused by pulling forces during activation, from the initial length L_0 to the length of tube in expanded state, L . Equation (1) is derived from the assumption of volume constance of plastified metal. Except for L , all factors can be determined before the test, so the specimen will not have to be disassembled after the test.

Testing

Tube dimensions must be measured before as well as after activation of the specimen. The change of the inner diameter must be carefully monitored, across the central portion along the tube. A 3-point digital internal micrometer (Bowers) may be used. It is advised to average three measurements along 40° positions. The change of length of the tube is not crucial for the accuracy, a simple caliper can be used. When testing in hot environments, a correction for the thermal expansion of metal tubes is necessary. Testing in wet environments require that the fibre is soaked with the proper constituent during activation, and accessed by suitable slots in the rubber.

It is advised to use a lathe or similar equipment to wind the fibre on the metal tube. The pitch should be slightly larger than the fibre thickness to allow for the axial shortening of the tube usually occurring during the activation.

The testing involves 2 or 3 distinct steps: activation of the specimen, acoustic monitoring of fibre fractures during environmental exposure, and, optionally, disassembling of the specimen. Disassembling is only required in order to maximize the accuracy of calculated strain via D_y , and equation (2) below, and to check the relevance of trig events.

During activation of the specimen, strain will be permanently applied to the fibre, also when having released the deformed tube. In this way, an unlimited number of specimens can be activated, at arbitrary occasions.

A working concept of test equipment is schematically shown in Figure 2. The capacity of a corresponding equipment used at Telia is about 6-fold the present need, including a 1 hp hydraulic pump, and a 300 kN hollow ram mounted below a bench. On top of the table is extending an axis, on which a 4-piece tube support and the complete specimen are put. The tool is placed on the specimen, followed by tightening the pulling nut. The tool is pulled once through the aluminium tube, and gets loose by pushing the tube-support pieces outwards. In this way, the specimen can be quickly moved to the measuring site. The time for activating a specimen varies between 20-60 seconds.

Monitoring during environmental exposure is accessed by piezoelectric sensors of the types frequently used in two-point bending- and mandrel tests. The high frequency sensor signal can be monitored using suitable sample-and-hold circuitry, a data logger, and a PC. (Here AE-R15 sensors, FiberSigma trigger boxes and Loring data logger LDL-12 were used). A dummy channel should be dedicated to measure false trig events.

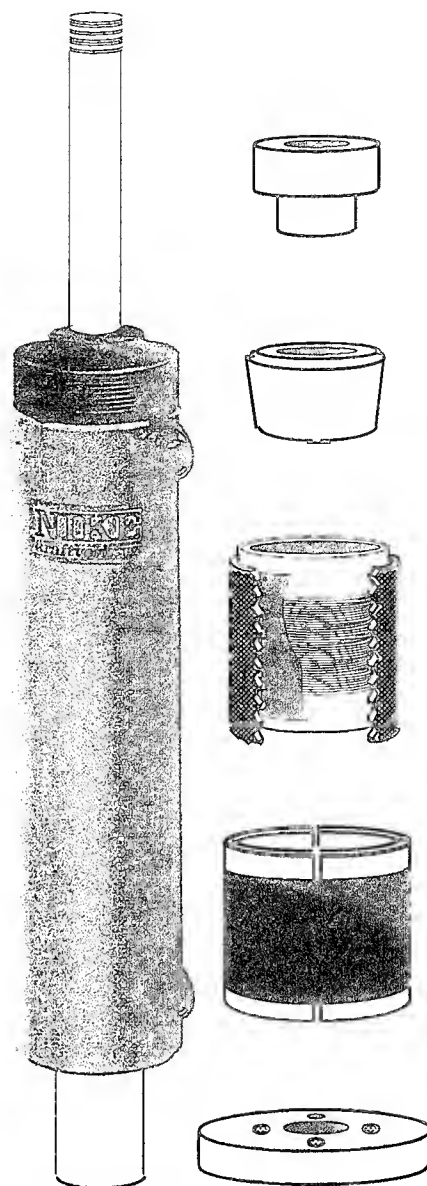


Figure 2. Ram and tools for the activation of specimen. Display cut of test specimen shown in center. Schematic.

During the test, fibre slippage adjacent to fractured fibre ends will be rejected by the rubber's friction, which is supported by pressure from the deformed plastic tube. Owing to this, a number of failures exceeding 100 may be obtained during a test, before slippage between fibre and rubber will start to significantly influence the fibre stress, and time-to-failure. See Figure 3.

Normally the test should be interrupted after a number of failures equal to half the number of turns of fibre wound on the tube. The left curve in Figure 3 intentionally shows the onset of fibre slippage by including excessive failure events.

The value of the Weibull modulus, m_s , falls closely to the value obtained from static testing in the "pilot expander", a prototype instrument having well documented properties and high repeatability, and being based on the same principle of straining a fibre wound on an expanding cylinder. The results shown are from one of the very first tube test experiments, in

December 1992, and clearly demonstrated the potential of the tube test. Later improvements have been on the application of machine winding and controlled winding tension.

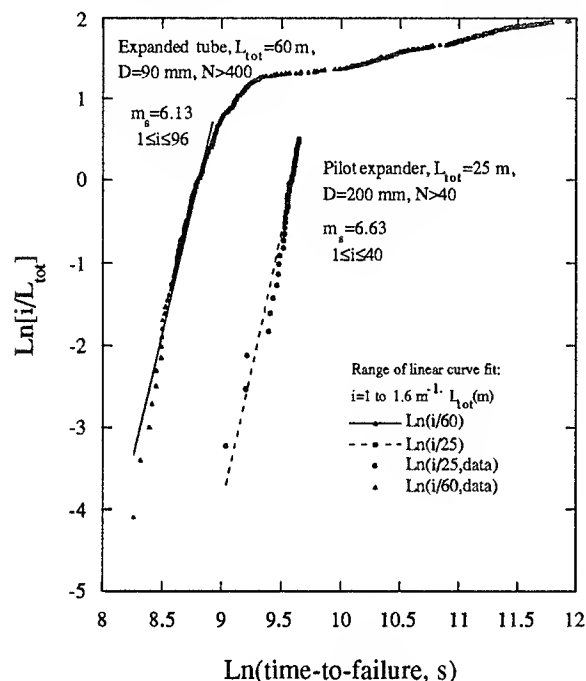


Figure 3. Tests results from pilot expander and tube test.

In Figure 3, due correction for the different fibre lengths used has been made. This is necessary only when carefully comparing data from different methods. In such cases, the reference failure time at unit length (the "site parameter") is obtained at the crossing point between the linear slope and the zero position of the ordinate, $\text{Ln}(i/L_{\text{tot}})=0$, just as in Weibull plots from regular tensile tests, where the ordinate $\text{Ln}(\text{Ln}(1/(1-F)))$ is used instead.

Tube tests

A few results from tube tests will be presented, in order to further enlight the compatibility with the pilot expander, using the same fibre. The environment was 23°C, 50% RH. The gauge length of each sample was 40 m (tube test) and 25 m (pilot expander). In tube tests, four levels of strain, 2.48, 2.95, 3.54, and 4.04% were applied to the fibre. All tubes were activated at the same occasion, and exposed to the same environment, humid atmosphere.

After successive completion of the tests, they were interrupted and evaluated. During seven months no failure had been observed in tube #14 (at 2.4% nominal strain). Weibull plots of the test data are shown in Figure 4.

The high strength of the fibres tested enabled the setting of a high and reliable triggering of failure events. Four equally sensitive channels had been activated, giving no indication of false trigger during the test period.

After the test period, the plastic tubes were discarded. The number of fractures in tube #15 was checked visually by disassembling the specimen after two months of monitoring. The number of fractured fibres and trig events did correspond well: 51 visible fractures vs 52 trig events.

The outer diameter, D_y was measured in the tubes #12, #13, and #15, in order to study the correspondence between the anticipated strain $\epsilon(1)$, due to equation (1), and the strain $\epsilon(2)$

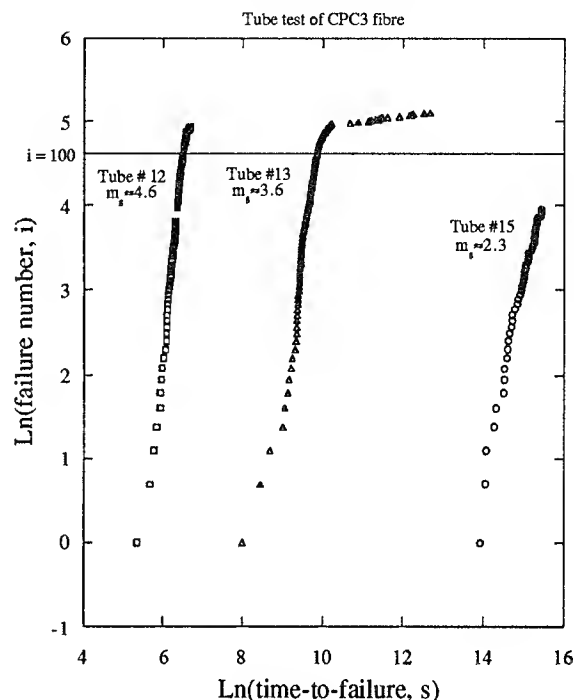


Figure 4. Weibull plot of tube tests

calculated from the outer diameter, equation (2) below:

$$\epsilon = \ln\left(\frac{D_y}{D_{y0}}\right) \quad ..(2)$$

This equation is exact for an infinitely thin fibre. Equation (2) is thus more accurate than eq (1). It is also simpler to apply, because knowledge of tube shortening is not required. However, equation (2) can not be used to determined the fibre strain, until the monitoring has been completed.

A minor strain from the bending of fibre, and the tension applied during winding, shall be added to the strain calculated from both equations. For 125 μm glass diameter and 50 gf tension the additional strains are about 0.14%, and 0.06% respectively.

Calculated values of strain according to equation (1) and (2) do closely correlate, the ratio of $\epsilon(2)/\epsilon(1)$ being 1.015 on average.

Comparison

Perhaps the most interesting comparison is made, by plotting average strength versus time data from tube- and pilot expander tests, as in Figure 5. One of the data points from testing in the pilot expander correspond to static measurements, the others are effective values, transformed from dynamic measurements^{5,6}. Tube test data all are static.

Smooth curve fits may be readily obtained through each series of data. In each series, the present data significantly indicate a usually observed increase of the n-value with time^{6,7}. Averaging the n-values yields 22.6 for expander

tests at short time, and 28.5 for tube tests at longer times. Though being slightly displaced, the two curves are parallel within the interval of overlapping times-to-failure. The only static data from the pilot expander also falls close to the tube test data.

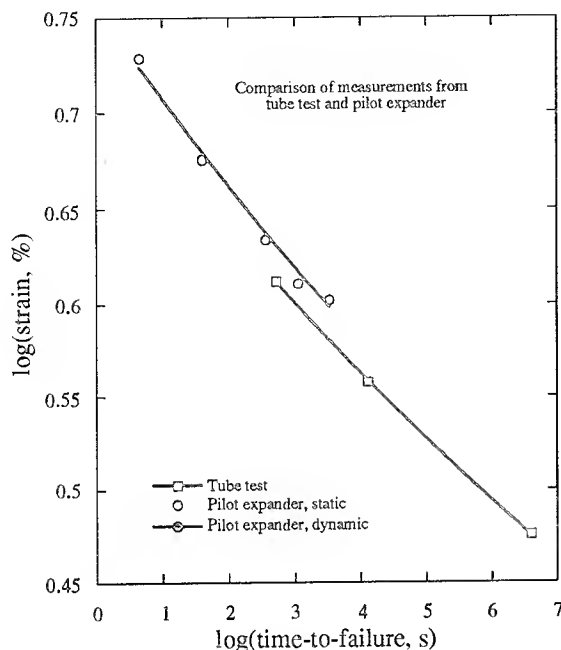


Figure 5. Effective time-to-failure as function of strain in expander- and tube tests

Testing in wet environment

Finally, a different test result will be presented. In Figure 6 is demonstrated the first tentative tube test performed in hot water. The fibre was wound on the tube in ambient environment, soaked in tap water and covered by a slotted

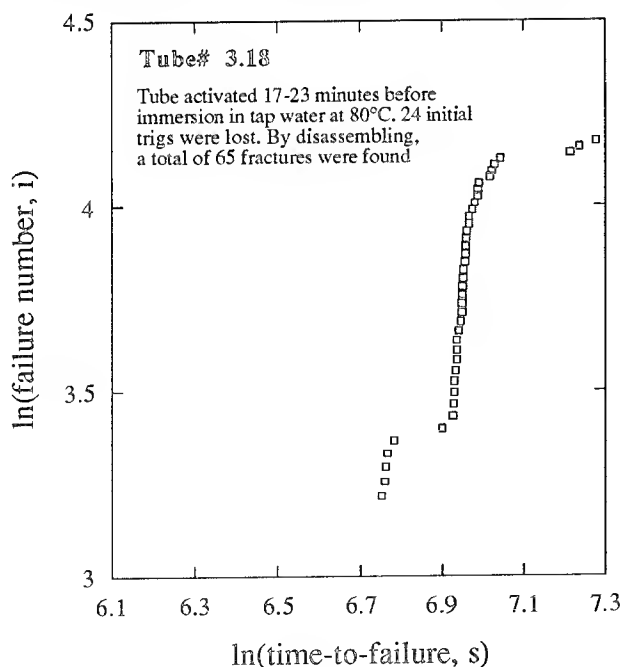


Figure 6. Failure of fibre during tube tests in 80°C water.

rubber sheath about 20 minutes prior to mechanical activation and immersion in 80°C water.

The hoop strain of the tube was 2.75%. An additional strain of 0.14% from the thermal expansion yields an estimated fibre strain of 2.89%. About 40 failures were observed after 20 minutes in hot water, a similar number of failures would expectedly have occurred at 4-10 hours in ambient conditions. Unfortunately, the early occurrence of trig events caused a loss of the initial 24 failures. After the test, the specimen was disassembled. A total of 65 fractures were found, randomly distributed along the fibre.

The comparatively short time-to-failure and the high static Weibull modulus may indicate the occurrence of a fatigue knee. More obvious however, was the distinct appearance of early failures, which were lost before monitoring was switched on. However, a few of these precursors are visible in the lower part of Figure 6.

Conclusions

Although the tube test has not yet been proved to yield an exact one-to-one correspondance with other uniaxial test methods, it apparently enables a reliable characterization of a fibre's time-dependent strength. Also, the occurrence of premature failures can be monitored, in detail. Early results indicate that the technique is useful for testing in adverse environments as hot water. A conclusion will be, that when searching for a test method combining small dimensions, easy aquisition of a significant amount of data output, including monitoring premature failures of fibre, the application of tube testing should be considered.

References

- 1 T. Svensson and A. Breuls, "Strength and fatigue of different kind of weak spots from the manufacture of optical glass fibres", *SPIE Vol 2290* (1994)
- 2 J. Björkman and T. Svensson, "Quick-Access to Fracture Statistics at Ultra-Wide-Range Tensile Test of Optical Fibers", *Proc of the 39th IWCS*, pp 373-378 (1990)
- 3 T. Svensson, L. Sundeman, and E. Sundberg, "Methods and Studies on Fibre Reliability at Swedish Telecom", *SPIE Vol 1973*, p 180-185 (1993)
- 4 T. Svensson, "The tube test", paper presented at COST 246 meetings in Martlesham, U.K., March 1994
- 5 T. Svensson, "Static fatigue of optical fiber using expander technique. A comparison between static and dynamic failure data", 10th Management Committee Meeting of COST 218, Berne, Schweiz, Oct. 1991
- 6 T. Svensson and E. Sundberg, "New approaches to measurement of strength and fatigue of optical fibers", *SPIE Vol 1791*, pp 117-121 (1992)
- 7 A. Breuls, "A COST 218 comparison of n-values obtained with different techniques", *Tech Digest OFMC '93*, Torino, Italy, Sept 1993

Biographies



Torbjörn Svensson received his MS and Ph.D. from the Royal Institute of Technology, Stockholm. In 1976 he joined the Dept of Physical Metallurgy at RIT where he worked on mechanisms of plastic deformation. In 1979 he joined the Dept of Materials at the National Defence Research Institute of Sweden, essentially working on high-strain-rate effects in solids. During his employment at the Swedish Telecom Technology Dept, in 1985-91, and later at the Networks Outside Plant Division, he has been engaged in quality assurance and techniques for testing fibers and cables. His present employment is at Telia Research AB, Sweden, where he is responsible for fiber mechanics and splicing technology. Dr. Svensson holds a number of patents, being the inventor of fiber optical test methods as the high-speed tensile test, the expander, the tube test, and the distributed strain technique.



Per-Olov Karlsson was employed at Swedish Telecom, the Networks Outside Plant Division in 1991, essentially working with fusion splice technology. Later, he joined the Systems Research Department at Telia Research, where he is responsible for passive optical components. Mr. Karlsson has a B.S. degree in Physics from the University of Stockholm. He is a member of the Swedish Optical Society.

DEVELOPMENT OF 16-FIBER PUSH-ON TYPE OPTICAL CONNECTOR

I. Matsuura, T. Ueda, M. Honjo, T. Yamanishi

Sumitomo Electric Industries, Ltd.

1, Taya-cho, Sakae-ku, Yokohama, Kanagawa 244 Japan

Abstract

The push on type optical connector which can connect 16-fiber ribbon was proposed.

The low insertion loss of less than 0.2dB and high return loss of more than 50dB were provided without index matching gel utilizing low-loss 16-fiber connector ferrule and novel endface structure for direct physical contact.

The characteristics of the developed push on type connector including long time reliability is described as well as the detail design concept.

1. Introduction

High-density optical fiber connectors are required for optical fiber subscriber network [1]. At the last year's IWCS, we reported about the low-loss 16-fiber connectors for high-speed low-loss cable connection [2]. On the other hand, multifiber push-on type connector (MPO connector) which can connect up to 8-fiber ribbon was proposed as shown in figure 1 [3]. This type of connector can be easily engaged by pushing it on and disengaged by pulling it off.

The MPO connector consists of an adaptor and two connector plugs, each of which has a plastic ferrule pressed by a coil spring from behind in the housing. It provides high return loss and low insertion loss without index matching gel due to eliminating of Fresnel reflection by endface polishing at an angle of 8 degrees and direct physical contact between ferrules.

For the purpose of the use in the high-density optical fiber network, we tried to design the

16-fiber Push-On type connector (16PO) based on the design concept of MPO connector such as 8 degrees endface polishing and direct physical contact.

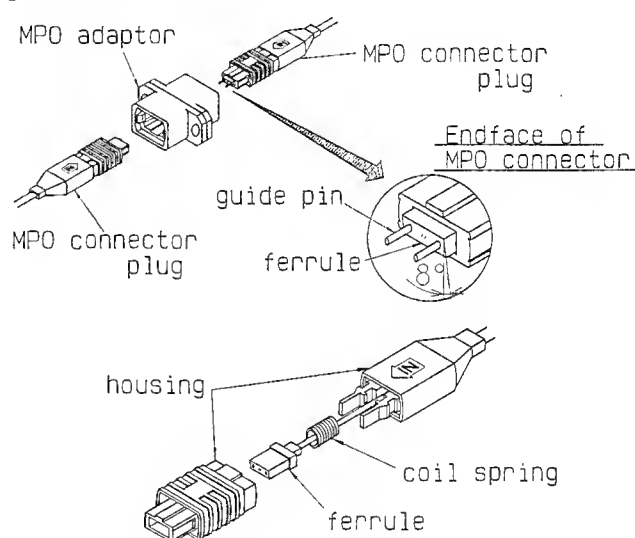


Figure 1. The structure MPO connector.

In this paper, we first describe how to reach the new PC structure. Next we design it and optimize its dimensions and materials. Results of critical dimensions are presented. And the process of the new PC structure is described. Following that, we report the characteristics and reliability.

2. Novel ferrule structure for 16PO

It is predicted that the 8 degrees endface polishing technique of MPO connector can be easily applicable to 16PO. But the direct physical contact of 16-fiber connector is

extremely difficult, because the contact area of PO connector should be much wider than that of MPO connector.

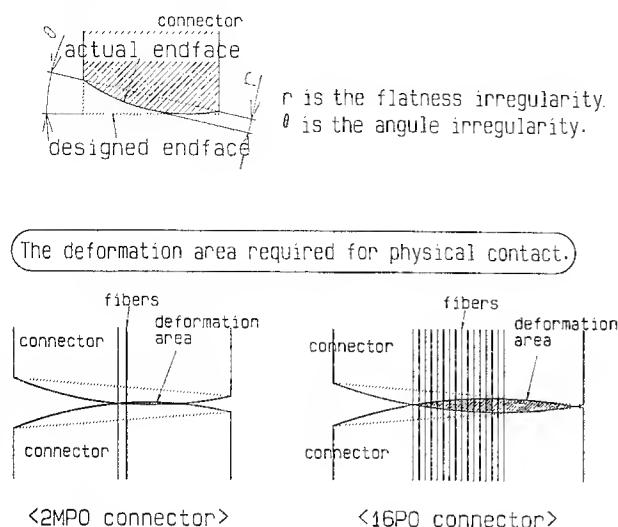


Figure 2. The irregularity of the connector endface and the deformation of ferrule material.

In case of 2MPO connector, the physical contact is realized by the microscopic deformation of ferrule material to eliminate the irregularity of the connector endface as shown in figure 2. The angular tolerance and the flatness of the endface should be within 0.15 degrees and $1.0 \mu\text{m}$ respectively for the 2MPO ferrule which has 2000kgf/mm^2 of Young's modulus. The calculation of the physical contact condition based on the contact theory of Hertz suggested that the angular tolerance and the flatness of endface must be less than 0.05 degrees and $0.1 \mu\text{m}$ respectively for 16PO. It is clear that these tolerance is impossible to attain considering commercial mass production of connector ferrules.

More deformation of an object generally requires to give more pressure or to use lower Young's modulus materials. The theoretical calculation also indicates that the pressure is three times as much as that of 2MPO connector and the Young's modulus is an half as high as that of 2MPO connectors in order to realize

physical contact of 16PO by the same endface precision with 2MPO.

To increase the connecting pressure in 16PO connector, we designed the contact area of less than a third as large as that of 2MPO connector instead of increase of the force of a coil spring in the housing. Because the increase of connecting force by the coil spring makes the housing larger.

The other hand, the connector ferrule is made from thermoset epoxy resin with silica fillers for dimensional stability and long time reliability. It is not easy to reduce Young's modulus of ferrule material without changing stability and reliability.

Finally, we concluded new ferrule structure which is satisfied two design requirements such as three times increase of connecting pressure and reduction of Young's modulus to less than a half.

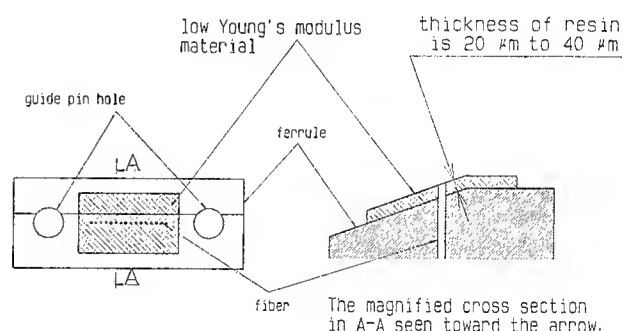


Figure 3. The structure of the new ferrule.

As shown figure 3, the new ferrule has thin resin layer on its endface, which covers only a third area of endface, and which Young's modulus is half of that of the ferrule material.

The trial production of 16PO with newly developed connector ferrule was conducted after polishing connector ferrules at an angle of 8 degrees, 16 fibers of ribbon cable were inserted into the ferrule and were fixed, then a third area of the endface was coated with low Young's modulus material. The low Young's modulus layer and the fibers were polished at 8 degrees

angle. The Young's modulus of the thin layer is 800kg/mm^2 , the thickness of the thin layer was controlled from $20\text{ }\mu\text{m}$ to $40\text{ }\mu\text{m}$ in polishing process. The precision of polishing process such as angular tolerance and flatness of endface almost same with the conventional MPO manufacturing process.

The structure of the housing for 16PO is almost same to that of MPO except that connector ferrule for 16PO is little larger than that of MPO. The cross section per fiber of this 16PO connector is only $18.1\text{mm}^2/\text{fiber}$, and is much smaller than that of conventional 2MPO's $122.4\text{mm}^2/\text{fiber}$ and of SC connector's $206.8\text{mm}^2/\text{fiber}$.

3. Characteristics

We have realized the 16PO connector with an average insertion loss of 0.18dB without index matching gel, shown in figure 4.

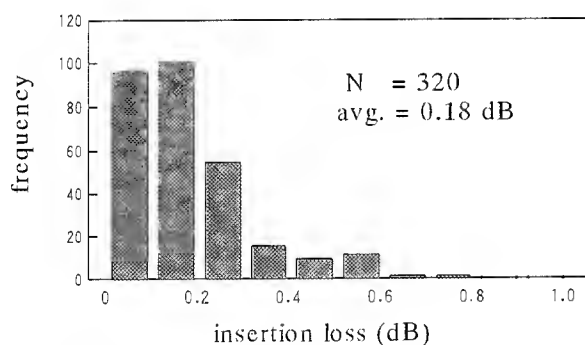


Figure 4. Insertion loss without index matching.

In order to evaluate the probability of physical contact of the 16PO connector, we produced two kinds of 16PO connectors, one has the developed structure and the other has the same structure with conventional MPO connector. As a method of evaluating the physical contact, we measured the insertion loss under the both condition of using index matching gel and without it. If the fibers

contact directly to each other, the measured insertion loss without index matching gel should be nearly equal to the loss with matching gel. The measured insertion loss relation between with and without the index matching gel is shown in figure 5, and figure 6. We have found that new ferrule structure is very effective for direct physical contact of fibers, compared with the conventional MPO connector.

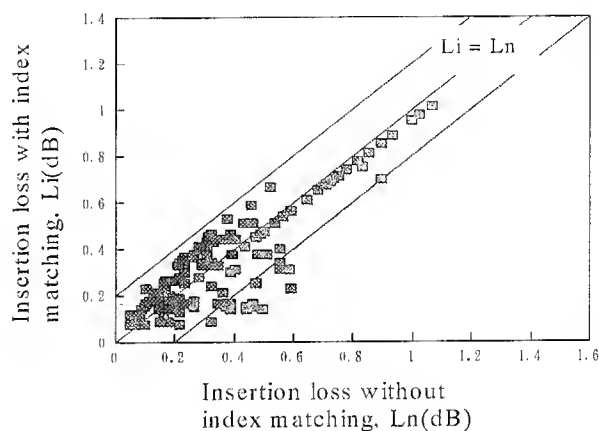


Figure 5. Relation between insertion losses with and without index-matching gel for 16PO connectors in the new structure.

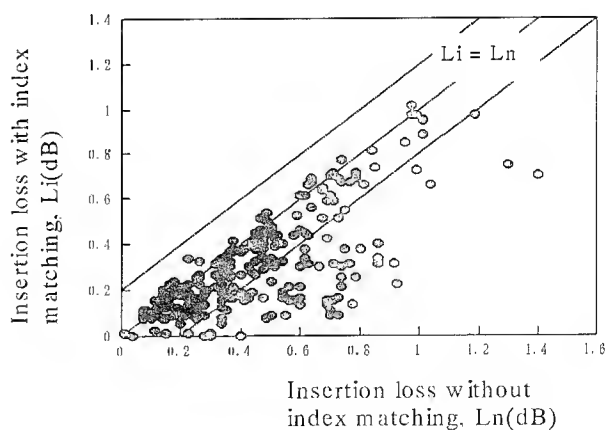


Figure 6. Relation between insertion losses with and without index-matching gel for 16PO connectors in the structure of polishing condition of 2MPO connectors.

The average return loss is 61.3 dB, as shown in figure 7, and is almost same as that of MPO connectors.

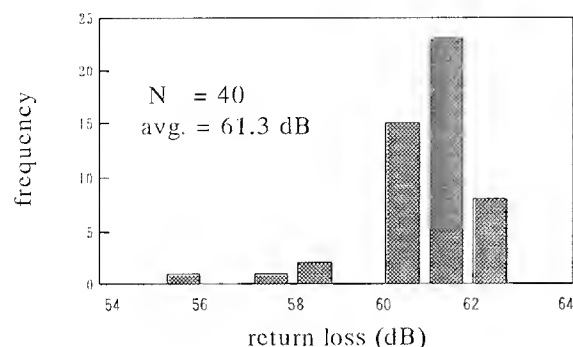


Figure 7. Return loss.

4. Reliability

As the environmental performance test of the 16PO connector, we evaluated the temperature cycling test. Two pair of the connectors were subjected to 10 six-hour temperature cycles, where the temperature ranged from -25 °C to +70 °C. Insertion loss was measured before (initial), during, and after (final) the tests for each of the 32-fiber pairs.

The insertion loss change for the typical fiber during the temperature cycling test is shown in figure 8.

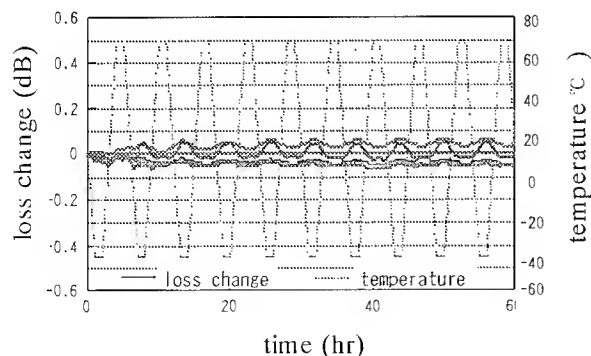


Figure 8. Insertion loss change for a few typical individual fibers during temperature cycle test.

The durability of the repeated matings of the connectors is very important for this connector use. One connector pair is subjected to 100 repeated matings to measure the insertion loss change as shown in figure 9. Average loss change was 0.17dB, with a standard deviation of 0.09dB.

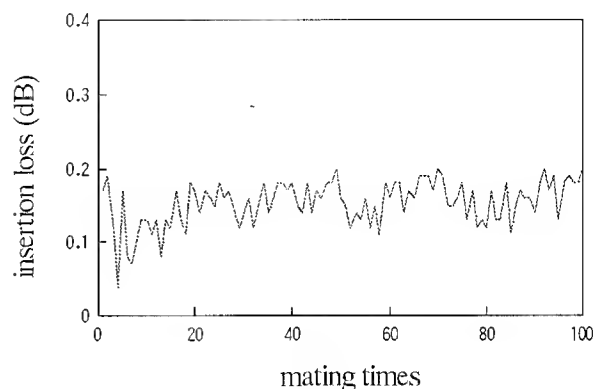


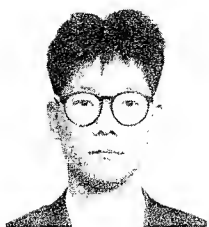
Figure 9. Insertion loss change for a typical individual fiber during durability test.

5. Conclusion

We proposed the push on type optical connector which can connect 16-fiber ribbon. The low insertion loss of less than 0.2dB and high return loss of more than 50dB were provided without index matching gel. We have conducted various performance tests and reliability tests. The test result indicates that 16PO utilizing the novel ferrule structure is effective in construction of future subscriber networks.

References

1. S.Tomita, M.Matsumoto, S.Nagasawa, T.Tanifuji, and T.Uenoya, 'Preliminary Research into High-Count Pre-connectorized Optical Fiber Cable', 41st IWCS, pp5-12, 1992.
2. T.Ueda, H.Ishida, I.Tsuchiya, T.Kakii, and T.Yamanishi, 'Development of 16-Fiber Connectors for High-speed Low-Loss Cable Connection', 42nd IWCS, pp244-249, 1993.
3. S.Nagasawa, Y.Yokoyama, F.Ashiya, and T.Satake, 'A Single-Mode Multifiber push-on type Connector with Low Insertion- and High Return-Loss', ECOC'91, pp49-52.
4. S.Nagasawa, T.Tanifuji, M.Matsumoto, and M.Kawase, 'Single-Mode Multifiber Connectors for Future Large Scale Subscriber Network', ECOC'93, pp29-32.
5. S.Iwano, R.Nagase, K.Kanayama, E.Sugita, K.Yasuda, and Y.Ando, 'Compact and Self-Retentive Multi-Ferrule Optical Backpanel Connector', IEEE, pp1356-1362, 1992.



Ichiro Matsuura

Sumitomo Electric
Industries, Ltd.

1, Taya-cho, Sakae-ku
Yokohama, Japan

Ichiro Matsuura received a B.E. degree from Keio University in 1988. He joined Sumitomo Electric Industries, Ltd. in 1988, and has been engaged in research and development of optical connectors. He is an engineer of Communication R&D Department in Yokohama Research Laboratories.



Makoto Honjo

Sumitomo Electric
Industries, Ltd.

1, Taya-cho, Sakae-ku
Yokohama, Japan

Makoto Honjo received a M.E. degree from Osaka University in 1984. He joined Sumitomo Electric Industries, Ltd. in 1984, and has been engaged in research and development of optical fiber, cable and jointing technologies. He is a senior engineer of Communication R&D Department in Yokohama Research Laboratories.



Tomohiko Ueda

Sumitomo Electric
Industries, Ltd.

1, Taya-cho, Sakae-ku
Yokohama, Japan

Tomohiko Ueda received a B.E. degree from Tokyo University in 1987. He joined Sumitomo Electric Industries, Ltd. in 1987, and has been engaged in research and development of optical connectors. He is an engineer of Communication R&D Department in Yokohama Research Laboratories.



Toru Yamanishi

Sumitomo Electric
Industries, Ltd.

1, Taya-cho, Sakae-ku
Yokohama, Japan

Toru Yamanishi received a B.E. degree from Hokkaido University in 1972. He joined Sumitomo Electric Industries, Ltd. in 1972, and has been engaged in research and development of optical fiber, cable and jointing technologies. He is a chief research associate of Communication R&D Department in Yokohama Research Laboratories.

Field Test Results for Pre-connectorized Cable with 16-fiber Ribbons

Hideyuki IWATA, Michito MATSUMOTO, Yasuo ISHINO,
Shigeru TOMITA, Shinji NAGASAWA and Tadatoshi TANIFUJI

NTT Access Network Systems Laboratories
Tokai, Naka, Ibaraki, 319-11 JAPAN

Abstract

Field test results are described for ultra-high density pre-connectorized cable containing thinly coated 16-fiber ribbons. A pre-connectorized U-groove unit cable containing 1600 fibers was successfully installed into conduits without any optical loss or fiber strain degradation. The average jointing loss change after the installation of the stacked 80-fiber connectors was less than 0.06 dB. The jointing time for 1600-fiber cable was less than 3 hours using stacked 80-fiber connectors.

1. Introduction

The construction of Fiber-To-The-Home (FTTH) networks supporting broadband integrated digital services, will require optical cable networks based on single-star(SS) architecture. Therefore, high count optical cables containing up to a few thousand fibers will be needed in order to realize FTTH.

We have been investigating ultra high density and high count optical fiber cables and multi-fiber jointing technologies using 16-fiber ribbons consisting of thinly coated optical fibers. Based on these technologies, the outer diameter of a 4000-fiber cable is reduced to less than 40 mm. Moreover, the cable jointing time is greatly reduced by using pre-connectorized cable with stacked or unit type 80-fiber connectors and compact joint boxes.

We performed a field test to confirm the compatibility of the ultra high density optical cable technologies for practical use. This paper describes the field test results.

2. Ultra high density optical cable technologies examined in the field test

Pre-connectorized cables were installed into conduits to evaluate their performance in the field. This section, outlines field test cable facilities, pre-connectorized cables and the jointing technologies and test items.

2.1 Cable and joint arrangement in the field test

Figure 1 shows a schematic view of the underground facilities used in the field tests. The conduit route length is 500m long, and there are two manholes at which the conduits intersect at right angles.

One pre-connectorized 1600-fiber cable was installed from manhole No.1 to manhole No.5 and the pulling head is placed at the manhole No.5 located in the middle of the route. Another pre-connectorized cable was installed from manhole No.9 to manhole No.5.

Pre-connectorized cables are jointed using a stacked 80-fiber connector. To make various measurements easier, round trip cables were installed with the same arrangement parallel to the first cables. At the left side end in the figure, 16-fiber ribbon connectors were used to investigate the joint time dependence on the jointing methods.

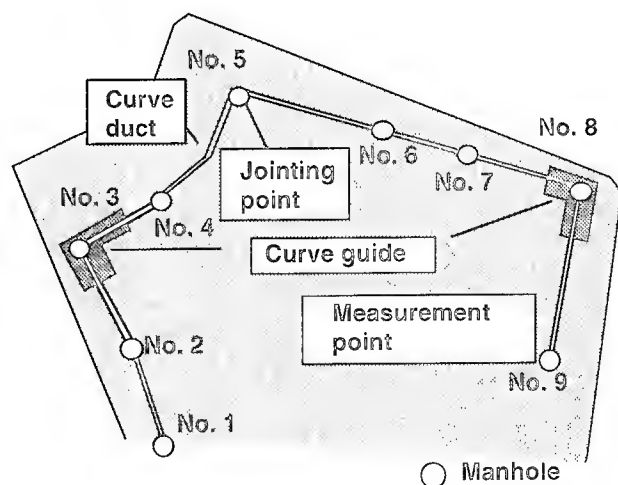
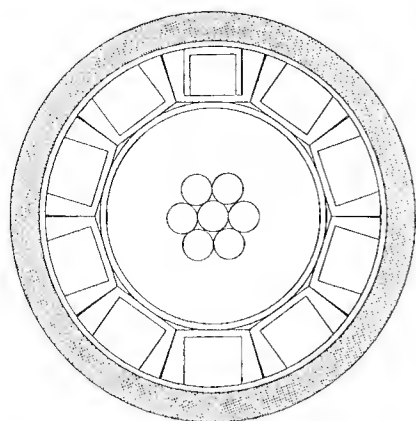
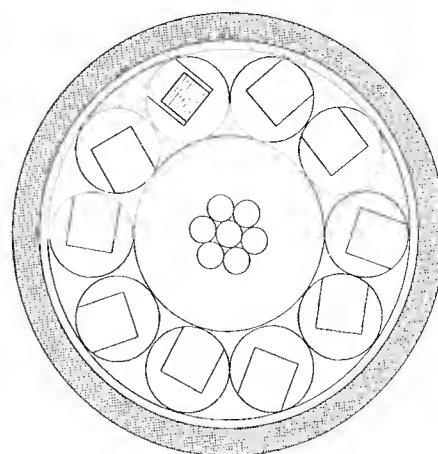


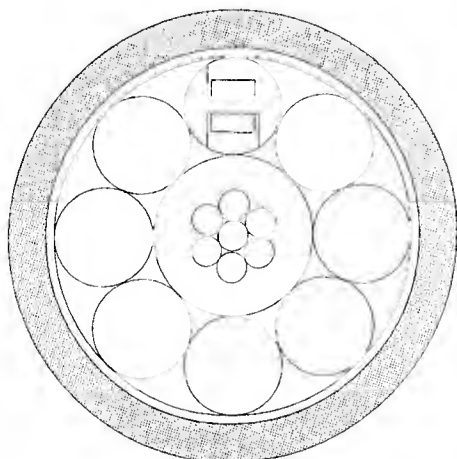
Figure 1 Underground facilities in the field test



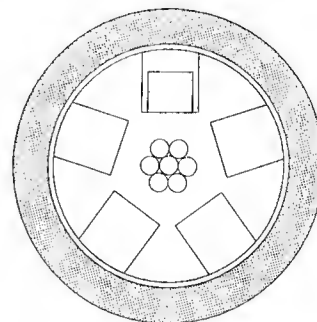
(a) 1600-fiber U-groove unit cable



(b) 1600-fiber single slot in a rod unit cable



(c) 1600-fiber double slot in a rod unit cable



(d) 800-fiber slotted rod cable

Figure 2 Structures of trial cables

2.2 Pre-connectorized cable and joint box structures

(1) Cable structures

The cable structures used in the field test are shown in Figs.2(a) to 2(d). Figure 2(a) shows a 1600-fiber U-groove unit cable. The U-grooves are filled with ten stacked 16-fiber ribbons consisting of thinly coated fiber 0.18 mm in diameter. Ten U-grooves are stranded around a central member and constitute the 1600-fiber cable. This cable has an outer diameter of 28mm.

Figure 2(b) shows a single slot in a rod unit cable whose slot is helically rotated around the rod. The U-grooves are filled with ten stacked 16-fiber ribbons. Ten rods are stranded around a central member and constitute the 1600-fiber cable. This cable has an outer diameter of 33mm.

Figure 2(c) shows a double slot in a rod unit cable in which the slots are stranded around the rod. Five 16-fiber ribbons are stacked in each slot. Ten rods are stranded around a central member and constitute the 1600-fiber cable. This cable has an outer diameter of 30 mm.

Figure 2(d) shows a slotted rod cable. As with the U-groove cable, the slots are filled with ten stacked 16-fiber ribbons constituting 800 fiber cable. This cable has an outer diameter of 19mm.

In these cables, specified fibers are used only in one unit. In the other units, unspecified fibers are used to confirm pulling head and joint box design.

(2)Pre-connectorized pulling head structure

A schematic view of a pre-connectorized pulling head is shown in Fig.3. Optical cables are installed by pulling force applied through the tension member located in the central part of the pulling head, which is joined to the tension member of the cable. In another solution, the housing of a pulling head protector is used as a tension member.

(3)Joint box structure

A schematic view of a joint box is shown in Fig.4. The stacked 80-fiber connectors shown in Fig.5 are located in the central part of a conventional closure. Five excess fiber ribbons are banded together to reduce excess fiber treatment time.

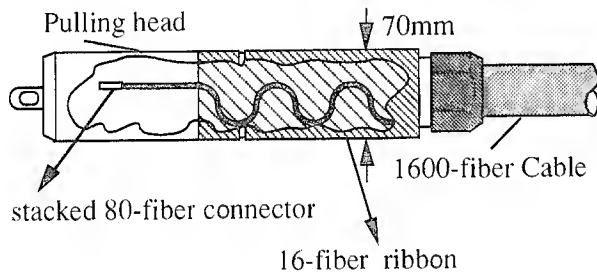


Figure 3 Pre-connectorized pulling head.

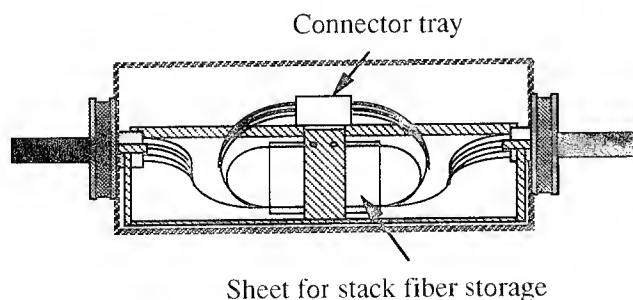


Figure 4 Joint box

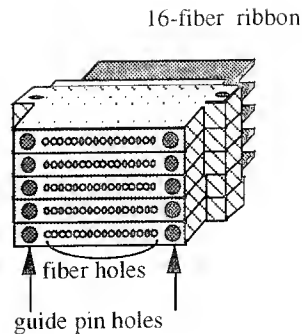


Figure 5 Stacked 80-fiber connectors

2.3 Test items

The following items were investigated in the field test.

(1)Optical loss change

Optical loss of the cable was measured before and after installation, and after removal from a conduit. In all cases, the optical cables were jointed in a similar way when installed in the conduits. The optical loss in each cable and the jointing loss were measured by OTDR at the wavelength of 1.31 and 1.55 μm . 160 specified fibers were measured at 1.31 μm . At 1.55 μm , corner fibers of the unit were measured in addition to central fibers of the unit.

(2)Strain distribution of fibers in cable

The strain distribution was measured by BOTDA (Brillouin Optical-Fiber Time Domain Analysis) before and after installation and after removal from the conduit. The measurement wavelength was 1.55 μm .

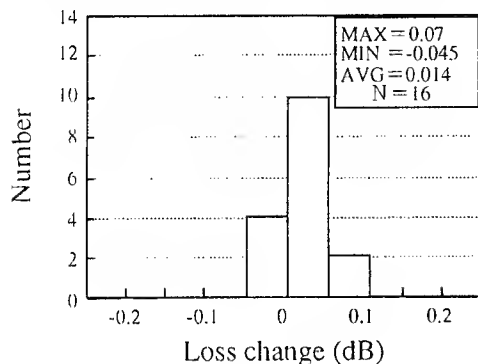
(3)Cable jointing time

Cable jointing time includes the time required to remove the pulling head, connect and accommodate the fiber and complete the enclosure.

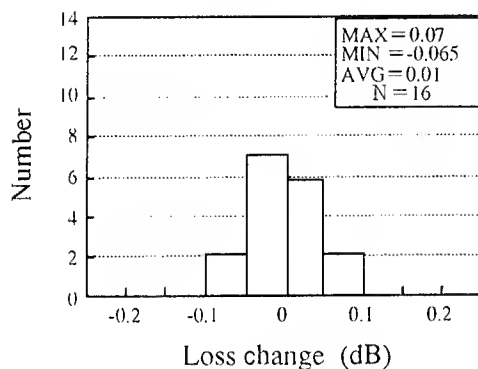
3. Field test results

(1)Optical loss change of cable

Figure 6 shows the optical loss change histogram after installation and after removal from conduit for U-grooved 1600-fiber cable. As shown in the figure, the optical loss change both at 1.31 and 1.55 μm is less than 0.1dB/km, which is within measurement accuracy. For the other cables shown in Fig.2(b)-2(d), the optical loss changes were less than 0.1dB/km.



(a)1310nm



(b)1550nm

Figure 6 Loss change after installation

(2)Optical loss change of multi fiber connector.

Figure 7 shows the jointing loss change for multi-fiber connectors after installation and removal from a conduit. The average connection loss was 0.2dB at 1.31 μm . The average connection loss change was 0.06dB, which is within the repeatability margin for connection loss.

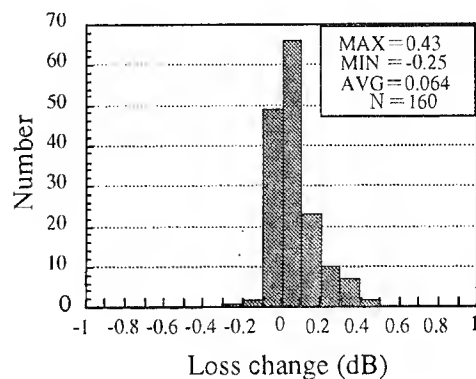


Figure 7 Jointing loss change
multi-fiber connectors

(3)Cable jointing time

Figure 8 shows, the jointing time for 1000-fiber cable using the present method (8-fiber ribbon connectors), and jointing time for 1600-fiber cable using 16-fiber ribbon connectors. The jointing time is 2.5 hours for 1600 fiber cable using stacked 80-fiber connector and this is much quicker than the conventional jointing procedure.

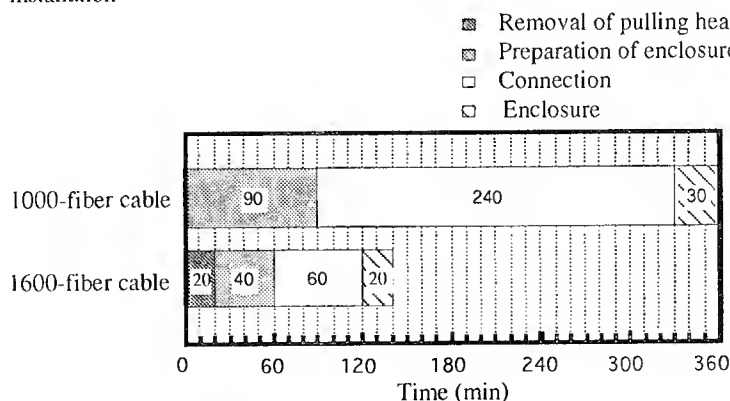


Figure 8 Jointing time for 1000 & 1600 fiber cable

(4) Strain distribution of fibers in cable

Figure 9 shows the strain distribution before and after installation for fibers both at the side and in the center of ribbons. As shown in the figure, the strain in the fibers before installation decrease between 0 and 0.07% after installation. Because there are the cyclic compression and extension on both side of the fiber in the ribbons caused by the bends in a reeled cable before installation.

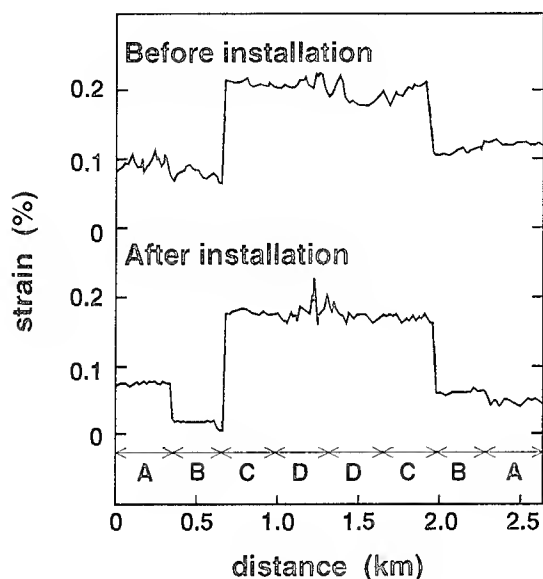


Figure 9 Strain distribution before and after installation

4. Conclusion

Ultra high density pre-connectorized optical cables have been field tested with a view to practical application.

It is clear that the optical and mechanical properties of the cables are sufficiently stable with the present installation methods. Cable jointing times are greatly reduced by using stacked 80-fiber connectors and newly developed closures.

5. References

- [1] S. Tomita, M. Matsumoto, T. Yabuta and T. Uenoya "Preliminary Research into Ultra High Density and High Count Optical Fiber Cables", 40th IWCS, pp.8-15, 1991
- [2] S. Tomita, M. Matsumoto, T. Tanifuji, S. Nagasawa and T. Uenoya; "Preliminary Research into High-count Pre-connectorized Optical Fiber Cable", Proc. of 41st IWCS pp. 5-12, 1992.
- [3] W. Katsurashima, Y. Kitayama, K. Oishi, T. Kakuta and N. Akasaka "Microbending Loss of Thin Coating Single Mode Fiber for Ultra-High-Count Cables", 41st IWCS, pp. 13-19, 1992
- [4] M. Hara, S. Okagawa, and A. Otake "Design of Downsized Coated Optical Fibers to Minimize Microbending Loss", 41st IWCS, pp.20-24, 1992
- [5] K. W. Jackson M. L. Pearsall "Design and Performance of a Compact 204-Fiber Ribbon Cable", OFC'90, p. 107, 1990
- [6] M. Kawase, T. Fuchigami, M. Matsumoto, S. Nagasawa, S. Tomita, and S. Takashima "Subscriber Single-Mode Optical Fiber Ribbon Cable Technologies Suitable for Midspan Access", J. of Lightwave Technology, Vol.7, No.11, November, 1989.
- [7] T. Haibara, S. Tomita, M. Matsumoto and T. Yabuta "High-Speed Low-Loss Connection Techniques for High Count Pre-Connectorized Cables", 40th IWCS, pp.296-302, 1991



Hideyuki IWATA

NTT
Access Network
Systems Laboratories
Tokai, Ibaraki,
319-11, JAPAN

Hideyuki Iwata was born in 1965 and received B.E. and M.E. degrees in electronic engineering from Yamagata University in 1989 and 1991 respectively.

He joined NTT in 1991. Since 1993 he has been engaged in research on high-density and pre-connectorized optical fiber cable.

Mr. Iwata is a member of IEICE of Japan.



Yasuo ISHINO

NTT
Central Training
Institute
Chofu, Tokyo,
182, JAPAN

Yasuo Ishino is a Research Engineer.

He was born in 1954 and graduated from Nagano Technical college in 1975.

He joined NTT in 1975. Since 1992 he has been engaged in research on high-density and pre-connectorized optical fiber cable.



Michito MATSUMOTO

NTT
R&D Management
Department
Chiyoda-ku, Tokyo,
100-19, JAPAN

Michito Matsumoto is an Executive Research Engineer. He was born in 1952 and received B.E. degree in electrical engineering from Kyushu Institute of Technology. He received M.E. and Ph.D. degrees in electronics engineering from Kyushu University in 1977 and 1987, respectively.

He joined NTT in 1977. Since 1990 he has been engaged in research on high-density and pre-connectorized optical fiber cable.

Dr. Matsumoto is a member of IEEE.



Shigeru TOMITA

NTT
Plant Planning
Department
Chiyoda-ku, Tokyo,
100, JAPAN

Shigeru Tomita is a Senior Research Engineer.

He was born in 1960 and received B.E. and Ph.D degrees in electronics engineering from Nihon University in 1983 and 1993 respectively.

He joined NTT in 1983. Since 1990 he has been engaged in research on high-density and pre-connectorized optical fiber cable.

Dr. Tomita is a member of IEEE.



Shinji NAGASAWA

NTT
Access Network
Systems Laboratories
Tokai, Ibaraki,
319-11, JAPAN

Shinji Nagasawa is an Executive Research Engineer. He was born in 1950 and received B.E. and M.E. degrees in electrical engineering from Chiba University in 1974 and 1976, respectively.

He joined NTT in 1976. Since 1990 he has been engaged in research on multi fiber connectors.

Mr. Nagasawa is a member of IEEE.



Tadatoshi TANIFUJI

NTT
Access Network
Systems Laboratories
Tokai, Ibaraki,
319-11, JAPAN

Tadatoshi Tanifuji is the leader of high count optical fiber cable research group. He was born in 1949. He received B.E. and M.E. degrees in electronics engineering from Hokkaido University in 1972 and 1974, respectively.

He joined NTT in 1974. Since 1991 he has been engaged in research on High-density and Pre-connectorized optical fiber cable.

Dr. Tanifuji is a member of IEEE.

AUTOMATED CONNECTORIZING LINE FOR OPTICAL CABLES

M.Tsuda R.Yuguchi T.Isobe K.Ito Y.Takeuchi
T.Uchida K.Suzuki T.Matsuoka K.Higuchi I.Kinoshita

The Furukawa Electric Co.,Ltd.
6, Yawata-kaigan-dori, Ichihara city, Chiba, 290, Japan

Abstract

Along with current rapid spread of bases for optical fiber networks, the explosive increase of demand for pre-connectorized optical fiber cables is expected. However, almost all connectors are mounted in a manual process, so we have developed the automated connectorizing line for optical fiber cables. This line can mount any one of 3 types of connectors to either of 2 types of single-fiber optical cords with different outer diameters. By combining the connectors with various optical fiber cables, which have stranded cords, the line can produce more than 100 kinds of pre-connectorized optical fiber cables. Although the quality of connectors mounted manually depends on the skill of workers, the line can assure stable and uniform quality of pre-connectorized optical cables.

Introduction

In order to accomplish an information highway plan in the near future, infrastructure for optical fiber networks are rapidly developed. Along with this development, it is expected that a demand for optical fiber connectors will increase abruptly. The optical fiber connectors are mainly used as pre-connectorized optical fiber cords/cables. Their connectorizing process is still largely manual, so its automation has been required to ensure uniform quality, reduction of connectorizing cost, and growth of production capacity.^{1), 2), 3)} Taking these circumstances into account, we have developed an automated connectorizing line for single-fiber cords/cables. The connectorizing process consists of the following stages;

- 1) ferrule insertion
- 2) fiber end polishing
- 3) connector body assembly
- 4) inspection

Of them, we have accomplished of automation of the stages 1) through 3). In order to improve transfer

efficiency of cords and cables, we have developed a special hanger, which can deal with some coiled forms of them, and its automatic transportation system. Fig.1 shows an outline of this line. The following describes the features of it.

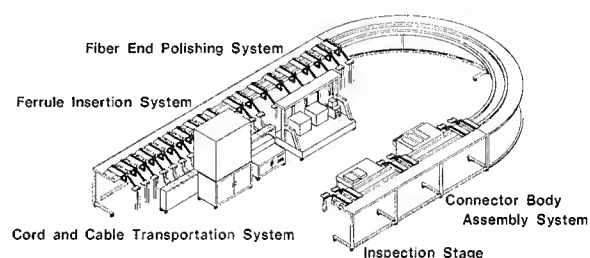


Fig. 1 Outline of the line

1.The Diversified Combination of Optical Fiber Cords/Cables and Connectors

This automated line is capable of connectorizing the single-fiber optical cords with an outer diameter of 2.0 or 2.8mm (major dimensions in Japan), which use either one of 2 kinds of optical fibers, SM and MM. Connectors are generally mounted to the single-fiber optical cords, and also, optical cables which are stranded. Therefore, we have made the line capable of dealing with single-fiber to a maximum of 32-fiber optical cables. The line can mount 3 types of connectors, that are FC, SC, and so called Plug-in type (connectors generally used in Japan). We have perfected the line as a diversified small-quantity production type which allows more than 100 kinds of pre-connectorized optical fiber cords/cables to be produced by combining these connectors with various multi-fiber optical cables. Fig.2 outlines the connectorized optical fiber cords/cables which can be produced by this line.

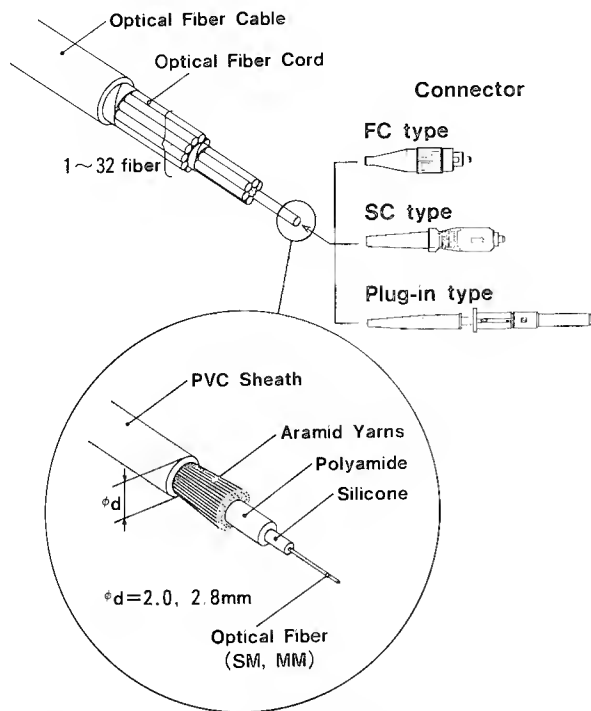


Fig. 2 The diversified combination of optical fiber cords/cables and connectors

2. Ferrule Insertion System

We have divided the ferrule insertion stage into 8 steps. We developed work stations for each step, and those are built in the automated line to form continuous process. The ferrule insertion system consists of "jacket stripping device," "aramid yarns cutting device," "silicone removing device," "fiber diameter measuring instrument," "epoxy resin mixer," "mixed epoxy resin injector," "fiber insertion device," and "epoxy resin hardening device." Fig.3 and Photo 1 shows an outline of processing for each step and an appearance of the system, respectively. Before placing cables in the system, its sheath is stripped to a required length in advance to expose cords. After putting connector body through each cord, it is hooked under the special hanger, and placed in the automatic transportation system. Each cable is labeled with a bar code which represents the data on a product type of connectorized optical cord/cable (that is, fiber type, cord outer diameter, connector type and so on). When it is loaded onto the line, the ferrule insertion system reads the data from this bar code. The system performs processing in each step by referring to this data.

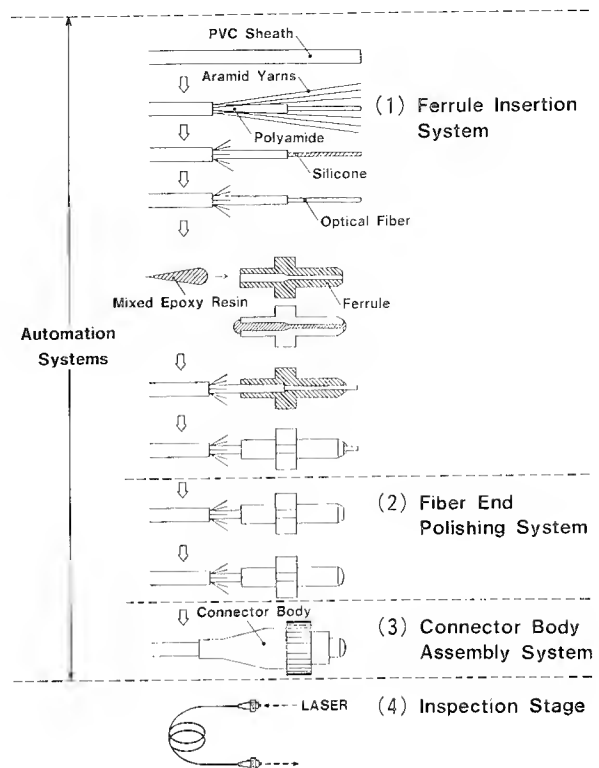


Fig. 3 Outline of connector mounting procedure

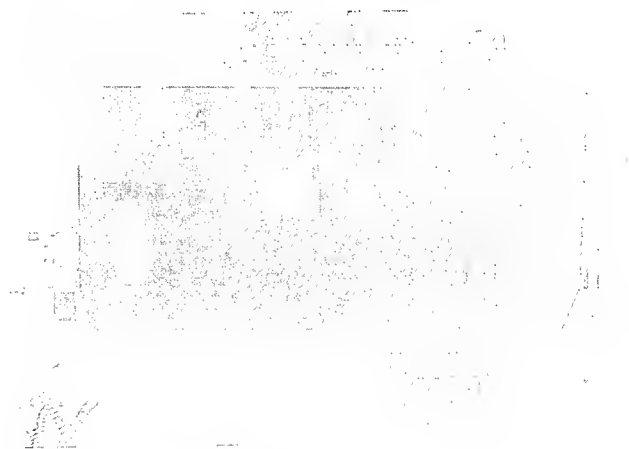


Photo 1 Ferrule insertion system

2-1. Jacket Stripping Device

This device strips the PVC sheath and polyamide coating of the cord to a specified length. When stripping the polyamide coating, the tension members existing between the PVC sheath and polyamide coating (aramid yarns are usually used) are obstructive. However, this device deals with it by spraying air to the cord end to separate the aramid yarns from polyamide coating. The

PVC sheath with outer diameter of 2.0 or 2.8mm can be stripped by an identical edge by adjusting a combination of a pulse motor and ball screw. Photo 2 shows an appearance of the device.

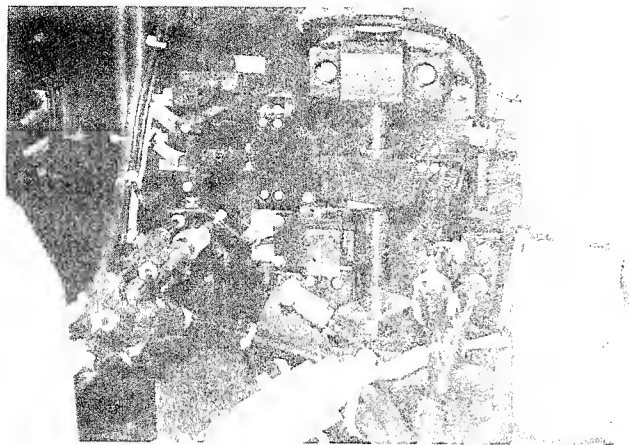


Photo 2 Jacket stripping device

2-2. Aramid Yarns Cutting Device

This device cuts the aramid yarns at a specified length, which was separated by the air at the jacket stripping device. Since the aramid yarns provides protection when a tension is applied to the cord, it is important to cut at a specified length in order to exhibit their protective capability. As a conventional blade is used to cut them, its sharpness will be quickly deteriorated and they may not be properly cut. Therefore, we have introduced a new method for this device, which cuts the aramid yarns by pressing against them a highly heated metal blade. By keeping a blade temperature and cutting speed at optimum values, there

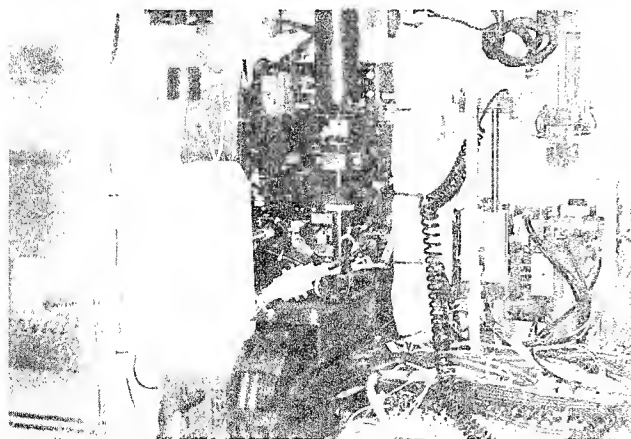


Photo 3 Aramid yarns cutting device

is hardly a trace of scorching left on the cut face of the aramid yarns. This method has a cutting life of over several thousand times, allows unchanged sharpness until the end of the cutting life, and hardly has any uncut yarns left. Photo 3 shows an appearance of this device.

2-3. Silicone Removing Device

Part of the silicone coating has been removed by the jacket stripping device. The remaining coating is completely removed by the silicone removing device to expose the optical fiber. Unless the silicone coating is completely removed, the fiber will be snapped when inserting into the ferrule or its strength will be lost adhered to the ferrule. This device is capable of completely removing the silicone coating, including the stripped edge of the polyamide coating.

2-4. Fiber Outer Diameter Mesuring Instrument

This instrument measures an exposed fiber outer diameter and selects a ferrule with an optimum hole diameter. If you use a ferrule whose hole is sufficiently larger than a fiber diameter, insertion of the fiber into the ferrule will be facilitated, however insertion loss will be increased. On the other hand, if you use a ferrule whose hole diameter is almost as large as the fiber diameter, the fiber may be snapped in process of insertion. To solve this problem, we have determined to keep 2 kinds of ferrules with different hole diameters for each fiber type in the system and select either one of them suitable to the fiber diameter measured by this instrument. This has reduced occurrences of fiber breakage and lowered insertion loss.

2-5. Epoxy Resin Mixer

Before inserting a fiber into a ferrule, the ferrule is filled with 2-liquid curable mixed epoxy resin in order to adhere and fix the fiber and ferrule. This device quantitatively discharges and mixes this epoxy resin. The epoxy resin consists of pre-cured epoxy resin and its hardener; they are mixed at a ratio of 10:1. Since a filling amount into one ferrule is about $1/100,000,000\text{m}^3$, high-accurate and repeatable mixing technique is required. As a basic structure, this device uses a 2-liquid mixing dispenser with micro-gear pumps system as shown in Fig.4. Basically, it sufficiently meets required performance such as a mixture ratio above. However, the

mixture ratio must be extremely accurate in order to obtain sufficient bonding strength, and it is very difficult to make this check in the postprocess. To solve this problem, we have developed a method which measures each inflow of pre-cured epoxy resin and its hardener into a mixer constantly to eliminate accumulation of measured errors. This enables high-accurate automatic mixing.

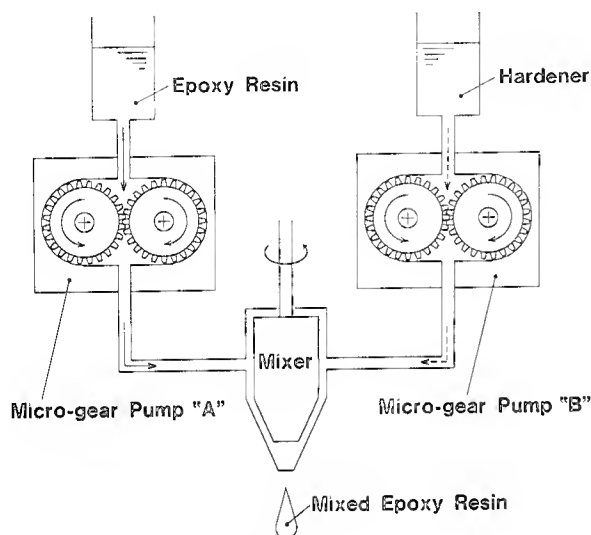


Fig. 4 Epoxy resin mixer

2-6. Mixed Epoxy Resin Injector

This device fills the ferrule with mixed epoxy resin. If air bubbles (void) exist in the resin, a stress may be applied to the fiber inside the ferrule after hardening of the epoxy resin, having some effect on reliability. So, we have improved a special injection method to enable filling which hardly allows a mixture of void into the ferrule. Although this epoxy resin has a bad effect on the skin of workers, depending on their physical constitutions, its effect is very little because they are hardly exposed to it thanks to this device and epoxy resin mixer.

2-7. Fiber Insertion Device

This device inserts the fiber into the ferrule filled with mixed epoxy resin. In order to be a lower insertion loss, the hole diameter of the ferrule has a minimum clearance for the outer diameter of the fiber. This makes insertion work very difficult. So this may cause incomplete insertion of the fiber, and as a result, it is

likely that more stress will be applied to the fiber in the ferrule after hardening of the epoxy resin. This device enables highly reliable insertion in terms of both success rate and quality, due to the use of split guides and improvement of inserting action.

2-8. Epoxy Resin Hardening Device

After inserting the fiber into the ferrule, this device heats and hardens the mixed epoxy resin. Since it is heated with the cord by placing on the conveyor in the cord and cable transportation system, the ferrule is slid on a heated plate as shown in Photo 4. While the ferrule moves from the front end of the plate to its rear end, the mixed epoxy resin will have been heated and hardened by heat conduction. Since the plate is successively heated even if the line is stopping halfway, the resin can be sufficiently hardened.

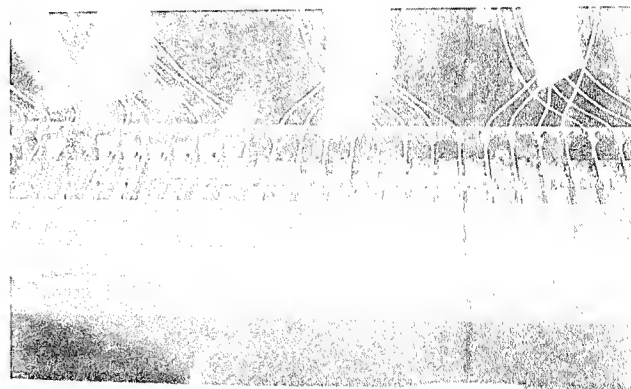


Photo 4 Epoxy resin hardening device

3. Fiber End Polishing System

This system polishes both end faces of the fiber and the ferrule whose main body consist of partially stabilized zirconia (PSZ).⁴⁾ Currently, the main method of polishing connectors is a PC (Physical Contact) which has the end face of the ferrule ground into a convex sphere and the fibers mutually brought into direct contact. This system also uses this method, and by adding to another polishing process,⁵⁾ a return loss can be higher than 45 dB. The system consists of "epoxy resin removing device" and "convex sphere polishing device." Adjacent to them, an automatic transportation system for a ferrule attached cord is installed. Between these systems, the cord attached ferrule is handled by

2-axis and 3-axis orthogonal actuators. Since the automatic transportation system is installed in series to the ferrule insertion system, the ferrule attached cord can be automatically transferred between them, thus we have built the fully automated connectorizing line from ferrule insertion to fiber end polish. Photo 5 shows an appearance of the fiber end polishing system. The following describes each component device of the system. (for outline machining, refer to Fig.3)



Photo 5 Fiber end polishing system

3-1. Epoxy Resin Removing Device

After attaching the ferrule to the fiber, this device removes the hardened epoxy resin and excess fiber adhered to its end face. Normally, a grindstone is used to remove them. This method, however, scratches the fiber or ferrule deeply, or if the resin is not completely removed, quality of their end faces will be worsened in the subsequent end polishing process. This device hardly has a bad effect on the postprocess, because of some control items set under optimum conditions, such as a load to press the ferrule against the grindstone, fixing method and grinding time.

3-2. Convex Sphere Polishing Device

Many kinds of polishers have been sold, which are designed to polish both end faces of the ferrule and fiber into convex spherical shapes. From a viewpoint of easy handling, we have employed a semiautomatic polisher developed by NTT. Adding of 3-axis orthogonal actuators allows to automatically bring the ferrule attached cord in and off the polisher.

4. Connector Body Assembly System

In a connector body assembly process, work time and product quality greatly differs depending on proficiency of each worker. It is one of most difficult processes to automate. We have enabled machining which is not affected by proficiency of the worker, by automating the processes except for handling of the cord. Fig.5 shows a schematic diagram of the processes. In this system, we have determined to manually shift onto the end of the cord and set in the system the connector body which is let through the cord prior to attaching the ferrule to it. What has been automated is the postprocesses which will affect the product quality. This equipment switches 3 units, depending on types of connectors. Photo 6 shows its appearance.

Important points on product quality are taking out and fixing of the aramid yarns. Taking out of the aramid yarns refers to exposing the yarns which are covered by a bush, and fixing of the aramid yarns refers to covering them with a stopper and fixing them by applying an adequate pressure. These processes are required to prevent a tension from being applied to the fiber itself when the cord is pulled. Conventionally, a worker uses to pull out the aramid yarns through a gap between the bush and the cord, using a needle. With this method, however, they may damage the cord or leave some yarns inside the bush after fixing, and need a

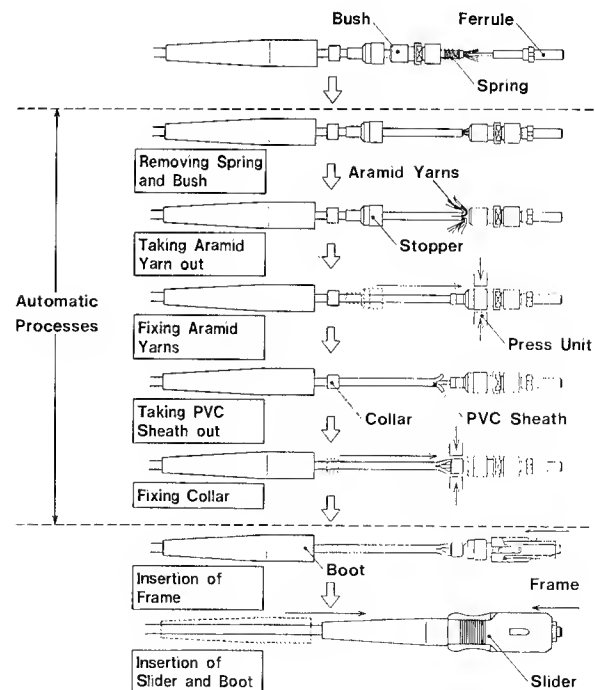


Fig. 5 Connector body assembling processes

considerable work time. This system allows unhurt, secure taking out of the aramid yarns in a short time. When these yarns are covered with the stopper and fixed by a 2-split-type press unit, if a fixing force is insufficient, they will come off, and if too strong, the stopper will be crushed. Although an optimum fixing force differs depending on the materials of the cord and parts of connector body, this system allows an optimum fixing for machining at any time.

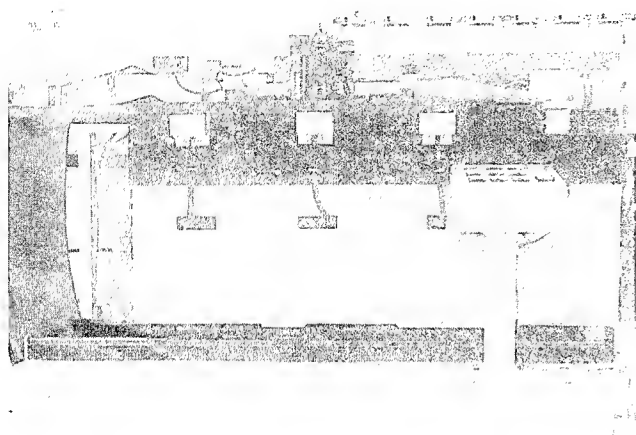


Photo 6 Connector body assembly system

5. Cord and Cable Transportation System

This line can deal with single-fiber cord and 2 to 32-fiber cable. Their transfer and handling are troublesome and may damage the cords/cables and connectors. These problems have been solved by combining special cords/cables hanger and its automatic transportation system. The hanger can deal with the cords/cables in coil or coiled around a bobbin. By holding the cords/cables vertically, it can be stored in a small space. Since the automatic transportation system has been designed to include the automation systems (ferrule insertion, fiber end polishing and connector body assembly system) and inspection stage, a transfer of the cords/cables becomes very easy between them.

6. Conclusion

We have developed an automated line which is designed to connectorize single-fiber optical cord and cable which some cords are stranded. This line is diversified small-quantity production line which can deal with more than 100 kinds of pre-connectorized optical fiber cables. Conventionally, the product quality used to differ depending on worker's proficiency in manual works such as "ferrule insertion" and "connector body assembly." However, automation of mounting connectors has made it possible to assure uniform quality of products

7. References

- 1) S. Nakamura, et al., "Automated Assemble Technique for Optical Fiber Connector." Technical Report of IEICE of Japan, EMC88-11, pp.17-23, 1988.
- 2) S. Nakamura, et al., "An Automated Assembly Machine for Optical Connector", Spring National Convention of IEICE of Japan, 1988.
- 3) Johann Schulte, "Automated Mounting of Connectors to Fiber Optic Cables", Proceedings of 40th, International Wire and Cable Symposium, pp.303-308, 1991.
- 4) N. Suzuki, et al., "Low-Insertion and High Return-Loss Optical Connectors with Spherically Convex-Polished End", Vol. 22, Electronics Letters, pp.110-112, 1986.
- 5) K. Matsunaga, et al., "Study on Polishing Method for Optical-Fiber", National Conference of Semiconductor Devices and Materials of IECE of Japan, 1985.



Masamichi Tsuda

The Furukawa Electric Co., Ltd.
6, Yawata-kaigan-dori,
Ichihara city, Chiba, Japan

Mr. Tsuda graduated from Hokkaido University in 1991 with a B. E. in applied physics. Then he joined the Furukawa Electric Co., Ltd. and has been engaged in development of optical fiber connectors.

Mr. Tsuda is now an engineer of Production Engineering Section of FC Center of Fiber Optics & Telecommunications Division.



Tatsuya Isobe

The Furukawa Electric Co., Ltd.
6-1, Marunouchi 2-chome,
Chiyoda-ku, Tokyo, Japan

Mr. Isobe graduated from Kobe University of Merchant Marine in 1988 with a B. E. in engineering. Then he joined the Furukawa Electric Co., Ltd. and has been engaged in development of optical fiber connectors.

Mr. Isobe is now an engineer of Engineering Department of Network Integration Division.



Renichi Yuguchi

The Furukawa Electric Co., Ltd.
6, Yawata-kaigan-dori,
Ichihara city, Chiba, Japan

Mr. Yuguchi graduated from Tokyo Institute of Technology in 1984 with a M. Sc. in mechanical engineering. Then he joined the Furukawa Electric Co., Ltd. and has been engaged in research and development of optical fiber connectors and fiber optic apparatus.

Mr. Yuguchi is now an assistant manager of Production Engineering Section of FC Center of Fiber Optics & Telecommunications Division.



Kyoichi Ito

The Furukawa Electric Co., Ltd.
6, Yawata-kaigan-dori,
Ichihara city, Chiba, Japan

Mr. Ito graduated from Meiji University in 1992 with a M. Sc. in industrial chemistry. Then he joined the Furukawa Electric Co., Ltd. and has been engaged in development of optical fiber cables and connectors.

Mr. Ito is now an engineer of Submarine Cable Engineering Section of Optical Fiber Production Department of Fiber Optics & Telecommunications Division.



Yosinori Takeuchi

The Tohoku Furukawa
Electric Co., Ltd.
1-41, aza-tanosawagasira,
Ichikawa-machi, Hachinohe
city, Aomori, Japan

Mr. Takeuchi graduated from Hachinohe National College of Technology in mechanical engineering in 1992. Then he joined the Tohoku Furukawa Electric Co., Ltd. and has been engaged in development of connectorizing systems for optical fiber cables.

Mr. Takeuchi is now an engineer of Equipment & Devices Department in The Tohoku Furukawa Electric Co., Ltd.



Kenji Suzuki

The Furukawa Electric
Co., Ltd.
6, Yawata-kaigan-dori,
Ichihara city, Chiba, Japan

Mr. Suzuki graduated from Tokyo Institute of Technology in 1978 with a B. E. in manufacturing mechanical engineering. Then he joined the Furukawa Electric Co., Ltd. and has been engaged in development of power cables, heat pipes and production facilities.

Mr. Suzuki is now a manager of Precise Machining R&D Section of R&D Department of Plant & Facilities Division.



Teruyoshi Uchida

The Furukawa Electric
Co., Ltd.
6, Yawata-kaigan-dori,
Ichihara city, Chiba, Japan

Mr. Uchida graduated from Kyusyu University in 1987 with a B. E. in mechanical engineering. Then he joined the Furukawa Electric Co., Ltd. and has been engaged in development of automation systems of connectorizing.

Mr. Uchida is now an engineer of Automation R&D Section of R&D Department of Plant & Facilities Division.



Takayuki Matsuoka

The Furukawa Electric
Co., Ltd.
6, Yawata-kaigan-dori,
Ichihara city, Chiba, Japan

Mr. Matsuoka graduated from Shizuoka University in 1991 with a B. E. in mechanical engineering. Then he joined the Furukawa Electric Co., Ltd. and has been engaged in development of automation systems of connectorizing.

Mr. Matsuoka is now an engineer of Automation R&D Section of R&D Department of Plant & Facilities Division.



Kazuhiro Higuchi

The Furukawa Electric
Co., Ltd.
6, Yawata-kaigan-dori,
Ichihara city, Chiba, Japan

Mr. Higuchi graduated from Mukai-no-oka Highschool of Technology in mechanical engineering in 1984. Then he joined the Furukawa Electric Co., Ltd. and has been engaged in development of cable facilities and automation systems of connectorizing.

Mr. Higuchi is now an engineer of Automation R&D Section of R&D Department of Plant & Facilities Division.



Isamu Kinoshita

The Furukawa Battery
Co., Ltd.
23-6, Kuidesaku, Jyouban-
shimofunao-machi, Iwaki
city, Fukushima, Japan

Mr. Kinoshita graduated from Waseda University in 1981 with a B. E. in electronics and communication engineering. Then he joined the Furukawa Electric Co., Ltd. and has been engaged in development of control systems of power cable facilities and automation systems of connectorizing.

Mr. Kinoshita is now an assistant manager of Production Engineering R&D Section of R&D Department in Furukawa Battery Co., Ltd.

RELIABILITY OF EPOXY ADHESIVES IN CERAMIC-FERRULE OPTICAL CONNECTORS

L.A. Reith, R.A. Frantz, P.B. Grimado, I.M. Plitz*,
O.S. Gebizlioglu*, and D.A. Dolinoy

Bellcore, 445 South St., Morristown, N.J. 07960

*Bellcore, 331 Newman Springs Rd., Red Bank, N.J. 07701

ABSTRACT

To achieve low-reflectance performance in optical connectors, it is imperative to maintain physical contact at the interface between the fiber cores. Typically, fiber contact is initially ensured by using a radiussed connector ferrule endface, carefully polished so that the glass fiber is not undercut with respect to the ceramic. While this ensures initial contact, failure of the epoxy can allow the fiber to withdraw or be pushed back into the ferrule over its service life. By experimentally simulating ferrule endface loading conditions using radiussed zirconia indentors, we can compare fiber pushback for different epoxies under a variety of stress levels to ascertain which factors play a critical role. Aging of ferrule assemblies at high temperatures and high humidities indicates that some epoxies can degrade in these severe environments, increasing the possibility of in-service failure. In addition, differences in the performance of factory-assembled and field-assembled connectors have led us to investigate the effects of assembly processes. In particular, the use of inadequate or improper cleaning techniques may result in connector plugs with an increased potential for fiber pushback and subsequent failure.

1. INTRODUCTION

Physical contact at the fiber cores must be maintained in optical connectors to ensure low-reflectance performance. In the majority of optical connectors today, epoxies are used to mount the fibers in ceramic ferrules, and ferrule endfaces are radiussed to ensure good physical contact. When two connector plugs are mated, the fibers experience a loading force dependent not only on the spring-loading force, but also on the details of the ferrule endface geometries. Previous work has shown that the ability of the epoxy to withstand the loading force and hold the fiber in place is determined by epoxy properties and processing factors such as the epoxy cure level and glass transition temperature (T_g).¹⁻³ If the epoxy is not fully cured initially, it may cure later during its service life. The epoxy can then shrink and pull the fiber back into the ferrule. If the connector experiences temperatures approaching the epoxy T_g while under load, the epoxy can creep and the fiber will be pushed back into the ferrule.

In this work, we have expanded the number of epoxies under test to verify our earlier conclusions concerning epoxy T_g dependence. In addition, we begin the process of identifying other critical factors, including high humidity and assembly process cleanliness. Other studies have indicated that a high humidity environment can apparently cause temporary fiber withdrawal at high temperatures.⁴ In this paper we investigate the effect of high humidity on permanent fiber pushback under loaded conditions. Although it is reasonable to assume that epoxy adhesion will suffer if the fibers are not properly cleaned, we are not aware of any published data in this area. We therefore completed a brief study to compare the results of two different fiber cleaning techniques. We will describe the experimental setup and measurement procedure in the next section, give results in Section 3, and present conclusions in Section 4.

2. EXPERIMENT

2.1 Test Fixtures

The test fixtures allow us to apply simulated mating loads to the ferrule assemblies under test and to measure fiber pushback after exposure to a variety of different environmental conditions. The fixtures utilize a lever arm with moveable weights, which can be used to apply different static loads.¹ In the experiments described here, the total load is fixed at 0.9 kg (2 lb), which is a typical spring-loading force in ceramic-ferrule connectors.

Figure 1 shows in detail how the load is applied to the ferrule assembly endface. Radiussed zirconia rods, or indentors, are used to transfer the load to the ferrule assemblies under test. There are two sets of indentors: one with nominal radii of 10 mm, and the other with nominal radii of 24 mm. The radiussed indentors simulate an ideal connector endface in the sense that the fiber is locked in place and cannot be pushed back into the ferrule. At the indenter/ferrule assembly interface, the total load applied to the ferrule assembly is shared between the fiber and ferrule. Since zirconia is stiffer than glass, the fiber loading force applied by an indenter is somewhat greater than that of another ferrule assembly.

Copyright © 1994 Bellcore
All rights reserved

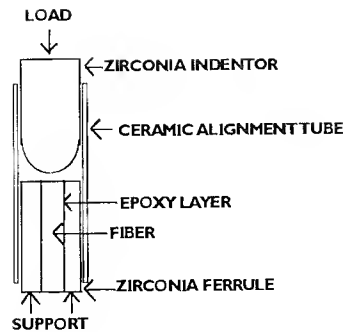


Figure 1. Detail of application of loading force. A radiussed zirconia rod, or indenter, is used to apply the load of 0.9 kg to the ferrule assembly.

Figure 2 shows values of the fiber load as a function of the total load, calculated using a boundary element analysis.² Fiber loads for several different configurations are compared. The upper and lower dashed curves represent the loads for mated ferrule assemblies with 10 mm and 30 mm radii, respectively. Most commercially-available connectors have radii lying within this range; the shaded area between these two curves therefore represents the range of fiber loads expected in service. The solid curves represent fiber loads for ferrule assemblies when the load is applied by an indenter. Data are plotted for indentors with 10 mm and 24 mm radii, loading ferrule assemblies with flat endfaces, which is characteristic of the

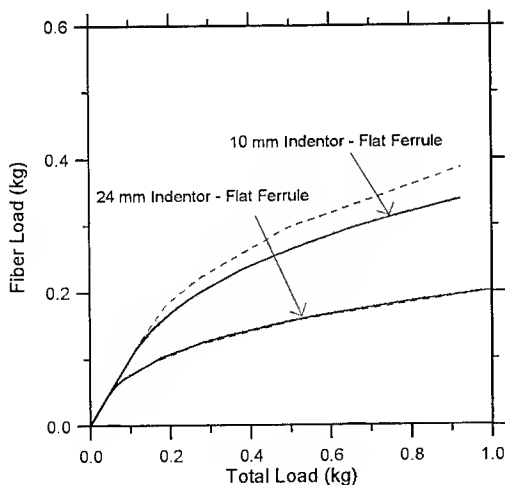


Figure 2. Fiber load for various mating configurations. The shaded area represents typical loading forces in mated connectors. For our experiments we used 10 and 24 mm radiussed indentors mated to flat-ended ferrule assemblies.

assemblies used in our tests. The ferrule assemblies are assumed to have fibers polished flush to the flat surface. For the 24 mm radiussed indenter, the estimated load the fibers will experience under test are almost identical to the actual loading forces expected for mated connectors with 30 mm radii. For the 10 mm radiussed indenter, the estimated fiber loads are greater, but still well within the range expected for mated connectors. Our experiments therefore provide realistic simulations of fiber loading forces in actual connectors.

2.2 Ferrule Assembly

Complete connector plug assemblies were simulated by using 10.5 mm-long zirconia ceramic ferrules. The ferrules had nominal dimensions of 2.5 mm O.D. and 126 μm I.D. Ferrule assemblies were fabricated using the same techniques and procedures as for field-installable connectors. Commercial fibers were epoxied into the ferrules using cure schedules recommended by the epoxy manufacturers. After the epoxy cured, the fiber was cleaved and the ferrule assembly endface was polished until the fiber was approximately flush with the flat endface of the ferrule.

Ferrules were assembled using four different types of epoxy. For epoxies with short cure schedules, the time in the oven was increased to ensure that the samples were at the proper temperature over the full curing time. Five ferrule assemblies were prepared using each type of epoxy. Four of each type were put on test under load.

An additional set of ferrule assemblies was fabricated to determine the effect of the fiber cleaning procedure on fiber pushback. Three ferrule assemblies were prepared using a typical procedure in which the fiber was cleaned with an alcohol-wetted, lint-free cloth. Four other ferrule assemblies were prepared using fibers that were cleaned by wiping with the fingers, which might be expected to leave behind an oily residue.

2.3 Data Collection

The initial position of the fiber with respect to the ferrule was measured immediately before putting the ferrule assemblies on test. A contact profilometer with an accuracy of $\pm 0.02 \mu\text{m}$ was used to make a single-line scan across the center of each ferrule. The calibration of the profilometer was checked on a weekly basis.

The ferrule assemblies were then placed under load, first for at least a week at ambient conditions, and then at 65 °C for approximately four weeks. The assemblies were then placed under load at 65 °C/95 % relative humidity (RH) for three more weeks. The assemblies were removed from test at intervals throughout the testing period and allowed to return to ambient conditions. The loads were then removed and the fiber position with respect to the ferrule remeasured to determine the amount of fiber pushback.

2.4 Epoxy Characterization

When the ferrule assemblies were placed in the curing oven, 5-10 mg samples of the epoxy were also cured in small pans. These epoxy samples were later analyzed by differential scanning calorimetry (DSC) to determine their level of cure and effective glass transition temperature, T_g .¹ In the DSC analysis, samples were heated from -30 °C to 200 °C at a rate of 10 °C/min.

The epoxy adhesives used in fiber optic connectors may relax under mechanical loads when exposed to temperatures close to their T_g . Under constant mechanical stress, they tend to creep (deform), and this tendency can be expressed as creep compliance (deformation or creep strain divided by constant stress). Although the adhesive film in a ferrule may be under a complex deformation condition, it is customary and convenient to measure creep compliance in tension. Therefore, epoxy samples were also separately prepared in films 400-800 μm thick, 10 mm wide, and 10 mm long, using the same cure schedules as the ferrule assemblies. These samples were subjected to dynamic mechanical analysis using a dynamic mechanical thermal analyzer (DMTA).⁵ The analysis provided creep compliance values at 65 °C as well as an independent measure of the epoxy T_g . To measure T_g , the samples were scanned at 1 and 10 Hz from -50 °C to 125 °C at 2 °C/min.

3. RESULTS

3.1. Epoxy Properties

Table I gives the results of the T_g measurements from DSC and DMTA scans for the epoxies used in our experiments.

TABLE I. T_g for Fully Cured Epoxies Used in Fiber Pushback Experiments

EPOXY TYPE	T_g (°C)(DSC)	T_g (°C)(DMTA)
1	62	59
2	90	84
3	100	93
4	120	115

Both the DSC and DMTA measurements give the same rank ordering of T_g for the four epoxies. This suggests that the amount of creep, and therefore fiber pushback, will decrease for Epoxies 1, 2, 3, and 4, in that order. We expect creep compliance to be inversely correlated to the epoxy T_g , and in fact, the creep compliance ranged from a high of 0.24 MPa^{-1} for Epoxy 1 to a low of 0.04 MPa^{-1} for Epoxy 4.

3.2 Fiber Pushback

Figure 3 shows, the fiber pushback for Epoxies 1, 2, and 3 (dashed, solid, and bold lines, respectively) at 25 °C (Days 0-11) and 65 °C (Days 12-34). All ferrule assemblies were mated against 24 mm radiussed indentors. At 25 °C all epoxies performed well and the fibers experienced very little pushback. At 65 °C, however, there were clear differences in the performance between different epoxies. Epoxy 1, with the lowest T_g , showed the most fiber pushback, consistent with our earlier findings. The fibers were pushed back close to the maximum amount possible, which is $\approx 0.15 \mu\text{m}$ recess with respect to the ferrule.² Epoxy 3 had good performance; the fibers were pushed back to $\approx 0.04 \mu\text{m}$. Epoxy 2 showed mixed results. On average, however, the fiber was pushed back to $\approx 0.08 \mu\text{m}$ recess. Ferrules assembled using Epoxy 4 (the highest T_g epoxy) initially had slightly protruding fibers, and the fibers were still protruding by $\approx 0.02 \mu\text{m}$ after exposure to 65 °C. The total amount of pushback in this case was only $\approx 0.03 \mu\text{m}$.

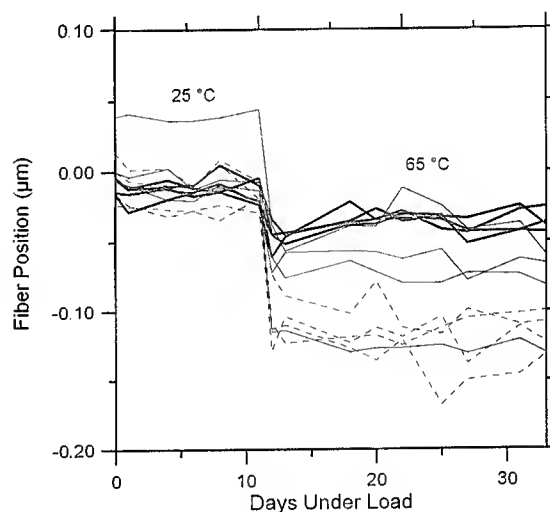


Figure 3. Fiber pushback for three different epoxies: Epoxy 1 (dashed), Epoxy 2 (solid), and Epoxy 3 (bold).

Results of preliminary tests on Epoxy 4 at 95 % RH, shown in Figure 4, indicate that fiber pushback can increase when the epoxy is exposed to high humidity levels. The change in fiber pushback is shown here when the RH is increased to 95 % for ferrule assemblies loaded with 10 mm radiussed indentors.

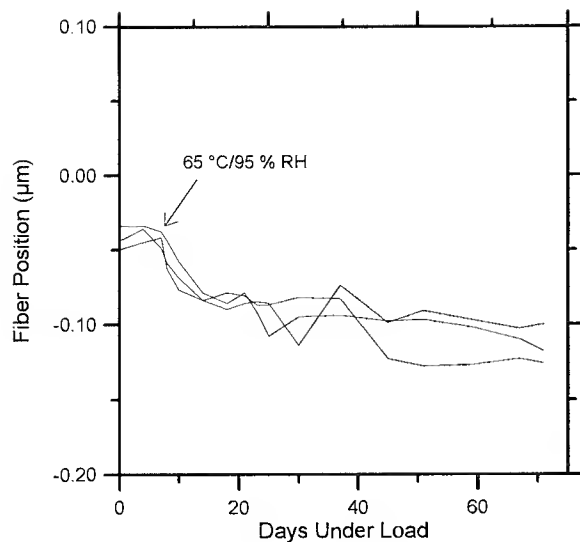


Figure 4. Increased fiber pushback for Epoxy 4 after exposure to 95 % RH.

Ferrule assemblies using epoxies 1, 2, and 3 were loaded with 24 mm radiussed indentors and exposed to 65 °C/95 % RH. There was no additional fiber pushback due to high humidity exposure for epoxies 1, 2 and 3 after a four week exposure.

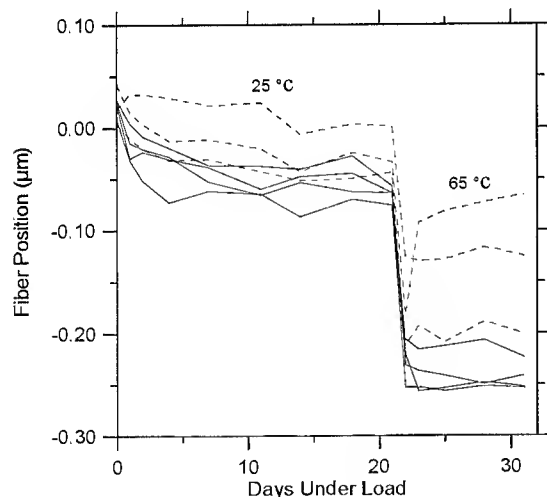


Figure 5. Fiber pushback for fibers cleaned using an alcohol wipe (dashed lines) and using a finger wipe (solid lines) in the ferrule assembly process.

Finally, Figure 5 compares the fiber pushback for ferrule assemblies in which the fiber was cleaned using a typical alcohol wipe procedure (dashed lines) with ferrule assemblies in which the fiber was cleaned by a finger wipe (solid lines). The ferrule assemblies were mated against 10 mm radiussed indentors. Clearly, inadequately cleaned fibers do experience a greater amount of fiber pushback than those cleaned with the standard technique.

4. CONCLUSIONS

It is our hypothesis that each epoxy can support some minimum load below which the fiber pushback will be negligibly small. The minimum load will depend on epoxy properties such as T_g , adhesion, and cohesive strength. In previous work we have noted a strong dependence of fiber pushback on T_g . The present work supports the earlier conclusion that it is important to use an epoxy whose T_g is well above the operating temperature range of the connector. In these experiments, the ability of the epoxy to prevent fiber pushback was directly correlated to the epoxy T_g . If fibers become recessed more than about 0.10 μm , physical contact of the fiber cores becomes marginal, and can result in large reflectances.^{2,3} For example, ferrule assemblies using Epoxy 1 had unacceptably large fiber pushback when loaded at 65 °C. This epoxy had a $T_g < 65$ °C, which is within the operating range of the outside plant environment.⁶ Current Bellcore Generic Requirements for optical connectors call for an epoxy T_g for a fully cured epoxy, measured using a DSC analysis, to be ≥ 95 °C.⁷

Additional fiber pushback after exposure to high humidity occurred for one epoxy (Epoxy 4) that we tested. Epoxy 1 showed no additional pushback, but the fibers had already been pushed back into the ferrules to approximately the maximum possible recess. Therefore no further pushback was possible. Epoxies 2 and 3 showed little change after exposure to high humidity over a four week period. Therefore, high humidity will not necessarily result in fiber pushback for appropriately-chosen connector epoxies. Some epoxy chemistries will be more susceptible to high humidities, and the determination of epoxy types that are most resistant is important. More testing also needs to be done to determine whether or not there are short-term reliability problems (e.g., only in certain temperature ranges), or non-epoxy related reliability problems.

Finally, fiber pushback was measured for ferrule assemblies using fibers cleaned with an alcohol wipe compared with ferrule assemblies in which the fibers were finger wiped. Those fibers cleaned by finger wiping experienced more fiber pushback, and point to the necessity of cleanliness in the connector assembly process. The additional fiber pushback is likely caused by lack of good adhesion at the fiber/epoxy interface.

5. ACKNOWLEDGMENTS

We would like to thank Chris Burpee for completing many of the fiber pushback measurements in these experiments.

6. REFERENCES

1. L.A. Reith, R.A. Frantz, I.M. Plitz, and W.W. Wood, "Fiber Withdrawal in Ceramic-Ferrule Optical Connectors," *Proc. of the 42nd IWCS*, St. Louis, MO, Nov. 15-18, pp. 256-264, 1993.
2. L.A. Reith, P.B. Grimado, R.A. Frantz, I.M. Plitz, W.W. Wood, and D.A. Dolinoy, "Effects of Fiber Pushback in Ceramic-Ferrule Connectors on Connector Intermateability," *Proc. of the 10th Annual NFOEC*, Vol. 3, San Diego, CA, June 12-16, pp. 225-240, 1994.
3. R. Ziebol, H. Roberts, and B. Daniel, "Permanent Fiber Withdrawal in Fiber Optic Connectors," *Proc. of the 8th Annual NFOEC*, Washington, DC, Vol. I, pp. 211-230, April, 1992.
4. T. Shintaku, E. Sugita, and R. Nagase, "Highly Stable Physical-Contact Optical Fiber Connectors with Spherical Convex Ends," *J. Lightwave Tech.*, vol. 11, pp. 241-248, 1993.
5. I.M. Plitz, O.S. Gebizlioglu, and M.P. Dugan, "Reliability Characterization of Adhesives Used in Passive Optical Components," *SPIE Proc.*, Vol. 2074, Boston, MA, Sept. 8-10, pp. 288-299, 1993.
6. T.N. Bowmer, R.J. Miner, and R.L. Coker, "Field Temperature in Outside Plant," *Proc. of the 39th IWCS*, Reno, NV, Nov. 13-15, pp. 335-342, 1990.
7. Bellcore, "Generic Requirements for Optical Fiber Connectors," TA-NWT-000326, Issue 4, December, 1993.



Leslie A. Reith received a BA degree from New York University in 1975, the M.Phil. degree from the City University of New York in 1979, and the Ph.D. degree from The University of Texas at Austin in 1981, all in physics. In 1981 she joined AT&T Bell Laboratories as a Member of Technical Staff. In 1984 she subsequently joined Bellcore, where she is presently a member of the Fiber Media and Component Reliability Group in Morristown, NJ. Her research at Bellcore is primarily concerned with reliability issues related to optical splices and connectors.



Rolf A. Frantz is a Distinguished Member of Technical Staff in the Fiber Media and Component Reliability Group at Bellcore. He holds BS and MEng degrees from Cornell University and received his PhD at Brown University. He spent eleven years at Bell Laboratories, working principally on applications problems of dielectric materials, and he continued working in this area when he came to Bellcore in 1983. Since 1988, he has been concerned with the applications and reliability problems of fiber coatings, adhesives, coloring inks, gels, and related materials used in manufacturing optical fibers, cables, connectors, and splices.

Philip B. Grimado received the BS degree in civil engineering from the City University of New York and the MS and PhD degrees in applied mechanics from Columbia University, New York, in 1962 and 1968, respectively. He joined Bell Laboratories in 1968 where his responsibilities included vulnerability studies of antiballistic missile systems, fire protection studies involving fire-risk analyses, heat transfer calculations, development of standard fire testing methods for telephone company equipment and development of algorithms for optimum control of building environmental equipment. Since 1983, he has been with Bellcore, engaged in outside plant activities concerned with fiber optic cable placement, damage assessment, and fiber optic cable and optical fiber stress analyses.



Irene M. Plitz is a Member of Technical Staff in the Metals and Plastics Technology Group at Bellcore. She graduated from Morgan State University in 1970 with a BS degree in chemistry and then joined AT&T Bell Laboratories. Since becoming part of Bellcore in 1983, her interests have centered around the degradation, characterization, and reliability of polymeric materials used in the telecommunications industry.



Osman S. Gebizlioglu is a Member of Technical Staff in the Metal and Plastics Technology Group at Bellcore. He holds BSc and MSc degrees in Chemical Engineering from the Middle East Technical University in Ankara, Turkey. After receiving his PhD in the Polymer Materials Program of the Chemical Engineering Department at Princeton University, he did postdoctoral research as a Monsanto Fellow in the Department of Mechanical Engineering at MIT. Since he joined Bellcore in 1987, he has conducted research on the mechanical reliability of polymeric materials in fiber optic cables, devices, and connectors.

RELIABILITY OF OPTICAL FIBER CABLES FOR NEW CONNECTOR SYSTEMS

J.R. Holman, A.C. Jenkins, N.T. Subh, and R. Travieso

AT&T Bell Laboratories
2000 N.E. Expressway
Norcross, Georgia 30071

ABSTRACT

New optical fiber connectors have been developed that are more robust and easier to use. Many of these connector systems employ pull-proof cable-retention mechanisms that maintain the optical performance when axial and side loads are applied to the fiber-optic cable. The improved performance of pull-proof connectors must be balanced with a reliable connector and cable design to avoid failures resulting from undesirable permanent bending stresses. Upon mating, the ferrule assembly travels with respect to the cable jacket and strength members, resulting in excess fiber length within the cable assembly. This excess buffered fiber length will either bend within the connector or be forced back into the cable. The extent of bending depends on the connector design as well as the mechanical and physical properties of the buffered fiber and cable. Single and duplex cables were designed to meet the requirements of pull-proof connectors by allowing free movement of the buffered fiber into the cable's core when connectors are mated. The designs are more robust and pass both cable and connector requirements.

PULL-PROOF CONNECTORS

Bellcore's^[1] generic requirements of optical fiber connectors include active tension tests that require the use of pull-proof cable-retention mechanisms. The required travel for the ferrule assembly results in excess buffered fiber length within the cable assembly. Bent-fiber configurations for pull-proof connectors have been estimated using elastic buckling analysis. Calculations indicate that bending stresses in excess of 100 ksi may be produced if the buckling is confined to the connector. To reduce the fiber stress, it is desirable that the displaced buffered fiber segment move into the cable upon connector mating. Therefore, complimentary improvements in the optical-fiber connector and cable designs were required.

The SC connector employs a simple push-pull latching mechanism (Figure 1). Connector plugs may be yoked together with a duplex clip for duplex applications and the connector is easily tunable providing lowest insertion losses. The pull-proof ST® connector features a positively locking ramped bayonet latch. Each of these connector systems employ pull-proof cable-retention mechanisms that maintain the optical performance when axial and side loads are applied to the fiber optic cable. In pull-proof connectors, the cable jacket and strength members are isolated from the ferrule assembly. Upon mating, the ferrule assembly travels, resulting in an excess fiber length within the cable assembly.

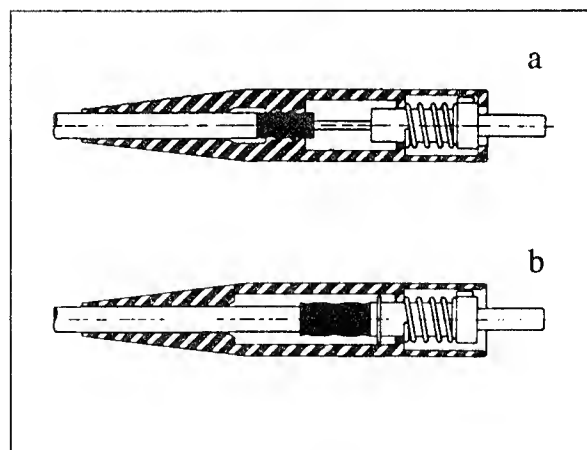


Figure 1 : Comparison of Connectors (a) Pull-Proof
(b) Not Pull-Proof

CONNECTOR RELIABILITY

The pull-proof connectors have passed a variety of optical, mechanical, and environmental tests. Additional work was undertaken to ensure the long-term reliability of these connector systems. The connector housing contains a channel wherein the buffered fiber

has only limited confinement. Upon the mating of two connectors, the ferrule is displaced some distance which provides a corresponding displacement of the buffered fiber in the channel. An undesirable stress state may occur during the installation of a pull - proof connector . The excess buffered fiber will either bend within the connector or be forced back into the cable. The extent to which bending occurs depends on the connector design as well as the mechanical and physical properties of the buffered fiber and cable.

Bent-fiber configurations for pull-proof connectors have been estimated by King using elastic buckling analysis^[2]. Figure 2 shows a representation of the limiting case where the buffered fiber is fixed on the end near the interconnection cable and all of the deformation takes place in the channel. King has developed a closed-form solution to these bent-fiber configurations for $w < g$ and for finite-length contact at the wall. The maximum curvature and corresponding stress in the bent fiber was determined.

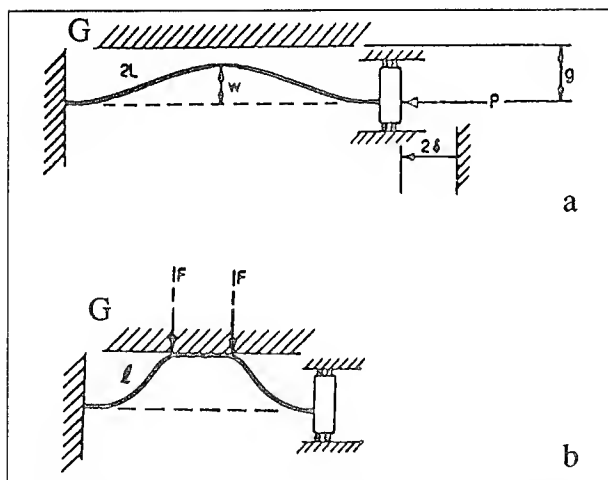


Figure 2: Limiting Case of Fiber Bent within Housing for (a) $w < g$ and (b) contact at G

The model assumes that the fiber is uniform, linearly elastic, and sufficiently slender that the bending moment is proportional to curvature of the inextensible centerline. Thus the underlying model is that of the classical elastica. King has proven that for a clamped fiber where the fiber is not restrained by the surface G as shown in Figure 2a , the curvature ($1/R$) is

$$1/R = 2\pi\sqrt{\delta/l^3}.$$

The stress σ in the fiber is then computed as

$$\sigma = Er/R,$$

where

E is the modulus of the glass fiber (10^7 psi ; 68,800 Mpa), r is the radius of the glass fiber (.0025 in.; 0.064 mm), and R is the radius of curvature.

The graph shown in Figure 3 shows how stress varies with ferrule displacement 2δ for a fixed channel length $2l$. Results show that substantial stresses are produced for slight displacements.

King has also developed a solution for the condition where the buckled fiber is constrained by a wall G as shown in Figure 2b. For this case, the maximum curvature is given by

$$1/R = (32\pi/9)\delta^2/g^3$$

Once again, the stress σ in the fiber is given by

$$\sigma = Er/R.$$

Proof-test levels of fibers are typically 100,000 psi (688 MPa) or less. Long-term stresses are normally kept to a fraction of the proof-test level to ensure that the connector will meet its intended life.

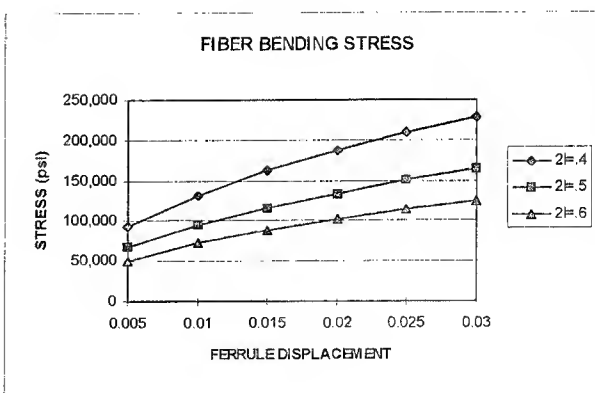


Figure 3 : Variation of Stress With Ferrule Displacement 2δ (No confining wall $w < g$)

For a typical SC connector, $2\delta = .015$ in. (.38 mm), $2l = 0.50$ in. (12.7 mm), and $g = .045$ in. (1.14 mm). For this case, there is no contact at the wall ($w < g$). The maximum stress level for this "typical" SC connector is

located at the clamped ends and at the midpoint of the span and is approximately 108,800 psi (749 MPa).

A typical SC connector with maximum ferrule displacement $2\delta = 0.024$ in. (0.61 mm) would result in a case where the fiber is constrained by the wall G. This case results in maximum bending stresses as high as 440,000 psi (3027 MPa).

CABLE ASSEMBLY

Figure 2 shows an extreme case of fiber deformation. The amount of fiber deformation is a function of buffer type, and cable design. A representation of an interconnection cable design is shown in Figure 4. The buffered fiber is the core of the interconnection cable design. It has an industry standard 0.035 in. (0.89 mm) outer diameter. The buffer is surrounded by a soft layer of aramid yarn which serves as a buffer from mechanical loads and provides the tensile strength of the cable. An outer jacket is extruded over the core.

Mathis et al [3] performed an analysis on this design and determined that the following relationship can be employed to explain the interaction of the assembly components.

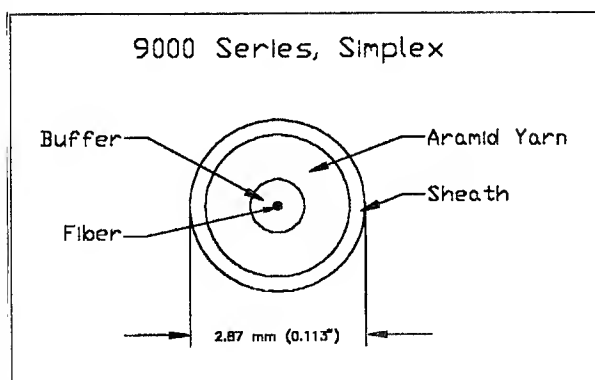


Figure 4 : Interconnection Cable

$$EI' = \frac{P_r(2l)^2 \mu A}{4\pi^2}$$

EI' is the minimum flexural rigidity of the buffered fiber at which it can be pushed into the jacket. μ and P_r are dependent on the physical properties of the buffered fiber and cable, respectively. The coefficient of friction

between the aramid yarns and the buffer jacket is defined by μ and P_r is the radial pressure exerted on the buffered fiber by the aramid yarns and outer jacket. A is the surface area of the buffered fiber in the jacket. $2l$ is the length of the buffered fiber in the channel.

When load is applied to the ferrule, two cases are possible depending on the physical make up of the interconnection cable. The first is similar to that shown in Figure 2. The force to buckle the buffered fiber is less than the force to slide the buffered fiber into cable. This occurs when the buffered fiber has a low flexural rigidity, the cable is too tight, or the coefficient of friction is high between the buffer and the aramid yarns. There are designs on the market that would produce this response. The second case occurs when the buffered fiber slides into the jacket. This is possible with a stiff buffer (higher flexural rigidity), looser core and lower friction between the buffer and the aramid yarn. Of course, the latter gives the lowest stress levels and therefore would provide a more reliable connector.

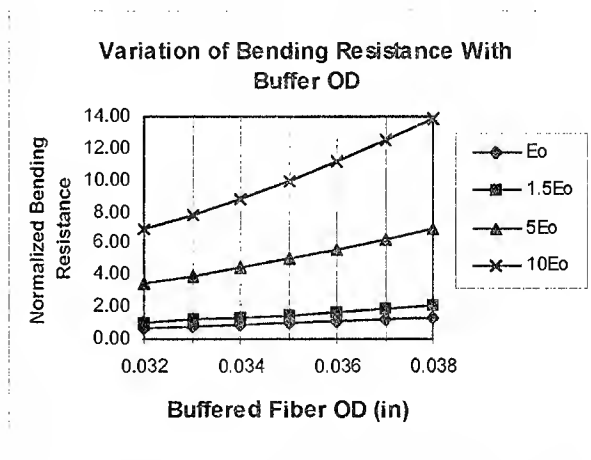


Figure 5: Variation of Bending Resistance With Buffer OD and Modulus

A design falling in the first case should be redesigned to reduce potentially life-shortening stress levels. Several changes are possible including employing a higher modulus buffer and decreasing the tightness of the core. There are several commercially available materials on the market to improve modulus. The tightness of the jacket can be controlled using proprietary process conditions and materials. The flexural rigidity of a buffered fiber can be increased by either increasing the modulus or the diameter. Figure 5 shows how the bending resistance of a buffered fiber can be increased or decreased by changing the jacket modulus and buffer diameter. The graph shows how the resistance to

bending varies over an allowable buffer diameter of 0.035 ± 0.002 in. ($0.89 \text{ mm} \pm 0.05 \text{ mm}$). The interconnection cable should be designed to work over this range.

QUANTITATIVE ANALYSIS

Quantitative analysis is required to determine if a cable assembly adequately addresses these questions. Apparatus was developed to determine the buckling resistance of various buffered fibers and the push-in resistance of various cable designs. The goal was to ensure that in any design, the force to buckle the free length of buffered fiber behind the ferrule was greater than the force to push the buffered fiber into the cable jacket. Figure 6 shows a representation of the buckling apparatus. The apparatus was designed to determine the relative differences of the various buffer designs evaluated. A buffered fiber is placed in the apparatus which has a 0.5 inch (12.7 mm) free space and a load is slowly applied and recorded until the buffered fiber buckles. The load recorded indicates the critical buckling load of the fiber.

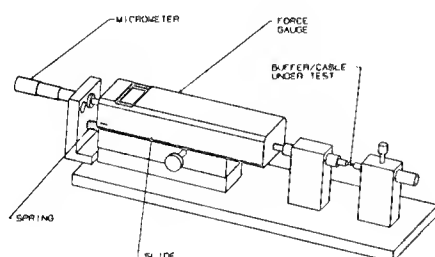


Figure 6: Representation of Apparatus to Measure Force to Buckle Buffered Fiber

The push-in test was developed employing the same apparatus to determine the amount of load required to push a 0.5 in. (12.7 mm) section of buffered fiber into the cable for a distance of 0.050 in. (1.27 mm). A cable of length of 18 inches (0.46 m) is tied in a knot at one end (simulates remote mechanical coupling) and then stripped back to expose the buffered fiber at the other end. The test is performed by inserting the buffered fiber in the buckling apparatus such that approximately 0.5 in. (12.7 mm) is exposed. Turning the micrometer causes the fiber to move. The buffered fiber will either buckle or move into the cable. The maximum load is measured employing the force gauge. The value of this test is that it allows the operators on the cabling line to

determine immediately the cable quality. Any significant variations in the process are sensed by the device.

A third test was also developed to determine the tightness of the cable structure. The test is particularly important when testing a design which contains a buffered fiber with low flexural rigidity. The goal was to develop a structure that is loose enough to permit the sliding of the buffered fiber, yet sufficiently tight to retain sufficient dimensional integrity for connectorization. The pull-out test was developed using a tensile testing machine. A sample was prepared by cutting an 18 in. (0.46 m) sample of cable with one inch of buffered fiber exposed. The jacket and yarn were clamped on one end of the sample and the buffered fiber on the other. The load was recorded as the sample was pulled. The load recorded should also indicate the amount of force required to push the buffered fiber into the cable.

Figure 7 shows the results on four different interconnection cable designs. Designs A, B, and C contain nylon buffered fibers. Design D contains a PVC buffered fiber. The push-in force could not be determined for Design D due to the low flexural rigidity of the PVC buffered fiber. It is clear that the designs containing the nylon buffered fiber did very well in meeting the requirement that the force to buckle the buffered fiber be greater than the force to push the buffered fiber into the cable.

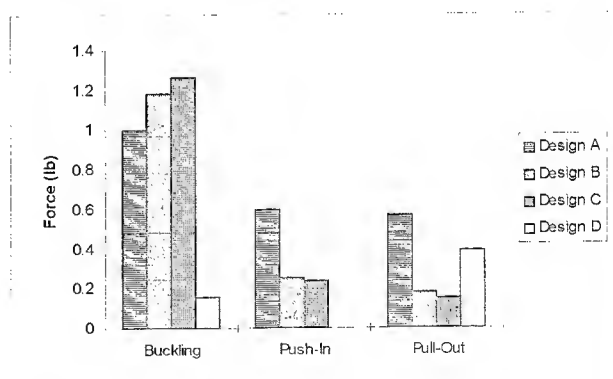


Figure 7: Quantitative Results on Four Cable Designs

CABLE QUALIFICATION

Figure 8 shows a duplex cable designed for use with the pull-proof connectors. The duplex design contains two single-fiber cable designs. Each single-fiber design

has a nylon-buffered fiber, sufficiently tight core, and flexible PVC jacket. The duplex design was developed by choosing proper tooling, processing conditions and aramid yarn content that provides low-friction single-fiber cordage surrounded by a PVC jacket. The cables were measured for loss after processing, then submitted to mechanical, environmental, and safety tests. The cable passed all mechanical and environmental tests as specified by TR-NWT-000409. In addition, the cable passed the UL 1666 riser fire test and the FT4 riser fire test. Table I contains some of the test results for TR-NWT-000409 for the single-mode cable at 1550 nm wavelength transmission.

These designs although developed for the pull-proof connectors can be employed with most connector designs on the market.

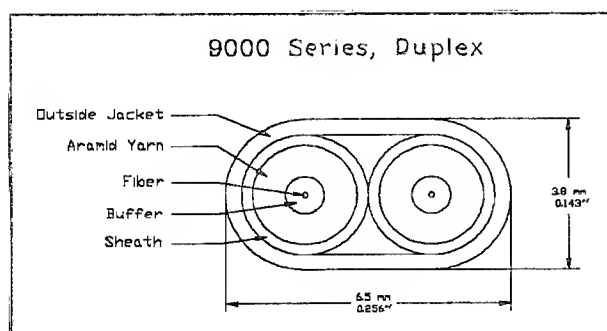


Figure 8: Interconnection Cable Design for Pull-Proof Connectors

CONCLUSION

When employing pull-proof connector designs, one must consider the reliability of the assembly. A properly designed cordage product must be employed to ensure the reliability of the cable assembly due to potentially high bending stresses resulting from ferrule displacement. The design must also be sensitive to human factors to ensure that performance features are not achieved at the expense of a user-friendly, easy-to-strip buffered fiber, and flexible cable. Apparatus has been designed and tests developed to determine a cordage design's compatibility and reliability with pull-proof connectors. The design also works with other connector designs including biconic, ST-compatible, SMA, D4, BNC, or DIN. The design functions in a

single or duplex configuration. The cables passed a complete battery of tests.

REFERENCES

- (1) TR-NWT-000326, Generic Requirements of Optical Fiber Connectors, Issue 3 (Bellcore, June 1992)
- (2) W. King: Displacement-Limited Buckling of an Optical Fiber, Journal of Electronic Packaging, Vol 115, March 1993, p. 39
- (3) D. Mathis, M. Viriyayuthakorn, J. Holman, L. Graham, R. Reagan: Miniature Optical Fiber Cables For Jumper Applications, November 1994, International Wire and Cable Symposium



Artis C. Jenkins is a Distinguished Member of Technical Staff in the Fiber Optic Cable, Materials Development and Engineering Department at AT&T Bell Laboratories in Norcross, Georgia. He is responsible for the development of Fiber Optic Premises Cable products.

Dr. Jenkins joined AT&T Bell Laboratories in 1980. He has a B.S. degree in Mechanical Engineering from North Carolina State University and a M.S. and Ph.D. in Mechanical Engineering from the Georgia Institute of Technology.

He has been granted two patents.



Jim Holman is a Senior Development Engineer in the Fiber Optic Cable, Materials Development and Engineering Department at AT&T in Norcross, Georgia. He is responsible for the development of manufacturing processes for Fiber Optic Premises Cable products.

Mr. Holman began his career with AT&T Bell Laboratories in 1966 and later transferred to Network Cable Systems. He has a B.S. degree in Electrical Engineering from the Georgia Institute of Technology.

He has been granted three patents with one pending.



Naif T. Subh is a Member of Technical Staff in the Fiber Optic Apparatus Department at AT&T in Norcross, Georgia. He is responsible for the development of manufacturing processes for Fiber Optic Connector products.

Mr. Subh began his career with AT&T Bell Laboratories in 1969 and later transferred to Network Cable Systems. He has a B.S. degree in Electrical Engineering from the Georgia Institute of Technology.

He has been granted 3 patents.



Ruben Travieso is a Member of Technical Staff in the Fiber Optic Apparatus Department at AT&T Bell Laboratories in Norcross, Georgia. He is responsible for the development of Fiber Optic Connector Products

Mr. Travieso joined AT&T Bell Laboratories in 1986. He has a B.S. degree in Mechanical Engineering from the Georgia Institute of Technology and a M.S. in Mechanical Engineering from Stanford University.

He has been granted four patents.

Table I
Qualification Results
 (Single mode , 1550 nm)

TEST	CRITERIA	MAXIMUM LOSS (dB)
IMPACT FOTP-25A , IEC 794-I-E4	δ loss < 0.20 dB .54ft-lb; 20 cycles	.00
COMPRESSIVE (CRUSH) STRENGTH FOTP-41 , IEC-794-I-E3	δ loss < 0.20 dB 20 lb/in	.00
TENSILE LOAD/BEND FOTP-33A , IEC-794-I-E1	δ loss < 0.20 dB 350 lb	.01
CABLE TWIST (TORSION) FOTP-85 , IEC-794-I-E7	δ loss < 0.20 dB	.00
CYCLIC FLEXING FOTP-104 , IEC-794-I-E6	δ loss < 0.20 dB	.00
TEMPERATURE CYCLING THERMAL AGING	δ loss < 0.30 dB 0° C to 50° C	.01 before aging .20 after aging
HIGH / LOW TEMPERATURE BENDING FOTP-37 , IEC-794-I-E11	δ loss < 0.20 dB 50° C / 0° C	.05 / .06

A "UNIVERSAL" BUILDOUT SYSTEM FOR FIBER-OPTIC CONNECTIONS

*W.W. King, B.G. LeFevre, D.L. Stephenson,
C. Gonzalez, S.C. Perry*

AT&T Bell Laboratories
Norcross, Ga. 30071, USA

ABSTRACT

Reported here is the development of a family of coupling products that accommodates FC, SC, and ST fiber-optic connections. The key attribute is that, with access available to only one side of an optical interface, the connector type employed on that side can be changed easily as can be the level of attenuation when the attenuator form of the system is employed.

Except for standard ceramic alignment sleeves, components are composed of injection-molded plastic parts fastened together by mechanical latches so that neither adhesive nor ultrasonic bonding is needed in the manufacturing process. Because a coupling here comprises a "buildout" and a "block", only loosely joined, and because individual parts are plastic, testing has focused on environmental performance and on response to mechanical loading. Test results indicate apparent absence of any environmental problem. Mechanical strength and stiffness are generally consistent with Bellcore specifications, and exceptions are noted.

INTRODUCTION

Currently, the most popular singlemode fiber-optic connectors, FC, SC, and ST, are all based on 2.5 mm alignment ferrules into which fibers are bonded.^{1,2,3} This commonality, and that of the corresponding alignment sleeves, facilitates coupling these otherwise dissimilar connectors. Consequently, a number of manufacturers include hybrid couplings (adapters) in their product lines. This paper deals with components that allows formation of such adapters with great flexibility.

The capability for mixed or matched connections is of particular importance when a connection is to be made at the faceplate of a transmitter or receiver. Then a manufacturer can standardize on a single connector to be mounted inside a circuit pack, while at the same time offering a customer the choice, from among several types of connector to be mounted externally. The manufacturer reaps the benefits of standardization, and the customer is relieved

of any need for hybrid jumpers. An important additional level of flexibility is acquired by using a "buildout system". There, a "block", permanently mounted in a faceplate, serves as the inside-connector port. A detachable "buildout" serves as the outside-connector port, and there is one buildout for each of the connector types. A buildout must be easily engaged into (or disengaged from) a block so as to facilitate the formation of one of several hybrid couplings. This allows a connector type to be changed without accessing the interior of a transmitter/receiver package. In Fig. 1 is depicted a faceplate for which the two internal connectors are ST, and the outside is one FC and one SC.

A second application, in which the flexibility of a buildout system is apparent, is that of preterminated shelves. Here all the fibers in a relatively short section of cable are connectorized at one end, and the connectors are plugged into panel-mounted adapters in a cabinet-like panel-mounted housing. This factory-assembled package is then shipped to its point of application, where the cable is spliced and where jumper interconnections can be made at the adapters. By installing the blocks of a buildout system in the panels, as illustrated in Fig. 2, cable connectorization can take place without restricting the end-user's choice of jumpers. This is particularly useful at the present time when each of the three principal connector types has its technical advocates.

Alignment sleeves could be mounted either in blocks or in buildouts, and arguments can be made for each of the alternatives. However, a particularly compelling reason for using buildouts is the possibility of mounting attenuator elements in the alignment sleeves. These buildout attenuators can be formed, and attenuation can be changed by removing only one of the two connectors, and requiring access to only one side of a panel (or faceplate).

Most of the attributes ascribed to a buildout coupling system have been available in a family of products offered for several years by AT&T Network Systems. Their development predated the rising popularity of the SC connector in the United States and was motivated principally by the needs of AT&T Transmission Systems. Consequently, there was developed only an ST block and only ST and FC buildouts. The present paper reports the

design of a second-generation family that accommodates the SC connector and, as will be seen, falls only one short of all possible interconnections amongst FC, SC and ST connectors.

DESIGN

Objectives and Constraints

The rather narrow need for an ST-to-SC buildout coupling would have been met by design of an SC buildout to interface with the already existing ST block mentioned earlier. However, the geometry and dimensions of an SC coupling are incompatible with those of that ST-ST/FC system, which is based on the cylindricity of the ST and FC connectors (and couplings). The problem here is the rectangularity of the SC connector system. To satisfy the need for maximum flexibility in transmission equipment, as illustrated in Fig. 1, an ST block, to be coupled with any one of FC, SC, and ST buildouts, was sought. In light of the increasing popularity of SC connectors, an SC block was also sought. The resulting family of products is shown in Fig. 3. Notably missing is an FC block, and so FC-to-FC connections are not possible. The absence of this element is somewhat a reflection of the declining popularity of the FC connector, it being the precursor of the SC in the family of NTT-designed connectors. More important, though, is a geometric compatibility problem which will be discussed later.

Significant constraints and objectives of the design process were:

1. Conformance to existing geometric standards for FC, SC and ST couplings.
2. Use of standard components when possible - in particular the same ceramic alignment sleeves commonly used with these connectors.
3. Accommodate space available on AT&T transmission faceplates - "double-D" hole mounting of ST block.
4. Accommodate one-half-inch spacing of connector centerlined for panel applications.
5. Satisfy performance specifications of Bellcore TR-NWT-000326, Generic Requirements for Optical Fiber Connectors.⁴
6. Attachment (detachment) of buildouts of (from) blocks without special tools.
7. Accommodate AT&T sleeve-mounted attenuator elements.⁵
8. Low cost!

Satisfaction of Item 7 means that Fig. 3 not only depicts a family of buildout couplings but three families of attenuators - 5, 7, 10, 15 and 20 dB in each of the buildouts.

Functional Features

Referring to Fig. 3, as a buildout is fixed to a block a cylindrical portion, containing the alignment sleeve, is inserted into a circular hole in the block. Behind that hole is the ferrule of the block-side connector. So the sleeve, surrounded by this "sleeve holder", accepts that ferrule as the buildout is advanced into place. The ferrule in an ST connector extends about 0.8 mm beyond the connector body; this in the case of an ST block, enough unrestricted ferrule is available for insertion into the buildout sleeve regardless of fine details of the sleeve-holder part. The situation is quite different for the SC connector, where the ferrule is mostly surrounded by the connector body, and the annular gap between them provides part of the nested-cylinders alignment structure associated with that connector and its standard adapter. This severely restricts the outside diameter of the sleeve holder in each of the buildouts. A similar structure, but with different dimensions, is found in the standard FC connector/adapter system. These differences probably relate to the facts that the earlier designed FC has a machined metal adapter and the relevant part of the SC adapter is molded plastic. In any event, the decision here to use molded plastic parts and the consequent minimum wall thicknesses along with a functional need for snug fit rendered the development of an FC block not feasible.

Retention of a buildout in a block is accomplished by wedge-like stops on the parallel walls of the blocks (see Fig. 3). Part of a buildout body is caused to be trapped between these stops and the body of a block. The stops, once final engagement is effected, prevent axial motion of the buildout relative to the block. Attachment is achieved in two steps: first the buildout, with orientation about 15 counterclockwise of final position, is advanced into flush contact with the blocks; second the buildout is rotated into final position where its orientation is maintained by a locking beam, which can be seen on the side of each of the buildouts of Fig. 3. Disengagement is effected by depressing the locking beam and reversing the steps above. These kinematics are illustrated in Fig. 4.

Design for Manufacturing

The inherent geometric complexity, primarily driven by the SC's rectangularity, taken together with the deformation required of the locking beam and the need for low cost have dictated that components, other than the alignment sleeve, be injection-molded plastic. The material chosen was polysulfane with 20 percent glass-fiber filler.

A characteristic of the design is that neither adhesive nor ultrasonic bonding is needed in the manufacturing process. All joining of plastic parts is done by mechanical latches. Fig. 5 illustrates the ease of assembly of an ST buildout attenuator. An attenuator element is mounted in a sleeve, the sleeve is dropped into the housing, and then

the sleeve retainer is snapped in place. Similarly, the FC buildout is, excepting attenuator, sleeve and sleeve retainer, a plastic part.

The SC buildout is one-part more complicated than either of the others. Because of the internal latching beams which grip the SC connector and other details it is necessary to mold two parts - a sleeve holder and a housing, as shown in Fig. 6. These are snapped together as shown in the figure.

Construction of the blocks is similar. The ST block is one piece, with a threaded section to accommodate retention in a panel by a nut. Because of the interior latching structure, the SC block is of two parts which are snapped together at assembly in a manner similar to the sleeve holder and housing of the SC buildout.

CRITICAL TESTING

Performance standards to be found, say, in Bellcore documents necessarily pertain to an optical connection - that is, two connectors and an adapter. For the most part, the buildout couplings have been found to be indistinguishable from unitized adapters when mated to the same quality connectors. This should not be at all surprising since the key element is the common ceramic alignment sleeve, presuming of course that one hasn't missed the mark on connector - retention geometry. Nonetheless, the fact that a buildout adapter comprises two plastic assemblies only "loosely" joined stimulates concern about environmental behavior and about mechanical strength. When testing to the levels of Bellcore TR-NWT-00326 no environmental problem has been found; and an example of response to very severe thermal cycling will be presented to illustrate robustness. Naturally, the strengths and stiffnesses of these coupling systems, when a connection is subjected to cable tension, are less than to be expected from standard (particularly metallic) adapters; relevant data is present later in this section.

Thermal Cycling

The effect of thermal cycling on reflectance is shown in Fig. 7 for an ST-to-SC connector using an ST block and SC buildout. The most benign range (-40°C to $+75^{\circ}\text{C}$) is that specified by Bellcore and is shown at the left side of the figure. Moving from left to right on the figure, we observe that no meaningful change in reflectance occurs until the peak temperature reaches about 100°C . This is entirely consistent with what is often observed in standard connections, the reflectance change usually being attributed to thermally stimulated relative motion between fibers and ferrules. The point here is that these plastic modular couplings exhibit no added component of environmental vulnerability, within the range of stability of standard connections

Cable Tension

Tension applied to a jumper may cause degradation of signal through a connection or it may even cause permanent damage to some component of the connection. Bellcore tests addressing the first concern are called "straight pull" ("side pull") if the load is applied axially (transversely). Insertion loss and reflectance are monitored while several levels of loading are applied. Adapter stiffness is very important here, but so is the manner in which the cable and connector are joined. Extensive testing has shown that when connectors mated with standard adapters conform to the Bellcore standard then so do these connectors when mated with buildout couplings conform.

Bellcore tests addressing the probability of permanent damage to a connection are called "proof Tests" - "0°" if the load is axially applied and "90°" if the load is transversely applied. For axially applied loads, the TR-NWT-000326 standards are 10-pounds "requirement" and 15-pounds "objective". Substantial data collected during product development and during qualification testing confirm that the FC and ST buildouts easily support the 15-pounds load. However, early testing during the design phase of this project revealed what Wood, et al,⁶ have reported - that is, an axial pull-out load that is sensitive to small details of the coupling and connector. Decoupling, under axial load, if a connector from an FC or ST buildout is achieved by fracture (or severe distortion) of either the buildout on the connector. However, such decoupling in an SC system is typically nondestructive, and, while this is good news, the bad news is that the load distribution may be statistically broad.

The axial decoupling (0° proof test) load for SC buildouts mounted on ST blocks was determined by testing a sample of 40 assemblies. The mean and standard deviation were 26.1 and 5.75 pounds respectively. Assuming a lognormal fit to the data, the estimated percentiles corresponding to the 10 pound requirement and 15 pound objective are 0.00 and 0.74 respectively, i.e., virtually none of the units should fail the requirement and greater than 99% of the product should meet or exceed the objective.

The Bellcore proof-test standards for transverse loading are 7.5-pounds requirement and 10-pounds objective. Perhaps not surprisingly, these have been the performance standards with which we have had greatest difficulty during the development process. FC and SC housing are most vulnerable to this loading, and Figs. 8 and 9 show housing failures. Those failures occurred under dead-load conditions and naturally were accompanied by cracking of ceramic alignment sleeves. These failure modes in light of obvious stress concentrations would appear to provide grounds for some redesign of detail. However, controlled-displacement loading has demonstrated that sleeve

fracture precedes housing failure, indicating that small perturbations on design of the housings would not be helpful.

The performance under 90° loading was determined for each of the three buildout designs mounted on ST blocks. The failure loads are summarized in the table below.

Transverse Failure Loads (pounds)				
	ST		FC	SC
	A	B		
Mean:	13.9	11.1	7.39	11.1
Std Dev:	1.11	1.45	0.53	1.96
N:	10	10	10	10
Estimated Percentile				
5 pounds:	0.00	0.00	0.00	0.00
7.5 pounds:	0.00	0.14	59.6	1.72
10 pounds:	0.00	22.1	99.9	31.4

Note: A and B denote loading parallel and at right angle to the the coupling slot.

The ST data indicates a moderate dependence of failure on loading direction with respect to the housing slot. A test of statistical significance shows that the 2.8 pound difference between samples A and B has less than a 0.05% chance of occurrence if the two population means were actually equal, i.e., there is a high probability that the ST is stronger in the A direction as indicated by the data. The FC is the weakest of the three designs. From the percentiles (based on a lognormal fit) one can estimate the reliability of each design at various loads. We would expect, for example, that greater than 99.8% of ST units and greater than 98% of SC units would meet or exceed a 7.5 pound criterion. We would expect about 40% of FC's to meet 7.5 and virtually all to meet or exceed 5.

CONCLUSIONS

A coupling system that facilitates hybrid connections and readily-changed fixed levels of attenuation has been designed and successfully put into production. The design employs, where possible, standard components, and assemblies of injection-molded parts are accomplished without adhesives, so the manufacturing costs are low. Environmental stability is excellent, and, for the most part, mechanical strength exceeds Bellcore requirements.

REFERENCES

1. G.M. Alameel and A.W. Carlisle, "The Performance of the AT&T Single-Mode ST Connector and Its Enhanced Features", Fiber and Integrated Optics, vol. 8, pp. 45-59, 1988.
2. E. Sugita, R. Nagase, K. Kanayama and T. Shinkatu, "SC-Type Single-Mode Optical Fiber Connectors", J. of Lightwave Technology vol. 7, no. 11, pp. 1689-1696, 1989.
3. N. Suzuki, Y. Iwahara, M. Saruwatari and K. Nawata, "Ceramic Capillary Connector for 1.3-um Single-Mode Fibers", Electronics Letters, vol. 15, no. 25, pp. 809-810, 1979.
4. Bellcore Technical Reference TR-NWT-000326, "Generic Requirements for Optical Fiber Connectors", Issue 3, June 1992.
5. R.R. Cammons, A.W. Carlisle and N.R. Lampert, "Optical Fiber Connecting Device Including Attenuators", U.S. Patent No. 5,082,345, Jan. 1992.
6. W.W. Wood, G.D. Kiss, L.A. Reith, E.M. Vogel and H.H. Yuce, "Reliability of Interconnection Devices", Proc. 9th NFOEC, pp. 209-221, June 1993.

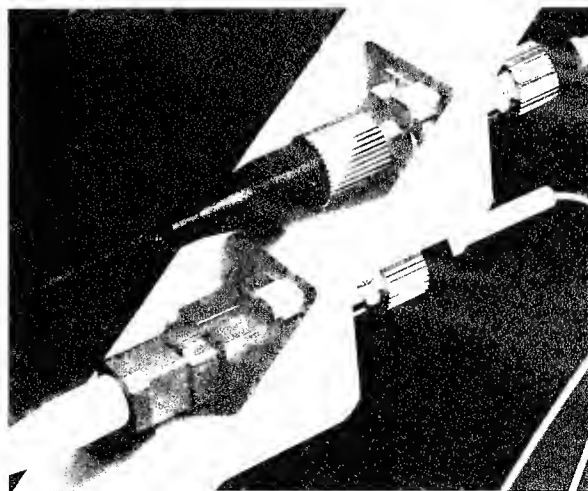


Fig. 1. Hybrid Couplings at Faceplate of Transmission Equipment

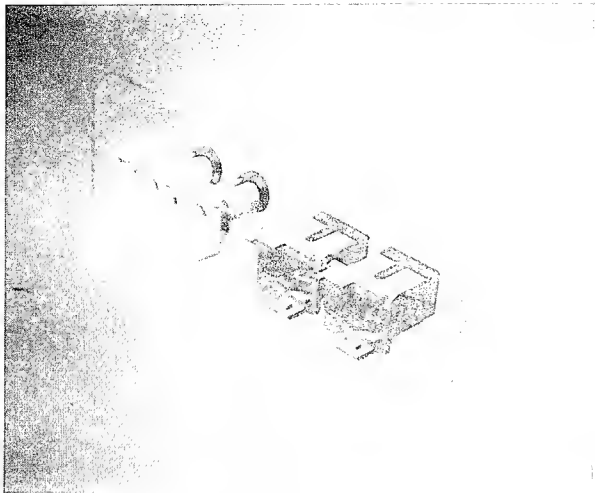


Fig. 2 Panel-Mounted blocks

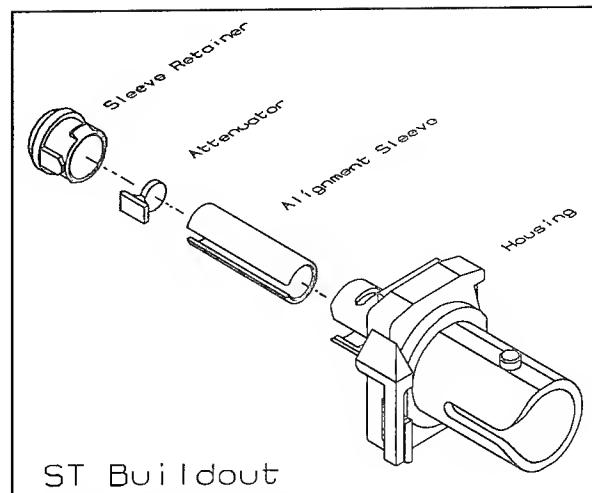


Fig. 5. ST Buildout Assembly

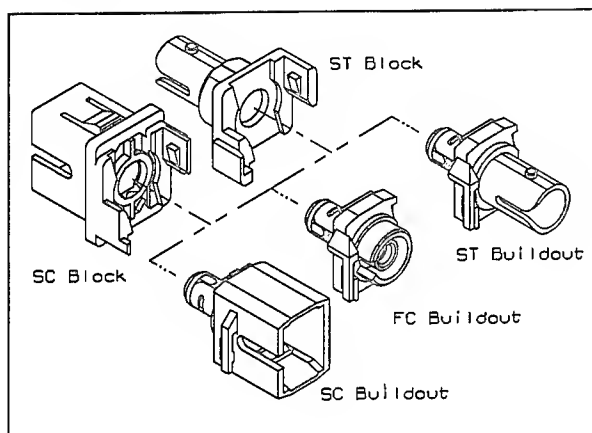


Fig. 3. The Universal Buildout System

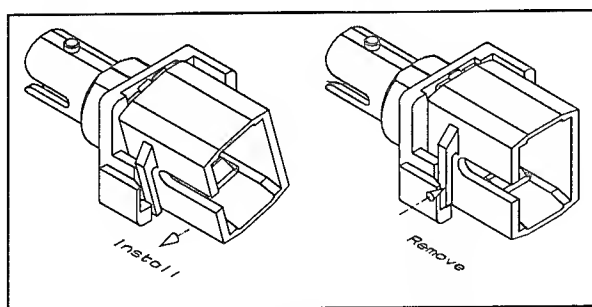


Fig. 4. Kinematics of Engagement/Disengagement

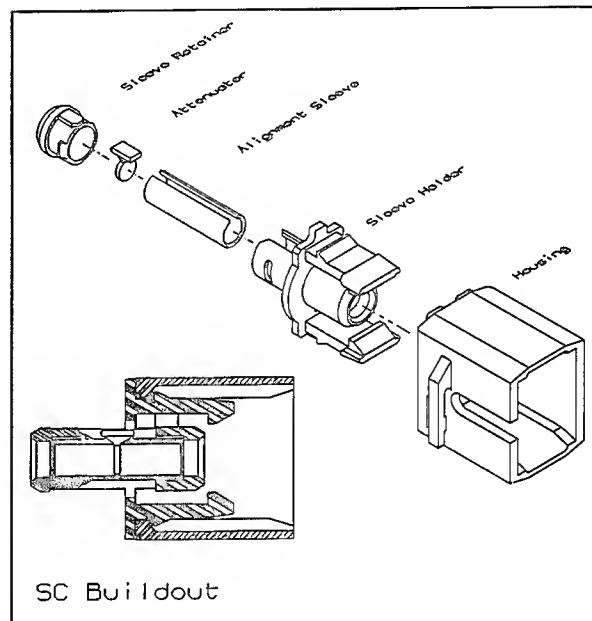


Fig. 6. SC Buildout System

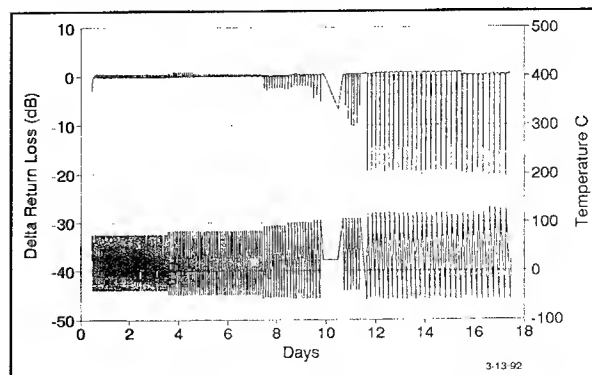


Fig. 7. Thermal Cycling: ST Block, SC Buildout

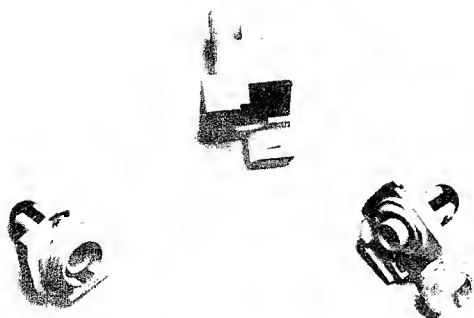


Fig. 8. FC Housing Failure: Transverse Cable Tension



Wilton King is Emeritus Professor at the Georgia Institute of Technology, where he served on the faculty for twenty seven years. In 1991 he joined AT&T Bell Laboratories in Norcross, Georgia, where he designs and analyzes fiber-optic connector products.



Fig. 9. SC Housing Failure: Transverse Cable Tension



Bruce G. LeFevre is a Member of Technical Staff at AT&T Bell Laboratories, Norcross, Georgia. He received his B.S. (Colorado School of Mines) and Ph.D. (University of Florida) in Physical Metallurgy. He joined AT&T Bell Laboratories in 1976 after ten years on the faculty of Georgia Institute of Technology. He has been involved in the study of metals and alloys used in the manufacture of cables and connectors; and is currently working with fiber-optic interconnections, with emphasis on design and reliability.



Charlene Gonzalez obtained her B.S. degree in Mechanical Engineering in 1994 from the University of Puerto Rico at Mayaguez. She worked for AT&T Bell Laboratories in Norcross, Georgia as a summer intern in 1993 and 1994, being involved in mass fusion splicing and fiber-optic interconnections studies. She will pursue a M.S. degree in Mechanical Engineering at Stanford University.



Dan L. Stephenson is a member of Technical Staff in Design Engineering at AT&T Network Systems, Norcross, Ga. He is responsible for rapid prototype parts and tooling. He joined Bell Labs in 1969 as a graduate of Alamance Community College with an Associate in Machine Design.



S. Carolyn Perry is a Senior Technical Support Analyst in the Adversarial Test Group at AT&T Bell Laboratories, Norcross, Georgia. A graduate of the University of Georgia, she joined AT&T in 1971. For the past two years, she has been involved with the accelerated life testing and failure analysis of Fiber Optic Apparatus products.

HIGH FREQUENCY CHARACTERISTICS OF OUTSIDE PLANT MULTIPAIR TELEPHONE CABLES

J. Schulte, Ch. Chojetzki, G. D. Maltz, G. Verdenhalven

Kabelmetal Electro GmbH
Postfach 260
30002 Hannover, Germany

Summary.

Subscriber loop telephone cables have gained new attention as media for high bandwidth switched services. We investigated unit-stranded plastic-insulated copper cables, designed for voice frequency use, from different countries to determine their high frequency properties. At IWCS 1993 we reported results on crosstalk measurements. In this paper we are concentrating on input impedance, structural return loss and excess loss. We are showing results of computational simulations of input impedance for incidental and systematic inhomogeneities in the cable structure and compare them to measured results. Altogether, standard telephone cables do not reach the performance level of Category 5 data cables. This type of application calls for special designs. The connection technique in the central office, in the field and at the subscriber has considerable effect on crosstalk and on the frequency-dependent behavior of input impedance and excess loss. This requires optimizing the complete installation for high frequency applications.

Introduction.

Subscriber loop telephone cables have gained new attention as media for high bandwidth switched services. In the future, symmetrical outside plant telephone cables will have to carry high bit rate or high frequency signals within the entire subscriber loop. Examples are the (Very) High Bit Rate Digital Subscriber Line, (V)HDSL, or the Asymmetrical Digital Subscriber Line, ADSL. Applications with even higher bit rates are carried out over short distances in FTTC (Fiber to the Curb) concepts. Modern transmission techniques also allow for video transmission over symmetrical cables.

The question therefore arises whether the subscriber loop copper cables manufactured today and designed for voice frequency use are capable of carrying high bandwidth signals. We investigated unit-stranded, plastic-insulated copper cables from different countries.

The transmission behavior is defined by the impedance Z , the propagation constant $\gamma = \alpha + i\beta$ (wherein α is the attenuation constant and β the phase constant) and the near-end and far-end crosstalk properties (NEXT and ELFEXT). We report measurements of these properties up to 20 MHz.

We demonstrate further that today's conventional telephone cables exhibit quite acceptable high frequency properties. However, these cannot be compared to those of Category 5 data cables which are designed for frequencies up to 100 MHz. In the case of outside telephone lines that require electrical performance similar to that of data cables, special, more elaborate designs, are available.

Measurement Facility.

The test equipment used was the Hewlett-Packard Model 4194A Impedance/ Gain Phase Analyzer. This system includes an auto-balancing bridge for the determination of the impedance and propagation constant through open- and short-circuit measurements. In addition, the attenuation was determined by feeding a signal into one cable end and detecting it at the other end by using the gain-phase measurement capability of this equipment. The cables were connected through suitable North Hills baluns. For the purpose of these measurements the cable ends were stripped back about 15 cm.

It should be noted that open- and short-circuit measurements at high frequencies tend to indicate primarily the properties just near the beginning of the cable. The test set-up selected for the measurement of attenuation, on the other hand, covers the properties over the entire length of the cable.

Thus, inhomogeneities occurring in the middle of a cable can remain unnoticed during open- and short-circuit measurements while they are picked up completely in the direct attenuation measurement.

Characteristic Impedance and Input Impedance.

The characteristic impedance Z_C is defined for a homogeneous cable. The input impedance Z_{in} of such a cable, when terminated by Z_C equals Z_C . Since an actual cable consists of many individual short sections, each of which may have a different characteristic impedance, the measured input impedance of the actual cable will deviate from the nominal characteristic impedance, even when the last section is properly terminated. These deviations are caused by reflections inside the cable. The input impedance was determined as follows from open- and short-circuit measurements:

$$Z_{in} = \sqrt{Z_{sc} \cdot Z_{oc}} \quad (1)$$

wherein Z_{sc} and Z_{oc} are input impedances with shorted or open remote ends of the cable, respectively. To understand the behavior of Z_{in} we shall first report the results of numerical evaluations on different models of cables with selected inhomogeneities and their influence on Z_{in} . These calculations were done by numerical concatenation of several different quadripole cable sections. The measurement results can then be interpreted based on these computational results.

Simulation of Input Impedance.

A standard multipair telephone cable incorporates the following possible phenomena that may lead to a variation of the local characteristic impedance:

- Variation in the spacing of the conductors within a quad or a pair. It is possible that the conductors of a telephone circuit are locally separated during subsequent fabrication steps. In star-quad construction and assuming the worst-case scenario, the insulated conductors can be pushed together to the point where they touch and therefore assume the characteristics of a pair.
- Uneven density of the cable core: this can result from compacting variations during stranding of the units.

- Proximity to the shield: in cables with single-layer stranded units and in the case of outer layer units in high-pair cables, the pairs or quads approach the shield at repeated intervals.

- Uneven foam factor or fill factor which may lead to local variations of the effective dielectric constants.

Actual measurements for the determination of these individual local effects on cables are difficult. In their stead we estimated and calculated their realistic magnitude (Table 1).

possible cause for Z-variation	variation of Z [%]	
	pairs	quads
conductor separation (estimate)	+5	+5/-3
packing density (estimate)	±2	±2
proximity to shield (estimate)	+1/-3	-4
foam factor (±5%)	±2	±1.5
fill factor (maximum, no filling)	+10	+9
fan-out (maximum)	+57	+36

Table 1: Variations (Estimates and Maxima) of the Characteristic Impedance as a Result of various Influences.

All these effects may have their influence on the cable cumulatively and in varying degrees. They may be periodical, as a result of machine properties used in fabrication, or random. To evaluate the effect on Z_{in} and for a quantitative determination, we calculated the following models for a 300 m-long cable (Fig. 1):

Model No. 1. Random variation of the characteristic impedance at 0.1 m periodic intervals with an amplitude change up to ±2.5% around 100 ohms.

Model No. 2. Subsequent periodic intervals of 0.9 m with 100 ohms followed by 0.2 m with 105 ohms.

Model No. 3. Subsequent periodic intervals of 10 m with 100 ohms followed by 2 m with 105 ohms.

Model No. 4. Subsequent periodic intervals of 25 m with 100 ohms followed by 2 m with 105 ohms.

Model No. 5. A 130 ohm cable of 0.2 m length is followed by 300 m of a 100 ohm cable.

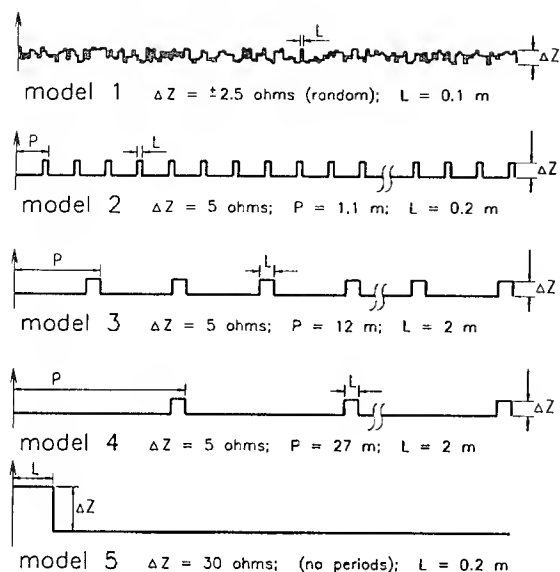


Fig. 1 Models of calculated Cables with Inhomogeneities (not to scale). Total Cable Lengths abt. 300 m.

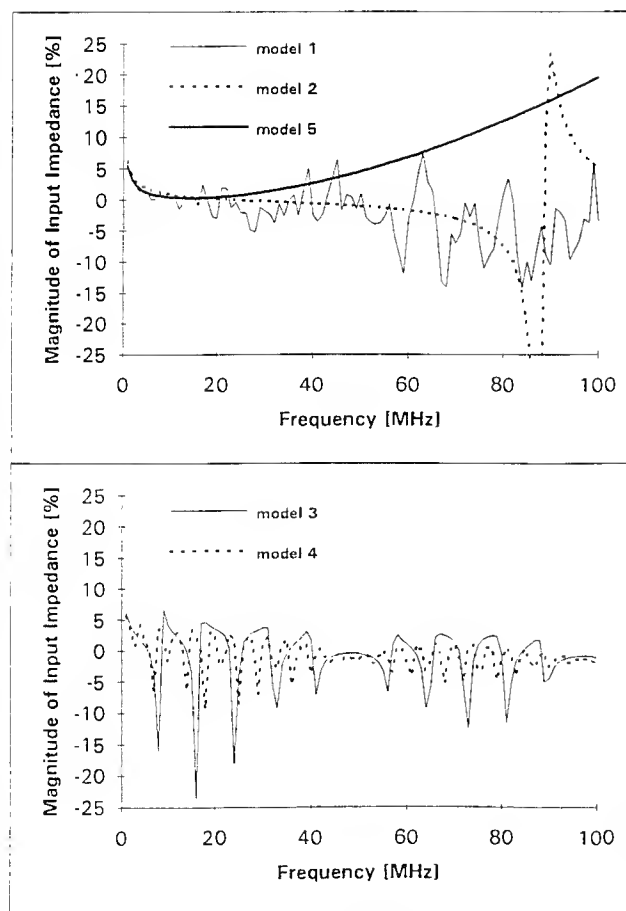


Fig. 2 Calculated Magnitude of Z_{in}

Models 1, 3 and 4 simulate, for example, different displays of irregularities in conductor separation and foam or fill factor. Model 2 simulates, for example, the proximity to the shield. Model 5 simulates a condition that may arise during the cable end preparation for testing of a filled cable or in the course of normal installation.

The simulation of the cable is computed with series-connected 4-pole networks, representing the individual short and homogeneous sections. Fig. 2 shows the calculated variation of the magnitude of Z_{in} . Fig. 3 illustrates the phase of Z_{in} as a function of frequency f .

The following conclusions may be drawn from Figs. 2 and 3:

- Random variations of the characteristic impedance in 0.1 m periodic intervals up to several MHz are not affecting $|Z_{in}|$; they average themselves out. As the frequency increases, $|Z_{in}|$ oscillates with ever-increasing amplitude around the characteristic impedance.

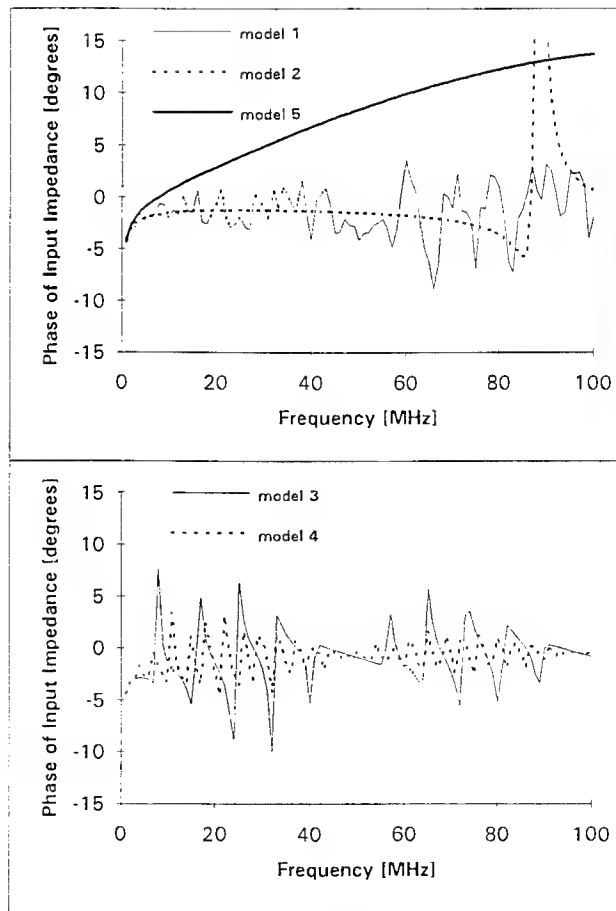


Fig. 3 Calculated Phase of Z_{in}

- Systematic variations of the characteristic impedance in small sections L and short periodic intervals P become noticeable only at higher frequencies (about 90 MHz in the case of model 2 with $P = 1.1$ m). Longer sections ($L = 2$ m) with irregular characteristic impedance in long periodic intervals of $P = 27$ m (model 4) cause $|Z_{in}|$ to oscillate at a 3.6 MHz frequency. The same variations of the characteristic impedance over shorter intervals of $P = 12$ m (model 3) double the amplitude of the variations of $|Z_{in}|$ but at 8 MHz frequency intervals. The length over which the characteristic impedance assumes a change in value (in the case of models 3 and 4, $L = 2$ m) manifests itself through a modulation of the amplitude of the $|Z_{in}|$ deviations of about 50 MHz.

- Also as a result of reflections within the cable Z_{in} has an imaginary component with alternating polarity. The phase of Z_{in} therefore varies around the zero-reference (Fig. 3).

- Model 5 shows a short piece of cable with higher characteristic impedance connected in series with 300 m of the 100 ohm cable (modeling the preparation of the cable end for testing). This causes an apparent increase of $|Z_{in}|$ with frequency and a phase increase going positive.

A distinct maximum value of $|Z_{in}|$ at 100 MHz may result if the cable piece in front is longer (approx. 1 m). This maximum value shows up if the short length connected in series equals $\lambda/4$. Disregarding losses, we obtain⁵:

$$Z_{in}'' = Z_s^2 / Z_{in}' \quad (2)$$

wherein Z_{in}' and Z_{in}'' is the input impedance without and with a series-connected length, respectively and Z_s is the characteristic impedance of the series-connected length. This result proves that the fan-out must be as short as possible during installation and testing.

Measurements of Characteristic Impedance.

This paper reports the results of measurements on unit-stranded, polyolefin-insulated copper cables from various European countries and the U.S.A. The cables consisted of 100 pairs, 50 quads or 56 quads as stranding elements (Table 2). They were fabricated to different national standards and using different manufacturing techniques. We limited our measurements to a frequency of 20 MHz because, in our judgment, standard outside multipair telephone cables will not be used at much higher frequencies.

cable	pairs or quads per unit	number of units	filled	type of insulation	conductor diameter
I	25 pairs; 12 or 13 pairs per subunit	1 unit	yes	foam skin	0.41 mm
II		+	yes	foam skin	0.41 mm
III		6 subunits	yes	solid	0.4 mm
IV	10 pairs	3 + 7	yes	foam skin	0.4 mm
V	10 pairs	3 + 7	yes	solid	0.4 mm
VI	4 + 10 quads	4	yes	solid	0.4 mm
VII	5 quads	3 + 7	no	solid	0.35 mm

Table 2 Measured Cable Types

cable	$ Z_{in} $ [Ω]	$ (Z_{in} - Z_{in}') / Z_{in}' \max$ [%]	$ \Delta\varphi \max$ [°]	ω/β (20 MHz) [10 ⁸ m/s]	α (20 MHz) [dB/100 m]
I	99.3	14.7	8.2	1.99	10.8
II	104.4	9.9	4.7	1.81	10.3
III	113.8	12.1	8.5	1.89	9.1
IV	101.1	8.7	8.2	2.05	11.1
V	105.0	12.0	6.6	1.82	10.1
VI	110.4	8.9	4.9		10.9
VII	132.0	14.0	8.0	1.96	10.3

Table 3 Measurement Results

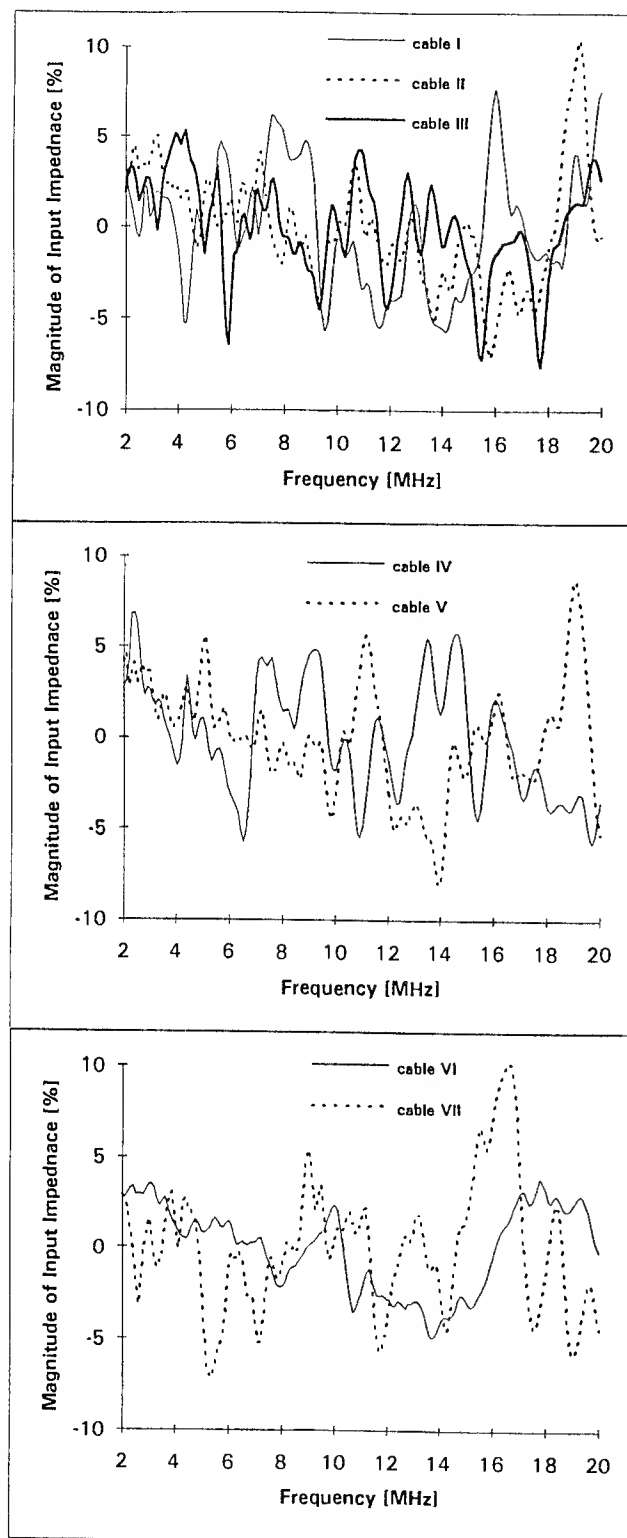


Fig. 4 Measured Magnitude of Z_{in}
(referenced to $|Z_{in}|$, as given in
Table 3)

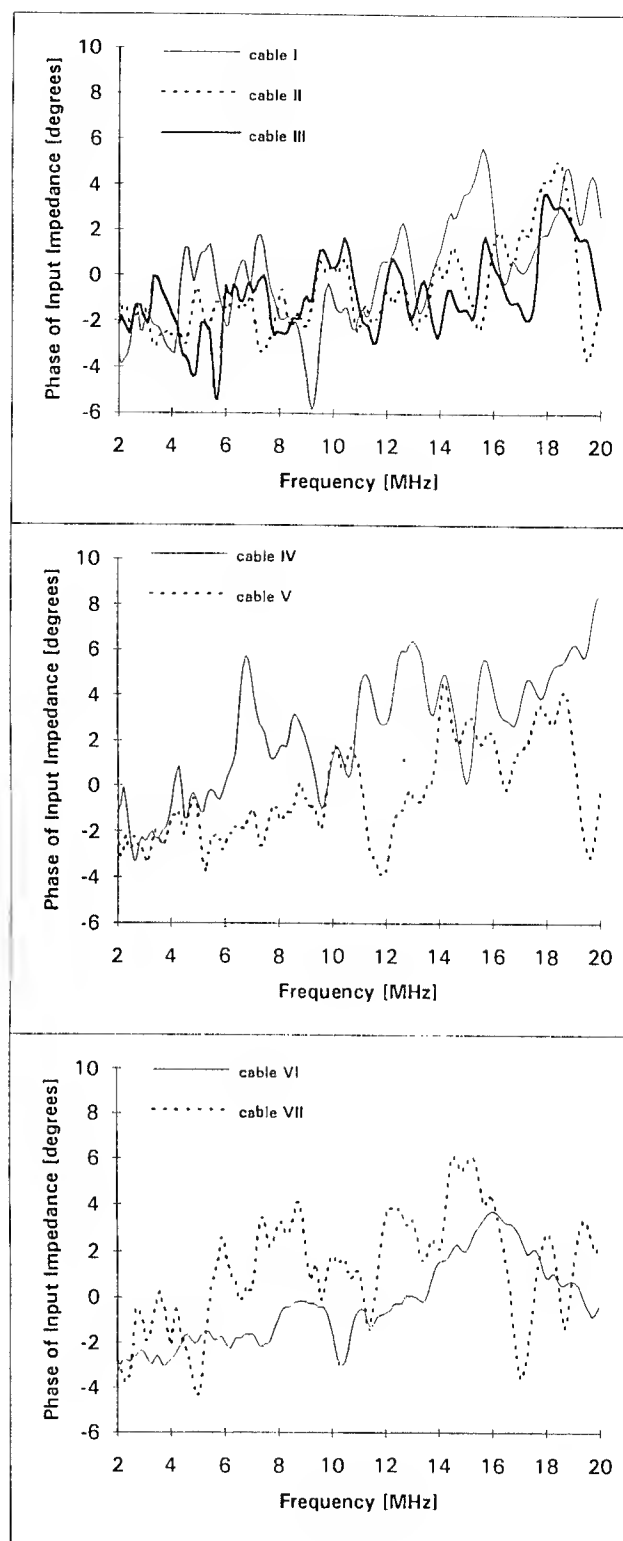


Fig. 5 Measured Phase of Z_{in}

Figs. 4 and 5 illustrate the results of the magnitude and phase of Z_{in} for a typical pair from each of the investigated cables. The $|Z_{in}|$ curves oscillate with slowly increasing amplitude over the investigated frequency range. They do not contain any clear reference to a possible Z-periodicity in the cable. Non-systematic, incidental or random disturbances in the cable predominate.

Table 3 lists the averaged $|Z_{in}|$ values of each cable. The averaging was conducted over all measured pairs/sides of the cable and in the frequency range between 2 and 20 MHz. The average values lie between 99.3 and 132 ohms. They are the result of different specification requirements. The maximum measured percentage deviations of $|Z_{in}|$ from the average value up to 20 MHz are also shown in Table 3. They amount up to 14.7%.

Also as a result of reflections the phase φ of $|Z_{in}|$ is non-zero. Instead, it fluctuates around zero as a function of frequency. A few pairs indicate a slight phase rise with respect to zero. This may be the result of the previously mentioned preparation of the cable ends for testing. Table 3 lists the maximum phase deviations with respect to the average curve up to 20 MHz for each cable; they amount to 8.5° .

In order to evaluate the reflections in the cable the structural return loss (SRL) has been determined using ^{3,4}:

$$SRL = -20 \log \frac{|Z_{in} - Z_0|}{|Z_{in} + Z_0|} \quad (3)$$

wherein Z_0 is the characteristic impedance of the undisturbed cable, as derived from the measurement curves through the generation of an average curve.

Fig. 6 illustrates typical SRL curves of the individual cables. For high frequencies, Z_0 was determined with the mutual capacitance C from the formula

$$|Z_0| = \beta / \omega C \quad (4)$$

The structural return loss at 2 MHz has its minimum value near 30 dB and at 20 MHz near 23 dB. The SRL for Category 5 data cables is specified at 23 dB¹ up to 20 MHz. Taking into account some necessary safety margin we conclude that standard multipair telephone cables do not fulfill this requirement.

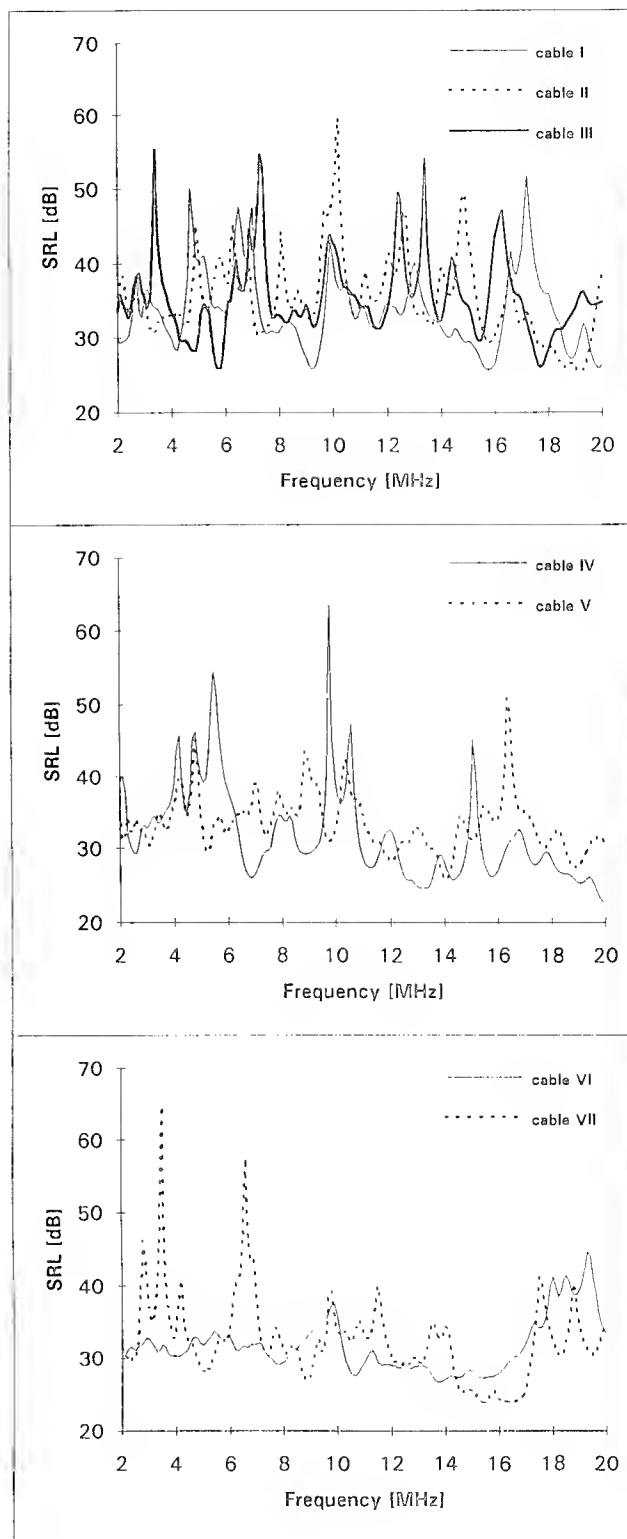


Fig. 6 SRL of measured cables

The SRL together with a smooth-fitted curve of Z_{in} serves as a useful characterization of the cable.

Characteristic Impedance and Cable Installation.

The significant effects of the cable connection technique and of accessories like connectors and splices on the crosstalk behavior of symmetrical cables are well known. Twisting the conductors after removing the cable shield may reduce the crosstalk but it increases the characteristic impedance of the pair or side of the quad because of the lack of the electrical shield and, if applicable, the filling compound. The difference amounts up to 30 ohms for quads and 50 ohms for pairs (Table 1 and model 5). Periodic changes of the characteristic impedance may also be caused by the installation (joints at regular intervals). The resulting effect on Z_{in} can be gathered from Figs. 2 and 3. Fig. 7 illustrates the measured $|Z_{in}|$ of a pair from a 322 m-long cable line consisting of 12 cable pieces, each 25 m long, the pairs of which are spliced together in 2 m long unscreened splicing sections. Fig. 8 shows the measured attenuation. The effect of the periodic disturbance is clearly evident.

Propagation Constant.

Attenuation is primarily determined by the cable design and the materials used. In multipair outside plant cables it may be to some degree higher than that of data cables which are designed for higher frequencies¹. Inhomogeneities of the characteristic impedance result in an additional attenuation component generated by

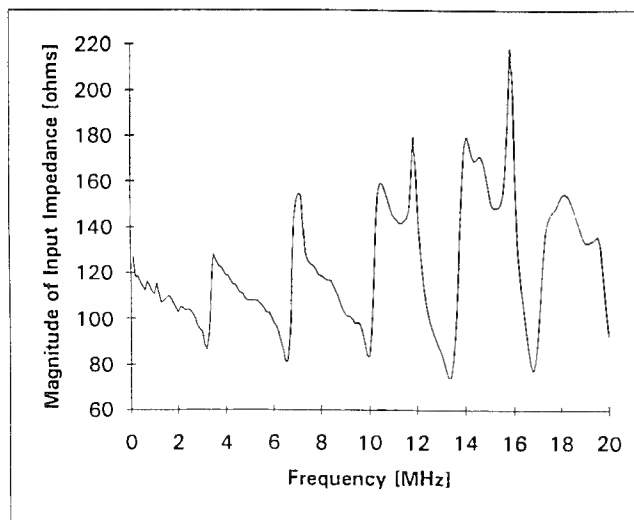


Fig. 7 Measured Magnitude of Z_{in} of a Trial Cable Installation

multiple reflections. Periodic inhomogeneities in $\lambda/2$ distances lead to attenuation peaks at the corresponding frequency. By comparing the magnitude of the SRL and the irregularities of the attenuation one must consider that the latter is the result of double-reflections.

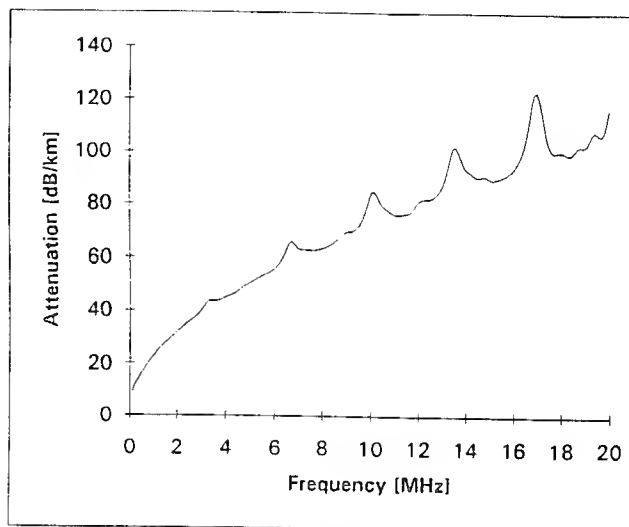


Fig. 8 Measured Attenuation of a Trial Cable Installation

The average measured attenuation value which is determined by the requirements of the respective cable specifications, is illustrated in Table 3 for 20 MHz. The attenuation curves of individual pairs within a given cable show a smooth progression. Some roughness becomes visible at higher frequencies. For a more precise evaluation of excess loss we subtracted the \sqrt{f} -proportional contribution, as expected from theory, showing now only the difference.

Fig. 9 illustrates two differential plots. In addition, we included for both curves straight lines which reflect a frequency-proportional component of the attenuation. This component is attributable to reflections and dielectric loss α_G (dB/km):

$$\alpha_G = 8.686 \cdot \pi f \cdot C \cdot Z_0 \cdot \tan \delta \quad (5)$$

We used $6 \cdot 10^{-4}$ and $10 \cdot 10^{-4}$ for the dissipation factor $\tan \delta$, the measured value for the mutual capacitance C and the average value for Z_0 for the analyzed cables.

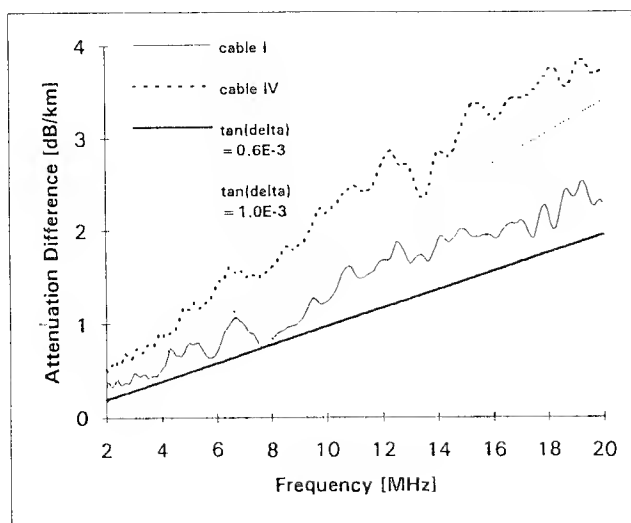


Fig. 9 Attenuation Difference $\alpha - A\sqrt{f}$ of Cables I and IV

The two curves in Fig. 9 grow to about 2 and 4 dB/km, respectively, at 20 MHz. The maximum roughness is about 0.6 dB/km, that is less than 1% of the attenuation α . This deviation from the \sqrt{f} -proportional progression is due both to dielectric loss and reflections within the cable.

Table 3 lists the calculated phase velocities ω/β obtained from the measured phases. These velocities approach $3 \cdot 10^8 (2.3)^{-1/2} = 1.98 \cdot 10^8$ m/s in solid and filled cables.

Near-End and Far-End Crosstalk.

We have reported the results of measurements of near-end crosstalk attenuation (NEXT) and compared them with the requirements of ICEA Specification No. S-84-608-1988 in ². This specification contains power sum requirements for five discrete frequencies. In view of the severe fluctuations of the individual NEXT-curves, it is questionable whether it is adequate for the characterization of the cables or whether it would not be better to state the requirements within a given frequency range.

Fig. 10 shows typical results of NEXT measurements in a 10-pair unit. Similar curves with correspondingly higher crosstalk attenuation are obtained between adjoining and non-adjoining units. Contrary to the individual NEXT or ELFEXT

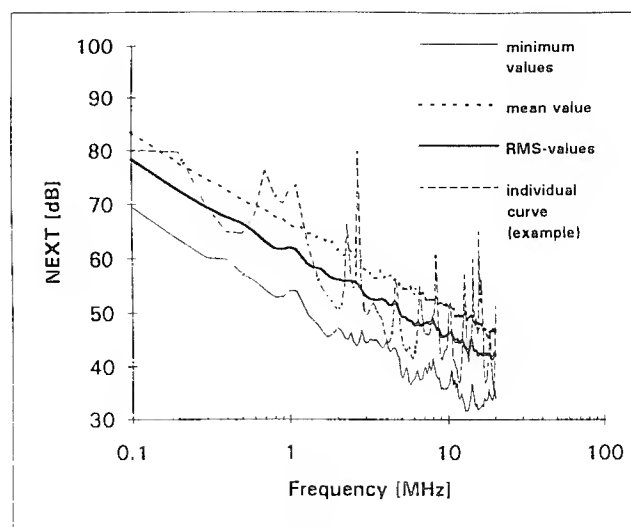


Fig. 10 NEXT Results

curves the RMS and mean value curves run smoothly. The standard deviation (in dB) was found to be nearly independent of frequency for all cables. It was 8 dB in the example of Fig. 10. The standard deviation for NEXT of the different cables was between 7 and 10 dB in the unit, about 7 dB between adjoining units and about 6 dB between non-adjoining units. Not all of the measured NEXT values correspond to those specified for Category 5 data cables, that is: 62 dB for individual values at 1 MHz.

This behavior of crosstalk attenuation curves averaged over enough pair combinations is found in all cables and for all calculated curves. Because of the smooth progression of the curves it is fully adequate, in the case of multi-pair cables, to set NEXT requirements only at discrete frequencies for average values or for power sum such as is the case, for instance, in the afore-mentioned REA/ICEA specification.

Fig. 11 shows average values of far-end crosstalk attenuation (ELFEXT) obtained from all combinations in the unit. In this case, too, the standard deviation was found to be independent of frequency. It measured 7 to 8 dB in the unit and 6 to 7 dB between units for the different cables. In addition, we show a straight line of the theoretically-expected decrease of the averaged ELFEXT curves. Due to the length of the cable, some of the curves reveal noise at high frequencies. The side/side crosstalk inside the quad was included. The measured curves of the average values run smoothly. At higher frequencies they show a decrease of about 20 dB/decade. This is particularly true for the cables with star quads. Here, some

literature cites considerably steeper ELFEXT-losses with frequency. Quadded Cable VI discloses particularly good ELFEXT values.

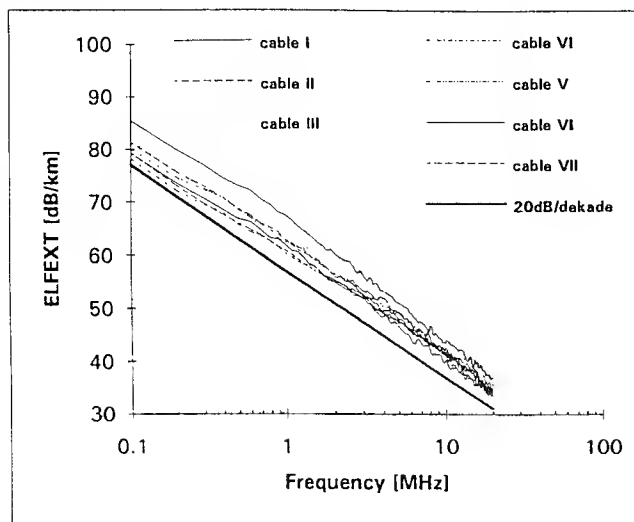


Fig. 11 ELFEXT Results

Conclusion.

Unit-stranded polyolefin-insulated local cables of different countries and specifications were investigated. The effect of unsystematic and possible systematic inhomogeneities in the cable on input impedance and attenuation are presented. As expected, the investigated cables do not meet the requirements for Category 5 data cables. Such electrical requirements for outside plant cables can only be met through special design and fabrication. But up to 20 MHz all investigated cables show quite adequate transmission properties.

The input impedance Z_{in} varies with frequency. Therefore, a cable cannot be characterized based on measurements at discrete frequencies. On the other hand, the SRL is insensitive to the phase of the reflected wave. Therefore, together with a smooth approximation of Z_{in} , the SRL is a more suitable description of a cable.

Attenuation follows the theoretically expected \sqrt{f} -proportional progression rather closely. Further examination reveals an f -proportional contribution to attenuation which becomes visible at higher frequencies. It is caused in part by dielectric loss and, in part, by reflections in the cable.

In the case of NEXT and ELFEXT requirements in multi-pair cables, it is entirely sufficient to set the mean value or power sum conditions at discrete frequencies.

In high frequency operation of installed cables it is important to optimize the properties of the total installation. The connecting techniques (splices, joints, sleeves, branches) in the local office, in the field and at the subscriber have considerable effect on input impedance, crosstalk and attenuation.

Acknowledgments.

The authors gratefully acknowledge the cooperation of Messrs. Dimitri R. Stein and Henry Hofheimer of Cable Consultants Corp., Larchmont NY in the review and editing of this paper.

References.

1. ISO/IEC DIS 11801
2. "Performance of current Local Cable Designs in High Bit Rate Applications", G. D. Maltz, Ch. Chojetzki, J. Schulte, G. Verdenhalven, K. Verlande, Proceeds. IWCS 1993, pp. 270-282
3. "An Evaluation of Measurement Techniques for determining Copper Cable structural Effects", H. W. Friesen, Proceeds. IWCS 1991, pp. 93-104
4. "An improved characteristic Impedance Measurement Technique", H. W. Friesen, Proceeds. IWCS 1990, pp. 608-617
5. "Elektromagnetische Wellen auf Leitungen", H.G. Unger, Hüthig Verlag, Heidelberg, 1991



Christoph Chojetzki
Kabelmetal Electro GmbH
Gubener Strasse 1
31644 Stadthagen
Germany

Christoph Chojetzki was born in 1963. He graduated in 1988 with a degree in electrical engineering (Dipl.-Ing.) from the Friedrich-Schiller-University in Jena. He joined Kabelmetal Electro in 1991, where he is currently engaged in the engineering of telecommunications cables.



Georg Maltz
Kabelmetal Electro GmbH
Postfach 260
30002 Hannover
Germany

Georg Maltz received his degree in communications engineering from the Technical University Hannover in 1958. During the same year he joined Kabelmetal Electro GmbH. Since 1965 he is responsible for research and development of telephone and carrier frequency cables and, since 1978, also in R & D of fiber optic cables.



Johann Schulte
Kabelmetal Electro GmbH
Gubener Strasse 1
31644 Stadthagen
Germany

Johann Schulte received his physics degree in quantum optics in 1981 and his Ph.D. in engineering in 1986 from the Technical University Hannover. After a research fellowship at IBM, Yorktown Heights, he joined Kabelmetal Electro in 1987, where he is currently in charge of cable engineering.



Gerd Verdenhalven
Kabelmetal Electro GmbH
Gubener Strasse 1
31644 Stadthagen
Germany

Gerd Verdenhalven joined Kabelmetal Electro in 1969 after completing his studies in communication engineering at the Technical University Hannover. He was active in R & D of telecommunications cables and measuring techniques both in the carrier frequency and digital range. In the 1980s he became responsible for the design and testing of fiber optic cables and, since 1985, he is head of the group for design of telecommunications cables in the Stadthagen plant.

Symmetrical copper trunk cables for use up to 20 MHz optionally to be combined with optical fibres

Paul E. Gregor, Georg Hög, Peter E. Zamzow, Günter Thönneßen †

KABELRHEYDT AG Mönchengladbach Germany

Abstract

A new hybrid cable design has been introduced in order to meet demands upon future transmission systems.

Data rates to be transmitted are increasing strongly.

Therefore adequate cable constructions are to be manufactured. Basically 2 Mbit/s transmission systems have to be applied and also various advanced link technologies for instance for HDSL, ADSL or VHDSL. It is moreover extremely important to create the most favourable cable design solution as a compromise between lowest possible cable diameter and high grade transmission characteristics.

Longitudinal and lateral watertight cables have been tested up to 20 MHz and it has been found possible to achieve sufficient electrical properties by using certain production measures and employment of suitable materials.

1. Introduction

There is a certain tendency on market to use telecommunications outdoor trunk hybrid cables which are able to serve for various transmission systems.

Particular railway authorities and pipeline operators respecting their typical route structure exhibit different subscribers requirements regarding electrical performance.

Transmission of electrical signals VF, HF and even DC are necessary. For higher data rate performances and high electrical immunity demand optical fibres are necessary to be used.

This contribution describes a universal applicable cable design consisting of a cable core with different stranding elements. On one hand star quads for use up to at least 20 MHz and on the other hand optical fibre elements to fulfil above mentioned criteria.

A possible particular system application in which copper and optical fibre elements cooperate is shown in fig. 1.

This cable design philosophy enables the user to install a cable link which fulfils the needs for several decades.

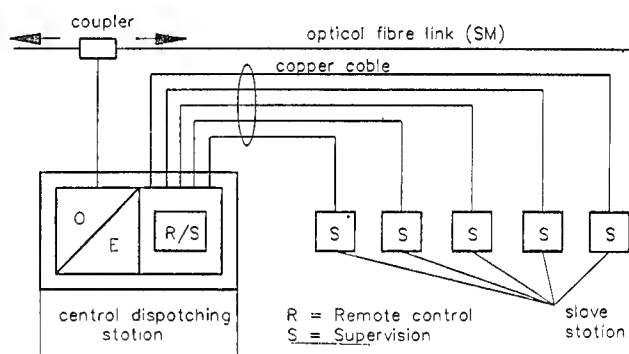


figure 1: Possible application for hybrid cables considering VF/TDM systems

2. Cable design

2.1 Star quads for HF-applications

Generally the cable design at present has to be more than ever a compromise between high grade transmission quality bridging the needs for different systems on the one hand and a little cable diameter regarding favourable mounting and transportation properties on the other hand.

The most important criteria are

- low attenuation coefficient
- high crosstalk attenuation

In order to achieve high crosstalk attenuation resp. low capacitance unbalance values production of insulated conductors with high concentricity and low wall thickness tolerances are fundamental to be obtained. Modern electronically controlled extrusion lines meet the needed design accuracy.

The geometrical configuration of conductor within starquads have to maintain a square cross section along the whole length of cable. This is the presupposition for an ideal electrical behaviour showing capacitance unbalance values towards zero.

As an most favourable insulation material polyethylene foam skin material is employed. The cellular degree of the inner part of insulation is performed close to 50 %.

The mutual capacitance of the circuit within a star quad has been chosen upon international established levels for paper insulated cables, this is around 30 nF/km.

Since there is an optimum ratio respecting lowest possible attenuation depending from geometrical dimensions as distance between conductors and conductor radius within a quad this matter is important to be obtained. The physical background are the criteria skin effect and effects caused by adjacent circuits and the metallic sheath. The optimum ratio calculated and proved by measurements has been found in the range of 6,0 and 7,5 which has been taken into account accordingly.

2.2 Cable core and sheath design

Star quads are stranded together in concentric layers.

There are basically two categories of elements. Those are quads used for voice frequency links and quads applicable for PCM systems primarily.

Additionally optical fibre elements can be combined with metallic stranding elements.

The optical fibre unit with single mode fibres has been designed in such a way that it comprises the same volume compared to a star quad.

Up to 6 multifibre buffer are stranded around a central fibre reinforced plastic (FRP) strength member kept together by an open plastic spiral. During stranding operation it has to be made sure that no unacceptable pulling load occur upon the optical unit.

The pitch length and the dimensions of the components are selected in such a way that no unallowed expansion and constraint during later installation procedure occur. The design and properties of singlemode optical fibres are in accordance to CCITT Rec. G652 resp. IEC 794-1.

Figure 2 shows a cross section of an optical fibre unit.

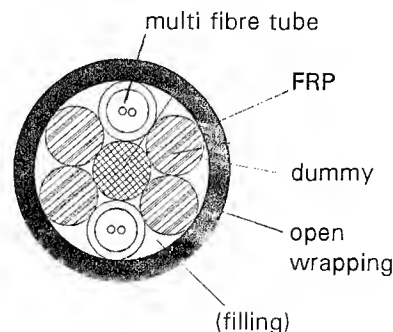


figure 2: optical fibre unit

Typical cable cross sections under application are shown in figures 3a und 3b:

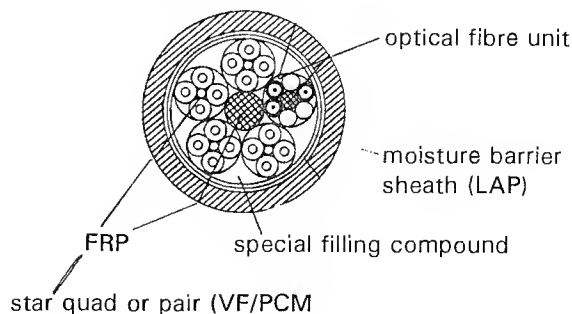
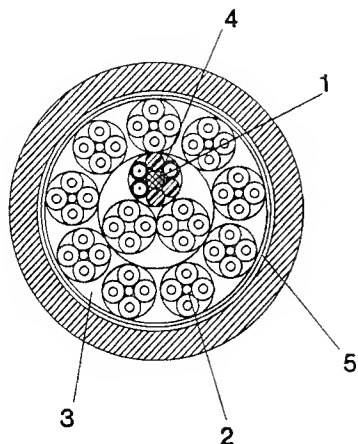


figure 3a: Typical cross sections of hybrid cables with 4 quads and 2 O.F.



- 1 = FRP
- 2 = star quad or pair (VF/PCM)
- 3 = special filling compound
- 4 = optical fibre unit
- 5 = moisture barrier sheath (LAP)

figure 3b: Typical cross sections of hybrid cables with 11 quads and 6 O.F.

The interstices of the cable core have to be filled with a special mass in order to obtain longitudinal watertightness. Normally conventional filling material increases the mutual capacitance by approximate 25 %.



figure 4: Real composite copper/optical fibre cable with 6 quads and 4 O.F.

To avoid this remarkable portion a special compound is being used. The dielectrical constant is 1,6 instead of 2,3 with petrojelly. By using this filling compound the mutual capacitance is only increased by less than 10 % compared to an unfilled cable.

As sheath construction a laminated aluminium polyethylene (LAP) performance is normally under application.

Figure 4 and figure 5 show examples of composite copper/optical fibre cable types.

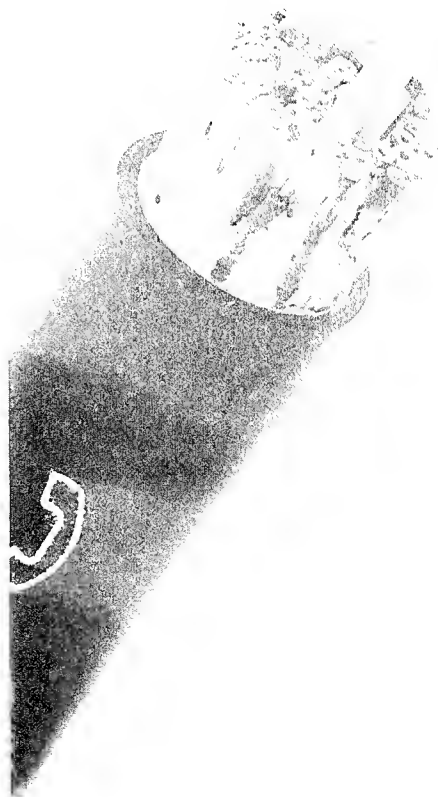


figure 5: Actual hybrid cable sample with 11 quads and 6 O.F.

Table 1 summarizes the most important design criteria for cables with copper conductors diameter of 0,9 mm and 1,2 mm.

conductor diameter [mm]	0,9	1,2
mutual capacitance [nF/km]	31	29
diameter over insulated conductor [mm]	1,9	3,2
diameter over star quad [mm]	4,6	7,7
number of star quads/fibres (typical)	4/5/6/10	4 + 2 SM fibres 6 + 4 SM fibres 11 + 6 SM fibres
cable core	stranded in concentric layers	
filling of cable core	special mass with low dielectric constant	
sheath	laminated aluminium polyethylene moisture barrier sheath (LAP)	
nom. outer diameter of cable [mm]	17,8 (5 quads)	28,8 (11 quads + 6 fibres)

table 1

For particular purposes special armouring design with respect to improved pulling strength, lightning stability and electromagnetic shielding performance should be manufactured. Normally copper wires and steel tapes applied helically shall be used.

2.3 Shielding of individual stranding elements

In order to improve crosstalk attenuation between PCM circuits star quads or units shall be shielded separately by a special metal foil normally applied longitudinally together with an open binder. Considering a high production economy only one filling process is acceptable. Therefore the shielding tapes shall be configured with a suitable perforation enabling the filling compound to be penetrated through the total cable core during the filling procedure obtaining a longitudinal watertightness.

With respect to a certain dielectric strength the metal foil shall be combined with a paper or plastic layer. As a further measure for increase of dielectric strength a suitable plastic grid shall be wrapped below the shielding material.

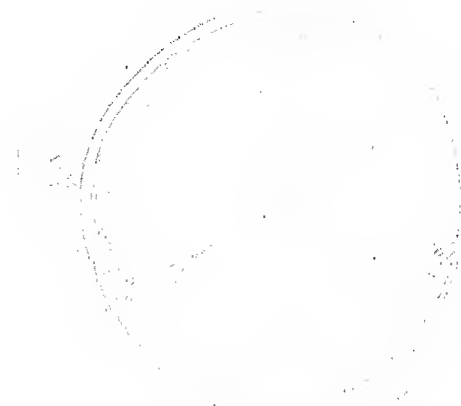


figure 6a: cable cross section with separate shielding of copper units

Moreover it should be pointed out that inspite of unit wrapping an advantageful desired segmentation of stranding elements (cable samples shown in figure 6a) and 6b) has been achieved caused by application of relatively long lay length and suitable wrapping design.



figure 6b: cable sample with individual shielding of copper units

3. Characteristics of cable delivery lengths

3.1 DC and VF properties

Table 2 exhibits DC and VF data for cables with copper conductors of 0,9 mm and 1,2 mm diameter.

property at 20°C	value		test method according to	
	0,9 mm	1,2 mm	DIN VDE 0472	IEC
DC loop resistance of copper conductors	$\leq 56,6$ Ω/km	$\leq 31,8$ Ω/km	part 501 item 2.1	189-1 sub-cl. 5.1
DC resistance unbalance	$\leq 3 \%$		part 501 item 2.2	708 Am.3 cl. 24
dissipation factor at 800 Hz	$\leq 5 \times 10^{-3}$		part 505	
DC insulation resistance	$\geq 1,5 \text{ G}\Omega \cdot \text{km}$		part 506	189-1 sub-cl. 5.3
mutual capacitance at 800 Hz	≤ 31 nF/km	≤ 29 nF/km	part 504	189-1 sub-cl. 5.4
capacitance unbalance at 800 Hz	$\leq 100 \text{ pF/km}$		part 502	189-1 sub-cl. 5.5
dielectric strength 50 Hz/1 min cond./cond. cond./shield	500 V		part 509	189-1 sub-cl. 7.1

table 2: DC and VF data for delivery length

3.2 HF characteristics of cable delivery lengths

3.2.1 Attenuation coefficient

In order to achieve the lowest possible attenuation coefficient considering economy the favourable foam skin polyethylene insulation material and a special filling compound with low dielectric constant have been combined.

In figure 7 the results regarding the attenuation coefficient up to 20 MHz for side circuits of quads with copper conductor diameters of 0,9 mm and 1, 2 mm have been recorded under application of a short/open circuit test method.

Compared to conventional trunk cable with paper insulation the achieved attenuation level of the new cable generation is nearly identical. A fully substitution of the classical paper trunk cable technique has been reached regarding attenuation (for instance compared to CCITT Rec. G.612 (Fase. III.3, Blue book)).

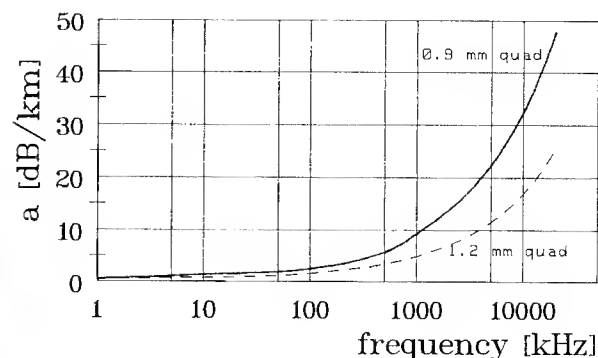


figure 7: attenuation coefficient curve respecting delivery length

3.2.2 Near end crosstalk attenuation

Figure 8 shows the near end crosstalk attenuation (NEXT) up to 20 MHz between side circuits of quads without shielding of stranding elements. In the case of elements with individual shielding the average value has been tested with the result of 98 dB with a standard deviation of 7 dB.

The test have been performed as a level measurement up to 20 MHz.

In comparison to ISO/IEC DIS 11801, cat. 5 gained NEXT level has been realized well above specified values.

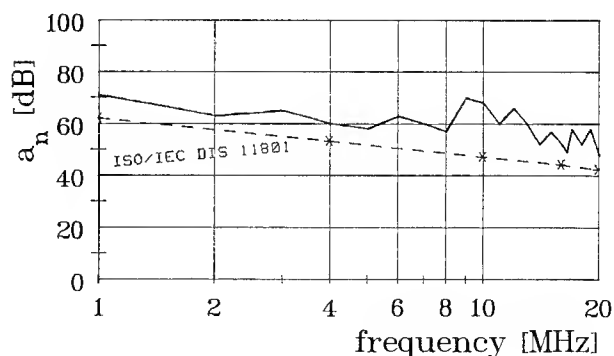


figure 8: Near end crosstalk attenuation

3.2.3 Characteristic impedance

In figure 9 the characteristic impedance up to 20 MHz for both star quads with conductor diameter of 0,9 mm and 1,2 mm has been drawn using the open/short circuit test method.

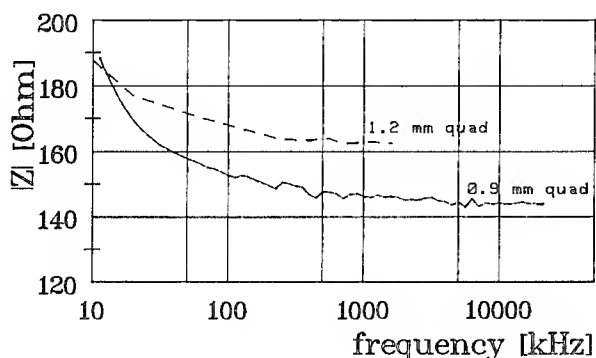


figure 9: characteristic impedance of delivery length

3.2.4 Phase velocity

Figure 10 gives the result for the phase velocity up to 20 MHz.

It shows that above 1 MHz the value maintains at a level of $2,2 \times 10^5$ km/s (resp. 0,73 c).

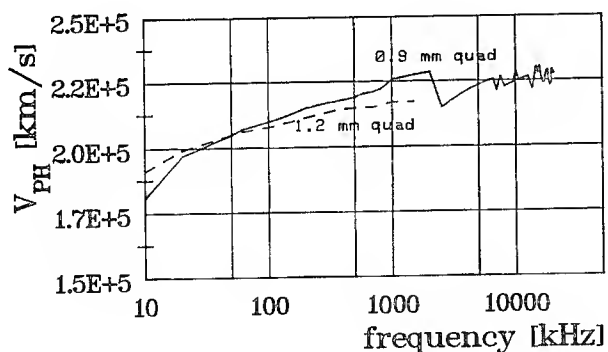


figure 10: phase velocity due to delivery length

4. System considerations

In order to clarify the possible repeater spacing following test configuration has been made up (figure 11):

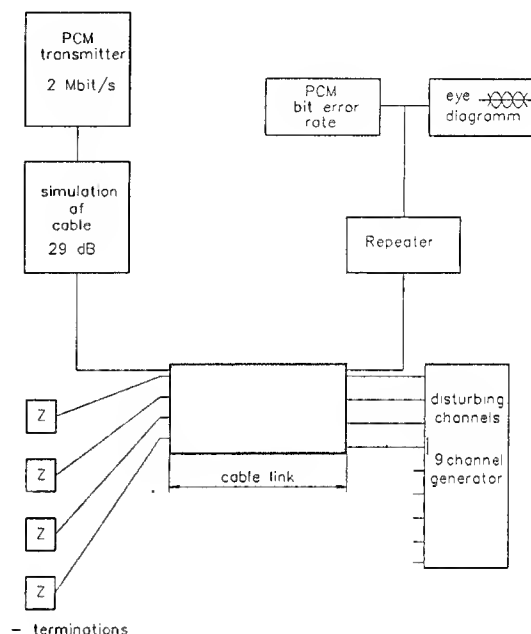


figure 11: Test configuration of PCM transmission link

Following results have been taken together:
Based on the formular

$$a_{\max} = \frac{\text{NEXT} - 0,115 \sigma^2 - \log n - S/N}{a} = [\text{km}]$$

NEXT = Near end crosstalk attenuation
 σ = standard deviation
 a = attenuation coefficient
 S/N = Signal/Noise ratio

a maximum repeater spacing according to values in table 3 has been calculated and compared to test results gained within measurements upon procedure according to principle in figure 11.

copper conductor diameter	repeater spacing for 2 Mbit/s-System
0,9 mm Ø	3,2 km
1,2 mm Ø	8 km

table 3: repeater spacing

5. Jointing material

In figure 12 the inner part of a jointing sleeve is sketched. In principle a metal frame bridges the two cable ends and takes over the fibre splicing cassette on one side and the splices for copper elements on the other side. In case of additional shielding material the latter will be connected through as well. The total jointing sleeve is configured cylindrically.

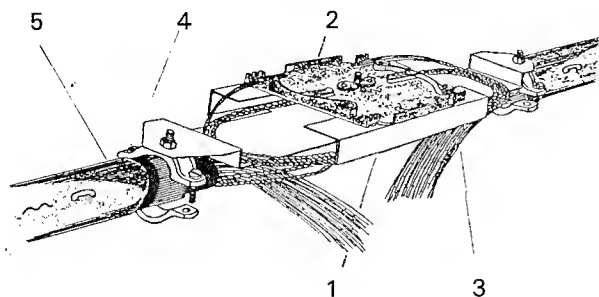


Fig. 12: Jointing sleeve for hybrid cable consisting of copper and optical fibre elements

- 1 = metal supporting frame
- 2 = O.F. splicing frame
- 3 = copper conductors
- 4 = cable clamp
- 5 = cable

6. Conclusion

A new composite trunk cable design for multifunctions for instance used along typical railway or pipeline links have been introduced.

High grade symmetrical copper elements for use within digital systems up to 20 MHz are suggested to be used.

Favourable low attenuation level has been obtained by selection of advanced material technologies on the one hand and comparable high crosstalk attenuation behaviour has been achieved by employment of a particular shielding of individual transmission circuits on the other hand.

Optical fibre elements for most modern and economical aspects may be combined with copper quads or pairs according to the needs of subscribers within link.

This paper is a result of team work. We earnestly thank the individuals with a special mention to H.Kuhnen from the testing department.

7. Literature

- /1/ IEC 794-1 Optical fibre cables, Part 1 Generic Specification
- /2/ DIN VDE 0888 Lichtwellenleiter für Fernmelde- und Informationsverarbeitungsanlagen
- /3/ DIN VDE 0816 Außenkabel mit Kupferleitern
- /4/ H.G. Dageförde / P. Gregor / G. Thönneßen Glassfibre armoured PIC Trunk Cable assembled with connecting plugs IWCS 1975
- /5/ Gregor, P.; Lehan, K; Mühlen, H: Normen für Meßmethoden an Kupfer- und Lichtwellenleiterkabeln, ET2 19/1993
D. F. Dekker/H. G. Dageförde/P. E. Zamzow Ausgleichsfreies Sternviererkabel für Pupinisierung und für Breitbandbetrieb (techn. Mitteilung 1/75)

Authors

Peter E. Zamzow
KABEL RHEYDT AG
Mönchengladbach, Germany

Peter E. Zamzow (54) is director of the Telecommunication Division. After finishing his postgraduate studies in telecommunications in München and Graz as Dipl.-Ing. he joined AEG KABEL in 1970. He has been engaged in development and production of telecommunications cables. In 1980 he became head of the fiber optic division at AEG KABEL and in 1982 he was nominated as a senior engineer. From 1992 on he was plant manager of the new Optical Fiber Cable Plant Rheydt. Since 01. July 1994 he is general manager for CATV activities worldwide.



Georg Hög
KABEL RHEYDT AG
Mönchengladbach, Germany

Georg Hög was born in 1950. After studying electrotechnics at the Technische Hochschule Aachen he joined KABELRHEYDT as a development engineer for copper cables in 1977. In 1980 he became responsible for the development of symmetrical telecommunication cables. In this position he was also busy in the standardisation for copper cables for the German Telekom. In 1985 he became the head of the development for optical fiber cables. From 1987 to 1988 he was the head of the technique department of BETEFA (special cables for telecommunications). Since 1989, back to KABELRHEYDT, he is responsible for the development and construction department for optical fibre cables. He is also responsible for the standardisation for optical fibre cables for the DBP Telekom and a member in the standardisation bodies in VDE ETSI AND IEC for optical fibre cables.



Paul E. Gregor
KABEL RHEYDT AG
Mönchengladbach, Germany

Paul E. Gregor (52) is head of the Technical Sales Department for Telecommunications cables. He reached his Ing. from Ingenieurschule Duisburg in 1966 and joined Kabelwerk Duisburg, now a part of KABELRHEYDT AG.

After ten years activities in development department he took over the position as head of design branch for copper and optical fibre cables. Since 1989 he is engaged in his present position.

He is also a member of the standardisation bodies in DIN VDE AND ISO/IEC.



Günter Thönneßen (†
14.06.94)
KABEL RHEYDT AG
Mönchengladbach, Germany

Günter Thönneßen was head of the Development Department for Telecommunication Cables. He finished his studies at Technische Hochschule Aachen in 1964. After a 3 years employment as a development engineer for CF measuring instruments he returned to Technische Hochschule Aachen, where he graduated as a Dr.-Ing. In 1971 he joined KABELRHEYDT.



POWERING STUDY OF BROADBAND COAXIAL CABLE DISTRIBUTION PLANTS

Henry D. Pixley

CommScope, Div. of General Instrument
Catawba, North Carolina 28609

ABSTRACT

This paper describes system powering field studies of the broadband coaxial cable distribution plant and laboratory corrosion testing of the connector and cable system, in order to address the concerns of system reliability and performance and how they relate to the future powering schemes being considered.

These studies have confirmed the presence of multiple return paths within the buried plant, indicating that a portion of the return current travels to the utility company's ground at the subscriber's home via the drop cable. Laboratory corrosion testing involved subjecting the connector and cable system to the salt fog chamber, while being powered with 60V/15A AC and DC waveforms. Electrical performance measurements have confirmed that currents have an effect on corrosion and that DC currents appear to have more of an effect than AC.

INTRODUCTION

Today's telecommunication systems are quickly evolving into full service networks, with the deployment of hybrid fiber and coax architectures. These systems, due to their providing life-line services, will demand system reliability and performance.

With the requirements of having to provide power to the RF actives, node and possibly even going to the home, different powering schemes are presently being considered. These schemes consist of both AC and DC waveforms with levels of 60, 90 and 145 volts.

Due to the concerns of system reliability and performance on the future powering schemes being considered, it is important to understand the powering system of today's broadband coaxial cable distribution plant and the effects

of these future powering schemes on corrosion within the plant.

TRADITIONAL CATV POWERING SCHEME

The traditional CATV coaxial cable plant consists of a tree and branch type architecture and delivers power to the RF active components via the inner and outer conductors of the trunk and distribution coaxial cable. Typical CATV power supplies include both non-standby and standby designs and output a 60Vrms 60Hz AC square waveform with maximum current draw ratings ranging from 6 to 15 amperes.

The load for the CATV power supply is the power supply of the RF active component. The power supply of the RF active component must draw current during each voltage eye and convert the AC square wave to DC and provide the appropriate regulated voltage, typically 24 volts, to the amplifier circuitry. Two types of amplifier power supplies found within the CATV plant are the linear power supply and the Switch Mode Power Supply (SMPS). The linear power supply behaves as a linear load, such as a resistor, drawing more current when the AC voltage increases and less current when the AC voltage decreases. The SMPS, on the other hand, constantly adjusts its input current draw in order to maintain a constant power consumption. For example, if the input voltage to the SMPS is decreased, the input current draw increases, in order to maintain the constant power output to the amplifier.^[1] SMPS's are usually found in trunk amplifiers, while linear power supplies are still found in line extenders.

SYSTEM DESIGN

In system design, when using the coaxial cable to deliver power to the active components, a low DC resistance between actives is desirable, in order to reduce the IR voltage drop. A low voltage drop between actives is desirable in order to be able to: 1) Load the power supply

70 to 80 percent of its name plate rating, while still being able to provide adequate voltage to the last active in the cascade with reasonable safety margin. 2) Increase the number of actives per power supply, therefore, reducing power supplies. 3) Reduce power consumption.

The power is usually inserted on a section of coaxial cable where an equal split of current draw will result on both legs, commonly referred to as a balanced system. The parallel loading architecture shown in Figure 4 is also a common circuit design useful in reducing long cascades. These designs aid in being able to effectively load the power supply without dropping below the useful voltage range. Depending on the density of subscribers within the area, however, the dc loop resistance of the coaxial cable may not always be of concern. For example, in a high density area where the actives are spaced close together, there is usually not enough cable footage to create a resistance problem between active components.

FIELD STUDY

Introduction

In the past, there have been several excellent articles written on CATV system powering, however, they have all been in regards to the aerial plant. These articles have confirmed the presence of multiple return paths within the aerial plant, indicating that the return current travels to ground via the CATV strand, utility company's neutral and the coaxial cable's outer conductor. Because few powering studies have been performed on the buried plant, it is the intent of this study to investigate and characterize the CATV system powering circuit of the buried coaxial cable distribution plant. The following sections detail the procedure and findings of this study.

Procedure

In order to be able to characterize the CATV powering circuit of the buried coaxial cable distribution plant, several buried plants within different parts of the United States have been studied and a number of measurements performed. These measurements consisted of 1) voltage measurements at each of the actives 2) current draw of each of the actives 3) current on each span of coaxial cable and 4) coaxial cable footage measurements between actives. From knowing the voltage drop and footage between actives along with the current on the coaxial cable, the effective resistance between actives can be

calculated and compared to the DC loop resistance of the coaxial cable. If the effective resistance is less than the DC loop resistance of the coaxial cable, this would infer that multiple return paths could exist.

Measurement Equipment

Current and voltage measurements were made using the Fluke 97 scopemeter (digital storage type). The scopemeter was capable of displaying two waveforms and performing calculations such as rms, phase difference, etc. Also necessary to perform current measurements were current probes and current probe amplifiers with power supply. The current probe, when placed around a wire carrying current, measures the flux generated from the current. The current probe amplifier then converts this signal to a voltage level and its waveform is displayed on the scopemeter. When the current probe is placed around a coaxial cable that has equal and opposite current flow on the inner and outer conductor, the resulting flux measurement is zero, due to the cancellation of flux. Therefore, the current measurements made by placing the probe around the coaxial cable are actually differential currents, meaning that they are a measure of the difference in current between the inner and outer conductor.

Measurements

Voltage measurements were easily conducted by opening the amplifier housing and measuring the voltage potential between the center conductor pin of the coaxial cable and the amplifier housing. Measurements of current draw of the active components and of the current traveling on the coaxial cable were more difficult.

Current draw measurements of the line extender's power supply were not possible, due to the power supply being integrated into the amplifier circuitry. Due to this reason and because not all amplifiers were accessible with current measurement equipment, the cable operator's current draw specifications were used and were verified to be very accurate when measurements were possible. Coaxial cable current measurements were also difficult, due to the phenomena of flux cancellation. The current probe was capable of only being able to measure the difference in current between the inner and outer conductor, when placed around the coaxial cable. The footage between actives was taken from the system map and was verified to be very accurate.

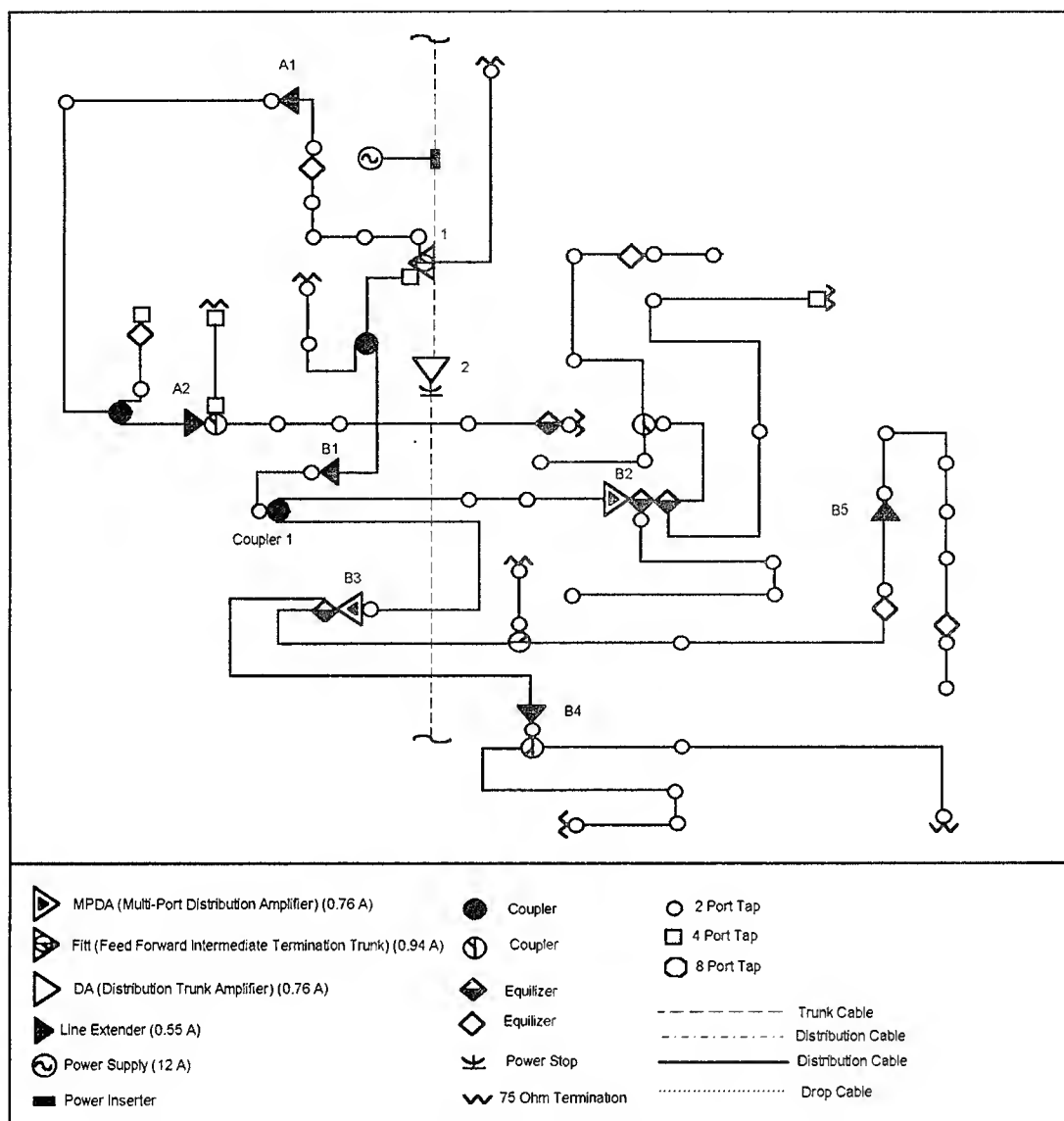


FIGURE 1. - Buried CATV Coaxial Cable Distribution Plant System Layout

Findings

Figure 1 shows the system layout for a section of buried CATV coaxial cable distribution plant which is located on the Central East Coast of the United States and will be used to demonstrate the findings of this study.

All of the buried plants that were studied showed the presence of differential currents on the trunk and distribution coaxial cables as well as on the drop cables. These differential currents consisted of both 60 Hz AC square and narrow sinusoidal waveforms, depending on

their location within the plant. The square waveform was closely in phase with the center conductor's square voltage waveform, while the narrow sinusoidal waveform was usually out of phase, by a few degrees. Differential current measurements measure the difference in current traveling on the inner and outer conductors, i.e., they measure the net current. The direction of current can be determined relative to the direction of voltage or other currents traveling on the coaxial cable system, by viewing both waveforms on the scope at the same time. In doing this, the net current was found to be traveling in the direction of the center conductor current, indicating that

Cable Span	A2-A1	Cable Span	A1-1
Cable Type	P3 500	Cable Type	P3 500
Footage, ft	937	Footage, ft (m)	1127
Voltage Drop, volts	0.7	Voltage Drop, volts	1.9
Current Through Cable (Cat.), Amps.	0.55	Current Through Cable (Cat.), Amps.	1.1
DC Loop Resistance (Cat.), ohms/kft	1.72	DC Loop Resistance (Cat.), ohms/kft	1.72
Effective DC Loop Resistance	1.36	Effective DC Loop Resistance	1.53
Effective Resistance, % of Cat.	79	Effective Resistance, % of Cat.	89
Cable Span	B5 - B3	Cable Span	B4 - B3
Cable Type	P3 500	Cable Type	P3 500
Footage, ft (m)	896	Footage, ft (m)	615
Voltage Drop, volts	0.6	Voltage Drop, volts	0.4
Current Through Cable (Cat.), Amps.	0.55	Current Through Cable (Cat.), Amps.	0.55
DC Loop Resistance (Cat.), ohms/kft	1.72	DC Loop Resistance (Cat.), ohms/kft	1.72
Effective DC Loop Resistance	1.22	Effective DC Loop Resistance	1.18
Effective Resistance, % of Cat.	71	Effective Resistance, % of Cat.	69
Cable Span	B3 - Coupler 1	Cable Span	B2 - Coupler 1
Cable Type	P3 500	Cable Type	P3 500
Footage, ft (m)	607	Footage, ft (m)	886
Voltage Drop, volts	1.7	Voltage Drop, volts	0.9
Current Through Cable (Cat.), Amps.	1.86	Current Through Cable (Cat.), Amps.	0.76
DC Loop Resistance (Cat.), ohms/kft	1.72	DC Loop Resistance (Cat.), ohms/kft	1.72
Effective DC Loop Resistance	1.51	Effective DC Loop Resistance	1.34
Effective Resistance, % of Cat.	88	Effective Resistance, % of Cat.	78
Cable Span	Coupler 1 - B1	Cable Span	B1 - 1
Cable Type	P3 500	Cable Type	P3 500
Footage, ft (m)	120	Footage, ft (m)	767
Voltage Drop, volts	0.48	Voltage Drop, volts	3.3
Current Through Cable (Cat.), Amps.	2.62	Current Through Cable (Cat.), Amps.	3.17
DC Loop Resistance (Cat.), ohms/kft	1.72	DC Loop Resistance (Cat.), ohms/kft	1.72
Effective DC Loop Resistance	1.53	Effective DC Loop Resistance	1.36
Effective Resistance, % of Cat.	89	Effective Resistance, % of Cat.	79

TABLE 1. - Effective Resistance Calculations

either the return current on the outer conductor was less than the center conductor current or that some other current was traveling on the outer conductor in the direction of the center conductor current.

In order to determine which was the case, the effective resistances between actives were measured and compared against the DC loop resistance of the coaxial cable. In doing this, the effective resistances were found to be between 70 to 90 percent of the cable's DC loop resistance, indicating that the outer conductor current was less than the center conductor current. Refer to Table 1 for these results.

Differential currents of up to 3.0 A were measured on the distribution coaxial cable from one side of the power inserter, while ground currents of up to 0.32 A were measured going from the tap to the ground block at the subscriber's home, via the outer conductor of the drop cable. Low currents of around 0.046 A were measured going to the ground at the tap, indicating that these grounds were not as low in resistance compared to those at the home and are mainly used for lightning protection.

In order to determine if these ground currents were a portion of the CATV power supply's return current, further measurements were conducted.

These measurements involved comparing the center and outer conductor current waveforms of the distribution coaxial cable to each other as well as to the current waveform traveling on the outer conductor of the drop cable. In order to do this, one leg of the distribution coaxial cable was removed from the input of a line extender and reconnected using two wires as shown in Figure 2. This enabled the inner and outer conductor currents to be measured separately and compared. These measurements showed the center conductor current to be 2.96 A, while the outer conductor current was only 1.64 A, thus agreeing with the differential current measurement of 1.32 A which was taken earlier. These currents were in phase and identical in waveform, both being narrow sinusoidal in shape. The current on the drop cable was measured to be 0.34 A which had made sense, since the difference in the differential currents entering and leaving the tap was also 0.34 A. The drop cable current waveform was also found to be in phase and

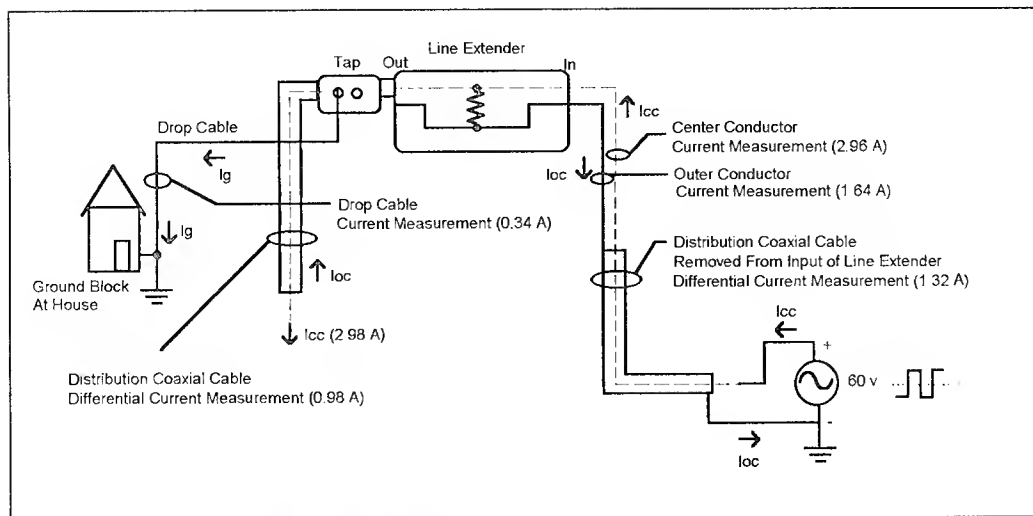


FIGURE 2. - Current Measurement Diagram

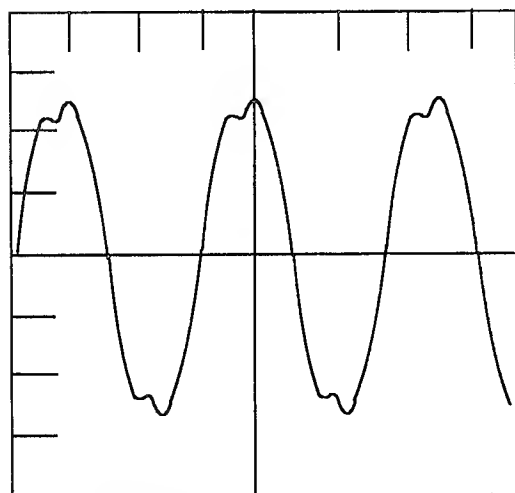


FIGURE 3. - Current Waveform

identical to the center conductor current waveform on the distribution coaxial cable.

These current waveforms are representative of the linear and SMPS power supplies loading at that particular location. They are usually narrow sinusoidal in shape and at times, depending on the load, the SMPS draw can be seen within the waveform as shown in Figure 3.

Conclusion

From the findings of these studies, it is evident that a portion of the CATV power supply's return current is returning to ground at the ground block at the

subscriber's home, via the outer conductor of the drop cable. These multiple return paths reduce the amount of return current on the outer conductor, reducing the effective resistance and hence voltage drop between active components.

Discussion

By characterizing and understanding the CATV system powering circuit of the buried coaxial cable distribution plant, one can design a more efficient powering system and coaxial cable to be used for powering.

Figure 4 shows the electrical powering circuit model of the buried CATV coaxial cable distribution plant of Figure 1. From looking at the model it is evident that multiple return paths are present, however, these grounds are not necessarily all at the same potential. The ground resistance depends on many factors such as soil content, moisture, quality of the ground installation, etc. Therefore, before designing the powering system, sample measurements should be taken of the ground resistances at a few of the homes within the area, in order to be able to characterize the flow of return currents within the system. Taking into consideration the presence of these multiple return paths, when designing the powering system, will allow the power supplies to operate at optimum efficiency.

The presence of multiple return paths also has an effect on the design of a coaxial cable that is to be used for powering. In coaxial cable design, the most effective way to reduce the cable's DC loop resistance is to add material

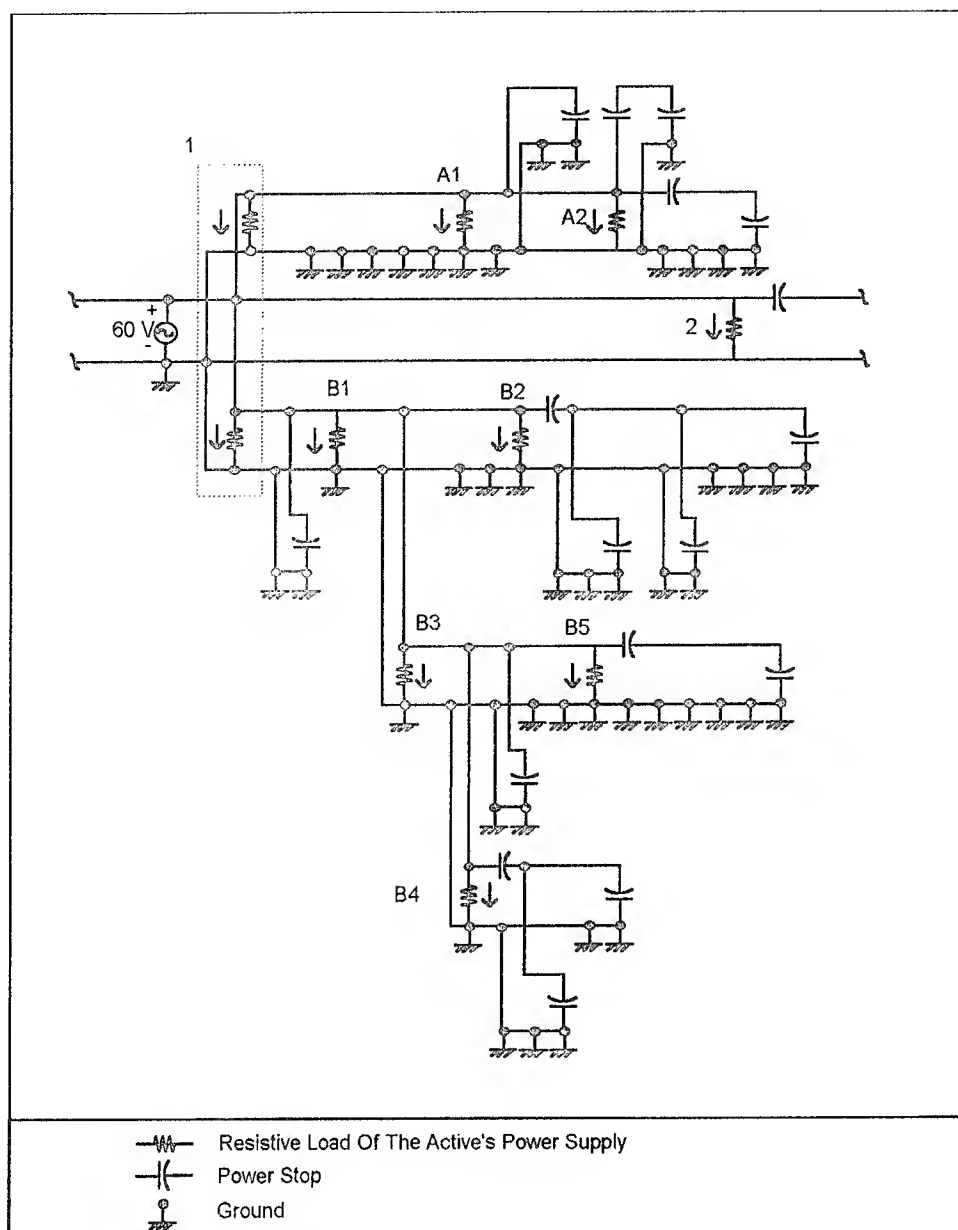


FIGURE 4. - Electrical Powering Circuit Model
(Buried CATV Coaxial Cable Distribution Plant)

to the center conductor, rather than to the outer conductor. This is because of several reasons: 1) The center conductor contributes approximately 70% of the total DC loop resistance. 2) Multiple forward paths do not exist in the CATV powering circuit, indicating that the majority of current will reside on the center conductor. 3) The addition of material to the cable's outer conductor will adversely affect the cable's handling performance, weight and reliability, without having any

other electrical improvements such as attenuation, SRL, impedance, etc.

CORROSION TESTING

Introduction

In order to address the concerns of system reliability and performance and how they relate to the future powering schemes being considered for the broadband coaxial cable

distribution plant, it is important to understand the effects of these powering schemes on corrosion. Because electrochemical (wet) corrosion is the most common type and involves the presence of two dissimilar metal surfaces, the corrosion testing performed herein focuses on comparing the effects of both AC and DC powering waveforms on corrosion at the connector and cable system.

Electrochemistry Background

In order for an electrochemical reaction to occur, two dissimilar metal surfaces must exist at the site and be in electrical contact with each other and an electrolyte, i.e., liquid solution, must be present and in contact with the two metal surfaces.

The electrochemical reaction can be modeled by a simple voltaic cell, as shown in Figure 5. The ions in the liquid solution react with one of the metal surfaces, cathode, causing positively charged metal ions to enter the solution, giving the cathode a negative charge (oxidation reaction). The free electrons from the other metal surface, anode, react to the positive ions in the solution, leaving this metal with a positive charge (reduction reaction). Due to the difference in charge, a voltage potential occurs between the two metals and a current flow results. In freely corroding systems, however, such as the connector and cable system, there is no external electrical circuit, therefore, the oxidation reaction must occur in local proximity to the accompanying reduction reaction.

Galvanic Corrosion

Corrosion is an electrochemical process and is driven by

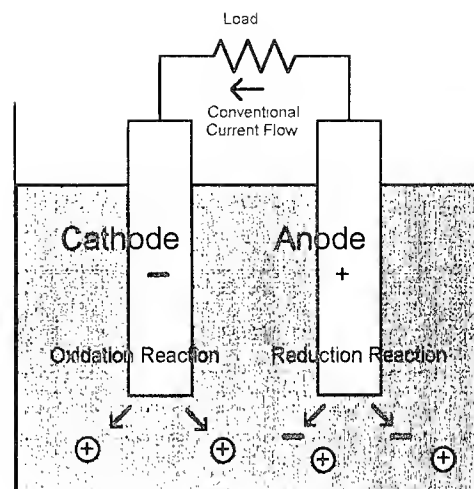


Figure 5. - Voltaic Cell Model

the voltage difference between the oxidation reaction and the reduction reaction. Therefore, by changing the voltage potential of a given metal surface, a change in the rate of corrosion will occur for that metal, relative to its freely corroding state. This is referred to as galvanic coupling.

A typical galvanic couple at the interface of a CATV Pin-type connector and distribution coaxial cable as shown in Figure 6, involves copper of the center conductor (cathode) and tin of the center conductor seizure mechanism (anode). When a galvanic cell develops, the anodic material usually deteriorates at an accelerated rate relative to its freely corroding state. ^[2]

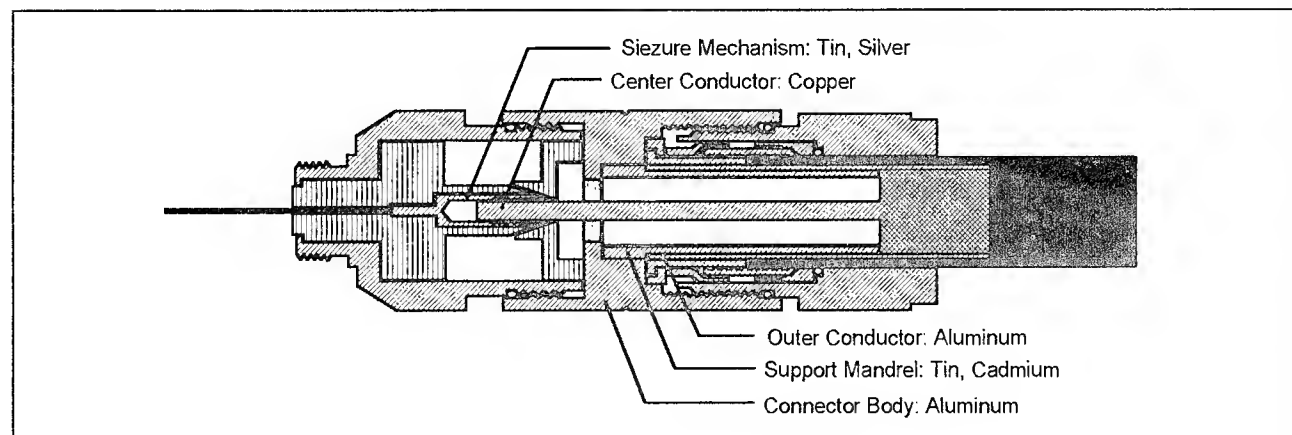


FIGURE 6. - Connector and Cable Interface (Pin Type)

Procedure

The connector and cable samples were subjected to the salt fog chamber per ASTM B 117 for a duration of thirty days, while being powered by both AC and DC waveforms.

Four control samples were without power, twelve samples were powered with AC (60 Vrms, 15 Arms) and 24 samples were powered with DC (60 Vrms, 15 Arms) as shown in Table 2.

Power	Moisture Seal	No. of Samples
No Power	With/Without	4
AC* (60V, 15A)	With/Without	12
DC (60V, 15A) Forward/Reverse	With/Without	24

* 60 Hz Sinusoidal

TABLE 2. - Connector and Cable Samples

Half of the samples had their moisture seal (O-rings) removed in order to insure that their insides were equally conditioned by the salt fog, while the other half was protected by their O-rings and the application of a shrinkboot. Half of the DC powered samples had current traveling in one direction, and the other half had current traveling in the opposite direction, in order to compare the effects of current direction. The connector and cable samples under test were 500 series and identical to that shown in Figure 6. The integral support mandrel and center conductor seizure mechanism of the connector were brass with bright acid tin plating.

In order to deliver power to the connector and cable samples under test, each sample consisted of two three-foot sections of coaxial cable with connectors spliced together at one end using a female pin-type barrel. Each end of the connector and cable sample was then connected to a six foot length of twelve gauge copper pair insulated industrial wire which extended outside of the salt fog chamber. The connections not being tested were carefully protected with silicon so as not to create any variables within the test. The samples were connected in series as shown in Figure 7 and the voltage and current were monitored daily for proper loading. The resistive load for both the AC and DC circuit consisted of heat resistor bars rated at 1500 Watts.

The effects of powering on corrosion were determined both electrically and physically. The electrical evaluation consisted of measuring the contact resistance of both the inner and outer conductor. The contact resistance

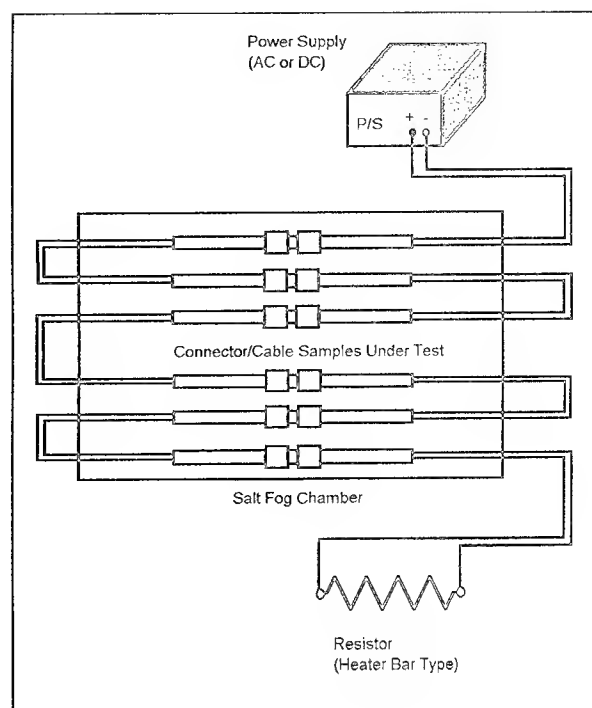


FIGURE 7. - Power Loading Scheme

depends on the contact area, pressure and surface conditions. The contact resistance will, therefore, increase with the development of corrosion on the contact surfaces. The physical evaluation consisted of dissecting the connector and cable sample and viewing it under the microscope for the presence of corrosion.

Findings

After thirty days of conditioning the connector and cable samples in the salt fog chamber while under power, their inner and outer conductor contact resistances were measured and compared to a sample that had not been powered. Figure 8 summarizes these results as shown in Table 3.

Figure 8	Contact Resistance	Moisture Seal
A	Center Conductor	w/o
B	Center Conductor	w
C	Outer Conductor	w/o
D	Outer Conductor	w

TABLE 3. - Figure 8 Plots

Because the contact resistances of the connector and cable sample are of such small values, the wires used to deliver power to the sample were removed from the

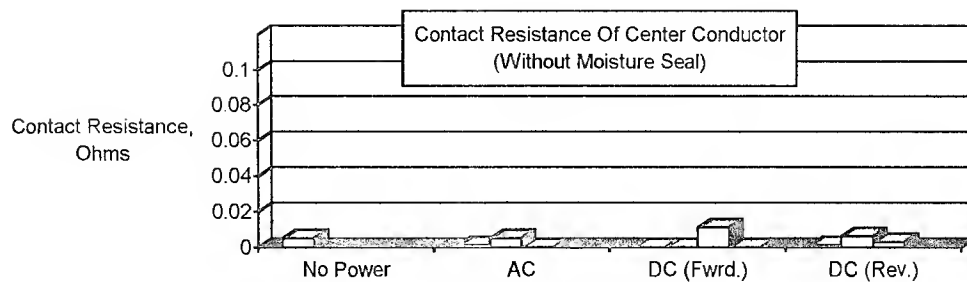


FIGURE 8A

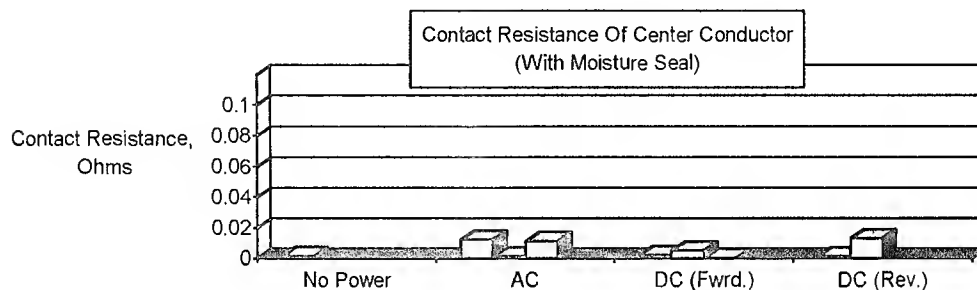


FIGURE 8B

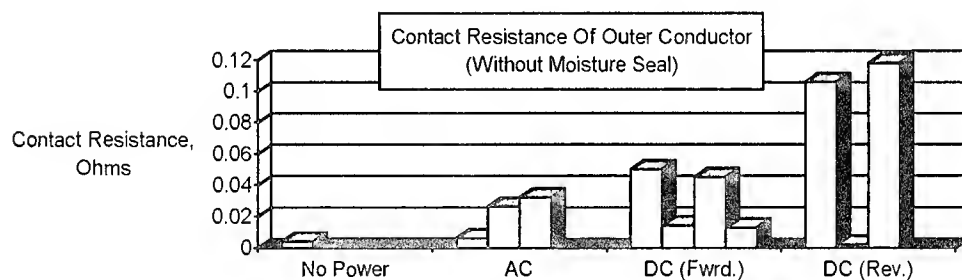


FIGURE 8C

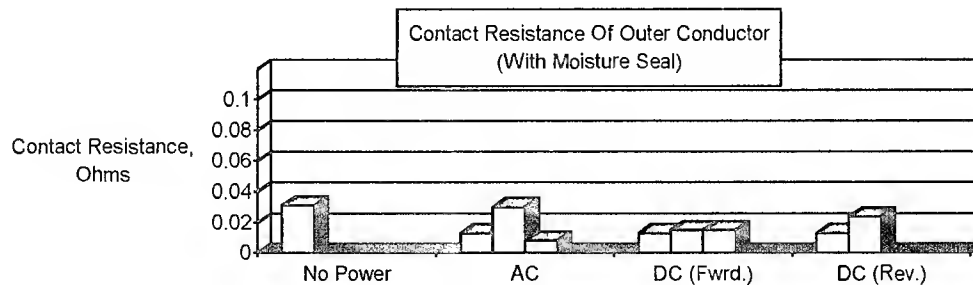


FIGURE 8D

measurement. The contact resistance measurements shown in Figure 8 are, therefore, of the three foot section of coaxial cable and the connector under test.

The contact resistances measured were all of small values, however, they do indicate that currents have an effect on corrosion and that DC currents appear to have more of an effect than AC. The contact resistance measurements also indicate that currents had more of an effect on the outer conductor than on the center conductor and that the direction of current had an effect on the outer conductor contact resistance. The sealed connectors showed less of an effect, compared to samples without moisture seal, as expected.

Visual examination of the connector and cable samples did not show any signs of corrosion, however, there were traces of salt within the unsealed samples as expected. Samples that were sealed did not show any signs of salt fog migration.

Conclusion

From the findings of the thirty day corrosion test, there was no visual appearance of any corrosion present and the inner and outer conductor contact resistances had very little effect. The contact resistances did indicate, however, that currents do have an effect on corrosion and that DC currents have more of an effect than AC.

From these findings it is recommended that a more severe corrosion test be conducted, such as CASS (Copper Acetic Acid Salt Spray) testing, in order to accelerate the development of corrosion or that the duration of time be extended for the salt fog testing.

ACKNOWLEDGMENTS

The author would like to thank Mr. Bruce Carlson, Product Development Manager, for his support and direction and the field support from Mr. M. Pennell and Mr. J. Elko. The author would also like to extend his sincere appreciation to the cable operators for their cooperation in letting these studies be performed on their systems.

Finally, the author is grateful to the management of CommScope, Inc. for supporting the publication of this paper.

REFERENCES

- [1] T. Osterman. "Grounding, sheath current and reliability: A CATV power distribution analysis". Communications Technology, 1992.
- [2] B. Bauer. "Hidden Influences on Drop Reliability: Effects of Low Level Currents on F-Interface Corrosion and Performance". Technical Papers of the NCTA, 1992.



Henry D. Pixley,
Product Development Engineer
CommScope, Inc.
General Instrument Corporation
6519 CommScope Rd.
Catawba, North Carolina 28609

Henry graduated from SUNY New Paltz, NY with a Bachelor of Science in Electrical Engineering in 1991 and joined Cablewave Systems, Div. of RFS to design and develop a line of radiating coaxial cables.

He joined CommScope, Inc. in the beginning of 1994 and is responsible for the development of new trunk and distribution and coaxial drop cable products. He is also a member of the Society of Cable Television Engineers (SCTE).

PROCESS CONTROL OF MULTIPAIR CABLE FOR CROSSTALK PERFORMANCE

Dai Kang, Zhou Fengqi

Chengdu Cable Plant, China
P.O.BOX 351, 610042, Chengdu, P.R.China

Abstract

The effect of pair lay design, core and unit constructions and stranding process etc. on crosstalk is evaluated based on the basic theory of crosstalk and our practice. Some random factors are analyzed, such as the deformation of pair lay and pair jumping in the course of helical stranding with respect to the reasons, characteristics and influence.

1. Introduction

In China, even in many countries all over the world, multipair cable plays a main part as the transmission media in local communications at present and even in a long time to come. For instance, PIC telephone cables laid in China are increasing year after year. In the forthcoming modern telecom network, full use must be made of existing and yet-to-be-laid cables to realize digital transmission.

--In junction line and the line from switching office to distribution points in a subscriber loop, a single cable-four wire system allows for PCM system to be transmitted at 2.048 Mbits/s, requiring more systems to be in transmission, i.e., more pairs available over a given transmission distance.

--In the line from distribution point to subscribers in a subscriber loop, by means of time compression multiplex (TCM) technique, all pairs are used to transmit ISDN in the form of 2B+D, requiring longer transmission distance on condition that transmission quality is ensured.

The above two applications are not only restricted by the high frequency attenuation of cable, but also by its NEXT and FEXT respectively. To diminish high frequency crosstalk has been a difficult point, but also a hot subject concerning the techniques of manufacturing multipair cable. This paper is intended to analyze in an all-around way various factors affecting crosstalk in the course of design and production of a cable.

2. Basic Theory of Crosstalk^{[1][2]}

The essence of crosstalk between loops is electromagnetic coupling. The direct electrical coupling coefficient c' and

magnetic coupling coefficient m' on a unit length between loops made up of two pairs are respectively the following:

$$c' = \frac{\pi \epsilon \xi}{2 \ln \frac{a_{12}}{r} \ln \frac{a_{34}}{r}} \cdot \ln \left(\frac{a_{14} \cdot a_{23}}{a_{13} \cdot a_{24}} \right) \quad (1)$$

$$m' = \frac{\mu}{2\pi} \cdot \ln \left(\frac{a_{14} \cdot a_{23}}{a_{13} \cdot a_{24}} \right) \quad (2)$$

where, r : conductor radius

a_{ij} : the distance between the centers of conductors i and j . 1 and 2 constitute pair I; 3 and 4, pair II.

ϵ : equivalent dielectric constant

μ : permeability

ξ : correction coefficient necessary since conductors between two pairs function as electric field shield.

The more these conductors, i.e., the greater the distance between I and II, the smaller ξ is. When I is adjacent to II, $\xi = 1$.

When transmission frequency is close to or more than 50kHz, the influence of the shield will gradually become predominant. By shield, herein, we mean the conductors of pairs in the vicinity of and surrounding pairs I, II, (or cable shield tape). In the case of the multipair cable constructed of compact core, the shield can be taken as a continuous seamless closed circle. Its influence can be expressed by electromagnetic coupling between the mirror image I' of the disturbing pair I versus the shield and disturbed pair II. Similarly, the coupling coefficients are respectively as follows:

$$c'' = \frac{\pi \epsilon \xi}{2 \ln \frac{a_{12}}{r} \cdot \ln \frac{a_{34}}{r}} \cdot \ln \left(\frac{a_{1'4} \cdot a_{2'3}}{a_{1'3} \cdot a_{2'4}} \right) \quad (3)$$

$$m'' = \frac{\mu}{2\pi} \cdot \ln \left(\frac{a_{2'3} \cdot a_{1'4}}{a_{1'3} \cdot a_{2'4}} \right) \quad (4)$$

The total electric and magnetic coupling coefficients are obtained on the unit length between the two circuits.

As the value of the fourth power and more of $\left(\frac{d}{2D}\right)$, $\left(\frac{d}{2D'} \cdot \frac{R}{a}\right)$ is much smaller than 1, only the case where $\alpha, \beta = 1$ is taken into account, thus, we get:

$$L_{\alpha\beta} \approx L_{11} = 4\left(\frac{d}{2D}\right)^2 \quad (12)$$

$$L'_{\alpha\beta} \approx L'_{11} = 4\left(\frac{d}{2D'}\right)^2 \cdot \left(\frac{R}{a}\right)^2 \quad (13)$$

Pair lay length can be selected by calculating the minimum crosstalk loss, that is, to find the maximum value K of the integral term in equation (9):

$$\begin{aligned} K &= \left| \int_0^l [L_1(z) - L_2(z)] dz \right|_{\max} \\ &= \left| \int_0^l L_1(z) dz \right|_{\max} + \left| \int_0^l L_2(z) dz \right|_{\max} \\ &= \frac{4}{\pi} \cdot \left(\frac{d}{2D}\right)^2 \cdot \left(\frac{1}{h_a} + \frac{1}{h_b}\right)^{-1} + \frac{4}{\pi} \cdot \left(\frac{d}{2D'}\right)^2 \cdot \left(\frac{R}{a}\right)^2 \cdot \left|\frac{1}{h_a} - \frac{1}{h_b}\right|^{-1} \end{aligned} \quad (14)$$

where, $D' = \frac{1}{a} \cdot \sqrt{R^4 + a^2 b^2 - R^2 \cdot (a^2 + b^2 - D^2)}$.

AutoCAD software can be used to instantly draw Fig.1, in which the distance of the center of each pair layer from point 0 is 0.68, 2.1 and 3.25mm. Use DXFOUT command to transmit graphic information to a sequential file. Then several lines of program in BASIC language will read the coordinates of the centers of 25 circles in the file. Enter the scheme of pair lay design to find out D , D' and K of 300 combinations.

The pair lay design can be optimized in the following two ways:

--Decrease the average value \bar{K} of K . It largely depends on the size range of pair lay length. We adopt 50.8 ~ 140.2mm. The ratio of adjacent lays is 1.040 ~ 1.053. It is helpful to reduce crosstalk in its entirety by adopting short lay scheme. But the disadvantage is that twinning speed is slower, too small difference of lays may likely occur between the adjacent pairs in a unit and pair lays are required to be perfectly accurate.

--Due to the fairly wide dispersion of the K values of 300 combinations, the basic principle of the distribution of pair lays is to avoid the occurrence of relatively great K value ($K > 20.0$ mm). The lay difference of two closer pairs should be larger, and even larger when the two lay lengths are comparatively great.

To appropriately distribute pair lays can also reduce \bar{K} . The authors substituted 44.96mm for one pair lay in our previous design and worked out a new lay design scheme with the aid of computer. As for SA 0.4 cable, K decreases from the original 5.356mm to 4.891mm, while the number of $K(>20.0$ mm) from 6 to 1, --the K value of pair 3-22 is

21.80mm. As the pairs in the middle layer separate pair 3 from pair 22, this combination will suffer less risk.

In the above computation, ξ is considered as constant 1, despite the fact that it is actually a function of D . FEXT loss at 150kHz of the combination composed of pair 2 and 8 is for many times, lower than 58dB/km, for reasons that no pair separates them, in addition to the comparatively great K (18.93mm).

2.2 General Analysis of the Effect of Random Factors on Crosstalk

Crosstalk is conventionally divided into systematic crosstalk and random crosstalk. The former can be analyzed quantitatively as described above while the latter is more influential, though not predictable.

The random phenomenon that the position of a pair is not fixable should be given an all-round analyze based on equations (1)-(4). The most desirable case is:

$a_{23} \cdot a_{14} = a_{13} \cdot a_{24}$, $a_{2'3} \cdot a_{1'4} = a_{1'3} \cdot a_{2'4}$. However, there exists no such absolute "symmetry" at all. The comparatively ideal and available case is a great distance between pairs, so $a_{23} \cdot a_{14} / (a_{13} \cdot a_{24}) \rightarrow 1$, $a_{2'3} \cdot a_{1'4} / (a_{1'3} \cdot a_{2'4}) \rightarrow 1$ and ξ is very small, k will be extremely small.

The majority of combinations have to rely on the cross-over of loops to diminish crosstalk. The function of twinning is to make the positions of the wires in a pair ceaselessly alternate, causing $a_{23}(z) \cdot a_{14}(z) / (a_{13}(z) \cdot a_{24}(z))$, $a_{2'3}(z) \cdot a_{1'4}(z) / (a_{1'3}(z) \cdot a_{2'4}(z))$ to fluctuate to-and-fro between >1 and <1 , as a result, $L_1(z)$, $L_2(z)$ are sometimes positive, sometimes negative, thus, in the entire length of a cable, c , m are themselves partially counteracted. The more frequently, the change between the positive and negative values of logarithm term takes place and the more uniform the magnitude, the smaller c , m in the entire length of a cable is. This requires the lays of two pairs to be uniform in size and appropriate in combination.

However, some random factors such as the deformation of pair lay, sharp twist along the cable length impair the counteraction degree of c , m . For multipair cable, the effect of the distance between pairs on crosstalk is more obvious. Following is an extreme example: during the production of a batch of cables, two pairs twinned with identical lay lengths were incorporated into a U-unit. In the quality inspection of this batch, FEXT loss at 150 kHz between the pairs was found to be greater than 58dB/km.

Of FEXT loss, RMS value is more apt to be affected by some combinations of lower FEXT loss than average value (Avg). And of NEXT attenuation, average value minus standard deviation (Avg - S) can also be affected to a certain extent owing to the tremendous difference in the test values of

individual combination. Therefore, it is desirable that the coupling loss of each combination is distributed as evenly as possible. To fix the position of a pair and optimize pair lays can not satisfactorily fulfill this requirement. Other approach is to allow of the same average distance among all the pairs in the U-units along the entire cable length. This is just the basic theorem of cross stranding^[3].

3. Practical Application

Our production equipment consists of $\Phi 1600$ and $\Phi 2400$ drum strander and cabler, both made by Pourtier Co. . Helical stranding process is adopted. The two lines are respectively packaged with 4-row and 8-row pay-off stands, each accommodating the pairs for one U-unit. The pairs are stringed with reference to Fig.1 through the eyelets in the array of "3 + 9 + 13" on oscillators. After oscillation, the U-unit (or subunit) is bound with two 125tex PP binders. Then, over the core(200 and less pairs) is longitudinally covered a layer of PET film, on which a binding thread is in turn applied. In the case of SD- or S-unit, a 250tex binder is applied.

The core of 300 and more pairs, are bunch-stranded of the units after each arranged in accordance with specific construction.

3.1 Unfixed Position of Pair

The pairs in the U-unit in concentric construction are arranged according to color code sequence as required in the cable specification. A long-term observation verifies that this requirement has never been attained.

The reason is that when pairs are going through closing die A after the oscillators, those in the central and middle layers are apt to jump to the inner wall of the die, especially when the inner diameter (ID) of the die is relatively large. The IDs of the dies B, C, D from die A to binding head with 125tex binder are so large that the pairs are allowed to jump almost without any limitation. Another reason is that 125tex binder fails to fix the positions of the pairs. The binder breaks frequently ascribed to a little too much tension. So the operators often release the tension on the binder. A core of 25 and less pairs is not bound with any binder, furthermore, the binding head is some distance away from the oscillator, there is still no way to hold the pairs in place.

In order to find out the actual effect of the unfixed positions of pairs on crosstalk, in the stranding of SD unit of HYA 2400 \times 2 \times 0.4 cable, we handled U1,U2 of the unit in the following different ways:

--U1: substantially the same way as in normal production. IDs of dies A, B, C, D were $\Phi 20.0\text{mm}$; 125tex binder was under loose tension. The positions of pairs were somewhat jumbled up.

--U2: IDs of dies A, B, C, D are $\Phi 8.5\text{mm}$. 125tex binder was under relatively great tension. A slight modification was made of the oscillator, that is, to shorten the distance from eyelets "3 + 9" to the center of the oscillator. Besides, enlightened by the practice that a large sized cable was stranded by closing its units layer by layer, we added a transit die between the oscillator and closing die A, through which pairs 1 ~ 12 were closed in advance. After start-up, we stopped the machine to check the pairs at intervals of a certain production length. The phenomenon that pairs 1 ~ 12 jumped to the outer layer was dramatically reduced. And the pairs in the same layer tended to be assembled in sequence of color code. However, there were pairs that jumped off their positions all the time, and the pairs were not assembled in full conformance with Fig.1. This indicates that compared with a unit, a tiny pair jumps off its position very easily.

The typical data of the crosstalk tests for trial cables are listed in Table 1.

Table 1 Data of the crosstalk tests for trial cables

	Coupling Losses (dB/km) ELFEXT@150kHz ALL Combinations (n=300)		Coupling Losses (dB/km) NEXT@1024kHz ALL Combinations (n=300)	
	U1	U2	U1	U2
IND MIN	59.6	57.1	48	47.8
IND MAX	109.4	111.5	96.8	107.5
Avg	78.3	78.7	71.5	71.5
STD DEV	9.2	10.1	10.5	11.1
RMS	71.4	70.2	61.4	61.3
Avg-S	69.1	68.6	61	60.4

The test results of U1 are not quite different from those of U2. One of the reasons is that there still exists the case that the positions of pairs in U2 remain unfixed. Anyhow, this test is convincing enough to dispel people's worry about the unfixed positions of pairs. This is of great importance to cable production.

In China, some manufacturers have already imported from Sweden cross-stranding equipment, on which twinning and stranding are completed in one operation. It is introduced that 40 ~ 100mm pair lay lengths are adopted. The typical data of ONEXT(1024kHz) in the U-unit of SA 0.4 cable produced therewith are: Avg = 64.97dB/km, STD DEV = 5.65dB/km. The dispersion extent of crosstalk attenuation is tremendously reduced, conformable with our expectation in this study. Their comparison test between cross stranding and concentric layer stranding came to the same conclusion. But it is somewhat beyond our expectation that the average value is lower. This might be attributed to the loose control of the quality exerted in the insulating procedure. As NEXT loss is less affected by some random

factors, it increases due to the random alternation of pair positions not so markedly as FEXT loss.

The data the authors collected display that both the average value and standard deviation of the crosstalk attenuation of a cross-stranded cable are lower than those of a concentric-lay cable. So RMS value of FEXT loss and Avg--S of NEXT attenuation of the above two cables do not differ greatly. The difference depends principally on pair lays. The above conclusion need to be further verified on account of limited source of data.

Over a long period of time, in testing FEXT and the capacitance unbalance pair-pair (CUPP) of a concentric-lay cable, only special combinations are selected among the adjacent and alternate pairs in the same layer and among the pairs in the central layer and those in the other layers. This has become a customary practice in the cable industry. As there exists above case that the positions of pairs are not fixed, some minimum, even non-conforming FEXT loss and maximum CUPP that might occur in those untested combinations will certainly be missed. China's national standard that is about to be implemented 《Local Telecommunication Cables with Polyolefin Insulation and Polyolefin Sheath》 sets forth a definite requirement that the verification of minimum individual value (58dB/km) of FEXT loss at 150kHz should cover all the pair combinations in a basic unit. But the verification of RMS value falls into two cases: for cross stranding, statistics should be made for all the combinations, while for concentric-lay stranding, only for special combinations -- RMS value thus obtained is generally lower by over 1dB/km than the whole combination.

The statistics of a large quantity of our test data exhibits that there are both higher FEXT loss and minimum value between the closer pairs (including those adjacent pairs in the middle and outer layers), as shown in Fig.1. The latter has greater probability, which shows that they have more chances to draw close in a unit. The positions of pairs remain somewhat stable on the local length of a cable and in partial pairs, their random degree can, after all, not be as great as that in cross-stranding. This is also one of the reasons for the slight difference of our comparison tests as described above. Therefore, to optimize the pair lay design has not yet lost its significance. The authors once analyzed a lay length scheme provided by a certain manufacturer, which basically has the same equipment and adopts the same process as our plant. We found in the tests that FEXT loss at 150kHz of between pairs 6 and 16 in Fig.1 was lower than 58dB/km for many consecutive times, agreeable to the larger K value of this combination ($h_a = 60.4\text{mm}$, $h_b = 57.4\text{mm}$, $R = 4.55\text{mm}$, $D = 0.93\text{mm}$, $D' = 5.45\text{mm}$, $K = 26.38\text{mm}$)

3.2 Deformation of Pair Lay

The twist lays of pairs increase and decrease alternatively along the core length with big or small magnitude. This

situation is related to the factors, such as backtwist, forwardtwist of pairs and tension fluctuation during the stranding of a unit.

On-site observation found that the lay lengths of the twinned wires between pay-offs and oscillators were popularly shortened and then gradually resumed to a different extent while going between the oscillators and the stranding cabinet, even greater prior to stranding. The longer the pair lay is, the more liable it deforms.

It was also found that the farther, the pairs away from the oscillators, the more sharply they deformed. For example, in the measurement of the lay lengths of a 3m cable, the variation of the average lay length of a violet/slate pair often exceeds 30mm and has been more or less reflected in the test of FEXT, based on which appropriate adjustment should be made in finalizing the pair lay lengths.

However, it is almost impossible to change the lays of the pairs made up of conductors sized 0.7, 0.8 and 0.9mm once having been twisted. This might probably be one of the reasons why it is easier for the cable with larger DOD to have better crosstalk attenuation performance.

On the other hand, in the core of a longer length, the average lay length of individual pair remains the same as that before stranding. The twist points do not change with regard to the total number, but slide along the cable length, and no longer distribute evenly. So it is still necessary to have the pair lays under rigid control in the twinning procedure.

3.3 Effect of Oscillator and Unit Binder

They both have some effect on NEXT between U-units in the same SD-unit.

Oscillation can prevent the two pairs between the adjacent U-units (especially, the pairs with identical lay length) from keeping adjacent in parallel throughout. In case the positions of the pairs in U-unit are in the status of random variation on the whole, it will be no need to oscillate.

Unit binders should ensure to keep SD-unit and 4 U-units therein round in contour and symmetrical in construction. Taking the SD-unit of SA 0.4 as an example, the numbers of U-units assembled clockwise are assumed to be 1, 2, 3, 4, as regards the Avg--S value of NEXT loss between U1-U3 and between U2-U4, one with a higher value is usually accompanied by another with a lower value ($<79\text{dB/km}$). This is attributed to the loose tension and large lay length of the unit binder. It is incidentally pointed out that a considerable number of people hold that all the U-units in the same SD-unit have a relation of being adjacent to each other. They even do not at all test the NEXT attenuation between U1-U3, U2-U4.

3.4 Cable Constructed of Subunits

The U-unit of the cable containing 30, 50, ... pairs is usually composed of subunits: 8 + 8 + 9 or 12 + 13. The crosstalk attenuation measured is often lower than the requirements set in the standard. The reasons is that the distance between pairs in a subunit generally becomes shorter, the probability of two pairs being adjacent in parallel over a long distance along cable length becomes more. The pair lay design optimized according to Fig. 1 is no longer "optimized".

The authors believe that it is not reasonable to make a SD-unit, using 10 subunits^[4]. It is recommended that no subunits should be used in the core as the case may be.

But the cable containing conductors sized 0.7, 0.8 or 0.9mm is an exception. The use of subunits in a cable can give a round and compact core. Compared with the subunits containing conductors sized 0.4, 0.5mm, their K values are generally lower, so the crosstalk attenuation performance of the cable is better.

4. Conclusion

Our study mainly relates to the high frequency crosstalk performance of PIC telephone cable composed of helically stranded units. However, part of the conclusion is also applied to multipair cable of other constructions or types.

1) During the course of producing a cable, some random factors impose dominant and complex influence on crosstalk. An overall analysis should be given of hard-to-eliminate problem like pair jumping instead of simply following traditional viewpoint that crosstalk is separately considered as systematic crosstalk and random crosstalk.

2) It is still essential in a certain sense to optimize the pair lay design. The adoption of CAD method can make design procedure quite convenient and fast. Those factors like the deformation of pair lay should also be taken into consideration in the design. Different manufacturers can develop different designs.

3) Importance should be attached to the effect of core construction on crosstalk.

4) The crosstalk performance of a cable comprehensively reflects the level of a manufacturer in regard to its production process and quality control, which can be appraised in the following respects:

--whether the test values can extensively satisfy or exceed the requirements of the standards.

--whether the minimum individual value of FEXT loss of the whole combination often arises from a few combinations thereof.

--whether simply rely on the adoption of shorter lays to partially counteract the influence of other adverse factors.

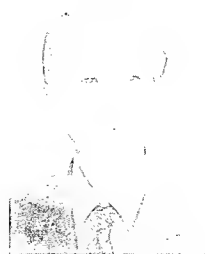
References

- [1] (德) Wilhelm..Klein, 《通信线路的串音理论》 (中译本), 人民邮电出版社, 1959年
- [2] 《通信电缆的设计与制造》, 南京邮电学院, 1977年
- [3] Sigurd Nordblad, "Multi-Paired Cable of Non Layer Design For Low Capacitance Unbalance Telecommunication Network.", 22nd IWCS, 1973
- [4] E.Esposito, "Test and Measurement Parameters for Telephone Multipair Copper Cables", 38th IWCS, 1989



Dai Kang
Chengdu Cable Plant,
Chengdu, Sichuan,
China

Mr. Dai was born in 1966 and graduated from Electrical Engineering Department of Xian Jiao Tong University in 1987. He joined Chengdu Cable Plant after graduation and having been engaged in cable design and manufacture technology.



Zhou Fengqi
Chengdu Cable Plant,
Chengdu, Sichuan,
China

Mr. Zhou graduated from Harbin Institute of Electrical Technology in 1963 and joined Chengdu Cable Plant in the same year, having been engaged in research, development, design and manufacture technology of telecom cable since then. He is the member of China's Telecommunications Society and the Chief Engineer of Chengdu Cable Plant.

TV AND THE TWISTED PAIR

David J. Meskell, Jr.

DJM Techniques
Eatonton, Georgia

ABSTRACT

Video transmission and telephone twisted pair cables are both ubiquitous in the USA but, until now, they have never met. With recent advances in dynamic equalization, echo canceling, signal compression and digital coding, in combination with the inherent transmission capabilities of twisted pair, they may well be the best way to carry video services the last couple of kilofeet to the residence. Asymmetrical Digital Subscriber Line (ADSL) systems are a family of digital twisted pair systems that are capable of delivering up to four independent, switchable VCR-quality video-on-demand streams, along with POTS and data, over at least 8,000 feet of unloaded unconditioned twisted pair. Combine this easily implemented technology with fiber feeders and one has a quick, flexible and economical entrance into the Information Age.

INTRODUCTION

As the United States embarks upon the construction of the Information Highway of Tomorrow, the proposed building methods have undergone several changes. First to be proposed was the Fiber-to-the-Home (FTTH) concept, delivering a huge bandwidth potential. However, it proved to be too expensive and was also plagued with questions as to how the customer premises equipment (CPE) would be operated in the case of local power failures. To reduce costs and to ease this powering problem, Fiber-to-the-Curb (FTTC) was suggested. This system would provide service for four to eight homes from one fiber terminal using a twisted pair (TP) and coaxial drop.

Another design studied was a fiber feeder/passive coaxial system that moved the fiber node back as far as possible without requiring line extender amplifiers in the coaxial runs. (Amplifiers are considered a source of service failures and maintenance problems.) Because a passive coaxial system required small serving areas and many fiber optic nodes, the cost again came out too high. The cable television industry meanwhile looked at proposals to do it all on coaxial, Coaxial-to-the-Home (CTTH).

Today both the telcos and the cable industry seem to be focused on the same technology. This technology is the hybrid fiber coaxial (HFC) system which lets the fiber node serve about 500 homes, uses coaxial cable with one or two line extender amplifiers for distribution (a balance of cost and reliability) and eases the powering problem because of the coaxial's ability to carry power. Proponents of this latter system claim it can be built in selected neighborhoods at the same cost as the traditional twisted pair systems.

While any of these systems may be a cost-effective solution for some set of housing densities, take ratios, and service requirements, each requires the building of a new distribution plant with its accompanying costs, time delays in attaining ubiquity, customer aggravations due to construction disruptions and service problems as the new technologies are shaken out.

Almost ignored in this competition is a solution that requires a minimum of rebuilding in the loop (in most cases none), has a cost competitive to the best of the above proposed systems and can be implemented very quickly. The system solution, developed by Bellcore in the late 1980s, is called Asymmetrical Digital Subscriber Line (ADSL) which can deliver to each residence over 6 megabits per second (Mb/s) of bandwidth on a single non-loaded, 24 gage twisted pair for distances of up to 8,000 ft. It also features up to 384 kilobits per second (kb/s) of two-way capability for POTS lines, video phone, work-at-home environments, etc. The downstream 6 Mb/s of bandwidth will deliver either four independently switchable VCR (MPEG-1) quality channels of video on demand (VOD); or two MPEG-1 and one 3 Mb/s full motion channel (MPEG-2), all switchable; or two MPEG-2 switchable channels.

While 6 Mb/s is not as flashy as 750 Mb/s, it is certainly adequate to address the needs and willingness to pay of a large segment of the residential market.

When OSP construction is necessary for ADSL applications, it will be in the form of fiber feeder to a carrier serving area, which is already a telco priority. Further, the ADSL electronics have the flexibility to be installed and relocated as demand shifts. Thus the

service providers not only can provision service sooner, they can also re-arrange their plant should the demand not materialize as planned.

One of the major advantages mentioned for the FTTH, FTTC, and HFC solutions is that they are self-testing and have automated provisioning, which can significantly reduce life-cycle management and maintenance costs. The ADSL subscriber terminals are capable of these same attributes and ability to reduce costs.

Before discussing further the potentials of Asymmetrical Digital Subscriber Line systems, let us first review how ADSL works and what it is capable of doing.

CAPABILITIES OF TWISTED PAIRS

Basic information theory has long shown that twisted pairs have far greater information-carrying capabilities than just the 4 kilohertz (kHz) of bandwidth required for "plain old telephone service" (POTS). However, utilizing these inherent capabilities required adaptive electronics to maximize throughput. With advances in very-large-scale integrated circuit technology (VLSI), a fuller realization of TP's capabilities has now become feasible.

To start, let us look at an information-theory analysis of twisted pairs and estimate their maximum capacity. The theory states that the capacity of a TP, expressed in bits/second (b/s) is found by summing the received signal over the frequency range where the desired signal is stronger than the noise (interference). This is shown mathematically below.

$$\text{Capacity} = \int_0^{\text{frequency}} \log_2 \left(1 + \frac{\text{received power}}{\text{noise power}} \right) df$$

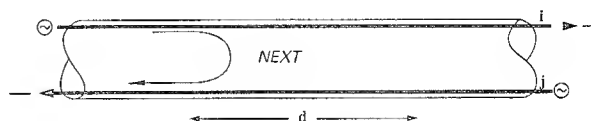
The ratio in the parentheses is called the signal-to-noise ratio (SNR). The received power is the power of the desired information signal at the end of the cable or, in other words, it is the originally transmitted signal modified by the transfer characteristics of the TP. The magnitudes of these changes are functions of the TP's gage, loop length, temperature and the frequency of the signal. For example, 26 gage (0.0159-inch diameter) pairs cause 40% more attenuation than the larger 24 gage (0.0201-inch diameter) pairs which contain about 60% more copper.

The noise power in the denominator of the ratio arises from many sources, such as echoes from bridged taps, impulse noise from switches, electromagnetic interference (EMI) from nearby equipment and crosstalk from other cable pairs. Of these multiple sources of interference, crosstalk is almost always the dominant noise source.

Crosstalk Limits

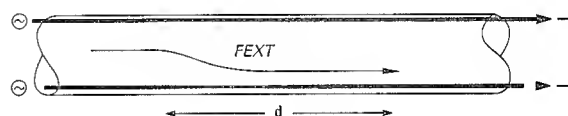
There are two types of crosstalk, as shown in Figure 1. In the upper half of the figure the noise is generated by a high-level transmitter signal from one wire pair leaking over into a low-level receiver signal in another wire pair in the same cable at the same end of the cable.⁽¹⁾ This type of crosstalk is called Near End Crosstalk (NEXT).

Near End Crosstalk



$$\text{CAPABILITY (NEXT)} = \int_0^{\text{freq}} \ln \left(\frac{K_e}{X \sqrt{f}} \right) df$$

Far End Crosstalk



$$\text{CAPABILITY (W/FEXT)} = \int_0^{\text{freq}} \ln \left(1 + \frac{K_e}{\sqrt{f}} \right) df$$

Figure 1

The bottom half of Figure 1 illustrates Far End Crosstalk (FEXT). In this case the interfering transmitter signals are from the opposite end of the cable from the receivers they disturb. To be exact, this is called equal-level FEXT because both the disturbing and disturbed signals experience the TP attenuation equally, having traveled the same distance along their respective wires, so are at the same relative power level. How much signal leaks over in either case depends on how well the cable is designed, built and installed.

Because of the signal level difference—that is, a relatively strong signal at the transmitting end of the circuit interfering with a relatively weak, attenuated signal coming from the far end—NEXT is the major noise contributor on loop circuits. Only where there are transmitters distributed along the cable's length, and the equal-level condition is thus violated, does FEXT become the major concern.

The NEXT of TP cables has been studied extensively and models of its form developed. NEXT is not a strong function of circuit length, but does grow in magnitude with increasing frequency, at about 14 decibels (dB) per decade. That is, if the NEXT level is at -57 dB with respect to the transmitter output level at 80 kHz, as specified by the Bellcore model, then it will be at -43 dB at 800 kHz.⁽²⁾ With this NEXT model and the known loss characteristics of TP cables, the usable bandwidth can be determined.

Bandwidth

Figure 2 illustrates how, for a "non-loaded" 24 gage pair 12,000 feet long, the transmitted signal's power decreases with frequency until the NEXT noise power exceeds it (at about 400-500 kHz). The point in the frequency spectrum where the curves meet defines the usable bandwidth of that gage and system length. Above this frequency the receiver is getting more noise than desired signal. Finer gages or longer lengths will cause the crossover frequency to decrease. Heavier gages and shorter lengths will of course result in a higher crossover frequency.

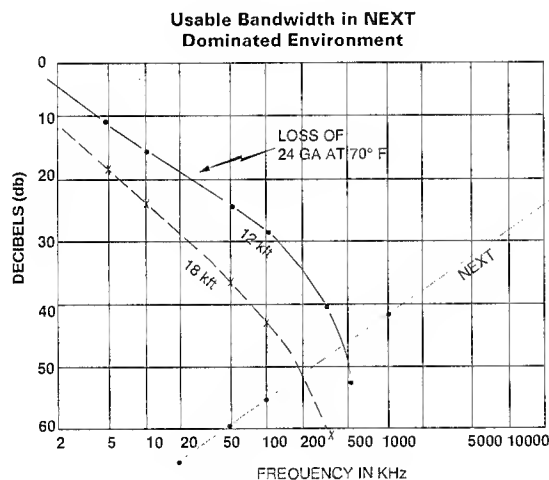


Figure 2

With all the elements defined, and assuming some optimum conditions, an upper bound on capacity can be calculated for non-loaded loops. Because loaded loops have such sharp cut-offs just above the 4 kHz band, they cannot be used for broadband purposes until the load coils are removed.

Figure 3 illustrates the results of the calculations and is called a Shannon Capacity Curve.⁽³⁾ Figure 3 shows both the bandwidth and digital capacity that can be supported by 24 and 26 gage TP as a function of

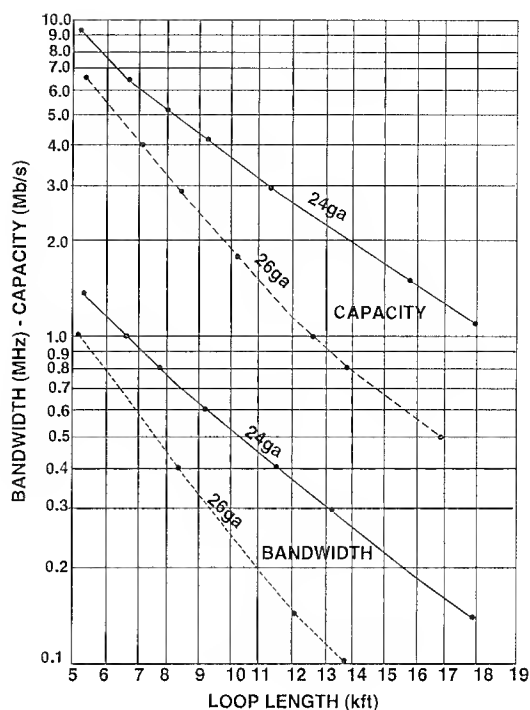


Figure 3

loop length. Of interest is the fact that the capacity of a 26 gage pair at 9,000 ft. is very close to that of a 24 gage pair at 12,000 ft. This capacity equivalency was the basis for defining the size of a Carrier Serving Area (CSA).

The Shannon curves represent bounds on the twisted pair's digital symbol line rate. In the real world attenuation variations, phase distortion, unequal level FEXT, impulse noise, echoes and EMI all work to limit the maximum uncoded rates to less than those given by the Shannon curves.

However, advances in Very Large Scale Integrated (VLSI) circuit technology have facilitated the development of adaptive equalizers and echo cancelers that do very effective jobs of mitigating these disturbing factors and optimizing the TP's performance.

Signal Compression

This new wider-band capability of the TP has worked in synergy with two other technologies to produce a broadband capability. First is the development of compression technology. In the early 1980s a digitalized video signal required 90 Mb/s. Today the ISO Motion Picture Expert Group (MPEG) has defined a VCR equivalent video picture (full motion) standard that can be transmitted at 1.5 Mb/s (MPEG-1). A second standard (MPEG-2) defines a 3

Mb/s video picture that can transmit real-time, fast-action pictures (e.g. sporting events).

These reductions of over 30 to 1 are achieved with picture quality much better than most of us normally see on our analog cable systems, and certainly far superior to antenna-based signals. These compression advances will continue, not because they help ADSL, but because they greatly facilitate the use of regional program sourcing via asynchronous transfer mode (ATM) systems. Nevertheless, each compression achievement will significantly increase the TP system's capability.

Coding

Complementing the advances in compression technology have been the equally important developments in more efficient coding schemes that reduce the required line rate (baud rate).

Several of the more popular coding schemes are shown in Figure 4. The first is the code used in integrated services digital network (ISDN) systems and is called *2B1Q*. In this code two bits are paired. The first bit determines the sign of the transmitted signal. The second bit determines the signal's magnitude. So

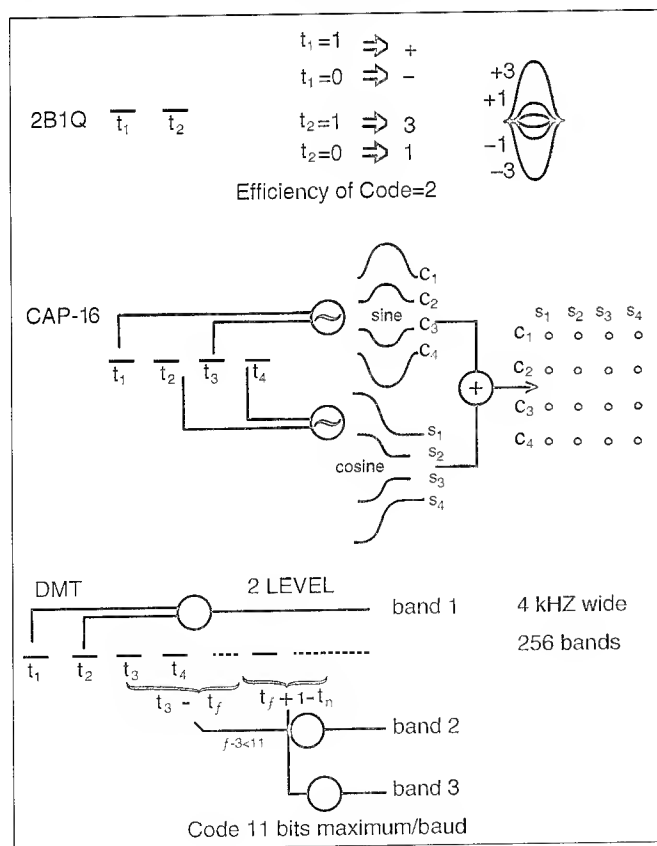


Figure 4

two bits are transmitted by one four-level signal. Thus the code has an efficiency of 2.

Two examples of the higher efficiency codes are also shown. *CAP-16* stands for *Carrierless Amplitude/Phase Modulated* code that transmits 4 bits of information ($2^4 = 16$) in one line pulse that can have 16 configurations.^(4,5) There is also a *CAP-64* that encodes six bits ($2^6 = 64$ possible combinations) into one line pulse.

The CAP-16 coding scheme is in some ways similar to 2B1Q in that bit pairs are used to generate signals of different forms that are orthogonal. These orthogonal signals are added and transmitted. Because orthogonal functions can be easily separated the receiver separates the orthogonal signals and then decodes them into bits.

A second high-efficiency coding method is called *Discrete Multi Tone (DMT)*. In this coding scheme, the available spectrum is divided into a series of 4 kHz channels. The transmitter electronics sample each channel's performance and determine how many encoded bits (i.e. how many signal levels) can be transmitted successfully in each channel. It then assigns the appropriate number of bits to that channel. The maximum number of bits per baud is 11 and some channels may even be shut off at times.⁽⁶⁾ One can picture this system as though one had a number of 4 kHz telephone lines and a collection of modems (4.8, 9.6 and 19.2 kb/s). After testing the line for loss and noise one selects the modem with the highest rate that will work in each 4 kHz channel. Since the noise and loss will vary with time, one would continuously test and assign modems. If there were 256 such 4 kHz channels, frequency multiplexed onto one pair, one would have a DMT system.

Figure 5 illustrates how the CAP and DMT coding schemes would be multiplexed onto a TP in the loop.⁽⁶⁾ Since both codes are bandpass they can be

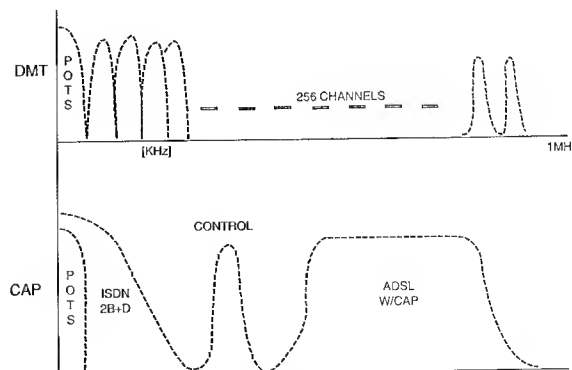


Figure 5

designed to let POTS and/or ISDN exist on the same pair.

After much testing and discussion, the standards being developed by ANSI will be based on the DMT coding scheme.

Asymmetry

The final innovation leading up to the ADSL system was proposed by Bellcore in the late 1980s. Their proposal was to send a broadband signal out from the wire center to the residence and limit the return signal from the residence to a few hundred bits per second. This signal asymmetry eliminates the potential for self-NEXT and thus significantly enhances the system's capabilities (i.e. range times bit rate).

ADSL SYSTEMS

The integration of the technology advances discussed in the previous section has led to three Asymmetrical Digital Subscriber Line systems. These systems are shown in Figure 6 and listed in Table 1. As shown in Table 1, ADSL-1 has a range of 18,000 ft and can carry two-way voice and basic ISDN (160 kb/s) plus one VCR-quality video-on-demand (VOD). Its range covers essentially all the non-loaded (NL) loops, which means it can provide service to over 100 million homes in the USA without a carrier system.

ADSL-2's range exactly matches a Carrier Servicing Area (CSA) and it can carry up to 384 kb/s two ways (H0 channel) plus two MPEG-1 or one MPEG-2. It will cover about 55% of the NL loops without a carrier system.

The newest version, ADSL-3, has a range of 8,000 ft with T-1 in adjacent binder groups on 24 gage cable and 6,000 ft on 26 gage cable with T-1. If the T-1 disturbers are not present the range is even larger. A recent study indicates that, even with T-1 in adjacent binder groups, the probability that ADSL-3 can be deployed over a CSA is greater than 90%.⁽⁷⁾ ADSL-3's payload includes up to a 384 kb/s two ways (H0 channel), which permits such services as video conferencing, access to business local area networks (LANs) for the work-at-home environment and a host of other ISDN services. The downstream-only payload has 6-8 Mb/s of bandwidth and can carry up to four video-on-demand or two real-time, fast-action programs, or combinations of both.

ADSL Supporting a Video Dial Tone Network

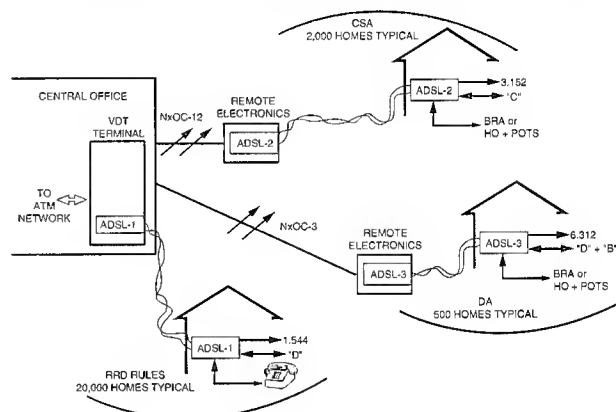


Figure 6

Table 1. ADSL System Options

System	Range	Two Way Rates	Downstream Rate	Video Capability	Reach
ADSL-1	18 kft	POTS or Basic ISDN	1.5 Mb/s	One MPEG-1	≈ 100% of Non-Loaded Loops >100 million homes
ADSL-2	9 kft on 26 ga. 12 kft on 24 ga.	POTS or ISDN or H0	3-4 Mb/s	Two MPEG-1 or One MPEG-2	CSA's 55% of NL Loops
ADSL-3	6 kft on 26 ga. 8 kft on 24 ga.	POTS or ISDN or H0	6-8 Mb/s	Four MPEG-1 or Two MPEG-1 and One MPEG-2 or Two MPEG-2	SUB-CSA 40 - 50% of NL Loops

All this ADSL capability is provided over a single non-loaded twisted pair without the need for line conditioning. The ADSL equipment is designed so that the units are flexible enough to configure for any of the three rates, which simplifies service changes, inventory and maintenance functions. While not the capacity of the FTTH or the HFC, ADSL-3 certainly has the ability to serve the VOD and TV access needs of a large market sector.

Why Use ADSL?

It has been asked, "Why design a system based on the older twisted pair technology when newer and broader band technologies are available?" The answer is not just "because it is there," even though the telcos continue to spend large sums on new copper plant every year and expect to do so well into the next century (≈ 2010). The reasons to build TP/ADSL into the information network plan are:

- Even if the new systems are built at accelerated rates it will be decades before some areas of the country will get access to the information highway. With ADSL the construction requirements are significantly lower, with often no outside plant (OSP) construction at all, so the implementation will be much quicker and less disruptive to customers.
- With volume deployment the cost of ADSL (projected to be in the \$500-800 range per system) competes very well with the other system options, even at high take rates. At lower take rates and spot markets, ADSL will have a large economic advantage.
- ADSL will complement any large systems that are built. For example, if a service provider, for reasons of bandwidth requirements, customer density, copper plant condition, or other reason decides to overbuild with fiber or coaxial, the enhanced services then available might be of limited value unless the people their customers want to interact with (such as regional offices) also have these services. Since ADSL can be applied incrementally, it could be applied in areas outside the rebuild zone to fill this need and complete the highway.
- A major justification for many of the new systems is that they can be easily

reconfigured (connects and disconnects) and service performance can be monitored remotely. These same functions can be built into the ADSL terminals.

- A survey by Bellcore showed that most residences would want a maximum of three to four channels at a time.⁽⁸⁾ ADSL-3 is well matched to this need and, with further advances in compression and/or coding techniques, will have even more capability. The pair's digital capability may be enhanced further by one of its competitors, fiber optics. As fiber optic costs decrease, optic nodes can be justified in smaller serving areas and, with the decreased range from the node to the home, the TP's capacity will increase.
- Since ADSL is not a broadcast system, the service provider has full control of what a customer is sent and thus eliminates the potential for cheating.
- ADSL systems could be used to get an early reading on customer reaction to video dial tone (VDT) without the need for large construction outlays. Some US trials are now starting.
- And, of course, the use of twisted pair solves the problem of POTS powering in power failures.

CONCLUSIONS

The copper twisted pair distribution plant and ADSL provide the telcos with an opportunity to increase revenues from their embedded base and also a means to rapidly, incrementally and economically build sections of the information highway. No one can predict when and what the information highway will turn out to be: FTTH, FTTC, HFC, wireless or TP/ADSL. In all likelihood it will be a mixture of all five, and others not yet conceived, with the TP/ADSL option playing a significant role in providing data and video access to the home. Therefore, it would be unwise to overlook the TP/ADSL potential, the quality of new pair cables, and the maintenance of the existing distribution plant. While twisted pair cables are a mature technology, they aren't "over the hill" yet. They still have a major role to play in the communications systems of tomorrow.

REFERENCES

1. The HDSL Environment. J.-J. Werner, AT&T Bell Labs, IEEE Journal on Selected Areas in Communications, Vol. 9, No. 6, August 1991.
2. High Bit Rate Digital Subscriber Lines: A Review of HDSL Progress. J. Lechleider, Bellcore, IEEE Journal on Selected Areas in Communications, Vol. 9, No. 6, August 1991.
3. The Asymmetrical Digital Subscriber Line (ADSL): A New Transport Technology for Delivering Wideband Capabilities to the Residence. D. Waring, Bellcore, Globecom, 1991.
4. Tutorial on Carrierless AM/PM (CAP). J.-J. Werner, AT&T Bell Labs, UTP-3 Working Group of the ATM Forum Report, April 1993.
5. Tutorial on CAP-Part 2. J.-J. Werner, AT&T Bell Labs, ANSI Report, February 1993.
6. ADSL: The On-Ramp to the Information Highway. S. Fleming and M. McLaughlin, Northern Telecom, Inc., Telephony, July 12, 1993.
7. Application of ADSL Technology to the North American Copper Loop Plant in Support of Video Dial Tone. W. Chen & D. Waring, Bellcore Report, February 1994.
8. Fiber Upgrade Strategies Using High Bit Rate Copper Technologies for Video Delivery. D. Wilson, D. Waring, & T. R. Hsing, Bellcore, Journal of Lightwave Technology, Vol. 10, No. 11, November 1992.



David J. Meskell, Jr. received his Bachelor of Science degree from the US Coast Guard Academy in 1957, an MSME degree from Stevens Institute of Technology in 1963, and an MSEE degree from the University of Maryland in 1968. He was with AT&T Bell Labs from 1961 until 1990, where his main responsibilities were in the design of land and ocean cables (coaxial, paired and fiber) and cable systems. He retired in 1990 as Director of the Transmission Media Laboratory in Atlanta. Presently he operates DJM Techniques, a telecommunications consulting company.

AUTHORS INDEX

Name	Page	Name	Page
ABE, H.	402	COCCHINI, F.	66
ABE, K.	678	CONSONNI, E.	96
AIHARA, K.	715	COOKE, H. G.	12
AIKAWA, H.	644	CORYELL, L. A.	291
AKASAKA, N.	552	COUVRIE, G.	368
AKASAKA, T.	234	CUOMO, D.	66
ANDO, T.	721	CYR, M. J.	256
ARAKI, S.	651	DAMSGAARD, H.	105
ARVIDSSON, B.	545	DANESHVAR, O.	678
ASAKAWA, M.	440	DANZUKA, T.	644
ATOBE, N.	608	DAVIDOW, T.	559
AU, K. C.	582	DÍA, C.	499
BAGUER, L.	499	DOLINOY, D. A.	790
BARK, P. R.	12	DWIVEDI, A.	728
BAUMANN, E.	672	EDGE, C.	281
BEAUCHAMP, W. N.	509	ELKO, J.	694
BELAND, W. D.	256	EOLL, C. K.	12, 728
BÉLANGER, M.	328	ERIKSSON, M.	545
BERTHELSEN, G.	249	ESCRIBANO, F.	499
BEST, A. B.	9	FABIAN, H.	105
BISHOP, J.	408	FACE, D. W.	155
BIZEUL, J. C.	203	FENGQI, Z.	837
BJÖRKMAN, J.	388, 478	FERGUSON, S. T.	227
BLASCO, P.	499	FERINA, JR., R. J.	620
BLYLER, L.	256	FERRI, G.	66
BLYLER, L. L.	241	FLEGAL, W. M.	105
BONICEL, J. P.	368	FLOR, E.	5
BOSAK, J. E.	559	FONTAINE, G. N.	256
BOSCHER, D.	203	FORD, J. R.	265
BOSCHER, G.	633	FORSBERG, S.	478
BOTELHO, J. W.	89	FRANTZ, R. A.	522, 564, 742, 790
BOTTANELLI, M.	528	FRANZ, M.	684
BOTTON, C.	203	FRIDERICH, B.	750
BOWMER, T. N.	742	FRIEBELE, E. J.	310
BOYER, G. R.	11	FUDAMOTO, K.	440
BRAMBILLA, G.	710	FUJUI, T.	440
BROKKE, B. M.	559	FUKAWA, M.	440
BROWN, C. J.	273	FUKUNAGA, S.	440
CARR, J. J.	678	FURUKAWA, H.	627
CHANG, T.-C.	513	GANTT, K.	694
CHANG, W. H.	291	GAO, L.	174
CHAWLA, C. P.	78	GEBIZLIOGLU, O. S.	538, 564, 790
CHEN, H.-T.	483	GIANGROSSI, R.	256
CHEN, K.-Y.	483, 488, 494, 504, 513	GIBSON, F. C.	241
CHEN, T. H.	672	GINOCCHIO, A.	96
CHEN, W.-J.	513	GLAESEMANN, G. S.	728
CHIEN, C.-K.	89	GLODIS, P. F.	105
CHIEN, W.-S.	483	GONZALEZ, C.	802
CHOJETZKI, C.	809	GOTO, S.	608
CHU, C. W.	174	GRAHAM, L.	183
COBO, J.	499	GREGOR, P. E.	363, 819

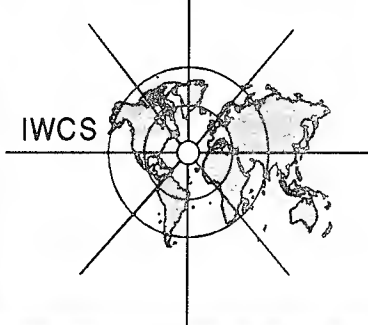
Name	Page	Name	Page
GRIDLEY, C. F.	105	KANG, D.	837
GRIFFIOEN, W.	750	KAR, G.	89
GRIMADO, P. B.	538, 790	KARLSSON, J. O.	134
GRIP, N. E.	388	KARLSSON, P.-O.	763
GROSSO, P.	203	KASHIHARA, Y.	376
GUBSER, D. U.	179	KATSURASHIMA, W.	36, 423
HAAG, H. G.	380, 710	KATZ, C.	450
HAMADA, M.	638	KEESE, J. R.	430
HAMADE, T.	473	KEITH, W. M.	241
HARA, M.	22	KEON, B. J.	522, 742
HASEGAWA, T.	440	KIKUCHI, Y.	627
HASHIGUCHI, Y.	72	KINARD, M. D.	219
HATTORI, T.	552	KING, W. W.	802
HIGUCHI, K.	781	KINOSHITA, I.	781
HINOSHITA, S.	341	KISS, G. D.	538
HIRANO, H.	593	KITAYAMA, Y.	36
HISANO, S.	715	KIUCHI, M.	234
HÖG, G.	134, 380, 819	KLEIN, A. A.	105
HOGARI, K.	593	KNOP, H.	363
HOLMAN, J.	183	KNUDSEN, G.	105
HOLMAN, J. R.	795	KOBAYASHI, K.	28
HOLSTEIN, W. L.	155	KOHTALA, J.	116, 545
HONGO, H.	423	KOUNTZ, D. J.	155
HONJO, M.	768	KOYAMADA, Y.	593
HORIGUCHI, T.	593, 608	KUKUREKA, S. N.	121
HORNG, Y.-T.	488	KURASHIMA, T.	593
HORSKA, J.	50	KURKI, J.	116
HSH, H.-P.	488	KURKJIAN, C. R.	736
HSIAO, J.-M.	513	LAI, K.-H.	494
HSIEH, C.-H.	504	LANDERS, A.	672
INNISS, D.	736	LAUDER, A.	155
INOUE, H.	440	LE NOANE, G.	203
ISBERT, J.	298	LEE, C.-C.	494
ISHI, S.	341	LEE, T.	256
ISHIHARA, K.	3	LEETHAM, R.	121
ISHII, K.	341	LEFEVRE, B. G.	802
ISHIKAWA, H.	644	LIAN, T.-J.	494
ISHINO, Y.	774	LIDÉN, L.	388
ISOBE, T.	781	LIESE, W.	571
ITO, K.	781	LIN, H.-F.	504
IWATA, H.	774	LIN, Y.-C.	504, 513
JABLONOWSKI, D. P.	105	LINDOEF, S.	388
JACKSON, K. W.	126	LIVINGSTON, R. O.	12
JAMET, P.	196	LJUNGQVIST, G.	589
JANSEN, U.	380	LOCH, M.	633
JARLOT, A.	196	LOCHKOVIC, G. A.	12, 430
JENKINS, A. C.	795	LORD, B.	328
JIA, W. S.	672	LUUKKALA, M.	116
JOHANSSON, M.	589	LUX, R. A.	291
JOHNSON, G. E.	241	MA, C. S.	241, 256
JONES, M. W.	241	MAISONNEUVE, J.-M.	298
JUDY, A. F.	658	MALTZ, G. D.	809
KAKUTA, T.	423, 552	MARIETTE, N.	134
KALISH, D.	105	MARUOKA, T.	43, 651
KALOMIRIS, V. E.	315	MATHIS, D.	183
KANAI, K.	614	MATHIS, T. D.	219

Name	Page
MATSUDA, Y.	423, 552
MATSUHASHI, S.	593
MATSUMOTO, M.	774
MATSUOKA, R.	22
MATSUOKA, T.	781
MATSUURA, I.	768
MCALISTER, T.	694
MCALPINE, W. W.	12
MCCALLUM, W. J.	227
MCGURK, G.	265, 273
MCMANUS, S. J.	533
MENG, R. L.	174
MESKELL, JR., D. J.	843
MILLER, G. C.	265
MITSUMI, H.	700
MIYAMOTO, M.	28, 43, 189, 211
MULLANEY, J. S.	509
MULLER, A. J.	126
MURASE, T.	700
MURPHY, C. E.	241, 256
MUTH, H.	315
NAGASAWA, S.	774
NAKAMURA, M.	644
NAKANISHI, H.	468
NANNI, F.	96
NOMURA, Y.	627
NORIMATSU, N.	402
NUNOKAWA, M.	234
OAKLEY, K.	8
OHTA, J.	376
OISHI, K.	423, 552
OKADA, N.	28, 43, 189, 211
OKAMOTO, Y.	638
ONO, S.	700
OOHASHI, K.	651
OSAKA, K.	638
OSAWA, S.	440
OTAKE, A.	22
PANG, P. S. W.	155
PANUSKA, A. J.	219
PARKER, L. J.	265
PATEL, P. D.	219
PATERNOSTRO, G.	134
PERRY, S. C.	802
PETISCE, J. R.	126
PFANDL, W.	413
PIXLEY, H. D.	827
PLITZ, I. M.	564, 790
POLHEMUS, L. G.	142
PORTINARI, A.	96
POWER, J.	395
PUDIA, A.	66
RÄIKÖNEN, H.	116
RALSTON, R. W.	150
RAPEBACH, L.	368
RAUCHS, J.	134, 368

Name	Page
REAGAN, R.	183
REICHERT, W. F.	355
REITH, L. A.	790
RIDD, B. R.	273
ROBA, G.	96
ROCHESTER, C.	395
RUE, R.	256
SAITO, M.	22
SAITO, N.	72
SAITO, S.	189
SAITO, T.	376
SAITO, Y.	665
SAKABE, I.	376, 715
SAKATA, M.	473
SAKATA, Y.	715
SANKAWA, I.	608
SATO, Y.	700
SCHANK, F.	603
SCHAPER, H.	105
SCHMIDT, G. A.	142
SCHÖNFELD, H.	571
SCHULTE, J.	134, 380, 809
SCHULTZ, P. C.	105
SCHULZE-BUXLOH, K.	710
SCHWEIGER, G.	684
SEARS, F. M.	12
SEGA, K.	473
SEKITO, T.	665
SHEN, Z. Y.	155
SHEU, T. J.	483
SHIGEMATSU, T.	614
SHIMO, Y.	473
SHIMOMICHI, T.	651
SHIONO, T.	700
SJÖLIN, K.	388
SMITH, D.	430
SMITH, O. E.	167
SODHI, S. S.	12
SOLLENBERGER, N. W.	126
SORBY, A.	105
STATHUM, R.	256
STEIN, D. R.	684
STENSLAND, L.	589
STEPHENSON, D. L.	802
STÖCKLEIN, W.	413
STORMBOM, L.	116
STROUMBAKIS, D.	256
SUBH, N. T.	795
SUDO, S.	700
SUETSUGU, Y.	665
SULTAN, B. Ä.	460
SUMITA, J.	376
SUZUKI, K.	781
SUZUKI, S.	234, 715
SVENSSON, T.	750, 759, 763
SZUM, D. M.	59

Name	Page	Name	Page
TAGUCHI, T.....	638	WANG, J.-H.	488
TAKASE, H.	72	WANG, S.-I.	504
TAKASHIMA, T.	582	WANN, B.-H.	494
TAKASUGI, Y.	72	WATANABE, K.....	28, 189, 211
TAKEUCHI, Y.	781	WATANABE, T.	638
TANAKA, S.	36	WATARI, T.	721
TANIFUJI, T.	774	WATERWORTH, G.	533
TANSKANEN, J.	545	WATSON, I. G.	533
TATAT, O.	134, 368	WEISS, A.	710
TAYAG, T. J.	291	WENSKI, W.	571
TAYLOR, C. R.	126	WERMKE, T. H.	509
THOLEN, T.	363	WESSELS, JR., R. A.	351
THÖNNESSEN, G.	819	WILKER, C.	155
TOLER, J. R.	89, 430	WOLF, S. A.	164
TOMITA, S.	774	WORTHINGTON, P.	395
TRAUT, R. T.	241, 256	WRIGHT, J. G.	291
TRAVIESO, R.	795	WRIGHT, W. F.	256
TREBER, N.	105	XUE, Y. Y.	174
TSAI, F.-Y.	483, 494	YAMADA, T.	582
TSUDA, M.	781	YAMAKAWA, J.	614
UCHIDA, T.	781	YAMAMOTO, H.	402
UEDA, T.	768	YAMAMOTO, K.	468
UKACHI, T.	72	YAMANAKA, M.	43
UNAMI, Y.	582	YAMANISHI, T.	768
UNGER, C.	413	YAMAZAKI, Y.	665
UNTERBERGER, S.	413	YANAGASE, H.	614
URANO, A.	644	YANAGI, T.	638
URRUTI, E. H.	89	YANG, R.	603, 672
USHIKI, M.	700	YIN, H. B.	620
VANDERLAAN, P. Z.	320	YOKOSUKA, H.	627
VERDENHALVEN, G.	809	YOSHIDA, K.	678
VERGEZ, C.	368	YOSHIDA, Y.	402
VINTERMYR, I.	249	YOSHIOKA, H.	234
VIRIYAYUTHAKORN, M.	183	YUCE, H. H.	742
VOGEL, E. M.	742	YUGUCHI, R.	781
WAGMAN, R. S.	12	ZAMMIT, M. J.	538
WAKUI, Y.	3, 593	ZAMZOW, P.	368
WALE, M. J.	281	ZAMZOW, P. E.	380, 819
WALKER, M.	450	ZHONG, Q.	736
WALLING, J.-H.	328		
WANCHUN, Z.	603		
WANG, C.-Y.	483		

NOTES



44th International Wire and Cable Symposium (IWCS)

Mariott Hotel

Philadelphia, Pennsylvania

November 13-16, 1995



REQUESTS FOR ABSTRACTS

TECHNICAL SESSIONS

Candidate papers for technical sessions should cover subjects of interest to the wire and cable industry. The industry typically consists of manufacturers, suppliers, OEM's and users who are involved with telecommunication (inside building, outside plant, submarine), control and signaling, quality control, processes, process control, manufacturing systems, interconnections, computers, electronic wiring, digital data systems, local area networks, data links, utilities for electrical power transmission and distribution. Papers are solicited covering both copper and fiber optic cable technology.

TRACK 1 - FIBER OPTIC CABLES

Papers in these sessions should involve areas such as: optical wave-guides, buffering techniques, cable designs, processing improvements, fiber coatings, new materials, fire considerations, installation, splicing developments, and field experience.

TRACK 2 - COPPER CABLES

As in the past, the IWCS will give special attention to advances in the design and manufacturing of copper cables. Papers in these sessions should involve areas such as: new developments in wire and cable design, shielding, wire harnesses, cable assemblies, connectorized cables, splicing and terminating techniques; new and improved materials, fire considerations, installation experience, cost reduction programs, and quality improvement programs; manufacturing techniques and use of copper cable network for higher level services, e.g. use of symmetrical copper network for data and high frequency applications.

POSTER SESSION

Papers in this session generally focus on developments in materials, measurement techniques, test procedures, installation practices or results of other brief investigations for both copper and fiber optic cables. Presentation of a paper in a Poster Session provides an opportunity for effective one-to-one communication and display of your material. Poster Session papers will be printed in the IWCS Proceedings and should not exceed five pages.

RELATED INTEREST SUBJECTS

Subjects of interest in these sessions include: global marketing strategies, domestic and international market surveys, future network plans, future industry needs and experience surveys.

Papers in the previously described areas are solicited. The listing below shows some typical categories for guidance purposes only and are not limited to these categories:

Applications and Field Evaluation

Future requirements in electronic systems; transmission characteristics; environmental performance, electromagnetic compatibility and interconnections; terminations, splices and couplers.

Process and Manufacturing

Insulating, shielding and sheathing; twisting, stranding, cabling, filling, taping, marking and automation; armouring and water blocking; round, flat and composite cables; quality-control methods.

Disposal, Recycling and Reutilization of Copper Cables

National regulations, environmental considerations, disposal techniques, separation of cable materials, physical/chemical analysis techniques, reutilization of materials.

Systems

Integration of wire, cables, fiber optics and other components; data cables, local area networks, inter- and intra-facility data distribution and management systems; computer and peripheral equipment wires, interconnections, optical waveguides and cable considerations, EMI and RFI considerations; testing and test procedures.

Design and Testing

Unique cable constructions; new measuring techniques, quality assurance and field tests.

Military Applications

Fixed plant, tactical communications, aircraft, shipboard, undersea applications and rapid deployment.

Power and Industrial Cables

Low, medium and high voltage a.c. and d.c. cables and accessories, joints and terminations, materials, processing, flame and radiation resistance, design, testing, installation, service restoration and experience, aerial and underground applications in transmission and distribution.

Cost Reduction and Quality Improvement Programs

Manufacturing equipment and processes improvements, maintenance programs, scrap reduction programs, supplier relationships, quality control practices and quality assurance testing.

Related Interest

Domestic and International marketing, surveys, future network and technological planning.

Author's Name(s) & Association _____

Contact for Correspondence _____

Company _____

Address _____

City _____ State _____ ZIP _____

Country _____

Telephone _____ Fax _____

Check the appropriate session:

☐ Fiber Technical

☐ Copper Technical

☐ Poster

Mail 25 copies before March 17, 1995 to:
International Wire and Cable Symposium, Inc.
174 Main St
Eatontown, NJ 07724
USA

AUTHOR'S SCHEDULE

Abstracts Due:	March 17, 1995
Acceptance Notification:	May 19, 1995
Complete Manuscript Due:	August 11, 1995
Symposium:	November 13-16, 1995

To submit a technical or poster session paper, prepare a comprehensive abstract using the format below:

1. TITLE OF PAPER: _____

2. PRIMARY CONCLUSION OR RESULT (One Paragraph):

3. BACKGROUND - WHY WAS WORK UNDERTAKEN? (One Paragraph)

4. ABSTRACT (Use additional pages as needed. See Note Below)

NOTE: Items 2, 3 and 4 should not be less than 300 words nor more than 500 words total in order to be considered by the Committee. The substance of submitted papers shall not have been previously published or presented and must satisfy the Committee's criteria for content, originality and minimal commercial content.

Acceptance by the Committee will be based on the abstract. Notification of acceptance will be mailed by May 19, 1995. The full manuscript will be required by August 11, 1995. The committee reserves the right to reject any final paper manuscript, if in its judgement, it does not comply with the guidelines on content, originality and minimal commercial content.